INTERNATIONAL ASTRONOMICAL UNION

SYMPOSIUM No. 169

UNSOLVED PROBLEMS OF THE MILKY WAY

Edited by LEO BLITZ and PETER TEUBEN

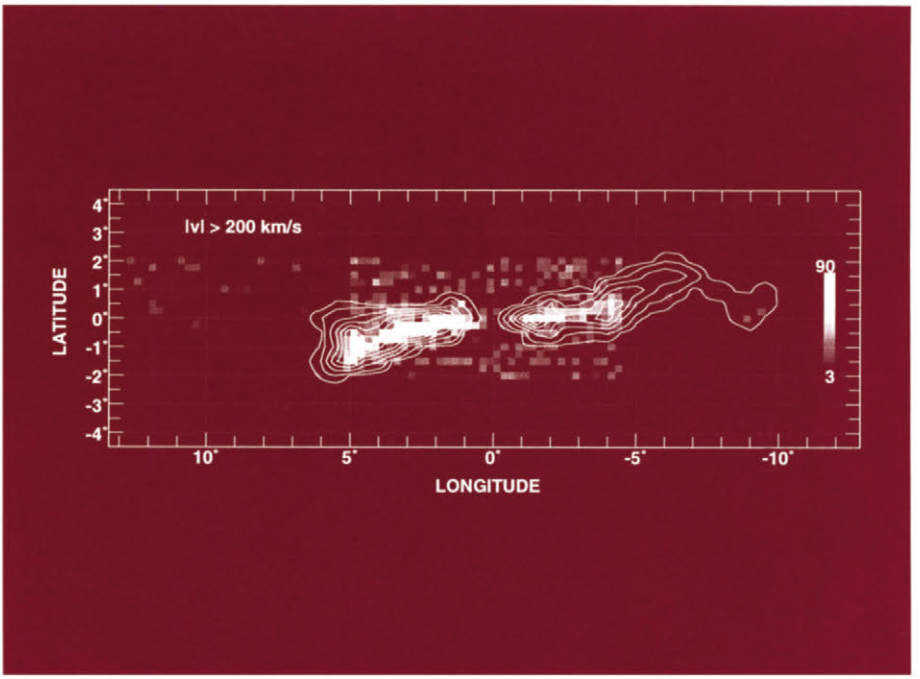

INTERNATIONAL ASTRONOMICAL UNION

SPRINGER-SCIENCE+BUSINESS MEDIA, B.V.

UNSOLVED PROBLEMS OF THE MILKY WAY

INTERNATIONAL ASTRONOMICAL UNION

UNION ASTRONOMIQUE INTERNATIONALE

UNSOLVED PROBLEMS OF THE MILKY WAY

PROCEEDINGS OF THE 169TH SYMPOSIUM OF THE
INTERNATIONAL ASTRONOMICAL UNION,
HELD IN THE HAGUE, THE NETHERLANDS, AUGUST 23–29, 1994

EDITED BY

LEO BLITZ

and

PETER TEUBEN

Department of Astronomy,
University of Maryland,
College Park, Maryland, U.S.A.

Springer-Science+Business Media, B.V.

A C.I.P. Catalogue record for this book is available from the Library of Congress.

ISBN 978-0-7923-4040-9 ISBN 978-94-009-1687-6 (eBook)
DOI 10.1007/978-94-009-1687-6

Printed on acid-free paper

All Rights Reserved
©1996 Springer Science+Business Media Dordrecht
Originally published by Kluwer Academic Publishers in 1996
Softcover reprint of the hardcover 1st edition 1996

No part of the material protected by this copyright notice may be reproduced or utilized in any form or by any means, electronic or mechanical including photocopying, recording or by any information storage and retrieval system, without written permission from the publisher.

CONTENTS

Preface ..... **xi**

Introduction

A. BLAAUW: Oort in Memoriam ..... **xv**

Chapter 1: Are the Disk and Halo Axisymmetric?

J.J. BINNEY: Should the Outer Milky Way be Axisymmetric? .. 1

M.D. WEINBERG: The Shape of the Disk: Clues from the Kinematics of Disk Stars 11

H.-W. RIX: The Shapes of Dark Halos 23

J.A. SELLWOOD: The Axisymmetric Stability of the Milky Way 31

C. PRITCHET, S. VAN DEN BERGH: Faint Surface Photometry of the Halo of M31 39

S.M. KENT: A Survey of Surveys 47

U. HAUD: Ellipticity of Outer Regions of Galactic Disks 57

J.E. RHOADS: Near Infrared Star Counts as a Probe of Asymmetries in the Galaxy's Disk 59

Chapter 2: Is the Milky Way a Barred Spiral Galaxy?

E. DWEK: Morphology of the Galactic Bulge from COBE DIRBE Observations 61

K. KUIJKEN: Is There a Bulge Distinct from the Bar? 71

O.E. GERHARD: Dynamics of the Bar at the Galactic Centre .. 79

B. PACZYŃSKI, *et al.*: Results from the Optical Gravitational Lensing Experiment (OGLE) 93

K.Z. STANEK, *et al.*: Evidence for the Galactic Bar from the Two Color Photometry of the Bulge Red Clump Stars 103

R.D. BLUM, *et al.*: M Giant Kinematics in Off-axis Fields between 150 and 300 PC from the Galactic Center 111
S. DEGUCHI, *et al.*: Results of the SiO Maser Survey of the Galactic Bulge IRAS Sources 119
R. FUX, *et al.*: 3D N-Body Simulations of the Milky Way 125
F. COMBES: Comparison with External Galaxies Dynamics ... 133
B.J. WEINER, J.A. SELLWOOD: Properties of the Galactic Bar from Hydrodynamical Simulations 145
K. WADA, *et al.*: Position-Velocity Diagrams as a Probe of the Bar in Edge-on Galaxies 147

Chapter 3: What is the Nature of the Center of the Galaxy?
C.H. TOWNES: Is There a Compact Central Mass Concentration in our Galaxy? 149
H. FALCKE: What is Sgr A*? 169
L.M. OZERNOY, R. GENZEL: Is Sgr A* Underfed, Undereffi-cient, or Underdone ? 181
L. OZERNOY: Recurrent Starbursts or Intermittent Starburst/ AGN Phenomena at the Galactic Center ? 189
D.C. BACKER: Diameter and Proper Motion of Sgr A* 193
W.J. DUSCHL, H. LESCH: The Radio Spectrum of Sgr A* 199
M.G. BURTON: Evolution in the Nucleus 205
H.M. LEE: Dynamical Evolution of Galactic Center Star Cluster and Importance of Stellar Collisions 215
R.D. BLUM, D.L. DEPOY, K. SELLGREN: A Comparison of Near Infrared Spectra of the Galactic Center He I Emission Line Sources and Early Type Mass Losing Stars 225
D. GEZARI, E. DWEK, F. VAROSI: Mid-Infrared Imaging of the Galactic Center 231
A.M. FRIDMAN, *et al.*: Mini-Spiral at the Galactic Center: a Link between its Structure and the Value of a Central Point Mass 241
M. MORRIS: What are the Radio Filaments near the Galactic Center? 247
E. SERABYN: The Nature of the Galactic Center Arc 263
F. YUSEF-ZADEH, *et al.*: The Nature of the Scattering and Faraday Screens Toward the Galactic Center 271
D. SCHAEItER: The Galactic Center Star Cluster: Normal Evolution!? 279
M. LINDQVIST, *et al.*: $C^{18}O$ and HNCO in the Galactic Centre 281

D.T. JAFFE, R. PLUME, S. PAK: Two New Views of the Galactic Center 283
E.J.A. MEURS: Possible Evidence for a Binary Massive Black Hole in the Galactic Nucleus 285

Chapter 4: Is there a Consistent Picture of the Inner kpc of the Milky Way?
K. KOYAMA, Y. MAEDA: The Hot Gas in the Galactic Bulge .. 287
H.S. LISZT, W.B. BURTON: Motions and Deformations of the Inner-Galaxy Neutral Gas Layer 297
P.J. BOYCE, R.J. COHEN: A Survey of OH in the Galactic Centre Region 311
H.J. HABING: Stellar Populations in the Galactic Bulge 317
D. MINNITI: Metallicity, Structure and Kinematics of the Milky Way's Bulge 329
R.-J. DETTMAR: Galactic Bulges as an Evolutionary Phenomenon 335
H. IZUMIURA: Observational Properties of SiO Masers in the Galactic Bulge IRAS Sources 341
D.A. LEVINE, M. MORRIS: Report on a Survey of H_20 Masers Towards the Galactic Center 343
M.N. SEVENSTER, *et al.*: Dynamical Properties of Galactic OH/IR Stars 345
M. SCHULTHEIS, et al.: Semiregular Variables in the Galactic Bulge 347
P. VAUTERIN, H. DEJONGHE: Instabilities of Uniformly Rotating Disks 349
W. DEHNEN: $F(E,L_z)$ for Kent's Model of the Galactic Bulge .. 351

Chapter 5: How Did the Milky Way Form?
J.E. NORRIS: The Age Structure of the Older Parts of the Galaxy 353
F. MATTEUCHI: Is the Dynamical History at odds with the Chemical History? 367
S. VAN DEN BERGH: Globular Clusters and the Formation of the Galactic Halo 381
I.F. BIKMAEV, *et al.*: Chemical and Dynamical History of the Milky Way 389
M. SAMLAND, G. HENSLER: The Metal Pre-Enrichment of the Galactic Disk: Solving the G-Dwarf Problem 395
R.M. RICH: Did the Bulge Form All at Once? 402
P. WHITELOCK: Late-Type Giants in the Bulge, at High Galactic Latitudes and in the Plane 411

W.J. SCHUSTER, C. ALLEN: Effects of Chaos in the Galactic Halo 419
Y. KAN-YA, *et al.*: The Velocity Dispersion in the Cold Collapse 423
T. TSUJIMOTO, *et al.*: The Chemodynamical Evolution of Spheroidal Systems and the Resultant Stellar Abundance Distribution Function 425
R. BUSER, J. RONG: Metallicity Structures of the Milky Way. . 427
M. SAMLAND, G. HENSLER: The Formation of the Galactic Bulge 429
B. FUCHS, C. DETTBARN, R. WIELEN: The Scatter of Metallicities of Stars in the Solar Neighbourhood 431
A.M. FRIDMAN, *et al.*: Different Laws of Increasing of Stellar Dispersion 433
M.G. LEE: UBVI CCD Photometry of an old Open Cluster AM-2 435

Chapter 6: How are we to Understand the Large Scale Structure of the ISM?

H. BLOEMEN: What do Gamma Rays tell us about the ISM?: New Insight from the Compton Observatory 437
W.B. BURTON, *et at.*: HI in the Milky Way 447
D.T. JAFFE: How Important is Neutral Carbon to an Understanding of the Dense Interstellar Medium? 469
A. FERRARA: Why is the HI Scale Height Constant with Galactocentric Radius? 479
J.M. DICKEY: The Z Velocity Dispersion of Outer HI Disks ... 489
H. OKUDA, *et al.*: Diffuse [CII] Emission in the Galaxy 497
S. MALHOTRA: Vertical Equilibrium of HI in the Galactic Disk 499
S. SAKAMOTO, *et at.*: Physical Conditions of Molecular Gas in the Galaxy 501
A.M. FRIDMAN, *et at.*: Does a Rotation Velocity Jump Generate the Outer Spiral Structure? 505
P.A. PATSIS, P. GROSBØL: Dynamics of Thick Spirals 507
D.J.D. EARN: Potential-Density Basis Sets for Three-Dimensional Disks 509
H. DEJONGHE, *et al.*: The Dynamics of Planetary Nebulae in the Galaxy: Evidence for a Third Integral 511
B. CHEN, *et al.*: The Existence of Moving Groups and the Disk Heating Problem 513
M. WAHDE, K.J. DONNER, B. SUNDELIUS: The Influence of Velocity Dispersion on Dynamical Friction in Stellar Discs 515

X. ZHANG: On the Spiral-Induced Nonlinear Dissipative Process to the Evolution of the Galactic Disk 517
E. GRIV: Stability of a Collisionless Stellar Disk 519
E. GRIV: Stability of a Collisional Galactic Disk 521
L.P. OSSIPKOV, S.A. KUTUZOV: Galactic Orbits of Different Galactic Population Objects 523
M. MORENO, J. TORRA, E. OBLAK: Local Variations of the Velocity Ellipsoid 525
J. ANOSOVA, *et al.*: Escape Velocities from Unstable Triple Stars 527
J. ANOSOVA, *et al.*: Hierarchical and Non-Hierarchical Triples 529
L. KISELEVA, J. ANOSOVA: Criteria of Dynamical Isolation of Binaries and Multiples 531

Chapter 7: How are we to Understand the Small Scale Structure of the ISM?
C.J. LADA: The Unsolved Problem of Stellar Origins 533
B.G. ELMEGREEN: What do we really know about Cloud Formation? 551
J. BRAND, J.G.A. WOUTERLOOT: Far-Outer Galaxy Molecular Clouds 561
W.T. REACH: Far-Infrared Spectral Observations of the Galaxy by the Far-Infrared Absolute Spectrophotometer 567
E.J. DE GEUS, J.A. PHILLIPS: The Search for Cold Molecular Gas in the Outer Galaxy 575
J. PALOUŠ: How does Star Formation Affect the Large Scale Structure of the ISM? 583
A. WHITWORTH: The Structure of the Neutral Interstellar Medium: A Theory of Interstellar Turbulence 591
A.M. FRIDMAN, *et al.*: Are there Giant Vortices near Solar Circle? 597
B.P. WAKKER, *et al.*: Distance and Metallicity of HVCs 605
S.J. CAREY, K.N. MEAD, M.L. KUTNER: Molecular Mass Distribution in the Outer Galaxy 607
B.M. DEISS, A. JUST: A Hydromagnetic Model for the Hierarchical Structure of Molecular Clouds 609
A.J. GREEN, *et al.*: Galactic Fine Structure at 843 MHz 611
S.J. PETUCHOWSKI, C.L. BENNETT: Neutral Gas Contributions to [S II] Galactic Background Emission 613

V.R. SHOUTENKOV: Study of the Magnetic Field of the Galaxy using Correlation Functions of the Intensity of Synchrotron Background Radio Emission 615
C. CAPPA DE NICOLAU, *et al.*: HI Bubbles around NGC 6888 617
C. CAPPA DE NICOLAU, *et al.*: Search for HI Bubbles around WR Stars: WR 149 619
S. EHLEROVÁ, *et al.*: GS64-01-97: Expanding Supershell in the Milky Way 621
L.G. BALÁZS, P. ÁBRAHÁM: Multi-Wavelength Study of the Giant Bubble in Cepheus 623
A.M. BYKOV: Non-Thermal Particles near OB Associations ... 625
N. JUNKES: G54.4-0.3 – Multi-Frequency Investigation of an SNR in Interaction with the ISM 627
R.H. RUBIN, *et al.*: HST Spectroscopy of the Orion Nebula ... 629

Chapter 8: How do we put it together?
P.L. SCHECHTER: How ought one Parameterize the Milky Way? 633
K.C. FREEMAN: Does Our Galaxy have a Massive Dark Corona? 645
A. GOULD: Mass near the Sun 651
F. PONT, *et al.*: Outer Disc Rotation from Cepheid Variables ... 661
F.D.A. HARTWICK: Where Does the Galaxy End? 669
A.C. ROBIN, M. CRÉZÉ, V. MOHAN: How do the Stellar Disc and Thick Disc Stop? 681
B. FUCHS, *et al.*: Proper Motion Study of the Galactic Rotation Curve 689
B. DAUPHOLE, *et al.*: The Mass Distribution of the Milky Way Deduced from Globular Cluster Dynamics 697
D.M. PETERSON, D. SLOWIK: The Rotation Curve from A-F Supergiants 703
R. BUSER, J. RONG: The Structural Parameters of the Milky Way 707
S. NINKOVIĆ: A System of Galactic Constants Based on Stellar Dynamics 709
S.A. KUTUZOV: Estimation of Galactic Model Parameters by Interval Method 713

Subject Index **715**

Object Index **723**

PREFACE

Prior to the IAU Symposium 169, it had been 11 years since the IAU held a major meeting on the topic of the Milky Way. Although some of the problems that astronomers were addressing in the literature were similar to those that were at the forefront at the last Milky Way IAU, there seemed to be a considerable shift in the areas of interest since then. For example, the nature of the Galactic center and the Galactic nucleus remain today active and compelling areas of research as they were ten years ago. However, the strong interest in the possibility that the Milky Way has a central bar, and the entire question of non-axisymmetric mass distributions throughout the Galaxy were little discussed then but have enjoyed a large surge of interest in the last five years.

It seemed fitting, therefore, that rather than have a meeting that simply assessed the progress of Milky Way research since the last IAU symposium, a meeting be held in which the subjects of most compelling current interest would be discussed and debated. Hence the title of the meeting, "Unsolved Problems of the Milky Way." There are of course more unsolved problems than could be addressed at the meeting, and an attempt was made to identify those problems that not only hold strong interest even for those astronomers not directly engaged in Milky Way research, but for which there is some hope of either being solved or having significant progress made in the next five to ten years. Even still, not all problems of wide interest could be accommodated. There was nothing in the program, for example, on high velocity clouds, or directly relating to spiral structure.

The meeting was one of six scientific symposia held in conjunction with the 22nd IAU General Assembly in the Hague. The organization was a bit different from most meetings in that each major topic was organized by one or two people on the scientific organizing committee in consultation with the chairs. Each session had the normal complement of invited speakers,

but the session organizers also chose from the papers contributed as posters, a number to be given orally. This allowed the organizers to identify those papers presenting the research most relevant to the chosen topics so that they could be aired for the entire audience. The process seemed to work well and made it possible to have a reasonably large number of relatively new faces make presentations to the entire symposium. The scientific organizing committee included: James Binney (co-chair), Leo Blitz (co-chair), Butler Burton, Francesca Matteucci, Mark Morris, Jan Palous, Paul Schechter, David Spergel, and Scott Tremaine. Hans Bloemen was the local organizer, and Hugo van Woerden did an outstanding job in making sure that meeting ran smoothly.

The organization of this volume follows reasonably closely the organization of the meeting itself. The order of the papers, however, has been changed somewhat so that speakers who have presented closely related topics have their papers appear together. Poster papers are presented at the end of each chapter which covers the most closely related topics. We have made an effort to reproduce as well as we could the discussion after each paper. In twenty years, the discussion will probably be the most widely read part of the book. We have also provided a subject and object index.

The year and a half prior to IAU 169 saw the passing of Jan Oort, whose towering contributions to the understanding of the Milky Way date back to the 1920s. Oort probably did more to lower the number of unsolved problems of the Milky Way than any other astronomer, not to mention the important work he did in many other areas. It therefore seemed particularly appropriate to dedicate the meeting to Oort, especially since the IAU was being held in his native Holland. As it turned out, two others who made enormous contributions to our understanding of the Milky Way also passed away the year the IAU was held: W.W. Morgan, and David Allen. It is perhaps a fitting tribute to all three that the Galaxy that they did so much to help us understand remains an object that even now harbors mysteries engaging a new generation of Oorts, Morgans, and Allens.

Leo Blitz and Peter Teuben
College Park, Maryland

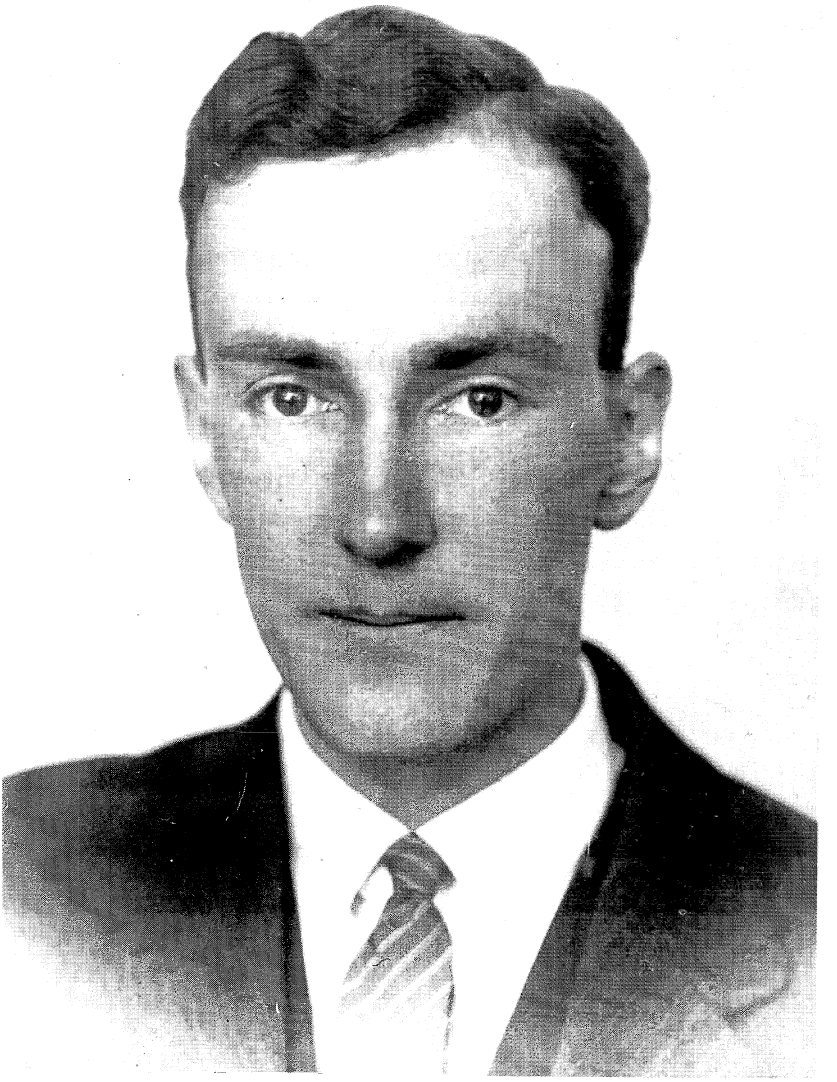

Dr. J.H. Oort.
"Courtesy Sterrewacht Leiden"

OORT IN MEMORIAM

ADRIAAN BLAAUW
Kapteyn Laboratory, University of Groningen

Jan Hendrik Oort died in November 1992 after a life devoted to astronomy. A life that brought him, and his beloved wife Mieke, the happiness of family life and innumerable honours, and the affection and admiration of colleagues all over the world. It is fitting that we devote this Symposium to the memory of a man to whom students of galactic research owe more, I think, than to any other astronomer of the 20th century.

Oort studied at Groningen under J.C. Kapteyn, whose approach to astronomical research has deeply influenced Oort's own work: always aiming at close confrontation of theory with observation, with a critical look at the real value of the observations, and keeping the theoretical treatment as transparent as possible. And always alert, with an open eye for that unexpected, easily overlooked feature that might contain the clue for opening a new field of interest. He was a man of extraordinary perception and perseverance.

If I ask youngest astronomers about Oort's work, the chances are that they will mention him as the discoverer of the "Oort Cloud" of comets; this has been referred to frequently in relation to recent, widely publicized events. If I ask the generation that entered astronomy in the 1960s and 1970s, they will mention his pioneering work in radioastronomy: the establishment of the radio observatories at Dwingeloo and Westerbork, the 21-cm surveys of the Galaxy, and subsequent extragalactic work. My own first acquaintance with Oort's work dates from still farther back: the mid-1930s, less than a decade after Oort's fundamental work on differential galactic rotation and the implications for the dimensions and dynamics of the Galaxy - and I

subsequently witnessed his interest shifting to the role of the interstellar medium in the context of galactic and extragalactic structure in the 1940s and 1950s. For me, this first phase of Oort's career has always remained the most impressive. All he did arose from his deepest motivation: curiosity about the structure and history of the all-embracing Universe.

Apart from his pure research, we owe to Oort initiatives that led to some of the most impressive facilities now accessible to the observational astronomer: the radio observatories at Dwingeloo and Westerbork and the European Southern Observatory. And we remember how deeply he has inspired the work of new generations of astronomers with these radio-astronomical facilities!

For those of us who have been privileged to be associated with Jan Oort, be it as student or as a colleague, there will remain the long lasting memory of a man of extraordinary leadership and inspiration, and of a dearly loved friend.

COLOR PLATES

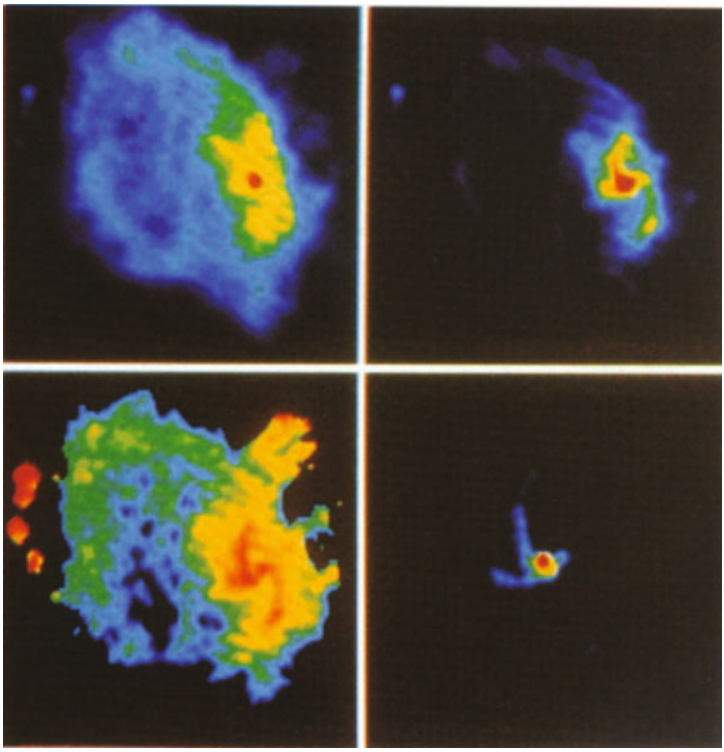

Figure 1. Radio continuum maps from the VLA of the central 10×10 pc^2 of our galaxy. Lower left: Spectral index map from images at 20 and 6 cm with 8 arcsec resolution. The blue region represents synchrotron radiation, the yellow and red various intensities of free-free thermal emission. Upper left: 20 cm image with 8 arcsec resolution. Upper right: 6 cm image. lower right: 2 cm image, resolution 4 arcsec. (Courtesy Ekers, R.D., Schwarz, U.J., Goss, W.M., and van Gorkom, J.H.).

(Figure belongs to the article by C.H. Townes, page 149)

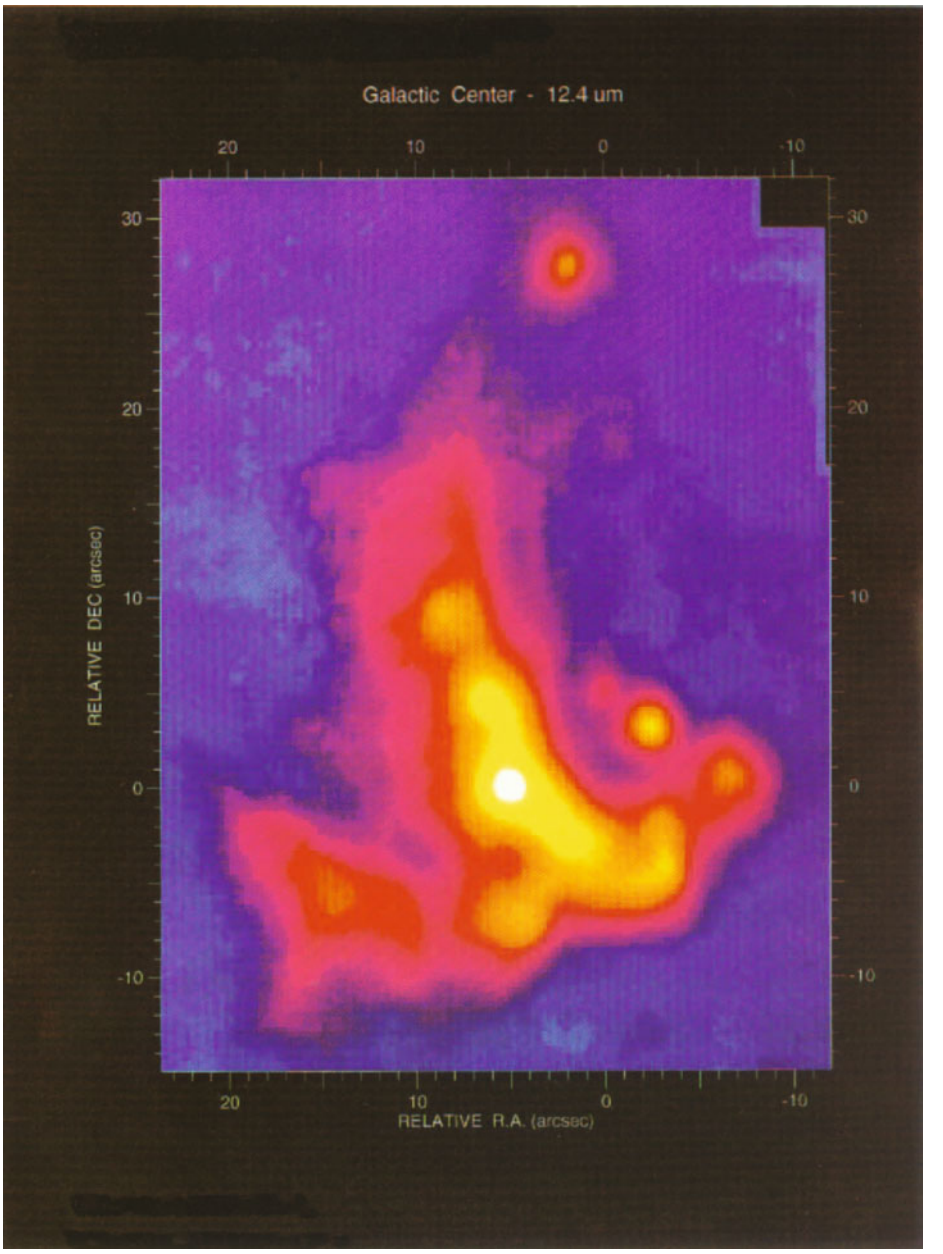

Figure 2. 12.4 μm continuum mosaic of the central 2 pc of the Galactic Center Sgr A West complex obtained with the 58 x 62 array camera (Gezari et al. 1992) at the 3-m NASA/IRTF Telescope at Mauna Kea. The intensity display is logarithmic to show details in regions of extended faint emission. The mosaic was assembled from 50 overlapping 1 min integration frames (15 x 16 arcsec field of view, pixel size 0.26 arcsec) which were aligned, matched and coadded to make up the final mosaic. Positions are measured relative to Sgr A*. The strongest infrared emission is very similar to the ionized gas distribution observed in 2-cm and 6-cm VLA maps of the region.

(Figure belongs to the article by D. Gezari et al., page 231)

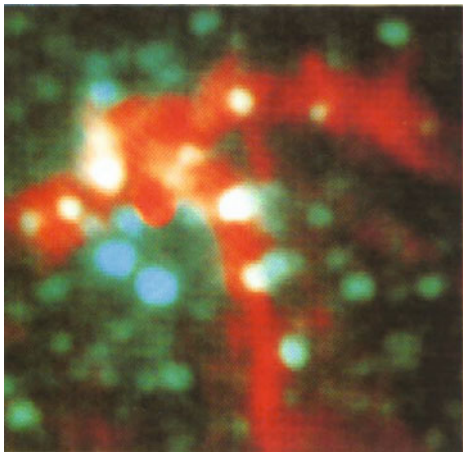

Figure 3. The IRPS 3.8μm image (from [5]) in blue, overlaid on the 6-cm radio continuum image of Lo & Claussen (1983) in red, tying together the radio and infrared reference frames via the emission from IRS 2/13, seen in both frames. This image demonstrated clearly that IRS16-C (which is not priminent at these wavelengths) and SgrA* were two separate sources. SgrA* is the rbight red soiurce just to the right of the center and IRS 7, the brightest sources at 2μm, is the blue star directly above it. IRS 2/13 are the pair of white sources just below right from SgrA*
(Figure belongs to the article by M.G. Burton, page 205)

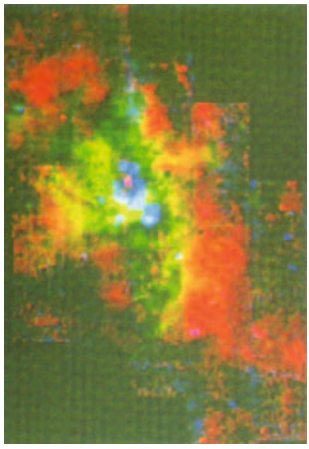

Figure 4. An image of the hot stars and gas in the centeral 2 parsecs of the Galaxy, obtained with the method of spectroscopic drift scanning of IRIS (from [8].) Blue denotes emission from a HeI line at 2.06μm, and shows a cluster of a dozen massive stars in the nucleus. They are surrounded by the ionized ghas ofthe radio "mini-spiral", here seen in green through the ermission of hydrogen Brγ at 2.17μm. Surroudning the ionized cavity is a hot clumpy molecular ring, seen in red through the light of molecular hydrogen at 2.12μm.
(Figure belongs to the article by M.G. Burton, page 205)

Chapter 1

Are the Disk and Halo Axisymmetric?

SHOULD THE OUTER MILKY WAY BE AXISYMMETRIC?

JAMES BINNEY
Department of Physics
1 Keble Road, Oxford, OX1 3NP, England

Abstract. The shape of the outer Milky Way should be heavily influenced by the shape of our heavy halo. Simulations of the formation of collisionless halos indicate that they should be highly triaxial, with a tendency to prolateness. If our halo were as strongly triaxial as these simulations suggest, the outer disk would have ellipticity $\epsilon_{\rm disk} \simeq 0.06$.

Simulations of galaxy formation which include an appropriately small fraction of gaseous matter give rise to halos of much smaller ellipticity, and predict $\epsilon_{\rm disk} \lesssim 0.02$. These simulations are not as reliable as purely collisionless simulations, and we should treat their results with some caution. However, it is not incredible that a small fraction of gas could radically reduce the ellipticity of a halo by making the system's potential more centrally concentrated.

The distribution of the apparent ellipticities of spiral galaxies indicates that their disks have slightly eliptical disks, $\epsilon_{\rm disk} \simeq 0.05$. This may merely reflect ephemeral features such as spiral arms, however. The velocity fields of disks provide a more robust probe of the ellipticity ϵ_Φ of galaxy potentials. The narrowness of the Tully–Fisher relation places an interesting upper limit $\epsilon_\Phi < 0.1$. More detailed studies of individual velocity fields will be required if we are unambiguously to demonstrate $\epsilon_\Phi > 0$ in some cases.

1. Introduction

It is now generally accepted that elliptical galaxies are not axisymmetric and it is natural to wonder whether the same might be true of disk galaxies such as the Milky Way. Of course, at least a half of all disk galaxies are clearly non-axisymmetric at small radii because they contain a bar. There is steadily accumulating evidence that the Milky Way has a central bar too.

L. Blitz and P. Teuben (eds.), Unsolved Problems of the Milky Way, 1–10.
© 1996 *International Astronomical Union.*

But the dynamical effects of this bar would be very small at the solar radius, R_0, and beyond. What I want to discuss here is the possibility that the outer galaxy is not so much barred as mildly elliptical. The main motivation for this proposition is theoretical and connected with the existence of massive halos. In Section 2 I review these arguments. Since these are of a general nature and would apply to any disk galaxy, it is natural first to test them by examining in Section 3 the evidence for ellipticity in external disk galaxies. Weinberg (this volume) examines the evidence for and against the Milky Way's being elliptical.

2. Theoretical arguments

Until recently it has been assumed that disk galaxies are fundamentally round rather than elliptical in shape, even though their images are usually elliptical – by Ockham's razor the ellipticity of their images was entirely ascribed to the effects of projection rather than to some combination of intrinsic ellipticity and projection.

From the mid 1970s this traditional view has been undermined by the suspicion that disk galaxies are embedded in dark halos (Ostriker & Peebles 1973, Trimble 1987). The Milky Way's dark halo is reputed to contribute on the order of half the galactocentric force on the Sun, and to contain the overwhelming majority of the Milky Way's total mass (Fich & Tremaine 1991). In 1978 Binney pointed out that it would be natural for dark halos to be triaxial bodies, independently of how they formed or of what they are made, and investigated the consequences of this triaxiality for the embedded visible galaxies.

The argument for the triaxiality of halos is simple. These systems (unlike disks) probably formed collisionlessly. Numerical experiments show that the 'violent' relaxation that takes place during the virialization of a collisionless system, is never so efficient as completely to erase memory of the initial conditions. In any plausible scenario of galaxy formation, the latter will have been significantly anisotropic, and the numerical experiments (Binney 1976, Aarseth & Binney 1978) indicated that this anisotropy will have bequeathed to the final halo a triaxial form.

Over the last decade and a half the sophistication of the numerical experiments has increased enormously, and we have achieved a moderate understanding of the internal dynamics of triaxial systems, although the topic is still very much under study.

The greatest advance in the numerical experiments has been the simulation of galaxy formation in realistic cosmological contexts and the inclusion, in a crude way, of gas. Barnes (1992, 1994), Hernquist (1993) and others have studied mergers in small groups of galaxies, Frenk *et al.* (1988),

Dubinski & Carlberg (1991) and Warren *et al.* (1992) have studied the formation of galaxy halos through hierarchical clustering in large cosmological simulations, and Katz & Gunn (1991) have studied the formation of individual galaxies from lumpy protoclouds along the lines pioneered by van Albada (1982). The purely collisionless simulations confirm Binney's original contention that halos will be generically triaxial – they prove strongly triaxial with a tendency to prolateness rather than oblateness. Moreover, the structures of merger remnants frequently deviate from axisymmetry in more exotic ways than mere triaxiality (Barnes 1992).

Simulations that contain even a little mass in 'gas' particles yield significantly different results (Katz & Gunn 1991, Barnes 1994). Collisional particles rapidly sink to the centres of merger remnants, greatly increasing the density there. This seems to drive the dark halo away from prolateness towards oblateness. For example, Barnes (1994) describes two merger simulations that initially differed only in that 1.5% of the mass of one simulation was gaseous. In the gas-free simulation the innermost quartile of the dark halo ended with axis ratios 1:0.88:0.80, while in the gas-rich simulation the inner dark halo finished with axis ratios 1:0.96:0.87 (Barnes, private communication). Thus 1.5% of gas reduced the ellipticity in the equatorial plane by a factor of ~ 3.

2.1. SELF-GRAVITY OF THE DISK

What makes the ellipticity ϵ_h of dark halos sensitive to the inclusion of so little gas? One factor to consider, which is certainly an important one in the Milky Way, is the self-gravity of the disk. Given that the pattern speed of the halo's figure must be very slow, it is straightforward to derive two results from the epicycle approximation: (i) the nearly closed orbits of the disk align such that their major axes coincide with the minor axis of the halo; (ii) the ellipticity ϵ_d of these orbits is nearly equal to that of the ellipticity ϵ_Φ of the isopotential contours. The ellipticities of disk and the closed orbits are strictly different but at the radii of interest very similar: for an exponential disk of scale-length R_d, $\epsilon_{\rm disk} \simeq (1 + R/R_d)\epsilon_d$ (Franx & de Zeeuw 1992). I shall identify ϵ_d with $\epsilon_{\rm disk}$.

Since it is characteristic of solutions of Poisson's equation that ϵ_Φ is roughly a third of the ellipticity of the generating mass distribution, we may write

$$\epsilon_\Phi \simeq \tfrac{1}{3}\Big(\frac{M_h}{M_h + M_d}\epsilon_h - \frac{M_d}{M_h + M_d}\epsilon_d\Big), \qquad (1)$$

where M_h and M_d are the masses of the halo and disk interior to the radius

under consideration. Inserting $\epsilon_d \simeq \epsilon_\Phi$ into this relation, we find

$$\epsilon_d \simeq \epsilon_\Phi \simeq \frac{M_h}{3M_h + 4M_d}\epsilon_h. \tag{2}$$

Near the Sun, $M_h \simeq M_d$ and $\epsilon_d \simeq \frac{1}{7}\epsilon_h$, while at radii so large that $M_h \gg M_d$, $\epsilon_d \simeq \frac{1}{3}\epsilon_h$. In other words, near R_0 the self-gravity of the disk diminishes the ellipticity of the potential by a factor $\frac{3}{7}$. Moreover, this is an underestimate of the true diminution, because our simple calculation has not allowed for the fact that the halo will be made rounder by this rounding out of the potential. Barnes' pair of simulations with and without gas may reflect this effect. In any event, taking the mean ellipticity $1 - b/a \simeq 0.4$ of the halos studied by Dubinski (1992) and one third of this value $\epsilon_h = 0.13$, as typical for simulations with and without gas, we find $\epsilon_d = 0.04, 0.13$ in the case $M_h \gg M_d$ discussed by Binney (1978) and $\epsilon_d = 0.019, 0.06$ in the more realistic case $M_h \simeq M_d$.

It is, in fact, likely that for a sufficiently large value of M_d/M_h both disk and halo become perfectly round. It would be interesting to determine this value of M_d/M_h.

2.2. CENTRALLY CONCENTRATED SYSTEMS

The effect of the disk's self-gravity just described will be small outside a few effective radii, R_e. Yet Dubinski (1994) has shown that adding the potential of a luminous galaxy to a dark halo can diminish the halo's ellipticity at several R_e. In his experiments an analytic disk or bulge potential placed at the centre of an n-body halo has a slowly increasing mass. While the flattening c/a of the halo is only slightly reduced by the growth of the analytic potential, the halo's axis ratio b/a increases from $b/a \simeq 0.6$ to $b/a \simeq 0.8$ at $r \simeq 25\,\mathrm{kpc} = 3.1R_e$, and from from $b/a = 0.7$ to $b/a = 0.85$ as far out as $r = 40\,\mathrm{kpc} = 5R_e$. The analytic potential has these far-reaching effects because the orbital structure of a triaxial system depends qualitatively on the system's degree of central concentration. This phenomenon deserves close attention because real galactic potentials are more centrally concentrated than that of any n-body model.

The landmarks in our understanding of the internal dynamics of triaxial systems are Schwarzschild's (1979) analysis of the orbit mix of a typical triaxial system, and de Zeeuw's (1985) demonstration that Stäckel potentials provide analytic models of the orbits identified by Schwarzschild. Wilkinson & James (1982), Barnes (1992) and others have demonstrated that the bars formed in collisionless n-body experiments conform to the pattern established by Schwarzschild and de Zeeuw. In particular, the backbones of these systems comprise stars on 'box' orbits.

The conversion of even a small fraction of the total mass to collisional 'gas' particles radically changes the structure of merger remnants because the great increase in the final central density to which these particles give rise, radically restructures parts of phase space. No analytic counterparts are known for the orbits in a centrally concentrated potential which take over the part of phase space which is occupied by box orbits in a Stäckel potential. Consequently, the dynamics of these crucial orbits is not properly understood.

For want of a better framework, one usually discusses the dynamics of centrally concentrated triaxial potentials by reference to Stäckel potentials. In this perhaps inappropriate language, as an initially Stäckel-like potential is made more centrally concentrated, more and more box orbits become either trapped by resonances, or become stochastic through competition between resonances for their adherence (Gerhard & Binney 1985, Lees & Schwarzschild 1992, Schwarzschild 1993). Physically, what is happening here is that orbits that pass close by the centre are scattered by the strong gravitational field there and are classified as stochastic orbits. Meanwhile other orbits perpetually avoid the centre by coordinating their motions parallel to the potential's principal axes; that is, by being trapped by some resonance.

Schwarzschild (1993) determined the orbital structure of the potential generated by the density distribution $\rho \propto m^{-2}$, where $m^2 = x^2/a^2 + y^2/b^2 + z^2/c^2$ is an elliptical radius. He showed that in this scale-free limit no non-resonant regular box orbits survive. He was nevertheless able to reproduce the underlying density distribution by superposing orbits in the given potential, provided he employed stochastic as well as regular orbits. This exercise suggests that realistically centrally concentrated triaxial halos may be possible, but it does not demonstrate that they will form in the real universe.

There are two potential problems with the orbit distribution of Schwarzschild's self-consistent scale-free model: it may be too special to form during violent relaxation or merging; or it may not be the distribution that emerges as dissipation makes a Stäckel-like system more centrally concentrated. I think it will be hard convincingly to eliminate these two anxieties because the enormous range in time- and length-scales of realistically centrally concentrated systems makes them difficult to simulate accurately. On the other hand, the approach pioneered by Schwarzschild cannot be used to study how slowly an initially triaxial system evolves towards axisymmetry in the event that a strict triaxial equilibrium is impossible. My hunch is that at the end of the day it will be found that centrally concentrated triaxial halos do form and survive for much longer than the Hubble time. I base this hunch on two facts. (i) Gerhard & Binney (1985) estimated the

time required for the triaxiality of an elliptical galaxy to disappear as a consequence of stars being scattered off the all important box orbits by a nuclear cusp. They concluded that in the Hubble time this process would only destroy triaxiality inside $\sim 3\,\mathrm{kpc}$. (ii) The central concentration of the potential is important only for stars whose apocentres lie many core radii out. But these are the stars which are most sensitive to any figure rotation of the potential; if the potential has non-zero pattern speed, as it surely has, the Coriolis force will deflect them from the nucleus, with the consequence that they are never scattered by it.

Before turning from dynamics to phenomenology, I must make explicit the spectre implicit in the discussion above. There must be a largest radius $r_{\rm max}$ at which a galaxy may safely be treated as a relaxed quasi-equlibrium object that may be plausibly characterised by a pair of ellipticities. Beyond $r_{\rm max}$ the system will be lop-sided and irregularly time-dependent as a consequence of long local dynamical times and regular passages by lumps of material (mostly dark) moving on highly elliptical orbits. We have no reliable estimate of $r_{\rm max}$. A lower estimate would be the radius, $r_{\rm warp} \simeq 1.2R_0$, at which warps become pronounced. In the popular normal-mode theory of warps (Dekel & Shlosman 1983, Toomre 1983), $r_{\rm warp}$ would be an underestimate of $r_{\rm max}$, but as Kuijken & Tremaine (1994) have pointed out, the Milky Way's warp is significantly too asymmetric to be accounted for by the normal-mode theory, and we should seriously consider the possibility that $r_{\rm max} \simeq r_{\rm warp}$ as an alternative theory (Ostriker & Binney 1989) requires. Beyond $r_{\rm max}$ the disk will not merely be elliptical, but lop-sided as well. Richter & Sancisi (1994) have recently demonstrated that most disk galaxies are significantly lop-sided at a few R_e.

3. Are the disks of external galaxies elliptical?

If disk galaxies are triaxial rather than axisymmetric, one would expect the principal axes of their isophotes to 'twist' from one isophote to the next. Bertola, Vietri & Zeilinger (1991) have sought such isophote twists in a sample of 32 nearby spirals. They find that the majority of these galaxies display isophote twists, from which it follows that in these galaxies at least one of the bulge and the disk must be triaxial.

There are two obvious observational tests of the conjecture that galactic disks are circular. One is to examine the distribution of apparent ellipticities. When a flat disk is viewed in projection, its image may have any axis ratio $q_{\rm app}$ from 1 (circular) to 0 (linear). If the disk is circular, the probability distribution $P(q_{\rm app})$ is independent of $q_{\rm app}$, but if the disk has intrinsic axial ratio $q_{\rm true} < 1$, $P(q_{\rm app})$ peaks at $q_{\rm app} = q_{\rm true}$ and falls away quite steeply at larger values of $q_{\rm app}$. This has the effect of reducing the number

of apparently round galaxies one expects to find if a significant fraction of disks are intrinsically elliptical. Binney & de Vaucouleurs (1981) found marginal evidence for this effect in the 650 spirals in second Reference Catalogue of Galaxies, while Lambas, Maddox and Loveday (1992) detected it in the 13 500 spiral galaxies in the APM survey. The data favour many disks having axis ratio $q_{\rm true} \simeq 0.95$, with few disks more elliptical than $q_{\rm true} = 0.9$. Huizinga & van Albada (1992) and Franx & de Zeeuw (1992) have reached similar conclusions.

The apparent ellipticities of spiral galaxies must be influenced by spiral structure, so it is not clear whether the results reported in the last paragraph reflect fundamental ellipticity or the ephemeral effects of spiral arms. A more robust test of the conjecture that disks are intrinsically round is to examine the velocity fields of galaxies (Binney 1978, Franx & de Zeeuw 1992, Franx, van Gorkom & de Zeeuw 1994). The kinematic minor axis is the line on which the projected velocity equals the systemic velocity, while the kinematic major axis is the line along which the projected rotation velocity is largest for a fixed galactocentric distance. Since the stars of an elliptical disk are on elliptical rather than circular orbits, the kinematic axes usually do not coincide with the photometric principal axes when the velocity field generated by stars on elliptical orbits is examined in projection. Unfortunately, warping of the disk also causes the kinematic axes to deviate from the photometric axes. The effects of warping and ellipticity can in principle be distinguished because the former keeps the kinematic axes mutually perpendicular, while the latter does not. However, separating warps from ellipticity requires detailed modelling of the data, and the sample of galaxies that have been analyzed in the requisite detail is still small. Begeman (1989) studied eight galaxies in detail and found misalignments of the kinematic and photometric axes compatible with those expected if the galaxies had potentials of ellipticity $\epsilon_\Phi \simeq 0.1$, but the offsets detected were comparable to the errors. Franx *et al.* (1994) have analyzed HI data for a filled ring at $R \simeq 6.5R_e$ around an early-type galaxy in Fornax cluster, IC 2006. Although the circular-speed curve appears to be roughly flat to this radius, Franx *et al.* find that the potential of IC 2006 is axisymmetric to within the errors: $\epsilon_\Phi = 0.012 \pm 0.026$. On the other hand dark halos do not as a rule prove to be spherical: Sackett *et al.* (1994) deduce from observations of a polar ring that the halo of NGC 4650A is as flattened as the luminous galaxy.

Franx & de Zeeuw (1992) pointed out that disk ellipticity would contribute to the scatter in the Tully–Fisher relation, $L \propto v_c^n$, between luminosity and maximum circular speed v_c, by making the inferred value of v_c dependent on the orientation of the disk. The magnitude of this effect depends on how v_c is inferred from the data – whether the disk's orientation

is determined by fitting a ring model to the velocity field, or by fitting an axisymmetric model to the photometry; a ring model yields the smaller error. The magnitude of the error also depends on the inclination angle i – the error in v_c becomes large for nearly face-on galaxies. Franx & de Zeeuw calculated the ellipticity ϵ_Φ that would give rise to a scatter in $L \propto v_c^n$ as large as that reported, and found that $\epsilon_\Phi \simeq 0.1$ sufficed because even the small errors in v_c (10%) give rise to significant scatter in L ($\simeq 40\%$). Since it seems unlikely that disk ellipticity is the only contributor to the scatter in $L \propto v_c^n$, Franx & de Zeeuw conclude that $\epsilon_\Phi < 0.1$.

4. Conclusion

The shape of outer Milky Way will be heavily influenced by the shape of the heavy halo. N-body simulations of the formation of collisionless halos indicate that such halos would be strongly triaxial, and the dynamics that underlies this result is understood in some detail. Disk ellipticities of order $\epsilon_{\rm disk} \simeq 0.06$ are predicted by these simulations for radii near R_0 (where half of the radial force is contributed by the disk) rising to $\epsilon_{\rm disk} \simeq 0.13$ at $R \gg R_0$.

The halos that form in galaxy-formation simulations that include gas are significantly rounder than those that form in purely collisionless simulations. These still pioneering simulations are undoubtedly less trustworthy than are purely collisionless simulations, but we do expect the inclusion of gas to reduce significantly the ellipticities of halos. One mechanism for this reduction is the tendency of disks to anti-align with the potential in which they move, thus diminishing the ellipticity of both the overall potential and the halo. A second more far-reaching mechanism arises from the fact that orbits in very centrally concentrated triaxial potentials are not structured in the same way as orbits in less centrally concentrated systems. Because of this, very centrally concentrated self-consistent triaxial systems may not even exist.

Notwithstanding these anxieties, our best guess at the moment is that halo potentials are at least mildly triaxial, with the consequence that the embedded disks will have ellipticities $\epsilon_{\rm disk} \simeq 0.015 - 0.03$, with larger values ruling at larger radii. Studies of the apparent-ellipticity distribution of spiral galaxies suggest that most disks are elliptical, with ellipticities near 0.05. In principle the velocity fields of disks provide much more reliable probes of disk ellipticity than photometry, and this line of attack should be increasingly exploited in the future as good quality velocity data become available. At the moment is hard to draw a firm conclusion from detailed studies of individual data, although these do seem to be compatible with an ellipticity distribution centred on $q = 0.05$ of width $\delta\epsilon \simeq 0.05$. Signifi-

cantly more elliptical disks seem to be ruled out by the narrowness of the Tully-Fisher relation.

References

Aarseth, S.J., Binney J.J., 1978. MNRAS, 185, 227
Barnes, J.E., 1992. ApJ, 393, 484
Barnes, J.E., 1994. In *The Formation of Galaxies*, ed. Munoz-Tunon, C., (Cambridge, Cambridge University Press)
Begeman, K., 1989. A&A, 223, 47
Bertola, F., Vietri, M., Zeilinger, W.W., 1991. ApJ, 374, L13
Binney, J.J., 1976. MNRAS, 177, 19
Binney, J.J., 1978. MNRAS, 183, 779
Binney, J.J., de Vaucouleurs, G., 1981. MNRAS, 194, 679
Dekel, A., Shlosman, I., 1983. In *IAU Symposium 100, Internal kinematics & dynamics of galaxies* ed. Athanassoula, E., pp. 187–188. Dordrecht: Reidel
de Zeeuw, P.T., 1985. MNRAS, 216, 273
Dubinski, J., 1992. ApJ, 401, 441
Dubinski, J., 1994. ApJ, 431, 617
Dubinski, J., Carlberg, R.G., 1991. ApJ, 378, 496
Fich, M., Tremaine, S., 1991. ARA&A, 29, 409
Franx, M., de Zeeuw, P.T., 1992. ApJ, 392, L47
Franx, M., van Gorkom, J.H., & de Zeeuw, P.T., 1994. ApJ, 000, 000
Frenk, C.S., White, S.D.M., Davis, M., Efstathiou, G., 1988. ApJ, 327, 507
Gerhard, O.E., Binney, J.J., 1985. MNRAS, 216, 467
Hernquist, L., 1993. ApJ, 409, 548
Huizinga, J.E., van Albada, T.S., 1992. MNRAS, 254, 677
Katz, N., Gunn, J.E., 1991. ApJ, 377, 365
Kuijken, K., Tremaine, S.D., 1994. ApJ, 421, 178
Lambas, D.G., Maddox, S.J., Loveday, J., 1992. MNRAS, 258, 404
Lees, J., Schwarzschild, M., 1992. ApJ, 384, 491
Ostriker, E.C., Binney, J.J., 1989. MNRAS, 237, 785
Ostriker, J.P., Peebles, P.J.E., 1973. ApJ, 186, 467
Richter, O.-G., Sancisi, R., 1994. A&A, 000, 000
Sackett, P.D., Rix, H-W., Jarvis, B.J., Freeman, K.C., 1994. ApJ, 000, 000
Schwarzschild, M., 1979. ApJ, 232, 236
Schwarzschild, M., 1993. ApJ, 409, 563
Toomre, A., 1983. In *IAU Symposium 100, Internal kinematics & dynamics of galaxies* ed. Athanassoula, E., pp. 177–186. Dordrecht: Reidel
Trimble, V., 1987. ARA&A, 25, 425
van Albada, T.S., 1982. MNRAS, 201, 939
Warren, M.S., Quinn, P.J., Salmon, J.K., Zurek, W.H., 1992. ApJ, 399, 405
Wilkinson, A., James, R.A., 1982. MNRAS, 199, 171

DISCUSSION

K. Freeman: Early in your talk, you suggested that the large size of the halo would limit its possible pattern speed. Could you say more about such limits on the halo pattern speed, please?

Binney: One cannot speak confidently of a perimeter of something one

cannot see. Bars in N-body models end by co-rotation at the latest. So the simple argument is to say $\omega_p < V_c/R_{halo}$ where $R_{halo} > 50$ kpc at least. Logically this upper limit could be too small because the halo could have a fast rotating subsystem inside it, and be axisymmetric beyond the boundary of the subsystem. But N-body models give no indication that halos, which being dissipationless cannot concentrate their angular momentum, are structured like that.

THE SHAPE OF THE DISK: CLUES FROM THE KINEMATICS OF DISK STARS

MARTIN D. WEINBERG
Department of Physics and Astronomy
University of Massachusetts
Amherst, MA 01003-4525

1. Introduction

It is a tall task to determine the structural parameters of one's own galaxy much less any deviations from axisymmetry. Nonetheless, after hard work, the existence of asymmetries has been reported and discussed in the literature from a wide variety of sources (most recently, Nakai & Nishiyana 1994). Now, in order to understand Milky Way evolutionary history, it is our job to determine the origin and intrinsic structure of these asymmetries.

In the first part of this talk, I will explore the correlation between morphology, pattern speed and kinematics. I will do this using the properties of a particular structure producing mechanism. James Binney has presented arguments for a triaxial halo (this volume). It is worth bearing in mind that one of the main arguments for the existence of the halo was to stabilize the disk (Ostriker & Peebles 1973). Conversely, if the halo itself is not axisymmetric, this will be communicated to the disk. With this motivation, I will demonstrate with a simple model for the Milky Way that a small halo ellipticity may cause a large response in the galactic disk which is remarkably similar to that observed with and features similar to models presented in the literature. More importantly, the generic features of these models corroborate the general finding that pattern speed and kinematics are closely coupled; both the shape of the response and its kinematic signature seem to be insensitive to changes in the amplitude and profile of the perturbation. Although one can already reject some scenarios as unlikely using local kinematic data, many possibilities remain.

In the second part of this talk, I will discuss observational tests, focusing on the importance of stellar kinematics in further discriminating between

L. Blitz and P. Teuben (eds.), Unsolved Problems of the Milky Way, 11–21.
© 1996 *International Astronomical Union.*

possible dynamical hypotheses. Velocities together with photometric distances play two roles:

1. testing velocity signatures predicted by the dynamical scenarios; and
2. improving, statistically, the photometric distance determinations.

We will discuss each in turn, but the distinction is heuristic; in practice both tasks should be combined. To conclude, I will put both the dynamics and observational tests together and, with a simulation, determine how proposed asymmetry producing mechanisms might be tested.

2. Dynamical scenario

What is the response of the disk to an elliptical halo? Asymmetries on large scales, especially if they originate in the kinematically hot halo/spheroid component, are likely to be smooth and well-represented by low-order harmonic components ($l = 1, 2$ say). If we now insert an axisymmetric stellar disk into this halo it will distort (e.g. Thielheim & Wolff 1984).

To illustrate the response here, I chose a distortion whose scale could be varied, chose a pattern speed, and solved the linearized Boltzmann equation for the response of the disk. For computational ease, I chose a Toomre (1963, Model No. 1) disk with Kalnajs (1976, 1/8 model) analytic distribution function. The resulting model is stable and is a passible fit to the galaxy, although the rotation curve rises a bit slowly from the center and begins to fall past the solar circle (Kalnajs 1976, his Fig. 3). Future work will include a realistic Milky Way profile.

Fig. 1 shows the response of the disk to an elliptical distortion in the halo which peaks near the solar circle, rotated to put the bar in the first quadrant. The y-axis coincides with $l = b = 0°$ in galactic coordinates. The isodensity contours are linearly spaced. Corotation is at roughly 4 kpc; the bar ends inside of this point (≈ 3 kpc); stars orbit clockwise. The peak perturbation is 20% of the initial axisymmetric disk density. The asymmetric features are a forced response; if I slowly removed the halo asymmetry, the bar would go away.

The arrows show the velocity of each standard of rest (SR) relative to circular motion; the largest arrow corresponds to 10 km s^{-1}. Notice that the kinematic major axis is skew to the photometric/density major axis. The small circle marks the position of the Sun. Notice that the Sun sits near an inward radial velocity flow and that the kinematic major axis is skew to the photometric/density major axis. Fig. 2 shows the cut through this diagram along $l = b = 0°$. The trough occurs near the solar position and would result in the outer galaxy appearing to recede at about 8 km s^{-1}, which is only slightly larger and has the same sense as the 6 km s^{-1} as recently measured

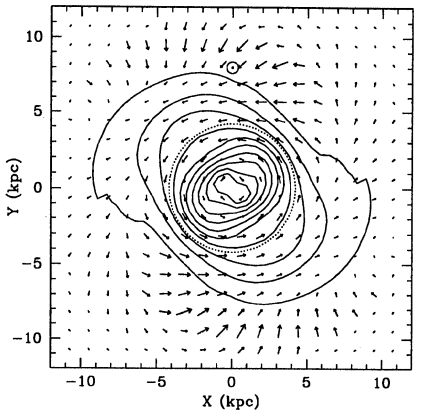

Figure 1. Arrows show velocity of the standard of rest due to fast-pattern bar perturbation. The largest arrow corresponds to $\approx 10\,\mathrm{km\,s^{-1}}$. Contours show the total density including the $m = 2$ perturbation. The dotted line shows the corotation circle and the estimated solar position is indicated ($\odot$).

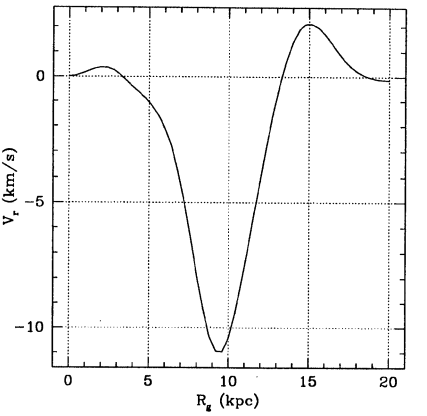

Figure 2. Cut at $l = b = 0°$ for the $m = 2$ perturbation shown in Fig. 1.

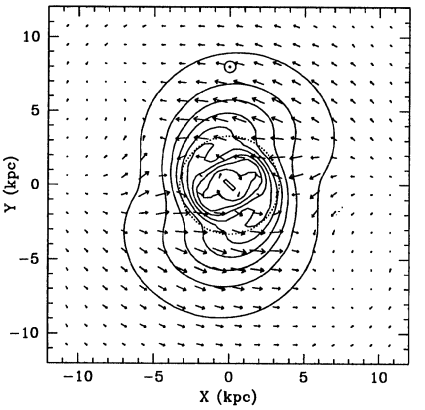

Figure 3. As in Fig. 1 but for a slower pattern speed; the dotted curve now shows the position of the ILR.

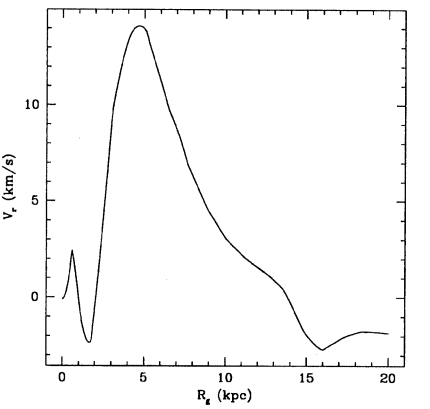

Figure 4. Cut at $l = b = 0°$ for for the slow pattern speed model in Fig. 3.

by Metzger & Schechter (1994) using carbon stars. With no doubt, the measured value could be matched by decreasing the bar amplitude.

This general velocity field appears to be a generic signature of a bar with a corotation inside the solar circle. For example, I reported the same trend using a different approach and for a different model (Weinberg 1993). But these features are not obtained for the slowly rotating pattern (e.g. that of a "classical elliptical") shown in Fig. 3. In this case, there is no corotation and the bar now ends at the ILR (which occurs on the rising part of the rotation curve). Compared to Fig. 1, the bar is a bit smaller and the larger scale oval distortion has changed position, but most significantly, the SR velocity field is qualitatively different (Fig. 4). In the slow pattern speed scenario, the LSR is moving outward and from our vantage point the inner galaxy is approaching. Note that there is no first quadrant bar which matches the kinematics (similar lines of argument have been presented by Blitz & Spergel 1992, Kuijken 1992, Kuijken & Tremaine 1994).

The relative orientation and sign of the velocity field relative to the density pattern, appears to be largely independent of the scale of the halo disturbance. Increasing or decreasing this scale by a factor of 1.5 makes very little qualitative difference in the overall features of the response.

For reference, the elliptical distortion in a halo five times more massive than the disk requires an axis ratio of $q = 0.96$ to produce the response seen in Figs. 1 and 3. This "elliptical" would have to be rapidly rotating to match the local kinematics which according to current thinking is unlikely. More generally, this simple scenario suggests that mild halo ellipticity may have dramatic consequences for the disk. For example, if the halo is structured as Binney suggests, the response of the disk provides a probe even if the halo is dark. This issue is far from closed but suggests to me that the connection between the disk and halo is more intimate than implied by the rigid potential invoked to provide the observed rotation curve. Of course, there is the straightforward possibility we are observing an isolated—not externally forced—bar. Clearly what is needed are methods for testing these various hypotheses.

3. Observational tests

In order to probe global structure, one wants to use a tracer that reflects this structure. Although gas is good because it is reactive, for this purpose it can be *too* reactive by responding to small-scale structure. Stars on the other hand are likely to give a fairer picture of the overall gravitational potential. This is illustrated by U- and R- or I-band images of your favorite spiral galaxy (e.g. NGC 4535).

TABLE 1. Candidate tracers

Star	Standard Candle	Tracer
K-giant	poor, $-1 \lesssim V \lesssim 2$ but v. good with metalicity	need low-absorption windows
Cepheid	v. good, v. bright	young pop, in spiral arms
Planetary nebula	fair (20% to 10 kpc)	intermediate pop, systematics?
AGB–OH/IR	fair, bright but $\sigma \sim 1$ mag	inner galaxy/bulge
AGB–Mira/LPV	fair (good if P-L relation)	good, but long-term search
AGB–Carbon	fair→good, $\sigma \sim 0.4$ mag	good, but spectral ID

3.1. TRACER STARS

Table 1 lists the stars most commonly used for kinematic and structural studies with comments on their properties. Although not ideal standard candles because their photometric precision depends on metallicity, K-giants are a work horse. They are plentiful, easily identified spectroscopically and are excellent kinematic targets (see Lewis & Freeman 1989). They are too faint to overcome extinction at small longitudes $|l|$, requiring low-absorption windows; a surmountable but thorny problem for a statistical study. Of all the stars on the list, Cepheids are the best standard candles. Their one disadvantage is their youth; they therefore tend to trace spiral arms and have low scale heights. Planetary nebulae are reported to be fair distance indicators and kinematic targets although systematic effects are still debated in the literature. The last three in Table 1 are the same class of stars, distinguished more by their means of detection. If a period-luminosity relationship holds in the Milky Way as reported for LMC Mira-like stars, the suitability as standard candles improves but this requires a long term search. The carbon stars are bright and with no other information are probably the best tracer among the AGB stars.

3.2. USING VELOCITIES

3.2.1. *Method*

Although, any of the candidates listed in Table 1 might be profitably used, AGB stars are a promising compromise. They are representative of the mixed disk (progenitors have $1\,\mathrm{M}_\odot \lesssim M \lesssim 2\,\mathrm{M}_\odot$) and what they lack as a standard candle can be recovered by either acquiring a larger sample or using velocities. Velocity information refines the distance estimate in much the same way as HI or CO rotation curves are constructed.

The process is depicted in Fig. 5. For this cartoon, we observe an AGB star at longitude $l = 10°$. For a particular rotation curve, the line-of-sight

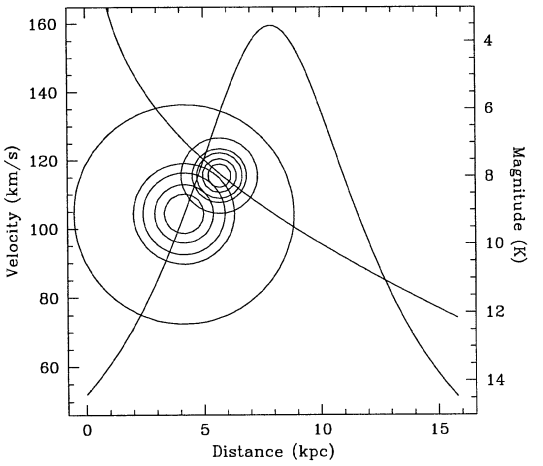

Figure 5. Decreasing curve: m_K vs. distance for an AGB star (right axis). Peaked curve: line-of-sight velocity (v_{los}) vs. distance (left axis). The 50%, 75%, 95% and 99% confidence contours are shown for measured values $v_{los} = 105\,\mathrm{km\,s^{-1}}$ and $m_K = 8$. The joint probability of the two measurements is the product of the two distributions.

velocity is determined as a function of distance (left-hand scale). Similarly, for a given extinction gradient, the apparent magnitude may be computed as a function of distance (right-hand-scale). Assume stars are on circular orbits for argument only. If our model is correct, the star must be at one of the intersections between the two curves. Now, a star is measured with $v_{los} = 105\,\mathrm{km\,s^{-1}}$ and $m_K = 8$ mag. If the velocity measurement error is $10\,\mathrm{km\,s^{-1}}$ and the combined intrinsic dispersion and measurement error for m_K is 0.5, we may compute the joint probability that the star is at either intersection. Not surprisingly, for a gaussian error model, the relative probability that the star is at the closer distance is larger by more than 20 orders of magnitude; this is true for the case depicted in Fig. 5.

For more marginal cases and real world error distributions, there will be considerably less confidence but the lack of symmetry in the two curves gives remarkable statistical leverage. Finally, with many stars and using Bayes theorem, the relative probability of the hypothesis θ is the product of these joint probabilities for each star: $P_{i,\theta} \propto P_{vel}(v_i) \times P_{mag}(m_i)$. The total probability for all stars is then

$$P_{tot} = \prod_i P_{i,\theta}$$

or

$$\log L = \sum_i \log P_{i,\theta}. \quad (1)$$

The 'most likely' hypothesis θ maximizes $\log L$: this is the well-known M-L method. For only hundreds of stars, one can do extremely well in estimating parameters, as the following examples will show (see also Schechter et al. 1987).

3.2.2. *Example*

For a simple demonstration, let us estimate the scale length and extinction coefficient from a sparsely selected sample of bright stars ($m_K \leq 6$) with an intrinsic brightness dispersion of $\sigma = 1.0$ mag (this is worse than reality). I assume the galaxy has a flat rotation curve with $V_o = 200\,\mathrm{km\,s^{-1}}$, an exponential disk scale length of 3.5 kpc, $A_K = 0.15$ mags/kpc, and an isotropic velocity ellipsoid with $\sigma = 20\,\mathrm{km\,s^{-1}}$. The photometric and kinematic measurement errors are $\sigma_m = 0.2$ and $\sigma_v = 10\,\mathrm{km\,s^{-1}}$. Fig. 6[1] shows contours of $\log L$ (cf. eq. 1) for different sample sizes. With $N \gtrsim 400$ stars, one has determined the parameters quite well.

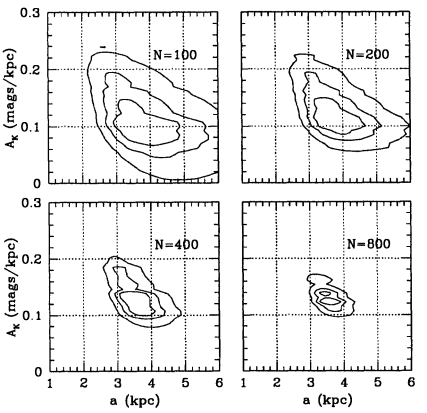

Figure 6. Estimates of scale length and extinction coefficient for different sample sizes. Shown are contours at 75%, 90% and 95% confidence.

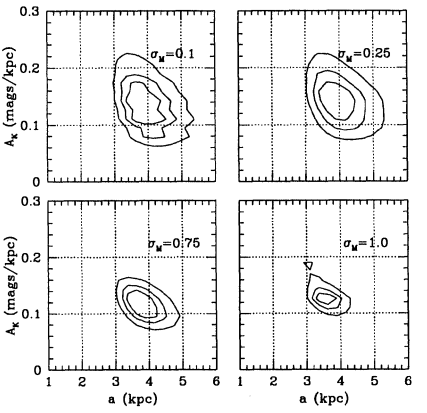

Figure 7. As in Fig. 6 but for various values of σ_M.

A quick aside. Fig. 7 repeats the experiment for $N = 800$ stars but now varies the dispersion of intrinsic tracer star brightness. The confidence improves with *increasing* σ_M. Although somewhat counterintuitive at first

[1]The likelihood surface is often steep; the knotty appearance in some contours is the resulting artifact of the plotting algorithm with an undersampled grid.

glance, larger σ_M means that there are brighter stars and therefore more distant probes. As long as the tracer population is distinguishable and well understood, it need not be a high-quality standard candle.

3.3. TESTING DYNAMICAL HYPOTHESES

We now want to compare our dynamical scenarios to real data. In order to do this we need to know the probability function (cf. eq. 1). We may think of Figs. 1 and 3 as the probability that we have a star with a given density from a population with mean velocity relative to the rotation curve shown by the arrows. More precisely, the proper probability function to use is the phase-space distribution function used to make these figures.

Let's look at some examples. Synthetic data sets are easily generated from the theoretical distribution function shown in Fig. 1 whose disturbance has orientation and amplitude 45° and $\epsilon = 0.2$, respectively. Each star is an AGB star with an intrinsic dispersion in magnitude of 0.75 with a standard K-mag extinction gradient. A sparsely-selected flux-limited sample of stars is then "observed" with 5% photometry and $10\,\mathrm{km\,s^{-1}}$ spectroscopic resolution to a limiting magnitude of $K = 10$ (stars at the mean brightness are roughly at the distance of the galactic center). We assume all pattern orientations and positive amplitudes are possible and maximize eq. 1 to determine these parameters.

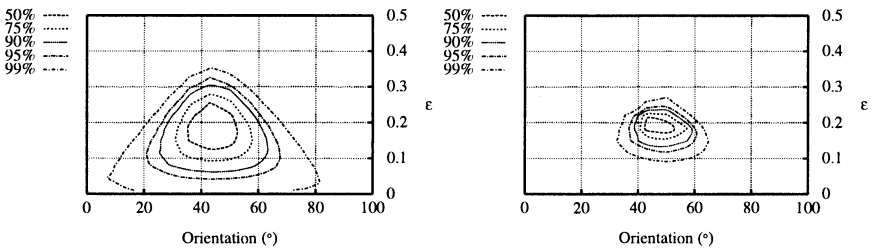

Figure 8. Likelihood contours showing confidence limits on estimates of orientation (in degrees) and bar amplitude (ϵ) and for a simulation with 400 AGB stars and population variance of 0.75 magnitudes. Left: uses photometry only. Right: uses full phase-space distribution.

The M-L estimates based on a sample of 400 stars are shown in Table 2 with 95% confidence error bars (a.k.a. "2–σ"). The likelihood contours are shown in Fig. 8. The panels show the results with photometry only (i, left) and photometry and the full velocity field (ii, right). In case (i), there is a clear detection (zero amplitude is ruled out with 99% confidence) but poor amplitude determination. If I add knowledge of the background rotation curve, the amplitude improves but the estimate of pattern orientation is

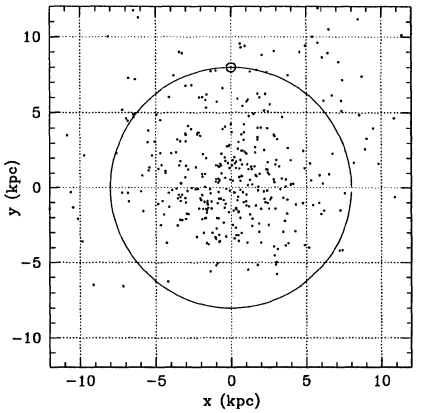

Figure 9. Distribution of AGB stars used in the simulation described by Figs. 8 and 10.

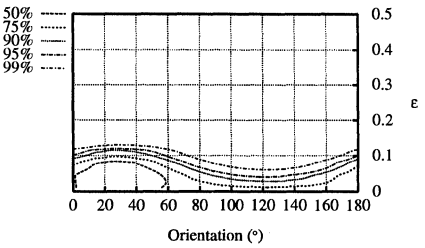

Figure 10. As in Fig. 8 but for slow pattern speed, full phase-space distribution.

TABLE 2. M-L Test Results

Case	Orientation (°)	Amplitude (ϵ)
i	43 ± 15	0.18 ± 14
ii	46 ± 11	0.20 ± 0.07
iii	24 ± 180	0.03 ± 0.05

somewhat worse (not shown). However, using the full distribution function (case ii) improves the estimation dramatically. Should you be unimpressed with the size of the error bars, attempt the estimate by eye from the true distribution of stars on the galactic disk (Fig. 9). With 1200 stars, the estimated orientation and amplitude further improves: $47° \pm 3$ and $0.2^{+0.01}_{-0.05}$. Even with poor standard candles, one can learn about global structure if kinematic information is available.

However, the most useful aspect of this analysis is its power to discriminate between or reject hypotheses. As an example, we can use the same simulated data set to estimate the parameters of the "slow" pattern described in §2 and Fig. 3. One finds that there are no good amplitudes and orientations (Fig. 10). That is, the maximum likelihood solution has amplitude consistent with zero with undetermined position angle. Furthermore, based on the relative values of $\log L$, one can reject the "slow" pattern hypothesis in favor of the the "fast" pattern (case ii) at confidence of 1 part in 10^4.

4. Summary

Over the last 10 (and especially 3) years, the textbook picture of the axisymmetric galaxy has faded. The myriad of asymmetries uncovered by observational advances points to the complexity of interactions between structure at different scales and components; the results in §2 are a simple example.

To trace this structure, stars have the advantage of providing both distance and kinematic data simultaneously. In addition, since the information added by the velocity data effectively improves the distance determination, we can tolerate moderate to poor standard candles.

To test the plethora of hypotheses—halo interaction and the more traditional self-consistent disk bar are only a few—I strongly advocate using both spatial and kinematic data together, since the peak signal in their respective fields occur in different places and are sensitive to different parameters (e.g. scale and pattern speed in the case of the $m = 2$ response discussed above). Although there are many possible strategies to this end, the simulations above suggest that a sparsely selected sample $\sim$ 1000 stars with $10\,\mathrm{km\,s^{-1}}$ velocity resolution and limiting K magnitude of 10–12, which roughly penetrates to the galactic center, is sufficient to begin to test some of these dynamical scenarios.

Acknowledgements

I thank the IAU for travel support. This work was supported in part by NASA grant NAG 5-1999 and the Alfred P. Sloan Foundation.

References

Blitz, L. and Spergel, D. N. 1991, Astrophys. J., 370, 205.
Kalnajs, A. J. 1976, Astrophys. J., 205, 751.
Kuijken, K. 1992, Publ. Astron. Soc. Pac., 104, 809.
Kuijken, K. and Tremaine, S. 1994, Astrophys. J., 421, 178.
Lewis, J. R. and Freeman, K. C. 1989, Astron. J., 97, 139.
Metzger, M. R. and Schechter, P. L. 1994, Astrophys. J., 420, 177.
Nakai and Nishiyana 1994, *Radial Distributions of Hα in Barred Galaxies. M83, NGC 4321, NGC 1365, and the Galaxy*, preprint.
Ostriker, J. P. and Peebles, P. J. E. 1973, Astrophys. J., 186, 467.
Schechter, P. L., Aaronson, M., Blanco, V. M., and Cook, K. H. 1987, in L. Blitz and J. Lockman (eds.), *The Outer Galaxy*, pp 31-39, Springer-Verlag.
Thielheim, K. O. and Wolff, H. 1984, Astrophys. J., 276, 135.
Toomre, A. 1963, Astrophys. J., 138, 385.
Weinberg, M. D. 1994, Astrophys. J., 421, 481.

DISCUSSION

P. Schechter: My recollection of the work of Gerhard, Binney and collaborators is that their bar, with a corotation radius of 2.4 kpc produces little kinematic signature at the Sun's position. Is your larger signature the result of your having assumed a larger corotation radius?

Weinberg: Partly; corotation for the fast pattern speed model is nearly 4 kpc. In addition, the self-gravity is to blame for the phase shift between the kinetic and photometric axes, placing the sun near the peak inward velocity. Finally, remember that bar is not self-consistent but a response to a halo ellipticity which is largest near the solar circle.

J. Binney: Can you give some more detail on your bar- in particular, to what radius does your bar's non-axisymmetry rock?

Weinberg: The peak halo asymmetry occurs near the solar circle in both cases presented (fast and slow pattern speeds). Since they are linear solutions, the degree of halo ellipticity depends on the halo to disk mass ratio. For a ratio of 5:1, the axis ratio in the disk plane is Qtrue= 0.96. This value depends on the location of the peak asymmetry; if the location is beyond the solar circle, presumably Qtrue must decrease.

T. de Zeeuw: How sensitive is your method to the assumption of uniform extinction?

Weinberg: It depends on the magnitude of the fluctuation. Variations of $\lesssim$ 1 mag along any line of sight would probably not cause problems. The beauty of this method is that velocities help resolve poor photometric distances. Larger extinction variations can be incorporated as long as they are well characterized a priori. Hopefully, the upcoming infrared surveys will help us do this.

THE SHAPES OF DARK HALOS

HANS-WALTER RIX
Institute for Advanced Study, Princeton, NJ 08540, USA
and
Max-Planck-Institut für Astrophysik, 85740 Garching, Germany

1. Introduction

Galactic and extragalactic astronomers often mean different things by "halo"; the former mean the spheroidal distribution of metal poor stars around the Milky Way (MW), the latter mean the massive, dark component providing the large dynamically inferred mass in and around galaxies. This review will focus on massive, dark halos. Despite the title of this conference, we cannot restrict our attention to the shape of the MW halo: very little would be to say. We must turn to cosmological simulations and to observations of external disk galaxies in the hope of deriving a representative picture.

Extensive effort has gone into studying the radial mass profile of dark halos, $\rho = \rho(r)$. In comparison, the question of the shapes of the halo isodensity surfaces ("the shapes of halos") has received little attention. Even if the shapes of these surfaces were restricted to concentric ellipsoids, a full determination of the axis ratios and orientation angles at each radius would be beyond reach of observational tests for the foreseeable future. Therefore we must turn to simpler questions:

- Are halos approximately spherical ($a \sim b \sim c$), oblate ($a \sim b > c$) or triaxial ($a > b > c$)?
- Are the axis ratios, $a(r) : b(r) : c(r)$, a strong function of radius?
- Are the axes of the isodensity ellipsoids aligned as a function of radius? Is the symmetry plane of the halo aligned with the galaxy's disk?
- How can observations determine "characteristic" axis ratios?

Halo shapes are of interest chiefly for two reasons. First, in order to relate local properties in the MW [*e.g.* the halo mass density at the position of the Sun, $\rho(R_\odot, z = 0)$] to global properties [*e.g.* the rotation curve, $v_c(R)$], the halo flattening must be known. For a given value of $v_c(R_\odot)$ the

L. Blitz and P. Teuben (eds.), Unsolved Problems of the Milky Way, 23–30.
© 1996 *International Astronomical Union.*

value of $\rho(R_\odot, z = 0)$ will be much higher, if the total distribution is highly flattened rather than spherical. Similarly, the fraction of the circular speed attributed to different components in "disk–halo" fits of other galaxies, can depend sensitively on the shape of the halo. Second, the flattening of dark halos may provide a crucial clue to the nature of the dark matter (DM). If the DM were dissipational (e.g. baryonic MACHOs, cold molecular gas), then it should be distributed in disk-like structures. This is not the case for models with dissipationless DM.

2. Theoretical Expectations

What shape is predicted for the halos arising in hierarchical structure formation scenarios? For dissipationless DM this question can be addressed by cosmological N-body simulations (Katz, 1991; Dubinski and Carlberg, 1991; Warren *et al.* , 1992; Katz and Gunn, 1992; Summers, 1993; Dubinski, 1994). Competing requirements make even collisionless calculations difficult: on the one hand, they should be "cosmologically correct", i.e. should properly simulate the generation of angular momentum and the merging history for each halo. This requires large simulation volumes. On the other hand, the simulations must resolve galactic scales, $\lesssim$ 5kpc, in order to make predictions in a radial range where observational tests are feasible.

Despite an ongoing discussion about numerical techniques and proper initial conditions, all *dissipationless* simulations agree on a number of important results: (a) The resulting halos are strongly triaxial, closer to prolate than oblate. (b) The net angular momentum is aligned with the shortest axis. (c) In the virialized parts ($\lesssim$ 50kpc) the isodensity ellipsoids are aligned as a function of radius. (d) The axis ratios of the isodensity ellipsoids vary only weakly with radius, and the distribution of halo flattenings, $(c/a)_{halo}$, peaks near 0.7.

Dissipational material will affect the halo shape in several ways. A mass concentration at small radii will round the equipotentials by increasing the monopole. The concentration of mass towards a (disk) plane, will adiabatically compress the halo in the disk normal direction. Further, dissipative matter will settle onto loop orbits in a disk. These loop orbits will be elongated *perpendicularly* to the imposed distortion of the halo, and make the total (disk + halo) potential closer to axisymmetric than it would be due to either component (see Section 3).

Simulation including gas dynamics (e.g. Katz and Gunn 1992; Summers, 1993) or the slow growth of a disk component (Dubinski, 1994), bear out these expectation: the halos become slightly flatter and much closer to oblate ($b/a \sim 1$). The surprising result of the simulations is that these changes in halo shape extend to large radii, where $M_{dissipative}/M_{total} \ll 1$.

Hence the reshaping cannot be solely attributed to adiabatic orbit changes, but must be due to a decrease in the abundance of the box orbits, which originally sustained the triaxial shape.

3. Observational Signatures of Non-Spherical Halos

Rotation curves measure the monopole structure of the mass distribution, while the halo shapes are described by the higher mass multi-poles. Observational tests can only measure the shape of the *potential*, which is much rounder than the generating *mass distribution* and which has correspondingly smaller multipole terms. Therefore it should come as no surprise if shape measurements proved much more difficult than rotation curve measurements.

Most observational tests designed to measure the halo shapes are based on the following ideas:
(1) estimating the MW halo flattening through dynamical modelling of collisionless tracers. As a first step, one identifies a population of kinematic tracers that probe the potential at large distances and high above the disk, such as "extreme Population II" stars. Then one obtains the shape of the *local* velocity dispersion ellipsoid, the mean radial density profile and the flattening for the tracer population (not the total mass!). With these data and the run of the (equatorial) rotation curve, one can ask which flattening of the mass distribution, $(c/a)_{mass}$, is consistent with all these constraints.
(2) determining the shape of closed loop orbits. In any given potential there is a unique set of *closed loop orbits*. For a specific example, consider a non-rotating, logarithmic potential of constant distortion, ϵ_{pot},

$$\Phi(R,\varphi) \equiv \frac{v_c^2}{2}\left(\ln R^2 - \frac{\epsilon_{pot}}{2}\cos 2\varphi\right), \tag{1}$$

where $\epsilon_{pot} \sim \frac{1}{3}(1-(b/a)_{halo})$. In this potential the closed loops are simple ovals of the same ellipticity, ϵ_{pot}, which are elongated *perpendicularly* to the equipotentials:

$$R(\varphi) = R_0(1 - \frac{\epsilon_{pot}}{2}\cos 2\varphi). \tag{2}$$

The velocities, (v_φ, v_R), of any particle moving along these orbits differ from the circular motion $(v_c, 0)$ by a fractional amplitude of $2\epsilon_{pot}$. This very restricted set of orbits acquires its importance, because it constitutes the only orbits on which gas can move without getting shocked by other gas elements in the galaxy. Hence cold ($T \ll T_{virial}$) gas will populate these orbits after a few dynamical periods (Rix and Katz, 1991). Note that material on such loop orbits (Eq. 2) will produce a potential whose quadrupole distortion

has the opposite sign of the input distortion (Eq. 1). In this sense the response of the embedded disk "counter-acts" the imposed halo distortion. Whenever disk and halo are of comparable dynamical importance, their combined potential will be much closer to axisymmetric than it would have been due to either component.

Other observational methods to measure the shape of halos include:
(3) studying the shape of the X-ray gas in halos. This technique has been applied to measuring the shape of several galaxy clusters (Buote and Canizares, 1992) and of one individual elliptical galaxy, NGC 720 (Buote and Canizares, 1994). If the X-ray gas is in quasi-hydrostatic equilibrium and if it is nearly isothermal, then the map of the projected gas emissivity provides a good map of the projected potential. However, it is unlikely that this method can be extended to halos around disk galaxies, since those do not seem to have smooth X-ray coronae.
(4) studying the flaring of neutral hydrogen disks (e.g. Maloney, 1993; Olling and van Gorkom, *in prep.*). The neutral hydrogen disks around spiral galaxies are observed to have a universal velocity dispersion of $\sigma \sim 8$km/s. In edge-on disks a comparison of the rotation curve (radial centrifugal equilibrium) to the vertical gas scale height (vertical hydrostatic equilibrium) can constrain the shape of the halo. In such an analysis only the potential in the immediate disk vicinity is probed and warps may be difficult to untangle from flaring. Nonetheless, this method may eventually test whether the DM at large radii is in a disk-like configuration.

4. Are Halos Flattened?

4.1. MILKY WAY

All existing estimates for the flattening of the dark MW halo arise from the dynamical modelling of extreme Population II stars (see Section 3). The observational constraints are: $(\sigma_R : \sigma_\phi : \sigma_z)_{trc} \sim 1.5 : 1 : 1$ at the position of the sun (Hartwick 1983, Sommer-Larsen and Zhen 1990, Morrison *et al.* 1990), $(c/a)_{trc} = 0.6 - 0.85$ (Wyse and Gilmore, 1986, Sommer-Larsen and Zhen 1990), $\rho_{trc} \propto R^{-3.5}$ and $v_c(R) = const.$

This observational input, however, is far from determining a unique model and further "plausible" assumptions need to be made. Binney, May and Ostriker (1987) constructed approximately self-consistent disk halo models with Stäckel potentials and find that $(c/a)_{halo} \sim 0.5$ fits the observations best. For a sample of local halo stars with known space motions, Sommer-Larsen and Zhen (1990) retraced the orbits in a Stäckel potential, favoring a nearly spherical halo, $(c/a)_{halo} \sim 0.9$. Van der Marel (1991) used the Jeans equations to show that halo flattenings of $0.4 \leq (c/a)_{halo} \leq 1$ were consistent with the data, depending on the tilt of the velocity el-

lipsoid away from the disk plane. Amendt and Cuddeford (1994) derived higher order closure relations for the Jeans equations and applied those to Hawkin's (1984) sample of RR Lyrae stars, finding a preferred value of $(c/a)_{halo} \sim 0.7$.

In summary, these tests show that the data permit a wide range of halo flattenings, with only very flat halos disfavored by the data. It is unlikely that these tests can be much improved in the foreseeable future, because the dominant source of uncertainties is our ignorance about the shapes of the stellar tracer orbits.

4.2. POLAR RING GALAXIES

Polar ring galaxies are a relatively rare species of disk galaxies in which a ring of stars and gas orbits over the galaxy's pole. In such polar rings of varying radial extent, $0.1 \lesssim \Delta R/\langle R \rangle \lesssim 2$, the neutral and ionized gas provide an excellent probe of the halo flattening: (a) the gas moves in a plane including the z-axis, and (b) the gas often extends to radii where the dark halo is expected to dominate. The halo flattening can be estimated either by comparing the kinematics in the polar and equatorial (disk) plane or by studying the shape of the (closed loop) orbits in the polar plane. Sackett and Sparke (1990) and Sackett *et al.* (1994) built global dynamical models for NGC4650A to match simultaneously the kinematics of the stellar disk and of the polar ring and found $(c/a)_{halo} \sim 0.4 \pm 0.1$. For A0136-0801, where Hα observations provide a high quality, two dimensional velocity field, Sackett and Pogge (*in prep.*) show that the halo must also be oblate. In UGC 7576 (Sackett, Rix and Peletier, *in prep.*), the ionized gas appears to form a thin ($\Delta R/\langle R \rangle \ll 1$), edge-on annulus. If gas is on circular orbits (in a spherical potential) then the line-of-sight velocities and the projected positions are related by $v_{l.o.s.}(R_{proj}) \propto R_{proj}$. If the potential is oblate, the closed gas orbits are oval and this relation becomes non-linear in a unique way. The gas velocities along the polar ring in UGC 7576 do indeed show such non-linearities and a very preliminary analysis points to flattening of $(c/a)_{mass} \sim 1/2$ at the radius of the ring.

In summary, the three disk galaxies with polar rings studied to date all show that their halos are flattened perpendicular to the stellar disk, with characteristic flattenings of $(c/a)_{halo} \sim 0.5$.

5. Are Halos Axisymmetric?

There are no direct constraints on deviations of the MW *halo* from axisymmetry in the disk plane. In part, this is due to the partial compensation of disk and halo distortions, discussed in Section 3. Even for significantly triaxial halos this will make the combined disk-halo potential much rounder

than it would be due to either of its components, as long as the disk and the halo contribute comparably to the rotational support at the solar radius.

To address the axisymmetry of halos we must turn to external galaxies and rely on the Copernican principle for any inference about the MW. All existing observational tests for external disk galaxies are based on the shape of closed loop orbits. Franx and de Zeeuw (1993, FZ93) proposed a very powerful statistical way to limit $(b/a)_{pot}$, using the small scatter in the linewidth-luminosity relation ("Tully-Fisher" relation) for spiral galaxies. If the HI disks in these galaxies are oval then the same (edge-on) galaxy seen at different azimuthal angles, φ, will have linewidths, $W_{20}(\varphi)$, varying by $(1+\epsilon_{pot}\cos 2\varphi)$. Averaged over all viewing angles the line width scatter, ΔW_{20} will be at least $\Delta W_{20}/W_{20} = \epsilon_{pot}/\sqrt{2}$. If the luminosity, L varies as $L \propto (W_{20})^{\gamma}$, with $\gamma \sim 4$, this will result in a luminosity scatter of $\Delta L/L = \gamma\epsilon_{pot}/\sqrt{2}$. Using the observed scatter in published galaxy samples, Franx and de Zeeuw derive $\epsilon_{pot} < 0.1$. Unfortunately, it is unclear whether W_{20} probes a radius where the halo dominates. This problem could be, and should be, remedied by considering the full two-dimensional velocity field in a small subsample of galaxies rather than only the HI linewidth.

Alternatively, one can use the shape of stellar disk isophotes to constrain the potential distortion in the disk plane. Even though stars to not move on *closed* loop orbits, an extension of this analysis is possible as long as most stars move on loop orbits at all (Rix and Zaritsky, 1994). If an exponential disk with scale length R_{exp} is embedded in a logarithmic potential, its isophote shapes, ϵ_{iso}, are related to the potential shape by $\epsilon_{iso}(R) = \epsilon_{pot}(1 + R_{exp}/R)$ (FZ93). This relation can be applied statistically (Binney and de Vaucouleurs, 1981; Huizinga and van Albada, 1992; Fasano *et al.* 1993, FZ93), comparing the distribution of apparent isophotal axis ratios of disk galaxies to the expected uniform distribution expected for randomly oriented, circular disks. All these authors all find $\langle\epsilon_{pot}\rangle \lesssim 0.1$.

Rix and Zaritsky (1994) tried to improve on these analyses by using near-infrared K($2.2\mu m$) images (reducing the distorting impact of dust and hot stars on the isophote shapes), by selecting the sample galaxies to be face-on on a purely kinematic basis and by fitting $\epsilon_{iso}(R)$ over the whole disk rather than measuring the disk ellipticity at one single radius. They found a tighter limit for the characteristic potential ellipticity, $\langle\epsilon_{pot}\rangle \lesssim 0.05$ for $R_{exp} \leq R \leq 4R_{exp}$. But even this measurement constrains $(b/a)_{halo}$ only weakly. If disk and halo contribute comparably to v_c, then their quadrupole distortions will cancel in part and $\langle\epsilon_{pot}^{halo}\rangle \sim 2\langle\epsilon_{pot}\rangle$ (Dubinski 1994). This makes $(b/a)_{halo} \sim 1 - 3\langle\epsilon_{pot}^{halo}\rangle \sim 0.7$ still consistent with the data.

The most compelling constraint on the shape of any halo exists for the elliptical galaxy IC 2006 (Franx, van Gorkom and de Zeeuw, 1994): $\epsilon_{pot} = 0.015\pm0.025$ at $R = 7R_e$. Since the halo shape seems to be affected by

the orbital structure of the luminous mass (the disk-halo "counter-action"), it is not clear whether the halo shapes in elliptical and disk galaxies should be the same.

6. So, What is the Shape of Dark Halos?

Cosmological simulations of halo formation predict that they are flattened by $\langle c/a \rangle \sim 0.7$, and that their axis ratios $\langle b/a \rangle$ depend sensitively on the amount of dissipative matter in the halo.

Our position within the MW complicates measurements of the halo shape for the MW. Consequently, a wide range of shapes is consistent with the data. Some progress has been made on constraining the shapes of halos in external disk galaxies. In particular, flattening estimates are now becoming available for several polar ring galaxies. In these galaxies the halos are definitely flattened perpendicular to the stellar disk (with $(c/a)_{halo} \sim 0.5$), consistent with cosmological formation simulations of dissipationless DM halos. Some more work would be desirable to see whether very flat halos (e.g. from dissipational DM) can be ruled out observationally. Constraining deviations of the halo from axisymmetry in the disk plane, is complicated by the counter-action of halo and disk distortions. This problem is best remedied by going to large radii, where the halo dominates (see e.g. the tight constraint on the shape of the halo around the elliptical galaxy IC 2006; Franx, van Gorkom and de Zeeuw, 1994).

If the MW halo is typical, then observations of the halos around other galaxies and the cosmological simulations lead us to adopt an axisymmetric halo with $(c/a) \sim 1/2$ as a better "default" shape than spherical when modelling the MW.

It is a pleasure to thank Penny Sackett and E. Q. Reade for extensive help in preparing this review.

References

Amendt, P. and Cuddeford, P., 1994, *preprint.*
Binney, J., May, A. and Ostriker, J. P., 1987, MNRAS, 226, 149.
Binney, J. and de Vaucouleurs, G., 1981, MNRAS, 194, 679.
Buote, D. and Canizares, C., 1992 ApJ, 400, 385.
Buote, D. and Canizares, C., 1994 ApJ, 427, 86.
Dubinski, J. and Carlberg, R., 1991, Ap.J., 369, 13.
Dubinski, J., 1994, *preprint.*
Dubinski, J. and Kuijken, K., 1994, *preprint.*
Fasano, G. *et al.*, 1993, MNRAS, 262, 109.
Franx, M. and de Zeeuw, T., 1992, ApJL, 392, 47.
Franx, M., van Gorkom, J. and de Zeeuw, T., 1994, ApJ, *in press.*
Hartwick, F. D. A., 1983, MmSocAstIt, 54,51.
Hawkins, M. R. S., 1984, MNRAS, 206, 433.
Huizinga, J.E. and van Albada, T.S., 1992, MNRAS, 254, 677.

Katz, N., 1991, Ap.J., 368, 325.
Katz, N. and Gunn, J. E., 1991, Ap.J., 377, 365.
Maloney, P., 1993, ApJ, 414, 41.
Morrison, H., Flynn, C. and Freeman, K., 1990, A.J., 100, 1191.
Rix, H.-W. and Katz, N., 1991, in *Polar Rings and Inclined Disks in Galaxies*, Cambridge Univ. Press, Eds: S. Casertano, P. Sackett and F. Briggs.
Rix, H.-W. and Zaritsky, D. F., 1994, Ap.J. *submitted.*
Sackett, P. and Sparke, L., 1990, ApJ, 361 408.
Sackett, P., Rix, H.-W., Jarvis, B. and Freeman, K., 1994, Ap.J., *in press.*
Sommer-Larsen, J. and Zhen, C., 1990, MNRAS, 242, 10.
Summers, F., 1993, Ph.D. Thesis, Univ. of California, Berkeley.
van der Marel, R. P., 1991, MNRAS, 248, 515.
Warren, M. S., Quinn, P. J., Salmon, J. K. and Zurek, W. H., 1992, Ap.J., 399, 405.
Wyse, R. F. G, and Gilmore, G., 1986, A.J., 91, 855.

THE AXISYMMETRIC STABILITY OF THE MILKY WAY

J. A. SELLWOOD
Rutgers University
Department of Physics & Astronomy, Piscataway, NJ 08855

1. Motivation

The problem of axisymmetric Jeans stability of a stellar disk was essentially completely solved in the classic paper by Toomre (1964). While his analysis was strictly local, the stability criterion it yielded has been found to be remarkably reliable in global studies; I review earlier results and give a further example in Sellwood (1995, hereafter S95). Toomre (1974) concluded that the MW is safely stable to axisymmetric Jeans modes.

Here, however, I am principally concerned with bending instabilities which were again first considered by Toomre (1966) also using a local approximation. He showed that random motion can cause an infinitesimal corrugation to grow exponentially, but that the instability can be shut off by gravitational restoring forces on large scales and by finite thickess on small scales. His analysis, and one more detailed by Araki (1985), indicated that the vertical random velocities need be no larger than some 30% of the in-plane random velocities for a uniform slab to be stable.

Large-scale bending instabilities have been reported in a number of recent N-body simulations of thin stellar systems, which ultimately caused them to thicken. At first this behavior was seen only in bars (e.g., Combes & Sanders 1981; Combes *et al.* 1990; Raha *et al.* 1991; Merritt & Hernquist 1991) but Sellwood & Merritt (1994, hereafter SM) and Kalnajs (unpublished) found that large-scale bends could also occur in axisymmetric disks. The instability had been missed in many other simulations either because the particles were confined to a plane, or random motions were too small to drive any but small-scale instabilities, which are easily suppressed by a modest disk thickness or poor spatial resolution. The bending instability can, however, even outpace the more familiar bar instability in a fully self-

L. Blitz and P. Teuben (eds.), Unsolved Problems of the Milky Way, 31–37.
© 1996 *International Astronomical Union.*

gravitating disk with a single directly rotating population, when random motions are large enough.

Merritt & Sellwood (1994, hereafter MS) showed that the Toomre-Araki stability criterion breaks down when the dominant bending mode has a radial wavelength comparable to, or greater than, the scale on which the surface density varies, and argued that it fails because the gravitational restoring force at the disk center arising from the displaced outer disk is weaker than the Toomre-Araki analysis assumes. From much higher quality simulations, but restricted to axial symmetry, I (S95) was able to show that the local stability criterion fails significantly only where pressure support is comparable to, or exceeds, that from rotation.

MS concluded that the bending instability precludes the existence of elliptical galaxies more flattened than about E7, as Fridman & Polyachenko (1984) had speculated. On the other hand, only the very centers of most disk galaxies would have enough in-plane random motion to thicken significantly; the instability therefore offers a potentially important process for bulge formation, as noted in the above cited papers.

While the local stability criterion is not strongly violated in rotationally supported parts of the disk, it seemed to MS at least possible that some overshoot may occur on all scales. They therefore wondered whether the Milky Way could after all be locally close to the bending stability boundary and that the current thickness might have been set by bending instabilities, rather than through some other mechanism. This consideration prompted the present study in which, however, I find that these suspicions were unfounded and that Toomre (1966) concluded correctly that "the Galaxy is well clear of this stability boundary" also.

2. A Milky Way Model

The Kuz'min-Toomre disk I used in S95 is a poor model of the Milky Way; I have therefore tried here to simulate a more realistic model, both to verify the stability of the MW directly and also to determine the scale height of the local disk if bending instabilities were the sole thickening agent.

The model for the Milky Way I have used in this study is based on a Rybicki (unpublished) disk model which has the surface density distribution

$$\Sigma(r) = \frac{M}{2\pi a^2}\left(1+\frac{r^2}{a^2}\right)^{-1/2}, \tag{1}$$

and squared circular velocity

$$v_c^2 = \frac{GM}{a}\left(1-\frac{a}{\sqrt{a^2+r^2}}\right). \tag{2}$$

Here, a is the core radius and M is a mass unit, but the total disk has infinite mass and extent, as it must have if it is to give rise to an asymptotically flat rotation curve without a halo component. Evans & Collett (1993) have given a family of DFs for this model characterised by an index n which determines the degree of pressure support; $n = 1$ yields a hot disk (but still with significant rotation) while all orbits become circular as $n \to \infty$.

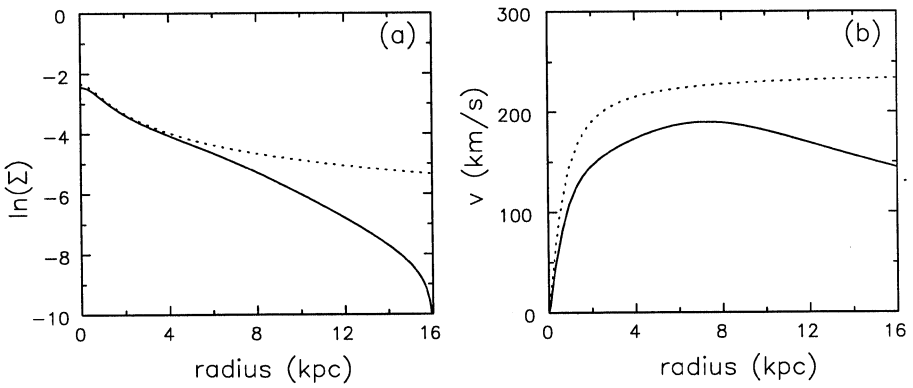

Figure 1. Properties of the adopted Milky Way model. (a) The dotted curve shows the surface density profile of a 60%, untruncated Rybicki disk, the full-drawn curve that obtained after applying the truncation rule described in the text. (The surface density unit is M/a^2.) (b) The circular velocity (km s^{-1}) arising from the truncated, disk only (full drawn) and total rotation curve of the model (dotted).

Since the surface density (1) declines too slowly for a realistic galaxy, and the disk anyway has to be truncated for use in a simulation, I applied the following rules to limit its radial extent: I multiplied the DF by the taper function

$$T(h) = \left[1 + \left(\frac{h}{h_0}\right)^4\right]^{-1}, \tag{3}$$

where h is the specific angular momentum and $h_0 = 10\sqrt{GMa}$. I also applied the further restriction that no particle has sufficient energy that its unperturbed orbit would take it beyond an outer cut-off radius of $r_{\max} = 20a$. With these rules, and choosing $n = 15$, I obtained the surface density profile of active matter shown in Figure 1(a), which is approximately exponential with a mean scale-length of about $4a$. The rotation curve of this considerably altered disk is, of course, no longer given by (1) and it is necessary to supplement the self-consistent central attraction with an additional function in order to maintain the equilibrium of this truncted DF.

A reasonable scaling of this model to the Milky Way would be to choose $a = 0.8$ kpc and $\sqrt{GM/a} = 240$ km s^{-1}, which implies that $M \simeq 1.07 \times 10^{10}$ M$_\odot$ and one dynamical time ($= \sqrt{a^3/GM}$) is 3.26 Myr. With this scaling, the radial velocity dispersion at the position of the Sun ($r = 8$ kpc) is approximately 47 km s^{-1} and the asymmetric drift is 18.5 km s^{-1}.

There are two undesirable features of the full disk mass distribution arising from this DF. First, the central attraction of the truncated disk *exceeds* that of the untruncated disk at radii between $4a$ and $13a$ (because the missing exterior mass would pull outwards locally); the correcting forces to restore the radial balance would therefore have to be repulsive over this range. Second, the radial velocity dispersion is too low to prevent axisymmetric Jeans instabilities in the truncated disk; the locally defined Q has a minimum of about 0.75 around $r = 6a$. I therefore reduced the active surface density of the disk to 60% of that given by the above description; the extra forces required to restore the radial balance of the disk now arise from a mass distribution (assumed spherical) having a positive density everywhere, and the disk is locally Jeans stable. The rotation curves of the active disk mass and of the total disk-plus-halo distributions are shown in Figure 1(b). The total mass of the disk in this model is $\sim 6.1 \times 10^{10}$ M$_\odot$ and the surface density at the position of the Sun is ~ 83 M$_\odot$ pc^{-2}, which is deliberately on the high side.

Thus far, the vertical structure of the disk has not been specified. The purpose of this study is to determine whether the Milky Way is locally stable to bending modes and whether bending instabilities could in fact have thickened the disk to something close to its current value. These questions can both be answered by a single simulation which is initially thin enough that bending instabilities are certain to be provoked; the non-linear evolution will reveal the extent to which instabilities can thicken the disk and indicate the thickness at which instabilities are shut off. I have therefore adopted the very low value of $z_0 = 0.04a = 32$ pc for the Gaussian scale height of the disk. The vertically integrated, vertical velocity dispersion resulting from this choice is no more than one quarter of the radial dispersion anywhere.

3. Results

I computed the evolution of this model using the grid-based axisymmetric N-body code described in S95. The grid had 200 points in radius and 135 vertically, the spacing in each direction was separately constant but the vertical spacing was 0.16 that in the radial direction in order to ensure five mesh spaces per initial Gaussian scale height of the disk. I employed 50 K particles and a time step of 0.02 dynamical times. Tests indicated that the

results were insentive to changes in grid resolution and other numerical parameters.

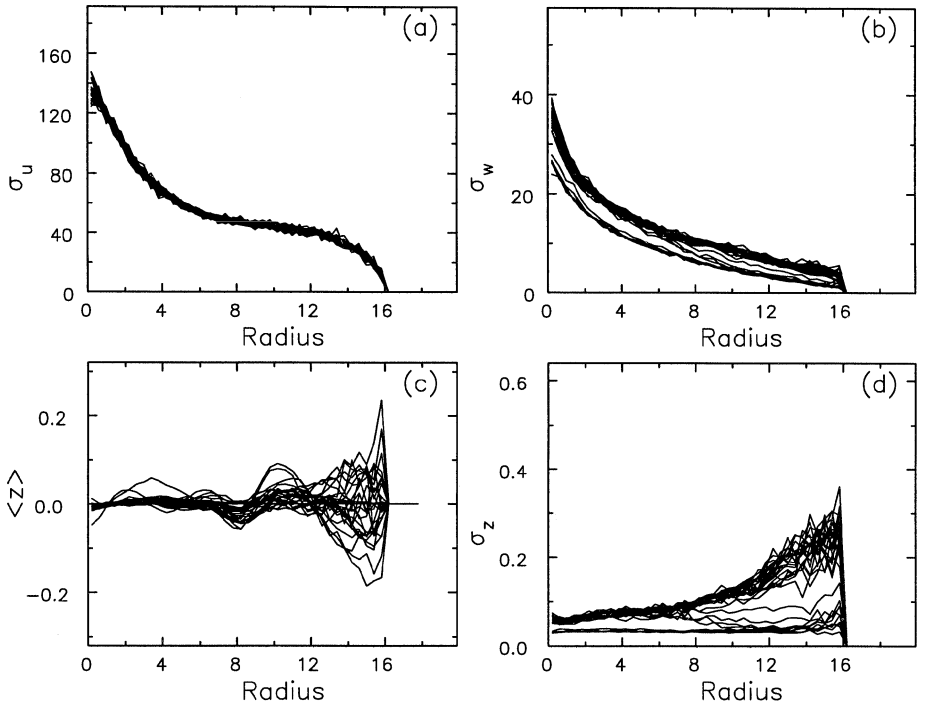

Figure 2. Properties of the Milky Way model, as functions of radius (in kpc), measured at intervals of 20 dynamical times. (a) The radial velocity dispersion (km sec^{-1}) does not change significantly throughout the evolution. (b) The vertical velocity dispersion rises by some 60% at the solar radius ($r = 8$); the vertical scale is set to have a full extent precisely 30% of that in (a). (c) The mean z displacement of the particles (kpc), showing a long lived bend. (d) The rms vertical thickness which started out at a small constant value and increased most at large radii.

The evolution of the model reavealed a number of bending modes which caused a peak displacement of the mid-plane of almost 200 pc, but bending activity appeared to cease after about 1 Gyr. Figure 2 shows profiles of the radial and vertical velocity dispersions and of the mean displacement and rms thickness of the plane at a number of equally spaced moments during the run. The vertical velocity dispersion rises during the first Gyr of evolution only, but does not reach even 30% of the radial dispersion, because the additional restoring force to the plane from the spherical rigid material alters the Toomre-Araki stability criterion. An additional experiment with a less massive disk led to a still flatter final ellipsoid.

Figure 2(d) shows that the disk flares outwards, while Figure 2(c) indicates that it does not flatten completely immediately after the final instability saturates, but maintains a long-lived bend which shows little sign of decay for at least a further Gyr. The persistence of this feature suggests that the observed departures from a perfect plane of the Milky Way may possibly have been created by bending instabilities in the distant past when the plane might have been thinner. I would caution, however, that rings which form in Jeans-unstable models are very persistent when non-axisymmetric forces are inhibited but quickly dissolve when the evolution is unrestricted; if bending modes behave analogously, the bend in the present model might not persist in an unrestricted simulation.

This result confirms Toomre's (1966) conclusion, based on his local criterion alone, that the disk of the Milky Way is sufficiently thick to be well clear of the bending stability boundary. The observed vertical velocity dispersion of old disk stars in the solar neighborhood, some 18–20 km s^{-1} (e.g. Mihalas & Binney 1981), is almost twice that which the simulation indicates could have been created through bending instabilities, even with a high disk surface density. The current thickness must therefore have developed through some other mechanism, probably scattering by gas clouds.

Admittedly this study has been restricted to axial symmetry; non-axisymmetric instabilities are possible, though the prospects of a violation of the Toomre-Araki criterion in the azimuthal direction seems less likely because the azimuthal dispersion is lower and surface density varies only in the radial direction.

I wish to thank David Merritt for many helpful conversations. This work was supported by NSF grant AST 9318617.

References

Araki, S. 1985, Ph.D. thesis, MIT
Combes, F., Debbasch, F., Friedli. D. & Pfenniger, D. 1990, *A&A*, 233, 82
Combes, F. & Sanders, R. H. 1981, *A&A*, 96, 164
Evans, N. W. & Collett, J. L. 1993, *MNRAS*, 264, 353
Fridman, A. M. & Polyachenko, V. L. 1984, *Physics of Gravitating Systems*, (Springer-Verlag: New York)
Merritt, D. & Hernquist, L. 1991, *Ap.J.*, 376, 439
Merritt, D. & Sellwood, J. A. 1994, *Ap.J.*, 425, 551
Mihalas, D. & Binney, J. 1981, *Galactic Astronomy*, (Freeman: San Franciso)
Raha, N., Sellwood, J. A., James, R. A. & Kahn, F. D. 1991, *Nature*, 352, 411
Sellwood, J. A. 1995, *Ap.J.*, submitted
Sellwood, J. A. & Merritt, D. 1994, *Ap.J.*, 425, 530
Toomre, A. 1964, *Ap.J.*, 139, 1217
Toomre, A. 1966, *Geophysical Fluid Dynamics*, notes on the 1966 Summer Study Program at the Woods Hole Oceanographic Institution, ref. no. 66-46, p 111
Toomre, A. 1974, *Highlights of Astronomy*, 3, ed Contopoulos, G. (Reidel: Dordrecht) p 457

DISCUSSION

K. Chamcham: Observations of Kennicutt (89) show that there is a close correlation between the stability properties of discs at the onset of star formation i.e. star formation starts when the disc becomes unstable and therefore you should include the effect of stars in your criterion. Moreover, once star formation starts, you should also include the effect of cosmic rays and magnetic fields. Don't you think that these effects will change your results?

Sellwood: You are obviously thinking of Jeans-type instabilities, whereas my principal interest in these stellar dynamical simulations was the stability into bending modes. It is well known that Jeans instabilities in discs are significantly affected by a cool dissipative gas component, but I would not expect it to have much effect on the bending stability boundary.

FAINT SURFACE PHOTOMETRY OF THE HALO OF M31

CHRIS PRITCHET
Department of Physics and Astronomy, University of Victoria, P.O. Box 3055, Victoria, BC, Canada V8W 3P6

AND

SIDNEY VAN DEN BERGH
Dominion Astrophysical Observatory, 5071 W. Saanich Road, Victoria, BC, Canada V8X 4M6

Abstract. We have obtained counts of stars near the tip of the red giant branch of M31, and have used these counts to estimate the surface brightness of the halo of M31 down to a level of $\mu_V \simeq 30$ mag arcsec^{-2} ($R \approx 20$ kpc). The surface brightness along the minor axis of the M31 halo is well-represented by a single de Vaucouleurs law ($0.2 \lesssim R$[kpc] $\lesssim 20$). Alternatively, the *outer* halo of M31 can also be modelled by a power-law density distribution of the form $\rho(R) \propto R^{-5}$. This result suggests that the globular cluster component of the halo of M31 (for which $\rho \propto R^{-3}$) is more extended than the stellar halo of this galaxy. At $\mu_V \approx 28$ mag arcsec^{-2} ($R \approx 10$ kpc), the axial ratio of the halo of M31 is found to be $c/a = 0.55 \pm 0.05$.

1. Introduction

A paper on M31 might seem a somewhat odd choice for a meeting on the Milky Way. Yet very little is known about the structure of the Milky Way stellar halo, primarily because we are immersed in it, and are locally swamped by stars belonging to the disk. It therefore seems reasonable to see what can be learned about stellar halos by studying other galaxies, in particular M31, which is close enough that its stellar halo can be resolved.

In this paper we use a method involving counting individual stars to determine the surface brightness distribution of the halo of M31. Surface brightness levels $\mu_V \approx 30$ mag arcsec^{-2} are reached; we predict that ~ 32

L. Blitz and P. Teuben (eds.), Unsolved Problems of the Milky Way, 39–45.
© 1996 *International Astronomical Union.*

mag arcsec^{-2} is within reach of future observations. Further details of this work can be found in Pritchet and van den Bergh (1994, hereafter PV94).

2. From Star Counts to Surface Brightness

Observations were obtained with the Canada-France-Hawaii 3.6 m Telescope, in conjunction with CCD detectors with field size $2\farcm2 \times 3\farcm3$. Total exposures were $\sim$1 hr through B and V filters. Seeing was typically $\sim 1''$ FWHM for all exposures.

Most of the program fields were chosen to lie along the minor axis of M31 (fields M0–M5, 40′–5°); two fields (E1 and E2) were observed at position angle between the major and minor axes, and three fields (R1–R3) were observed at large distances ($\sim 10°$) from M31 as "reference" fields, to monitor foreground and background contamination. The data were analyzed using DAOPHOT (Stetson 1987). Completeness fractions and photometric errors were evaluated with artificial star experiments (typically 5 runs of 100 added stars for each field and bandpass). Image moments (Kron 1980) were used to find and reject extended objects.

Luminosity distributions in the V band were computed by counting each star as $1/\mathrm{f}(\mathrm{m}_i)$, where f is the completeness fraction at m_i, the magnitude of star i. Examples of some luminosity distributions can be found in PV94. Our analysis of the surface brightness of the fields is confined to the magnitude range $22 < V < 24$, and avoids both unnecessary contamination by field stars at the bright end, and severe incompleteness problems at the faint end (since 50% completeness is at $V = 24.5$).

The true surface brightness in each field is determined by *(1)* subtracting the contribution of contaminants in the magnitude range $22 < V < 24$, and *(2)* correcting for the missed light from M31 halo stars outside the magnitude range $22 < V < 24$. Correction *(1)* is $\mu_V = 30.26 \pm 0.11$ mag arcsec^{-2} for the contaminant luminosity distribution that was derived above. Correction *(2)* depends on metallicity, and is about -1.64 mag (appropriate to a 47 Tuc metallicity – *cf.* Mould and Kristian 1986, Pritchet and van den Bergh 1988, Christian and Heasley 1991, van den Bergh and Pritchet 1992). The reader is referred to PV94 for further details on the above corrections.

3. Luminosity Profile and Flattening of M31 Halo

Fig. 1 shows our observed surface brightness data for the M31 halo; filled squares represent minor axis data, and open squares represent fields E1 and E2 (between major and minor axis – to be discussed below). Also shown in Fig. 1 are data from Walterbos and Kennicutt (1987). Our observations join smoothly onto an extrapolation of these data, and also onto the data of de Vaucouleurs (1958).

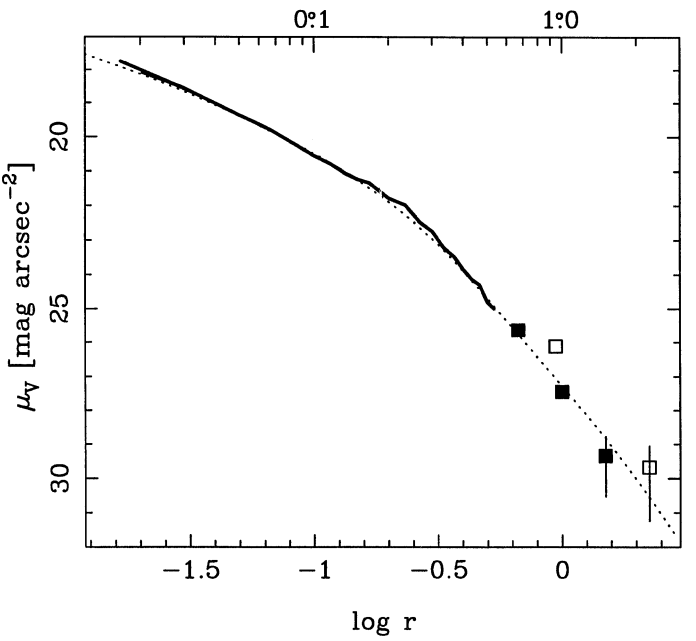

Figure 1. Surface photometry of M31 plotted against angle (degrees) from the centre of M31. The solid squares represent minor axis photometry, and the heavy solid line represents minor axis photometry of Walterbos and Kennicutt (1987). The dotted line represents a sum of the disk plus $r^{\frac{1}{4}}$ spheroid model. The open squares refer to our fields that are between the major and minor axis of M31. These latter fields are brighter than fields on the minor axis, indicating that the halo is flattened.

The disk contribution is estimated from Walterbos and Kennicutt (1988, WK88) to be quite small in Fig. 1; it is at most 40% of the light at about 15′ , but drops to less than 10% for our outer fields. The dotted curve in Fig. 1 shows the sum of the disk plus de Vaucouleurs (dV) law spheroid contributions from the WK88 model. This model provides an *excellent* fit to the data plotted in Fig. 1. It also provides a reasonable fit to the data of Kent (1983) and WK88 at smaller radii (at least for $r \gtrsim 1'$).

We conclude that *a single de Vaucouleurs law luminosity profile* (with minor axis effective radius $b_{eff} \simeq 1.3$ kpc) *can fit the spheroid of M31 from the inner bulge* ($r \approx 1', R \simeq 200$ *pc) all the way out to the halo* ($r \gtrsim 1°.5, R \gtrsim 20$ *kpc).* The behavior of the luminosity profile within 1′ is much more complicated (*e.g.*, Light, Danielson, and Schwarzschild 1974; Kent 1983).

A single power law *cannot* represent the run of surface brightness in Fig.

1. The outer minor axis observation require a power-law in projected surface brightness $I \propto r^{-4}$, or a density profile $\rho \propto R^{-5}$. These $\rho(R)$ distributions are clearly much steeper than the $\rho \propto R^{-2.5}$ observed at $r < 0.^{\circ}1$, and also steeper than the $\rho \propto R^{-3.5}$ observed for the Milky Way.

Two of our fields (E1 and E2) are situated well away from the minor axis of M31, at position angles between 30° and 45°. Fig. 1 shows that these fields possess an excess of light relative to minor axis fields at the same radial distance from the center of M31. This clearly demonstrates that the halo of M31 is flattened, with $c/a = 0.55 \pm 0.05$ (after correcting for disk light).

4. Comparison of M31 with the Milky Way and Other Galaxies

How does the minor axis profile of M31 compare with that of the Milky Way? To answer this question, we consider surface photometry of the bulge of the Milky Way by de Vaucouleurs and Pence (1975). They showed the bulge of the MW is well-fitted by a de Vaucouleurs law; however, extrapolating this dV law to the Galactic poles overestimates the known surface brightness from halo stars by more than 2 mag! A similar effect is seen for NGC 4565: the bulge of this galaxy is much brighter than would be predicted by extrapolating the halo light profile (van der Kruit and Searle 1981*a*). On the other hand, the halo of the edge-on Sbc galaxy NGC 891 (which resembles the MW quite closely) obeys an $r^{\frac{1}{4}}$ law from 1.5 to 8 kpc (van der Kruit and Searle 1981*b*). The situation with the halos/bulges of other galaxies is confusing: some do, and some don't, follow a single dV law (PV94). This seems to suggest (but does not prove) that (i) bulge and halo formation is decoupled; and (ii) the continuity of the bulge and halo light in M31 may be an accident. It should be noted that M31 now possesses the best surface photometry of any bulge/halo system, so that a comparison with other galaxies is not easy.

Expressing the halo density law as a power-law $\rho(r) \propto r^n$, we find an exponent n approaching -5; this is very different from the values of $n = -3$ to -3.5 that are often quoted for the Milky Way. Now, it seems unlikely that M31 would have a shallower power-law density drop-off than the Milky Way, given its earlier morphological type (which folklore dictates should imply a more prominent spheroidal population). Nor do we consider the canonical MW power-law values of n to be reliable, since they are mostly based on globular clusters (which do not necessarily follow the density law of the stellar halo in other galaxies), or RR Lyrae stars (whose density law may be strongly modulated by population dependent [second parameter] effects). Thus we consider it to be entirely possible that the MW stellar halo may follow a density law as steep as that implied for M31. Given the

steepness of the implied exponent ($n \simeq -5$), this would have important ramifications for the spatial extent of the MW halo. Clearly it would be of enormous interest to obtain better estimates of the run of density in the MW stellar halo based on subdwarfs.

The flattening c/a that we have obtained for the M31 halo is quite comparable to that observed for other g· laxies. NGC 891 possesses $c/a \approx 0.5$, with a considerable dependence on radius (van der Kruit and Searle 1981*b*). The halo of NGC 4565 may be even more flattened, reaching $c/a \simeq 0.4$ (van der Kruit and Searle 1981*a*). On the other hand, the earlier type (Sab) galaxy NGC 7814 has $c/a \simeq 0.57$ at $\mu_J \lesssim 26$ mag arcsec^{-2}, with little or no radial variation (van der Kruit and Searle 1982) . This latter result is more similar to that which is observed for M31, and also for the Milky Way (*e.g.*, Wyse and Gilmore 1989 and references therein).

The globular cluster system of the M31 halo has a density profile $\rho \propto R^{-3}$ (Racine 1991), identical to that observed for Milky Way globulars (Racine and Harris 1989). This should be compared with the density profile $\rho \propto R^{-5}$ observed for M31 halo stars at $R \gtrsim 10$ kpc, or with $\rho \propto R^{-4}$ at smaller radius. We conclude that the globular cluster system of M31 is more extended than the stellar halo of this galaxy. This conclusion is confirmed by the work of Fusi Pecci *et al.* (1993), who show that the M31 globular cluster system follows an $r^{\frac{1}{4}}$ law in projected density, with effective radius $r_{eff} = 4.6$ kpc. The fact that this value of r_{eff} is significantly larger than the value of 2.0 kpc measured for the stellar halo (§4) again suggests that the M31 globular cluster system is more extended than its stellar halo.

A similar effect has been noted for several well-observed giant ellipticals in the Virgo cluster (*e.g.*, Harris and Racine 1979; Forte, Strom, and Strom 1981; McLaughlin, Harris, and Hanes 1993). This observation has been used as an argument in favor of the view that the formation of globular clusters predates the formation of the field spheroidal population in galaxies. Although not all galaxies show this effect, it appears that most well-observed galaxies in fact have different globular cluster and stellar halo density distributions (*cf.* Harris 1991).

5. Conclusions

We have traced the halo of M31 out to a surface brightness level ~ 30 mag arcsec^{-2} in V, corresponding to a radial distance of ~ 20 kpc from the center of M31. The spheroid (bulge plus halo) of M31 is well-described by a single de Vaucouleurs law, with constant (or slightly decreasing) c/a, from $r \simeq 1'$ all the way out to the limit of our observations at $r \simeq 1°.5$. The axial ratio of the M31 halo is $c/a \simeq 0.55$ at $\mu_V \simeq 28$ mag arcsec^{-2}. There is a hint of a possible cutoff in the surface brightness distribution beyond

20 kpc.

This work was supported by the Natural Sciences and Engineering Research Council of Canada.

References

Christian, C.A., & Heasley, J.N.; 1991, AJ, 101, 848.
Forte, J.C., Strom, S.E., & Strom, K.M.; 1981, ApJL, 245, L9.
Fusi Pecci, F., Cacciari, C., Frederici, L., & Pasquali, A.; 1993, in *The Globular Cluster Connection*, ed. G.H. Smith and J.P. Brodie, A.S.P. Conference Series (San Francisco: ASP), p. 410.
Harris, W.E.; 1991, ARA&A, 29, 543.
Harris, W.E., & Racine, R.; 1979, ARA&A, 17, 241.
Kent, S.M.; 1983, ApJ, 266, 562.
Kron, R.G.; 1980, ApJS, 43, 305.
Light, E.S., Danielson, R.E., & Schwarzschild, M.; 1974, ApJ, 194, 257.
McLaughlin, D.E., Harris, W.E., & Hanes, D.A.; 1993, ApJ, in press.
Mould, J., & Kristian, J.; 1986, ApJ, 305, 591.
Pritchet, C.J. & van den Bergh, S.; 1988, ApJ, 331, 135.
Pritchet, C.J. & van den Bergh, S.; 1994, AJ, 107, 1730 (PV94).
Racine, R.; 1991, AJ, 101, 865.
Racine, R., & Harris, W.E.; 1989, AJ, 98, 1609.
Stetson, P.B.; 1987, PASP, 99, 191.
van den Bergh, S., & Pritchet, C.J.; 1992, in *The Stellar Populations of Galaxies*, ed. B. Barbuy & A. Renzini (Dordrecht: Reidel), p. 161.
van der Kruit, P.C., & Searle, L.; 1981*a*, A&A, 95, 105.
van der Kruit, P.C., & Searle, L.; 1981*b*, A&A, 95, 116.
van der Kruit, P.C., & Searle, L.; 1982, A&A, 110, 79.
Vaucouleurs, G. de; 1958, ApJ, 128, 465.
Vaucouleurs, G. de, & Pence, W.D. 1978, AJ, 83, 1163
Walterbos, R.A.M., & Kennicutt, R.C.; 1987, A&ASuppl, 69, 311.
Walterbos, R.A.M., & Kennicutt, R.C.; 1988, A&A, 198, 61 (WK88).
Walterbos, R.A.M., & Schwering, P.B.W.; 1987, A&A, 180, 27.
Wyse, R.F.G., & Gilmore, G.; 1989, Comm. Ap., 13, 135.

DISCUSSION

I. King: These are fascinating results, but I would like to remind everyone here that this paper is not related to the preceding ones. It has become a firm astronomical practice to use the word "halo" to refer to two completely distinct components of the Milky Way (or of other galaxies): the stellar halo and the dark halo, which have completely different spatial distributions.

Pritchet: Good point. I emphasize that our work refers to the stellar halo.

A. Gould: The last point at 18 kpc seems very insecure. Could the radial profile be even steeper?

Pritchet: Yes. The detection is clear but the value is uncertain. The profile could be steeper.

B. Burke: King mentioned that there were two kinds of halo, but there is a third halo, the high-energy halo, observed at meter wavelengths. The origin of the high-energy halo, and its dynamical behavior, are still not clear, but it probably is generated by supernova remnants bubbling up from the plane? After that, its behavior should be governed by the gravitational field in the halo. The system looks more flattened than the 2:1 flattening mentioned here- perhaps 4:1, but in view of our present lack of knowledge, one probably can only conclude that it supports the notion of flattened gravitational isopotentials in the halo.

Pritchet: What is the radial dependence?
(reply by Burke): Most, but not all, of the radiation is within R_o.

A SURVEY OF SURVEYS

S. M. KENT
Fermi National Accelerator Laboratory
MS 127
P. O. Box 500
Batavia, IL 60510 USA†

Abstract. A new era for the field of Galactic structure is about to be opened with the advent of wide-area digital sky surveys. In this article, I will review the status and prospects for research for 3 new ground-based surveys: the Sloan Digital Sky Survey (SDSS), the Deep Near-Infrared Survey of the Southern Sky (DENIS) and the Two Micron All Sky Survey (2MASS). These surveys will permit detailed studies of Galactic structure and stellar populations in the Galaxy with unprecedented detail. Extracting the information, however, will be challenging.

1. The Surveys

The SDSS is a project to produce a digital photometric map of half the northern sky to about 23 mag in the V band. This map will be used to select about a million galaxies and 100,000 quasars for which high resolution spectra will be obtained with the same wide-field special-purpose telescope. The imaging survey will also be used to produce a catalog in five colors (u' to z') of all detected objects, about 100 million galaxies and a similar number of stars, and a million quasar candidates. The survey will be conducted with a special purpose telescope to be built at Apache Point Observatory in New Mexico. The instrumentation will consist of a mosaic of 30 Site 2048 X 2048

*Work supported by the U. S. Department of Energy under contract No. DE-AC02-76CH03000.
†Work supported by the U. S. Department of Energy under contract No. DE-AC02-76CH03000.

L. Blitz and P. Teuben (eds.), Unsolved Problems of the Milky Way, 47–55.
© 1996 *International Astronomical Union.*

CCDs and a pair of multi-fiber spectrographs which can obtain spectra of 600 objects simultaneously.

The DENIS project will provide a uniform survey of the southern sky at three near-infrared bands: I, J, and K. The expected data products are a set of elementary images (12' X 12') and specialized catalogs of point and extended sources comprising 10 million stars and 250,000 galaxies. The survey will be used to investigate stellar populations (particularly low temperature stars, brown dwarfs, and red giants and asymptotic giant branch stars, and Galactic bulge stars) and the properties and distribution of external galaxies. The instrumentation will consist of a single Tektronix CCD for the I band and two 256 X 256 HgCdTe array detectors for the J and K bands.

The 2MASS project will provide a uniform survey of the entire sky at three near-infrared bands: J, H, and K' (a modified K). A major goal of the survey is to probe large scale structures in the Milky Way and in the Local Universe, exploiting the relatively high transparency of the interstellar medium in the near-IR and the high near-IR luminosities of evolved low- and intermediate-mass stars. Approximately 100 million stars and 1 million galaxies will be detected. Two special purpose telescopes will be built and sited at Mount Hopkins Arizona in the northern hemisphere and Cerro Tololo in the southern hemisphere. The instrumentation will consist of a camera with a mosaic of 256 X 256 HgCdTe array detectors.

2. Comparison of Surveys

The two near-infrared surveys have rather similar capabilities. The SDSS survey is complementary to the other two. Table 1 compares a number of characterstic parameters among the three surveys.

A comparison of the SDSS with the IR surveys reveals that:

1. Sky Coverage - the SDSS will cover primarily the north Galactic pole region down to b=30 degrees (and a smaller portion of the southern sky). The IR surveys will cover the entire sky, particularly the Galactic plane and bulge. The SDSS will overlap with only the northern half of the 2MASS survey.
2. Detection limits - A comparison of the detection limits for point sources of the 3 surveys is shown in Figure 1. Also plotted are a sample of spectra for "normal" stars. Because the SDSS is a bigger telescope and will have longer integration times, it will be more efficient at detecting stars earlier than spectral type M5. Table 2 gives typically maximum distances out to which stars of various classes will be detected by the surveys. The SDSS actually has a more serious problem in that it will

TABLE 1. Comparison of Major Optical/IR Surveys

	SDSS	2MASS	DENIS
Coverage	NGP $b > 30$ deg	All Sky	$\delta < 0$ deg
Telescope	2.5 m	1.3 m	1 m
Detector	30×CCDs	3×HcCdTe	1×CCD 2×HgCdTe
Bands	$u'g'r'i'z'$	JHK'	IJK
Pixel size	0.4″	2″	1.5″(I) 3″(JK)
Integration Time (s)	55	8	9
Duration (Yrs)	5	3	3-4
Location	APO	FLWO + CTIO	ESO
Institutions	8	9	20
Phot. Error (rms mag)	0.02	0.05	0.05
Astrometric Error (rms)	$< 0.2''$	$\geq 0.5''$	
Limiting Mag	$V = 22$	$K = 14$	$K = 14$
Dynamic Range (mag)	8	10	

saturate for stars brighter than about V=14. This renders it of minimal use for studies of giants at distances of less than a few kpc.

3. Filter Bands - One weakness of the SDSS for Galactic research is that it is being conducted with very non-standard bandpasses. The g' filter, centered at 0.44 microns, is especially wide. Interpreting the SDSS data in the context of existing stellar photometry will be complicated.

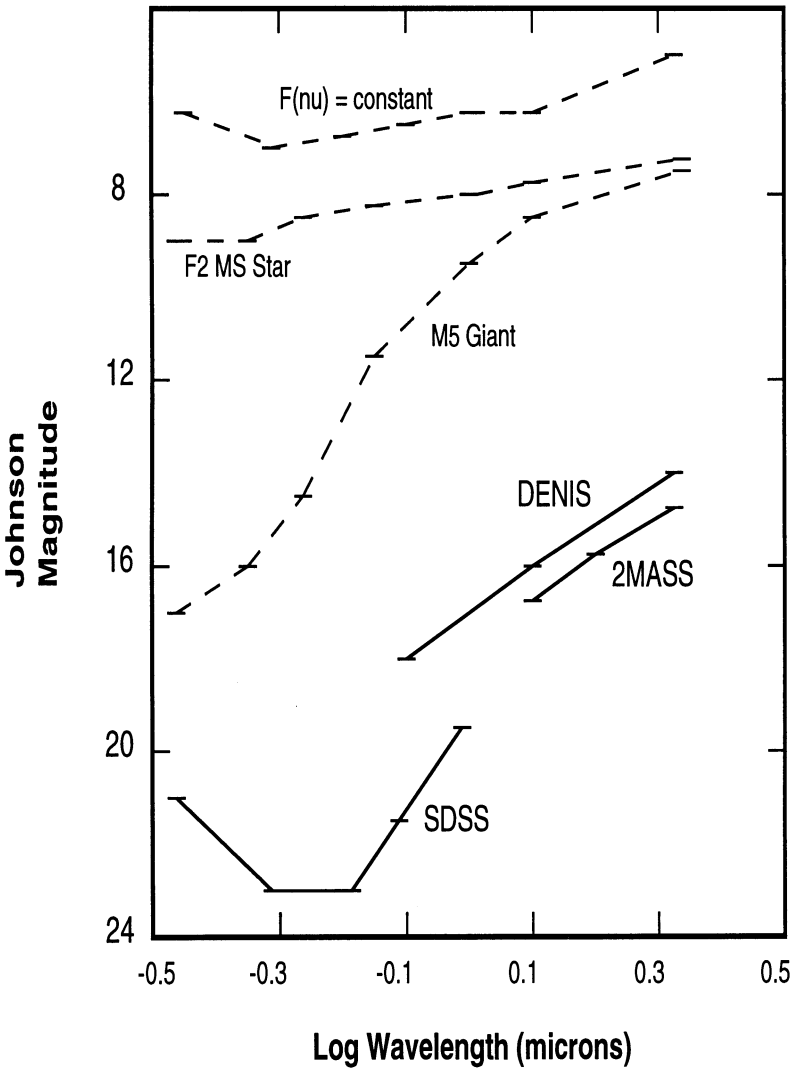

Figure 1. Sensitivity Limits of Optical and IR Sky Surveys

DENIS and 2MASS use standard bands with the exception of K, where each has its own minor variation.

3. Advantages for Galactic Research:

1. Uniformity - The SDSS has a goal of about 2% systematic error over the sky. The IR surveys do not have stated goals but should achieve an error of order 5%. For studies such as number counts of stars, errors

TABLE 2. Comparison of Survey Depths

Star Type	SDSS (kpc)	2Mass/DENIS (kpc)
OH/IR ojbect	–	100
Mira Giant	1000	300
M5 Giant	126	50
Horizontal Branch Star	275	4.4
F subdwarf	50	1.2
M5 dwarf	0.5	0.1
Brown Dwarf	–	0.01-0.10

in the counts from survey non-uniformity become negligible compared with other uncertainties.

2. Multi-color data - Such data are invaluable for distinguishing stars of different types and metallicities.
3. Coverage - The usefulness of this property is self-evident. The combination of wide angular coverage, depth, and uniformity will permit quantitative probes of Galactic structure that have not been possible up to now.

4. Hazards of Galactic Structure

In principle, star count data, such as will be collected by the three surveys, provide much more information on Galactic structure than integrated light maps from surveys such as the *DIRBE* experiment on *COBE*. The extra information consists of differential counts as a function of both color and magnitude at each position in the sky, One learns about the distribution of stars in the Galaxy from both the distribution of stars along the line of sight and from the variation of the counts with direction in the sky. However, in order make use of this information, one must have some model for the distribution of stars in the H-R diagram. In the absence of *a priori* information about this distribution, the number of additional knowns introduced by having star counts is matched by the additional unknowns, and so, compared with integrated light maps, one actually gains no additional information about Galactic structure at all! In practice we do have a priori knowledge, but interpretation of star count data is as much an exercise in modeling stelllar populations as it is in modeling Galactic structure, and ambiguities are often present in such analyses (e.g., Habing 1988; Wainscoat *et al.* 1992; Ortiz and Lepine 1993). Nevertheless, the new wide angle surveys will provide enough new information that some of the ambi-

guities will be resolved. particular for populations with with axisymmetric distributions such as the old disk or halo.

In detail, it is convenient to look at halo and disk components separately.

4.1. HALO

The canonical model of the halo is a slightly flattened de Vaucouleurs profile, with parameters given by Bahcall and Soneira (1980). This model works well in reproducing existing star counts at high Galactic latitude for $V < 19$, but predicts too many stars at fainter magnitudes (Reid and Majewski 1993). Some combination of a flatter spheroid and/or a shorter scale length is indicated. The Reid and Majewski paper also illustrates the value to having color information: their "standard model" reproduces the star counts at the NGP reasonably well for $V < 19$, but fails to reproduce the color distribution at a fixed magnitude, indicating that the relative ratios of disk and halo stars is incorrect.

The SDSS should provide the most useful information on the halo. It will detect main sequence turnoff stars to a distance of 50 kpc. For stars fainter than V=17, halo stars are dominant in star counts, and one can further distinguish them on the basis of their blue color (Kron 1980). Some problems that can be addressed are:

1. An improved measure of the density profile with radius.
2. A proper measure of the flattening of the halo, plus a measure of its triaxiality.
3. From multicolor data, an improved measure of the variation of metallicity with radius.

The SDSS u' filter lies shortwards of the Balmer discontinuity at 0.36 microns, and so the SDSS will be able to detect and distinguish blue horizontal branch stars throughout the halo.

4.2. DISK

A number of models for the distribution of stars in the Galaxy incorporate complex models for the disk above and beyond the nominal exponential disk with a sech^2 vertical profile of constant scale height (e.g., Bahcall and Soneira 1980; Hayakawa *et al.* 1981; Gilmore and Reid 1983; Robin & Creze 1986; Habing 1988; Ruelas-Mayorga 1991a,b; Wainscoat *et al.* 1992; Ortiz and Lepine 1993). A composite of such models might incorporate a young thin disk, an old thin disk, a thick disk, and multiple spiral arms. Each component has its own spatial distribution, stellar population, and kinematics. Such complexity seems to be required to explain the cumulative observations of the disk so far, but the number of free parameters required

to characterize each component is larger than can be constrained by existing observations. To date, global star counts have played little role in contraining these parameters, primarily because the existing data are sporadic, do not go very deep, and are nonuniform. Data for the southern hemisphere are particularly sparse. DENIS and 2MASS will completely reverse this situation. They should detect all AGB stars in the Galaxy and all late type giants to a distance at or beyond the Galactic center. The counts should be dominated by disk giants for all positions in the disk except near the bulge.

Any interpretation of star count data in the Galactic plane must contend with two effects: extinction by dust and confusion due to high star densities in the Galactic plane. Both effects can be minimized by looking just outside of the plane, but the loss of information is high: at a latitude of just 2 degrees, a line of sight to the Galactic center is 280 pc above the Galactic plane and already missing over half the stars in the disk. Even at K band, the extinction to the Galactic center is of order 3 mag. Thus, careful modeling of the dust distribution is necessary. Fortunately, the dust distribution in the Galaxy seems to follow the gas density rather closely, so one can do kinematic modeling of the gas distribution from HI and CO observations and thus construct a 3 dimensional map of extinction over a substantial range of Galactic longitude (roughly 20 to 60 degrees) where extinction problems are most severe (e.g., Kent, Dame and Fazio 1991) A rough estimate of the confusion limit suggest that one will do 10% photometry on $K = 10$ stars at position $b = 0, l = 20$. 2MASS, with its smaller pixels, will be better off than DENIS, and both with be confusion limited well above their sensitivity limits.

A sample of problems that can be attacked by the sky surveys includes:

1. Comparison of starcounts with existing models: Detailed Galaxy models of infrared star counts exist already (e.g., Ortiz and Lepine 1993), but are untested due to a paucity of data. The new surveys will rectify that shortage. It may be possible to probe the dependence of characteristic scale lengths and scale heights on stellar population.
2. Non-axisymmetric Galactic structure: DENIS and 2MASS data will be well suited to probes of nonaxisymmetric structure in the Galaxy. Here, one can use lines of sight outside of the plane itself in order to probe N-S asymmetries and thus overcome the extinction/confusion problems. Of major interest is whether our Galaxy has a classical bar and/or a triaxial bulge. Tantalizing evidence exists (Blitz and Spergel 1991; Weinberg 1992) but at present it is ambiguous as to what the nature of the bulge/bar is, its radial extent, and its thickness. If the Milky Way has a bar of size 1 scale length (3 kpc) which is typical for external barred galaxies, then in projection it will extend to a longitude

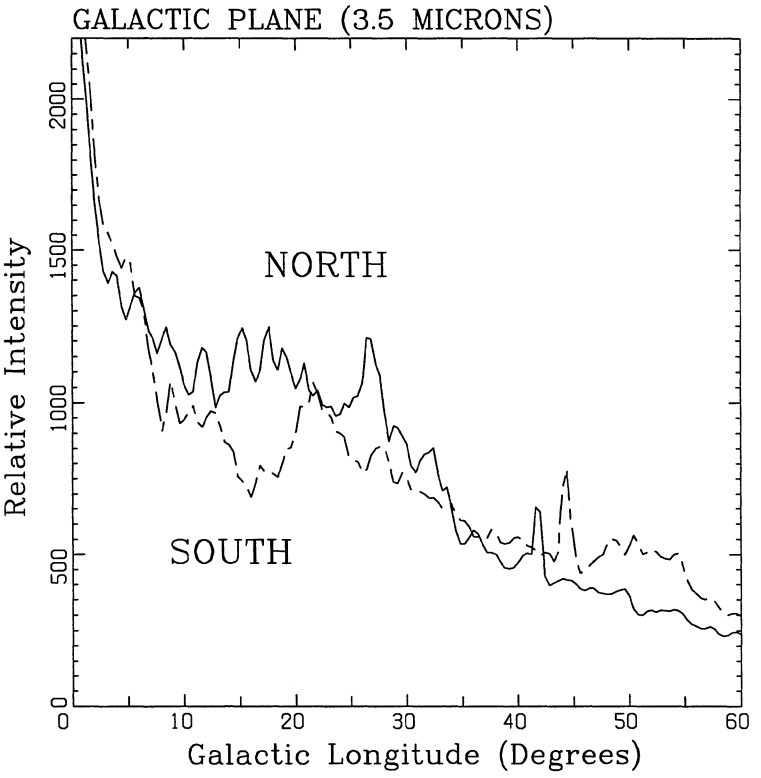

Figure 2. DIRBE 3.5 micron luminosity profiles of Galactic plane. Profiles are integrated over $\pm 1^\circ$ of latitude.

of between -20 and 20 degrees, depending on the orientation to the line of sight. The difference in distance modulus for stars at opposite ends of the bar will be between 0 and 1.7 mag. Current opinion is that the bar is closer to end on than sideways, so there should be a large asymmetry in the star distribution in the longitude range -10 to 10 degrees.

3. Spiral Structure: In addition to possible asymmetries due to a bar, near-IR integrated light maps (e.g. Hayakawa *et al.* 1981) show that light in the Galactic plane is very asymmetric out to longitudes of $|l| \approx 30^\circ$. Figure 2 shows a plot from the *DIRBE* experiment on *COBE*

(Boggess *et al.* 1992; Hauser 1992) of the 3.5 micron luminosity profile along the Galactic plane for the northern and southern Galactic hemispheres, illustrating the asymmetry. This asymmetry might be due to spiral structure. Such structure should be reflected in star counts. One might be able to use JHK colors and/or extinction modulations (Karawa *et al.* 1982) to identify a young population of stars assocated with spiral arms. Paczinski *et al.* (1994) have already used *visual* color-magnitude diagrams derived from observations of fields in the direction of the Galactic bulge as part of the *OGLE* survey to identify main sequence stars in a nearby spiral arm.

I wish to thank Andy Gould, Martin Weinberg, and Hans-Walter Rix for valuable discussions.

References

Bahcall, J.N., and Soneira, R.M. (1980) *Astrophys. J. Suppl.* 44, 73
Blitz, L., and Spergel, D. (1991) *Astrophys. J.*, 379, 631
Boggess, N.W., Mather, J.C., Weiss, R., Bennett, C.L., Cheng, E.S., Dewk, E., Gulkis, S., Hauser, M.G., Janssen, M.A., Kelsall, T., Meyer, S.S., Moseley, S.H., Murdock, T.L., Shafer, R.A., Silverberg, R.F., Smoot, G.F., Wilkinson, D.T., and Wright, E.L. (1992) *Astrophys. J.*, 397, 420
Gilmore, G.F., and Reid, I.N. (1983) *Mon. Not. Roy. Astron. Soc.*, 202, 1025
Habing, H. *Astron. Astrophys.*, 200, 40
Hauser, M. (1992) In AIP conference *Back to the Galaxy*, 201
Hayakawa, S., Matsumoto, T., Murakami, H., Uyama, K., Thomas, J.A., and Yamagami, T. (1981) *Astron. Astrophys.*, 100, 116
Karawa, K., Kozasa, T., and Sato, S. (1982) *Publ. Astron. Jap.* 34, 389
Kent, S.M., Dame, T.M., and Fazio, G. (1991) *Astrophys. J.*, 378, 131.
Kron, R.G. (1980) *Astrophys. J. Suppl.*, 43, 305
Ortiz, R., and Lepine, R.D. (1993) *Astron. Astrophys.*, 279, 90
Paczynski, B., Stanek, K.Z., Udalski, A., Szymanski, M., Kaluzny, J., Kubiak, M., Mateo, M., and Krzeminski, W. (1994) preprint
Reid, N., and Majewski, S.R. (1993) *Astrophys. J.*, 409, 635
Robin, A.C., and Creze, M. (1986) *Astron. Astrophys., 157*, 71
Ruelas-Mayora, R.A. (1991a) *Rev. Mexicana Astron. Astrophys, 22*, 27
Ruelas-Mayora, R.A. (1991b) *Rev. Mexicana Astron. Astrophys, 22*, 43
Wainscoat, R.J., Cohen, M., Volk, K., Walker, H.J., and Schwartz, D.E. (1992) *Astrophysical Journal Supplement* 83, 111
Weinberg, M. (1992) *Astrophys. J.*, 384, 81

DISCUSSION

M. Balcells: Could you tell us something about data processing strategy?

Kent: It would take more time than I have here to give a complete answer. Basically, data will be recorded at the mountain on magnetic tape and returned to Fermilab for processing.

ELLIPTICITY OF OUTER REGIONS OF GALACTIC DISKS

URMAS HAUD
Tartu Astrophysical Observatory
EE2444 Toravere, Estonia

In hierarchical cosmologies, dark matter coronas arise from the gravitational collapse of density peaks in a random perturbation field. The result is a **triaxial**, slowly rotating, centrally concentrated dark corona (Dubinski and Carlberg, 1991; Dubinski, 1992). Binney (1978) was the first to consider the effects of triaxial coronas around disk galaxies, showing that they might explain the observed warps and apparent twists seen in many disks. In external galaxies these deformations of density and velocity fields are modeled with a system of **circular** annuli, each of which has its own inclination and line of nodes (LON). By examining warped systems in a variety of reference frames, Briggs (1990) has mentioned that galaxy kinematics uniquely specifies a new reference frame in which there is a common LON for orbits within the transition radius and also a differently oriented straight LON for the gas outside the transition radius, which is approximately equal to the Holmberg radius of the galaxy.

In a complete picture of galaxy formation, baryons become segregated from the collisionless dark matter through the dissipation of their gravitational energy and sink to the center of the dark corona (Katz and Gunn, 1991; Evrard, Summers and Davis, 1992). The resulting rotationally supported disk will be ovally distorted or **elliptical** (Kuijken and Tremaine, 1992; Dubinski, 1993). The long axis of the orbits is perpendicular to the long axis of the corona potential. Due to this antialignment, if the disk mass is comparable to the halo mass within the disk, the combined potential there becomes considerably rounder (Dubinski, 1993). As there is a distinct trend towards rounder axial ratios of the corona at larger radii (Dubinski, 1992), we may expect the highest triaxiality of the potential somewhere in the transition region from disk to corona.

Van Albada, Kotanyi and Schwarzschild (1982) have shown that there exist stable orbits of various tip-angles in a triaxial potential which under-

L. Blitz and P. Teuben (eds.), Unsolved Problems of the Milky Way, 57–58.
© 1996 *International Astronomical Union.*

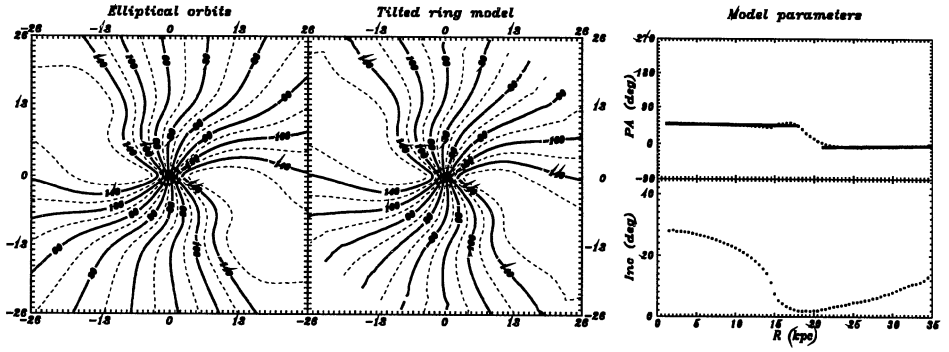

Figure 1. Left: the velocity field of the warped model galaxy with elliptical orbits having a common LON and the highest ellipticity at optical boundary of the galaxy; middle: the approximation of the velocity field with the standard circular orbit model; right: the plots of the tip angle and LON in the circular orbit model as a function of the radius of the ring, directly comparable to Fig. 3 by Briggs (1990).

goes figure rotation. The warp produced by such a system would have a constant line of nodes. In this model the findings by Briggs can be explained by the fact that most elongated gas orbits are found somewhere around the Holmberg radius of the system, where the gravitational potential of the corona becomes dominating. We illustrate this in Figure 1. As we can see, our model yields a simple explanation to the otherwise strange behavior of the tilted ring models for galactic warps, discussed by Briggs (1990).

Acknowledgements This work was supported in part by the International Science Foundation grant number LCH000 and by the Estonian Science Foundation grant number 180.

References

Binney, J. J.: 1978, *Monthly Notices Roy. Astron. Soc.*, 183, 779.
Briggs, F. H.: 1990, *Astrophys. J.*, 352, 15.
Dubinski, J.: 1992, *Astrophys. J.*, 401, 441.
Dubinski, J.: 1993, *SISSA*, 9309001.
Dubinski, J., Carlberg, R. G.: 1991, *Astrophys. J.*, 378, 496.
Evrard, A. E., Summers, F. J., Davis, M.: 1993, *preprint.*
Katz, N., Gunn, J. E.: 1991, *Astrophys. J.*, 377, 365.
Kuijken, K., Tremaine, S.: 1992, in *Dynamics of Disk Galaxies*, B. Sundelius (ed.), Göteborg Univ. Press, Göteborg, 71.
van Albada, T. S., Kotanyi, C. G., Schwarzschild, M.: 1982, *Monthly Notices Roy. Astron. Soc.*, 198, 303.

NEAR INFRARED STAR COUNTS AS A PROBE OF ASYMMETRIES IN THE GALAXY'S DISK

JAMES E. RHOADS
Princeton University Observatory, Princeton NJ 08544, USA.
email: rhoads@astro.princeton.edu

I have recently started an observing program to study the distribution of dynamically old giant stars in the disk, looking for *(i)* large amplitude spiral arms and *(ii)* small amplitude corrugations.

(*i*) Theoretical studies of spiral density waves usually assume that the mass density contrast is weak and the waves linear. Recent observations in red and near-IR light (e.g., Elmegreen and Elmegreen 1984; Rix and Zaritsky 1994), coupled with stellar population models, suggest otherwise. In the Galaxy, we can compare observations of diffuse NIR light and of individual stars, eliminating the need for population modeling. Moreover, we can estimate distances to stars to learn about 3D structure.

(*ii*) Recent work by Malhotra (1994a; 1994b) has shown that the midplane of the molecular and atomic gas differs from the nominal (Galactic latitude $b = 0°$) plane by up to 50 pc in the inner Galaxy. Various observations (Djorgovski & Sosin 1989, Freudenreich et al 1994, Carney & Seitzer 1993) show that the stellar distribution also deviates from $b = 0$. We will choose fields to test the possibility that the stars behave like the gas. This constrains theories of the corrugations; e.g., if old stars participate then magnetic fields aren't the cause.

We use the 3.5m telescope at Apache Point Observatory in NIR and optical bands. We use giant stars as tracers; they are common, can be seen to distances $\sim$ 17 kpc, and have a fairly narrow luminosity function (FWHM $\sim$ 2 mag, cf. table 2 of Wainscoat et al 1992) so are somewhat useable as standard candles. At fixed apparent magnitude, giant stars are further away than cool dwarfs. They will therefore suffer more reddening and will lie in a different region of the CMD (cf. figure 1).

Further details on the methods can be found in Rhoads 1995.

L. Blitz and P. Teuben (eds.), Unsolved Problems of the Milky Way, 59–60.
© 1996 *International Astronomical Union.*

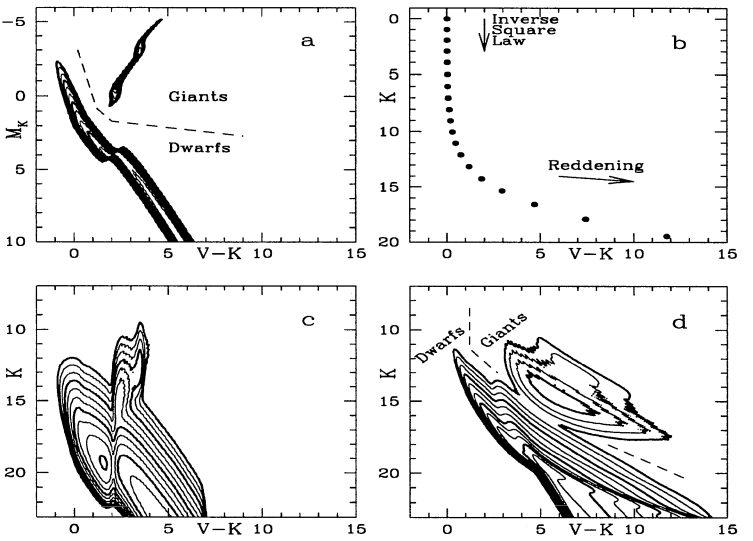

Figure 1. Model stellar densities in K, $(V-K)$ color-magnitude diagrams illustrate our sample selection procedure. Contours are logarithmically spaced by factors of $10^{1/3}$; every third contour is emphasized. (a) Contours are for unreddened stars at $d = 10$ pc. (b) The reddening vector for $A(V) = 0.5$ mag is shown. The solid circles mark the location of an A0V star at distance moduli $0, 1, 2, \ldots$, assuming extinction $A_V = 0.33$ mag/ kpc. (c) CMD for $l = 60°$, $b = 0°$ assuming no extinction. The lowest contour level is 1 star/ $\left[(2')^2(K\,\mathrm{mag})(V-K\,\mathrm{mag})\right]$. (d) As (c), but assuming $A_V = 0.33$ mag/ kpc.

Acknowledgements

I thank my advisor David Spergel and the Princeton area observing community for discussion and advice. Also, I thank Richard Wainscoat for his model of the IR sky. Financial support for this work is provided by NSF grant AST91-17388 and by NASA grant NAG5-2693.

References

Carney, B. W. & Seitzer, P. 1993. *AJ* 105, 2127.
Djorgovski & Sosin 1989. *ApJ Lett* 341, L13.
Elmegreen, D. M. & Elmegreen, B. G. 1984. *ApJS* 54, 127.
Freudenreich et al 1994. *ApJ Lett* 429, L69.
Malhotra, S. 1994a. *ApJ* 433, 687.
Malhotra, S. 1994b. *ApJ*, submitted.
Rhoads, J. E. 1995. In the proceedings of the *"Formation of the Milky Way" workshop*, E. Alfaro, ed., Cambridge University Press.
Rix, H.-W. & Zaritsky, D. 1994. *ApJ*, submitted.
Wainscoat, R. J. et al 1992. *ApJS* 83, 111.

Chapter 2

Is the Milky Way a Barred Spiral Galaxy?

MORPHOLOGY OF THE GALACTIC BULGE FROM COBE DIRBE OBSERVATIONS

E. DWEK
Code 685, NASA/Goddard Space Flight Center, Greenbelt, MD 20771

1. Introduction

The Diffuse Infrared Background Experiment (DIRBE) on-board the Cosmic Background Explorer (*COBE*) satellite has provided striking new images of the Galactic bulge at effective wavelengths of 1.25, 2.2, 3.5, and 4.9μ (Hauser 1993, plate 3; Arendt et al. 1994; Weiland et al. 1994). The bulge, defined here as the spheroid within the $|l| < 20°$ and $|b| < 10°$ region around the Galactic center, and its stellar content have been subjects of considerable interest since they contain important clues about the dynamical and star-formation history of our Galaxy. The morphology of the Galactic bulge is much harder to ascertain than that of bulges in many external galaxies, because of our location in the Galactic plane amid the obscuration by interstellar dust. In spite of this difficulty, there has recently been an accumulating body of evidence that the stellar distribution in the bulge is bar shaped, i.e. that the bulge is not rotationally symmetric in the plane of the disk (see Blitz 1993 for a review of the subject). The existence of a bar in our Galaxy would have important implications for the dynamics of the Galaxy. A bar would provide a mechanism for sweeping gas from the disk into the Galactic center "feeding" a central black hole (e.g. Shlosman, Frank, & Begelman 1989). It would also provide a mechanism for generating spiral arms, and a basis for estimating the mass of the halo relative to that of the disk (e.g. Combes & Sanders 1981 and references therein).

The evidence for a bar at the Galactic center is drawn from: (1) stellar and gas dynamics in the Galactic center region (Liszt & Burton 1980; Bahcall, Schmidt, & Soneira 1982; Vietri 1986; Binney et al. 1991; de Zeeuw 1992; Binney & Gerhard 1993); (2) asymmetries in the photometric image of the bulge (Blitz & Spergel 1991, based on the 2.4μ image obtained by

L. Blitz and P. Teuben (eds.), Unsolved Problems of the Milky Way, 61–69.
© 1996 *International Astronomical Union.*

Matsumoto et al. 1982; and Weiland et al. 1994, from DIRBE images at 1.25, 2.2, 3.5, and 4.9μ); (3) the analysis of stellar tracers of the large-scale Galactic structure (Habing et al. 1985; Rowan-Robinson & Chester 1987; Blanco 1988; Nakada et al. 1991; Whitelock & Catchpole 1992; Weinberg 1992a,b); (4) the excess of gravitational microlensing events in the direction of the Galactic bulge over earlier theoretical expectations (Paczynski et al. 1994); (5) the presence of a hotspot off-center from the Galactic center in the 1.8 MeV COMPTEL sky map (Chen, Gehrels, & Diehl 1994); and (6) the asymmetric distribution of bulge red clump stars detected by the OGLE (Stanek et al. 1994). However, the exact morphology of the bar, its orientation with respect to the disk are still issues that need to be resolved.

2. DIRBE Observations

The DIRBE images of the Galactic center region provide a new, and much improved data base, in terms of spatial and simultaneous wavelength coverage, and in sensitivity, for studying the bulge. After the subtraction of radiation scattered and emitted by interplanetary dust and emission from the galactic disk, and including a correction for interstellar extinction, the DIRBE data show a longitudinal asymmetry in the intensity maps of the bulge, and a flattening of the light distribution in the north and south polar regions of the bulge, giving it a "boxy" appearance (see Weiland et al. 1994 for a detailed description of the unveiling of the bulge morphology).

The 1.25, 2.2, 3.5, and 4.9μ data used in this investigation are a specially processed subset of the DIRBE data consisting of DIRBE weekly-averaged maps, selected at 2 week intervals over a 6 month period to achieve complete sky coverage. (Weiland et al. 1994). The calibration applied is preliminary, and the same as that used in the publicly-released DIRBE Galactic Plane Maps. To prepare the data for comparison with bulge models, we: (1) subtracted a simple empirical model describing the intensity of the interplanetary dust emission and scattering component; (2) created extinction corrected maps for $|l| > 3°$ at 1.25, 2.2, and 3.5μ, and for $|l| > 2°$ at 4.9μ; and removed the emission of the Galactic disk. Details of these procedures, and a discussion on the related uncertainties can be found in Dwek et al. (1994).

3. Bar Models and Their Characteristics

3.1. MATHEMATICAL CHARACTERIZATION OF THE BULGE

The calculated intensity of light from the bulge region in a given direction is given by an integral of the volume emissivity of the sources along the line of sight. We assumed that the volume emissivity can be described by

an analytical function subjected to three consecutive rotations: the first, a counterclockwise rotation by an angle α around the z-axis, giving rise to a longitudinal asymmetry in the projected intensity; the second, a clockwise rotation by an angle β around the new y-axis, tilting the source distribution out of the Galactic plane and giving rise to both longitudinal and latitudinal asymmetries in the projected intesity; and the third, a roll, defined here as a counterclockwise rotation of the bar by angle γ around the new x-axis. Such a rotation is degenerate for prolate spheroids, but will change the projected intensities for triaxial systems.

3.2. AN OBLATE SPHEROID MODEL

Before resorting to triaxial models, we examined to what extent the bulge can be approximated by an axisymmetric distribution of sources such as an oblate spheroid. Such a simple model will provide a first order estimate of the minor-to-major axis ratio of the system. The latter quantity is of great interest, since it contains clues to the dynamical history of the formation of the bulge (Statler 1987; Combes & Sanders 1981; Combes et al. 1990; Raha et al. 1991; Sellwood 1993). We therefore adopted an axisymmetric Gaussian-type function to describe the source density distribution in the bulge, and calculated the apparent intensity of this density distribution as seen by an observer located at a distance D from the Galactic center. The results showed that in spite of the relatively good agreement between this model and the data, it fails to account for the observed longitudinal asymmetry of the bulge. The asymmetry is apparent in the DIRBE data (Weiland et al. 1994; Figure 3a in Dwek et al. 1994), which shows the systematic deviations of the data from the longitudinal symmetric model at positive Galactic longitudes. This led us to examine various triaxial models for the bulge.

3.3. TRIAXIAL BULGE MODELS

We have selected from the literature several functional forms, previously chosen to fit the observed surface brightness profile of the Galactic bulge or bulges in external galaxies, to characterize the source distribution of the Galactic bulge. Some functions have been used to describe an axisymmetric source distribution, and their radial coordinate was modified to allow for a triaxial bulge morphology. The various functions considered for the density distribution of bulge sources fall into three categories which characterize their general behavior: Gaussian-type functions (G), exponential-type functions (E), and power-law type functions (P). For a list of the various functional forms and their equations see Dwek et al. (1994).

In these functional forms, the bulge is characterized by its axes x0, y0,

and z0; by its normalization constant $\rho 0$; and by its orientation, which is characterized by three rotation angles described before: the in-plane rotation, out-of-plane tilt, and out-of-plane roll. We determined the best fitting model by a search for the minimum reduced chi-square in the multi-dimensional space spanned by these parameters. The results of the modeling efforts are discussed below.

4. The Resulting Bulge Morphology

4.1. GENERAL RESULTS

Table 1 in Dwek et al. (1994) presents the parameters and their 1σ statistical uncertainties of the best fitting models for the 2.2μ intensity with no roll, for the various triaxial functional forms discussed above (see also Figure 1). Not surprisingly, considering the flattened appearance of the bulge, the best fitting models have intrinsically a "boxy" geometry which flattens the shape of the bulge both in the z direction and in the Galactic plane. Models which have "exponential" radial density distributions generally fit as well as the Gaussian functions, with the exception of model E1 used by Blitz & Spergel (1991) which was somewhat worse. The "power law" functions generally fit relatively poorly, since they have difficulty in fitting the outer portions of the bulge.

4.2. BULGE AXIS RATIOS

The scale lengths and densities have different meanings for the different functional forms and therefore cannot be directly compared to each other. However, a quantity that can be compared between the different functional forms is the ratio of various axes. The results show that regardless of the functional form and the wavelength of the observations, $x0/y0 = 3\pm1$, $z0/y0 = 0.7\pm0.3$, $z0/\mathrm{sqrt}(x0^2 + y0^2) = 0.74\pm0.4$. The latter ratio is somewhat larger than that derived for an axisymmetric bulge model or from the observed drop-off in the projected intensities along the x and z axes of the bulge (Weiland et al. 1994). The average axis ratios derived here translate to axial ratios of $\{x0: y0: z0\} = \{1: 0.33\pm0.11: 0.23\pm0.8\}$. Another quantity of interest is the bulge triaxiality, defined here as the ratio $T = [1 - (y0/x0)^2]/[1 - (z0/x0)^2]$. Note that T is equal to 0 and 1 for oblate and prolate spheroids, respectively. The triaxiality of the bulge is in the range: $T = 0.81 - 0.94$, close to that of a prolate spheroid.

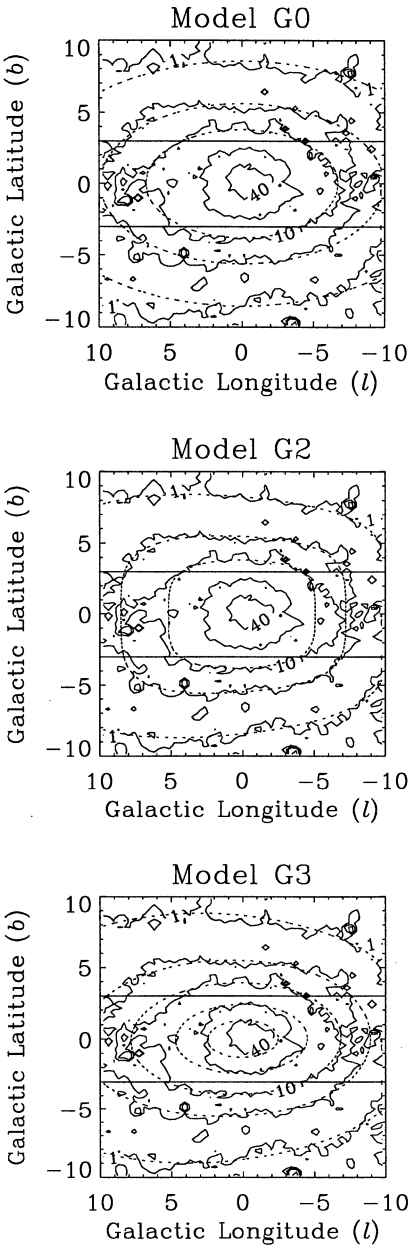

Figure 1. Comparison of the DIRBE observations (solid contours) with the projected 2.2μ intensity of selected models (dotted contours).

4.3. BULGE ORIENTATION

The rotation and tilt angles are defined in the same way for each model, and also allow for a direct comparison between the various models. The best fitting models G2 and E3 give values of $\alpha = 74$ and $50°$, respectively. The rotation angles of all models lie in the range $\alpha = 50 - 90°$, with an average of $\alpha = 65°$ if the power law functions are excluded, and with a $\pm 15°$ uncertainty reflecting the variance of the different models. Binney et al. (1991) have argued from studies of the kinematics of the H I, CO and CS gas in the central region of the Galaxy that the flow of the gas is dominated by a bar which should have a viewing angle of $16 \pm 2°$. Weinberg (1992a), on the other hand, suggested a viewing angle of $36 \pm 10°$ for the bar. These "viewing" angles correspond to values of $\alpha = 74 \pm 2°$ and $\alpha = 54 \pm 10°$, respectively, in our notation (see Figure 2 in Dwek 1994). The Binney et al. kinematic model therefore favors the Gaussian-type function G2 which has $\alpha = 70.7 \pm 4.4°$, over the functional form E3 that was used by Kent et al. which gives $\alpha = 49.8 \pm 9.4°$. Weinberg's model, however, favors the modified Bahcall & Soneira function, G3, which has a value of $\alpha = 59.0 \pm 9.5°$.

From an observed tilt in the streamlines of the H I and CO gas located within 2 kpc of the Galactic center, Liszt & Burton (1980) argued that the bulge should be tilted out of the Galactic plane as well. The data allow for an out-of-plane tilt of the bulge; however, at 2.2μ the tilt angles of the various models are small, typically less than $0.6°$, and are never larger than 3σ from zero. Results from 3.5 and 4.9μ suggest that the tilt may be increasing with wavelength; however, the tilt angle is always less than $2°$. Such small tilt angles could be caused by a non-uniform distribution of foreground stars. Our conclusion is therefore consistent with that reached by Weiland et al. (1994), who found no evidence for a tilt in the data. Blitz & Spergel argued from the Matsumoto et al. data that the bar should be tilted by as much as $7°$. Tilting any of the models by that amount will produce a longitudinal difference map that is inconsistent with the DIRBE data. The difference between our result and that of Blitz & Spergel can probably be attributed to the improved data used in the current modeling effort, especially the improved correction for interstellar extinction.

4.4. THE EFFECT OF A ROLL

We have examined the effect of a roll, initially surpressing any tilt of the bulge, on two select functional forms, E1 and G2 in the notation of Dwek et al. (1994), and found that the roll had a minor effect on the quality of the fit of the function G2, and actually worsened the fit to the data. The effect of the roll was most dramatic for the function E1. By rolling the function by $\approx 45°$ the projected intensity attained an almost "boxy"

character, distinctly different from its otherwise elongated appearance. The effect of the roll on E1 is peculiar to that function because of its definition of the radial coordinate. Similar results for these models were obtained for cases in which all three angles were allowed to vary simultaneously. Again, the 45° roll preferred by model E1 represents the peculiar definition of its radial coordinate, rather than an intrinsic roll of the Galactic bulge.

5. Conclusions and Comparison to Previous Work

We have modeled the Galactic bulge morphology and derived its luminosity and mass using the DIRBE observations of its projected surface brightness in the $|l| < 10°$, and $|b| > 3°$ region at 2.2μ, and in the $|l| < 10°$, and $|b| > 2°$ region at 3.5, and 4.9μ. The main results of the paper, and their relation to previous investigations can be briefly summarized as follows:

1) The bulge is a bar with its closest edge in the first Galactic quadrant. Even though an axisymmetric oblate spheroid provides a reasonable fit to the observed intensity, it fails to reproduce the longitudinal asymmetry observed in the DIRBE data (Weiland et al. 1994). This reconfirms the results of Weiland et al. and previous photometric studies of the bulge (Blitz & Spergel 1991), as well as studies of stellar populations and stellar and gas kinematics in the Galactic center region.

2) Triaxial models provide an improved fit to the data, and produce a longitudinal asymmetry in the projected intensity maps. Of the list of triaxial models studied (see Dwek et al. 1994) the Gaussian-type models (G1-G3), and the triaxial version of the modified spheroid used by Kent, Dame, & Fazio (1991), model E3, provided the best fits to the data.

3) Triaxial models produced axis ratios of $\{x0{:}y0{:}z0\} = \{1{:}\ 0.33{\pm}0.11{:}\ 0.23{\pm}0.08\}$. Thus the bulge resembles a prolate spheroid with a triaxiality between 0.81 and 0.94. For comparison, Vietri (1986) derived axis ratios of $\{1{:}0.7{:}0.4\}$ from dynamical constraints on model G3.

4) Comparison of the results of model E2 with the fit of Whitelock & Catchpole to the population of bulge Mira variables suggests that the IRAS selected Mira distribution is significantly flatter than the population of bulge K and M giants. This morphological discrepancy is puzzling considering the widely held view that M stars evolve into Miras. However, the difference in the morphology of these two populations probably arises from the fact that the IRAS Miras used in their analysis form an incomplete sample of all Miras with respect to their periods and spatial distribution.

5) The in-plane rotation angle α (see Figure 2 in Dwek et al. 1994) is between 50 - 80°, the range of values reflecting the variance between the different models. This corresponds to a range of viewing angles (the angle between the solar radius and the bar's major axis) between 10 - 30°.

This range is consistent with the value of $16 \pm 2°$ suggested by Binney et al. (1991), and the value of $36 \pm 10°$ suggested by Weinberg (1992a). The models most consistent with Binney et al. are G1 and G2, whereas Weinberg's results favor models G3 and E3. The bar could intrinsically be peanut-shaped but appears boxy because of the nearly end-on viewing angle (Combes & Sanders 1981).

6) The models are consistent with a slight tilt in the bar by an angle of about $0.6°$ at 2.2μ and by an angle of about $2°$ at 3.5 and 4.9μ. However, these tilts are statistically insignificant, and can be accounted for by a non-uniform distribution of foreground stars.

7) A roll can affect the projected intensity of a given functional form. The effect of a roll was most noticeable for model E1, giving an intensity that was initially flattened along the galactic plane a "boxy" appearance.

Acknowledgements

The National Aeronautics and Space Administration / Goddard Space Flight Center (NASA/GSFC) is responsible for the design, development, and operation of the Cosmic Background Explorer (*COBE*), under the scientific guidance of the COBE Science Working Group.

References

Arendt, R. G., et al. 1994, ApJ, 425, L85
Bahcall, J. N., Schmidt, M., & Soneira, R. 1982, ApJLett, 258, L23
Binney, J. J., & Gerhard, O. 1993, in Back to the Galaxy, eds. SS. Holt & F. Verter, (New York: American Institute of Physics), p. 87
Binney, J. J., Gerhard, O. E., Stark, A. A., Bally, J., & Uchida, K. I. 1991, MNRAS, 252, 210
Blanco, V. 1988, AJ, 95, 1400
Blitz, L. & Spergel, D. N. 1991, ApJ, 379, 631
Blitz, L. 1993, in Back to the Galaxy, eds. SS. Holt & F. Verter, (New York: American Institute of Physics), p. 98
Chen, W., Gehrels, N., & Diehl, R. 1994, ApJ, submitted
Combes, F., & Sanders, R. H., 1981, 96, 164
Combes, F., Debbasch, F., Friedli, D., & Pfenniger, D. 1990, A&A, 233, 82
de Zeeuw, T. 1992, in The Stellar Populations of Galaxies, ed. B. Barbuy & A. Renzini (Dordrecht, Kluwer), 51
Dwek, E. et al. 1994, accepted for publication in the ApJ
Habing, H. J., Olnon, F. M., Chester, T., Gillett, F., Rowan-Robinson, M., &
Neugebauer, G. 1985, A&A, 152, L1
Hauser, M. G. 1993, in Back to the Galaxy, eds. S. S. Holt & F. Verter, (New York: American Institute of Physics), p. 201
Kent, S. M., Dame, T. M. & Fazio, G. 1991, ApJ, 378, 131
Liszt, H. S., & Burton, W. B. 1980, ApJ, 236, 779
Matsumoto, T. et al. 1982, in The Galactic Center, ed. G. Riegler & R. Blandford (New York: American Institute of Physics), 48
Nakada, Y., Deguchi, S., Hashimoto, O., Izumiura, H., Onaka, T., Sekiguchi, K., & Yamamura,JI. 1991, Nature, 353, 140

Paczynski, B., Stanek, K. Z., Udalski, A., Szymanski, M., Kaluzny, J., & Kubiak, M., Mateo, M., & Krzeminski, W. 1994, ApJ, in press
Raha, N., Sellwood, J. A., James, R. A., & Kahn, F. D. 1991, Nature, 352, 411
Rowan-Robinson, M. & Chester, T. 1987, ApJ, 313, 413
Sellwood, J. A.1993, in Back to the Galaxy, eds. SS. Holt & F. Verter, (New York: American Institute of Physics), p. 133
Shlosman, I., Frank, J. & Begelman, M. C. 1989, Nature, 338, 45
Stanek, K. Z., Mateo, M., Udalski, A., Szymanski, M., Kaluzny, J., & Kubiak, M. 1994, ApJ, 429, L73
Statler, T. S. 1987, ApJ, 321, 113
Vietri, M. 1986, ApJ, 306, 48
Weiland, J. et al. 1994, ApJ, 425, L81
Weinberg, M. D. 1992a, ApJ, 384, 81
Weinberg, M. D. 1992b, ApJLett, 392, L67
Whitelock, P. & Catchpole, R. 1992, in The Center, Bulge, and Disk of the Milky Way, ed. L. Blitz (Dordrecht : Kluwer), p. 103

IS THERE A BULGE DISTINCT FROM THE BAR?

KONRAD KUIJKEN
Kapteyn Instituut
P.O. Box 800, 9700 AV, Groningen, Netherlands
and
Harvard-Smithsonian Center for Astrophysics
60 Garden Street, Cambridge MA 02138, USA

1. Introduction

It seems by now well-established that in the central kpc the Galaxy is not axisymmetric (Gerhard 1995, Dwek 1995). The kinematics of many different tracers, as well as the distribution of sources on the sky, all point to an elongated distribution of matter and of the potential, with the long axis of the distortion pointing somewhere in the first Galactic quadrant. It is therefore tempting to reconsider our data concerning this part of the Galaxy in terms of 'the' Bar. But to what extent should we (or is it useful to) distinguish between the bar and the stellar bulge of old?

There are two philosophies that one can adopt. The first is that of the classifier, who divides the Galaxy into as many simple components as seem warranted by the data. This approach is often guided by a preconceived notion of what the components look like: for instance, one might decide a Galaxy contains an outer ring because its disk is not exponential, or a bulge might require a second nuclear component because its profile does not follow the $r^{1/4}$ law, etc. This description of the system in terms of basic building blocks is very useful, but it is often not clear in how far one should think of the blocks as different *physical* entities with their own colours, ages, metallicity, etc., especially since they often overlap considerably in several coordinates (position, velocity, metallicity, age...) A possible second approach is more agnostic: to try to describe the different parts of the Galaxy as they are observed, without necessarily splitting the system into a superposition of components that are familiar or mathematically convenient. From this point of view, one would only talk of different com-

L. Blitz and P. Teuben (eds.), Unsolved Problems of the Milky Way, 71–77.
© 1996 *International Astronomical Union.*

ponents if their properties were clearly disjoint in one or more observable coordinates.

Clearly the approach to the topic of this review will depend greatly on one's philosophy.

2. Terminology

Before we can address the issue of whether there are various components in the central kpc, we need to discuss terminology.

2.1. WHAT IS A BAR?

The prerequisite for labelling an object a bar is that it be elongated instead of axisymmetric. Bars were also often said to be as flat as disks. The usual argument is that some 30% of face-on galaxies are clearly barred, but 30% of edge-on galaxies do not show an anomalous thickening (Kormendy 1982). However, recent numerical simulations (see section 3 below) have shown that bars are in fact very unlikely to remain thin for very long. Bars are thought to be pattern-rotating, and are kinematically quite hot.

2.2. WHAT IS A BULGE?

By a bulge is usually meant a central thickening of a disk (when seen edge-on) or a central brightening of a disk above the exponential Freeman law. Bulges may or may not be related to the metal-poor stellar halo that is seen in the Milky Way. Kinematically, bulges are about as hot as the immediately surrounding disk, and they are often well-described as oblate axisymmetric rotators (Kormendy & Illingworth 1982). The stellar populations are generally old.

2.3. DISTINCT IN WHAT SENSE?

What criteria can we use to decide whether there truly are two distinct components (as opposed to there being a convenient mathematical two-component description of the distribution of stars in some coordinates)?

Many physical criteria are possible, and a reasonable fraction of them would have to argue in favour of a separation before it is profitable to distinguish two components.

The following might be reasons in favour of separate components:

- *Formation Mechanism* With a good understanding of galaxy formation, we might be able to show that bars and bulges are formed by different mechanisms. In that case, it would clearly be important to

be able to decide on a star by star basis which component to assign objects to.

- *Stellar Populations* It might be the case that the stellar population nicely splits up into two components. If one of these is characterized as being non-axisymmetric, whereas the other one bulges out above the disk, this would be evidence for two components.
- *Shape* The spatial structure of a galaxy might naturally split into two very different components. This is a dangerous criterion to use, though, since the rotating potential in a barred galaxy can dictate abrupt changes in orbit shapes near resonance radii. For example, the perpendicular 'inner bar' seen in many face-on SB0 galaxies can be caused by an inner Lindblad resonance (accross which the orientation of the orbits changes by 90°), and does not imply separate origin or nature of the stars there.
- *Kinematics* Finally, the velocity distribution might naturally split into two components. However, once again it is important to note that the resonances due to the bar potential may also cause abrupt changes in star and gas kinematics.

Unfortunately, none of the above form very clear-cut practical criteria.

3. The buckling instability of bars

It has long been supposed that bars form as a result of an instability in differentially rotating disks (e.g., Sellwood 1981) whereas bulges are a primordial galactic component. In such a scenario, it certainly makes sense to search for ways of separating the two components, in terms of age, chemistry or kinematics. However, it has become clear in the last few years that the picture is not that simple: N-body bars appear to be generically susceptible to a buckling instability which thickens them considerably, and makes them look quite a lot like the box- or peanut-shaped bulges seen in some 30% of edge-on galaxies (Combes & Sanders 1981, Combes et al. 1990, Raha et al. 1991). The picture that bars are flat, non-axisymmetric photometric components whereas bulges are vertically extended does not fit in with this theory: so, if the N-body results hold, they imply that a physical bar component must be taken to be vertically extended too.

The fact that the Galaxy has both a boxy bulge and a bar argues for this theory. A numerical simulation of a bar-unstable Milky-Way like model in fact produces a structure which resembles the COBE bulge maps quite well (Sellwood 1993). There are also a few external galaxies known which exhibit both a bar and a boxy bulge: NGC 4442 (Bettoni & Galletta 1994), which is seen at such an orientation that the bar and the box shape are both visible photometrically, and NGC 5965 and NGC 5746 (Kuijken & Merrifield

1994), both edge-on S0 galaxies with boxy bulges whose kinematics provide clear evidence for a barred potential. We are currently developing further the kinematic signature of a bar in edge-on systems, with a view to investigating the link between box-shaped bulges and bars in a larger sample of edge-on galaxies. Without a kinematic test it is difficult to demonstrate the association of the two phenomena, since they are best observed from very different orientations: without kinematic information, detecting or disproving the existence of a bar in an edge-on boxy-bulge galaxy is about as hard as deciding whether a face-on barred galaxy has a boxy bulge!

It is clear that the buckling instability thoroughly complicates the issue of whether there are separate bulge and bar components, since it implies that bars have significant vertical extent. How then can we usefully distinguish between a lone bar and one with a 'separate' bulge?

3.1. RECURRING BAR INSTABILITY

One possible scenario which might lead to distinct components is a recurring bar instability (Hasan, Pfenniger & Norman 1993). If a disk forms a central bar, then one of the effects is to drive any gas towards the center. Eventually, this gas may form a sufficiently concentrated mass that the orbit structure of the bar is drastically altered: the main orbit family that supports the bar breaks up, as a result of which the bar dissolves. The result of such an episode will then be a fairly axisymmetric thick 'bulge', hotter than the original disk. If the disk now acquires more cold gas, the bar instability may restart, eventually leading to a new buckling bar, and hence a second high-latitude population. Then the term 'bulge' might refer to the material that was formed before the last buckling, and 'bar' to the disk material that formed later and is presently undergoing the bar instability. The bar would then have to be younger than the bulge.

4. The Milky Way: Two components or not?

We now turn to a discussion of the available evidence for the Milky Way.

4.1. STELLAR POPULATIONS

The bar material after the instability will be found at high latitudes, contaminating any pre-existing 'bulge' material, and unless the stellar populations are very different the result will be a broader spread in age and/or metallicity, not a clear two-component distribution. The data of Tyson & Rich(1993) show that there is indeed a vertical metallicity gradient on the Galactic minor axis, but it only sets in above a height of 1.5kpc. Above this height the metal-poor stars found at larger radii become quickly dominent.

Moreover, the distribution of metallicities is well fit by a closed box model. This result therefore argues for a chemically uniform, isolated formation of the bulge material, though a more inhomogeneous evolution followed by mixing (e.g. by a bar instability) may also explain the data.

There is evidence for non-uniformity as well. The late-M giants are very tightly concentrated to the Galactic plane, and to the bulge region (Blanco 1988). This implies that there is at least one thin component in the center of the Galaxy: it therefore has not undergone the buckling instability (yet). Is this evidence for a later burst of star formation? Unfortunately, the kinematics and space distribution of these stars are not sufficiently well-known to be able to decide if they lie in a bar or not. Since the M-giant luminosity function is a sensitive function of metallicity, it is possible that a moderate metallicity gradient is responsible for this strong observational effect. Nevertheless, it is expected that if the bar buckles, it thickens all populations, so it remains to be seen if the metallicity gradient implied by the M giant observations is not too strong.

In external galaxies, it is observed that faint and bright bulges have systematically different colour gradients (Balcells & Peletier 1994). This suggests that the disk exerts some influence in the fainter bulge galaxies, whereas the brighter ones form a more orderly sequence which may indicate a uniform formation scenario. At its most extreme, the disk 'influence' on the fainter bulges may be that the bulge actually forms out of the disk via the bar and buckling instabilities.

4.2. MORPHOLOGY

From our vantage point, it is hard to make a convincing case for two superimposed components of different shape in the bulge region. It is clear, though, from perspective effects in near-IR maps, that the distribution of stars above the disk is not axisymmetric, but rather barred (Blitz & Spergel 1991, Weiland et al. 1994). Of course, a box-shaped bar/bulge superimposed on a primoridal rounder bulge will simply look like a slightly less boxy bulge, unless the radial scale lengths are very different. Only star counts can be used as a way of probing the three-dimensional distribution of stars at all, and the accuracy presently obtainable is barely up to the task. Perhaps the most thorough analysis was made by Weinberg (1992), who analysed IRAS points sources near the Galactic plane: he clearly detects a bar-like distortion, with a central concentration that is probably rounder. It is not clear whether this morphology is usefully described as a two-component structure, though.

Many, but not all, external SB0 galaxies show a perpendicular 'inner bulge', aligned orthogonal to the bar: while these may be consequences

of the effects of stellar-dynamical resonances, detailed study of this phenomenon is lacking.

4.3. KINEMATICS

We would naively expect that a barred population would have a larger velocity dispersion along the bar than perpendicular to it. Therefore, the distributions of radial velocity and of proper motion in longitude in a bar would be expected to be different. A bar seen at 45° will have identical dispersions in both directions, whereas a more end-on bar (as appears to be favoured by the star count and by the gas kinematics results) should have higher radial velocity dispersion than tangential. The data appear to favour a more or less isotropic velocity distribution, and in fact are well fit by an isotropic oblate axisymmetric rotator model (Kent 1992, Kuijken 1995): stellar dynamical evidence for a bar in the center of the Milky Way are at this point almost non-existent. Only the properties of a sample of stars in Baade's Window with measured three-dimensional velocities (Zhao et al. 1994; Rich 1995, this volume) indicate that the kinematics may not be axisymmetric.

The OH/IR stars in the bulge region exhibit quite a clear two-component kinematic structure (Lindqvist et al. 1992), though the sample is not as yet complete. Superimposed on a distribution of stars which broadly follows other kinematic tracers of the disk, in the central 100pc a fast-rotating group of stars is seen. It has quite a high velocity dispersion too. Some if not most of this may be due to projection of the closed orbits in the barred potential: comparison with the CO emission over the same region shows that the closed orbits (as identified by Binney et al. 1991) project to velocity widths of 200–300km/s. Thus these stars may in reality constitute a very cold component, associated with the molecular gas.

4.4. CONCLUSION: IS THERE A BULGE AS WELL AS A BAR?

Few of the data for the Milky Way indicate a strong need for a two-component description. All signatures of triaxiality agree on the quadrant in which the long axis lies, plausibly establishing the reality of the bar. The starlight above the disk is elongated in the same direction as the gas orbits close to the plane. There is therefore no need for a two-component description in terms of a more-or-less axisymmetric bulge with a superimposed bar. However, there remains the puzzle of how to fit the (presumably more metal-rich) late-M giants into the picture: these stars are confined close to the plane, and therefore somehow avoided the buckling instability of the bar which presumably caused the boxy shape of the bulge.

References

Balcells, M., & Peletier, R., 1994, preprint
Bettoni, D. & Galletta, G. 1994, A&A, 281, 1
Binney, J., Gerhard, O.E., Stark, A.A., Bally, J. & Uchida, K.I. 1991, MNRAS, 252, 210
Blanco, V.M., 1988, AJ, 95, 1400
Blitz, L. & Spergel, D.N., 1991, ApJ, 379, 631
Combes, F., Debbasch, F., Friedli, D. & Pfenniger, D. 1990, A&A, 233, 82
Combes, F. & Sanders, R.H. 1981, A&A, 96, 164
Dwek, E., 1995. This volume
Gerhard, O.E., 1995. This volume
Hasan, H., Pfenniger, D. & Norman, C., 1993, ApJ, 409, 91
Kent, S.M., 1992, ApJ, 387
Kormendy, J. & Illingworth, G. 1982, ApJ, 256, 460
Kormendy, J., 1982 in Morphology and Dynamics of Galaxies, ed. L. Martinet & M. Mayor, (Geneva Observatory), 237
Kuijken, K., 1995, preprint
Kujken, K. & Merrifield, M.R., 1994, ApJL, submitted
Lindqvist, M., Winnberg, A., Habing, H.J. & Matthews, H.E. 1992, A&AS, 92, 43.
Raha, N., Sellwood, J.A., James, R.A. & Kahn, F.D. 1991, Nature, 352, 411
Rich R.M., 1995, this volume
Sellwood, J., 1981, A&A 99, 362
Sellwood, J., 1993, in Galactic Bulges, IAU Symposium 154, eds. H. Dejonghe & H.J. Habing, 391
Tyson, N.D. & Rich, R.M., 1993, in Galactic Bulges, IAU Symposium 154, eds. H. Dejonghe & H.J. Habing, 333
Weiland, J.L., et al., 1994, ApJ 425, L81
Weinberg, M.D., 1992, ApJ, 384, 81
Zhao, Spergel, D.N. & Rich, R.M., 1994, preprint

DISCUSSION

M. Balcells: When comparing the kinematic predictions of the various Milky Way bulge models (bar, axisymmetric structure) you did not mention extinction. Shouldn't we always extinct our models before comparing to optical tracers? And, can we make extinction play in our favour to further discriminate among models? E.g., if the back side of the bar is dimmer than the near side, we may observe non-zero mean velocity at the bar center.

M. Weinberg: I am worried that the inference of a perpendicular bulge component based on the figure from my 1992 paper (ApJ 384, 81) may be an artefact of the 2 Jy cutoff. Although a 1Jy cutoff is certainly incomplete, it does not show such a pronounced perpendicular component.

DYNAMICS OF THE BAR AT THE GALACTIC CENTRE

ORTWIN E. GERHARD
Astronomisches Institut, Universität Basel
Venusstrasse 7, CH-4102 Binningen

1. Introduction

There is now substantial evidence for a rotating bar in the inner Galaxy. This is an important change in our perception of the Galaxy because it changes the ways in which we have to think about its evolutionary history.

The idea of a Galactic bar is not new; that motion on elliptic orbits in a barred potential might explain various aspects of the atomic and molecular gas observations near the Galactic Centre has been suggested a number of times (e.g., Peters 1975, Cohen & Few 1976, Liszt & Burton 1980, Gerhard & Vietri 1986, Mulder & Liem 1986, Sanders 1989).

What has changed in the past few years is (i) that the evidence now comes from several fronts, including the NIR light distribution as measured by COBE, IRAS source counts, atomic and molecular gas kinematics, the first indications for triaxiality in the stellar kinematics of the bulge, and perhaps the large optical depth to microlensing in the OGLE experiment; and (ii) that there is a dynamical model which provides a physical basis for explaining a number of independent features in the observed gas kinematics, is consistent to zeroth order with the other pieces of evidence for a bar that we now have, and promises to be extendable towards including these into one coherent picture.

In this review I give a brief summary of the current evidence for the bar in the inner Galaxy. Then I discuss in more detail the subject of gas flows in bars and in the Galactic Centre. The integrated NIR photometry is described in the paper by Dwek. Finally, several evolutionary processes are briefly discussed which become relevant for Galactic evolution because of the presence of the bar, such as gas infall, angular momentum transfer, subsequent central star formation, and the formation of peanut-bulge-like stellar systems from bars through a bending instability.

L. Blitz and P. Teuben (eds.), Unsolved Problems of the Milky Way, 79–91.
© 1996 *International Astronomical Union.*

2. Evidence for the Galactic Centre Bar

Near-infrared photometry, IRAS source counts, and modelling of the atomic and molecular gas in the inner Galaxy all point to the existence of a $\sim 3:1$ elongated bar at the Galactic Centre with major axis length $2-4\,\mathrm{kpc}$ and near side in the first quadrant of galactic longitude. Table 1 lists individual sources of evidence, references, length and axial ratios of the inferred bar, and the angle ϕ_{maj} between the near side of the bar major axis and the line Galactic Centre - Sun, such that positive ϕ_{maj} corresponds to position in the first quadrant. No information is listed when not constrained well or not known to this author. A short discussion of these observations follows.

The older balloon data (Matsumoto *et al.* 1982) and more clearly the COBE-DIRBE photometry (Weiland *et al.* 1994, Dwek *et al.* 1995) show that the Galactic bulge is both brighter and more extended in latitude at given positive longitude than at the same negative longitude, except for a region close to the Galactic Centre where the first effect is reversed. These signatures are just as expected for a triaxial bulge with its long axis in the first quadrant (Blitz & Spergel 1991), because then a line-of-sight at fixed positive l cuts the the bar major axis at smaller galactocentric distance than one with the same negative longitude. The length given for the COBE bar is inferred from where the longitude asymmetry ends; it is not apparent in the Dwek *et al.* model fits. The apparent shape of the COBE bulge was matched by an N-body simulation of a peanut bulge formed from a disk-bar-bending instability (Sellwood 1993; see Section 4 below); this resulted in the parameters given in the third row. The vertical extent of the N-body bar is uncertain because of limited grid resolution.

Source counts in the bulge region come mostly from the IRAS data which is not restricted to a small number of special fields where the extinction is low. However, the very large number of survey stars in the OGLE experiment has allowed constraints on the spatial distribution to be obtained from just a few of these fields (Stanek *et al.* 1994). In the source samples listed in Table 1, the evidence for the bar comes from a distribution that is asymmetric in longitude with respect to the Sun-Galactic Centre line in either its number surface density or flux distribution, or both, as expected for an intrinsically barred distribution of objects observed at finite distance from the Sun. To determine the bar parameters accurately from such a sample requires sophisticated modelling (Weinberg 1992), taking into account the sample selection function, and large spatially extended samples.

Modelling the gas kinematics has the advantage of also constraining the pattern speed of the bar, $\Omega_p \simeq 60\,\mathrm{km s^{-1}\,kpc^{-1}}$. These results are described in more detail in the next Section. The detailed comparison to observations depends on the choice of mass distribution for the bulge and bar (which is

Evidence	from	Refs.	ϕ_{maj}	a (kpc)	a:b:c
NIR	Balloon	1,2	positive	>1.8	
	COBE DIRBE	3,4	$20° \pm 10°$	2.2	$10:3\pm1:2\pm1$
	N-body vs. COBE	5	30°	2.3*	$10:3-4:2?$
Discrete	IRAS Mira variables	6	45°	~ 1.5	4 : 1 : 1
Sources	IRAS sample	7	positive		
	AGB stars	8	$36 \pm 10°$	~ 4	3 : 2 : ?
	Red clump stars	9	$< 45°$	>1	
	Disk Glob. clusters	10	25°	~ 3	3 : 1 : ?
Gas	Parallelogram, HI	11	16°	2.2*	
	HI-envelope	12	$\sim 30°$		
Kinematics	Bulge K-giants	13			
Microlensing	OGLE	14-16	$\lesssim 20$		$\gtrsim 3:1:?$

TABLE 1. Evidence for the bar in the inner galaxy. References are: 1. Matsumoto *et al.* 1982, 2. Blitz & Spergel 1991, 3. Weiland *et al.* 1994, 4. Dwek *et al.* 1995, 5. Sellwood 1993, 6. Whitelock & Catchpole 1992, 7. Nakada *et al.* 1991, 8. Weinberg 1992, 9. Stanek *et al.* 1994, 10. Blitz 1993, 11. Binney *et al.* 1991, 12. Weiner & Sellwood, these proceedings, 13. Zhao *et al.* 1994, 14. Paczynski *et al.* 1994a, 15. Evans 1994, 16. Zhao *et al.* 1995. *: Estimated as $0.9\times$ corotation radius.

different for the two analyses listed). The BGSBU-model of Binney, Gerhard, Stark, Bally & Uchida (1991) is based on modelling the molecular paralellogram, HI terminal curve, and galactic centre cloud orbits, and uses a barred bulge with density $\propto r^{-1.8}$. The model of Weiner & Sellwood is described elsewhere in these proceedings.

Indications for a barred bulge also come from the kinematics of bulge K-giant stars in Baade's window (Zhao, Spergel & Rich 1994), although the stellar sample is small and cannot be used to constrain the bar parameters quantitatively. The bar has been proposed as a key ingredient for explaining the high optical depth to gravitational lensing towards the bulge seen in the OGLE results (Paczynski *et al.* 1994a). In this case the bar must have its long axis near the Sun-Galactic Centre line. However, modelling results to-date are still controversial (Evans 1994, Zhao, Spergel & Rich 1995).

In summary, there now appears to be good evidence from several different sets of observations that our Galaxy contains an elongated ($\sim 3:1$) nuclear bar/bulge of length $2-4$ kpc, with its nearby long axis in the first longitude quadrant at $\phi_{maj} = 15-45°$. However, not all observations may measure the same physical bar population; e.g., the vertical scale-length of the Mira variables is significantly smaller than that of the COBE NIR emission. The bar parameters will undoubtedly be constrained much better when dynamical models based on the combined COBE NIR light distribu-

tion and HI and molecular gas dynamics have been constructed and have been used to predict source count results and microlensing probabilities.

Previously unknown central bars have recently been seen in a number of external galaxies with large-scale bars (*e.g.*, Wozniak *et al.* 1995, Shaw *et al.* 1995). The nuclear bar in the oval-disk galaxy M94 (Möllenhoff, Matthias & Gerhard 1995), e.g., has axis ratio in the galaxy plane $\sim 3:1$, ends at $\sim 1.2\,\mathrm{kpc}$ somewhat inside an inner star-forming gas ring, and is less centrally concentrated and more flattened to the plane than the co-spatial axisymmetric part of the bulge. This example shows that also the structure of the Galactic bulge/bar could be considerably more complicated than the simple one-component triaxial models used sofar.

3. Gas Flow in the Inner Galaxy

Observations of cold gas in the inner galactic disk show a clumpy, asymmetric distribution, with large non-circular velocities up to $\sim 200\,\mathrm{km\,s^{-1}}$. Only a small fraction ($\sim 10^7\,\mathrm{M_\odot}$) of the cold gas in the Galactic Center (GC) region is in the form of neutral HI, measured at 21 cm (Burton & Liszt 1978, 1983; Sinha 1979; Braunsfurth & Rohlfs 1981). The dominant component ($\sim 10^8\,\mathrm{M_\odot}$) is the cold molecular gas observed in mm-emission lines of molecules such as ^{12}CO, ^{13}CO, CS (Bania 1977, Sanders *et al.* 1984, Heiligman 1987, Dame *et al.* 1987, Bally *et al.* 1988). Despite the clumpiness and asymmetry of the gas distribution, the non-circular motions follow a coherent pattern whose gross properties can be described by assuming that the gas flows on tilted elliptical orbits (Peters 1975, Liszt & Burton 1980).

The *dynamical* understanding of such flow patterns comes from hydrodynamic simulations in gravitational fields. The key observation is that, if a quasi-equilibrium flow is established, it is generally a good approximation to think of such a flow in terms of the closed ballistic orbits in the underlying gravitational potential. This is independent of whether the simulations use sticky particles (Schwarz 1981, 1984; Habe & Ikeuchi 1985) or smooth fluids (Sanders & Huntley 1976; van Albada 1985; Mulder & Liem 1986; Athanassoula 1992). Physically, a cloud of gas released into a gravitational potential will shear and then settle onto closed orbits, because the energy in epicyclic motions is dissipated by collisions between fragment cloudlets. Subsequently, dissipation is reduced and the gas slowly drifts inwards along a sequence of closed orbits.

Only near resonances or where closed orbits intersect, do hydrodynamic forces significantly change this simple flow pattern. The location of the resonances in a barred potential is determined by the bar's pattern speed Ω_p and the circular velocity curve $v_c(R)$. These two parameters

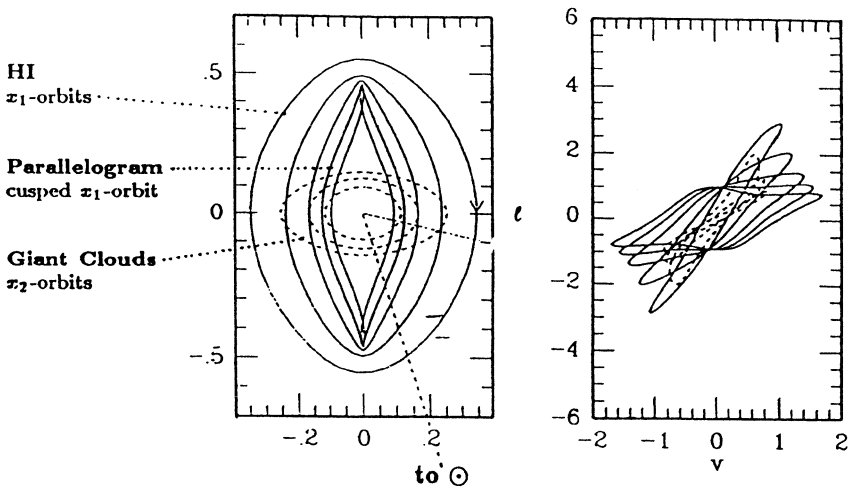

Figure 1. Closed orbits in a rotating barred potential and their projection into the (l, v)-diagram for an observer near the long axis of the bar. (From Gerhard 1992, after BGSBU).

are therefore of primary importance for shaping the gas flow in a barred galaxy. For example, if the density and circular velocity curve scale as $\rho \propto R^{-\alpha}$ and $v_c(R) \propto R^{1-\alpha/2}$, then the corotation radius is proportional to $R_{\rm CR} \propto \Omega_p^{-2/\alpha}$, and the ratios of the inner (ILR) and outer (OLR) Lindblad resonance radii to corotation is given by $R_{\rm ILR}/R_{\rm CR} = (1-\frac{1}{2}\sqrt{4-\alpha})^{2/\alpha}$ and $R_{\rm OLR}/R_{\rm CR} = (1+\frac{1}{2}\sqrt{4-\alpha})^{2/\alpha}$. Notice that these ratios are fairly sensitive to the parameter α.

Fig. 1 shows the sequence of prograde closed orbits inside corotation in a barred potential with circular velocity curve $v_c \propto R^{0.1}$, similar to that in the inner Galaxy. Gas inside corotation follows the main prograde 'x_1' family until these orbits becomes self-intersecting near the inner Lindblad resonance. When the inflowing gas reaches the highest-energy self-intersecting x_1-orbit (the 'cusped orbit' in Fig. 1), the hydrodynamic simulations show that a shock forms, which causes it to switch to the closed 'x_2' orbits deeper in the potential well. These are elongated along the potential's short axis.

The structure of such a shock near the ILR is shown in Fig. 2. The gas in this SPH-simulation is isothermal, and flows in a fixed rotating bar potential like that used by Athanassoula (1992). The velocity field outside the ILR region is clearly reminiscent of the closed orbit shapes in Fig. 1. Gas flowing inwards along the sequence of x_1-orbits eventually reaches the 'cusped' orbit. At pericentre on the 'cusped' orbit it crashes into gas at apocentre on the largest embedded x_2 orbit, producing a spray of material,

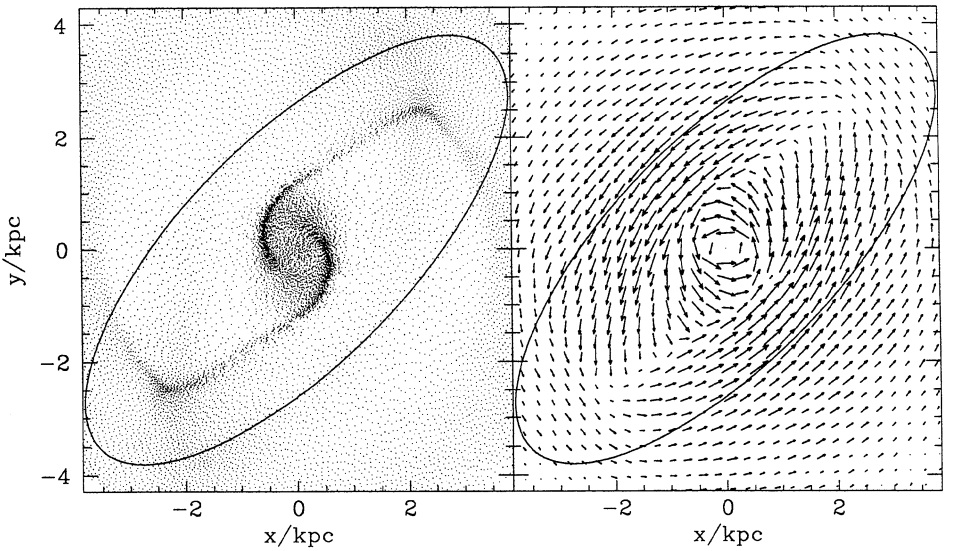

Figure 2. Morphology and velocity structure of gas flow in a rotating barred potential. Smooth Particle Hydrodynamic (SPH) simulation from Englmaier & Gerhard (in preparation).

which in turn causes a shock at the far side of the 'cusped' orbit. From there, material moves onto deeper-lying x_2 orbits, which are not affected by the shock. Across the shock in Fig. 2 the density jumps by a factor of $\simeq 5$, and the transverse velocity decreases by a similar factor. Van Albada (1985) and Athanassoula (1992) find similar velocity and density structures in their grid-based simulations. In fact, with enough resolution the results from the two different methods of solving the hydrodynamic equations are very similar.

BGSBU have argued that the key to interpreting the observations of cold gas in the inner Galaxy is the striking parallelogram in the (l, v) plane seen in surveys of ^{12}CO (Bania 1977) and ^{13}CO (Heiligman 1987, Bally *et al.* 1988). BGSBU argue that this structure, shown in Fig. 3, is formed in a 'cusped' orbit shock like that in Fig. 2. In their model, the outermost x_1 orbits parallel to the long axis of the bar are mostly occupied by HI clouds. These clouds gradually drift inwards, onto more elongated orbits. Eventually they reach the cusped orbit, encounter the shock, in which most of the gas condenses into molecular form, and then plunge onto the small central x_2-orbits.

The projection of the sequence of closed x_1 and x_2 orbits into the (l, v)-diagram for an observer near the long axis of a rotating bar is shown in

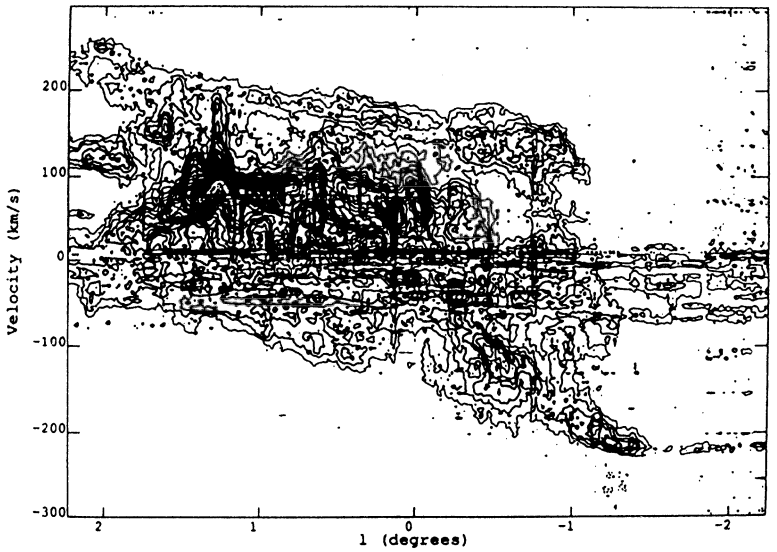

Figure 3. (l, v) digram of ^{12}CO $J = 1 \rightarrow 0$ averaged over $|b| < 0.1°$. The contours (spaced at intervals of 1 K) show a striking parallelogram. (From BGSBU.)

Fig. 1. Requiring that the (l, v) trace of the 'cusped' orbit resemble the observed parallelogram determines that observers near the Sun must view the GC bar at a narrowly constrained angle around $\phi_{\rm maj} = 16°$. By contrast, only a weak limit on the bar's axial ratio q can be obtained, as this does not influence the orbit shapes near the ILR much. With the same viewing angle, it is also possible to account for the rapid fall-off in the HI terminal velocity observed near $l = 2°$ and the subsequent slower decline out to $l = 12°$. For a given scale of the parallelogram and bulge mass profile, the HI data determine the pattern speed of the bar such that corotation is at $R_{\rm CR} \simeq 2.4 \pm 0.4\,$kpc. In the region $R \lesssim 1.2\,$kpc, where the HI terminal-velocity curve decreases outwards, the circular velocity is, in fact, rising. The inferred potential in the bulge region is given in Gerhard & Binney (1993).

The strong points of the BGSBU model are that it can fit the (l, v) distribution and the associated large non-circular motions of the molecular parallelogram and the HI terminal curve. The locations of the giant molecular clouds at the GC, such as Sgr B and Sgr C, in the (l, v)-diagram are successfully predicted by the x_2-orbits in the model (Fig. 6 in Binney 1994). The model naturally accounts for the absence of cold gas between $R \sim 1.5\,$kpc and $R \sim 3.5\,$kpc, since in the neighbourhood of corotation no

stable closed orbits exist on which cold gas could settle. The molecular ring at $R \sim 3.5\,\mathrm{kpc}$ may be associated with gas accumulating near the bar's outer Lindblad resonance. Finally, the predicted perspective asymmetry in the gas distribution goes in the same sense as that observed, and in the sense expected from the bulge infrared photometry (Blitz & Spergel 1991, Weiland *et al.* 1994).

However, it also appears that some essential ingredients are still missing from the model. On the one hand, the observed lopsidedness of the GC molecular gas is probably too great to be accounted for just in terms of perspective effects. We are currently investigating whether asymmetries in the initial gas distribution can be enhanced by hydrodynamic clumping when the self-gravity of the gas is included. This problem is important in a wider context since many external barred galaxies show strong asymmetries in their gas flows. Another, probably harder, problem with the BGSBU model that it has no explanation for the tilt in the HI gas distribution (Liszt & Burton 1980). While simulations show that some gas in peanut-bulge potentials may settle on non-planar closed orbits (Friedli & Benz 1993, Friedli & Udry 1993), no obvious explanation of the HI tilt has yet emerged, mainly because the vertical parity of the orbits in these simulations is different from that of the tilt in the Galactic Centre.

A further uncertainty is the choice of 'correct' description for the interstellar gas in such simulations, as interstellar cloud hydrodynamics may not necessarily be very well described by the standard Euler equations (Binney & Gerhard 1993, Jenkins & Binney 1994). Jenkins & Binney have explored simple interaction schemes in sticky particle-hydrodynamic simulations of the Galactic gas flow. In these particle simulations, the interpretation of the molecular parallelogram in terms of the transition from x_1 to x_2 orbits is only partially born out, mainly, because no strong shocks form. This shows that the chosen description of interstellar gas does matter, and raises the interesting possibility of using observed gas flows to enhance our understanding of cloud fluids and *calibrate* the simulation schemes.

4. Evolutionary Processes in a Barred Milky Way

The presence of a bar in the inner Galaxy makes a number of evolutionary processes relevant for Galactic evolution. Some are briefly discussed in this Section.

4.1. GAS INFALL

In the rotating Galactic bar potential, molecular gas is moving inwards through the cusped orbit shock. Simple estimates for the present mass inflow rate through the ILR give $\sim 0.1\,\mathrm{M}_\odot/\,\mathrm{yr}$ (Gerhard 1992). Further in,

the massive GC clouds on x_2-orbits, such as Sgr B, circulate with speeds greater than the pattern velocity of the bar. Thus they tend to lose further angular momentum to the bulge/bar stars, both by gravitational torques from the rotating quadrupole, and by dynamical friction. The latter process alone causes gas inflow to yet smaller radii at a comparable rate (Stark *et al.* 1991). Thus the present population of Galactic centre clouds must be transient, and for the next Gyr material will be accreting onto the GC at an average rate of $\sim 0.01 - 0.1\,M_\odot/\,\mathrm{yr}$. Gas in the bulge region may be replenished by mass loss from the bulge stars ($\sim 0.2\,M_\odot/\,\mathrm{yr}$; Ciotti *et al.* 1991), and perhaps from gas moving inwards through corotation (if the medium is sufficiently dissipative to outweigh the spin-up from the bar there, or if the potential is time-varying; see, e.g., Schwarz 1981, Noguchi 1988, Pfenniger & Norman 1990, Friedli & Benz 1993). The frequent observation of central gas concentrations with associated non-circular motions in nearby barred spirals suggests that radial gas inflow is a common phenomenon (Kenney 1994).

4.2. ANGULAR MOMENTUM TRANSFER

The infalling gas must lose its angular momentum to the stars in the bar/bulge. For a hot stellar component the dynamical importance of this angular momentum transfer is enhanced by the fact that the typical circular velocity for gas in the bulge region is $\sim 180\,\mathrm{km\,s^{-1}}$, while the streaming velocity of the stars in, say, an oblate-isotropic bulge model is only $\sim 65\,\mathrm{km\,s^{-1}}$ (estimated from the model in Kent 1992). For a rapidly rotating stellar bar, the gas-driven angular momentum accretion may reverse the tendency of the bar to lose angular momentum to the surrounding spheroid or halo, which is predicted by dynamical friction calculations (Weinberg 1985, Hernquist & Weinberg 1992), as shown in the coupled gas- and stellardynamical simulations of Friedli & Benz (1993).

4.3. BUILD-UP OF THE INNER DISK

If accretion rates of $0.1\,M_\odot/\,\mathrm{yr}$ can be maintained over prolonged periods of time, and the material be mostly converted into stars, then significant additions to the mass budget of the inner disk will result. Over the age of the bulge $0.1\,M_\odot/\,\mathrm{yr}$ correspond to of order one third of the total mass inside 500 pc. The present star formation rate in the central few 100 pc is normal for the amount of gas there (as inferred from FIR and thermal radio emission, Güsten 1989). It may currently be surpressed by the pressure from a very hot, 10^8K gas (Spergel & Blitz 1992, Blitz *et al.* 1993), but it is hard to see how this hot medium can be maintained over long time-scales without converting a significant fraction of the accreted material into stars,

unless unusually many massive stars are produced. Kenney (1994) discusses the triggering of burst-like star formation by gas inflow in external barred galaxies.

4.4. BAR DISSOLUTION BY A CENTRAL MASS CONCENTRATION

By funneling material to its centre, the bar may generate the cause of its own destruction: Hasan & Norman (1990) and Hasan, Pfenniger & Norman (1993) have shown that a central mass with a few percent of the bar mass ($\sim 10^8\,M_\odot$ in our Galaxy) would destroy the bar. For a mass of this order the outer ILR has moved outwards sufficiently, so that there no longer exist the elongated x_1-orbits to self-consistently support the bar's elongated shape. While the Galaxy's central point mass is not (yet) relevant for such evolution of the bulge/bar, Friedli & Benz (1993) and Friedli & Martinet (1993) have shown that bar-driven gas inflow may form sufficiently concentrated gas disks or secondary bars which can have similar effects.

4.5. LATE BULGE FORMATION FROM DISK INSTABILITIES

It has recently emerged from N-body simulations that two-dimensional bars are often unstable to a bending instability and evolve to form peanut-shaped bulges (Combes *et al.* 1990, Raha *et al.* 1991, Pfenniger & Friedli 1991; for a review see Sellwood & Wilkinson 1993). Pfenniger & Friedli (1991) show that the final peanut-shaped bulge is largely supported by a 2:2:1 resonant orbital family antisymmetric with respect to the equatorial plane. The instability appears to be wide-spread; most strong bars also quickly become three-dimensional. The mechanism appears to work for thin and thick initial disk bars, and for a range of initial disk-to-preexisting bulge ratios. After their formation, these peanut-bulges apparently do not evolve significantly (Pfenniger & Friedli 1991).

The resulting peanut bulges are centrally concentrated, substantially flattened bodies. Seen edge-on, they show clear peanut-shapes, but have more normal, nearly elliptical shapes when viewed end-on, and boxy shapes at intermediate angles (Combes *et al.* 1990). Their dynamical structure is closer to the dynamics of disks than classical spheroidal bulges; it is governed by fast rotation nearly constant on cylinders. This is similar as in some observed peanut bulges such as in NGC 4565 (Kormendy & Illingworth 1982). Sellwood's (1993) model has a remarkably similar morphology to the COBE bulge/bar, and a kinematic anisotropy that is not too dissimilar to that deduced from the observed radial velocities (summarized by Kent 1992) and proper motions in Baade's window (Spaenhauer, Jones & Whitford 1992).

One may speculate that, integrated over the age of the Galaxy, a significant part of the Galactic bulge/bar might have been made in the disk and scattered out of the galactic plane in this way. The test of this hypothesis will come from observations of ages, abundances, and kinematics of bulge stars, a difficult subject reviewed by Rich (1993) and other papers in Dejonghe & Habing (1993). While the evidence points towards stellar ages of $\sim 5-10$ Gyr in Baade's window, with an age spread (e.g., Holtzman *et al.* 1993, Paczynski *et al.* 1994b), the situation at lower latitudes is less clear. The correlations between kinematics and [Fe/H] argue for dissipative, perhaps extended formation of the bulge (Rich 1990, Minniti 1995). Clearly, much remains to be learned here.

References

Athanassoula E., 1992, MNRAS 259, 345
Bania T.M., 1977. ApJ 216, 381
Bally J., Stark A.A., Wilson R.W., Henkel C., 1988, ApJ 324, 223
Binney J.J., 1994, in The Nuclei of Normal Galaxies, NATO ASI Ser. C, Vol. 445, Genzel R., Harris A.I., eds, Kluwer, Dordrecht, 75
Binney J.J., Gerhard O.E., 1993, in Back to the Galaxy, AIP Conf. Proc. 278, Holt S.S., Verter F., eds, AIP, New York, 87
Binney J.J., Gerhard O.E., Stark A.A., Bally J., Uchida K.I., 1991, MNRAS 252, 210 (BGSBU)
Blitz L., 1993, in Back to the Galaxy, AIP Conf. Proc. 278, Holt S.S., Verter F., eds, AIP, New York, 98
Blitz L., Binney J., Lo K.Y., Bally J., Ho P.T.P., 1993, Nature 361, 417
Blitz L., Spergel D.N., 1991, ApJ 379, 631
Braunsfurth E., Rohlfs K., 1981, A&AS 44, 437
Burton W.B., Liszt H.S., 1978, ApJ 225, 815
Burton W.B., Liszt H.S., 1983, A&AS 52, 63
Ciotti L., D'Ercole A., Pellegrini S., Renzini A., 1991, ApJ 376, 380
Cohen R.J., Few R.W., 1976, MNRAS 176, 495
Combes F., Debbasch F., Friedli D., Pfenniger D., 1990, A&A 233, 82
Dame T.M. etal, 1987, ApJ 322, 706
Dejonghe H., Habing H.J., eds, 1993, Galactic Bulges, Proc. IAU Symp. 153, Kluwer, Dordrecht
Dwek E. *et al.* , 1995, ApJ , in press
Evans N.W., 1994, ApJL 437, L31
Friedli D., Benz, W, 1993, A&A 268, 65
Friedli D., Martinet L., 1993, A&A 277, 27
Friedli D., Udry, S., 1993, in Galactic Bulges, Proc. IAU Symp. 153, Dejonghe H., Habing H.J., eds, Kluwer, Dordrecht, 273
Gerhard O.E., 1992, Reviews in Modern Astronomy 5, 174
Gerhard O.E., Binney J.J., 1993, in Galactic Bulges, Proc. IAU Symp. 153, Dejonghe H., Habing H.J., eds, Kluwer, Dordrecht, 275
Gerhard O.E., Vietri M., 1986, MNRAS 223, 377
Güsten R., 1989, in The Center of the Galaxy, Proc. IAU Symp. 136, Morris M., ed, Kluwer, Dordrecht, 89
Habe A., Ikeuchi S., 1985, ApJ 289, 540
Hasan H., Norman C., 1990, ApJ 361, 69
Hasan H., Pfenniger D., Norman C., 1993, ApJ 409, 91

Heiligman G.M., 1987, ApJ 314, 747
Hernquist L., Weinberg M.D., 1992, ApJ 400, 80
Holtzman J.A. *et al.* , 1993, AJ 106, 1826
Jenkins A., Binney J.J., 1994, MNRAS 270, 703
Kenney J., 1994, in Astronomy with Millimeter and Submillimeter Wave Interferometry, Proc. IAU Coll. 140, Ishiguro M., ed, ASP Conf. Series, ASP, San Francisco
Kent S.M., 1992, ApJ 387, 181
Kormendy J., Illingworth G., 1982, ApJ 256, 460
Liszt H.S., Burton W.B., 1980, ApJ 236, 779
Matsumoto T. *et al.* , 1982, in The Galactic Center, AIP Conf. Proc. 83, Riegler G.R., Blandford R.D., eds, AIP, New York, 48
Minniti D., 1995, ApJ , submitted
Möllenhoff C., Matthias M., Gerhard O.E., 1995, A&A , in press
Mulder W.A., Liem B.T., 1986. A&A 157, 148
Nakada Y., Deguchi S., Hashimoto O., Izumiura H., Onaka T., Seki- guchi K., Yamamura I., 1991, Nature 353, 140
Noguchi M., 1988, A&A 203, 259
Paczynski B., Stanek K.Z., Udalski A., Szymanski M., Kaluzny J., Kubiak M., Mateo M., Krzeminski W., 1994a, ApJL 435, L113
Paczynski B., Stanek K.Z., Udalski A., Szymanski M., Kaluzny J., Kubiak M., Mateo M., 1994b, AJ 107, 2060
Peters W.L., 1975, ApJ 195, 617
Pfenniger D., Norman C., 1990, ApJ 363, 391
Pfenniger, D., Friedli, D., 1991, A&A 252, 75
Raha N., Sellwood J.A., James R.A., Kahn F.D., 1991. Nature 352, 411
Rich R.M., 1990, ApJ 362, 604
Rich R.M., 1993, in Galactic Bulges, Proc. IAU Symp. 153, Dejonghe H., Habing H.J., eds, Kluwer, Dordrecht, 169
Sanders D.B., Solomon P.M., Scoville N.Z., 1984, ApJ 276, 182
Sanders R.H., 1989, in The Center of the Galaxy, Proc. IAU Symp. 136, Morris M., ed, Kluwer, Dordrecht, 77
Sanders R.H., Huntley J.M., 1976, ApJ 209, 53
Schwarz M.P., 1981, ApJ 247, 77
Schwarz M.P., 1984, MNRAS 209, 93
Sellwood J.A., 1993, in Back to the Galaxy, AIP Conf. Proc. 278, Holt S.S., Verter F., eds, AIP, New York, 133
Sellwood J.A., Wilkinson A., 1993, RepProgPhys 56, 173
Shaw M., Axon D., Probst A., Gatley I., 1995, MNRAS , in press
Sinha R.P., 1979, A&AS 37, 403
Spaenhauer A., Jones B.F., Whitford A.E., 1992, AJ 103, 297
Spergel D.N., Blitz L., 1992, Nature 357, 665
Stanek K.Z., Mateo M., Udalski A., Szymanski M., Kaluzny J., Kubiak M., 1994, ApJL 429, L73
Stark A.A., Gerhard O.E., Binney J.J., Bally J., 1991. MNRAS 248, 14P
van Albada G.D., 1985, A&A 142, 491
Weiland J.L. *et al.* , 1994, ApJL 425, L81
Weinberg M.D., 1985, MNRAS 213, 451
Weinberg M.D., 1992, ApJ 384, 81
Whitelock P., Catchpole R., 1992, in The Center, Bulge, and Disk of the Milky Way, Blitz L., ed, Kluwer, Dordrecht, 103
Wozniak H., Friedli D., Martinet L., Martin P., Bratschi P., 1995, A&A , in press
Zhao H.-S., Spergel D.N., Rich R.M., 1994, AJ 108, 2154
Zhao H.-S., Spergel D.N., Rich R.M., 1995, ApJ , submitted

DISCUSSION

J. Sellwood: It is obviously a good idea to try many different numerical schemes to model the ISM and to compare and contrast the results. But we should bear in mind which component we are trying to model with each code. I'd like to suggest that fluid codes would do a better job of modeling the low density HI while particle code may be better for the high density molecular clouds.

RESULTS FROM THE OPTICAL GRAVITATIONAL LENSING EXPERIMENT (OGLE)

B. PACZYŃSKI AND K. Z. STANEK
Princeton University Observatory
Princeton, NJ 08544-1001

A. UDALSKI, M. SZYMAŃSKI, J. KAŁUŻNY AND M. KUBIAK
Warsaw University Observatory
Al. Ujazdowskie 4, 00-478 Warszawa, Poland

M. MATEO
Department of Astronomy, University of Michigan
821 Dennison Bldg., Ann Arbor, MI 48109-1090

W. KRZEMIŃSKI
Carnegie Observatories, Las Campanas Observatory
Casilla 601, La Serena, Chile

AND

G. W. PRESTON
Carnegie Observatories, Institution of Washington
813 Santa Barbara Street, Pasadena, CA 91101

Abstract. The analysis of the first three years of the OGLE data revealed 12 microlensing events of the Galactic bulge stars, with the characteristic time scales in the range $8.6 < t_0 < 80$ days, where $t_0 = R_E/V$. A complete sample of nine events gave the optical depth to gravitational microlensing larger than $(3.3 \pm 1.2) \times 10^{-6}$, in excess of current theoretical estimates, indicating a much higher efficiency for microlensing by either bulge or disk lenses. The lenses are likely to be ordinary stars in the Galactic bar , which has its long axis elongated towards us. At this time we have no evidence that the OGLE events are related to dark matter . The OGLE color magnitude diagrams reveal the presence of the Galactic bar and a low density inner disk region ~ 4 kpc in radius. A catalogue of a few thousand variable stars is in preparation.

L. Blitz and P. Teuben (eds.), Unsolved Problems of the Milky Way, 93–102.
© 1996 *International Astronomical Union.*

1. Introduction

The OGLE project (Optical Gravitational Lensing Experiment) is a collaboration between the Warsaw University Observatory, Carnegie Observatory, and Princeton University Observatory. All observations are done with the 1 meter Swope telescope at the Las Campanas Observatory, operated by the Carnegie Institution of Washington. We have the telescope available to the OGLE about 70 nights each season, which lasts from early April to early September, when the Galactic bulge can be observed. The detector is a single Loral CCD with $(2k)^2$ pixels. A somewhat modified DoPhot photometric software (Schechter, Mateo & Saha 1993) is used to extract stellar magnitudes from the CCD frames. All data is processed at the observing site with a Sparc 10/512 computer within 24 hours of the acquisition, and the summary of the results is e-mailed to the Warsaw University Observatory for evaluation, off-loading the observer who is on duty. All technical details and the journals of the observations are provided in Udalski et al. (1992, 1994a). The project covered three observing seasons: 1992, 1993, and 1994, and it is likely to continue in the same form through 1995.

Some time in 1995 a new 1.3 meter R/C telescope will be put into operation at the Las Campanas site. It will be managed by the Warsaw University Observatory, and it will be dedicated to massive CCD photometry, the search for gravitational microlensing being one of the prime projects. Two other large collaborations are involved in a search for gravitational microlensing of the LMC stars as well as the Galactic bulge stars (Alcock et al. 1993; Aubourg et al. 1993; see also these Proceedings).

2. Results

Whenever the Galactic bulge was observable and the seeing was adequate we were monitoring 13 fields in the bulge region in 1992, and 20 fields in 1993 and 1994, each field being $\sim 15' \times 15'$ in size. The distribution of the fields in the sky is shown in Stanek et al. (1994b, cf. Fig. 1., these Proceedings) The total of 12 lensing events was discovered: 7 in 1992, 3 in 1993 and 2 in 1994 (Udalski et al. 1993a, 1994b,c,d,e). The location of 11 of those lenses in the color magnitude diagram (CMD) is shown in Fig. 1. It is clear that the lenses are scattered over the part of the diagram where the Galactic bulge stars are found.

A careful statistical study of a complete sample of nine events found in the data from 13 fields observed in 1992 and 1993 confirmed the impression that the distribution of those nine events was random in the CMD, and their amplitude distribution was random as well, allowing for known biases in the detection procedure (Udalski et al. 1994e). In the same paper the optical depth to microlensing was found to be larger than $(3.3 \pm 1.2) \times$

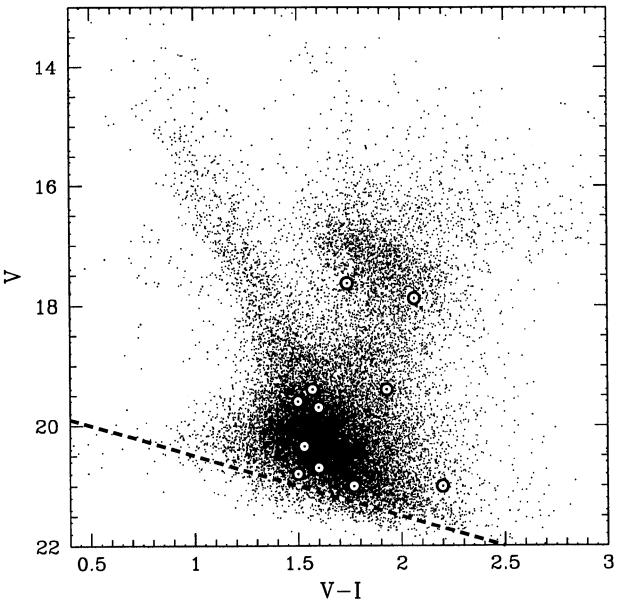

Figure 1. The locations of the 11 OGLE lensing events (large circles) are shown in the color – magnitude diagram for Baade's Window and the Galactic bar fields combined. Only $\sim$ 5% of all stars are shown. The dashed line shows the limit of lenses detectability given by the condition $I < 19.5$. A calibrated photometry of one of the 12 OGLE events is not available at this time.

10^{-6}, in excess of original theoretical estimates, indicating a much higher efficiency for microlensing by either bulge or disk lenses. We argued that the lenses are likely to be ordinary stars in the Galactic bar, which has its long axis somewhat inclined to the line of sight (Paczyński et al. 1994b). Two examples of the microlensing events are presented in Fig. 2.

Another major highlight was the development and implementation in the 1994 season of the "early warning system", EWS (Paczyński 1994a, Udalski et al. 1994c). The data from every clear night were automatically analyzed by the on-site computer system (Sparcstation 10/512), and the summary of results was automatically forwarded by e-mail to Warsaw. Two lensing events, OGLE #11 and OGLE #12 (Fig. 3), were detected on their rise on July 8 and August 20, 1994, respectively, making it possible to follow them up in detail.

The first fairly spectacular case of a microlensing by a double star, OGLE #7, was found in the 1993 data (Udalski et al. 1994d). The observed light curve, shown in Fig. 4, exhibits a sharp peak due to the source star crossing an optical caustic in the lensing system. Theoretical modeling predicted that a second sharp peak should be present in the gap of the

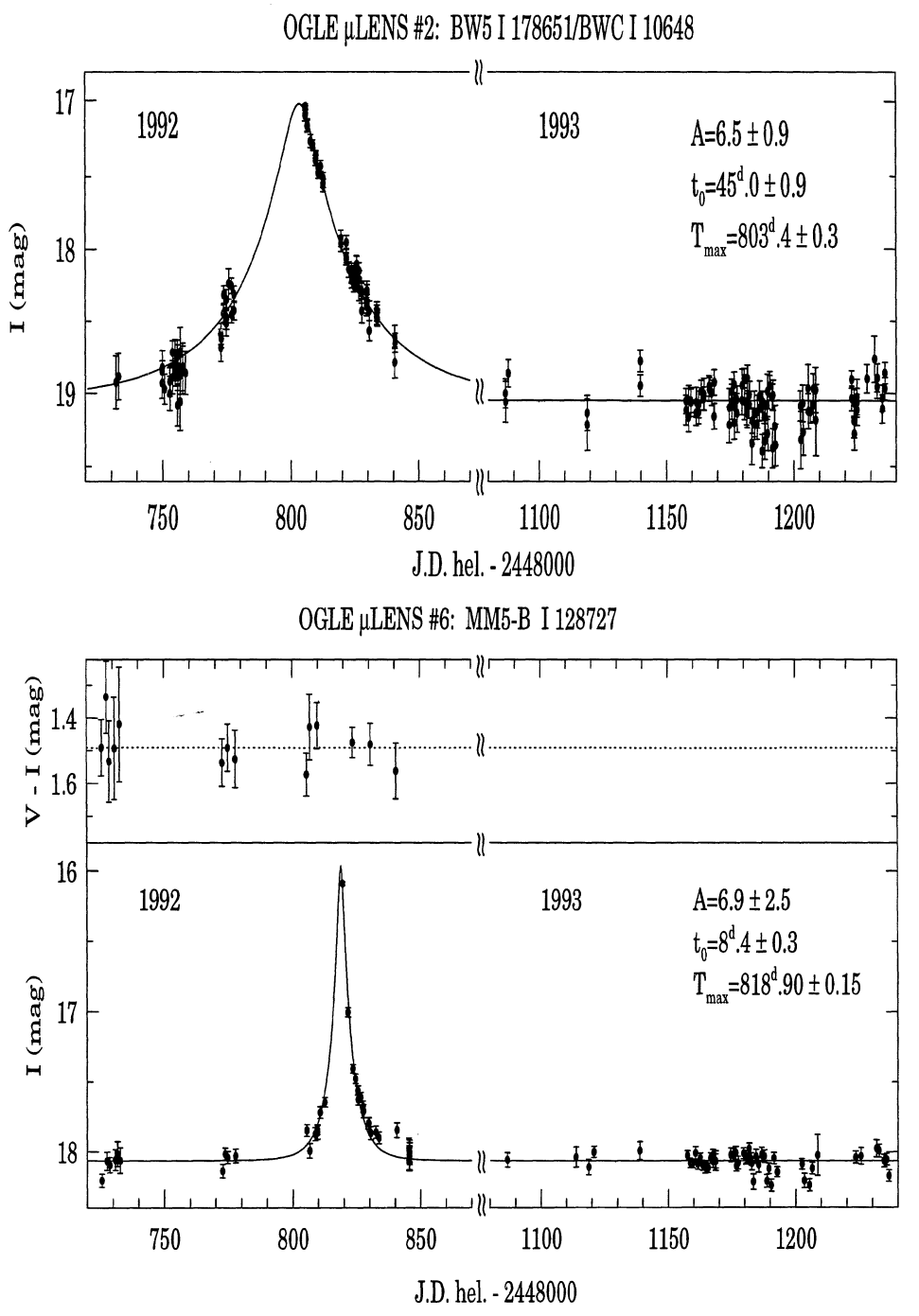

Figure 2. Examples of two microlensing events: long-lasting (upper panel) and short-lasting (lower panel) (Udalski et al. 1994b,e).

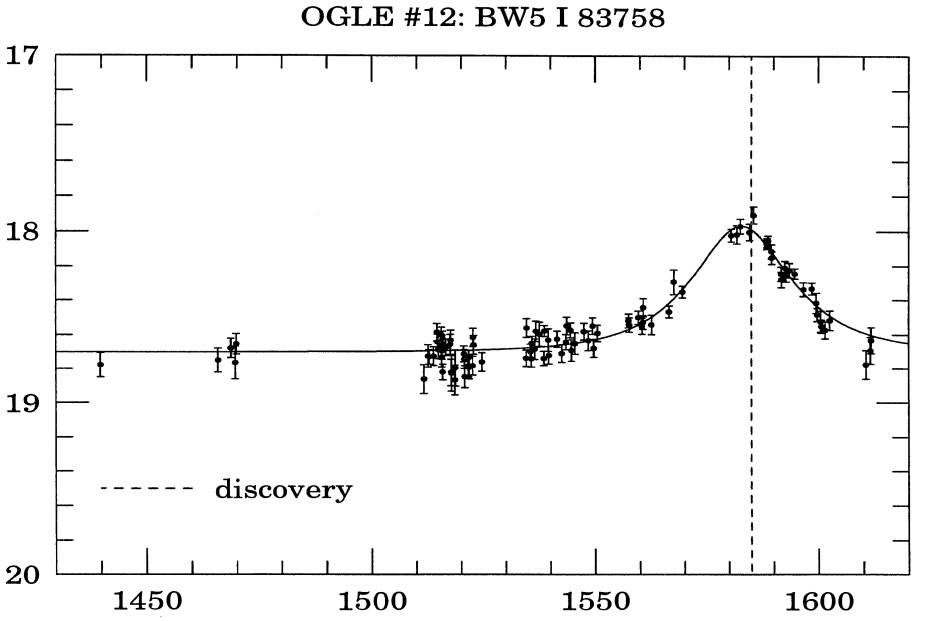

Figure 3. The second microlensing event detected by the OGLE Early Warning System and observed in real time (Udalski et al. 1994c). The dashed vertical line marks the date the event crossed the detection threshold – August 20, 1994. The first event ever to be detected in real time, OGLE #11, crossed the detection threshold on July 8, 1994.

OGLE data. Following the OGLE discovery of the event #7 the MACHO collaboration found the object in their data, and the presence of the second sharp peak of the light curve has been confirmed (Ch. Alcock, private communication). Thanks to the "early warning system" it will be possible in the future to obtain very good time coverage of such peaks in the light curves of double lensing events, which in turn will allow detailed studies of normally very faint stars. Events like that resolve the disks of the lensed stars just like stellar eclipses do. Brightening by more than five magnitudes is possible in some cases.

The color magnitude diagrams of the bulge region (Udalski et al. 1993b) turned out to be very useful source of information about the galactic structure. Stanek et al. (1994a,b) found that the red clump stars (the cloud of points around $V - I = 1.9, V = 17$ in Fig. 1) in the Galactic bulge were 0.37 ± 0.025 mag brighter at (l,b) = $(+5.5^o, -3.5^o)$ than at $(-5.0^o, -3.5^o)$, indicating the bulge is shaped as a bar, with the end at positive galactic longitude being closer to us.

The distribution of the galactic disk stars turned out to be unexpected. The disk main sequence stars form a surprisingly narrow band, traceable from $(V-I, V) = (0.9, 15)$ to $(1.4, 19)$ in Fig. 1. The analysis of the observed

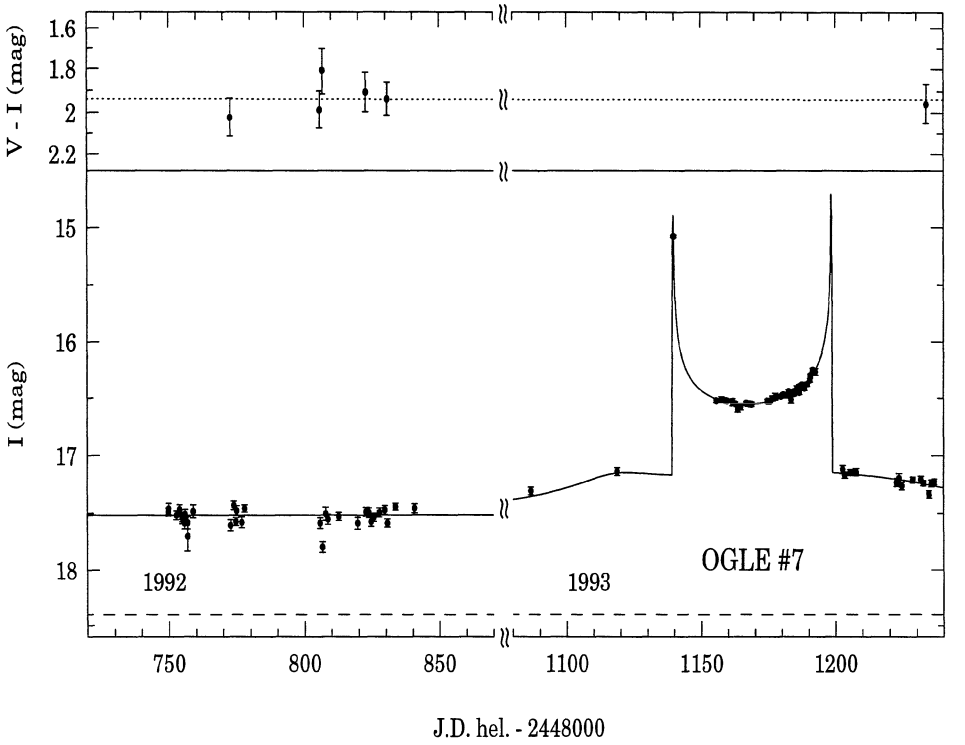

Figure 4. OGLE #7 – the first clear case of lensing by a binary system (Udalski et al. 1994d).

distribution pointed to a rapid drop in the number density of disk stars at a distance $\sim$ 3 kpc from the Sun (Paczyński et al. 1994a). These are the disk stars which may contribute to the lensing of the bulge stars, and the structure is apparent down to at least $M_V \approx 7$, i.e. it includes the old disk population. The evidence that the inner disk may have very few moderate age stars was available for some time (Baud et al. 1981, Blommaert et al. 1994).

In a systematic search for periodic variable stars thousands were found, and the catalogues are in preparation using the database of the OGLE photometry (Szymański & Udalski 1993). These are mostly contact binaries, other eclipsing binaries, RR Lyrae and SX Phenicis stars.

When the Galactic bulge could not be observed we had a number of secondary targets. In 1992 a few dozen clusters of galaxies were monitored for about four months in an attempt to detect supernovae – none were found.

In 1993 one field in the Sculptor dwarf galaxy was monitored and over

200 RR Lyrae stars were detected (Kałużny et al. 1994). Some examples are shown in Fig. 5. A correlation was detected between the period and average V magnitude of RRab type variables. Also, two globular clusters, 47 Tuc and Omega Cen, were monitored in a search for detached eclipsing binaries. At least one such system was found in Omega Cen, approximately one magnitude above the main sequence turn-off point (Kałużny et al., in preparation).

In 1994 Omega Cen and 47 Tuc were monitored, and in addition some frames of one field in the recently discovered Sagittarius dwarf (Ibata, Gilmore and Irwin 1994) were taken. We detected seven RR Lyrae variables belonging to the dwarf, and these were used to determine the distance: 25.2 ± 2.8 kpc (Mateo et al. 1994). The color magnitude diagram was used to estimate the age to be ~ 10 Gyr.

Preliminary results from the OGLE were presented at a number of conferences (Szymański et al. 1993, Udalski et al. 1992b, 1993c)

3. OGLE Related Papers

There was a number of papers written as a consequence of the OGLE observations. Kiraga & Paczyński (1994) noticed that the major contribution to the optical depth to gravitational microlensing of the Galactic bulge stars is from the Galactic bulge stars themselves. Kiraga (1994) presented theoretical maps of the optical depth as a function of galactic coordinates. The high optical depth found by the OGLE was reproduced theoretically by Zhao, Spergel and Rich (1994) with their dynamical model of the Galactic bar, strengthening the case for the presence of the bar and for the bar origin of the majority of OGLE lensing events. Stanek (1994) noticed that the 'red clump' stars that are lensed should be systematically fainter than the general population of the red clump stars , and the shift in the median magnitude is directly proportional to the radial depth of the bulge/bar.

In general there is no unique relationship between the observed time scale of a microlensing event t_0 and the lens mass (e.g. Kiraga and Paczyński 1994). However, there is a case where the relation between t_0 and the lens mass is simple and unique. This is lensing of the Galactic bulge stars and LMC stars by globular clusters which are in front of them (Paczyński 1994b). This may be the most robust (though rather time consuming) way to determine the mass function of stars and brown dwarfs of which the globular clusters are made.

Renzini (1994) noticed that the very high number of the red clump stars observed by the OGLE in the Galactic bulge can be explained with the enhanced helium abundance of those stars, the enhancement related to their high heavy element content.

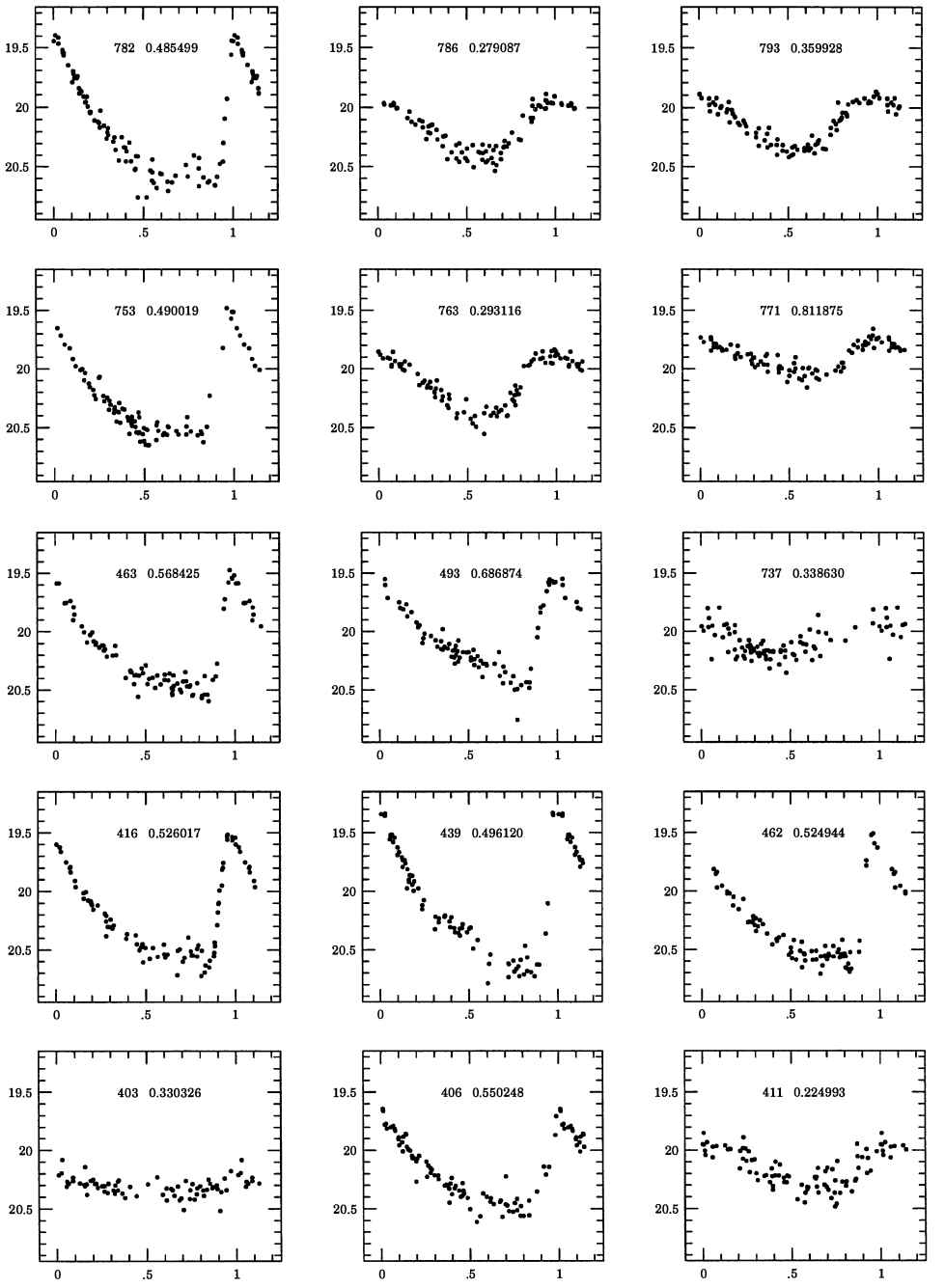

Figure 5. Examples of variable stars found in Sculptor dwarf galaxy (Kałużny et al. 1994) in *V mag*-phase diagrams.

Mao and Di Stefano (1995) developed a code to fit theoretical double lens light curves to the data, and noticed that the OGLE #6 event might be due to a double lens. The code was used to fit the observations of the OGLE #7 (Udalski et al. 1994d).

Many theoretical interpretation papers about the OGLE and MACHO events were written, but they are beyond the scope of this mini-review.

4. OGLE by Internet

Since the beginning of the 1994 observing season the OGLE project is capable of near real time data processing (Paczyński 1994, Udalski et al. 1994c). The new computer system automatically signals the events while they are on the rise, making it possible to carry out photometric and/or spectroscopic follow-up observations. The observers who would like to be notified about the on-going events should send their request to A. Udalski (udalski@sirius.astrouw.edu.pl). Two microlensing events have already been discovered with this system (Udalski et al. 1994c).

The photometry of the OGLE microlensing events, their finding charts, as well as a regularly updated OGLE status report, including more information about the "early warning system", can be found over Internet from "sirius.astrouw.edu.pl" host (148.81.8.1), using the "anonymous ftp" service (directory "ogle", files "README", "ogle.status", "early.warning"). The file "ogle.status" contains the latest news and references to all OGLE related papers, and the PostScript files of some publications, including Udalski et al. (1994c,e). The OGLE results are also available over "World Wide Web": "http://www.astrouw.edu.pl/".

This project was supported with the NSF grants AST 9216494 and AST 9216830 and Polish KBN grants No 2-1173-9101 and BST438A/93.

References

Alcock, C. et al. 1993, Nature, 365, 621
Aubourg, E. et al. 1993, Nature, 365, 623
Baud, B., Habing, H. J., Matthews, H. E., & Winnberg, A. 1981, A&A, 95, 156
Blommaert, J. A. D. L., van Langevelde, H. J., & Michiels, W. F. P. 1994, A&A, in press
Ibata, R. A., Gilmore, G., & Irwin, M. J. 1994, Nature, 370, 194.
Kałużny, J., Kubiak, M., M. Szymański, A. Udalski, Krzemiński, W., & Mateo, M. 1994, A&A, submitted.
Kiraga, M. 1994, Acta Astronomica, 44. 241.
Kiraga, M., & Paczyński, B. 1994, ApJ, 430, L101.
Mao, S., & Di Stefano, R. 1995, ApJ, 440, ...
Mateo, M., Udalski, A., Szymański, M., Kałużny, J., Kubiak, M., & Krzemiński, W. 1994, AJ, in press.
Paczyński, B. 1986, ApJ, 304, 1
Paczyński, B. 1991, ApJ, 371, L63
Paczyński, B. 1994a, IAU Circular No. 5997

Paczyński, B. 1994b, Acta Astron., 44. 235.
Paczyński, B., Stanek, K. Z., Udalski, A., Szymański, M., Kałużny, J., Kubiak, M., & Mateo, M. 1994a, AJ, 107, 2060
Paczyński, B., Stanek, K. Z., Udalski, A., Szymański, M., Kałużny, J., Kubiak, M., Mateo, M., & Krzemiński, W. 1994b, ApJ, in press.
Renzini, A. 1994, A&A, 285, L5.
Schechter, P. L., Mateo, M., & Saha, A. 1993, PASP, 105, 1342
Stanek, K. Z. 1994, ApJ, submitted
Stanek, K. Z., Mateo, M., Udalski, A., Szymański, M., Kałużny, J., & Kubiak, M. 1994a, ApJ, 429, L73
Stanek,K. Z., Mateo, M., Udalski, A., Szymański, M., Kałużny, J., Kubiak, M., & Krzemiński, W. 1994b, these Proceedings
Szymański, M., & Udalski, A. 1993, Acta Astron., 43, 91.
Szymański M., Udalski, A., Kałużny, J., Kubiak, M., Mateo, M., Krzemiński, W., Preston, G.W., Paczyński, B. 1993, in: "Gravitational Lenses in the Universe" – Proceedings of 31st Liege International Astrophysical Colloquium, eds. J. Surdej et al., p. 503.
Udalski, A., Szymański, M., Kałużny, J., Kubiak, M., & Mateo, M. 1992, Acta Astron., 42, 253.
Udalski, A., Szymański, M., Kałużny, J., Kubiak, M., Mateo, M., Preston G. W., Krzemiński, & W. Paczyński, B. 1992, in "Galactic Bulges", eds. H. Dejonghe & H. Habing (Dordrecht: Kluwer), p. 311
Udalski, A., Szymański, M., Kałużny, J., Kubiak, M., Krzemiński, W., Mateo, M., Preston, G.W., & Paczyński, B. 1993a, Acta Astron., 43, 289.
Udalski, A., Szymański, M., Kałużny, J., Kubiak, M., & Mateo, M. 1993b, Acta Astron., 43, 69.
Udalski A., Szymański, M., Kałużny, J., Kubiak, M., Mateo, M., Preston, G. W., Krzemiński, W., Stanek K. Z. & Paczyński, B. 1993c, in "Relativistic Astrophysics and Particle Cosmology", eds. C. W. Akerlof & M. A. Srednicki, Ann. N.Y. Acad. Sci., 688, 626
Udalski, A., Szymański, M., Kałużny, J., Kubiak, M., Mateo, M., & Krzemiński W. 1994a, Acta Astron., 44, 1.
Udalski, A., Szymański, M., Kałużny, J., Kubiak, M., Mateo, M., & Krzemiński W. 1994b, ApJ, 426, L69.
Udalski, A., Szymański, M., Kałużny, J., Kubiak, M., Mateo, M., Krzemiński, W., & Paczyński, B. 1994c, Acta Astron., 44, 227.
Udalski, A., Szymański, M., Mao, S., Di Stefano, R., Kałużny, J., Kubiak, M., Mateo, M., & Krzemiński, W. 1994d, ApJ , in press.
Udalski, A., Szymański, M., Stanek, K.Z., Kałużny, J., Kubiak, M., Mateo, M., Krzemiński W., Paczyński, B., & Venkat, R. 1994e, Acta Astronom., 44, 165.
Zhao, H. S., Spergel, D. N., & Rich, R. M. 1994, ApJ, submitted.

DISCUSSION

L. Blitz: Have you checked to see whether you have any triggering by events at the threshold level below the mean as a check to see that you are not getting similar events that would be spurious?

Paczynski: *answer not recorded.*

EVIDENCE FOR THE GALACTIC BAR FROM THE TWO COLOR PHOTOMETRY OF THE BULGE RED CLUMP STARS

K. Z. STANEK
Princeton University Observatory
Princeton, NJ 08544-1001

M. MATEO
Department of Astronomy, University of Michigan
821 Dennison Bldg., Ann Arbor, MI 48109-1090

A. UDALSKI, M. SZYMAŃSKI, J. KAŁUŻNY AND M. KUBIAK
Warsaw University Observatory
Al. Ujazdowskie 4, 00-478 Warszawa, Poland

AND

W. KRZEMIŃSKI
Carnegie Observatories, Las Campanas Observatory
Casilla 601, La Serena, Chile

1. Introduction

The Optical Gravitational Lensing Experiment (OGLE, Udalski et al. 1994a; Paczyński et al. 1994b – these proceedings; and references therein) is an extensive photometric search for the rare cases of gravitational microlensing of Galactic bulge stars by foreground objects. It provides a huge data base (Szymański & Udalski 1993), from which color-magnitude diagrams have been compiled (Udalski et al. 1993, 1994b). Here we discuss the use a of well-defined population of bulge red clump stars to investigate the presence of the bar in our Galaxy. The results of our earlier studies are described by Stanek et al. (1994).

There are now a number of photometric and dynamical indications that the Galaxy is barred (de Vaucouleurs 1964; Blitz & Spergel 1991; Binney et al. 1991; Whitelock & Catchpole 1992; Weinberg 1992; for a review see Blitz 1993). The bar is clearly present in the COBE DIRBE data (Weiland

L. Blitz and P. Teuben (eds.), Unsolved Problems of the Milky Way, 103–109.
© 1996 *International Astronomical Union.*

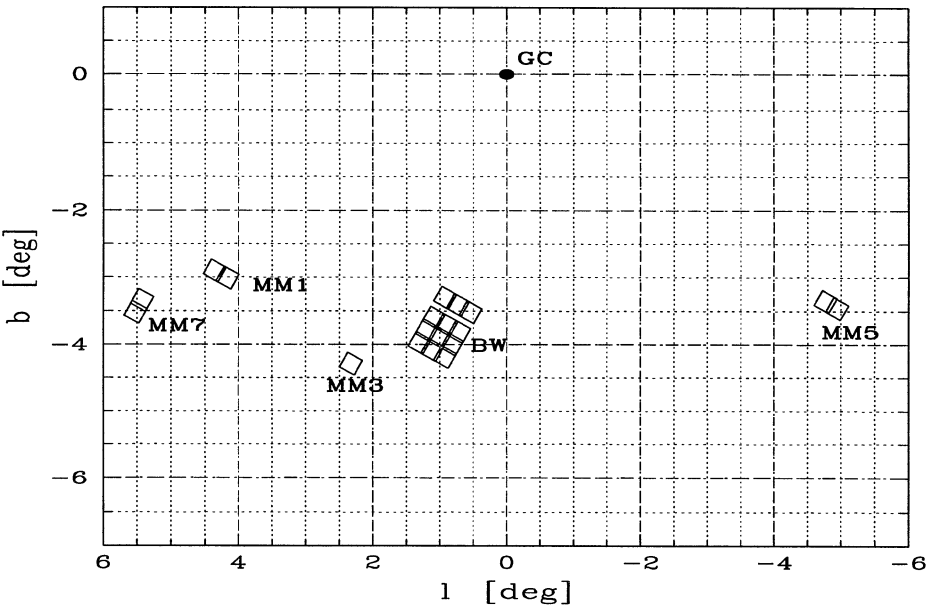

Figure 1. Positions in the Galactic coordinates of 19 fields discussed in this report, for which the $V - I$ color-magnitude diagrams were obtained by the OGLE experiment (Udalski et al. 1993, 1994b).

et al. 1994), which was used by Dwek et al. (1994; also this proceedings) to constrain a number of analytical bar models existing in the literature.

2. The Data

Udalski et al. (1993, 1994b) present color-magnitude diagrams (CMDs) of 19 fields in the direction of the Galactic bulge, which cover nearly 1.5 square degrees and contain about 8×10^5 stars. Fig.1 shows the positions of all 19 fields in galactic coordinates. As an example, the CMD for one of the positive galactic longitude fields (MM7-A) is shown in Fig.2, with main populations of stars schematically illustrated. The part of the diagram dominated by the disk stars was recently analyzed by Paczyński et al. (1994a). Here we use a well-defined population of bulge red clump stars to investigate the presence of the bar in our Galaxy. The results of our earlier studies are presented by Stanek et al. (1994).

To analyze the distribution of bulge red clump stars in a quantitative manner, we define the extinction-insensitive V_{V-I} parameter

$$V_{V-I} \equiv V - 2.6\,(V - I), \tag{1}$$

where we use reddening law $E_{V-I} = A_V/2.6$. The parameter V_{V-I} has been defined so that if A_V/E_{V-I} is independent of location then for any

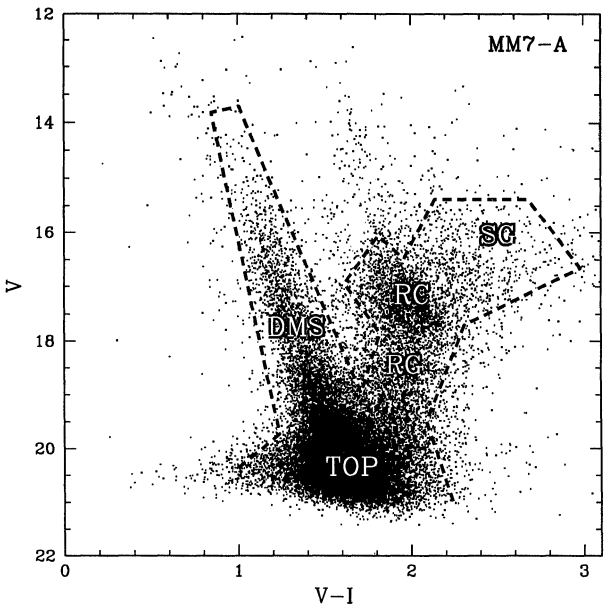

Figure 2. The $V - I$ color-magnitude diagram for stars in the MM7-A field of the OGLE experiment (Udalski et al. 1993). Schematically shown are main populations of stars: TOP – Turn-Off Point, RG – Red Giants, RC – Red Clump, SG – Super-Giants and DMS – Disk Main-Sequence.

particular star its value is not affected by the unknown extinction (see Stanek et al. 1994). The part of the CMD dominated by bulge red clump stars is shown, for six out of all 19 observed fields, in Fig.3. The fields were ordered from top-left to bottom-right by decreasing galactic longitude l. Also shown are two lines corresponding to the V_{V-I} values equal to 11.5 and 13.0. It is clearly visible that the red clump stars from fields with larger l group near to the $V_{V-I} = 11.5$ line, while red clump stars from the fields with smaller (negative) l have, on average, larger values of this parameter.

To quantify the effect observed in Fig.3, for all 19 fields we select the region of the CMD clearly dominated by the bulge red clump stars:

$$1.4 < V - I \;\; ; \;\; 10.5 < V_{V-I} < 14.0 \qquad (2)$$

For every field all stars that satisfied the inequalities (2) were counted in bins of $\Delta V_{V-I} = 0.05$. The result appears in Fig.4, where we show the number of stars as a function of V_{V-I} for the same six fields as in Fig.3. The distributions shown in Fig.4 are similar in shape, with red clump stars forming a pronounced peak. There is however a clear shift between the distributions, in the sense that stars from fields with bigger value of l have on average smaller values of V_{V-I} parameter. To quantify this shift, for every

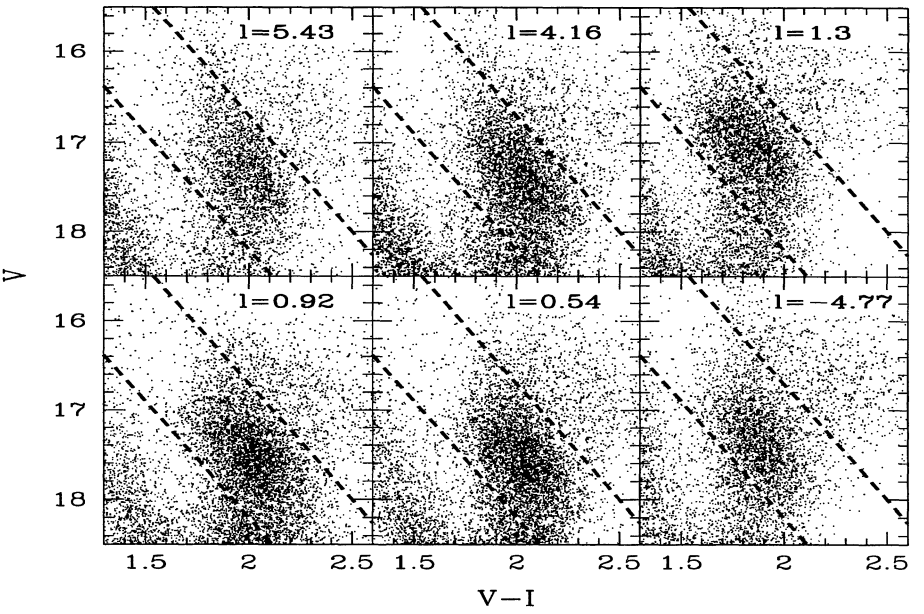

Figure 3. Region of the $V - I$ color-magnitude diagrams dominated by bulge red clump stars for six out of all 19 observed fields, ordered from top-left to bottom-right by decreasing galactic longitude l. The two straight lines correspond to the value of extinction-insensitive parameter V_{V-I} equal to 11.5 and 13.0 (Eq.1).

field we found the mode of the V_{V-I} distribution (see Stanek et al. 1994). The resulting plot of the mode as a function of galactic longitude l for every field is shown in Fig.5. There is a clear anti-correlation between the V_{V-I} value of the mode and the Galactic longitude l for a given field that corresponds to decrease of V_{V-I} value of $\sim 0.04\ mag/$ deg.

3. Discussion

In the previous section we have shown that the distributions of bulge red clump stars, observed in various fields, as a function of extinction-adjusted apparent magnitude are similar in shape but are systematically shifted. This is likely due to the difference in the distance to the bulge red clump stars in various fields, an indication that the bulge is not axially symmetric. If we assume that the peaks of the V_{V-I} distributions correspond to the stars lying at the major axis of the bar, we can obtain the angle of inclination of the bar to the line of sight, $\theta \approx 45$ deg. For a very thin bar such an inclination angle corresponds directly to the true inclination angle, but if the bar is thick then the true inclination angle is smaller (Stanek et al. 1994). It is possible to use the observed luminosity function of red clump

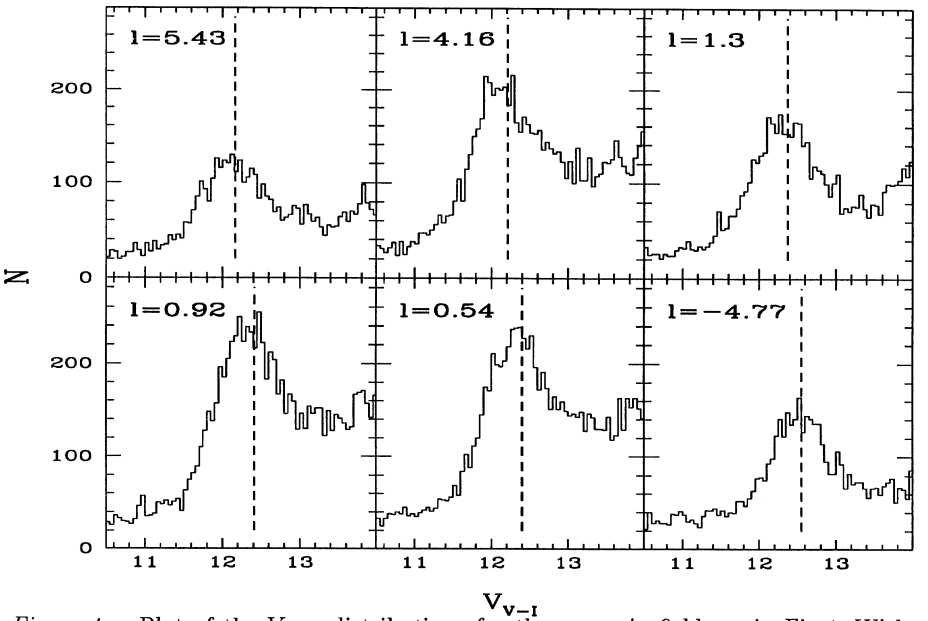

Figure 4. Plot of the V_{V-I} distributions for the same six fields as in Fig.4. With the vertical dashed lines we mark the position of the mode of the distributions.

stars to put constraints on various models of the Galactic bar. This have the advantage over the studies using surface brightness measurements (Dwek et al. 1994) that the red clump stars provide us with information about the depth of the bar along the line of sight. Such information was recently used by Stanek (1994) in his study of the magnitude offset between gravitationally lensed stars and observed stars. The preliminary results from the modelling of the Galactic bar by fitting the observed red clump luminosity function (Stanek et al., in preparation) indicates that the inclination of the Galactic bar to the line of sight is about ~ 20 deg, but it is too early to say how robust this result is.

The presence of the bar in the Galaxy seems to be firmly established by various authors and methods, but there are still considerable differences as to details of the bar structure or angle of inclination to the line of sight. We have shown that the red clump stars can be very useful for investigating the Galactic bar, being both numerous and relatively bright. We are now extending the work presented here, by incorporating more information provided by the red clump region of CMDs, to test a variety of Galactic bar models (Stanek et al., in preparation).

We would like to thank B. Paczyński, the PI of the OGLE project, for encouragement, many stimulating discussions and comments. We acknowledge comments from J. E. Rhoads, who read an earlier version of this

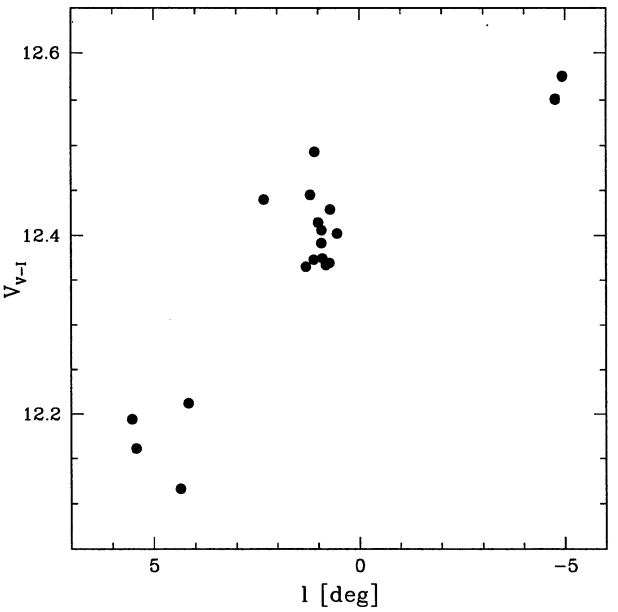

Figure 5. Correlation between the mode of the V_{V-I} distribution and the Galactic longitude l for all observed fields.

report. This work was supported with the NSF grants AST 9216494 and AST 9216830 and Polish KBN grants No 2-1173-9101 and BST438A/93.

References

Binney, J., Gerhard, O. E., Stark, A. A., Bally, J., & Uchida, K. I., 1991, MNRAS, 252, 210

Blitz, L., & Spergel, D. N., 1991, ApJ, 379, 631

Blitz, L. 1993, in "Back to the Galaxy", AIP Conference Proceedings 278, eds. S. S. Holt & F. Verter, (New York: AIP Conference Proceedings), p.98

de Vaucouleurs, G. 1964, in IAU Symp. No. 20, eds. F. J. Kerr and A. W. Rodgers (Australian Acad. Sci.: Canberra), p.195

Dwek, E., et al. 1994, ApJ, submitted (also these Proceedings)

Paczyński, B., Stanek, K. Z., Udalski, A., Szymański, M., Kałużny, J., Kubiak, M., & Mateo, M., 1994a, AJ, 107, 2060

Paczyński, B., et al. 1994b, these Proceedings

Stanek, K. Z., Mateo, M., Udalski, A., Szymański, M., Kałużny, J., Kubiak, M., 1994, ApJ, 429, L73

Stanek, K. Z., 1994, ApJ, submitted

Szymański, M., & Udalski, A. 1993, Acta Astron., 43, 91

Udalski, A., Szymański, M., Kałużny, J., Kubiak, M., & Mateo, M. 1993, Acta Astron., 43, 69

Udalski, A., Szymański, M., Stanek, K. Z., Kałużny, J., Kubiak, M., Mateo, M., Krzemiński, W., Paczyński, B., & Venkat, R. 1994a, Acta Astron., 44, 165

Udalski, A., et al. 1994b, Acta Astronomica, submitted

Weiland, J. L., et al., 1994, ApJ, 425, L81

Weinberg, M. D., 1992, ApJ, 384, 81
Whitelock, P., & Catchpole, R., 1992, in The Center, Bulge, and Disk of the Milky Way, ed. L. Blitz, (Dordrecht: Kluwer Academic), p. 103

DISCUSSION

I. King: Are your red-clump stars good enough standard candles that they can tell you anything about the extent of the bar/bulge along the line of sight?

Stanek: Without any knowledge about the intrinsic properties of the red clump stars we can roughly say only that the FWHM indicates that the depth of the bar along the line of the sight is $\lesssim$ 4kpc.

M GIANT KINEMATICS IN OFF-AXIS FIELDS BETWEEN 150 AND 300 PC FROM THE GALACTIC CENTER

R. D. BLUM, J. S. CARR, K. SELLGREN AND D. M. TERNDRUP
The Ohio State University
174 W. 18th Ave., Columbus, Oh, 43210, USA

Abstract. We present radial velocities for approximately 40 stars in each of four optically obscured, off-axis fields toward the Galactic bulge. The mean heliocentric radial velocity and velocity dispersion are -75 ± 24 km s^{-1} and 127 ± 16 km s^{-1}, 2 ± 23 km s^{-1} and 127 ± 14 km s^{-1}, -14 ± 22 km s^{-1} and 126 ± 14 km s^{-1}, and -31 ± 28 km s^{-1} and 153 ± 17 km s^{-1} for fields located at 299, 288, 171, and 160 pc projected radius, respectively. The dispersions generally match Kent's (1992) axisymmetric mass model but may be higher than the model's predictions at small projected radius.

1. Introduction

Recent photometric studies have produced strong evidence that the inner Galaxy is barred (Blitz and Spergel 1991, Weiland et al. 1994, Stanek et al. 1994, and Dwek et al. 1994). In addition, dynamical modeling of observed gas kinematics also indicates that the inner Galaxy is non-axisymmetric (Binney et al. 1991). However, clear evidence for a non-axisymmetric potential has not been found in the observed stellar kinematics. Indeed, Kent's (1992) axisymmetric dynamical model of the Galactic bulge fits the available data well.

To better constrain the inner Galaxy mass distribution, we have obtained radial velocities for stars in each of four fields located at off-axis positions between 150 and 300 pc projected radius from the Galactic Center (GC). Kent's model predicts a change in the projected dispersion as a function of distance at these radii, but until now, no stellar kinematic data were available here. The large amount of extinction toward the GC at optical wavelengths requires spectroscopic observations at near infrared or

L. Blitz and P. Teuben (eds.), Unsolved Problems of the Milky Way, 111–117.
© 1996 *International Astronomical Union.*

longer wavelengths. We obtained the radial velocities using spectra centered near the 2.3 μm CO bandhead, a strong photospheric absorption feature in M giants.

The data for one of the fields shown here has been presented earlier by Blum et al. (1994).

2. Observations

The program stars were selected from the brighter and redder stars on K and J band images obtained with the Ohio State Infrared Imaging System (OSIRIS) on the Perkins 1.8m telescope near Flagstaff, Arizona during May 1992 and March 1993. OSIRIS employs a 256×256 NICMOS III array.

The majority of the spectroscopic observations were made on the CTIO 1.5m telescope in July 1992 and 1993 using the facility infrared spectrometer (IRS) which employs an SBRC 58×62 InSb detector. The spectral resolution was 84 km s^{-1} (42 km s^{-1} pix^{-1}) at the 2.3 μm CO bandhead. The velocities for stars in one field were obtained in July 1994 using the IRTF 3m infrared telescope and facility echelle spectrometer, CSHELL. The spectral resolution was 25 km s^{-1} (2.5 km s^{-1} pix^{-1}).

Figure 1 shows the spectra of a radial velocity standard and program star measured on each system. The uncertainty in an individual velocity is approximately $\pm$ 15 km s^{-1} as determined from the rms difference of measurements of 15 program stars on both systems.

3. Color Magnitude Diagram

The mean intrinsic $J - K$ can be estimated from the measured CO absorption strengths which are independent of reddening. The mean intrinsic $J - K$ can then be combined with the mean observed $J - K$ to derive the reddening for each field. Comparison of our mean CO strength with the disk M giant spectra in Kleinmann & Hall (1986) and the bulge giant spectra from Terndrup et al. (1991) suggests a mean spectral type of about M5-M7 III or later. This corresponds to an intrinsic $J - K$ of about 1.15 for the stars in Terndrup et al. (1990). The derived reddening given in Table 1 is based on the interstellar reddening curve of Mathis (1990).

The de-reddened color-magnitude diagram (CMD) for the program stars is shown in Figure 2. The left panel depicts the CMD for stars in the four fields for which $K \lesssim 9$. The right hand panel shows those stars for which we obtained spectra. The stars in Figure 2 were corrected for extinction as described above. The derived extinction at K is given for each field in Table 1. The photometric uncertainties in J and K are $\lesssim \pm$ 0.10 mag.

In Figure 2, we also show the unreddened mean and median color v. magnitude relations for the Baade's Window M giants measured by Frogel

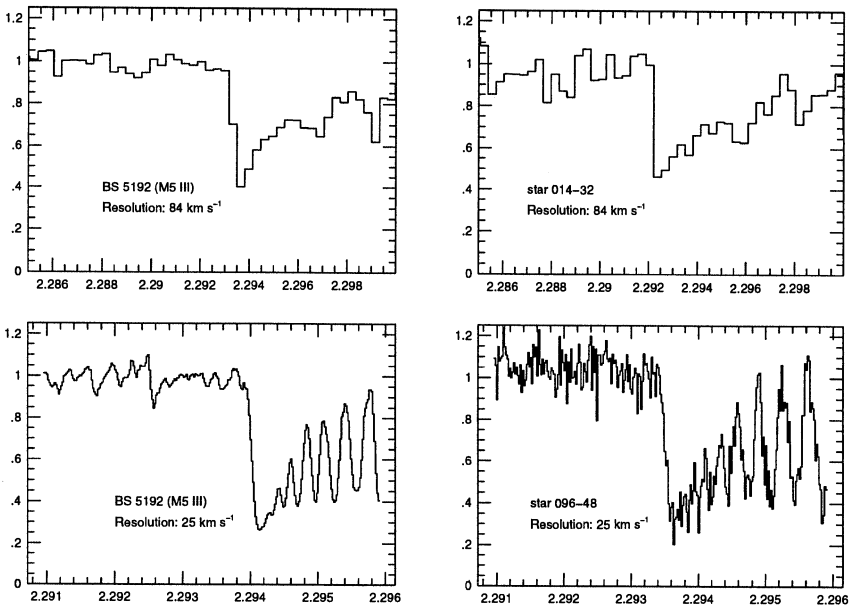

Figure 1. Upper panels, CTIO IRS spectra: resolution = 84 km s^{-1} (42 km s^{-1} pix^{-1}). Lower panels, IRTF CSHELL spectra: resolution = 25 km s^{-1} (2.5 km s^{-1} pix^{-1}). A typical radial velocity standard (BS 5192, M5 III) is shown along with two program stars.

& Whitford (1987). The majority of our stars lie near the Frogel & Whitford relations, suggesting they are also in the inner Galaxy.

4. Kinematics

The velocity dispersion and mean heliocentric radial velocity for each field is shown in Table 1. The distribution of velocities for each field is shown in Figure 3 along with the expected number from a Gaussian distribution of the same mean and dispersion. Kolmogorov-Smirnov (KS) tests show no statistical evidence that any of the observed distributions is different from Gaussian. However, because of the small number of stars in each field, we have not attempted to uniquely determine the form of the intrinsic distributions. There is no reason to expect *a priori* that the distribution of observed velocities should be Gaussian. Kuijken (1994) computed the distribution function for stars in the Kent (1992) isotropic oblate rotator model and found that the distribution in Baade's Window is well represented by a Gaussian. However, the predicted distribution of velocities for stars in another part of the bulge was not Gaussian.

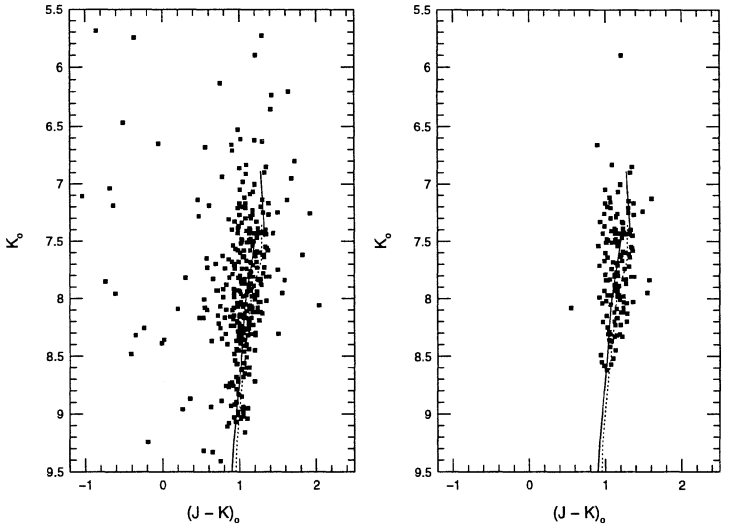

Figure 2. De-reddened color-magnitude diagram for the four program star fields. The extinction correction assumes the interstellar relation from Mathis (1990) and relies on using the observed CO strengths to determine the mean intrinsic color in each field. The left panel depicts the CMD for stars in the four fields for which observed $K \lesssim 9$. The right panel shows the stars for which we obtained spectra; their selection was based on color and magnitude. The lines are the mean (solid) and median (dashed) relations for Baade's Window taken from Frogel and Whitford (1987).

Table 1. M Giant Observed Properties

Field	l (deg)	b (deg)	R[a] (pc)	A_K[b]	v[c] (km s^{-1})	σ (km s^{-1})
1	−0.59	0.98	160	0.99	−31 ± 28	153 ± 17
2	0.85	−0.88	171	0.74	2 ± 23	127 ± 14
3	1.21	−1.67	288	0.23	14 ± 22	126± 14
4	−1.14	1.81	299	0.59	−75 ± 24	127 ±17

Notes to Table 1: a) Assuming $R_o = 8$ kpc. b) Derived using the extinction law of Mathis (1990) and intrinsic color based on CO strength; see text. c) Mean heliocentric velocity.

A rough comparison to the observed kinematics can be made by comparing our projected velocity dispersions to Kent's prediction for the minor axis of the bulge (Figure 4). Three of our positions are consistent with Kent's model. The fourth position shows a dispersion which is larger than Kent's prediction (2 σ). The observed dispersion in Field 1 is possibly in-

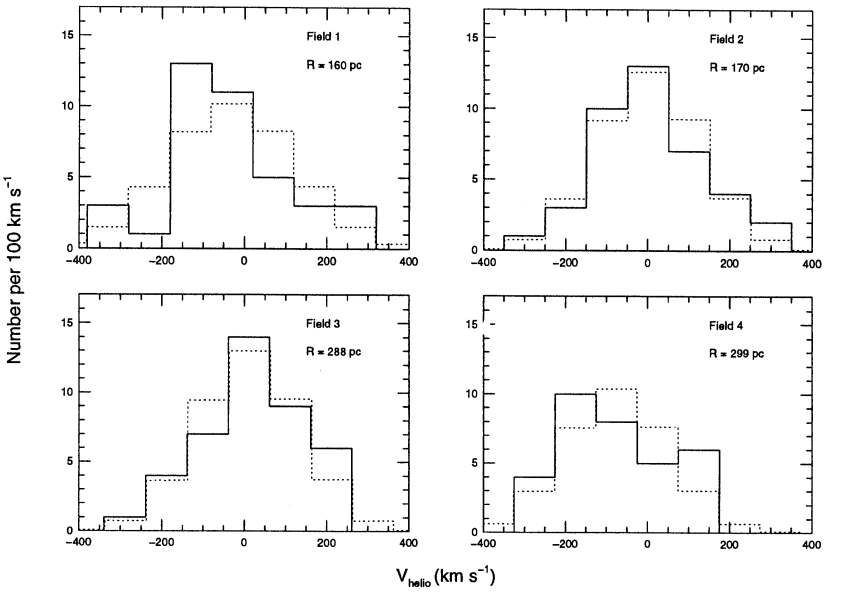

Figure 3. Observed heliocentric velocity distributions for each field (solid line). Distribution of velocities for a Gaussian of the observed FWHM and mean velocity (dashed line). Application of a Kolmogorov-Smirnov test shows no statistical evidence that the observed distributions are non-Gaussian.

consistent with a constant M/L ratio axisymmetric model since it would require a somewhat more peaked density distribution within about 100 pc. A more peaked density distribution with constant M/L is probably ruled out, however, by a preliminary comparison of recent COBE data (Dwek et al. 1994, Weiland et al. 1994) with the original Kent model (Kent, private communication). We note that the data shown in Figure 4 suggests that the line of sight dispersion may be constant or increasing at R $\lesssim$200 pc where Kent's model is decreasing.

A second possibility is that the higher line of sight dispersion in Field 1 results from a barred potential which we observe along a line of sight near its major axis. The dynamical model of Binney et al. (1991), derived from fitting the envelope of gas velocities in the l vs. v diagram, has a barred potential oriented with its major axis only 16° from our line of sight. Dwek et al. (1994) find a best fit triaxial model for the bulge by modeling the near infrared surface brightness distribution in the inner Galaxy. Their best fit model has its major axis oriented at 20° $\pm$ 10° to our line of sight. However, until realistic non-axisymmetric dynamical models that predict stellar kinematics are produced, no direct comparison can be made to the observations, and the mass distribution derived from stellar kinematics remains uncertain.

The mean velocities for three of the four fields are consistent with Kent's model. The velocity in field 4 is significantly more negative (2 σ) than

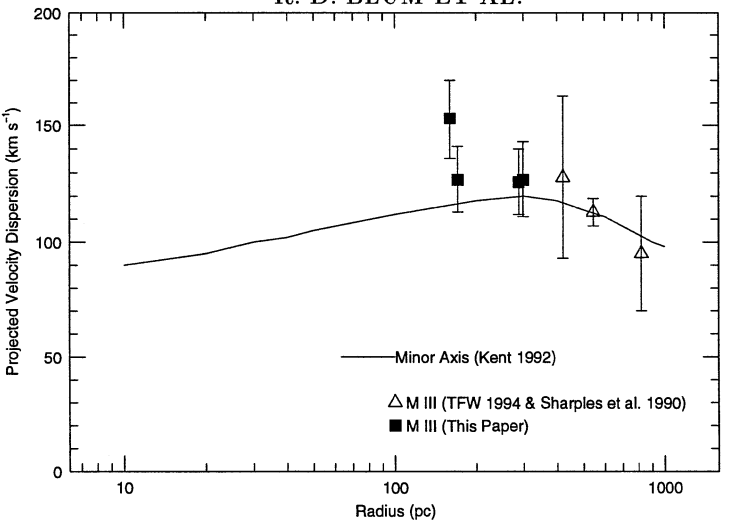

Figure 4. Comparison of observed and predicted line of sight velocity dispersions. The solid curve is taken from the oblate isotropic rotator model of Kent (1992).

predicted (-25 km s^{-1} for this line of sight, Kent, private communication). A gradient in mean velocity along the minor axis would be evidence for triaxiality. However, our fields lie along neither axis, so we can not easily separate the components of velocity along the two axes.

References

Binney, J., Gerhard, O. E., Stark, A. A., Bally, J., & Uchida, K.I., 1991, MNRAS, 252, 210
Blitz, L. & Spergel, D.N., 1991, ApJ, 379, 631
Blum, R. D., Carr, J. S., DePoy, D. L., Sellgren, K., & Terndrup, D. M., 1994, ApJ, 422, 111
Dwek, E., et al., 1994, ApJ, submitted
Frogel, J. A. & Whitford, A.E., 1987, ApJ, 320, 199
Kent, S.M., 1992, ApJ, 387, 181
Kleinmann, S.G. & Hall, D.N.B., 1986, ApJS, 62, 501
Kuijken, K., 1994, preprint
Mathis, J.S., 1990, ARA&A, 28, 37
Sharples, R., Walker, A., & Cropper, M., 1990, MNRAS, 246, 54
Stanek, K. Z., Mateo, M., Udalski, A., Szymanski, M., Kaluzny, J. & Kubiak, M., ApJL, 429, L73
Terndrup, D.M., Frogel, J.A., & Whitford, A.E., 1991, ApJ, 378, 742
Terndrup, D.M., Frogel, J.A., & Whitford, A.E., 1990, ApJ, 357, 453
Terndrup, D. M, Frogel, J. A., & Wells, L., 1994, in preparation (TFW)
Weiland, J., et al., 1994, ApJL, 425, L81

DISCUSSION

J. Sellwood: Some people may be surprised at how well Kent's axisymmetric model matches up to the kinematic data on the bulge which we believe to be triaxial. In order to fit the observations, an axisymmetric model must have kinematics intermediate between those on the major and minor axes. But we observe the bar at an intermediate angle, so intermediate kinematics should not be surprising.

Blum: No answer.

T. de Zeeuw: It is useful to compare not only the measured σ_{los} to Keitt's model but also the actual histogram of μ_{los}. Konrad Kuijken, e.g. has calculated expected distributions.

Blum: We would be happy to make comparisons between the observed velocity distribution and the predictions from Kuijken's analysis of the Kent model. We have already compared the observed distributions to gaussians of the observed width and mean velocity and find no significant statistical difference between them.

RESULTS OF THE SIO MASER SURVEY OF THE GALACTIC BULGE IRAS SOURCES

S. DEGUCHI AND N. UKITA
Nobeyama Radio Observatory,
National Astronomical observatory
Minamimaki, Minamisaku, Nagano 384-13, Japan

H. IZUMIURA AND T. ONO
Department of Astronomy and Earth Sciences,
Tokyo Gakugei University
4-1-1 Nukii-kita, Koganei, Tokyo 184, Japan

Y. NAKADA
Kiso observatory, The University of Tokyo
Mitake, Kiso, Nagano 397-13, Japan

T. ONAKA AND I. YAMAMURA
Department of Astronomy, The University of Tokyo
Bunkyo-ku, Tokyo 113, Japan

AND

O. HASHIMOTO
Department of Applied Physics, Seikei University
3-1-1 Kichijouji-kita, Musashino, Tokyo, 180, Japan

1. Introduction

Evidence for the bar structure in our Galaxy has been shown by Blitz and Spergel (1991b) based on the near-infrared maps of the bulge, by Nakada et al. (1991) based on IRAS point source catalogue, and more clearly by recent COBE maps. However, no clear "dynamical" signature of the bulge bar has been found yet. At optical wavelengths, stellar radial velocities of the bulge stars were observed only at the optical windows and were not observed for the entire region of the bulge because of the dust extinction in this direction.

L. Blitz and P. Teuben (eds.), Unsolved Problems of the Milky Way, 119–124.
© 1996 *International Astronomical Union.*

The Galactic bulge contains a number of late-type stellar objects which emit maser radiation, for example, the OH 1612 MHz maser, and 43 GHz SiO masers. The galactic disk is tranparent at radio wavelengths. We can survey the bulge stars by SiO masers and obtain the radial velocities of bulge stars. We can simultaneouly observe two lines of SiO near 43 GHz, i.e., the J=1-0 rotational lines at the first and the second vibrationally excited states. The Nobeyama 45-m radio telescope has a highest sensitivity at 43 GHz. A part of the result of this survey has been published by Nakada et al. (1993), and Izumiura et al. (1994ab). Radio maser surveys by OH have been conducted by several groups. These surveys were mostly devoted to the special small region of the sky, for example, one square degrees near the galactic center with VLA by Lindqvist et el. (1990), or to the entire sky, for example, with Dwingeloo-Effelsberg-Parkes (te Lintel- Hekkert et al. 1990), Arecibo (Lewis et al. 1990), and Nancay (Le Squeren et al. 1992) telescopes. These previous surveys are very extensive and sensitive but not devoted to the bulge stars.

2. Source selection

The surveyed region is within 15 degrees from the galactic center and the sources near the galactic plane ($|b| < 3°$) are omitted because there are a lot of galactic disk sources and contamination is severe. Sources are selected by colors, i. e., logarithmic ratio of IRAS 12 and 25 μm intensities to be approximately zero. This enables us to pick up the infrared sources with a dust shell of about $T = 300K$. Also we impose the IRAS 12 μm intensity approximately between 2 and 15 Jy. This condition leads us to pick up the infrared sources at the distance of about 8 kpc if the stellar luminosity of the sources is $3 \times 10^3 L_\odot$.

Two-color diagram of the observed IRAS sources indicates that the detected and undetected sources are uniformly distributed in the selected color range. According to the Van der Veen and Habing classification of IRAS stars, these sources belong mainly to the type IIIa, oxygen-rich Mira variables with optically thick dust. Some sources belong to type IIIb, stars with very thick envelope, and to type VIb, the stars thicker at 60 micron. The selected stars have dust shell temperature of about 200-400 K.

2.1. DISCRIMINATION OF THE DISK SOURCES

Although we primary select the sources in terms of IRAS colors and intensities, disk sources may contaminate in the samples. To discriminate the disk sources, we further use near infrared photometric data and the period-luminosity relation if available. Whitelock, Feast and Catchpole (1991) measured the period of bulge IR stars in the JHKL bands, especially for stars in

the galactic latitude between 7 and 8 °. The distance to the stars are therefore known from period-luminosity relations for the $|b| = 7 - 8°$ strips. For this reason we observed the stars in these strips much more than anywhere else.

For sources in regions other than $|b| = 7 - 8°$, we have calculated the probability of a source being the bulge object. The luminosity distribution function of of the bulge IRAS sources can be obtained from the period-luminosity relation given by Whitelock et al. (1991). From this luminosity distribution, we can calculate the probability of the distance to the particular source being within 3 kpc from the galactic center. We have regarded the sources with the bulge probability of more than 50 % as bulge sources and omit the sources with probabilities less than 50 % as disk sources. By this method, we have assigned about 25 % of sources as disk sources.

3. Observations

The intensities of the two lines, SiO J=1-0 rotational lines from the v=1 and 2 states are comparable. In most of sources, two lines of SiO appear at the same radial velocity. This fact secures detections very much for weak sources in this survey. The maser intensity varies very much. For example, we have observed IRAS 17042-2833 several times. In the first two observations, we could not detect the line. However, at the third observation, two years later from the first observation, we got the clear SiO signals. We have repeated the observations several times for undetected sources.

3.1. SIO-OH VELOCITY COMPARISON

The SiO maser velocity is a good indicator of the stellar velocity (Jewell et al. 1991). About 27 SiO sources have OH 1612 MHz masers with the typical double peak profile which is considered to form in the front and receding part of the expanding shell of the star. The center velocity of OH double peaks has been considered as the stellar velocity. For 27 sources, the SiO velocity lies within a $2\,km\,s^{-1}$from the center velociy of OH. This is a strong indication of the SiO velocity equals to the stellar velocity.

3.2. ROTATION OF THE BULGE STELLAR SYSTEM

The main result of this survey is the plot of radial velocities of SiO masers with galactic longitude (figure 1). The radial velocity used here is the velocity in the galactic standard of rest, in which the galactic rotation of $220\,km\,s^{-1}$ of the local standard of rest is subtracted. The best linear fits are shown with the solid line (bulge sources) and dot-dash line (disk sources). The dots deviate from the best fit line appreciably by about $80\,km\,s^{-1}$ and

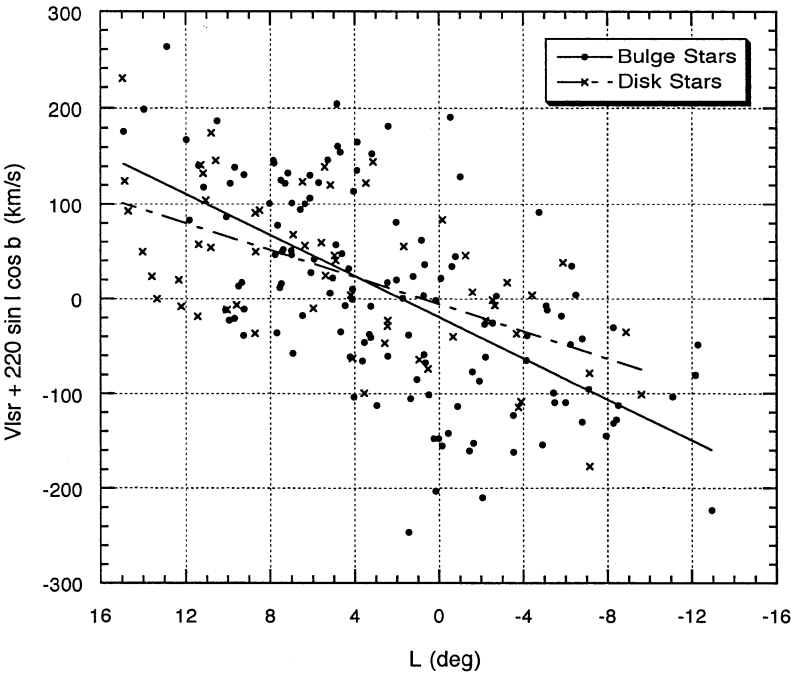

Figure 1. Velocity-Longitude plot for the bulge and disk SiO maser sources.

this would be a random motion of stars in the bulge. The inclination of the best fit line is about $10\,km\,s^{-1}$ per degree for bulge sources. This means the galactic bulge stellar system is rotating around the galactic center. A simple computation leads to a rotation period of approximately $9 \times 10^7 yr$ and an approximate bulge mass of about $1.4 \times 10^{10} M_\odot$ in 2.6 kpc.

One peculiarity imediately recognizable in figure 1 is that the radial velocity is shifted by about $20\,km\,s^{-1}$ from zero at l=0° . This is quite peculiar because we have a net movement of bulge stars. If we see the best fit to the disk sources, the average shift at the zero longitude is nearly equal to zero. So that the radial velocities of disk stars behave as expected.

3.3. WHAT CAUSES THE VELOCITY SHIFT ?

We can consider three explanations for the average overall velocity shift. One is a motion of the local standard of rest, which may be moving toward the galactic center direction. However, this contradicts to the conclusion derived from classic works of HI rotation curve. Kerr (1962) or a recent result of Blitz and Spergel (1991a) concluded that the local standard of rest is moving away from the galactic center with about $14\,km\,s^{-1}$. Of course, this is based on the measurements of HI profile, so that it reflects

the gas motion. Our measurements are based on the stars, so that the gas may have a peculiar motion to the stars.

3.4. TILT OF THE BULGE

The other potential explanation of the velocity shift is observational selection. If the bulge is tilted, the radial velocity must be shifted to the negative side for north strip sources and to the positive side for south strip sources. When we observe the bulge from the nothern hemisphere (at Nobeyama), the negative latitude sources may be undersampled. In such a case, the average velocity may be shifted to the negative side.

To check this possibility, we have plotted the north and south bulge sources separately in the Velocity-Longitude diagram. The best fit curves show that the radial velocities for north bulge sources are shifted by about $10\,km\,s^{-1}$ on average from the radial velocities for the south bulge sources. This indicates that the axis of the bulge stellar system is tilted by about 6 degree from the galactic longitude circle. This result concides with the previous measurement of the tilt of nuclear disk within a observational error, for example, by Burton and Liszt (1978), using HI 21 cm line. However, we have to stress that taking into account the tilt of the bulge, we still get a net shift, i.e., the average of two rotation curves of north and south bulge sources, of about $19\,km\,s^{-1}$.

3.5. POSSIBILITY OF THE BAR STREAMING MOTION

The other possible cause for the velocity shift is another observational selection effect, that is, the streaming motion of stars in the bar-like potential. When the bulge is elongated, the stars observed from the sun must take an elliptical orbit in Velocity-Longitude diagram. When the ellipticity parameter of the bar varies, the orbit changes. If observers selectively pickup forefront stars, that is, brighter stars, we have more stars with negative radial velocities on average. So that the streaming motion may cause the average velocity shift in the Velocity-Longitude map. Probably this is a signature of the dynamics of the bar-like bulge, unless the local standard of rest is moving toward the Galactic center.

3.6. PRESENCE OF FOBIDDEN REGIONS

Another peculiarity to be mentioned is that there are forbidden regions in V-L diagram. There are regions in which no star falls at $(V, l) = (60 \pm 35\,km\,s^{-1}, 3.5 \pm 1°)$ and $(70 \pm 45\,km\,s^{-1}, -3.3 \pm 1.5°)$. This may be an indicator of streaming motion of the bulge which is caused by the bar-like or elongated structure of the bulge potential. These holes are not so large,

and not so clear, so that it may be regarded as statistical fluctuations. The probability of the hole being present in the figure is approximately 0.3 % if the star distribution is random.

We have compared the longitude-velocity map of bulge SiO maser stars with the map of the 21 cm HI line in the nuclear disk with the same galactic longitude. The HI map was taken from Burton and Liszt (1978). The location of SiO holes are quite close to the location of the contour dips of HI. HI therefore shows similar dynamical behavior in terms of the forbidden regions. We should note that the HI nuclear disk is on the galactic plane, that is, in $|b| < 2°$. However, the bulge SiO maps shown here is the data with $|b| > 3°$. So that there are no reason to believe that the dynamics of the disk HI gas is similar to the dynamics of SiO maser stars in the bulge if the gas and stars move independently. Only one explantion for this coincidence is that the bulge is bar-like and the streaming motion of bulge stars influences to the gas motion in the nuclear disk.

4. Conclusion

We have observed 313 IRAS sources on the bulge direction and detected SiO masers in 194 sources. The average rotation velocity is obtained as $-18.7(\pm 7.6)+10.8(\pm 1.2)\,(l/deg)\,km\,s^{-1}$. From this rotation curve, we compute the bulge mass within 2.6 kpc as $1.4 \times 10^{10} M_{\odot}$. The bulge rotation axis is considered to be tilted by about 6°. The presence of holes in V-L map may indicate the streaming motion of the stars.

References

Blitz, L., & Spergel, D. N. (1991a) *ApJ*, 370, 205
Blitz, L., & Spergel, D. N. (1991b) *ApJ*, 379, 631
Burton, W. B., & List, H. S. (1978) *ApJ*, 225, 815
Izumiura, H., Deguchi, S., Hashimoto, O., Nakada, Y., Onaka, T., Ono, T., Ukita, N., & Yamamura, I. (1994a) *ApJ*, (Dec. 10 issue in press)
Izumiura, H., Catchpole, Deguchi, S., Hashimoto, O., Nakada, Y., Onaka, T., Sekiguchi, K., Ono, T., Ukita, N., & Yamamura, (1994b) *ApJ*, (submitted)
Jewell, P. R., Sneyder, L. E., Walmsley, C. M., Wilson, T. L., & Gensheimer, P. D. (1991) *A&A*, 242, 211
Kerr, F. J. (1962) *MN*, 123, 327
Le Squeren, A. M., Sivagnam, P., Dennefeld, M., & David, P. (1992) *A&A*, 254, 133
Lewis, B. M., Eder, J., & Terzian, Y., (1990) *ApJ*, 362, 634
Lindqvist, M., Habing, H. J., & Winnberg, A. (1990) *A&A*, 259, 118
Nakada, Y., Deguchi, S., Hashimoto, O., Izumiura, H., Onaka, T., Sekiguchi, K., & Yamamura, I. (1991) *Nature*, 353, 140
Nakada, Y., Onaka, T., Yamamura, I., Deguchi, S., Ukita, N., & Izumiura, H., (1993) *PASJ*, 45, 179
te Lintel-Hekkert, P., Caswell, J. L., Habing, H. J., Haynes, R. F., & Norris, R. P. (1990) *A&AS*, 90, 327
Whitelock, P., Feast, M., & Catchpole, R. (1991) *MN*, 248, 276

3D N-BODY SIMULATIONS OF THE MILKY WAY

R. FUX, L. MARTINET AND D. PFENNIGER
Geneva Observatory
Ch. des Maillettes 51, CH-1290 Sauverny, Switzerland

1. Introduction

While the existence of a central bar in our Galaxy now seems to be well established, its parameters (such as position angle, extension, axis ratio, angular speed etc...) still remain controversial. The large amount of photometrical and stellar kinematical data becoming now available within $\sim 30°$ of the Galactic Centre should provide potentially new constraints on these parameters. Unfortunately, a detailed barred model of the Milky Way, which would offer a powerful work frame to interpret such observations, does not exist yet. We therefore report here on a first attempt at constructing a 3D dynamically self-consistent barred model of the Galaxy. The idea is to follow the time evolution of a set of 400,000 particles initially distributed according to a plausible axisymmetric mass model of the Milky Way and in virial equilibrium, hoping that a bar will form spontaneously. Gas is not included so far, but will be introduced as a next step in this ongoing work. Some results presented at this meeting will be only quickly summarised here and explained in some more details elsewhere (Fux *et al.* 1995 and *A&A* paper in preparation).

2. Initial conditions

The initial axisymmetric mass distribution includes three components (see Table 1): a radially and vertically exponential disc, representing mainly the Galactic old disc (no division into subpopulations), a so-called nucleus-spheroid (NS) with mass density scaling as $R^{-1.8}$ near the centre, as is observed in the near IR, and as $R^{-3.3}$ in the outer part, as is for example the case for the globular cluster system, and a dark halo (DH) to ensure a flat rotation curve up to at least 30 kpc. All parameters of this mass

L. Blitz and P. Teuben (eds.), Unsolved Problems of the Milky Way, 125–131.
© 1996 *International Astronomical Union.*

model have been adjusted to several observational constraints, assuming $R_o = 8$ kpc.

For each component, we have assumed an isotropic Maxwellian velocity distribution and solved numerically the hydrodynamical Jeans equations for the (isotropic) velocity dispersion σ and the mean azimuthal velocity $\overline{u_\phi}$ (no streaming motion in the other directions). Before starting the main simulation, we let the DH relax for 3 Gyr imposing axisymmetry, and the kinematics of the other components, kept fixed during that time, was in fact calculated with the *final* DH mass distribution. The resulting rotation curve and disc velocity moments are shown in Fig.2a.

TABLE 1. Initial mass model of the simulation. The scale length of the disc is taken from Robin *et al.* (1992) and Fux & Martinet (1994). The oblate NS and DH have a common axis ratio $e = 0.5$

Component	# particles	Space density	Parameters
Disc	150,000	$\propto \exp(-R/h_R - z/h_z)$	$h_R = 2.5$ kpc $h_z = 250$ pc $M = 4.6 \cdot 10^{10}$ M$_\odot$
NS	50,000	$\propto \frac{m^p}{1+m^{p-q}}$, $m^2 = (R^2 + e^2 z^2)/a^2$	$p = -1.8, \quad q = -3.3$ $a = 1$ kpc $(M/L)_K = 0.75$ (solar units)
DH	200,000	$\propto \exp(-\mu)$, $\mu^2 = (R^2 + e^2 z^2)/b^2$	$b = 9.1$ kpc $M = 3.2 \cdot 10^{11}$ M$_\odot$

3. Time evolution

The time integration is achieved using the polar-cylindrical PM code of Pfenniger & Friedli (1993) with a central resolution of 38 pc and a rather short time step of 0.1 Myr because of the strong density peak of the NS component in the centre. We also impose two symmetries, namely reflexions about the z axis and about the Galactic plane. The total integration time is 5 Gyr and thus requires 50,000 time-steps.

The simulation, illustrated in Fig.1, leads to the formation of a bar after about 1 Gyr and then strong spiral arms appear and persist until about 2 Gyr. The extension of the bar is ~ 5 kpc and its axis ratio in the plane ~ 0.5. As one could expect, the spiral arms do heat the disc very efficiently: its radial velocity dispersion almost doubles from 1 to 2 Gyr, while its scale height outside the bar region increases by a factor 1.3. However, the innermost disc ($R < 1$ kpc) does not follow this thickening and surprisingly

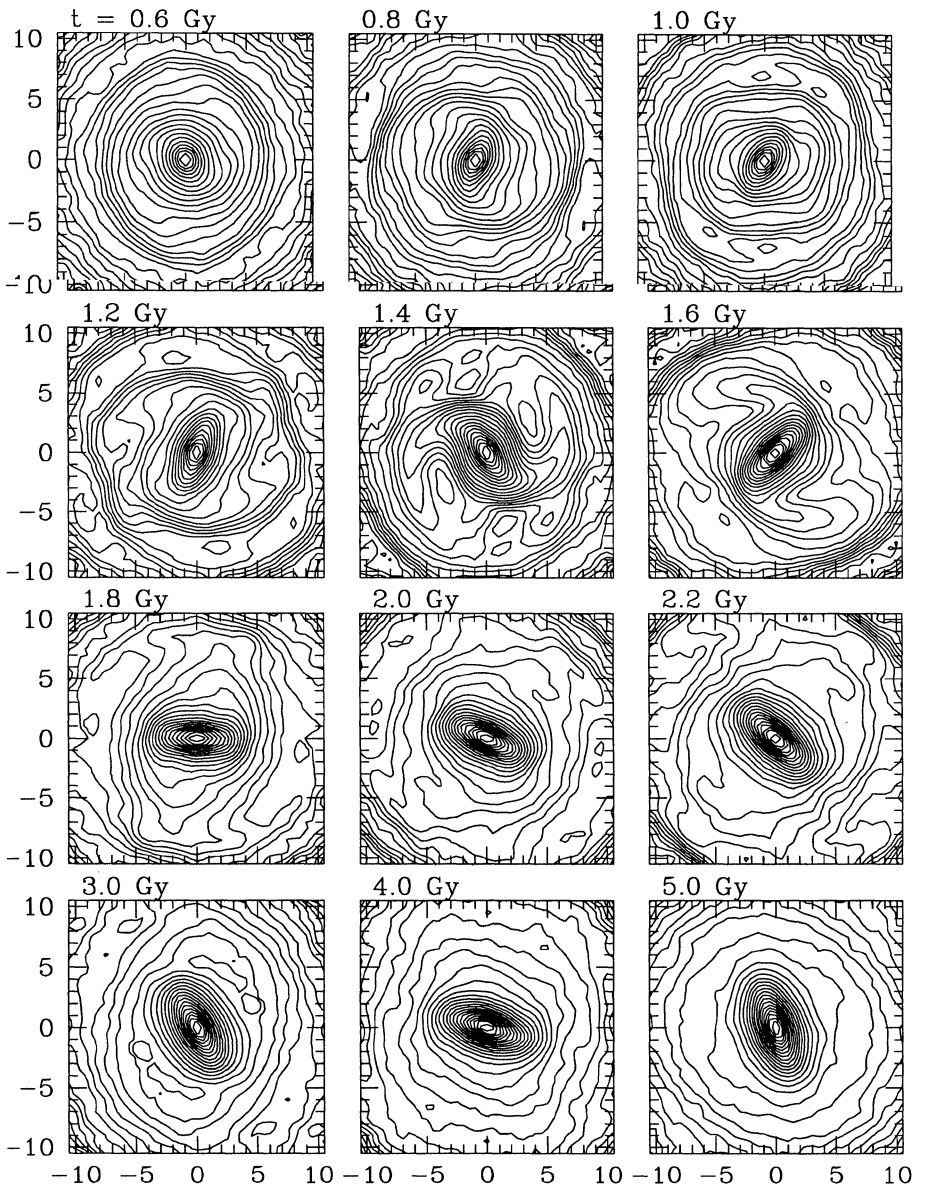

Figure 1. Face-on isodensity curves of the visible components at several times. The length unit is one kpc

becomes the thinnest part of the whole disc.

The velocity dispersion of the disc is closest to the observed one for the Galactic old disc stars at about 1.2 Gyr (see Fig.2b) and then the disc becomes substantially too hot (we expect however that a gas component,

not included in the simulation yet, will reduce this heating). In Fig.2 we also notice that, although we have started with a rather unrealistic isotropic velocity dispersion, the kinematics of the disc evolves spontaneously to anisotropy, with the components of the velocity dispersion just ordered in the same way as observed in the solar neighbourhood, i.e. $\sigma_{RR} > \sigma_{\phi\phi} > \sigma_{zz}$.

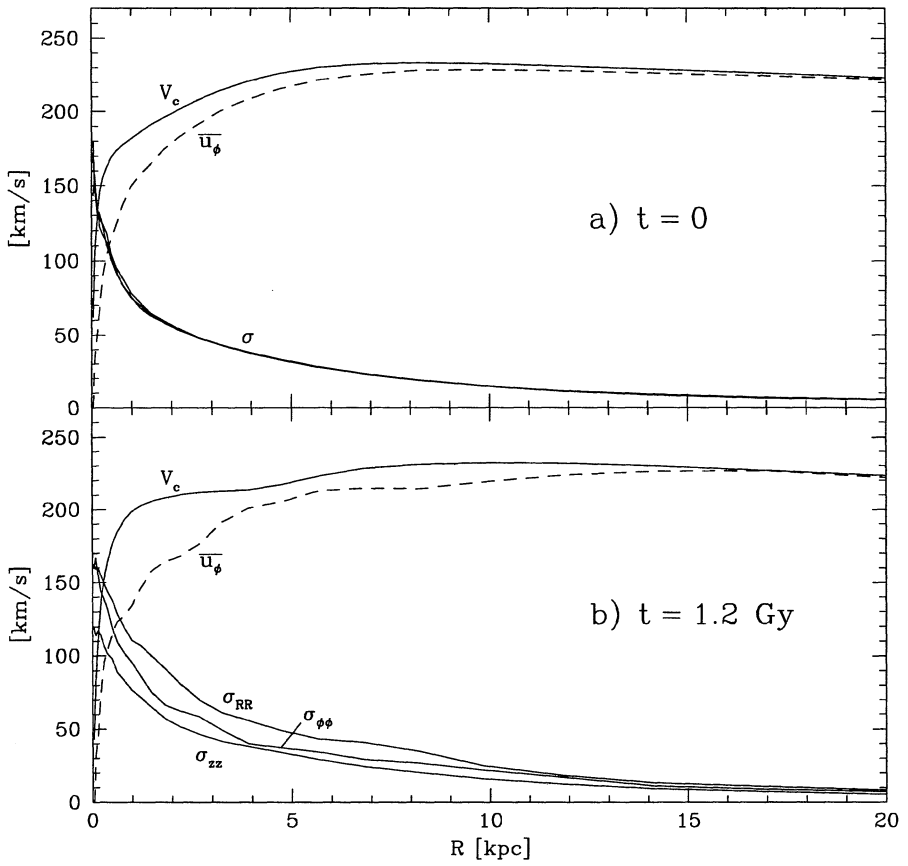

Figure 2. Rotation curve (V_c), and mean azimuthal motion ($\overline{u_\phi}$) and velocity dispersion (σ_{ii}) of the disc

4. Kinematics along Baade's Window

The central radial velocity dispersion of the disc in Fig.2b is not directly comparable to existing observational data in Baade's Window, for example

those given by Lewis and Freeman (1989) for K giants, because the line of sight through this field passes more than 500 pc away from the Galactic Centre. The radial velocity dispersion computed so as to mimic observations in Baade's Window is shown in Fig.3. The result depends within 30% on the position angle of the fictive observer with respect to the bar, the maximum velocity dispersion occurring when the bar is seen end-on. All viewing angles lead to lower velocity dispersions than at $R = 0$.

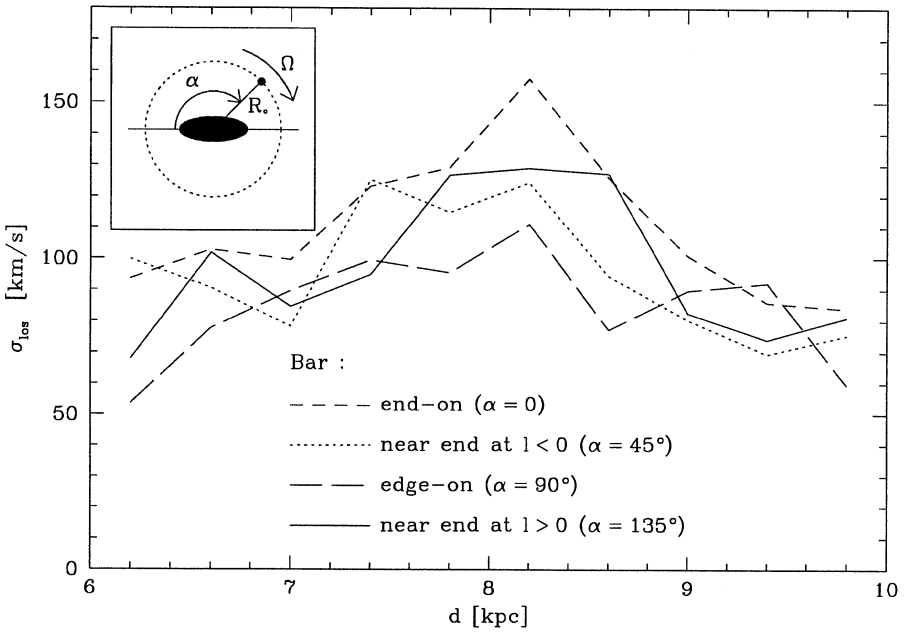

Figure 3. Line of sight velocity dispersion at $t = 1.2$ Gyr when looking towards Baade's Window ($l = 0.9°$, $b = -3.9°$) from points on the solar circle with various position angles relative to the bar. d is the distance from the observing point ($d \approx 8$ kpc close to the Galactic Centre) and α is the angle defined in the small embedded box

5. Isophotes from the Sun's position

During the simulation, the bar pumps disc stars into a peanut bar/bulge over a time scale of 1 Gyr. Fig.4 gives the "isophotes" as they would appear to our fictive observer moving along the solar circle a few Gyr after the formation of the bar. The peanut shape is clearly visible in the edge-on case and the intermediate case with the near end of the bar in the first Galactic quadrant qualitatively resembles COBE's image.

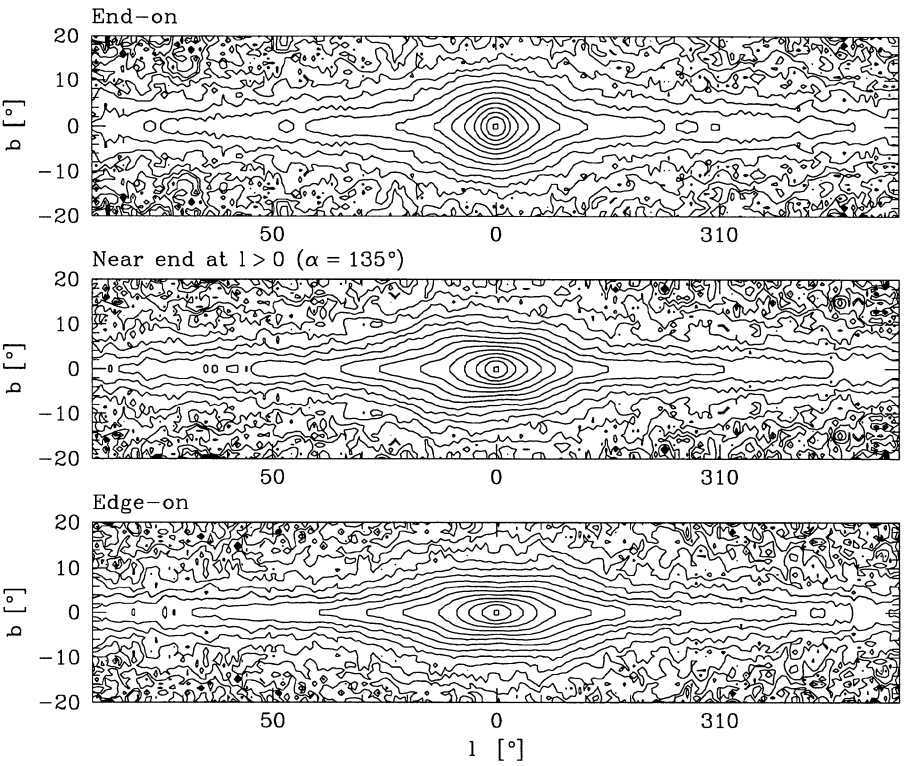

Figure 4. Surface brightness contours of the simulation at $t = 5$ Gyr from various view points located on the solar circle. The contours are obtained from the visible components, assuming that the apparent luminosity of each particle is proportional to its mass divided by the square of its distance

6. Other results

- The corotation radius is close to 5 kpc and the bar angular speed, of 45 km/s/kpc at $t = 2$ Gyr, decreases by $\sim$5 km/s/kpc every Gyr.
- From the velocity field analysis all around the solar circle in our simulation and the commonly accepted position angle of the Sun relative to the bar in the Milky Way (i.e. $\alpha \sim 135°$), one could expect an outward mean radial motion of the disc stars in the Solar Neighbourhood.

References

Fux, R. and Martinet, L. 1994, *A&A*, 287, L21
Fux, R., Martinet, L. and Pfenniger, D. 1995, in *Proceedings: The Formation of the Milky Way*, Granada, september 1994, Cambridge University Press
Lewis, J.R. and Freeman, K.C. 1989, *AJ*, 97, 139
Pfenniger, D. and Friedli, D. 1993, *A&A*, 270, 561
Robin, A.C., Crézé, M. and Mohan, V. 1992, *A&A*, 265, 32

DISCUSSION

J. Palous: May we conclude anything about the bar from the observed vertex deviation of A stars in the solar vicinity?

Fux: The disc in our simulation does not separate into subpopulations like the young A stars. We may therefore only investigate the possible connection between the bar and the local kinematical properties of the dominant disc population, i.e. the old disc stars. The results will be published in a future paper.

COMPARISON WITH EXTERNAL GALAXIES DYNAMICS

F. COMBES

DEMIRM, Observatoire de Paris
61 Ave. de l'Observatoire
F-75014 Paris, FRANCE

Many features of the Milky Way appear weird or unique, because of the peculiar point of view. However the same features are observed more easily and clearly in nearby galaxies. The Milky Way appears to cumulate many dynamical features, such as a bar, a nuclear disk, a perpendicular nuclear bar (?), lopsidedness, an inner ring (molecular ring at 5kpc), a peanut-shape bulge, a warp, and a polar ring. By comparison with external galaxies, and also results from N-body simulations, we can infer the most probable bar angular velocity and length, and interpret the ring features.

1. Bar, nuclear bar

1.1. PRESENCE OF A BAR

It is now widely recognized that our Galaxy is barred, from non-circular motions: 3kpc arm, for instance (Peters 1975, Liszt & Burton 1980), $l - v$ CO parallelogram in the Galactic Center (e.g. Binney et al. 1991), but also from its perspective view (Blitz & Spergel 1991a & b; COBE-DIRBE 2 μm survey Weiland et al. 1994, Hammersley et al. 1994), and even microlensing (Kiraga & Paczynski 1994, Stanek et al. 1994). However, the various authors don't agree on the length, and orientation of this bar (Weinberg 1992). The presence of a bar is not surprising, since the majority of spiral galaxies are barred, more than 2/3 if oval distortions are taken into account. Some bars are only visible in the old stellar component, and revealed in the near-infrared (e.g. Block et al. 1994). It is likely that our bar is not only a Pop II bar, with the Pop I component decoupled, since the bar is so obvious in the molecular component.

L. Blitz and P. Teuben (eds.), Unsolved Problems of the Milky Way, 133–143.
© 1996 *International Astronomical Union.*

1.2. BAR LENGTH AND PATTERN SPEED

According to orbits theory, the bar length can be predicted with respect to the bar resonances (corotation, Lindblad resonances). For instance, a bar cannot extend outside its corotation (cf. Contopoulos 1980). Bars can be considered as standing waves, or the eigen modes of the galaxy host: their characteristics do not depend on the triggering mechanism, for instance an external companion that helps to transfer angular momentum outwards. So the bar pattern speed, at steady equilibrium, depends only on the mass distribution of the galaxy; it slowly evolves in time with increasing mass concentration.

Within the first order epicyclic approximation, stellar orbits can be considered as ellipses precessing at the rate $\Omega - \kappa/2$ (in the rotating frame with precisely that speed, orbits are closed and run two epicycles for one turn). Since $\Omega - \kappa/2$ is a slowly varying function of radius, differential precession is not large, which helps the formation of a density wave. Self-gravity will force equality of all precessing rates. As was shown in the density wave theory (e.g. Lin & Shu 1964), the equivalent epicyclic frequency κ' is lowered by self-gravity, i.e. $\kappa' < \kappa$. This implies a larger precessing rate $\Omega - \kappa'/2$, which is indeed confirmed by N-body simulations: at the beginning of bar formation, still in the linear regime, the bar pattern speed is slightly larger than the maximum of the $\Omega - \kappa/2$ curve. During its growth, however, the bar slows down, loosing angular momentum through the trailing spiral wave. At steady state, the bar pattern speed is usually lower than the maximum of the $\Omega - \kappa/2$ curve. Then two inner Lindblad resonances exist, as testified by the presence of the perpendicular x2 orbits (Sellwood & Sparke 1988). This is always the case in concentrated mass distribution, corresponding to early-type galaxies. The bar extends then up to half the optical disk radius, where the spiral structure takes over, which corresponds to the bar ending a little inside its own corotation (CR).

But a completely different situation can occur in late-type galaxies, with no central mass concentration, where the rotation curve is very slowly rising all over the galactic disk (cf. Combes & Elmegreen 1993). The $\Omega - \kappa/2$ curve is then very flat (it is even zero for $V \propto r$, where $\kappa = 2\ \Omega$). The corresponding low bar speed pushes corotation out of the optical disk, which prevents the bar from growing, by lack of stars near CR. These bars are therefore "truncated" and much shorter relative to their corotation. Direct measurements of the pattern speed from kinematical signatures support this theory, in NGC 4321 and NGC 7479 (Sempere et al. 1994a & b).

In our Galaxy of rather early-type (Sb), the mass concentration is sufficient to be in the first category, i.e. we expect that the bar will extend up to its CR. From the observed rotation curve, the corresponding $\Omega - \kappa/2$

curve (fig. 1), and N-body simulations with stars and gas including similar bulge and disk components, we can infer a bar pattern speed of 40-50km/s, putting the CR at about 4-5 kpc. The bar length would then be 4-5kpc, which corresponds better to the Weinberg (1992) or Hammersley et al. (1994) propositions. This corresponds also to the global gas-dynamical model of our Galaxy by Mulder & Liem (1986).

1.3. NUCLEAR BAR

The much higher pattern speed inferred by Binney et al. (1991) from the CO $l - v$ diagram in the very center could be related to the existence of a nuclear bar in the center of the Galaxy. Indeed, it is very frequent, when the mass concentration is very high in the inner kpc, and when there exists a large central gas fraction (as it appears to be the case for the Milky Way), that a second bar decouples from the first one, and is amplified by non-linear interaction at a common resonance (Tagger et al. 1987): typically the corotation of the small bar is the inner Lindblad resonance (ILR) of the big one. Nuclear bars are observed in external galaxies through isophote twists. They are even more obvious at near-infrared wavelengths (cf. Shaw et al. 1993).

Two main interpretations can be proposed for these isophote twists: first, in the presence of two inner Lindblad resonances, the family x2 of perpendicular periodic orbits is the cause of phase shifts in the gas component; once enough gas is gathered in the center, a fraction of the stellar component follows its potential (Shaw et al. 1993). Second, a nuclear bar decouples from the main bar, with a larger pattern speed: it is the bar within bar phenomenon, as suggested by Shlosman et al. (1989), and demonstrated by Friedli & Martinet (1993) and Combes (1994a). This second mechanism occurs in simulations with a more viscous gas, i.e. with a large velocity dispersion. The presence of the second fast bar is difficult to predict. It is a relatively transient phenomenon, its life-time being of the order of a few 10^8 yrs, and depends on gas accretion. When gas accretion is fast enough, the consequent star formation yields enough energy in the central gas that its equivalent viscosity then can trigger the nuclear bar decoupling.

Parallel (x1) and perpendicular orbits (x2 in the notation of Contopoulos & Mertzanides 1977) are clearly observed in our Galaxy, through the $l - v$ diagram of the HI and CO emission. The x1 periodic orbits aligned parallel to the bar, and in particular, the cusped ones delineate a parallelogram in the $l - v$ plot, that is reminding of the shape of the $l - v$ CO diagram from the survey of Bally et al. (1988). The orbits x2, perpendicular to the bar between the two inner Lindblad resonances, also seem to fit the line of enhanced CO intensity following the diagonal of the parallel-

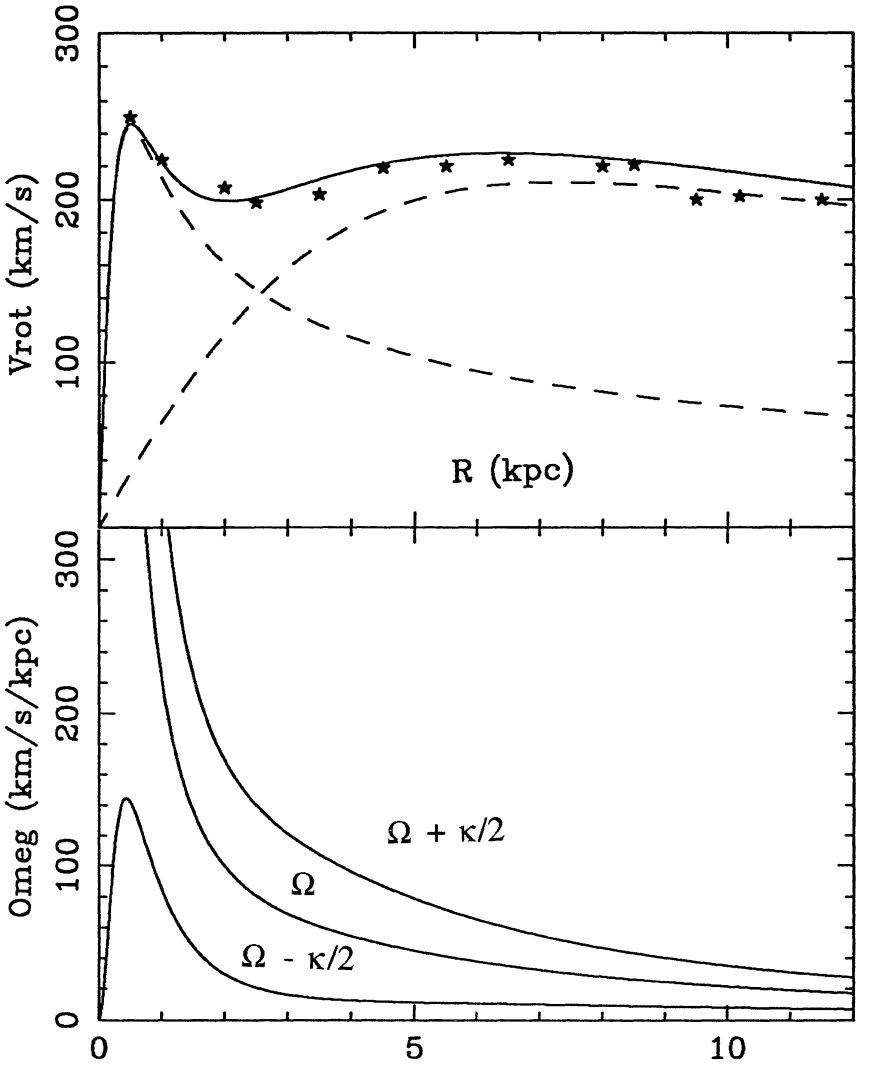

Figure 1. Rotation curve fit of the Galaxy: a) the stars are the average of observed points, as compiled by Fich & Tremaine (1991); the dashed lines represent the contributions of the bulge (1.1 10^{10} $M_\odot$) and disk (7.2 10^{10} $M_\odot$ within 12kpc). It was not necessary to add any dark halo within 12kpc. b) The corresponding frequencies Ω, $\Omega - \kappa/2$, and $\Omega + \kappa/2$, and the suggested value of the bar pattern speed Ω_p.

ogram. In early-type external galaxies possessing a nuclear bar, the latter is confined inside the nuclear ring, which corresponds to the wide location of the inner resonance; the nuclear ring is formed by the x2 orbits, which are much rounder than the x1. Since it is likely that the nuclear disk in the

Milky Way center corresponds also to orbits trapped around the x2 family, their excentricity is not large; this implies that the velocities are not highly non-circular, and supports the validity of the observed rotation curve of fig. 1.

The deformation of the parallelogram when different latitudes are taken into account in the $l-v$ diagram suggests that the elongated x1 orbits are slightly tilted, such that their extremities (at quasi zero velocity) do not lie at zero latitude. A slight tilt of 3° would be sufficient to explain the observations (Combes 1994b).

2. Nuclear disk

A nuclear disk is often apparent in galaxies as a separate dynamical component, revealed by large rotational velocities towards the center (inner kpc). It is a large mass concentration, mainly gaseous. When seen almost face-on, these objects reveal frequently a nuclear ring of star formation, i.e. the Hα regions are concentrated in an annulus centered on the nucleus. Conspicuous examples are NGC 4321 (Arsenault et al. 1988), NGC 1097 (Hummel et al. 1987). A large amount of molecular hydrogen has been traced in these galaxies, with large velocity gradients (Garcia-Burillo et al. 1994, Gerin et al. 1988).

When seen almost edge-on, these objects are peculiar from their large radial velocity gradients, as in the Milky Way (fig.2a, Dame et al. 1987). This peculiar kinematical behaviour in the center is not an exception, but is frequently encountered in external galaxies. This has been revealed by the high resolution observations in the CO emission of the central molecular component. NGC 891 (fig. 2b), which has been called the "sosie" of the Milky Way from its morphological type, presents a position-velocity diagram along the major axis very similar to the $l-v$ diagram of fig. 2a: there is a sharp velocity gradient inside the central 20"=1kpc, and the maximum apparent rotational velocity (260km/s) is reached there, while the outer disk has a flat rotation at 225km/s (Garcia-Burillo et al. 1992); it forms a separate component, in the sense that there is a shortage of CO emission between the nuclear disk (of radius 230pc) and the outer molecular ring, as in the Milky Way. The nuclear disk has a counter part in IR and radiocontinuum emission, as well as in Hα emission (Garcia-Burillo et al. 1992).

Such sharp gradients are also obtained through HI absorption in NGC 660 (van Driel et al. 1994) and NGC 1808 (Koribalski et al. 1993), as well as in the CO emission for NGC 3079 (Sofue & Irwin 1992), NGC 4945 (Dahlem et al. 1993), or even NGC 6946 (Casoli et al. 1989). Table 1 summarises the best evidences for gaseous nuclear disks in external spiral galaxies.

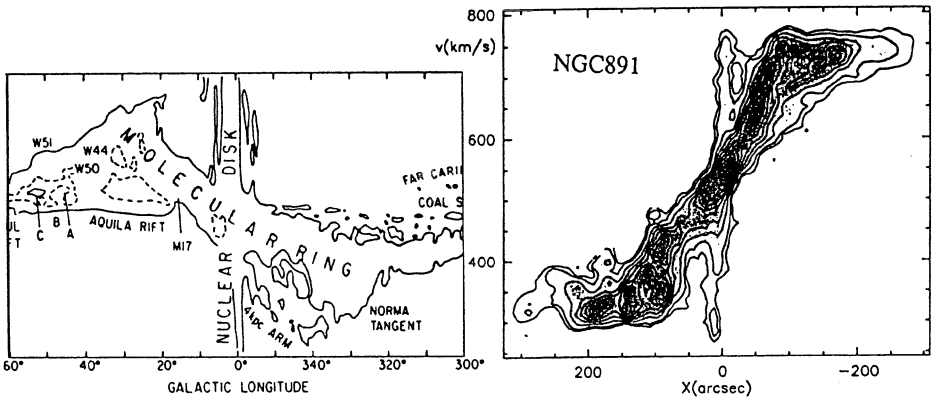

Figure 2. a) CO $l - v$ diagram of the central Milky Way, from Dame et al. (1987); b) CO(2-1) position-velocity diagram of NGC 891, from Garcia-Burillo et al. (1992).

3. Lopsidedness

The nuclear disk of the Milky Way appears strongly off-center: about 3/4th of the CO emission is at positive longitudes (and positive velocities, e.g. Bally et al. 1988). Lopsidedness is very frequently observed in external galaxies (e.g. recent images in Block et al. 1994). Already de Vaucouleurs & Freeman (1970) noticed that M33 and M101 have nuclei not-coinciding with mass centers of the galaxies. Baldwin et al. (1980) discuss properties of m=1 deformed galaxies. The nucleus of our nearest spiral neighbour M31 is displaced by 3-5 pc from the gravity center (Light et al. 1974, Nieto et al. 1986, Kormendy 1988). Recently, observations with high spatial resolution, with the 2D TIGER spectrograph, have shown that the velocity field, although regular, is displaced with respect to the light peak (Bacon et al. 1994). HST observations (Lauer et al. 1993) also suggest the presence of two components (nuclei?) in the center.

Off-centering is so frequent that it cannot be explained by transient phenomena, such as tidal effects for instance, but a physical mechanism must explain their persistence. Miller & Smith (1992) have revealed the existence in simulated disks of a density wave of the m=1 symmetry, corresponding to an oscillatory motion of the nucleus with respect to the galaxy disk. Weinberg (1994) has shown that the m=1 instability is in fact not as quickly damped as previously thought; there can exist very weakly damped m=1 modes, that persist during 10-100 crossing times, in which the peak density slowly revolves about the mass center.

This lopsidedness in the center could be related to the tilt of orbits with respect to the Galactic plane (e.g. Burton & Liszt 1993). The central gas

TABLE 1. Nuclear Disks in Spiral Galaxies

Galaxy	Type	Nuclear disk size	Ref
Milky Way	Sb	250pc	1
NGC 660	SBa	800pc	2
NGC 891	Sb	250pc	3
Maffei 2	Sbc	200pc	4
NGC 1068	Sb	1.5kpc	5
NGC 1097	SBb	800pc	6
IC342	Sc	100pc	7
NGC 1808	SABbc	250pc	8
M82	Irr	250pc	9
NGC 3079	Sc	600pc	10
NGC 3351	Sb	350pc	11
NGC 4314	SBa	350pc	12
NGC 4321	Sc	900pc	13
NGC 4945	SBc	400pc	14
M51	Sc	550pc	15
NGC 5236	SBc	200pc	16
NGC 6946	Sc	500pc	17

1- Dame et al. (1987); 2- van Driel et al. (1994); 3- Garcia-Burillo et al. (1992); 4- Ishiguro et al. (1989); 5- Planesas et al. (1991); 6- Gerin et al. (1988); 7- Ishizuki et al. (1990); 8- Koribalski et al. (1993); 9- Lo et al. (1987); 10- Sofue & Irwin (1992); 11- Devereux et al. (1992); 12- Combes et al. (1992); 13- Garcia-Burillo et al. (1994); 14- Dahlem et al. (1993); 15- Rand & Kulkarni (1990); 16- Handa et al. (1990); 17- Casoli et al. (1990)

disk might be warped, and the m=1 wave associated to a precession.

4. Inner ring

A conspicuous feature in our galaxy is the presence of the molecular ring, between 4 and 8kpc (see fig. 2a). Such rings are very precious in external galaxies as indicators of the pattern speed of the bar, since they correspond to resonances with the bar (or spiral).

Binney et al. (1991) in their fast bar model, interpret this ring as the outer Lindblad resonance (OLR), corresponding therefore to the usual outer rings observed in external barred galaxies. However, OLR in general occur at the outskirts of optical disks, and have no CO emission (because of metal deficiency), but are rich in atomic gas. The position of the OLR in the middle of the disk would then be unique. We prefer to interpret the molecular ring as the inner ring occuring at the ultra-harmonic resonance UHR, just inside the corotation region. These inner rings are frequent in

barred galaxies, and encircle the bar (Buta & Combes 1994). This will correspond to the 4-5 kpc bar model. The main feature here is the depletion of the region inside CR by the gravity torques, where no molecular gas is seen (e.g. Combes 1988).

5. Box-Peanut

The COBE-DIRBE maps have revealed not only the bar (Weiland et al. 1994, Arendt et al. 1994), but also a very conspicuous box-peanut shape bulge in the center of the Galaxy. This shape is frequently observed in edge-on external galaxies (de Souza & dos Anjos 1987), and can be explained by a z-resonance effect with the bar (Combes et al. 1990). This feature confirms the existence of a strong bar in the center, and could help to determine its length. Since the box should end with the bar at R_b, its final longitude l is related to the angle θ between the bar and the Sun-Galactic Center axis, and to the solar radius R_0 by:

$$R_b = R_0 sin(l) sin(l - \theta)(sin^2 l - sin^2 \theta)^{-1}$$

If we adopt R_0=8.5 kpc, $\theta = 20°$, and $l = 21°$, this yields $R_b = 4.6$ kpc. This is only an order of magnitude, since a complete model, including the bar thickness in the plane, is necessary.

6. Warp and polar ring

The Galaxy plane appears clearly warped in the HI distribution (e.g. Burton 1992), but also in the interstellar dust layer and stellar disk, as revealed by COBE-DIRBE maps (Freudenreich et al. 1994). The stellar disk is warped at half the amplitude, which is certainly due to the radial truncation of the stellar disk. This is currently observed in external galaxies. Although almost every HI disk is warped, the stellar disks are much less frequently warped, and present only small distortions (Sanchez-Saavedra et al. 1990). The correspondence in azimuth of the stellar and HI warp indicates that the line of nodes is straight in the Milky Way, as for most of the galaxies (Briggs 1990). This straight line of nodes is still an unsolved problem, when account is taken of differential precession. The warp is however not symmetrical, being 4 times higher in the northern part (Burton 1992). This asymmetry could be attributed to the tidal perturbations of the Magellanic Clouds. Finally, the Galaxy has also a ring of matter similar to polar rings around external galaxies, orbiting around its poles: the Magellanic stream and related matter. The ring is in the settling process (Lin et al. 1993).

7. Conclusions

Our Galaxy is most probably barred, but the orientation, dimensions and pattern speed of the bar are difficult to obtain directly. By comparison with external galaxies and from the experience gained by N-body simulations, we can infer the bar length and speed from the observed mass distribution. If we believe the observed rotation curve, our Galaxy has a high central mass concentration, and the nature of its bar should correspond to the early-type barred galaxies: its pattern speed can be scaled from N-body simulations to 40-50km/s/kpc, corresponding to corotation at 4-5 kpc. The bar length is then expected to be 4-5 kpc in radius. If the molecular ring is real (i.e. not only spiral arms accumulation on the line of sight), it can then easily be interpreted as the inner ring encircling frequently the bars in external galaxies, and corresponding to UHR (ultra-harmonic resonance).

A nuclear disk component is obvious in the central gas kinematics: a large gas mass is observed with high rotation, with velocity not so far from circular. Its position corresponds to the wide region of inner Lindblad resonance, and evidence is found of x2 perpendicular orbits. External galaxies with such a nuclear disk or ring display a nuclear bar confined in the ring, aligned or not with the main bar. Because of the large mass concentration, and large gas fraction in the center, our Galaxy is also a good candidate for a nuclear bar, decoupled or not in velocity from the main one.

There is a significant lopsidedness in this nuclear component, which is not centered on the center-of-mass of the large-scale Galaxy. These asymmetries are also frequent in external galaxies. This could be related to the inner disk tilt. The box-peanut shape of the bulge might be a consequence of the bar, and gives a constraint between the bar orientation and length.

References

Arendt R.G. et al. : 1994, ApJ 425, L85
Arsenault R., Boulesteix J., Georgelin Y., Roy J-R.: 1988, A&A 200, 29
Bacon R., Emsellem E., Monnet G., Nieto J.L.: 1994, A&A 281, 691
Baldwin J.E., Lynden-Bell D., sancisi R.: 1980, MNRAS 193, 313
Bally J., Stark A.A., Wilson R.W., Henkel C.: 1988, ApJ 324, 223
Binney J., Gerhard O.E., Stark A.A., Bally J., Uchida K.I.: 1991, M.N.R.A.S 252, 210
Blitz L., Spergel D.N.: 1991a, ApJ 370, 205
Blitz L., Spergel D.N.: 1991b, ApJ 379, 631
Block D.L., Bertin G., Stockton A., et al.: 1994, A&A 288, 365
Briggs F.H.: 1990, ApJ 352, 15
Burton W.B., Liszt H.S.: 1993, A&A 274, 765
Burton W.B., 1992, in "The Galactic Interstellar Medium", SAAS-FE, ed. D. Pfenniger & P. Batholdi, p. 126
Buta R., Combes F.: 1994, Fundamental of Cosmic Physics, p.
Casoli F., Clausset F., Viallefond F., Combes F., Boulanger F.: 1990, A&A 233, 357
Combes F.: 1988, in "Galactic and Extragalactic Star Formation", ed. R.E. Pudritz & M. Fich, Kluwer, p. 475-494

Combes F., Debbasch F., Friedli D., Pfenniger D.:1990, A&A 233, 82
Combes F., Gerin M., Nakai N., Kawabe R., Shaw M.: 1992, A&A 259, L27
Combes F.: 1994a, in "Mass-transfer induced activity in galaxies", ed. I. Shlosman, Lexington conference, Cambridge University Press, p. 170
Combes F.: 1994b, in "Nuclei of normal galaxies" ed. R. Genzel, Ringberg conference, p.
Combes F., Elmegreen B.G.: 1993, A&A 271, 391
Contopoulos G.: 1980, A&A 81, 198
Contopoulos G., Mertzanides C.: 1977, A&A 61, 477
Dahlem M., Golla G., Whiteoak J.B. et al.: 1993, A&A 270, 29
Dame T.M., Ungerechts H., Cohen R.S. et al.: 1987, ApJ 322, 706
de Vaucouleurs G. Freeman K.C.: 1970, IAU 38, 356
de Souza R.E., dos Anjos S: 1987, A&AS 70, 465
Devereux N.A., Kenney J.D.P., Young J.S.: 1992, AJ 103, 784
Fich M., Tremaine S.: 1991, ARAA 29, 409
Friedli D., Martinet L.: 1993, A&A 277, 27
Freudenreich H.T. et al. : 1994, ApJ 429, L69
Garcia-Burillo S., Guélin M., Cernicharo J., Dahlem M.: 1992, A&A 266, 21
Garcia-Burillo S., Sempere M., Combes F.: 1994, A&A in press
Gerin M., Nakai N., Combes F.: 1998, A&A 203, 44
Handa T., Sofue Y., Nakai N., Hayashi M., Fujimoto M.: 1990, PASJ 42, 1
Hammersley P.L., Garzon F., Mahoney T., Calbet X.: 1994, MNRAS 269, 753
Hummel E., van der Hulst J.M., Keel W.C.: 1987, A&A 172, 32
Ishiguro M., Kawabe R., Morita K-I et al. : 1989, ApJ 344, 763
Ishizuki S., Kawabe R., Ishiguro M. et al. : 1990, Nature 344, 224
Kiraga M., Paczynski B.: 1994, ApJ 430, L101
Koribalski B., Dickey J., Mebold U.: 1993, ApJ 402, L41
Kormendy J.: 1988, ApJ 325, 128
Lauer T.R. et al.: 1993, AJ, 106, 1436
Light E.S., Danielson .E., Schwarzschild M.: 1974, ApJ 194, 257
Lin C.C., Shu F.H.: 1964, ApJ 140, 646
Lin D.N.C. et al. : 1993, BAAS
Liszt H.S., Burton W.B.: 1980, ApJ 236, 779
Lo K.Y., Cheung K.W., Masson C.R. et al.: 1987, ApJ 312, 574
Miller R.H., Smith B.F.: 1992, ApJ 393, 508
Mulder W.A., Liem B.T.: 1986, A&A 157, 148
Nieto J.L., Macchetto F.D., Perryman M.A.C et al. : 1986, A&A 165, 189
Peters W.L.: 1975, ApJ 196, 617
Planesas P. Scoville N.Z., Myers S.T.: 1991, ApJ 369, 364
Rand R.J., Kulkarni S.R.: 1990, ApJ 349, L43
Sanchez-Saavedra M.L., Battaner E., Florido E.: 1990, MNRAS 246, 458
Sellwood J.A., Sparke L.S.: 1988, MNRAS, 231, 25P
Sempere M., Garcia-Burillo S., Combes F.: 1994a, A&A, in press
Sempere M., Combes F., Casoli F.: 1994b, A&A, in press
Shaw M.A., Combes F., Axon D.J., Wright G.S.: 1993, A&A 273, 31
Shlosman I., Frank J., Begelman M.: 1989, Nature 338, 45
Sofue Y., Irwin J.: 1992, PASJ 44, 353
Stanek K.Z. et al.: 1994, ApJ 429, L73
Tagger M., Sygnet J.F., Athanassoula E., Pellat R.: 1987, ApJ 318, L43
van Driel W., Combes F., Casoli F., et al.: 1994, A&A submitted
Weiland J.L. et al. : 1994, ApJ 425, L81
Weinberg M.D.: 1992, ApJ 384, 81
Weinberg M.D.: 1994, ApJ 421, 481

DISCUSSION

O. Gerhard: We have recently analyzed the oval-disk galaxy of M94. This contains a nuclear bar with half-length ~20" (Mollenholft et al. AA submitted), inside the well-known inner ring at r=45" Assuming that this bar extends to somewhat inside its corotation radius we obtain a pattern speed which places the new ring at the OLR of the bar. According to your models, it is also at the ILR of the outer rotating oval. Is this ratio of pattern speeds also seen in some of your simulations? If not, what physical mechanism causes the preferred coincidence of inner bar-CR with outer bar-ILR that you described?

Combes: There are not yet enough N-body runs to have encountered all cases possible. However, I will guess that in the case you propose, the ratios of the two pattern speeds is then much larger, which necessitate a much larger mass concentration.

P. Schechter: If the orbits at the center of the arc are nearly circular, they imply a larger value for the stellar velocity dispersion than is observed. Is this cause for discomfort?

Combes: I don't think it raises a problem. The main distribution in the center, determined from stellar kinematics and IR photometry essentially, gives already rotational velocity of 200-250km/s at 100pc ($1\text{-}2\times10^9$ $M_\odot$ within 100pc).

PROPERTIES OF THE GALACTIC BAR FROM HYDRODYNAMICAL SIMULATIONS

BENJAMIN J. WEINER AND J.A. SELLWOOD
Dept. of Physics and Astronomy, Rutgers University
P.O. Box 849, Piscataway, NJ 08855, USA

It is well known that the existence of H I and CO gas at "forbidden" velocities in longitude-velocity (l–V) diagrams of the inner Galaxy (*e.g.* Liszt & Burton 1980, Liszt 1992) is inconsistent with circular motion in an axisymmetric potential. Gas flow in a barred potential could be consistent with the observations, however. We have compared the observations to 2-D hydrodynamical simulations of gas flows in a family of barred potentials. The gas flow pattern is very sensitive to the assumed potential, and the l–V distribution of cool gas in the inner Galaxy places strong constraints on several parameters of the Milky Way bar.

We use a 2-D grid-based hydrodynamical code (kindly provided by E. Athanassoula) to model the gas flow (van Albada 1985, Athanassoula 1992). This is an Eulerian grid code for an isothermal gas in an imposed potential, taken to be due to the stellar component and halo. We use a mass model with three components: a modified Hubble bulge, a Rybicki disk (representing both the disk and the halo), and a prolate Ferrers $n = 1$ bar. Each model is specified by seven parameters for these components, and the pattern speed of the bar. The velocity field of the gas reaches a steady state by about 0.15 Gyr; we continue the simulation to roughly 0.4 Gyr, and then project the density and velocity data into l–V diagrams as would be seen by an observer at the solar radius, at various viewing angles to the bar.

We concentrate our attention on the shape of the extreme–velocity envelope of the Galactic H I l–V diagram (see Liszt 1992, Fig. 2); the H I should probe the maximum velocity attainable and the outer contour is unaffected by clumpiness. As the band of emission at $|v| < 80$ km s^{-1} is due to foreground (Liszt, private communication), we compare only to the shape of the contour at higher velocities. Notable features of the l–V diagram are (1) sharp peaks at $l = +3°$ and $-4°$, which require either a peak in the rotation curve or strong non-axisymmetric motions, and (2)

L. Blitz and P. Teuben (eds.), Unsolved Problems of the Milky Way, 145–146.
© 1996 *International Astronomical Union.*

emission in the "forbidden" quadrants – there is gas at positive longitude, out to $l = 6°$, with negative (approaching) velocities, and vice versa; this is impossible in a stationary axisymmetric system.

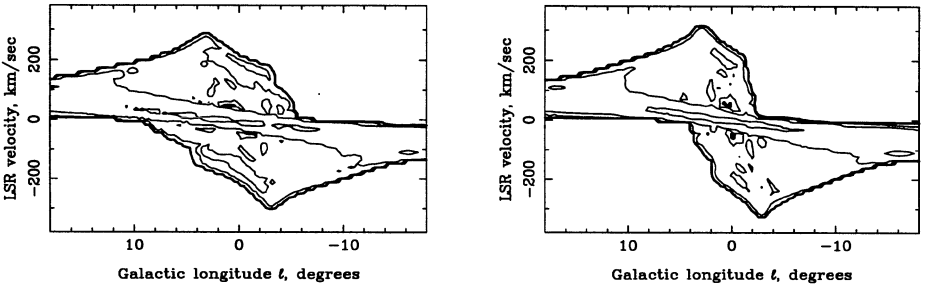

Figure 1. (a) Longitude-velocity diagram for our best-fitting model of the Galactic bar, viewed at 35° to the major axis of the bar. The contours are stepped logarithmically by a factor of 10. (b) The same model viewed at 20° to the major axis.

We have run over 40 models, varying the parameters of the potential, and constructed l–V diagrams. The l–V diagram of our best model is shown in Figure 1(a); this model has a bar with semimajor axis 3 kpc, axis ratio 4:1, mass $8 \times 10^9 M_\odot$, and Lagrangian radius 3.6 kpc, and best matches the data when viewed at 35° to the major axis of the bar. The emission at the peaks in the l–V diagram tends to come from gas streaming along the bar, relatively close to the center. The model has straight shocks at an angle to the major axis of the bar, as in many of Athanassoula's (1992) models. The emission in the forbidden quadrants comes from gas which is approaching these shocks from behind. Hence the lengths of the shocks limit the angular extent of the emission in the forbidden quadrants. If the bar is too small, or too close to end-on, the shocks subtend a smaller angle in longitude and the emission in the forbidden quadrants is cut off, as seen in Figure 1(b).

In order to match the data we have had to do considerable fine–tuning of the parameters; we do not claim that ours is a unique model for the Galactic potential. However the sensitivity of the l–V diagram to the assumed potential and the need for fine-tuning suggest that large regions of parameter space are inconsistent with the observations. In particular we suggest that a bar which is closer than 20° to end-on cannot generate the emission observed in the forbidden quadrants of the l–V diagram.

References

Athanassoula, E. 1992, *MNRAS* 259, 345.

Liszt, H.S. 1992, in *The Center, Bulge, and Disk of the Milky Way,* ed. L. Blitz, (Dordrecht: Kluwer), p. 111.

Liszt, H.S., & Burton, W.B. 1980, *Ap. J.* 236, 779.

van Albada, G.D. 1985, in *The Milky Way Galaxy, IAU Symp. 106,* ed. H. van Woerden et al. (Dordrecht: Kluwer), p.547.

POSITION-VELOCITY DIAGRAMS AS A PROBE OF THE BAR IN EDGE-ON GALAXIES

The Face-on View of our Galaxy

KEIICHI WADA
Center for Information Processing Education, Hokkaido Univ., Sapporo 060, Japan

TETSUO HASEGAWA, YOSHIAKI SOFUE
Institute of Astronomy, The Univ. of Tokyo, Mitaka, Tokyo 181, Japan

YOSHIAKI TANIGUCHI
Astronomical Institute, Tohoku Univ., Sendai 980-77, Japan

AND

ASAO HABE
Dep. of Physics, Hokkaido Univ., Sapporo 060, Japan

Analyses of the distribution of far infrared point sources in the Galactic bulge have suggested that from a face-on perspective the bulge has a bar like shape. Here, we investigate how a rotating bar-like bulge affects the global gas dynamics in a disk and compare the longitude-velocity (LV) maps from selfgravitating hydrodynamical simulations[1] with observed maps of neutral hydrogen and carbon monoxide in the Galaxy. We found that the features on the numerical LV maps depend strongly on four factors: the pattern speed of the bar, the position angle of the Sun, the strength of the bar potential and the ratio of the gas mass to total dynamical mass. We conclude that our Galaxy has a rotating, weak, bar-like bulge ($a/b \sim 0.8$) observed from nearly end on ($\theta_p < 20°$). The allowed range of pattern speed of the bar is surprisingly narrow ($\sim$ 20 km s^{-1} kpc^{-1}) and is consistent with recent observations of bulge stars. Selfgravity of the interstellar matter is needed to account for some of the observations.

We can also apply the presented method to the studies of external edge-on galaxies. For example, the well-studied nearby edge-on disk galaxy NGC 891 also has a central high velocity component and a molecular ring on its observed HI and CO [2]. The present study suggests that NGC 891 is quite similar to our Galaxy not only from the edge-on view, but also the face-

L. Blitz and P. Teuben (eds.), Unsolved Problems of the Milky Way, 147–148.
© 1996 *International Astronomical Union.*

on view. Note that our Galaxy and NGC 891 are not necessarily 'barred' galaxies but are ordinary spiral galaxies classified as Sb $\sim$ Sc in the classification scheme of Hubble. Our Galaxy and NGC 891 should look like NGC 309 (Sc) which has a weakly-distorted bar with two open spiral arms in the infrared light but shows very rich star forming regions in the disk[3].

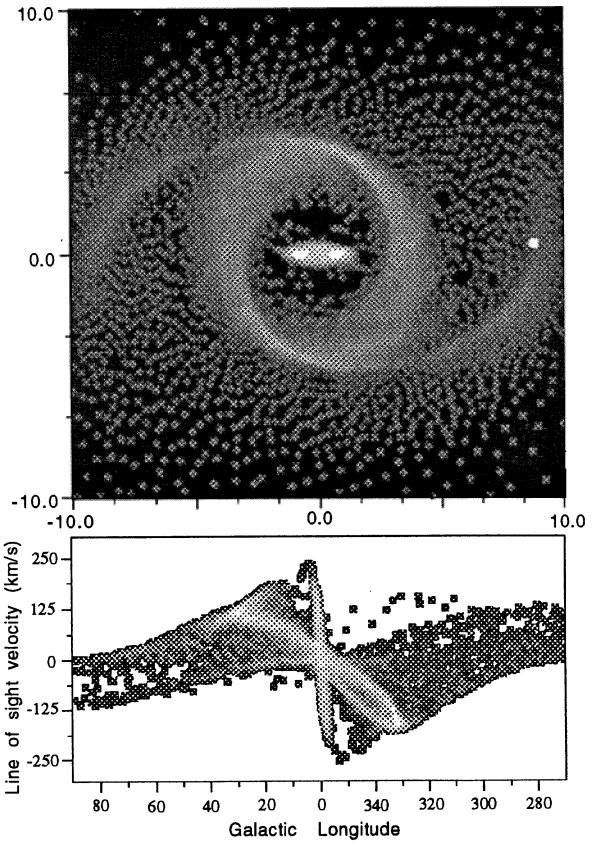

Figure 1. (Top) Gas density distribution of our Galaxy. The most probable position of the LSR is shown by a white filled circle. (Bottom) Position-Velocity diagram from the LSR.

One of the authors (KW) would like to thank the Nukazawa Science Foundation for their travel support.

References

Wada, K. & Habe, A. 1992 MNRAS, 258, 82.
Sofue, Y. & Nakai, N. 1993, PASJ, 45, 139.
Block, D.L., & Wainscoat, R.J. 1991, Nature, 353, 48.

Chapter 3

What is the Nature of the Center of the Galaxy?

IS THERE A COMPACT CENTRAL MASS CONCENTRATION IN OUR GALAXY?

CHARLES H. TOWNES
University of California at Berkeley
Berkeley, CA 94720

1. Introduction

Since the center of our own galaxy is the closest region of this type, it should provide a proving ground for our understanding of such regions. And fortunately, recent developments in radio, infrared, and x-ray astronomy allow us to look at the center of our galaxy in considerable detail – a privilege not possible in the visible region because of the rather dense dust clouds surrounding it. We find there many complex and interesting phenomena, including evidence for a compact central mass of a few million solar masses from the dynamics of stars and gases. However, its existence has been doubted because the radiant energy coming from the very center is much less than normal theoretical expectations for a black hole of such a mass. This discrepancy has led to speculation whether the velocity measurements could be misleading, whether the concentrated mass is in some form other than the expected black hole, whether the radiation might be taking place in an exotic form, being directed away from us or happening to be low at the moment, or whether our theories of such radiation are as yet incomplete. The general characteristics of the very central region of our galaxy will be reviewed along with the dynamic evidence for a large concentrated mass and comparison of the radiation it emits with that of various theoretical models.

2. The Central Region of our Galaxy and Sgr A*

Radiation from the center of our galaxy was first seen in the radio region in 1932 by Jansky (1932), but it was only in the recent few decades that the growing fields of radio interferometry and infrared astronomy have allowed

L. Blitz and P. Teuben (eds.), Unsolved Problems of the Milky Way, 149–168.
© 1996 *International Astronomical Union.*

us to see details of composition and structure in this region. Plate 1 provides high resolution radio maps of the region made with the VLA, showing four panels of different intensity levels. The blue color is used to indicate synchrotron type radiation and red color for thermal radiation from ionized gas. At the lowest exposure, the intense point source known as Sagittarius A* shows up very prominently. This point source is a strong candidate for a black hole, and is possibly the heavy black hole indicated by dynamical measurements. However, its radiated intensity is orders of magnitude weaker than first expectations for such an object.

Surrounding the ionized region of Plate 1 is relatively warm molecular gas, of temperature about 200-300K. Figure 1 shows a map by Güsten et al. (1987) of the HCN $0 \rightarrow 1$ transition in this warm, dense, and clumpy gas. Large variations in density are indicated on the map. The dark central region in its center contains very few molecules, but is occupied by the ionized gas shown in Plate 1 along with some atomic material. At increasing radii from the center of the galaxy, the HCN radiation fades out. This does not mean that no HCN is present, but rather that the temperature and densities are too low for this particular transition of HCN to be strongly excited. In fact, clumpy clouds and somewhat turbulent motion continue for some distance from the center, as shown by observations of CO and other molecules.

The hole in the center of the molecular cloud immediately raises the question as to how it was formed. The energy required to form it has been estimated to be as large as about 10^{53} ergs. While the clouds containing HCN are in general circulating around the center, they do not all move at the same speed, and hence should collide with each other and make a more uniform motion and distribution after a period of time of about 100K years. Hence, some very energetic phenomenon must have occurred within the last 100K years, quite possibly the same one which produced the central hole. While this may immediately suggest infall of material into a black hole and a subsequent explosion, it might instead be due to a series of supernovae, or an intense starburst.

Sagittarius A* is unique in our galaxy in terms of its intensity and radio characteristics, and has been intensively examined since its discovery. Rogers et al. (1994) have found it's size to be about 1.4×10^{13} cm at 3 mm wavelength. Position measurements over a period of about 10 years shows that is velocity across the field of view is smaller than about 15km s^{-1} (Backer, 1994). This rather low velocity, compared to the velocity of the many stars nearby of about 150 km s^{-1} or more, indicates that it must be substantially heavier than the average such star. The probability of its having such a low cross-field velocity is less than about 1% if its mass is equal that of the average nearby star, but about 25% if its mass if 40 time

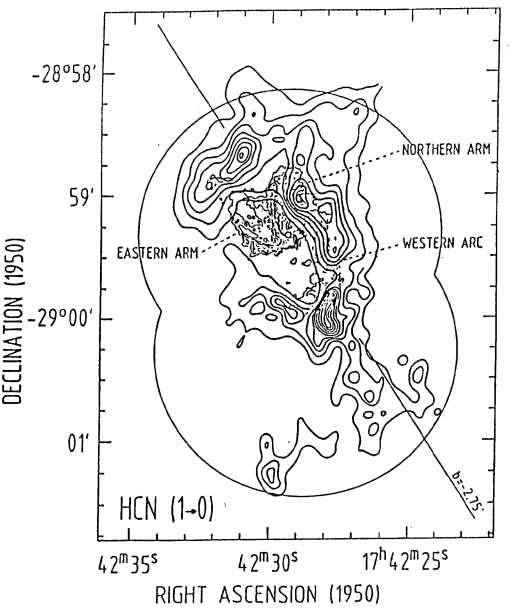

Figure 1. A map of the HCN 1 → 0 transition, with contours representing successively higher intensity, superimposed on thin-line contours of the radio continuum. The latter is intense in the central hole where there is no HCN radiation and also borders the cloud of molecular gas surrounding the hole. (After Güsten et al., 1987).

larger. Thus, one can say that its mass is large, but while it may indeed by very massive, there is no overwhelming case that its mass is larger than a star of some tens of solar masses. Clearly it is a special object from the point of view of its characteristics and its location, which is not further from the exact dynamic center than a couple of arcsecs, the probable error in such a determination. It is a strong candidate for the putative massive black hole.

Considerable effort has been directed towards detecting Sgr A* in the infrared, since an accreting black hole is expected to radiate strongly in the infrared. Eckart et al. (1993) have succeeded in obtaining excellent resolution of an object coinciding in position with Sgr A*, as shown in Figure 2. The object appears to have an effective temperature about 35,000K, a luminosity of $10^{5.4\pm.5}$ $L_\odot$ (Eckart et al., 1993), and is elongated. However, there are enough bright stars in the vicinity to make some of the apparent elongation and even any certain identification with Sgr A* open to some question in the absence of other identifying characteristics because of the possible coincidence of other stars.

Nearby phenomena also indicate something special about Sgr A*. Figure 3 shows a map of radio radiation around the infrared star IRS 7, which is

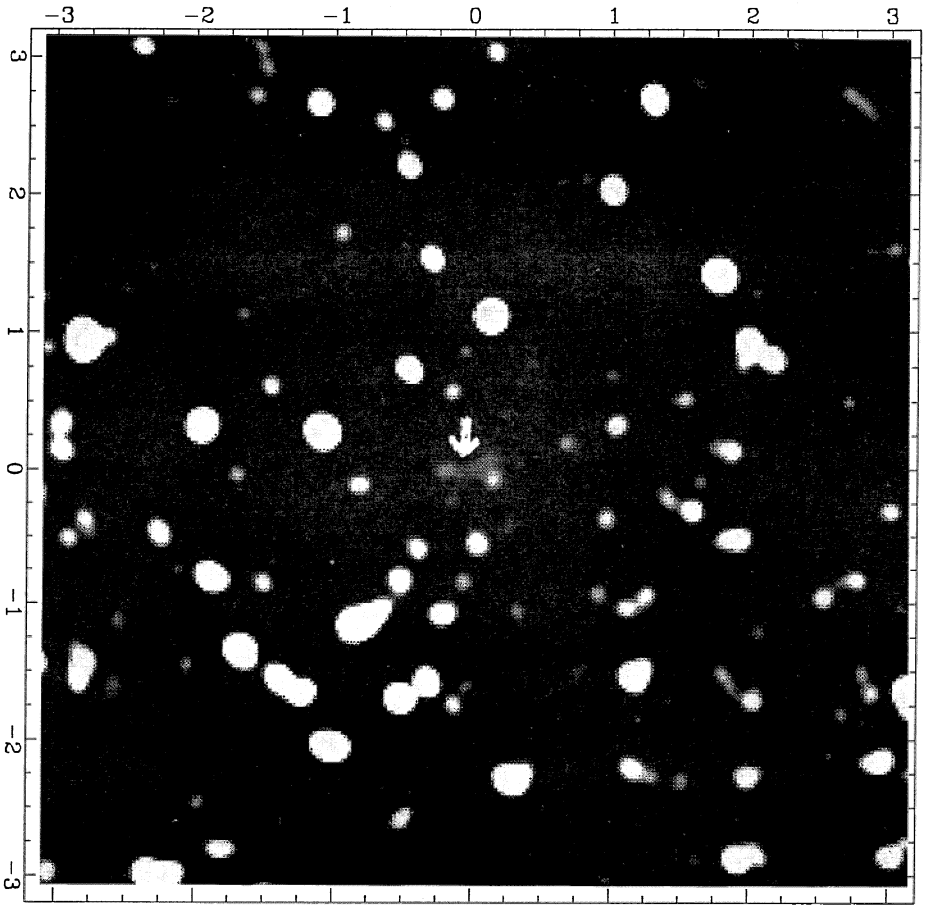

Figure 2. A high resolution near IR image of the galactic center showing an elongated object (marked by arrow) at the position of Sgr A*. Resolution is approximately 0.15 arcsec. (Courtesy Eckart, A., Genzel, R., Hofmann, R., and Tacconi-Garman, L.E.).

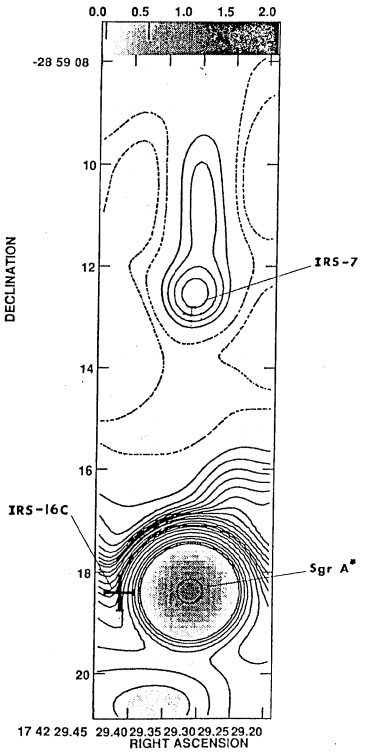

Figure 3. IRS7 and the vicinity of Sgr A* at 2 cm wavelength. The intensity contours show a tail on the star IRS7 pointed away from Sgr A*, indicating a wind from the direction of the latter source (Yusef-Zadeh and Morris, 1991).

near Sgr A*. There is a tail of material leaving IRS 7 pointing exactly away from Sgr A*, and hence indicating a strong wind from that object. Figure 4 shows what is known as the "minicavity" in nearby ionized material. This represents a remarkably circular region low in ordinary ionized material. Its opening is not precisely in the direction of Sgr A*, but velocities in the region may have moved this "minicavity" about 2 arcsecs in a few hundred years. Hence it might have been more centered on Sgr A* not too long in the past.

Figure 5 is a cartoon to provide an overall view of the central region. This shows the circulating molecular clouds, the hole in the center, Sgr A*, ionized streamers, IRS7 and its tail, the "minicavity", and an aggregate of some rather unusual bright blue stars very near the center. Many of these stars are rich in helium and emit stellar winds of velocities near 1000 km s^{-1}. Clearly, they are short-lived, and their type is very rare in any region far from the galactic center.

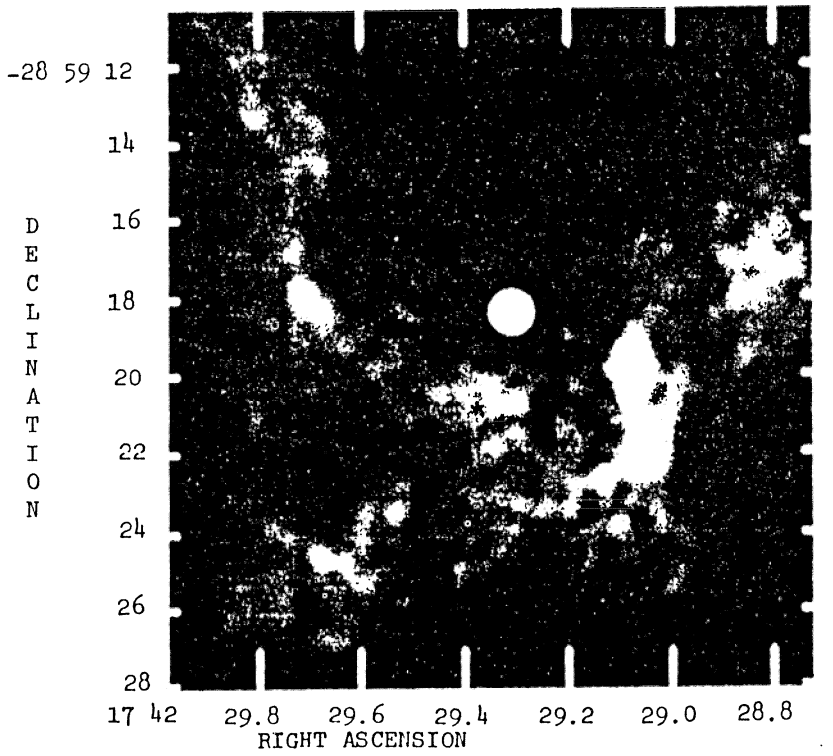

Figure 4. The "minicavity" , a circular pattern with an opening, in the radio continuum radiation (at 2 cm) near Sgr A*. The latter point source is the bright circular object near the "minicavity" (Morris and Yusef-Zadeh, 1987).

3. Dynamic Evidence for a Strong Central Gravitational Field

While some of the features already discussed certainly suggest that Sgr A* may be a massive black hole, the evidence discussed so far is only qualitative and not conclusive. More specific evidence comes from dynamics of the region. Initial measurements of velocities of ionized gas near the galactic center were made by a several students at Berkeley, including Lacy and Serabyn who have also done more recent work of this type (Serabyn et al., 1985). The fine structure transitions of the ground state of NeII and AIII were first measured, since they provide convenient lines in the ionized material from which excitation temperature and densities as well as velocities can be determined. Other measurements have been made of hydrogen recombination lines (Roberts et al., 1993) at radio frequencies and of the Brγ line (Herbst et al., 1993). Figure 6 shows positions where velocities of NeII were measured by Serabyn et al. (1985). These include an examination of the ionized ellipse which is clearly evident on the western side of the cavity

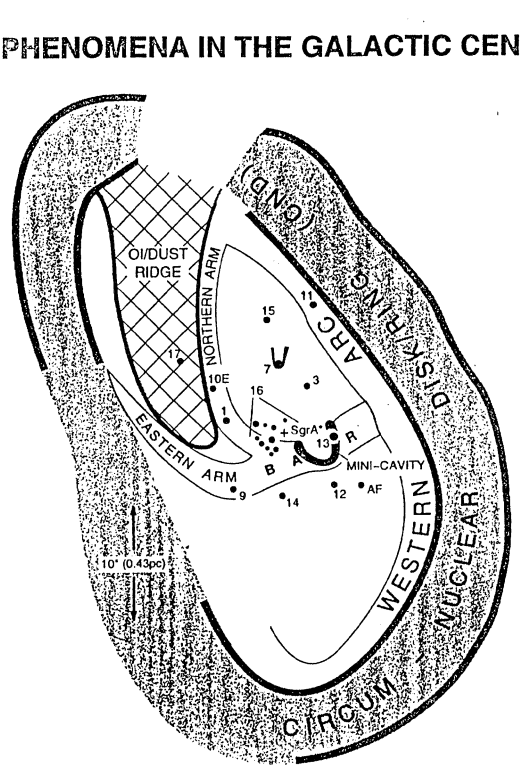

Figure 5. A cartoon diagram showing phenomena near the galactic center, including the circumnuclear disk of molecular gas, the ionized western arc, and eastern and northern arms. The northern arm is probably part of an atomic cloud shown to the east of it. Also shown are the radio point source Sgr A*, IRS7 and its ionized tail, the "minicavity" in ionized gas, and a number of bright stars. Distance from top to bottom of the circumnuclear disk shown here is approximately 65 arcsec, or 2.7 pc. (After Genzel and Townes, 1994).

and which can be traced somewhat further around the center, and even more detailed measurements of the "northern arm", or streamer running north and south within this cavity. Figure 7 is a plot of velocities in this elliptical structure as a function of north-south displacement from the center. To a good approximation these velocities vary linearly from north-to-south and are near zero at the center. This is easily interpreted as the projection of a circular distribution of ionized gas around the center with a velocity of rotation about 110 km s^{-1}. Since the distance from the center of the ellipse is approximately 1.4 parsecs, the mass enclosed within its radius is found to be 4.0×10^6 $M_\odot$. Variations in velocity from an ideal constant rotation can be seen from Figure 7 to be about 20 km s^{-1}. This is one of the observations which indicates that the clouds have been recently disturbed since this nonuniformity would tend to be smoothed out by collision in the

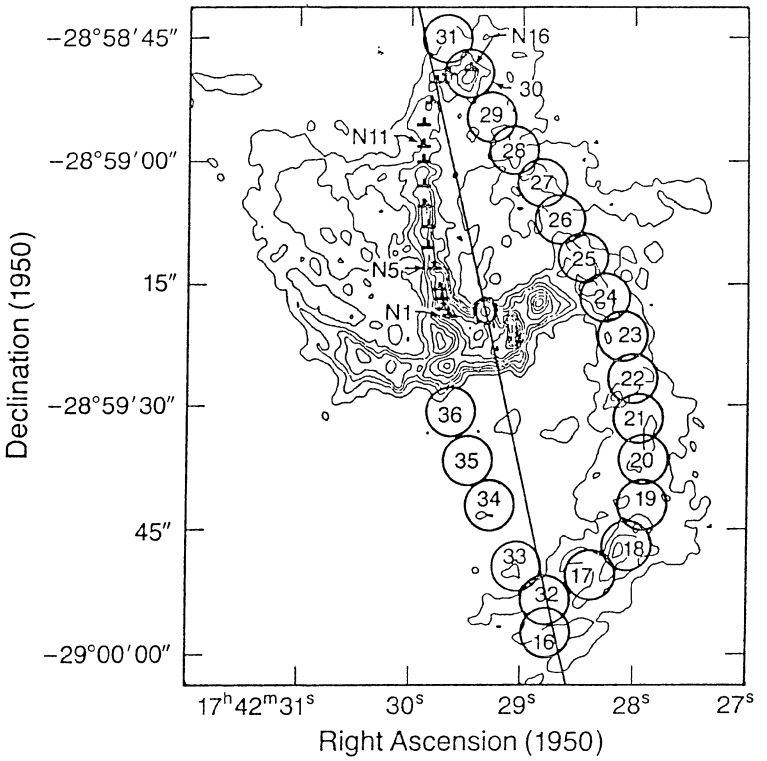

Figure 6. Radio intensity contours of the western arc and the northern northern arm with positions where the NeII spectra were measured by Serabyn and Lacy (1985).

course of about 50K years.

The "northern arm" has a very different pattern of velocities. It has been fitted by Serabyn and Lacy (1985) to a parabolic orbit, representing infall of material towards a central mass of about 4×10^6 $M_\odot$, and the orbit indicates that this mass is still enclosed within a radius as small as 0.5 parsecs. Herbst et al. (1993) have recently made measurements of this northern arm in the Brγ line. Their measurements agree well with those of Serabyn et al. (1985), but they were able to extend the velocity measurements still closer to the center and find that the orbit corresponds to a parabolic one about a mass of 4×10^6 $M_\odot$ even as close as 0.2 parsecs. The attractive center for this orbit is within one arcsec of Sgr A*, a distance about equal to the uncertainty in location of this center.

Although the northern arm provides a very strong suggestion that there is a large concentrated mass and also a measurement of its magnitude, an important question can be raised about the rigor of such a conclusion. Jackson et al. (1993) have found a large cloud of atomic gas to the northeast

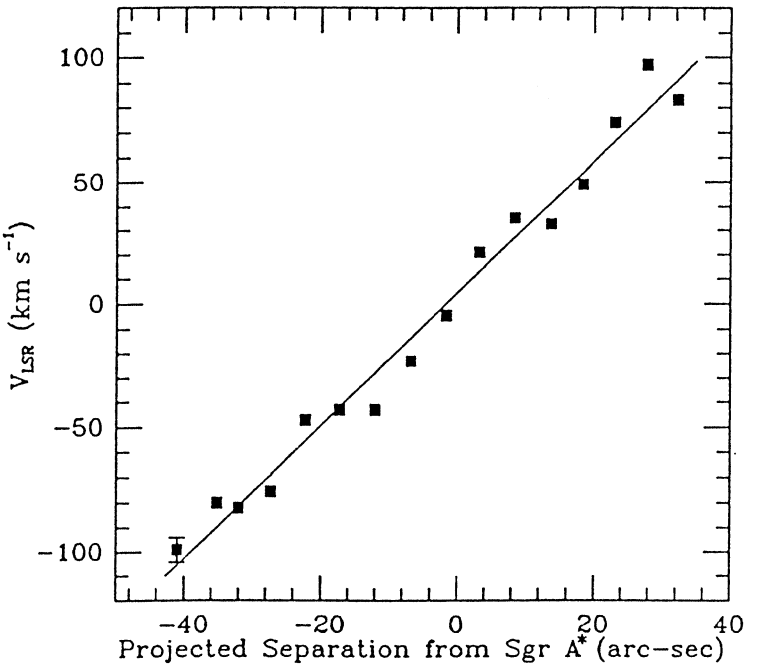

Figure 7. Plot of NeII velocities along the western arc versus the offset in declination from Sgr A* (Serabyn and Lacy, 1985).

of the northern arm, as if in fact a large amount of material has been falling towards the center and the northern arm is simply its edge, ionized by UV radiation from the center. This is also taken as an explanation why the ionized ellipse is not seen to the northeast, since the atomic cloud is dense enough to shield the molecular ring from ionizing radiation coming from the center. If the northern arm is thus the edge of infalling material, its pattern does not necessarily represent an orbit of free falling material. The fact that it fits a parabolic orbit so well is impressive and may correctly represent the gravitational field, but this pattern could be accidentally produced by rather more complex motions of the entire cloud.

There is considerable additional high velocity gas very near the galactic center. Most of this other gas does not clearly fit any recognizable orbit, but may simply represent blobs of gas which are moving in the gravitational field. One can see from Figure 8 that there is a considerable amount of rather high velocity gas, with velocities frequently 200-300 km s^{-1} and becoming as high as 400 km s^{-1}. These are substantially larger than ve-

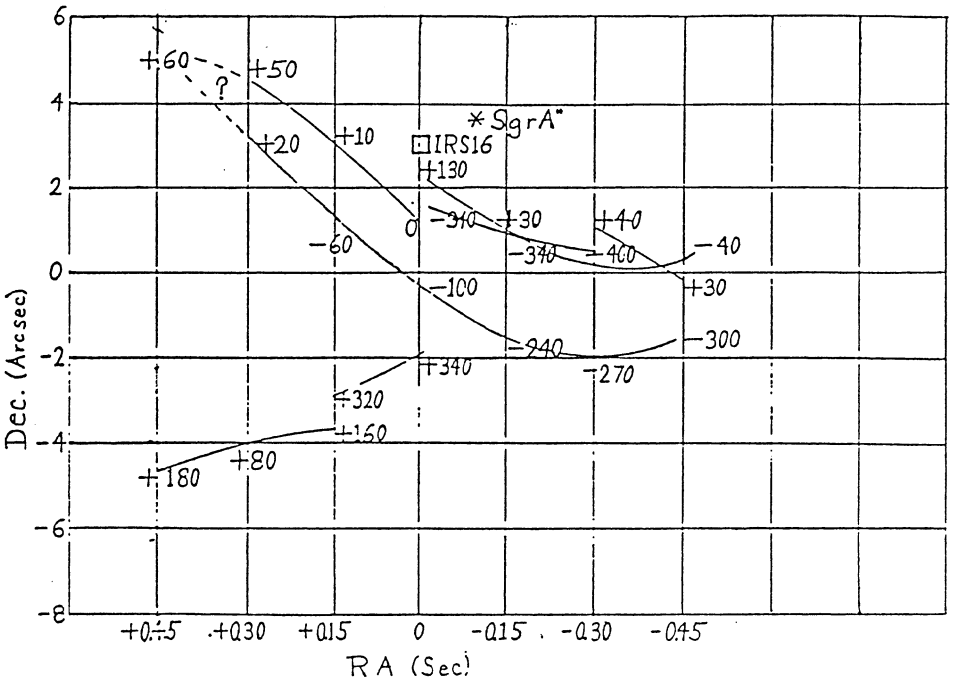

Figure 8. Velocities in km s^{-1} of ionized gas near Sgr A* as determined from NeII spectra (Adapted from Serabyn et al., 1988). Lines connect what may be parts of various gas flows, though the presence of gas flows rather than simply motion of individual batches of gas is uncertain.

locities of typical material found in the circulating molecular clouds, and appear to represent motions of gas in a rather strong gravitational field, corresponding again to a central mass near 4×10^6 $M_\odot$.

Gas velocities can be misleading indicators of gravitational fields since gas may be accelerated by a variety of mechanisms such as variable magnetic fields and winds, or the gas may fall in from a long distance. However, we now have reasonable evaluations of magnetic fields in this general region from polarization measurements (Aitken et al., 1991) and Zeeman effects (Roberts and Goss, 1993). While they are strong enough to somewhat effect the motion of ionized gas found in the galactic center, they are not strong enough to dominate the kinetics or produce the velocities observed. There are also high winds present; some emanate from the hot blue stars near the center and some may come from Sgr A*. These can have effects on the velocities of gas clouds but the present winds would not be strong enough to give the observed cloud velocities and patterns. Neither can infall

from a long distance produce the particular patterns and velocities seen, since such an infall would be expected to produce long streamers, such as the northern arm, and in any case for the high velocities involved, if there were no large central mass the infall would have to come from such a long distance that there would be many collisions to impede the accumulation of the observed velocity.

While gas measurements appear to give substantial information about strong gravitational fields, and possible questions about their interpretation do not discount the essence of this information, stellar velocities are open to somewhat fewer questions than those of the ionized gas. For that reason the stellar measurements of Sellgren et al. (1990), Haller (1992) and Haller et al. (1992) have been particularly valuable. Both of these groups have measured the near IR lines of CO in the atmospheres of red giants. Haller et al. have measured individual red giant stars. Sellgren et al. have measured the average velocity of a collection of stars within a given field of view, so that somewhat weaker stars could be utilized. The velocities obtained by Sellgren et al. as a function of distance from the center are shown in Figure 9 where the velocity is seen to increase toward the center rather than remaining constant as would be expected for a normal cluster of uniform stars. The evidence that there is a substantial increase in velocity as one approaches the center can be described as approximately a 6σ result. In presenting the evidence for a concentration of dark mass, Sellgren et al. also note that the mass to luminosity ratio increases towards the center to a value of about 10. They find $5.5 \pm 1.5 \times 10^6$ $M_\odot$ within the radius of 0.6 parsecs. Haller, Rieke, and Rieke (1992), not only have proceeded with their measurements in a rather different way, they have also made an independent analysis of results. They conclude there is evidence for a mass of $2.0 \pm .4 \times 10^6$ $M_\odot$ within a radius 0.17 parsecs and obtain a signal to noise ratio of 6σ.

An additional method for obtaining information on motions near the center is now becoming available through the measurement of proper motions of the peculiar bright blue stars near Sgr A*. These stars appear, from Doppler shifts of gases near their photospheres, to have velocities of the order of 1,000 km s^{-1} but the Doppler shifts may be produced primarily by stellar winds rather than stellar motion. Careful measurement of stellar positions, using a high resolution near-IR camera, has been used by Eckart et al. (1994) to show that two of these stars appear to have proper motions corresponding to velocities near 1,000 km s^{-1}. They are substantially closer to the very center than most of the other stars observed, and this high velocity of course again indicates a large concentrated mass. At present one can still claim some uncertainty in these results: one possible objection is that since stars are very dense in this region and some of them are of vari-

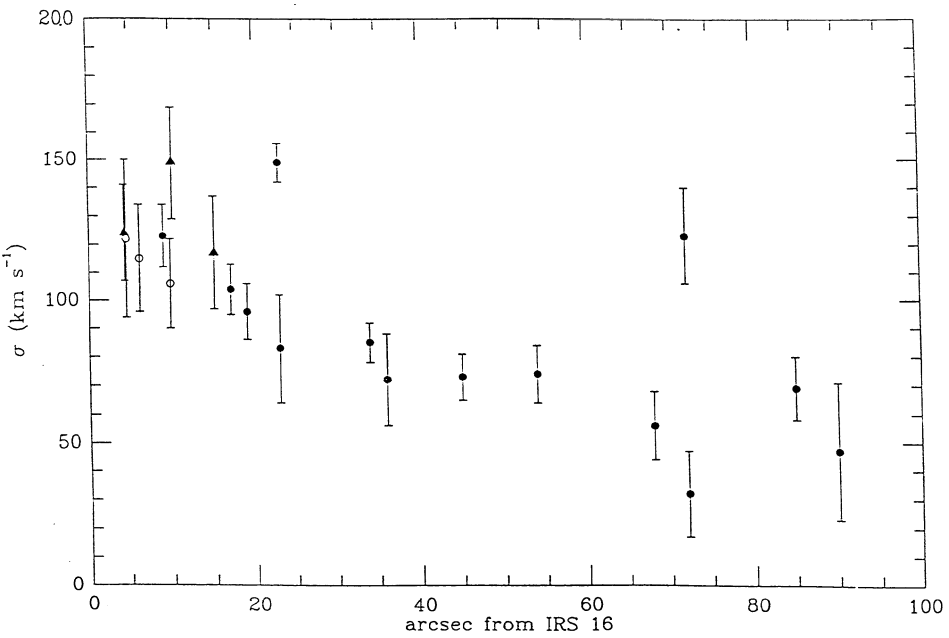

Figure 9. Stellar velocities as a function of distance from IRS16, and hence also approximately distance from Sgr A* (Sellgren et al., 1990).

able luminosity, the apparent proper motion might be caused by a near coincidence along the line of sight of two stars and the variable intensity of one of them. This type of measurement has only recently been realized, but it does appear that in the long run measurement of a number of stars should provide conclusive results. So also may very precise measurement by radio interferometry of the position of gaseous components near the center.

As an overall summary of these dynamic results, Figure 10 shows the mass which would be inside a given radius from the center, using the velocity results for the various components which have been measured. The data include spectra of OH maser stars, most of which are at some distance, CO spectra of red giants, and IR spectra of gaseous components. The results are compared with curves representing a normal cluster of stars. Two such curves are shown, with the two possible core radii of the cluster of stars near the galactic center which have been estimated by Rieke et al. (1988) and by Eckart et al. (1993). It is clear that observations do not fit these ideal stellar clusters, but instead indicate a concentrated central mass of

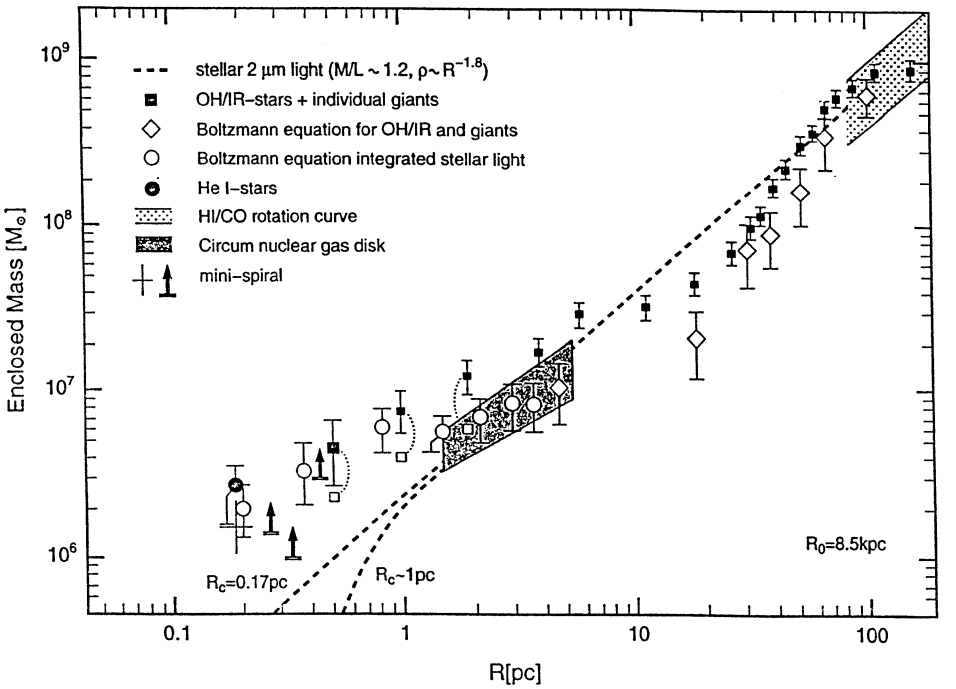

Figure 10. Mass inside a given radius from the galactic center as judged from velocities of gas and stars. The two dotted lines are the expected values for stellar clusters with core radii of 0.17 pc and 1.0 pc respectively (Genzel et al., 1994).

$2 - 3\times 10^6$ $M_\odot$. Furthermore, a wide variety of measurements appear to consistently indicate such a value.

4. Radiation from the Central Region

The Eddington luminosity limit of a black hole having the mass indicated by dynamics in the galactic center is about 3×10^{44} ergs s^{-1}. But the actual radiation observed in the x-ray region is only about 2×10^{36} ergs s^{-1}, in the radio region about 10^{34} ergs s^{-1}, and in the infrared about 10^{38} ergs s^{-1}, more than six orders of magnitude below the Eddington limit. Of course, the Eddington limit need not be reached. However, considerable ionized gas is found in the immediate region near Sgr A* and it has been estimated from this and from the local stellar winds that there should be a mass infall of about 10^{-3} $M_\odot$ per year (Lacy et al., 1982) which, for 10% energy conversion efficiency, would produce a luminosity within two orders of magnitude of the Eddington limit.

One reason the apparent black hole in the galactic center may not be radiating as much as is expected at present is that the amount of mass infall can be variable. It has been estimated that a star would fall into the central mass once every few thousand years (Lacy et al., 1982), and Rees (1988) has pointed out that such an infall might last only a few years. Hence there may be a probability as low as about 10^{-3} that infall into the black hole would be radiating actively at any one time. However, some evidence against such episodic radiation has been given by Sunyaev et al. (1993), who have examined Compton scattering of x-rays in the 9-20 keV range from gas in the galactic plane. They give an upper limit to the x-ray radiation scattered a certain distance from the galactic center, and conclude that there has been no x-ray radiation from the center in the wavelength range measured with an intensity greater than about 10^{38} ergs s^{-1} averaged over the last 400 years, and that the Eddington limit could not have been in effect for as much as one day during this time. With somewhat less restrictive numbers, their work indicates that no intense x-ray radiation has been emitted over the last few thousand years, requiring any strong emission episode to have been rather far in the past.

Ozernoy (1989) models infall of material into a black hole and finds that, for the amount of gas present and the radiation seen in the radio and infrared regions, the black hole must have a mass less than a few hundred $M_\odot$ rather than $2 \times 10^6 M_\odot$. Falcke et al. (1993) model the radiation with a rotating black hole of mass $\leq 2 \times 10^6$ M $_\odot$ and the very low infall rate of $< \ 10^{-7}$ $M_\odot yr^{-1}$. Melia (1992) has calculated a model of a uniform wind striking a black hole of $1 - 2 \times 10^6 M_\odot$ which, because the angular momentum is very small, accretes into the black hole with relatively little radiation. In fact, he fits the observed radiation throughout the spectral region observed with just such a gas falling into the black hole at a rate of about 10^{-3} $M_\odot$ per year. Radiation is produced in part because of turbulence in the accretion, which effectively provides some angular momentum, and produces variations in the intensity of radiation consistent with the minor variations which have been seen. Of course, the actual flow of gas will not be completely uniform. Ruffert and Melia (1994) have refined Melia's model to allow an inflow of gas from about 30 stars surrounding the black hole which are emitting stellar winds and providing about a 3% gradient in the velocity over the accretion radius of 10^{16} cm. They find the radiation in this case more or less consistent with what has been observed, but about twice as large as that for the uniform flow. The Falcke et al. model may be satisfactory as a model at this particular time, but with an improbably small inflow which cannot be typical. The Ozernoy model does not at present appear consistent with the Melia or Ruffert and Melia models, and the discrepancy must remain open until further work is done.

There have been a number of suggestions that perhaps the concentrated mass indicated by dynamics in the central region is not a black hole, but another form of dark mass, such as neutron stars, other small black holes, or even some new form not yet envisaged. Morris (1993) has calculated that if the region within about 10 parsecs of the galactic center produces stars at a normal rate, there should in the past have been a number of rather heavy, short-lived stars which in their supernova stage produced black holes of about 10 $M_\odot$. A large fraction of these black holes would migrate much closer to the center of the galaxy and Morris suggests they might form the concentrated heavy mass, as well as perhaps some of the unusual stars found there by their merger with more ordinary stars. These proposals also have difficulties. The lighter stars such as neutron stars should be evicted from the center by collision and in addition, either neutron stars or black holes should be expected to form some binaries and capture material to produce individual x-ray sources in the central region – sources which are not observed. A large concentration of 10 solar mass black holes with density about 10^8 per pc^3 which is suggested has been shown by Goodman and Lee (1989) and by Lee (1994) to be unstable, and in fact to collapse into a large black hole. Morris' estimate of a large number of black holes migrating towards the center as the result of local supernova is, however, not easy to dismiss and the lack of evidence for them in the form of mergers or x-ray sources suggests either very little stellar formation in the region during the last 10^9 years or that black hole formation by heavy supernovae explosions is much less frequent than expected.

There should indeed be merger stars in the neighborhood of the galactic center, since the density there is quite high. Mergers with some neutron stars or small black holes could produce types of stars which are not otherwise very familiar. Since there are some few tens of unusual intense blue stars near the galactic center it has been suggested that at least some of these may be merger stars, which is an attractive suggestion. However, a group of rather similar stars has been found about 100 parsecs away from the galactic center near the radio continuum striations to the northeast where the density is not particularly high. This gives credence to the more every-day suggestion that these stars have been produced by a starburst. On the other hand, this explanation also leaves questions because at least at present the region near the galactic center is quite unsuitable for much stellar formation.

We are thus left with rather convincing evidence based on velocity measurements that there is indeed a concentrated mass in the center of our galaxy of about $2 \times 10^6 M_\odot$ but with the puzzle that it does not radiate as much as it expected, considering the amount of material surrounding it. A similar dilemma occurs in a number of nearby galaxies for which there

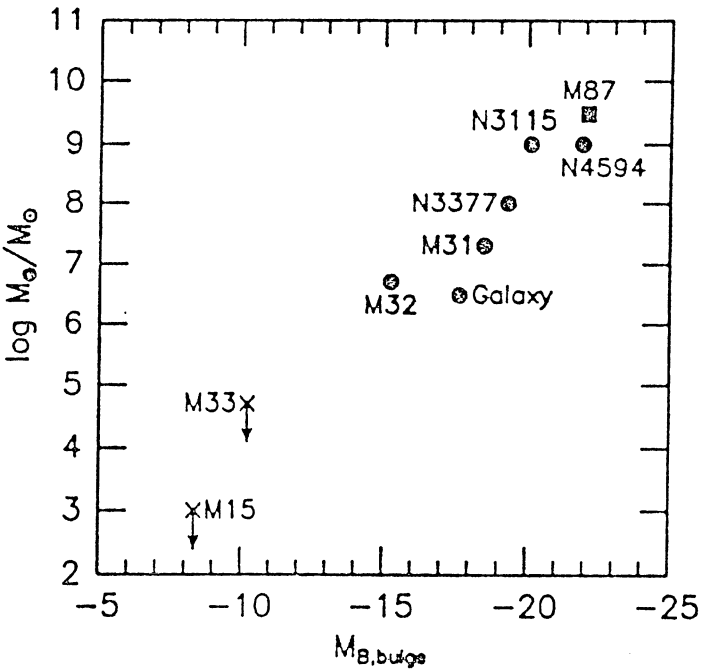

Figure 11. Magnitude of the apparent black hole mass at the center of nearby galaxies as a function of the bulge absolute magnitude (Kormendy, 1994).

appears to be good dynamic evidence for heavy black holes but which are emitting even less radiation than the center of our own galaxy. Among the local galaxies which have been studied, Kormendy (1993) has shown that the mass of the apparent central black hole, as judged from velocity measurements, is closely related to the luminosity of the galactic bulge, as shown in Figure 11. It can be seen from this figure that the apparent black hole mass in the center of our own galaxy and its luminosity are rather consistent with this plot of the black hole masses and bulge luminosities for other galaxies. The black hole in M87 has recently been confirmed by Ford et al. (1994), with measurements of high velocity gas surrounding its center. Figure 12 provides a plot of velocities for the galaxy NGC 3115, showing rather good evidence that in fact the velocity increases sharply near the center, indicating a central black hole of mass about 10^8 $M_\odot$. Evidence for the other galaxies also seems reasonably convincing. Of the five nearby galaxies for which there appears to be reasonable evidence of heavy black holes in their central regions only two, the Sombrero Galaxy

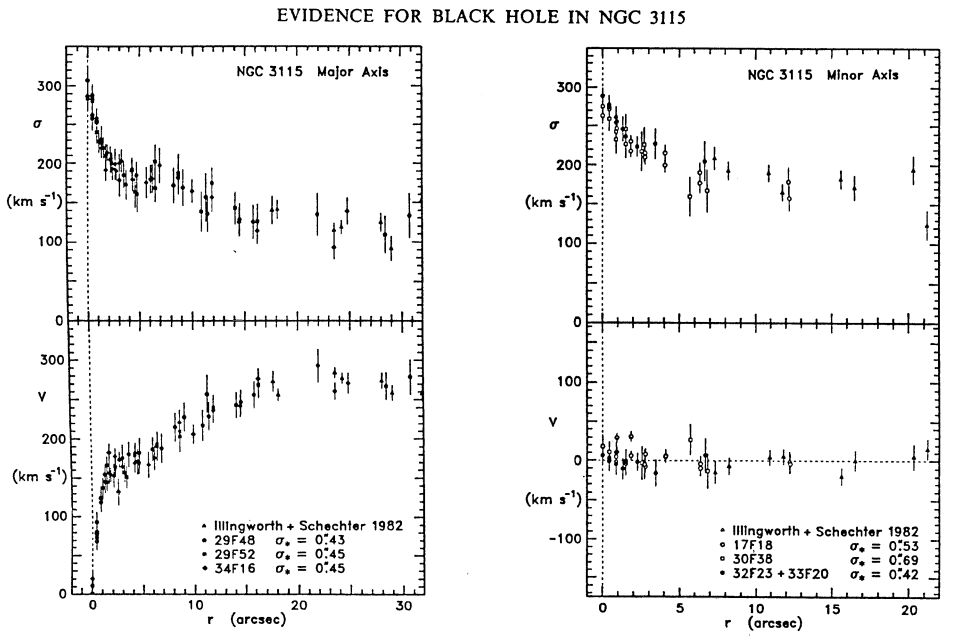

Figure 12. Stellar velocity dispersion (upper diagrams) and rotational velocities (lower diagrams) as a function of distance from the center of NGC 3115 (Kormendy and Richstone, 1992). The velocity dispersion strongly indicates a massive central black hole.

(NGC 4594) and M87, are producing intense radiation. The others produce even less than does our own galaxy, though their black holes as judged from dynamics near their centers are substantially larger. One can appeal to the argument of episodic behavior for these galaxies which are not emitting strongly, that is, the supposition that not much material is presently falling into the black holes. Unfortunately, we cannot study the nature of the very centers of these galaxies as well as we can the center of our own galaxy. However, M31 has recently been found by Lauer et al. (1994) to have a double nucleus which is thought to indicate a merger of two galaxies, and this would lead one to expect that substantial material would be falling into the two nuclei.

5. Summary

Despite the great amount of detailed information which has been accumulated by many different research groups about the center of our galaxy, we

are left with several dilemmas:

1) There is a sizable group of bright blue and unusual stars, many of them with a high He abundance, in the center of our galaxy whose origin is unclear.

2) One would expect a number of black holes of size of about 10 $M_\odot$ to have migrated towards the galactic center if such black holes are formed by the supernova explosions of heavy stars as is expected (Brown and Bethe 1994), but the lack of x-ray sources in the center indicate that these are missing. Does this indicate that the formation of black holes by supernova explosions is not as abundant as has been expected, or instead that there has been no recent stellar formation near the galactic center other than possibly the peculiar stars mentioned above?

3) Finally, there seems to be positive dynamic evidence indicating a large central mass in our galaxy and also in a number of nearby galaxies, masses so concentrated that there are no models for them other than black holes. Yet the radiation expected from these black holes, according to most of the accepted theoretical models, is not observed. Is the dynamic information misleading us about heavy central masses, or do we simply not yet understand sufficiently well the many complex phenomena connected with infall of material into massive black holes?

My personal inclination is to believe the apparent results of the kinetic information, which are in the case of our own galaxy indicated by several different types of measurements of reasonable surety and involve a somewhat simpler use of theory than does the possibly complex dynamics of infall into a black hole and energy conversion during infall. However, further measurements will be needed to settle this question in a really satisfactory way. Fortunately, there are methods envisioned, particularly measurements of proper motions, which in time should allow a convincing settlement of this question.

References

Aitken, D.K., Gezari, S., Smith, C.H., McCaughrean, M., and Roche, P.F. (1991) Ap.J., Vol. 380, pp. 419

Backer, D.H. private communication

Brown, G.E. and Bethe, H.A. 1994, to be published

Eckart, A., Genzel, R., Hofmann, R., Sams, B.J. and Tacconi-Garman, L.E. 1993, Ap.J., 407, L77.

Eckart, A., Genzel, R., and Tacconi-Garman, L.E. 1994, private communication

Falcke, H., Biermann, P.L., Duschl, W.J., and Mezger, P.G. 1993, Astr.Ap., 270, 102

Ford, H., Harms, R., Tsvetanov, Z., Davidson, A., Kriss, G., Bohlin, R., Hartig, G., Dressel, L., Kochbar, A.K., and Morgan, B. 1994, to be published

Genzel, R. Hollenbach, D., and Townes, C.H. 1994, Reports of Progress in Physics

Goodman, J. and Lee, H.M. 1989, Ap.J. 337, 84

Güsten, R., Genzel, R., Wright, M.C.H., Jaffe, D.T., Stutski, J., and Harris, A.I. 1987, Ap.J., 318, 124

Haller, J.W. 1992, Ph.D. Thesis, Univ. of Arizona
Haller, J.W., Rieke, M.J., and Rieke, G.H. 1992, BAAS, 24, 1178 Herbst, T.M., Beckwith, S.V.W., Forrest, W.J., and Pipher, J.L. 1993, A.J. 105, 956
Jackson, J.M., Geis, N., Genzel, R., Harris, A.I., Madden, S., Poglitsch, A., Stacey, G.J., and Townes, C.H. 1993, Ap.J. 402, 173
Jansky, K.G. 1932, Proc. I.R.E. 20, 1920
Kormendy, J. 1993, Ann. Rev. Astr. Ap.
Kormendy, J., and Richstone, D. 1992, Ap.J. 393, 559
Lacy, J.H., Townes, C.H., and Hollenbach, D.J. 1982, Ap.J. 262, 120
Lauer,T.R. 1994, to be published
Lee, H.M. 1994, MNRAS, to be published
Melia, F. 1992, Ap.J., 387, L25
Morris, M. 1993, Ap.J., 408,496
Morris, M. and Yusef-Zadeh, F. 1987, AIP Conference Proceedings 155, ed. D.C. Backer. 127
Ozernoy, L.M. 1989, The Galactic Center, ed. M. Morris, Kluwer (Dordrecht), 555
Rees, M.J. 1988, Nature 333, 523
Rieke, G.H. and Rieke, M.J. 1988, Ap.J. 330, L33
Roberts, D.A. and Goss, W.M. 1993, Ap.J. (Suppl.), 86, 133
Rogers, A.E.E., Doeleman, S., Wright, M.C.H., Bower, G.C., Backer, D.C., Padin, S., Phillips, J.A., Emerson, D.T., Greenhill, L., Moran, J.M., and Kellermann, K.I. 1994, Ap.J., to be published
Ruffert, M., and Melia, F. 1994, private communication
Sellgren, K., McGinn, M.T., Becklin, E.E., and Hall, D.N.B 1990, Ap.J. 359, 112
Serabyn, E. and Lacy, J.H. 1985, Ap.J. 293, 445
Serabyn, E., Lacy, J.H., Townes, C.H., and Bharat, R. 1988, Ap.J. 326, 171
Sunyaev, R.A., Markevitch, M., and Pavlinsky, J. 1993, Ap.J., 407, 606

DISCUSSION

W. Kundt: Before calling SgrA East a "SNR", one should notice that it is some 10 times too small, and some 10^2 times too energetic for a SNR, and may instead be part of the outflow phenomenon from SgrA* through the pc-scale sets into the Gal-Center Chimney; see A & SS 172, 109 (1990). And: when trying to distinguish between an unresolved nuclear mass of a few 10^6 $M_\odot$ via stellar velocities, care should be taken at radii $\lesssim$ 1 lyr that their line-opaque windzones may have large relative velocities, as indicated by IRS 7,10, 6, and 21.

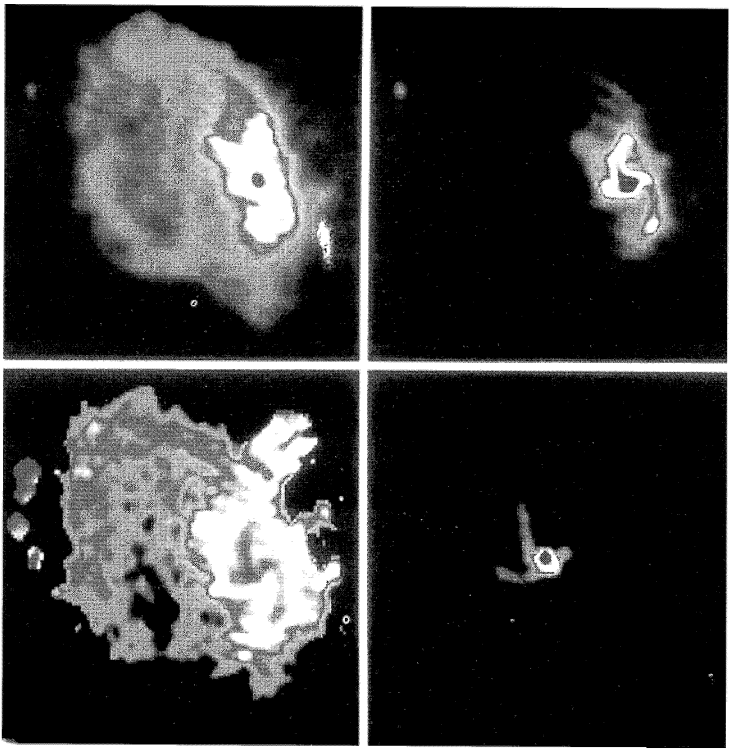

Figure Radio continuum maps from the VLA of the central 10×10 pc^2 of our galaxy. Lower left: Spectral index map from images at 20 and 6 cm with 8 arcsec resolution. The blue region represents synchrotron radiation, the yellow and red various intensities of free-free thermal emission. Upper left: 20 cm image with 8 arcsec resolution. Upper right: 6 cm image. lower right: 2 cm image, resolution 4 arcsec. (Courtesy Ekers, R.D., Schwarz, U.J., Goss, W.M., and van Gorkom, J.H.).
(For colour plate of figure see page xviii)

WHAT IS SGR A*?

The Starved Black Hole in the Center of the Milky Way

H. FALCKE
Max-Planck-Institut für Radioastronomie (MPIfR)
Auf dem Hügel 69, D-53121 Bonn, Germany
E-mail: HFalcke@mpifr-bonn.mpg.de (hfalcke@astro.umd.edu)

1. Introduction

Sgr A* is the unique 1 Jy flat spectrum radio point source located at the dynamical center of the Galaxy and in the very center of the central star cluster (Eckart et al. 1993). Due to its unusual appearance it has long been speculated that this source is powered by a supermassive black hole – an object whose presence has been suspected to reside in the nuclei of many other galaxies as well. Its mass is believed to be as large as $M_\bullet \sim 2 \cdot 10^6 M_\odot$ (e.g. Genzel & Townes 1987) while a lower limit of $M_\bullet > 200 - 2000 M_\odot$ can be inferred from the low proper motion of Sgr A* (Backer – this volume). The currently best dynamical arguments for the million solar mass black hole stem from detailed stellar kinematic studies (Haller et al. 1995).

The enormous increase in observational data obtained for Sgr A* in recent years has enabled us to develop, compare and constrain a variety of models for the emission characteristics of this source. Because of its relative proximity and further observational input to come Sgr A* may therefore become one of the best laboratories for studying supermassive black hole candidates and basic AGN physics. This paper briefly summarizes our current understanding of this enigmatic radio source.

2. Observational Input

2.1. RADIO-SUBMM SPECTRUM

The radio spectrum of Sgr A* has been extensively studied in the range 1-600 GHz where it mostly shows substantial variability. As there are only very few quasi-simultaneous flux density measurements available (see Wright & Backer 1993) an exact description of the radio spectrum is very

L. Blitz and P. Teuben (eds.), Unsolved Problems of the Milky Way, 169–180.
© 1996 *International Astronomical Union.*

uncertain at the moment. An averaged spectrum combined of various data sets available in the literature (Duschl & Lesch 1994) may be fitted by a single powerlaw with spectral index $\alpha \sim 1/3$ ($S_\nu \propto \nu^\alpha$). However, it appears as if the submm regime is less variable than the radio regime (Zylka et al. 1995) and there might even be a weak submm-excess (Zylka et al. 1992; compare also Rogers et al. 1994 with Zylka et al. 1995). Sgr A* is not seen at IR wavelength and hence the spectrum must cut-off towards 12μm (Zylka et al. 1992; Gezari – this volume). The spectrum also cuts off below 1 GHz.

2.2. HIGH ENERGIES

Evidence has grown substantially that Sgr A* is also an X-ray emitter. Art-P/GRANAT detected an x-ray source coinciding with the position of Sgr A* within 40″ (Sunyaev et al. 1991). It shows variability within a factor 2 over a period of several months. The identification as Sgr A* is corroborated by a ROSAT detection of this source with a positional uncertainty of only 10" (Predehl & Trümper 1994). The ROSAT flux, however, was lower than expected from the Art-P measurements and prompted the interpretation of additional intrinsic absorption in Sgr A* – if the ROSAT and the Art-P source are identical. The spectrum in the Art-P band (4-20 keV) is a hard powerlaw with $\alpha \sim -0.6$ and breaks already in the range 35-100 keV (Goldwurm et al. 1994). The situation, however, seems to have changed now, after the launch of ASCA. Koyama (1994) and Maeda et al. (1996) report that the hard source at the Galactic Center (GC) and the soft ROSAT source are offset by 1.3 arcmin. They claim that the hard souce – which is most likely the source detected by Art-P – is not Sgr A*, but a transient x-ray binary. This means that the total x-ray luminosity of Sgr A* could be as low as $10^5 L_\odot$ and lower.

There is also a gamma-ray detection of the GC with EGRET (Mattox et al. 1992) but at present it is not clear whether this is a point source or extended emission.

2.3. LUMINOSITY CONSTRAINTS

The bolometric optical-UV luminosity of Sgr A* can be estimated from the fact that a luminous point source should contribute to the heating of the surrounding dust and thus be visible in submm-IR data (Falcke et al. 1993a) – which is not the case. Hence, we estimated that Sgr A* cannot be very luminous with $L_{\rm UV} \leq$ a few $10^5 L_\odot$. Recently Zylka et al. (1995) have updated their submm measurements of the Sgr A region and concluded from the low temperature gradients in the dust that the dust heating can not be dominated by a single point source but is more likely

due to a cluster of luminous stars (e.g. Krabbe et al. 1991). This would also indicate that Sgr A* has a bolometric luminosity of not more than a few $10^5 L_\odot$, but this estimate could be uncertain by a factor 10. A lower limit derived from the claimed detection of Sgr A* at NIR wavelengths (Eckart et al. 1992) has become uncertain as this source was now resolved into a cluster of stars (Genzel – this volume; Eckart et al. 1995) making it difficult to identify Sgr A* with the present uncertainties between the radio and optical reference frame. Provided the separation of the 5 sources is real, the upper limit for Sgr A* in the K band could be $L_\nu < 3 \cdot 10^{21}$ erg/sec/Hz. In the IR Gezari (this volume) has reported an upper limit at 12.4μm of $0.9 \cdot 10^{22}$ erg/sec/Hz. With all these upper limits one starts to wonder whether Sgr A* is actually there, and without the compact radio source we would have not the slightest clue that there is something. However, we have argued earlier that in order to explain the radio emission, one needs $L_{\rm UV} > 10^4 L_\odot$ (Falcke et al. 1993b) and there is still hope that finally Sgr A* will reveal itself unambiguously at other wavelengths as well.

2.4. SOURCE SIZE

The mm-submm size of Sgr A* is constrained at least within one order of magnitude. From the absence of refractive scintillation Gwinn et al. (1991) have argued that Sgr A* must be larger than 10^{12} cm at $\lambda 1.3$ and $\lambda 0.8$ mm. Krichbaum et al. (1993 & 1994) obtained source sizes for Sgr A* of $4.2 \cdot 10^{13}$ cm at 86 GHz and $9.5 \cdot 10^{13}$cm at 43 GHz with VLBI – the latter well above the expected scattering size as extrapolated from lower frequencies. This claim is challenged by Rogers et al. (1994) who only get $2 \cdot 10^{13}$ cm at 86 GHz in an experiment with a factor 2 shorter baseline. Krichbaum et al. (1993) also found additional weak components and a somewhat elongated source structure at 43 GHz VLBI not seen by Backer et al. (1993). A possibility to reconcile the results could be source variability and elongation of the internal structure which would lead to different sizes if observed with differently oriented baselines. It will be very interesting to see the results of further mm-VLBI experiments.

3. Properties of the Radio Source

3.1. A HOMOGENOUS BLOB?

Recent submm measurements (see Zylka et al. 1995) indicate that the radio spectrum of Sgr A* continues up to several hundred GHz with peak fluxes around 3.5 Jy and a sharp cut-off towards the IR. The submm spectrum can no longer be explained by thermal dust emission as this would require extremely cold dust ($\sim$ 15K) which is very unlikely because of the intense

(stellar) radiation field in the Galactic Center. To explain the flat submm spectrum with synchrotron emission one needs either a combination of self-absorbed components (requiring high compactness) or an electron distribution where the bulk of the electron energy is concentrated in a narrow energy interval. The latter could be either a very flat electron powerlaw distribution ($dN/d\gamma \propto \gamma^{-p}$) with $p < 1/3$ and sharp high-energy cut-off, a steep powerlaw with low-energy cut-off, a monoenergetic (e.g. an electron beam) or a thermal distribution.

Duschl & Lesch (1994, also this volume) suggested that the radio emission of Sgr A* can simply be explained with a single homogenous blob of monoenergetic electrons. Although this cannot be quite true in its most rigorous formulation, as argued below, one can use this approach to get a fairly good idea of the basic parameters of the Sgr A* radio source: the required model parameters are the magnetic field B, the Lorentz factor γ_e, the electron density n_e, the volume $V = \pi R^2 Z$ (assumed to be cylindric) and the distance set to 8.5 kpc. On the other side we have three measurable input parameters: the peak frequency $\nu_{\max} \sim \nu_c/3.5$ of a monoenergetic synchrotron spectrum, the peak flux $S_{\nu_{\max}}$ and the VLBI source size (see above). A fourth parameter can be gained if one assumes that magnetic field and relativistic electrons are in equipartition, i.e. $B^2/8\pi = k n_e \gamma_e m_e c^2$ with $k \sim 1$. With this condition we obtain (averaged over pitch angle) that

$$\gamma_e = 326\, k^{1/7} \left(\frac{F_{\nu_{\max}}}{3.5\mathrm{Jy}}\right)^{-1/7} \left(\frac{\nu_{\max}}{10^{12}\mathrm{Hz}}\right)^{3/7} \left(\frac{R}{10^{13}\mathrm{cm}}\right)^{2/7} \left(\frac{Z}{4\cdot 10^{13}\mathrm{cm}}\right)^{1/7}$$

$$B = 10\,\mathrm{G}\, k^{-2/7} \left(\frac{F_{\nu_{\max}}}{3.5\mathrm{Jy}}\right)^{2/7} \left(\frac{\nu_{\max}}{10^{12}\mathrm{Hz}}\right)^{1/7} \left(\frac{R}{10^{13}\mathrm{cm}}\right)^{-4/7} \left(\frac{Z}{4\cdot 10^{13}\mathrm{cm}}\right)^{-2/7}$$

$$n_e = \frac{1.4\cdot 10^4}{\mathrm{cm}^3} k^{2/7} \left(\frac{F_{\nu_{\max}}}{3.5\mathrm{Jy}}\right)^{5/7} \left(\frac{\nu_{\max}}{10^{12}\mathrm{Hz}}\right)^{-1/7} \left(\frac{R}{10^{13}\mathrm{cm}}\right)^{-10/7} \left(\frac{Z}{4\cdot 10^{13}\mathrm{cm}}\right)^{-5/7}$$

Apparently the 'non'-equipartition parameter k enters only weakly and as long as one is not very far from equipartition the parameters are basically fixed: $\nu_{\max}$ is known within a factor three, $S_{\nu_{\max}}$ within 50% and the source size within a factor 10. This means that models advocating very high electron Lorentz factors ($\gamma_e \sim 10^4$, Kundt 1990) deviate from equipartition by ~ 10 orders of magnitude!

Because of the high compactness of Sgr A* synchrotron self-absorption becomes another important point to be considered. Using an absorption

coefficient of $\kappa_{\rm sync} = 1.4 \cdot 10^{-9}{\rm cm}^{-1}(n_{\rm e}/{\rm cm}^{-3})(B/{\rm G})\gamma_{\rm e}^{-5}(\nu/\nu_{\rm c})^{-5/3}$ one finds the synchrotron self-absorption frequency to be

$$\nu_{\rm ssa} = \frac{2.5\,{\rm GHz}}{k^{0.09}} \left(\frac{F_{\nu_{\rm max}}}{3.5{\rm Jy}}\right)^{0.69} \left(\frac{\nu_{\rm max}}{10^{12}{\rm Hz}}\right)^{-.46} \left(\frac{R}{10^{13}{\rm cm}}\right)^{-.77} \left(\frac{Z}{4 \cdot 10^{13}{\rm cm}}\right)^{-.69}$$

Here we took the *maximum* sizes allowed by mm-VLBI; if further studies show that Sgr A* is even more compact at submm then $\nu_{\rm ssa}$ will increase further making it completely impossible to describe the whole spectrum with a single component.

3.2. SUBMM SOURCE SIZE

We can now make very solid arguments about the possible source size of Sgr A* at submm wavelengths. As VLBI measurements are only available at higher wavelengths one could still postulate arbitrarily large submm source sizes. However, if Sgr A*(submm) were optically thin and larger than $4 \cdot 10^{13}$ cm we should have seen the low frequency $\nu^{1/3}$ part of its spectrum with 3mm VLBI already. This could only be avoided if the submm component becomes optically thick below $\sim$ 100 GHz. As shown above this is possible only for a very compact source where the dimensions of Sgr A* at submm wavelengths are substantially *smaller* than at λ3mm. *Consequently Sgr A* has to be equal or smaller at submm wavelengths than at λ3mm.*

Once $\nu_{\rm ssa}$ can be determined, e.g. from broadband variability studies, we can specify the compactness of Sgr A* from its spectral characteristics alone. Arguing that the bulk of the emission at submm and mm wavelengths comes from two separate components, i.e. requiring $\nu_{\rm ssa} \sim 100$ GHz for the submm component, would imply a source size of only

$$R \sim 1.5 \cdot 10^{12}{\rm cm} \quad k^{-1/17} \left(\frac{F_{\nu_{\rm max}}}{3.5{\rm Jy}}\right)^{8/17} \left(\frac{\nu_{\rm max}}{10^{12}{\rm Hz}}\right)^{-16/51} \left(\frac{\nu_{\rm ssa}}{100{\rm GHz}}\right)^{-35/51}$$

for $R \sim Z$. This corresponds to $5R_{\rm g}$ $(= 5\frac{GM_\bullet}{c^2})$ of a $2 \cdot 10^6 M_\odot$ black hole and hence to the innermost parts of an accretion disk or the very base of a jet. The fact that the non-thermal spectrum cuts-off towards the IR indicates that the submm regime indeed corresponds to the smallest spatial scale. Do we touch the supermassive black hole at these wavelengths directly?

3.3. MULTIPLE COMPONENTS

Although the single, monoenergetic, homogenous blob hypothesis clearly is the simplest description it appears not to be sufficient to explain Sgr A* and there are several observational indications suggesting a non-homogenous source structure, i.e.

- ▷ different core sizes at λ7mm and λ3mm (Krichbaum et al. 1994)
- ▷ different variability at radio and submm (Zylka et al. 1995)
- ▷ varying simultaneous spectral indices (Wright & Backer 1993).

Thus inhomogenous models (with gradients in size, B and n_e, e.g. in a jet or an accretion disk) are required to describe Sgr A*.

4. Spherical Wind Accretion Models

If we now want to go beyond a mere description of Sgr A*, we have to ask how this source is powered and what the underlying engine producing the radio and x-ray emission actually is? One idea is that if Sgr A* is a black hole it should swallow some fraction of the strong stellar winds seen in the GC through Bondi-Hoyle accretion.

The rate of infall depends only on the mass of the black hole and the wind parameters. Once we know the latter we can determine the black hole mass from the estimated accretion rate, which in turn could be derived from the spectrum of Sgr A*. The general validity of the Bondi-Hoyle accretion (without angular momentum) under these assumptions was recently demonstrated by 3D numerical calculations (Ruffert & Melia 1994) and the main uncertainties are related to the plasmaphysical effects associated with the infall. It is usually assumed that the magnetic field in the accreted plasma is amplified by compression up to a point where it reaches the equipartition value. Beyond this point the excess magnetic field is assumed to be dissipated and used to heat the plasma. The electron temperature is determined by the equilibrium between heating and cooling via cyclo-synchrotron radiation where one has to consider two domains for the solution of this problem: (1) hot electrons, where the typical electron Lorentz factors are of the order 100-1000 and (2) warm electrons, where the electron Lorentz factor is still close to unity.

The first domain is in a regime where synchrotron emission is important and also very effective. This requires only low accretion rates ($\dot{M} \sim 10^{-10} M_\odot/\mathrm{yr}$) and hence permits only moderately high black hole masses of the order $M_\bullet \simeq 10^3 M_\odot$ (Ozernoy 1992). The second domain is in the transition regime between cyclotron and synchrotron radiation, which is less effective than pure synchrotron radiation and hence requires higher accretion rates ($\dot{M} \sim 10^{-4} M_\odot/\mathrm{yr}$) and a higher black hole mass of the order $M_\bullet \simeq 10^6 M_\odot$ (Melia 1992 & 1994).

The big advantage of the wind-accretion approach is that it, firstly, appears unavoidable and, secondly, self-consistently ties observable parameters and accretion rate to the mass of the central object. The radio spectrum is well reproduced and initially Melia also was able to account for the x-ray flux.

On the other hand there are several counter arguments to be considered: Firstly, it is not at all clear that the wind has zero angular momentum, which would diminish the accretion rate and lead to a circularization of the accretion flow further away from the central object. There also could be residual angular momentum in Sgr A* itself, e.g. because of a fossil accretion disk which could catch the inflow further out, filling a reservoir of rather dense matter instead of directly feeding the black hole. The viscous time scales of such a disk can be very long – up to 10^7 years (Falcke & Heinrich 1994). More detailed calculation (Falcke & Melia 1996), show that in fact an intrinsically large angular momentum in the wind is required – a fossil disk alone is not sufficent, as the disk/wind interaction would produce too much NIR emission – to stop (and circularize) the infall at a scale of 10^{16} cm and to avoid a strong luminosity output.

There are also problems specific to each model. Ozernoy predicts a very compact source which, as shown above, would become self-absorbed already at high radio frequencies and hence requires the presence of other emission components. Melia on the other hand needs a very high accretion rate and, as Ruffert & Melia (1994) have shown, fluctuations will always lead to the formation of an accretion disk close to the black hole even for the case of initially zero angular momentum. As most of the energy of an accretion disk is produced very close to the black hole it seems impossible to avoid a high luminosity output from this accretion process. The luminosity produced by a Schwarzschild hole ($R_{\rm in} = 6R_{\rm g}$) is $L_{\rm disk} = 0.8 \cdot 10^8 L_\odot \dot{M}/(10^{-4} M_\odot/{\rm yr})$ and even if the outer disk radius is only two times larger than $R_{\rm in}$, $L_{\rm disk}$ reduces only by a factor 3. Given the strong limits on the luminosity of Sgr A* of $L_{\rm disk} \ll 10^6 L_\odot$ it is very unlikely that such a high accretion rate is *currently* flowing onto the black hole. Finally, the recent SIGMA results (Goldwurm et al. 1994) and especially the ASCA results seem to be in contradiction with the predicted X-ray spectrum of the Melia model.

An alternative to the models mentioned above was proposed by Narayan et al. (1995), who explain the discrepancy between high accretion rate and low luminosity by the effects of an advection dominated disk. In this model more than 99% of the energy is not radiated but transported through the disk by advection and finally swallowed by the black hole. And in fact it appears as if advection is non-negligible in many accretion disks, but whether indeed such a high fraction of the energy is transported by advection alone is not at all clear. One also has to make sure that not a substantial fraction of the energy is released in the inner parts of the disk and the energy is swallowed quietly by the black hole. Even if an advection dominated disk is not the whole story, it may be an interesting part of it.

5. Jet-disk Models

5.1. THE BASIC IDEA

Already in 1980 Reynolds and McKee argued that it is very difficult to confine the synchrotron emitting particles in Sgr A* and proposed a wind or jet model to explain the radio spectrum. Rees (1982) tried to explain Sgr A* by accretion from the interstellar matter as discussed in the previous section, however, invoking an accretion disk where the synchrotron emission stems from a relativistic electron gas in its inner parts.

We recently suggested to consider a coupled jet disk system for Sgr A* (Falcke et al. 1993a&b, Falcke & Biermann 1994&1995). The basic concept behind this approach – which has also successfully been applied to AGN – is to postulate a fundamental symbiosis between jets and disks around compact objects, i.e. that both always exist and both are energetically important. As the typical escape speed close to a black hole is scale invariant and always a large fraction of c we expect at least mildly relativistic outflows irrespective of the black hole mass. The power of the jet should be mainly governed by the accretion rate.

We extended the classic Blandford & Königl (1979) jet-emission model by adding mass and energy conservation in a jet-disk system also defining scale invariant parameters for the plasma flow. A more refined model spectrum which includes the effects of adiabatic losses and non-conical jet geometry (see Reynolds 1982) but uses the same basic principles is shown in Fig. 1. Here we also accounted for the presence of a cylindrical region at the base of the jet which we termed 'nozzle', assuming that this is the region where the jet is accelerated and the electrons are injected. Hence the spectrum consists of three regions:

a) the *nozzle*, dominated by a single, quasi monoenergetic electron distribution producing the *submm* bump;
b) the *jet* itself, producing an inverted radio spectrum at *cm* wavelengths where the exact spectral index depends on the jet shape and
c) an *intermediate* region at *mm* wavelengths where both contribute equally.

The turnover frequencies between those regions depend on the self-absorption frequency of the submm component and as discussed above on the source size of jet and nozzle. Therefore one expects these parameters to be fixed by either mm-submm VLBI or simultaneous variability studies at cm-submm wavelengths.

The main finding of this kind of model is that size and flux of Sgr A* are compatible with it being a radio jet, i.e. the low accretion rate results in a very compact jet but still can yield a 1 Jy source. Although the overall power of the jet is fairly low due to the low accretion rate, the ratio between

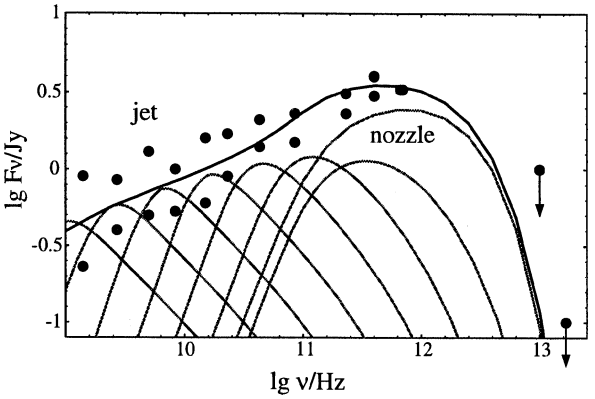

Figure 1. Model spectrum for jet and nozzle coupled to an accretion disk in Sgr A*. Parameters are: $R_{\rm nozz} = 3 \cdot 10^{11}$ cm, $Z_{\rm nozz} = 4.25 \cdot 10^{12}$ cm, $\gamma_{\rm e} = 70$, $q_{\rm j/l} = 0.35$, $L_{\rm disk} = 10^{39}$ erg/sec, $x_{\rm e} = 1$, $\gamma_{\rm j} = 2$, $i = 60°$ (see Falcke & Biermann 1995). We included adiabatic losses, a nozzle where electrons are injected monoenergetically and a jet with shape $R_{\rm j} = R_{\rm nozz} + (Z_{\rm j}/Z_{\rm nozz})^{0.55}/\mathcal{M}$ slowly reaccelerating electrons into a $p = 2.5$ powerlaw.

jet power $Q_{\rm jet}$ and $L_{\rm disk}$ appeared relatively high ($\sim 0.3-1$). This can easily be checked by crudely estimating the magnetic luminosity of Sgr A* which is $L_{\rm B} \sim 0.125(10\,{\rm G})^2(10^{13}{\rm cm})^2 c \sim 10^4 L_\odot$. Now, one only has to remember that the total jet power including relativistic particles and kinetic energy is at least 3-4 times higher and that probably $L_{\rm disk} \leq 10^5 L_\odot$.

5.2. THE AGN CONNECTION - THE CASE FOR HADRONIC CASCADES

We found that the same kind of model can not only explain Sgr A* but also the jets in AGN and even account for the tight UV-radio correlation in radio weak quasars (Falcke et al. 1995b).

Once more the limits imposed by the accretion disk played a crucial rôle. Again one infers injection of relativistic electrons (positrons) at high energies above $\gamma_{\rm e} = 100$ for radio loud jets and we argued that perhaps the difference between radio loud and radio weak quasars could be understood by the lack of this efficient injection mechanism in radio weak quasars (Falcke, Gopal-Krishna, Biermann 1995a). Anyway, the similarity of the high electron Lorentz factors found (directly) in Sgr A* and (indirectly) in AGN is more than striking. Hence we suggested that this typical Lorentz factor has a basic physical reason, namely the π-decay following hadronic cascades initiated by *pp*-collisions between relativistic protons in the jet and thermal protons surrounding the jet. Because of the high rest mass of the π the secondary pairs produced in the cascade will have a characteristic energy of $> 35 MeV$ ($\gamma_{\rm e} > 70$) (see also Biermann et al. 1995). Jets interacting with

a dense medium can inject additional high energy secondary electrons and become radio loud, while those which do not interact remain radio weak with only primary electrons injected at thermal energies – in this respect Sgr A* is *radio loud*. The latter remains true if one extends the $L_{\rm disk}$-radio correlation of AGN to lower luminosities and includes nearby Galaxies with detected radio cores and even stellar mass black holes (Falcke 1994, Falcke & Biermann 1996): again one finds something like a radio loud/radio weak dichotomy, smoothly connecting to AGN, with Sgr A* beeing fairly loud.

Where exactly those *pp*-collisions might occur in Sgr A* is still uncertain: they may happen in an interaction zone between the jet and infalling wind or the dense absorbing material discovered by ROSAT (Predehl & Trümper 1994), but even the disk or the wind (Mastichiadis & Ozernoy 1994) itself could be a site for proton (shock-)acceleration. If *pp*-collisions are the dominant cooling process for relativistic protons being accelerated in a dense medium this would naturally yield monoenergetic secondary electrons. Below the π-production threshhold at 140 MeV *pp*-collisions are inelastic and neither produce secondaries nor lead to cooling of the protons. Once the protons are accelerated above the threshhold energy for π-production, they will instantaneously cool by *pp*-collisions until they fall below the threshhold energy thus bouncing back and forth around this energy. The resulting secondary electrons would be injected in a narrow energy interval at roughly 1/4 of the the *threshold* energy yielding $\gamma_{\rm e} \geq 70$.

6. Summary

Considering the dynamical and spectral evidences I have no doubt that indeed Sgr A* is the very center of the Galaxy and hence will have the coordinates $l_3 = 0$ and $b_3 = 0$ after the next revision of the galactic coordinate system (to be proposed at a future IAU assembly). Current observational data constrain models for Sgr A* already much stronger than for any other galactic nucleus – we will never get closer to a supermassive black hole. Although many question are still disputed, there is now some consensus that Sgr A* is currently put on a starvation diet – despite its high mass and strong stellar winds in the surroundings. A coupled jet/disk system can explain the spectral and structural characteristics of Sgr A* quite well and its smallest source size is close to the typical size of a black hole of mass $M_\bullet \sim 10^6$, while the typical electron Lorentz factor of $\gamma_{\rm e} \sim 100$ may be indicative of hadronic cascades. Crucial future experiments will be simultaneous variability studies and mm-submm VLBI observations. Both, however, will require joined efforts to face a single but promising challenge – *understanding Sgr A**.

References

Backer D.C., Zensus J.A., Kellermann K.I. et al. 1993, Science 262, 1414
Biermann P.L., Strom R., Falcke H. 1995, A&A 302, 429
Blandford R.D., Königl A. 1979, ApJ 232, 34
Duschl W.J., Lesch H. 1994, A&A 286, 431
Eckart, A., Genzel, R., Krabbe, A., Hofmann, R., van der Werf, P. P., Drapatz, S. 1992, Nat 355, 526
Eckart, A., Genzel, R., Hofmann, R., Sams, B.J., Tacconi-Garman, L.E. 1993, ApJ 407, L77
Eckart, A., Genzel, R., Hofmann, R., Sams, B.J., & Tacconi-Garman, L.E. 1995, ApJ 445, L23
Falcke H. 1994, PhD thesis, RFW Universität Bonn
Falcke H., Biermann P. L. 1994, in "Mass Transfer Induced Activity in Galaxies", Shlosman, I. (ed.), Cambridge University Press, p. 44
Falcke H., Biermann P.L. 1995, A&A 293, 665
Falcke H., Heinrich O. 1994, A&A 292, 430
Falcke H., Biermann P.L. 1996, A&A in press
Falcke H., Melia F. 1996, ApJ submitted
Falcke H., Biermann P. L., Duschl W. J., Mezger P. G. 1993a, A&A 270, 102
Falcke H., Mannheim K., Biermann P. L. 1993b, A&A 278, L1
Falcke H., Gopal-Krishna Biermann P. L. 1995a, A&A 298, 395
Falcke H., Malkan M., Biermann P.L. 1995b, A&A 298, 375
Genzel R., Townes R., 1987, ARA&A 25, 377
Goldwurm A. et al. 1994, Nat 371, 589
Gwinn C.R., Danen R., Middleditch J., Ozernoy L., Tran T. 1991, ApJ 381, L43
Haller J., Rieke, M., Rieke, G., Tamblyn, P. Close, L. & Melia, F. 1995, Ap.J., in press
Krabbe A., Genzel R., Drapatz S., Rotaciuc V., 1991, ApJ 382, L19
Krichbaum T.P., Zensus J.A., Witzel A., et al. 1993, A&A 274, L37
Krichbaum T.P., Schalinski C.J., Witzel A., Standke K., Graham D.A., and Zensus J.A. 1994, in "The Nuclei of Normal Galaxies: Lessons from the Galactic Center", eds. Genzel R. & Harris A.I., Kluwer, Dordrecht
Kundt W. 1990, A&ASS 172, 130
Koyama, K. 1994, in: New Horizon of X-ray Astronomy - first results from ASCA, Universal Academy Press, p. 181
Maeda Y., Koyama K., Sakano M., Takeshima T., Yamauchi S. 1996, to appear in PASJ
Mastichiadis A., Ozernoy L. 1994, ApJ 426, 599
Mattox J.R., Bertsch D.L., Fichtel C.E. 1992, BAAS 24, 1296
Melia F. 1992, ApJ 387, L25
Melia F. 1994, ApJ 426, 677
Narayan R., Yi I., Mahadevan R. 1995, Nat 374, 623
Ozernoy L. 1992, in AIP Conf. Proc. 254, Testing the AGN Paradigm, ed. S.S. Holt et al., New York, p. 40,44
Predehl P., and Trümper J. 1994, A&A 290, L29
Rees M. 1982, in: "The Galactic Center", AIP Conf. 83, eds. Riegler & Blandford, p. 166
Reynolds S.P. 1982, ApJ 256, 13
Reynolds S.P., McKee C.F. 1980, ApJ 239, 893
Rogers A.E.E., Doeleman S., Wright M.C.H. et al. 1994, ApJ 434, L59
Ruffert M., Melia F. 1994, A&A 288, L29
Sunyaev R. et al. 1991, ApJ 383, L49
Wright M.C.H., Backer D.C. 1993, ApJ 417, 560
Zylka R., Mezger P.G., Lesch H. 1992, A&A 261, 119
Zylka R., Mezger P.G., Ward-Thomson D., Duschl W., Lesch H. 1995, A&A 297, 83

DISCUSSION

C. Townes: There are strong stellar winds in the GC. How can you avoid a high mass inflow – like in the Melia model – if Sgr A* is a supermassive black hole?

Falcke: Given the bolometric luminosity constraints for UV and X-rays, I think that accretion rates as high as $10^{-4} M_{\odot}/\mathrm{yr}$ are already ruled out by observations. Why Sgr A* does not accrete more matter remains a mystery. Obviously we do not yet understand angular momentum distribution and transport in the inner 0.1 pc around Sgr A*. On the other hand I can not completely rule out that Sgr A* is less massive than we think it is.

C. Townes: Does the mass of Sgr A* play an important rôle in your models.

Falcke: Not really. Besides the dynamical estimates, only the fact that the limits for the submm source size – giving the smallest scale – are so close to what we expect for a $10^6 M_{\odot}$ black hole seems very suspicious. A sign for a low mass black hole would be thermal x-ray emission from an accretion disk and heating of the ambient gas.

T. Hasegawa: Do you have any comments on the accretion history of the black hole? Do we see any signs of episodes of higher accretion rate in the past, or has it been starving from the very beginning of its formation?

Falcke: There is a weak feature – the so called GC spur (Sofue, Reich & Reich 1989, ApJ 341, L47) – which could be the smoke trail of past jet activity. A single giant molecular can turn the GC into a Seyfert nucleus at any time and this could have happened already in the past. If the winds of the surrounding stars really are captured by a fossil accretion disk around Sgr A* and are stored in a close orbit than this could also lead to recurrent activity on a time scale of $10^5 - 10^7$ years.

IS SGR A*

UNDERFED, UNDEREFFICIENT, OR UNDERDONE ?

Why the Milky Way Galaxy Is NOT a Seyfert Galaxy ?

LEONID M. OZERNOY
Inst. for Computational Sciences and Informatics & Dept. of Physics, George Mason University, Fairfax, VA 22030-4444
also
Laboratory for Astronomy and Solar Physics, NASA/GSFC Greenbelt, MD 20771, USA
e-mail: *ozernoy@hubble.gmu.edu, ozernoy@stars.gsfc.nasa.gov*

AND

REINHARD GENZEL
Max-Planck Institut für Extraterrestrische Physik, Garching, Germany
e-mail: *genzel@mpe.mpe-garching.mpg.de*

Abstract. We argue that the wind from IRS 16 and He I stars in the central 1 pc of the Galaxy is responsible for the peculiar features of accretion onto a putative black hole at the Galactic center. What makes Sgr A* unique is not that it is just underfed but, in addition, it has a much lower efficiency of accretion and possibly a lower mass, compared to the AGN case.

1. Starvation Paradox of the Galactic Center

The Galactic center used to be considered a scaled-down version of active galactic nuclei (AGN), and Sgr A* – as a template for nuclear 'engines', presumably massive black holes (BHs). A drastic difference with AGN can be seen by evaluating the ratio of the total accretion luminosity of Sgr A* , L_{ac}, to the inferred Eddington luminosity, L_{Edd}:

$$\frac{L_{ac}}{L_{Edd}} \lesssim 4 \cdot 10^{-5} \left(\frac{M_h}{10^6\ \mathrm{M}_\odot} \right)^{-1} \ll 1, \qquad (1)$$

L. Blitz and P. Teuben (eds.), Unsolved Problems of the Milky Way, 181–187.
© 1996 *International Astronomical Union.*

whereas for AGN this ratio is thought to be much closer to unity. In evaluating Eq. (1), we assume $L_{ac} = L_{obs}$, the total observed luminosity, for which only a rough upper limit of $L_{obs} \lesssim 5 \cdot 10^{39}$ erg/s (Zylka *et al.* 1994) is available so far. The difference between Sgr A* and AGN might similarly be emphasized by evaluating the inferred dimensionless accretion rate

$$\frac{\dot{M}_{ac}}{\dot{M}_{Edd}} \lesssim 4 \cdot 10^{-3} \left(\frac{\epsilon}{0.1}\right)^{-1} \left(\frac{M_h}{10^6\ \mathrm{M}_\odot}\right)^{-1} \ll 1, \qquad (2)$$

where ϵ is the accretion efficiency. The small value of the l.h.s. in Eqs. (1) or (2) is what is usually meant by the "starvation" of the Galactic-center BH (Falcke & Biermann 1994). However, this is only part of the story! Paradoxically, the inflow rate into the central 10 pc or so is not small at all: $\dot{M}_{inflow} \simeq 10^{-2}\ \mathrm{M}_\odot/\mathrm{yr}$ (Blitz *et al.* 1993, Genzel *et al.* 1994). This implies

$$\frac{\dot{M}_{inflow}}{\dot{M}_{ac}} \gtrsim 10^4 \left(\frac{\epsilon}{0.1}\right) \left(\frac{M_h}{10^6\ \mathrm{M}_\odot}\right) \gg 1, \qquad (3)$$

in a sharp contrast with Eq. (2). Thus the "starvation paradox" can be formulated in this way: why is the Galactic-center BH accretion luminosity so weak although the feeding rate does not seem to be small?

2. Possible Routes to Solve the Problem

Eqs. (1) - (3) include three poorly known quantities – $\dot{M}$, ϵ, and M, *i. e.* accretion rate, accretion efficiency, and black hole mass. Accordingly, three principally different routes are possible to resolve the starvation paradox:

- $\dot{M}_{ac} \ll \dot{M}_{inflow}$ **(a True "Starving Monster")**
- $\frac{\epsilon}{0.1} \ll 1$ **(a Low Efficiency)**
- $M_h \ll 10^6\ \mathrm{M}_\odot$ **(a Smaller Black Hole Mass)**

The last two options have been widely discussed in literature. A very low efficiency, $\epsilon \ll 0.1$, is known to occur in the conditions of quasi-spherical accretion when the inflow time might become much shorter than the radiation cooling time (Ipser & Price 1982, Chakrabarti 1990, Narayan *et al.* 1994). This results in advection of an appreciable part of the energy released in due course of accretion and therefore in a low output of accretion luminosity. If the feeding of Sgr A* is provided by accretion of the wind from IRS 16 (Ozernoy 1989, Melia 1992, Ozernoy 1993) this proceeds in a quasi-spherical fashion as a Bondi accretion with a very low efficiency. Furthermore, a low BH mass, $M \ll 10^6\ \mathrm{M}_\odot$, would also weaken inequalities in Eqs. (1) - (3); for a review of this option, see Ozernoy (1994a,b) and refs. therein.

Whichever case – a low ϵ, or a low M, or both – takes place, it seems impossible for Sgr A* to have $\dot{M}_{ac}$ as large as $\dot{M}_{inflow} \simeq 10^{-2}\ M_\odot\ \mathrm{yr}^{-1}$, otherwise in order L_{ac} not to exceed $L_{obs} \lesssim 5 \cdot 10^{39}$ erg/s the accretion efficiency

should be $\epsilon \lesssim 10^{-6}$, which is unlikely. Therefore, one of the central issues to resolve seems to be the origin of a strong inequality: $\dot{M}_{ac} \ll \dot{M}_{inflow}$.

Two specific mechanisms could, in principle, explain a vast difference between $\dot{M}_{ac}$ and $\dot{M}_{inflow}$: (i) a low transport rate of angular momentum in the CNR and (ii) the wind from IRS 16 + He I stars. The next two sections discuss these mechanisms in detail.

3. Transport of Angular Momentum in the CNR

An issue to be addressed first is whether the above mentioned gas inflow into the central 10 pc with the rate $10^{-2}\ M_\odot\,\mathrm{yr}^{-1}$ can be transferred inward and, if so, with what rate. Between $r \sim 10$ and $r \sim 1.5$ pc the rotating molecular 'circum-nuclear ring' (CNR) is located, which consists of many magnetized clumps. Two basic mechanisms contribute to the transfer of angular momentum: turbulent viscosity and magnetic stresses ("magnetic viscosity"). The net mass inflow rate is given by (Ozernoy & Genzel 1994, Ozernoy, Fridman, & Biermann 1994):

$$\dot{M} = \frac{2\pi r}{v_\varphi}\Sigma\left(\xi v_A^2 + \nu_{\mathrm{eff}}\Omega\right)\left[1 - \left(\frac{R_i}{r}\right)^{1/2}\right]^{-1}, \qquad (4)$$

where $v_\varphi \simeq 110$ km s^{-1} is the rotational velocity, $\Sigma \simeq 2 \cdot 10^{-2}$ g cm^{-2} is the CNR surface density, $\xi \sim 1$ is the $(-B_r/B_\varphi)$ averaged over z-coordinate, $v_A \simeq h\Omega \simeq 30$ km/s is the Alfven velocity, $\nu_{\mathrm{eff}} \simeq 1 \cdot 10^{24}$ cm^{2}s^{-1} is an effective viscosity in the clumpy CNR, and $R_i \simeq 1.5$ pc is the inner radius of the ring. Eq. (4) yields $\dot{M} \simeq 10^{-2}\ M_\odot\,\mathrm{yr}^{-1}$ at a fiducious distance of $r = 2$ pc, *i. e.* the value of the same order of magnitude as the infalling mass rate. Therefore the CNR cannot be responsible for any drastic reduction of the accretion rate compared to the inflow rate entering Eq. (3). Moreover, the inflow rate as high as about $10^{-2}\ M_\odot\,\mathrm{yr}^{-1}$ can be traced down to the distance of 1 pc or so from Sgr A* as it follows from the presence of clumps like the "Tongue" at such distances (Genzel *et al.* 1994). Thus of the two alternative sites, where a substantial reduction in $\dot{M}$, from $\dot{M}_{inflow}$ to $\dot{M}_{ac}$, might occur – the CNR and the central wind – the first one is ruled out. Let us address the second option.

4. Wind from IRS 16 + He I Stars

Considerations of momentum and energy balances in the inflowing gas and in the central wind produced by the IRS 16 and He I stars in the inner 1 pc demonstrate that this wind creates an effective obstacle for the high-rate mass inflow from the CNR (Genzel *et al.* 1994, Ozernoy & Genzel 1994). In respect to the central black hole, the role of the wind is two-fold: On

one hand, outflow of momentum and energy with the wind is able to shrink substantially the inflow thereby suppressing a high accretion rate. On the other hand, the wind itself serves as a source of accretion onto the BH as a Bondi accretor, which intercepts a part of the wind at the rate that depends on the BH mass as well as on the density, n_w, and velocity, v_w, of the wind far from the BH:

$$\dot{M}_{ac} \simeq 3 \cdot 10^{-5} A M_6^2 \frac{\mathrm{M}_\odot}{\mathrm{yr}}; \; A \equiv \frac{n_w}{10^4 \; \mathrm{cm}^{-3}} \left(\frac{v_w}{700 \; \mathrm{km/s}} \right)^{-3}. \qquad (5)$$

Besides the energy-momentum arguments, there is one more, although indirect, evidence that the accreting gas is intercepted by Sgr A* as a BH from a local wind and does not result from an inflow through the CNR: Indeed, if the accreting gas originated in the CNR, it would possess a huge angular momentum and form an extensive disk around Sgr A* , which is not seen. There are serious reasons to believe that the accretion onto Sgr A* proceeds in a quasi-spherical fashion, which could explain the origin of its radio (Melia 1992, Ozernoy 1993) and X-ray emissions (Mastichiadis & Ozernoy 1994).

Meanwhile the orbital velocities of IRS 16 and He I stars are responsible for a non-zero net angular momentum of the wind although, due to the unknown character of those orbits as well as non-homogeneity and velocity gradients in the flow, it would be rather difficult to evaluate how large it is. Moreover, a significant part of the angular momentum might dissipate and be cancelled in the post-bowshock region (Ruffert & Anzer 1994). As a result, it is yet unclear whether the residual angular momentum of the accretion disk formed from a part of the quasi-spherical flow would be Keplerian or sub-Keplerian. Still, it is instructive to compare the expected parameters of a Keplerian disk around Sgr A* in the two cases – with and without the wind at the Galactic center. In the next section, we make this comparison.

5. What if there were no wind available...

Although this section serves mainly for illustrative purposes, its starting point seems to be rather firm: an accretion disk around Sgr A*, both at the present time and at a time when there were no mass-losing massive stars in the Galactic center, is expected to be magnetized. (This assertion hardly needs to be substantiated here, given the well-known facts that the winds from massive stars are known to contain magnetic fields *and* that the CNR possesses a strong magnetic field as well). Therefore the structure of the accretion disk should be dominated by magnetic stresses rather than by viscosity. Using the recent models of magnetized accretion disks (e.g. Field

& Rogers 1993), we estimate below the parameters of the accretion disk around Sgr A* under different conditions (Ozernoy & Genzel 1994).

5.1. SGR A* AT A HYPOTHETICAL SEYFERT PHASE

If there were no wind from IRS 16 and He I stars, it would be a continuous inflow of matter from the CNR down to the accretion disk (AD) around Sgr A* with the rate $\dot{M} \simeq 10^{-2}\ M_\odot\ \mathrm{yr}^{-1}$. A link between the parameters of the CNR and AD could be easily established and the accretion luminosity of the central black hole would be straightforward to evaluate. In particular, the toroidal magnetic field in the disk midplane at the radius $R_{1/2} = 3.6 \cdot 10^{12}\ M_6$ cm, where half of the disk luminosity is produced, is given by $B_0 \simeq 10^5 \left(\frac{L_{43.7}}{M_6^2}\right)^{2/5}$ G. The total accretion luminosity is expected to be $L \simeq 5 \cdot 10^{43}$ erg/s, which is of the order of a typical Seyfert luminosity.

5.2. SGR A* IN ITS PRESENT STATE

Fortunately we live in a much more quiescent and quiet environment! And this is thanks to the wind in the Galactic center, which prevents the accretion rate onto the central black hole from being as high as the above inflow rate. Although the BH is able to intercept a part of that wind, which results in the accretion rate given by Eq. (5), the accretion disk turns out to be meager. The bulk of accretion luminosity is produced by a quasi-spherical accretion, whose efficiency is very low, which makes the entire situation drastically different from what would happen in the absence of the wind. In particular, the wind-induced accretion rate results in the accretion luminosity $1.5 \cdot 10^{41} \epsilon_{-1} M_6^2$ erg/s, where the efficiency of accretion $\epsilon_{-1} \equiv \epsilon/0.1 \ll 1$. The magnetic field in the corona around the disk is estimated to be $B_c \simeq 2 \cdot 10^2\ \frac{L_{39.7}^{1/2}}{M_6}$ G.

6. Conclusions

If the current paradigm about Sgr A* as an accreting BH is correct, there is an important feature that makes the center of our Galaxy unlike any active galactic nucleus. The feature is *not* that the Galactic center is just a *micro*-quasar (as its total luminosity hardly exceeds 10^{-6} of a Seyfert galaxy's emission). The basic difference with an AGN is that the Sgr A* luminosity is substantially lower than the inferred Eddington luminosity as shown by Eq. (1). We suggest three possible options to explain that difference, *viz.* a low accretion rate $\dot{M}$, a low efficiency ϵ, and a low BH mass M. In other words, is Sgr A* underfed, underefficient, or underdone ?

In this paper, we have explored why an otherwise high inflow rate of $\sim 10^{-2}\ M_\odot\,\mathrm{yr}^{-1}$ into the central 10 pc or so turns out to be much higher than the inferred accretion rate [see Eq. (3)]. The following specific results discussed above are worth mentioning:

- Magnetic + turbulent transport of angular momentum in the circumnuclear ring (CNR) allows $\dot{M} \simeq 10^{-2}\ \frac{\mathrm{M}_\odot}{\mathrm{yr}}$ down to $\lesssim 1$ pc.
- Strong wind from IRS 16 + He I stars prevents further accretion with such a high rate onto Sgr A* .
- However, the black hole acting as a Bondi-Hoyle accretor intercepts a part of this wind, which results in the accretion rate $\dot{M}_{ac} \simeq 3 \cdot 10^{-5}\ AM_6^2\ M_\odot\,\mathrm{yr}^{-1}$, depending upon the BH mass $M = 10^6 M_6\ \mathrm{M}_\odot$.
- Along with a quasi-spherical accretion flow, a magnetized accretion disk emerges, which has $B \sim 10^3$ G. The structure, radiation, and evolution of the magnetized disk differ substantially from a standard viscous disk.

Thus Sgr A* is definitely underfed in a sense that, in the absence of central wind, the accretion rate would be the same as the inflow rate from the CNR, $\dot{M}_{inflow} \sim 10^{-2}\ M_\odot\,\mathrm{yr}^{-1}$, which greatly exceeds the expected feeding rate given above. The wind that is responsible for such a "confinement diet" could provide the total accretion luminosity of Sgr A* to be as high as $1.5 \cdot 10^{41} \epsilon_{-1} M_6^2$ erg/s. Therefore, even if the accretion efficiency and the BH mass were as high as, correspondingly, $\epsilon_{-1} \sim 1$ and $M_6 \sim 1$, then in this wind-fed "starvation" case the Sgr A* luminosity would be comparable with that of some AGN, which is clearly not the case. Therefore the starvation of the BH at the Galactic center seems to not be the entire story: besides being underfed, the BH should also be either underefficient ($\epsilon_{-1} \ll 1$) or underdone ($M_6 \ll 1$), or both. In any case, the small value of the factor $\epsilon_{-1} M_6^2 \ll 1$ is what technically makes Sgr A* underluminous compared to the AGN situation if the accretion rates were the same.

The efficiency issue seems to be straightforward: as discussed in Sec. 4, the wind accretion onto Sgr A* is quasi-spherical and hence its efficiency is very small indeed, as it follows from the accretion models of the Sgr A* radio and X-ray luminosities. Meanwhile in the AGN case, at least for Seyfert galaxies and QSO's, accretion is usually assumed to have a disk character and hence to possess $\epsilon_{-1} \sim 1$.

It remains to be seen whether a very small efficiency is the only cause which makes Sgr A* underluminous or a smaller than $\sim 10^6\ \mathrm{M}_\odot$ mass of this source needs to be incorporated as well. Several methods to evaluate the actual mass of this enigmatic source have been recently reviewed in Genzel *et al.* (1994) and Ozernoy (1994). We would like to emphasize the importance of the direct methods proposed in those papers, such as the measurements of proper motions of stars *and* the radio emitting plasma

blobs in the Sgr A* vicinity. Besides, further constraining or detecting the infra red luminosity of Sgr A* would be very helpful for constraining its mass.

References

Blitz, L., Binney, J., Lo, K.Y., & Ho, P.T.P. 1993, Nature 361, 417
Chakrabarti, S.K. 1990, "Theory of Transonic Astrophysical Flows". World Scientific Publ. Co. Genzel, R., Hollebach, D., & Townes, C.H. 1994, Rep. Progr. Phys. 57, 417
Falcke, H. & Biermann, P.L. 1994, in "Mass Transfer Induced Activity in Galaxies". I. Shlosman, Ed. Cambridge Univ. Press, p. 44
Field, G.B. & Rogers, R.D. 1993, ApJ 403, 94
Ipser, J.R. & Price, R.H. 1982, ApJ 255, 654
Melia, F. 1992, ApJ 387, L25
Narayan, R. & Yi, I. 1994, ApJ 428, L 13
Ozernoy, L.M. 1989, in "The Center of the Galaxy". M. Morris, Ed. Kluwer Acad. Publ., p. 555
Ozernoy, L.M. 1993, in "Back to the Galaxy". S.S. Holt and F. Verter, Eds. AIP Conf. Proc. 278, 69
Ozernoy, L.M. 1994a, in " Multi-Wavelength Continuum Emission of AGN". T.J.-L. Courvoisier and A. Blecha, Eds. Kluwer Acad. Publ., p. 351
Ozernoy, L.M. 1994b, in "The Nuclei of Normal Galaxies: Lessons From the Galactic Center". R. Genzel & A. Harris, Eds. (in press)
Ozernoy, L.M., Friedman, A.M. & Biermann, P. 1994, A&A (to be submitted)
Ozernoy, L.M. & Genzel, R. 1994, A&A (to be submitted)
Ruffert,M. & Anzer, U. 1994, A&A preprint
Zylka, R., Mezger, P.G., Ward-Thompson, D., Duschl, W.J., & Lesh, H. 1994, A&A (submitted)

RECURRENT STARBURSTS OR INTERMITTENT STARBURST/AGN PHENOMENA AT THE GALACTIC CENTER ?

LEONID M. OZERNOY
Inst. for Computational Sciences and Informatics & Dept. of Physics, George Mason University, Fairfax, VA 22030-4444
and
Laboratory for Astronomy and Solar Physics, NASA/GSFC Greenbelt, MD 20771, USA
e-mail: *ozernoy@hubble.gmu.edu, ozernoy@stars.gsfc.nasa.gov*

Abstract. Recently, I summarized arguments, both old and new, that the Galactic center has experienced a starburst in a recent past (Ozernoy 1994a). Here I propose a likely mechanism – collisions between giant molecular clouds – that might induce (recurrent) starbursts. Taken together, these two approaches seem to indicate that the history of the central part of our Galaxy can be described as recurrent starbursts or intermittent Seyfert activities/starbursts.

1. The Problem

Analyses of recent data on the 10 KeV gas in the central 200 pc and on star formation history at the Galactic center both make a starburst episode very likely in the recent past (Ozernoy 1994a). Here I address an issue what a mechanism could trigger such a starburst.

2. Collisions between the GMCs as a Mechanism for Recurrent Starbursts

Giant Molecular Cloud Collisions. There are about 200 giant molecular clouds (GMCs) in the inner kiloparsec of the Galaxy, each containing 10^5

L. Blitz and P. Teuben (eds.), Unsolved Problems of the Milky Way, 189–192.
© 1996 *International Astronomical Union.*

to 10^6 $M_\odot$ of gas, usually on the verge of gravitational instability (Jog & Solomon 1984). Many of these clouds have peculiar velocities which deviate significantly from circular orbits around the Galactic center, with radial motions that are comparable to the circular velocity (*e. g.* Heiligman 1987). Having highly elongated orbits and a low angular momentum, those molecular clouds should experience mutual collisions. The average time interval between two successive collisions is $T_c = 2\pi/\omega_c = 2\left(a^2 n_c \sigma_v\right)^{-1} \simeq 2 \cdot 10^8$ yr, where $\sigma_v \simeq 30$ km/s is the radial velocity dispersion of GMCs whose typical radius is $a = 20$ pc, and the spatial density is $n_c \simeq 10^{-6}$ pc^{-3}. Despite the presence of magnetic fields in the clouds, the collisions of GMCs turn out to be highly dissipative.

GMC Collisions As Triggers for Star Formation at the Galactic Center. A single collision between two GMCs gives rise to the dissipation of a substantial part of the angular momentum of each of the clouds; as a result, they end up on much lower orbits. Furthermore, after the collision and dissipation of internal turbulent motions the clouds become gravitationally unstable, they could fragment and experience star formation. Therefore, a "wave of star formation" could start at comparatively large distances from the Galactic center and gradually propagate towards the center, accompanied by the fall of the remnants of the clouds onto the center.

The presence at the Galactic center of a rotating molecular circumnuclear ring, which extends between 1 and 10 pc in radius, could be considered as evidence for a recent collision between the molecular clouds in the central several tens of parsecs. The ring whose mass is estimated between 10^4 to 10^5 $M_\odot$ (Genzel et al. 1994) seems to be what is left after a comparable mass, which had its angular momentum dissipated by the collision, fell into the central parsec. Short-lived spurs like *O*I/dust ridge between the Eastern and Northern arms in Sgr A West ("the Tongue") might be one of manifestations of this collision.

A Recent Starburst. The latest starburst within the central parsec has involved no more than $\sim 4 \cdot 10^5$ $M_\odot$ (Tamblyn & Rieke 1993), which is just what is expected to be involved in a star formation process resulting from a GMC collision. Tamblyn & Rieke have found the age of the starburst to be $7 - 8$ Myr and an average SN production rate to be 1 SN/$7 \cdot 10^4$ yr. The latter implies more than 100 SN during the entire starburst, which is marginally consistent with what is required to produce the bubble of ultra hot gas (Ozernoy 1994a). Sgr A East which has been interpreted as a product of a SN explosion might be a part of that starburst provided that the SN exploded into a progenitor bubble created by a wind (Mezger *et al.* 1989).

Inhomogeneities in the eventual products of GMC collisions unavoidably give rise to non-uniform dissipation and fragmentation processes and, as a

result, to non-coeval star formation. Different ages of stars which originated in different sites of the same starburst may explain why the estimates of the Galactic center starburst are somewhat contradictory. SN explosions can also occur non-instantaneously in different places. This might explain the existence, along with the 150-pc expanding molecular ring, of two other large-scale structures ("40-pc molecular ring" and the "20-pc barrel") with kinetic energies of 10^{52-53} ergs and the age of 10^{5-6} yr (Tsuboi *et al.* 1989).

Collisions of GMCs as a Mechanism for Recurrency of Starbursts. The time between two successive GMC collisions, $T_c \simeq 200$ Myr, defines the characteristic time interval of starburst reccurency. A possibility of repeating starbursts at the Galactic center has been envisioned by Loose *et al.* (1982) who considered evolution of a massive gaseous cloud into stars and found that, due to feedback from SN explosions, the star formation process stops and could be repeated, after some (non-specified) dissipation of turbulence induced by supernovae, on the time scale of several hundred Myr. The GMC collisions considered above offer a natural mechanism of dissipation necessary to make the starbursts repetitive.

3. Why Starburst(s), and not AGN Event(s) ?

Oort (1977) was the first who summarized evidence in favor of explosive phenomena at the Galactic center. Could those events be interpreted in terms of a compact 'monster' such as a black hole believed to operate in active galactic nuclei (AGN) ? To answer this question, a careful examination of various phenomena associated with the black hole concept needs to be done. In particular, several different methods have been employed to evaluate or constrain the black hole mass (for detail, see Ozernoy 1994b and refs. therein). The derived upper limits seem to be too small ($\ll 10^6$ $M_\odot$) to allow the black hole to serve as an 'engine' for a Seyfert galaxy at the Galactic center.

The lack of an appropriate mass for the 'engine' is not the main reason why our Galaxy is currently not a Seyfert one. Neither is there insufficient mass supply in the central part of the Galaxy: the mass flux into the central parsec is estimated to be $\sim 10^{-2}$ $M_\odot\,\mathrm{yr}^{-1}$(*e.g.* Blitz *et al.* 1993, Genzel *et al.* 1994) which, paradoxically, is rather large even on AGN scale. However, the lion's share of this flux is not going to 'feed the monster' (whatever it is), otherwise it would result in accretion luminosity much exceeding the available upper limit. The main reason is the presence of the *wind from IRS 16 and He I stars* in the central parsec, which prevents the accretion rate from being as high as the inflow rate. If a recent starburst at the Galactic center is responsible for the formation of these stars (Tamblyn & Rieke 1993), then the starburst and an AGN-type activity are anti-correlated

here.

Such a prevention of a Seyfert-type activity could not last longer than the life-time of the wind-creating massive stars, *i. e.* several Myr. After that, the total accretion luminosity of Sgr A* would be as high as $L \simeq 5 \cdot 10^{43}$ erg/s, provided that the inflow rate were kept the same as the current one. (The current mass flux onto the galactic nucleus, however, might be just a transient phenomenon responsible for feeding the starburst). This power does not depend upon the value of Sgr A* mass unless it is smaller than $4 \cdot 10^5$ M$_\odot$ (for this mass, $L \simeq L_{\rm Edd}$).

It remains to be seen whether or not the Galactic center has experienced such a Seyfert-type activity in the distant past. Meanwhile the evidence summarized above demonstrates that, in the recent past, the Galactic center has passed through a starburst. It is worth emphasizing that the energy production by supernovae averaged over time during the starburst phase was as high as $\sim 3 \cdot 10^{42}$ erg/s, which is comparable with the above accretion luminosity, especially if $L \ll L_{\rm Edd}$.

4. Conclusions: AGN/Starburst Dilemma

To sum up, the main conclusions of the present paper are the following:
• Rather than being a 'dormant' version of an AGN, the Galactic nucleus seems to be a scaled-down version of a starburst nucleus.
• There are reasons to believe that the starbursts at the Galactic center are recurrent. Intermittence *starburst/AGN* seems possible but the expected level of non-thermal activity would be not too spectacular.

Acknowledgements. I am thankful to S. Ames for careful reading of the manuscript.

References

Blitz, L., Binney, J., Lo, K.Y., Ho, P.T.P. 1993, Nat 361, 417
Genzel, R., Hollebach, D., Townes, C.H. 1994, Rep. Progr. Phys. 57, 417
Heiligman, G.M. 1987, ApJ 314, 747
Jog, C.J., Solomon, P.M. 1984, ApJ 276, 114
Loose, H.H., Krügel, Tutukov, A.V. 1982, A&A 105, 342
Mezger, P.G., Zylka, R., Salter, C.J., Wink, J.E., Chini, R., Kreysa, E., Tuffs, R. 1989, A&A 209, 337
Oort, J.H. 1977, ARA&A 15, 295
Ozernoy, L.M. 1994a, In "Multi-Wavelength Continuum Emission of AGN". T.J.-L. Courvoisier and A. Blecha, Eds. Kluwer Acad. Publ., p. 351
Ozernoy, L.M. 1994b, In "The Nuclei of Normal Galaxies: Lessons From the Galactic Center". R. Genzel & A. Harris, Eds. Kluwer Acad. Publ.
Tamblyn, P., Rieke, G.H. 1993, ApJ 414, 573
Tsuboi, M., Handa, T., Inoue, M., Inatani, J., Ukita, N. 1989, In "The Center of the Galaxy". M. Morris, Ed. Kluwer Acad. Publ., p. 135

DIAMETER AND PROPER MOTION OF SGR A*

D. C. BACKER

Astronomy Department & Radio Astronomy Laboratory
University of California
Berkeley, CA 94720 USA

Abstract. The best hypothesis for the energy source of the compact, non-thermal radio source in the center of our galaxy, Sagittarius A* (Sgr A*), is accretion onto a massive black hole from winds emanating from nearby luminous stars. The hole mass, accretion rate, and ultimate fate of accreted matter are uncertain. In this report I give a summary of recent critical observations. The interpretation of these results supports this general hypothesis, and begins to place constraints on model parameters. If so, then Sgr A* is a miniature version of extragalactic AGNs in a quiescent state.

1. Introduction

Infrared speckle imaging results of the central stellar distribution, reported by Eckart *et al.* (1993) and updated by R. Genzel during this IAU meeting, lead to the strong conclusion that Sgr A* is *at* the dynamical center of the Galaxy. However, in spite of its location and the summary remarks in the abstract, Sgr A* remains an enigmatic object: we have no firm information on the *intrinsic* brightness distribution of Sgr A*; there is no widely accepted estimate of the mass of the underlying body; and there is no convincing model for the emission mechanism(s). In this short account I will summarize recent measurements of its angular diameter at millimeter wavelengths and the proper motion of Sgr A*. A longer account may be found in Backer (1994), and a review of our understanding of the central 100 parsecs may be found in review article by Genzel, Hollenbach and Townes (1994).

L. Blitz and P. Teuben (eds.), Unsolved Problems of the Milky Way, 193–198.
© 1996 *International Astronomical Union.*

2. Models

Models for the radio emission from Sgr A* have varied widely. Reynolds & McKee (1980) considered mass outflow from a stellar mass energy source. Rees (1987) discusses a model involving accretion onto a massive black hole from the disruption of stars in the central stellar cluster. Ozernoy (1989; 1993; 1994) concludes that if the radiation arises in matter accreting onto a massive black hole from nearby stars, then the hole mass is less than 10^3 $M_\odot$. In his model a spherical halo of electrons, which are heated to relativistic speeds as they fall into the hole's deep potential well, emit optically thin synchrotron radiation. Melia (1992; 1994) and Ruffert & Melia (1994) calculate that a 10^6 $M_\odot$ black hole will accrete $\dot{M}$ of 10^{-4} $M_\odot$ y^{-1} with low specific angular momentum from the wind emanating from the nearest object in the IRS 16 complex. He computes the flux spectrum from electrons that are heated to near relativistic temperatures as they fall spherically into the black hole potential. The embedded magnetic field is an additional energy source as it is assumed to stay in equipartition during infall. Additionally he identifies the source observed by Sigma/GRANAT at the position of Sgr A* (Sunyaev *et al.* 1991) as the thermal bremsstrahlung counterpart of the electrons which create the radio spectrum via magnetic bremsstrahlung. Goldwurm *et al.* (1994) conclude from the extremely low level of Xray flux above 30 keV that the mass is much less then 10^6 $M_\odot$ in spite of Melia's calculations. Falcke *et al.* (1993) provide a third view. They assume a much lower accretion rate of 2×10^{-8} $M_\odot$ y^{-1} onto a 10^6 $M_\odot$ hole, and form the radio emission spectrum in a relativistic jet that is expelled from a disk around the hole and whose length is below observability.

3. Intrinsic Brightness Distribution and Interstellar Scattering

High angular resolution VLBI techniques have been used to probe the brightness distribution of radiation from Sgr A* (Lo *et al.* 1985; Jauncey *et al.* 1989; Alberdi *et al.* 1992; Lo *et al.* 1993). These long wavelength results indicate an apparent East-West diameter of (1.40 ± 0.05) $(\frac{\lambda}{\mathrm{cm}})^{2.0}$ mas. The visibility data at λ 3.6cm fit a profile that is very closely gaussian along both major and minor axes of the apparent source brightness distribution. The ellipticity is 2:1. Observations with the inner VLBA antennas at λ 7mm are very consistent with the extrapolation of the anisotropic image sizes (Backer *et al.* 1993; Krichbaum *et al.* 1993). VLBI measurements on the HSTK-KTPK-OVRO baselines in 1994 April at λ 3mm place limits on the diameter of the source and strongly suggest that scattering is still dominant along the major axis at these short wavelengths (Fig. 1; Rogers *et al.* 1994). Krichbaum *et al.* (1994) have resolved Sgr A* at λ 3mm on the Pico Velata-Effelsberg baseline (PA 245°), and suggest that intrinsic struc-

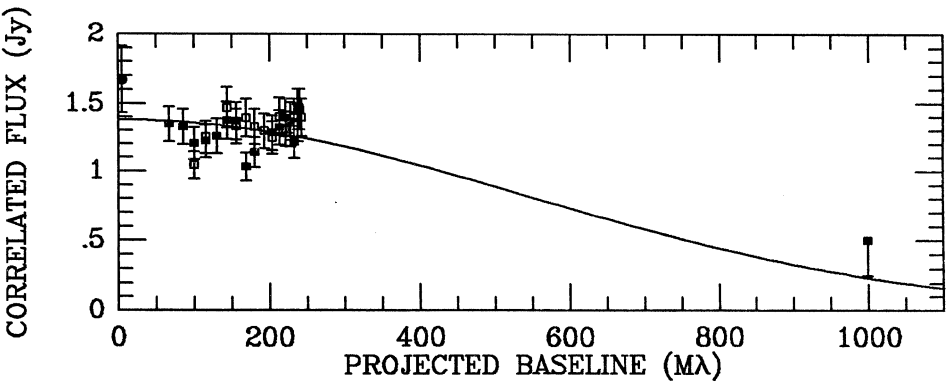
CORRELATED FLUX (Jy)
2
1.5
1
.5
0
0
200
400
600
800
1000
PROJECTED BASELINE (Mλλλ

4. Proper Motion

NRAO's VLA has been used from 1981 to 1988 to measure the apparent proper motion of Sgr A* relative to three compact radio sources with separations from Sgr A* of less than 1° (Backer & Sramek 1987). The estimated proper motion and estimated 2σ errors is:

$$(\mu_l,\ \mu_b) \ = \ (-6.55 \pm 0.34,\ -0.48 \pm 0.23) \text{ mas y}^{-1}.$$

These values can be compared to those that one would expect for an object at rest at the galactic center – a secular parallax – $(-6.21,\ -0.19)$ mas y^{-1} for a choice of the solar motion of 220 km s^{-1} and a choice of the solar distance $R_\odot$ of 8.0 kpc (Reid 1993). The measured value agrees closely with the secular parallax. An upper limit on the transverse peculiar motion of Sgr A* is then, $(-13 \pm 13, -11 \pm 9)$ km s^{-1}.

If Sgr A* is 'just' a star buzzing around in the equipotential well of the galactic center, then it is most likely in equipartition with the detected IR stars. Sellgren *et al.* (1990) have shown that low (solar) mass stars in the central parsec have a velocity dispersion of about 125 km s^{-1}. On the other hand, if the presumed higher mass He stars in the central 0.3 pc have a similar, or even higher, velocity dispersion (Eckart *et al.* 1993), then the equipartition energy for Sgr A* could be at least an order of magnitude higher. The lower limit to the mass of Sgr A* is then at least 100 $M_\odot$, and could be larger by an order of magnitude.

5. Conclusions

Sgr A* is a unique radio source in the very center of the galaxy. It spectrum suggests an inhomogeneous, optically thick synchrotron source. VLBA observations show that the intrinsic size of the λ 3mm source is not more than one AU. The mass of the central body most likely exceeds 100 $M_\odot$ based on a proper motion measurement and the observed stellar velocity dispersion. A black hole that is large in stellar mass units is indicated, and starved accretion onto this object is the leading candidate for energy source that generates the spectrum of Sgr A*. There is wide disagreement on further details. Variations of the accretion rate and instabilities in the inflow can easily be associated with the observed variability.

There is considerable room for improvement of our knowledge of Sgr A* from cm/mm observations: searches for linear polarization with extremely large Faraday rotation, a more accurate estimate of its peculiar velocity with VLA and VLBA measurements, analysis of temporal variability, investigation of structure on the scale of our solar system with higher dynamic range VLBI observations, and investigation of structure on the AU

scale with shorter wavelength VLBI observations are all possible with new instrumentation and new techniques within our grasp.

Acknowledgements

Support for this work was provided by NSF grant AST-9003404.

References

Alberdi, A., Lara, L., Marcaide, J.M., Elosegui, P., *et al.* (1993) *Astron. Astrophys.*, 277, pp. L1-4.
Backer, D. C., & Sramek, R. A. (1987) *AIP Conf. Proc.*, 155, pp. 163-5.
Backer, D. C. (1988) *AIP Conf. Proc.*, 174, pp. 111-6.
Backer, D.C., Zensus, J.A., Kellermann, K.I., Reid, M., *et al.* (1993) *Science*, 262, pp. 1414-16.
Backer, D. C. (1994) in *Nuclei of Normal Galaxies : Lessons from the Galactic Center*, ed. A. Harris & R. Genzel, [Kluwer : Dordrecht], in press.
Carlstrom J.E., Lay, O.P., & Hills, R.E. (1993), *BAAS* , 25, pp. 859.
Eckart, A., Genzel, R., Hofmann, R., Sams, B.J., *et al.* (1993) *Astrophys. J.*, 407, pp. L77-80.
Falcke, H., Biermann, P.L., Duschl, W.J., & Mezger, P.G. (1993) *Astron. Astrophys.*, 270, pp. 102-6.
Frail, D.A., Diamond, P.J., Cordes, J.M., & van Langevelde, H.J. (1994) *Astrophys. J.*, 427, pp. L43-6.
Genzel, R., Hollenbach, D., & Townes, C.H. (1994) *Rep. on Progr. in Physics*, 57, pp. 417-79.
Goldreich, P., & Sridhar, S. (1994) *Astrophys. J.*, in press.
Goldwurm, A., Cordler, B., Paul, J., Ballet, J., *et al.* (1994) *Nature*, 371, pp. 589-91.
Higdon, J.C. (1984) *Astrophys. J.*, 285, pp. 109-23.
Higdon, J.C. (1986) *Astrophys. J.*, 309, pp. 342-61.
Jauncey, D.L., Tzioumis, A.K., Preston, R.A., Meier, D.L., *et al.* (1989) *Astron. J.*, 98, pp. 44-8.
Krichbaum, T.P., Witzel, A., Graham, D.A., Standke, K.J., *et al.* (1993) *Astron. Astrophys.*, 275, pp. 375-89.
Krichbaum, T. (1994) in *Nuclei of Normal Galaxies : Lessons from the Galactic Center*, ed. A. Harris & R. Genzel, [Kluwer : Dordrecht], in press.
Lo, K.Y., Backer, D.C., Ekers, R.D., Kellermann, K.I., *et al.* (1985) *Nature*, 315, pp. 124-6.
Lo, K.Y., Backer, D.C., Kellermann, K.I., Reid, M., *et al.* (1993) *Nature*, 362, pp. 38-40.
Melia, F., Jokipii, J.R., Narayanan, A. (1992) *Astrophys. J.*, 395, pp. L87-90.
Melia, F. (1992) *Astrophys. J.*, 387, pp. L25-8.
Melia, F. (1994) *Astrophys. J.*, 426, pp. 577-85.
Ozernoi, L. (1989) in *Proc. of IAU Symp. No. 136*, ed. M. Morris, [Kluwer : Dordrecht], pp. 555-66.
Ozernoi, L. (1993) *AIP Conf. Proc.*, 278, 69-72.
Ozernoi, L. 1994, in *Nuclei of Normal Galaxies : Lessons from the Galactic Center*, ed. A. Harris & R. Genzel, [Kluwer : Dordrecht], in press.
Rees, M. (1987) *AIP Conf. Proc.*, 83, pp. 166-76.
Reynolds, S.P., & McKee, C.F. (1980) *Astrophys. J.*, 239, pp. 893-7.
Rogers, A.E.E., Doeleman, S., Wright, M.C.H., Bower, G.C., Backer, D.C. *et al.* (1994) *Astrophys. J.*, 434, L59-62.
Ruffert, M., & Melia, F. (1994) *Astron. Astrophys.*, 288, pp. L29-32.

Sellgren, K., McGinn, M.T., Becklin, E.E., Hall, D.N.B. (1990) *Astrophys. J.*, 359, pp. 112-20.
Sunyaev, R., *et al.* (1991) *Sov. Astr. Lett.*, 17, 42-5.
van Langevelde, H.J., Frail, D.A., Cordes, J.M., & Diamond, P.J. (1992) *Astrophys. J.*, 396, pp. 686-95.
Wright, M.C.H., & Backer, D.C. (1993) *Astrophys. J.*, 417, pp. 560-4.
Yusef-Zadeh, F., Cotton, W., Wardle, M., Melia, F., & Roberts, D.A. (1994) *Astrophys. J.*, 434, L63-6.
Zylka, R., Mezger, P.G., & Lesch, H. (1992), *Astron. Astrophys.*, 261, pp. 119-29.

THE RADIO SPECTRUM OF SGR A*

WOLFGANG J. DUSCHL[1,2] and HARALD LESCH[1]
1: Max-Planck-Institut für Radioastronomie
Auf dem Hügel 69, D-53121 Bonn, Germany
2: Institut für Theoretische Astrophysik
Im Neuenheimer Feld 561, D-69120 Heidelberg, Germany

Abstract. We discuss the radio spectrum of Sgr A* in the frequency range between ≈ 1 GHz and $\approx 1\,000$ GHz, show that it can be explained by optically thin synchrotron radiation of relativistic electrons, and point toward a possible correlation between the spectrum of Sgr A* and larger-scale ($\lesssim 50$ pc) radio emission from the Galactic Center region.

1. Introduction

Duschl and Lesch (1994 = DL94) have shown that one can understand the radio spectrum of Sgr A* between ≈ 1 and $\approx 1\,000$ GHz as being due to a single physical process, namely optically thin synchrotron radiation of relativistic electrons. In this contribution, we will shortly discuss their results (sect. 2), especially in the light of new observational results (Zylka *et al.*, 1995), and compare it with other models for Sgr A* (sect. 3). Finally, we will comment on the large-scale radio emission of the Galactic Center and its implications for the radiation mechanism in the Galactic Center (sect. 4).

2. Optically Thin Synchrotron Radiation of Relativistic Electrons

For the frequency range from ≈ 1 GHz up to a few hundred GHz, the time averaged flux density F_ν shows a dependency on frequency ν of $F_\nu \propto \nu^{1/3}$ (fig. 1; for details, and for a compilation of the then available observations in this frequency range, see DL94). While MIR observations ($8\,\mu\text{m} \leq \lambda \leq 20\,\mu\text{m}$) give only upper limits for the flux densities, nonetheless they

L. Blitz and P. Teuben (eds.), Unsolved Problems of the Milky Way, 199–204.
© 1996 *International Astronomical Union.*

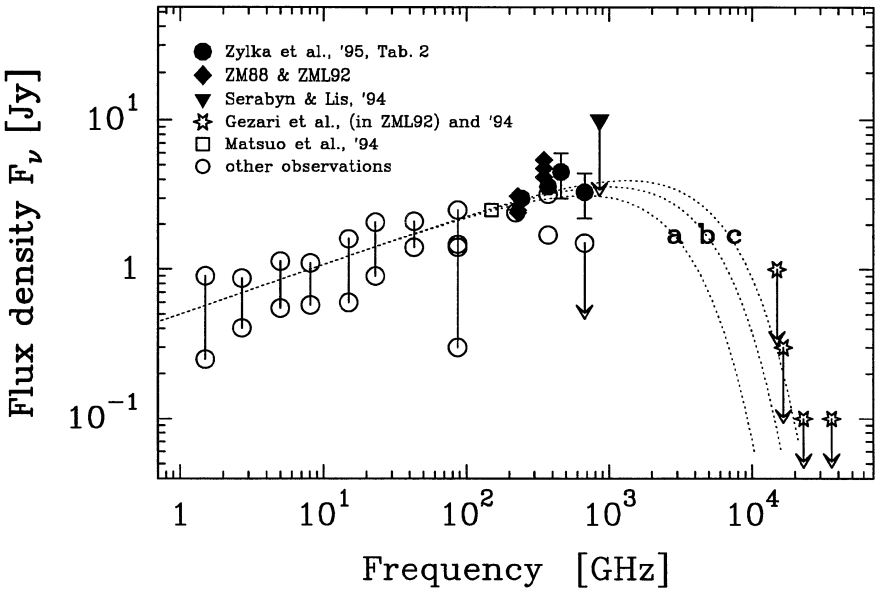

Figure 1. The radio spectrum of Sgr A*. Vertical arrows indicate upper limits; vertical lines around individual symbol indicate error bars; vertical lines connecting symbols indicate observed variability ranges [ZM88: Zylka and Mezger (1988); ZML92: Zylka, Mezger, and Lesch (1992); for details on "other observations", see DL94]. The dotted lines are optically thin synchrotron model spectra for three different sets of physical parameters (a, b, and c; see table 1). [Figure after Zylka *et al.*, 1995]

show that the radio spectrum must attain its maximum somewhere around 10^3 Ghz with a sharp drop of the flux density toward higher frequencies. DL94 have demonstrated that one can interpret the spectrum of Sgr A* in the radio to submillimeter range as due to a single physical process: optically thin synchrotron emission of relativistic electrons. In fig. 1 we show three model spectra for the extremal case of monoenergetic electrons (labelled a, b, and c). For the flux density F_ν we get in this case

$$F_\nu \propto \nu^{1/3} \exp\left(-\nu/\nu_c\right)$$

with a cut-off frequency ν_c. The physical parameters for the three model spectra are summarized in table 1. We find that we need typically magnetic fields of $\approx 5\,\mathrm{G}$ and electron energies $\approx 120\,\mathrm{MeV}$, only weakly dependent of the frequency $\nu_{\max}$ where the flux density attains its maximum. Values for $\nu_{\max}$ considerably lower than $\approx 500\,\mathrm{GHz}$ are excluded by the measured flux densities, while $\nu_{\max} \gtrsim 1500\,\mathrm{GHz}$ would lead to contradictions with the upper limits of the MIR observations.

TABLE 1. Physical parameters for the synchrotron emission models of Sgr A* as shown in fig. 1. [ν_c: cut-off frequency; ν_{max}: frequency of maximum flux density; B: magnetic field strength; E: energy of (monoenergetic) electrons; L: resulting radio luminosity of Sgr A*]

Model	ν_c	ν_{max}	B	E	L
	[GHz]	[GHz]	[G]	[MeV]	[$L_\odot$]
a	$2\,10^3$	$6.7\,10^2$	5.1	111	$2.5\,10^2$
b	$3\,10^3$	$1.0\,10^3$	5.6	121	$4.3\,10^2$
c	$4\,10^3$	$1.3\,10^3$	6.0	127	$6.3\,10^2$

The exact values for, e.g., the magnetic field strength and the electron energy depend on the volume from which the emission comes; here we have taken a spherical volume with a radius of $4\,10^{13}$ cm, according to Krichbaum *et al.*'s (1993) VLBI resolution of Sgr A*. A magnetic field strength of the required order of magnitude can easily be achieved in an accretion disk around a black hole of a few $10^6\,M_\odot$ and an accretion rate of $\approx 10^{-7\ldots-6}\,M_\odot$/yr, i.e., a situation presumably typical for the immediate vicinity of Sgr A* (Falcke *et al.*, 1993a). Recent observations at $\lambda\,1\,300$, 800, 600, and 450 μm (Zylka *et al.*, 1995), and at $\lambda\,2$ mm (Matsuo*et al.*, 1994) are in good agreement with this picture and help to constrain the frequency where the spectrum attains its maximum to $\nu_{max} \in [700\,\mathrm{GHz}, 1\,200\,\mathrm{GHz}]$.

While in the lower frequency range ($\nu \lesssim 100$ GHz) Sgr A* clearly shows variability over time scales ranging down to weeks (Zhao *et al.*, 1992), at higher frequencies the situation is less clear yet. If any, only the variability at $\nu \lesssim 10$ GHz is attributed to interstellar scintillation. Thus, at least the variability at frequencies $\gtrsim 10$ GHz most likely is due to Sgr A* and/or its immediate vicinity. Interestingly enough, the time scale of the viscous evolution of the inner radii of an accretion disk around a $10^6\,M_\odot$ black hole at an accretion rate of around $10^{-6}\,M_\odot$/yr is of the same order as that of the observed variability of Sgr A*. However, our new observations show, at best, marginal evidence for variability at $\lambda\,1\,300\,\mu$m within a time scale of ten days. This clearly warrants a longer term monitoring of the spectrum of Sgr A* in this spectral range.

It is important to note that for the applicability of our model a strictly monoenergetic energy distribution for the electrons is not required (Crusius and Schlickeiser, 1988; Beckert *et al.*, 1995).

3. Other Models for Sgr A*

Falcke *et al.* (1993b; also this volume) interpret the radio emission as due to a jet, which has been observed at $\lambda 7$ mm by Krichbaum *et al.* (1993). In their model the observed synchrotron radiation is the result of an evolving electron spectrum injected into a supersonic, freely expanding conical jet, convecting a tangled magnetic field. The electrons, accelerated via shock waves in the jet, follow a power law energy distribution with $n(\gamma) \propto \gamma^{-2}$, with a low and a high energy cut-off (γ: Lorentz factor; n: volume density of electrons). They obtain a flat spectrum by integrating over optically thin and thick jet components .

Melia (1994) explains the radio spectrum of Sgr A* as due to magnetic bremsstrahlung of a plasma with temperatures of $\sim 10^{10}$ K descending toward the horizon with a rate of $\sim 1.5\,10^{-4} M_\odot$/yr. According to his figure 8, the observed radio spectrum would be produced by very hot electrons in a magnetic field of far more than 1 000 G, in order to produce a break frequency of $\sim$ 1 000 GHz.

Whereas the two above mentioned models also favor a scenario with a black hole mass of $\sim 10^6\,M_\odot$, Mastichiadis and Ozernoy (1994) obtain an upper limit for the black hole mass of $\sim 3\,10^3\,M_\odot$ by considering X-ray and γ-ray emission from the Galactic Center region. However, concerning the radio emission their model seems to us to be not applicable. Their estimated magnetic field due to spherical accretion from the surrounding stars is $\sim 4\,10^4$ G at the Schwarzschild radius. Electrons emitting in such a strong magnetic field must have Lorentz factors of the order unity, which means they radiate in a cyclotron line but not in a synchrotron continuum. Furthermore, they give a minimum Lorentz factor for the electrons $\sim 10^4$. These electrons would only allow for a field strength of less than 10^{-3} G to emit at 100 GHz. For their spherical model such a field strength is obtained at $\sim 4\,10^{14}$ cm, i.e., at 10^6 Schwarzschild radii for a $10^3\,M_\odot$ black hole. But the observations at $\lambda 7$ and 3 mm (Krichbaum *et al.*, 1993, 1994) already resolved source sizes of $\sim 0.13 - 0.33$ mas ($1.6 - 4\,10^{13}$ cm).

Summarizing, any synchrotron interpretation of the radio spectrum of Sgr A* sets a constraint on its size. The observed luminosity is proportional to the volume and to the square of the magnetic field strength. If one favors smaller black hole masses, the volume decreases, whereas the field strength increases. To emit still at the same frequency, the particles' energy has to decrease. However, a particle with a Lorentz factor of around unity radiates cyclotron line emission instead of a synchrotron contiuum spectrum.

4. The large-scale radio emission of the Galactic Center

The large-scale ($\simeq$ 50 pc) radio emission of the galactic center region was observed by Reich *et al.* (1988). These observations include the very center Sgr A* and the extended components up to a distance of 40 pc, often referred to as "Bridge" and "Arc" (Brown and Liszt, 1984), located north of Sgr A*. They measured a similarly flat or inverted spectrum in the frequency range betwen 843 MHz and 43 GHz in the Bridge and Arc as in Sgr A*. After a separation of thermal/nonthermal emission they find, that most of the nonthermal emission has an inverted spectrum with $\alpha \simeq 0.3$ ($\alpha = d\log F_\nu / d\log\nu$). Whereas the spectrum of the Arc can be explained by local acceleration (Lesch and Reich, 1992), the spectral index $\alpha \sim 0.3$ in the Bridge strongly suggests a very close physical connection between the extended emission and the radio source Sgr A*, which was investigated by Lesch *et al.* (1988).

If Sgr A* is the source of the electrons which radiate in the Bridge – as may be indicated by the common spectral index – this has important implications. It makes it highly unlikely that the emission of Sgr A* is due to superposed optically thick synchrotron components. This can be seen as follows: let us assume the emission of Sgr A* is composed of optically thick synchrotron sources. When they move into the extended regions, they become optically thin. At frequencies higher than the turnover frequency, which defines the transition from optically thin to optically thick, the spectrum is a power law with negative spectral index. Such a behaviour is well known from the time evolution of synchtrotron components in active galactic nuclei (see, e.g., Marscher and Gear, 1985). The finding that α is not only positive but even still 0.3 contradicts the assumption that the emission is optically thick synchrotron radiation.

References

Beckert, T., *et al.* (1995) in preparation

Brown, R.L., Liszt, H. (1984), *Annual Reviews in Astronomy and Astrophysics*, 22, pp. 223–265

Crusius, A., Schlickeiser, R. (1988) *Astronomy & Astrophysics*, 196, pp. 327–337

Duschl, W.J., Lesch, H. (1994) *Astronomy & Astrophysics*, 286, pp. 431–436 [=DL94]

Falcke, H., Biermann, P.L., Duschl, W.J., Mezger, P.G. (1993a) *Astronomy & Astrophysics*, 270, pp. 102–106

Falcke, H., Mannheim, K., Biermann, P.L. (1993b) *Astronomy & Astrophysics*, 278, pp. L1–L4

Gezari, D.Y., Ozernoy, L., Varosi, F., McCreight, C., Joyce, R. (1994) in: *The Nuclei of normal galaxies: Lessons from the Galactic Center* (eds.: R. Genzel & A.I. Harris), in press

Krichbaum, T.P., Zensus, J.A., Witzel, A., Mezger, P.G., Standke, K., Schalinski, C.J., Alberdi, A., Marcaide, J.M., Zylka, R., Rogers, A.E.E., Booth, R.S., Rönnang, B.O., Colomer, F., Bartel, N., Shapiro, I.I. (1993) *Astronomy & Astrophysics*, 274, pp. L.37–L40

Krichbaum, T.P., Standke, K.J., Graham, D.A., Witzel, A., Schalinski, C.J., Zensus, J.A. (1994) in: *Multi-wavelength continuum observations of AGN* (Proceedings of IAU symposium 159; eds.: T.J.-L. Courvoisier, A. Blecha), pp. 187–188

Lesch, H., Schlickeiser, R., Crusius, A. (1988) *Astronomy & Astrophysics*, 200, pp. L9–L12

Lesch, H., Reich, W. (1992) *Astronomy & Astrophysics*, 264, pp. 493–499

Marscher, A.P., Gear, W.K. (1985) *Astrophysical Journal*, 298, pp. 114–127

Mastichiadis, A., Ozernoy, L.M. (1994) *Astrophysical Journal*, 426, pp. 599–603

Matsuo, H., *et al.* (1994) in preparation

Melia, F. (1994) *Astrophysical Jornal*, 426, pp. 577–585

Mezger, P.G. (1994) in: *The Nuclei of normal galaxies: Lessons from the Galactic Center* (eds.: R. Genzel & A.I. Harris), in press

Reich, W., Sofue, Y., Wielebinski, R., Seiradakis, J.H. (1988) *Astronomy & Astrophysics*, 191, pp. 303–312

Serabyn, E., Lis., D. (1994) quoted by Mezger (1994)

Zhao, J.-H., Goss, W.M., Lo, K.-Y., Ekers, R.D. (1992) in: *Relationships between active galactic nuclei and starburst galaxies* (ed.: A.V. Filipenko), pp. 295–299

Zylka, R., Mezger, P.G. (1988) *Astronomy & Astrophysics*, 190, pp. L25–L28 [=ZM88]

Zylka, R., Mezger, P.G., Lesch, H. (1992) *Astronomy & Astrophysics*, 261, pp 119–129 [=ZML92]

Zylka, R., Mezger, P.G., Ward-Thompson, D., Duschl, W.J., Lesch, H. (1995) *Astronomy & Astrophysics*, in press

EVOLUTION IN THE NUCLEUS

A review of David Allen's research into the nature of the Galactic Centre

M.G. BURTON
University of New South Wales
School of Physics
Sydney, NSW 2052
Australia

Abstract. A personal reflection is presented of David Allen's research into the content of our Galactic nucleus.

1. Introduction

David Allen's contributions to astronomy are legend, and encompassed a depth and breadth that is staggering. From public populariser to innovative researcher, David's achievements were exceptional at every level, through virtually every field of astronomy, from planetary atmospheres to quasar evolution. A few themes, however, coursed especially strongly through his work. One of these was the nature of our Galactic nucleus. I have had the great privilege to work closely with David during the last four years of his work in this arena, and would like to reflect upon some of the insights we have gleaned as a result of his perception.

Two intertwined threads run through his work, the evolution in IR detector technology and the evolution in ideas. During a decade where IR instruments evolved from single element bolometers, through simple linear arrays, to the sophisticated array detectors now available, David developed the IRPS, the FIGS and finally IRIS for use on the Anglo Australian Telescope. He used these in novel ways to extract just that information of interest from the vast data stream pouring into the telescope. Through its interpretation we witnessed an evolution of ideas about the core of the Galaxy. They moved from that of an ailing nucleus dominated by old giants surrounding a massive black hole centred on IRS 16, to that of a youthful, vigorous nucleus, the product of a mild starburst, and perhaps only a low mass, passive black hole, in its core.

L. Blitz and P. Teuben (eds.), Unsolved Problems of the Milky Way, 205–214.
© 1996 *International Astronomical Union.*

David Allen's bibliography contains over 500 articles, and those on the Galactic Centre are listed at the end of this article. This review will attempt to summarise their achievements. David, of course, would never claim the credit for this work on his own, and fully acknowledged the contributions of his co-workers. He would also pay close regard to the work of others in the field, and allow their ideas to influence his work. I am afraid I am unable to adequately attribute all the credit that David would give to his colleagues here. This is not an historical treatise, and a proper treatment of the evolution of our understanding of the Galactic centre would naturally provide a more comprehensive review of the contributors to the field. But as all who worked with David well knew, he was the driving force behind it, whatever the field.

2. The Evolution in Observational Technique

David's first instrument in the 80's was the IRPS (Infrared Photometer Spectrometer), a single channel instrument with broad band filters, and a 1% CVF for low resolution spectroscopy. With the genius of John Barton's electronics this could work in simple DC mode, averting the need for spatial chopping, a facet that David quickly realised would allow him to readily map IR sources. Accumulating data as the telescope scanned rapidly back and forth across a source, complete with allowance for telescope inertia, the maps obtained were both unprecedently deep and had better spatial integrity than any other group was achieving [*eg.* 2, 3, 5]. For instruments of its type, the IRPS was never beaten. Though it has been far surpassed by the technology now available, it gave David great satisfaction in his final months to know that the IRPS was still being put to good use. It had been redeployed to the South Pole, and was spending the winter sitting outside at $-60°$ C, site testing the Antarctic Plateau for a future IR observatory!

By the middle of the decade a linear array was available, and FIGS (the Fabry-Perot Infrared Grating Spectrometer) was born. Though FIGS was never quite the success it was originally hoped to be, it still produced its fair share of exciting new science. David's innovation was an extension of DC imaging, to develop imaging spectroscopy. However this time the chopping secondary was scanned across a source, instead of the telescope. Readouts were synchronised to the scan speed, and a 3D data cube built up, containing 2 spatial and one spectral dimension [*eg.* 6, 11].

Finally in the 90's the AAO obtained an infrared array, and with the help of Peter Gillingham's brilliant optical design, David came up with IRIS (the Infrared Imaging Spectrometer, though David will insist that there is no acronym, simply a name), an all-singing, all-dancing IR camera / spectrometer. The innovative use this time was again drift scanning, but

now slowly drifting the spectrometer slit across the source to build the data cube. The entire H (1.6μm) and K (2.2μm) bands could be measured simultaneously [*eg.* 8, 9, 10, 12, 13, 14, 15, 16], and spectral maps at any desired wavelength obtained from the resultant cube. It might perhaps be noted, though, that the full data reduction, involving correcting for the tiny tracking inaccuracies of the telescope over a 2 hour scan, could be a little tedious at times!

3. The Evolution in Ideas

Perhaps surprisingly, David's first venture in the field of the Galactic Centre [1, 4] in fact involved a discovery and then a retraction! But it was an error he freely admitted to. An L'-band (3.8μm) spectrum towards IRS7 revealed a broad absorption. In particular, there were several discrete features in the absorption trough. It was speculated that their origin might indicate the presence of complex organic molecules in the interstellar grains. However, follow up work with the UKIRT telescope later showed no evidence for these features! David eventually convinced himself that he had been the victim of a rather obscure systematic error, the result of the light path of the standard and source passing through a slightly different part of the CVF on the IRPS.

The next piece of research moved to the nature of the black hole presumed to lurk at the centre of the Galaxy. A sub-arcsecond 'image', obtained via scanning with the IRPS [2], revealed new details in the central parsec. First, was the obvious presence of some regions of particularly heavy obscuration, presumed to signal the presence of small molecular clouds. We now easily recognise these as the circumnuclear ring. Second, there was the surface brightness profile, shown to continue as an $r^{-0.7}$ power law to 1" from the (presumed) centre. This did not conform to an isothermal model ($r^{-1.0}$), unless the core was much smaller than that of any globular cluster known. Any core radius would have to be < 2" or < 0.08 pc. It suggested to him a density cusp, with a massive central object. To account for $10^7 M_\odot$ in the central parsec, as deduced from [Ne II] kinematics (Lacy *et al.*, 1980), implied a core density of $> 10^8 M_\odot pc^{-3}$.

A companion paper [3] with John Storey took this work further. A 1μm CCD image, plus J (1.2μm) and K band maps, were used to determine stellar types from colours, and to achieve better astrometric precision between the radio position for SgrA* and the IR image. IRS16 was resolved into 3 components, with the designated IRS16–C 1.0 ± 0.4" E from the best astrometric position they could determine for SgrA*. While with hindsight we can see that this difference is significant, so strong was the belief that SgrA* must be associated with a stellar-like source, they concluded IRS16–

C represented the centre of the Galaxy. Making this identification allowed the cusp-like distribution inferred in [2] to be extended to within 0.6" of the centre, strengthening the case for a massive black hole. From its colour, significantly 'bluer' than the M–supergiant IRS7, the mean spectral type was estimated to be around mid–K. Thus, from the flux of IRS16–C they deduced that approximately 100 giants inhabited the 1" region around the nucleus. Storey and Allen must have had an inkling that all might not be right with this conclusion, however, for they very wisely finished off their paper with a recommendation that improved astrometry be obtained to better tie together the radio and infrared reference frames!

David's next contribution to the Galactic Centre was the one that really made his mark on the field, and has a controversy still raging today. With Bob Saunders he indeed obtained the better data needed above. They asked the question in the title of a provocative Nature paper "the galactic centre black hole: only a dwarf?" [5]. Having identified common features in L' and M (4.8μm) band images to the radio 6-cm image of Lo & Claussen (1983), it was clear that SgrA* was over 1" W of IRS16–C. While in agreement with the earlier result in [4], this time it was certain the offset was for real.

The implications were considerable. A faint IR source was associated with SgrA*, but now the complex structure around IRS16 could no longer be identified as the core of a cusp around the central object. Any black hole associated with SgrA* must have low luminosity. To provide the UV energy required to heat the dust and produce the far–IR emission would have needed a K band flux at least 20 times greater. Thus SgrA* could not be providing the bulk of the luminosity from the nucleus. This then raised the question of the source of the ionizing radiation? Allen & Saunders argued that the M supergiants present implied a burst of star formation about 10^7 years ago, leaving a concentration of B stars there now. They thus concluded that around 100 B stars made up IRS16, split into the four components then identified, which together provided the luminosity for the Galactic centre. However, this raised a severe problem for the massive black hole model. The proximity of the IRS16 'clumps' to SgrA* would result in their dispersion within a few hundred years, unless star formation was continuously occurring. But the tidal field of a massive black hole would inhibit the latter process. Allen & Saunders provided us with a coherent picture; an isothermal core with radius 0.1 pc and central stellar density $> 10^7 M_\odot pc^{-3}$, a few small associations of newly formed B stars within that core, and an accreting black hole with a mass of no more than 100 $M_\odot$.

The next piece of work [6, 11] developed this idea further. On the scene came FIGS, and the ability to obtain spectral images. A spectral cube in Brα (4.05μm) showed both broad and narrow components to the line, with

striking changes in only 1.5". The broad component, over 1000 km/s in extent, was likened to the profiles seen in Wolf-Rayet stars. Images in and outside the CO bandhead absorption features (at 2.3μm) revealed a bimodal population of hot (no absorption) and cool (with absorption) stars. The hot star distribution was strongly peaked on IRS16. It was concluded this represented a population of early-type stars, whereas the cool stars were M giants and supergiants. The most interesting feature in the spectral cube, however, turned out to be that of He I (2.06μm), where a single bright star (the 'AHH' star) was apparent. With a profile similar to the broad hydrogen lines, and a strength twice that of the 2.16μm Brγ line, such a spectrum had only been seen before in supergiants classified as WN9 and Ofpe in the Magellanic Clouds (McGregor, Hillier & Hyland, 1988). Finally, an unidentified line was discovered at 2.22μm, confined to the radio 'mini-cavity' 3" to the SW of SgrA*. This has only recently been identified as due to [Fe III] (Lutz *et al.*, 1994). Folding all this into the picture, their conclusion was that a burst of star formation occurred in the Galactic Centre a few million years ago, leading today to the hot, evolved wolf-rayet-type AHH star, and a cluster of 10-100 $B_{[e]}$ stars associated with IRS16. With temperatures ~30,000 K, luminosities in the range $10^{5-6} L_{\odot}$ and masses in the range 20-60 $M_{\odot}$, together they account for virtually all the UV and bolometric luminosity of the central parsec. They suggested our galaxy be regarded as a weak starburst.

Technology development marched on, and in the early 90's the AAO finally obtained a Rockwell IR array detector. IRIS was built to house it, and a new camera turned to the Galactic centre. Through drift scan imaging, 3D data cubes were again built up containing the entire K–band spectrum. They were both considerably more extensive, had better spatial resolution, and went much deeper, than the FIGS variety. David was first involved in some perhaps incidental work before he resumed the study of the stellar population. Better images of the H_2 (2.12μm) and Brγ lines were obtained [8, 13], illustrating the hot molecular gas in the circumnuclear disk and showing a close correspondence between the IR and radio recombination lines (but not exact, which lead an interesting study by Roberts and Goss (1993) on the 3D geometry). The spectra lead some support to the PDR model for the excitation of the molecular ring, and helped rule out a hot, ionized bar. On the discovery of a transient radio source, IRIS was used to search for a stellar counterpart [7]. Curiously, the transient appeared in the middle of one of the dense clouds of the circumnuclear ring, leading to speculation of a SN. However no source was identified, and the limits placed on its IR luminosity made such a scenario look unlikely.

The delay in receiving an array meant that David missed being the actual discoverer of the cluster of He I stars (Krabbe *et al.*, 1991), and the

demonstration that these could provide the UV to power the $10^7 L_\odot$ far–IR luminosity from the central parsec. But IRIS soon confirmed this result [8], and quickly extended the range of stellar types that make up the young cluster through images in the line of [Fe II] 1.64μm [13] and by extending the technique of hot and cool star separation previously demonstrated with the FIGS [10, 16]. Some 30 or so hot emission line stars were identified in the Galactic core from their He I, Brγ, [Fe II] and/or lack of CO bandhead emission. They are surrounded by the ionized gas of the radio 'mini-spiral', also seen clearly in the Brγ image. This ionized gas abutts the inside edge of a hot, clumpy molecular ring, seen in the light of H_2 [8].

Most intriguing, however, was David's last piece of analysis, from the hot and cool star separation [10, 14]. It revealed that the hot, population I stars formed a tight cluster, with a very much more compact core than that of the population II stars of the Galactic bulge, seen in the cool star picture. The comparison with Eckart *et al's* (1993) speckle data was fascinating. They saw 350 individual sources in the inner parsec, contributing at least 90% of the flux there, and each brighter than K$\sim$ 14. These sources also formed a tight core, of radius about 4" (0.2 pc), and their absolute absolute magnitude required them to be either M giants or OB stars. The *flux* distribution of hot stars was virtually identical to the *number* distribution of Eckart *et al.* David concluded that they represented the same population.

The implications were considerable. It would imply these 350 stars were essentially all OB stars; young, massive stars that only recently formed, with the most massive just starting to evolve off the main sequence. They form a population I core to the centre of the Galaxy, with a combined mass in the range $10^{3-4} M_\odot$. They would not, however, dominate the mass in the centre. This would be either from the cool stars, or from a massive central object. But the comparison could be taken further. From the $\sim$ 100 km/s velocity dispersion seen in CO (Sellgren *et al.*, 1990), and the 20" (1 pc) core radius of the cool star flux distribution, a mass density of $10^6 M_\odot pc^{-3}$ is derived for the inner parsec, similar to that obtained from dynamical arguments of the gas motions. If SgrA* were to weigh $10^6 M_\odot$ then the central parsec would be virtually devoid of stars (other than the 350 seen by Eckart *et al.*). The (simpler) alternative is that there is no large central object, and the combined mass of the cool, bulge stars dominates.

This conclusion is, to say the least, controversial! Its validity depends on whether the flux and number distributions can indeed be equated. Already some evidence has been presented at this conference by Reinhard Genzel to suggest that this might not be the case. If not, and the core radius really is as small as 4", then the central mass density would rise to $\sim 10^8 M_\odot pc^{-3}$, easily accommodating the requirements of a massive black hole.

While the argument over the central mass continues, the evidence for a starburst grows. David used IRIS to explore selected regions in the central 50 parsecs [9, 12, 15], initially to seek an ionization source for the arched radio filaments. Instead, a number of new star clusters were discovered, and spectroscopic imaging has shown they also contain similar emission line stars as those in the nucleus. Not as many, but still suggesting a recent episode of massive star formation, which has now left WN and $B_{[e]}$ stars. The conditions in these clusters are not extreme, and no other reasonable explanation other than star formation has been given for their presence. It suggests the conditions of the central parsec are not unique, and thus calls into question explanations other than star formation for the massive stars found there.

4. Conclusions

I have tried to describe David Allen's immense contributions to the debate on the Galactic nucleus, though any such account can only be incomplete. Although David knew his own picture would surely evolve as observations continued to improve, he left us believing he had given us a view which was both self-consistent and simple. It is one of life's tragedies that he will no longer be able to respond to the latest data, and develop his own theories to accommodate them. I would like to use David's own words to summarise his picture, as presented in his own unique style at the last conference he attended, a workshop on the Galactic Centre held at Sydney University in November 1993.

> "The Galactic centre is a retirement village where old population II stars go to live out their closing years. But we see a second, younger population in the central parsec. Why? A group of young stars formed there $\sim 10^7$ years ago, presumably as the result of a molecular cloud collision. Dynamical interactions have pushed the population II stars outwards. In other words, when the hooligans arrived the old folk feared for their well being and moved out!"

And David leaves us with two questions:

- Why the small spread in mass and spectral type?
- Is the dynamical timescale adequate?

To end, I would like to pass on two pieces of wisdom that David was fond of telling us about. The first was the principle of Ockham's Razor. Now that SgrA* is no longer at the centre of the light distribution, nor is needed to account for the luminosity and the mass loss rate, why do we still need to use it account for the mass (since this is why a large central mass was first postulated)? The second is that the inner cluster, for which we now observe

such complex structure, would only subtend 0.1" even at the distance of the nearby Andromeda Galaxy. Yet we cannot claim to understand its origin. Surely therein lies cautionary advice for active galaxy pundits.

5. Bibliography

5.1. PAPERS IN REFEREED JOURNALS

Allen, D. A. and Wickramasinghe, D. T. (1981) 'Diffuse interstellar absorption bands between 2.9 and 4.0 μm', *Nature*, 294, 239. [1]
Allen, D. A., Hyland, A. R. and Jones, T. J. (1983) 'High-resolution images of the Galactic centre', *Mon. Not. R. Astr. Soc.*, 204, 1145. [2]
Storey, J. W. V. and Allen, D. A. (1983) 'The Galactic nucleus', *Mon. Not. R. Astr. Soc.*, 204, 1153. [3]
Jones, T. J., Hyland, A. R. and Allen, D. A. (1983) '3μm spectroscopy of IRS 7 towards the Galactic centre', *Mon. Not. R. Astr. Soc.*, 205, 187. [4]
Allen, D. A. and Sanders, R. H. (1986) 'The Galactic centre black hole: only a dwarf?' *Nature*, 319, 191. [5]
Allen, D. A., Hyland, A. R. and Hillier, D. J. (1990) 'The source of luminosity at the Galactic centre'. *Mon. Not. R. astr. Soc.*, 244, 706. [6]
Zhao, J-H., Roberts, D. A., Goss, W. M., Frail, D. A., Lo, K. Y., Subrahmanyan, R., Kesteven, M. J., Ekers, R. D., Allen, D. A., Burton, M. G. and Spyromilio, J. (1992) 'A transient radio source near the center of the Milky Way Galaxy', *Science*, 255, 1538. [7]
Burton, M. G. and Allen, D. A. (1992) 'Imaging the hot molecular gas at the centre of the Galaxy', *Proc. Astr. Soc. Aust.*, 10, 55. [8]
Cotera, A. S., Erickson, E. F., Allen, D.A., Colgan, S. W. J., Simpson, J. P., and Burton, M. G. (1994) 'A cluster of hot stars near the galactic center arched filaments', *Astrophys. J.*, in preparation. [9]
Allen, D. A. and Burton, M. G. (1994) 'The population I core of the Galaxy', *Proc. Astr. Soc. Aust.*, 11, 191. [10]

5.2. PAPERS IN CONFERENCE PROCEEDINGS

Allen, D. A., Hyland, A. R., Hillier, D. J. and Bailey, J. A. (1989) 'The stars that power the Galactic centre', *Int. Astr. Union Symp.*, 136, 513. [11]
Cotera, A. S., Erickson, E. F., Simpson, J. P., Colgan, S. W. J., Allen, D. A. and Burton, M. G. (1992) 'A new cluster of hot stars near the Galactic center', *Bull. Amer. Astr. Soc.* 24, 1262, *ABSTRACT*. [12]
Burton, M. G. and Allen, D. A. (1993) 'Near–IR imaging spectroscopy of the hot gas in the centre of the Galaxy'. In *Astronomical Infrared Spectroscopy: Future Observational Directions*, ed. S. Kwok, *Astr. Soc. Pacif. Conf. Ser.*, 41, 289. [13]
Allen, D.A. (1994) 'The central stellar cluster', Ringsberg conference on *The Galactic Centre*, in press. [14]
Cotera, A. S., Erickson, E. F., Allen, D.A., Colgan, S. W. J., Simpson, J. P., and Burton, M. G. (1994) 'The discovery of hot stars in the vicinity of the thermal filaments', Ringsberg conference on *The Galactic Centre*, in press. [15]
Burton, M.G. and Allen, D.A. (1994) 'The population I core at the centre of the Galaxy', *Proc. Airborne Astronomy Symp. on the Galactic Ecosystem: From Gas to Stars to Dust*, ed. M. R. Haas, J. A. Davidson and E. F. Erickson, (San Francisco: ASP), in press. [16]

5.3. POPULAR ARTICLES

Allen, D. A. (1983) 'The heart of our Galaxy', *Yearbook of Astronomy 1984*, 147. [17]
Allen, D. A. (1993) 'What lurks at the centre of our Galaxy?', *Yearbook of Astronomy 1994*, 125. [18]

References

Eckart, A., Genzel, R., Hofmann, B., Sams, B.J and Tacconini-Garman, L.E. (1993) *Ap. J. Lett.*, 407, L77.
Lacy, J.H., Townes, C.H., Geballe, T.R. and Hollenbach, D.J. (1980) *Ap. J.*, 241, 132.
Lo, K.Y. and Claussen, M.J. (1983) *Nature*, 306, 647.
Lutz, D., Krabbe, A. and Genzel, R. (1994) *Ap. J.*, in press.
Krabbe, A., Genzel, R., Drapatz, S. and Rotaciuc, V. (1991) *Ap. J. Lett.*, 382, L19.
McGregor, P.J., Hillier, D.J. and Hyland, A.R. (1988) *Ap. J.*, 334, 639.
Roberts, D.A. and Goss, W.M. (1993) *Ap. J. Supp.*, 86, 133.
Sellgren, K., McGinn, M.J., Becklin, E.E. and Hall, D.N.B. (1990) *Ap. J.*, 359, 112.

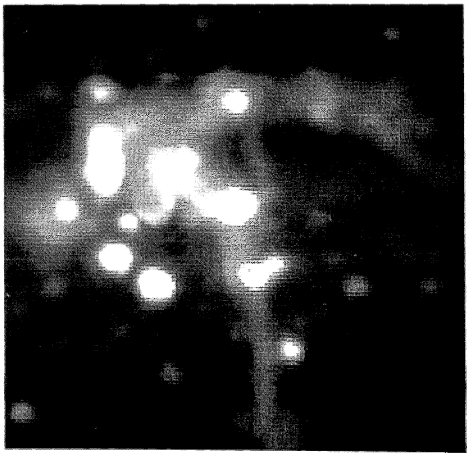

Figure The IRPS 3.8μm image (from [5]) in blue, overlaid on the 6-cm radio continuum image of Lo & Claussen (1983) in red, tying together the radio and infrared reference frames via the emission from IRS 2/13, seen in both frames. This image demonstrated clearly that IRS16-C (which is not priminent at these wavelengths) and SgrA* were two separate sources. SgrA* is the rbight red soiurce just to the right of the center and IRS 7, the brightest sources at 2μm, is the blue star directly above it. IRS 2/13 are the pair of white sources just below right from SgrA*

(For colour plate of figure see page xx)

Figure An image of the hot stars and gas in the centeral 2 parsecs of the Galaxy, obtained with the method of spectroscopic drift scanning of IRIS (from [8].) Blue denotes emission from a HeI line at 2.06μm, and shows a cluster of a dozen massive stars in the nucleus. They are surrounded by the ionized ghas ofthe radio "mini-spiral", here seen in green through the ermission of hydrogen Brγ at 2.17μm. Surroudning the ionized cavity is a hot clumpy molecular ring, seen in red through the light of molecular hydrogen at 2.12μm.

(For colour plate of figure see page xx)

DYNAMICAL EVOLUTION OF GALACTIC CENTER STAR CLUSTER AND IMPORTANCE OF STELLAR COLLISIONS

HYUNG MOK LEE
Pusan University
Department of Earth Sciences, Pusan 609-735, Korea

1. Introduction

The Galactic Center (GC) star cluster is a compact stellar system. The *surface brightness distribution* at infrared has core radius of about 0.8 pc (Rieke & Lebovsky 1987) when the contribution from bright stars are removed. On the other hand number counts of infrared sources in the high resolution speckle image by Eckart et al. (1993) at 2.2 μm gives 0.15 pc for the core radius of the *surface density distribution.* At present it is not clear which is more appropriate for the *mass distribution.* If we assume that the central star cluster is an isothermal sphere, the central density and the core radius are related via

$$\rho_c = \frac{9\sigma^2}{4\pi G r_c^2} \approx \begin{cases} 2.7 \times 10^6\,\mathrm{M}_\odot\,\mathrm{pc}^{-3} & \text{if } r_c = 0.8 \text{ pc;} \\ 7.4 \times 10^7\,\mathrm{M}_\odot\,\mathrm{pc}^{-3}. & \text{if } r_c = 0.15 \text{ pc.} \end{cases} \quad (1)$$

where we have assumed one-dimensional velocity dispersion $\sigma = 100\,\mathrm{km/sec}$. Therefore the central density depends sensitively on the measured value of the core radius. The central relaxation time of the cluster also varies greatly depending on the central density,

$$t_{rel} \approx \begin{cases} 6 \times 10^8 \mathrm{yrs}, & \text{if } r_c = 0.8 \text{ pc;} \\ 2 \times 10^7 \mathrm{yrs}, & \text{if } r_c = 0.15 \text{ pc.} \end{cases} \quad (2)$$

where we have assumed that the mass of individual star is $1\,\mathrm{M}_\odot$. Since core collapse takes place in many multiple of the central relaxation time (i.e., 20$\sim$ 300, e.g., Cohn 1980) one does not expect much evolution during Hubble time if the core radius is 0.8pc while significant evolution should have occurred if the core radius is 0.15 pc.

L. Blitz and P. Teuben (eds.), Unsolved Problems of the Milky Way, 215–223.
© 1996 *International Astronomical Union.*

For the case of high stellar density core (i.e., $r_c = 0.15\,\mathrm{pc}$), one also expects very frequent stellar collisions. The consequences of close encounters depend on the relative velocity at infinity (v_{rel}); merger for $v_{rel} < v_{esc}$ and complete disruption for $v_{rel} > v_{esc}$, where v_{esc} is the escape velocity from the stellar surface. Since $\sigma \approx 100\,\mathrm{km/sec}$ in the GC, merger is a natural consequence of stellar collisions. It should be noted that the relaxation time is usually short if the collision time is short. This means that the dynamical evolution must be taken into account if one wants to consider the time dependent stellar mergers.

Recently Brown & Bethe (1994) proposed that stars with main-sequence mass greater than $\sim 25\,\mathrm{M}_\odot$ would leave black holes of $\sim 10\,\mathrm{M}_\odot$ behind at the end of stellar evolution. Such black holes would comprise around 0.5 $\sim$ 1 % of the stellar mass if Salpeter mass function with relatively large high mass cut-off is assumed. Even such a small amount of black holes could be dynamically important as discussed by Lee (1995).

In this review, we discuss two aspects of the dynamical evolution of GC star cluster: (a) effects of the stellar merger and (b) effects of $10\,\mathrm{M}_\odot$ black holes.

2. Dynamical Evolution with Successive Mergers

The stellar merger may be regarded as an alternative process of forming high mass stars. About 15 HeI/HI emission line stars have been identified in GC region (e.g., Krabbe et al. 1991) and they are interpreted as $20 \sim 40\,\mathrm{M}_\odot$ stars by Najarro et al. (1993). Since lifetimes of these stars are fairly short, there might have been star formation activity in the past 10^7 years. However, the strong tidal field in GC region requires very high density ($n_H \gtrsim 10^7\,\mathrm{cm}^{-3}$) for gravitational collapse. Such high density clouds are not completely ruled out by the present observations (Jackson et al. 1993), but there is no convincing evidence for the star formation activity either.

Is it possible that the high mass stars are born outside the center and segregated to the present location via dynamical friction? The answer is clearly no because the time scale for dynamical friction is longer than the lifetime of these stars. Thus the difference in the core radii for *surface brightness distribution* and *surface density distribution* has not been caused by the equipartition process alone. We examine merger scenario as an alternative for the formation of high mass stars below.

2.1. MODELS FOR SUCCESSIVE MERGERS

The formation process of high mass stars via stellar mergers may be modeled by simple rate equations (Lee 1989). However, other dynamical effects

such as relaxation and dynamical friction should be taken into account. One also has to consider the fact that stars live only finite amount of time.

Rather crude modeling for successive mergers including relaxation, dynamical friction, and evolution of high mass stars was introduced by Lee (1987) in the context of globular cluster evolution by integrating (modified) Fokker-Planck equation. Application of this method to denser stellar systems of galactic nuclei was done by Quinlan & Shapiro (1990). The main purpose of these studies are to test the possibility of 'runaway merger' which could lead to the formation of a central black hole followed by the formation of very massive star which is dynamically unstable.

More specific study towards the GC in an attempt to estimate the number of high mass stars formed through successive merger was performed by Lee (1994). The result of this study is negative since the number of stars exceeding $20\,M_\odot$ is of order of 1 at most. Because of indirect heating effect due to the stellar evolution, the core collapse stops at some point and the cluster begins to expand as the heating rate eventually exceeds the rate of conductive outflow of the energy. Numbers of merger products reach maxima just after the maximum density.

The number of high mass stars is rather sensitive to the stellar lifetime. The stars formed by successive mergers may be rapidly rotating and the stellar lifetime could be longer than non-rotating stars. In Table 1, we have compared the maximum number of stars formed by mergers for two different assumptions in lifetimes: the case with standard values and the case with twice the standard values. Other model parameters are chosen to resemble the GC (see Lee 1994 for details). As can be seen from this table, the number of stars with $> 20\,M_\odot$ can be as large as 5. The observed number of HeI/HI stars of about 15 is larger by only a factor of few. Since the HeI/HI stars are in temporary phase of the stellar evolution, actual number of $M > 20\,M_\odot$ stars are likely to be much larger then 15. Thus the successive merger does not appear to be a dominant process of forming high mass stars.

TABLE 1. Maximum Number of Stars Formed by Mergers

Mass ($M_\odot$)	Standard Lifetime	2× Standard Lifetime
1.4	4.5×10^5	4.6×10^5
2.8	2.0×10^4	2.6×10^4
5.6	940	1960
11.2	30	160
22.4	0.3	5.3

In the Fokker-Planck calculations, we have assumed that the mass lost by stellar evolution would leave the entire cluster in a short amount of time. If the gas can stay in the vicinity of cluster's core, the heating rate would not be enough to stop the core collapse. The stellar merger then would take place in an accelerated manner. It is possible to have much more high mass stars ($M > 20\,M_\odot$) than the values tabulated in Table 1. However, the core radius of the cluster should be very small.

2.2. SHORTFALLS AND POSSIBLE SOLUTIONS

There are two serious problems in the merger scenario for the formation of high mass stars. First, in order to form 20 $M_\odot$ stars, there must be a much larger number of slightly lower mass stars (i.e., 10 $M_\odot$). Table 1 shows the maximum number of 11.2 $M_\odot$ stars can be 50 to 100 times larger than that of 22.4 $M_\odot$ stars. These stars could be observed from the GC region. Second, the velocity dispersion of the high mass stars should be smaller than the 'average' velocity dispersion. Since stellar merger is completely inelastic process, the velocity dispersion of the merged stars dictates that of the equipartition (i.e., $m_1 < v_1^2 >= m_2 < v_2^2 >$). Such a behavior of velocity dispersion has not been observed.

If there is a black hole in the center of the Galaxy, the velocity dispersion would not depend on the mass. The stellar distribution within $r_b = GM_B/v^2$ would follow $r^{-7/4}$ (e.g., Bahcall & Wolf 1976). The collisional frequency then becomes much larger than that for the case with flat core. Actual calculation of stellar merger with a central black hole has not been carried out yet, but it would be interesting to see if the presence of black hole would solve the problems mentioned above.

3. Effects of Remnant Stars

The stellar evolution inevitably produces remnant stars such as white dwarfs, neutron stars and black holes. The white dwarfs may not give important effects on dynamical evolution but neutron stars and black holes could be important.

If there are significant number of 10 $M_\odot$ black holes in the GC, dynamical friction will bring the black holes into the central parts in $(m_*/m_B)\,t_{rel} \ll t_{rel}$, where m_* and m_B are masses of normal stars and black holes, respectively. After the formation of a black hole subsystem, it evolves quickly because the relaxation time becomes very short. There are many interesting physical processes within the black hole clusters.

3.1. BLACK HOLE BINARIES AND DYNAMICAL EVOLUTION

After the subsystem of black hole is formed, the black hole cluster undergoes core collapse like ordinary stellar systems. Binaries via three-body processes can form rather efficiently because the rate of binary formation is proportional to $m_B^5 n_B^3 \sigma_B^{-9}$, where n_B is the number density and σ_B is the velocity dispersion of the black holes.

The binaries become heat source when they interact with other black holes. The core collapse eventually stops and the central core of black hole subsystem begins to expand. The 'post-collapse' expansion driven by binaries formed via three-body processes (three-body binaries in short) can be characterized by self-similar evolution for the case of single-component, isolated clusters. The core and the half-mass radii expand at the same rate. However, since the black hole cluster is embedded in a much larger stellar cluster, the time scale for the expansion is set by the half-mass relaxation time of the surrounding cluster which is much longer than the Hubble time. Thus the energy released from the black hole binaries can be absorbed by the stellar cluster. It might be possible to maintain nearly static two-component structure for a very long time as discussed by Goodman & Lee (1989). Since the size of the black hole cluster is very small, the cluster of black holes may be indistinguishable from a single massive black hole in the center.

However, there may be a destabilizing affect. Ordinarily binaries are eventually ejected from the stellar system when the hardness (ratio of orbital kinetic energy to average kinetic energy of background stars) becomes very large ($\sim$ a few 100). For the tight black hole binaries the gravitational radiation effect can be quite important. In the stellar system with $\sigma \gtrsim 100\,\mathrm{km/sec}$ the binaries are found to 'merge' due to gravitational radiation reaction before they are ejected.

Lee (1993) showed that a runaway merger would produce a 'seed' black hole in the center of a dense stellar system composed of neutron stars. Such a runaway merger is also a possible product in the black hole subsystem if the the 'merger time scale' is short.

Numerical modeling for two-component clusters composed of $0.7\,M_\odot$ main-sequence stars and $10\,M_\odot$ black holes was carried out by Lee (1995) using Fokker-Planck equation. Heating by three-body binaries enables the post-collapse evolution, which is characterized by rapid oscillations of core density. The black hole cluster expands rather slowly because the surrounding star cluster absorbs the energy.

It is difficult to judge if the runaway merger is possible because of the statistical nature of Fokker-Planck calculations. More realistic N-body calculations are necessary to determine the merger instability.

If a seed black hole of mass comparable the core mass of the black hole subsystem forms, it can grow by absorbing surrounding black holes and stars.

3.2. OBSERVATIONAL CONSEQUENCES

If the two-component phase of star-black hole configuration is long-lived, black hole subsystem may be kinematically similar to a massive central black hole. One of the argument against the massive black hole in the GC is the lack of X-ray radiation (e.g., Ozernoy 1994). Similar arguments can be applied to the two-component cluster for GC (and possibly for other nearby galaxies). The least violent interaction between a black hole and a main-sequence star will be tidal capture. Large fraction of tidally captured main-sequence stars will be destroyed during the circularization process because the energy to be deposited to the normal star exceeds star's gravitational binding energy if mass ratio between the black hole and the normal star is large (Lee 1992). We now estimate the rate of tidal capture.

Suppose that the black hole cluster is embedded in a flat core of normal stars. Then the total number of tidal capture per unit time can be expressed as

$$\frac{dN_{tc}}{dt} = \int_V n_* n_B < \Sigma_{tc} v_{rel} > dV \approx n_* N_B < \Sigma_{tc} v_{rel} >, \tag{3}$$

where n_* and n_B are number densities of normal stars and black holes, respectively, N_B is the total number of black holes, and Σ_{tc} is the tidal capture cross section. The relative velocity between a normal star and a black hole can be replaced by the velocity of normal star, and the brackets represent the average taken over the velocity distribution. Using the overlap integrals for tidal interactions tabulated by Lee & Ostriker (1986), we obtain $R_{min} \approx 8.6 R_*$ for $m_B/m_* \approx 14$ (i.e., $m_* \approx 0.7\,\mathrm{M}_\odot$) and $v_{rel} = 100\,\mathrm{km/sec}$. If we assume that the cross section is dominated by gravitational focusing we may write

$$\frac{dN}{dt} \approx 8.6\pi R_* n_* N_B 2G m_B \left\langle \frac{100\,\mathrm{km/sec}}{v_{rel}} \right\rangle \tag{4}$$

$$\approx 5 \times 10^{-6} \left(\frac{n_*}{10^6\,\mathrm{pc}^{-3}}\right) \left(\frac{N_B}{10^4}\right) \left(\frac{100\,\mathrm{km/sec}}{\sigma}\right) \mathrm{yr}^{-1} \tag{5}$$

where we have assumed $R_* = 0.7\,\mathrm{R}_\odot$. If we accumulate the above rate over Hubble time, the number of black hole binary would be over 10^4 for GC. Such a large number of binaries may not be compatible with the observations.

If the large fraction of tidal capture leads to the disruption of main-sequence stars, more appropriate quantity is the *instantaneous* luminosity from accretion. Some fraction ($\lesssim 50\%$) of the gas released from the star will be bound to the black hole. They will eventually be accreted to the black hole and radiation will be released. The tidal capture rate estimated above can thus be translated into the upper limit of $2.5 \times 10^7\,L_\odot$ on accretion luminosity. Here we have assumed efficiency of 10% for the conversion of rest mass energy into radiation. Clearly this is also too large compared to the upper limit of 250 $L_\odot$ on X-ray luminosity see Genzel et al. 1994 for a summary). However, the total UV luminosity of about $10^7\,L_\odot$ is not much different from the accretion luminosity estimated above. The central cluster of hot stars are assumed to be liable for the entire UV luminosity, but it is tempting to postulate that the HeI/HI stars are Thorn-Zytkow type (Thorne & Zytkow 1977) accretion flows around the black holes (Morris 1993).

4. Summary

The observed characteristic of the GC cluster is examined in view of dynamical evolution theories. If the core radius of the *mass distribution* is as small as 0.15 pc, one expects rather frequent collisions between stars. High mass stars can be formed through successive mergers. However, we found that the number of high mass stars ($\gtrsim 20\,M_\odot$) are not enough to explain HeI/HI stars observed in GC region. Also the merger scenario predicts small velocity dispersion for high mass stars than what is observed. These difficulties may be relieved by the introduction of central black hole, but actual calculation has not been carried out yet.

The possible effects of 10 $M_\odot$ black holes, which might have formed in early history of the Galaxy through the collapse of He core of high mass stars, are examined. These black holes would evolve separately by forming a subsystem within the flat core of star cluster. The black hole cluster undergoes rapid core oscillation after the core collapse but the general expansion is very slow because the surrounding star cluster effectively absorbs the expansion energy generated by black hole binaries. During this near static two-component phase, a central seed black hole might form through runaway merger of black holes followed by formation of binaries via three-body processes.

If the runaway merger does not take place within Hubble time, the two-component cluster should give some interesting observational consequences. First, the kinematic signature of central massive black hole will also be observable because the size of black hole subsystem is very small. Second, the tidal interactions between main-sequence stars and black holes will

inevitably lead to the accretion of stellar mass. The estimated upper-limit for accretion luminosity is close to the total UV luminosity in the central cluster of hot luminous stars.

Acknowledgements

This work was supported in part by the Korea Science Engineering Foundation under Grant No. 941-0200-001-2 and in part by National Science Foundation under Grant No. PHY89-04035.

References

Bahcall, J. N., & Wolf, R. A., 1976, ApJ, 209, 214.
Brown, G. E., & Bethe, H. A., 1994, ApJ, 423, 659.
Cohn, H., 1980, ApJ, 242, 765.
Eckart, A., Genzel, R., Hofmann, R., Sams, B. J., Tacconi-Garman, L. E., 1993a, ApJ, 122, 433.
Genzel, R., Hollenbach, D., & Townes, C. H., 1994, Rep. Prof. Phys, 57, 417.
Goodman, J., & Lee, H. M., 1989, ApJ, 337, 84.
Jackson, J. M., et al. 1993, ApJ, 402, 173.
Krabbe, A., Genzel, R., Drapatz, S., & Rotaciuc, V., 1991, ApJ, 382, L19.
Lee, H. M., 1987, ApJ, 319, 801.
_____, 1989, in *Dynamics of Dense Stellar Systems*, ed. D. Merritt, Cambridge Univ. Press, p105.
_____, 1992, J. Korean Ast. Soc., 25, 47.
Lee, H. M., 1994, in *Nuclei of Normal Galaxies: Lessons from Galactic Center*, eds. by R. Genzel & A. I. Harris, (Dordrecht:Kluwer) in press.
Lee, H. M., 1995, MNRAS, in press.
Lee, H. M., & Ostriker, J. P., 1986, ApJ, 322, 123.
Lee, M. H., 1993, ApJ, 418, 147.
Morris, M., 1993, ApJ, 408, 496.
Najarro, F., Hillier, D. J., Kudritzki, R. P., Krabbe, A., Lutz, D., Genzel R., Drapatz, S., & Geballe, T. R., 1993, A&Ap,
Ozernoy, 1994, in *Nuclei of Normal Galaxies: Lessons from Galactic Center*, eds. by R. Genzel & A. I. Harris, (Dordrecht:Kluwer) in press.
Quinlan, G. D., & Shapiro, S. L., 1990, ApJ, 356, 483.
Rieke, G. H., & Lebovsky, M. J., 1987, in *The Galactic Center, AIP Conference Series, No. 155*, ed. D. C. Backer, p91.

DISCUSSION

J. Grindlay: Let me point out that your estimate of $\sim 10^4$ (to even $\sim 10^5$) as a possible total number of $\sim 10 M_\odot$ BH remnants in the central cluster is unlikely - since in this case formation of LMXBs containing a $\sim 10 M_\odot$ BH and $\lesssim 1 M_\odot$ companion would be expected and these, in turn, would be detected as either (or both) persistent and transient bright ($\geq 10^{37}$ ergis) x-ray sources. In particular, these would show up as "x-ray novae", whereas in $\sim$20 year of x-ray coverage (since UHURU) no such transients

(now recognized to be BH LMXBs) have been detected from the Galactic Center. Similar constraints can be derived for the central cusp of neutron stars, although these are less likely to form and to be retained given their power mass and higher velocity than for $\sim 10 M_{\odot}$ BHs.

Lee: The expected number of black holes is $\sim 10^3$. Still you expect quite frequent encounters between black holes and normal stars. Because of large mass ratio between black holes and normal stars, and because of high velocity environment, the likely consequence of BH-normal star interaction is a total disruption of the star. Accretion of disrupted material is likely, but there are many uncertainties regarding physical processes after the disruption.

R. Sunyaev: Did you compute neutron star distribution? If they are numerous $\sim 10^5$ in the central cluster, they must form some amount of binaries with strong accretion. We do not see with GRANAT no traces and no place for such bright close as Neutron Star-normal star or Black Hole-normal star x-ray emitting binaries. At the same time they are observed practically in every globular cluster.

Lee: I haven't included neutron stars here. First of all, since neutron stars are much less massive than blackholes, their distribution will be less concentrated than black holes. Second, the probability of forming binaries is very small. The stars will be just disrupted as a result of close encounters.

A COMPARISON OF NEAR INFRARED SPECTRA OF THE GALACTIC CENTER HE I EMISSION LINE SOURCES AND EARLY TYPE MASS LOSING STARS

R. D. BLUM, D. L. DEPOY AND K. SELLGREN
The Ohio State University
174 W. 18th Ave., Columbus, Oh, 43210, USA

Abstract. We have obtained R $\approx$ 570 resolution K band spectra of eight sources in the Galactic Center, including four sources within the IRS 16 cluster, IRS 13, IRS 1W, and the compact He I emission line sources AF (also known as AHH) and AHH NW. We have also obtained R $\approx$ 570 H and K band spectra of nine galactic and LMC early–type mass–losing stars, including Ofpe/WN9 and WN stars. The spectra of both the Galactic Center sources and the comparison stars show a wide range of behavior in the He I (1.70 μm, 2.06 μm, 2.11 μm) and H I (Brackett series) lines. We find significantly larger He I equivalent widths in the AF source and two galactic early type mass losing stars than in any of the LMC stars. Several of the Galactic Center He I sources are found to have higher He I velocity widths than any of the galactic or LMC early type mass losing stars. At least one source, IRS 13, shows a strong red wing to the He I 2.06 μm emission.

1. Introduction

What is the source of radiation that ionizes the gas and powers the emission from dust at the Galactic Center? Two primary models have long been debated: (1) accretion onto a massive black hole and (2) young ($\lesssim 10^7$ yr) massive stars (see Genzel and Townes 1987 and Genzel, Hollenbach, and Townes 1994 for extensive reviews). Lebofsky, Rieke, & Tokunaga (1982) identified M supergiant stars in the Galactic Center (GC), supporting the recent star formation model. More recently, Forrest et al. (1987), Allen,

L. Blitz and P. Teuben (eds.), Unsolved Problems of the Milky Way, 225–230.
© 1996 *International Astronomical Union.*

Hyland, and Hillier (1990) and Krabbe et al. (1991) have identified compact He I sources and/or Brα emission sources with no radio counterparts in the GC. Allen et al. (1990) and Krabbe et al. (1991) interpreted the He I and accompanying H I emission as arising in the extended mass-losing envelopes of hot massive post-main-sequence stars. This interpretation is based on the similarity of the K band (λ=2.2 μm) spectrum of the GC He I source AF and the relative He I to Brγ line measurements of other GC He I sources compared to the near infrared (NIR) spectra of optically classified stars in the Large Magellanic Cloud and elsewhere in the Galaxy. In particular, the AF source has been classified as an Ofpe/WN9 star based on its K band spectrum as compared to similar spectra of a number of the LMC stars with this classification (Allen et al. 1990). If correct, this interpretation provides the most substantial evidence to date for the star formation model.

2. Observations

The majority of observations were obtained on the nights of 11 and 12 July, 1993 and 6 and 22 September, 1993 on the CTIO 4m telescope. The observations were made using the Ohio State Infrared Imager/Spectrometer (OSIRIS) in low resolution mode (R $\approx$ 570). OSIRIS employs a 256$\times$256 HgCdTe array and may be used in crossed-dispersed (simultaneous I (partial), J, H and K) mode. The GC sources (Figure 1) were observed solely in the K band (except AF) with a 120″$\times$1.3″ slit. The AF source and comparison stars (Figures 2,3) were observed in cross–dispersed mode with a 20″$\times$1.3″ slit. The spatial scale was 0.45″ pix^{-1}. A higher resolution (R $\approx$ 1350) 2.0 - 2.24 μm spectrum of IRS 13 was obtained in July, 1994 on the CTIO 4m. The spatial scale for this spectrum was 0.17″ pix^{-1}.

3. Discussion

The LMC Ofpe/WN9 stars were first classified by Walborn (1977) and they now number ten stars in all (Bohannan and Walborn 1989). These mass–losing stars are believed to be precursors to the Wolf-Rayet stage and hence are likely to be helium enriched and massive.

The defining characteristic of the Ofpe/WN9 stars in the NIR has been taken as a He I 2.06 μm / Brγ integrated line flux ratio greater than one, with broad line width in He I. Beyond this simple criterion, what more can quantitatively be said regarding the nature of the GC sources in the absence of optical spectra? To begin, we have analyzed the H I and He I emission lines in a number of LMC and galactic (Ofpe/WN9 and other hot supergiant) stars and those in the GC for a direct comparison. A full description of the GC and LMC spectra and their analysis is given in Blum et al. (1994).

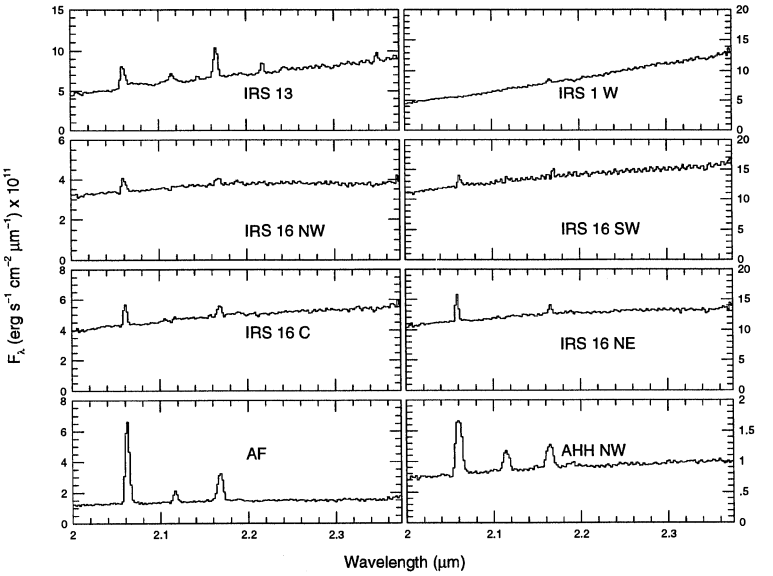

Figure 1. K band spectra of He I emission line sources in the Galactic Center showing the He I 2.06 μm and Brγ (2.17 μm) emission lines. Several sources also show He I emission at 2.11 μm. The lines near 2.14 μm, 2.22 μm, 2.24 μm, and 2.35 μm in IRS 13 are due to [Fe III]. These spectra were extracted from $\approx 1.8'' \times 1.4''$ apertures and include background subtraction from nearby ($\lesssim 2''$) apertures.

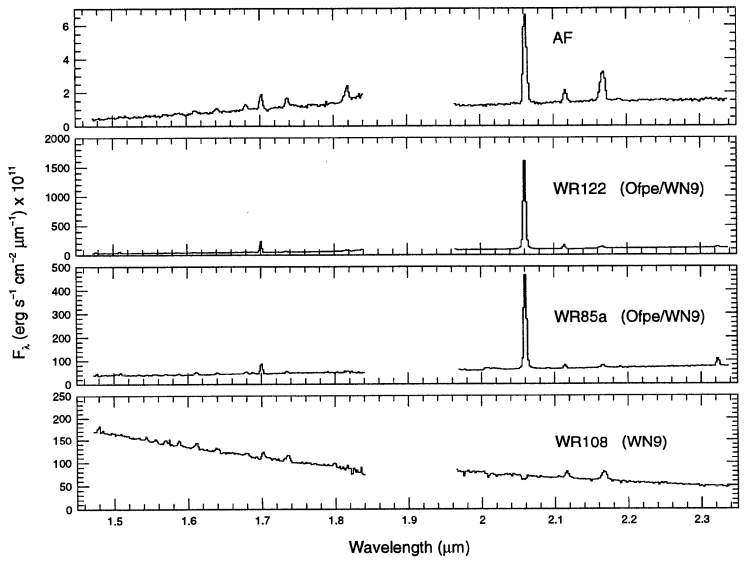

Figure 2. H and K band spectra of He I emission line sources in the Galaxy showing the He I 1.70 μm, 2.06 μm and 2.11 μm and Brackett series emission lines. Reliable detections are made for Brγ (2.17 μm) ,Br9 (1.82 μm), Br10 (1.74 μm), Br11 (1.68 μm), and Br12 (1.64 μm). These spectra were extracted from $\approx 2.3'' \times 1.4''$ apertures and include background subtraction from nearby ($\lesssim 5''$) apertures.

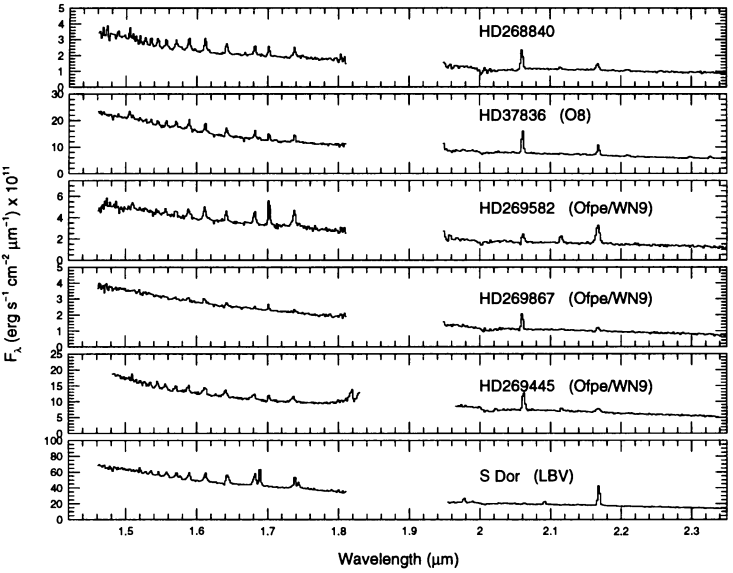

Figure 3. Same as Figure 2 but for He I Emission Line Sources in the LMC. Spectra of the Luminous Blue Variable, S Dor, which shows no He I, is shown for comparison. The lines near 1.69 μm, 1.74 μm, and 2.09 μm are due to Fe II.

The emission line analysis leads to the following results:

1.) The H I Brackett line ratios with respect to Brγ are larger than predicted for case B recombination (Hummer and Storey 1987; T_e=10^4 °K, $n_e > 10^4$) for the LMC stars and the galactic star WR85a. This suggests that the lines are optically thick (McGregor, Hyland, and Hillier 1988; Simon et al. 1983). The Brackett lines in the AF source are also interpreted as optically thick, if the extinction to this source is typical of the GC ($A_K \approx 3$ mag). The galactic Ofpe/WN9 star WR122 may be consistent with case B or optically thick line ratios depending on the extinction.

2.) The AF, AHH NW, WR85a, and WR122 stars have about an order of magnitude greater He I 2.06 μm equivalent width, W_λ, than the LMC stars. The range of W_λ, 109 to 715 Å, for these stars may be compared to the average W_λ=34 $\pm$10 Å for the LMC stars. The remainder of the GC sources have much smaller equivalent widths, on average a factor of 2 less than the LMC stars.

3.) All the highest velocity widths are observed in the GC; the galactic and LMC emission-line stars are unresolved at our resolution in the He I lines The GC He I widths range from unresolved to $\approx$ 1200 km s^{-1} (this is the observed FWHM, uncorrected for instrumental broadening).

4.) Several of the GC stars appear to have extended emission to the red of the He I 2.06 μm line. IRS 13 (Figure 1) is the most prominent example. The emission may result from blending of unknown lines or may

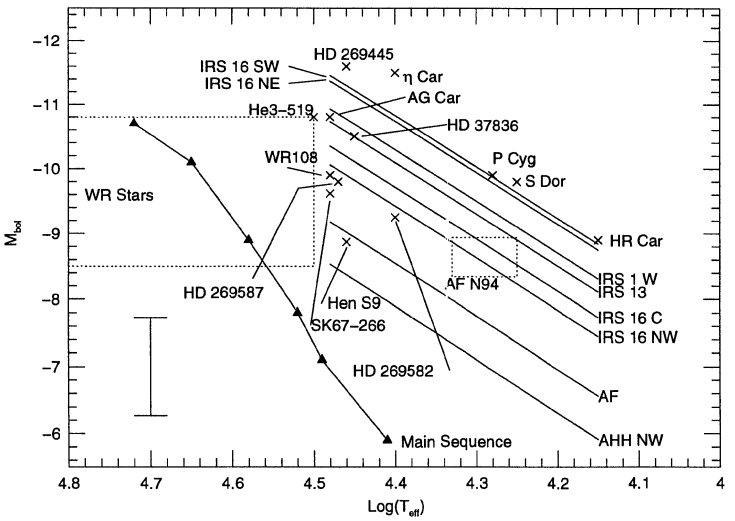

Figure 4. HR diagram for the GC sources and early-type mass-losing stars. The GC sources are shown as solid lines using the bolometric correction v. effective temperature relationship derived in Blum et al. (1994). Data for the individual comparison sources (crosses) are taken from the literature. The larger box (dashed lines) labeled "WR Stars" is reproduced from Humphreys and Davidson (1994). The smaller box (dashed lines) labeled "AF N94" depicts the model results of Najarro et al. (1994) for the AF source. The error bar shown is for the GC sources and corresponds to a $\pm$ 0.71 mag uncertainty in M_{bol} estimated from the derived bolometric correction relation added in quadrature to an assumed $\pm$ 0.5 mag uncertainty in the adopted reddening. The main sequence (Schmidt-Kaler 1982) is shown for comparison (filled triangles).

be associated with the 2.06 μm line. A high resolution spectrum of IRS 13 was obtained to further investigate this red wing emission (see Figure 4 of Blum et al. 1994). The wing does not break up into individual lines in the higher resolution spectrum.

5.) Subtraction of nearby background apertures is important in the GC where diffuse gas and unresolved stellar light contaminate the spectra. We find no He I emission in IRS 1W after background subtraction (see Figure 1). The embedded source(s) suggested by Rieke and Lebofsky (1982) and Rieke, Rieke, and Paul 1989, in IRS1 W does not appear to be a He I emission-line source. Krabbe et al. (1991) indicate that this source is contaminated by H II emission, but include it as a compact He I source. Libonate et al. (1994) also find no compact He I source at the position of IRS1 W.

Unambiguous spectral types for the GC sources would allow us to place them in the HR diagram and thus, better understand their impact on the GC environment. Our results clearly show significant differences between the LMC stars and the GC He I sources, so we can not yet assign de-

tailed spectral types; however, their spectra do show broad similarities. Therefore, we have placed the GC stars in the HR diagram (Figure 5) by deriving a bolometric correction at K from data in the literature and by considering a range of effective temperatures for the GC sources. The details of the construction of the HR diagram may be found in Blum et al. (1994). We consider an upper temperature limit based on temperatures of the Ofpe/WN9 stars and a lower limit based on mass losing stars that show no He I 2.06 μm emission. The HR diagram suggests that some of the GC sources may be among the brightest and most massive stars in the Galaxy.

References

Allen, D. A., Hyland, A. R., & Hillier, D. J., 1990, MNRAS, 244, 706
Blum, R. D., DePoy, D. L., & Sellgren, K., 1994, ApJ, submitted
Bohannan, B. & Walborn, N. R., 1989, PASP, 101, 520
Forrest, W. J., Shure, M. A., Pipher, J. L., & Woodward, C. E., 1987, in "The Galactic Center," ed. Backer, D. C., AIP, New York
Genzel, R. & Townes, C. H., 1987, ARAA, 25, 377
Genzel, R., Hollenbach, D. & Townes, C. H., 1994, "Reports on Progress in Physics, " in press
Hillier, D. J., 1984, ApJ, 280, 744
Hummer, D. G. & Storey, P. J., 1987, MNRAS, 224, 801
Humphreys, R. M. & Davidson, K., 1994, PASP, submitted
Krabbe, A., Genzel, R., Drapatz, S., & Rotaciuc, V., 1991, ApJL, 382, L19
Lebofsky, M. J., Rieke, G. H., & Tokunaga, A. T., 1982, ApJ, 263, 736
Libonate, S., Pipher, J. L., Forrest, W. J., & Ashby, M. L. N., 1994, ApJ, in press
McGregor, P. J., Hyland, A. R., & Hillier D. J., 1988, ApJ, 324, 1071
Najarro, F., Hillier, D. J., Kudritzki, R. P., Krabbe, A., Genzel, R., Lutz, D., Drapatz, S., & Geballe, T. R., 1994, A&A, in press.
Rieke, G. H. & Lebofsky, M. J., 1982, in "The Galactic Center," ed. Riegler & Blandford, AIP, NY, 194
Rieke, G. H., Rieke, M. J., & Paul, A. E., 1989, ApJ, 336, 752
Schmidt-Kaler, T., 1982, in *Landoldt-Bornstein, Numerical Data and Functional Relationships in Science and Technology*, Vol 2, Springer-Verlag, p. 453
Simon, M., Felli, M., Cassar, L., Fischer, J., & Massi, M., 1983, ApJ, 266, 623
Walborn, N. R., 1977, ApJ, 215, 53

DISCUSSION

A. Underhill: Have you considered the possibility that the emission lines you are observing may be formed in a disk driven wind?

MID-INFRARED (4.8 - 12.4 AND 20.0 μm) IMAGING OF THE GALACTIC CENTER: MODELING THE DUST EMISSION AND ENERGETICS OF THE CENTRAL PARSEC

DAN GEZARI, ELI DWEK AND FRANK VAROSI
NASA/Goddard Space Flight Center
Infrared Astrophysics Branch (Code 685)
Greenbelt, MD 20771

Abstract. We have modeled the mid-infrared emission from the Galactic Center using our array camera images at eight wavelengths. The results suggest that the high infrared luminosity of the region is provided by a cluster of luminous stars. There is no direct indication in the new model results of a very luminous object or "central engine" near Sgr A*.

1. Introduction

Two schools of thought have emerged which explain the high infrared luminosity and the apparent mass distribution in the Galactic Center. One contends that a recent episode of massive O star formation has occured (Rieke and Lebofsky 1982, Allen et al. 1990) which would account for the luminosity and ionizing radiation in the central few parsecs of the Galaxy. The other argues that the luminosity and central mass concentration are evidence for a "central engine" associated with Sgr A*, and that this object may be a massive black hole surrounded by an accretion disk (e.g. Lynden-Bell and Rees 1971, Rees 1982, Melia 1992).

The total infrared luminosity observed in the inner 2 parsecs of the Galactic Center is about 10^7 $L_\odot$ (Low et al. 1969, Becklin, Gatley and Werner 1982). There is evidence for the presence of a compact mass of $\approx 10^6$ $M_\odot$ within the central 0.1 pc (at or near Sgr A*) inferred from 12.8 μm Neon II emission line studies (Lacy et al. 1980) and 2.3 μm CO band observations (McGinn et al. 1989). These observations suggest that a very

L. Blitz and P. Teuben (eds.), Unsolved Problems of the Milky Way, 231–240.
© 1996 *International Astronomical Union.*

energetic, compact object may exist at the nominal Galactic Center.

Several new results now make the idea of a single, exotic, luminous object at the Galactic Center seem somewhat less appealing. A cluster of luminous Helium I emission line stars has been detected in the central parsec (Krabbe et al. 1991, Krabbe 1993) which represent a significant source of luminosity for Sgr A West. These stars were found to be correlated with infrared brightness features and the details of the color temperature distribution (Gezari 1992). The modeling of the infrared emission presented here, using our new diffraction limited (1 arcsec resolution) array camera images at eight wavelengths between 4.8 and 20.0 μm, gives the distribution of dust temperature, emission opacity, line-of-sight extinction, and total infrared luminosity are computed over the central 15 arcsec field-of-view (1 parsec = 24 arcsec at 8.5 kpc), providing a basis for detailed analysis of the energetics and morphology of the central parsec of the Galaxy.

2. Instrumentation and Observations

The image data were obtained with the 58 x 62 pixel mid-infrared array camera developed at NASA/Goddard. The camera uses a gallium doped silicon (Si:Ga) direct readout (DRO) photoconductor detector array manufactured Hughes/Santa Barbara Research Center, with six fixed interference filters between 7.8 - 12.4 μm ($\Delta\lambda/\lambda = 0.1$). A complete description of the array camera system is presented by Gezari et al. (1992).

The structure of the core of Sgr A West at 12.4 μm is shown in Figure 1 and Color Plate 2, part of a large-scale 12.4 μm mosaic image of the Galactic Center was assembled from 50 individual array camera exposures. The images were made at the 3.0-meter NASA Infrared Telescope Facility (IRTF) at Mauna Kea, image quality was seeing-limited at typically 1.1 arcsec (FWHM) and pixel size was 0.26 arcsec. Point source positions can be measured to a relative astrometric accuracy of $\pm$ 0.1 arcsec. The mosaics are assembled using our MOSAIC image analysis software package (Varosi and Gezari 1993). An image set in eight colors between 4.8 and 20.0 μm (Figure 2) was obtained for the central 15 arcsec array field of view, each with typically 5 minutes of integration time. This data set provided low resolution spectra for each pixel position in the central $\approx$ 15 arcsec field of view, which were as input to the model.

3. Modeling the Infrared Emission

We have modeled the dust emission from the central parsec using the "stack" of eight 4.8 - 20.0 μm images, further constrained by 2.2 and 3.8 μm images by Herbst, Beckwith and Shure (1993). The spectrum for each 0.26 arcsec resolution element (pixel) within the field-of-view is obtained

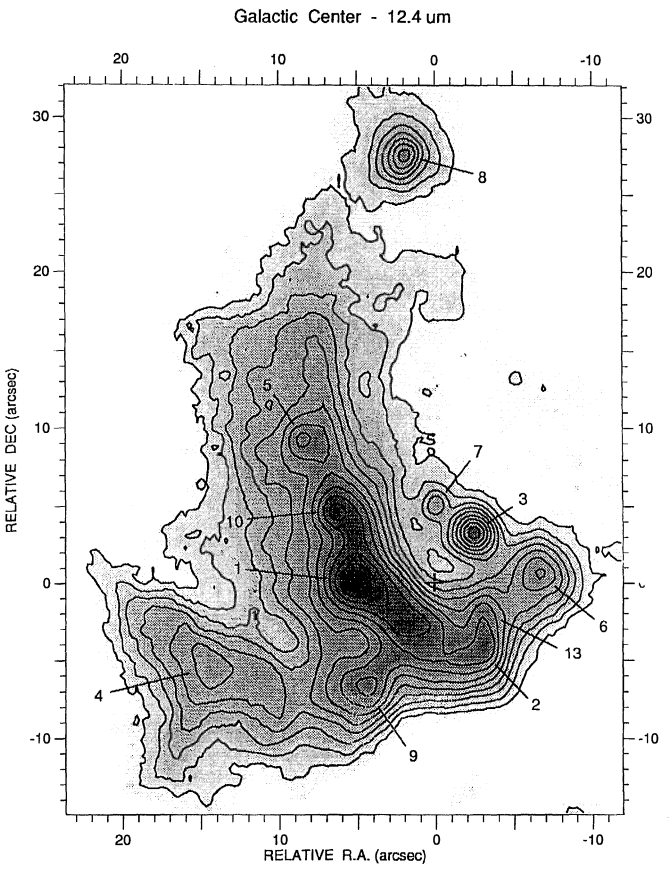

Figure 1. Contour map of the 12.4 μm continuum mosaic image of the Galactic Center Sgr A West complex obtained with our 58 x 62 Si:Ga array camera, developed at NASA/Goddard Space Flight Center (Gezari et al. 1992), at the 3-m NASA/IRTF Telescope at Mauna Kea. The mosaic was assembled from 50 overlapping 1 min integration frames (15 x 16 arcsec field of view, pixel size 0.26 arcsec), plotted with 30 contour intervals between the 3s noise level of 0.3 Jy/arcsec^2 and the peak brightness of 16 Jy/arcsec^2 at IRS 1. The prominent IRS sources are labled, and the cross shows the position of the non- thermal point source Sgr A* at the nominal Galactic Center. Deep integrations at 12.4 μm show no indication of infrared emission from Sgr A* (3s upper limit 0.1 Jy/arcsec^2 at 12.4 μm)

through the stack of aligned images. Because of limited spatial coverage at some wavelengths, the modeling calculations were restricted to an image overlap region common to all wavelengths of about 15 arcsec.

The spectrum of each pixel stack is modeled as arising from an isothermal source of mixed interstellar silicate and graphite dust, radiating at some temperature T. The emitted radiation is attenuated by an identical mixture of dust along the line of sight. Dust to gas mass ratios and dust

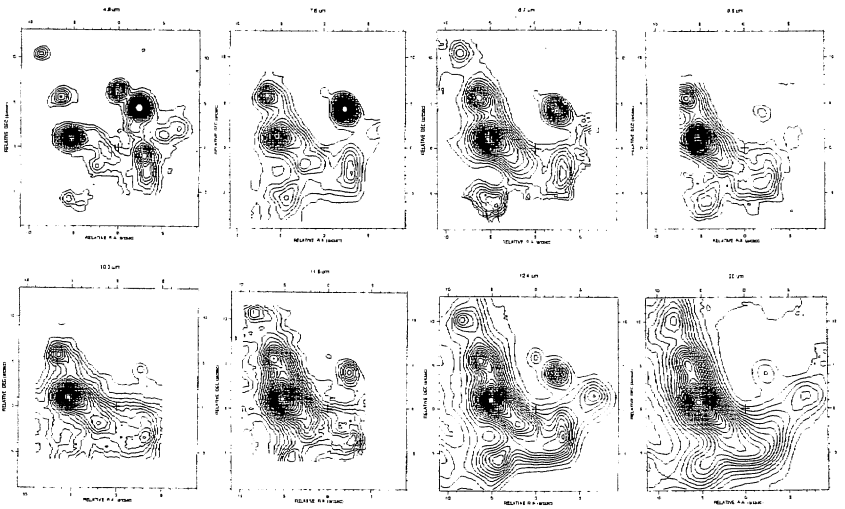

Figure 2. Galactic Center image set comprising the data "stack" used in the model, obtained with our 58 x 62 array camera. Top row: a) 4.8 μm. The ridge-like 4.8 μm emission just east of Sgr A* (cross) is the remnant of the IRS 16 cluster. b) 7.8 μm, c) 8.7 μm, and d) 9.8 μm array images. Local silicate extinction effects are dramatic at 9.8 μm; IRS 3 practically disappears in the image, where 95% of the 9.8 μm continuum flux is absorbed. The least silicate absorption is still very large, 80%, at IRS 1. Bottom row: e) 10.3 μm, f) 11.3 μm, g) 12.4 μm, and h) the 20.0 μm image, made with an Si:Sb array installed in the camera (Gezari et al. 1993).

optical constants were taken from Draine & Lee (1984). The observed infrared intensity I_ν from each source element (pixel) is then simply given by

$$I_\nu = (1 - e^{-\tau_S})B_\nu(T)e^{-\tau_{LOS}} \approx \tau_S B_\nu(T)e^{-\tau_{LOS}} (for \ \ \tau_S << 1)$$

where $\tau_S(\nu)$ is the source opacity of the emitting dust grains, $B_\nu(T)$ is the Planck function at the dust temperature T, and $\tau_{LOS}(\nu)$ is the line-of-sight (LOS) dust extinction opacity.

The model applies to the warm (T = 150 - 400 K) dust component in the galactic center region. Unfortunately, no high spatial resolution far-infrared photometry exists which could further constrain the fitting of model spectra longward of 20 μm. Despite this difficulty, model temperature resolution of 20K was achieved. We have not included 2.2 and 3.5 μm observations in our modeling, since strong sources in this wavelength range represent a different, much hotter dust component. The derived luminosity and dust mass results could be neglecting small contributions from cold (T $\approx$ 30 K) or hot (T > 400 K) dust not modeled. However, the color temperature

calculated from the 2.2/4.8 μm flux ratio was considered when interpreting of the model results. More detailed description of the modeling effort will be presented by Gezari, Dwek, & Varosi (1994).

4. Results

The model results are presented in Figure 3(a-d). We find that IRS 1, 3, 5, 7, 10, 13, 21 and 29 all coincide with local peaks in the modeled dust temperature (Figure 3a) and are generally 100K warmer than the surrounding extended ridge material. IRS1 and IRS10 both have source temperatures T = 325K. IRS 13 is relatively warmer (T = 450K), as is IRS2 (T = 375K). The hottest sources are IRS 7 (T = 1300K), IRS3 (T = 600K), and the near infrared point source IRS29 (T = 600K) located 3 arcsec south of IRS3. The temperature peaks seem to be shifted slightly from the peaks of the IRS sources. It should be noted that positional shifts have been found (Gezari 1992) between the 12.4 μm IRS sources and the corresponding peaks in VLA 2-cm ionized gas maps, which could be interpreted as the influence of a central, luminous, ionizing source. These shifts are small, but real, well above the astrometric precision of the comparison.

The emitting dust (source) opacity distribution (Figure 3b) shows peaks which are anti-correlated with the 12.4 μm IRS sources. This contradicts the conclusion drawn by Gezari et al. (1985) that the observed infrared emission was due primarily to dust density structure. The present study resolves greater source detail, showing that the principal IRS sources are located between the opacity peaks, in regions of locally lower dust density. For the mixed silicate-graphite grain source case the peak 12.4 μm emission opacity in the region is $\tau_S \approx 0.3$, corresponding to a peak dust mass surface density of about 5×10^{-3} $M_\odot$/arcsec^2.

The opacity of extincting silicate-graphite dust along the line-of-sight is shown in Figure 3c. The extinction opacity distribution is rather smooth compared to the silicate feature strength image, with typical extinction opacity at 12.4 μm of about $\tau_{LOS} \approx 2$ across the extended ridge, peaking at $\tau_{LOS} = 2.5$ at IRS3. In the 9.8 μm silicate feature the extinction opacity is about $\tau_{LOS} \approx 4$ on the ridge, peaking at $\tau_{LOS} = 6$ at IRS3.

The model luminosity distribution result for the mixed silicate-graphite grain case (Figure 3d) shows peak values of 1×10^5 $L_\odot$/arcsec^2 at IRS1 and IRS3, and 5×10^4 $L_\odot$/arcsec^2 in typical regions of the extended ridge. The total luminosity integrated over the 15 arcsec (0.6 parsec) region modeled is about 5×10^6 $L_\odot$.

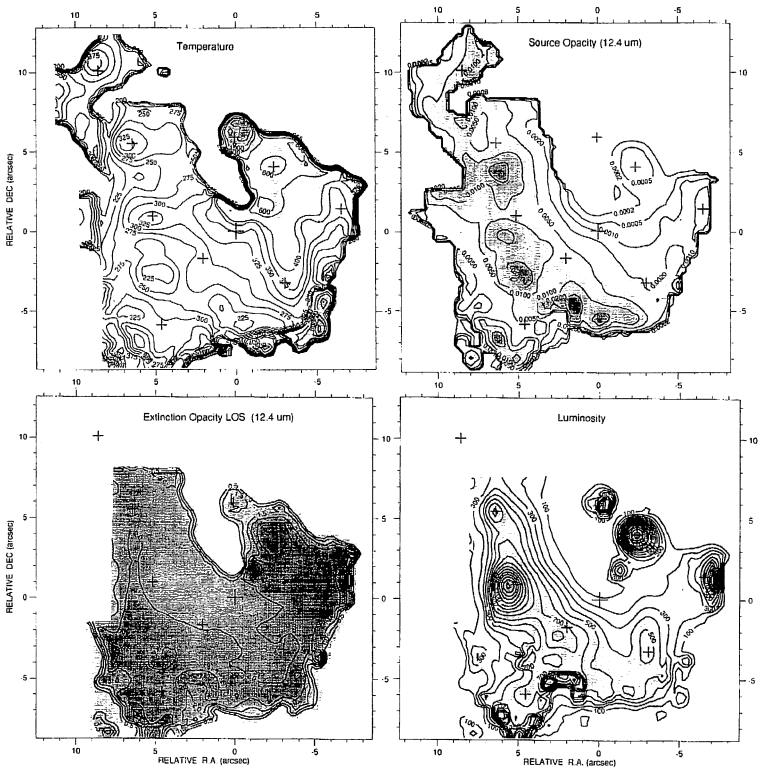

Figure 3. a) Dust temperature distribution modeled in the central 0.6 pc, calculated for mixed silicate-graphite grains. Darker colored regions are hotter. The positions of the IRS sources and Sgr A* are shown (crosses). Temperature enhancements are seen at the positions of the IRS sources, and correlations are seen at the positions of luminous Helium I line stars (see Figure 4). The model temperature is T = 325K at IRS1 and IRS10, and the hottest source is IRS7 where T = 1300K. b) Opacity of emitting dust grains showing anti-correlation with IRS source positions. Darker colored regions are more opaque, with peak opacity of $\tau_S \approx 0.3$ (or mass surface density 5×10^{-3} $M_\odot/arcsec^2$) close to IRS1, and minimum opacity level of $\tau_S \approx 0.02$. c) Extinction opacity of mixed silicate-graphite dust along the line-of-sight, with typical extinction opacity at 12.4 μm of about $\tau_{LOS} \approx 2$ across the extended ridge, peaking at $\tau_{LOS} = 2.5$ at IRS3. At 9.8 μm the extinction opacity is about $\tau_{LOS} \approx 4$ on the ridge, peaking at $\tau_{LOS} = 6$ at IRS3. d) Model luminosity distribution showing peak values of 1×10^5 $L_\odot/arcsec^2$ at IRS1 and IRS3, and 5×10^4 $L_\odot/arcsec^2$ in the extended ridge. The total luminosity integrated over the 15 arcsec (0.6 parsec) region modeled is about 5×10^6 $L_\odot$.

5. Discussion

The model results (temperature, opacity and luminosity distributions of the emitting dust) can be used in an attempt to discriminate between the "central engine" and "embedded stellar cluster" heating mechanisms. Since

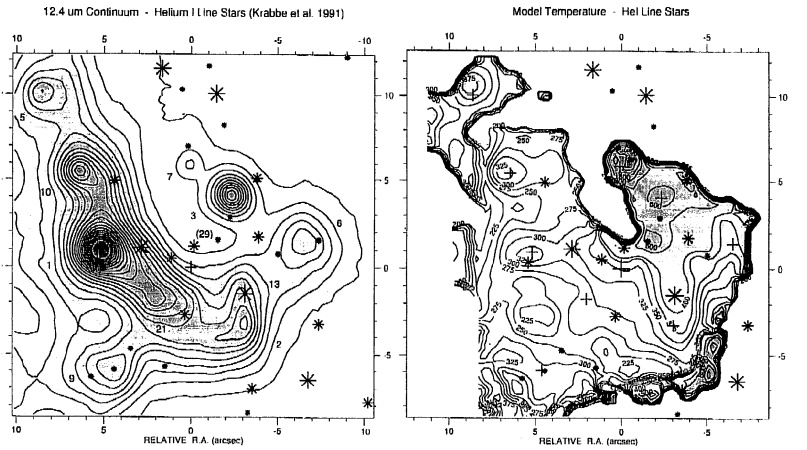

Figure 4. a) Positions of the more prominent Helium I emission line stars (asterisks, size proportional to brightness) in the central parsec found by Krabbe et al. (1991), shown with our 12.4 μm continuum brightness contours. These star data are new recent results provided by Krabbe (private communication). Positions are measured relative to Sgr A* (cross). b) Helium I star positions plotted on the modeled temperature distrubution of warm dust modeled in the Galactic Center. Darker regions are hotter. Note that the HeI stars are correlated with temperature enhancements, and occasionally with temperature minima in regions depleted of dust.

the source temperature distribution is determined by the density of the local ambient radiation field, a central luminosity source near Sgr A* should cause a large- scale temperature gradient radially across the extended infrared ridge, whereas embedded luminous stars should produce numerous local temperature "hot spots" throughout the ridge. The fact that the mid-infrared IRS sources all coincide with compact, symmetrical temperature peaks suggests that the IRS sources are heated by luminuos stars embedded at those positions, which is supported by the result that the dust density is lower near the IRS sources on the extended ridge (implying depletion of dust).

A detailed comparison between the positions of the HeI line stars imaged by Krabbe et al. (1991, 1993) and the mid-infrared model results shows that the HeI star positions are not well correlated with the compact 5 - 20 μm IRS source positions (see Figure 4a) or with the modeled source opacity and dust mass distributions (Figure 3b).

However, there is surprisingly good correlation between the HeI star positions and the modeled dust temperature features (Figure 4b). In almost every instance where the HeI stars lie in regions modeled, they are asso-

ciated with local temperature enhancements or perturbations of the temperature contours. Considering the weakness of the correlation between the stars and dust density features, we conclude that the HeI stars are located between (rather than embedded within) the dense dust clouds in the Sgr A West complex. These stars would appear to heat the dust clouds externally, from dust-depleted regions between the IRS sources. But the HeI stars apparently are not embedded within the IRS sources themselves, which must contain other internal luminous objects.

The HeI stars are thought to be late-type blue supergiants stars (Najarro et al. 1993) with high mass-loss rates (10^{-5} to 10^{-4} $M_\odot$/yr) and high outflow velocities ($\approx$ 1000 km/s). These stars have predicted individual luminosities in the range $0.1 - 2 \times 10^6$ Lo resulting in a total luminosity of 1.2×10^7 $L_\odot$ for the entire $\approx$ 1 pc cluster (Krabbe et al. 1991). The new two-composition dust model fit indicates that the luminosity of all sources in the central 15 arcsec (0.6 pc) field-of-view modeled is 5×10^6 $L_\odot$, about half of the total infrared and far-infrared luminosity observed in the greater Sgr A West complex (central $\approx$ 2 parsecs). Thus radiation from the HeI emission line stars could account for the luminosity observed with the array camera from the central 15 arcsec field-of-view, and the total luminosity observed in the far infrared from the central few parsecs of the Galaxy.

We have seen that the compact IRS sources are warm spots in the dense Galactic Center dust complex. The temperature structure also suggests that the IRS sources contain embedded luminous stars which are not members of the HeI star cluster. The luminous HeI emission line stars must be co-located with the emitting dust in the Sgr A West infrared source complex, heating the dust clouds externally. However, there is little in the new model results to suggest the presence of a central luminosity source near Sgr A*. The weight of observational evidence thus seems to be falling on the side of luminous stars located in and among the dense dust clouds as the origin of the $\approx$ 10^7 $L_\odot$ luminosity. The present observational picture does not require that an exotic "central engine" be invoked to account for the high infrared luminosity of the Galactic Center.

Acknowledgements

This work was supported by NASA/OSS RTOPs 188-44-23-08 and 188-44-53-05.

References

Allen, D. A., Hyland, A. R., and Hillier, D. J. 1990, M. N. R. A. S., 244, 706.
Becklin, E. E., Gatley, I., and Werner, M. W. 1982, Ap. J., 258, 135.

Draine, B. T. and Lee, H. M. 1984, Ap. J., 285, 89.
Gezari, D. Y. 1992, in "The Center, Bulge and Disk of The Galaxy", ed. L. Blitz, Kleuwer Academic Publishers, Doecrecht, 23.
Gezari, D. Y., Dwek, E., and Varosi, F. 1994, (in preparation for Ap. J.).
Gezari, D. Y., W. Folz, L. Woods and Varosi, F. 1992, P. A. S. P., 104, 191.
Gezari, D. Y., Tresch-Fienberg, R., Fazio, G. G., Hoffmann, W. F., Gatley, I., Lamb, G., Shu, P., and McCreight, C. 1985, Ap. J., 299, 1007.
Gezari, Ozernoy, Varosi, McCreight, and Joyce 1993, "Nuclei of Normal Galaxies: Lessons Learned fronm the Galactic Center" ed. Genzel, R. and Harris, A., Kluwer Pub. Co. (Dordrecht), in press.
Herbst, R., Beckwith, S. V. W. and Shure, M. 1993, Ap. J. (Letters), 411, L21.
Krabbe, A., Genzel, R., Drapatz, S. and Rotaciuc, V. 1991, Ap. J. (Letters), 382, l19.
Krabbe, A. 1993 (private communication).
Lynden-Bell, D. and Rees, M. J. 1971, M. N. R. A. S., 152, 416.
McGinn, M. T., Becklin, E. E., Sellgren, K., and Hall, D. N. B. 1989, Ap. J., 338, 824.
Melia, F. 1992, Ap. J. (Letters), 387, L25.
Najarro, F., Hillier, D. J., Kudritzki, R. P., Krabbe, A., Genzel, R., Lutz, D., Drapatz, S., Geballe, T. R. 1993, Proc. "Nuclei of Normal Galaxies: Lessons Learned from the Galactic Center," ed. Genzel, R. and Harris, A., Kluwer Academic Pub. Co. (Dordrecht), in press.
Rees, M. J. 1982, "The Galactic Center", ed. G. Riegler and R. Blanford, American Institute of Physics, Conf. Series, 83, 166.
Rieke, G. H. and Lebofsky, M. J. 1982, "The Galactic Center", ed. G. Riegler and R. Blanford, American Institute of Physics, Conf. Series, 83, 194.
Varosi, F. and Gezari, D. Y. 1993, "Astronomical Data Analysis Software and Systems II", P. A. S. P. Conf. Series, 52, 393.

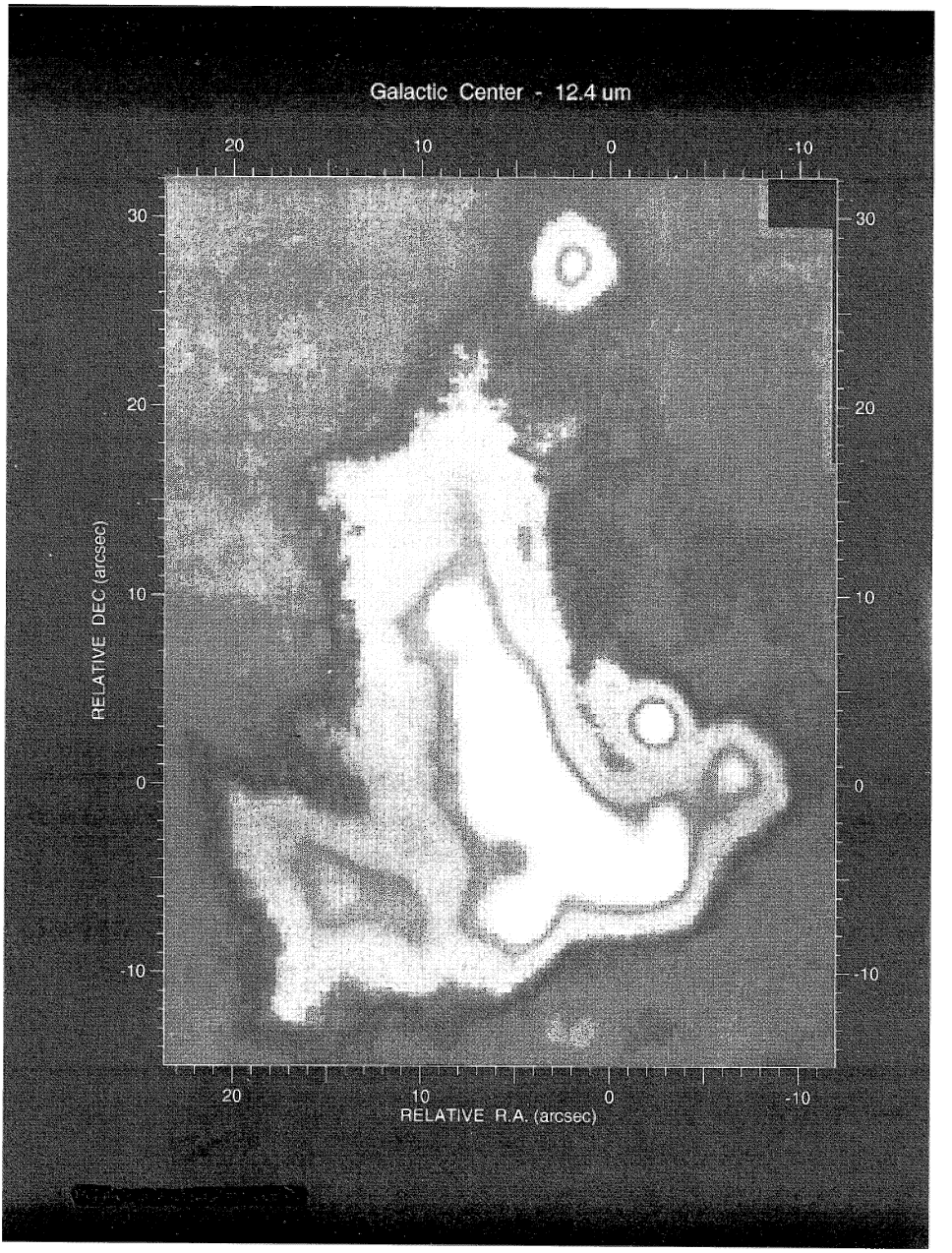

Figure 2. 12.4 μm continuum mosaic of the central 2 pc of the Galactic Center Sgr A West complex obtained with the 58 x 62 array camera (Gezari et al. 1992) at the 3-m NASA/IRTF Telescope at Mauna Kea. The intensity display is logarithmic to show details in regions of extended faint emission. The mosaic was assembled from 50 overlapping 1 min integration frames (15 x 16 arcsec field of view, pixel size 0.26 arcsec) which were aligned, matched and coadded to make up the final mosaic. Positions are measured relative to Sgr A*. The strongest infrared emission is very similar to the ionized gas distribution observed in 2-cm and 6-cm VLA maps of the region.

(For colour plate of figure see page xix)

MINI-SPIRAL AT THE GALACTIC CENTER: A LINK BETWEEN ITS STRUCTURE AND THE VALUE OF A CENTRAL POINT MASS

A.M. FRIDMAN, O.V. KHORUZHII AND V.V. LYAKHOVICH
Institute of Astronomy, Russian Academy of Sciences, 48 Pyatnitskaya St., Moscow, 109017, Russia

L. OZERNOY
Inst. for Computational Sciences and Informatics & Dept. of Physics, George Mason U., Fairfax, VA 22030-4444, USA

AND

L. BLITZ
Department of Astronomy, University of Maryland, College Park, MD 20742, USA

The innermost 2 pc contain a rotating ring ("circumnuclear disk") of molecular gas, neutral hydrogen, and dust with an embedded H II region called Sgr A West; a dense stellar cluster; and a compact nonthermal radio source Sgr A* (for a recent review, see Blitz *et al.* 1993). The clumped, spiral-shaped morphology of Sgr A West, sometimes called "the mini-spiral", has been a subject of numerous speculations concerning its origin (for a review, see Genzel & Townes 1987). Lacy *et al.* (1991) demonstrated that both the kinematics and shape of a part of Sgr A West can be fairly well approximated using an one-armed density-wave model.

In this paper (and a related one by Fridman *et al.* 1994), we make a next step in this direction and consider the observed structure of the mini-spiral as a result of hydrodynamical instability of the gaseous disk rotating in the gravitational field of the stellar cluster with an embedded central point mass. Self-gravitation of the disk is negligible as its gravity is small compared to hydrodynamical forces (see Lacy *et al.* 1991).

The rotation curve of the disk outside $r \sim 1.5$ pc is fairly well approximated by $V_\varphi = \text{const} \sim 110$ km/s (Serabin *et al.* 1986; Güsten *et al.* 1987; Sutton *et al.* 1990). Closer to the center, in the region where the

L. Blitz and P. Teuben (eds.), Unsolved Problems of the Milky Way, 241–246.
© 1996 *International Astronomical Union.*

central point mass could dominate, it should go up into the Keplerian law $V_\varphi \propto r^{-1/2}$. Therefore, somewhere inside 1.5 pc a kink on the rotation curve should appear. In the work by Fridman *et al.* (1994), we have analytically shown that a kink of the rotation curve can lead to instability, which results in the generation of a spiral density wave. As it follows from our study, in the disk with a sharp kink the modes with a large number of spiral arms are the most unstable. In the disk with a smooth kink, as numerical simulations (Lyakhovich *et al.* 1994) have shown, the azimuthal number of the most unstable mode decreases with an increase in the kink width. For a very smooth kink, a mode with one spiral arm is only unstable.

The hydrodynamical model predicts that the generated density wave must have the shape of an Archimedes spiral outside R_{res}, the corotation radius. Observational data indicate that the morphology of the mini-spiral has, indeed, the shape of an Archimedes spiral outside 0.1-0.3 pc (Lacy *et al.* 1991). Therefore, the morphology of the mini-spiral could serve an argument in favor of the hydrodynamical origin of this structure.

The morphology of the mini-spiral can provide information about its corotation radius and pattern speed. Indeed, since the generated density wave must have the shape of an Archimedes spiral outside the corotation radius *only*, the minimal distance down to which the shape of the density wave is approximated by an Archimedes spiral can be used to evaluate the corotation radius. It follows from the shape of the mini-spiral that the corotation radius equals to 0.1-0.3 pc.

As shown by Fridman *et al.* (1994), a simple relationship exists between the pattern speed, Ω_{res}, and the pitch angle, i, of the spiral arm:

$$\Omega_{res} = -\frac{c}{r \tan i}, \tag{1}$$

where c is the "sound speed" (the chaotic velocity of the clouds) and r is the radial distance. Parameters c and i are given by observations outside the corotation region: for the mini-spiral $|r \tan i| = |dr/d\varphi| \gtrsim 0.1$ pc rad^{-1} in the region $r \sim 1$ pc (see Lacy *et al.* 1991) and for the disk $c \leq$ 30-50 km/s (Lacy *et al.* 1991, Roberts and Goss, 1993). ¿From this we obtain $\Omega_{res} \lesssim$ (300 - 500) km pc^{-1} (rad) s^{-1}.

The mini-spiral parameters, R_{res} and Ω_{res}, can be determined more accurately by comparison of the shape of the observed mini-spiral with that for the model spiral obtained by numerical simulations. Below, some results are given of numerical simulations for the mini-spiral generation in the gaseous disks with a smooth kink in the rotation curve.

In our numerical simulations, we used the code described in Fridman *et al.* (1994). The profile of the unperturbed rotational velocity with a kink was modelled by

$$\frac{V_\varphi(r)}{V_1} = \left(\frac{r}{R_0}\right)^{\frac{n_1+n_2}{2} - \frac{n_1-n_2}{\pi}\arctan\left[\frac{2(r-R_0)}{l}\right]+1}. \quad (2)$$

Here R_0 is the radial distance to the kink in the rotation velocity, l is the characteristic width of the kink; V_1=110 km/s; n_1=-1.5 and n_2=-1 are to match the approximations V_φ = const = V_1 for $r \gg R_0$ and $V_\varphi \propto r^{-1/2}$ for $r \ll R_0$. The profile of the unperturbed surface density of the gaseous disks was, for simplicity, approximated by $\Sigma(r)$ = const (for the other cases, see Lyakhovich *et al.* 1994 and Fridman *et al.* 1994). The profile of the sound speed was taken to be $c(r)$ = const, which is consistent with an isotermal model of the disk. The value of sound speed was taken in the range of 30 km/s $< c <$ 50 km/s. Numerical simulation showed that the maximum value of the kink smoothing, l, at which the mini-spiral is still generated for these parameters, is as large as $l = (0.3 - 0.4)\ R_0$. Thus the instability can take place even at a rather smooth rotation curve.

Fig. 1 shows the numerical model superimposed onto the observed contour map of the mini-spiral. Fig. 2 demonstrates the rotation curve used for the modelling of the spiral wave shown in Fig. 1. A visual inspection of Fig. 1 suggests that the model is able to describe the data fairly well.

By changing the sound speed in the range (30 - 50) km/s we obtain the values of other parameters of the disk for which our model fits the observed mini-spiral fairly well. While doing so one obtains the position angle of the disk 17°-25°, the inclination of the disk 59°-67°, and the position of the center of rotation 0″-2″ West and 0″-2″ South off Sgr A*. These results are consistent with the observational data (see Table 1).

In the frame of our model we determine the other parameters of the mini-spiral: Ω_{res} = (400-500) km pc^{-1} s^{-1} and $R_{res} = 0.2 - 0.3$ pc.

It follows from our analytical and numerical studies that the corotation radius and the radial distance of the kink are close to each other. Thus the rotation velocity is approximately constant outside r = 0.3 pc, which is also consistent with the data presented in Lacy *et al.* (1991).

The above parameters of the mini-spiral allow us to determine the total enclosed mass inside R_{res}. In the disk the pressure force can be neglected compared to the centrifugal one (since their ratio is $\sim c^2/V_\varphi^2 \lesssim 0.2 - 0.07$). The balance of the centrifugal force with the outer gravitating forces induced by both the stellar cluster and a central point mass yields

$$M(r) = \Omega^2(r) r^3/G, \quad (3)$$

where G is the gravitational constant. Substituting the values of $r = R_{res}$ and $\Omega = \Omega_{res}$ we obtain the total enclosed mass inside the radius (0.2-0.3) pc to be $(3 - 7) \times 10^5$ M$_\odot$. Bearing in mind that the inferred core mass of

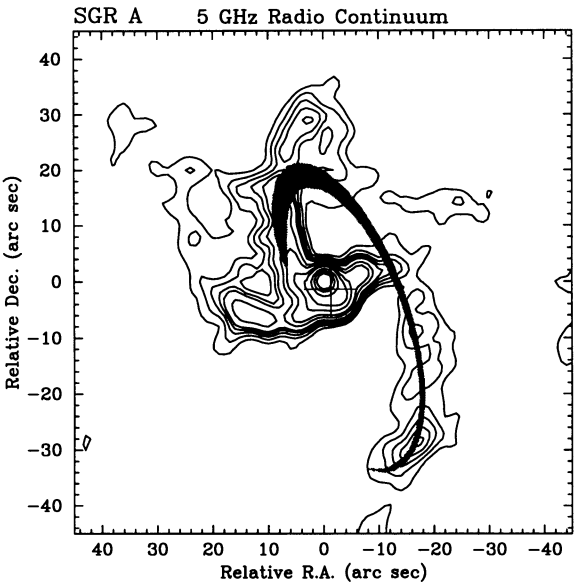

Figure 1. The mini-spiral: the contour map is the observational data (Blitz *et al.* 1993), the filled region is the computer simulation, the cross is the center of rotation. The offset for the rotational center with respect to Sgr A* is 0.″6W and 1.″3S [the rotational center coincides with the center of the stellar cluster, 0.″6W ± 0.″7, 1.″3S ± 1.″0 (3 σ errors), as given by Eckart *et al.* 1993]. The sound speed $c = 50$ km/s. The inclination of the disk is 60°, the position angle of the disk is 20°.

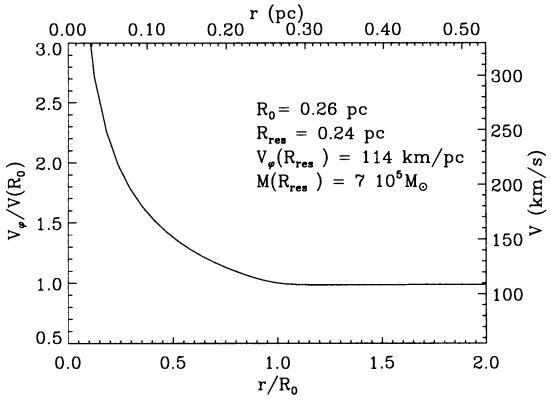

Figure 2. The rotation curve used for the modelling of the spiral wave shown in Fig. 1. The parameters of the curve (see Eq. 2) are $n_1 = -1.5$, $n_2 = -1$, $l/R_0 = 0.3$, and $V_1 = 110$ km/s.

TABLE 1. The mini-spiral parameters

Model Parameter	1	2	3	4	5	6
Position angle	$21° \pm 4°$	$15° \pm 2°$	$22° \pm 5°$	$\approx 20°$	$\approx 12°$	$15° \pm 15°$
Inclination	$63° \pm 4°$	$65° \pm 5°$	$65° \pm 5°$	$65° \pm 5°$	$65° \pm 5°$	$65° \pm 5°$
Position of center (relative to Sgr A*)						
Right Ascension	$1''W \pm 1''$	$0'' \pm 1''$	$1''W \pm 4''$	$0'' \pm 2''$	$\approx 0''$	$\approx 0''$
Declination	$1''S \pm 1''$	$1''N \pm 1''$	$7''S \pm 7''$	$0'' \pm 2''$	$\approx 0''$	$\approx 0''$

[1] our parameters for the mini-spiral
[2] Lacy *et al.* (1991) for the mini-spiral
[3] Roberts & Goss *et al.* (1993) for the western arc
[4] Serabyn & Lacy *et al.* (1985) for the northern arm
[5] Serabyn & Lacy *et al.* (1985) for the western arc
[6] Serabyn *et al.* (1986); Güsten *et al.* (1987); Sutton *et al.* (1990) for the molecular disk

the central stellar cluster believed to be isothermal is 5×10^5 $(10^{\pm 0.3})M_\odot$, the core radius is (0.15±0.05)pc (Eckart *et al.* 1993), the central point mass (a putative black hole?) is severely constrained to a value of the order of $10^5 M_\odot$. This upper limit is consistent with the other approaches employing various physical processes (Ozernoy 1992, 1993). A comparatively small central mass makes it understandable why the radial distance of the kink on the rotational curve turns out to be rather close to the core radius of the stellar cluster.

We note in passing that the shape of the generated spiral wave outside the corotation radius does scarcely depend upon a concrete hydrodynamical mechanism of its generation. In particular, Eq. (1) could be appropriate for other hydrodynamical mechanisms as well. For instance, in Fridman *et al.* (1994) we have explored in detail the generation mechanism associated with a jump in the surface density and have obtained the same rotation curve ($V_\varphi = \text{const}$) outside 0.2-0.3 pc (and also the same total enclosed mass). The method employed here is only valid for the determination of the rotation curve outside the central 0.2-0.3 pc and therefore gives only an upper limit to the point mass.

References

Blitz, L., Binney, J., Lo, K.Y., & Ho, P.T.P. 1993, Nature, 361, 417.
Eckart, A., Genzel, R., Hoffmann, R., Sams, B.J., & Tacconi-Garman, L.E. 1993, ApJ, 407, L77.
Fridman, A.M., Khoruzhii, O.V., Lyakhovich, V.V., Ozernoy L., & Blitz L., 1994, in "Physics of the gaseous and stellar disks of the Galaxy", ed. I. King, ASP Conference Series, v.66, p. 305.
Genzel, R. & Townes, C.H. 1987, ARA&A, 25, 377.

Güsten, R., Genzel, R., Wright, M. C. H., Jaffe, D.T., Stutzki, J., & Harris, A. I. 1987, ApJ, 318, 124.
Lacy, J.H. 1989, in IAU Symp. 136, The Center of the Galaxy, ed. M.Morris (Dordrecht: Kluwer), 493
Lacy, J.H., Achtermann, J.M., & Serabyn, E. 1991, ApJ, 380, L71.
Lyakhovich V.V., Fridman A.M., Khoruzhii O.V., 1994, in "Non-stable Processes in the Universe", ed. A.G. Masevich , Moscow, p.194 (Russia).
Ozernoy, L.M. 1992, in "Testing the AGN Paradigm", eds. S.S. Holt, S.G. Neff and S.M. Urry, AIP Conf. Proc., 254, pp. 40 and 44.
Ozernoy, L.M. 1993, in "Proc. 16th TEXAS/3rd PASCO Symp. on Relativistic Astrophysics", eds. C. Akerlof and M. Srednicki; Ann. New York Acad Sci. 688, 596
Roberts, D.A., & Goss, W.M. 1993, ApJS, 86, 133.
Serabyn, E., & Lacy, J.H. 1985, ApJ, 293, 445
Serabyn, E., Güsten, R., Walmsley, C.M., Wink,J.E., & Zylka,R. 1986, A&A, 169,85.
Sutton, E.C., Danchi, W.C., Jaminet, P.A., & Masson, C.R. 1990, ApJ, 384, 503

WHAT ARE THE RADIO FILAMENTS NEAR THE GALACTIC CENTER?

MARK MORRIS
Department of Physics and Astronomy
UCLA, Los Angeles, CA 90024, USA

Abstract. A population of nonthermally-emitting radio filaments tens of parsecs in length has been observed within a projected distance of ~130 pc of the Galactic center. More or less perpendicular to the Galactic plane, they appear to define the flux lines of a milligauss magnetic field. The characteristics of the known filaments are summarized. Three fundamental questions raised by these structures are discussed: 1) Do they represent magnetic flux tubes embedded within an ubiquitous, dipole magnetic field permeating the inner Galaxy, but which have been illuminated by some local source of relativistic particles, or are they instead isolated, self-sustaining current paths with an approximately force-free magnetic configuration in pressure equilibrium with the interstellar medium? 2) What is the source of either the magnetic field or the current? and 3) What is the source of the relativistic particles which provide the illuminating synchrotron radiation? We are nearer an answer to the the last of these questions than to the others, although several interesting models have been proposed.

1. The State of our Knowledge

Filaments of various kinds and having various appelations, including streaks, streamers, strands, strings, striations and fibers, can be found in numerous astrophysical situations, so one must begin by clarifying the particular characteristics of the radio filaments being considered in this paper. These polarized nonthermal radio emission structures are tens of parsecs long, and only a fraction of a parsec wide. They may occur in isolation (in which case they have been called "threads") or in bundles. Morphologically, they are strikingly uniform in brightness and curvature, and therefore are quite dif-

L. Blitz and P. Teuben (eds.), Unsolved Problems of the Milky Way, 247–261.
© 1996 *International Astronomical Union.*

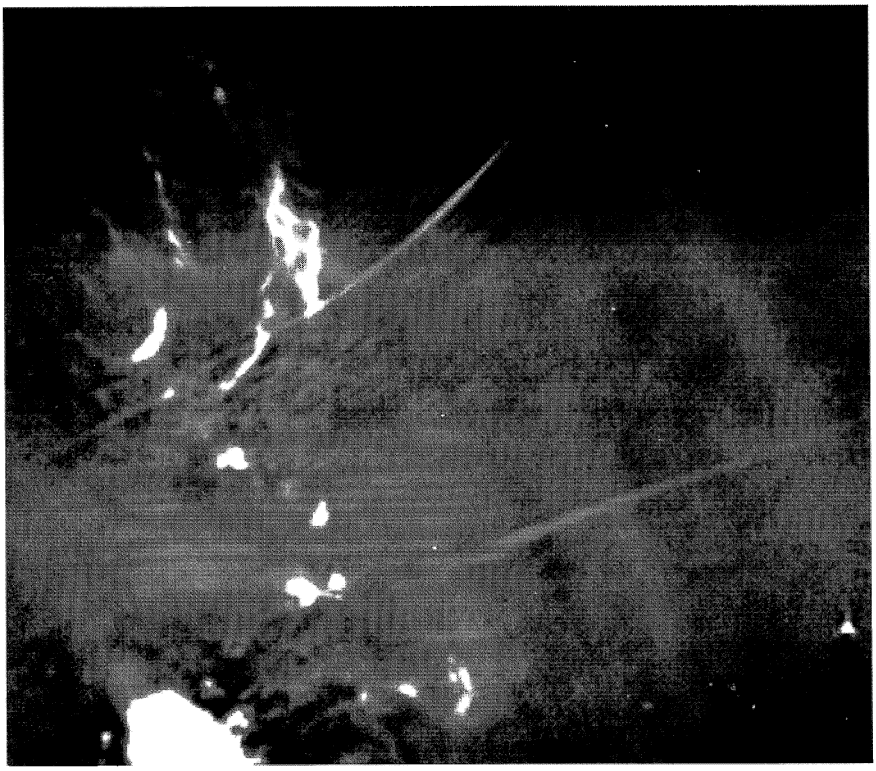

Figure 1. Radiograph at λ20cm of the radio "threads", first identified by Morris & Yusef-Zadeh (1985). Sgr A lies at the bottom left.

ferent from the meandering, contorted filamentary structures one may find in supernova remnants and emission-line nebulae. Examples of filaments are shown in figures 1 through 3.

1.1. A CATALOG OF KNOWN FILAMENTS

A catalog of known, nonthermal filaments is quickly completed*:

1. The "Snake" (G359.1-0.2) (Gray *et al.* 1991)
2. Sgr C (Liszt 1985)
3. G359.54+0.18 (Bally & Yusef-Zadeh 1989)
4. G359.96+0.09, a thread which merges in projection with the halo of Sgr A (Morris & Yusef-Zadeh 1985; Echevarria & Morris 1995)
5. G0.08+0.15, the northernmost thread (Morris & Yusef-Zadeh 1985)

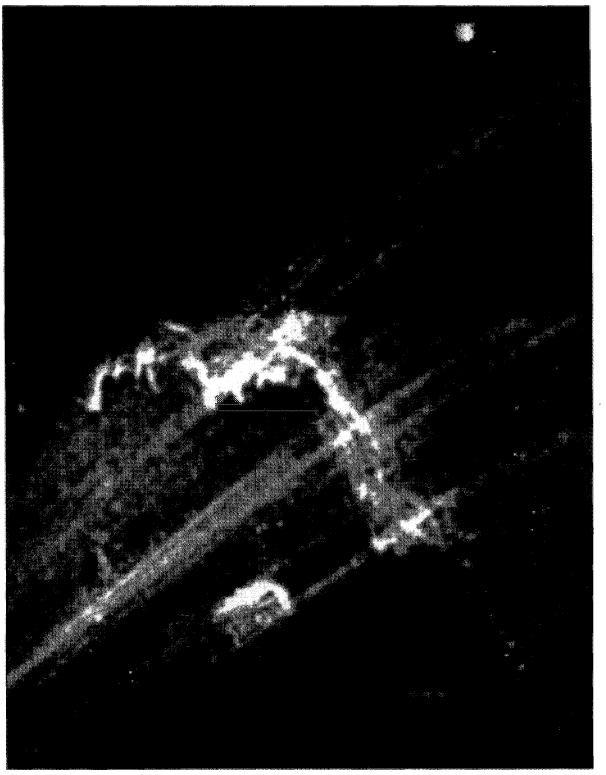

Figure 2. Radiograph at λ6cm of G0.18-0.04, located at the center of the Radio Arc – a prominent bundle of filaments. Numerous nonthermal filaments run diagonally through the figure, and interact with the thermal source, G0.18-0.04

6. The Radio Arc, l = 0.2° (Yusef-Zadeh, Morris & Chance 1984), including:
   • the bundle of ~ a dozen filaments between b = ±0.2° (Yusef-Zadeh & Morris 1987a,b)
   • the few northern filamentary extensions to at least b = ~0.4° (Yusef-Zadeh & Morris 1988)
   • a few southern filamentary extensions of the Arc (Yusef-Zadeh *et al.* 1990)
7. G0.25-0.2 (Yusef-Zadeh *et al.* 1990)
8. G0.29-0.22 (Yusef-Zadeh *et al.* 1990)

*some consider G359.79+0.17 to be a filamentary thread like the others, but it may be a superimposed, partial nonthermal shell source.

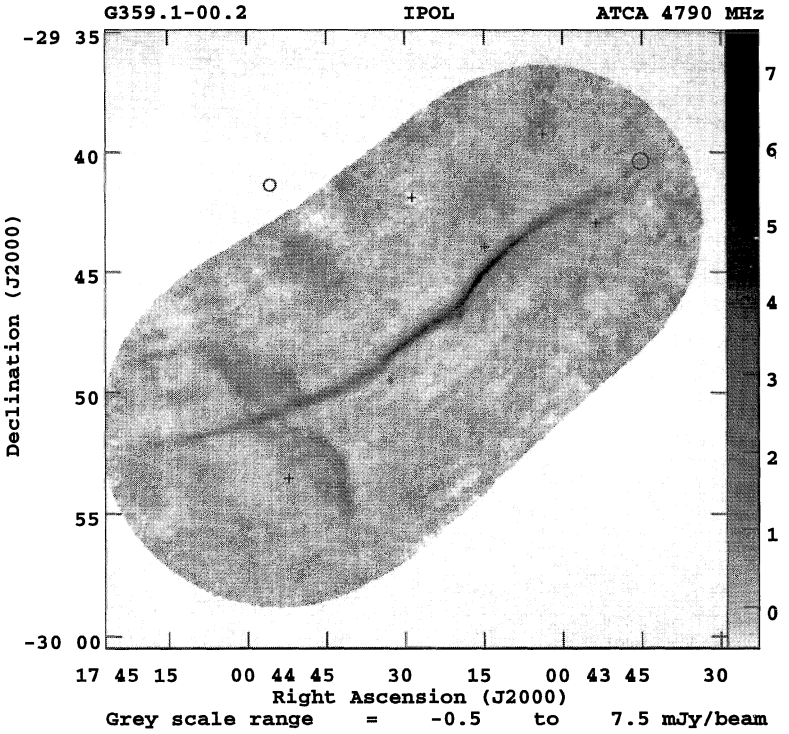

Figure 3. 6.3-cm radiograph of the "Snake" resulting from a four-field mosaic made with the Australia Telescope (from Gray 1994 and personal communication). This is the only filament showing such prominent cusps, or directional discontinuities, and the furthest from the Galactic center.

1.2. THE ARCHED FILAMENTS

Not included in this accounting are the "arched filaments" or "bridge", which define the thermal part of the Radio Arc. They represent a different kind of filament from the ones of primary concern in this paper, but they warrant mentioning because they are intimately linked to the nonthermal portion of the Radio Arc (Yusef-Zadeh & Morris 1988; Morris & Yusef-Zadeh 1989). The appellation "bridge" was originally introduced because, in low-resolution radio maps, the arched filaments appeared to connect the Radio Arc with Sgr A, although VLA maps clearly illustrate that there is no such connection (Morris & Yusef-Zadeh 1989). While the arched filaments are clearly filamentary structures, they are somewhat fleecy and less well-defined than the nonthermal filaments. Their thermal nature is revealed by their radio recombination line emission (Pauls *et al.* 1976; Yusef-Zadeh,

Morris, & van Gorkom 1987), and by their far-IR fine structure line emission (Erickson *et al.* 1991).

The arched filaments lie at or near the surface of a massive molecular cloud observed in CO (Bally *et al.* 1987), CS (Serabyn & Güsten 1987) and CII (Poglitsch *et al.* 1991). The exceptionally luminous ($\sim 3 \times 10^7$ $L_\odot$) far-IR continuum emission from this cloud is aligned with, but is more broadly distributed than, the arched filaments. A particularly curious, and perhaps important property of this cloud is that it has velocities which are forbidden, in the sense of Galactic rotation, and the molecular and recombination lines show a strong velocity gradient: -20 to -80 km $\cdot$ s^{-1}. The molecular cloud extends well beyond the arched radio filaments; Poglitsch *et al.* (1991) have argued it may be physically linked to the circumnuclear disk within Sgr A. Thus, this cloud may constitute the "bridge". At the northern extreme of the molecular cloud underlying the arched filaments, these thermal filaments and the nonthermal, quasi-linear filaments of the Radio Arc meet in a right-angle junction . Along a very well-defined line constituting the edge of the molecular cloud, the arched filaments end and the brightness of the nonthermal filaments undergoes an abrupt discontinuity (Yusef-Zadeh & Morris 1988). Thus, the geometrical evidence for a real physical interaction is quite strong.

1.3. ARE THE FILAMENTS REALLY AT THE GALACTIC CENTER?

There can be little doubt that the filaments are located at the Galactic center. First, they are known in only that direction. Ten years ago when they were first found, there was a serious question about whether they may be found anywhere in galactic plane, but now, with the passage of time and the acquisition of a great deal of data with the VLA and other telescopes, further examples have only been found in the inner degree of the Galaxy. Second, the molecular clouds found to be interacting with the filaments all have the broad lines (FWHM $>$ 20 km $\cdot$ s^{-1}) characteristic of the Galactic center cloud population, and are quite rare elsewhere. Third, Uchida *et al.* (1992) have used HI absorption line data to place one filament – the Snake – behind high-velocity molecular gas that is part of the Galactic center's dynamical system, so it is likely that this feature arises from within a few hundred parsecs of the center.

1.3.1. *Characteristics of the Filaments*

The properties of the galactic center radio filaments, those which define them more explicitly and differentiate them from other kinds of linear structures, are as follows:

1. All of them are oriented roughly perpendicular to the Galactic plane.

Their orientation may, in fact, be a function of Galactic latitude, with the perpendicularity being almost exact at b = 0°, and with the orientation deviating from this more and more up to and beyond b= 0.25°. This statement requires some extrapolation of the curvature of those filaments which do not pass through the galactic plane or which do not extend very far in latitude.

2. They generally have a smoothly and slowly-varying curvature, and a surface brightness which varies only slowly along their length. (The Snake is a notable exception to this, inasmuch as it has two apparent directional discontinuities. This unusual characteristic may be related to the fact that the Snake is substantially further from the Galactic center, in projection, than any other filament.)

3. Their radio emission is strongly linearly polarized.

4. The filament defines the magnetic field direction. This is more of a presumption than a demonstrated fact. The intrinsic direction of the magnetic field has only been determined for the filaments of the radio Arc. Tsuboi *et al.* (1986) made rather large corrections of the observed polarization angle for Faraday rotation, and deduced that the intrinsic field lies along the filaments. This was confirmed by Reich (1994), who measured the polarization angle at such a high frequency that the Faraday rotation angle (proportional to λ^2) is small.

5. The spectra of the filaments, where they have been measured, is either falling with frequency ($I_\nu \ \alpha \ \nu^{-0.6}$), or is flat or slowly rising (Anantharamaiah *et al.* 1991). In either case, a nonthermal emission mechanism is indicated, as was already implied by the linear polarization. The filaments with the flat or rising spectra are possibly the ones into which fresh, high-energy electrons are still being accelerated.

6. There are no obvious radio point sources associated with the filaments, such as might be invoked to provide the illuminating relativistic particles.

7. In every sufficiently well-studied case, an interaction with a molecular cloud somewhere along the length of the filament is suspiciously in evidence. In spite of these interactions, the filaments are only sightly bent or distorted at the location of the interaction. The fact that the magnetic pressure must therefore be at least as large as the turbulent pressure in the cloud, or the ram pressure of the interaction, led to an estimate of > a few milligauss for the magnetic field strength in the filaments of the radio Arc (Yusef-Zadeh & Morris 1987a,b; Morris & Yusef-Zadeh 1989); a similar estimate can be derived from all of the filamentary systems where a molecular cloud has entered the picture.

2. Unsolved Problems

There is little doubt that the filaments represent magnetic structures – flux tubes – in which relativistic electrons are trapped, and along which they are presumably streaming. However, there are really two major problems which need to be solved before we fully understand the nature of the filaments. The first involves the geometry and the origin of the magnetic filaments. Are the apparently strong fields local to the filaments, do they form a cylindrical wall about the Galactic nucleus, or are they ubiquitous throughout the inner 100 parsecs or so? A related question is how the magnetic field structures originated. The answer to this is quite different for the different field geometries.

If the magnetic field is dipolar and ubiquitous, as I have previously argued (Morris 1990, 1994), then the total magnetic energy within a radius of 100 pc is $> 4 \times 10^{54}\ B^2_{mG}$ ergs, comparable to the energy of the hot coronal gas occupying about the same volume (Koyama, these proceedings). Furthermore, the pressure balance of the interstellar medium near the Galactic center is dominated in this case by the magnetic pressure, $B^2/8\pi \sim 4 \times 10^{-8}$ ergs cm^{-3}. This hypothesis may also help account for the paucity of cosmic rays near the Galactic center (Blitz *et al.* 1993).

The second major, unanswered question is, "What is the source of the relativistic electrons in the filaments?" Are they accelerated *in situ* by some magnetic mechanism, or do they have a discrete source? I think we are closer to solving the second of these two problems than we are to the first.

3. Models

Six models of the filamentary phenomenon have been offered to date, although not all of them address the same unsolved problem. I will describe each of them briefly in turn and comment on its strengths or weaknesses.

3.1. EXPANDING MAGNETIC LOOPS

Heyvaerts, Norman, & Pudritz (1988) propose that the Galactic nucleus contain a generator of magnetic loops, presumably a differentially rotating accretion disk around a central black hole. Once formed, the loops shear off from the central disk and expand away from it, provoking observable phenomena on a variety of scales. On the largest scale (~40 pc), the loops are invoked to account for the filaments of the Radio Arc as a result of a collision with a hypothetical, vertical magnetic wall surrounding the nucleus at this distance. The asymmetry of the Arc about the galactic center and the apparently random distribution of filaments about the center can be explained in terms of the stochastic nature of the loop ejection phenomenon.

The nonthermal emission from the filaments is attributed to particle acceleration to relativistic energies as a result of magnetic field line reconnection taking place along the colliding interface between the loop and the wall. The difficulty with this hypothesis lies in understanding how loops can survive their trajectory through the busy and tumultuous Galactic center medium without suffering energy loss (other than that owed to expansion) and consequent disruption. Perhaps the interior of the 40-pc-radius magnetic cylinder is relatively empty. Additionally, however, this hypothesis does not incorporate any explanation of the role of the molecular cloud underlying the arched filaments of the Arc, which, according to others, is an essential component of the Radio Arc. The anomalous velocity of this cloud would simply be coincidental.

However, some elements of this hypothesis have appeared in subsequent discussions of the filaments: the possibility of a cylindrical, magnetic wall surrounding the Galactic nucleus, and the notion that field line reconnection may be an important mechanism for accelerating particles.

3.2. INDUCED ELECTRIC FIELDS, CURRENTS, AND MHD-INDUCED IONIZATION

Benford (1988) and Morris & Yusef-Zadeh (1989) describe a model for the Radio Arc which can be generalized to the threads. They note that a molecular cloud moving through a strong, uniform field can induce an electric field at its surface via the $\mathbf{v}\times\mathbf{B}$ interaction. They identify the arched filaments as the resulting current sheets at the surface of the negative velocity cloud. The rarity of this phenomenon can be ascribed to the rarity of massive clouds which have such a large anomalous velocity as the one underlying the arched filaments. Indeed, if the ambient magnetic field lines move with approximately the circular orbital velocity at the location of the Radio Arc, then the arched filament cloud is moving at $\sim 10^2$ km $\cdot$ s^{-1} with respect to the field lines. This will induce a strong electric field within a layer at the cloud surface having a depth governed by the ability of the magnetic field to penetrate the cloud as a result of diffusion and shredding of the cloud surface. The electric field, in turn, drives a current. The resistance of the medium can be decreased, and thus the current can be increased, in proportion to the fractional ionization of the medium. Morris & Yusef-Zadeh (1989) suggested that the cloud surface would be naturally ionized by the critical ionization velocity phenomenon, although more recently, a cluster of stellar ionizing sources has been found nearby (Cotera *et al.* 1994). It remains to be seen whether the stellar sources of ionizing photons are sufficient to account for the ionization of the arched filaments, both in terms of geometry and in terms of the required ionization rate (Morris 1994).

Once created, the current moving along the cloud surface does not, ac-

cording to the model, simply end at the cloud extremity, but instead turns to follow the magnetic field lines. The filaments in the linear portion of the radio Arc are identified with the current system following the field lines. According to Benford (1988), the filaments represent the coalescence of a large number current-carrying pinches. They presumably form a locally force-free magnetic field configuration (Yusef-Zadeh and Morris 1987b). After flowing through the Galactic plane and reaching some critical position coinciding with the end of the bright portion of the linear filaments, the current turns away from the magnetic field, and flows back to the origin of the circuit (the opposite extremity of the cloud providing the electromotive force) through a relatively low-density medium, forming the weak radio counter-arches (Seiradakis *et al.* 1985; Morris & Yusef-Zadeh 1989). It is not obvious how, or whether, this circuit model can be applied to filaments other than those in the Arc, although some of its elements may be relevant to all the filaments, including the idea that an induced electric field and the consequent current may be important where clouds interact with a magnetic field, and the notion that the filaments may represent locally force-free magnetic field configurations.

3.3. PARTICLE ACCELERATION BY FIELD LINE ANNIHILATION AROUND CURRENT PINCHES

Lesch & Reich (1992) adopt the notion that the filaments result from the coalescence of current-carrying pinches to form locally force-free, cylindrically symmetric configurations. Where there is a multiplicity of nearby filaments, as in the radio Arc, they attract each other for the same reason that parallel current-carrying wires having currents in the same direction attract each other: the locally toroidal component of the magnetic field surrounding each filament, induced by the axial component of the current, exerts a Lorentz force on the current-carrying particles in the other filament toward the first filament. However, the toroidal components of the two filaments are opposed in the region between the approaching filaments, so as they encounter each other, a large current density results as the field lines undergo reconnection. While ohmic dissipation transforms much of the magnetic energy into heat, the induced electric field accelerates some of the electrons to relativistic energies. These electrons then follow the magnetic field lines and define the synchrotron-emitting filaments. It remains to be seen how the particles which are accelerated between the filament cores, where the current flows along the straight symmetry line of the filament, migrate into the filament cores. Furthermore, this mechanism is not obviously operational in the case of the isolated threads.

One of the goals of the Lesch and Reich treatment is to account for the slowly rising spectral slope of the filaments in the radio Arc. They point

out that the slope can be accounted for by an approximately monoenergetic electron energy spectrum or by an energy spectrum with a sharp lower cut-off energy. Noting that the reconnection mechanism gives an approximately equivalent acceleration to each electron, they identify this as the means to achieve a monoenergetic electron spectrum, and thus the slowly rising radio slope.

3.4. FILAMENT FORMATION BY THERMAL INSTABILITY IN A RELATIVISTIC GAS

Rosso & Pelletier (1993) note that the electric field induced by cloud motions through a magnetic field, as suggested in the earlier models, is sufficient, by itself, to accelerate electrons to relativistic energies. The reason for this is that, whereas most of the accelerated particles suffer frequent collisions and thereby dissipate their energy as ohmic heating, those particles which reach high velocities are less likely to suffer collisions because of the v^{-3} dependence of the collision cross-sections. They can thus become "runaway" electrons and may be identified with those responsible for the synchrotron radiation. This idea is more appealing for the G0.18-0.04 cloud and HII region (see Serabyn, in these proceedings), which is associated with the synchrotron filaments of the Arc than it is for the arched filament HII region, which shows no clear signature of synchrotron emission, except where it is tied to the synchrotron filaments at its northern extreme.

The nonthermal filaments are produced, according to the model of Rosso & Pelletier (1993), by a thermal instability accompanying the synchrotron losses of the relativistic particles. They find that the diffusion of relativistic electrons across the magnetic field lines is generally dominated by the contribution of electrostatic turbulence, described by a Bohm-like diffusion coefficient. This form of the diffusion law leads to a prediction for the width of the filaments which depends only on the magnetic field strength. For a milligauss field, they deduce a maximal width of 0.004 pc. The measured widths are more nearly a few tenths of a parsec, although there are insufficient studies to determine whether the filaments have smaller-scale substructure.

3.5. PARTICLE ACCELERATION BY FIELD LINE ANNIHILATION AT THE SURFACES OF MOLECULAR CLUMPS

The model which is most closely tied to the full set of existing observations is the one by Serabyn & Morris (1994), described separately by Serabyn in these proceedings. According to this model, the synchrotron-emitting electrons are accelerated by magnetic field line reconnection at the ionized

surfaces of molecular cloud clumps as they move through a uniform, ambient field. Such molecular cloud clumps should thus be found to lie at the origin of all of the filaments.

3.6. COSMIC STRINGS

Chudnovsky *et al.* (1986) consider the hypothesis that the Galactic center filaments are low-mass-density cosmic strings which have been concentrated at the Galactic center. Indeed, the surprising rigidity and large radius of curvature of the filaments makes this hypothesis worth considering. The very large tension in cosmic strings would rapidly smooth out irregularities and eliminate all but the largest-scale curvature. This same tension, however, would accelerate the string laterally as it acts to straighten it. The string would then oscillate about its equilibrium position at relativistic speeds, notwithstanding the inertia of the plasma to which it is coupled. Such motion should be readily detectable, even at the Galactic center, but it is in fact not seen. In a study with a 4-year time base, Echevarria & Morris (1995) set limits of 0.03c – 0.06c on the lateral motion of two isolated threads.

Another argument against a superconducting string is that the magnetic field surrounding it should be predominantly azimuthal; that is, its projection onto the plane of the sky should be perpendicular to the filament rather than parallel, whereas a parallel field is observed in the Arc and in G359.54+0.18 (Yusef-Zadeh *et al.* in these proceedings). Another complication of cosmic string hypotheses is the apparent splitting of some of the filaments (*e.g.*, Fig. 4). It is easier to understand this as a diffusion of relativistic electrons between neighboring magnetic flux tubes, than it is to imagine and invoke split cosmic strings.

4. Some Implications of a Strong Magnetic Field

If the Galactic center filaments are an indication of a large-scale magnetic field of milligauss strength, they carry profound implications for physical processes taking place in this arena. Consequently, it is extremely important to demonstrate whether the field is truly ubiquitous and whether it is participating in galactic rotation.

As an example, if the presumed dipole magnetic field is not anchored in the disk clouds (and there is no evidence that it is), then the field may be rotating with a small or even zero velocity, in which case clouds orbiting near the Galactic center have a considerable velocity, on the order of 10^2 km $\cdot$ s^{-1}, in the rest frame of the field. The magnetic viscosity of the medium is then quite large, causing clouds to lose angular momentum at such a large rate that they spiral inwards on relatively short time scales. More

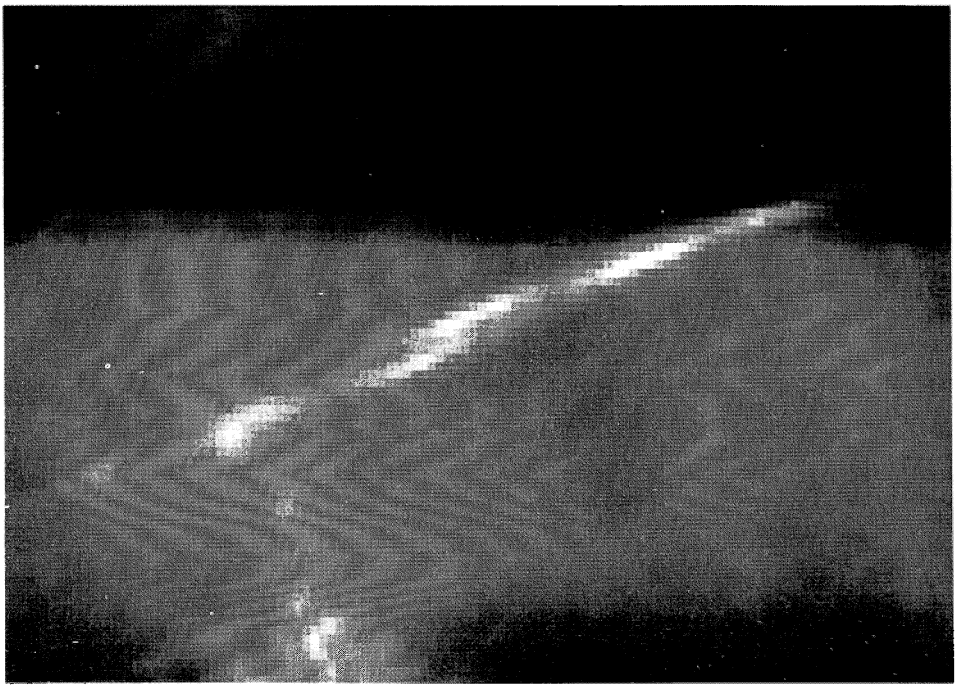

Figure 4. Radiograph at λ20cm of a split radio thread, from Echevarria & Morris 1995.

precisely, the viscous force on a cloud of radius r moving at speed v through an intercloud medium of density ρ_{icm} and magnetic field of strength B is $(\pi\rho_{icm})^{1/2}Bvr^2$. The dependence on ρ_{icm} occurs because of its effect on the Alfvén velocity. Therefore, for a cloud of diameter d and number density n, orbiting through an ambient medium of number density n_{icm} at a relative velocity equal to half the orbital velocity, the time scale for angular momentum loss by magnetic viscosity is

$$2.6 \times 10^7 \left(\frac{d}{7pc}\right)\left(\frac{n}{2\times 10^4 cm^{-3}}\right)\left(\frac{10\ cm^{-3}}{n_{icm}}\right)^{1/2}\left(\frac{10^{-3}\ G}{B}\right)\ years,$$

or ~25(R/25 pc) orbital times, at galactocentric radius R. This would add to the already rapid angular momentum loss by dynamical friction (Stark *et al.* 1991) to bring clouds into the Galactic center quickly.

The dynamical effects of a strong magnetic field on the low-density interstellar medium can be much more drastic. If the radial scale length of the vertical field is R_B, then radial magnetic forces equal gravitational

forces when

$$\rho_{icm} = \left(\frac{B^2}{8\pi V_c^2}\right)\left(\frac{R}{R_B}\right) \sim 100\ cm^{-3}\left(\frac{B}{1\ mG}\right)^2\left(\frac{R}{R_B}\right),$$

where $V_c \sim 150$ km $\cdot s^{-1}$ is the circular orbital velocity in the region of interest. Thus, in the presence of a pervasive milligauss field, the interstellar medium will settle into corotation with the magnetic field when its density is on the order of tens of particles per cm^3. Data on the 21-cm HI line from the inner magnetosphere of the Galaxy may provide a useful probe of the strength and behavior of the central magnetic field, inasmuch as it is presumably formed in such a low-density medium.

References

Anantharamaiah, K.R., Pedlar, A., Ekers, R.D. & Goss, W.M. 1991, *MNRAS*, 249, 262.
Bally, J., Stark, A.A., Wilson, R.W. & Henkel, C. 1988, *Ap.J.*, 324, 223.
Bally, J. & Yusef-Zadeh, F. 1989, *Ap.J.*, 336, 173.
Benford, G. 1988, *Ap.J.*, 333, 735.
Blitz, L., Binney, J., Lo, K.Y., Bally, J. & Ho, P.T.P. 1993, *Nature*, 361, 417.
Chudnovsky, E.M., Field, G.B., Spergel, D.N. & Vilenkin, A. 1986, *Phys. Rev. D*, 34, 944.
Cotera, A.S., Erickson, E.F., Simpson, J.P., Colgan, S.W.J., Allen, D.A. & Burton, M.G. 1994, in "The Nuclei of Normal Galaxies: Lessons from the Galactic Center" eds: R. Genzel and A. Harris, (Dordrecht: Kluwer).
Echevarria, L. & Morris, M. 1995, in preparation.
Erickson, E.F., Colgan, S.W.J., Simpson, J.P., Rubin, R.H., Morris, M. & Haas, M.R. 1991, *Ap.J. Lett.*, 370, L69.
Gray, A.D., Cram, L.E., Ekers, R.D. & Goss, W.M. 1991, *Nature*, 353, 237.
Gray 1994, PhD Thesis, School of Physics, The University of Sydney.
Heyvaerts, J., Norman, C. & Pudritz, R.E. 1988, *Ap.J.*, 330, 718.
Lesch, H. & Reich, W. 1992, A&A, 264, 493.
Liszt, H.S. 1985, *Ap.J. Lett.*, 203, L65.
Morris, M. 1990, in IAU Symp. No. 140: "Galactic and Intergalactic Magnetic Fields," eds: R. Beck, P.P. Kronberg, & R. Wielebinski, Dordrecht: Kluwer, p. 361.
Morris, M. 1994, in "The Nuclei of Normal Galaxies: Lessons from the Galactic Center" eds: R. Genzel and A. Harris, (Dordrecht: Kluwer).
Morris, M., Davidson, J.A., Werner, M., Dotson, J., Figer, D.F., Hildebrand, R., Novak, G. & Platt, S. 1992, *Ap.J. Lett.*, 399, L63.
Morris, M. & Yusef-Zadeh, F. 1985, *A.J.*, 90, 2511.
Morris, M. & Yusef-Zadeh, F. 1989, *Ap.J.*, 343, 703.
Pauls, T., Downes, D., Mezger, P.G. & Churchwell, E. 1976, *Astr. and Ap.*, 46, 407.
Poglitsch, A., Stacey, G.J., Geis, N., Haggerty, M., Jackson, J., Rumitz, M., Genzel, R. & Townes, C.H. 1991, *Ap.J. Lett.*, 374, L33.
Reich, W. 1994, in "The Nuclei of Normal Galaxies: Lessons from the Galactic Center" eds: R. Genzel and A. Harris, (Dordrecht: Kluwer), p. 55.
Rosso, F. & Pelletier, G. 1993, *Astr. and Ap.*, 270, 416.
Seiradakis, J.H., Lasenby, A.N., Yusef-Zadeh, F., Wielebinski, R. & Klein, U. 1985, *Nature*, 317, 697.
Serabyn, E. & Güsten, R. 1987, *Astr. and Ap.*, 184, 133.
Serabyn, E. & Morris, M. 1994, *Ap.J. Lett.*, 424, L91.

Stark, A.A., Gerhard, O.E., Binney, J. & Bally, J. 1991, *MNRAS*, 248, 14p.
Tsuboi, M., Inoue, M., Handa, T., Tabara, H., Kato, T., Sofue, Y. & Kaifu, N. 1986, *A.J.*, 92, 818.
Uchida, K., Morris, M. & Yusef-Zadeh, F. 1992, *A.J.*, 104, 1533.
Yusef-Zadeh, F. & Morris, M. 1987a, *A.J.*, 94, 1178.
Yusef-Zadeh, F. & Morris, M. 1987b, *Ap.J.*, 322, 721.
Yusef-Zadeh, F. & Morris, M. 1988, *Ap.J.*, 329, 729.
Yusef-Zadeh, F., Morris, M. & Chance, D. 1984, *Nature*, 310, 557.
Yusef-Zadeh, F., Morris, M. & van Gorkom, J. 1987, in AIP Conf. Proc. No. 155: "The Galactic Center", ed: D.C. Backer, New York: AIP, p 190.
Yusef-Zadeh, F., Morris, M. & van Gorkom, J. 1989, in IAU Symp. No. 136: "The Center of the Galaxy", ed: M. Morris, Dordrecht: Kluwer, p 275.
Yusef-Zadeh, F., Morris, M., Lasenby, A.N., Seiradakis, J.H. & Wielebinski, R. 1990, in IAU Symp. 140: "Galactic and Intergalactic Magnetic Fields," ed: R. Beck *et al.* , Kluwer, p. 373.

DISCUSSION

B. Gustafsson: As regards the question concerning abundance signatures that would show a tine span between the halo and the formation of the disk, I think one would expect a discontinuity in the α/Fe abundance ratios when passing from halo to disk stars of similar metallicities. One should look for that.

W. Jaffe: If the 1ρG fields are global in GC, is the material bound? ie is $\triangle B^2 < \frac{GMP}{r}$ ie $V_A^2 \lesssim V_{orbit}^2$

Morris: If the field is poloidal, as is indicated, then the magnetic pressure need be confined only parallel to the galactic plane. One might imagine that this is accomplished by a ring current which is somehow driven by an inflow of matter, or simply by the inflow of matter itself, as a result of inevitable momentum losses. The field cannot diffuse outward through this matter. The answer to the question, "where is the field anchored?" is an interesting one. Perhaps it is bound to bulge & halo gas, but it does not seem to be anchored to gas in the plane.

I. King: Is there evidence that the arches and the filaments are not at separate points along the line of sight?

Morris: The evidence for interaction is circumstantial, but strong. Yusef-Zadeh & Morris (1988) point out that, along a well-defined line where the molecular cloud underlying the arched filaments ends, both filamentary systems undergo sharp discontinuities in brightness and/or polarization. Furthermore, one can draw a detailed one-to-one correspondence between filaments in the two systems.

G. Verschuur: I am concerned that you maintain that these filaments are unique to the galactic center. The WSRT has been used to map the

distribution of galactic polarized radiation and very long thin filaments are common. This is seen in the work of Wieringa & de Bruyn, as well as the work of Spoelstra & myself. I would suggest that it would might be fruitful to treat filaments as common and consider only that the source of illumination is unique to the galactic center. Are you aware of the filaments I am referring to?

Morris: –

THE NATURE OF THE GALACTIC CENTER ARC

E. SERABYN
Department of Physics, Mathematics and Astronomy
California Institute of Technology, Pasadena, CA 91125

Abstract. Ever since the Galactic Center Arc was resolved into its component filaments a decade ago, it has been clear that its linear structure arises from the influence of a strong magnetic field. However, the origin and nature of the contributory phenomena have remained elusive. Since what is seen is synchrotron emission from relativistic particles, of prime interest is a knowledge of the acceleration mechanism involved. Interferometric imaging of the molecular gas in the vicinity of the Arc has now provided a tantalizing clue to the Arc's origin: molecular clumps coinciding with the endpoints of a number of the Arc's filaments point to these clumps as the source of the relativistic particles. This suggests that as dense molecular clumps course through the ambient magnetic field at the Galactic Center, magnetic energy is liberated in their leading layers via field reconnection, precipitating rapid acceleration of free charges to high energy.

1. Introduction

The resolution of the Galactic Center Arc (the "Arc" in the following) into a set of a dozen or so linear nonthermal filaments (NTFs) has contributed to a gradual, but fundamental change in our view of the Galactic center environment. While the synchrotron nature of the Arc's radio emission demands the presence of both a strong magnetic field and a copious supply of relativistic particles, numerous observations of the central molecular cloud layer have brought additional insights, particularly concerning the turbulent nature of these clouds. As is outlined in the following, an understanding of the nature of the Galactic Center Arc can be achieved from a synthesis of our knowledge in these two areas. I begin with a short review of both topics. A more complete review, including a compendium of extant models,

L. Blitz and P. Teuben (eds.), Unsolved Problems of the Milky Way, 263–269.
© 1996 *International Astronomical Union.*

is provided by M. Morris in this volume.

The presence of a high strength magnetic field in the central hundred or so parsecs of our Galaxy is observationally well supported (Morris 1994), but the field morphology and strength nevertheless remain subject to considerable uncertainty. Thus, while it is now known that the ambient field is oriented roughly perpendicular (vertical) to the plane of the Galaxy in the NTFs making up the Arc, as well as in several other 'threads' of nonthermal emission in the vicinity of the Galactic Center (Morris, this volume), it is not yet known if these nonthermal filaments correspond to regions of enhanced field strength (flux tubes), or to sites of particle injection in a more or less uniform vertical field. In terms of field strengths, although estimates for the central region span a large range, from tens of μG to several mG (Yusef-Zadeh *et al.* 1984; Sofue *et al.* 1987), all of the measured values are well above typical μG Galactic disk values. Thus, the general picture of a strong, vertically oriented magnetic field in the central region of our Galaxy has become established.

Concurrently, our views of the molecular cloud layer at the Galactic center have evolved, from earlier resolution-limited overviews of the large scale gas distribution and kinematics, to quite detailed views of the physical conditions and kinematics of individual clouds, and of the molecular cloud population as a whole. Thus, it is now clear that molecular clouds in the central few hundred parsecs differ considerably from their counterparts in the large-scale Galactic disk. Physically, the Galactic Center clouds are both hotter and denser (Güsten 1989). Moreover, external forces acting on the clouds are much larger in the Galactic Center: both tidal gravitational forces and magnetic pressures are much higher. Finally, the Galactic Center clouds are invariably more turbulent: they have both higher internal velocity dispersions and also a much higher random component to their systemic velocities, with some clouds following orbits decidedly at odds with systematic rotation (Bally *et al.* 1989). Indeed, many clouds show radial velocities which are "forbidden", i.e., opposite in sign to Galactic rotation. Thus, the molecular medium in our Galactic nucleus consists of an ensemble of clouds which is much more chaotic, more highly excited, and more affected by large scale external forces than are the clouds in the Galactic disk.

Given a strong vertical magnetic field and a sub-population of anomalously orbiting molecular clouds (i.e., clouds on orbits not in accord with corotation of the interstellar medium and the magnetic field), it is natural to ask how the two interact. In particular, what happens as these anomalously orbiting clouds (which presumably have some fractional ionization level) attempt to traverse the vertical magnetic field lines? This question becomes all the more interesting when it is revealed that an anomalously orbiting molecular cloud is located at the approximate midpoint of the

Galactic Center Arc. I return to this issue after briefly discussing some of the most relevant observational data relating this cloud to the Arc.

2. Molecular Observations

The molecular cloud in question, M0.20-0.033 or the 25 km s^{-1} cloud, lies roughly in the true Galactic plane, near the midpoint of the nonthermal filaments which comprise the Galactic Center Arc (Lasenby *et al.* 1989; Serabyn & Güsten 1991 — hereafter SG). Its radial velocity, 25 km s^{-1}, is difficult to reconcile with simple Galactic rotation if the Arc is actually as close to the Galactic Center as it appears in projection. Two lines of argument suggest that this cloud is interacting with the Arc. The most obvious mode of interaction is through the mediation of the HII region G0.18-0.04 (Yusef-Zadeh & Morris 1987), which appears to 'wrap around' the sheaf of NTFs making up the Arc. As this HII region represents the ionized surface of the 25 km s^{-1} cloud (SG), the molecular cloud is obviously also involved in the interaction. Moreover, as molecular material seems to 'protrude' from the main body of the 25 km s^{-1} cloud along the direction of the NTFs in the single dish CS map (SG), a more direct interaction between the molecular medium and the NTFs is also intimated.

While single dish observations thus provided an overview of the molecular cloud morpholgy and suggested the model components to be discussed below (SG), recent observations with the OVRO mm-wave interferometer have provided further clues which have put these hypotheses on a stronger observational footing (Serabyn & Morris 1994 — hereafter SM). Fig. 1 presents the interferometric image of the emission from the 25 km s^{-1} cloud in the CS J = 2-1 line. Because of the small primary beam, the mapped fields cover only a small fraction of the cloud, but the three fields available are nevertheless quite revealing.

As discussed in more detail in SM, several molecular clumps are seen in the mapped fields, all of which lie athwart one or more of the nonthermal filaments. Indeed, only a few of the filaments pass by these clumps without crossing one or another of them, and of course even these filaments may encounter a molecular clump outside of the mapped interferometer fields. More importantly however, the observed clumps all lie close to the locations at which the NTFs either fade from view, or change direction slightly. Thus, in brief, it is possible to conclude that the endings and bendings of the NTFs near G0.18-0.04 are intimately related to the presence of molecular gas clumps.

Does this mean that these clumps are sites of relativistic particle generation, or absorption? Based on the molecular cloud's central location relative to both the NTFs and the Galactic plane, on the observed increase in en-

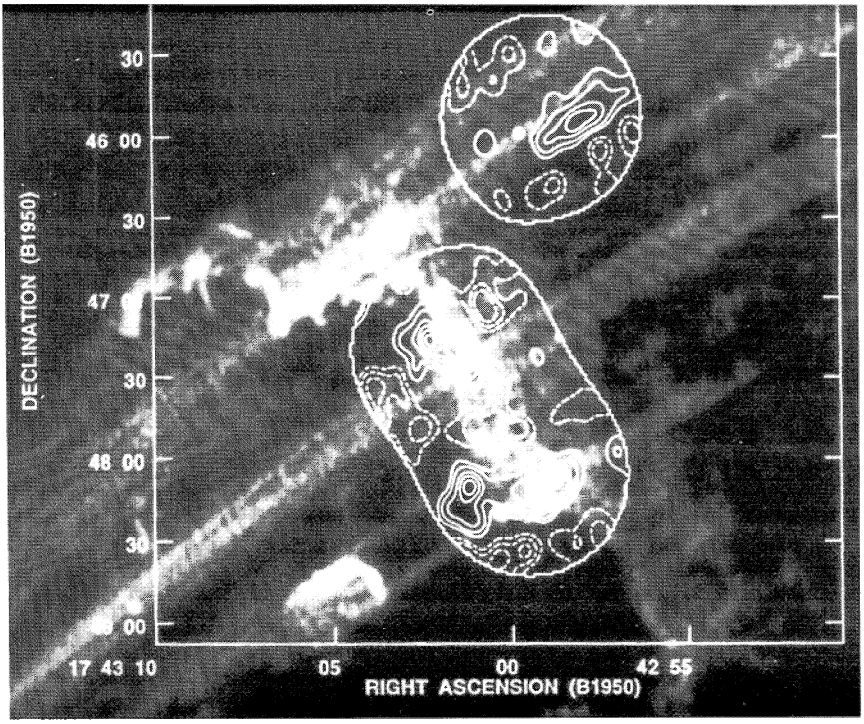

Figure 1. Superposition of the OVRO CS J=2-1 three-field mosaic of the 25 km s^{-1} cloud (contours) on a 5 GHz radiograph of the G0.18-0.04 HII region and the nonthermal filaments in the Arc (from Serabyn and Morris 1994).

tropy of the Arc away from the Galactic plane (only amorphous plumes are seen at Galactic latitudes $> 0.2°$; Seiradakis *et al.* 1985; Tsuboi *et al.* 1986), and on the observed decrease in the Arc's spectral index away from the Galactic plane (Reich 1990), which argues for a more aged population of electrons far from the Galactic plane, it is possible to conclude that the molecular clumps are the generation sites of the relativistic electrons.

3. Reconnection Scenario

Because the Arc's synchrotron emitting filaments attest to the presence of a strong magnetic field, it is natural to look to the magnetic field for the particle acceleration mechanism. This then brings us back to the question raised earlier — as a partially ionized molecular cloud attempts to traverse a region of high magnetic field, how does it interact with the field? The problem of course is that the cloud's internal field is frozen in by the small ionized component present, and so as the cloud traverses the ambient field,

both the internal and external fields must deform to enable the passage of the intruding cloud (unless the ionization level is very low). The external field ahead of the cloud is thus compressed by ram pressure, and then swept around and past individual dense clumps, while at the same time, the clumps' internal field lines are dragged through the ambient medium. In analogy to the case of a magnetized planet making its way through the solar wind, a contact discontinuity develops ahead of each advancing cloud clump, wherein the compressed external field is forced into contact with the clump's own internal field. (In this analogy, we must of course remember that an interstellar cloud is not a rigid body, so that the external magnetic pressure likely leads to cloud fragmentation and interpenetration of the field and the clumps, and also that such a cloud's internal magnetic field is not internally generated, as in the case of a magnetized planet, but is instead a relic of the cloud's own history as part of the ISM). Thus, a structure resembling a planetary magnetopause is set up ahead of each advancing clump, in which particle acceleration may occur. However, due to the fluid nature of molecular clouds, this 'magnetopause' is likely not a stable surface — indeed it likely distorts markedly as a result of spatial density and ionization variations, rotational and turbulent motions in individual clumps, and fragmentation resulting from magnetic pressure gradients.

In the boundary layer ahead of the advancing clumps, the external and internal fields, which are likely dissimilar both in magnitude and orientation, are forced into contact, leading to the "reconnection" of the two fields. Briefly (Parker 1979), the two fields diffuse through the partially ionized medium toward the boundary, and this diffusion of flux induces an electric field which rapidly accelerates the free charges present. A more formal way to describe the phenomenon is that the curl of the magnetic field across the boundary necessitates a current flow (and so an electric field) along the boundary. Of course shocks may aid in the acceleration process. Once out of the interaction zone, the accelerated particles attach themselves to the nearest large scale field lines, and spiral vertically out of the plane of the Galaxy. Given the high frequency spectral cutoff of the NTF emission (between 15 and 43 GHz; Sofue *et al.* 1992), Gev electron energies and roughly 10^4 yr radiative lifetimes are indicated, implying that the relativistic electrons can easily travel the length of the filaments during their lifetimes.

In this scenario, the observed nonthermal filaments result from the local injection of particles onto ambient field lines from 'hot spots' corresponding to individual molecular clump surfaces. As a result, there is no need to rely on special magnetic field configurations based on the existence of a high field flux tube at the location of the Arc (which would raise pressure balance problems). Instead, even with a uniform magnetic field structure, all that is required is a clumpy molecular medium, which is in fact observed. Since

reconnection likely also occurs at a lower level in the more diffuse interclump medium, this scenario can also explain the more extended 'background' of nonthermal emission seen around the individual nonthermal filaments. Indeed, fewer collisions near the generation site may allow electrons from more diffuse gas to escape with higher energies, consistent with the higher cutoff frequency seen outside of the well-defined filaments (Sofue *et al.* 1992).

The details of the reconnection and acceleration processes are beyond the scope of this paper (and also occur on a scale too small to be directly observable at the distance of the Galactic center), but two general questions can be addressed. First, is the process energetically feasible — i.e., is the magnetic energy swept up by the advancing cloud sufficient to power the luminosity seen from the relativistic particles in the Arc? Second, since the process described is quite general, why is the Arc such a unique source?

To address the first question, a cloud coursing thru an ambient field encounters a magnetic energy flux of $10B^2v$ $L_\odot/pc^2$, where B is the external field in mG, and v is the cloud-field relative velocity in km s^{-1}. Allowing for a cloud cross-section of 10 pc^2, a field of 1 mG, and a relative velocity of 100 km s^{-1} (all of which are subject to large uncertainties), the 25 km s^{-1} cloud then encounters magnetic energy at a rate of $\sim 10^4$ $L_\odot$. In contrast, the luminosity of the Arc is only of order 10^2 $L_\odot$, requiring an efficiency for magnetic to kinetic energy conversion of only 1%, a level consistent with theoretical expectations for field reconnection (SM).

Concerning the second question, since the rate of accessing magnetic energy depends on the ambient magnetic energy density, as well as on the cloud-field relative velocity, clearly a large luminosity in relativistic particles can be produced only in the central high-field, high-turbulence region of our Galaxy. However, while this volume includes many molecular clouds, the instances of filamentation are relatively few, leading one to suspect that the picture is not yet complete. Indeed, a further variable is involved — the ionization structure of the cloud. This enters in two opposing ways, as the reconnection rate is inversely proportional to the conductivity of the medium (and so is low if the ionized fraction is high), but free charges must be present to provide an ionized population susceptible to acceleration.

Presumably what occurs is then the following. If the ionization level is low, a projectile cloud or clump can easily be accomodated by the fields, although some very low level reconnection may occur. If however, a cloud has an ionized surface layer (presumably due to photoionization, but perhaps aided by Alfven's critical ionization effect), the cloud's projectile motion will be strongly opposed by the ambient field. With ionized surfaces which are oriented more or less along the direction of motion, the ionized layers can shear off of the bulk of the neutral medium, disrupting the cloud,

but likely leading to little in the way of reconnection. This may in fact explain the elongated appearance of the nearby thermal "arched filaments" (Morris, this volume). On the other hand, if a cloud's leading surface were ionized, the results would be dramatic: the approaching fields would be pressed against each other, and prolific reconnection and particle acceleration would occur at the interface, as discussed above. Thus, by combining the need for a high magnetic field, a high cloud-field relative velocity, and also surface ionization in the leading cloud layers, the phenomenon seen as the Galactic Center Arc should indeed be rare.

References

Bally, J., Stark, A.A., Wilson, R.W., & Henkel, C. 1988, *Ap. J.* 324, 223.
Güsten, R. 1989, in IAU Symp. 136, "The Center of the Galaxy", ed. M. Morris (Dordrecht: Kluwer), 89.
Lasenby, J., Lasenby, A.N., & Yusef-Zadeh, F. 1989, *Ap. J.* 343, 177.
Morris, M. 1994, in "The Nuclei of Normal Galaxies: Lessons from the Galactic Center", eds. R. Genzel & A. Harris (Dordrecht: Kluwer).
Parker, E.N. 1979, Cosmical Magnetic Fields (Oxford: Clarendon Press).
Reich, W., 1990 in IAU Symp. No. 140, "Galactic and Intergalactic Magnetic Fields", eds. R. Beck, P. Kronberg and R. Wielebinski (Dordrecht: Kluwer), 369.
Seiradakis, J.H., Lasenby, A.N., Yusef-Zadeh, F., Wielebinski, R., & Klein, U. 1985, *Nature* 317, 697
Serabyn, E. & Güsten, R. 1991, *Astr. and Ap.* 242, 376.
Serabyn, E. & Morris, M. 1994, *Ap.J. Lett.* 424, L91.
Sofue, Y., Murata, Y. & Reich, W. 1992, *Publ. Ast. Soc. Japan*, 44, 367.
Sofue, Y., Reich, W., Inoue, M., & Seiradakis, J.H. 1987, *Publ. Ast. Soc. Japan* 39, 95.
Tsuboi, M., Inoue, M., Handa, T., Tabara, H., Kato, T., Sofue, Y., & Kaifu, N. 1986, AJ, 92, 818.
Yusef-Zadeh, F. & Morris, M. 1987, *Astron. J.* 94, 1178.
Yusef-Zadeh, F., Morris, M., & Chance D. 1984, *Nature* 310, 557.

THE NATURE OF THE SCATTERING AND FARADAY SCREENS TOWARD THE GALACTIC CENTER

F. YUSEF-ZADEH, P. PARASTARAN
Northwestern University
Department of Physics and Astronomy
Evanston, Il. 60208

M. WARDLE
University of Rochester
Department of Physics and Astronomy
Rochester, N.Y. 14627

AND

K. UCHIDA
Max-Planck-Institute fur Radioastronomy
Bonn, Germany

Abstract. We probe the relationship between the scattering and Faraday screens toward the Galactic center by examining the scattering properties of Sgr A* and OH/IR stars and by measuring the rotation measure distribution of an extended nonthermal filament. The unusually large rotation and scattering measures, the evidence for anisotropic scattering, and the anisotropy in the rotation measure structure function, suggest that the Faraday and scattering media are located near the Galactic center. The results presented here are consistent with a turbulent medium of magnetized thermal electrons with the outer scale of electron density and magnetic field fluctuations being of the order of 5×10^{-4} and 2 pcs, respectively.

1. Introduction

The apparent size of the bright compact radio source, Sgr A*, as a function of wavelength has been extensively studied at a number of frequencies using VLBI measurements (Lo 1993). These high-frequency measure-

L. Blitz and P. Teuben (eds.), Unsolved Problems of the Milky Way, 271–277.
© 1996 *International Astronomical Union.*

ments indicate that the EW diameter of the source scales as $\lambda^{2.0}$ suggesting that interstellar diffractive scattering is responsible for the broadening. The interstellar scattering hypothesis has received strong confirmation by the measurement of a similar amount of scattering for nearby OH masers (van Langevelde et al. 1992). Recent VLBA measurements at λ7mm have shown that scattering still dominates the brightness distribution at short wavelengths (Backer 1994).

Recent VLA observation of Sgr A* at λ20cm show that the NS diameter has the same wavelength dependence as in the EW direction (Yusef-Zadeh et al. 1994). The scatter-broadened image is elongated in the EW direction, with an axial ratio of 0.56 ± 0.22 and a position angle of $82^0\pm1.8^0$. The conclusion is that there is a 2:1 asymmetry in the scatter-broadened image of Sgr A* at a number of wavelengths with a position angle that ranges between 80 to 90^0. Elongation of the scattered image with nearly constant PA and ellipticity is explained by propagation through anisotropic turbulent distribution of thermal electrons (Higdon 1984). Similar effects have been observed in radio wavelengths through the outer solar corona where the magnetic field dominance over plasma pressure leads to highly anisotropic turbulence (Narayan et al. 1989; Armstrong et al. 1990).

Recent observations show that the scattering of the OH masers within the inner 45′ of the Galactic center is also anisotropic (Frail et al. 1994). Yusef-Zadeh et al. argue that the scattering occurs within HII regions lying in the central 100 pc of the Galaxy. The magnetic field in this region must be organized and have a strength of at least a milliGauss. Such a high value of the magnetic field is not unexpected since a number of large-scale magnetized filaments in the Galactic center region are thought to have milliGauss field strengths in the direction perpendicular to the Galactic plane. The inferred magnetic field from the scatter-broadened sources indicate a strong magnetic field with a random orientation within the inner 45′ and therefore, they do not follow the organized poloidal geometry of the field which is expected to dominate the Galactic center region (Yusef-Zadeh 1989; Morris 1994). The anisotropic scattering results complement polarization and Zeeman measurements in characterizing the magnetic field in a turbulent medium of thermal electrons.

2. The Scattering Medium

The anisotropy of OH/IR stars and Sgr A* is probably caused by a magnetic field permeating the scattering medium, but the location of the scattering screen has not been determined. The strong, anisotropic scattering extending over a 40′ region aligned with the Galactic center is suggestive of a scattering medium near the Galactic center. However, scattering be-

comes less effective when the distance from the source to the screen is much smaller than their distance to the observer because the broadening must overcome the spherical divergence of the wavefront incident on the screen. If the scattering medium is located near the Galactic center the electron density fluctuations (for an outer turbulent scale of 1 pc) would produce more free-free emission than is observed from the galactic center and in addition, the screen would become optically thick to low radio frequencies (Backer 1978). This argues for the coincidental alignment of a screen that lies outside the central regions of the Galaxy (e.g. van Langenvelde et al 1992)

An important point is that the angular broadening reflects the power in the screen at the smallest length scales (perhaps 10^7 cm), whereas the size of the density fluctuations depends on the power on the largest scales. Estimates of the electron density fluctuations are obtained from the observations by extrapolating the power spectrum of the fluctuations from 10^7 cm to an unknown outer scale, typically assumed to be of order 10^{18} cm or more (a typical HII region size). It is possible for the scattering screen to lie within a few tens of parsecs of the Galactic center if the outer scale is much smaller than 1 pc. One possibility is that the scattering occurs in thin ionized surface layers of molecular clouds lying in the central 100 pc of the Galaxy (Yusef-Zadeh et al. 1994). The outer scale of turbulence in this model is identified with the thickness of the ionized layers, about 4×10^{-4}pc for the intense UV radiation field in the region.

The assumptions made in the above model are that the UV radiation field is strong enough to photoionize the outer layer of the molecular clouds and that the outer scale of turbulence is identified with the thickness of the photoionized layer. Thus, measuring the radiation field will test this scenario. One method of investigating the nature of the UV radiation field in the inner Galaxy is to search for radio continuum emission from the outer envelopes of the population of OH/IR stars that are known to lie in the Galactic center region (Lindqvist et al. 1992). The ionized surfaces of the stellar envelopes should emit an amount of free-free emission dependent on the value of the ambient UV flux near the Galactic center. The strength of the free-free emission can be compared to theoretical estimates of the fluxes from photoionized surfaces of mass-losing stellar envelopes (Serabyn et al. 1991). The continuum fluxes from these cool stars will reflect the variation in the local UV flux with distance from the Galactic center.

3. The Faraday Screen

It is plausible that the scattering screen and Faraday screens should be identified with one another. In order to examine the relationship between

these two screens, we analyzed polarization data of a nonthermal radio continuum filament, G359.5+0.18 (Bally and Yusef-Zadeh 1989). This source is located within the region where strong anisotropic scattering of thermal emission from OH/IR stars has been found, and allows us to measure the variation of Galactic Faraday rotation over small angular scales along its 3′ length.

Multifrequency VLA observations reveal the magnetic field geometry, and detailed rotation measure distributions of this system of nonthermal filaments with a spatial resolution of ≈3". The projected magnetic field follows predominantly along the filaments except in its western boundary where the intrinsic field runs perpendicular to the direction of the linear filaments. In addition, the filaments show very high rotation measures (RM) ranging between -370 and -4200 rad m^{-2}. The plots of the RM values vs. λ^2 demonstrate that the Faraday screen is external to the source (Yusef-Zadeh et al. 1995).

The high variability of the rotation measure along G359.5+0.18 is a powerful probe of the structure of the ionized magnetized medium that constitutes the Faraday screen (and probably the scattering screen). The variation in RM over an angular scale ($\delta\theta$) is described by the structure function, which for a Kolmogorov spectrum increases as $\delta\theta^{5/3}$ for small angular scales and flattens at scales larger than the outer turbulent scale (Simonetti and Cordes 1988; Clegg et al. 1992). The observed structure function has a power-law index of approximately 2 for small scales and flattens above 10". The RM structure function distribution indicates that for $\delta\theta < 20$", the RM gradient along the Galactic plane appears to be lower by a factor 2 than in other directions.

This anisotropy is roughly consistent with the anisotropic scattering seen toward Sgr A* and the Galactic center OH/IR stars, suggesting that the same magnetized medium is responsible for the large anisotropic scattering and the variation of the RM on small angular scales. Further evidence is provided by the high RM found for a number of other sources located within a degree from the Galactic center (Inoue et al. 1984; Yusef-Zadeh and Morris 1987; Gray 1994).

Both the magnitude of the RM and its small scale structure argue against the ionized screen being an extended local HII region coincidentally aligned with the Galactic center. The RM toward G359.5+0.18 is more than two orders of magnitude higher than other sources outside the Galactic center region, requiring $n_e B_{\|} L \approx 3000\,\mathrm{cm}^{-3}\mu\mathrm{G\,pc}$, where L is the thickness of the screen. For magnetic fields in the screen of a few micro-Gauss, the emission measure $n_e^2 L$ exceeds the value $2 \times 10^4\,\mathrm{cm}^{-6}\,\mathrm{pc}$ seen towards the galactic center (Mezger and Pauls 1979) unless L is in excess of 50 pc. Further, the RM fluctuates wildy on angular scales of a few arc-

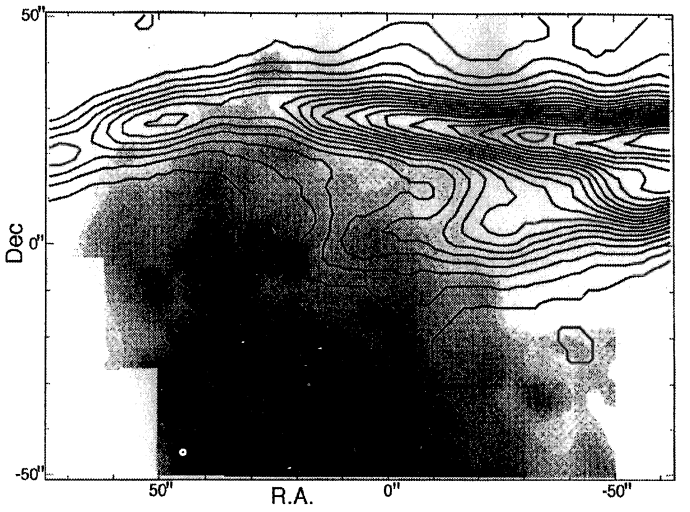

Figure 1. Contours of the λ6cm continuum image superimposed on a grayscale J=2-1 ^{12}CO line emission integrated from -160 to -122 km s^{-1}based on IRAM observations. It is slightly to the east of this region where the linear filaments, as seen in Figure 2, lose their coherent appearance.

seconds. L cannot be much greater than the corresponding spatial scale otherwise averaging along the line of sight would substantially reduce the amplitude of the fluctuations.

In summary, the RM observations strongly suggest that the Faraday screen is located near the Galactic center, where the electron density and magnetic field fluctuations are expected to have large values relative to the rest of the Galaxy. If the Faraday screen is to be identified with the photoionized surfaces of clouds in the region, the 10" angular scale must represent the outer scale of the fluctuations in the magnetic field (about 0.5 pc) rather than the electron density fluctuations.

4. G359.5+0.18 and Its Adjacent Molecular Cloud

A number of molecular clouds lying within the inner few hundred pcs of the Galaxy appear to be outlined by nonthermal filaments. The interaction hypothesis between the molecular gas and the energetic electrons associated with synchrotron-emitting filaments has been discussed (*e.g.*, Serabyn 1994), though the evidence for such an interaction is still not convincing. As a point of illustration, we show J=2-1 CO observations of the molecular cloud that lies at the edge of G359.54+0.18. Earlier J=2-1 CS and J=1-0

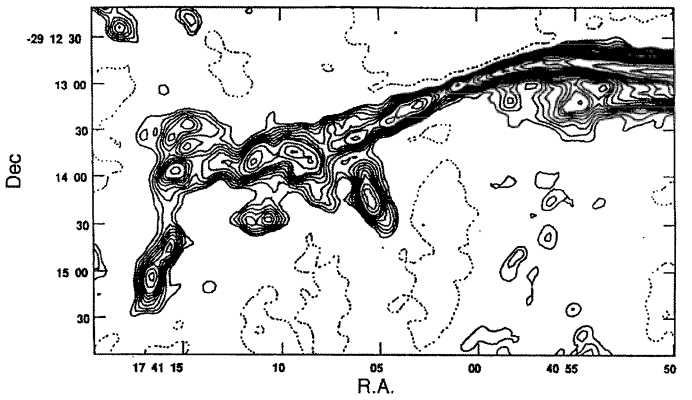

Figure 2. The λ6cm total intensity images of the eastern region of the filaments with a resolution of 10" × 10" are displayed.

^{13}CO measurements from the Bell Labs survey data with a resolution of about 100" (Bally and Yusef-Zadeh 1989) and J=2-1 ^{12}CO measurements based on observations made with the NRAO 12m telescope with a resolution of 30" (Bally, Yusef-Zadeh and Hollis 1989) suggested the possible association between the filaments in G359.54+0.18 and the adjacent -140 km s^{-1} molecular cloud. Motivated by the results of earlier low-resolution measurements, J=2-1 ^{12}CO observations were carried out toward the filament G359.54+0.18 with a resolution of 12" using the IRAM 30m telescope. The new CO map which is superimposed on the radio continuum image of G359.5+0.18 is shown in Figure 1. There is an apparent anti-correlation of the continuum nonthermal filaments with the molecular cloud suggesting that these two features maybe physically interacting with each other. Figure 2 shows contours of continuum emission at λ6cm from a region slightly east of the area that CO distribution was shown in Figure 1. The distorted filaments lose their coherent appearance as their morphology strengthens the argument for the interaction of G359.5+0.18 with its adjacent cloud. A more detailed presentation of these observations will be given elsewhere.

References

Armstrong, J., et al. 1990, *ApJ, 358*, 685.
Backer, D.C. 1994, *this conference*

Bally, J., Yusef-Zadeh, F. 1989, *ApJ, 336*, 173.
Clegg, A.W., Cordes, J.M., Simonetti, J.H. and Kulkarni, S.R. 1992, *ApJ, 386*, 143.
Frail, D.A., Diamond, P.J., Cordes, J.M. and van Langevelde, H.J. 1994, *ApJ, 427*, L43.
Gray, A.D. 1994, *PhD. Thesis*, University of Sydney.
Higdon, J.C. 1993, *ApJ, 285*, 109.
Inoue, M. et al. 1984, *Pub.Astron.Soc.Japan., 36*, 633.
Lindqvist, M., Habing, H.J. and Winnberg, A. 1992, *A.A., 259* 118.
Lo et al. 1993, *Nature, 362*, 38.
Morris, M. 1994, *this conference.*
Narayan, R., et al. 1989, *MNRAS*, 241, 403.
Mezger, P.G., and Pauls, T. 1985, in *IAU Symposium No. 84*, ed. W.B. Burton, Reidel, Dordrecht, p. 357.
Morris, M. 1994, *this conference.*
Serabyn, E., Lacy, J.H., and Achtermann, J.M. 1991, *ApJ, 378*, 557.
Simonetti, J.H. and Cordes, J.M. 1988, in *AIP 174, Radio Waves Scattering in the Interstellar Medium*, ed. B.J. Ricket and D.C. Backer (NY:AIP)
van Langevelde, H.J., Frail, D.A., Cordes, J.M. and Diamond, P.J. 1992, *ApJ, 396*, 686.
Yusef-Zadeh, F., 1989, *IAU Symposium No. 136, The Center of the Galaxy*, ed. M. Morris, Kluwer, Dordrecht, p. 243.
Yusef-Zadeh, F. et al. 1995, *in preparation.*
Yusef-Zadeh, F. and Morris, M. 1987, *ApJ, 322*, 721.

THE GALACTIC CENTER STAR CLUSTER: NORMAL EVOLUTION !?

DANIEL SCHAERER
Geneva Observatory, CH-1290 Sauverny, Switzerland

1. Introduction

The star cluster in the Galactic center (GC) provides an exceptional testground for the evolution of stars in extreme environments. Its understanding is an important step for the study of stellar populations in starburst galaxies and AGN's. In this work we address the question if the central cluster can be understood by standard evolutionary scenarios, or whether other processes (collisions, mergers, atmosphere stripping etc.) need to be invoked. A more detailed account of this work will be published elsewhere.

2. Normal evolution

Evidence for the massive star population comes from the ionising radiation field and the first direct K-band observations. Let us now combine both informations to obtain a quantitative estimate of the different stellar types. *(i)* The number of Lyman continuum photons is $\log Q_0$=49.6 to 50.4, and $\log Q_1$=48.4 to 49.2 (Krabbe et al. 1991, Genzel et al. 1993). To reproduce the ionising radiation field thus only requires 2 to 22 equivalent O7 V stars (cf. Vacca & Conti 1992). Note that the contribution of the emission line stars to Q_0 and Q_1 is negligible (Najarro et al. 1994). *(ii)* The recent spectral analysis of the HeI/HI emission line star (spectral type Of/WN, henceforth called AF; Najarro et al.) yields stellar parameters, including surface abundances, which show a very good agreement with the evolutionary grids of Meynet et al. (1994) at Z=0.04 (cf. Shields & Ferland 1994), indicating that the AF star can be attributed to the socalled WNL phase of our tracks, with an initial (present) mass of $\sim$ 25 (10) $M_\odot$. Note that the mass loss rates used in these models are supported by the extensive

L. Blitz and P. Teuben (eds.), Unsolved Problems of the Milky Way, 279–280.
© 1996 *International Astronomical Union.*

comparisons of Maeder & Meynet (1994) showing a good agreement with observations in regions with constant star formation.

Assuming the AF star to be representative for the other $\sim$ 14 emission line stars, we thus derive a number ratio of these stars (called WNL*) to O7 V stars of WNL*/(WNL* + O7V) = 0.4 to 0.9, which is of the same order as observed in WR galaxies (Vacca & Conti 1992). This value can directly be compared to the predictions of Meynet (1994) for instantaneous star formation, which are based on the same tracks as used above. From his Fig. 3 (high mass loss) one obtains that the massive star population of the central star cluster can be explained by standard evolutionary models and adopting a normal IMF. The age of the cluster is then found to be 7–8 Myr, younger ages being excluded by the absence of WC stars and the stellar parameters of the AF star.

3. Discussion

Using simple observational constraints we have shown that with the present knowledge about the massive star population the GC star cluster can be explained by standard evolutionary models and a normal IMF yielding an age of 7 to 8 Myr. No particular processes like mergers etc. seem to be required. In fact this simple picture is also compatible with the integrated K, and the total IR luminosity. Several late type stars are also present in the cluster, their nature being partly disputed (cf. Genzel et al. review). The presence and the number of M-K supergiants can also be explained within the above scenario. It is clear, however, that if some cluster members are in fact AGB stars, the picture must be revised.

Clearly more detailed studies on both the late and the early type stars in the cluster are required to obtain more quantitative determinations of its stellar content. Concerning the emission line stars, calculations of Schaerer (1994) in particular show the large importance of line blanketing on the spectral analysis of AF like stars. This may also be of importance to understand the seeming differences of the GC emission line stars with normal Of/WN stars.

References

Genzel R., Hollenbach D., Townes C.H., 1993, MPE preprint 276
Krabbe A., Genzel R., Drapatz S., Rotaciuc V, 1991, *ApJ* 382, L19
Maeder A., Meynet G., 1994, *A&A* 287, 803
Meynet G., 1994, *A&A*, in press
Meynet G., Maeder A., Schaller G., Schaerer D., Charbonnel C., 1994, *A&AS* 103, 97
Najarro F. et al., *A&A* 285, 573
Schaerer D., 1994, *PhD thesis*, Geneva University
Shields J.C., Ferland G., 1994, *ApJ* 430, 236 Vacca W.D., 1994, *ApJ* 421, 140
Vacca W.D., Conti P.S., 1992, *ApJ* 401, 543

$C^{18}O$ AND HNCO IN THE GALACTIC CENTRE

M. LINDQVIST
Sterrewacht Leiden,
Postbus 9513, 2300 RA Leiden, The Netherlands

AA. SANDQVIST
Stockhom Observatory, S-133 36 Saltsjöbaden, Sweden

A. WINNBERG, L.E.B. JOHANSSON
Onsala Space Observatory, S-439 92 Onsala, Sweden

L.-Å. NYMAN
ESO, Casilla 19001, Santiago 19, Chile

F. COMBES
DEMIRM, Observatoire de Paris,
61 Av. de l'Observatoire, F-75014 Paris, France

R. GENZEL
MPIfEP, D-8046 Garching bei München, Germany

M. GERIN
Radioastronomie ENS,
24 Rue Lhomond, F-75231 Paris CDX 05, France

AND

P.G. MEZGER
MPIfR, Auf dem Hügel 69, W-5300 Bonn 1, Germany

Using the SEST, we have observed 554 positions with a spacing of 45″ in the $C^{18}O(J = 1 \rightarrow 0)$ and $HNCO(J_{kk'} = 5_{05} \rightarrow 4_{04})$ lines. The data covers most of the Sgr A region including the Arc. Many of the dominant clouds in the GC region (see e.g. Güsten et al. 1981, A&A 103, 197; Bally et al. 1987, ApJS, 65, 13) are readily identified in the total integrated $C^{18}O$ and HNCO maps (Fig. 1). The results will be published in A&AS and will include intensity maps with $5\,km\,s^{-1}$ velocity resolutions, as well as galactic longitude-velocity and galactic latitude-velocity maps. $J = 2 \rightarrow 1$ $C^{18}O$ ob-

L. Blitz and P. Teuben (eds.), Unsolved Problems of the Milky Way, 281–282.
© 1996 *International Astronomical Union.*

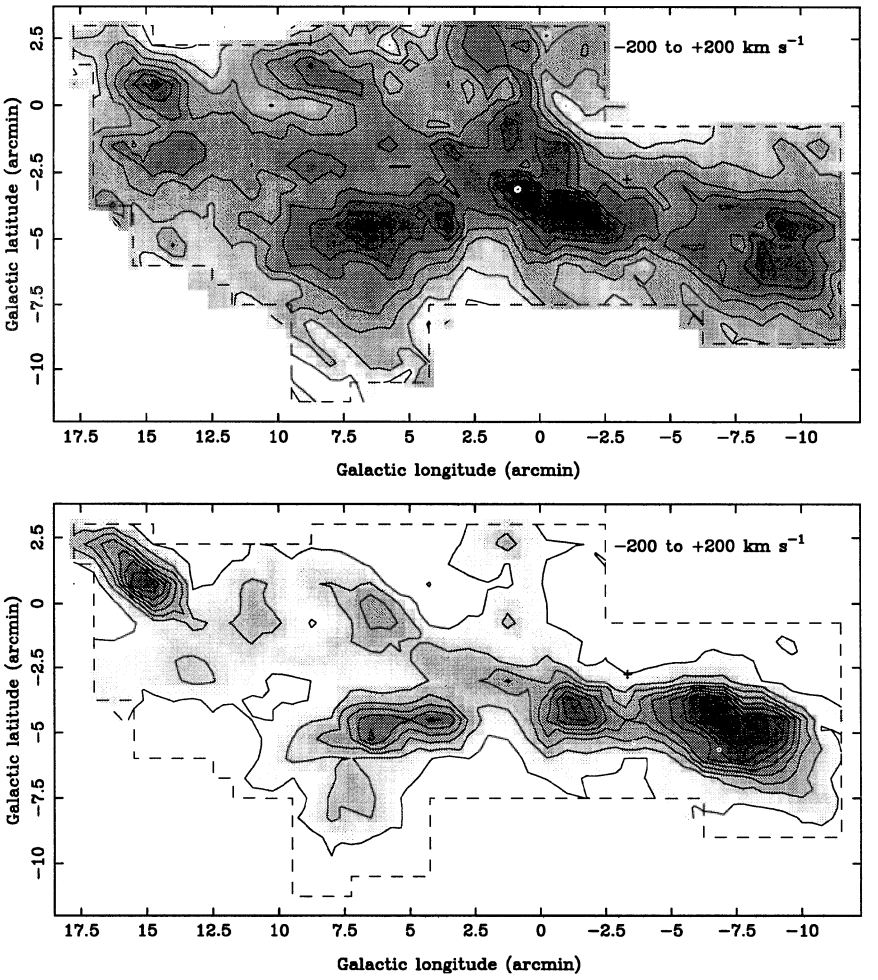

Figure 1. $C^{18}O(J=1\rightarrow 0)$ (top) and $HNCO(J_{kk'}=5_{05}\rightarrow 4_{04})$ (bottom) intensity maps covering the velocity interval $V_{LSR} = -200$ to $+200\,km\,s^{-1}$. The lowest contours are $5.0\,K\,km\,s^{-1}$. The increments are 5.0 and $10\,K\,km\,s^{-1}$ for $C^{18}O$ and HNCO, respectively. Units are in T_{mb} (K). The + sign marks the position of Sgr A*.

servations are planned for selected regions. The objectives of the project are twofold: 1. Geometrical, morphological, and dynamical relationships between the molecular regions and the radio continuum sources. 2. Heating mechanisms in GC molecular clouds.

Acknowledgements

ML is supported by an ESA external fellowship. This project is supported by the Swedish Natural Science Research Council (NFR)

TWO NEW VIEWS OF THE GALACTIC CENTER

D.T. JAFFE, R. PLUME, AND S. PAK
Department of Astronomy, University of Texas at Austin
Austin, Texas 78712 USA

The inner few hundred parsecs of the Galactic Center contains ~10% of the molecular ISM in the Galaxy. The conditions in this gas are significantly different from those in molecular clouds elsewhere in the Galaxy. Typical temperatures, densities, and internal velocity dispersions are higher (Güesten 1989). There is also evidence for a large amount of molecular gas which is not bound to distinct clouds (Stark et al. 1989). High velocity bulk gas motions and velocity discontinuities open up the possibility of a role for powerful large-scale shocks in ISM excitation. The very different nature of the dense ISM in the inner Galaxy make it useful as a laboratory for physical effects in the interstellar medium and a proving ground for ideas about the interaction of gas and stars in the nuclei of other galaxies.

We present here two new views of the inner 300 pc of the Milky Way. We have surveyed along the galactic plane in the 609 μm $^3P_1 \rightarrow ^3P_0$ line of C I and the v=1→0 S(1) line of H_2 at 2.12 μm. We made the 3' beam C I observations with a reimaging device at the Caltech Submillimeter Observatory (Plume & Jaffe 1995). We obtained the H_2 strip map on the McDonald Observatory 0.9m telescope with a 3.5′ beam using a Fabry-Perot spectrometer (Luhman et al. 1995a).

Figure 1 shows a longitude–velocity plot for the 492 GHz C I line. C I was detected everywhere along the plane in the region surveyed (l=-0.5 to +1.5 degrees) and its spatial-velocity distribution agrees fairly well with that of CO and ^{13}CO J=2→1. N(C I)/N(CO) ~0.5 near the peaks and is higher elsewhere implying that a large fraction of carbon in the neutral gas is atomic. Figure 2 shows the distribution of H_2 v=1→0 S(1) intensity along the same strip. The H_2 emission peaks at SgrA* where it had been previously detected by Gatley et al. (1986) and is present at a lower level (a few 10^{-6} erg cm^{-2} s^{-1} sr^{-1}) along much of the 2.5° strip we observed. Although extinction strongly affects the emergent intensity distribution, the low level and ubiquity of the H_2 emission argue for UV-fluorescence rather

L. Blitz and P. Teuben (eds.), Unsolved Problems of the Milky Way, 283–284.
© 1996 *International Astronomical Union.*

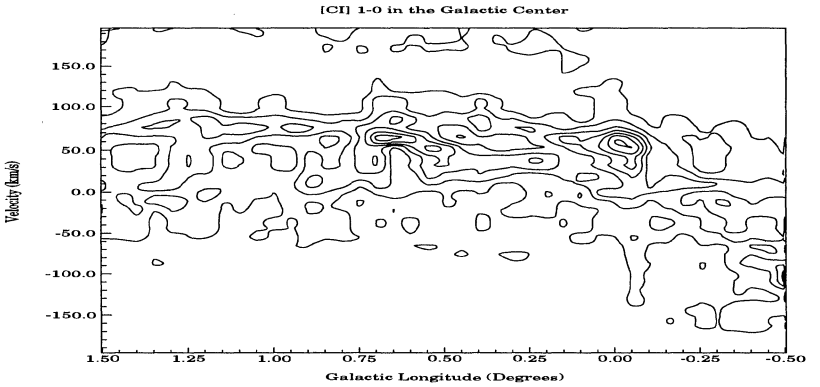

Figure 1. Longitude–velocity diagram for the 492 GHz [C I] $^3P_1 \rightarrow {}^3P_0$ transition along a cut at b=-3′. Contour intervals are 2 K km s^{-1} to 41 K km s^{-1} in steps of 6.5 K km s^{-1}.

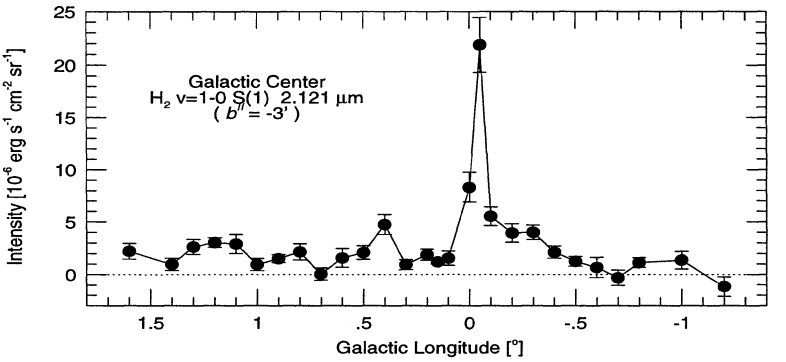

Figure 2. Intensity distribution of the H_2 v=1→0 S(1) line along a cut at b=-3′.

than shocks as the dominant excitation mechanism (see also Luhman et al. 1995b).

We thank our collaborators: John Bally, Neal Evans, Luke Keller, and Michael Luhman, for their contributions to the results discussed here. This work was supported in part by NSF grant AST-9117373 and a David and Lucile Packard Foundation Fellowship.

References

Gatley, I., Jones, T.J., Hyland, A.R., Wade, R., Geballe, T.R., & Krisciunas, K. 1986, MNRAS, 222, 299

Güsten, R. 1989, in IAU 136 , The Center of the Galaxy, ed. M. Morris, 89

Luhman, M.L., Jaffe, D.T., Keller, L.D., & Pak, S. 1995a, PASP, submitted

Luhman, M.L., Jaffe, D.T., Keller, L.D., & Pak, S. 1995b, ApJL, in press

Plume, R., & Jaffe, D.T. 1995, PASP, submitted

Stark, A.A., Bally, J., Wilson, R.W., & Pound, M.W. 1989, in IAU 136, The Center of the Galaxy, ed M. Morris, 129

POSSIBLE EVIDENCE FOR A BINARY MASSIVE BLACK HOLE IN THE GALACTIC NUCLEUS

E.J.A. MEURS
Dunsink Observatory
Castleknock, Dublin 15, Ireland

Abstract. The Galactic Centre candidate Sgr A* may exhibit a 40 km/s radial velocity component, which is not observed for OH/IR stars around the centre. This could be interpreted as orbital motion of one member of a binary massive black hole. In other galaxies such pairs may be inferred from radio jet precession and emission line profiles.

1. The Galactic Centre

The intricate radio source Sgr A West is commonly considered as the centre of our Galaxy (e.g. Genzel 1987). Within this region, the unique, strong radio source Sgr A* is the main candidate for a central black hole (cf. Lo 1987). Mass estimates for such an object have been derived from the overall emission properties of Sgr A* (for example, Melia et al. 1992, Ozernoy 1995) and from the inferred mass distribution in the Galactic Nucleus (for example, Townes 1995). The available mass determinations appear to separate between either $\sim 10^6 \mathcal{M}_\odot$ or $\sim 10^2 \mathcal{M}_\odot$.

2. Binary Black Holes in the nuclei of galaxies

Theoretical modelling of galaxy mergers suggests that pairs of massive black holes may dwell in the centremost region of galaxies, as a result of past mergers. Their masses probably depend on the previous history of the core in each of the merging galaxies. Normally they would stay at a distance of a few parsec apart, until a next merger takes place. Then the separation of the two black holes may decrease, followed by coalescence, after which a

L. Blitz and P. Teuben (eds.), Unsolved Problems of the Milky Way, 285–286.
© 1996 *International Astronomical Union.*

new pair of black holes is established with the incoming galactic nucleus. This scenario is described more in detail by Roos (1988).

The close location of two such black holes renders it difficult to recognize the binarity when other galaxies are concerned. VLBI might detect this if both black holes would emit radio radiation. Otherwise, more indirect methods will stand a better chance. One example of this is the temporal variability pattern of suitable optical emission lines (Halpern & Filippenko 1988). An appropriate indication for binary compact objects is also the precessional behaviour of radio jets (e.g. Rees 1984). How the dynamical evolution of a binary massive black hole may be reflected in a changing precession period is elaborated by Roos (1988) and Roos et al. (1993).

3. Possible evidence for binarity in the Galactic Centre

Of course, the centre of our Galaxy offers the best spatial scale to search for binary compact objects. An intriguing observation exists (see Clube 1986) of the radial velocities of two H_2 emission regions straddling the Galactic Centre (a likely torus shaped geometry). The observed radial velocity asymmetry between these two peaks implies a radial velocity component of 40 km/s with respect to the sun. Yet, no such difference is noticeable from the distribution of radial velocities of OH/IR stars around the Galactic Centre (measured from radio maser lines). These objects show evidence of rotation around the Centre, but have essentially no offset in radial velocity (Habing 1995). An alternative interpretation of the H_2 radial velocity asymmetry would be that the observed difference originates from the orbital motion of one member of a binary massive black hole. The apparent dichotomy in the mass estimates for a central compact object (see Section 1) could find a natural explanation in this way.

References

Clube, S.V.M. (1986) *The Observatory*, 106, 166
Genzel, R. (1987) in *The Galaxy*, Eds R. Carswell and G. Gilmore, *NATO ASI Series*, p. 51
Habing, H. (1995) this volume
Halpern, J.P., Filippenko, A.V. (1988) *Nature*,, 331, 46
Melia, F., Jokipii, J.R., Narayanan, A. (1992) *ApJ*, 395, L87
Lo, K.Y. (1987) in *The Galactic Centre*, Ed. D.C. Backer, *AIP Conf. Proc.*, 155, 30
Ozernoy, L. (1995) this volume
Rees, M.J. (1984) *AnnRevAA*, 22, 123
Roos, N. (1988) *ApJ*, 334, 95
Roos, N., Kaastra, J.S., Hummel, C.A. (1993), *ApJ*, 409, 130
Townes, C.H. (1995) this volume

Chapter 4

Is there a Consistent Picture of the Inner kpc of the Milky Way?

THE HOT GAS IN THE GALACTIC BULGE

- Diffuse X-rays with complex K-shell transition lines from the Bulge -

K. KOYAMA AND Y. MAEDA
Department of Physics, Kyoto University, Sakyo-ku, Kyoto, 606-01 Japan

Abstract. X-ray imaging spectroscopic observations near the Galactic center region were carried out with the ASCA satellite. We found two bright spots very close to the Galactic center (Sgr A*); one is extended and has a soft spectrum associated with strong emission lines from highly ionized irons, while the other is a point-like object with a harder spectrum and a larger absorption. We also found extended emission with K-shell transition lines from highly ionized Si, S, Ar, Ca and Fe. Remarkable feature found with ASCA is an extended emission of 6.4 keV lines of low ionization irons. The 6.4 keV line fluxes are found to be well correlated to the region of cool clouds. We interpret that the 6.4 keV line is due to florescence from the cool clouds irradiated by strong (and obscured from our line of sight) X-ray beams.

1. Introduction

With the Ginga satellite, we found 6.7 keV lines from a highly ionized iron near the Galactic center. This indicates that the Galactic center region is surrounded by a thin hot plasma with a tilting elliptical distribution. The plasma temperature is determined to be about 10 keV, with the total luminosity in the 6.7 keV line and 2-10 keV bands to be 1×10^{36}, and 2×10^{37} erg s^{-1} , respectively. With a simple assumption that the plasma density is uniform, we can estimate that the energy of the plasma is as large as 10^4 SN and the dynamical age is 10^{4-5} yr (Koyama et al. 1989, Yamauchi et al., 1990). Due to a limited spatial and energy resolution of Ginga, we cannot study further detail of the Galactic center plasma. Using the ASCA satellite, we have obtained new pictures near the Galactic center. We will review the early ASCA results. Brief descriptions of the ASCA satellite and onboard instruments are found in Tanaka et al. (1994).

L. Blitz and P. Teuben (eds.), Unsolved Problems of the Milky Way, 287–295.
© 1996 *International Astronomical Union.*

2. Results

2.1. SGR A* AND HARD SOURCE NEAR THE GALACTIC CENTER

Figure 1 shows an X-ray mosaic picture near the Galactic center region of about 1°×1° in the 0.7-10 keV band obtained with the GIS instrument. Although no correction of non-uniform efficiency over the detector field was made on the mosaic picture, we see several bright spots as well as an extended emission. The three brightest spots correspond to the point-like objects, which are already catalogued with the Einstein and Ariel 5 satellites (Watson et al. 1981). Another bright source at the center of the map corresponds to the Galactic center (Sgr A*). In addition to these point like sources, we found a diffuse emission extending very largely. The peak flux of the extended emission comes near Sgr A*.

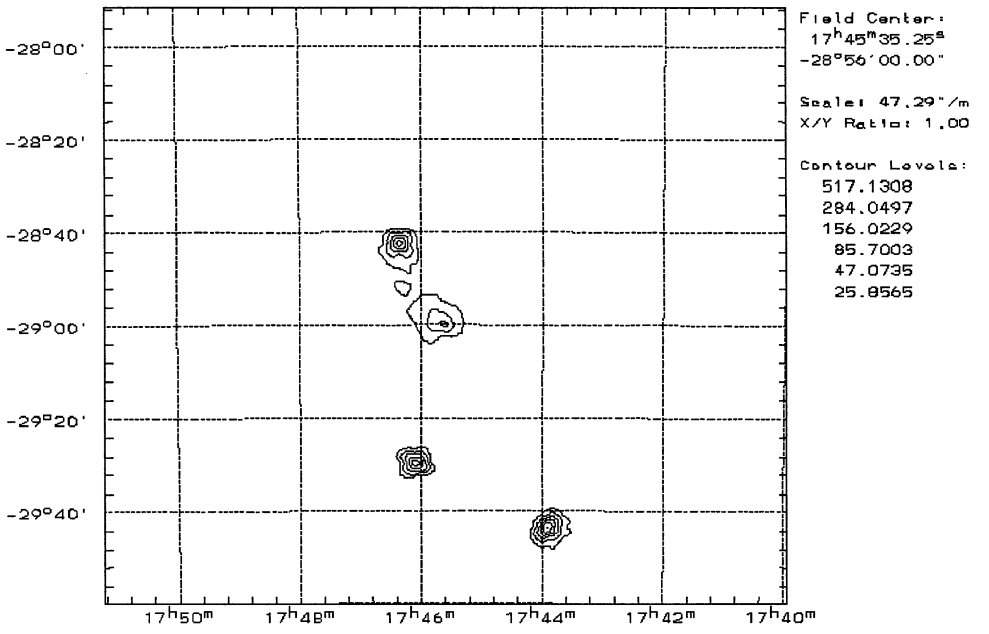

Figure 1. GIS image (1° × 1°)

Fig. 1. The mosaic picture in the 0.7 - 10 keV band with GIS2 & GIS3. The background is not substracted. The image is smoothed with σ=4pixel (1 pixel ~ 15") with the angular resolution of about ~ 1'. Four bright peaks are respectively (in the order from north to south) 1E1743.1-2843, SgrA, A1742-294, and 1E1740.7-2942. $(RA,Dec)_{2000}$

In figure 2, we show a zoomed-up SIS picture near Sgr A* with the energy band of 3-10 keV. One bright part (north east) is elliptically extended, in which our Galactic center Sgr A* lies. Since this emission region seems extended, we refer to be the Center plasma. The other bright spot (south west) is point-like. This source is clear only in the hard X-ray band, hence is referred to be the Hard source in this paper.

The X-ray spectrum from the Center plasma exhibits many emission lines. This indicates that the X-rays come from a high temperature thin hot plasma. On the other hand, the line fluxes of the Hard source are about 3 times smaller than that of the Center plasma. These lines would be due to the diffuse X-rays in which the Hard source is also embedded. If we assume that the X-ray spectrum of the Hard X-ray source is composed of two components; one is the similar shape as the Center plasma and the other is a power-law spectrum with no line emission, we found that the power-law component should be highly absorbed with N_H value of $\sim 2 \times 10^{23}$ H cm^{-2}. Therefore, the Hard source would be behind a gas of high column. Unabsorbed X-ray luminosity in the 2 - 10 keV band is estimated to be about 4×10^{35} erg s^{-1}. Recently the Hard source emitted a type 1 X-ray burst (Maeda et al. private communication) and therefore is classified to be a neutron star binary. From the positional conicidence, we suggest the Hard source to be in a quiescent state of the transient source A1742-289 (Eyles et al. 1975).

Figure 2 & 3
SIS image (20' × 20')

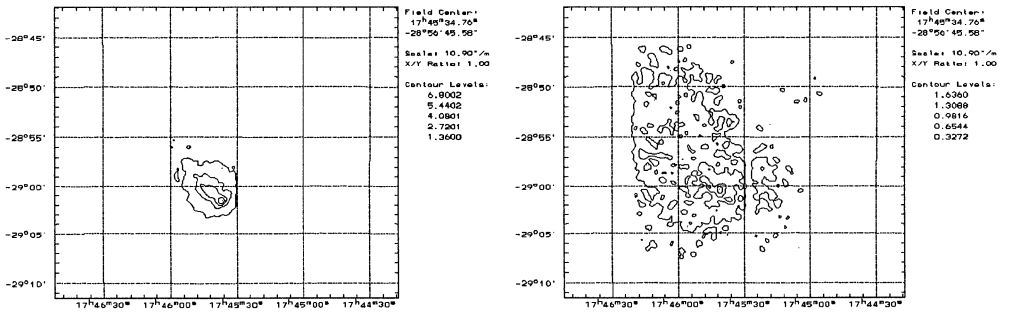

Fig. 2. : SIS0 image near SgrA* in the hard band (3-10 keV). A bright elliptical shape region is associated with SgrA-West. $(RA,Dec)_{2000}$
Fig. 3. : SIS0 image near SgrA* in the soft band (0.7-3 keV). $(RA,Dec)_{2000}$

2.2. SPECTRUM OF DIFFUSE HOT PLASMA

If we make the X-ray image with a lower energy band, we can see clear diffuse emission as is given in figure 3 (0.7-3 keV). This diffuse emission is extended to nearly 1-2 degree, consistent with the Ginga results. Therefore we refer to this as the Bulge plasma. We have made a spectrum using all the data of the Bulge plasma and compared it to the Center plasma. A remarkable difference was found only in the Fe line feature as is shown in figure 4.

Figure4
Bulge plasma spectrum

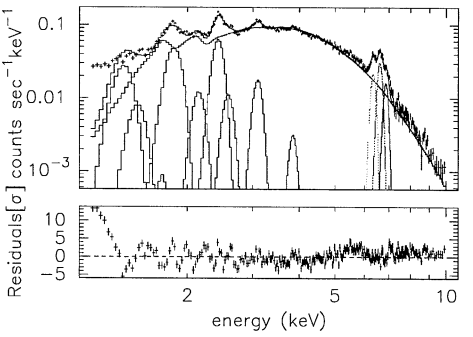

Table 1

Line Energy	Identification
(1.35 keV)	He-like Mg Kα
(1.47 keV)	H-like Mg Kα
1.86 keV	He-like Si Kα
(2.00 keV)	H-like Si Kα
(2.18 keV)	He-like Si Kβ
2.45 keV	He-like S Kα
(2.63 keV)	H-like S Kα
(2.93 keV)	He-like S Kβ
3.14 keV	He-like Ar Kα
3.90 keV	He-like Ca Kα
6.40 keV	Neutral Fe Kα
6.70 keV	He-like Fe Kα
6.95 keV	H-like Fe Kα

Fig. 4: The SIS0 & SIS1 spectrum of the Bulge region. Emission lines are He-like Si, S, Ar, Ca and Fe Kα and H-like Fe Kα line and cold Fe Kα line (see Table 1). $(RA,Dec)_{2000}$

In table 1, we listed emission lines found from the Bulge plasma. We have never seen so many lines from any object of X-ray astronomy except for the very young SNRs such as Cas A and Tycho. All these lines other than the 6.4 keV line are attributable to the K-shell transitions from H-like or He-like Si, S, Ar, Ca and Fe. The co-existing of these lines from wide range of atomic numbers indicates that the plasma is multi-temperature. For example, K-shell resonance lines from He-like Si are most prominent

at 0.8 keV temperature while those from H-like iron become dominant at a temperature of about 15 keV.

Another possibility is non equilibrium ionization (NEI) plasma as is often found in the young supernova remnants. We tried NEI model fits to the Bulge plasma excluding 6.4 keV line and found reasonable fits with roughly solar abundance (except for Si). The best fit temperature (kT) and ionization parameter nt (n is the electron density and t is the elapsing time after the plasma was heated up to the temperature kT) are estimated to be about 5-10 keV and 10^{10} cm^{-2} s, respectively. This indicates that the plasma is very young.

2.3. SPATIAL DISTRIBUTION OF HOT PLASMA

Fig 5 shows narrow band energy maps including important emission lines: He-like S, Fe and 6.4 keV iron. Since the first two of these lines come mainly from a thin hot plasma, these images show a spatial distribution of the thin hot plasma. The shape of the 6.7 keV line emitting region is elliptical, while that of S has more complicated structure. The complicated structure may be due absorption, because the energy of this line comes critical values of the low energy-cut by a typical Galactic absorption of 10^{23} H cm^{-2}. We tried to compare the ^{12}CO map with two different velocity taken by Hasegawa et al.(private communication) at Nobeyama 45m radio telescope and found an indication that expanding molecular clouds are in front at negative latitude and in behind at positive latitude.

2.4. SCATTERING X-RAYS - POSSIBILITY OF OBSCURED LUMINOUS X-RAY SOURCE-

Molecular clouds also play another important role to the X-ray emission from the Galactic Bulge. A new (and important) discovery with ASCA is a strong 6.4 keV line from the Bulge region. This line is due to neutral or low ionization states of iron. Therefore we need cool gas and high energy source to excite the K-shell electron of the cool iron. The source of the cool iron would be molecular clouds. In fact, we see good spatial correlation of the molecular cloud and the 6.4 keV line distribution. Since the Sgr B2 cloud is near the edge of the Bulge plasma which emits the 6.7 keV line, contribution of the hot plasma may be relatively small and therefore suitable for the study of the origin of the 6.4 keV line. Fig 6 is the spectrum of the Sgr B2 region. A strong 6.4 keV line emission is found with an equivalent width (EW) of about 2 keV. This large EW of the 6.4 keV line can resonably be predicted by the scattering X-rays model (see also Mrkevitch, M. et al. 1993). Suppose that the X-ray spectrum of Sgr B2 is due to the scattering, optical depth of the scattering material is estimated

to be 0.1 using the radio data. The absorption corrected luminosity in the $10' \times 10'$ region is 5×10^{35} erg s^{-1} (at 8.5 kpc distance). Then we can estimate the contribution of the nearby bright sources to the Sgr B2 emission to be only a few percent. Larger contribution is due to the thin thermal Bulge emission. The estimated value depends on the shape of the Bulge plasma. Our best estimate for the contribution of the Bulge emission to Sgr B2 does not exceed about 10 % of the observed flux. Thus we need unseen bright X-ray source. If we put the source at the Galactic center, the X-ray luminosity of the source is estimated to be larger than 10^{39} erg s^{-1}. This exceeds the luminosity of Eddington limit of any Galactic binary sources. Thus our suggestion is that the Galactic center would be either a low luminosity Seyfert 2 (obscured AGN) or an AGN which was bright in near past but quiescent at present.

Acknowledgements

We thank the ASCA team for the support of this fantastic observation. We owed much to Mr. Sonobe and Prof. Tanaka for the data reduction and discussion.

References

Eyles, C.J., Skinner, G.K., Willmore, A.P., and Rosenverg, F.D. 1975, Nature, 257, 291.
Koyama, K., Awaki, H., Kunieda, H., Takano, S., Tawara, Y., Yamauchi, S., Hatsukade, I. and Nagase, F. 1989, Nature, 339, 603.
Mrkevitch, M., Sunyaev R.A. and Pavlinsky, M. 1993, Nature 364, 40.
Tanaka, Y., Inoue, H. and Holt, S.S. 1994, PASJ, 46, L49.
Watson, M.G., Willingale, R., Grindlay, J.E., and Hertz, P. 1987, ApJ, 250, 142.
Yamauchi, S., Kawada, M., Koyama. K., Kunieda, H., Tawara, Y. and Hatsukade, I. 1990, ApJ, 365, 532.

DISCUSSION

J. Binney: Prof. Sunyaev has argued, I believe, that all the diffuse radiation is scattered and that there is no diffuse hot plasma. What is the strongest argument against this point of view, or is it one or sympathetic too.

Koyama: Since we definitely found many emission lines from highly ionized atoms and the overall spectrum can be fitted with NEI model with reasonable abundance, we are quite sure that the most of the diffuse emission is thin hot plasma. Of course some part of the X-Ray emission such as the 6.4 keV line is due to scattering.

M. Morris: Do the ASCA data give the same picture for the extended (200×300 pc) bulge X-ray source as Ginga had previously given?

Koyama: Yes, ASCA data surely indicate the similar picture of largely extended X-ray emission. In this talk, we have concentrated on the fine structure near the Galactic Center.

L. Ozernoy: An important question t! at you raised in your talk as to why the temperature of hot gas looks the same for the hot bubbles of different ages finds an answer in the starburst interpretation of the origin of the hot gas developed by Ozernoy, Ramaty and Titarchuk 1993 ("Back to the Galaxy", AIP Conf. Proc. 278, 73). The temperature of the gas passing through a shock at the adiabatic stage of the hot bubble is $T \sim 10^8$ K $(E_{SN}/10^{51}$ erg$)(M_{ej}/10M_\odot)^{-1}$ and it is kept the same as long as the parameters of a SN explosion are more or less identical. Interestingly, similar temperatures of hot gas have been observed in the near by starburst galaxies NGC253 and M82 (for details, see Ozernoy 1994 in "multi-Wave length Continuum Emission of AGN", Ed. T. J.-L. Courvoisier and A. Blecha, eds. Kluwer Acad. Publ., p. 351)

Figure 5
Nallow band images

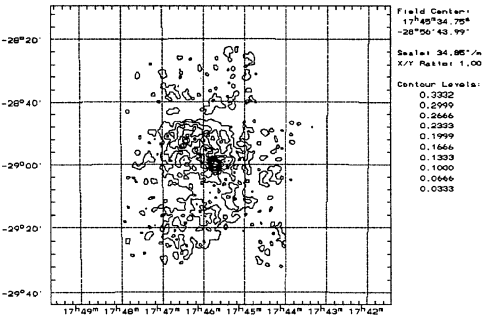

Figure 5-a
S-He like K-shell transition line
(2.46 keV)

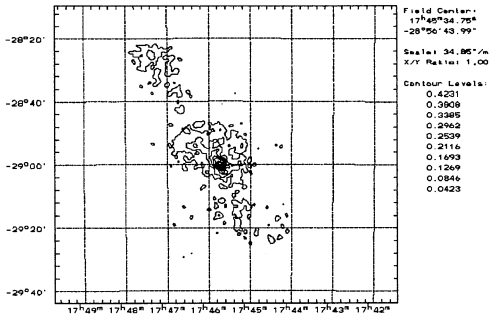

Figure 5-b
Cold Fe K-shell transition line
(6.4 keV)

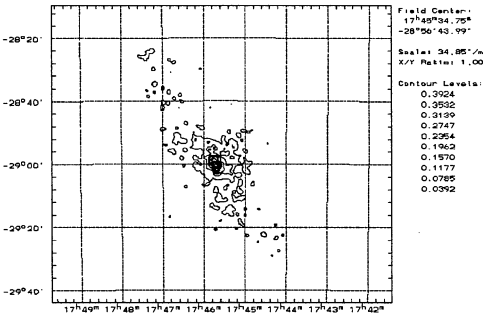

Figure 5-c
He-like Fe K-shell transition line
(6.7 keV)

Fig. 5 : X-ray images of the energy band 2.37-2.54 keV (5-a), 6.20-6.55 keV (5-b),and 6.55-6.90 keV (5-c). The bright X-ray binaries A1742-294, 1E1743.1-2843 and A1742-289(Hard source) are removed from these images. $(RA,Dec)_{2000}$

Figure 6
SgrB2 spectrum

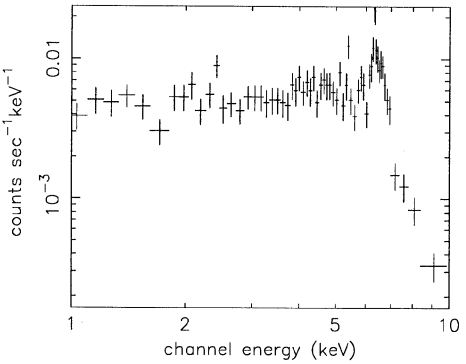

Fig. 6 : The spectrum of Sgr B2 cloud obatined with SIS0 & SIS1.

MOTIONS AND DEFORMATIONS OF THE INNER-GALAXY NEUTRAL GAS LAYER

H. S. LISZT
National Radio Astronomy Observatory
520 Edgemont Road
Charlottesville VA USA 22903

AND

W. B. BURTON
Sterrewacht, Leiden
Postbus 9513
2300 RA Leiden, Netherlands

Abstract.

Neutral gas in the inner few kpc of the Milky Way is notable for showing strong non-circular motions, large excursions from the nominal galactic plane, and an overwhelming preponderance of molecular (rather than atomic) neutral gas. Here, we discuss the coherent nature of the kpc-scale tilts seen in H I and CO emission and demonstrate the congruence of the inner-Galaxy atomic and molecular gas distributions, out more than 1 kpc in radius and 300 pc vertically from the center. We point out that features in inner-Galaxy spectra can usually not be identified with discrete, underlying material entities, but instead arise solely as the result of kinematic projection effects.

1. Introduction

In 1977, Jan Oort published a long review ('The Galactic Center'), mostly concerned with interpretation of atomic and molecular gas in the inner few kpc of the Galaxy. At that time, the first H I maps were twenty years old and molecular (OH) absorption profiles had been known for more than 10. An important result of this interpretational effort, presented in Table 1 on

L. Blitz and P. Teuben (eds.), Unsolved Problems of the Milky Way, 297–310.
© 1996 *International Astronomical Union.*

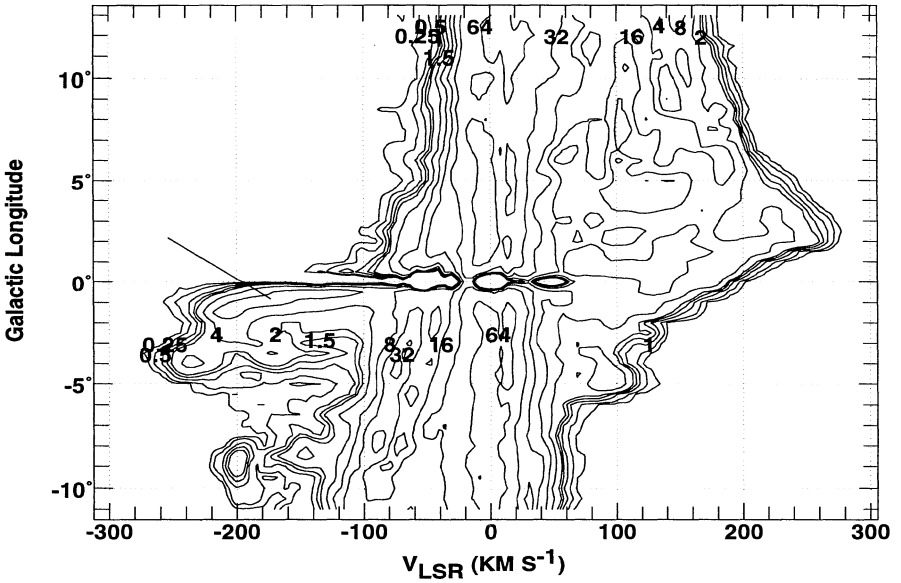

Figure 1. H I emission at b = 0° from the 21′-resolution, 0.5°-spacing survey observations of Burton and Liszt (1983). The nuclear disk of Rougoor and Oort (1960) is marked by a line.

the first page of the article, was derivation of the galactic rotation curve and mass distribution at galactocentric radii 50 pc $\leq$ R $\leq$ 1000 pc from H I data, continued inward using the $\lambda 2\mu$ intensity distribution of Becklin and Neugebauer (1968).

In Oort's summary, there are sharply-etched distinctions between H I gas seen in and out of the galactic plane and between gas seen at so-called 'permitted' and 'forbidden' velocities (*i.e.* consistent or inconsistent with direct circular motion about the center). The gas seen out of the plane was not just the expected plane-parallel stratified continuation of lower-latitude material, but was often remarked to have large (> 100 km s^{-1}) forbidden velocities directed away from the nucleus. This out-of-plane gas had a preferred axis such that it appeared in the two opposed quadrants with b $< 0°$, $l > 0°$ and b $> 0°$, $l < 0°$, and at b $< 0°$ (b $> 0°$) on the near (far) side of the center (van der Kruit 1970, Cohen and Davies 1976). The preferred explanation for this material, which in the aggregate is quite massive, was ejection from the nucleus as in classical radio galaxies. The gravitational potential of the inner galactic regions could not possibly have been as tipped as the apparent pole of the ejected gas.

In the galactic plane, a welter of features rendered generalization difficult but one feature at permitted velocities and negative longitudes was

singled out for special attention. The 'rotating nuclear disk' of Rougoor and Oort (1960), shown in Figure 1, was the source of the all-important gravitational potential in Oort's Table 1. There clearly is much gas at b = 0° which does not accord with simple rotation, for which various dynamical interpretations might be invoked (ejection, spiral arms, a bar, resonance orbits to name a few); the rotating nuclear disk is *invisible* at $l > 0°$. Nonetheless, Oort (and many others) felt that the appearance of a feature having behaviour consistent with pure rotation provided one case where a simple interpretation was both fully justified and amply rewarded.

If we associate the permitted terminal-velocity edge of the H I emission with the circular rotation speed at each projected sub-central point, which is the usual manner of derivation in the disk of the Milky Way, a peculiarly-shaped rotation curve results (Figure 2). The inner peak requires a separate, concentrated mass component or other contrivance but is easily accounted for if the potential is strongly non-circular (*i.e.* barred, see Gerhard and Vietri 1986). In fact the usual assumptions for deriving the rotation curve from the terminal velocity are *not* met in the central region and the appearance of the rotating nuclear disk feature is heavily modulated by absorption against the Sagittarius radiocontinum source complex (Burton and Liszt 1993). Roughly speaking, the difference in Figure 2 between the odd galactic rotation curve and the $R^{0.1}$ behaviour is probably ascribable to non-circular motion out to at least R = 2 kpc. The H I terminal velocity may be determined by equilibrium gravitational forces, but the motions are non-circular nonetheless.

So studies of the atomic and molecular neutral gas have provided early and continuing indications that the Galaxy is barred, as discussed at length elsewhere in this volume and dating to the earliest attempts to understand such features as the 3-kpc arm *cf.* Peters (1975). However, the makeup of the bar is uncertain (where is co-rotation? where does the bar point?) and attempts to reproduce observed velocity patterns in the Galaxy, even with barred potentials, have generally shown that success in the disk precludes agreement in the center and *vice-versa* (see Mulder and Liem 1986 and Burton and Liszt 1993).

The present discussion concerns some of the clearest and yet most puzzling aspects of the inner-Galaxy neutral gas distribution. The distribution is strongly inclined with respect to the galactic plane, so that the tilts seen earlier and ascribed to the ejected H I are a general feature of all the gas, both atomic and molecular, over the entire central region. The inner-Galaxy is filled with both H I and CO, but the distribution is *extraordinarily* molecular in nature, with the CO and H I emission patterns coinciding in space, velocity, and *intensity* over the inner 20° of longitude: less than 1% of the gas is atomic.

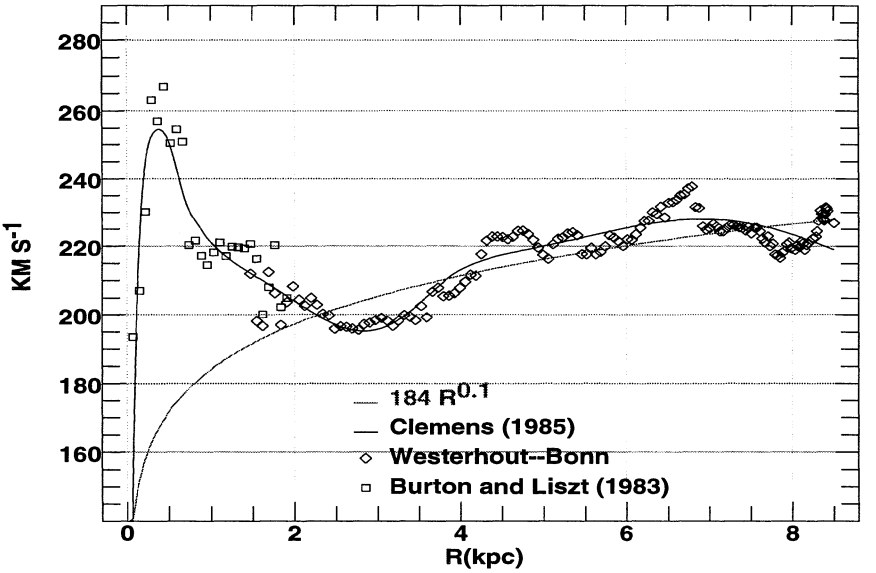

Figure 2. The Galactic rotation curve of Clemens (1985), superposed on H I terminal velocities as noted. The gray curve represents the circular velocity corresponding to a galactic density distribution which varies as $R^{-1.8}$ (see Burton and Liszt 1993).

In Section 2 of this work, we show how the tilt of the forbidden-velocity ejected H I gas came to be seen as a general property of inner-Galaxy gas, how recognition of this tilt leads to the introduction of non-circular motion into the kinematics of the low-latitude permitted-velocity features (including the rotating nuclear disk), and how the permitted and forbidden-velocity H I emission can be unified into a large-scale, coherent, pattern. As satisfying as this demonstration of consistency may be, it begs the question of why such an unusual distribution persists in the center.

In Section 3, we show that the large-scale CO and H I distributions are identical, with the inner-Galaxy filled by both gases out to (at least) 1 kpc from the nucleus and 300 pc from the galactic equator. We discuss the *apparent* differences between the atomic and molecular gases (see Oort's Figure 22, due to Bolton, meant to highlight these differences) and the origin of a chimerical feature known as the 'expanding molecular ring'.

2. The Tilted Inner-Galaxy H I layer

Oort's discussion included Figure 15 due to Kerr (1968) which was recreated later to great effect by Burton and Liszt (1978), Sinha (1978), and Liszt and Burton (1980). If we follow the terminal-velocity H I ridge–the gas from

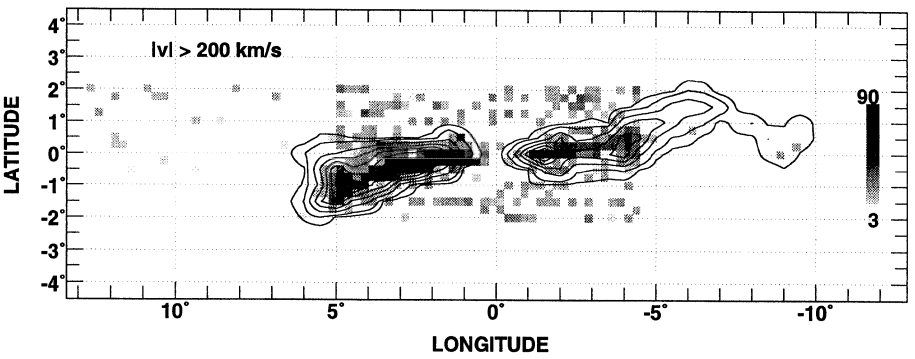

Figure 3. Contours of integrated, permitted-velocity H I emission seen at $|v| > 200$ km s^{-1} (levels are 20, 40, 80 ... K km s^{-1}), with a superposed gray-scale of the analogous CO emission from the survey of Bitran (1986).

which the circular velocity was supposedly derivable–something like our Figure 3 results. But Figure 3 shows precisely the out-of-plane behaviour and orientation ascribed to the isolated and supposed ejected H I features, with several immediate implications. The low-latitude permitted-velocity gas is neither purely rotating nor aligned with the larger galactic disk; the high-latitude forbidden velocity gas has more in common with the 'normal' emission than can be accomodated by the ejection hypothesis.

The disposition of the H I is shown in Figure 4 as a series of latitude-velocity cuts across the H I survey of Burton and Liszt (1983). For a galactocentric distance of 8.5 kpc, 1° corresponds to 150 pc, so that the outermost of these diagrams, at $|l| = 7°$, come no closer than 1 kpc to the nucleus. In the oral presentation it was easier to 'walk' the audience across several aspects of the distribution. Here only a self-guided tour can be suggested.

2.1. THE SELF-GUIDED TOUR OF FIGURE 4

To begin, follow the permitted terminal-velocity ridge from $l = 7°$, b = -1°, v = 160 km s^{-1} inward toward $l = 0°$, noting two things: the velocity increases toward the center, at least into $l = 3°$, while the mean latitude moves closer to 0°. At $l = 0°$, pretend that the gas is purely rotating and cross over to $l = -1°$, v = -200 km s^{-1}. Continue to follow the outer negative-velocity gas as it moves out in velocity and up in latitude to $l = -7°$, b = 1°. The gas is noticeably weaker at $l < 0°$. The slope indicated by this behaviour is perhaps 1/7, for a tilt of 8°, but see below; the tilt cannot be derived with recourse to the permitted velocity gas alone.

Next, proceed as before to follow the positive-velocity gas inward and upward from $l = 7°$, but do not cross over to negative velocity at the

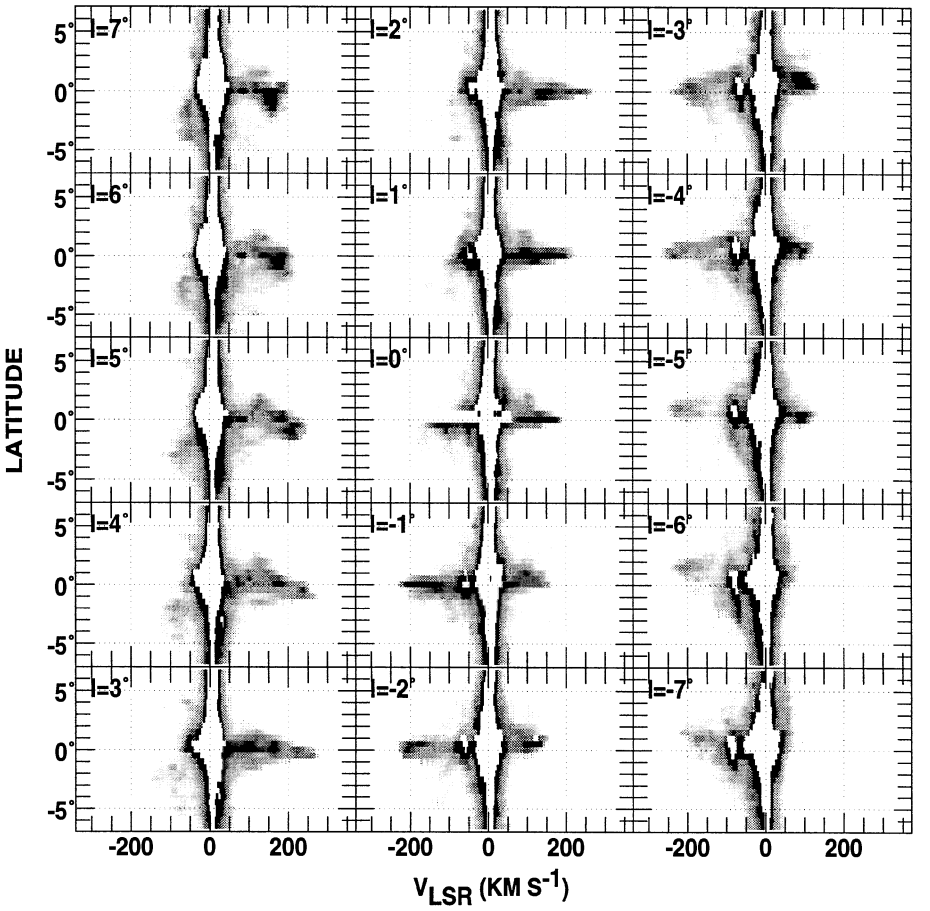

Figure 4. Latitude-velocity diagrams of H I emission at l = 7°,6°... -7°. Antenna temperatures above 20 K have been blanked. Note the unusual distribution of the 3 kpc arm gas, although this lies outside the region of interest here. See Section 2.1 of the text for a description of the other behaviour shown here.

galactic divide (l = 0°); follow the outermost positive-velocity contours at each longitude. See how this gas is continuous across l = 0°, in both velocity (see Figure 1) and space, moving gradually upward in latitude at more negative longitudes. Although difficult to see in the Figure, the forbidden-velocity gas at l = −3° extends up to b = 3.5° in a feature once known as J2 (Jodrell 2). J2 appeared in Oort's (1977) Figure 13 demonstrating the tilted pole of the H I ejection, along with Feature VII which is the stronger

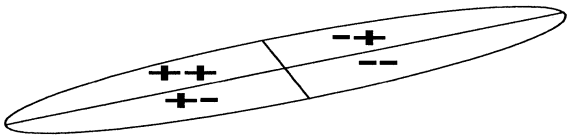

Figure 5. Schematic projection of circular and non-circular motions in an inclined disk. The left-hand and right-hand signs in each quadrant describe the sense of projection of rotation and outward-directed non-circular motion, respectively. Velocities inconsistent in sign with rotation (the so-called 'forbidden velocities') can only occur where the signs are opposite, and so appear to be more highly inclined with respect to the horizontal.

forbidden-velocity ridge at $l = -3°$, b = 1°, v = 100 km s^{-1}. If the reader *can* see J2 in Figure 4, it is apparent that it is the positive-velocity tip of a finger of H I emission extending continuously (at $l = -3°$) to b = 0.5°, v = -200 km s^{-1}. This behaviour is shown in more detail in Figure 8.

2.2. THE TILT

The demonstration by Burton and Liszt (1978) that high-latitude 'ejected' H I features had nearby, permitted-velocity extensions/counterparts played a large role in showing that they could be understood in terms of a coherent geometrical and kinematic pattern valid across the entire center region. The ejection hypothesis fell into disuse once this was noted, and it is no longer the case, as was once common, that individual forbidden-velocity H I features are invested with much importance. In Section 2.1, our purpose was to show that the same continuities apply as well to lower-latitude material which is often seen as the strong permitted-velocity gas. But a tilt clearly applies to *all* the gas and it is not a subtle effect; it is pronounced and very consistent across the region.

If the tilt angle is estimated from the permitted-velocity terminal velocity gas alone, the slope is 1/7; Oort (1977) cited a communication from R. Davies estimating a tilt of 6°. However, the forbidden velocity material is more strongly tilted (Cohen and Davies 1976) and a complete explanation melding the two will necessarily have a larger tilt than 6°. There is a simple geometrical explanation for this. As is well known from extragalactic studies, the circular component of the perceived velocity changes sign across the apparent minor axis of the gas and is of one sign on either side. Any non-circular component of the motion changes sign across the apparent major axis, however, so that the kinematics are split into four distinct quadrants. In two of these, appearing on opposite sides of both the minor and major axes, the circular and non-circular components have the same sign and

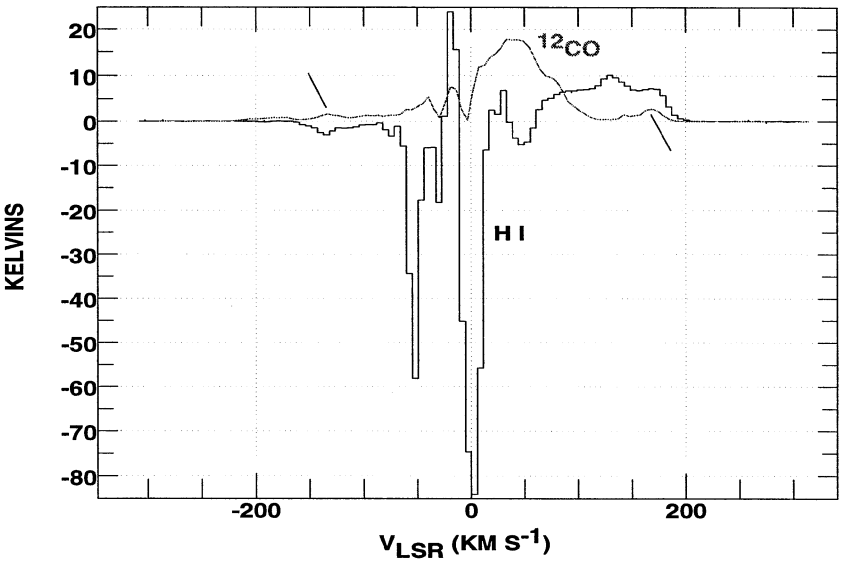

Figure 6. H I and CO spectra observed toward Sgr A* with 21′ and 1′ resolution, respectively. The so-called expanding molecular ring emission is marked by lines in the CO spectrum.

permitted velocities are augmented. In the other two, the components have opposite signs and forbidden velocities may appear. The situation relevant to the Milky Way is shown in Figure 5. For the case of apparent outward non-circular motion (the old ejection idea), the net result is that forbidden velocities appear to be more highly tilted while permitted velocities appear closer to the galactic plane (albeit with larger |v|). The kinematic models made by Burton and Liszt (1978) and Liszt and Burton (1980) typically needed total tilts of 20° to mimic the observations.

3. Congruence of the Large-Scale Atomic and Molecular Gas Distributions

Another distinction sharply drawn in Oort (1977), and one which continues to exert a strong hold on the popular imagination, concerned profound differences in the distributions of the atomic and molecular gases. Emission-line mapping of CO, which was very new in 1977, could probe the inner parts of the gas distribution with exquisitely high 1′ (2.5pc) resolution, or some 2–3 orders of magnitude smaller beam area than was used for H I . CO also was free of the absorption which bedeviled H I in the inner degree of longitude. Spectra of H I and CO taken toward Sgr A are presented in

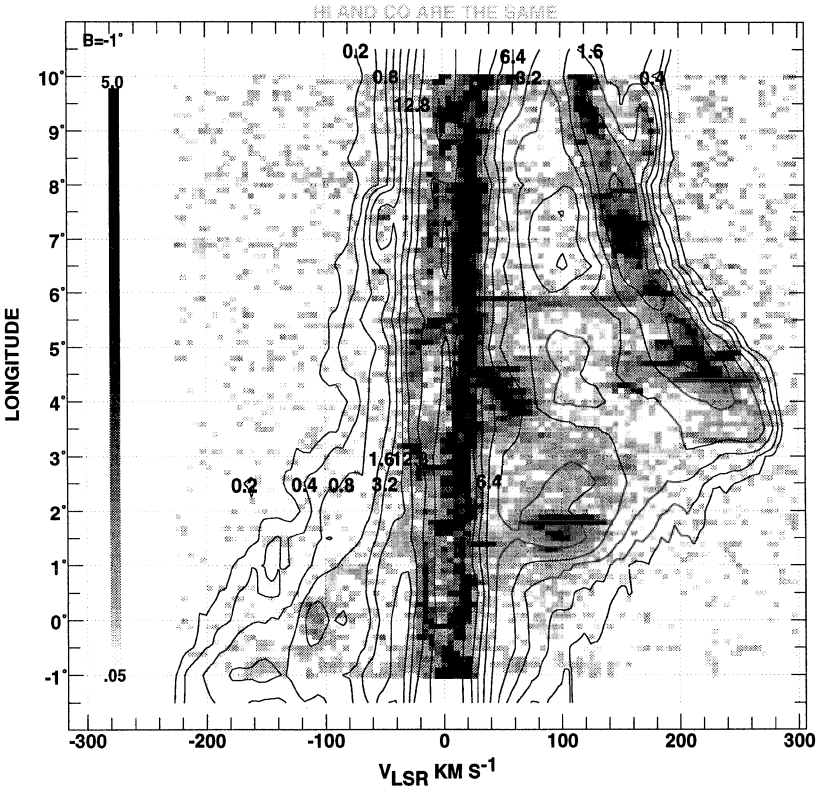

Figure 7. Contours of H I emission at b = -1°, with superposed CO emission gray-scale. The 1′ resolution CO spectra are spaced by 6′.

Figure 6; are they similar or dissimilar?

But the differences were seemingly more basic than mere questions of resolution, or the presence or absence of absorption, because crucial features of the H I distribution–the nuclear disk!–were just not dominant in any molecular species. Conversely, some important molecular features (the so-called 'expanding molecular ring') had been previously ignored in H I (although they are certainly present; see Figure 6 here). Oort's Figure 22, due to Bolton, Gardner, McGee, and Robinson (1964) compared H I and OH absorption. The former showed strong features only at -53 and 0 km s^{-1} (as in our Figure 6), while the OH was strongest at -135 km s^{-1} and 50 km s^{-1} (which are weak in H I). Strikingly, the OH absorption profile extended to significantly more negative and positive velocities.

3.1. LARGE-SCALE CONGRUENCE OF H I AND CO EMISSION

In Figure 3 we showed contours of the highest permitted-velocity H I to illustrate the pervasive nature of the tilt. Overlaid on those contours is a gray-scale representation of the large-scale CO J=1-0 distribution from the work of Bitran (1986); some of the most extreme negative longitude and velocity emission was not covered in the CO. Perhaps surprisingly, given the prevailing view that CO and H I are so different, the CO fills the H I contours out even to $l = 5°$, b = -1°. The peak integrated intensity of the CO is about 100 K km s^{-1}, while that of the H I is twice greater. But this can be compared with observations of the galactic disk, in which the integrated H I intensity is typically more than an order of magnitude greater (Burton and Gordon 1978).

This congruence of the large-scale CO and H I distributions is illustrated further in Figure 7. There, we compare H I with CO data taken with a 1′ beam spaced every 6′ over a large swath of the inner Galaxy at b = -1°. The strong positive-velocity, positive-longitude ridge with $dv/dl < 0$, mimicking the peculiar shape of the rotation curve in Figure 2, has been called the H I 'connecting arm' between the galactic center and disk.

The H I features in Figure 7 are galactic in scale, extended over several degrees. Their appearance in CO, observed with a 400 times smaller beam (continuously and in detail) implies that the inner few kpc of the Milky Way are filled with molecular material. There is another striking aspect of this congruence, namely the similarity of the CO and H I *brightnesses* in the inner-Galaxy material; the 2–3 K CO signals appear nested within H I contours of similar value. This could be an accident, but a more straightforward explanation is that the H I emission originates in an atomic residue within a molecular gas, and that the H I is fairly cold.

If 1 K km s^{-1} of integrated H I intensity represents 1.8×10^{18} H-nuclei cm^{-2}, while the same conversion for ^{12}CO is $2 - 3 \times 10^{20}$ H_2 cm^{-2}, less than 1% of the gas is atomic. Viewed another way, there is about as much molecular material represented in the 1′ CO beam as atomic material within the 21′ H I beam. The molecular distribution can easily be followed several hundred pc from the nominal galactic plane in Figure 8, where CO and H I are again overlapped in a latitude-velocity cut at $l = -3°$ (compare with the panel in Figure 4). The J2 feature discussed previously is easily seen above b = 2.5° but the CO observations do not extend this far. However, the old H I feature VII at v = 100 km s^{-1}, mentioned above, is also well populated with forbidden-velocity molecular emission.

If the high mass of anomalous H I features was problematical for the ejection hypothesis two decades ago (Oort 1977), it pales in comparison with their presence in CO. Figure 8 is perhaps the first time that the presence

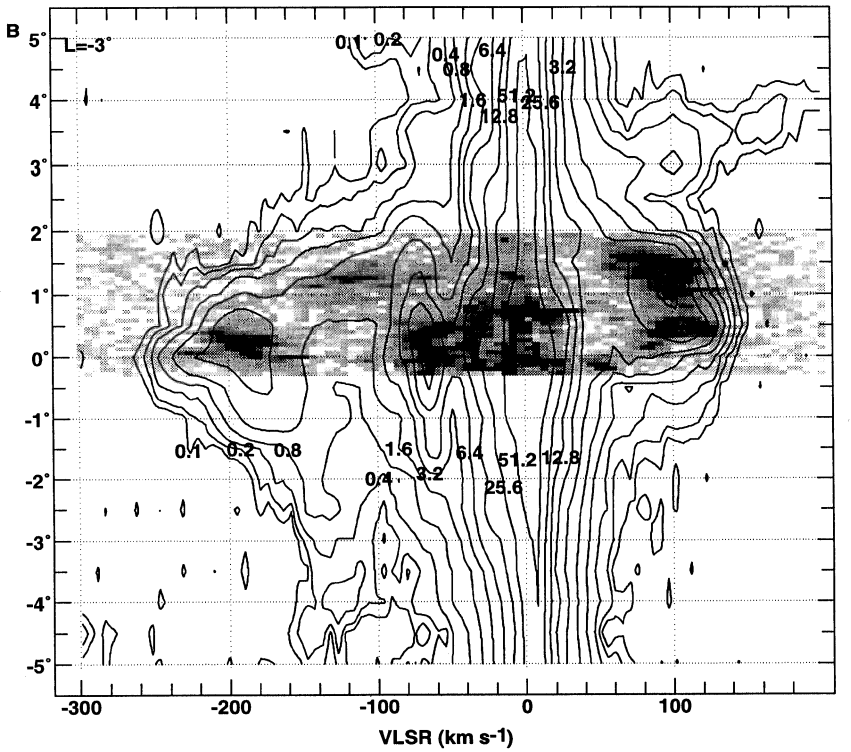

Figure 8. Contours of H I emission at l = -3°, with superposed CO emission gray-scale. The feature at v $\geq$ 100 km s^{-1}, b $\geq$ 2.5° is known as J2 (Jodrell 2); CO was not observed there. The emission just below J2 was another example of H I ejecta, feature VII. VII is clearly full of CO which, due to the inner-Galaxy tilt, is carried well above the local 0-velocity CO emission.

of molecular gas in the old H I ejecta has been explicitly noted. Note how the tilt of the inner-Galaxy CO distribution carries it above the local (0-velocity) gas in latitude (2°, corresponding to 300 pc). A derivation of the vertical thickness of the molecular material which ignored the tilt would ascribe to the gas an inordinately large scale-height.

3.2. THE EXPANDING MOLECULAR RING

Demonstration of the large-scale congruence of the atomic and molecular gas is as direct as making and overlaying the maps. How then does it occur that they have been widely supposed to be so disparate?

Part of the answer concerns the scales on which they have been observed. Large-scale surveys of CO are relatively recent and more attention (at mm-wavelengths) has been lavished on the inner few degrees of galactic

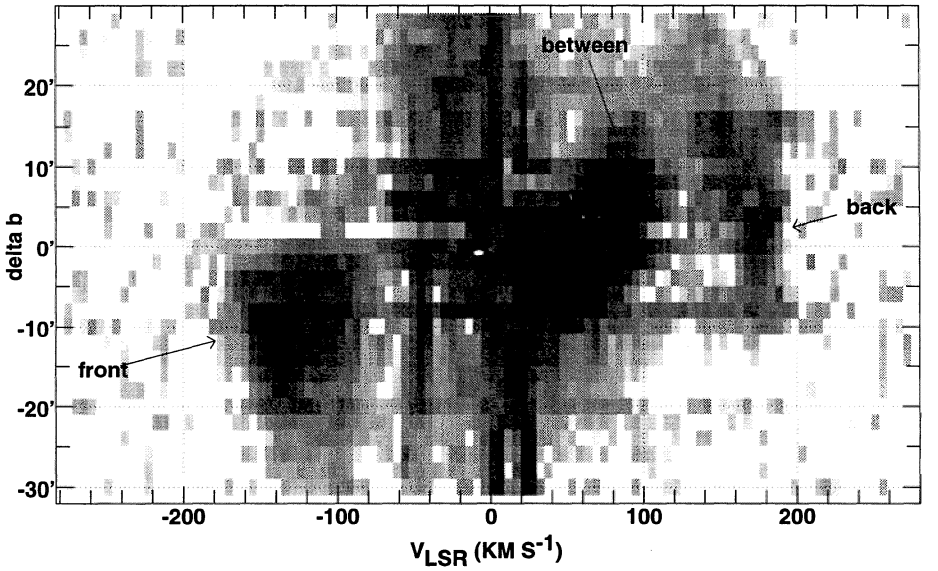

Figure 9. ^{12}CO emission in a cut across the galactic plane through Sgr A*. The vertical axis is galactic latitude measured with respect to Sgr A*. Note that the positive- and negative-velocity emission identified with the 'expanding molecular ring' has the up-down reflection symmetry originally discussed in H I.

longitude where star formation and strong molecular emission are concentrated. These inner regions are both difficult to resolve and distorted by absorption at cm-wavelengths. But even when looking at the Sagittarius source complex, it is impossible to avoid seeing features which are widely distributed. One of the most important and prominent of these is the 'expanding molecular ring'.

Although OH absorption at -135 km s^{-1} against Sgr A had been known for some time, it remained for Scoville and Solomon (1973), while studying H_2CO, to trace a convincing pattern in the gas. They posited an expanding ring of (molecular) gas with a radius of about 75′ (190 pc now), rotating at 50 km s^{-1}, with an outflow velocity of 140 km s^{-1}. Oort (1977) discussed this body in terms of the same ejective phenomena then used to characterize high-latitude H I. Because of the high molecular masses derived, and the weakness or absence of analogous behaviour in H I, this ring was supposed to be a genuinely new phenomenon prominent only in molecular material.

From absorption measurements alone the far side of the ring feature was not apparent, but an analogous band of CO emission was soon found crossing $l = 0°$ at +165 km s^{-1} by Sanders and Wrixon (1974; see Figure 6 here). Association of the two slightly asymmetric halves of the ring with each other was made by Bania (1977) and Liszt and Burton (1978): this

was not entirely straightforward because the two have an unusual symmetry introduced by the tilt of the inner-Galaxy gas (see Figure 3 of Liszt and Burton 1978). The back-side emission clearly extends out to $l = 2.2°$ near $b = 0°$.

As the CO was mapped more fully, the true nature of the 'ring' became more apparent. Its negative- and positive-velocity portions quite obviously have the front-down, back-up reflection symmetry originally supposed to apply to the tilted H I ejecta and now known to apply generally (Figure 9). It should be clear from comparison of the H I and CO spectra in Figure 6 that the expanding molecular ring gas is nothing more than the molecular expression of the H I terminal velocity, and that this gas is broadly distributed over the center region as the inescapable consequence of geometry.

The continuity and coherence of the large-scale inner-Galaxy gas distribution are plainly on display in Figure 4 (Section 2). Despite this, we may note that the positive-velocity envelope of the gas has generally been given a different name and supposed to be a different body and phenomenon at each and every latitude at which we have shown it here. In Figure 7 at $b = -1°$ it was the old H I 'connecting arm' (Section 3.1). In Figure 8 at $l = -3°$ it was VII at $b = 1°$ or J2 at $b > 2.5°$. At $b = 0°$ it is the back side of the expanding molecular ring. The appearance of each and every one of these is a simple consequence of the same tilted inner-Galaxy geometry and non-circular motion (Burton and Liszt 1978; Liszt and Burton 1980). None of is a material body having the properties originally ascribed to it in isolation from the others.

Acknowledgements

The authors are grateful to P. Thaddeus and T. Dame for providing the unpublished CO survey data of Bitran (1986)

References

Bania, T. M. 1977, *ApJ*, 216, 381
Becklin E. E., & Neugebauer, G. 1968, *ApJ*, 151, 148
Bitran, M. 1986, PhD Dissertation, U. Florida
Bolton, J. G., Gardner, F. F., McGee, R. X., & Robinson, B. J. 1964, *Nature*, 204, 30
Burton, W. B. & Gordon, M. A. 1978, *A&A*, 63, 7
Burton, W. B. & Liszt, H. S. 1978, *ApJ*, 225, 815
Burton, W. B. & Liszt, H. S. 1983, *A&A Suppl.*, 52, 63
Burton, W. B. & Liszt, H. S. 1993, *A&A*, 274, 765
Clemens, D. P. 1985, *ApJ*, 295, 422
Cohen, R. J. & Davies, R. D. 1976, *MNRAS*, 175, 1
Gerhard, O. E., & Vietri, M. 1986, *MNRAS*, 223, 337
Kerr, F. 1968, in *Radio Astronomy and the Galactic System, IAU Symp No. 31.*, ed. H. van Woerden, (Dordrecht: Reidel) 239
Liszt, H. S. & Burton, W. B. 1978, *ApJ*, 226, 790

Liszt, H. S. & Burton, W. B. 1980, *ApJ*, 236, 779
Mulder, W. A. & Liem, B. T. 1986, *A&A*, 157, 148
Oort, J. 1977, *ARAA*, 15, 295
Peters, W. L. 1975, *ApJ*, 196, 617
Rougoor, and Oort J., 1960, *Proc. Nat. Acad. Sci. USA*, 46, 1
Sanders, R. H. & Wrixon, G. T. 1974, *A&A*, 33, 9
Scoville, N. Z. & Solomon, P. M. 1973, *ApJ*, 180, 55
Sinha, R. P. 1978, in The Large-Scale Characteristics of the Galaxy, IAU Symposium No. 84, ed. W. B. Burton, (Dordrecht: Reidel) 341
van der Kruit, P. C. 1970, *A&A*, 4, 462

A SURVEY OF OH IN THE GALACTIC CENTRE REGION

P.J. BOYCE

Department of Physics and Astronomy,
University of Wales College of Cardiff
5 The Parade, PO Box 913, Cardiff CF2 3YB

AND

R. J. COHEN

University of Manchester,
Nuffield Radio Astronomy Laboratories,
Jodrell Bank, Macclesfield, Cheshire SK11 9DL

1. Introduction

The galactic centre contains the largest concentration of molecular clouds in the Galaxy. The clouds in the central region are unusual in having large linewidths and masses, and large non-circular motions. Previous surveys of their distribution in the central region have been carried out in OH (Robinson & McGee 1970; Cohen & Few 1976), H_2CO (Whiteoak & Gardner 1979; Cohen & Few 1981), CO (Bania 1977; Dame et al. 1987; Bally et al. 1987, 1988) and CS (Bally et al. 1987, 1988). The OH groundstate lines at 18cm wavelength have certain advantages for such a survey. The OH lines appear in absorption against the galactic centre continuum sources, and against the continuum emission from the disk of the Galaxy. The absorption spectra are sensitive to relatively small molecular column densities. In addition they can give information on the relative positions of the molecular gas and the radio continuum sources. This paper describes results from an absorption line survey of the galactic centre region in the OH main lines at 1667.359 MHz and 1665.402 MHz (Boyce & Cohen 1994).

L. Blitz and P. Teuben (eds.), Unsolved Problems of the Milky Way, 311–316.
© 1996 *International Astronomical Union.*

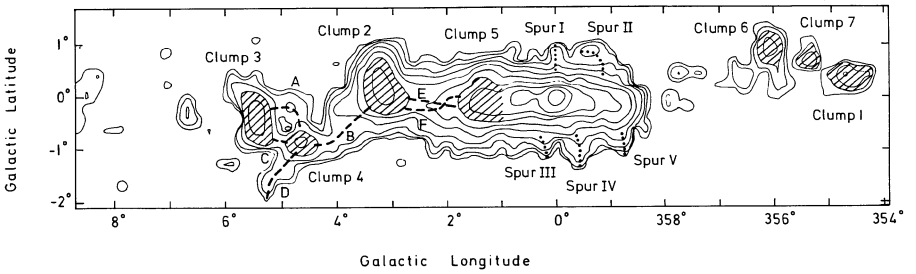

Figure 1. Map of integrated OH absorption with the positions of the broadline clumps (cross-hatched), filaments (dashed lines) and molecular spurs (solid lines) marked.

2. Observations

The survey was made using the 250ft Lovell Telescope at Jodrell Bank which has a beamwidth of 10 arcmin at 1666 MHz. Spectra were taken on a grid with 0.°2 spacing. The entire region between $354° \leq l \leq 8.°6$ and $-1.°0 \leq b \leq +1.°0$ was surveyed with extensions out to $b = -2.°0$ and $b = +1.°6$ at some longitudes. The spectra were taken using an autocorrelation spectrometer with spectral bandwidth 5 MHz, a velocity range of 900 km s^{-1} and a resolution of 3.1 km s^{-1}. The rms noise level achieved was typically 80–90 mK. The data are presented by Boyce & Cohen (1994) as a series of longitude–velocity (l–V), latitude–velocity (b–V) and longitude–latitude (l–b) contour maps of line temperature and apparent opacity.

3. Results

The results are summarized here in Figures 1 and 2. Figure 1 shows the integrated OH absorption, with some the individual features labeled. Figure 2 shows a longitude-velocity map of the OH absorption integrated over all latitudes of the survey.

The OH survey clearly reveals the full extent of the molecular gas distribution in the galactic centre region. The molecular nuclear disk can be traced over the entire region $354° < l < 6°$, corresponding to a projected diameter of ~1.8 kpc. The structure is warped, lying preferentially below the galactic plane at positive longitudes, and above the plane at negative longitudes. The warp extends to at least $\pm 1.°6$ in latitude, corresponding to z–distances of ± 240 pc. The warp is in the same sense as the warp seen on a larger scale in the HI distribution (Cohen & Davies 1976).

It is possible that the OH survey has not traced the full z–extent of the

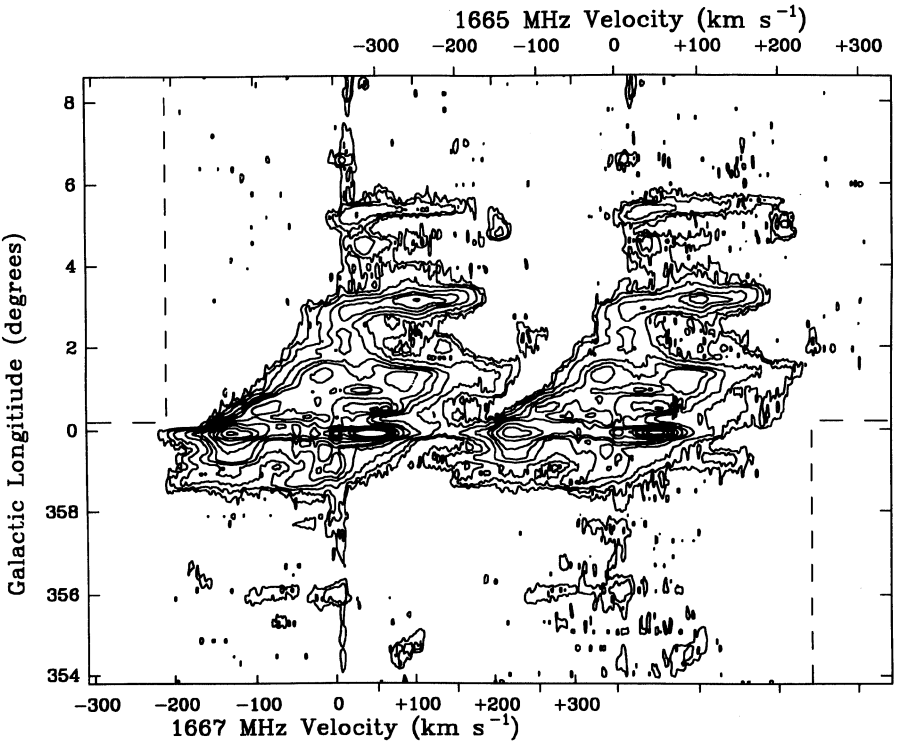

Figure 2. Longitude-velocity map of OH absorption integrated over galactic latitude. Contour levels are in units of antenna temperature and are set at –0.75, –1.5, –3, –6, –9, –12, –18, –24, –30, –36 and –42 K. The resolution is 3.1 km s^{-1} × 12′.

molecular distribution. There are a few positions where OH absorption was detected at the outermost latitudes of the grid, for example at the lower extremities of Spurs IV and V. Furthermore the detection of OH absorption relies on a continuum background. In the present survey OH absorption was detected only at positions where the radio continuum was at least 5 K of antenna temperature (corresponding to 7.5 K of brightness temperature). Therefore it is possible that molecular gas could have been present far from the galactic plane in regions of low radio continuum emission, and not have been detected in the OH survey. The CO emission line observations by Dame et al. (1987) show that there is no large concentration of molecular gas far from the plane ($|b| < 8°$), but those observations would not have been sensitive to narrow filamentary structures such as the molecular spurs

reported here.

The OH survey has revealed three new phenomena. Perhaps the most striking are the broadline clump features, of which there are at least 7. These are concentrations of molecular gas with angular sizes of typically 0.°6 and velocity extents of typically 200 km s^{-1}. The clumps have positive gradients of velocity with longitude. The clumps are easily recognized in the longitude-velocity diagram Figure 2. The clump parameters are listed in Table 1.

TABLE 1. Properties of broadline clumps

Feature	l range deg	b range deg	V range km s^{-1}	N_{OH}/T_{ex} $\times 10^{14}$ cm^{-2} K^{-1}	M_{OH} $M_\odot$
Clump 1	354.4→355.2	0.0→+0.6	+55→+120	2.6±0.7	1.0±0.1
Clump 2	2.8→3.8	−0.4→+0.8	−45→+245	16.0±2.3	21.6±2.4
Clump 3	5.2→6.0	−0.8→+0.2	−30→+210	6.7±2.3	6.0±0.7
Clump 4	4.4→4.8	−1.2→−0.4	+15→+195	6.7±2.3	2.4±0.3
Clump 5	1.0→2.0	−0.6→+0.4	−45→+220	18.4±2.3	18.4±2.1
Clump 6	355.8→356.4	+0.2→+1.2	−120→+30	3.4±1.1	2.1±0.7
Clump 7	355.4→355.6	+0.4→+0.6	+15→+95	2.4±0.9	0.30±0.05

At positive longitudes the clumps appear to be connected by filaments which have typical widths of 30 km s^{-1}, much narrower than those of the clumps. The filament parameters are listed in Table 2. Together the clumps and filaments appear to form an organized structure which accounts for most of the molecular gas at $|l|>2°$. The clumps at negative longitudes have lower apparent opacities, and it is possible that filaments connecting them would have been below our detection limit.

The third new phenomenon is the existence of molecular spurs near $l=0°$ which point out of the galactic plane and extend to latitudes of at least $\pm 1°$. The spurs all appear to be associated with radio continuum features. Spurs I and II follow the galactic centre lobe (Sofue & Handa 1984), Spur III follows the southern galactic centre lobe (Seiradakis et al. 1989), and Spurs IV and V are associated with the shell source G359.1–0.5 (Uchida et al. 1992). Figure 3 presents a comparison of the molecular spurs with the continuum features. CO observations of these spurs would be desirable to trace their full extents and to study at higher angular resolution their association with the radio continuum features.

TABLE 2. Properties of filaments

Feature	l range deg	b range deg	V range km s^{-1}	$\Delta V_{1/2}$ km s^{-1}	N_{OH}/T_{ex} cm^{-2}K^{-1}	M_{OH} $M_\odot$
Filament A	4.6→5.0	−0.4→0.0	+20→+50	30	1.5×10^{14}	0.4
Filament B	3.4→4.2	−1.0→−0.4	+40→+70	18	3.7×10^{14}	1.7
Filament C	5.0→5.4	−0.8→−0.6	+170→+220	19	1.4×10^{14}	0.3
Filament D	4.8→5.4	−1.6→−1.2	+185→+220	20	1.7×10^{14}	0.4
Filament E	1.8→3.0	−0.2→+0.4	−40→+50	35	1.2×10^{14}	9.6
Filament F	1.8→2.6	−0.4→−0.2	+115→+160	16	3.3×10^{14}	0.9

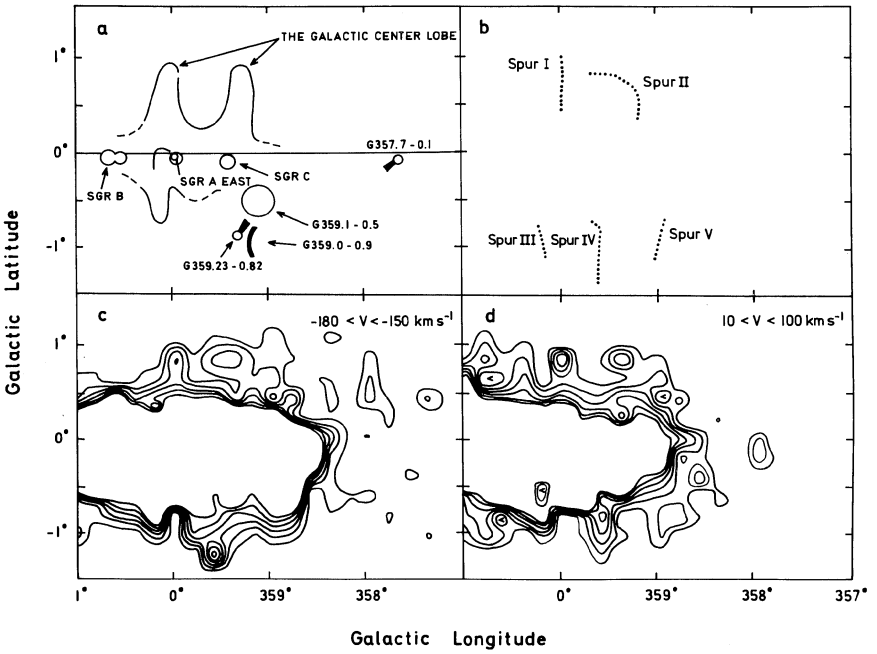

Figure 3. a) a schematic chart of continuum features close to the nucleus (from Uchida et al. 1990), b) a schematic chart of the locations of the molecular spurs, c) a map of the spurs obtained by integrating the 1667 MHz line over V=−180→−150 km s^{-1}. Contours are set at 2, 4, 6, 8, 10 and 12 K km s^{-1}, d) a map of the spurs obtained by integrating the 1667 MHz line over it V=+10→+100 km s^{-1}. Contours are set at 2, 4, 6, 8, 10 and 12 K km s^{-1}.

4. Discussion of clumps

The most difficult features to explain are the broadline clumps, which appear to be a new phenomenon confined to the galactic centre. The masses

of the clumps can be estimated in various ways to be about 10^7 $M_\odot$. They usually contain substructure, with length scales of 15 pc and velocity widths of 20 km s^{-1}. Recent measurements at Jodrell Bank reveal that the clumps also have a substantial component of neutral atomic hydrogen with a mass of typically 3 x 10^5 $M_\odot$ (Nixon 1994). The large number of these clumps, and the fact that they show positive gradients of velocity with longitude, put strong constraints on their possible origin. From an observational point of view the clumps have some similarities to the enormous concentrations of molecular gas seen in the nuclei of starburst galaxies and megamaser galaxies. However if the clumps are considered as compact entities then they would have enormous kinetic energies of expansion, typically 10^{54} ergs. On the other hand if they were to be incorporated into a bar-type model for the gas kinematics of the central region then they would translate from wide lines in l–V space to long dust lanes in the central region, all pointing exactly towards the Sun. Neither of these models seems entirely satisfactory at the present time.

References

Bally, J., Stark, A.A., Wilson, R.W., Henkel, C., 1987, ApJS 65, 13
Bally, J., Stark, A.A., Wilson, R.W., Henkel, C., 1988, ApJ 324, 223
Bania, T.M. 1977, ApJ 216, 381
Boyce, P.J., Cohen, R.J. 1994 A&AS 107, 563
Cohen, R.J., Davies, R.D. 1976, MNRAS 175, 1
Cohen, R.J., Few, R.W. 1976, MNRAS 176, 495
Cohen, R.J., Few, R.W. 1981, MNRAS 194, 711
Dame, T.M., Ungerechts, H., Cohen, R.S., et. al. 1987, ApJ 322, 706
Nixon, C.A. 1994, MSc thesis, University of Manchester
Robinson, B.J., McGee, R.X. 1970, Aust.J.Phys 23, 405
Seiradakis, J.H., Reich, W., Sofue, Y. 1989, ed. M. Morris, The Centre of our Galaxy, I.A.U. Symp. No.136 (Kluwer Academic Publishers, Dordrecht) 237
Sofue, Y., Handa, T. 1984, Nature 310, 568
Uchida, K.I., Morris, M., Bally, J., Pound, M., Yusef-Zadeh, F. 1992, ApJ 398, 128
Whiteoak, J.B., Gardener, F.F. 1979, MNRAS 188, 445

STELLAR POPULATIONS IN THE GALACTIC BULGE

H.J. HABING
Sterrewacht, Leiden

1. What we want to know, and why.

In this review I discuss stars in the bulge of our Milky Way, but I exclude stars within a few parsec from Sgr A West; they are the subject of other reviews at this Symposium. We should, however, not forget that there may be an intimate connection between the central cluster and the bulge: bulge stars may eject matter that feeds the monster at the center and eruptions by this monster may have an important effect on the bulge.

Over the last years several separate reviews and several conferences have been dedicated (at least in part) to bulges and to the bulge of our Milky Way Galaxy: see references below. It is quite a task to read all reviews on the topic! King's stimulating introduction to the Ghent symposium on galactic bulges leads us directly into what we want to know, and what we don't: "The problems of the bulge fall into four general areas: what is there, how it is distributed, how it moves and how it got that way". Phrased in a mathematical way, we want to know the distribution function $f(\mathbf{x}, \mathbf{v})$ for each astrophysical object (star, cluster, planetary nebula) defined by an age, a metallicity and a ZAMS–mass (and ideally: with a multiplicity index). Here $\mathbf{x}$ is the position vector in galactic coordinates and $\mathbf{v}$ the 3-d velocity vector. Ultimately this knowledge will give us the mass–distribution in the bulge and the formation history.

I owe to King's introduction an obvious warning, that however needs repetition: the galactic center is not only a place of its own, but also the center of other galactic components. Thus the discovery of halo objects inside the bulge may have no other meaning than that this place is the center of the halo. Are the metal–poor and the metal–rich stars near the center accidentally together or is there a relation? To answer such type of

L. Blitz and P. Teuben (eds.), Unsolved Problems of the Milky Way, 317–327.
© 1996 *International Astronomical Union.*

questions we need first a good insight in the distribution functions $f(\mathbf{x}, \mathbf{v})$ of metal–rich and metal–poor stars.

In the concluding remarks of my talk I will check the recent progress against King's four question areas. At this place allow me this side remark: if an unresolved scientific problem can be formulated in such a complete set of very general questions as given by King, we do not yet know a hell of a lot.

2. What we learned in the last few years.

2.1. COLOUR–MAGNITUDE DIAGRAMS (CMD'S).

Star counts made in one colour have been obtained by several authors, but I will not discuss them here; CMD's are more informative and I gave their discussion higher priority. Surface photometry by the Spacelab Infrared Telescope (Kent *et al.*, 1991) and especially by COBE will be discussed, I presume, elsewhere is this book.

Going from brighter to fainter stars the appearance of the CMD's is dominated successively by foreground main-sequence stars in the galactic disk, red giants in the bulge, horizontal–branch or core–helium burning stars (especially red HB stars), and main sequence stars in the bulge. Because our understanding of the red giant branch and of the HB is well advanced some conclusions can be drawn without a discussion of the faintest objects, the main sequence stars in the bulge.

One of the new, and perhaps firm conclusions is that the number of foreground disk stars is smaller by factors of order two than those predicted by the Bahcall and Soneira model. The shortage of foreground stars becomes obvious at the higher latitudes (let me say above 5° latitude) where the numbers of bulge stars have dropped strongly (Paczynski *et al.*, 1994; Ng *et al.*, 1994; Bertelli *et al.*, 1994).

2.1.1. *CMDs in wavelength bands below 1 μm.*

Colour–magnitude diagrams in the V, R, I–bands have appeared of stellar fields at different longitudes and latitudes containing large numbers (tens of thousands) of stars measured photometrically down to sometimes 21st or 22nd magnitude with accuracies of a few hundredths of a magnitude. CCD's yield the best measurements, but photographic surveys are still significant, even when they go much less deep (Ng, 1994). The CMDs are affected by incompleteness because the surveys are often confused by crowding of the stellar images at the fainter magnitudes; therefore there is a role in this game for HST (after the repair).

The diagrams contain a mix of main-sequence and evolved (FGB and HB) stars of varying distance and extinction and of different metallicities.

Often the true nature of an individual star is unknown: is it a reddened G dwarf in the galactic disk or a distant G giant in the bulge? The statistical analysis is thus more complex than those of stellar clusters, although cluster CMDs are at the heart of all analyses. The extinction has to be known as a function of distance and a galactic model is needed to describe the distribution of the stars in space. The Bahcall and Soneira model is often used but it is inadequate at low latitudes (for which it was never designed). Recently a new galactic model has been proposed by the Padua group of Chiosi (see Ng *et al.*, 1994) as part of a software package that predicts galactic field CMDs and is called "HRD–GST": "a Hertzsprung–Russell Diagram Galactic Software Telescope". The package consists of three parts: I. A library of evolutionary tracks for stars of different masses and different helium and metal abundances; II. A galactic model that defines the spatial distribution of the stars and the extinction; III. A simulator that creates CMDs from the two previous parts by a Monte Carlo process. Predicted and observed CMDs are compared by some statistical technique and the parameters of the galactic model are varied until a satisfactory fit is obtained. Application of this tool requires a good confidence in the library of evolution tracks, which has been obtained by checking the library against cluster observations. However, as the galactic center is likely to be a high–metallicity environment the lack of observed CMDs of super–metal rich clusters is a weakness. For example, strong blanketing effects e.g. in the $V-$ and $I-$ band observations of red giants are believed to exist, but have not at all been quantitatively described. Another weakness of the computed CMDs is that they do not contain multiple stars, although in reality these will be present in significant numbers.

I now summarize some recent results:

CMDs have been measured mostly in V and I of several metal–rich globular clusters in the inner Galaxy; from the same CCD frames CMDs were produced of field stars. Ortolani *et al.* (1993a and 1993b) give a summary of these field CMDs and Bertelli *et al.* (1994) discuss the results further (and revise at least one of the earlier conclusions).

Extinction plays a major role in shaping the diagrams, and not only the total amount of extinction is important, but also its distribution along the line of sight. In the end Bertelli *et al.* conclude that the two CMDs at (respectively) $l = -31°$ and $12.9°$ contain mainly disk stars, but in the field near $l = -2.4°$ one recognizes many bulge stars (red giants and clump stars). By removing the disk stars a CMD is produced for this field that contains only bulge stars. An age of 12.5 to 15 Gyr can then be assigned to the bulge stars and a star formation rate that decreased exponentially with an e-value of 2.5 Gyr. A conclusion that satisfied me greatly is the existence of a hole in the galactic stellar disk with a radius of 2.5 kpc around

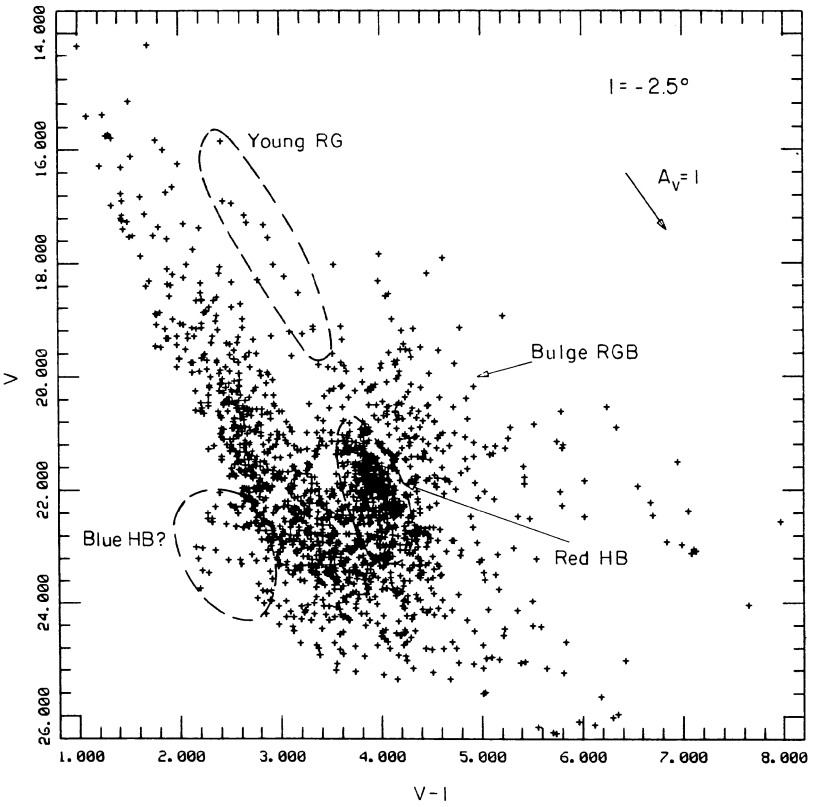

Figure 1. V versus $(V - I)$ diagram of field stars near the open cluster Terzan 1 at $l = -357.5°$, $b = +1.0°$; Ortolani *et al.*, (1993b)

the galactic center; this hole agrees nicely with that found in the OH/IR star distribution (thus: in the distribution of the most luminous AGB stars; Baud *et al.*, 1981; Blommaert *et al.*, 1994). The hole is encircled by a ring of disk stars. Ages between 1 and 7 Gyr are assigned to the disk stars, based on the ratio between the numbers of main-sequence and giant stars. A few much younger stars are also present.

V vs. $V - I$ diagrams of 300,000 stars in Baade's window have recently been published by the OGLE consortium (Paczynski *et al.*, 1994). This is a side product from the search for dark matter via mini-gravitational-lens effects. Paczynski will discuss these observations in one of the next invited reviews, and I skip discussing the interesting CMDs. But I note the conclusion that the number of foreground stars (disk stars) seem to disappear abruptly at a distance of only a few kiloparsec. This conclusion agrees in general terms with those reached by others (see above) but there

are differences that will hopefully be resolved in the near future.

A first CMD based on HST measurements, before its repair, in Baade's window been presented by Holtzmann *et al.* (1993). This is a crowded field and it is no surprise that the conclusions reached (a.o. that the bulge contains star less than 10 Gyr old) differ from e.g. those of Bertelli *et al.* (see above).

2.1.2. *CMD's in the near–infrared.*

In the near-IR (J, H, K, L) one can penetrate all the way to the galactic center; extinction continues to cause problems but is no longer as devastating as it is below 1 μm. The near IR bands have the disadvantages of less sensitivity and a smaller number of pixels per exposure; both disadvantages are now rapidly disappearing. An early piece of work is by Catchpole *et al.* (1990) who mapped an area of $1^\circ \times 2^\circ$ around the center with a photometer working simultaneously at J, H, K, but with only one pixel per band and with poor angular resolution ($6'' \times 12''$). The detection limit $K = 12$ and thus only bright stars are detected ($M_K \leq -2.5$), probably all late–type giants; the brightest stars ($K < 7.0$) cluster more strongly to the center than the fainter giants.

Ruelas–Mayorga and Teague (1993) give a CMD of K versus $J - K$ of ≈ 160 stars down to $K \approx 11$ in Baade's Window showing a giant branch. This work is surpassed in importance by Davidge (1991) who produces a CMD from J, H, K–measurements on 76 stars in Baade's Window down to $K \approx 16$. The RGB is clearly seen; it matches very well the RGB of 47 Tuc and of M67 (if these are shifted according to distance and extinction differences). Horizontal Branch stars appear below $K \approx 13.2$. There are less HB stars with respect to the red giants than as seen in the I–band.

Nagata *et al.* (1993, 1994) made a survey simultaneously in the H and the K band of a strip of $112' \times 18'$ containing the galactic center and discuss more extensive photometry (in a few cases to 20 μm) of a sample of 50 stars brighter than K=9.45; this sample contains *all* stars with $K < 7.6$. Several objects have $M_{bol} < -5.0$ ($L > 7700\ L_\odot$), which is also the maximum for M giants in the bulge (Frogel and Whitford, 1987). The number of bright objects is consistent with an exponential disk and there is no indication of a concentration of M–supergiants in the central region. A few objects could be very young.

2.2. ABUNDANCES AND AGES.

There are several indications that the bulge contains stars of much higher metallicity than the Sun, but the indications are all indirect: a detailed spectroscopic analysis of stellar atmospheres has been lacking until recently.

The stars easiest detected in the bulge are M–giants, but unfortunately their atmospheric structure is poorly known and until now a detailed spectral analysis has been impossible; a breakthrough may have been achieved recently by Tsuji *et al.* (1994) in their detailed analysis of SiO–abundances in bright and nearby M-giants.

McWilliam and Rich (1994) analyse spectra of 12 K giants in Baade's Window taken between 617 and 760 nm with a resolution of $R \approx 17000$. Judging from their magnitude and their radial velocity the stars are not in the foreground and belong almost certainly to the bulge. McWilliam and Rich perform a detailed spectroscopic analysis. The conclusion is that the distribution of [Fe/H] abundances of stars in Baade's Window agrees very well with the distribution in solar neighborhood stars. The same is true for Ca and Si, but Mg and Ti are enhanced by about 0.3 dex. The [Fe/H] abundances derived before by Rich (1990) are about 0.3 dex (a factor of 2) too high; this is mainly because Mg played a tricky role: the [Mg/Fe] abundance is higher in the bulge stars than in the solar neighborhood stars. The conclusion of solar–like Fe abundance resolves a few outstanding problems; for example the conclusion by Davidge (1991) that the giant branch in K vs. $J - K$ CMDs of Baade's Window agrees so well with that of 47 Tuc; but solar–like abundances contradict (indirectly) abundances obtained by others. These differences are discussed at length in the McWilliam and Rich paper and lead to the conclusion "that the others were wrong"; the arguments convinced me but some further discussion by "*affecionados*" is to be expected.

In detailed analyses like those by McWilliam and Rich one element is outstandingly absent: helium. Yet helium plays a key role in determining the stellar properties, for example in the determination of the age of a red giant. Indirectly one may estimate the helium abundances from the ratio between horizontal branch stars and red giants, a technique propagated already by Schwarzschild (1970) in his George Darwin lecture. In a recent paper Renzini (1994) discusses this ratio for the bulge stars; its value is read from the OGLE CMD. There appear to be relatively fewer red giants in the bulge than e.g. in globular clusters and this leads Renzini to the suggestion that the helium abundance is enhanced in the bulge; he estimates Y to be between 0.31 and 0.35. Another consequence is that these HB stars could be very old, at least as old as the globular clusters.

Other old stellar objects in the bulge that permit detailed spectroscopic analysis are the planetary nebulae. Clegg (1993) surveys recent abundance determinations in the Bulge, elsewhere in the Galaxy and in other, nearby galaxies. Concerning planetary nebulae in the bulge solar abundances are found.

There are other, more indirect means for the determination of abun-

dances: the CO– and H_2O–indices; the absence of carbon stars; the ratios of number densities of FGB (First Giant Branch), RHB, BHB stars; Preston's ΔS for RR Lyrae. I like to add a new one to this list: the v_{out}–method for OH/IR stars, discovered in model calculations of the transfer of momentum from photons to dust to gas in circumstellar envelopes (Netzer and Elitzur, 1993; Habing, Tignon and Tielens, 1994); the results are supported by several observational facts. The models show that the mass loss rate, $\dot{M}$, of a Mira or OH/IR star is determined by the pulsational properties of the star and *not* by the light pressure on grains, but the light pressure does determine the *momentum* obtained by the outflow, $\dot{M}v_{out}$. As a consequence the outflow velocity, v_{out} is determined by two factors: the luminosity L and the dust–to–gas ratio, δ, at least in stars with a high value of $\dot{M}$; the relation is $v_{out} \propto \delta^{0.5} L^{0.25}$ (Habing *et al.*, 1994). Thus if one knows L and v_{out}, one derives δ. In OH/IR stars the dust–to–gas ratio is determined by the Si–abundance and δ is a measure for [Si/H].

2.3. VARIABLES AT THE TOP OF THE AGB AND THEIR OFF–SPRING.

Long Period Variables (Mira variables, "IRC Miras" and OH/IR stars) are very bright AGB stars. Planetary Nebulae develop at constant luminosity from these top-AGB stars. For a thorough discussion of the presence of these populations in the bulge I refer to the conference proceedings listed at the end of this review.

Given the little time available I turn my attention to the distribution of OH/IR stars in the innermost parts of our Milky Way, that is within 200 pc from the center. OH/IR stars are direct relatives of Miras and these two kinds of Long Period Variables overlap in luminosity between 5000 and 8000 $L_{\odot}$, that is for M_{bol} between -4.5 and -5.1; Miras with longer periods (and higher luminosity) equal in luminosity the OH/IR stars of shorter periods (and lower luminosity) and probably the Miras develop into these OH/IR stars. A considerable fraction of the OH/IR stars (4 out of 17 measured by Blommaert, 1992; 8 out of 17 measured by Jones *et al.*, 1994) are brighter than M_{bol}= -5.1 and this appears to be the upper limit of the stars detected by optical means in the various windows. Such luminous AGB stars must be, at least in part, rather young (say younger than 1-2 Gyr)– if the stars are single. Renzini (1992) has suggested that the OH/IR stars result from mergers of double stars and thus may be much older than this low age; the small number of these stars is to be expected under this merged–double hypothesis. An interesting case is the star that is most luminous (by far): OH 359.762+0.120; M_{bol}=-7.2 or L= 60,000 $L_{\odot}$(Jones *et al.*, 1994), P = 760^d, v_{out}= 15 km/s. The star cannot be a foreground object, because the 1612 MHz (18 cm) image of the maser

is strongly deformed (= smeared out) by interstellar scintillation and this effect, we think, occurs only close to the galactic center (van Langevelde, *et al.* 1992; Frail *et al.* 1994). Renzini's suggestion is quite welcome in explaining the high luminosity of this star. Yet, I feel some reservation (see below) against applying the merged–double explanation to *all* OH/IR stars.

After a search lasting several years Lindqvist *et al.* (1991, 1992) have now obtained a sample of 136 OH stars within 150 parsec from the galactic center. The sample is complete down to a well defined sensitivity limit and as such it is probably the only complete stellar sample known in this inaccessible region of the Galaxy. Subsamples have been monitored in the near IR (Jones et al, 1994) and in the maser line (van Langevelde *et al.*, 1993) and prove that the majority, though not all, are long period variables with periods up to 800 days. Infrared measurements made from the ground lead to reasonably accurate estimates of the stellar luminosities (Jones *et al.*1994; Blommaert, 1992). If this sample is divided in two subsamples based on the value of the outflow velocity, v_{out}(an easily and accurately measured quantity) there are pronounced differences in the distribution of these two samples in the plane of the sky and in the longitude/velocity diagram:

—Stars with lower expansion velocities are distributed in a spheroidal distribution with a flattening of 0.7. The radial velocities may correlate with longitude, but the slope of the regression line is small (0.01 km/s/pc). Its value agrees nicely with that seen in Mira variables (e.g. in Baade's Window) or in the recent near IR measurements of M–giants by Blum *et al.* (1994). The dynamical model by Kent (1992) accounts quite well for these velocities and for the spatial distribution by assuming a relaxed stellar population with an isotropic velocity distribution and small systematic rotation, enough to flatten the bulge by a modest amount.

—In contrast to the stars with lower outflow velocities, one finds for the stars with higher outflow velocity a flatter distribution on the sky and a rapid rotation around the galactic center like a solid body with a speed of about 1 km/s/pc; thus a rotation much faster than Kent's spheroid.

Kinematic differences prove that these two subsamples of OH/IR stars represent two different galactic populations. The distinction between the populations is made on basis of by the outflow velocity. As mentioned above a difference in δ or L or in both determines the outflow velocity, v_{out}. The luminosities of several OH/IR stars have been determined via broad-band photometry between 4 and 20 μm (Blommaert, 1992); the stars with higher v_{out} have somewhat higher luminosity, but not enough to explain the difference in v_{out} between the two samples. The conclusion is that the stars with larger v_{out} have higher dust–to–gas ratios and higher Si–abundance. Thus the stars with larger outflow velocity behave as if they have formed

out of a disk of (significantly enriched) gas and have kept their state of motion since then, and that this formation was an event different from and more recent than the one that formed Kent's spheroid: the OH/IR stars near the center are a mix originating from two different populations, each with its own formation history.

To close off this subject allow me a few additional remarks.

(i) M-giants near the center studied o far all appear to belong to the flattened spheroid discussed by Kent. Where are the M-giants/precursors of the OH/IR stars with large outflow velocities? If Renzini (see above) is right about the fact hat the OH/IR stars are mergers from a population of old stars with maximum AGB luminosity M_{bol}=-5.1, then the high outflow–velocity OH/IR stars should have also many counterparts of lower luminosity. Where are they?

(ii) Each OH/IR star appears to have a SiO-maser but the reverse is not true: there are many more stars with an SiO and without an OH maser than stars that have both. The somewhat small sample of OH/IR stars can thus be expanded by a significant factor by concentrating on SiO masers. Izumiura *et al.* (1994) have just completed a study with the Nobeyama telescope and detected SiO masers in a large number of bulge LPV's. Clearly here is a new opening to the field of research of LPV's in the galactic bulge.

2.4. BULGE AND BAR.

If our Galaxy contains a bar (and the kinematics of the gas in the inner Galaxy clearly point in that direction) it will be important to find out what stellar population it contains. The only "definite suggestion" (apologies for the contradiction) has been made by Whitelock (1993) who finds a concentration of Long Period Variables associated with the bar.

3. What remains to be learned.

There has been significant progress in recent years. The large and thorough work by McWilliam and Rich has now established somewhat more firmly that the bulge or at least the K–giants in Baade's Window have Fe abundances comparable to those in the solar neighborhood but a higher Mg/Fe abundance ratio. This conclusion about solar type abundances then agrees with those about the abundances in bulge planetary nebulae. The solar metallicity conclusion solves other outstanding problems but disagrees with much earlier work, mostly based on indirect and modestly accurate metallicity estimators. McWilliam and Rich's words will not be the last to be said about abundances in the bulge. Deep Hertzsprung–Russell diagrams for bulge stars, with the foreground stars removed, and in fields in

different directions are now available; detailed studies on individual stars in these diagrams are the next step (e.g. detailed spectroscopy of red horizontal branch stars in the bulge). It is to be hoped that accurate spectroscopic determinations of metallicities in M–giants will become doable. Whereas Kent's spheroidal model explains most of the bulge data, one finds in part of the OH/IR stars a population that is clearly different; it seems to have a high metallicity and an origin different from that of Kent's spheroid.

4. A concluding and irrelevant remark.

Jan Oort established his fame in 1927, in his 27th year, when he concluded that stars in the solar neighborhood rotate around a distant center in Sagittarius. This conclusion is still a major anchor that secures the study of the Galaxy we live in. For about 65 years Oort continued to solve problems of the Galaxy. But clearly he did not solve all of them, otherwise we would not have a symposium with the title "Unsolved problems of our Milky Way". To me there is irony in the fact that we dedicate a symposium with this title to him, who has solved more galactic problems than anybody else; it almost looks as if we have a cause for complaints. Well, I may find this ironical, but I think that he would have felt differently and that is what counts.

5. Conference Proceedings and general review lectures:

"Bulges of Galaxies", 1990, eds. B.J. Jarvis, D.M. Terndrup (ESO publications).

"The Stellar Populations of Galaxies", IAU Symposium # 149, 1992, eds. Barbuy and Renzini, Kluwer Academic Publishers, Dordrecht.

"Galactic Bulges" IAU symposium # 153, 1993, eds. H. Dejonghe and H.J. Habing, Kluwer Academic Publishers, Dordrecht.

"Planetary Nebulae", IAU Symposium # 155, 1993, eds. R. Weinberger, A. Acker, Kluwer Academic Publishers, Dordrecht.

"The Nuclei of Normal Galaxies: Lessons from the Galactic Center" (Conference at Schloss Ringberg), 1994, eds R. Genzel and A. Harris, NATO ASI series, Kluwer Academic Publishers, Dordrecht.

"The Center, Bulge and Disk of our Milky Way", 1992, ed L. Blitz, Kluwer Academic Publishers, Dordrecht.

References

Baud, B., Habing, H.J., Matthews, H.E., Winnberg, A. (1981), *A.& A.*, 95,p. 156
Bertelli, G., Bressan, A., Chiosi, C., Ng, Y.K., Ortolani, S. (1994), *A.& A.*, submitted
Blommaert (1992),*thesis, Leiden University*
Blommaert, J.A.D.L., van Langevelde, H.J., Michiels, W.F.P. (1994), *A.& A.*, 287,p. 479

Blum, R.D., Carr, J.S., DePoy, D.L., Sellgren, K., Terndrup, D.M. (1994), *Ap.J.*, 422,p. 111
Catchpole, R.M., Whitelock, P.A., Glass, I.S. (1990), *Mon. Not. R.A.S.*, 247, p. 479
Clegg, R.E.S. (1993), *in "Planetary Nebulae", IAU Symposium # 155, eds. R. Weinberger and A. Acker*,Kluwer, Dordrecht,p. 549
Davidge, T. (1991), *Ap. J.*, 380,p. 116
Frail, D.A., Diamond, P.J., Cordes, J.M., van Langevelde, H.J. (1994), *Ap.J.let*, 427,p. L43
Frogel, J.A., Whitford, A.E. (1987),*Ap. J.*, 320,p. 190
Greggio, L., Renzini, A. (1990), *Ap. J.*, 364,p. 35
Habing, H.J., Tignon, J., Tielens, A.G.G.M. (1994), *A.& A.*, 286,p. 523.
Holtzman, J.A., Light, R.M., Baum, W.A., Worthey, G., Faber, S.M., Hunter, D.A., O'Neil, E.J., Kreidl, T.J., Groth, E.J., Westphal, J.A. (1993), *Astron. J.*, 106, p. 1826
Izumiura, H., Deguchi, S., Hashimoto, O., Nakada, Y., Onaka, T., Ono, T., Ukita, N., Yamamura, I. (1994), *Ap. J.*, in press
Jones, T.J., McGregor, P.J., Gehrz, R.D., Lawrence, G.F. (1994), *Astron. J.*, 107, p. 1111
Kent, S.M. (1992), *Ap. J.*, 387, p. 181
Kent, S.M., Dame, T., Fazio, G. (1991), *Ap. J.*, 378,p. 131
Lindqvist, M., Winnberg, A., Habing, H.J., Matthews, H.E. (1991), it A.& A. Sup. Ser.,bf 92,p. 43
Lindqvist, M., Habing, H.J., Winnberg, A., (1992),*A.& A.*, 259, p. 118
McWilliam, A., Rich, R.M. (1994), *Ap. J. Sup*, 91,p. 749
Nagata, T., Hyland, A.R., Straw, S.M., Sato, S., Kawara, K. (1993), *Ap. J.*, 406,p. 501
Nagata, T., Kobayashi, N., Sato, S. (1994), *Ap.J.let*, 423,p.L113
Netzer, N., Elitzur, M. (1993), *Ap.J.*, 410, p. 701
Ng, Y.K. (1994), *thesis, Leiden University*
Ng, Y.K., Bertelli, G., Chiosi, C., Bressan, A. (1994), *A.& A.*,submitted
Ortolani, S., Bica, E., Barbuy, B. (1993a), *A.& A.*, 267,p. 66
Ortolani, S., Bica, E., Barbuy, B. (1993b), *Ap. J.*, 408,p. L29
Paczynski, B., Stanek, K.Z., Udalski, A., Szymanski, M., Kaluzny, J., Kubiak, K., Mateo, M. (1994), *Astron. J.*, 107,p. 2060
Renzini, A. (1994), *A.& A. Lett.*, 285,p. L5
Rich, R.M. (1990), *Ap. J.,362*,p. 604
Ruelas-Mayorga, R.A., Teague, P.F. (1992), *A.& A. Sup. Ser.*, 93,p. 61
Schwarzschild, M. (1970), *Quart. J. R.A.S.*, 11,p. 12
Tsuji, T., Ohnaka, K., Hinkle, K.H., Ridgway, S.T. (1994), *A.& A.*,submitted
van Langevelde, H.J., Frail, D.A., Cordes, J.M., Diamond, P.J. (1992), *Ap.J.*, 396,p. 686
van Langevelde, H.J., Janssens, M., Goss, W.M., Habing, H.J. Winnberg, A. (1993), *A.& A.*, 101,p. 109
Whitelock, P.A., *in "Galactic Bulges", IAU Symposium # 153*, eds. H. Dejonghe and H.J.Habing,Kluwer, Dordrecht, p. 39

METALLICITY, STRUCTURE AND KINEMATICS OF THE MILKY WAY'S BULGE

DANTE MINNITI
European Southern Observatory
Karl-Schwarzschild-Str. 2
D-85748 Garching bei München
Germany

1. Introduction

One of the unsolved problems of the Milky Way is the interplay between the different components (disk, bulge and halo) in the inner regions, where they may all reach their maximum density. As a first approach to attack this problem, we summarize the results of a photometric and spectroscopic study of the Galactic bulge based on ~700 K and M giants in 3 fields (Minniti 1993a). Table 1 lists the position of the fields, their projected Galactocentric distance, number of stars with spectra at present, and estimated disk contamination.

TABLE 1. Caption text

Field	l , b	R (kpc)	N	N_{disk}/N_{tot}
F588	8 , 7	1.5	300	5%
M22	10 , -8	1.7	100	6%
F588	12 , 3	1.7	300	40%

2. Metallicity of the Bulge

We determine metallicities for a large number of K giants in these 3 fields based on medium resolution spectra. These abundances are derived by mea-

L. Blitz and P. Teuben (eds.), Unsolved Problems of the Milky Way, 329–334.
© 1996 *International Astronomical Union.*

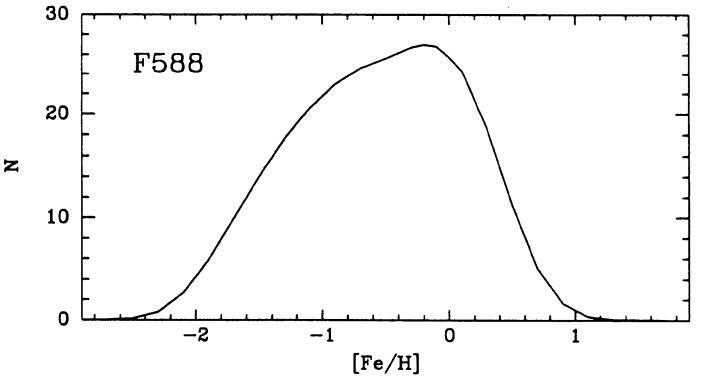

Figure 1. "True" metallicity distribution in field F588 obtained by Lucy deconvolution using the estimated errors, normalized to the total number of stars observed.

suring the strength of spectral indices, calibrated with a grid of giants observed in clusters with well–known abundances (Minniti et al. 1992). Our calibration is based on the globular cluster metallicity scale of Armandroff (1989). The mean metallicities for the fields with small disk contamination (M22 and F588) is between $[Fe/H] = -0.5$ and -0.6. McWilliam & Rich (1994) find a higher mean metallicity ($[Fe/H] = -0.25$) in Baade's Window, at 0.5 kpc from the Galactic center.

From these data we conclude that: 1) There is a metallicity gradient within the inner 2 kpc of the Galaxy, confirming previous photometric determinations (e.g. Terndrup 1988); 2) At any given distance from the Galactic center there is a large spread in metal abundances (Figure 1); and 3) The bulge is not super metal–rich as thought before. In particular, if the disk metallicity gradient continues or flattens out towards the Galactic center, the bulge itself would be more metal poor than the inner disk.

3. Structure of the Bulge

For the sample in the M22 field, we not only have abundances and optical photometry, but also proper motions measured by Cudworth (1986) and IR photometry. From these data we can estimate distances for the giants in this field if we assume ages for them. As a first guess, we adopt a mean age of 15 Gyr, for stars of all metallicities. The distribution of distances measured for the metal poor and metal rich giants is different (Figure 2a). Even though these distances can be uncertain, it is clear that: 1) the metal rich giants are closer in the mean than the metal poor giants, and 2) the metal rich giants have a more peaked distance distribution than the metal poor giants.

We compare the observed distributions with the ones predicted by the

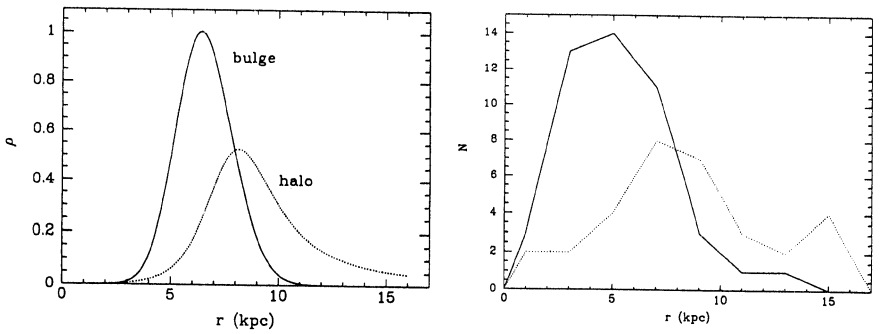

Figure 2. Left) Expected density distribution along the line of sight in the M22 field for both the halo (dotted line) and bulge (solid line), from the models described in the text. These densities have not been convolved with the error bars. Right) Observed distribution of stars as function of distance for the metal rich ([Fe/H] ≥ -1, solid line) and metal poor ([Fe/H] ≤ -1, dotted line) giants in the M22 field.

best fitting bar models for the bulge data from the DIRBE experiment on board the COBE satellite (Dwek et al. 1994), and by an axisymmetric halo with power law density distribution $\rho_h \propto r^{-3.2}$ (Figure 2b). The two observational results can be explained if there is a triaxial bulge consisting of stars with [Fe/H] ≥ -1, and a halo that is more axisymmetric. This would be the first indication that the inner halo is not barred as the bulge. We also argue that in order to match the observed mean distance of bulge giants to models of the bar, the bulge must be significantly younger than the halo.

4. Kinematics of the Bulge

We also measured radial velocities with an accuracy of $\sim$ 10 km s^{-1} for all K and M stars. We will examine the kinematics of stars again in two groups: stars more metal–rich than [Fe/H] $= -1.0$, and metal–poor stars with [Fe/H] ≤ -1.0. This division is chosen arbitrarily to reflect the transition between true halo stars and disk stars in the neighborhood of the Sun (e.g. Carney et al. 1989), and using the fact that there is no metallicity gradient in the halo (e.g. Zinn 1985).

For any given field there is a marked trend of kinematics with metallicity, in the sense that the metal–poor population has a higher velocity dispersion and a lower rotational velocity than the metal–rich population. An example of this is given in Figure 3. subsequently, we then look at the radial dependences of kinematics (Figure 4). It is found that the K giants with $[Fe/H] \leq -1$ have halo–like kinematics, with no significant rotation and $\sigma \sim 120$ km s^{-1} independent of Galactocentric distance. The velocity dispersion of the giants with [Fe/H] ≥ -1 decreases with increasing

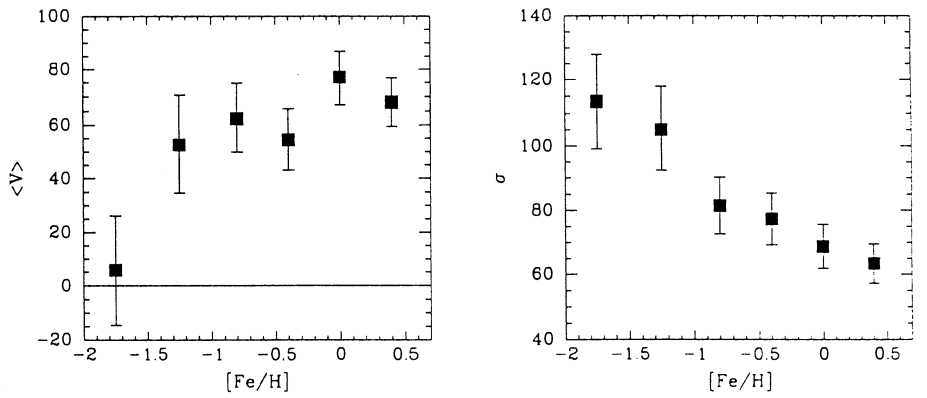

Figure 3. Mean Galactocentric velocities V, and velocity dispersions σ *vs* metallicity for K giants in the F588 bulge field, located at l,b = (8, 7), at projected distance of 1.5 kpc from the Galactic center. Each bin includes 30 to 55 stars.

Galactocentric distance, and this population is rotating with $V \sim 9$ km s^{-1} degree^{-1}.

The velocity dispersions and rotational velocities of the metal–poor stars observed in bulge fields have similar values to those of the nearby halo stars, to those of the halo globulars and to those of the bulge RR Lyraes. On the basis of this comparison, it is then plausible to conclude that the metal–poor stars in this study, and the RR Lyraes in Baade's Window, are the extension of the halo population within 3 kpc. We would then conclude that the halo is isothermal all the way to the center.

The metal–rich population has substantial rotation, and we identify these stars with the bulge. The PN, Miras and SiO masers are kinematic tracers of the bulge and not the halo. Disk contamination would have a negligible effect in fields F588 and M22. Paczynski et al. (1994) model the number density of disk stars as constant up to some distance, and vanishing beyond that distance, as if the disk were hollow in the inner few kiloparsecs.

5. The Formation of the Bulge and Halo

Figure 5 shows the location of the halo and the bulge in a classical V/σ *vs* ϵ diagram (Binney 1978), where V is the peak rotation, σ is the central velocity dispersion, and ϵ is the flattening ratio. This figure suggests that somehow during the formation of the Galaxy there was a change from an extended, pressure supported halo, to a flattened, more concentrated and rapidly rotating bulge. This leads to the following formation scenario: Only a small fraction of the gas in the proto–halo formed stars (e.g. Hartwick 1976). The rest of the gas was lost from the halo, sinking deep into the

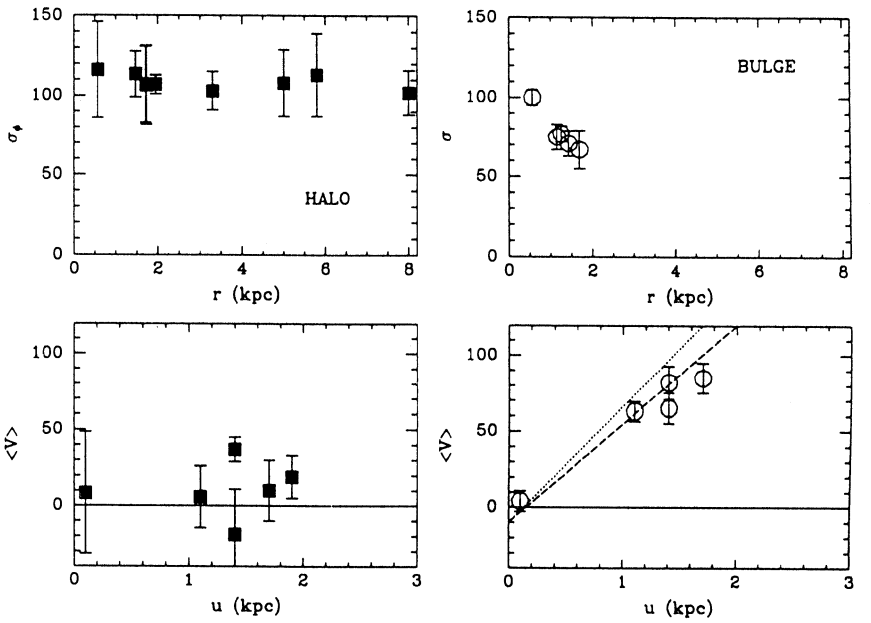

Figure 4. Run of the mean line of sight velocity V *vs* Galactocentric distance projected in the plane u and velocity dispersions σ *vs* Galactocentric distance for K giants with [Fe/H] ≤ -1.0 (left panels), and with [Fe/H] ≥ -1.0 (right panels) in different fields towards the Galactic bulge. The dashed line in the lower right panel shows the mean rotation of planetary nebulae from Kinman et al. (1990), and the dotted line shows the mean rotation of bulge Mira variables (Menzies 1990), and of bulge SiO masers (Nakada et al. 1993).

potential, due to energy loss by radiation and cloud–cloud collisions, but conserving angular momentum. The enriched gas collapsed towards the central parts of the Galaxy, due to its low angular momentum, forming bulge stars (e.g. Carney et al. 1990, see also Wyse & Gilmore 1992). In this model the bulge would have formed after the old halo stars (i.e. after most of the metal–poor RR Lyraes and globular clusters with blue horizontal branches).

The predictions from this scenario (and those from other models) can be tested with more data. In the nearby future we expect significant progress in the following areas: 1) Large number of proper motions in the bulge will lead to more refined dynamical models (e.g. Minniti 1993b, Zhao et al. 1994). 2) Accurate measurements of detailed chemical abundances for large numbers of bulge giants will lead to more refined models of chemical evolution (e.g. Matteucci & Brocatto 1989). 3) Accurate ages obtained from observations with the refurbished HST combined with the metallicity information will lead to a better understanding of the chronology of bulge formation (e.g. Holtzmann et al. 1993).

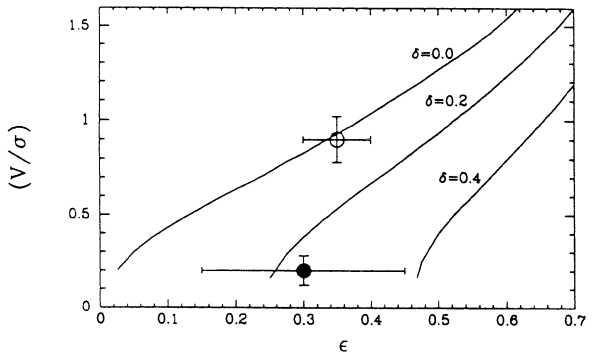

Figure 5. Relationship between rotation parameter V/σ and ellipticity ϵ for coaxial oblate spheroids with different anisotropy δ (solid lines), reproduced from Binney & Tremaine (1987, their figure 4–5 on p. 217). We have plotted the location of the Galactic bulge (open circle) and halo (filled circle). The bulge ellipticity is taken from Kent et al. (1991), and the halo ellipticity from the reviews by Bahcall (1986) and Freeman (1987). The 1 σ error bars shown are conservative.

Acknowledgements

I am very grateful to M. Rich for reading my contribution during the meeting. I also thank L. Kaper for carefully reading this manuscript.

References

Armandroff, T. 1989 *AJ* 97, 375.
Bahcall, J. N. 1986 *ARA&A* 24, 577.
Binney, J. 1978 *MNRAS* 183, 501.
Binney, J., & Tremaine, S. 1987 *"Galactic Dynamics"* (Princeton Univ.), p. 217
Carney, B. W., Latham, D. W., & Laird, J. B. 1990 *AJ* 99, 752.
Cudworth, K. M. 1986 *AJ* 92, 348.
Dwek, E. et al. 1994 *ApJ* , submitted.
Eggen, O. J., Lynden-Bell, D., and Sandage, A. 1962 *ApJ* 136, 748.
Hartwick, F. D. A. 1976 *ApJ* 209, 418.
Kent, S. M., Dame, T. M., & Fazio, G. 1991 *ApJ* 378, 496.
Kinman, T. D., Feast, M. W., and Lasker, B. M. 1988 *AJ* 95, 804.
McWilliam, A., & Rich, R. M. 1994 *ApJS* 91, 749.
Menzies, W. J. 1990 *in "Bulges of Galaxies"* , eds. B. J. Jarvis & D. Terndrup, p. 111.
Matteucci, F, & Brocatto, E. 1990 *ApJ* 365, 359.
Minniti, D., White, S.D.M., Olszewski, E., and Hill, J.H. 1992 *ApJ* 393, L47.
Minniti, D. 1993a PhD Thesis, Steward Observatory, Univ. of Arizona.
Minniti, D. 1993b *in "Galactic Bulges"* , B. J. Jarvis & D. Terndrup, p. 315.
Nakada, Y., et al. 1993 *PASJ* 45, 179.
Paczynski, B., et al. 1994 *AJ* 107, 2060.
Rich, R. M. 1988 *AJ* 95, 828.
Terndrup, D. M. 1988 *AJ* 96, 884.
Wyse, R. F. G., and Gilmore, G. 1992 *AJ* 104, 144.
Zhao, H.-S., Spergel, D., & Rich, R. M. 1994 *AJ* , in press.
Zinn, R. 1985 *ApJ* 293, 424.

GALACTIC BULGES AS AN EVOLUTIONARY PHENOMENON: OBSERVATIONAL EVIDENCE FROM THE STATISTICS OF "BOX/PEANUT" BULGES

R.-J. DETTMAR

*Space Telescope Science Institute**†
3700 San Martin Dr.
Baltimore, MD 21218 (USA)

1. Introduction

N-body simulations for stars in bar potentials have demonstrated over the last couple of years (e.g., Combes et al. 1990; Raha et al. 1991) that bars growing in z will lead to the presence of a bulge component. In such a scenario a central "bulge" component could develop as a resonance phenomenon caused by a bar and would be distinctly different from any "spheroidal" or "halo" component.

There is growing evidence that our Galaxy harbors such a "bulge–bar" structure. The box- or peanut shape of the bulge in the Milky Way as revealed by the DIRBE experiment on board of COBE is one of the typical signatures for the proposed "resonant phenomenon". In addition to morphology gas kinematics shows the presence of a bar and the Galaxy and extragalactic examples have been discussed extensively earlier at this conference (see, e. g., contributions by Blitz, Gerhard, Combes, and Kuijken). Here we discuss evidence for such an evolutionary scenario in the formation of bulges based on the frequency of box- and peanut-shaped (b/p) bulges observed in a CCD surface photometry of edge-on galaxies.

*affiliated with the Astrophysics Division in the Space Science Department of ESA
†present address: Astronomisches Institut der Ruhr-Universität, Universitätsstr. 150, D-44780 Bochum, Germany

L. Blitz and P. Teuben (eds.), Unsolved Problems of the Milky Way, 335–339.
© 1996 *International Astronomical Union.*

2. Statistics of b/p Bulges from CCD Photometry

We have obtained CCD images of ≈80 edge-on galaxies with the 2.2m-telescopes at ESO/La Silla and Calar Alto/Spain. Detailed surface photometry of a subset is presented in Barteldrees and Dettmar (1994).

As an example we show in Fig. 1 the surface photometry of ESO 321-G10. This example demonstrates that the peanut shape of the bulge can be identified by the double humped profile in cuts taken parallel to the major axis. This is true even in spirals of types as late as Sc. In total 35 or 43% of the objects in our sample show b/p bulges. In Fig. 2 we have scaled our sample to the distribution of morphological types as given by the ESO/Uppsala catalogue. The particular binning of types is for easier comparison with previous work (Jarvis 1986, Shaw 1987, de Souza and dos Anjos 1987). While for types in the range S0 – Sbc the agreement with Shaw and de Souza & dos Anjos is excellent, we find a significant fraction of later type spirals to show b/p bulges. The previous studies used the sky survey photographic material and the higher dynamic range of our CCD photometry easily explains the higher detection rate in Sc galaxies.

It is worthwhile to point out that some more b/p bulges in spirals of type Sbc–Sc can be found in the color images by Wray (1988). These images nicely represent the nuclear regions of galaxies and reveal well known objects such as NGC 5170 to have a b/p bulge.

The frequency of b/p bulges now can to be compared with the frequency of bars broken down by morphological type. These numbers are very uncertain and 25% – 35% seems to be a very conservative estimate for the fraction of barred galaxies (Sellwood and Wilkinson 1993) averaged over all spirals. With the large statistical errors from the small number of galaxies in our sample the frequencies seem to be compatible. However, the statistics of b/p bulges is not corrected for the aspect angle. Therefore either bars have to be more frequent than 35% to explain b/p bulges or other processes are contributing to the formation of b/p bulges, too. In our sample there is indeed evidence that some b/p bulges are caused by interaction and examples are presented elsewhere (Dettmar and Barteldrees 1990).

3. Minor Axis Profiles

The N-body simulations mentioned above (e.g., May et al. 1985; Combes et al. 1990) predict for the resulting "thick bar" surface brightness distributions that are significantly different from de Vaucouleurs profiles which well describe the spheroidal components in early type spiral galaxies. At least for some bulges of late type spirals the minor axis intensity profiles seem to fall of steeper than a de Vaucouleurs profile. For a large range in radius the de Vaucouleurs law is well represented by a simple r^{-2} power law (Kor-

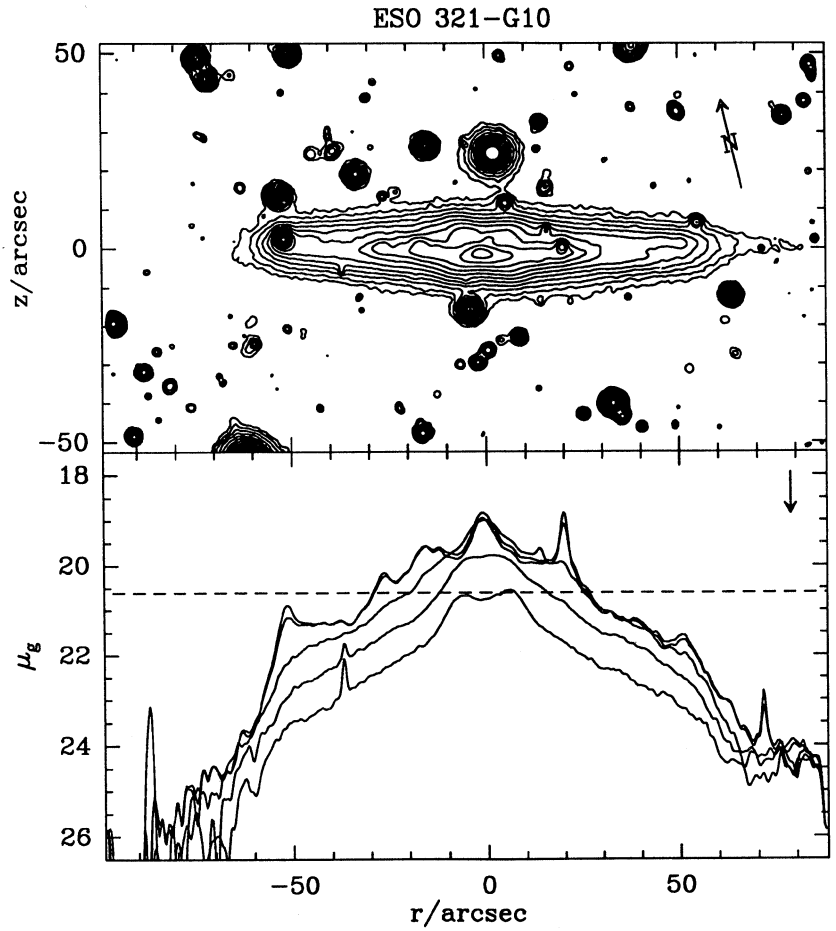

Figure 1. Top: Isophote map of the surface brightness distribution for ESO 310-G10. The faintest contour is at μ_g=24.0, steps between contours are 0.5 mag. Bottom: Cuts parallel to the major axis separated by 1.8 arcsec; the dashed line represents the brightness of the night sky. The double humped profile identifies the b/p bulge.

mendy 1982). Hamabe (1982) used a power law representation to compare spheroidal components for galaxies of morphological types ranging from E to Sc. The few late type cases in his diagram can be at most suggestive for a tendency showing steeper bulges in late type spirals. However, Dettmar and Wielebinski (1986) report that minor axis profiles of bulges in late type spirals, and in particular b/p bulges, are much steeper than spheroids in early type spirals and S0s. While this may support the idea of bulges in late type spirals being different from spheroids in early type spirals the result

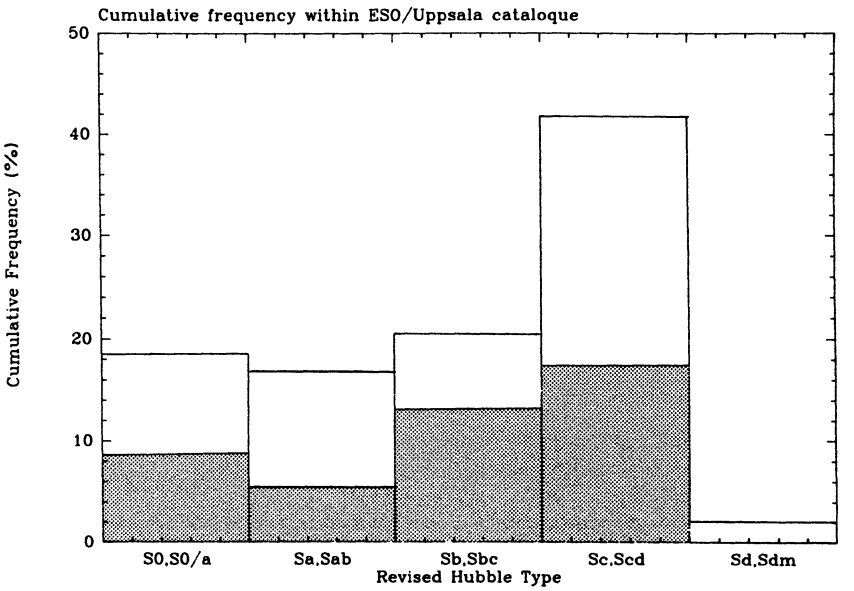

Figure 2. Cumulative frequency of morphological types (upper histogram) and b/p bulges within each bin (hatched histogram) scaled to the distribution of types in the ESO/Uppsala catalogue.

is, of cause, hampered by the influence of dust absorption. The availability of IR detector arrays will allow for a thorough reanalyses of this question in the near future.

4. Discussion and Conclusions

The high frequency (>35%) of the b/p bulge phenomenon requires a very common process to be at work. Various processes have been proposed: (1) external torques (May et al. 1985) , (2) bars (e.g., Combes et al. 1990), and (3) "soft" merging (Binney and Petrou 1985; Whitmore and Bell 1988). All these processes might contribute to the high frequency of b/p bulges, with bars explaining the largest fraction.

This is supported by the growing number of galaxies with b/p bulges that show in optical as well as radio high-resolution spectral line studies the complex gas motions characteristic for a bar. In addition to the cases mentioned before by F. Combes and K. Kuijken (this proceedings), I want to mention NGC 3268 and NGC 2683. Both objects are known for decades to show b/p bulges. The gas kinematics in the central region obtained in CO(J=2-1) in the case of NGC 3628 (Reuter et al. 1991) and in HI for NGC 2683 (Broeils 1992) again link the b/p bulges to the presence of a

bar.

The possibility of bulges being generated by bars as an evolutionary phenomenon in disks has, of course, important implications for understanding galaxy evolution and formation. The B/D ratio, for example, then does no longer constrain any primordial condition for galaxy formation.

Acknowledgments. I am greatful to A. Barteldrees, J. Christensen, and S. Gonzaga for help with the data reduction. Parts of this work have been supported by DFG at University of Bonn and DDRF at STScI.

References

Barteldrees, A., and Dettmar, R.-J. (1994) A&AS 103, 475
Binney, J., and Petrou, M. (1985) MNRAS 214, 449
Broeils, A. (1992) PhD thesis, Groningen
Combes, F., Debbasch, F., Friedli, D., and Pfenniger, D. (1990) A&A 232, 82
de Souza, R. E., and dos Anjos, S. (1987) A&AS 70, 465
Dettmar, R.-J., and Barteldrees, A. (1990) in Bulges of Galaxies, eds. B. J. Jarvis and D. M. Terndrup, ESO, p. 255
Dettmar, R.-J., and Wielebinski, R. (1986) A&A 167, L21
Hamabe, M. (1982) PASJ 34, 423
Jarvis, B. J. (1986) AJ 91, 65
Kormendy, J. (1982) in Morphology and Dynamics of Galaxies, eds. L. Martinet, M. Mayor, Geneva Observatory, p. 113
May, A., van Albada, T. S., and Norman, C. A. (1985) MNRAS 214, 131
Raha, N., Sellwood, J. A., James, R. A., and Kahn, F. D. (1991), Nature 352, 411
Reuter, H.-P., Krause, M., Wielebinski, R., and Lesch, H. (1991) A&A 248, 12
Sellwood, J. A., Wilkinson, A. (1993) Rep. Prog. Phys. 56, 173
Shaw, M. A. (1987) MNRAS 229, 691
Whitmore, B. C., and Bell, M. (1988) ApJ 324, 741
Wray, J. (1988) The Colour Atlas of Galaxies, Cambridge

DISCUSSION

P. Teuben: Have any multi wavelength IR studies been done to correct for dust absorption and check how persistent these P/B bulges are? Recall Dwek showed a few days ago that in our galaxy bulge it largely disappears.

Dettmar: For the few published cases of b/p bulges in edge-on galaxies studied in the IR (e.g., NGC 891) the b/p bulge is not disappearing in the IR. Bagett and Anderson have looked for the possibility to explain the b/p shape by dust absorption but could rule out this.

OBSERVATIONAL PROPERTIES OF SIO MASERS IN THE GALACTIC BULGE IRAS SOURCES

H. IZUMIURA
SRON Laboratory for Space Research Groningen
Landleven 12, P.O.Box 800, 9700 AV Groningen
The Netherlands

We surveyed 313 color-selected IRAS sources in the Bulge in the SiO J=1-0 (v=1,2) lines with the Nobeyama 45m telescope, which resulted in 222 detections (Nakada et al. 1992; Izumiura et al. 1994ab). The detection rates exceeded 80% for the brighter samples (Table 1). We discuss the observed SiO maser characteristics and the implications of the obtained l-v diagram.

SiO Maser Intensity: We examined the integrated SiO intensity against the 12μm flux density. On average, our sample stars show much stronger SiO intensities for a particular 12μm flux than found by Jewell et al. (1991) for stars in the solar neighborhood. The highest observed value of the SiO intensity for a fixed 12μm flux is 10 times as high as theirs. This large discrepancy should be confirmed with future observations of the nearby stars with the 45m telescope.

Completeness of our survey: In terms of 12μm flux, our survey is almost complete down to F_{12} ~1.5 Jy in the $|b|$ =7°-8° strips. According to Whitelock et al. (1991) our survey reached the far side of the Bulge, as far as 4 kpc away from the galactic center. Our sample, however, may be biased to the intrinsically brighter objects in the far-side. In the $|b|$ =4°-5° strips the sampling is complete down to F_{12} = 3 Jy, which means that our survey is almost complete in the near side of the Bulge (see Nakada et al. 1991). The far side has also been substantially sampled as far as 10 kpc from the Sun. In addition, these arguments are valid for the region of $l > -8°$ due to the declination limit at Nobeyama.

Implications of the l-v diagram: Izumiura et al. (1993) suggested a possible asymmetry in the l-v diagram. It has turned out to come mostly from sources in the 7°-8° strips in quadrant "A" of Figure 1. The 4°-5° strips sources are distributed rather symmetrically around the origin in the diagram, in spite of the somewhat smaller distance coverage. The asymmetry

L. Blitz and P. Teuben (eds.), Unsolved Problems of the Milky Way, 341–342.
© 1996 *International Astronomical Union.*

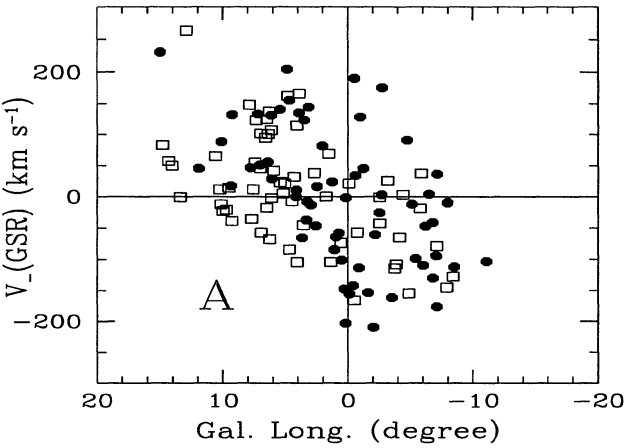

Figure 1. l-v diagram for the 4°-5° (filled circles) and 7°-8° (open squares) strips. All the sources which have a F_{12} less than 10 Jy are plotted.

is probably not due to the sampling effect but real. This suggests that either the 7°-8° strips have a significantly different velocity structure than the 4°-5° strips, or the 4°-5° strips will show a similar feature if the sampling becomes deeper. We might be seeing an extra kinematical component which becomes evident only away from the plane.

TABLE 1. Detection Rate (%) ($N_{detected}/N_{observed}$)

Color Range	Flux Range (Jy)			
$\log(F_{25}/F_{12})$	1.0-2.0	2.0-4.0	4.0-8.0	8.0-16.0
−0.10-0.00	56 (5/9)	67 (6/9)	78 (7/9)	67 (10/15)
0.00-0.10	52 (11/21)	65 (31/48)	79 (52/66)	88 (23/26)
−0.15-0.15	57 (24/42)	66 (44/67)	73 (74/101)	81 (43/53)

References

Jewell, P. R., Snyder, L. E., Walmsley, C. M., Wilson, T. L., & Gensheimer, P. D. 1991, *A&A*, 242, 211
Izumiura, H. et al. 1993, in *IAU Symp. 153, Galactic Bulges*, ed. H. Dejonghe & H. J. Habing, (Dordrecht:Kluwer), p.303,
Izumiura, H. et al. 1994a, *ApJ*, in press
Izumiura, H. et al. 1994b, *ApJS*, in press
Nakada, Y. et al. 1991, *Nature*, 353, 140
Nakada, Y. et al. 1992, *PASJ*, 45, 179
Whitelock, P., Feast, M, & Catchpole, R. 1991, *MNRAS*, 248, 276

REPORT ON A SURVEY OF H_2O MASERS TOWARDS THE GALACTIC CENTER

DEBORAH A. LEVINE
IPAC/UCLA
IPAC, MS 100-22, Caltech, Pasadena CA 91125

AND

MARK MORRIS
UCLA
Department of Physics & Astronomy,
8979 Math Sciences Bldg., Los Angeles, CA, 90024

1. Introduction

Galactic H_2O masers are associated either with the circumstellar shells of late-type stars or with star-forming regions (SFRs). Previous surveys for H_2O masers had revealed relatively few near the Galactic Center (GC). We report on the continuation of a survey using the VLA to make 22.2 GHz observations of IRAS point sources which lie within 2° of the GC and which have either 12 μm or 25 μm flux > 8 Jy. Taylor, Morris and Schulman (TMS, 1992, *AJ*, 106, 1978) previously observed 97 of 342 candidate sources. We have observed 160 more and plan to complete the survey in early 1995.

2. Results

54 new masers in the direction of the GC have been detected. The resulting sample contains both SFRs and circumstellar masers, which are distinguished by IR colors and by 22 GHz spectra. We have adopted the color criterion of TMS, which was validated by comparison to independent identifications. The survey sample also contains both masers located in the GC and relatively local masers lying along the line of sight to the GC. These two populations are distinguished by assuming that high-velocity (>30 km/s) sources in the direction of the GC are participating in the high

L. Blitz and P. Teuben (eds.), Unsolved Problems of the Milky Way, 343–344.
© 1996 *International Astronomical Union.*

velocity dispersion of the inner galaxy. The populations overlap at 0 km/s. 19 of the detected masers are in the high-velocity population.

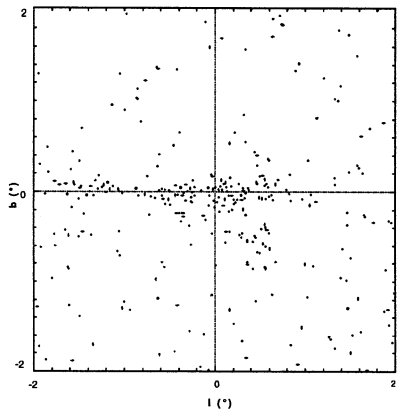

Figure 1–Distribution of IRAS Candidates

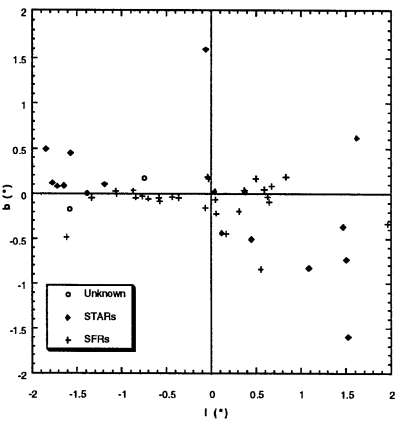

Figure 2–Distribution of Masers

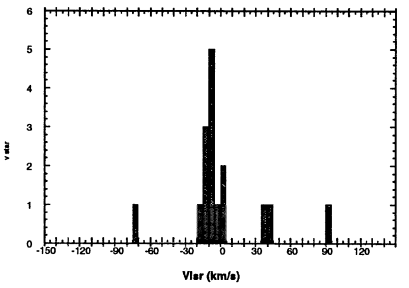

Figure 3–Velocity histogram for Circumstellar Masers

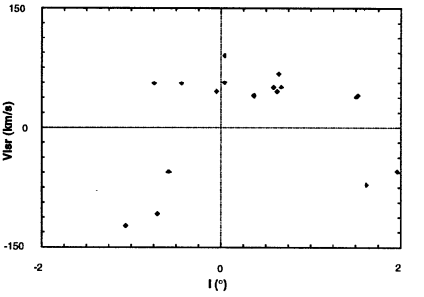

Figure 4–Longitude vs velocity for high-velocity masers

3. Conclusions

We note that there appears to be an offset in the peak of the circumstellar velocity histogram from 0 km/s, of about -13 km/s. Deguchi (1995, *these proceedings*) noted a similar offset in the Nobeyama SiO maser survey. This may represent motion of the local standard of rest, which would be a useful and sensitive diagnostic of Milky Way bar geometry (Weinberg, 1995, *these proceedings*).

If we continue with a similar detection rate for the remainder of the survey, we will have a final sample of 75 H_2O masers in the survey region, $\sim$32 of which are expected to be GC sources.

The resulting sample will provide valuable information about the mass distribution at the GC, GC star formation, H_2O maser luminosity functions, molecular cloud velocity dispersion, motion of the LSR and bulk motion of the material along the line-of-sight to the GC.

DYNAMICAL PROPERTIES OF GALACTIC OH/IR STARS

M. N. SEVENSTER, R. A. ARNOLD, L. O. SJOUWERMAN
Sterrewacht Leiden,
Postbus 9513, 2300 RA Leiden, The Netherlands

1. Introduction

An OH/IR star is an intermediate mass AGB star which loses mass and is optically obscured by its envelope. Such stars can be detected in the infrared and by radio maser lines. In particular the OH line (1612 MHz) is bright and has a distinctive profile, that allows us to determine the radial velocity of the central star. OH/IR stars are excellent tracers for the study of Galactic dynamics because they are bright, unaffected by extinction in the OH line – and therefore visible throughout the Galaxy – and because they represent a wide range of stellar masses. The outflow velocity of the circumstellar shell is most likely driven by radiation pressure from the central star on the dust. Therefore outflow velocity increases with stellar luminosity and metallicity, and decreases with age.

We have selected two samples of OH/IR stars for our present study. The first, the Central sample, is a set of 149 stars from Lindqvist *et al.* (1992). The second sample consists of 700 stars selected from IRAS PSC and observed by te Lintel Hekkert *et al.* (1991), covering the Galactic bulge and the better part of the galactic disc.

2. Kinematic properties

There is clear evidence of galactic rotation in both samples. One of the primary objectives of this study is to construct a model which can account for the velocity distribution of the two sets. In figure 1 we show the correlation of the observed rotation – measured by the product $v_c\ell$ – and the circumstellar shell expansion velocity $v_{\rm exp}$. We have ranked the stars in the two samples in order of increasing expansion velocity and plotted rank along the abscissa. The cumulative sum of $v_c\ell$ is plotted on the ordinate. If a star appears at upper right or lower left in figure 1(a) then $v_c\ell$ is positive

L. Blitz and P. Teuben (eds.), Unsolved Problems of the Milky Way, 345–346.
© 1996 *International Astronomical Union.*

– in which case it is rotating in a prograde sense – and in the other two quadrants the product $v_c\ell$ is negative. In both samples the set of stars with low expansion velocities does not have a strong rotation about the Galactic center, and the cumulate hovers near zero. At high expansion velocities however, the cumulate climbs steadily, indicating that it is primarily these stars which are responsible for the rotation seen in figure 1. The outflow velocities are significantly higher among the Central sample stars than those in the IRAS sample. The transitions of behavior in figure 1 occur at about 17 km/s for the Central stars and at 13.5 km/s for the IRAS stars.

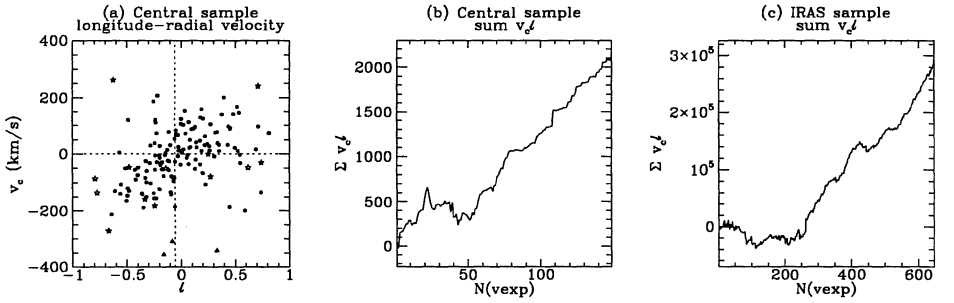

Figure 1. (a) Distribution of line of sight velocity v_c and Galactic longitude ℓ for the Central sample. (b) Cumulate sum of $v_c\ell$ plotted against $v_{\rm exp}$ rank for the Central sample and (c) for the IRAS sample.

Global dynamical distribution functions, derived from axisymmetric orbital components (Dejonghe 1989), show a compact, fast rotating circular disc in the Central sample. The IRAS sample contains an isotropic bulge distribution and a weak rotating component. In order to improve the kinematic constraints on the models we are extending the sample of OH/IR stars in the region $|l| < 45°$ and $|b| < 3°$, and in addition measuring proper motions for stars near the center.

If stars in the center are more metal rich than stars of the same age elsewhere and if we assume that expansion velocity is primarily determined by metallicity, then these two samples could have similar ages. Alternatively, the central stars may be genuinely younger than those found in the IRAS sample, in which case one would also expect them to have higher metallicities and higher expansion velocities. Our dynamical results favor the latter scenario.

References

Dejonghe, H., 1989. AJ 343, 242
Lindqvist, M., Habing, H. J. & Winnberg, A., 1992. A&A 259, 118
te Lintel Hekkert,P., Habing,HJ., Caswell,J., Norris,R., Haynes,R. 1991. A&AS 90, 327

SEMIREGULAR VARIABLES IN THE GALACTIC BULGE

M. SCHULTHEIS [1], Y. K. NG [2], J. HRON [1], H. HABING [2]
([1])*Institut für Astronomie, Wien, Austria*
([2])*Leiden Observatory, the Netherlands*

1. Observations[1]

Near Infrared photometry (JHKL'M) of 78 SRVs in field #3 (PG3) of the Palomar Groningen Variable Star Survey ($l = 0°$, $b = -10°$) was obtained at the ESO 1-m telescope, La Silla, Chile.

2. Results

The Bulge SRVs were compared with the Bulge Miras (Blommaert 1992) and the field SRVs (Kerschbaum&Hron 1994). In the (H–K)/(J–H) plane one can see some difference in the colour between the Bulge Miras and the Bulge SRVs. Bulge Miras are slightly redder in H–K and bluer in J–H than Bulge SRVs. The Bulge SRVs cover a wide range in this two colour diagram but are concentrated mainly in the same region as field SRVs. The position of M giants in a (J–H)/(H–K) plot is sensitive to surface gravity, atmospheric extension and chemical abundance. Metal-richer stars get a shift in the (J–H)/(H–K) plane towards bluer J–H and redder H–K. By photometric means there is no metallicity difference between Bulge stars and field stars visible.

In the (J–H)/(K–L) plane the field SRVs are intermediate between the field SRVs and the Bulge SRVs. There is a clear separation between the three groups in K–L as well as in J–H. This is caused partly by a temperature difference as well as a different atmospheric extension (Bessel et al. 1989). The separation in K–L could be enhanced by the different thickness of the circumstellar shell as with longer periods (Miras) the mass loss increases.

[1]supported by ASF project P9638-AST

L. Blitz and P. Teuben (eds.), Unsolved Problems of the Milky Way, 347–348.
© 1996 *International Astronomical Union.*

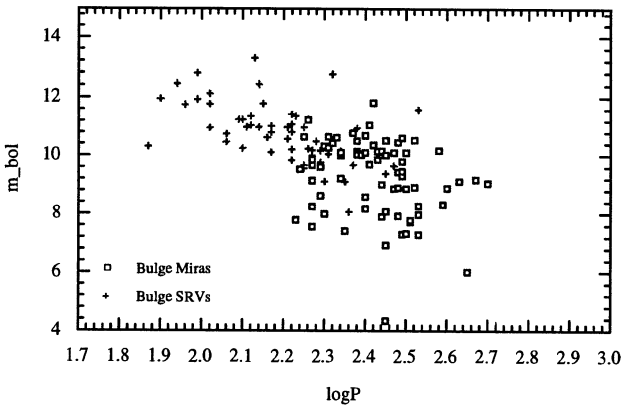

Figure 1. m_{bol} is plotted against logP. The apparent bolometric magnitudes were derived by fitting a blackbody curve through JHKLM. The large scatter for the Bulge Miras can be explained by contamination of foreground stars. By excluding them, Bulge Miras follow the same PL relation as Bulge SRVs

Bulge SRVs and Bulge Miras obey the same P/(J–K) relation, which is slightly above the P/(J–K) relation for Miras in the LMC (Feast 1989). For longer periods the stars are cleary off the relation, because the dust shell becomes dominant. Field SRVs are redder in J–K than Bulge SRVs. In contrast to the Bulge SRVs, the slope of the PC relation for field SRVs is flatter. The same behaviour shows up in a (J–H)/logP diagram where the separation of the three groups is even much clearer.

Bulge Miras as well as Bulge SRVs follow a period-luminosity relation (Fig. 1). This stresses the suggestion that Bulge SRVS are an extension of the Bulge Miras towards shorter periods. The scatter of the Bulge Miras is much higher than for the Bulge SRVs. This is caused by contamination of foreground stars and also by the much higher uncertainties in the determination of m_{bol}. Miras have larger amplitudes than SRVs and the scatter in the bolometric magnitude can reach nearly 1^m.

For all SRVs in PG3 low resolution spectra were obtained. Besides a spectral classification of these stars we are going to obtain radial velocities for these stars in order to compare the kinematics of Bulge SRVs and Bulge Miras.

References

Bessel, M. S., Brett, J. M., Scholz, M., Wood, P. R., 1989, A&A 213, 209
Blommaert J., 1992, thesis Leiden
Feast, M. W., Glass, I. A., Whitelock, P. A., Catchpole, R. M., 1989, MNRAS 241, 375
Kerschbaum, F., Hron, J., 1994, A&A 106, 397

INSTABILITIES OF UNIFORMLY ROTATING DISKS

P. VAUTERIN AND H. DEJONGHE

University of Ghent, Belgium

We explore a series expansion method to calculate the instabilities and the structure of the perturbations for a variety of uniformly rotating finite stellar disks. This survey focuses on the role of the distribution function in stability analyses. Although the potential does not show differential rotation, it will in many cases be a reasonable approximation for the disk in the central regions of galaxies without massive central mass concentration.

1. Method

In order to find normal mode perturbations, we have to find simultaneous solutions for the linearized Boltzmann equation and the Poisson equation. We use a power series expansion in the radius. The velocity coordinates enter as power series as well, choosing stars on circular orbits as the zero point. In addition, the angular and time dependence are combined in a rotating harmonic function. These expansions can be substituted in the linearized Boltzmann equation in order to collect the terms with equal powers, resulting in a linear set of equations for the unknown response. The method (Vauterin & Dejonghe, 1994) is very well suited for uniformly rotating disks, since these do not show any local resonances. Coupling this way of solving the Boltzmann with Hunter's (1963) set of potential-density pairs, self-consistent modes were calculated using a matrix method.

The described scheme can be used to study the stability of a wide variety of uniformly rotating stellar disks. The calculations start with an unperturbed distribution written as a linear combination of (nonintegral) powers of binding energy E and angular momentum J. Most of the unperturbed models which we have studied feature an inert, spherical halo.

L. Blitz and P. Teuben (eds.), Unsolved Problems of the Milky Way, 349–350.
© 1996 *International Astronomical Union.*

2. Results

All examined models which are isotropic in a rotating frame and have a distribution which is everywhere increasing with increasing binding energy were found to be stable, regardless the halo strength or the rotation speed. The simple analytical form of the perturbed distribution allows to quantify the vertex deviation due to the presence of a rotating bar.

We superimposed two components with opposite rotation speeds, which are on themselves stable. The result turns out to be unstable for modes with higher order of symmetry, resulting in somewhat patchy perturbations. Since the individual components are stable for all perturbations, these instabilities are clearly two-stream.

In the self-consistent isotropic case (Maclaurin disk), the distribution is proportional to $E^{-1/2}$. By adding an angular momentum dependence to this distribution, we constructed self-consistent unperturbed models which are not isotropic. The dominating mode, which was perfectly bar-shaped in the isotropic case, now shows a spiral structure. Other inverted models also show spiral instabilities. The disks become more unstable for increasing rotation Ω and increasing disk-to-halo proportion f.

3. Conclusions

It turned out that *the structure of the distribution has a big influence on the stability.* Even the "simple" quadratic potential we applied allows the construction of disks varying from totally stable to violently unstable ones. In addition, *this potential can generate bar instabilities as well as spiral structures.* It is reasonable to assume that most of these instabilities correspond to so-called "edge-modes" (Toomre, 1981).

All of the examined distributions which have an increasing number of stars for increasing binding energy are stable in a quadratic potential, even for a small halo component (some 20 % in mass). This might indicate that disks in the central parts of galaxies (where the potential is almost quadratic) are usually stable.

References

Vauterin, P. & Dejonghe, H., 1994, A & A, in press
Hunter, C., 1963, MNRAS, 126, 299
Kalnajs, A. J., 1972, ApJ, 175, 63
Toomre, A., 1981, Structure and Evolution of Normal Galaxies, eds. S. M. Fall & Lynden-Bell (Cambridge University Press), 111

F(E,L_Z) FOR KENT'S MODEL OF THE GALACTIC BULGE

WALTER DEHNEN
Theoretical Physics
Oxford, OX1 3NP
United Kingdom

Abstract. Using the Richardson-Lucy algorithm the two-integral distribution function (2I-DF) $f(E, L_z)$ for Kent's (1992) Bulge model has been constructed. It turns out to be negative (and hence unphysical) at $L_z \approx L_c$. The physical reason for this result and its implications are discussed.

The even part $f_e(E, L_z)$ of the 2I-DF that creates the axisymmetric density $\rho(R, z)$ is uniquely determined by $\rho(R, z)$ and the potential, but the analytic inversion formulae (e.g. Hunter & Qian 1993) require the knowledge of density and potential outside the physical domain (at complex z), and are numerically unstable, i.e. noise in ρ is amplified into noise in the DF. However, the Richardson (1972) -Lucy (1974) algorithm can be used to fast and accurately compute $f_e(E, L_z)$ for any axisymmetric stellar system, as I showed in Dehnen (1994), where M32 is modeled. Here this method is applied to Kent's (1992) mass model for the Bulge, which consists of a $s^{-1.85}$ cusp inside 0.9 kpc and falls off steeply outside, where

$$s^m = R^m + (z/0.61)^m, \qquad m = 4. \tag{1}$$

The potential is that of Bulge and disk. The 2I-DF comes out to be negative at high angular momenta for all energies. This is independent of the disk, which contributes only marginally to the potential inside the cusp, and of the presence of a central black hole, which affects only the innermost 10 pc.

In order to understand this result, consider the run of density along a potential contour, which for $f = f(E)$ simply is a constant. In case of a boxy density the potential will be rounder, and the "corner" of the boxy ρ-contours creates a peak in the run of ρ along a Ψ-contour, see the Fig. 1. To create this maximum, the 2I-DF has to strongly populate orbits with intermediate $L_z/L_c(E)$. However, these orbits also contribute to, and even

L. Blitz and P. Teuben (eds.), Unsolved Problems of the Milky Way, 351–352.
© 1996 *International Astronomical Union.*

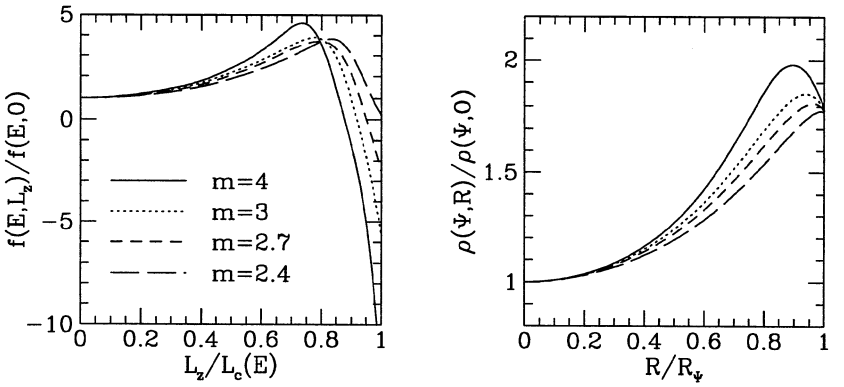

Figure 1. Left: run of the 2I-DF with L_z at the energy of the circular orbit at 100pc. Right: run of ρ along the potential contour of $\Psi(R{=}100\text{pc}, z{=}0)$. The lines correspond to different values of m in eq. (1), $m{=}4$ gives Kent's (1992) model.

overpopulate the density on the equator. Therefore, to gain the correct density there, $f_e(E, L_z)$ has to become negative for near-circular orbits. This is illustrated by Fig. 1 which shows $f_e(E, L_z)$ vs. L_z at fixed E (left) and ρ along a potential contour (right).

The outcome of a negative 2I-DF is an example for the danger in using the Jeans equations for galaxy modeling, which do not tell anything about the physicality of the underlying DF. Kuijken (1994) also found indications for negativity of the 2I-DF for Kent's Bulge model. Another hint comes from Evans' (1994) power-law models, which have spheroidal potentials and boxy densities. Using his model with $\rho \propto r^{-1.85}$, one finds that the 2I-DF is non-physical for axis ratios less than 0.65 (Kent's models has 0.61).

There are three possibilities, to alter the used mass distribution in order to gain a model with physical 2I-DF. As indicated by Evans' (1994) models, a greater axis ratio (i) or a shallower cusp (ii) will certainly help. A less boxy density (iii) should also alleviate the problem. Experiments with smaller powers m in eq. (1) showed, that for a modest boxiness with $m = 2.4$ the 2I-DF is just physical (see Fig. 1). However, physical 2I-DFs with peanut-shaped densities exist, which indicates, that Kent's parametrisation of the boxyness (eq. 1) is a bad choice, as it cannot create a peanut shape.

References

Dehnen W., 1994, MNRAS, submitted
Evans N.W., 1994, MNRAS 267, 333
Hunter C., Qian E., 1993, MNRAS 262, 401
Kent S.M., 1992, ApJ 387, 181
Kuijken K., 1994, preprint
Lucy L.B., 1974, AJ 79, 745
Richardson W.H., 1972, J. Opt. Soc. Am. 62, 55

Chapter 5

How Did the Milky Way Form?

THE AGE STRUCTURE OF THE OLDER PARTS OF THE GALAXY

JOHN E. NORRIS

Mount Stromlo and Siding Spring Observatories
Private Bag, Weston Creek P.O., ACT 2611, Australia

1. Introduction

The history of the Galaxy is encoded in the kinematic, chemical and age profiles of its various populations, and their inter-relationships. Of these, the age structure has proved to be the most problematic. The aim of the present paper is to discuss our understanding of the ages of the various components and to seek to understand the chronology of the system, highlighting along the way some of the unsolved problems.

For the purposes of discussion it is useful to identify the major components. We live in a disk galaxy with a prominent bulge. As we have heard at this meeting the bulge appears to encompass a bar like configuration: indeed, the bulge may be a bar. The masses of disk and bulge appear to be 6 $10^{10}M_{\odot}$ and 1 $10^{10}M_{\odot}$, respectively, and both are embedded in a much more tenuous, luminous, halo, the mass of which is 1 - 3 $10^{9}M_{\odot}$ (Bahcall 1986). The inter-relationship of halo and disk has been one of the driving challenges of the study of stellar populations since their identification by Baade. More recently we have come to appreciate that all of this luminous material is enshrouded in a vast unseen mass of dark matter which will be referred to here, following Schmidt (1985) in an effort to avoid ambiguity, as the dark corona. Many refer to it as the dark matter halo. The mass and extent of this component is not well defined, but current estimates suggest that it extends out to at least 50 kpc from the Galactic center at which point the interior mass is 5 $10^{11}M_{\odot}$ - 1 $10^{12}M_{\odot}$.

In what follows we shall discuss each of these components in turn, returning to their inter-relationships in the final sections.

L. Blitz and P. Teuben (eds.), Unsolved Problems of the Milky Way, 353–366.
© 1996 *International Astronomical Union.*

2. Dark Corona

No direct age determination of the dark corona exists. Current wisdom holds that the luminous parts of galaxies form within the potential wells of large aggregates of dark material which were the initial irregularities in the expanding Universe. As such they would be the oldest structures in the Universe. What remains unclear is how long after the existence of the deep potential well of the dark matter the luminous components first emerged.

Discussion of the formation of the luminous parts of galaxies has centered around two dominant themes. The first postulates a central gravitational contraction or collapse as suggested most persuasively in the context of the Milky Way system by Eggen, Lynden-Bell, & Sandage (1962, hereafter ELS) : "The oldest stars formed out of gas falling towards the galactic center in the radial direction and collapsing from the halo onto the plane. The collapse was very rapid and only a few times 10^8 years were required for the gas to attain circular orbits in equilibrium." The second questions the primacy of the central collapse in determining the observed structures, and postulates that the merging of fragments of material (both gaseous and astrated) plays a large role. Searle & Zinn (1978, hereafter Searle & Zinn) established the counterpoint to ELS with their suggestion for the origin of the halo: "the loosely bound clusters of the outer ... halo originated in transient protogalactic fragments that continued to fall into dynamical equilibrium with the Galaxy for some time after the collapse of its central regions had been completed". The timescale envisaged by Searle & Zinn was a few billion years.

These two themes have been rehearsed and expanded extensively during the past decades. The central collapse, with dissipation, has been modeled by many workers, beginning with Larson (1969) who first addressed the possible lumpy nature of the Galaxy, through to the recent works of Burkert, Truran, & Hensler (1992) who postulate an initial two phase situation involving clouds and intercloud medium, and Katz (1992) who follows the evolution of a disk galaxy in a lumpy medium of dark material. The role of merging of fragments with an already existing disklike Milky Way system is also the center of intense theoretical activity. As well as providing a possible explanation of the outer halo, it had been shown that accretion of fragments will heat an existing disk. The capture of a satellite of mass $0.1M_{disk}$ might be expected to heat the disk to a vertical velocity dispersion of $\sim$ 40 km/s (Quinn, Hernquist, & Fullagar 1993). Accretion of satellites may drive gas from the disk into the central region and trigger starbursts, with implications for the formation and/or modification of the bulge component (Mihos & Hernquist 1994).

What remains to be established is the relative importance of these two

phenomena. Sandage (1990) expresses the opinion "Searle and Zinn is ELS plus noise, all of which is staged within a play by Zurek, Quinn and Salmon, which is on a theme of Larson, after Toomre". Other recent views on the relative importance of the two effects may be found, for example, in Zinn (1993), van den Bergh (1993), and Norris (1994).

3. Halo

The reader will recall the basic parameters of the halo of the Galaxy: it is spatially extended with density decreasing radially as $R_G^{-3.5}$; is kinematically hot ($\sigma_{total} \sim 200$ km/s) with little systemic rotation ($V_{rot} \sim 30$ km/s); and is metal poor (-4 < [Fe/H] < -0.5). Most important for the present discussion, it is old, with 12 Gyr $\leq$ age $\leq$ 18 Gyr.

The determination of the ages of halo material centers almost entirely on the interpretation of the color-magnitude diagrams of globular clusters, and to a lesser extent on Strömgren photometry of near main sequence metal poor and high velocity stars. As is well known, increasing age leads to fainter turnoffs and bluer horizontal branches, and it is these dependencies which have been utilized to determine the age profile of the halo.

3.1. HORIZONTAL BRANCH AGE CONSTRAINTS

The most powerful claims concerning the age structure of the halo come from consideration of the horizontal branch (HB) morphology of the globular clusters. Searle & Zinn (their Figure 10) demonstrated very clearly that HB morphology is a function of Galactocentric distance, and more recently the subject has been closely re-examined by Lee, Demarque, & Zinn (1994, their Figure 7). Inside the solar circle there exists a tight relationship between HB type and [Fe/H] which may be readily explained solely in terms of a range in [Fe/H], while outside, the dependence of HB type on abundance becomes much looser and at a given [Fe/H] the horizontal branches are redder. While HB morphology depends on several parameters, Searle & Zinn put forward the hypothesis that the data were well explained in terms of age variations. They suggested that there was little age spread inside the solar circle (< 1 Gyr) but that outside the sun the clusters were on average younger by a few Gyr and showed an age spread of a similar amount. The synthetic horizontal branch calculations of Lee *et al.* (1994) confirm that the observations can be explained by age differences of order 2-4 Gyr.

The question that has exercised the minds of many workers over the past 15 years is whether age variations provide the only explanation of these observations. What seems clear is that age is not the only parameter affecting HB morphology in the globular cluster system. The classic example of this is NGC 2808 with its very bimodal horizontal branch (see Byun

& Lee 1991, and references therein). There is now, however, fairly convincing evidence that age differences of order 2-4 Gyr exist in the system, based on considerations of the main sequence turnoff. Several independent investigations of the critical pair NGC 288/NGC 362 all conclude that NGC 362 is younger than NGC 288 by 2-3 Gyr as might be expected from their HB morphologies (Bolte 1989; Green & Norris 1989; Sarajedini & Demarque 1990; VandenBerg, Bolte, & Stetson 1990). And while evidence is growing that the bulk of the clusters may be coeval to within 2-3 Gyr (see e.g. Figure 3 of Buonnano *et al.* 1994) there are currently four distant clusters with ages some 4 Gyr below average : Pal 12 (Stetson *et al.* 1989), Ru 106 (Buonnano *et al.* 1990), and Arp 2 and Terzan 7 (Buonanno *et al.* 1994).

The basic question for the hypothesis of Searle & Zinn, at least in the view of the present author, is not whether age is the only parameter affecting HB morphology. Rather, the question is this: is age the parameter which dominates the behavior of HB morphology as a function of Galactocentric distance. There are two independent pieces of evidence which support the contention that it is. The first is the result of Chaboyer, Sarajedini, & Demarque (1992, their Figure 3) who determine ages based on the luminosity of the main sequence turnoffs of globular clusters and find that on average clusters inside the solar circle are younger than those outside this limit, by some 2 Gyr. They also demonstrate (their Figure 5) that in the range -1.75 $\leq$ [Fe/H] $\leq$ -1.25 HB type is a function of age. The second point is that Marquez & Schuster (1994), using ages determined from Strömgren photometry of metal poor near turnoff stars, demonstrate that when age is plotted as a function of apogalactic distance, material with apogalacticon outside 10 kpc is younger on average by $\sim$ 2 Gyr than that inside this value.

3.2. MAIN SEQUENCE TURNOFF AGE DETERMINATIONS

There are several approaches to age determination from main sequence globular cluster photometry. One involves the fitting of the full turnoff region to stellar evolution isochrones. See, for example, the study of 47 Tuc by Hesser *et al.* (1987). A second, differential, method (Sarajedini & Demarque 1990; VandenBerg *et al.* 1990) involves comparison of the color difference between main sequence turnoff and subgiant branch at fixed abundance with model calculations. The third, and perhaps most widely used, method involves determination of the luminosity difference between the horizontal branch and main sequence turnoff, and assumptions about the luminosity of the horizontal branch in order to derive the luminosity of the turnoff which, from a theoretical viewpoint, is the best indicator of age. In what follows I shall refer mainly to the results of the second and third approaches, referred to as the $\Delta(B-V)_{TO,RGB}$ and ΔV(TO-HB) methods, respectively.

3.2.1. *Results from the ΔV(TO-HB) Method*
There is currently little concensus on the ages of the globular clusters determined with the ΔV(TO-HB) method, driven by disagreement on the dependence of the luminosity of RR Lyrae variables on metal abundance. Sandage (1993) favors a value of $dM_v(RR)/d[Fe/H] = 0.30$, and determines the same age, 14 Gyr, for all clusters. In contrast, Chaboyer *et al.* (1992) and Carney, Storm, & Jones (1992), who adopt $dM_v(RR)/d[Fe/H] \sim 0.20$, find an age, metallicity relation among the clusters, with the most metal poor objects being 2-4 Gyr older than the most metal rich. At [Fe/H] = -1.5, Chaboyer *et al.* report an age of 14 Gyr, while Carney *et al.* report values of 15 and 17 Gyr, depending on which of two assumptions they make regarding the value of [O/Fe]. Not all of the news, however, is bleak. This is a tractable problem. With the determination of horizontal branch magnitudes for globular clusters of different abundance in the Andromeda galaxy with HST much of this uncertainty will be resolved.

Uncertainty in the values of other physical parameters propagates into age uncertainties. Table 1 shows very roughly some of the effects. Given our understanding of the various parameters, it seems reasonable to suggest that our knowledge of cluster ages is uncertain at the 2-3 Gyr level.

TABLE 1. Sensitivity of Ages based on ΔV(TO-HB) (Age $\sim$ 14 Gyr, [Fe/H] $\sim$ -1.3)

Parameter	Δ(Parameter)	Δ(Age)
$[Fe/H]$	+0.2	-0.7
ΔV(TO-HB)	+0.1	+1.5
$[O/Fe]$	+0.3	-1.0
$[\alpha/Fe]$ (includes O)	+0.3	-1.5
Diffusion	On	-0.3
Rotation	On	Unimportant
Y	+0.03	-0.4

3.2.2. *Results from the $\Delta(B-V)_{TO,RGB}$ Color Method*
The color method has also yielded important results. VandenBerg *et al.* (1990) have presented evidence that at [Fe/H] = -2.1 the age spread appears to be less than 0.5 Gyr. They also report that there is a scatter in age which increases with increasing metallicity: at [Fe/H] = -1.3 they find a real spread of $\sim$ 2 Gyr. The importance of this clue cannot be overemphasized. We comment on one possible interpretation in §7.

3.3. ROLE OF ACCRETION/MERGERS

Given that the age spread is real, what does this tell us about the evolution of the Galaxy. There now seem to be many workers offering support for the general concept of accretion as advocated by Searle & Zinn, albeit to different degrees. Lin & Richer (1992) argue that Ru 106 may have been captured from the Large Magellanic Cloud. Zinn (1993) has presented a case for subsystems of old and young globular clusters, while van den Bergh (1993) has also identified subgroups in the halo cluster system, and suggested a past merger with a small galaxy to explain the systematics of the situation. Other observations consistent with the concept of relatively recent merger events are the young, blue metal poor stars discovered by Preston, Beers, & Shectman (1994), and the recently discovered dwarf spheroidal galaxy in Sagittarius reported by Ibata, Gilmore & Irwin (1994), which appears currently to be experiencing the merging process.

3.4. HALO SUMMARY

While there is no universal consensus on the age structure of the halo, the author's view is as follows. (a) The inner halo (R_G < 8 kpc) shows little evidence for an age spread (Δ(age) < 1 Gyr). Current best estimates suggest a mean age of 15 $\pm$ 2 Gyr. (b) The outer halo shows a real age spread ($\sim$ 2-4 Gyr), and appears to be younger on average than the inner halo by $\sim$ 2 Gyr. (c) There is evidence that the age spread increases with increasing [Fe/H]. (d) A significant part of the halo has been accreted, some at least of which appears to be relatively young.

4. Disk

For the purposes of the present discussion it is useful to recall that the disk density distribution is exponential in both the radial and vertical direction. The disk is kinematically cool and supported by rotation, with metallicity spanning the range -1.5 < [Fe/H] < 0.2, though it should be noted that the lower limit quoted here is still the subject of debate. Stars of all ages, up to that of the halo, are present in the disk. Here we shall consider only material older than a few Gyr.

The large range of properties of the disk has led to the description of its sub-populations in terms of young/old, metal-weak/metal-poor, and thick/thin (e.g. 'the' old disk, 'the' thick disk, metal-poor thick-disk stars). Many workers think in terms of a thick and a thin component, while others think in terms of an extended, continuous, configuration. It terms of the thick/thin description, which provides a useful working model, the relevant parameters in the solar neighborhood are:

TABLE 2. Parameters of the Thin & Thick Disks

Parameter	Thin	Thick
Relative proportion	1	0.02 to 0.10
$[Fe/H]$	-0.4 to +0.2	-1.5 to -0.4
Kinematics	$\sigma_z \sim 20$ km/s	$\sigma_z \sim 45$ km/s
	$V_{rot} \sim 220$ km/s	$V_{rot} \sim 180$ km/s
Scale height	300 pc	900-1300 pc

The relationship between the disk and halo is of considerable interest. Work over the past decade has established fairly convincingly that there is a fairly sharp transition between the metal poor, slowly rotating halo and the metal rich, rapidly rotating disk. See for example Carney, Latham & Laird (1990, Figures 2 and 3) and references therein. With the realization, however, that the halo may contain subcomponents (Zinn 1993; van den Bergh 1993; Norris 1994) one should be alive to the possibility that part of the material traditionally associated with the halo by virtue of its low abundance may in fact be connected in a complicated way with the disk.

Table 3 presents various age estimates for the older material of the disk. The most interesting fact about its age structure is that current estimates suggest that at the solar circle the *bulk* of the disk is significantly younger than the ~15 Gyr of the halo inside the solar circle. Note in particular the values in Table 3, clustering around 10 Gyr, determined from the white dwarf luminosity function, the chromospheric age indicators of local dwarfs, and the oldest open clusters. In some contrast, most results for the metal poorer, kinematically hotter material, which one associates with the thick disk, suggest ages not too different from that of the halo. Note here the disk globular cluster 47 Tuc and the results for the high proper motion stars.

The case of the disk globular clusters needs special emphasis. For 47 Tuc, which has [Fe/H] = -0.7 and R_G = 6 kpc, the results of Carney *et al.* (1992, with [O/Fe] = -0.3), Chaboyer *et al.* (1992) and Sandage (1993) yield an age of 13.9 Gyr, which is only 1.4 Gyr younger than the halo clusters inside the solar circle for which they have also determined ages. While one has to worry a little about possible systematic errors in these estimates, driven by abundance differences, one might hope that the differential result between disk and halo is not greatly in error. Apart from 47 Tuc, little information is available and there is an urgent need for more work on the age profile of the disk globular clusters. One should note the recent work of Fullton & Carney (1994) on NGC 5927, 6352, and 6723, and their intriguing result that the most metal-rich one (NGC 5927) is younger that the others by 3-5

TABLE 3. Age Estimates of the Disk

Method/Sample	Age	Comment
Globular cluster 47 Tuc	14 Gyr	R_G = 6 kpc
White Dwarf Luminosity Function (Winget *et al.* 1987, Wood 1992)	9.3 ± 2 Gyr	Bulk of disk locally
Chromospheric Ages (Barry 1988)	≤ 11 Gyr	Bulk of disk locally; calibrated with age(NGC 188) = 8 Gyr
Old open clusters (Demarque *et al.* 1992)	≤ 9 Gyr	Age(NGC 6791) = 9 Gyr caveat: clusters easily destroyed
Th/Nd ratio in stars (Butcher 1987)	≤ 10-12 Gyr	Beware Co I contamination. Lawler *et al.* (1990) find 15-20 Gyr
Red giants at z = 1-3 kpc (Norris & Green 1989)	< Age(47 Tuc) by several Gyr	Solar vicinity, no kinematic bias
High proper motion stars (Carney *et al.* 1989)	≥ Age(47 Tuc) to within 3 Gyr	Kinematically biased sample
Strömgren Photometry: (Edvardsson *et al.* 1993a,b)	Relatively few stars older than 10-12 Gyr formed in solar nbd. Small component with 12 < Age < 18 Gyr	Sample biased on abundance Ages accurate to 20%
(Marquez & Schuster 1994)	Thick disk stars younger than halo by 1-2 Gyr	Beware systematic differences driven by [Fe/H] difference

Gyr. This problem should be solved soon (at least from the point of view of obtaining the necessary high quality data) by observations with HST.

The results of recent Strömgren photometry based age investigations are also of considerable importance. While the Edvardsson *et al.* (1993a,b) sample of solar neighborhood dwarfs contains stars which appear to be as old as the halo clusters, they conclude that when one considers where the stars originated and the metallicity bias of the sample there are very few old stars in the sample and that "one might wonder whether disk stars formed this far from the galactic center more than 10-12 Gyr ago". A second particularly important result for the age chronology of the disk is their finding that [α/Fe] as a function of [Fe/H] depends on the place

of origin of stars in their sample: at [Fe/H] = -0.8 to -0.4 they report that stars which formed closer to the Galactic center appear more enriched in the α elements, suggesting that star formation and chemical enrichment occurred over a shorter period towards the center and proceeded more sedately further out.

The reader should note also that the question of the relative ages of thick disk and halo remains unresolved. Differences of 0-3 Gyr (in the sense of the thick disk being younger) appear not inconsistent with the observations, but it seems unlikely that the difference can be greater than this.

4.1. DISK SUMMARY

Inside the solar circle there appears to be only a small age difference between the oldest disk material and the halo. Thick disk material may be younger by $\sim$ 1-3 Gyr at most. On the other hand, the bulk of the material in the solar neighborhood appears younger than the halo by 4-5 Gyr. This is surely suggestive of an hiatus between an early epoch of star formation and the bulk of star formation in the solar neighborhood.

5. Bulge

The Galactic bulge is an agglomeration of populations with an extremely complicated age structure, which is not yet understood. As well as being the intersection of the halo and disk, there is now evidence that the center of the Galaxy contains a bar, and indeed perhaps what we refer to the bulge is really a bar. For a description of the bulge and its properties the reader is referred to Dejonghe & Habing (1993), and Rich in these proceedings. Here I shall say only a few words on some age determinations.

The existence of RR Lyrae stars at the Galactic center demonstrates that at least part of the bulge is old. Indeed, Lee (1992) has argued from the abundance distribution of the RR Lyraes in the bulge, in comparison with their distributions at larger Galactocentric distances, that they are older than the inner halo globular clusters by 1.3 Gyr. This has led him to support an inside-out chronology for the formation of the Galaxy.

Studies of K giants in the Galactic center, which presumably are representative of a significant amount of material there, suggest that the bulk of the bulge may be quite young. The work of McWilliam and Rich (1994) is particularly important in this regard. From a high resolution abundance analysis of 11 bulge giants they have recalibrated the abundance distribution of the bulge, and readdressed the significance of the relative blueness of its the color-magnitude diagram. They report: "use of our abundance scale ... suggests that the Frogel and Whitford (1987) infrared H-R diagram requires that the mean mass of the Baade's window giants can be no less than

about $1.1M_{\odot}$". From such a large mass one infers a significantly younger age than that of the disk globular clusters of similar metal abundance - presumably by several Gyr.

This result is supported by the work of Holtzman *et al.* (1993), who have analyzed HST based color-magnitude and luminosity function data which reach to below the bulge main-sequence turnoff for a region in Baade's Window. While these authors were commendably cautious in view of problems associated with the spatial distribution, photometric zero-points, abundance, and reddening of the material they were sampling, they were forced to the conclusion: "The location of the break in the luminosity function suggests that there are a significant number of intermediate age (< 10 Gyr) stars in the Galactic bulge."

The work of McWilliam and Rich (1994) is important in a second area. As emphasized by Matteucci and Brocato (1990), the dependence of [α/Fe] on [Fe/H] depends strongly on the rate and duration of star formation. If, for example, star formation in the bulge was an efficient and very rapid process one might expect relatively higher values of [α/Fe] (say 0.5) for [Fe/H] >-0.5 compared with values [α/Fe] < 0.1 found in the solar neighborhood. Unfortunately the data of McWilliam & Rich (their Figure 20) on the α elements is inconclusive on this point: for whereas Mg and Ti are suggestive of such a phenomenon, Si and Ca are not. Nevertheless, with more data for a considerably larger sample, strong constraints on the timescale for the formation of the bulge should be possible.

6. Order of Events

The observational data discussed in the preceding sections suggest the following chronology.

The bulk of the halo inside the solar circle, and part of the bulge, formed relatively quickly some 15 Gyr ago. This seems to have happened within 1 Gyr, and may have occurred as envisaged by ELS. The bulk of the outer halo assembled a little later, by $\sim$ 1-2 Gyr, over a longer time, $\sim$ 2-4 Gyr. Accretion of fragments played an important role in the outer halo, and continues to the present time, as shown by the capture of the Sagittarius dwarf spheroidal galaxy, apparently currently under way. A large part of the outer halo probably assembled as suggested by Searle & Zinn. The halo contained $\sim$ 1/30 of the mass to which the disk would grow.

A disk with <[Fe/H]> $\sim$ -0.6 existed inside the solar circle within 1-2 Gyr of the formation of the inner halo. (Witness the disk globular cluster population and the thick disk in the solar neighborhood. More work is, however, urgently needed on the age profile of the disk globular cluster population.) The disk at this stage contained $\sim$ 1/10 of the mass to which

it would eventually grow.

At the solar circle the bulk of the disk formed 4-5 Gyr after the inner halo and the oldest disk stars. The work of Edvardsson *et al.* (1993a) on [α/Fe] versus [Fe/H] indicates that the disk formed from the inside out.

The bulge remains a challenge. It contains material as old as, and probably older by $\sim$ 1 Gyr, than the inner halo. Current best estimates (by no means definitive) suggest that a large fraction of the bulge is relatively young ($\sim$ 10 Gyr), but much work is needed to place this on a firm footing.

7. Cosmogony

If the above chronology is correct, it suggests that some marriage of central contraction (ELS) and later accretion (Searle & Zinn) will explain the halo and disk observations. Some interesting questions, however, remain. What happens to the enriched gas (several times the mass of the stars which have formed [see eg Hartwick 1976]) and the supernova energy which escaped the star forming regions of the halo and thick disk. Carney *et al.* (1990) and Wyse & Gilmore (1992) suggest that the halo ejecta go to form the bulge, and similarly that the thick disk ejecta form the thin disk. An important possibility which has its origins with Berman & Suchkov (1991) and Burkert *et al.* (1992) is that the energy output during this phase completely ionized the remainder of the protogalaxy, precluding further star formation for a few Gyr. In the Burkert *et al.* two phase model (clouds, intercloud medium) the ionized material is heated to 2 10^{6}°K and is chemically enhanced to [Fe/H] = -1.5. If more globular clusters form in the second epoch of star formation this could contribute to an age, metallicity relation in the halo (as claimed by Chaboyer *et al.* 1992, and Carney *et al.* 1992), and to an age dispersion, metallicity relation similar to that reported by VandenBerg *et al.* (1990). Note that we now have two processes competing to explain the age spread in the halo - successive generations and accretion.

How seriously should one take the apparent hiatus of 4-5 Gyr between formation of the inner halo, thick disk, old bulge, on the one hand, and the bulk of the disk in the solar neighborhood, on the other. One possibility is that the evolutionary ages of the globular clusters have been overestimated, and their real age is $\sim$ 10 Gyr. While this has a certain attractiveness in the cosmological context, we shall not discuss it further, except to note that if this is the case some revision to basic ideas of stellar evolution will be necessary. Assuming the reality of the age difference we make four comments. First, we refer the reader to the work of Mathews & Schramm (1993) who present a model of the halo forming while the protogalaxy was still expanding as part of the general expansion of the Universe, with disk formation occurring some 4-5 Gyr later after the system had turned around

and contracted significantly. The small difference in age $\sim$ 1-2 Gyr discussed here between the thick disk material and the halo may prove difficult for this scenario. Second, it is interesting that the Carina dwarf spheroidal galaxy presents a nice example of a system with two main epochs of star formation at $\sim$ 6 and >10 Gyr (see Smecker-Hane *et al.* 1994). Hiatuses do happen! Third, the ionization concept of Berman & Suchkov (1991) mentioned above leads naturally to periods with little star formation. Fourth, perhaps the observed age difference is just the time that it takes the bulk of the disk to grow outwards, as suggested by models such as those of Larson (1976).

The implications of the age structure of the bulge and its bar are far from clear. By definition, the models of Larson (1976) contain a bulge which forms dissipatively over a period of a few Gyr. In counterpoint to this, as noted in §2, minor mergers provide an interesting way of moving gas from the disk into the bulge (Mihos & Hernquist 1994) and may have contributed to its development, while they also have the propensity to thicken disks. It is then important to note the growing observational evidence that there is no kinematic gradient in the thick disk (Soubiran, 1993; Onja *et al.* 1994), which tends to favor a merger rather than a dissipational origin of the thickening, and to recall the association made between bulges and thick disks by van der Kruit & Searle (1981), who first claimed that one generally accompanies the other. (There seems, however, to be some disagreement about the reality of the connection. On the one hand, Shaw & Gilmore (1990) have presented data which argues against it, while Morrison *et al.* (1994), on the other, implicitly appear not to accept this more recent result.) If bulges and thick disks are causally connected it may be that merger events play a role in the establishment of both.

References

Bahcall, J.N. 1986, ARA&A, 24, 577
Barry, D.C. 1988, ApJ, 334, 436
Berman, B.G. & Suchkov, A.A. 1991, Ap. Space Science, 184, 169
Bolte, M. 1989, AJ, 97, 1688
Buonanno, R., Buscema, G., Fusi Pecci, F., Richer, H.B., & Fahlman, G.G. 1990, AJ, 100, 1811
Buonanno, R., Corsi, C.E., Fusi Pecci, F., Fahlman, G.G., & Richer, H.B. 1994, ApJ, 430, L121
Burkert, A., Truran, J.W., & Hensler, G. 1992, ApJ, 391, 651
Butcher, H.R. 1987, Nature, 328, 127
Byun, Y.-I. & Lee, Y.-W. 1991, The Formation and Evolution of Star Clusters, ed. K. Janes (ASP Conf.Ser. 13), 243
Carney, B.W., Latham, D.W., & Laird, J.B. 1989, AJ, 97, 423
Carney, B.W., Latham, D.W., & Laird, J.B. 1990, AJ, 99, 572
Carney, B.W., Storm, J., & Jones, R.V. 1992, ApJ, 386, 663
Chaboyer, B., Sarajedini, A., & Demarque, P. 1992, ApJ, 394, 515
Dejonghe, H. & Habing, H.J. eds. 1993, IAU Symposium 153, Galactic Bulges (Dordrecht

: Kluwer)
Demarque, P., Green, E.M., & Guenther, D.B. 1992, AJ, 103, 151
Edvardsson, B., Andersen, J., Gustafsson, B., Lambert, D.L., Nissen, P.E., & Tomkin, J. 1993a, A&A, 275, 101
Edvardsson, B., Gustaffson, B., Nissen, P.E., Andersen, J., Lambert, D.L., & Tomkin, J. 1993b, preprint
Eggen, O.J., Lynden-Bell, D., & Sandage, A.R. 1962, ApJ, 136, 748 (ELS)
Frogel, J.A. & Whitford, A.E. 1987, ApJ, 320, 199
Fullton, L. & Carney, B.W. 1994, poster paper presented at IAU Symposium 164, Stellar Populations
Green, E.M. & Norris, J.E. 1989, ApJ, 353, L17
Hartwick, F.D.A. 1976, ApJ, 209, 418
Hesser, J.E., Harris, W.E., VandenBerg, D.A., Allwright, J.W.B., Shott, P., & Stetson, P.B. 1987, PASP, 99, 739
Holtzman, J.A., Light, R.M., Baum, W.A., Worthey, G., Faber, S.M., Hunter, D.A., O'Neil, E.J. Jr, Kreidl, T.J., Groth, E.J., & Westphal, J.A. 1993, AJ, 106, 1826
Ibata, R.A., Gilmore, G., & Irwin, M.J. 1994, Nature, submitted
Katz, N. 1992, ApJ, 391, 502
Larson, R.B. 1969, MNRAS, 145, 405
Larson, R.B. 1976, MNRAS, 176, 31
Lawler, J.E., Whaling, W., & Grevesse, N. 1990, Nature, 346, 635
Lee, Y.-W. 1992, AJ, 104, 1780
Lee, Y.-W., Demarque, P., & Zinn, R. 1994, ApJ, 423, 248
Lin, D.N.C. & Richer, H.B. 1992, ApJ, 388, L57
Marquez, A. & Schuster, W.E. 1994, A&A, in press
Mathews, G.J. & Schramm, D.N., 1993, ApJ, 404, 468
Matteucci, F. & Brocato, E. 1990, ApJ, 365, 539
McWilliam, A. & Rich, R.M. 1994, ApJS, 91, 749
Mihos J.C. & Hernquist, H. 1994, ApJ, 425, L13
Morrison, H.L., Boroson, T.A., & Harding, P. 1994, AJ, 108, 1191
Norris, J.E. 1994, ApJ, 431, 645
Norris, J.E. & Green, E.M. 1989, ApJ, 337, 272
Ojha, D.K., Bienaymé, O., Robin, A.C., & Mohan, V. 1994, A&A, 284, 810
Preston, G.W., Beers, T.C., & Shectman, S.A. 1994, AJ, 108, 538
Quinn, P.J., Hernquist, L., & Fullagar, D.P. 1993, ApJ, 403, 74
Sandage, A. 1990, JRASC, 84, 70
Sandage, A. 1993, AJ, 106, 719
Sarajedini, A. & Demarque, P. 1990, ApJ, 365, 219
Searle, L. & Zinn, R. 1978, ApJ, 225, 357
Schmidt, M. 1985, in IAU Symposium 106, The Milky Way Galaxy, ed. H. van Woerden, R.J. Allen, & W.B. Burton (Dordrecht : Reidel), 75
Soubiran, C. 1993, A&A, 274, 181
Shaw, M.A. & Gilmore, G. 1990, MNRAS, 242, 59
Smecker-Hane T.A., Stetson, P.B., Hesser, J.E., & Lehnert, M.D. 1994, AJ, 108, 507
Stetson, P.B., VandenBerg, D.A., Bolte, M., Hesser, J.E., & Smith, G.H. 1989, AJ, 97, 1360
VandenBerg, D.A., Bolte, M., & Stetson, P.B. 1990, AJ, 100, 445
Van den Bergh, S. 1993, ApJ, 411, 178
Van der Kruit, P.C. & Searle, L. 1981, A&A, 95, 116
Winget, D.E., Hansen, C.J., Liebert, J., van Horn, H.M., Fontaine, G., Nather, R.E, Kepler, S.O., & Lamb, D.Q. 1987, ApJ, 315, L77
Wood, M.A. 1992, ApJ, 386, 539
Wyse, R.F.G. & Gilmore, G. 1992, AJ, 104, 144
Zinn, R. 1993, in The Globular Cluster - Galaxy Connection, ed. G.H. Smith & J.P. Brodie (ASP Conf. Ser. 48), 38

DISCUSSION

I. King: I know that it's not fair to blame you for the hypothesis that the disk has been puffed up by mergers, but I wonder how you would reconcile this idea with the fact that the thick disk (as evidenced by 47 Tuc) seems to be older than the thin disk.

Norris: he age results show that the disk is thick only for ages greater than 10 Gyr, so the concept of mergers thickening the disk presumably applies to events which happened early in the life of the Galaxy.

K. Freeman: Are you convinced (regarding the hiatus between thin and thick disk etc.) that Edvardsson *et al* and others are on the same age scale.

Norris: No. Edvardsson *et al* quote an error of 20% for their ages. What does impress me, however, is that the white dwarf luminosity function result has stood the test of time now in spite of many efforts to increase the ages. Also, almost all of the diverse methods of age dating of the bulk of the disk in the solar neighborhood report $\sim$ 10 Gyr. This contrasts quite strongly with the 14 Gyr which stellar evolution methods yield for 47 Tuc.

A. Gould: The ages scale inversely with the adopted RR Lyrae luminosities. Have you accounted for this when comparing relative ages.

Norris: Each of the three groups whose ages I quoted employ a consistent treatment of the RR Lyrae luminosities as a function of [Fe/H]. Without knowing which formulation is correct, it doesn't make much sense to seek to make a correction.

F. Matteucci: If there was a big time interval between the halo and disk formation during which star formation stopped one should expect a signature of that in the abundance ratios. In particular, one should expect a decreasing trend for [α/Fe] ratios due to the fact that Fe continues to be produced during the absence of star formation whereas the αs are not.

Norris: That's clearly an important test. A comparison of data such as those of Edvardsson *et al.* with the predictions of models of disk formation should be able to constrain the extent of the hiatus.

IS THE DYNAMICAL HISTORY AT ODDS WITH THE CHEMICAL HISTORY?

F. MATTEUCCI
Dipartimento di Astronomia, Universita' di Trieste
Via G.B. Tiepolo, 11 TRIESTE

1. Formation and Evolution of the Galaxy as suggested by the correlation between abundances and kinematics

The paper of Eggen, Lynden-Bell and Sandage (1962)(hereafter ELS) titled "Evidence from the motion of old stars that the Galaxy collapsed" was the first attempt to understand the formation and evolution of our Galaxy. From a study of a kinematically selected sample of high velocity stars, ELS had found a remarkable correlation between chemical abundance and orbital eccentricity, in the sense that stars with the largest ultraviolet excess (a measure of stellar metallicity, in particular Fe), i.e. the lowest metallicity, are invariably moving in highly elliptical orbits. As the average $< [Fe/H] >$ (in the usual notation $[Fe/H] = log(Fe/H)_* - log(Fe/H)_\odot$)is expected to increase with time, as a consequence of the progressive chemical enrichment of the gas, stars with the lowest [Fe/H] are, on average, the oldest. ELS also found a correlation between abundance and motion of stars perpendicular to the Galactic plane. This correlation suggests a continuous decrease of the perpendicular velocity with decreasing [Fe/H]. To explain these relations ELS proposed that the Galaxy collapsed from a protocloud to a thin disk on a timescale of a few times 10^8 years, with progressive chemical enrichment as the collapse proceeded. This model was subsequently criticized mainly because of selection effects in their data, i.e. given the data available to ELS one would not expect the sample to contain low abundance, low orbital eccentricity objects even if they existed. They would be absent from the high velocity catalog they used. In addition, the ELS simple model did not account for the fact that almost half of the halo stars have retrograde orbits . This fact led Larson (1969) to consider models of clumpy and turbulent protogalaxies with collapse times that sometimes exceeded 1 Gyr.

L. Blitz and P. Teuben (eds.), Unsolved Problems of the Milky Way, 367–379.
© 1996 *International Astronomical Union.*

Searle and Zinn (1978) expressed a different point of view relative to ELS as a result of their studies of the globular cluster system of the Galaxy. First they found no gradient in metallicity in the globular clusters at galactocentric distances greater than 10 Kpc. However this observation per se does not argue against the rapid collapse proposed by ELS, since a metallicity gradient is favored by a slow dissipative collapse. The second point was the problem of the Horizontal Branch morphology in globular clusters, i.e. the fact that it appears to be a function of galactocentric distance. This was attributed to age differences implying that globular clusters in the outer halo have an age spread of a couple of billion years, whereas those of the inner halo have a spread in age of less than 1 Gyr. They also claimed that for halo abundances ($[Fe/H] < -1.0$) there is no dependence of the kinematics on abundance for subdwarf samples when all the velocity components are considered. Therefore, they proposed a major modification of the ELS picture in which as well as a central collapse they envisaged gaseous fragments in the outer halo which remained distinct and experienced their own star formation and chemical evolution over a relatively long period before falling into equilibrium with the inner Galactic regions. In this way, one should expect no gradient and no correlation between kinematics and abundance as well as an age spread for the globular cluster population of the outer halo.

Yoshii and Saio (1979), analysing a large sample of stars, concluded that the kinematics can be better explained by a slow collapse model, with the collapse lasting $3 \cdot 10^9$ years.

Later, Gilmore and Reid (1983) and Gilmore and Wyse (1985) have suggested the existence of a possible third major component of the Galaxy. This third component was called *thick disk*. This component, which possesses some properties of the disk subsystem of globular clusters discussed by Zinn (1985), was excluded by ELS since they used catalogs containing only samples of the kinematic extremes.

Sandage (1987) and Sandage and Fouts (1987) contested the view of Searle and Zinn (1978). They presented new kinematically selected data obtained to increase the ELS sample. The new feature, not contained in ELS, was the large population of intermediate velocity stars. This component has a metallicity distribution intermediate between that of the old thin disk (e-folding scale height of $\simeq 270pc$) and the extended halo (scale height $\simeq$ 3.2 Kpc) and an e-folding scale-height of 920 pc. The mean metallicity of the thick disk is [Fe/H]=-0.6 dex, whereas that of the halo is -1.5 dex and that of the thin disk -0.1 dex. They identified this component as the thick disk of Gilmore, Reid and Wyse. The main conclusion of Sandage was that the addition of the thick disk to the thin disk and halo changes the details of ELS picture but not its essential substance. The conclusions

of Sandage were again in contrast with those of Searle and Zinn and Norris (1986) who claimed no correlation between metallicity and kinematics below [Fe/H]< -1.0, while he instead found a continuous correlation. If Sandage is correct the chemical evolution of our Galaxy can be thought of as caused by separate processes or as part of a continuum which has different enrichment rates per unit gas mass relative to the collapse rate as a function of time. In the beginning the collapse must have been rapid with a very small energy dissipation rate, then the dissipation increased thus decreasing the collapse rate. The metal enrichment went up and so the ratio between the collapse and enrichment rate flattened thus giving higher metallicity per unit mass in stars in the flattened structures (thick disk and thin disk). Each component will therefore have a different average metallicity, chemical gradient and metallicity distribution.

On the other hand, in agreement with the previous study of Norris (1986), Ryan and Norris (1991) concluded from a kinematical study of metal poor stars that their data are not consistent with a model in which the halo formed from star formation in a dissipating collapsing cloud, unless the kinematics have since been modified by unstable orbits or violent relaxation. They suggest a picture in which numerous independently evolving clouds formed the halo stars, similar to Larson's (1969) early suggestion.

Therefore, a word of caution is in order concerning the interpretation of these kinematical data in terms of Galaxy formation mechanisms and timescales. As Gilmore et al. (1989) have pointed out, the presence or absence of a correlation between rotation velocity and stellar metallicity does not really allow one to distinguish between fast and slow collapse models of the Galaxy. So while we may learn something about the importance of energy dissipation and the efficiency of violent relaxation, the timescales enter the interpretation of the relation between rotational velocity and metallicity only by assumption.

Before trying to reach a conclusion about the halo formation we should, however, discuss another independent clock for establishing the timescale of the halo collapse, and this is given by purely chemical arguments, as will be seen in the next paragraph.

2. Formation and Evolution of the Galaxy as suggested by abundance ratios

An independent way of deducing the timescale for the halo collapse is to look at the evolution of abundance ratios determined for stars in the solar vicinity. In recent years, a great deal of observational work has been devoted to the study of the chemical abundances in solar neighbourhood stars. In particular, in the last ten years the development of efficient spectrom-

eters combined with powerful linear detectors have revolutionized stellar spectroscopy. At the same time, theoretical model atmosphere and synthetic spectrum calculations have been considerably improved, especially with improved treatment of the line blanketing by atoms and molecules. The claimed error in the derived abundances have decreased from roughly $\simeq$ 0.3 dex (a factor of 2) down to $\simeq$ 0.05 dex in the most recent studies (Edvardsson et al., 1993).

A particularly useful abundance ratio is that between α-elements and Fe since the α-elements (i.e. those synthesized from α particles such as O, Ne, Mg, Si and S) are almost entirely produced by massive short living stars ($M > 10M_{\odot}$ and lifetimes in the range 10^6-10^7 years) exploding as type II SNe, whereas Fe is produced both by type II supernovae (SNe) and by SNe of type Ia which are believed to originate from white dwarfs in binary systems (the lifetimes go from 10^7 to 10^{10} years and more). The most popular models for the progenitors of type Ia SNe all involve white dwarfs in binary systems which reach the Chandrasekhar mass limit by accretion from either another white dwarf or a red giant. Because of the time delay in the bulk of production of iron relative to the α-elements, the abundance ratio [α/Fe] can be used as a cosmic clock. Let us take oxygen as representative of α-elements. One can infer the timescale of the halo collapse and formation by looking at the observed [O/Fe] vs. [Fe/H] relation for solar neighbourhood stars. This relation shows a plateau extending roughly up to [Fe/H]=-1.0 (which is also the transition metallicity from halo to disk stars) and then the [O/Fe] ratio declines until it reaches the solar value. If we have a Galactic chemical evolution model following the evolution of single chemical abundances and we are able to reproduce the observed relationship, then we know at which time the gas has reached the metallicity -1.0 and this is the timescale for the formation of the halo, under the assumption that the various Galactic components formed in a continuous process. The theoretical [O/Fe] vs. [Fe/H] relation depends on the assumed SN progenitors, stellar nucleosynthesis and star formation history. For this reason, the observed abundance patterns, when compared to theoretical models, can constrain SN progenitors, nucleosynthesis and star formation. Chemical evolution models (Matteucci and François, 1992) suggest this timescale to be not longer than 1-1.5 Gyr. In particular, Matteucci and François (1992) tried to reproduce the change in slope of [O/Fe] vs. [Fe/H] relation at [Fe/H]$\simeq$-1.7, as claimed by Bessel et al. (1991). They presented models assuming different star formation laws and concluded that the data are best reproduced by a model where the star formation rate depends almost linearly upon the surface gas density. In this case the time necessary to reach the halo-disk transition metallicity [Fe/H]=-1.0 is between 1 and 1.5 Gyrs. On the other hand, if star formation has a quadratic dependence on

the surface gas density (Schmidt law) then this time scale is only $3 \cdot 10^8$ years and the change in slope in the predicted [O/Fe] vs. [Fe/H] relation occurs not before [Fe/H]=-1.0. Therefore, it is extremely important to have detailed abundance ratios involving oxygen and the other α-elements especially in halo stars. This timescale of 1-1.5 Gyr is longer than that inferred by ELS but is still too low to explain the age-gap of 3-4 Gyr claimed for the globular clusters by Bolte (1987). However, Vanden Bergh et al. (1990) have shown that most of the halo population of globular clusters should be coeval with a fraction of the more metal rich clusters showing ages which are perhaps 2-3 Gyr younger. More recently, Buonanno et al. (1994) showed that four globular clusters are unequivocally younger by 3-4 Gyr than others of similar metallicity and they are all at galactocentric distances larger than 20 Kpc, and concluded that is possible that they have all been accreted by the Milky Way since they are all on similar orbits. The same age spread seems to be suggested also for halo field stars (subdwarfs) (Schuster and Nissen, 1989). These authors found an age-metallicity relation for halo stars indicating a difference of $\simeq$ 3 Gyr passing from [Fe/H]=-3.0 to -2.0. If this result is real and is not affected by systematic errors, it is favoring a coherent very slow dissipative collapse of the halo. However, a time scale of the order of 2-3 Gyr is clearly at variance with that deduced from the [O/Fe] vs. [Fe/H] ratio. In order to have such a slow halo collapse there should be a much more restricted region of constant [O/Fe] for halo stars. In fact, if the halo collapse time is longer than 3 Gyr then SNe Ia had time to restore the bulk of Fe, since the characteristic time scale for this restoration is $\simeq$ 1 Gyr, and the change in the slope in the observed [O/Fe] should occur at much lower metallicities than observed([Fe/H]=-1.0 – -1.5), as has been shown by Matteucci and Brocato (1990). Recently Marquez and Schuster (1994) seem to find that there is not an age-metallicity relation in halo stars as found before, and that the inner part of the halo is older and with less age spread than the outer one, thus confirming the inside out scenario.

Another aspect of the [O/Fe] vs. [Fe/H] relation, which might be in contrast with the *chaotic scenario* of Searle and Zinn, is the small spread around [Fe/H]=-1.0. In fact, if the halo or part of it were the result of random evolution of independent clouds, we should perhaps expect a larger spread in the [O/Fe] ratio in halo stars, especially because of the different metallicities at which the change in the [O/Fe] ratio would occur in the different clouds (Wyse and Gilmore, 1993).

These discrepancies could be eliminated if we think not in terms of a unique timescale for the halo collapse but assume that the inner halo evolved more rapidly than the outer halo, and that the chemically derived timescale refers mostly to the inner halo, due to the fact that the halo stars

observed in the solar region are mostly those born inside the solar circle (Grenon 1987). This agrees with the fact that the observed spread in the age of globular clusters refers only to objects belonging to the outer halo. Recently, Zinn (1993) has suggested that the inner old halo clusters could have formed during a collapse not unlike the ones proposed by ELS, Larson (1976) or Sandage (1990) and Katz (1992), whereas the younger outer halo clusters could have formed in satellite systems that were accreted by the Galaxy. In the best model of Matteucci and François (1992) collapse timescales increasing with galactocentric distance are assumed. As a consequence, they predict that both halo and disk take longer to form in the outermost regions. In particular, they estimate from the chemical argument that the extreme outer halo should have formed in 3-4 Gyr as compared to the 1-1.5 Gyr predicted for the inner halo.

At present, most of the abundance data refer to stars in the solar neighbourhood, although recently abundances in disk stars at different galactocentric distances in the Galactic plane have become available. In principle, the analysis of the [α/Fe] vs. [Fe/H] curves for different galactocentric distances could give us an idea about the evolutionary rate in different Galactic regions.

The recent paper by Edvardsson et al. (1993) shows evidence for the [α/Fe] ratio in metal poor disk stars ([Fe/H]< -0.4) to be smaller in stars at larger galactocentric distances. This fact also suggests that the Galaxy must have evolved less rapidly in the outer regions than in the inner ones. In such a case, in fact, it has been predicted (Matteucci, 1992) that the [α/Fe] ratio would start decreasing at lower metallicities than in the inner regions where instead a longer plateau extending also to disk metallicities should be expected. Another claim of the paper of Edvardsson et al. is the existence of a big spread in the age-[Fe/H] relationship, which is larger than the spread observed in the [α/Fe] ratios. Several explanations have been proposed to explain this spread:

a) orbital diffusion combined with abundance gradients, i.e. some of the stars we observe now in the solar vicinity region have been born at different galactocentric distances where the chemical evolution had proceeded at different rates than in the solar region. In particular, the most metal deficient stars are those with the highest probability of having been born far away from the solar region. This can be the consequence of the diffusion of their orbits which amplifies the orbital eccentricity. Orbital diffusion may be the consequence of scattering of stars by molecular clouds, by massive black holes coming out of the Galactic halo, by density wavelets and their oscillations in the Galactic disk and by infalling disrupting satellite galaxies. The evidence for orbital diffusion comes from the observed relation between age and stellar velocity dispersion (Wielen 1977; Wielen et al., 1992).

b) Discontinuous infall of primordial material,

c) local chemical inhomogeneities,

d) overlapping of stars belonging to different populations (halo, thick and thin disk) which evolved simultaneously but at different rates.

Concerning orbital diffusion coupled with abundance gradients, François and Matteucci (1993) have suggested that most of the spread observed by Edvardsson et al. in the [Fe/H] vs. age as well as in the [α/Fe] vs. [Fe/H] relations can be due to the fact that some of the stars we observe at the present time in the solar neighbourhood might have been born in different regions of the Galactic disk and perhaps even in the Bulge. They assumed that the amplitude of the stellar orbits increases with the square root of their age (Wielen and Fuchs, 1985), and that the Galaxy formed from inside out, i.e. with collapse rate and star formation rate decreasing with increasing galactocentric distance. Edvardsson et al. (1993) have criticized this explanation of their data by arguing that they do not see any trend of an increasing velocity dispersion with age in the interval 3-10 Gyr, thus concluding that the heating of the disk saturates at a dispersion of about 20 km/sec after 3 Gyr. However, in this context one has then to find a different heating process for the thick disk stars, which are at least 10 Gyr old with a velocity dispersion of 40 km/sec. Their main argument is, however, that the spread does not change when one considers stars restricted to the solar circle. Their argument is as follows: since the mean galactocentric radius of the orbit does not change much during the history of the disk one should expect a smaller scatter for the solar circle stars if orbital diffusion was important. On the other hand, Fuchs et al. (1994) using Edvardsson et al.'s data and other data on local stars concluded that the velocity dispersion increases continuously with the stellar age, in very good agreement with predictions from the theory of orbital diffusion. In addition, by assuming an Fe gradient in the disk of the order of -0.1dex/kpc they found very good agreement between the observed and predicted spread in [Fe/H]. In addition, they argued that the assumptions concerning the mean orbital galactocentric distance cannot be used to trace past positions, since, while statistically the mean orbital galactocentric distance (i.e. the average between the pericentric and apocentric distance) is equal to its present value, there is an ever increasing probability looking backwards in time of scattering events from nearby orbits into the present one.

Concerning the overlapping of stars belonging to different Galactic components, Pardi et al. (1994) calculated a model for the chemical evolution of the solar neighbourhood region where the three components, halo, thick and thin disk were considered. The three components evolve at different rates but they are connected through gas flows, in the sense that during the halo formation gas is lost to form the thick disk which then accumulates

with a time delay relative to the halo. The thin disk forms with an even longer time delay since they assumed a progressively longer timescale for the formation of the different components. However, while the timescale for the formation of the thick disk is similar to that of the halo since the gas lost from the halo goes directly to form the thick disk, the difference between the thin disk and the halo, on the other hand, is larger since the rate of formation of the thin disk depends only on the gas lost from the thick disk. Thus the thick disk is an intermediate step which allows one to separate the halo from the thin disk evolution. As a result of this the thin disk forms out of already enriched material and on a timescale as long as 3-4 Gyr thus ensuring a fit to the G-dwarf distribution. In addition, this model predicts that the [O/Fe] vs. [Fe/H] relation is not unique but is given by the convolution of the [O/Fe] vs. [Fe/H] relations for each Galactic component. In other words, this kind of model assumes an evolution *in parallel*, as opposed to an evolution *in series* as in the model of Matteucci and François. In particular, no spread at low metallicities is predicted whereas for [Fe/H]> -1.0 a spread of the order of 0.3-0.4 dex is found. The reason for this spread resides in the fact that the chemical evolution of the gas in the halo and in the thick disk continues until the present time although the amount of star formation becomes negligible after 2 Gyr in the halo and after 8 Gyr in the thick disk. Therefore, very few halo stars for [Fe/H]>-1.0 and very few thick disk stars for $[Fe/H] > -0.5$ are predicted, so that they cannot explain all of the observed spread but probably part of it. A weakness of this model is represented by the thick disk which forms too quickly to fit well the metallicity distribution of thick disk stars, indicating that an even larger time delay between halo and thick disk formation is required. The physical reason for such a delay is the progressive increase of energy dissipation as the collapse proceeds.

3. Abundance gradients and the formation of the galactic disk

The existence of abundance gradients of O, N, Si and S along the galactic disk is shown by abundance measurements in HII regions (see Wilson and Matteucci, 1992 for a review). The existence of an iron gradient, on the other hand, is shown by stellar photometric studies of open clusters and from spectroscopic studies of late type supergiants. These gradients show that the chemical abundances decrease towards the outermost Galactic regions. From a theoretical point of view abundance gradients can be explained under different assumptions, but one of the most realistic is that the disk formed from inside out, in the sense that the star formation rate and the collapse rate were higher in the central than in the external parts. As a consequence of this, the external regions of the Galaxy may still be

collapsing now. Therefore, these different evolutionary rates create the differences in the abundances, due to the different age-metallicity relations in the different Galactic regions. This conclusion agrees with chemo-dynamical Galactic models (Burkert et al. 1992) and with the recent data from Edvardsson et al. (1993).

Concerning the time scale for the formation of Galactic disk in the solar vicinity, chemical models (Matteucci and Tornambè 1985; Matteucci and François 1989; Ferrini et al. 1992) suggest a value of the order of 3-4 Gyr. This value comes from fitting the G-dwarf distribution in the solar neighbourhood. In fact, the well known G-dwarf problem, i.e. the lack of metal poor disk stars in the solar neighbourhood relative to the predictions of the simple model, can be solved by assuming a slow dissipative formation of the disk. An even longer timescale (4-6 Gyr) is suggested by the chemodynamical models of Burkert et al. (1992). Unfortunately, Burkert et al. did not study the formation of the halo, but started from a hot protodisk and followed only the subsequent dissipative formation of the thick and thin disk.

4. Chemical evolution of the Galactic bulge

In the past, the formation and evolution of the Galactic bulge has not received much attention as the formation of the halo and the disk, perhaps because halo and bulge were considered as a single spheroidal component. Now we have evidence suggesting that the bulge might have evolved independently of the halo and this evidence is in the form of chemical and kinematical studies of the bulge stellar populations.

The Milky Way bulge is a region within 1kpc from the center, where a metal rich, rotationally supported stellar population resides. Rich (1988) determined [Fe/H] for 88 K giants in Baade's window and showed that the central stellar bulge of the Milky Way is a distinct stellar population with an age of the order of 10 Gyr and abundance range from -1.5 to +1.0 dex with a peak between +0.15 and +0.3 dex. This result was later confirmed by Geisler and Friel (1992). This stellar distribution is easily reproduced by models assuming a fast ($\simeq$ 0.5 Gyr) formation time for the bulge (Matteucci and Brocato, 1990). These same models predict that most of the stars should show enhanced α-elements relative to iron.

This result is due to the nucleosynthesis scenario presented before, coupled to the assumption of a rapid star formation and collapse.

Alternatively, if the Edmunds et al. (1991) suggestion that the [O/Fe] trend in the solar vicinity can be due to a secondary-like behaviour of Fe, in the sense that the Fe abundance increases with metallicity, then we should expect the metal rich Bulge stars to show low [O/Fe] ratios.

Recently, McWilliam and Rich (1994) measured abundance ratios in metal rich stars in the bulge and, although these measures need to be confirmed, they showed that elements such Mg seem to be overabundant with respect to iron (i.e. [Mg/Fe]>0), thus indicating that the timescale for the collapse of the Bulge must have been shorter than in the solar neighbourhood.

If this is true it implies that the Galactic bulge is older than the solar vicinity region and it again points to the conclusion that the Milky Way should have formed from inside out. Another important aspect of the McWilliam and Rich results is that the [Fe/H] abundances are all systematically lower by 0.25-0.3 dex than the abundances given for the same stars by Rich (1988). One of the reasons for this could be that Rich (1988), who derived [Fe/H] from the magnesium index M_{g_2}, had assumed [Mg/Fe]=0.0 in his stars. These lower [Fe/H] indicate that the Galactic bulge is not as metal-rich as previously thought and that the average [Fe/H] is roughly solar. Since the peak of Rich's (1988) distribution at +0.3 dex led Matteucci and Brocato (1990) to conclude that a flatter IMF than in the solar neighbourhood was required, this new result might mean that there is no necessity for claiming a different IMF in the bulge.

A very recent study by Minniti (1993) has shown that there is a correlation between kinematics and metallicity in Bulge stars, in the sense that the more metal-poor stars seem to have higher velocity dispersion and lower rotational velocity than the metal-rich population. On the basis of his results together with the existence of a Bulge metallicity gradient he concludes that the Bulge formed by dissipational collapse. As a consequence of this he argues that the Bulge should be younger than the halo. On the other hand, Renzini (1994) has argued that the existing data are consistent with the bulk of stars in the Bulge being at least as old as globular clusters stars.

5. Conclusions

It is still difficult to draw firm conclusions on the formation and evolution of our Galaxy. The dynamical and chemical evidence shown in the previous paragraphs give some idea of the complexity of the problem but they do not allow to distinguish between different hypotheses. Although we all agree that the formation of the Galactic disk must have been slow and dissipative, there is not a clear understanding about the timescale for the formation of the halo. Chemical arguments suggest that the halo collapse was fast, i.e. not longer than 1.5–2.0 Gyr, whereas dynamical and kinematical arguments alone do not allow one to understand this timescale. Estimates of the age of globular clusters together with the morphology of the Horizontal Branch

suggest that the globular clusters of the outer halo have an age spread of 3-4 Gyr. Can this be taken as a probe of long collapse time for the whole halo? Perhaps there was a different mechanism of formation operating in the inner and the outer halo, in the sense that the inner halo might have formed on a short timescale of the order of the chemical one, thus confirming a picture similar to that proposed originally by ELS, whereas the outer one could have formed in a more chaotic way by accretion of external material as suggested by Searle and Zinn (1978), or just more slowly. In order to better understand these issues we would need more data on abundance ratios and metallicities especially for halo stars since the chemical method of dating the halo is less ambiguous than the kinematical information.

In conclusion, by considering all the kinematical and chemical information available on the halo, disk and bulge, it seems to us that the most likely picture for the formation of our Galaxy is the *inside out* model, where the Galaxy collapsed differentially, being faster in the innermost regions. This model can in fact explain the abundance gradients in the Galactic disk, the metallicity distribution and abundance ratios in the Bulge, the possible age spread in globular clusters as well as the observed spread in the abundances of disk stars.

References

Bessel, M.S., Sutherland, R.S., Ruan, K. (1991) *Ap. J.*, 383, L7
Bolte, M. (1987) *Ap. J.*, 319, 760
Buonanno, R., Corsi, C.E., Fusi Pecci, F., Fahlam, G.G., Richer, H. (1994), *Ap. J. Lett.*, 430, 121
Burkert, A., Truran, J.W., Hensler, G. (1992) *Ap. J.*, 391, 651
Edmunds, M.G., Greenhow, R.M., Johnson, D., Kluckers V., Vila, M.B. (1991) *M.N.R.A.S.* 251, 33P
Edvardsson, B., Andersen, J., Gustafsson, B., Lambert, D.L., Nissen, P.E., Tomkin, J. (1993) *A.A.*, 275, 101
Eggen, O.J., Lynden-Bell, D., Sandage, A.R. (1962) *Ap. J.*, 136, 748
Ferrini, F., Matteucci, F., Pardi, C., Penco, U. (1992) *Ap. J.*, 385, 138
François, P., Matteucci, F. (1993) *A.A.*, 280, 136
Fuchs, B., Dettbarn, C., Wielen, R. (1994) *Ergodic Concepts in Stellar Dynamics*, eds. D. Pfenninger and V.G. Gurzadyan (Springer-Verlag)
Geisler, D., Friel, E.D. (1992) *Astron. J.*, 104, 128
Gilmore, G., Reid, N. (1983) *M.N.R.A.S.*, 202, 1025
Gilmore, G., Wyse, R.F.G. (1985) *Astr. J.*, 90, 2015
Gilmore G., Wyse, R.F.G., Kuijken, K. (1989) *Evolutionary Phenomena in Galaxies*, eds. J.E. Beckman and B.E.J. Pagel, (Cambridge University Press), p.172
Grenon, M. (1987) *J. Astrophys. Astr.*, **8**, 123
Katz, N. (1992) *Ap. J.*, 391, 502
Larson, R.B. (1969) *M.N.R.A.S.*, 145, 405
Larson, R.B. (1976) *M.N.R.A.S.*, 176, 31
Marquez, A., Schuster, W.J. (1994) preprint
Matteucci, F., Brocato, E. (1990) *Ap. J.*, 365, 539
Matteucci, F., François, P. (1992) *A. A.*, 262, L1
Matteucci, F., François, P. (1989) *M.N.R.A.S.*, 239, 886

Matteucci, F., Tornambè, A. (1985) *A. A.*, 142, 13
Mc William, A., Rich, R.M. (1994) *Ap.J. Suppl.*, 749
Minniti, D. (1993) *Ph.D. Thesis, Steward Observatory, University of Arizona*
Norris, J.E. (1986) *Ap. J. Suppl.*, 61, 667
Pardi, C., Ferrini, F., Matteucci, F. (1994) *Ap. J.*, in press
Renzini, A. (1994) *A.A.*, 285, L5
Rich, R.M. (1988) *Astron. J.*, 95, 828
Ryan, S.G., Norris, J.E. (1991) *Astron. J.*, 101, 1835
Sandage, A. (1987) *The Galaxy*, eds. G. Gilmore and B. Carswell, (Reidel, Dordrecht), p.321
Sandage, A. (1990) *J.R.A.S.C.*, 84, 70
Sandage, A., Fouts, G. (1987) *Astron. J.*, **93**, 74
Schuster, W.J., Nissen, P.E. (1989) *A.A.*, 222, 69
Searle, L., Zinn, R. (1978) *Ap. J.*, 225, 357
VandenBergh, D.A., Bolte, M., Stetson, P.B. (1990) *Astron. J.*, 100, 445
Wielen, R. (1977) *A.A.*, 60, 263
Wielen, R., Fuchs, B. (1985) *IAU N. 106*, The Milky Way Galaxy, eds. H. van Woerden et al., (Reidel, Dordrecht) p.481
Wielen, R., Dettbarn, C., Fuchs, B., Jahreiss, H., Radons, G. (1992) *IAU Symp. 149*, The Stellar Populations of Galaxies, p.81
Wilson, T.L., Matteucci, F. (1992) *Astron. Astrophys. Rev.*, 4,1
Wyse, R.F.G., Gilmore, G. (1993) *ASP Conf. Series N.48*, The Globular Cluster-Galaxy Connection, eds. J.Brodie and G. Smith.
Yoshii, Y., Saio, H. (1979) *Publ. Astron. Soc. Japan*, 31, 339
Zinn, R. (1985) *Ap. J., 293*, 424
Zinn, R. (1993) *ASP Conf. Series No. 48*, The Globular Cluster-Galaxy Connection, eds. J.Brodie and G. Smith, p. 38

DISCUSSION

B. Gustaffson: I wish to clarify that we (Edvardsson et al. 1993) for a given stellar age group and galactocentric mean distance found an astonishingly small scatter in [α/Fe], while the scatter in [Fe/H] is significant, about 0.2 dex. This may be explicable as the result of orbital diffusion and a metallicity gradient in the disk, but that would then imply a gravitational potential field that is varying with time or has a considerable roughness (cf. the poster paper by B. Fuchs and R. Wielen for this symposium).

L. Ozernoy: The phenomenon of high velocity clouds is seemingly consistent with the continuing build-up of the disk. However, it is unclear yet what is the rate of this process. Could you quantify somehow what is the current infall rate onto the Galaxy?

Matteucci: Most of the galactic chemical evolution models are consistent with an average infall rate in the disk now of $\sim 1 M_{\odot}/yr$.

H. van Woerden: *(about high-velocity clouds)[Remark made after Underhill and Gustaffson]* For the role of high velocity clouds (HVCs) in the formation and evolution of the Milky Way disk, the following facts are rel-

evant (cf. poster by Wakker et al. in this Symposium):
1. The mass inflow is of the order of a few solar masses per year.
2. The metallicities of individual HVCs are quite different, ranging at least from 10^{-3} to 10^{-1} times solar. This may include primordial origin, although for some HVCs no metal absorption lines have yet been found.
3. Distances are still unknown for most HVCs, although information is accumulating.
4. Both accretion of intergalactic material and circulation of gas, in a Galactic Fountain may play important roles in the diverse HVC phenomenon in addition to distance and metallicity information, we require models for the dynamics and evolution of HVCs (cf. Wakker 1990, thesis Groningen)

GLOBULAR CLUSTERS AND THE FORMATION OF THE GALACTIC HALO

SIDNEY VAN DEN BERGH
Dominion Astrophysical Observatory
National Research Council
Victoria, B.C., V8X 4M6
Canada

Abstract.

The radii of globular clusters are used to study the early evolution of the Galactic halo. It is found that such cluster radii increase with Galactocentric distance and depend on orbit shape. It is suggested that metal enrichment in the Galactic halo might have been mainly a local phenomenon, whereas cluster radii may have been determined by more global properties of the protogalaxy.

1. Introduction

Present ideas on the formation of the Galaxy and the evolution of the halo were largely shaped by the pioneering papers of Eggen, Lynden-Bell and Sandage (1962) and Searle & Zinn (1978), which will subsequently be referred to as ELS and S&Z. On the ELS picture the entire Galactic halo collapsed rapidly; in which the exact meaning of "rapidly" is explained by Sandage (1990). On the other hand Searle (1977) and S&Z envisage a situation in which halo globular clusters form within a number of more or less isolated fragments before, or during, the initial phases of Galactic collapse. In the S&Z scenario gas masses, clusters and stars of the outer halo continued to fall into the Galaxy for some time after the collapse of its central regions had been completed. The development of this model was influenced by (but not entirely driven by) the discovery that *the globular clusters with* $R_{gc} > 10$ *kpc do not exhibit a radial abundance gradient.*

L. Blitz and P. Teuben (eds.), Unsolved Problems of the Milky Way, 381–388.
© 1996 *International Astronomical Union.*

2. Cluster Radii Versus Galactocentric distance

N-body calculations by Spitzer & Thuan (1972), Lightman & Shapiro (1978) and Murphy, Cohn & Hut (1990) show that the half-light radii r_h of globular clusters change little over periods as long as 10 relaxation times. For many globulars r_h therefore provides information on conditions at the time of cluster formation. Fig. 1 shows a plot of r_h versus R_{gc} from data recently compiled by Djorgovski (1993). The figure shows that r_h for Galactic globulars grows with increasing Galactocentric distance, and that $r_h \propto R_{gc}^{\gamma}$, with $\gamma \approx 2/3$. A similar relation is found for the clusters associated with the Large Magellanic Cloud (van den Bergh 1994). The absence of very extended clusters at small values of R_{gc} might be partly due to destruction of such large objects by Galactic tidal forces. However, the present absence of compact clusters in the outer Galactic halo must be due to the fact that such objects never formed. In other words the data plotted in Fig. 1 suggest that *the Galaxy exhibits a real radial gradient in the dimensions of globular clusters located at* $R_{gc} > 10$ *kpc.* Fig. 1 also shows that clusters with a wide range in metallicity follow similar mean relations between r_h and R_{gc}. The existence of such a relationship, between cluster properties and distance from the Galactic center, is surprising and appears difficult to reconcile with the S&Z picture, in which the properties of halo "fragments" are not expected to depend on their distance from the center of the Galaxy.

Searle (1977) assumes "complete mixing within fragments and no mixing between them". This makes it improbable that proto dwarf spheroidal galaxies should be identified with Searle's fragments. This is so because individual stars within dwarf spheroidals often exhibit a wide range in metallicity. Furthermore van den Bergh (1994) finds that the globular clusters in the Fornax dwarf galaxy have $<r_h> = 3.2$ pc, whereas globular clusters in the outer halo of the Galaxy are much larger having $r_h > 10$ pc. It therefore appears safe to conclude that the globular clusters in the outer halo of the Galaxy did *not* form in "fragments" that resembled proto dwarf spheroidals. This line of reasoning is also supported by the observation that giant carbon stars are rather rare in the Galactic halo (Green *et al.* 1994), but quite common in dwarf spheroidals (Azzorpardi & Lequeux 1992). Van den Bergh (1994) also finds that the majority of the true globular clusters associated with the LMC have $r_h < 10$ pc, and therefore differ from globulars in the outer halo of the Galaxy. This indicates that Searle's "fragments" cannot be identified with objects resembling the proto LMC.

Fig. 2 shows the mean surface brightness of Galactic globular clusters within r_h, as a function of distance from the Galactic center. This figure also appears to show a radial gradient beyond R_{gc}= 10 kpc. Compact clusters with a high central surface brightness are expected to survive preferentially

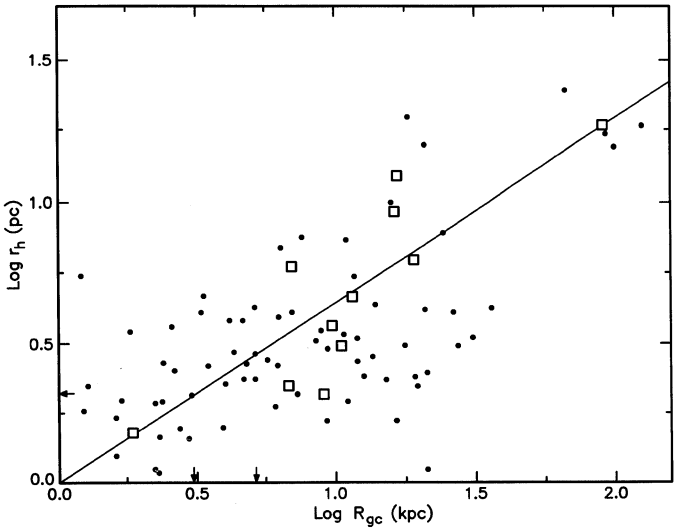

Figure 1. Cluster radius versus Galactocentric distance for globular clusters with -2.0 < [Fe/H] < -1.0 (dots) and [Fe/H] < -2.0 (squares). The fiducial line is the relation log r_h(pc) = 0.65 log R_{gc}(kpc). Clusters in both metallicity ranges appear to scatter about the same r_h versus R_{gc} relation.

in the outer halo. Their absence indicates that such objects were probably never formed in the outer halo of the Galaxy. Figs. 1 and 2 therefore suggest that *the properties of globular clusters, and hence of the "fragments" from which they formed, were a function of Galactocentric distance.*

It is curious that the globular cluster radii at $R_{gc} > R_\odot$ appear to exhibit a radial gradient, while cluster metallicities do not (Searle & Zinn 1978). This conundrum could, perhaps, be resolved by assuming that *metal enrichment in the Galactic halo was predominantly a local phenomenon, whereas cluster radii might have been mainly determined by global properties of the halo of the protoGalaxy.* Powerful UV radiation from a central source might be an example of a phenomenon that would produce mainly global, rather than local, effects.

3. Cluster Radii Versus Orbital Characteristics

Fig. 3 shows a plot of r_h versus R_{gc} for all globular clusters for which this information is given in Djorgovski (1993). The figure shows that clusters on circular orbits (van den Bergh 1993) have systematically larger radii than do other clusters at similar Galactocentric distances. A Kolmogorov-Smirnov test shows that the probability of the clusters in circular orbits

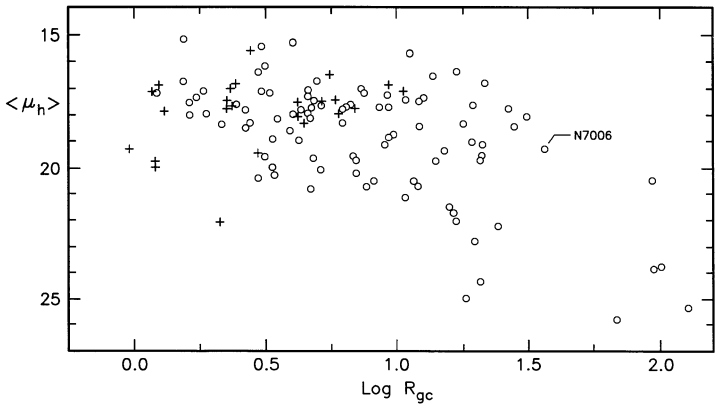

Figure 2. Average surface brightness (corrected for absorption) ¡h¿o, within the half-light radius r_h, versus Galactocentric distance R_{gc}. Clusters with collapsed cores are shown as crosses. Note the absence of high surface brightness clusters at large distances from the Galaxy.

having been drawn from the same parent population of distances from the fiducial line, as the other clusters in Fig. 3, is $< 1\%$. Globulars on circular, or nearly circular, orbits probably have above-average values of r_h because their orbits avoid the dense central regions of the Galaxy where clusters on more elongated orbits have their outer regions trimmed by tidal forces.

Fig. 4 shows that clusters on retrograde orbits (van den Bergh 1993) are, on average, smaller than other globulars. This difference might be due to the fact that many clusters on retrograde orbits dip deeply into the Galaxy, where tidal forces will trim off their envelopes. *Alternatively ram-pressure stripping of gaseous proto globular clusters might have preferentially removed the outer regions of retrograde objects moving through a (mostly prograde) gaseous halo.* On the latter hypothesis (Stetson 1994) one might have expected clusters on retrograde orbits to be fainter than globulars on prograde orbits. This is *not* observed to be the case. For 11 retrograde clusters

$< M_V >= -7.40 \pm 0.25$, compared to $< M_V >= -6.95 \pm 0.63$ for 12 clusters on prograde orbits. A third possibility is that some of the metal-poor clusters in retrograde orbits originally formed in dwarf spheroidal galaxies that were captured into retrograde orbits.

Available observations hint at the possibility that the youngest halo clusters [the α Population of van den Bergh (1993)] may be systematically smaller than other (mostly older) halo globular clusters at similar Galactocentric distances.

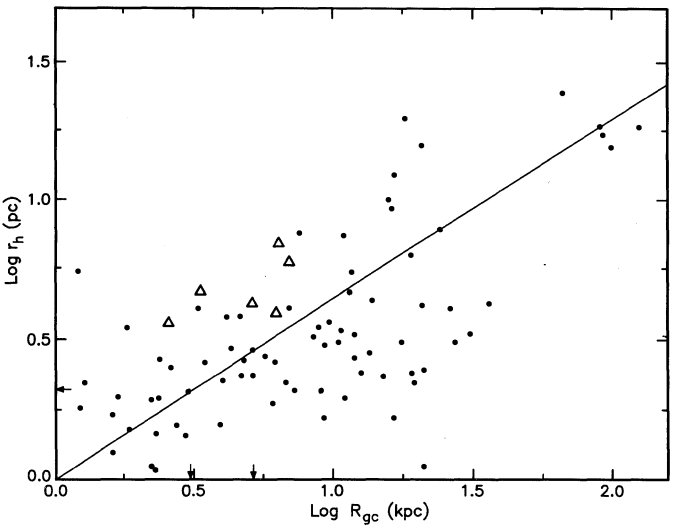

Figure 3. Metal-poor clusters on circular orbits (triangles), are seen to have above-average radii.

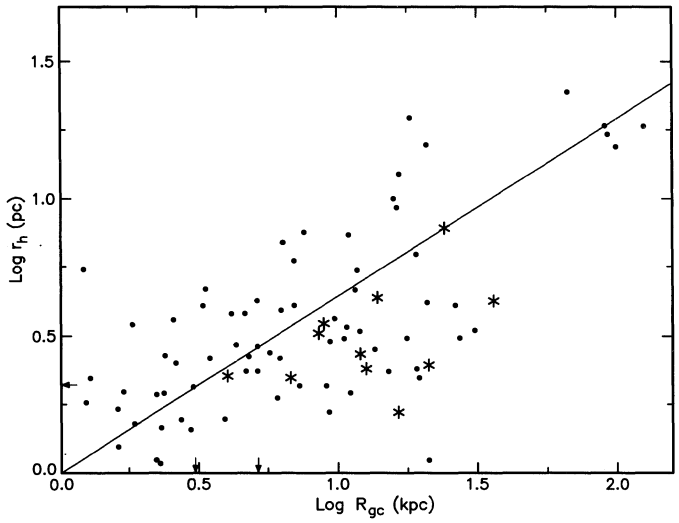

Figure 4. Clusters on retrograde orbits (asterisks) appear to have below-average radii and fall below the mean relation between r_h and R_{gc}.

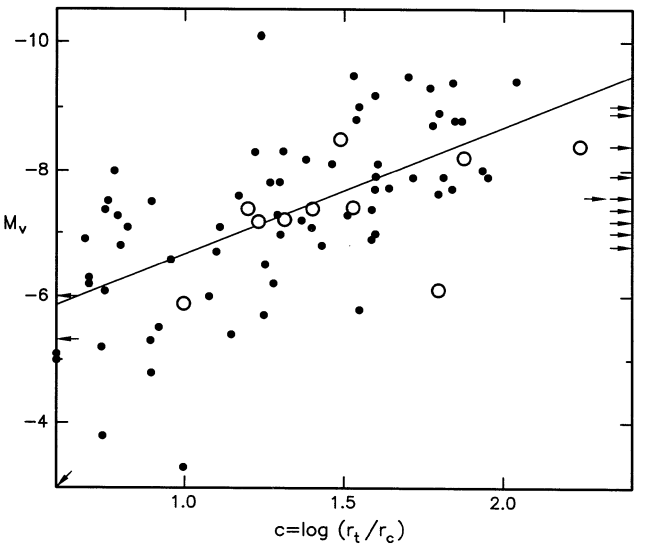

Figure 5. Relation between cluster luminosity MV and central concentration c = log (r_t/r_c). Clusters with collapsed cores, shown as arrows, do not follow this relation. Globulars on retrograde orbits (open circles) are seen to fall close to, or slightly below, the mean relation given by Eqn.(1).

4. Relation Between Structure and Luminosity of Globular Clusters

It was first pointed out by Shapley & Sawyer (1927) that the central concentration of light in globular clusters correlates with luminosity. Fig. 5 shows this same relationship using modern data compiled by Djorgovski (1993). The figure shows that, for clusters which do not have collapsed cores,

$$M_V \sim -4.7 - 2\log(r_t/r_c), \qquad 1$$

in which r_t and r_c are the clusters tidal and core radii, respectively. Van den Bergh (1994) has shown that both true globular clusters and old populous red clusters in the LMC appear to follow Eqn.(1). It is not yet understood why the luminosity (mass) and central concentration of clusters should be so well correlated.

5. Capture of Globular Clusters

Lin & Richer (1992) have argued that the globular clusters Ruprecht 106, and perhaps also Palomar 12, (which appear to be a few Gyr younger than typical halo clusters) were tidally captured from the Magellanic Clouds.

Some data on these two clusters are summarized in Table 1. Pal 12 ([Fe/H] = -1.14) falls outside the range -2.17 [Fe/H] - 1.37 observed for true globular clusters (Suntzeff 1992) in the LMC. With an age > 10 Gyr, Pal 12 is also too old (and too metal-poor) to be related to the old red populous cluster population in the Large Cloud. However, Pal 12 might have been stripped from the SMC, in which clusters with ages of 4 - 12 Gyr are observed to have [Fe/H] $\approx$ -1.3 (Da Costa 1991).

TABLE 1. Properties of Palomar 12 and Ruprecht 106

Cluster	r_c(pc)	[Fe/H]	ΔT(Gyr)
Pal 12	6.2	-1.14	3
Rup 106	5.8	-1.9	4.5

The relatively large core radii (Rodgers & Roberts 1994) of Pal 12 (r_c = 6.2 pc) and Rup 106 (r_c = 5.8 pc) are similar to that of NGC 2257 (r_c = 6.1 pc), which is located 8°.5 from the LMC. The observation that Rup 106 and Pal 12 have radii similar to those of clusters in the inner halo of the LMC [but which are larger than those in the core of the Large Cloud!] is compatible with the stripping hypothesis of Lin & Richer (1992).

References

Azzopardi, M., & Lequeux, J. 1992 in: The Stellar Populations of Galaxies, IAU Symposium No. 149, eds. B. Barbuy and A. Renzini (Kluwer: Dordrecht), p.201
Da Costa, G.S. 1991 in: The Magellanic Clouds, IAU Symposium No. 148, eds. R. Haynes and D. Milne (Dordrecht: Kluwer), 183
Djorgovski, S. 1993 in: Structure and Dynamics of Globular Clusters, ASP Conference Series No. 50 (ASP: San Francisco) p. 373
Eggen, O.J., Lynden-Bell, D., & Sandage, A., 1962, ApJ, 136, 748 (=ELS)
Green, P.J., Margon, B., Anderson, S.F., & Cook, K.H. 1994, ApJ, in press
Lightman, A.P., & Shapiro, S.L. 1978, Rev. Mod. Phys. 50, 437
Lin, D.C.N., & Richer, H.B. 1992, ApJ, 388, L57
Murphy, B.W., Cohn, H.N., & Hut, P. 1990, MNRAS, 245, 355
Rodgers, A.W., & Roberts, W.H. 1994, AJ, 107, 1737
Sandage, A. 1990, JRASC, 84, 70
Searle, L. 1977 in The Evolution of Galaxies and Stellar Populations, eds. B.M. Tinsley and R.B. Larson (Yale Observatory: New Haven), p.219
Searle, L., & Zinn, R. 1978, ApJ, 225, 357 (=SZ)
Shapley, H., & Sawyer, H.B. 1927 Harvard College Obs. Bull, No. 849
Spitzer, L., & Thuan, T.X. 1972, ApJ, 175, 31
Stetson, P.B. 1994, private communication
Suntzeff, N.B. 1992 in The Stellar Populations of Galaxies = IAU Symposium No. 149 eds. B. Barbuy and A. Renzini (Dordrecht: Kluwer), 23
van den Bergh, S. 1993, ApJ, 411, 178

van den Bergh, S. 1994 in preparation

DISCUSSION

K. Freeman: Concerning the comparison of luminosity functions for open and globular clusters: from the work of Weinberg and others, we know that young clusters of lower concentration or flatter mass function will evaporate. So perhaps one should include only clusters with ages greater than say 5×10^7yr in this comparison.

van den Bergh: I agree that both evaporation and interactions with GMCs will lead to the destruction of many low-mass clusters. However, the fact that globulars in very different environments (bulge, disk, halo, M31, giant ellipticals) have similar luminosity functions suggests to me that the faint end of the globular cluster luminosity function is not entirely determined by cluster destruction.

A. Renzini: I'd like to ask a very naive question – In the first picture you have shown the metal rich clusters are very concentrated towards the galactic center, rather than flattening about the Disc, with the vast majority of them physically lying within the Bulge – So, why are they called "Disc" rather than "Bulge" clusters?

van den Bergh: You are quite right! Another example of such poor nomenclature is that Supernovae at Type II belong to Population I.

CHEMICAL AND DYNAMICAL HISTORY OF THE MILKY WAY

I.F.BIKMAEV
Special Astrophysical Observatory, Nizhnij Arkhyz, Karachai-Circassian Republic, Russia, 357147

AND

L.I.MASHONKINA, N.A.SAKHIBULLIN, V.V.SHIMANSKIJ AND N.SHIMANSKAYA
Department of Astronomy, Kazan State University, Lenin Str.,18, Kazan, Russia, 420008

1. Introduction

F-G dwarf stars of different metallicity are used as tracers of chemical and dynamical history of the Galaxy. Observed ratios of element abundances "[X/Fe] versus [Fe/H]" (where "X" is a some of chemical element) are compared with theoretical ones and allow us to make the choice between models (or parameters of theoretical models) of the Galaxy chemical evolution, nucleosynthesis and processes of star formation. Our experience has shown (Bikmaev, 1991, 1994a,b; Bikmaev et al., 1990) that in some cases classical approaches in abundance determination are affected by methodical uncertainties and the spread in [X/Fe] ratios may be large even if high quality spectra used.

Our recent investigation based on: 1) high resolution spectra of 60 stars obtained on the 6-m telescope (Bikmaev, 1987) and carefully selected homogeneous list of published equivalent widths of spectral lines, 2) Kurucz's (1979) grid of model atmospheres and his WIDTH6 program, 3) temperature scale of the Infrared Flux Method and use of infrared (V-K) or red (R-I) color indices for effective temperature determination, 4) trigonometric parallaxes and the "temperature-mass-luminosity" dependence for obtaining surface gravity, 5) non-LTE computations for FeI, BaII, NaI and MgI lines, 6) use of FeII lines for metallicity determinations.

L. Blitz and P. Teuben (eds.), Unsolved Problems of the Milky Way, 389–394.
© 1996 *International Astronomical Union.*

2. Results of non-LTE computations

Deviations from LTE for FeI lines strongly depend on a number of levels in the FeI model atom and an adapted value of cross-section of collisions with hydrogen atoms (Bikmaev et al., 1990, Gehren et al., 1991, Steenbock, 1991). It was found (Bikmaev, 1994b) that problems in FeI-FeII ionization balance, probably, lie out of the classical methods of non-LTE computations using of homogeneous model atmospheres. Therefore, we used FeII lines for iron abundance determination taking into account that they show no any deviations from LTE (Steenbock, 1991) and are insensitive to possible effects of temperature inhomogeneities in the atmospheres of real stars (see Fig.2 of Bikmaev,1994a). Metallicity scale based on the FeII lines has changed for extremely metal-poor stars: a value of [Fe/H]=-2.5 in the classical case when FeI lines used, corresponds to [Fe/H]=-2.0 in our scale (Bikmaev et al., 1990), Figs. 1-8.

MgI lines (excluding 4571 Å and Mgb lines) show small deviations from LTE (0.04-0.12 dex) depending on adapted value of cross-section of collisions with hydrogen atoms. So we used LTE abundances in this study.

It was found (Mashonkina et al., 1993) that only 6154 Å and 6160 Å sodium lines have small (0.05-0.10 dex) non-LTE corrections. All other lines show large negative non-LTE effects (up to -0.3-0.5 dex for NaD and infrared lines in the case of metal-poor stars where they are only measurable in the spectra, see Fig.7).

Note that we used an estimate of the value of positive non-LTE correction for resonance aluminum lines (Fig. 8) from the paper of Gehren et al., 1991. Taking into account large non-LTE effects with a different sign for resonance sodium and aluminum lines solves the problem of a discrepancy in [Na/Mg] and [Al/Mg] ratios found for halo stars (Zhao and Magain, 1990).

All 4 measurable BaII lines show their own range of non-LTE corrections (0.05-0.20 dex) with a change of sign when metallicity and effective temperature change (Mashonkina and Bikmaev, 1994). Therefore we were forced to compute individual non-LTE corrections for all 140 stars in our sample. We used in this study only 4554 and 5853 Å lines showing smallest deviations from LTE. We did not take into account the hyperfine structure in 4554 Å line, trying to find this effect from difference in abundances obtained by using both these lines (Fig. 3).

3. Results and discussions

1) Fig.1 shows that distribution of subdwarfs by metallicity is a non-monotonic function and reflects the existence of three Galactic populations (halo, thick disk and disk) having their own ranges of metallicity.

2) There are the sharp boundaries in kinematic characteristics of halo, thick disk and disk stars at the metallicity values [Fe/H]=-0.9 and -0.4 (Figs. 2, 4, 10). Note that at these Figures each dot represents one star. The data of the ordinates in Figs. 2, 4 are taken from the paper of Carney et al. (1990) and from catalogues of Marsakov and Shevelev (1988) and of Shevelev (1988), obtained from Soviet Astronomical Data Center (Moscow). All data for Fig. 10 were taken from the paper of Edvardsson et al., 1993.

These kinematical boundaries occur at the positions of two main minima in Fig. 1 and support the reality of non-monotonic metallicity distribution. Halo, thick disk and disk have their own dynamical history.

3) Fig. 5-8 show that abundance ratios [O/Fe], [Eu/Fe], [Na/Mg], [Al/Mg] change their behavior near the metallicity value [Fe/H]=-0.9 which corresponds to kinematical boundary between halo and thick disk.

4) [Ba/Fe] ratio determined from resonance 4554 Å line shows non-linear dependence on [Fe/H] with breaks at [Fe/H]= -0.9-1.0 and -0.4-0.5 where changes in kinematics and in metallicity distribution are occurred (Fig.3). An excess in barium abundances obtained from 4554 Å line relative of those derived from 5853 Å line is the manifestation of influence the hyperfine structure to equivalent widths of resonance line as suggested by Cowley and Frey, 1989. According these authors part of barium isotopes are produced mostly during the r-process. Therefore, we, probably, have the indications of active phases in star formation and nucleosynthesis corresponding to periods of thick disk and disk stars formation. Decrease of [Ba/Fe] ratio inside of disk and thick disk with increase of [Fe/H] can be explained as interruption of active phases and "quiet" chemical evolution on the Galaxy space scales. Note that the same behavior as for barium 4554 Å line, can, probably, be seen in the data of Andersson and Edvardsson (1994) for carbon (Fig. 9) and data of Edvardsson et al. (1993) for zirconium. Naturally, this kind of result should be confirmed by additional investigations.

4. Conclusions

Our results support and develop the hypothesis of the existence an active phases during the Galaxy evolution (Suchkov, 1977, 1981, Marsakov and Suchkov, 1976, 1977, 1978). Active phases correspond to separate formation of three Galaxy stellar populations - halo, thick disk and disk, having their own chemical and dynamical history. Theoretical models should take into account the significant changes of chemical and dynamical properties at the boundaries (by metallicity) of each stellar population.

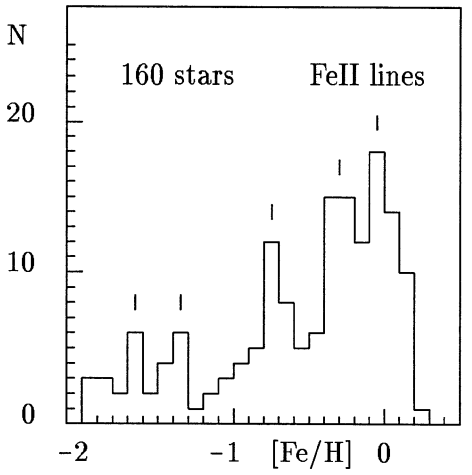

Fig. 1. Metallicity distribution of the sample of stars.

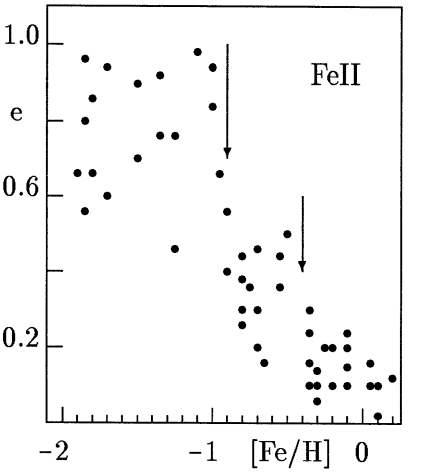

Fig. 2. Eccentricity versus metallicity.

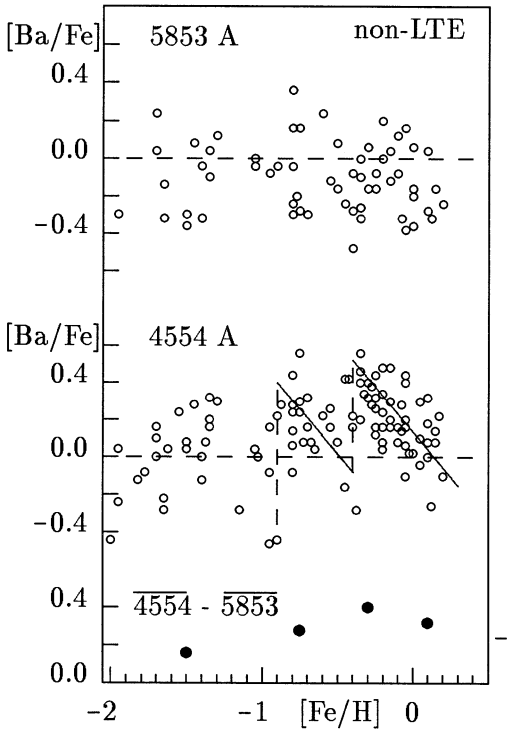

Fig. 3. [Ba/Fe] versus [Fe/H].

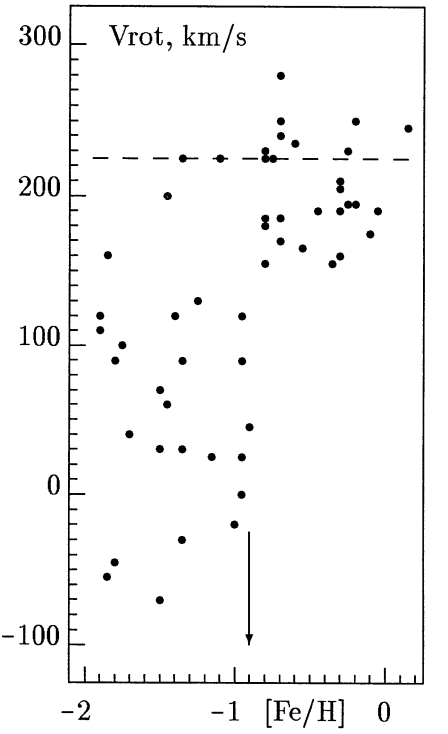

Fig. 4. Angular momentum versus metallicity.

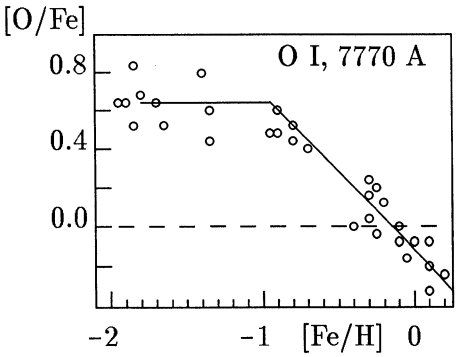

Fig. 5. [O/Fe] versus [Fe/H].

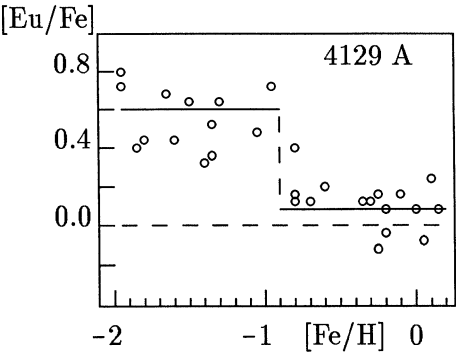

Fig. 6. [Eu/Fe] versus [Fe/H].

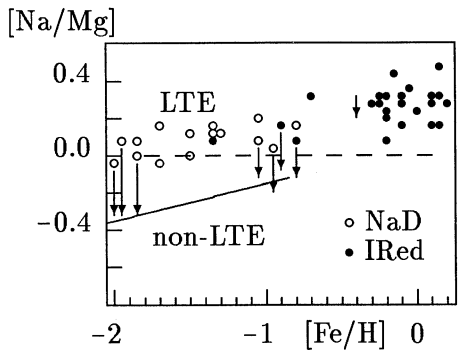

Fig. 7. [Na/Mg] versus [Fe/H].

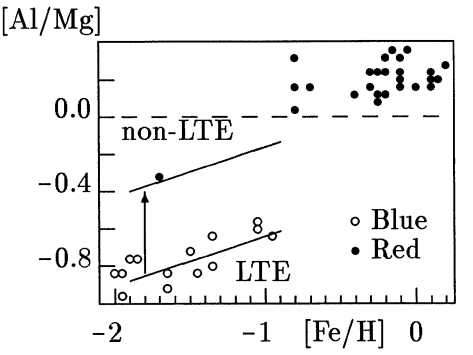

Fig. 8. [Al/Mg] versus [Fe/H].

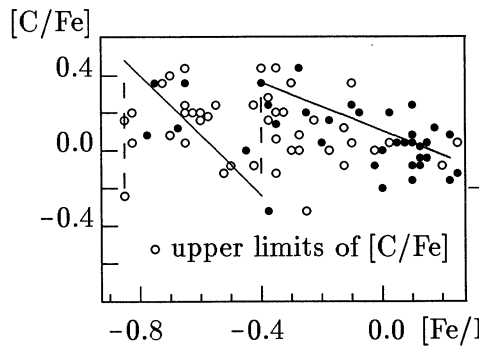

Fig. 9. [C/Fe] versus [Fe/H]. Data are taken from paper of Andersson and Edvardsson (1994).

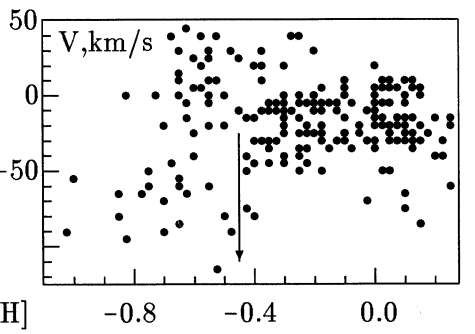

Fig. 10. V-component of space motions relative to the Sun (Vo=226 km/s) versus [Fe/H]. Data are taken from paper of Edvardsson et al. (1993).

Acknowledgements

This study was partly supported by grant of AAS to I.F.Bikmaev. This support is greatfully acknowledged. I.F.Bikmaev is also grateful to Drs. V.G.Klochkova and V.E.Panchuk for help during observational runs on the 6-m telescope and the IAU for travel grant allowing presentation of this report.

References

Andersson, H. and Edvardsson, B. (1994) *Astr.Astroph.*, 290, 590-598
Bikmaev, I.F. (1987) *Bull. of the Special Astrophys. Obs.-North Caucasus, Allerton Press Translation Series*, 25, 3-12
Bikmaev, I.F. (1991) *PhD Thesis, Nizhnij Arkhyz*
Bikmaev, I.F. (1994a) *in: ASP Conference Series, Physics of the Gaseous and Stellar Disks of the Galaxy, ed.I.R.King*, 66, 187-191
Bikmaev, I.F. (1994b) *in: IAU XXIInd General Assembly 1994 Poster Abstracts, ed. H. van Woerden, p.231*
Bikmaev, I.F., Bobritskij, S.S. and Sakhibullin, N.A. (1990) *Sov. Astr. Lett.*, 16, 91-95
Carney, B.W., Aguilar, L., Latham, D.W. and Laird, J.B. (1990) *Astron.J.*, 99, 201-220
Cowley, Ch.R. and Frey, M. (1989) *Astroph.J.*, 346, 1030-1034
Edvardsson, B., Andersen, J., Gustafsson, B., Lambert, D.L., Nissen, P.E. and Tomkin, J. (1993) *Astr.Astroph.*, 275, 101-152
Gehren, T., Reile, C. and Steenbock, W. (1991) *in: Stellar atmospheres: Beyond classical models, eds. L.Crivellari,I.Hybeny and D.G.Hummer, Kluwer, Dordrecht, p.387*
Kurucz, R.L. (1979) *Ap.J.S.Ser.*, 40, 1-340
Marsakov, V.A. and Shevelev, Yu.G. (1988) *Bulletin d'Information du CDS*, 35, 129-130
Marsakov, V.A. and Suchkov, A.A. (1976) *Sov.Astron.Lett.*, 2, 381-385
Marsakov, V.A. and Suchkov, A.A. (1977) *Sov.Astr.*, 54, 1232-1240
Marsakov, V.A. and Suchkov, A.A. (1978) *Sov.Astr.*, 55, 472-481
Mashonkina, L.I., Sakhibullin, N.A. and Shimanskij, V.V. (1993) *Sov.Astron.*, 70, 372-380
Mashonkina, L.I. and Bikmaev, I.F. (1994) submited to *Sov.Astr.Lett.*
Shevelev, Yu.G. (1988) *Bulletin d'Information du CDS*, 35, 135-136
Steenbock, W. (1991) private communication
Suchkov, A.A. (1977) *Sov.Astr.Lett.*, 3, 165-169
Suchkov, A.A. (1981) *Aph.Sp.Sci.*, 77, 3-22
Zhao, G. and Magain, P. (1990), *Astr.Astroph.*, 238, 242-248

THE METAL PRE-ENRICHMENT OF THE GALACTIC DISK: SOLVING THE G-DWARF PROBLEM

M. SAMLAND AND G. HENSLER
Institut für Astronomie und Astrophysik
Universität Kiel, D-24098 Kiel, Germany

1. Introduction

The stellar metallicity distribution of low-mass stars is one of the major touchstones for models describing the chemical evolution of our Galaxy. In contrast to the gaseous components, the abundances of the stellar components also reflect the temporal enrichment. Hence, the stellar metallicity distribution is a stringent test for evolutionary models of galaxies.
During the last decades many models describing the chemical evolution of galaxies have been developed. The majority of these models belong to the category of closed box models or modified ones, which only use a parametrized and a very rough description of gas infall or outflow, or neglect dynamical effects totally. Since the box models always have a number of free parameters like gas inflow/outflow, the stellar initial-mass function or heating processes which do not depend on local physical properties, it is not surprising that different evolutionary models can explain the observations with nearly the same accuracy. The paucity of old metal-poor stars in the solar neighbourhood can, for example, be a result of infall of processed gas (Ostriker & Thuan, 1975), metal-enhanced star formation (Talbot & Arnett, 1975), a prompt initial enrichment (Truran & Cameron, 1971), infall of unprocessed gas (Lynden-Bell, 1975) or a combination of these processes.
A different approach to describe the galactic evolution is provided by hydrodynamical and N-body models. The hydrodynamical simulations (Larson, 1975/1976, Burkert & Hensler, 1988), however, predict a too rapid collapse of a protogalactic cloud, which is inconsistent with observations, e.g. the age difference between halo and disk. The main reason for these discrepancies is the insufficient description of the interstellar medium (ISM) and its interactions with the stellar components. In order to understand the evolution

L. Blitz and P. Teuben (eds.), Unsolved Problems of the Milky Way, 395–401.
© 1996 *International Astronomical Union.*

of galaxies, it is therefore necessary to use self-consistent chemo-dynamical models including the dynamical treatment of the most important stellar and gaseous components and all interaction processes between them. So far these chemo-dynamical models have only been applied one-dimensionally to describe the evolution of giant and dwarf elliptical galaxies (Theis et al., 1992, Hensler et al., 1993).

2. The 2D chemo-dynamical model for disk galaxies

We have developed a 2D chemo-dynamical model in order to self-consistently simulate the evolution of disk galaxies. A detailed description of the model will be published soon (Samland & Hensler, 1994); the model will therefore be only roughly outlined here.

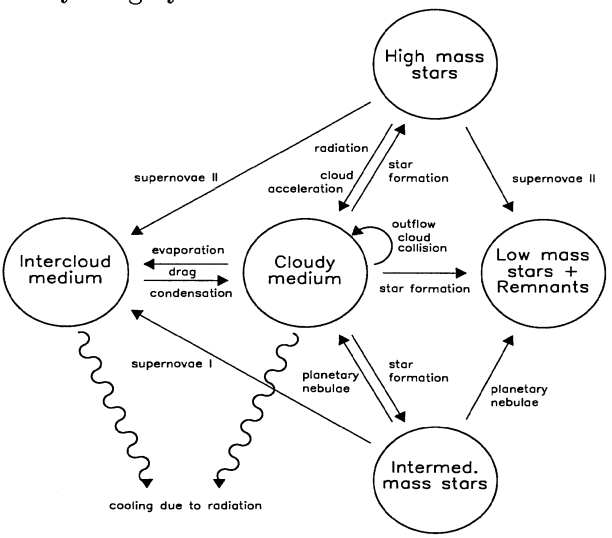

Figure 1. The different gaseous and stellar components are connected via mass, momentum and energy exchange. The most important interaction processes are shown in this diagram.

The ISM is divided into different phases, a cloudy phase (CM) consisting of cold cloud cores ($T < 100$K) with warm gas envelopes ($T \approx 8000$K) and a hot ($T \approx 10^5 - 10^7$K) intercloud medium (ICM). The CM and ICM are assumed to be in pressure equilibrium and connected by mass-, momentum-, and energy-exchange. Furthermore, the CM can dissipate kinetic energy by means of cloud collisions. Beside these gas-gas-interactions there are a number of star-gas-interactions. One of the most important processes is the star formation, which takes place in the cold cores of the CM. The formation itself is self-regulated (Köppen et al., 1994), because of the cloud heating by

the newly formed OB stars. As stars of distinct masses evolve very differently, a multi-component description of the stellar population is required. The model includes massive stars, with masses between $10-100\ M_\odot$, which evolve within $3\cdot10^6-2\cdot10^7$ years and explode as supernovae type II (SNII) and intermediate mass stars, with $1-10\ M_\odot$ and main-sequence lifetimes of $2\cdot10^7-1.2\cdot10^{10}$ years. The latter end their evolution with a significant mass loss in the red giant and planetary nebulae phase before they become white dwarfs. Stars with masses less than $1\ M_\odot$ have main-sequence lifetimes of the order of the Hubble time or more. Their influence during the galactic evolution restricts to gravitational forces. Therefore in the dynamical description they can be embraced with the stellar remnants in a third component. Apart from these interactions, the 2D chemo-dynamical model (see Fig. 1) includes supernovae of type I, molecular outflow in the star forming regions, heating of the CM due to Lyman-continuum photons, radiative cooling of the gaseous phases, and drag forces between clouds and the ambient medium.

3. Initial conditions and evolution of the galaxy

The initial model is a purely gaseous rotating Kuzmin-Plummer model (Satoh, 1980) consisting of 99% CM and 1% ICM without dark matter. The total mass and angular momentum of the protogalaxy is $3.7\cdot10^{11}\ M_\odot$ and $2\cdot10^{17}\ M_\odot pc^2 Myr^{-1}$, respectively. From this a spin parameter $\lambda = 0.05$ can be derived. Beginning from an equilibrium state the kinetic energy of the CM is dissipated due to cloud collisions and the protogalaxy begins to collapse. The violent collapse phase has a duration of about $2\cdot10^9$ years. During that time the density in the central region rises by more than a factor 100 to $0.2\ M_\odot pc^{-3}$. In the following $13\cdot10^9$ years the central mass density rises by another order of magnitude to a value of $3.6\ M_\odot pc^{-3}$. The duration of the collapse is much longer than the dynamical free-fall time ($\approx 2.5\cdot10^8$years), because the star formation rate (SFR) increases with the CM density and by this also the rate of SNII which stir up the CM efficiently and thus prevent the galaxy from a rapid collapse. The SNII, however, not only increase the velocity dispersion of the clouds, but also eject a large amount of hot metal-rich gas, which is driven, due to its high overpressure, out of the star-forming regions into the halo and the disk. Moreover, at that time the clouds which are embedded in the hot gas begin to evaporate, so that about 90 % of the outflowing material originates from the CM. Therefore the average metallicity of the outflow is approximately solar. During the first 10^9 years the heavy-element abundance increases almost independently of the radial distance from the galactic centre (Fig. 2). As most of the halo stars are formed during that time, they show no

significant abundance gradient. Subsequently, the abundances begin to rise faster in the outer parts of the galaxy than in the bulge, although most of the SNII explode near the galactic centre. This can be explained by a closer consideration of the enrichment process. The enrichment of the CM is determined not only by the number of SNII, but also by the mixing between their metal-rich ejecta and the star-forming clouds. The condensation of gas onto cloud surfaces or the cloud formation depends on the thermal energy density of the gaseous phases. During the collapse phase the total SFR is high ($30-50\ M_\odot/yr$) but peaks strongly in the center. Therefore the SN gas will not cool near the star forming regions, but is expelled into the halo or outer disk, cools efficiently there and condensates there on already existing clouds or forms new clouds. After $2.5 \cdot 10^9$ years the SFR begins to decrease while the collapse of the galaxy continues. Therefore the condensation front where the enrichment is effective moves inwards. At $t = 6 \cdot 10^9$ years most of the ejected metal-rich gas condenses close to the star-forming regions. Now the local enrichment exceeds that from gas coming from other parts of the galaxy.

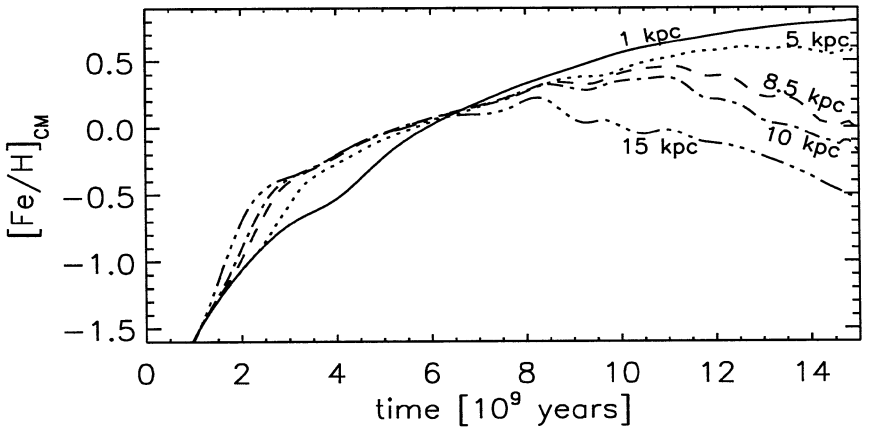

Figure 2. Temporal evolution of the iron abundance in the cloudy medium at different galactocentric radii in the equatorial plane.

4. Results

Fig. 3 shows the calculated oxygen gradient in the CM after $15 \cdot 10^9$ years in comparison with observed values of HII-regions in our Galaxy. It is clearly decernible that the observed abundance gradient is not simple linear and that within the error margin the chemo-dynamical models agree well with the observations. Especially at large galactocentric radii the model predicts a rather shallow gradient of only -0.01 dex/kpc. In the disk the

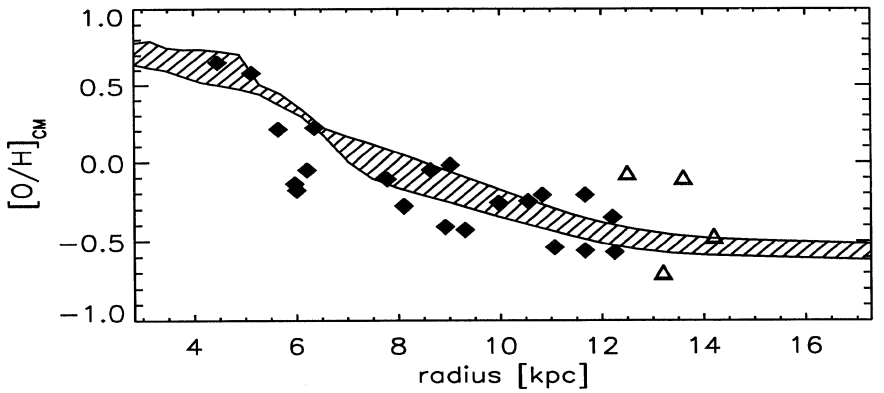

Figure 3. Oxygen abundance in the cloudy medium as a function of radial distance in comparison with the abundances of galactic HII regions. The observations are from Shaver et al., 1983 (rhombi) and from Fich & Silkey, 1991 (triangles). The result of the chemo-dynamical simulation is displayed as hatched area.

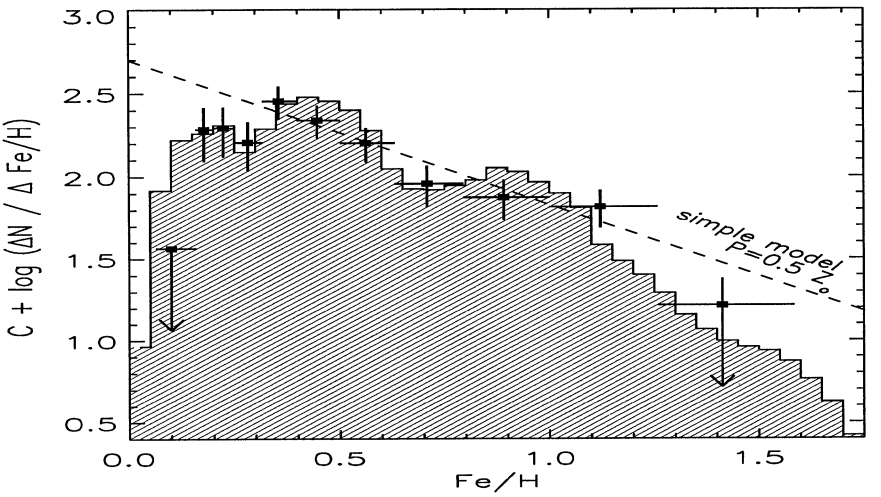

Figure 4. Differential distribution of iron abundances in G-dwarfs in the solar neighbourhood in comparison with the data from Pagel, (1989) which have been corrected for observational errors and cosmic scatter. The vertical error bars indicate the statistical errors in individual bins. The shaded histogram shows the iron distribution of G-dwarfs in our chemo-dynamical model. The dashed line corresponds to a simple closed-box model with an effective yield of $0.5Z_{\odot}$.

slope of the oxygen gradient depends strongly on the galactocentric radius. At radii less than 4 kpc the abundance gradients flattens again. The absolute values are more than one order of magnitude higher than in the halo.

A more severe test for galactic evolutionary models is the often cited differential metallicity distribution of long-living stars like the G-dwarfs. This represents not only the star-formation history but depends on the temporal development of the metal-enrichment, the star formation and the dynamical evolution of the stellar components. It is therefore not surprising that simple models of galactic evolution fail to explain the G-dwarf distribution. Fig.4 shows the result of the chemo-dynamical simulation in comparison with the observational data (Pagel, 1989) and with a simple closed-box model (dashed line) with an effective yield of 0.5 $Z_{\odot}$. Considering the quality of the observations, the agreement between the observations and the chemo-dynamical model is indeed remarkable. The model not only reproduces strikingly the deficiency of metal-poor G-dwarfs, but also self-consistently the variations with metallicity in the differential distribution. This result together with the metallicity gradient of the CM demonstrates convincingly, that the chemo-dynamical models appropriately describe the evolution of galaxies. Moreover, they are the only proper models to describe self-consistently different aspects of the galactic evolution and to provide a complete model for the different components of our Galaxy.

Acknowledgements

This work was supported by the DFG under grant He1487/5 (M.S.). The numerical calculations have been performed at the CRAYs of the HLRZ Jülich, the RZ Kiel and the ZIB Berlin.

References

Burkert, A., Hensler, G., (1988), *Astron. Astrophys.* 199,131
Fich, M., Silkey, M., 1991, *Astrophys. J.* 366,107
Hensler, G., Theis, C., Burkert, A., (1993), *Proc.* 3rd *DAEC Meeting*, eds. S. Stasinska, D. Alloin, p.229
Humphreys, R.M., (1978), it Astrophys. J. Suppl. 38,309
Köppen, J., Theis, C., Hensler, G., (1994), *Astron. Astrophys. in press*
Larson, R.B., (1975), *Mon. Not. R. Astr. Soc.* 173,671
Larson, R.B., (1976), *Mon. Not. R. Astr. Soc.* 176,31
Lynden-Bell, D.,, (1975), *Vistas in Astronomy* 19,299
Ostriker, J.B., Thuan, T.X., (1975), *Astrophys. J.* 202,353
Pagel, B.E.J., (1989) *Evolutionary Phenomena in Galaxies*, eds.: J.E.Beckman & B.E.J. Pagel, Cambridge University Press, Cambridge, p.201
Samland, M., Hensler, G., (1994), *submitted*
Satoh, C., (1980), *P.A.S.J.* 32,41
Shaver, P.A., McGee, R.X., Newton, M., Danks, A.C., Pottasch, S.R., (1983), *Mon. Not. R. Astr. Soc.* 204,53
Talbot, R.J., Arnett, W.D., (1975), *Astrophys. J.* 197,551
Theis, C., Burkert, A., Hensler, G., (1992), *Astron. Astrophys.* 265,465
Truran, J.W., Cameron, A.G.W., (1971), *Astrophys. Space Sci.* 14,179

DISCUSSION

C. Cowley: Have you made a comparison of the predictions of your SFR with the current mass function? If the SFR is dropping rapidly, you expect fewer massive stars than if the SFR is flat.

Samland: The number of massive stars ($M > 10\ M_\odot$) within a radius of 3 kpc of the sun is 950 (Humphreys, 1978), which is higher than the calculated number of 250. This indicates, that the SFR in the model at $t = 15 \cdot 10^{10}$ years is lower than the actual SFR in the Galaxy. Possible reasons for the discrepancy are e.g. the infall rate in the chemo-dynamical model is too small or because the disk of our Galaxy is not $15 \cdot 10^{10}$ years old.

S. van den Bergh: Do you have an angular momentum problem if you enrich the disk with supernovae in the bulge?

Samland: No, because the hot gas ejected by the supernovae contributes only a small mass fraction compared with the total mass of the cloudy medium. Another important point is, that the disk is not solely supported by rotation, but also by the velocity dispersion of the stars and clouds.

Ch. Trefzger: Can you produce the thick disk with your model?

Samland: Due to the limited spatial resolution of the grid (200 pc) it is not possible to resolve substructures of the disk.

DID THE BULGE FORM ALL AT ONCE?

R.M. RICH
Department of Astronomy, Columbia University, 538 W. 120th St. NY NY 10027

1. Introduction

It is reasonable to say that if Jan Oort were alive today, he would no doubt find recent developments in the study of the Galactic bulge to be fascinating. Oort considered the Galactic bulge in two contexts. First, he was interested in the use of the RR Lyrae stars as probes to determine the distance to the Galactic Center. No doubt, Oort would have been excited about the growing evidence of the bulge's triaxiality, as well as by the debate over the age of the bulge. His second interest was in the nature of activity at the center, an issue that I will not discuss in this review. The latter also remains an unsolved problem of the Milky Way, and (based on his work) one that might have been nearer to his heart than this one. Yet the question of when the bulge formed is ultimately a question about the formation history of the Galaxy. The oldest stars (those whose ages we are certain of) are found in Galactic globular clusters, the sum total of which are $\approx 5 \times 10^7 M_\odot$. The field population of the bulge is $\approx 2 - 3 \times 10^{10} M_\odot$, an order of magnitude more massive than the field population of the metal poor spheroid. So if the bulge formed all at once, and early, then the Milky Way had a luminous, even cataclysmic youth. But if the bulge formed later in the history of our galaxy, as a starburst or dynamical instability of the central disk, then the young Milky Way may have been inconspicuous and primeval galaxies may be hard to find indeed. If our bulge formed very early, its stellar population might have much in common with the giant ellipticals, while a late bulge might teach us much about processes that affect galaxy evolution.

The question "Did the bulge form all at once?" is really the question "does the bulge have an age range?". The two extreme populations in this regard are globular clusters, which have an age range too small to measure,

L. Blitz and P. Teuben (eds.), Unsolved Problems of the Milky Way, 403–410.
© 1996 *International Astronomical Union.*

and the local disk or dwarf spheroidals, where ancient stars are present but star formation is ongoing at the present epoch. There is also the question of what population we are discussing, when we refer to the bulge. The question of whether the Galaxy even has a bulge was possibly debatable until the *COBE* satellite produced a striking image at 2 microns that clearly shows a substantial bulge population (Weiland *et al.* 1994; Arendt *et al.* 1994). Does the Galactic Center belong to this population? If it does, then there is evidence that star formation is ongoing today, as has been discussed in this meeting in reviews by Sellgren, Genzel, and Becklin (see also Genzel *et al.* 1994). And the bulge has RR Lyrae stars (Baade 1951) which are an ancient population. Even if one excludes the Galactic center, there is a concentration of luminous stars within the central 100 pc (Catchpole *et al.* 1990) and there are a large number of Miras with periods in excess of 300 days (Glass *et al.* 1994).

Of course, the question actually is whether *most* of the bulge formed at the same time, and if so, when and how? In this review, I am going to discuss progress in 4 approaches toward answering this question. I will start out by stating that even early work (e.g. vanden Bergh, 1971, Rich, 1985) showed that there are few if any young turnoff stars in the bulge. The problem is difficult, and not just because of the extinction, crowding, superposition of stellar populations, and geometrical depth effects that we face in working toward the bulge. It is difficult because the population is older than 5 Gyr and has a narrow age range, features that greatly limit the precision of obvious age indicators like turnoff photometry and population synthesis.

We consider 4 methods that can be used to answer either or both of the questions "when?" and "how?" did the bulge form. The first approach is the frontal assault, age determination from the main sequence turnoff and comparison to globular clusters. We address a related approach (to which we have already alluded), the use of evolved stars such as Miras and RR Lyraes to constrain both the age and age spread in the population. Our third approach focuses more on the question of "how and how long?" than on the "when?". In this approach, we explore the chemical abundance ratios of the bulge stars, which may preserve the record of the type of supernovae (and therefore the timescale) of the enrichment. A fourth approach concerns dynamics, specifically asking what constraints observed dynamics places on formation scenarios. If we demand an age spread, or absolutely no age spread, does this make sense in terms of the observed structure and kinematics of the bulge?

2. Turnoff Photometry

In considering the bulge, one is most interested in the lower latitude fields where the mean metallicity is higher, and classic bulge indicators such as late-type M giants are found in large numbers (cf. Blanco, 1988). Further, the low-latitude fields are more dominated by bulge population and less likely to suffer contamination by either the disk or the metal poor halo. So while Baade's Window ($b = -4^o$) is the prime location to characterize the bulge, the population is so severely crowded that ground-based work on the main sequence turnoff was confined to higher latitude fields; vanden Bergh (1971), Rich (1985) and Terndrup (1988) found the main sequence population in fields no closer than $-8°$. Terndrup (1988) succeeded in fitting isochrones to the turnoff at $-8°$ and $-10°$ and found an age range of 8-12 Gyr (adjusted to $R_0 = 8$ kpc. But it could be argued that these higher latitude fields are mostly outside the inner bulge with lower metallicity and perhaps different age. Holtzmann *et al.* (1993) used the WFPC imager on the Hubble Space Telescope to explore the main sequence turnoff in Baade's Window. As Baum *et al.* (1993) so eloquently characterized, they found evidence for a "middle-aged" bulge in the Galaxy, perhaps dominated by stars as young as 8 Gyr. Mould (1992) analyzes the WFPC2 luminosity function to pose a credible argument that the bulge might be of order 13 Gyr old and this line of reasoning finds some new support (which is discussed below). While isochrone fitting is debated, Ortolani, Rich, & Renzini (1994) have spent the last few years obtaining deep images of bulge fields using the NTT and have succeeded in just reaching the Baade's Window turnoff from the ground. Most importantly, they have verified Holtzmann *et al.*'s calibration, an issue of some importance given the uncertainties of calibrating HST photometry.

A recent surprise has emerged (at the time of this writing). There is a population of metal rich globular clusters in the bulge; recent high dispersion work by Barbuy *et al.* (1992) shows that [M/H] for NGC 6553 is -0.2, a value close to the mean Baade's Window [Fe/H] (McWilliam & Rich, 1994). Using HST, Ortolani *et al.* (1995) obtain turnoff photometry for NGC 6553 and NGC 6528, an equally metal rich globular cluster. At once, they overcome many of the problems that hamper investigation of the bulge field: geometric depth, abundance spread, and differential reddening. They show that the turnoff to horizontal branch magnitude spread for these clusters is 3.6 mag, a value similar to that of other old halo clusters such as 47 Tuc. NTT images of Baade's Window cover a wide enough area to detect clump giants (horizontal branch stars) yet also go deep enough to reach the turnoff. When the luminosity function of the bulge globular clusters is broadened to simulate the depth of the bulge, the two can be aligned

(without reddening uncertainty) by a force-fit of the clump peaks (due to long-lived horizontal branch stars) in the luminosity function. The result is that the bulge and broadened cluster luminosity functions are identical, and age spreads as small as 10% at the turnoff appear to be ruled out by the data. At face value, this experiment provides the answer that the bulge was formed all at once (within any reasonable uncertainty) and that it is as old as the halo. However our other approaches (evolved stars, abundances, and kinematics) suggest that the bulge may have had a longer, more complex formation history than Ortolani *et al.*'s analysis implies. In the end, it is a worthwhile endeavor to seek agreement between all of the various approaches to this problem.

3. Evolved Stars

For the reasons cited above, turnoff photometry may fall short as an ideal age indicator in the Galactic bulge. It certainly falls short in M31, M32 and any galaxies more distant. Of great interest is the possibility of using the luminous evolved stars, particularly the AGB, as an age indicator. AGB tip luminosities well in excess of the first giant branch might signal the presence of an intermediate age population (cf. Renzini, 1993). Miras with periods exceeding 300 days have been shown (in the Solar neighborhood) to have disk kinematics, as opposed to the presumably halo population Miras of period 200 days or less. Again, long period Miras at the AGB tip would be the progeny of some kind of massive star population. Merged binaries (blue stragglers) could account for some of these, (Greggio & Renzini, 1990) although note that *most* of the Miras in the Sgr I bulge field exceed 300 day period (Glass *et al.* 1994). If the bulge is old, with a small age range, and approximately Solar metallicity (McWilliam & Rich, 1994) we have to wonder why its Miras differ so greatly from those of the Solar neighborhood. If surveys of Miras miss the reddest stars, they miss stars of the longest period. In any case, the surveys are presently complete enough that the period distribution is a serious problem. As Renzini (1993) points out, the most luminous giants have potential value in extending the "age ladder" to extragalactic populations. This is provided that such stars do not give misleading results locally. No doubt, the progeny of (massive) blue stragglers must account for some fraction of the population of Miras, but not all of them. So at face value, the presence of both RR Lyrae and Mira variables in the same stellar population would demand an age range, but we still do not know enough about the Miras to settle the question for certain.

4. Abundances

The question "Did the bulge form all at once?" could be taken to mean "Did the bulge form in a violent starburst?" It has long been felt that elliptical and bulge-like systems turn their gas into stars early and rapidly (cf. Matteucci & Brocato 1990) with consequent enhancement of oxygen and alpha-capture elements. The "smoking gun" for such a process would be to see stars with solar iron abundance and [O/Fe] > 0 and [α/Fe] > 0]. Actual high resolution spectroscopy of 11 bulge giants (McWilliam & Rich, 1994) finds a serious problem: Mg and Ti, well-known to be alpha-capture elements, are enhanced in the bulge, but Si and Ca follow the behavior characteristic of the solar neighborhood. Although difficult to measure, oxygen does not appear to show any dramatic enhancements in these stars (McWilliam, Tomaney, & Rich, 1995); while their sample is small, other groups working on different bulge giants have also failed to find extreme oxygen enhancements. On the other hand, the MgH molecule is strong in bulge giants. Rich (1988) used a combination of the Mg_2 index and strong Fe lines to estimate abundances of these stars compared to the Solar neighborhood; in retrospect it would appear that the high abundance scale of [M/H]=+0.3 was due to the apparent enhancement of Mg, which may be present in all bulge stars (Terndrup, Sadler, & Rich, 1995).

The McWilliam & Rich study also finds Solar [s/Fe] abundances in the bulge giants. If larger surveys of the bulge continue to find stars with normal s-process abundances, one is inclined to conclude that the bulge formed after an earlier generation of stars. In the extreme halo, the extreme drop of [Ba/Eu] at low [Fe/H] (Wheeler *et al.* 1989) is consistent with an early generation of massive star supernovae that occurred before any asmyptotic giant branch star had produced s-process elements in its He-burning shell. Had the starburst event from which the bulge formed been instantaneous ($< 10^8$ yr) one would expect to see only the products of massive star nucleosynthesis in the bulge giants. But this is not the case; the bulge is not identical to the solar neighborhood; the Mg enhancement does appear to reflect some kind of starburst history. But it seems attractive to consider the event to have been extended in time, also helping to understand the growing evidence for dissipative formation and enrichment.

5. Structure and Kinematics

High surface brightness, central concentration, and relative lack of flattening are the distinguishing characteristics of the bulge. Within the effective radius of the bulge, the density is $\approx$ 1000 atoms/cm^3 with a dynamical time $\approx$ 3Myr, and the cooling time is even shorter. The high density and consequent short cooling time have been advanced as arguments that L_*

elliptical galaxies should form quickly (Rees & Ostriker 1977, Silk 1977). These ideas, along with the $1/\sqrt{\rho}$ collapse timescale, have caused theorists to favor a rapid, early collapse for spheroids (cf. Renzini 1993). An early collapse and violent starburst is entirely consistent with the bulge metallicity distribution. However, distinguishing characteristic of the bulge is its triaxiality (Blitz & Spergel, 1990; Dwek *et al.* 1995) and it is very difficult to come up with an intuitive explanation for how such a scenario makes a triaxial bulge.

The question "Did the bulge form all at once?" might also be construed as asking whether the metal rich and metal poor stars formed at the same time. The work of Rich (1990), Minnitti (1992, 1994), and Rich *et al.* (1995) continues to find the metal rich bulge stars to be more rotation-supported than the metal poor stars. There is also some evidence that the lower metallicity RR Lyrae stars have a higher velocity dispersion than the metal rich bulge stars. The bulge and the extended metal poor halo evidently could not have formed at the same time, "all at once". If we insist that the bulge is as ancient as the oldest stars, we then must allow enough time for the proto-bulge gas to dissipate into the center. Both in its structure and metallicity, the bulge is distinguished from the metal poor halo. Even if these populations formed at the same time, their respective formation processes had to be very different.

6. Conclusions

Initial data from a small sample of bulge giants observed at high resolution suggests that the bulge does not show all of the chemical signs of a rapid starburst (cf. Matteucci & Brocato, 1990). There is continuing evidence as well that the bulge population has correlations between abundances and kinematics. These characteristics suggest that the full formation timescale was no less than 10^9yr. This is barely compatible with the analysis of Ortolani et al. (1995) which suggests that the largest admissible age spread is $\approx 5\%$. The population of luminous long period Miras that has been unequivocally established to be present in the bulge is incompatible with a bulge as old as the extreme halo, but has no bearing on the age *range* of the bulge. The high density of the bulge and correlations between abundances and kinematics are two powerful arguments in favor of a dissipative formation process, one that would have been extended in time. On the other hand, the data are now sufficiently good to rule out the idea that the bulge accumulated slowly from one or more mergers of satellite systems. Another idea for rapid bulge formation is that a massive stellar disk (formed in starburst?) became bar unstable; this structure could have thickened into a triaxial peanut-shaped bulge in < 1 Gyr (Combes & Sanders, 1981; Pfenniger &

Norman, 1990; Sellwood & Merritt, 1994). It is not clear whether such a process would preserve correlations between abundances and kinematics. In this last scenario, the bulge structure would have formed suddenly, but the stars comprising that structure could have formed over an extended period. It would appear that the present data support a timescale of order one Gyr for the formation of the bulge, but the chemical signatures of a violent starburst history are only partially present. Yet the most evolved stars stand as a problem, as they have since the subject began: How can RR Lyraes and 300+ day Miras coexist as part of the same population if the age range is narrow? While recent observations have advanced the subject greatly, we can only conclude that the time and timescale of bulge formation remain unsolved problems of the Milky Way.

Acknowledgements

RMR acknowledges financial support from NASA LTSARP grant NAGW-2479, and helpful discussions about dissipative bulge formation with David Spergel, and discussions with Alvio Renzini and Francesca Matteucci.

References

Arendt, R.G. *et al.* 1994, ApJ, 425, 530
Baade, W. 1951, Pub.Obs.Univ.Mich., 10, 7
Barbuy, B., Castro, S., Ortolani, S., & Bica, E., 1992 AA, 259, 607
Baum, W., Light, R.M., Holtzman, J.A. *et al.* 1993, in Galactic Bulges, Proc. IAU Symp. 153, Dejonghe H., Habing H.J., eds, Kluwer, Dordrecht, 289
Blanco, V.M., 1988, AJ, 95, 1400
Blitz, L, & Spergel, D.N., 1991, ApJ, 313, 59
Catchpole, R.M., Whitelock, P.A., & Glass, I.S. 1990, MNRAS, 252, 210
Combes, F., & Sanders, R.H. 1981, AA, 96, 154
Dwek, E. *et al.* 1995 ApJ in press
Glass, I., Whitelock, P.A., Catchpole, R.M., & Feast, M.W. 1995, MNRAS in press.
Greggio, L., & Renzini, A., ApJ, 364, 35
Matteucci, F., & Brocato, E., ApJ, 365, 539
McWilliam, A., & Rich, R.M. 1994, ApJS, 91, 749
McWilliam, A., Tomaney, A., & Rich, R.M. 1995, ApJ, submitted
Mould, J.R. 1993 in Science With the Hubble Space Telescope, Baia Chia Workshop
Minnitti, D.M., White, S.D.M., Olszewski, E.W., & Hill, J.M. 1992, ApJ, 393, L47
Minnitti, D., 1994, Ph.D. thesis, University of Arizona
Ortolani, S., Rich, R.M., & Renzini, 1994 in preparation
Ortolani, S., Renzini, A., *et al.* 1995, Nature, Submitted
Pfenniger, D., & Norman, C., 1990, Ap.J., 313, 391
Rees, M.J., & Ostriker, J.P. 1977, MNRAS, 179, 541
Renzini, A., 1993, in Galactic Bulges, Proc. IAU Symp. 153, Dejonghe H., Habing H.J., eds, Kluwer, Dordrecht, 391
Rich R.M., 1985, Mem.S.A.It., 56, 23
Rich R.M., 1988, AJ, 95, 828
Rich R.M., 1990, Ap.J., 362, 604.
Rich R.M., 1993, in Galactic Bulges, Proc. IAU Symp. 153, Dejonghe H., Habing H.J.,

eds, Kluwer, Dordrecht, 169
Rich R.M., Terndrup, D.M., & Sadler, E.M. 1995 in preparation
Sellwood, J.A., & Merritt, D., 1994, ApJ, 425, 530
Silk, J., 1977, ApJ, 211, 638
Terndrup, D.M., 1988, AJ, 96, 884
Terndrup, D.M., Sadler, E., & Rich, R.M. 1995, AJ, in press
van den Bergh, S., 1971, AJ, 76, 1082
Weiland, J.L. *et al.* 1994, ApJ, 425, L81
Wheeler, J.C., Sneden, C., & Truran, J.W., Jr. 1989, ARAA, 27, 279

LATE-TYPE GIANTS IN THE BULGE, AT HIGH GALACTIC LATITUDES AND IN THE PLANE

PATRICIA WHITELOCK
South African Astronomical Observatory
P O Box 9, Observatory, 7935 Cape, South Africa

Abstract. Mira and non-Mira M stars are easily distinguished by means of their near-infrared colours. The Miras show a large range of mass-loss rates, and the actual rates are a strong function of the K-[12] colour. The kinematics and scale heights of these Miras are a function of their pulsation periods. The period distribution of Miras in the South Galactic Cap is similar to that of Miras in the Bulge. Non-Mira M stars in the South Galactic Cap have similar colours to their counterparts in the Bulge but differ from bright M-giants in the solar neighbourhood. The galactic distribution and scale height of the M giants is a function of colour and it is suggested that differences in composition influence the colours.

1. Introduction

This paper summarizes some of the results from a survey of IRAS sources in the South Galactic Cap, selected on the basis of their IRAS 12 and 25 μm flux as high-mass-loss candidates. Details of the observations and their analysis can be found in Whitelock *et al.* (1994a,b hereafter Papers I and II, respectively).

IRAS sources with a 25 to 12 μm flux ratio of $F_{25}/F_{12} > 0.5$ were selected from galactic latitudes $b < -30°$. These criteria isolate stars with dust shells in the South Galactic Cap. Near-infrared, JHKL, photometry was obtained for all sources and repeated measurements for those with colours suggestive of something other than a normal M giant. Particular effort went into determining periods of previously unrecognized Mira variables. Spectra and optical photometry were also obtained for a significant fraction of the sample. This paper concentrates on the results for oxygen-

L. Blitz and P. Teuben (eds.), Unsolved Problems of the Milky Way, 411–417.
© 1996 *International Astronomical Union.*

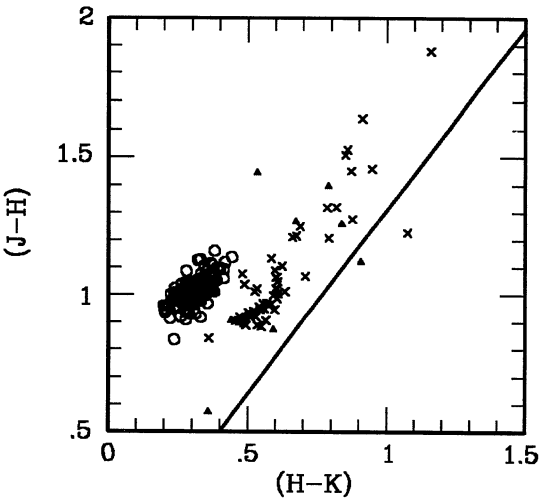

Figure 1. A near-infrared two-colour diagram of selected IRAS sources from the South Galactic Cap.

rich stars and distinguishes between Mira variables, which have pulsation amplitudes in excess of 0.4 mag at K, and non-Mira M-type giants (henceforth M giants), many of which are small amplitude variables.

Figure 1 shows the IRAS selected sample on a near-infrared two-colour diagram. The crosses are O-rich Mira variables, those higher up the diagram have thicker shells and their colours are therefore affected by circumstellar reddening. The crowded region on the left of the figure contains only the 154 M giants. The triangles represent peculiar stars which are not discussed further here. The diagram illustrates how effectively one can discriminate between Miras and other M stars on the basis of near-IR photometry alone. Our current understanding of these stars suggests that the Miras represent the last stage of Asymptotic Giant Branch (AGB) evolution for low and intermediate mass-stars. They are in the process of rapidly losing mass prior to crossing the HR diagram to become planetary nebulae. The M giants might be either on the first giant branch or on the AGB, but as they have moderately high mass-loss rates ($\gtrsim 10^{-8} M_{\odot} yr^{-1}$) most of them are probably on the AGB.

2. Mass-loss Rates

Figure 2 shows mass-loss rates for the Miras as a function of colour. These rates were calculated using a modification of the expression derived by Jura (1987) for carbon stars. This requires a knowledge of the distance, obtained from the period-luminosity relation, and the bolometric luminosity. Periods

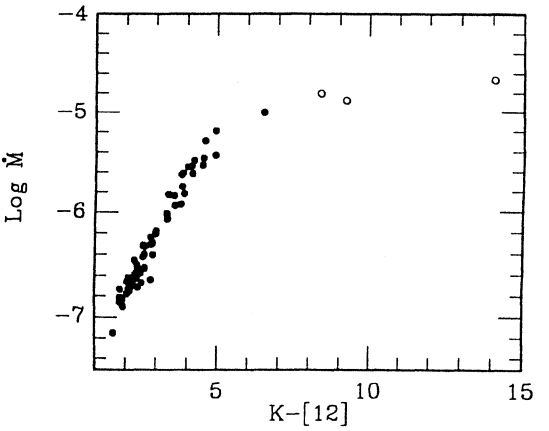

Figure 2. Mass-loss rates as a function of colour for IRAS Miras

were measured for all of the Miras, while the bolometric luminosity was derived from the combination of near-IR and IRAS photometry. As can be seen from Fig 2 the mass-loss rate is a very strong function of K-[12]. This is to be anticipated given that the 2.2 μm, K, flux originates almost exclusively from the star and the 12 μm flux from the dust. The turnover in the curve occurs where the dust becomes optically thick at 2.2 μm. The three stars with very high mass-loss rates (open circles) are carbon rich.

Assuming that the mass-loss rates for the M giants is a similar function of K-[12] then we find that the non-Miras typically have smaller mass-loss rates than do the Miras. There are, however, a few M giants with rather high rates ($\gtrsim 10^{-7} M_{\odot} yr^{-1}$). The nature of these stars was discussed in Paper II. It seems likely that they were undergoing more rapid mass-loss in the recent past than they are currently experiencing. The changed character of the mass-loss might be a consequence of helium shell flashes reducing their luminosity and forcing them out of the Mira instability strip. The remnant shell from mass-loss during the previous Mira phase is still evident in this diagram. Many of these stars may become Miras again later in their flash cycle if their luminosity rises as theory predicts.

3. Mira Pulsation Periods

The pulsation periods of the Miras are of particular interest because they are a function of the population to which the star belongs. A histogram of the periods of Miras in the South Galactic Cap was illustrated in Fig 8 of Paper I (this includes all Miras in the given volume, not just the IRAS selected sample). This can be compared with the distribution of Mira periods in various Bulge fields from Whitelock (1992 see also Glass *et al.*

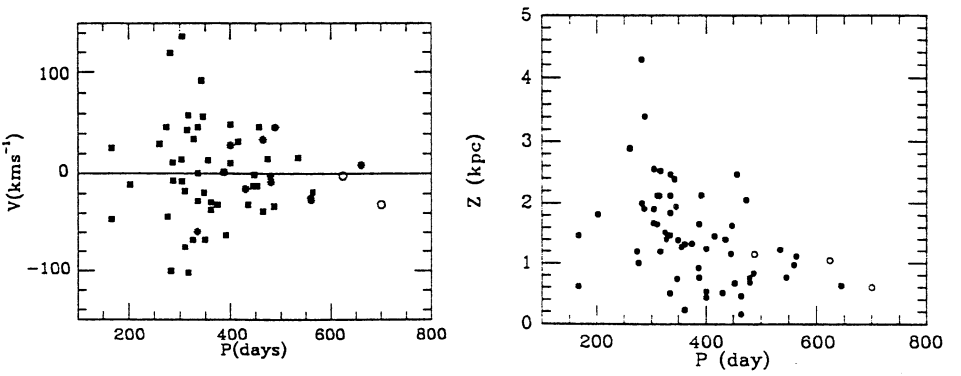

Figure 3. Radial velocity and height above the Galactic Plane as a function of pulsation period for Miras. Open-circles: carbon stars.

1994). Inclusion of the IRAS Miras extended the period distribution in the Galactic Cap towards longer periods. This distribution is very similar to that of Miras at a latitude of $b = -7°.5$ in the Bulge. The innermost Bulge field, Sgr I, seems to contain a somewhat larger proportion of long-period pulsators.

We now understand that the pulsation period tells us a good deal about the star. Figure 3 shows the radial velocity and height above the galactic plane as a function of the pulsation period. Distances were calculated from the period luminosity relationship. These data reinforce what we have known since Feast's (1963) spectroscopic work; i.e., the kinematics of the Miras are a function of their pulsation period. Longer-period Miras were either initially more massive or they are younger or they are more metal rich than short period ones. One of the obvious consequences of this is that we must not visualize Miras as evolving with large changes of period, an idea that is still prevalent. It is also clear from Fig 3 that we should expect a higher proportion of short period stars in the Galactic Cap than in the solar neighbourhood purely because the bulk of the volume examined in the Cap is at large distances from the Plane.

4. Non-Mira M giants

It is of considerable interest to look at the colours of the M giants and compare them with those of similar stars in the Galactic Plane and in the Bulge. Frogel *et al.* (1990) point out that the colours of the M giants in the inner Bulge differ from those of stars in the solar neighbourhood of the same spectral type. Furthermore they find a distinct difference in the colours of the giants in the inner and outer Bulge, with those in the outer Bulge resembling globular cluster giants. It is interesting to find therefore,

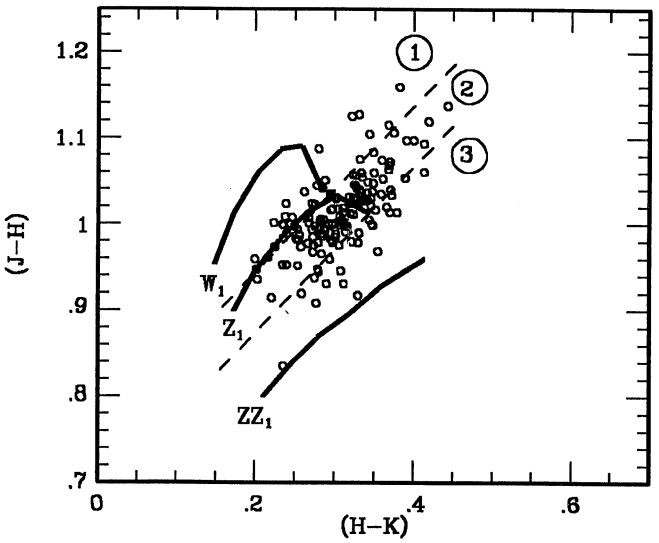

Figure 4. The M giants on a two-colour diagram; the colours have a precision of about ±0.03 mag. The solid lines are theoretical tracks from Bessell *et al.* (1989) for giants with metallicity, Z, of −0.5, 0.0 and +0.5, shifted as described by Feast *et al.* (1990). Two dashed lines divide the diagram into three parts and Table 1 lists the properties of the stars from each of these groups (see Paper II).

that the M giants from the South Galactic Cap IRAS sample have colours very similar to those of stars from the inner Bulge and quite distinct from those of stars in the solar neighbourhood or in globular clusters (Paper II). Although the colours are similar to those of the high-latitude late-M giants discovered by Stephenson (1986) and discussed by Feast *et al.* (1990) and Sharples *et al.* (1994). The critical difference between the local M stars and those from the Galactic Cap samples is probably in mass, those in the cap being less massive.

Figure 4 compares the observed colours of the M-giants with theoretical tracks. It is clear that many of the points lie outside the range of the models, so at best these models can provide only a qualitative interpretation of the data. Nevertheless, such a comparison does suggest possible reasons for the spread in the diagram. Although various factors play a role, it seems possible that metallicity is the dominant factor and that group 3 have a higher metallicity than group 2 which is higher than group 1. None of the models available allow for abundance anomalies of the type McWilliam & Rich (1994) found for K stars in the Bulge and it would clearly be important to investigate the effects on the M stars of altering abundances of α elements without changing [Fe/H].

$\Re$, (see Table 1) is the ratio of the number of stars in the hemisphere towards the Galactic Centre to the number in the opposite hemisphere.

TABLE 1. Mean properties of the M-stars from Fig 4

	Group 1	Group 2	Group 3
no. stars	27	101	26
Sp Type	5.2	5.9	7.0
J–K	1.30 ± 0.02	1.33 ± 0.01	1.30 ± 0.02
K–[12]	1.68 ± 0.13	1.47 ± 0.04	1.93 ± 0.13
V–K	6.33 ± 0.24	8.52 ± 0.88	7.31 ± 0.29
z_0 (pc)	> 500	> 330	> 560
$\Re$ (Y < 0/Y > 0)	0.8	1.9	4.2

Notice that stars from group 3, which has the latest mean spectral type and the highest mean mass-loss rate, are very strongly concentrated towards the Galactic Centre. For the purposes of calculating the distances to these stars, and hence the scale height, z_0, we assumed that they had the same absolute K magnitude as do stars in the Bulge with the same J–K colour. This assumption is unlikely to be correct for all of the stars in this sample and may result in an underestimate of some of the distances. However, the evidence points to these stars as having metallicities of solar or above and it is very interesting to see that they have rather large scale heights. A much deeper understanding of these stars should be possible after the completion of the DENIS and 2MASS near-infrared surveys which will provide a more complete survey of this type of star than was possible with IRAS.

Acknowledgements

I am very grateful to Michael Feast and John Menzies for helpful discussions.

References

Bessell, M. S., Brett, J. M., Scholtz, M., and Wood, P. R. (1989) *A& AS*, 77, p. 1
Feast, M. W. (1963) *MNRAS*, 125, p. 367
Feast, M. W., Whitelock, P. A. and Carter, B. S. (1990) *MNRAS*, 247, p. 227
Frogel, J. A., Terndrup, D. M., Blanco, V. M., Whitford, A. E. (1990) *ApJ*, 353, p. 494
Glass, I. S., Whitelock, P. A., Catchpole, R. M. and Feast, M. W. (1994) *MNRAS*, submitted
Jura, M. (1987) *ApJ*, 313, p. 743
McWilliam, A. and Rich, R. M. (1994) *ApJS*, 91, p. 749
Sharples, R. M., Whitelock, P. A. and Feast, M. W. (1994) *MNRAS* in press
Stephenson, C. B. (1986) *ApJ*, 301, p. 927
Whitelock, P. A. (1992) in: Dejonghe, H. and Habing, H. J., (eds.) *Galactic Bulges*, IAU Sym 153, Kluwer, p. 39

Whitelock, P. A., Menzies, J. W., Feast, M. W., Marang, F., Carter, B. S., Roberts, G. R., Catchpole, R. M. and Chapman, J. (1994a) *MNRAS*, 267, p. 711, Paper I
Whitelock, P. A., Menzies, J. W., Feast, M. W., Catchpole, R. M., Marang, F. and Carter, B. S. (1994b) *MNRAS* submitted, Paper II

DISCUSSION

S. van den Bergh: Can one tell from presently available data if Miras belong to two distinct subsystems, or is there a gradual transition from disk to halo objects?

Whitelock: There seems to be a gradual transition from the OH/IR stars with P>1000 day in the disk to the P~200 day Miras found in the metal-rich globular clusters.

EFFECTS OF CHAOS IN THE GALACTIC HALO

W.J. SCHUSTER AND C. ALLEN
Instituto de Astronomía, Universidad Nacional Autónoma de México

To study the way in which the principal periodic orbits in a Galactic potential determine orbital structure, horizontal and vertical surfaces of section, i.e. (dR/dt, R) and (dz/dt, z), are being used to explore the potential of Allen & Santillán (1991) and to investigate possible vertical structure in the Galactic halo. The chaotic "scattering" process due to the nearly spherical mass distribution close to the Galactic center in conjunction with the confinement of the chaotic orbits produces a vertical segregation of both chaotic and non-chaotic orbits in the halo. Certain z_{max}, z_{min} are preferred by the chaotic orbits over others as a result of the conservation of the total orbital energy and of the interaction and confinement of the chaotic orbits by the principal families of periodic orbits (Figure 1). Some of these periodic orbits have been identified. Correlations between the structure found in the observed W distribution and that of the numerically determined z_{max}, z_{min} histograms are shown for our sample of 280 halo stars (Schuster et al. 1993). W is the star's velocity perpendicular to the Galactic plane and z_{max}, z_{min} the maximum distances above or below the Galactic plane, respectively, reached by the star in the course of its orbit. This vertical structure may explain certain puzzling observations of the galactic halo, such as conflicting c/a values for the shape of the halo, and unusual velocity dispersions and/or distributions near the Galactic poles. These results are in good agreement with Hartwick's (1987) two component model for the halo.

Our main conclusions are as follows: 1. Chaotic scattering of Galactic halo stars can serve to hide or destroy correlations involving kinematic parameters, such as a possible chemical gradient in the halo. 2. Due to these chaotic processes, as well as to the coupling of vertical and horizontal motions, the W velocity component of halo stars does not give a good indication of the maximum height above or below the Galactic plane reached by a halo star in the course of its orbit. 3. Vertical Poincare sections (Figure 2) provide a good means of studying the effects of chaos as well as

L. Blitz and P. Teuben (eds.), Unsolved Problems of the Milky Way, 419–421.
© 1996 *International Astronomical Union.*

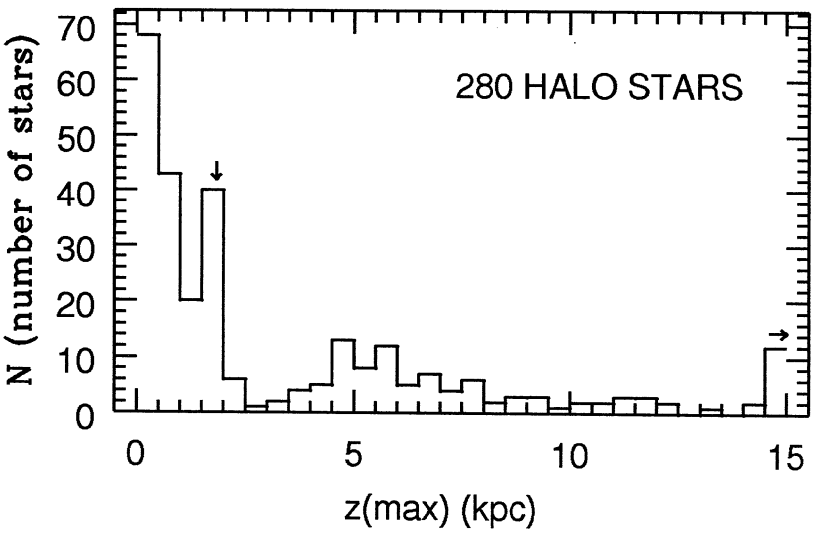

Figure 1. The calculated z_{max} histogram for the 280 halo stars obtained using the Galactic potential of Allen & Santillán (1991) with each orbit integrated for at least 15 radial or vertical oscillations. A minimum in the histogram is observed over the interval 2.5-3.0 kpc and a secondary maximum over 1.5-2.0 pc. This secondary peak is produced mainly by stars with chaotic orbits.

the velocity dispersions produced at the Galactic Poles by different Galactic potentials. 4. The observed W histogram for our 280 halo stars, the calculated z_{max} histogram, and various vertical Poincare sections all show structure, evidence for the interaction and confinement of chaotic orbits by families of periodic orbits. 5. Such interactions and confinements may help to explain the non-Gaussian "clumping in velocity space" that has been observed for halo stars near the Galactic Poles (Norris 1986), the possible existence of "moving groups" within the halo, as well as the differing shapes and velocity dispersions obtained for the galactic halo from different stellar samples.

References

Allen C., Santillán A., (1991) *Rev. Mexicana Astron. Astrof.* 22, 255.
Hartwich F.D.A., (1987), in: The Galaxy, eds. G. Gilmore and B. Carswell, Reidel, Dordrecht, p. 281.
Norris J., 1986, *ApJSS* 61, 667.
Schuster W.J., Parrao, L., Contreras Martínez M.E., (1993), *A&ASS* 97, 951.

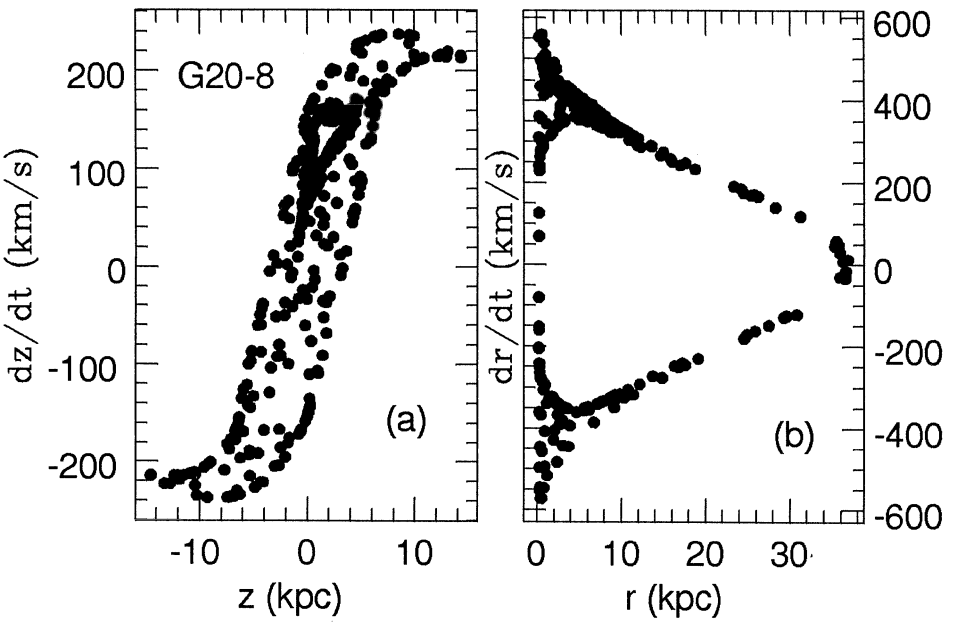

Figure 2. Vertical and horizontal Poincare sections for the halo star G20-8, which has a chaotic orbit. The vertical Poincare section (a) plots the W=dz/dt velocity against the vertical height each time the star crosses the Sun's radial distance traveling outward, while the horizontal Poincare section (b) the Galactocentric radial velocity against the radial position each time the star crosses the Galactic plane traveling upward.

THE VELOCITY DISPERSION IN THE COLD COLLAPSE

Y. KAN-YA AND M. SASAKI
Department of Physics, Kyoto University
Kyoto 606-01, Japan

T. TSUCHIYA
Division of Theoretical Astrophysics,
National Astronomical Observatory
Mitaka, Tokyo, 181, Japan

AND

N. GOUDA
Department of Earth and Space Science, Osaka University
1-1, Machikaneyama-cho, Toyonaka, Osaka 560, Japan

Abstract. We investigate the growth of the velocity dispersion in the initial stage of the cold dissipationless collapse of spherical collisionless systems by a perturbation theory. We show that the tangential velocity dispersion grows faster than the radial one for the system with centrally condensed initial density profile.

For the formation of the galactic halos cold collapses is often discussed, which is the collapse of the collisionless system whose initial virial ratio is much smaller than unity. It is known from N-body simulations that the cold collapse of the system results in a *prolate* final shape of the system (e.g. Min & Choi 1989, Aguilar & Merritt 1990), independent of its initial shape and initial density profile. These studies, however, are interested in the relationship between the initial condition and the final state of the system, so what made the system prolate still remains as a question. To make this point clear, the understanding of the internal dynamics in the collapsing collisionless system is important. As a first step we analyzed the behavior of the velocity dispersion as effective pressure by perturbation theory, in the outer region of spherical collisionless systems, for the initial free fall stage (Kan-ya *et al.* 1994). Apart from fluids we have no analog of the

L. Blitz and P. Teuben (eds.), Unsolved Problems of the Milky Way, 423–424.
© 1996 *International Astronomical Union.*

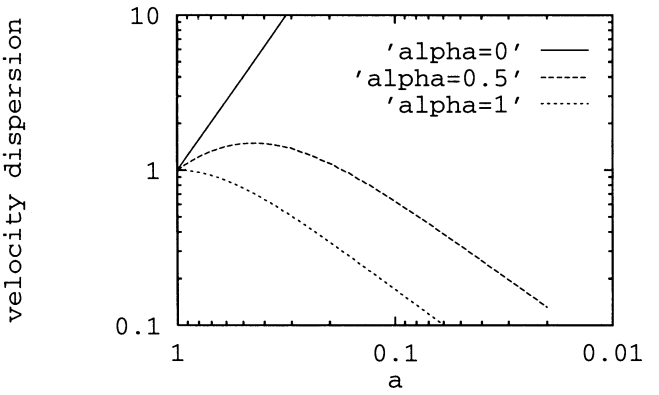

Figure 1. The radial velocity dispersions normalized by the initial values. The curves show for the initial density profile proportional to $r^{-\alpha}$ with indicated values of α. The tangential velocity dispersion is equal to the radial one with $\alpha = 0$, irrespective of the value of α.

equation of state for collisionless system. So we must solve the behavior of the velocity dispersion from the collisionless Boltzmann equation.

We assumed that initially the third moment of the distribution function is negligible with no cross correlation between the velocity of different directions. Then we solved the time evolution of the velocity dispersion from the moment equations of the collisionless Boltzmann equation, truncated until the second moment. This truncation is valid in this case. As a result we showed that the growth of the velocity dispersion is determined by the local compression of a mass shell. In Figure 1 we show the behavior of the solution in the system whose initial density profile is proportional to r^{α}. Our solution is depends on a, the scale factor of the collapse of a mass shell with $a(t = 0) = 1$, and the initial density profile of the system. From this figure we see the tangential dispersion grows faster than the radial one for centrally condensed initial density profile. This result implies that the radial-orbit instability is suppressed in the outer region for this stage of collapse (cf. Aguilar & Merritt 1990).

References

Aguilar, L.A., Merritt, D.R. (1990) *ApJ.*, 265, 33
Kan-ya, Y., Sasaki, M., Tsuchiya, T., Gouda, N. (1994) *submitted.*
Min, K.W., Choi, C.S. (1989) *M.N.R.A.S.*, 238, 253

THE CHEMODYNAMICAL EVOLUTION OF SPHEROIDAL SYSTEMS AND THE RESULTANT STELLAR ABUNDANCE DISTRIBUTION FUNCTION

T. TSUJIMOTO[1], T. SHIGEYAMA[2], AND K. NOMOTO[2]
[1] *National Astronomical Observatory*
Mitaka, Tokyo 181, Japan
[2] *Department of Astronomy, School of Science,*
University of Tokyo, Bunkyo-ku, Tokyo 113, Japan

We construct a chemo-dynamical model for galaxy formation using a three dimensional SPH method. We simulate the formation of two spheroidal systems, i.e., the elliptical galaxy and the Galactic bulge, based on the collapse scenario for protogalaxies. We obtain the chemodynamical formation and evolution models for the two systems during the first $\sim$ 1 Gyr. The relative ratio of kinetic to thermal energy of supernovae is found to heavily determine the outcome. By giving the explosion energy of supernovae to the interstellar gas with a physically meaningful relative ratio of kinetic to thermal energy, the elliptical galaxy model has the hot halo and the galactic wind, but it is not the case for the Galactic bulge model.

The chemical and dynamical properties of the model galaxies are found to depend mainly on the gravitational potential set by dark matter (Tsujimoto 1994). For the deeper potential, we obtain a model whose density profiles and velocity dispersions are consistent with the elliptical galaxies. On the other hand, the Galactic bulge-like structure, i.e., a compact core whose mass is $\sim 10^{10}\ M_{\odot}$ and radius is $\sim$ 2 kpc can be formed only in a much shallower potential. These results suggest that elliptical galaxies were formed in a deeper potential than spiral galaxies. Our calculations show that these two systems evolve as follows:

a) In the model for the elliptical galaxy, star bursts occur in the central part of dark matter. Eventually a core which consists of stars and the hot halo are formed. During the formation, the galactic wind with heavy elements (nearly solar abundance) occurs and $\sim$ 10 % of the initial gas escapes from the galactic potential.

L. Blitz and P. Teuben (eds.), Unsolved Problems of the Milky Way, 425–426.
© 1996 *International Astronomical Union.*

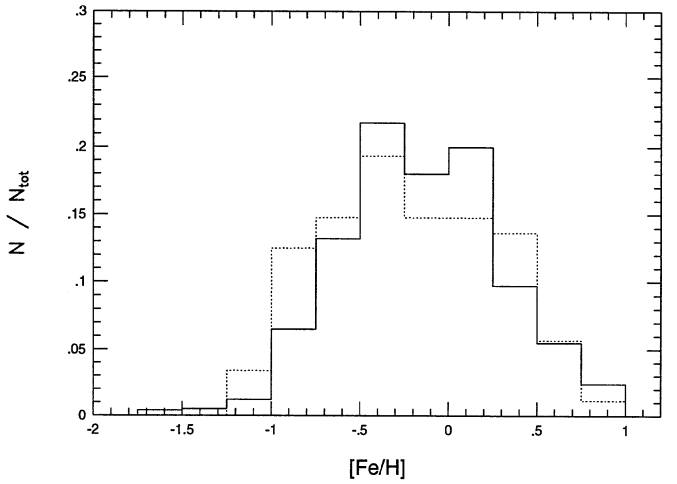

Figure 1. Calculated abundance distribution function of stars in the core for the Galactic bulge model (solid line) as compared with that of the bulge K-giants (dotted line:McWilliam & Rich 1994).

b) In the model for the Galactic bulge, (i) gases collapse in almost uniformly distributed dark matter, (ii) a small fraction of gases forms stars in the central part, and (iii) the residual gases make a bounce due to gas pressure, centrifugal force and the kinetic energy of supernova explosions.

Our model for the Galactic bulge is successful in reproducing the revised abundance distribution function of the bulge K-giants (McWilliam & Rich 1994). We find that the resultant stellar abundance distribution is produced by the inhomogenous enrichment. The wide range of metallicity and super metal-rich stars are made by the effect. The density inhomogenity in the core results in the inhomogenous metal enrichment. Such an inhomogeneity does not appear in one zone models. In addition, it is found that the distribution with its peak lying at a low metallicity ([Fe/H] ~ -0.5), despite the existence of super metal-rich stars, can be reproduced under the condition that the gas contaminated by heavy elements can easily escape from the core. If the bulge evolves in the closed system, the metallicity at the peak is shifted to higher and the abundance distribution function becomes similar to the observed one by Rich (1988). Not only the size and the mass of the Galactic bulge but also the abundance distribution function of the bulge K-giant implies that the bulge is formed in the shallow galactic potential.

References

McWilliam, A. & Rich, R.M., 1994, ApJS 91, 749
Rich, R.M., 1988, AJ 362, 606
Tsujimoto, T., 1994, submitted to ApJ

METALLICITY STRUCTURES OF THE MILKY WAY

ROLAND BUSER
Astronomical Institute, University of Basel, Switzerland
AND
JIANXIANG RONG
Astronomy Department, Nanjing University, China

Abstract. The metallicity-sensitive $(U-G)$ colors from the new homogeneous catalog of photographic RGU data in seven high-latitude fields have been used to determine the larger-scale metallicity distributions of the Galactic population components. For the *thick disk*, preliminary analysis based on our best structural models provides a mean metallicity $\langle[M/H]\rangle = -0.6 \pm 0.3 dex$ and a marginal vertical metallicity gradient $\approx -0.1 dex/kpc$. The observed color distributions are further consistent with the *(old) thin disk* having mean abundance $\langle[M/H]\rangle = -0.3 \pm 0.2 dex$ and abundance gradient $\partial[M/H]/\partial z = -0.6 dex/kpc$.

Based on the results obtained for the structural parameters [1], we have determined the metallicity structures of the different population components in a complementary analysis of the new RGU catalog [2]. In particular, parameter variation is confined to their optimized values and to within the constraints imposed by the relevant χ^2-curves and frequency distributions derived from the $(G, G-R)$ data. Model star count and color distributions are then calculated allowing for appropriate ranges of mean metallicities and vertical metallicity gradients for the different components and using the corresponding metallicity-dependent changes in the $(G, G-R)$ and $(G, U-G)$ color-magnitude calibrations [3]. Finally, the χ^2-analysis is performed by requiring the models to also provide *good matches to the observed distributions in the metal-sensitive* $(U-G)$ *color*, $N(U-G)$. Evaluation of the globally lowest-χ^2-models then leads to the determination of the optimum values for the mean metallicities, $\langle[M/H]\rangle$, and metallicity gradients, $\partial[M/H]/\partial z$, of the Galactic population components.

L. Blitz and P. Teuben (eds.), Unsolved Problems of the Milky Way, 427–428.
© 1996 *International Astronomical Union.*

TABLE 1. Mean metallicity and vertical metallicity gradient for thick disk

Field	l	b	Area (deg^2)	$m_{G,lim}$	No.**	$\langle[M/H]\rangle$	$\partial[M/H]/\partial z$
Praesepe	205.9	32.4	3.56	15.0	1228	-0.81	-0.20
M 101	101.0	60.0	2.00	18.5	1388	-0.60	-0.04
M 67	210.6	32.2	1.70	16.0	748	-0.78	-0.20
SA 54	200.1	58.8	2.56	18.5	1359	-0.52	-0.05
SA 57	65.5	85.5	2.61	19.0	1807	-0.49	-0.03
SA 141	245.0	-85.8	1.92	17.5	758	-0.76	-0.15
M 5	4.0	47.0	1.05	18.5	1819	-0.54	-0.03
Combined			15.40		9107	-0.58	-0.10

Table 1 gives a summary of the field data and the optimized values obtained for the mean metallicities and vertical metallicity gradients of the *thick disk* as derived from the $(U-G)$ color distributions in each individual field, plus the weighted mean for the combined survey. The present analysis suggests that the *thick disk* has mean metallicity $\langle[M/H]\rangle = -0.6dex$ (with dispersion $\sigma_{\langle[M/H]\rangle} = 0.3dex$) and only a marginal metallicity gradient $\partial[M/H]/\partial z = -0.1dex/kpc$.

For the *thin disk*, we find a relatively low optimized value of $\langle[M/H]\rangle = -0.3\pm0.2dex$, along with a vertical gradient of $\partial[M/H]/\partial z = -0.6dex/kpc$. No gradient, however, has been found for the halo ($\langle[M/H]\rangle = -1.5 \pm 0.5dex$), which, due to the relatively bright magnitude limit, is undersampled in the present survey.

These results are in good agreement with recent evidence from detailed studies of kinematic and chemical data for more local stellar samples. In particular, they corroborate and *extend to the larger-scale Galaxy* the conclusions drawn from photoelectric Walraven photometry for a small complete sample of the brighter SGP stars [4], and thus will help further constrain current models of the formation and early evolution of the Galaxy [5].

References

1. Buser, R. and Rong, J.X. 1994, this volume
2. Buser, R., Karaali, S., Topaktas, L., Karatas, Y. 1994, A&AS (in press)
3. Buser, R. and Fenkart, R.P. 1990, A&A 239, 243
4. Trefzger, Ch.F., Pel, J.W., Gabi, S. 1994, A&A (in press)
5. Majewski, S.R. 1993, ARA&A 31, 575

THE FORMATION OF THE GALACTIC BULGE

M. SAMLAND AND G. HENSLER
Institut für Astronomie und Astrophysik
Universität Kiel, D-24098 Kiel, Germany

The question is adressed whether the problem of the stellar metallicity distribution and the dynamics of the stellar components in the bulge as found out by refined observations during recent years can be understood within the context of the evolution of the whole Galaxy. A selfconsistent galaxy model has to explain the apparent differences in the effective yields of the enrichment of bulge, disk and halo. Moreover, it has to account for the observed age-metallicity distribution of the stellar components. It appears that chemo-dynamical infall models provide a consistent description of the bulge, in particular the metallicity distribution of the K giants. It should be emphasized that simple closed-box models are not appropriate, because during the bulge formation there is infall of cloudy medium (CM), as well as outflow of hot, ionized gas ejected by supernovae type II (SNII). Therefore dynamical processes have to be taken into account. For details of the chemo-dynamical description we refer to Samland & Hensler (1994) and references therein.

The chemo-dynamical models show that the early metal enrichment of the interstellar medium in the bulge by means of SNII remains initially confined to the hot gas phase because of the inefficiency of phase mixing. Since the SNII also heat the intercloud medium (ICM), a SN-driven wind sets in, so that the enriched gas leaves to some extent the bulge region and enriches the outer parts of the galaxy. Since the clouds embedded in the ICM evaporate, the outflowing gas has a metallicity which is nearly solar. Fig. 1 shows the infall rate of the CM, the outflow rate of the ICM and the sum of both processes for the central 2 kpc. It is obvious, that most of the bulge mass is accreted in the period of $2 \cdot 10^9 - 8 \cdot 10^9$ years. During the same time the iron abundance in the CM increases from [Fe/H] $= -1.0$ to [Fe/H] $= 0.5$ and due to an efficient star formation most of the CM is converted into stars.

Fig. 2 shows the calculated iron distribution of K giants in comparison with the data of Rich (1988) (left) and the corrected data of McWilliam &

L. Blitz and P. Teuben (eds.), Unsolved Problems of the Milky Way, 429–430.
© 1996 *International Astronomical Union.*

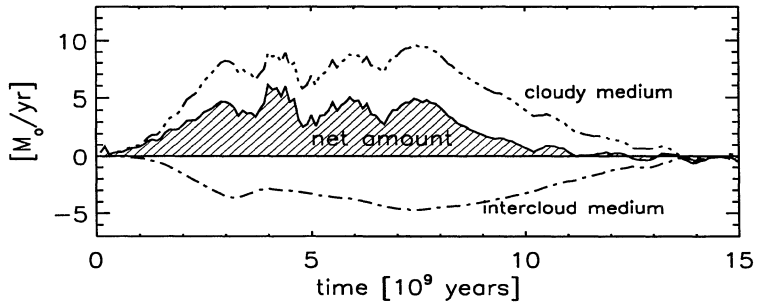

Figure 1. Infall rate of cloudy medium and outflow rate of intercloud medium for the central 2 kpc of the galaxy. The hashed area indicates the net effect of both processes.

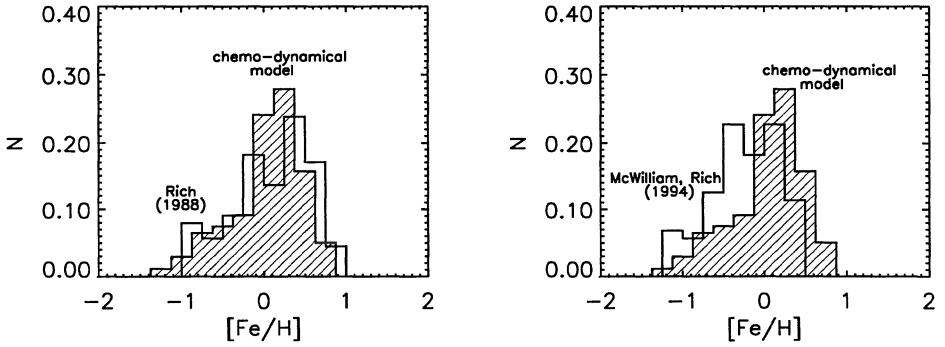

Figure 2. Abundance distribution of K giants in Baade's window in comparison with the distribution derived from a chemo-dynamical model (hatched area). The solid histogram outlined in the left diagram represents the original data from Rich (1988) and in the right diagram the corrected data by McWilliam & Rich, (1994).

Rich (1994) (right). Taking into account the uncertainities in the observational data and that the correction formula of McWilliam & Rich is only a rough fit, the model agrees convincingly well with the observations.

Moreover, the chemo-dynamical model explains the Fe, N and O distributions of bulge, halo and disk stars (Samland & Hensler, 1994). In contrast to the box-models, the chemo-dynamical models are self-consistent and there is no need of ad-hoc assumptions (e.g. different yields for bulge, disk and halo stars) to explain the stellar metallicity distributions.

References

McWilliam, A., Rich, R.M., (1994), *Astrophys. J. Suppl.* **91**,749
Rich, R.M., (1988), *Astron. J.* **95**,828
Samland, M., Hensler, G., (1994), *Metal Pre-Enrichment of the Galactic Disk* in: *IAU Symp. No. 169, Unsolved Problems of the Milky Way*, ed. L.Blitz

THE SCATTER OF METALLICITIES OF STARS IN THE SOLAR NEIGHBOURHOOD

B. FUCHS, C. DETTBARN AND R. WIELEN
Astronomisches Rechen-Institut Heidelberg, Germany

It is well known that the velocity dispersions of the stars in the solar neighbourhood increase with their ages (Wielen 1977). In Fig.1 we show $|W|$ weighted velocity dispersions (cf. Wielen 1977) of the stars in the Third Catalog of Nearby Stars (Gliese and Jahreiß 1994). Open symbols indicate main sequence stars and crosses indicate McCormick stars, a kinematically unbiased subset of the CNS3, respectively, whereas the filled symbols are the Edvardsson et al. (1993) data. Stars older than 14 Gyr are not shown because they are probably thick disk stars (Freeman 1991). We have assumed a maximum age of the old thin disk stars of 12 Gyr as suggested by the Edvardsson et al. data. As can be seen from Fig.1 both data sets fit ideally together. The solid line indicates a $\sigma \propto \tau^{1/2}$ law.

It is straightforward to derive from the epicyclic theory of stellar orbits the spatial dispersions corresponding to the velocity dispersions. For instance, the *rms* radial deviation of a stellar orbit from its original orbit is given by $\sigma_R = \sqrt{2.4}\sigma_U/\kappa$, if the galactic constants of the solar neighbourhood are used. σ_U is the dispersion of the radial velocity and κ is the epicyclic frequency, $\kappa = 36$ km s^{-1} kpc^{-1}.

If there is a galactic metallicity gradient it is quite obvious that the scatter of the metallicities of stars at a certain galactocentric distance, i.e. the solar neighbourhood, increases with the ages of the stars. Because older stars orbit on larger epicycles they can reach the solar neighbourhood from more distant parts of the galactic disk than younger stars. In Fig.2 we show metallicity dispersions determined from the Edvardsson et al. data versus radial dispersions calculated as described above. For this purpose the stars have been grouped into 5 age bins with about equal numbers of stars per bin. The mean ages of the groups are given in Gyr in Fig.2. The diagonal corresponds to a metallicity gradient of -0.1 dex/kpc. As can be seen from Fig.2 there is a very close correlation between the predicted and

L. Blitz and P. Teuben (eds.), Unsolved Problems of the Milky Way, 431–432.
© 1996 *International Astronomical Union.*

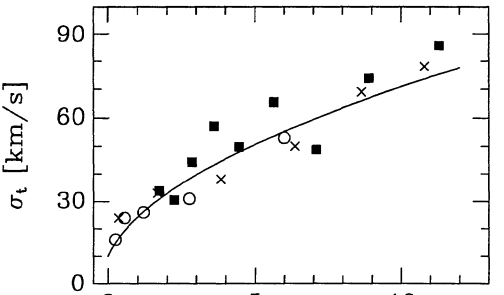

Fig. 1

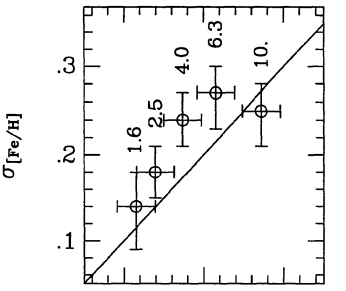

Fig. 2

actually observed metallicity spread. The deviations are of order of 0.1 dex which we interpret as the inherent cosmic dispersion of the star formation processes. Such a reduced scatter of [Fe/H] is expected in view of the low [α/Fe] scatter of the stars (cf. contributions of P. Nissen and R. Wyse at IAU Symp. No.164).

François and Matteucci (1993) have drawn the same conclusions concerning the role of orbital diffusion as major source of the observed [Fe/H] scatter. But Edvardsson et al. have put forward objections against this conjecture. They have considered a subset of stars in their sample which appear to lie on nearly circular orbits, and find that the metallicity scatter is essentially the same as for their full sample with no restrictions on the orbital parameters. They argue that these stars have always been close to the solar annulus so that the effect of orbital diffusion has been removed from the subset and that the large metallicity spread must be due to other effects. However the argument does not hold because stars which lie today on nearly circular orbits might have been scattered very recently onto them. We have derived elsewhere (Fuchs and Wielen 1987) the conditional probabilities for such cases and find that, looking backwards, the radial dispersion grows with age τ as $\sigma_R^2 = D_R\tau$. We have determined the diffusion coefficient D_R quantitatively and conclude that even in the restricted subset most of the observed metallicity scatter is due to orbital diffusion.

References

Edvardsson, B., Andersen, J., Gustafsson, B., Lambert, D.L., Nissen, P.E., Tomkin, J., 1993, *A&A* 275, 101.

François, P., Matteucci, F., 1993, *A&A* 280, 136.

Freeman, K.C. , 1991, in *Dynamics of Disc Galaxies*, B. Sundelius (ed.), Göteborg, Sweden, p.15.

Fuchs, B., Wielen, R., 1987, in *The Galaxy*, G.Gilmore, B. Carswell (eds.), Reidel, p.375.

Gliese, W., Jahreiß, H., in preparation.

Wielen, R., 1977, *A&A* 60, 263.

DIFFERENT LAWS OF INCREASING OF STELLAR DISPERSION: OBSERVATIONAL FLAWS OR NATURAL PROPERTY OF STELLAR POPULATION?

A.M. FRIDMAN, O.V. KHORUZHII AND A.E. PISKUNOV
Institute of Astronomy, Russian Academy of Sciences
48 Pyatnitskaya St., Moscow, 109017, Russia

Abstract. Observations show that in the solar neighborhood the velocity dispersions of disk stars increase with their age. In this work we present the results of a critical analysis of the existing interpretations of the data, as well as of previous theoretical explanations of the heating phenomenon. It is shown that different relaxation mechanisms based on star-cloud collisions can result in a wide set of age–velocity dispersion relations (AVDR). Thus the observed differing power laws of the heating of the stellar component can be a consequence of the different relaxation mechanisms.

The choice of a model of the motions of individual stars is crucial for a broad circle of astrophysical problems such as the dynamics and structure of galactic disks, their chemical evolution, and so on. Currently an agreement does not exist between different groups of investigators who have tried to construct the AVDR. (*e.g.* Wielen *et al.*, 1992, Meusinger *et al.* 1991).

The different constructions of the AVDR were done by different techniques. Thus the first possibility of explaining the disagreement in derived AVDRs is a simple choice between them. But the different results were also based on different disk-star samples. Thus a second possible explanation is that the different heating mechanisms, each of which has its own relaxation law, are more or less effective for different stellar classes or at different stages of relaxation. In this case the disagreement might not be the result of an error but might reflect instead the intrinsic properties of the system considered. In a recent paper (Fridman & Khoruzhii 1994) we show that star–cloud collisions can lead to various mechanisms of relaxation, each characterized by its own law of heating, and consequently the second possibility should be discussed.

Based on our analysis, main conclusions are as follows. (For details see Fridman & Khoruzhii 1994.)

L. Blitz and P. Teuben (eds.), Unsolved Problems of the Milky Way, 433–434.
© 1996 *International Astronomical Union.*

1. Star collisions with giant molecular clouds can be primarily responsible for the heating of the stellar population.
2. Different relaxation mechanisms based on these collisions exist, which can result in a wide set of age–velocity dispersion relations. So the observed various power laws of the heating of the stellar component can be a consequence of the different relaxation mechanisms.
3. These can cause two kinds of heating scenarios—saturated and unsaturated.
4. Saturated heating can occur both in a non-rotating collisional star–cloud system and in a differentially rotating one, independently of geometry, be it a mixture of stars and clouds or a thin layer of clouds and a thick layer of stars. Also this kind of heating can be caused by viscous stress in a differentially rotating stellar disk.
5. Mechanisms connected with differential rotation have not yet been studied. The classical works of Spitzer and Schwarzschild (1953) and Lacey (1984) take into account the effect of differential rotation only in words; the quantitative consideration in both works is inconsistent and describes only the "Maxwellianization" effect.
6. Unsaturated heating can be caused by at least two mechanisms: a) the friction due to the relative rotation of the gaseous and stellar disks, b) the heat transfer due to the spatial diffusion of stars.
7. The last two mechanisms are exemplified by the same characteristic time scale $\tau \simeq 10^{10}$ years and the same exponent of the age–velocity relation $p = 1/2$, that is consistent with Wielen's scenario (Wielen *et al.* 1992).
8. The relaxation mechanisms responsible for saturated heating (second scenario) are exemplified by similar values of the characteristic time scale $\tau \simeq 5 \cdot 10^7$–10^8 years, while the exponents in the age–velocity dispersion relations are very different: $p = 1/6$, $p = 1/5$, $p = 1/4$, $p = 1/3$, depending on the relaxation mechanism.

The main conclusion: Every stellar class can have its own intrinsic law of heating (relaxation), and this law need not be a power law with a unique exponent.

References

Fridman, A.M., & Khoruzhii O.V., 1994, In "Physics of the Gaseous and Stellar Discs of the Galaxy", ed. I.R.King, Astron. Soc. of the Pacific, 66,

Lacey, C. G. 1984, MNRAS, 208, 687.

Meusinger, H., Reimann, H.-G., & Stecklum, B. 1991, A.& Ap. , 245, 57.

Spitzer, L., & Schwarzschild, M. 1953, Ap. J., 118, 106.

Wielen, R., Dettbarn, C., Fuchs, B., Jahreiss, H., & Radons, G. 1992, in The Stellar Populations of Galaxies, ed. B. Barbuy & A. Renzini (Dordrecht: Kluwer), p. 81.

UBVI CCD PHOTOMETRY OF AN OLD OPEN CLUSTER AM-2

MYUNG GYOON LEE
Department of Astronomy, Seoul National University
Seoul, 151-742, Korea; mglee@astrog.snu.ac.kr

AM-2 is a sparse cluster located at low galactic latitude. It has been suspected to be a globular cluster. We present a study of AM-2 based on the deep $UBVI$ CCD photometry obtained using the Las Campanas duPont 2.5m telescope. The color-magnitude diagrams of AM-2 show (a) a main-sequence extending up to $V \approx 19$ mag at $(B-V) \approx 1.1$ mag, (b) a small number of red giant clump giants, (c) the brightest red giant at $V \approx 16.1$ mag and $(B-V) \approx 1.9$ mag, and (d) a small group of mysterious blue stars at $V \approx 16.6$ mag and $(B-V) \approx 0.9$ mag. We have estimated the reddening using the color-color diagram, $E(B-V) = 0.56 \pm 0.04$. The metallicity of the main-sequence stars has been estimated from the ultraviolet excess, $\delta(U-B)_{0.6} = 0.09 \pm 0.04$, to be [Fe/H] $= -0.4 \pm 0.2$ dex. The distance to the cluster has been measured using the Zero-Age-Main-Sequence fitting method, $(m-M)_0 = 14.8 \pm 0.3$ ($d = 9.1 \pm 1.4$ kpc). Finally we have estimated the age of the cluster using the Revised Yale isochrones and the Morphological Age Ratio (MAR) method, obtaining a value of 5 ± 1 Gyrs (Fig. 1). This shows that AM-2 is not a globular cluster, but an old open cluster.

L. Blitz and P. Teuben (eds.), Unsolved Problems of the Milky Way, 435–436.
© 1996 *International Astronomical Union.*

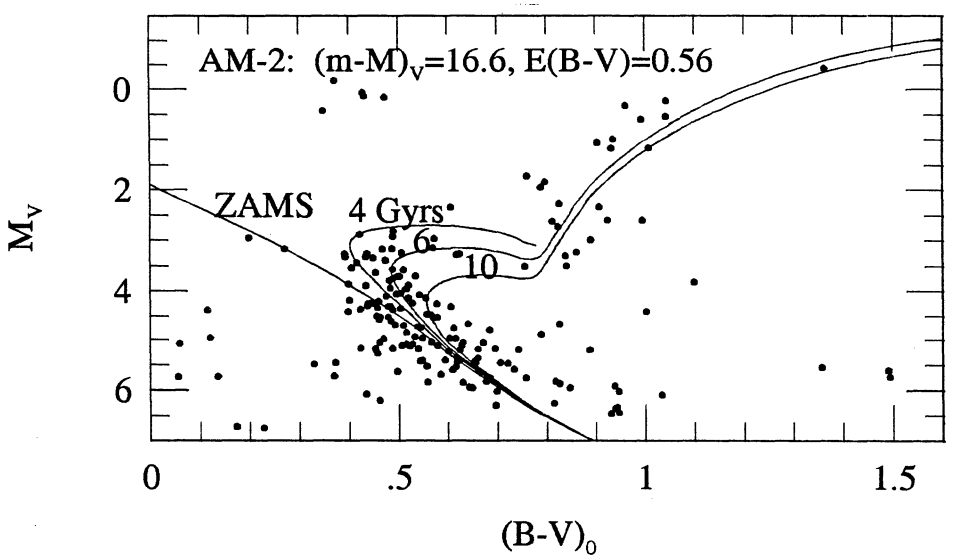

Figure 1. Estimation of the age of AM-2 using the Revised Yale isochrones for [Fe/H]=−0.4 dex and Y=0.28. Note that the age of AM-2 is estimated to be 5 ± 1 Gyrs.

Chapter 6

How are we to Understand the Large Scale Structure of the ISM?

WHAT DO GAMMA RAYS TELL US ABOUT THE ISM? NEW INSIGHT FROM THE COMPTON OBSERVATORY

HANS BLOEMEN
SRON-Utrecht[†]
Sorbonnelaan 2, 3584 CA Utrecht
The Netherlands

Abstract. Gamma-ray astronomy has become a rich field of research and matured significantly since the launch of NASA's Compton Gamma Ray Observatory in April 1991. Studies of the diffuse γ-ray emission of the Galaxy can now be performed in far more detail and extended into the MeV regime, including both continuum and line emission. These studies provide unique insight into various aspects of the interstellar medium, in particular of the cosmic-ray component. This paper gives a brief review on the diffuse Galactic γ-ray emission and summarizes early results and prospects from the Compton Observatory.

1. Introduction

The diffuse continuum γ-ray emission of the Milky Way is a unique tracer of cosmic rays. The observed radiation at energies above $\sim$50 MeV, well studied with the SAS-2 and COS-B satellites, seems indeed largely of diffuse origin. The basic findings are summarized in Section 2. The EGRET telescope aboard the Compton Observatory (Thompson et al. 1993) enables now more detailed studies, but these are largely in progress. A preliminary comparison with the COS-B observations is presented here. At low energies ($\lesssim$ 50 MeV) an important contribution from unresolved point sources cannot be excluded. The COMPTEL telescope on board the Compton Observatory (Schönfelder et al. 1993) provides for the first time extensive imaging possibilities in the 1–30 MeV range. First findings on the diffuse

[†]also Leiden Observatory

L. Blitz and P. Teuben (eds.), Unsolved Problems of the Milky Way, 437–446.
© 1996 *International Astronomical Union.*

continuum emission at these energies are discussed in Section 3. With an energy resolution of 5–8%, COMPTEL is capable of imaging in narrow energy bands, which has already proved to be of great value for studies of nuclear deexcitation γ-ray lines (Section 4). These lines either originate from nuclei of which the excited levels are populated in nuclear interactions (again providing unique information on cosmic rays) or from long lived radionuclei produced in various nucleosynthesis processes. Below $\sim$1 MeV, in the hard X-ray / low-energy γ-ray regime, very little is known about any diffuse emission from the Galactic disk (see e.g. Gehrels & Tueller 1993 and Ramaty & Skibo 1993). This paper is limited to energies above 1 MeV.

2. High-energy gamma-ray continuum — EGRET vs COS-B

The diffuse continuum γ-ray emission of the Galaxy largely originates from interactions of cosmic-ray (CR) particles with the interstellar gas. Beyond about 100 MeV, CR protons and α-particles with energies of typically 1–10 GeV play a dominant role through the decay of π°-mesons that originate from nuclear interactions. At lower γ-ray energies, the diffuse continuum emission is largely bremsstrahlung from low-energy CR electrons (typically 1–100 MeV). Away from the gaseous disk, a third emission component may be important, namely inverse-Compton radiation, which involves the scattering of high-energy electrons ($>$ 10 GeV) on low-energy photons (mainly optical and infrared photons and the 3 K background radiation).

A comprehensive review on high-energy γ-ray studies of the Milky Way using SAS-2 and COS-B observations is given by Bloemen (1989). Recent updates are presented by Strong (1994) and Bloemen (1993).

Several γ-ray studies have been aimed at determining the radial distribution of cosmic rays in the Galaxy. This requires independent information on the distribution of the target gas particles with which the cosmic rays interact. The results from the latest and most robust analyses (Bloemen et al. 1986; Strong et al. 1988) were obtained from correlation studies with HI and CO surveys, using the velocity information as a distance indicator. Only a weak Galactocentric gradient for the relevant CR particles (mainly protons) was found. Since all potential CR sources show a much steeper radial fall-off, a large CR halo seems required to explain the weak gradient. This is hard to reconcile with CR measurements near Earth, which indicate an effective CR scale height in the solar vicinity of $\lesssim$ 3 kpc (Webber et al. 1992, Bloemen et al. 1993). The lack of a strong CR gradient indicates that such a 'small' scale height can only be representative for the Galaxy as a whole if the CR source distribution has a weak gradient as well. On the other hand, the CR gradient may actually be underestimated due to hidden gas in the outer Galaxy (Lequeux, Allen, Guilloteau 1994).

Instead of adopting a CR distribution with a radial variation only, Bertsch et al. (1993) have considered a model that assumes cosmic rays to be preferentially located in regions of high gas density, based on the argument that the weight of the matter ties the magnetic fields and hence the cosmic rays to these regions (Bignami and Fichtel 1974; Fichtel and Kniffen 1984). This *coupling model* and the *gradient model* (as discussed above) appear to describe the γ-ray data equally well. This is basically due to the fact that the radial CR distribution in the gradient model (beyond a few kpc from the Galactic center) is similar to the radial distribution of the total gas surface density when smoothed over a few kpc (at least when the Columbia/CfA CO survey and the radial-unfolding method of Bronfman et al. 1988 are used). If the density of (GeV) cosmic rays and the matter density are correlated, it is indeed most realistic that this occurs on scales of a few kpc (also used by Bertsch et al.), because this is the characteristic CR diffusion path length. Melisse and Bloemen (1990) have shown that the gradient model fits the γ-ray data much better than a model in which CR and gas density are correlated on small scales of typically 100 pc, which appears to be mainly due to the small scale height of the γ-ray emitting disk inherent to this coupling model. This result is probably the most direct evidence from γ-ray astronomy for the existence of a (flat) halo distribution of GeV CR protons and confirms similar conclusions from radio synchrotron data for CR electrons (e.g. Baldwin 1976, Beuermann et al. 1985).

If independent information on the CR distribution throughout the Galaxy would be available, then γ-ray observations could be used as a tracer of the total gas column density. For some studies, the CR density is sufficiently constrained to derive meaningful information on interstellar gas components that is otherwise hard to obtain. This holds for the molecular gas and the extended warm ionized medium (the so called Reynolds layer). Valuable information on the CO-to-H_2 calibration factor has thus been obtained for the Galaxy at large (see e.g. reviews by Wolfendale 1988 and Bloemen 1989) and for regions that are of particular interest, such as the Galactic center (Blitz et al. 1985) and the Orion complex (Bloemen et al. 1984). Regarding the ionized medium (see Reynolds 1993 and references therein), it is interesting that almost half of the observed γ-ray emission at medium latitudes ($5° \lesssim |b| \lesssim 20°$) in the general direction of the inner Galaxy cannot be explained by CR-matter interactions if only atomic and molecular gas are involved. Although inverse-Compton emission can explain part of the excess, a significant fraction should probably be ascribed to the ionized gas which was not included in the γ-ray modeling (provided that this medium does not extend far beyond the solar circle).

Given the higher sensitivity, higher angular resolution, and lower instrumental background of the EGRET observations, the analyses previously

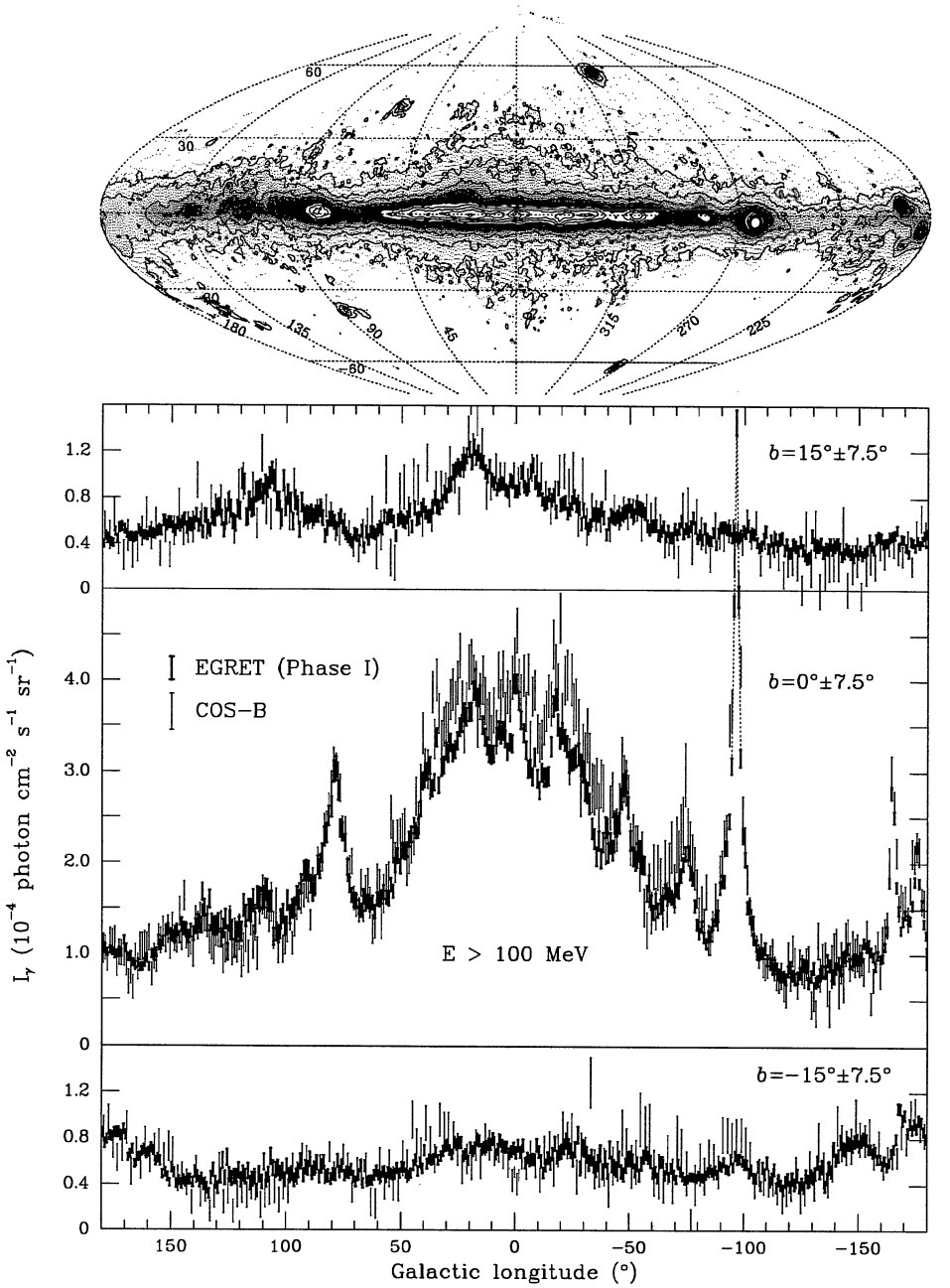

Figure 1. Top: Preliminary EGRET full-sky image (> 100 MeV) derived from a combination of all observations obtained during the first 18 months of the Compton Observatory mission (archival data). *Bottom:* Comparison of EGRET (archival data) and COS-B longitude profiles (> 100 MeV) for 15° wide latitude bands centered at $b = -15°$, 0°, and +15°. An instrumental (on-axis) background level of 7×10^{-5} photon cm^{-2} s^{-1} sr^{-1} has been subtracted from the COS-B intensities.

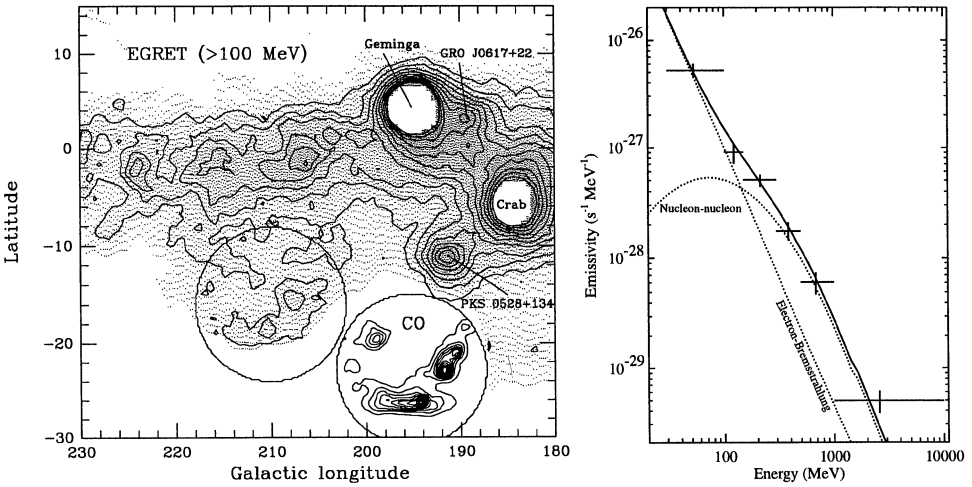

Figure 2. Left: EGRET image (> 100 MeV, archival data) of the Galactic anti-center, including the Orion complex (circle). Contour levels start at 8×10^{-5} photon cm^{-2} s^{-1} sr^{-1} with steps of 1.5×10^{-5}. The inset shows the Columbia CO observations. *Right:* EGRET spectrum of the Orion complex (Digel et al. 1995).

applied to the COS-B data can now be performed with higher accuracy and extended to small-scale regions and narrower energy bands. Very few results are available yet, but Figures 1 and 2 may illustrate what level of accuracy can be achieved with the EGRET observations. Figure 1 shows a comparison of the COS-B data and archival EGRET data (> 100 MeV). Since the EGRET observations are basically free of any instrumental background, whereas the COS-B observations are not, an instrumental (on-axis) background level of 7×10^{-5} photon cm^{-2} s^{-1} sr^{-1} (which appeared to be an optimum choice) was subtracted from the COS-B intensities. Long-term background variations during the COS-B mission were already accounted for in combining the individual observations — see Strong et al. 1987. Figure 1 shows that the EGRET and COS-B observations appear to be in good agreement, although the EGRET intensities seem to be systematically about 10% lower in the central radian of the Galactic disk. It should be emphasized, however, that the EGRET observations used here are considered to be preliminary. The level of detail that can be achieved with the EGRET observations is further illustrated in Figure 2, which shows a blow-up of the Galactic anti-center region, including the Orion region, together with a spectrum of the Orion complex (from Digel et al. 1995). Note that Figures 1 and 2 are based on data from the first observational phase only (about 18 months), so the statistical accuracy will significantly improve when further observations are added.

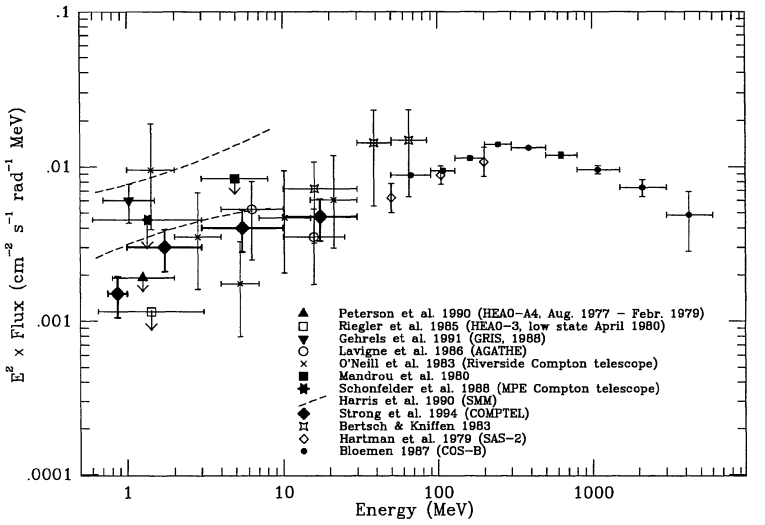

Figure 3. A compilation of flux estimates for the inner Galaxy, multiplied by E^2. An E^{-2} spectrum was assumed to calculate effective energies. The published fluxes from HEAO-3 and GRIS were converted to flux-per-radian by dividing by the FWHM of the instrument field of view. The references can be found in Bloemen et al. (1994a). The COMPTEL data points are from Strong et al. (1994).

3. Low-energy gamma-ray continuum — first COMPTEL results

For γ-ray energies < 50 MeV, our knowledge was very limited prior to COMPTEL because observations had mainly been made with non-imaging instruments with fields of view of typically tens of degrees. Figure 3 shows a compilation of flux estimates for the central radian of the Galactic disk. Preliminary broad-band images of the Milky Way obtained with COMPTEL (Bloemen et al. 1994a, Strong et al. 1994) show a structured ridge of emission along the Galactic equator (the integrated fluxes from the central radian are included in Figure 3). Starting from the assumption that the observed emission is of diffuse origin and due to electron bremsstrahlung, Strong et al. (1994) fitted a model based on HI and CO surveys and derived unique information on the low-energy CR electron spectrum ($\lesssim 100$ MeV), as shown in Figure 4. It should be emphasized, however, that the observed emission and model show distinct differences (Bloemen et al. 1994a). This may be due to an important contribution from unresolved point sources, but may also result from a very inhomogeneous distribution of low-energy CR electrons, which is largely determined by the distribution of the CR sources and the characteristics of the ambient interstellar medium. A closely related and very interesting preliminary finding from the analysis by Strong et al. is the indication for an energy dependence of the relative contribution from

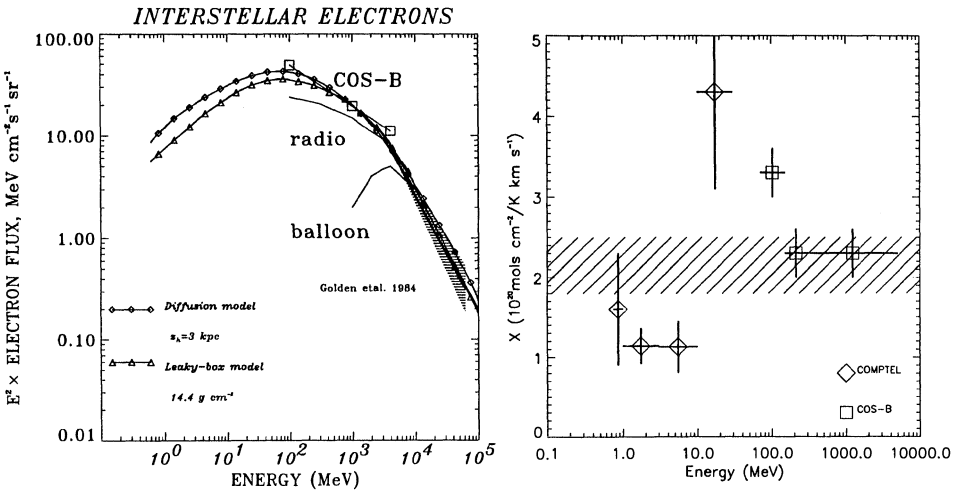

Figure 4. Left: Interstellar electron spectrum, illustrating the unique information that is provided by COMPTEL at low energies ($\lesssim$ 100 MeV). *Right:* Values of the "CO-to-H_2 conversion factor" derived from COMPTEL and COS-B studies, showing evidence for an energy dependence of the relative contribution from molecular clouds to the total γ-ray emission from the disk, with a peak contribution at 10-100 MeV. *From Strong et al. 1994.*

molecular clouds to the total γ-ray emission from the disk, with a peak contribution at 10-100 MeV (Figure 4). If confirmed in further analyses, this may have important implications for our understanding of the acceleration and propagation of CR electrons in/near molecular clouds.

4. Gamma-ray line emission

COMPTEL has good potentials for studies of de-excitation lines, which result from nuclear interactions and radioactive nucleosynthesis products (of which the lines from ^{26}Al and ^{44}Ti are of main interest for ISM studies).

Until recently, γ-ray lines resulting from accelerated particle interactions had been observed only from solar flares, namely the lines of ^{12}C at 4.44 MeV, of ^{16}O at 6.13 MeV, and of ^{20}Ne, ^{24}Mg, ^{28}Si, ^{32}S and ^{56}Fe in the 1–2 MeV range. COMPTEL has now detected intense emission in the 3–7 MeV range from the Orion complex, which was identified with the ^{12}C and ^{16}O de-excitation lines at 4.44 MeV and 6.13 MeV (Bloemen et al. 1994b), as illustrated in Figure 5. In view of early theoretical predictions (Meneguzzi and Reeves 1975, Ramaty et al. 1979), this discovery came as a pleasant surprise, the observed flux being much larger than anticipated. So far, Orion has revealed only upper limits in the 1–3 MeV range.

Bykov and Bloemen (1994) have shown that these results may find a novel explanation in the strong overabundance of oxygen in the supernova

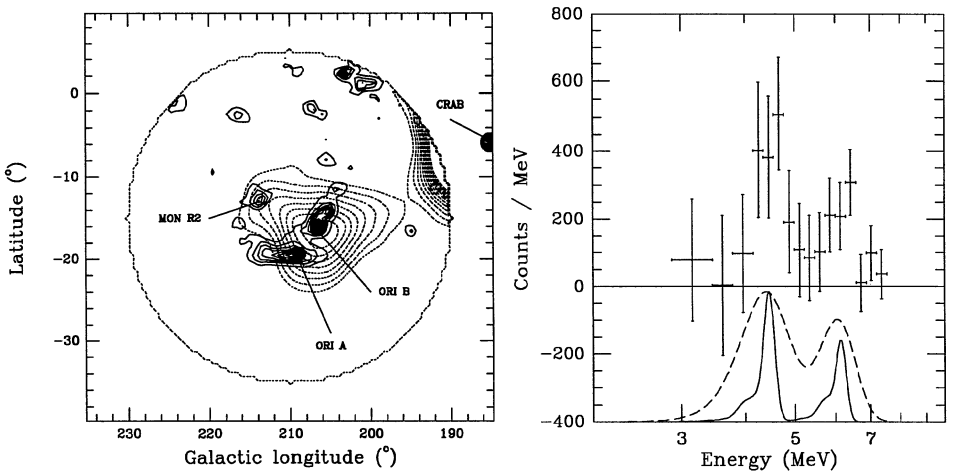

Figure 5. COMPTEL map (dotted contours) and spectrum of the Orion Complex, showing evidence for 3–7 MeV emission that can be attributed to the 4.44 MeV and 6.13 MeV de-excitation lines of carbon and oxygen following energetic nuclear interactions. The Columbia CO observations are superimposed in the map for comparison (solid contours). The excess in the upper right originates from the Crab pulsar. *From Bloemen et al. 1994b.*

ejecta from massive stars (Weaver and Woosley 1993, Woosley et al. 1993), in combination with the efficient acceleration of low-energy CR nuclei in regions with strong stellar winds and multiple supernova explosions (Bykov and Toptygin 1990, Bykov and Fleishman 1992). In this scenario, the γ-ray lines originate from energetic nuclei that are extracted from the enriched hot medium in regions of massive star formation and bombarding the ambient dense gas in clouds and shells. The width of nuclear interaction lines provides crucial information on the processes that occur, but the available COMPTEL observations of Orion are inconclusive. Detailed model spectra of the Orion region are presented by Ramaty et al. (1994). The study of nuclear interaction lines has broad applications: it provides direct insight into particle acceleration (in fact the very origin of cosmic rays), into the composition and enrichment of the ISM in regions of massive star formation (with important implications for nucleosynthesis studies), and into the role of cosmic rays in the ISM in general (such as CR ionization and heating).

The 1.809 MeV line emission from ^{26}Al ($\tau \simeq 10^6$ years) has now for the first time been mapped along the Milky Way by COMPTEL (Diehl et al. 1994, 1995a). Although the structured appearance of the observed emission (Figure 6) clearly excludes a dominant contribution from novae (Diehl et al. 1994, 1995a), alternative scenarios that have been proposed could so far not be distinguished. These scenarios largely invoke massive stars, as reviewed

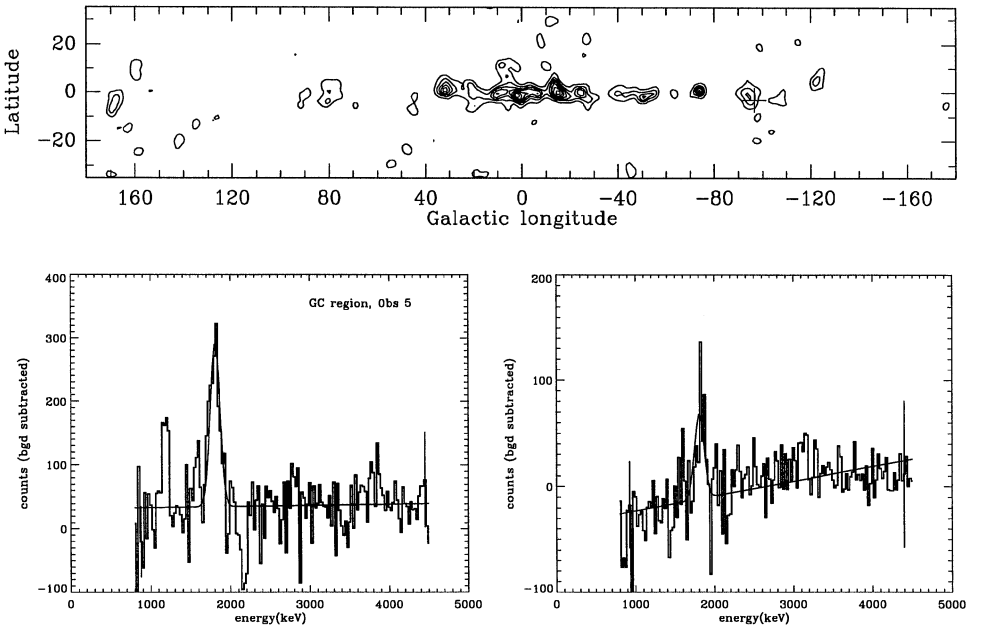

Figure 6. Top: COMPTEL map of the Galactic ^{26}Al 1.809 MeV emission, showing evidence for localized emission regions along the Milky Way (including a possible detection of the Vela supernova remnant at $\ell \simeq -97°$). The continuum radiation is removed using a model derived from the observed emission at adjacent energies. *Bottom:* Examples of background-subtracted counts spectra, obtained from one single observation of the inner Galaxy (left) and a combination of available observations of the Vela region (right). Typical statistical error bars are shown. *From Diehl et al. 1995ab.*

by Prantzos (1991). Apart from a possible detection of the nearby Vela supernova remnant (Diehl et al. 1994, 1995b), essentially all other localized emission regions that can be seen in Figure 6 must be due to an ensemble of sources. The intermittent nature of massive-star formation and the 1.809 MeV line, both on time scales of typically 10^6 years, may indeed explain the structured appearance of the 1.809-MeV Milky Way, but it remains to be seen which sources are prime contributors.

The 1.156 MeV line from the decay of ^{44}Ti into ^{44}Ca ($\tau \simeq 80$ years) is not only of importance for nucleosynthesis studies, but also provides an interesting possibility to search for obscured supernovae. The prime known candidate, Cas A, was already detected by COMPTEL (Iyudin et al. 1994).

Although this paper has only provided a first glance at the COMPTEL and EGRET observations of the Galactic diffuse emission, it may be clear from the above that γ-ray studies of the ISM have great potentials. With an expected mission lifetime of 6–10 years, the Compton Observatory will provide further insight into the γ-ray sky for several years to come.

Acknowledgements. I am grateful to all colleagues who have made the Compton Observatory such a great success and made this work possible. This study has made use of data obtained through the Compton Observatory Science Support Center GOF account, provided by NASA-GSFC.

References

Baldwin, J.E.: 1976, in *The Structure and Content of the Galaxy and Galactic Gamma Rays*, eds. C. Fichtel and F.W. Stecker, GSFC, p. 206
Bertsch, D.L., et al.: 1993, *Astrophys. J.* 416, 587
Beuermann, K., Kanbach, G., Berkhuijsen, E.M.: 1985, *Astron. Astrophys.* 153, 17
Bignami, G.F., Fichtel, C.E.: 1974, *Astrophys. J. Lett.* 189, L65
Blitz, L., Bloemen, H., Hermsen, W., Bania, T.M.: 1985, *Astron. Astrophys.* 143, 267
Bloemen, H.: 1989, *Ann. Rev. Astron. Astrophys.* 27, 469
Bloemen, H.: 1993, in *Back to the Galaxy*, eds. Holt & Verter, AIP Conf. Proc. 278, 409
Bloemen, H., et al.: 1984, *Astron. Astrophys.* 139, 37
Bloemen, H., et al.: 1986, *Astron. Astrophys.* 154, 25
Bloemen, H., Dogiel, V.A., Dorman, V., Ptuskin, V.: 1993, *Astron. Astrophys.* 267, 372
Bloemen, H., et al.: 1994a, *Astrophys. J. Suppl. Ser.* 92, 419
Bloemen, H., et al.: 1994b, *Astron. Astrophys.* 281, L5
Bykov, A.M., Bloemen, H.: 1994, *Astron. Astrophys.* 283, L1
Bykov, A.M., and Toptygin, I.N.: 1990, *Sov. Phys. JETP* 71, 702
Bykov, A.M., Fleishman, G.D.: 1992, *Mon. Notices Royal Astron. Soc.* 255, 269
Diehl, R., et al.: 1994, *Proceedings Second Compton Symposium*, eds. Fichtel et al., AIP Conf. Proc. 304, p. 147
Diehl, R., et al.: 1995a, *Astron. Astrophys.* , in press
Diehl, R., et al.: 1995b, *Astron. Astrophys.* , submitted
Digel, S.W., Hunter, S.D., Mukherjee, R.: 1995, *Astrophys. J.* , in press
Fichtel, C.E., Kniffen, D.A.: 1984, *Astron. Astrophys.* 134, 13
Gehrels, N., Tueller, J.: 1993, *Astrophys. J.* 407, 597
Iyudin, A., et al.: 1994, *Astron. Astrophys.* 284, L1
Melisse, J., Bloemen, H.: 1990, *Proc. 21st Int. Cosmic Ray Conf.* 1, OG 3.1-18
Meneguzzi, M., Reeves, H.: 1975, *Astron. Astrophys.* 40, 91
Prantzos, N.: 1991, in *Gamma-Ray Line Astrophysics*, AIP Conf. Proc. 232, p. 129
Ramaty, R., Kozlovsky, B., Lingenfelter, R.E: 1979, *Astrophys. J. Suppl. Ser.* 40, 487
Ramaty, R., Kozlovsky, B., Lingenfelter, R.E: 1994, *Astrophys. J. Letters* , in press
Ramaty, R., Skibo, J.: 1993, in *Back to the Galaxy*, eds. Holt & Verter, AIP Conf. Proc. 278, 399
Reynolds, R.J.: 1993, in *Back to the Galaxy*, eds. Holt & Verter, AIP Conf. Proc. 278, 156
Schönfelder, V., et al.: 1993, *Astrophys. J. Suppl. Ser.* 86, 657
Strong, A.W., et al.: 1987, *Astron. Astrophys. Suppl. Ser.* 67, 283
Strong, A.W., et al.: 1988, *Astron. Astrophys.* 207, 1
Strong, A.W.: 1994, *Proceedings Second Compton Symposium*, eds. Fichtel et al., AIP Conf. Proc. 304, p. 463
Strong, A.W., et al.: 1994, *Astron. Astrophys.* 292, 82
Thompson, D.J., et al.: 1993, *Astrophys. J. Suppl. Ser.* 86, 629
Webber, W.R., Lee, M.A., Gupta, M.: 1992, *Astrophys. J.* 390, 96
Weaver, T.A., Woosley, S.E.: 1993, *Physics Reports* 227, 65
Wolfendale, A.W.: 1988, in *Molecular Clouds in the Milky Way and External Galaxies*, eds. R. Dickman et al., Springer-Verlag, Heidelberg, p. 76
Woosley, S.E., Langer, N., Weaver, T.A.: 1993, *Astrophys. J.* 411, 823

HI IN THE MILKY WAY

Selected Problems Illustrated by the Leiden/Dwingeloo Survey

W.B. BURTON, DAP HARTMANN, AND S.R.D. WEST

Leiden Observatory
P.O. Box 9513, Leiden, 2300 RA, The Netherlands

Abstract. Some of the principal problems which can be confronted with HI observations of our Galaxy are illustrated here by a selection of maps showing the disposition on the sky of HI emitting in particular velocity ranges. The data are from the new Leiden/Dwingeloo survey of the entire sky north of $\delta \geq -30°$, which has occupied the 25–meter radio telescope of the Netherlands Foundation for Research in Astronomy for a period of five years. The tendency of the general gas/dust correlation to involve some HI structures with quite anomalous velocities is illustrated by comparing some λ21–cm data taken on a finer grid using the Arecibo 1000–foot telescope with IRAS data in the 100–micron band.

A survey of neutral atomic hydrogen in our Galaxy has been completed using the 25–meter radio telescope in Dwingeloo. The new observations span the entire sky down to $\delta = -30°$ with a true–angle grid spacing of 0.°5 in both l and b. The spectral resolution of the survey was set by the spacing of 1.03 km s^{-1} between each of the 1024 channels of the DAS digital autocorrelation spectrometer; the effective kinematic range of the material covers velocities (measured with respect to the Local Standard of Rest) between -450 km s^{-1} and $+400$ km s^{-1}. The characteristic *rms* limit on the measured brightness–temperature intensities is 0.07 K.

The data of the Leiden/Dwingeloo survey represent an improvement over that of earlier large–scale surveys by an order of magnitude or more in at least one of the principal parameters of sensitivity, spatial coverage, or spectral resolution. The observational and correction procedures are discussed in detail by Hartmann (1994).

L. Blitz and P. Teuben (eds.), Unsolved Problems of the Milky Way, 447–468.
© 1996 *International Astronomical Union.*

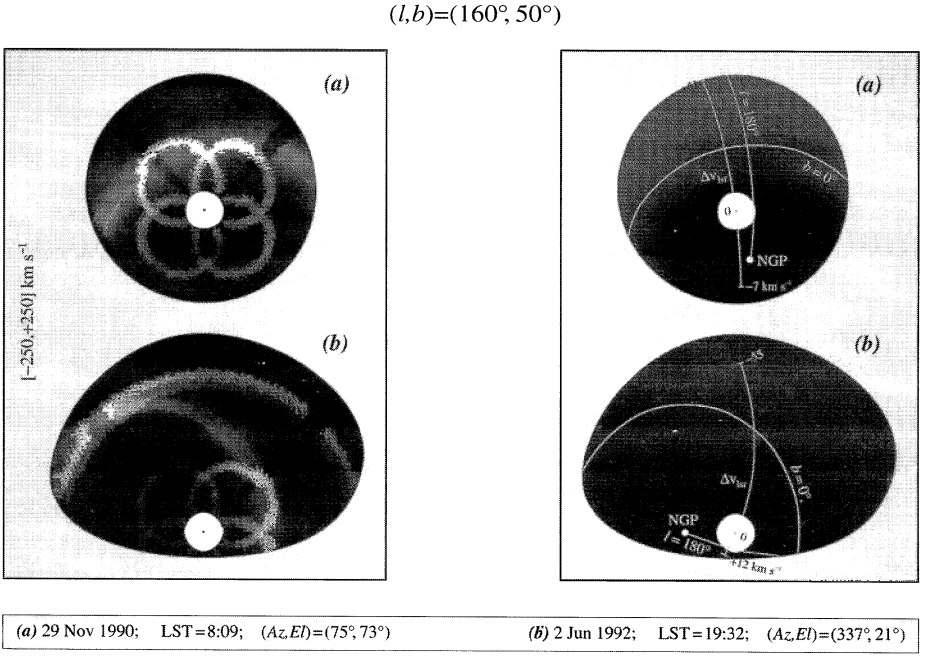

Figure 1. Illustration of the differing manner in which the stray radiation contaminates two observations made toward the single direction $(l, b) = (160°, 50°)$. The right–hand panel indicates the orientation of the Milky Way when the two spectra were taken. The white circle corresponds to the extent of the near sidelobes; the center of the circle indicates the pointing of the main beam. The placements of the galactic equator $b = 0°$, and of the anticenter line $l = 180°$, are indicated for the two observations. The left–hand panel shows the differing fluxes perceived by the far sidelobe pattern; the sensitive features of this pattern fall on quite different parts of the Milky Way, and thus contribute quite differently to the resulting spectra, shown in Figure 2.

The Leiden/Dwingeloo survey is the first major survey to be largely corrected for contamination by stray radiation. (The sensitivity of the earlier Hat Creek surveys did not warrant the correction; the influence of stray radiation on the Bell Labs data was only minor because the horn reflector is not blocked by a feed–support structure.) The nature of the stray–radiation correction is illustrated by Figure 1; its importance is demonstrated by Figure 2. The correction involved convolving the empirically–determined response of the Dwingeloo antenna with the measured all–sky λ21–cm distribution. The correction was applied in collaboration with P. Kalberla and U. Mebold of the University of Bonn, using a modified version of the algorithm described by Kalberla *et al.* (1980). A detailed description of the application of the stray–radiation correction to the Leiden/Dwingeloo data is given by Hartmann *et al.* (1995).

The input HI sky comprised the Leiden/Dwingeloo survey itself, reduced in all aspects except for the stray–radiation correction. (The correction could therefore only be applied after the entire accessible sky had been observed.) For each individual HI spectrum entering the final survey, the input sky was separately consulted so that the situation at the date and time appropriate to each observation could be accounted for.

A model of the Dwingeloo antenna response was based on interferometric measurements made earlier by Hartsuijker *et al.* (1972), on holographic measurements of the telescopes of the Westerbork Synthesis Radio Telescope reported by van Someren Greve (1991), and on our own measurements of bright continuum sources. Corrections were determined separately for the far sidelobes (*FSL*) and for the near sidelobes (*NSL*). The *FSL* contribution is largely due to reflections off the feed–support structure and to radiation entering the feed directly, for example after reflection off the ground. The *NSL* contribution (taken as that perceived within 16° from the pointing axis of the main beam) is largely due to imperfections in the main beam of the antenna pattern.

The amount of emission impinging upon the sidelobes, and its velocity structure, depends on the perception of the Milky Way by the extended antenna pattern during the course of the observation. Figure 1 shows that this perception varies fundamentally for different times and dates, and for different observed positions. When a particular position is tracked, different portions of the Galaxy radiate into different regions of the antenna response pattern; these differing portions of the Galaxy will also have varying relative motions with respect to those characteristic of the particular direction in question. Figure 2 shows that two observations made toward the same direction on the sky can return spectra which differ in accordance with the manner in which the antenna response perceives the kinematics and structure of the HI sky.

The 0.07 K *rms* sensitivity limit on the brightness temperatures measured in the new material depends crucially on the success of the stray–radiation correction. This limit is about an order of magnitude less than the peak intensity characteristically entering the far sidelobes of the Dwingeloo antenna; more importantly, at lower $|b|$ it is typically two orders of magnitude less than the peak intensity entering the near sidelobes. The emission entering the *FSL* pattern is always a concern: because it is largely contributed by the HI disk near the galactic equator, its velocity structure typically extends over some 150 km s^{-1}. Figure 2 shows that in regions where the total HI emission is exceptionally weak, for example in the direction of the HI–deficient region in Ursa Major discussed by Lockman *et al.* (1986), the flux entering the sidelobes may be as strong as, or even in excess of, that received by the main beam of the telescope.

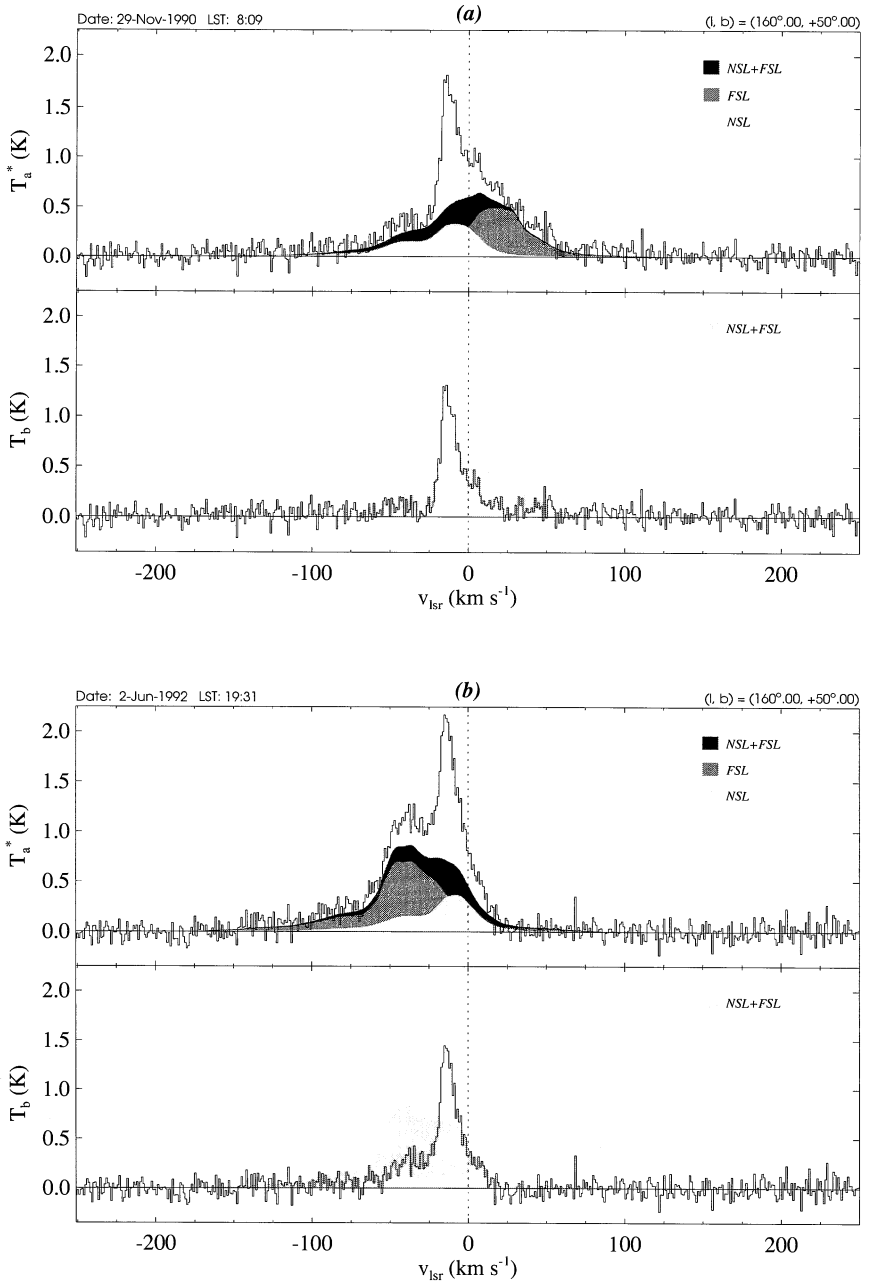

Figure 2. Illustration of the differing influence of stray radiation for two separate observations made on different dates toward the same direction, $(l, b) = (160°, 50°)$. (a) Observation made in November, 1990, at high elevation (73°). The *FSL* contribution is less prominent than in (b), because the spillover ring was directed toward the ground rather than toward the sky. (b) Spectrum observed in June, 1992, at an elevation of 21°. Here the spillover ring was pointing toward the sky. Figure 1 clarifies how *FSL* contamination entering the two spectra differs in intensity as well as in velocity.

The *NSL* contribution in a given direction shows little variation with time as the position of the main beam changes. The intensity of the near-sidelobe contamination can, however, be high. At low $|b|$, the contamination level is typically 10 K; although, unlike in the *FSL* case, the *NSL* contamination largely mimics the structure in the profile in question, correction for its total contribution is important to accurate determination of column depths, optical depths, and temperatures.

The Leiden/Dwingeloo HI survey is suited to a range of astronomical investigations; among those of most interest to us are the following:

- The survey is the first to embrace the kinematic regimes of the high– and intermediate–velocity clouds as well as that of gas at conventional velocities. There are a number of indications that the distinctions drawn between these regimes are arbitrary in important regards.
- Many dust cirrus features studied in the infrared have gas counterparts which can be traced to quite anomalous velocities. At least some interstellar cirri are evidently not quiescent objects with only modest energetics.
- The sensitivity and latitude coverage of the new data allow an improved description of the warp and flare of the gas layer in the outer Galaxy. It remains puzzling that the gas/dust correlation, which is so generally tight in the inner Galaxy and locally, apparently breaks down in the outer Galaxy; kinematic unraveling of the correlation as a function of galactocentric distance represents an important challenge.
- The relationship of HI intensity to interstellar extinction analyzed by Burstein and Heiles (1978) raised astrophysical questions which should be addressed again using modern data. Particularly important are the zero–point offset found in the relation between reddening and N_{HI}, and the variation in the gas–to–dust relationship found in different regions.
- Regions of exceptionally–low total N_{HI} in addition to the "hole" identified by Lockman *et al.* (1986) are being identified and their velocity characteristics studied. Regions of low N_{HI} are particularly of interest because of the role of interstellar HI in obscuring background X–rays.
- The extension of velocity information beyond the coverage and resolution available earlier will support determination of HI areal filling factors; important constraints can also be put on the more elusive volume filling factor. These factors are important to discussions of interstellar turbulence and scale–height maintenance, and of radiation penetration.
- The interstellar HI is largely marshaled into filamentary structures, variously named. Additional study of the form and motions of such structures will reveal the macroscopic energetics of the interstellar medium. Some structures have a kinematic span beyond the range of earlier data, suggesting a revision of the currently accepted energetics.

Figure 3. Distribution over the plane of the sky of integrated HI emission contributed over the full velocity range -450 km s^{-1} $\leq v \leq +400$ km s^{-1}. Integration over such a large velocity range measures the total column depth (assuming optical thinness) and shows some aspects of galactic morphology, but suppresses crucial kinematic information. $\Longrightarrow$

We illustrate a selection of these open problems (see also Burton, 1992) by representative slices through the Leiden/Dwingeloo HI data cube, supported by only cursory remarks. The deployment of astrophysically–relevant structures in a three–dimensional data cube is notoriously difficult to display (and, in consequence, also difficult to determine). Physical structures, not uncommonly with filamentary, or otherwise complicated, forms snake through any data cube constructed of orthogonal planes of l, b, and v; flat–plane cuts through such a data cube will not reveal the complete structural nature of the HI features. Nevertheless, such cuts are the most useful when displaying images of the entire sky. The slices shown here represent the distribution on the sky of integrated HI emission originating from the indicated velocity interval. (At high $|b|$, rectangular images are, of course, severely distorted; the principal advantage of rectangular images extending to the polar caps is that all the data can be displayed in a single map.)

Figure 3 shows the distribution of the total HI emission integrated over the full effective velocity range characterizing the new material, -450 km s^{-1} $\leq v \leq +400$ km s^{-1}. This map shows the sky coverage of the survey and displays some aspects of galactic morphology, but crucial kinematic information is suppressed by the large integration range.

Figure 4 shows the sky distribution of HI radiating between -90 km s^{-1} and -80 km s^{-1}. This range is particularly interesting because it falls between the regimes conventionally considered to separate the high–velocity–cloud objects from the intermediate–velocity ones. The distinction between these two classes of objects may be largely arbitrary; the high–velocity and the intermediate–velocity clouds merge rather continuously in velocity. The sky images at less extreme velocities show a smooth merger also of the IVCs with gas at conventional velocities; in fact, IVCs are not uncommonly associated with disturbances in the zero–velocity ambient gas, and there are some indications that the same conclusion holds for the HVCs. Perhaps the most important difference between the HVC and IVC objects is given by the failure to detect either dust emission or molecular emission from the HVC objects, despite substantial efforts to do so. IVCs, on the contrary, frequently have cirrus counterparts, and a few have associated molecular clouds; these few exceptions highlight the total lack of molecular–cloud and dust emission from the HVCs.

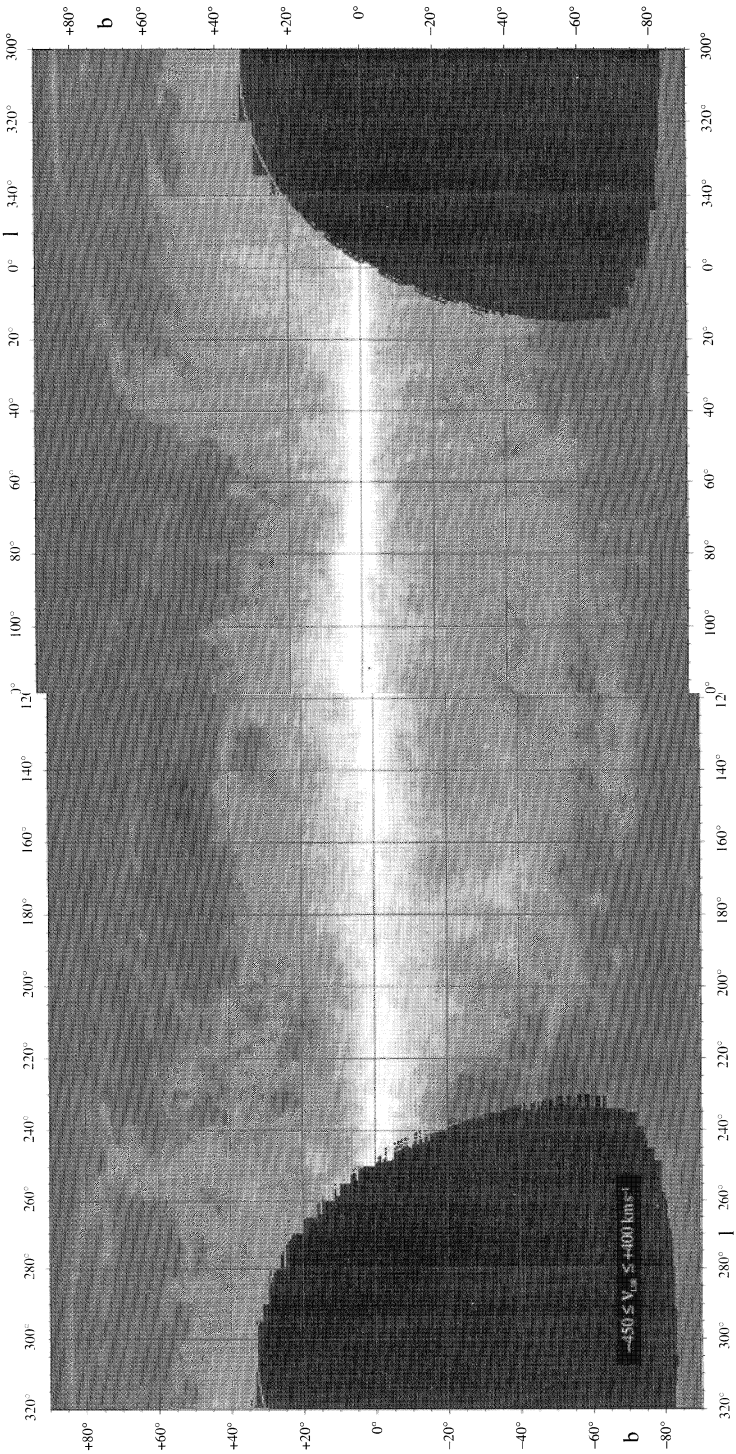
b
+80°
+60°
+40°
+20°
0°
−20°
−40°
−60°
−80°
l
300°
320°
340°
0°
20°
40°
60°
80°
100°
120°
140°
160°
180°
200°
220°
240°
260°
280°
300°
320°
−450 ≤ v_LSR ≤ +400 kms⁻¹

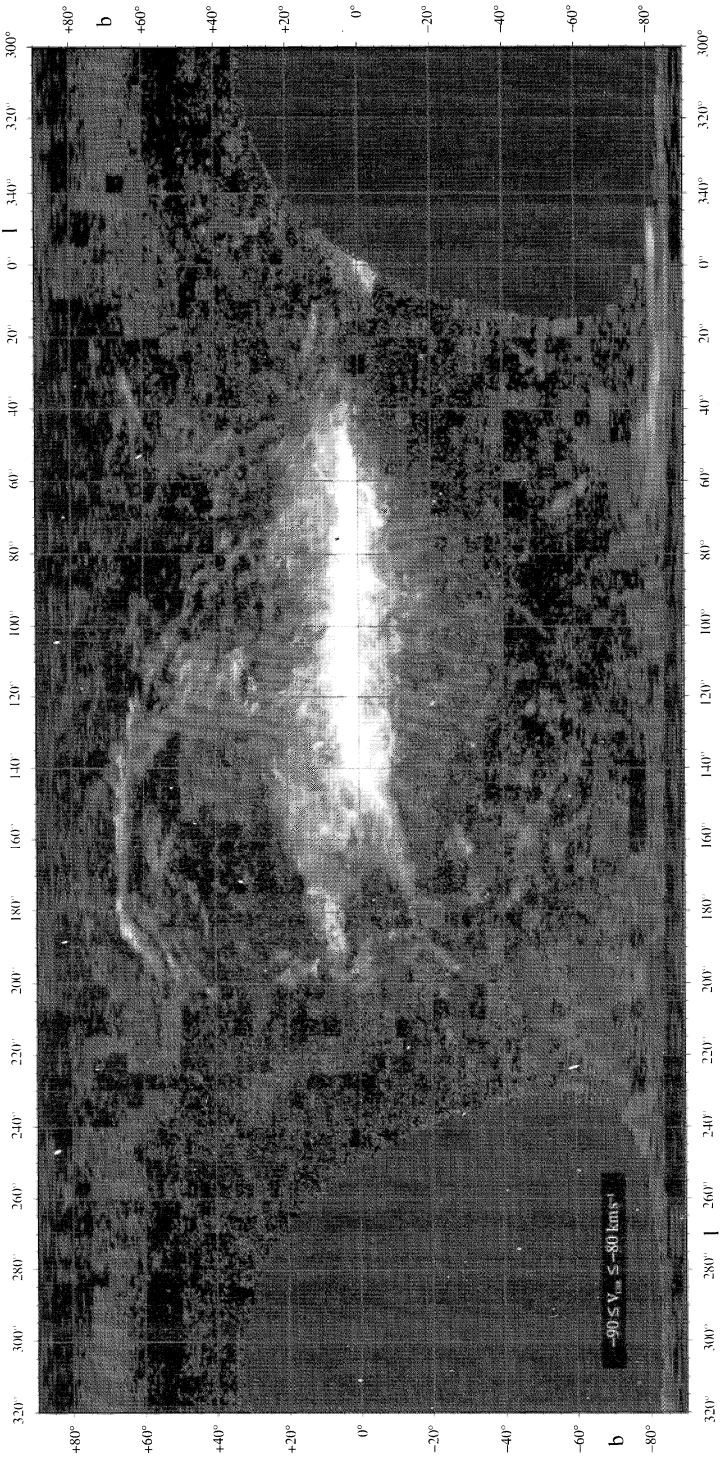
b
+80°
+60°
+40°
+20°
0°
−20°
−40°
−60°
−80°
l
300°
320°
340°
0°
20°
40°
60°
80°
100°
120°
140°
160°
180°
200°
220°
240°
260°
280°
300°
320°
−90 ≤ V_LSR ≤ −80 kms⁻¹

Figure 4. Sky distribution of HI column depths contributed over the velocity range -90 km s^{-1} $\leq v \leq$ -80 km s^{-1}. Except close to the galactic equator, gas emitting at these velocities is largely contributed by high–velocity–cloud objects and by the more extreme intermediate–velocity clouds. Emission from the HVC Complex M is evident as the arc crossing the central upper portions of this map. ⇐

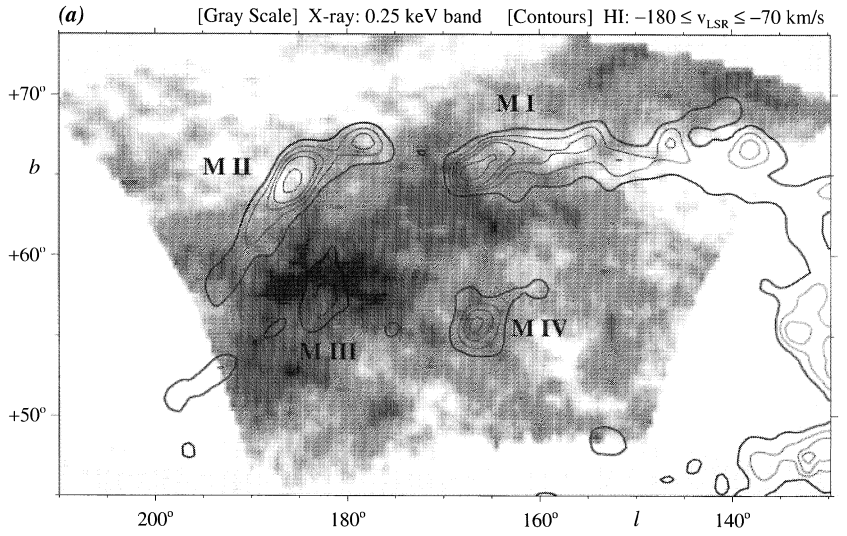

Figure 5. Grayscale plot of the ROSAT 1/4 keV X–ray image towards the HI HVC Complex M overlayed by contours showing the HI column–density distribution integrated between between -180 and -70 km s^{-1} (Herbstmeier *et al.* 1995). In this region of generally low N_{HI} column depths, enhanced X–ray emission is bounded by anomalous–velocity gas; the anticorrelation implies attenuation of the X–rays by foreground HI gas, and thus constrains the distances.

The material in the -90 km s^{-1} $\leq v \leq$ -80 km s^{-1} velocity range will enter studies of the galactic warp and flaring thickness. It is clear that measures of the thickness of the galactic gas layer, for example, or of the vertical line–of–sight velocity dispersion, must take account of possible distortion by the IVC emission.

The question of the distance to the HVC gas remains a difficult one. Figure 5 shows that the HI in the HVC Complex M evidently attenuates the soft X–ray background measured by ROSAT at 1/4 keV. Herbstmeier *et al.* (1995) have compared the X–ray distribution with that of the HI gas radiating in various velocity ranges, and found that high–velocity clouds are responsible for some of the X–ray attenuations. If the distance of the

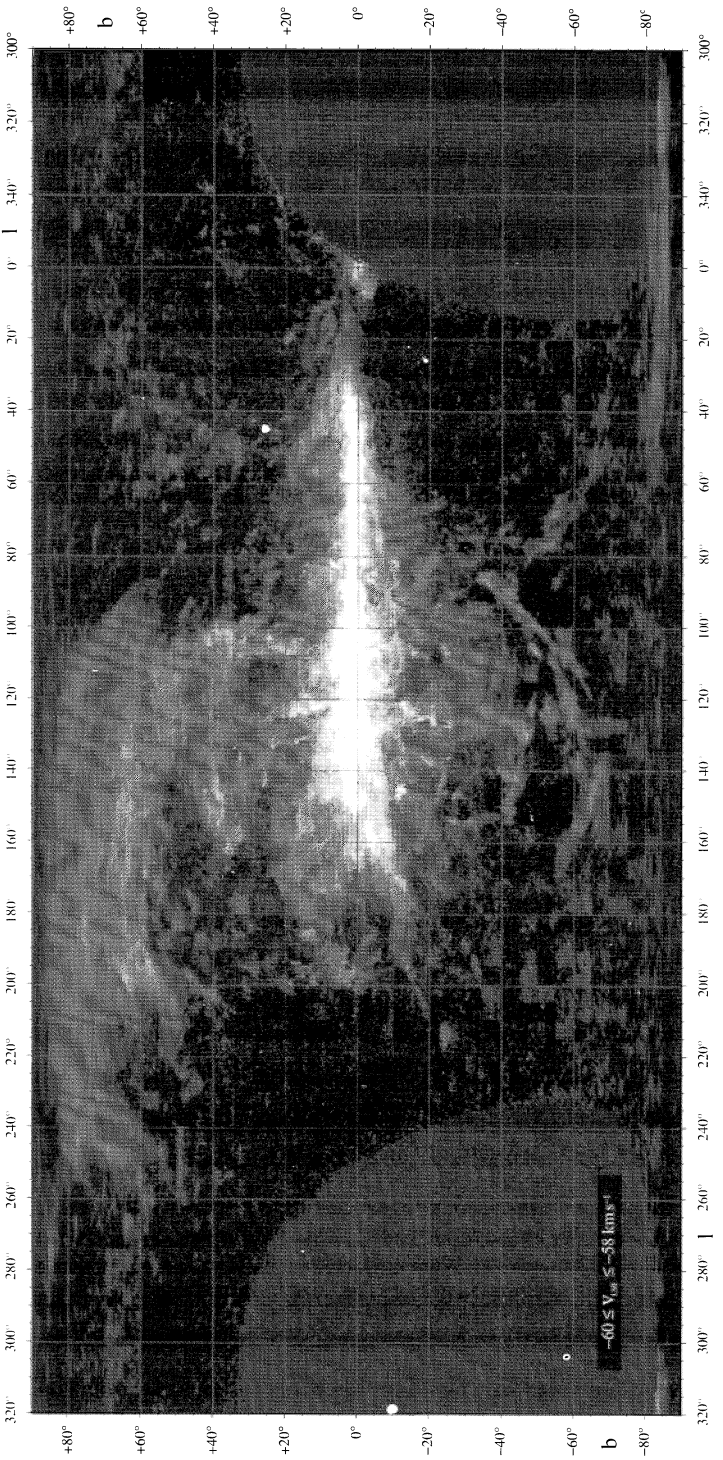
b
+80°
+60°
+40°
+20°
0°
−20°
−40°
−60°
−80°
l
300°
320°
340°
0°
20°
40°
60°
80°
100°
120°
140°
160°
180°
200°
220°
240°
260°
280°
300°
320°
−60 ≤ V_LSR ≤ −58 km s⁻¹

Figure 6. Distribution over the plane of the sky of HI column depths contributed over the narrow velocity range -60 km s^{-1} $\leq v \leq -58$ km s^{-1}. The so–called intermediate–velocity–cloud objects populating the higher $|b|$ region show a range of morphologies, still poorly understood in terms of filling factors, distance, origin, and energetics. Some, and maybe most, of these anomalous–velocity gas features have dust counterparts. ⇐

HVC complex has been correctly constrained to lie between 1.5 and 4.5 kpc, then the hot galactic corona extends at least several kiloparsecs from the galactic equator. Herbstmeier *et al.* also found evidence for an X–ray edge–brightening of the high–velocity clouds, suggesting that the clouds contribute to the heating of the corona.

Figure 6 shows the sky image of HI radiating in the narrow velocity range -60 km s^{-1} $\leq v \leq -58$ km s^{-1}. The situation at the moderate negative velocities (which were largely out of reach of the Hat Creek survey of Heiles and Habing, 1974) is evidently very interesting. Such velocity slices as the one shown in Figure 6 will provide substantial information on the various filling factors. The areal filling factor expresses the percentage of sky covered by HI structures, at specified velocities. The volume filling factor expresses the fraction of space occupied by the structures; requiring distance information, this factor will be more difficult to determine.

Data in the intermediate–velocity regime is also relevant to questions posed by the maintenance of the thickness of the galactic gas layer, especially that in the transition region between the lower halo and the conventional disk (see Dickey and Lockman 1990, and Lockman and Gehman 1991). Many of the "fast" clouds are in fact quite narrow in their σ_v measure. The concept of motions of separate entities forming an ensemble of structures only sparsely filling space, seems more realistic than the picture of a diffuse gas component at high $|b|$ with a large velocity dispersion. We note that the small scale–thickness and small line–of–sight σ_v measured in low $|b|$ in the inner Galaxy constrain a number of parameters of the IVC population.

The intermediate–velocity range, especially that at intermediate latitudes, is a rich source of information on the kinematic aspects of HI gas structures which are correlated with interstellar dust cirrus clouds. The kinematic structure can be unraveled by examining the gas/dust correlation as a function of velocity across the λ21–cm spectra of the associated gas (see Deul and Burton 1990, Burton *et al.* 1992, and West *et al.* 1995). All of the cirrus fields for which we have attempted kinematic unraveling using HI observations show relationships with the regime of intermediate–velocity gas. Evidently many cirri are not quiescent wisps, but involve substantial energetics.

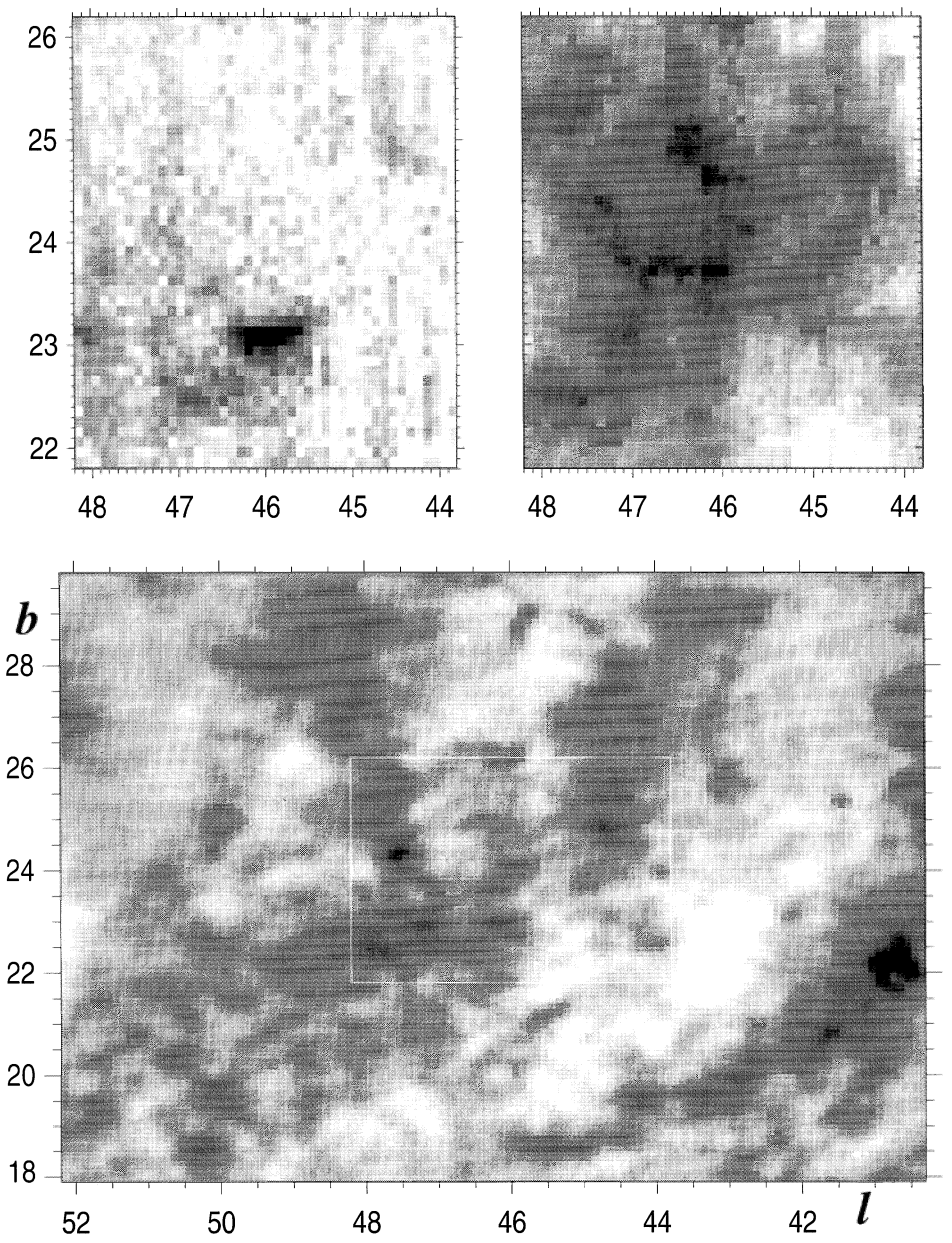

Figure 7. HI column densities, measured at Arecibo (West *et al.* 1995), corresponding to λ21-cm emission from the range -75 km s^{-1} $\leq v \leq -55$ km s^{-1} (left) and from the range -10 km s^{-1} $\leq v \leq +10$ km s^{-1} (right), compared with the IRAS 100-micron flux in the lower panel. (The boxed region in the lower panel delineates the extent of the Arecibo data.) The knot of HI emission at the anomalous velocities has a dust cirrus counterpart centered near $(l, b) = (46°, 23°)$. Cirrus filaments, with gas counterparts at velocities near zero, appear spatially associated with the IVC knot; if that association is a physical one, then the gas/dust association embraces more than 65 km s^{-1}. (Higher fluxes are blacker, for both the HI and the IR.)

Figure 7 shows the gas and dust emission from the vicinity of a cirrus feature centered near $(l, b) = (46°, 23°)$. The IRAS 100–micron map shows a dust feature with a filamentary morphology, centered on a knot of dust emission at $46°, 23°$. The dust filaments as well as the knot have gaseous counterparts, but at different velocities. The IR knot has a gas counterpart, centered near $v = -60$ km s^{-1}, radiating at velocities characteristic of a prototypical intermediate–velocity cloud. Furthermore, the HI column density corresponding to intensities integrated over the *conventional* velocity range -10 km s^{-1} $\leq v \leq +10$ km s^{-1} shows a deficiency of HI at the location of the IR knot. The gaseous counterparts of the filamentary structures, apparently focused toward the knot, radiate at the conventional velocities.

A satisfactory description of the $(l, b) = (46°, 23°)$ cirrus field will have to account for the relation of the HI IVC with its IR counterpart, as well as for the relationship of this pairing with the HI deficiency and apparent disturbance near zero velocity. It will also reckon with the appearance that filamentary dust features at modest velocities emanate from the position, and velocity, of the disturbance.

Figure 8 shows the sky image of HI radiating in the velocity range -40 km s^{-1} $\leq v \leq -38$ km s^{-1}; many of the points illustrated by Figure 6 pertain here also. We note in addition that some directions radiate more flux at these anomalous velocities than they do within, say, $|v| \leq 10$ km s^{-1}. Some of the individual HI features populating this velocity range have dispersions as small as $\sigma_v \simeq 1$ km s^{-1}. The measured widths are thus small enough to be relevant in estimating the kinematic temperature of HI clouds at high $|b|$. It appears promising to use the identification of narrow HI features (together with data on 100–micron excesses) as a finding chart for searching for high–latitude molecular clouds at these anomalous velocities.

Figure 9 shows the gas and dust emission from the vicinity of a cirrus feature centered near $(l, b) = (211°, 63°)$ in whose core Désert *et al.* (1990) found CO emission at -39 km s^{-1}. Molecular clouds at high latitude and at velocities differing from zero by more than 25 km s^{-1} are rare; only two are currently known in addition to the one found by Désert *et al.*, namely G90.0+38.6-25 (Heiles *et al.* 1988) and G135.3+54.5-45 (Mebold *et al.* 1989). Molecular gas associated with intense cirrus emission has frequently been observed, but generally confined to within about 5 km s^{-1} of zero velocity: the kinematic picture derived from most molecular emission associated with cirrus knots is a quiescent one.

The HI situation in the direction of the Désert *et al.* feature is particularly interesting. HI emission is intense near -40 km s^{-1}, and at these anomalous velocities it is well correlated with the 100–micron dust emission. The emission at velocities which would be associated with a quiescent

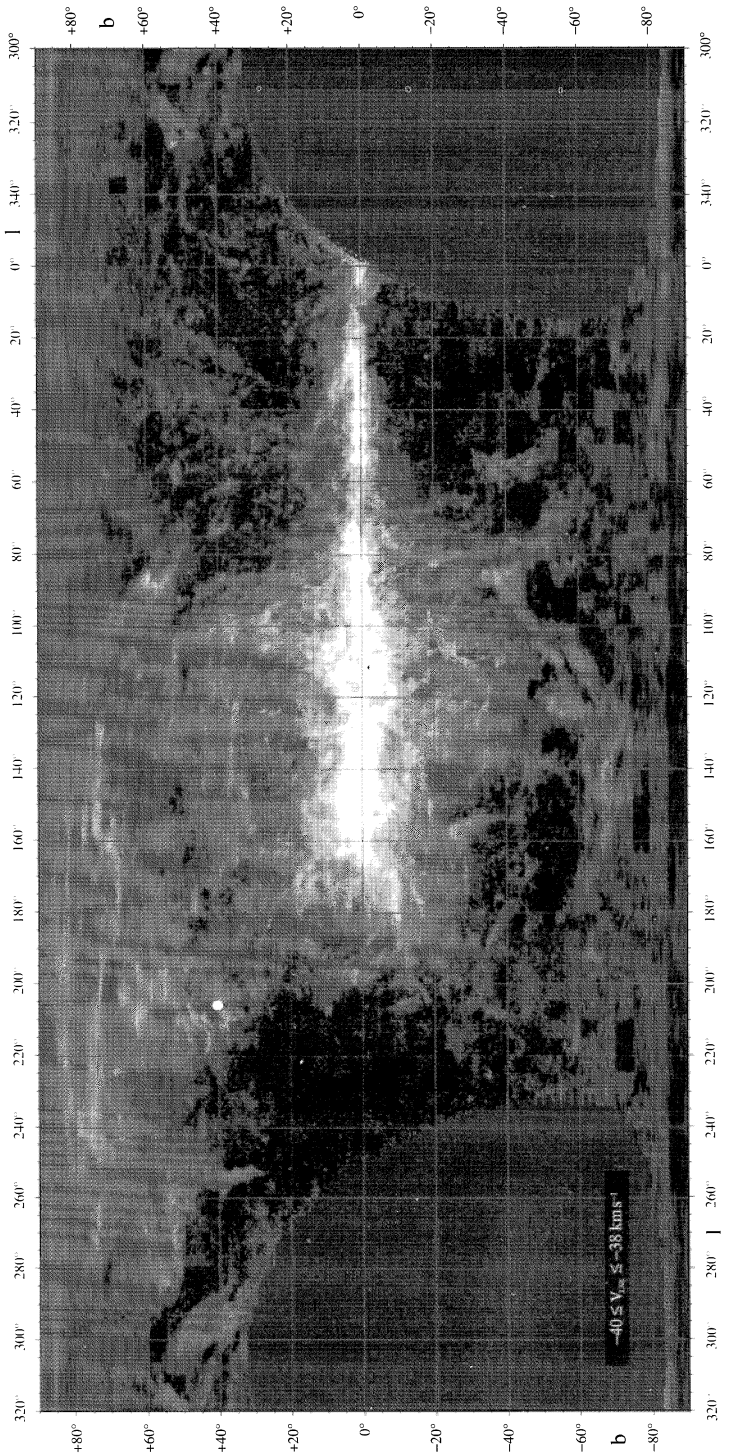
b
+80°
+60°
+40°
+20°
0°
−20°
−40°
−60°
−80°
l
300°
320°
340°
0°
20°
40°
60°
80°
100°
120°
140°
160°
180°
200°
220°
240°
260°
280°
300°
320°
−40 ≤ V_LSR ≤ −38 km s⁻¹

Figure 8. Distribution over the plane of the sky of HI column depths contributed over the narrow velocity range -40 km s^{-1} $\leq v \leq -38$ km s^{-1}. Some of the high-$|b|$ HI features are characterized by quite narrow velocity widths, as low as $\sigma_v \sim 1$ km s^{-1}. The small, narrow HI enhancement near $(l, b) = (211°, 63°)$ corresponds to the site where Désert *et al.* (1990) found a molecular cloud, one of only three molecular clouds known at $|v|$ more extreme than 25 km s^{-1}. The gas emitting at the anomalous velocities near -39 km s^{-1} dominates the total gas density budget in the direction of the associated cirrus structure. ⟸

ambient medium is exceptionally weak throughout the region. Just adjacent (on the north) to the IR knot and the molecular cloud, the total HI column depth approaches the exceptionally low values found in the direction of the Lockman *et al.* (1986) deficiency in Ursa Major. The HI spectral features associated with the IR knot and molecular cloud are quite narrow: the features near -39 km s^{-1} have Gaussian dispersions $\sigma_v \leq 1.4$ km s^{-1}. We note that the narrow measured dispersions are probably upper limits, not only because of the commonly-encountered possibility of blending of unrelated material, but also because the Arecibo data have not been corrected for stray-radiation effects: this correction systematically tends to render spectral features which are kinematically narrower than in the uncorrected case.

In addition to the HI feature emitting at -39 km s^{-1}, there is also a gaseous filament crossing the Arecibo map (in an unfortunately-sampled way, but confirmed in the Leiden/Dwingeloo data) just south of the Désert *et al.* cloud, at $b \sim 61°$, with $v \sim 0$ km s^{-1}. This conventional-velocity feature also has a dust counterpart. The IRAS 100-micron map shown in the lower panel of Figure 9 suggests that the two kinematic branches together form a single, shell-like structure; the HI data indicate kinematic continuity across some 40 km s^{-1}. The origin of the large total velocity extent of the shell-like structure which contains the peculiar-velocity molecular cloud remains a puzzle.

Most intermediate-velocity HI clouds have yet to be studied in detail. There are preliminary indications, however, that several of the characteristics of the gas/dust correlations pertaining for the $(l, b) = (211°, 63°)$ site may hold more generally, particularly the large total velocity span and the association of the anomalous-velocity occurrence with a perturbation in the conventional-velocity realm. We note that although intermediate-velocity HI features commonly trace extensive patterns over large angles on the sky, they also contain a great deal of small-scale structure, both spatially and kinematically. Many of these small-scale features are also quite cold, as indicated by the upper limits which can be placed on their velocity dispersions.

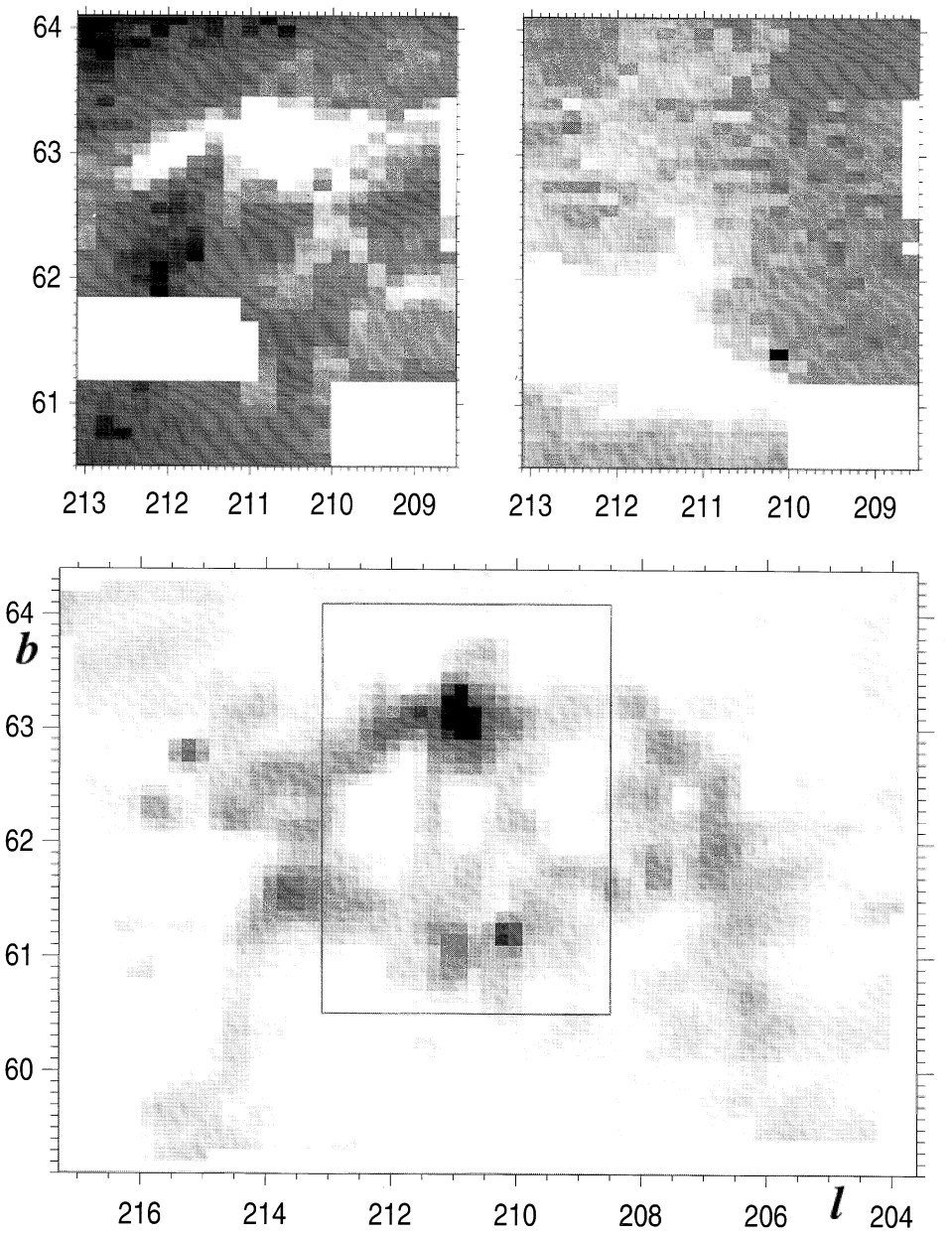

Figure 9. HI column densities, measured at Arecibo (West *et al.* 1995), corresponding to λ21–cm emission from the range -50 km s$^{-1} \leq v \leq -30$ km s^{-1} (left) and from the range -10 km s$^{-1} \leq v \leq +10$ km s^{-1} (right), compared with the IRAS 100–micron flux in the lower panel. (The boxed region in the lower panel delineates the extent of the Arecibo data.) The anomalous–velocity HI feature is correlated with a dust cirrus counterpart centered near $(l, b) = (211°, 63°)$; the strength of the HI emission at conventional velocities is, in this region, weaker than that of the peculiar–velocity material. (Higher fluxes are whiter in the HI case, but blacker in the IR representation.)

The matter of the characteristic distance to the IVC structures remains elusive. (Distances to HVCs are also only poorly established, but the particular importance of the IVC distances is emphasized by their clear association with cirri, which may be the principal carrier of the interstellar medium, and with perturbances in the conventional gas layer.) Substantial efforts have been directed to the detection of interstellar absorption lines in the directions of stars lying beyond IVC structures. Danly (1989) found ultraviolet absorption lines at about -50 km s^{-1} towards stars whose distances were evidently large, between 400 and 700 pc, but not towards stars nearer by.

Acceptance of distances of the order of 500 pc as being generally typically of the intermediate–velocity–cloud objects has a number of consequences. Such a characteristic distance is not compatible with the value of the vertical thickness of the galactic gas layer measured over much of the distant Galaxy. Values for the vertical thickness, measured as the Gaussian dispersion, σ_z, perpendicular to the galactic equator, are typically about 120 pc for both the HI and the dust layer radiating at 100–micron, and about half this value for the molecular–cloud ensemble. If the IVC HI gas (and the dust which at least to some extent is associated with that gas) were to be as distant as 400 to 700 pc, then the layer–thickness measures would have been larger, unless the IVC gas were confined to a very peculiar distribution. This peculiar distribution would involve two vertical, narrow cones with their vertices pointing toward the Sun. In other words, if the IVCs are quite distant, then they are, ironically, probably a *local* phenomenon, not a general aspect of the galactic gas layer. (Such localized HI disturbances have been seen in other galaxies.)

Acceptance of a large characteristic distance for the IVC gas led Lockman and Gehman (1991) to reject velocities $|v| \geq 30$ km s^{-1} from their discussion of the role of turbulence in the lower–halo gas. If the scale–thickness argument requires a smaller characteristic distance, then the turbulence of entities populating the IVC regime would in fact play an important role in the galactic–layer energetics. The motions in the lower–halo gas layer would then better be viewed in terms of turbulence of an ensemble of separate entities rather than in terms of high–dispersion wings from a diffuse gas component. We note that the anomalous velocities of the IVCs and their associated dust cirri are dominated by motions in the sense of infall, and are thus, in this regard, not indicative of normal turbulence. We note also that the measured motions are *vertical* ones, which evidently have no *horizontal* equivalent, at least at low $|b|$; measures of the bulk–motion turbulence at low $|b|$ are characterized by random–motion dispersions of less than about 5 km s^{-1}.

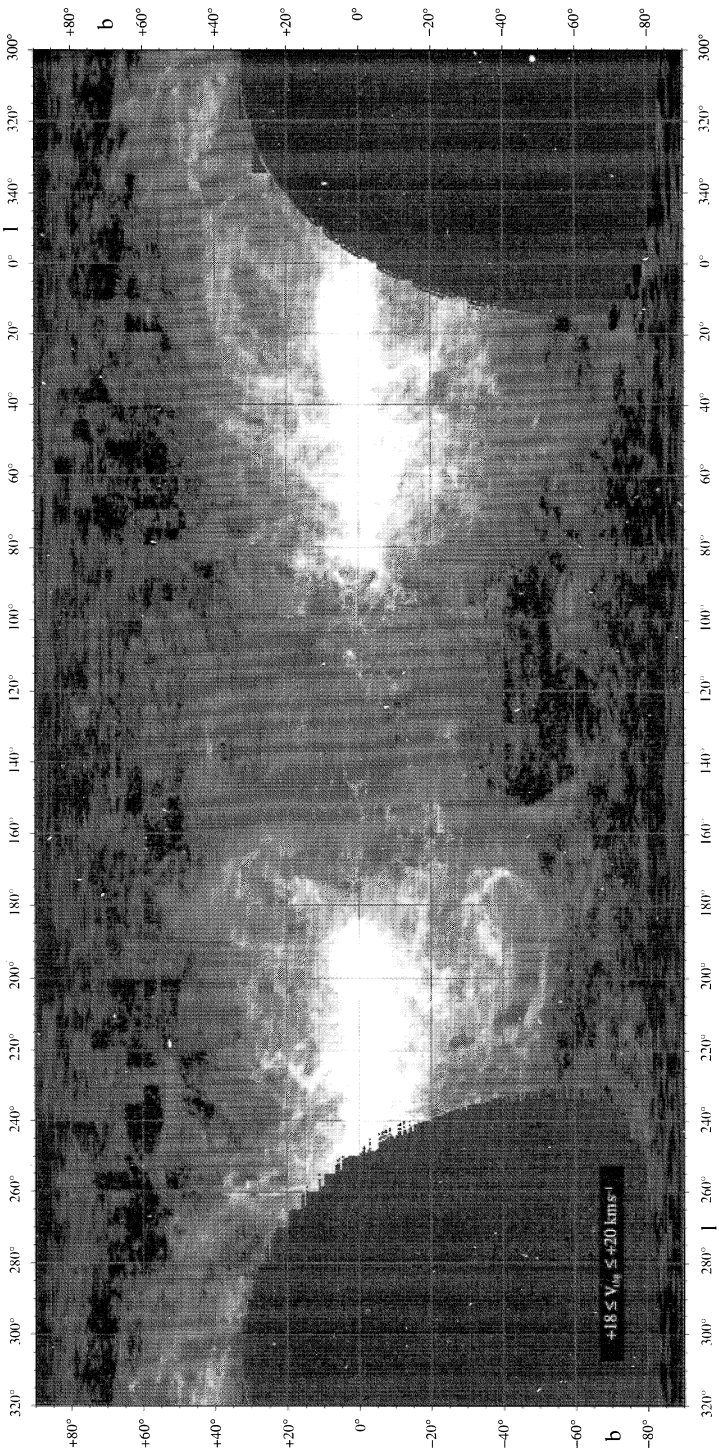
+18 ≤ V_lsr ≤ +20 kms⁻¹
l
b

Figure 10. Distribution over the plane of the sky of HI column depths contributed over the narrow velocity range $+18$ km s^{-1} $\leq v \leq +20$ km s^{-1}. Much of the HI gas is marshaled into filamentary structures such as that associated with the Orion/Eridanus bubble, and many of these cover a large total velocity expanse, implying substantial energetics. ⟸

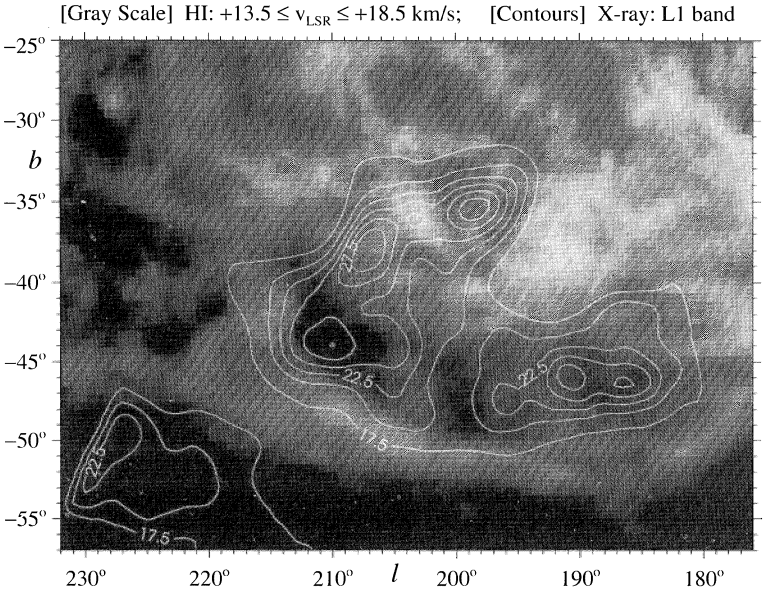

Figure 11. Confinement of 1/4 keV X–ray emissivities (from Burrows *et al.* 1992, shown by contours) by HI structures associated with the Orion/Eridanus bubble (Brown *et al.* 1995). The Orion OB1 association has caused a cavity filled with hot gas, surrounded by an expanding shell of HI. Comparison with the HI data in the range $+13.5$ km s^{-1} $\leq v \leq +18.5$ km s^{-1}shows an anticorrelation of the X–ray enhancement with kinematically–narrow HI features.

The sky–image moment map shown in Figure 10 represents the narrow positive–velocity range $+18$ km s^{-1} $\leq v \leq +20$ km s^{-1}. The most prominent of the remarkable structures seen in this image is the large shell–like Orion/Eridanus bubble, centered near $(l, b) = (200°, -40°)$. This feature is a prototypical example of the marshaling of various aspects of the kinematics and structure of the interstellar medium by consequences of star formation. HI and X–ray data from the region lead to a picture of a cavity filled with hot gas, surrounded by an expanding shell of neutral material. The HI material provides important information on the kinematics of the expanding shell.

Figure 12. Distribution over the plane of the sky of HI column depths contributed over the velocity range $+80$ km s^{-1} $\leq v \leq +90$ km s^{-1}. Comparison of this velocity slice with the one at complementary negative velocities shown in Figure 4 shows the well–known, but poorly understood, +/− kinematic asymmetry; there is also an obvious north/south asymmetry. The first galactic quadrant at these velocities displays some evidently violent ejecta; the third quadrant is populated by a number of high–velocity clouds, which generally are relatively scarce at positive velocities. $\Longrightarrow$

Brown *et al.* (1995) show a sequence of maps from the Leiden/Dwingeloo survey which indicate that the neutral hydrogen emission from the area surrounding the Orion/Eridanus bubble spans a total velocity extent of some 80 km s^{-1}. The enhanced X–ray flux in that area anticorrelates in a detailed way with narrow–dispersion HI features, clearly establishing the association of the X–ray enhancement with the bubble. Using models for wind–blown bubbles which incorporate the density stratification of the galactic HI layer, Brown *et al.* show that the Orion/Eridanus structure can be explained as a bubble blown by winds from Orion OB1.

The last moment–map image shown here is that in Figure 12 representing the HI emission from the positive–velocity interval $+80$ km s^{-1} $\leq v \leq +90$ km s^{-1}. Comparison of this image with the one at complementary negative velocities shown in Figure 4 indicates the kinematic asymmetry characterizing the HVC and IVC gas. High–velocity–cloud objects occur sparsely at positive velocities (see the review by Wakker, 1991); the positive–velocity HVC objects represented in this image in the third galactic quadrant differ also from those at complementary negative velocities in being quite isolated features, spanning angular scales typically less than 5°, rather than extended complexes spanning many tens of degrees. The features at anomalously–high positive velocities do share, however, the preference for positive latitudes shown by the negative–velocity HVCs.

The Figure 12 image also illustrates, in the first quadrant, several of the characteristic HI structures (variously called "worms", "chimneys", etc.) which appear to be associated with disturbances in the galactic–equator gas layer. Such disturbances are currently being studied by a number of groups; the nature of the responsible disturbance is still puzzling. Just as is the case at negative velocities, disturbances to the conventional gas layer may distort derived parameters such as the scale thickness. We note that these disturbances are *vertical* ones. The terminal–velocity cutoff of HI spectra at $b = 0°$ is a good kinematic measure of the line–of–sight *horizontal* turbulence; this measure constrains peculiar motions in the galactic equator to be quite small, with excursions away from the expected terminal velocity seldom greater than about 5 km s^{-1}.

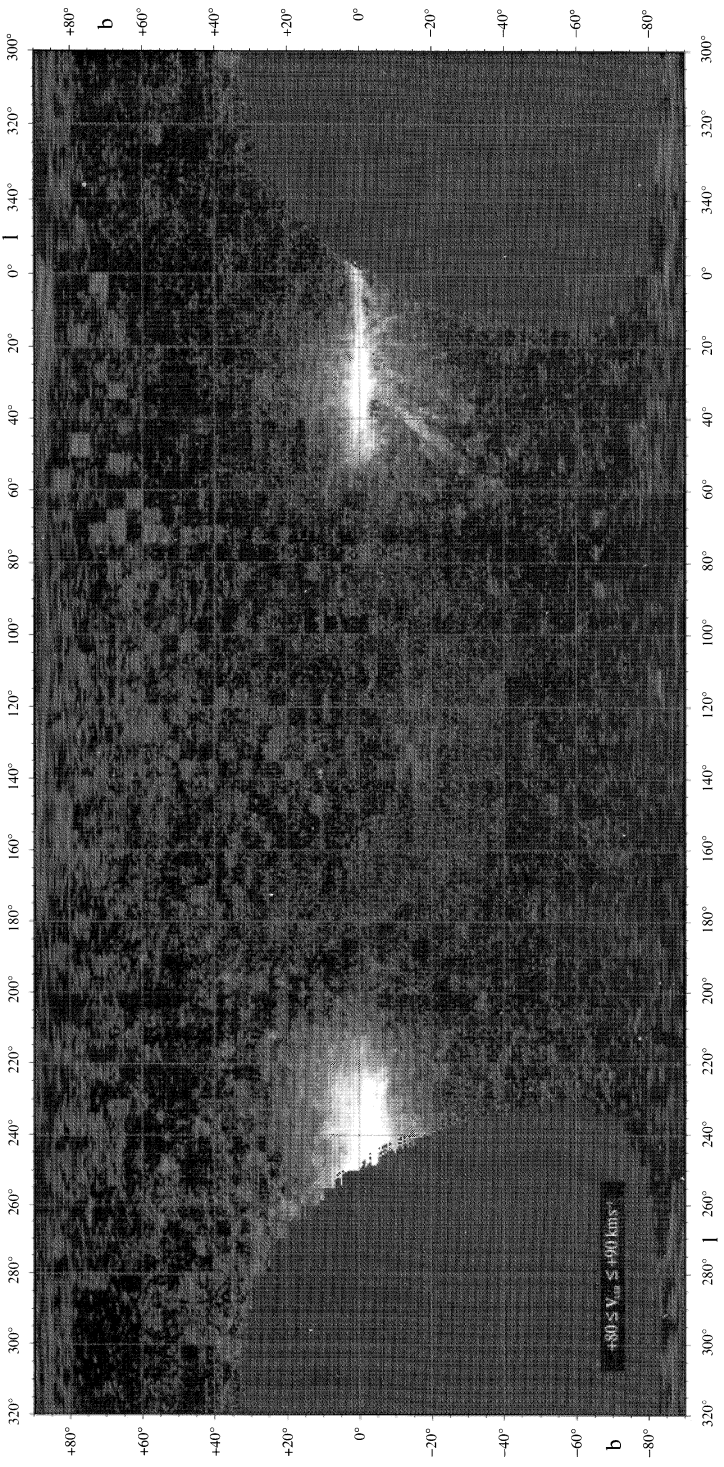
+80° b +60° +40° +20° 0° −20° −40° −60° −80°
320° 300° 280° 260° 240° 220° 200° 180° 160° 140° 120° 100° 80° 60° 40° 20° 0° 340° 320° 300° l
+80° +60° +40° +20° 0° −20° −40° −60° −80° b
320° 300° 280° 260° 240° 220° 200° 180° 160° 140° 120° 100° 80° 60° 40° 20° 0° 340° 320° 300° l
+80 ≤ V_LSR ≤ +90 km s⁻¹

The survey material is being published as an atlas of maps and as a FITS–format data cube on a CD–ROM (Hartmann and Burton, 1996).

The Leiden/Dwingeloo survey covers the sky accessible from the Netherlands. Southern extension of the coverage to include the region $\delta \leq -30°$ is underway at the Argentina Institute for Radioastronomy, where E. Bajaja and collaborators are using the 100–foot IAR telescope equipped with a receiver and spectrometer comparable to those used in Dwingeloo.

The Dwingeloo radio telescope is operated by the Netherlands Foundation for Research in Astronomy, under contract with the Netherlands Organization for Scientific Research. The Arecibo radio telescope is operated by the National Astronomy and Ionosphere Center, under contract with the U.S. National Science Foundation.

References

Brown, A.G.A., Hartmann, D., and Burton, W.B. (1995), *Astron. Astrophys.*, submitted.

Burrows, D.N., Singh, K.P., Nousek, J.A., Garmire, G.P., and Good, J. (1993), *Astrophys. J.* 406, 97.

Burstein, D. and Heiles, C. (1978), *Astrophys. J.* 225, 40.

Burton, W.B. (1992), in *The Galactic Interstellar Medium*, (D. Pfenniger & P. Bartholdi, eds.), Springer-Verlag, Heidelberg, p. 1.

Burton, W.B., Bania, T.M., Hartmann, D., and Tang, Y. (1992), in *Evolution of Interstellar Matter and Dynamics of Galaxies*, (J. Palous, W.B. Burton, & P.O. Lindblad, eds.), Cambridge University Press, Cambridge, p. 25.

Danly, L. (1989), *Astrophys. J.* 342, 785.

Deul, E.R., and Burton, W.B. (1990), *Astron. Astrophys.* 230. 153.

Désert, F.-X., Bazell, D., and Blitz, L. (1990), *Astrophys. J. Letters*, 355, L51.

Dickey, J.M., and Lockman, F.J. (1990), *Ann. Rev. Astron. Astrophys.*, 28, 215.

Hartmann, D. (1994), *The Leiden/Dwingeloo Survey of Galactic Neutral Hydrogen*, Ph.D. Thesis, University of Leiden.

Hartmann, D., and Burton, W.B. (1996), *An Atlas of Galactic Neutral Hydrogen*, Cambridge University Press, in press.

Hartmann, D., Kalberla, P.M.W., Burton, W.B., and Mebold, U. (1995), *Astron. Astrophys.*, submitted.

Hartsuijker, A.P., Baars, J.W.M., Drenth, S., and Gelato–Volders, L. (1972), *IEEE Trans. Antennas Propagation* 20, 166.

Heiles, C., and Habing, H.J. (1974), *Astron. Astrophys. Suppl.* 14, 1.

Heiles, C., Reach, W.T., and Koo, B.–C. (1988), *Astrophys. J.* 332, 313.

Herbstmeier, U., Mebold, U., Snowdon, S.L., Hartmann, D., Burton, W.B., Moritz, P., Kalberla, P.M.W., and Egger, R. (1995), *Astron. Astrophys.*, in press.

Kalberla, P.M.W., Mebold, U., and Reich, W. (1980), *Astron. Astrophys.* 82. 275.

Lockman, F.J. and Gehman, C., (1991), *Astrophys. J.* 382, 182.

Lockman, F.J., Jahoda, K., and McCammon, D. (1986), *Astrophys. J.* 302, 432.

Mebold, U., Herbstmeier, U., Kalberla, P.M.W., Souvatzis, I. (1989), in *Structure and Dynamics of the Interstellar Medium*, (G. Tenorio–Tagle, M. Moles, and J. Melnick, eds.), Springer Lecture Notes in Physics, p. 424.

van Someren Greve, H. (1991), in *Proc. Workshop "Holography Testing of Large Radio Telescopes"*, Nauka, Leningrad.

Wakker, B.P. (1991), *Astron. Astrophys.* 250, 499.

West, S.R.D., Burton, W.B., Hartmann, D., Bania, T.M., and Stark, R. (1995), in preparation.

HOW IMPORTANT IS NEUTRAL CARBON TO AN UNDERSTANDING OF THE DENSE INTERSTELLAR MEDIUM?

D.T. JAFFE
Department of Astronomy, University of Texas at Austin
Austin, Texas 78712 USA

1. Introduction

In virtually all of the dense interstellar medium, H_2 is the most abundant form of hydrogen, but it is not directly observable in the bulk of the gas. As a result, we are forced to use trace constituents of the gas as surrogates when we want to know the distribution of material in the dense ISM. Most commonly, we employ the lowest few rotational transitions of CO and its isotopes as the trace species. One of the most hotly debated issues in the study of the molecular ISM is the extent to which one can trust CO or isotopic CO lines to reflect reliably the underlying H_2 distribution (see Shier, Rieke, & Rieke (1994), Sodroski et al. (1995) for recent comments on the $I(^{12}CO)/N(H_2)$ ratio and Lada et al. (1994) for a recent analysis of the relationship between isotopic CO and total cloud column densities). CO becomes increasingly unreliable as a tracer of H_2 as the average column density between cloud surfaces exposed to ultraviolet photons and the shielded centers of clouds becomes smaller. Young stars in the galactic plane perfuse atomic and molecular clouds with far–UV ($\lambda > 91$ nm) radiation. This radiation tends to dissociate CO more readily than it dissociates H_2 (Van Dishoeck & Black 1988). The differences in susceptibility of H_2 and CO to photodissociation may lead to the existence of significant portions of the molecular medium where the usual trace species are underabundant or even absent. In addition, there is dense H I at the cloud boundaries, immediately outside the molecular material. In the UV–illuminated cloud surfaces, the gas-phase carbon is in the form of C I or C II. It is important, therefore, to determine the amount and location of large-scale C I emission

L. Blitz and P. Teuben (eds.), Unsolved Problems of the Milky Way, 469–478.
© 1996 *International Astronomical Union.*

if one hopes to know how much molecular and dense atomic gas is missing from studies using CO as a tracer and to what extent photodissociation is responsible for the absence of this CO. We discuss here some of the relevant theoretical and observational work on the relationship between C II, C I, CO and H_2. Our principal aim is to see if and how observations of C I might help us to improve our knowledge of the distribution of dense neutral gas in the Milky Way.

2. Origin of C I Emission: Photon Dominated Regions

Photon dominated regions (PDR's) form at the surfaces of molecular clouds wherever far–UV photons strike the gas. The PDR is a zone in a molecular cloud where UV photons dominate the energetics, chemistry, and ionization state (de Jong, Dalgarno, & Boland 1980, see Hollenbach & Tielens 1995 for recent references). At the PDR boundary, H rapidly makes a transition to H_2 as self-shielding begins to protect the molecules against photodissociation. In the outer part of the molecular cloud, CO cannot self-shield as effectively as H_2, so a region exists where the hydrogen is already molecular but C II and, somewhat farther in, atomic carbon are the dominant forms of gas–phase carbon. The transition from C II to C I comes at a depth into the cloud where the far-UV field has been sufficiently attenuated to allow C II to recombine (on the order of A_v=1 for a typical giant molecular cloud). The C I/CO transition occurs a bit farther in ($A_v \simeq$2–3) as re-formation of CO overcomes photodissociation. The exponential attenuation of far-UV radiation by dust results in a weak dependence of the C II column density on the incident UV field when the UV field is high (Tielens & Hollenbach 1985, Van Dishoeck & Black 1988). For weaker UV fields, the C II column density can vary somewhat more rapidly with the strength of the field. As an effect of its position in a transition zone, the column density of carbon in the neutral atomic region is relatively insensitive to variations in the strength of the incident UV field and the local density. The corresponding surface brightness in the lower C I transition also varies very slowly with cloud conditions (Hollenbach, Takahashi, & Tielens 1991).

Most PDR models consider the effects of far-UV radiation on uniform clouds, either plane parallel or spherical. These uniform models imply that a large fraction of the molecular ISM is photon dominated material. One can use the linewidth–size relation for molecular clouds (Solomon et al. 1987) to estimate the typical column density through the clouds. This column density corresponds to $A_v \sim$10. Given the thickness of typical C II and C I layers, this result implies that CO is the majority gas-phase carbon species in only 1/2 to 2/3 of the dense material.

The clumpy structure of real molecular clouds can lead to even higher

mass fractions of the cloud in regions where CO is not the dominant form of gas-phase carbon. Most clouds are highly clumpy with high density contrasts observable over a large range of scale sizes (see recent reviews by Blitz 1993, and Stutzki 1994). The clumpy nature of the clouds affects their interaction with far-UV radiation and therefore the pattern of C II, C I, and CO emission. Mapping of high column density molecular clouds reveals C II emission far within clouds where there are no embedded sources of far-UV radiation; the scale–length over which the C II intensity drops going into the cloud is 10–100 times longer than it would be for a uniform source (Howe et al. 1991). Models taking clumpiness into account can explain both the absolute intensity and distribution of the C II emission, if the volume filling factor of clumps in the clouds is modest (0.1–0.3) and if the area filling factor of clumps and the density of the interclump material allow UV radiation to penetrate through the cloud to reach clump surfaces 1–2 pc inside the cloud (Stutzki et al. 1988, Howe et al. 1991). In this case, each clump throughout the cloud has a PDR on its surface. For gas at a given density, then, clumpy clouds can have a much larger fraction of their volume in regions affected by UV photons than do correspondingly massive monolithic clouds.

3. Tracers of UV–Influenced Material

3.1. C II: THE IDEAL TRACER?

The structure of PDR's we have described here implies that the 158 μm C II line might be the best way to trace gas near UV illuminated surfaces. C II extends all the way from the H II/H I interface in to an $A_v \sim 2$. There are already extensive observations of the C II 158 μm line throughout the inner Galaxy which one might hope to use to study the distribution of UV–influenced molecular material (Shibai et al. 1991, Nakagawa et al. 1993, Bennett et al. 1994). Several problems combine, however, to limit the usefulness of the C II line as a quantitative PDR tracer. For the 158 μm transition, E_u/k is 92 K. Although electrons ejected from grains through the photoelectric effect heat the gas in the outer layers of the cloud significantly above typical dark cloud temperatures of 6–10 K, the temperature in these layers is not high enough to keep the emissivity of C II from varying rapidly over the range of far-UV fields incident on typical GMC's in the inner Galaxy. As a result, C II intensities do not reflect the amount of PDR material except near strong far–UV sources. A second problem is that ionized gas in extended, low density H II regions may contribute diffuse C II emission. For nebulae ionized by stars with surface temperatures below ~34,000 K, most of the carbon in the H II region will be C II (Rubin 1985). The critical density for electron collisions for the 158 μm line is only

$\sim$40 cm^{-3} (Hayes and Nussbaumer 1984) making significant emission possible even at low volume density. Estimates of the fractional contribution of diffuse ionized gas to the global C II emission vary from $\sim$0.1 (Stacey et al. 1985) to $\sim$ 0.5 (Shibai et al. 1991). There is also an observational problem with the C II line. Spectrometers relying on incoherent techniques do not have enough resolving power to examine line profiles or resolve different velocity components along the line of sight. Heterodyne spectroscopy at 2 THz is still in its infancy and does not offer enough sensitivity, in particular to extended C II emission, to be especially useful except in the brightest regions.

3.2. C I: A BETTER CHOICE

The C I ground state is a triplet. The two fine structure transitions arising from this state lie in the submillimeter at 492 GHz ($^3P_1 \rightarrow ^3P_0$, λ = 609 μm) and 810 GHz ($^3P_2 \rightarrow ^3P_1$, λ = 370 μm). The upper state of the 492 GHz transition is only 23 K above ground. For this transition, the critical density for collisions with H_2 molecules is only 1000 cm^{-3} (Schröder et al. 1991), comparable to the critical density of the CO J = 1$\rightarrow$0 transition.

The low upper state energy and critical density of the C I $^3P_1 \rightarrow ^3P_0$ transition mean that it is relatively easily excited. The line is detectable even when emitted by moderate density interstellar gas exposed only to a radiation field equal to the mean interstellar radiation field in the solar neighborhood. For the majority of clouds in the inner Galaxy, where the incident far–UV radiation field is 1-100 times the mean solar neighborhood field, the column density of the C I layer will have reached its asymptotic value as long as A_v through the cloud is $\geq$5 (Van Dishoeck 1994, personal communication). Although the strength of the 158 μm line varies quite a bit, the C II column density at cloud surfaces depends less strongly on the intensity of the incident UV field. We can therefore correct from the amount of C I observed to the total amount of C II plus C I in the molecular gas and use the 492 GHz C I transition to trace the substantial fraction of dense cloud material where most of the carbon is not in the form of CO.

Throughout the discussion in this paper, we assume that C I emission from PDR's dominates over any other possible sources. Is this a reasonable assumption? Most chemical equilibrium models indicate that the C I/CO ratio is very small in clouds without incident far–UV radiation. Recent calculations suggest, however, that in a part of temperature–density space, the chemical reaction network may have two stable solutions, one with high electron abundance and a large C I/CO ratio and another with low electron abundance and C I/CO ratio (Le Bourlot et al. 1993). The models yield C I/CO ratios in the range of 0.05–0.18 in the high ionization phase.

Several other groups are now searching for or have made searches for similar evidence of these effects in their own chemical equilibrium models.

From an observational point of view, the possible existence of shielded regions with substantial C I/CO ratios may be irrelevant. Plume, Jaffe, & Keene (1994) argue that PDR models produce enough C I column density to explain their observations of the large-scale 492 GHz emission from S140. Photon dominated regions can also explain the detailed morphology of the C I and ^{13}CO emission in S140 as well as the large-scale coincidence of the C II and C I distributions elsewhere (see Plume et al. 1995). In addition, the global C I/CO ratio in S140 is ~0.5, considerably higher than the most optimistic values quoted for the dark cloud models with higher electron abundance. The proponents of these models agree that PDR's will dominate the observable C I emission from clouds under most circumstances, even if the proposed high atomic carbon abundance in shielded regions really exists (Flower et al. 1994).

4. C I Observations and the Distribution of Dense, Neutral Gas

The 492 GHz C I line has been observed in a large variety of contexts in the dense interstellar medium (see Keene (1995) for a recent review). The bulk of the observations, however, consist of high angular resolution maps covering only small areas near known star forming cores or ionization fronts. For most observations, the beam sizes are only 10–20″ and the total mapped areas are no more than a few arc minutes on a side. The results show that the C I distribution is highly clumpy on small scales (White and Padman 1991, Büttgenbach 1993).

At the other extreme, there are very large scale C I observations of both our Galaxy and of the nuclei of a few nearby galaxies. The COBE satellite detected both ground-state C I lines along the Galactic Plane with a 7° beam (Bennett & Hinshaw 1993). C I is an important coolant of the neutral ISM; the ratio of C I $^3P_1 \rightarrow {}^3P_0$ to CO J=2→1 intensity is 2.3±0.6 (Wright et al. 1991), averaged over the whole Galaxy. The ratio is similar in the inner few hundred parsecs of IC342 (1.5±0.4; Büttgenbach et al. 1992) and M82 (1.3-1.6; Schilke et al. 1993, Wild et al. 1992).

For our own Galaxy, there is an enormous gap between the scale of the global COBE results and the small maps of selected cloud cores and ionization fronts. Several small, dedicated telescopes designed to plug this gap in spatial scales, the SWAS satellite and the ASTRO telescope for the South Pole, are now under construction. In the meantime, Plume and collaborators at the University of Texas and Caltech have been mapping the large-scale distribution of galactic C I emission using a reimaging device on

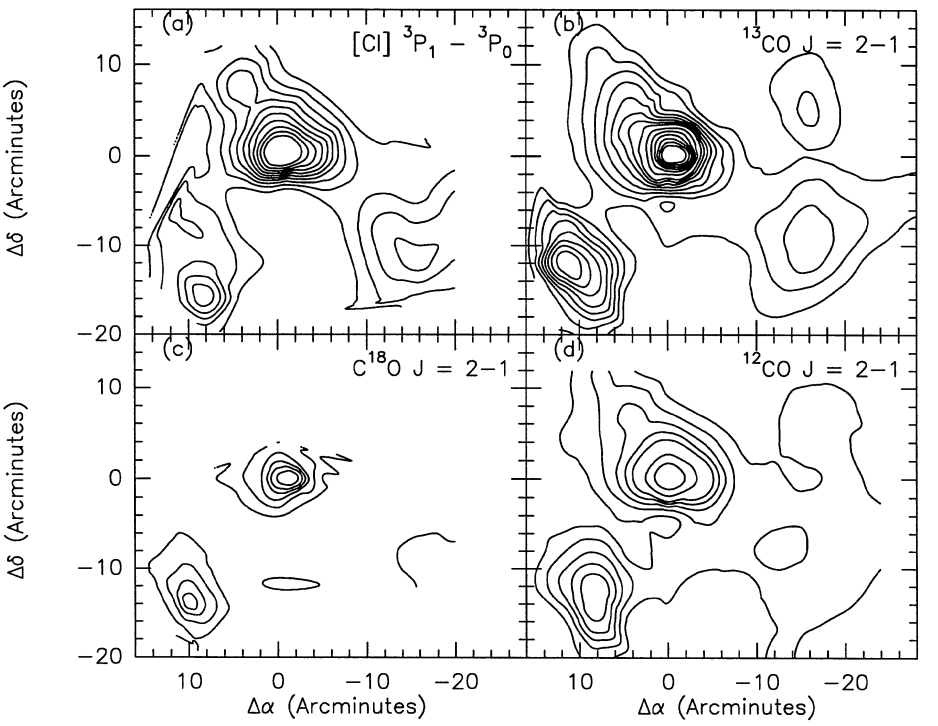

Figure 1. Integrated intensity distributions of C I and CO isotopomers toward W3 (Plume et al. 1995). The 0,0 position is (α=02^{h}21^{m}53.1^s, δ=61°52'22"), near W3 IRS5.

the Caltech Submillimeter Observatory 10.4m telescope. This device causes the facility receivers to underilluminate the primary mirror and creates a smaller telescope with 3 arc minute beams at both 220 and 492 GHz (Plume & Jaffe 1995). The reimaging device can be used in the daytime when the CSO telescope is normally idle. Since it is an off-axis system with good surface quality, the reimaging device has a clean beam which allows one to obtain an accurate representation of the very extended C I emission. In two, two-month observing seasons, the Texas group has used the reimaging instrument to map a sample of five GMC's over ~30′×30′(Plume, Jaffe, & Keene 1994; Plume et al. 1995) as well as to make a strip map of the Galactic Center (Jaffe, Plume, & Pak, this volume) and a crude survey of the first quadrant.

The large-scale distribution of 492 GHz C I emission is similar to that of CO and isotopic CO J=2→1 lines, in particular the ^{13}CO line. Figure 1 shows the distribution of C I $^3P_1 \rightarrow {}^3P_0$ and CO, ^{13}CO, and C^{18}O J=2→1 emission from the W3 molecular cloud complex (Plume et al. 1995). The

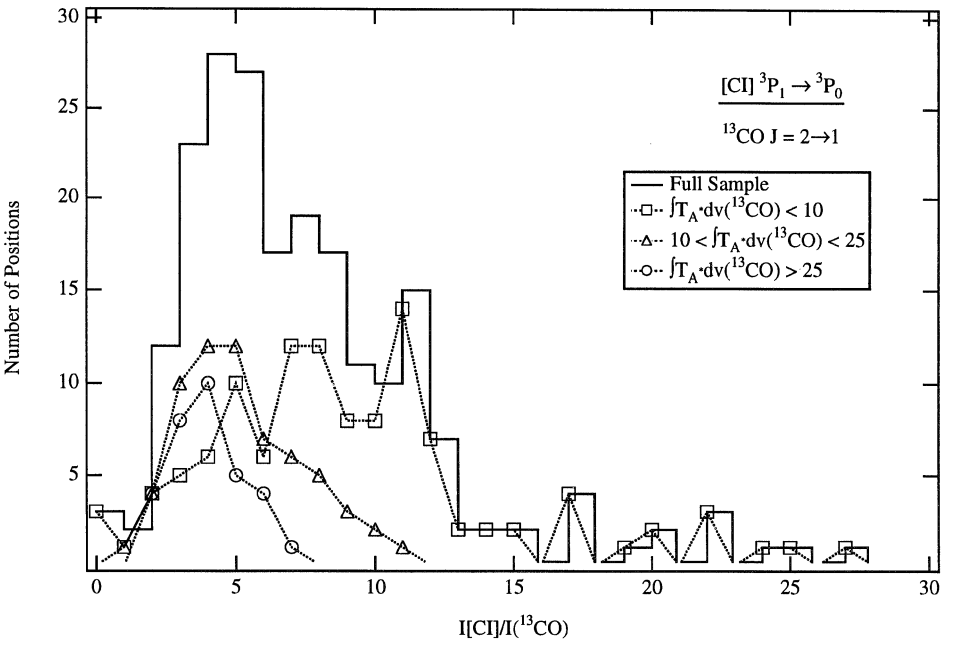

Figure 2. Frequency distribution of C I/CO intensity ratios for the molecular cloud sample of Plume et al. (1995). The three subgroups correspond fairly closely to macroscopic cloud edges (I_{13CO} <10 Kkms^{-1}), the bulk of the cloud (10<I_{13CO} <25 Kkms^{-1}), and dense, star forming cores (I_{13CO} >25 Kkms^{-1}).

lineshapes of C I and the lower opacity isotopic CO lines match fairly well. Plume, Jaffe, & Keene (1994) argue that the agreement in the lineshapes implies that the C I emission arises from the surfaces of individual clumps throughout the cloud rather than from an envelope belonging to the entire cloud. Globally, in the clouds we have surveyed, there is about half as much neutral atomic carbon as CO (Plume, Jaffe, & Keene 1994; Plume et al. 1995). If one takes into account the C II in the very outer part of the cloud, the majority of the gas-phase carbon in the clouds is in a form other than CO (Jaffe et al. 1994). Typically, the regions near the cloud cores have lower C I/CO ratios than the cloud edges (Figure 2).

The high observed fraction of neutral and ionized carbon in the gas in GMC's with typical column densities corresponding to A_v ~10 leads one to wonder whether there might be a population of clouds in which the vast majority of the gas-phase carbon is not in the form of CO. This could come about in two different ways. First, clouds with only somewhat lower A_v than typical will have disproportionately larger amounts of carbon in

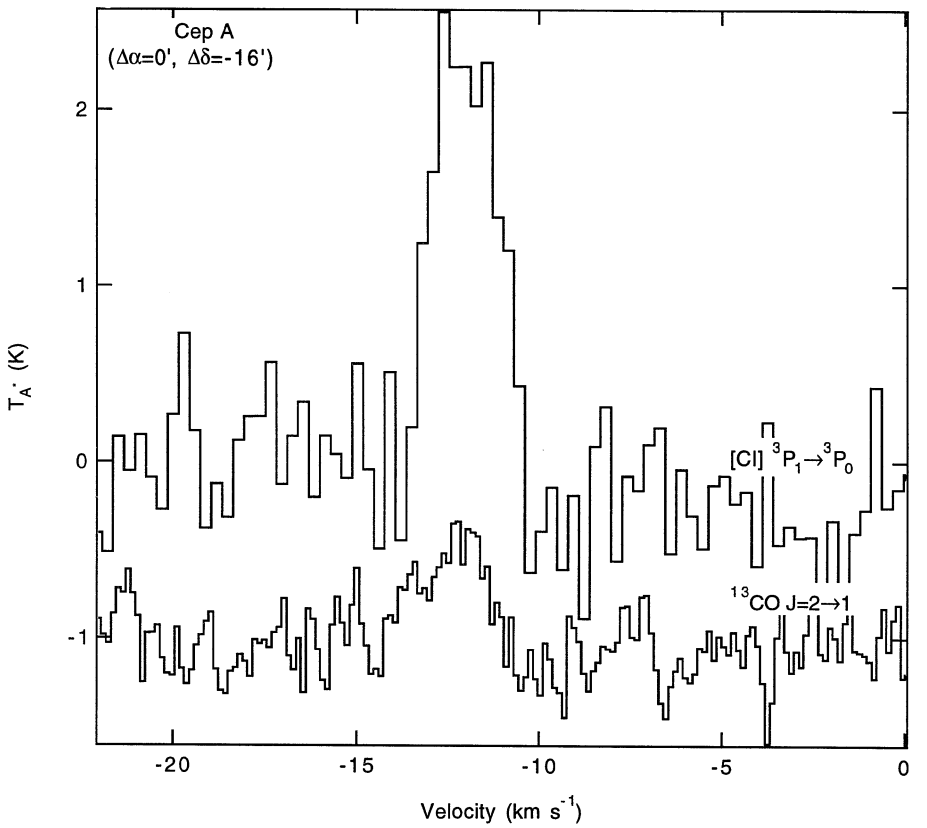

Figure 3. Spectra of C I $^3P_1 \rightarrow ^3P_0$ and ^{13}CO J=2→1 toward a secondary C I peak in CepA (Plume et al. 1995). The relative intensities imply a C I/CO column density ratio ~3. The 0,0 position for CepA was (α=22^{h}54^{m}19.2^s, δ=61°45'44").

atomic form. Second, the surface area to volume ratio of clouds can change, i.e., clouds can be more or less clumpy and therefore more or less subject to the influence of UV radiation. The huge variations in the N(^{13}CO)/A_v ratio for low A_v (Lada et al. 1994) indicate that, along some lines of sight, much of the carbon is in forms other than CO. Reach et al. (1994) present additional evidence for large molecular regions containing little CO. They have corrected 100 μm maps of diffuse clouds for the contributions of H I regions and compared the resulting "H_2" maps to the CO distribution in a sample of high latitude clouds. The "H_2" zone is much larger than the portions of the clouds in which there is detectable CO emission. In the GMC study of Plume et al. (1995), there is at least one example of a predominantly C I cloud core. Figure 3 shows C I and ^{13}CO spectra toward a

secondary maximum in the C I distribution toward CepA. At this position, the C I column density is $\sim 8\times10^{16}$ cm^{-2} while the CO column density inferred from ^{13}CO is $\sim 3\times10^{16}$ cm^{-2} (assuming ^{12}CO/^{13}CO=50).

5. Do We Really Need to Trace C I?

The basic result of our large-scale mapping of C I emission from GMC's is that a large fraction ($\sim 1/2$) of the gas-phase carbon in the dense interstellar gas is in C II or C I rather than CO. Since the variance of this fraction is not particularly large, one needs to decide if there is any reason not to simply go on using CO to trace H_2, correcting as necessary for additional material in the surface layers of clouds. In general, there is not a lot that speaks against this simple approach. There are, however, a few possible reasons why it may be a little too soon to give up on C I entirely:

(1) Even the Texas group's large-scale observations are biased toward regions known to have strong CO emission. A more unbiased large-scale survey may indicate a higher fraction of dense C II and C I bearing gas.

(2) If the characteristic column density between UV-exposed surfaces and the centers of clumps in GMC's were only slightly smaller, the fraction of molecular gas with carbon in C II, C I would rise dramatically. A more complete C I survey could show whether such clumpy, wispy regions are common.

(3) In addition to dissociating CO, the far–UV radiation also elevates the electron densities in the cloud surfaces by several orders of magnitude above the equilibrium level set by cosmic ray ionization and thereby lowers the ambipolar diffusion rate. If ambipolar diffusion plays a role in relaxing clouds toward a state where they are unstable to gravitational collapse (Shu, Adams, & Lizano 1987), the far–UV radiation may be an important inhibitor of star formation (McKee 1989). Observations of C I and CO together can provide an estimate of the fraction the gas in which the far–UV radiation affects the ambipolar diffusion rate (Plume et al. 1995).

I gratefully acknowledge the contributions to this work by R. Plume, K. Tatematsu, and J. Keene, the advice and assistance of T. Phillips, and the technical support of the Caltech Submillimeter Observatory. This work was supported in part by NSF Grants AST 9117373 and 9317567 and by the David and Lucile Packard Foundation.

References

Bennett, C.L., and Hinshaw, G. 1993, in Back to the Galaxy, ed. S.S. Holt and F. Verter (AIP Conf. Proc. 278) (New York: AIP), 257
Bennett, C.L. et al. 1994, ApJ, 434, 587.
Blitz, L. 1993, in Protostars and Planets III, ed. E.H. Levy & J.I. Lunine, (Tucson: Univ. of Arizona), 125
Büttgenbach, T.H. 1993, PhD Thesis, Caltech
Büttgenbach, T.H., Keene, J., Phillips, T.G., & Walker, C.K. 1992, ApJL, 397, 15
de Jong, T., Dalgarno, A., & Boland, W. 1980, A&A, 91, 68
Flower, D.R., Le Bourlot, J., Pineau des Forêts, G., and Roueff, E. 1994, A&A, 282, 225
Hayes, M.A., & Nussbaumer, H. 1984, A&A 134, 195
Hollenbach, D.J., & Tielens, A.G.G.M. 1995, in Proceedings of the 2nd Köln–Zermatt Symposium, ed. G. Winnewisser & G. Pelz, (Springer), in press
Hollenbach, D.J., Takahashi, T., and Tielens, A.G.G. M. 1991, ApJ 377, 192
Jaffe, D.T., Plume, R., & Pak, S. 1995, this volume
Jaffe, D.T., Zhou, S., Howe, J.E., Herrmann, F., Madden, S.C., Poglitsch, A., & van der Werf, P.P. 1994, ApJ, 435,
Howe, J.E., Jaffe, D.T., Genzel, R., & Stacey, G.J. 1991, ApJ 373, 158
Keene, J. 1995, in Proceedings of the 2nd Köln–Zermatt Symposium, ed. G. Winnewisser & G. Pelz, (Springer), in press
Lada, C.J., Lada, E.A., Clemens, D.P., & Bally, J. 1994, ApJ, 429, 694
Le Bourlot, J., Pineau des Forêts, G., Roueff, E., & Schilke, P. 1993, ApJL, 416, 87
McKee, C.F. 1989, ApJ, 345, 783
Nakagawa, T. et al. 1993, in AIP Conference Proceedings 278, *Back to the Galaxy*, ed. S.S. Holt & F. Verter, (AIP:New York), p. 303
Plume, R. & Jaffe, D.T. 1995, PASP, submitted
Plume, R., Jaffe, D.T., & Keene, J. 1994, ApJ, 425, L49
Plume, R., Jaffe, D.T., Tatematsu, K., & Keene, J. 1995, ApJ, to be submitted
Polk, K.S., Knapp, G.R., Stark, A.A., & Wilson, R.W. 1988, ApJ, 332, 432
Reach, W.T., Chu, B.-C., & Heiles, C. 1994, ApJ 429, 672
Rubin, R.H. 1985, ApJS, 57, 349
Schilke, P., Carlstrom, J.E., Keene, J., & Phillips, T.G. 1993, ApJL, 416, 67
Schröder, K., Staemmler, V., Smith, M.D., Flower, D.R., & Jaquet, R. 1991, J. Phys. B: At. Mol. Opt. Phys., 23, 2487
Shibai, H. et al. 1991, ApJ, 374, 522
Shier, L.M., Rieke, M.J., and Rieke, G.H. 1994, ApJL, 422, 9
Shu, F.H., Adams, F.C., & Lizano, S. 1987, ARAA, 25, 23
Sodroski, T.J. et al. 1995, ApJ, in press
Solomon, P.M., Rivolo, A.R., Barrett, J., & Yahil, A. 1987, ApJ, 319, 730
Stacey, G.J., Smyers, S.D., Kurtz, N.T., & Harwit, M. 1983, ApJL, 268, 99
Stutzki, J., Stacey, G.J., Genzel, R., Harris, A.I., Jaffe, D.T., & Lugten, J.B. 1988, ApJ, 332, 379
Tielens, A.G.G.M., & Hollenbach, D.J. 1985, ApJ, 291, 792
van Dishoeck, E.F., & Black, J.H. 1988, ApJ, 334, 771
White, G.J. & Padman, R. 1991, Nature, 354, 511
Wild, W., Harris, A.I., Eckart, A., Genzel, R., Graf, U.U., Jackson, J.M., Russell, A.P.G., & Stutzki, J. 1992, A&A, 265,447
Wright, E.L. et al. 1991, ApJ, 381, 200

WHY IS THE HI SCALE HEIGHT CONSTANT WITH GALACTOCENTRIC RADIUS ?

A. FERRARA
Osservatorio Astrosifico di Arcetri
Largo E. Fermi, 5 50125 Firenze, Italy

1. Introduction

The vertical distribution of neutral hydrogen has been studied over the last three decades (Schmidt 1957; Baker & Burton 1979; Lockman 1984; Savage & Massa 1987). The best fit curve to the HI z-distribution in the solar neighborhood has a FWHM of about 230 pc, and it extends appreciably beyond 500 pc (Dickey & Lockman 1990).

The support of the Galactic HI layer in the Galactic gravitational potential may be provided by bulk motions of the gas. Using a hydrostatic approach, Lockman & Gehman (1991) have demonstrated elegantly that, in order to reproduce the observed distribution, a number of isothermal components, with different one-dimensional velocity dispersion σ, must be considered. In these terms, a population of "very fast" ($\sigma_f \geq 25$ km s $^{-1}$) clouds seems to be necessary to explain the high-z tail of the distribution.

A population of fast clouds appears to be a basic ingredient of any model in which the vertical support of the HI is due to turbulent pressure alone, mainly to account for the extended tail of the distribution. The values of σ_f discussed above are certainly marginally sufficient to account for the observed HI scale height and distribution at $\varpi = \varpi_\odot$, but they are still quite controversial. In an analysis of the Galactic hydrostatic equilibrium, Bloemen (1987) uses a single value $\sigma = 9$ km s^{-1} for the HI dispersion; Boulares & Cox (1990) adopt a two population HI cloud model with $\sigma_s = 9$ km s^{-1} and $\sigma_f = 14.3$ km s^{-1} for slow and fast clouds, respectively. Supernovæ are generally considered to represent the major energy source for turbulent motions; nevertheless, an efficient conversion of the explosive energy injection into turbulent pressure relies on a high porosity parameter of the ISM, Q, which is far cry from being determined (McKee, 1990).

L. Blitz and P. Teuben (eds.), Unsolved Problems of the Milky Way, 479–487.
© 1996 *International Astronomical Union.*

In addition, the mechanisms accelerating the fast clouds - e.g. supernova shocks- are also likely to partially destroy them through fragmentation and evaporation (Klein, McKee & Colella, 1990). The two previous remarks underline that the origin, and perhaps even the very existence, of a class of very fast clouds ($\sigma_f \geq 25$ km s^{-1}) is troublesome. This complication can put pure turbulent pressure HI support models into some difficulty.

Apart from the large z-extension of the HI, its scale height is apparently constant of over a large range of galactocentric radii, ϖ, despite a sensible variation of the gravitational potential in the same range (Dickey & Lockman 1990; Heiles 1991). Also, the *shape* of the vertical HI distribution remains almost the same in $4 \leq \varpi \leq 8$ kpc.

In this paper we stress the relevance of the Galactic radiation field to account for the HI distribution in the Galaxy; in addition we present a simple model for the origin of turbulent motions that reproduces many of the features of the local, turbulent ISM.

2. Radiative/Turbulent Support of HI

In the following we present briefly the model for the radiative/turbulent support of the HI; a more extended description can be found in Ferrara (1993). Dust grains located at an optical depth $\tau < 1$ in an interstellar cloud immersed in a radiation field, feel a radiation pressure which depends on the field flux, F, and on the grain radiation pressure coefficient, Q_p (Franco *et al.* 1991; Ferrara 1993). The momentum transferred by the photons to the grains can be transmitted to the cloud gas provided that the dust-gas coupling, mainly represented by viscous and Coulomb drag, is strong enough. Hence, the requirement for a cloud to be effectively photolevitated by the radiation field is that its column density must be in the interval $10^{19} \leq N_H \leq 5 \times 10^{20}$ cm^{-2}.

If the photon field is anisotropic, the cloud receives a net acceleration which depends on the ratio $\gamma(r)$ between the average energy flux at z directed towards the disk, F_{down}, and the one directed upwards, F_{up}

$$\gamma(r) = \frac{F_{down}}{F_{up}} = \frac{\int_z^\infty F(z)\, dz}{\int_{-\infty}^z F(z)\, dz} = \frac{1 - W(r)}{1 + W(r)}, \qquad (1)$$

where $r = z/H_\star$, $W(r)$ and $H_\star$ are the distribution and scale height of the disk stars, respectively. Besides the average interstellar radiation field, a contribution to the radiation pressure on the cloud due to stellar clusters, P_{cl} is also included. The total radiation pressure, P_{rad}, therefore, can be written as

$$P_{rad} = P_{av} + P_{cl} = \left\{ \frac{Q_p F}{c} \left[\frac{1 - \gamma(r)}{1 + \gamma(r)} \right] + \frac{Q_p \langle L \rangle}{4\pi z^2 c} \right\} (1 - e^{-\tau_c}), \qquad (2)$$

where $F = F_{up} + F_{down}$ is the total power per unit surface from one face of the disk, $\langle L \rangle$ is the average cluster luminosity, and τ_c is the total optical depth of the cloud. A detailed evaluation of the galactocentric dependence of the parameters entering in eq. (2) is given by Ferrara (1993).

The radiative force adds to the gravitational one acting on the clouds, resulting in an "effective" potential ϕ_e. The expression for ϕ_e is

$$\phi_e(\varpi, z) = \int_0^z K_z(\varpi, z)dz - \int_0^z \frac{P_{rad}(\varpi, z)}{N\mu}dz = \int_0^z K_z(\varpi, z)dz, \quad (3)$$

where N is the cloud total column density along the z-axis, μ is the mean mass per gas particle, and $K_z(z)$ is the gravitational acceleration (Kuijken & Gilmore 1989).

The density distribution $n(z)$ can be obtained by solving the hydrostatic equilibrium equation

$$\nabla p = -\rho \nabla \phi_e. \quad (4)$$

If one admits that the pressure is provided solely by gas motions, then $p = \rho\sigma^2$; supposing also that the HI can be approximated as the sum of the "fast" and "slow" isothermal components, eq. (4) has the solution

$$\rho(z) = \sum_{j=f,s} \rho_{0,j} \exp\left[-\phi_e(z)/\sigma_j^2\right], \quad (5)$$

where the indexes f and s stand for fast and slow, respectively, and $\rho_{0,j}$ is the density at midplane. The total density profiles obtained from eq. (5) at different ϖ have been compared with the average observed profile given by Dickey & Lockman (1990) for all galactocentric radii considered (Ferrara 1993). The fits are remarkably good in the entire range $4 \leq \varpi \leq 8.5$ kpc assuming a slightly increasing value for σ_j (both for the fast and the slow clouds) towards the Galactic center: for $\varpi = \varpi_\odot = 8.5$ kpc ($\sigma_f = 13.0, \sigma_s = 5.0$) km s^{-1}, whereas for $\varpi = 4.0$ kpc ($\sigma_f = 22.0, \sigma_s = 8.0$) km s^{-1}.

We conclude that:

- The vertical support of the galactic HI may be completely provided by turbulence- *e.g.*, bulk motions of the gas- without requiring any additional pressure due to magnetic fields and cosmic rays when the average Galactic and cluster radiation fields acting on the clouds are included. The photolevitation mechanism tends to create a lower "effective" gravitational potential, as described above.
- The observed constancy of the HI scale height with ϖ is naturally explained by the model in terms of the similar radial dependence of the average luminosity and mass distribution found in spiral galaxies and, in particular, in the Milky Way.

• The increase in the velocity dispersion of the fast clouds implied by the fit parameters towards the Galactic center closely resembles the global distribution of the HII regions in the disk. This is also consistent with the suggestion by Dickey & Lockman (1990) that the dispersion may increase toward the inner Galaxy.

In the following we investigate the origin and the energy budget of the turbulent motions in the ISM.

3. Sources of Turbulent Energy

The kinetic energy stored in turbulent motions can be estimated from observational data to be $E_k \sim 6 \times 10^{51}$ ergs (Lockman & Gehman 1991). The most plausible sources of this energy are supernova explosions, which are likely to occur in a correlated manner, producing supershells. Correlated supernovæ can inject kinetic energy into the ISM at a rate

$$\dot{E}_{SN} \sim 10^{39} \left(\frac{N_{ss}}{10^3}\right) \left(\frac{E_0}{10^{51}\mathrm{erg}}\right) \left(\frac{\Delta\tau}{2 \times 10^5 \mathrm{yr}}\right) \left(\frac{\eta}{0.01}\right) \ \mathrm{erg\ s^{-1}}, \quad (6)$$

where N_{ss} is the number of supershells in the disk, E_0 is the total energy of a supernova, $\Delta\tau$ is the time interval between explosions, and η is the efficiency of the conversion of E_0 into kinetic motions. According to this estimate, the supply time for the turbulent energy is roughly 2×10^5 yr; in order to have a steady-state the decay time of the turbulent spectrum must be of the same order. Our approach to determine this quantity is to use the local interstellar medium (LISM). Since accurate measurements are possible for this environment, it represents an ideal laboratory to understand the decay of turbulence.

3.1. A FEW POINTS ABOUT THE LOCAL BUBBLE

The Local Bubble (LB) is an oval-shaped cavity filled with hot ($T_h \sim 10^6$ K), tenuous ($n_h \sim 5 \times 10^{-3}$ cm^{-3}) gas surrounding the sun. Its origin probably requires a supernova (SN) explosion that occurred close to the sun $\sim 2 - 10 \times 10^5$ yr ago (Cox & Reynolds 1987). This hypothesis has found strong support after the identification of the γ-ray source Geminga with the x-ray source 1E0630+178 (Bignami *et al.* 1983), recently discovered to be a pulsar by ROSAT observations. The age of the pulsar, as derived from its period, is $3.2 - 3.4 \times 10^5$ yr (Gehrels & Chen 1993); its distance from the sun is estimated to be 40-400 pc. On this basis, Gehrels & Chen conclude that the origin of the LB can well be ascribed to the Geminga supernova explosion.

In addition to the hot gas, several low-density HI clouds are interspersed in the ionized medium; the sun itself is located at the edge of the so-called

Local Cloud (LC). A likely possibility is that these structures are remnants of clouds that have been engulfed by the interstellar shock produced by the explosion, as predicted by the McKee & Ostriker (MO:1977) model. During this process, turbulence generation is expected as a result of noncoherent overlapping of the secondary shocks created by the interaction of the primary one with the clouds. The very complex velocity structure seen in the LC (Lallement *et al.* 1986) is suggestive of a turbulent pattern and of the fact that the cloud has been shocked (Bruhweiler & Vidal-Madjar 1987).

Recent absorption line studies (Linsky *et al.* 1993) have exploited the high-resolution, high signal-to-noise data from the *Hubble Space Telescope* Goddard High-Resolution Spectrometer to observe the line of sight toward the star Capella, located 13.2 pc away from the sun. In brief, the results of interest here are the determination (for the first time based on a direct analysis of the absorption line profiles rather than on equivalent widths) of an average hydrogen density $n_{HI} = 0.047$ cm^{-3}, a temperature $T = 7000 \pm 200$ K and a turbulent velocity $\xi = 1.66 \pm 0.03$ km s^{-1}. This last result is noticeably interesting, as ξ is substantially lower than the values inferred for the mean cloud velocity dispersion in the general ISM (see above).

3.2. EVOLUTION OF THE TURBULENT SPECTRUM IN THE LOCAL BUBBLE

In the following we present a model for the evolution and decay of the turbulent spectrum injected by a SN explosion in the LB. The aim is to reproduce the low velocity dispersion observed locally in a self-consistent manner. The interested reader may find a more extended presentation in Ferrara (1994).

Let's assume homogeneous, isotropic turbulence: this approximation is rather crude but still useful for the present aim; in addition, the results can be used at least as a guide when discussing compressible turbulence.

Next, we introduce a spectral representation of the velocity field in the fluid: the energy contained in eddies with wavenumber between k and $k+dk$ is given by $\rho E(k,t)dk$, where ρ is the density of the fluid and $E(k,t)$ is the (tridimensional) spectrum of the turbulence.

To study the evolution of the spectrum when the energy source is turned off (*i.e.*, after the supernova explosion) it is necessary to take into account the dynamic equation governing the time evolution of $E(k,t)$. In its integral form this equation reads (Batchelor 1986)

$$\frac{\partial}{\partial t}\int_0^k dkE(k,t) = \int_0^k dkF(k,t) - 2\nu\int_0^k dkk^2E(k,t); \qquad (7)$$

here $F(k,t)$ is the energy-transfer function, $\nu = \mu/\rho$ is the kinematic viscosity. The physical meaning of eq.(7) is transparent and can be understood in the following way. The lhs term describes the change in the kinetic energy and the dissipation occurring in large eddies with wavenumber less than k. The flow of energy from large eddies is split in two different contributions: part of it is transmitted in form of kinetic energy to smaller eddies, and part is directly dissipated into heat through viscosity. The first two terms on the rhs describe these two processes, respectively.

A complete solution of the dynamic equation in its general form has not yet been found and therefore it is necessary to postulate an explicit form of $F(k,t)$; this is usually done on the basis of some physical/dimensional arguments. We have adopted the formulation proposed by Kovasznay (1948),

$$\int_0^k dk F(k,t) = -\alpha E^{3/2}(k,t)k^{5/2}, \tag{8}$$

since this form automatically satisfies the condition of a local interaction in *every* region of the spectrum (Ferrara 1994). Given the adopted form of the transfer function it follows that eq.(7) can be more fruitfully written in its differential form

$$\frac{\partial E(k,t)}{\partial t} = -\alpha \frac{\partial}{\partial k}(E^{3/2}k^{5/2}) - 2\nu k^2 E(k,t), \tag{9}$$

where α is a constant of the order of unity.

Eq.(9) completely describes the evolution of the turbulent spectrum, provided the appropriate boundary and initial conditions are specified. A solution of eq. (9) is found using the method of characteristics. Introducing the auxiliary variable $\Psi(k,t)$, such that $E(k,t) = \Psi^2(k,t)k^{-5/3}$ we obtain

$$\frac{2}{\Psi(k,t)}\frac{\partial \Psi(k,t)}{\partial t} + 3\alpha k^{5/3}\frac{\partial \Psi(k,t)}{\partial k} + 2\nu k^2 = 0. \tag{10}$$

The solution of eq. (10) along a characteristic is

$$\Psi(k,t) = \frac{\Psi_0(k)}{k_r^2}\frac{k^2}{(1+2\nu k^2 t)}, \tag{11}$$

where k_r defines the intersection point of the characteristic with the axis $t = 0$. The characteristics are parametrically defined by the implicit equation

$$\frac{\Psi_0(k)}{k_r^2}\frac{k^2}{(1+2\nu k^2 t)} - \frac{\nu}{2\alpha}(k_r^{4/3} - k^{4/3}) + \Psi_0(k) = 0; \tag{12}$$

each value of k_r defines a specific characteristic. Since the curves defined by eq.(12) have a dependence of the type $t \propto 1/k^2$, they define in the $k-t$

plane a family of hyperbolas having the axis $k = 0$ as one of the asymptotes. This means that the spectrum will contract in time towards smaller wavenumbers, which is to be expected since energy is mostly dissipated in small ($k \gg k_0$, where k_0 is the injection wavenumber) eddies. The initial condition $E_0(k)$ is the interpolation formula given by von Karman (1948) for the case of negligible viscosity, which not only reproduces the right $k^{-5/3}$ behavior of the spectrum in the inertial regime, but also in the small k region, where it is known to be $\propto k^4$.

We can now compare the predictions of the present model with the degree of turbulence in the local ISM determined by the Linsky *et al.* (1993) experiment. The actual energy density inside the LB is $\epsilon_t = 2.76 \times 10^{-12}$ erg cm^{-3} and it is presumably the same in the hot and in the neutral gas (Cox & Reynolds 1987). If the explosion has taken place in a rarefied medium of density $n_0 \sim 4 \times 10^{-3}$ cm^{-3}, as suggested by Cox & Reynolds (1987), and assuming for the total energy of the explosion $E = 10^{51}$ ergs, then from case B of Chevalier (1974), the fraction η of the total energy converted in kinetic energy is $\eta \sim 0.1$. Therefore, the kinetic energy density is $\epsilon_k = \eta\epsilon_t/(\chi - 1) = 3.06 \times 10^{-13}$ erg cm^{-3}. This value can be used to fix the initial condition.

The time evolution of $E(k,t)$ is completely determined by the dynamic equation (9) when k_0, the energy injection wavelength, is specified. A considerable uncertainty remains in the determination of k_0 (for an instructive discussion see Spangler 1991); Spangler (1991) suggests $k_0 = 2\pi/10^{18}$ cm^{-1} as the most suitable value from observational arguments.

The most probable velocity ξ_{k^*} measured at the time t can be expressed in terms of the turbulent spectrum as

$$\xi_{k^*}(t) = \left[\int_{k^*}^{\infty} dk E(k, t - t_0)\right]^{1/2}, \tag{13}$$

where t_0 is the time of the explosion, and $k^* \sim 2\pi/d$, where d is the distance on which the turbulence is sampled, in this case the distance to Capella ($d = 13.2$ pc).

The time evolution of the spectrum for $k_0 = 2\pi 10^{-18}$ cm^{-1} is followed up 10^7 yr after the explosion, for a density $n = 0.047$ cm^{-3} and temperature $T = 7000$ K appropriate for the local HI (Linsky *et al.* 1993). In the first stage, lasting about 10^5 yr, energy is dissipated only in small eddies ($k \gg k_0$). An equilibrium spectrum is maintained through several wavelength decades while k_s rapidly approaches the injection wavelength and the Reynolds number decreases accordingly; in this stage, however, ξ_{k^*} decreases very slowly because most of the energy is stored in the large eddies with $k \sim k_0$.

In the second stage, energy starts to be dissipated also in large eddies with $k \sim k_0$ at a rate $\propto t^{-2}$. At the end of the calculation ($\tau = 10^7$ yr), $\xi_{k^*} = 0.039$ km s^{-1}.

The calculated ξ_{k^*} can be compared with the observed one for different values of k_0 and τ. If the explosion took place $2 - 10 \times 10^5$ yr ago (Cox & Reynolds 1987), then a narrow range of outer scales satisfies the limits on ξ_{k^*}. This range is very much in agreement with the value suggested by Spangler (1991): $0.9 \times 10^{18} \lesssim \ell_0 \lesssim 6 \times 10^{18}$ cm; generally, it appears possible to consistently match the observed degree of turbulence in the local environment with the scenario of the LB created by a SN explosion. In fact, the use of $\tau = 3.2 \times 10^5$ yr, suggested by Gehrels & Chen (1993) from the "Geminga hypothesis", implies $\ell_0 = 1.5 \times 10^{18}$ cm.

4. Summary

We have explored the effect of the photolevitation process, through which dusty diffuse clouds can rise to considerable high Galactic latitudes, on the global vertical distribution of the HI in the Galaxy. It is shown that the vertical support may be completely provided by turbulence in the lower effective gravitational potential determined by the Galactic radiation field. In addition, the apparent observed constancy of the HI scale height with galactocentric radius is naturally explained by the model in terms of the similar behavior of the Galactic radiative and gravitational fields.

We have investigated the origin and evolution of the turbulence taking the Local Bubble as a typical supernova-regulated environment. The evolution and decay of the turbulent spectrum injected by a supernova explosion in such an environment is studied through an analytical solution of the dynamic equation. The results, when compared with *HST* high resolution absorption line data, support the idea that the turbulent motions have been produced by a supernova explosion that occurred a few times 10^5 years ago, as indicated also by other evidences.

References

Baker, P.L., & Burton, W.B. 1979, *A&AS*, 35, 129
Batchelor, G. K. 1986, *The Theory of Homogeneous Turbulence*, (Cambridge: Univ. Press)
Bignami, G. F., Caraveo, P. A. & Mereghetti, S. 1993, *Nature*, 361, 704
Bloemen, J.B.G.M. 1987, *ApJ*, 322, 694
Bruhweiler, F. C. & Vidal-Madjar, A. 1987, *Scientific Accomplishment of the IUE*, ed. Y. Kondo, (Dordrecht:Reidel), 467
Boulares, A., & Cox, D.P. 1990, *ApJ*, 365, 544
Chevalier, R. 1974, *ApJ*, 188, 501
Cox, D. P. & Reynolds, R. J. 1987, *ARA&A*, 25, 303
Dickey & Lockman 1990, *ARA&A*, 28, 215
Ferrara, A., 1993, *ApJ*, 407, 157

Ferrara, A, *MNRAS*, submitted
Franco, J., Ferrini, F., Ferrara, A., & Barsella, B. 1991, *ApJ*, 366, 433
Gehrels, N. & Chen, W. 1993, *Nature*, 361, 706
Heiles, C. 1991, in *The Interstellar Disk-Halo Connection in Galaxies*, ed. H. Bloemen, (Dordrecht:Kluwer), 433
Klein, R.I., McKee, C.F., & Colella, P. 1990, in *The Evolution of the Interstellar Medium*, ed. L. Blitz, (San Francisco:PASP), 117
Kovasznay, L. S. G. 1948, *J. Aeronaut. Sci.*, 15, 745
Kuijken, K., & Gilmore, G. 1989, *MNRAS*, 239, 605
Lallement, R., Vidal-Madjar, A. & Ferlet, R. 1986, *A&A*, 168, 225
Linsky, J. L., Brown, A., Gyley, K., Diplas, A., Savage, B. D., Aires, T. R., Landsman, W, Shore, S. N. & Heap, S. R. 1993, *ApJ*, 402, 694
Lockman, F.J. 1984, *ApJ*, 283, 90
Lockman, F.J., & Gehman, C.S. 1991, *ApJ*, 382, 182
McKee, C.F. 1990, in *The Evolution of the Interstellar Medium*, ed. L. Blitz, (San Francisco:PASP), 3
McKee, C. F. & Ostriker, J. P. 1977, *ApJ*, 218, 148 (MO)
Schimdt, M. 1957, *Bull. Astron. Inst. Neth*, 13, 247
Savage, B.D., & Massa, D. 1987, *ApJ*, 314, 380
Spangler, S. R. 1991, *ApJ*, 376, 540
von Karman, T. 1948, *Proc. Natl. Acad. Sci. U.S.*, 34, 530

DISCUSSION

A. Whitworth: I recently estimated the mass-to-light ratio required for radiation pressure acting on dust to be comparable with gravity. If the gas is coupled to the dust, I obtain $(M/L) \sim 0.1 (M_\odot/L_\odot)$ using standard dust parameters. Have you made such an estimate for your model?

Ferrara: I agree qualitatively with your estimation. The bulk of the support is provided by turbulence and radiation pressure contributes a $\sim 20\%$ fraction. However, the mass and light distribution in the Galaxy conspire, through the radiative support, to give a constant scale height of HI in spite of the change in the gravitational potential and turbulent properties of the ISM.

THE Z VELOCITY DISPERSION OF OUTER H I DISKS

JOHN M. DICKEY
University of Minnesota
116 Church St. SE, Minneapolis, MN 55455, USA

Abstract. The velocity dispersion of the interstellar gas measured perpendicular to the disk in face-on spiral galaxies shows a remarkable consistency. Typically the width of the velocity distribution decreases monotonically with increasing galactic radius through the luminous, stellar disk; but in the outer disk where there is gas but no stars the velocity dispersion is $\sigma_v \simeq 7$ km s^{-1} with a scatter of 2 km s^{-1} at most from one position to another and from one galaxy to another. Trying to understand this number raises questions about the thermal state of the H I in outer, gaseous disks. The most important issue is to understand the dominant heating and cooling processes for the atomic gas.

1. Background

The velocity distribution perpendicular to the disk of a spiral galaxy provides a useful measure of the kinematics of a population of objects. For stars in the Milky Way the relationship between the disk scale height and the z-velocity dispersion (σ_v, z being the direction perpendicular to the disk) provides a measure of the local gravitational potential, as pointed out by Oort (1932). For gas the situation is more complicated since clouds are not ballistic; the pressure of the cosmic rays and the magnetic field, which are bound to the ionized component of the gas, also contributes to the scale height (Lockman and Gehman, 1992). For other galaxies we cannot observe both the scale height and the velocity dispersion in the same system, so to determine the gravitational potential of spiral disks we must generalize over statistical samples of face-on and edge-on spirals (van der Kruit and Shostak, 1983). Observing the λ 21-cm line of neutral hydrogen in face-on galaxies we can measure the z-velocity distribution function of the inter-

L. Blitz and P. Teuben (eds.), Unsolved Problems of the Milky Way, 489–495.
© 1996 *International Astronomical Union.*

stellar atomic gas, which is of interest as a measure of the cloud velocity distribution and the temperature of the warm phase of the medium. In this contribution I discuss unsolved problems of the Milky Way, and of spiral galaxies in general, which are raised by measurements of the z-velocity profile in outer, gaseous disks.

2. Observations

In the luminous regions of spiral disks, where young stars are common, the interstellar gas is stirred up by stellar winds, supernova remnants, and larger scale dynamical processes associated with stars, such as spiral shocks. The effect of these processes on the interstellar gas is traced morphologically in both Hα and H I; it appears also in the velocity distribution function of the interstellar gas. In the outer disks of spirals, where there is little or no evidence for stars, the gas is much more quiescent. Its motion can be very well described by a differentially rotating disk with gas on circular orbits. Even in the most face-on galaxies, the projected velocity structure on large scales is dominated by this rotation; for example, a galaxy rotating at 250 km s^{-1} inclined at only 5° to the line of sight will show a range of 44 km s^{-1} in projected velocity. A telescope must have a beam small enough to resolve away the spatial variations of this projected rotation pattern in order to measure the z-velocity distribution; in practice the beam size must be less than about 30" for even the most face-on, nearby galaxies. So we have good λ21-cm data for only a few galaxies so far, although at least two research groups have surveys of more candidates underway.

The few galaxies which have been well studied show a surprising consistency in the form of their z-velocity distributions. The basic result of all studies of face-on spirals so far published is that the z-velocity distribution of the atomic gas is very nearly a perfect Gaussian. In the inner, stellar part of the disk, this Gaussian is modified by the presence of very faint wings, roughly exponential in shape, extending several times the width of the Gaussian. (These are so weak that to see them generally requires that all spectra in an annulus be shifted to a common center velocity and then added. The velocity offset for each position is determined from the model rotation field as described by Dickey, Hanson and Helou, 1990.) In the outer, dark portion of the disk no such wings have been detected; there the Gaussian fit to the mean emission profile is nearly perfect. The widths of the fitted profiles decrease with increasing radius through the stellar disk, but beyond a radius where the blue surface brightness is about 25 mag (arc sec)$^{-2}$ the H I linewidths remain constant at $\sigma_v \simeq 7$ km s^{-1}. This value seems to be a very general quantity, many different face-on spirals in different environments show similar behavior, with outer disk z-velocity

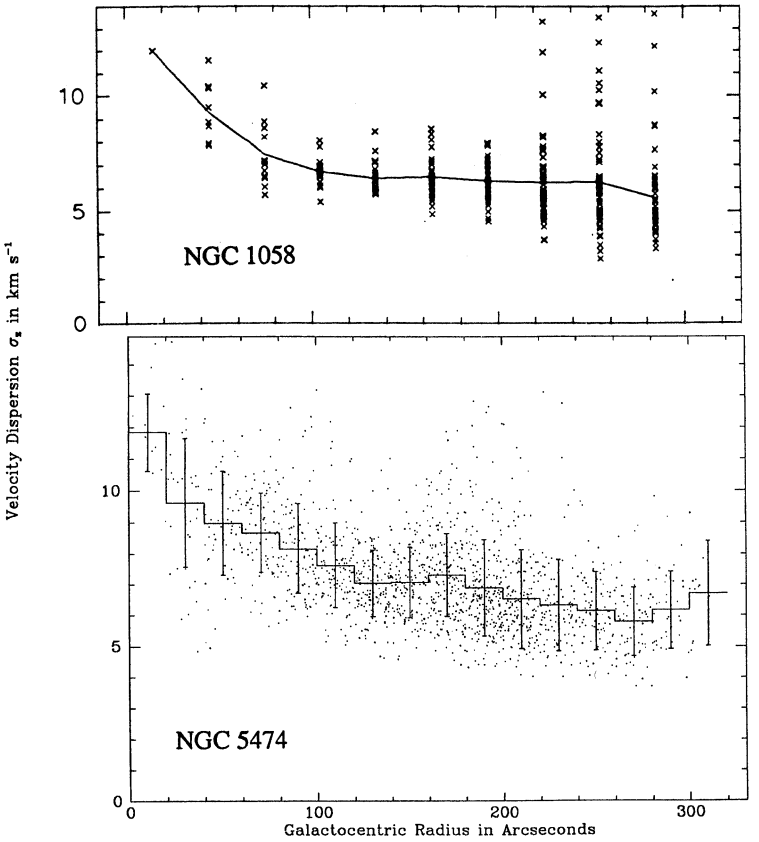

Figure 1. Examples of the radial variation of the H I linewidth, σ_v in two face-on galaxies. The top panel shows data for NGC1058 (Dickey, Hanson, and Helou, 1990), the lower panel for NGC5474 (Rownd, Dickey, and Helou, 1994). Symbols mark the results of Gaussian fits to independent beam areas in each annulus, while the line segments join the mean values for each radius.

dispersions in the range 6 to 9 km s^{-1} (Rownd, Dickey and Helou, 1994; Boulanger and Viallefond, 1992). Two examples are shown on figure 1.

3. Interpretation

This behavior of the velocity distribution is not hard to understand in general terms. The radial variation of σ_v in the stellar disks reflects the stirring of the interstellar medium by supernovae and stellar winds; the non-Gaussian tail of the velocity distribution function corresponds to the galactic fountain process (Bregman 1980, Norman and Ikeuchi 1988, Heiles 1990). A similar intermediate velocity cloud population is seen in the solar neighborhood of the Milky Way (Kulkarni and Fich 1985, Wakker 1991). In

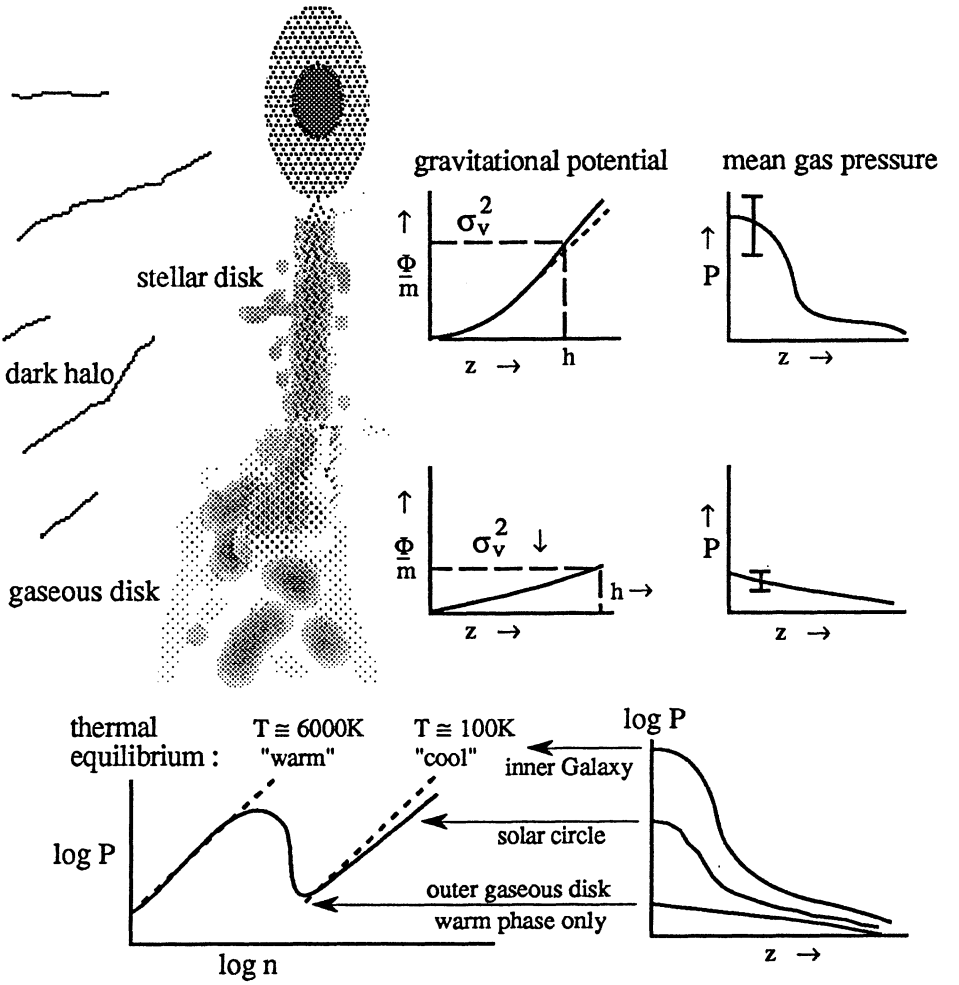

Figure 2. A schematic cross section of a spiral galaxy disk. As explained in the text, gas in the stellar disk probably has a very different pressure environment than gas in the outer part of the disk where there are no stars.

the outer disk, where there are no stars to inject turbulent kinetic energy, σ_v is smaller, and there is no intermediate velocity tail. It remains a question why the value of 7 km s^{-1} is so common, this must reflect the outcome of some physical process at work in the outer disks to regulate σ_v.

A possible explanation for the ubiquity of the 7 km s^{-1} value for σ_v is

sketched on figure 2. The upper part of this figure shows a cartoon of how the changing gravitational potential of the disk, as a function of z, influences the time-averaged interstellar pressure. On the left is a schematic cross-section of a galactic disk. Next to this are two graphs of the gravitational potential vs. z; plotted here is the potential per unit projectile mass, ϕ/m, whose derivative is the gravitational acceleration, K_z. In the inner disk the dynamics are dominated by disk stars, so the gravitational potential is parabolic in z near the midplane, where the density is roughly constant, and changes to a linear increase with z high above the plane where the mass density of disk stars is negligable. Even at high z there is some mass density due primarily to the dark matter halo, so the potential rises slightly faster than linearly; the disk alone would give something like the short-dashed line. The scale height, h, is set by the velocity dispersion, σ_z; for gas this is modified by magnetic fields and cosmic rays, a factor of $(1 + \alpha + \beta)$ in the notation of Spitzer (1977).

The time-average pressure of the interstellar gas must reflect the z dependence of the gravitational potential, as suggested in the right-hand plots. At any point, the pressure fluctuates as a function of time due to the occasional passage of supernova remnants, spiral density waves, and other processes, hence the large error bar on the pressure graph in the inner disk. But the time-average pressure must drop with z roughly as the potential rises, simply to keep the system in hydrostatic equilibrium on long time scales.

In the outer disk the gravitational potential is much weaker, the gas is only weakly self-gravitating in z and the dark halo does not help to confine it to a plane. As a result the gaseous disk warps and flares. The gravitational potential rises so slowly with z that even though the velocity dispersion is much less than in the stellar disk, the scale height is greater. The pressure must be much lower in this region, and, in the absence of stars to stir it up, there is very little fluctuation in the pressure as a function of time.

At the bottom of figure 2 is a sketch of how the pressure determines the thermal phase of the atomic medium. On the left is a plot of the heating-cooling equilibrium, in the style of Field, Goldsmith and Habing (1969). The solid line sketches the form of a typical equilibrium curve; thermally stable points correspond to positive slopes of this line, which are near $T \simeq 6000$ K (the warm phase) or $T \leq \sim 100$ K (the cool phase). In the solar neighborhood, at low z, the average pressure is in the range where both phases can coexist, but at higher z where the pressure is lower only the warm phase is a possible equilibrium state. In the outer galaxy the pressure may be below the minimum for which the cool phase can exist even at midplane, so we might expect that all the gas in outer, gaseous disks of spiral galaxies should be in the warm phase.

4. Questions

The values of σ_v that are actually measured are uncomfortably low for a disk of gas in the warm phase. If this one dimensional velocity dispersion is translated directly to a thermal velocity, then 7 km s^{-1} gives kinetic temperature T_{kin} = 5900 K, which is reasonable. However there are many other possible contributions to the linewidth besides microscopic thermal motions; these include both instrumental effects such as beam smearing of the projected rotation field and finite spectrometer channel widths as well as dynamical processes in the gas, such as cloud motions, shocks, and random departures from circular orbital motion. In the Milky Way where we can measure separately the kinetic temperature and the velocity dispersion of the gas in some regions we typically find that the total linewidth is about twice the contribution from thermal motions alone. These considerations suggest that a linewidth of 7 km s^{-1} should correspond with a kinetic temperature of about 1500 to 2000 K, which is low for a stable thermal equilibrium unless the heating and cooling processes are quite different from what we are familiar with in the solar neighborhood.

A more vague question concerns the role of cool, diffuse clouds in outer gaseous disks. There must be some H I in the cool phase in outer disks, as there are isolated spots of star formation and occasionally molecular clouds are seen even well outside the optical disks of spiral galaxies. The σ_v for a population of cool clouds will be determined primarily by the random velocity distribution of the clouds, as the thermal linewidth for gas at 100 K is slightly less than one km s^{-1}. If a significant amount of the outer disk gas is in the form of clouds, then it is hard to understand the constancy of the value $\sigma_v \simeq 7$ km s^{-1}, unless there is some physical process which regulates the cloud random velocity distribution. But such a process must work only in outer disks, since we know that in stellar disks the cloud population has a tail in velocity reaching much higher than 7 km s^{-1}.

In conclusion, I feel that there are a lot of unsolved problems associated with the outer, gaseous disks of spiral galaxies. The dark matter which dominates their large scale dynamics is a problem in itself. On smaller scales, the z velocity distribution raises issues of cooling, heating, and ionization, some of which have been discussed in other talks at this meeting. As new telescopes come on-line with greatly improved sensitivity and resolution, particularly for observing tracers of the interstellar medium in the radio, millimeter-wave, sub-millimeter, and infrared bands, we may hope in the next decade to vastly expand our knowledge of the astrophysics of the gas in the outer, dark regions of spiral disks.

References

Boulanger, F. and Viallefond, F. (1992), *Astron. Astrophys.* 266, 37.
Bregman, J.N. (1980), *Ap. J.* 236, 577.
Dickey, J.M., Hanson, M.M., and Helou, G. (1990), *Ap. J.* 352, 522.
Heiles, C. (1990), *Ap. J.* 354, 483.
Kulkarni, S.R. and Fich, M. (1985), *Ap. J.* 289, 792.
Lockman, F.J. and Gehman, C., (1991), *Ap. J.* 382, 182.
Norman, C.A. and Ikeuchi, S. (1989), *Ap.J.* 345, 372.
Oort, J.H. (1932), *Bull. Astron. Inst. Neth.* 6, 249.
Rownd, B.K., Dickey, J.M., and Helou, G. (1994), *A.J.* 108, 1638.
Spitzer, L. Jr. (1977), Physical Processes in the Interstellar Medium, (New York : John Wiley), chap. 11.
van der Kruit, P., and Shostak, S. (1984), *Astron. Astrophys.*, 134, 258.
Wakker, B. (1991), *Astron. Astrop.* 250, 499.

DISCUSSION

Shull: I believe that if one goes far enough out in the disk, the metagalactic radiation field can provide the heating necessary for $\sigma_v \simeq 7$ km s^{-1}. (This may require dust in this H I , for photoelectric heating.)

Dickey: Yes, then the metagalactic radiation field is crucial not only for ionizing the outer edges of gas disks, but also for heating the regions which remain neutral.

DIFFUSE [C II] EMISSION IN THE GALAXY

[1]H.OKUDA, [1]T.NAKAGAWA, [1]H. SHIBAI, [1,2]Y. DOI,
[1,2]K. MOCHIZUKI, [1,2]Y.YAMASHITA-YUI, [1]M. YUI,
[3]T. NISHIMURA AND [4]F.J. LOW

[1]*Inst. Space Astronaut. Science, Sagamihara by Tokyo, 229 Japan*
[2]*Dept. of Astronomy, Univ. Tokyo, Hongo, Tokyo, 113 Japan*
[3]*Natinal Astronomical Observatory, Mitaka, Tokyo, 181 Japan*
[4]*Steward Obs. Univ. Arizona, Tucson, AZ 85721 USA*

An extensive survey of [C II] line emission at 158 microns using the balloon borne telescope (BICE) has provided a complete map of the emission intensity distribution in the first and the fourth quadrants of the galactic plane ($280° < l < 80°$, $-5° < b < 5°$: Okuda et al. 1993). The emission is very extended throughout the galactic plane in which three intensity maxima are seen towards the tangential directions of the Scutum and the Norma arms as well as in the Galactic center region. However the Galactic center maximum is much less prominent compared with the two other distributions, unlike the case of far infrared continuum and CO emissions.

It has been previously shown that the [C II] emission is well correlated with FIR emission as well as CO (J = 1 – 0) emission (Stacey et al. 1991, Crawford et al. 1985). However, our observations show that the correlation varies from place to place. In Fig. 1, the correlations are plotted on the [C II]/FIR vs CO/FIR diagram used by Wolfire (1985) in his PDR emission model. As noted in the figure, the distribution of dots is highly dispersive and changes collectively from region to region. Some points are evidently spread out in the region where his model cannot explain, in particular, the points of the Cyg-X region are mostly present in the forbidden region. This should mean that the emission mechanism of [C II] line cannot be explained simply by the standard PDR model so far proposed. Doi et al. (1994) has shown that the emission from ionized gas should be dominant in the Cyg-X region. The noticeable depression of [C II]/FIR ratio in the Galactic center is explained partly by the additional heating of dust by low temperature star light which supplies extra FIR emission but not effective for ionization of carbon atoms. It should be partly caused by self-shielding

L. Blitz and P. Teuben (eds.), Unsolved Problems of the Milky Way, 497–498.
© 1996 *International Astronomical Union.*

of photodissociation region (Nakagawa et al. 1994). It is also interesting to remark that the distribution of [C II] emission in the Galactic center region is very similar to that of thermal radio continuum emission. This would indicate a substantial part of the emission is generated in ionized gas clouds. On the other hand, Yamashita et al. (1994) has shown the emission in the rho-Oph region is mostly generated in the region where B-stars are dominant UV sources.

In conclusion, our high resolution observations have resolved the locality of the diffuse [C II] line emission and suggested a large variety of its emission mechanisms.

One of the authors (HO) would like to dedicate this paper to Prof. Oort remembering his kind guidance and encouragement given in his stay at Leiden observatory more than twenty years ago.

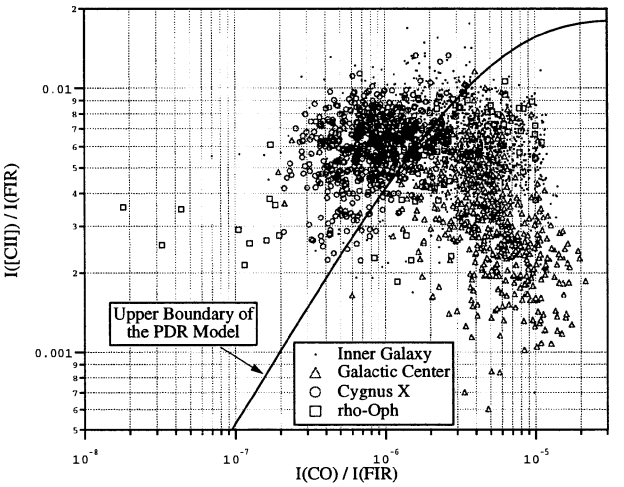

Figure 1.

References

Crawford, M.K. et al. 1985, ApJ, 291, 755
Doi, Y. et al. 1994, private communication
Nakagawa, T. et al. 1994, The 2nd Cologne-Zermat Symposium "The Physics and Chemistry of Interstellar Molecular Clouds"
Okuda, H. et al. 1993, Infrared Physics, 35, 391
Stacey, G.J. et al. 1991,ApJ. 373,423
Wolfire, M.G. et al. 1990, ApJ. 358, 116
Yamashita-Yui, Y. et al. 1994, ApJ. 419, L37

VERTICAL EQUILIBRIUM OF HI IN THE GALACTIC DISK.

Implications for mass models of the disk

S. MALHOTRA
Princeton University
Department of Astrophysical Sciences
Princeton NJ08544, USA.

1. Introduction

The analysis of vertical distribution and kinematics of disks of galaxies can yield the local mass density in the disk, distinct from the integrated mass inside a radius, derived from a rotation curve. HI is a particularly good tracer because of its ubiquity, ease of observation, and near isothermal nature. In the simplest case one considers the turbulent pressure gradient of the gas balancing the gravitational force in the z-direction. But the atomic gas may be subject to other pressures, for example, magnetic, cosmic ray or radiation pressure. The relative contributions of these are essentially unconstrained. The mass densities obtained from the analysis of HI vertical equilibrium can be verified with a similar analysis only in the solar neighborhood, where the vertical distribution and kinematics of stars can give an independent measure of the total midplane mass density (ρ_0).

2. Tangent Point Analysis and Results

The velocity dispersion and the scale heights are obtained from a full modeling of tangent point emission of HI as seen in the 21 cm transition in the inner Galaxy ($R \simeq 3-8$ kpc). The model used takes into account emission from a large path length along the line of sight, corresponding to an interval (ΔR) of typically ≤ 1 kpc in galactic radius; and is parametrized by the scale height of the gas, the centroid in z, the rotation velocity and the velocity dispersion. These parameters are assumed to be constant over the interval ΔR. This modeling is carried out for the 21 cm surveys of Weaver & Williams(1974), Bania & Lockman (1984), and Kerr et al. (1986) to measure these parameters. Similar modeling has been done for molecular gas (Malhotra 1994a)

L. Blitz and P. Teuben (eds.), Unsolved Problems of the Milky Way, 499–500.
© 1996 *International Astronomical Union.*

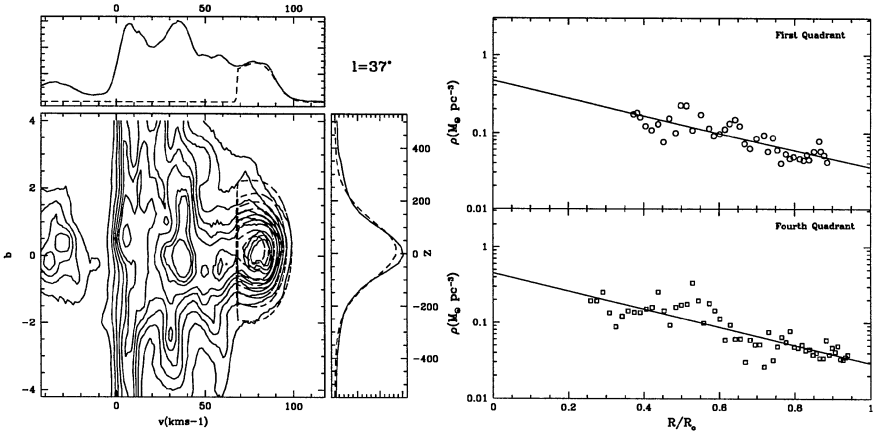

Figure 1. (a)Latitude-velocity maps of the 21 cm emission at the $l = 37°$. The best fit model is shown superposed on the data. Contour levels are defined at 10, 20, 30, .. 90% of the peak temperature in the best-fit model. The fitting is done only for $V > V_{\rm crit}$.(b)The midplane mass density of the disk $\rho_0 = \sigma_v^2/4\pi G\sigma_z^2$ (open circles: WW survey, open squares: Parkes survey). Exponential disk models are fitted to the WW data in the first quadrant and Parkes data in the fourth. The best fit scale-lengths are 3.4 ± 0.3 kpc and 3.1 ± 0.3 kpc for the first and the fourth quadrant respectively. The error bars on the scale-length are calculated by bootstrapping the measurements of $\rho_0(R)$.

Figures 1 shows the HI 21cm emission for one of the longitudes, and the best-fit model having velocity dispersion $\sigma_v = 9\,{\rm km\,s^{-1}}$, and a Gaussian scale height $\sigma_z = 95\,{\rm pc}$. The scale height of HI increases with radius while the velocity dispersion remains constant at $9 \pm 1\,{\rm km\,s^{-1}}$. The total midplane total mass density $\rho_0 = \sigma_v^2/4\pi G\sigma_z^2$, and is determined for each Galactic radius ($R = R_0 \sin l$). The radial profile of the midplane mass density is an exponential with a scale length of 3.3 ± 0.3 kpc (figure 1b), and extrapolates to $\rho_0 = 0.03\,M_\odot\,{\rm pc}^{-3}$, factor of $\simeq 3$ smaller than the ρ_0 measured for stars. This is consistent with a constant mass-to-light ratio of the disk, and extra pressure support for the HI layer constant with radius.

A more complete analysis can be found in Malhotra (1994b). This research was supported by by NSF grant AST89-21700 to Princeton University. Attendance at the meeting was supported by the IAU and a travel grant from the American Astronomical Society.

References

Bania, T. M., Lockman, F. J., 1984, ApJS, 54, 513
Kerr, F.J., Bowers, P.F., Jackson, P.D., Kerr, M., 1986, A&AS, 66, 373
Malhotra, S., 1994a, ApJ, 433, 687.
Malhotra, S., 1994b, preprint.
Weaver, H., Williams, D.R.W 1973, A&AS, 132, 20

PHYSICAL CONDITIONS OF MOLECULAR GAS IN THE GALAXY

S. SAKAMOTO, T. HASEGAWA, T. HANDA AND T. OKA
Institute of Astronomy, University of Tokyo
Osawa, Mitaka, Tokyo 181, Japan

AND

M. HAYASHI
National Astronomical Observatory
Osawa, Mitaka, Tokyo 181, Japan

1. The Tokyo-NRO Survey of the Galaxy in CO (J=2–1)

Physical conditions of molecular gas are key parameters to the formation rate and initial mass function of stars formed in molecular clouds. The ongoing Tokyo-NRO survey has been observing the Galactic CO (J=2–1) emission with a beamsize matched to the Columbia CO (J=1–0) survey. Intensities of the two lines should reflect physical conditions of the CO-emitting gas. An out-of-plane survey of the inner Galaxy which covers from 20° to 60° in galactic longitude and from −1° to +1° in galactic latitude with grid spacings of 0.25° has already been made (Sakamoto et al. 1994). Its coverage is large enough to draw conclusions on global properties of molecular gas in the inner Galaxy.

2. Meaning of the CO (J=2–1)/CO (J=1–0) Intensity Ratio

Through a numerical calculation based on a large velocity gradient approximation, the CO (J=2–1)/CO (J=1–0) intensity ratio ($\equiv R_{2-1/1-0}$) was found to be a useful tracer of physical conditions of molecular gas. Molecular gas can be classified into four classes in terms of the $R_{2-1/1-0}$ value; very high ratio gas (VHRG; $R_{2-1/1-0} \gg 1$), high ratio gas (HRG; $R_{2-1/1-0} \sim 0.8$), low ratio gas (LRG; $R_{2-1/1-0} \sim 0.5$), and very low ratio gas (VLRG; $R_{2-1/1-0} < 0.4$). The VHRG is optically thin, dense, and warm gas. The

L. Blitz and P. Teuben (eds.), Unsolved Problems of the Milky Way, 501–503.
© 1996 *International Astronomical Union.*

HRG is opaque and dense enough for low-J transitions of CO to be excited to local thermodynamical equilibrium through collisions, while the LRG is less dense and these low-J transitions are not thermalized. The VLRG is faint and usually not detected in quick surveys. For usual molecular gas, i.e., the HRG and the LRG, the $R_{2-1/1-0}$ value is sensitive to gas density rather than to gas kinetic temperature.

3. Distribution of Dense Molecular Gas in The Galaxy

Through comparison of the CO (J=2–1) data with the CO (J=1–0) data of Cohen, Dame, & Thaddeus (1986), we found a systematic variation of the $R_{2-1/1-0}$ value across the Galactic plane. The ratio varies from $\sim$0.75 at 4 kpc to $\sim$0.6 at 8 kpc in galactocentric distance, which implies large-scale variation in gas density across the Galactic disk by the factor of 2. This trend agrees quantitatively with that obtained with the pilot in-plane survey by Handa et al. (1993). There is little, if any, evidence for the difference of physical conditions between the in-plane gas and the out-of-plane gas.

Concentration of the HRG is found predominantly along arm-like structures called the Sagittarius arm and the Scutum arm in the inner Galaxy. This supports an idea that strong arms in the inner Galaxy compress molecular gas to contain much of the HRG. This, as well as the deficiency of atomic gas in the inner Galaxy, indicates that the predominance of dense molecular gas traced by the HRG is caused by compression processes such as shock compression by density waves followed by gravitational collapse, and not by dissociative stripping of low-density molecular gas due to UV photons.

4. Smaller Scale Height of Molecular Gas in Spiral Arms

Thickness of molecular gas in a disk galaxy reflects midplane total mass density and velocity dispersion of molecular gas. The Galaxy is a unique target to date for exact measurements of vertical extent of molecular gas. Analysis of the CO (J=1–0) data of Cohen, Dame, & Thaddeus (1986) and Bronfman et al. (1988) and of our CO (J=2–1) data at tangential points gives consistent results which indicate that the scale height of molecular gas layer in interarm regions is larger by a factor of 1.2 than in the arms. This fact requires either (1) that the arm-interarm contrast of midplane total mass density is larger than 1.5 or (2) that the velocity dispersion of molecular gas is smaller in arms.

References

Bronfman, L., Cohen, R. S., Alvarez, H., May, J., & Thaddeus, P. 1988, ApJ, 324, 248

Cohen, R. S., Dame, T. M., & Thaddeus, P. 1986, ApJS, 60, 695
Handa, T., Hasegawa, T., Hayashi, M., Sakamoto, S., Oka, T., & Dame, T. M. 1993, in Back to the Galaxy, ed. S. S. Holt & F. Verter (New York : AIP), 315
Sakamoto, S., Hasegawa, T., Hayashi, M., Handa, T., & Oka, T. 1994, ApJS, submitted

DOES A ROTATION VELOCITY JUMP GENERATE THE OUTER SPIRAL STRUCTURE?

A.M.FRIDMAN, O.V.KHORUZHII AND V.V.LYAKHOVICH
Institute of Astronomy, Russian Academy of Sciences
48 Pyatnitskaya St., Moscow, 109017, Russia

We investigate a stability of the gaseous disk in the Milky Way. The rotation curve with smooth two kinks in the Solar vicinity (Fig.1) was adopted in accordance with the observations (Fridman et al., 1994a). Such a gaseous disk is unstable. The instability can generate the four-armed spiral (Fig.2) and four-vortex structure (Fig.3). The method of the analysis is described by Fridman et al., 1994b. The generation mechanism is similar to that described by Glatsel, 1987.

The four-armed spiral is located outside its corotation circle with a radius about 8 kpc. Four vortices can be seen near the corotation radius. For the velocity dispersion of the gaseous clouds 10 km s^{-1}, a pitch angle of the spirals is $\sim 20^o$ (Blitz, 1983).

Acknowledgements. We thank the Russian Fund of Fundamental Investigations (grant 93-02-17248) for financial support.

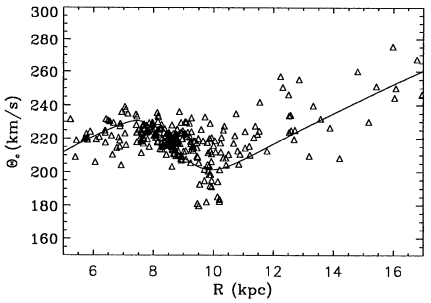

Figure 1. Rotation curve. Triangles are observations. The line is used for the simulation.

L. Blitz and P. Teuben (eds.), Unsolved Problems of the Milky Way, 505–506.
© 1996 *International Astronomical Union.*

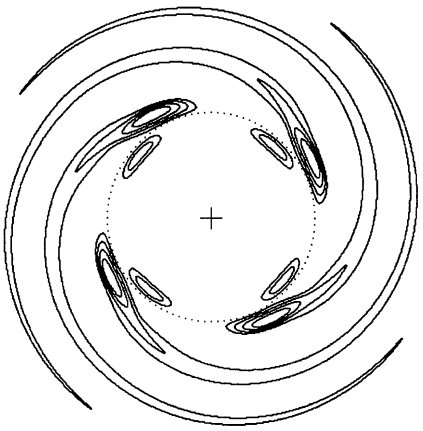

Figure 2. The four-armed density wave. A corotation circle is marked by a dotted line.

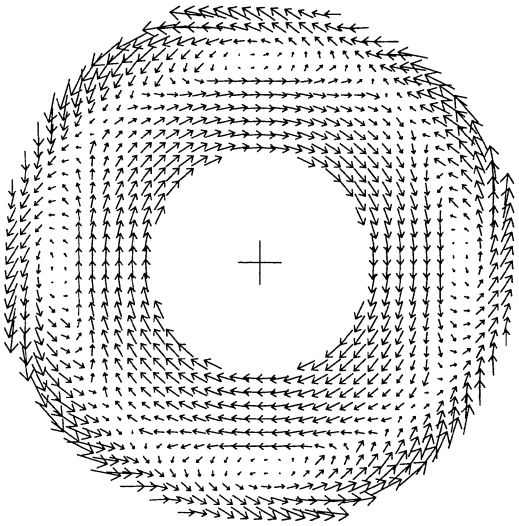

Figure 3. The velocity field which describes four anticyclones. For a clarity we increase the scale in two times in comparison with the Fig.2

References

Blitz, L. (1983) In "Surveys of the Southern Galaxy", eds. W.B.Burton and F.P.Israel, Dordrecht, 117.

Fridman, A.M., Khoruzhii, O.V., Lyakhovich, V.V., Avedisova, V.S. (1994a) in this volume.

Fridman, A.M., Khoruzhii, O.V., Lyakhovich, V.V. (1994b) In "Physics of the Gaseous and Stellar Disks of the Galaxy", ed. I.R.King, Astron. Soc. of the Pacific, 66, 285.

Glatzel, W. (1987) Mon. Not. R. Astr. Soc., 228, 77.

DYNAMICS OF THICK SPIRALS

P.A. PATSIS AND P. GROSBØL
ESO, Karl Schwarzschild Str. 2, D-85748, Garching, Germany

1. Introduction

Most studies of spiral structure in galaxies use 2D models, since the motion of the stars is supposed to be confined very close to the plane of symmetry. However, galactic disks have a finite thickness and the vertical variation of spiral perturbations should be considered. The effect of 3D orbits in the dynamics of normal spiral galaxies is examined in this paper. We present the basic orbital behavior of the families of periodic orbits, which support a thick spiral pattern.

2. The potential

The potential used for the calculations has the form: $\Phi = \Phi_d + \Phi_h + \Phi_s$, where the axisymmetric part consists of a Miyamoto disk Φ_d (Miyamoto and Nagai 1975) and a halo:

$$\Phi_h(r,z) = \frac{v_h^2}{2} \ln\left(1 + \frac{1}{r_c^2}(r^2 + z^2)\right) \tag{1}$$

The constants v_h and r_c are the maximum rotational velocity and the core radius of the halo respectively. The spiral perturbation is:

$$\Phi_s(r,\theta,z) = A\, r \exp(-\epsilon_s\, r)\, [\cos(2(\frac{\ln r}{\tan i}) - 2\theta)]\, \mathrm{sech}^2\left(\frac{z}{z_0}\right), \tag{2}$$

where A is the amplitude of the perturbation, ϵ_s is the inverse radial scale length of the spiral, i is its pitch angle and z_0 its scale height. We have calculated the orbits in a frame rotating around the z-axis. The angular pattern speed was taken so that corotation was located close to the R_{max} distance of van der Kruit and Searle (1982). The parameters used for the axisymmetric part attempted to fit the profiles proposed by van der Kruit and

L. Blitz and P. Teuben (eds.), Unsolved Problems of the Milky Way, 507–508.
© 1996 *International Astronomical Union.*

Searle (1982) (*Model A*) and by Barnaby and Thronson (1994) (*Model B*) for the surface photometry of NGC 5907. We added a strong open spiral with $i = 30°$.

3. Conclusions

The main conclusions for the 3D models are:

- A thick spiral pattern is supported by 3D families of periodic orbits with elliptical projections on the equatorial plane. These families are bifurcations of the 2D central periodic family at the vertical resonances of the model.
- The structure of 3D periodic orbits makes it difficult to create self-consistent models of spirals reaching corotation.

We found two different types of orbital behavior in the examined cases corresponding to the two different models of the photometry of NGC 5907.

- In *Model A* the successive 3D families which support the pattern are producing a "stair-type" edge-on profile. The most important 3D families of periodic orbits are bifurcated at the vertical 2/1, 3/1 and 4/1 resonances. This way it is possible for peanut shaped structures to appear in the central regions of the response model without invoking any bar in the imposed potential.
- In *Model B* the 3D families are characterized by similar mean z values of their orbits. Thus no "stair-type" effect appears. The most important families of 3D periodic orbits are bifurcated at the vertical 4/1, 5/1 and 6/1 resonances. Their projections on the equatorial plane are identical with the central family even after several kpc beyond the bifurcating point.

The above differences reflect the different locations of the vertical resonances in the models (Patsis and Grosbøl 1995).

Acknowledgements

This work was supported by the program "Human Capital and Mobility" of the EU, through the contract CHRA-CT93-0330.

References

Barnaby D., Thronson H.A.Jr, 1994, AJ 107, 1717
Miyamoto M., Nagai R., 1975 PASJ 27, 533
Patsis P.A., Grosbøl P., 1995 - A&A submitted
van der Kruit P.C., Searle L., 1982 A&A 110, 61

POTENTIAL-DENSITY BASIS SETS FOR THREE-DIMENSIONAL DISKS

DAVID J.D. EARN
Racah Institute of Physics
The Hebrew University, Jerusalem 91904, Israel

Poisson's equation, $\nabla^2\psi = 4\pi G\rho$, can be solved approximately using basis sets of potential-density pairs. A given density is approximated by a truncated expansion; the computed expansion coefficients immediately yield the corresponding potential since each basis density function is paired with a basis potential function, and Poisson's equation is linear.

This idea leads to a powerful N-body simulation technique (Clutton-Brock 1972) and is fundamental to semi-analytical normal mode analyses of stellar systems (Kalnajs 1977). The first step required before implementing these methods is to find a basis set that is well-suited to the model of interest. Some new basis sets for three-dimensional disks are presented here.

The standard potential-density basis set in cylindrical polar coordinates is given by the Laplacian eigenfunctions, $\psi_{kmh}(r,\phi,z) = J_m(kr)\,e^{im\phi}\,e^{ihz}$, which are obtained by the method of separation of variables. J_m is the cylindrical Bessel function of order m where m is an integer, and k and h range over all real values. The associated density function is $\rho_{kmh}(r,\phi,z) = -\frac{k^2+h^2}{4\pi G}\,\psi_{kmh}(r,\phi,z)$. These form a complete, orthogonal set for the space of square-integrable functions, $L^2(\mathbb{R}^3)$, but they are not especially well suited for numerical work with density distributions that are nearly flat, like disk galaxies. At the very least we want ρ_{kmh} to decay as $z \to \pm\infty$.

More suitable basis sets can be derived by seeking separated potential and density functions that are not necessarily eigenfunctions of the Laplacian operator. Instead, we can specify the vertical density profile $\rho_z(z)$ in advance and seek solutions of Poisson's equation with $\psi(r,\phi,z) = R(r)\Phi(\phi)Z(z)$ and $\rho(r,\phi,z) = \frac{1}{4\pi G}\,R(r)\Phi(\phi)\rho_z(z)$. Then $R(r) = J_m(kr)$, $\Phi(\phi) = e^{im\phi}$ and $Z(z)$ is the solution of

$$\frac{d^2Z}{dz^2} - k^2 Z = \rho_z(z)\,, \tag{1}$$

L. Blitz and P. Teuben (eds.), Unsolved Problems of the Milky Way, 509–510.
© 1996 *International Astronomical Union.*

where we impose the boundary conditions that the potential factor $Z(z) \to 0$ as $z \to \pm\infty$. The first row of Table 1 gives Green's function for Eq. (1) and yields the standard Bessel function basis set for flat disks. Rows 2–5 give solutions of Eq. (1) that allow us to construct 3-D basis sets for realistic disk galaxy models. To form basis sets we observe that ∇^2 is invariant under the translation $z \to (z-h)$ for any h, so if we replace $Z(z)$ by $Z(z-h)$ and $\rho_z(z)$ by $\rho_z(z-h)$ then we have another potential-density pair. As will be shown elsewhere, if we take $\rho_z(z)$ from any row in Table 1 and let h vary from $-\infty$ to ∞ then the density functions, $\rho_{kmh}(r,\phi,z) = \frac{1}{4\pi G} J_m(kr)\, e^{im\phi}\, \rho_z(z-h)$, form an L^2-complete basis.

TABLE 1. Vertical Factors for New Basis Sets

	Density factor $\rho_z(z)$	Potential factor $Z(z)$
1	$k^2\,\delta(kz)$	$-e^{-k\lvert z\rvert}$
2	$k^2\,e^{-k\lvert z\rvert}$	$-\frac{1}{2}(1+k\lvert z\rvert)\,e^{-k\lvert z\rvert}$
3	$k^2\,\mathrm{sech}(kz)$	$kz\,e^{kz} - \cosh(kz)\log(1+e^{2kz})$
4	$k^2\,\mathrm{sech}^2(kz)$	$1+\sinh(kz)\,\arctan[\sinh(kz)] - \frac{\pi}{2}\cosh(kz)$
5	$k^2\,e^{-(kz)^2}$	$-\frac{1}{4}e^{1/4}\sqrt{\pi}\,[e^{kz}\,\mathrm{erfc}(1/2+kz) + e^{-kz}\,\mathrm{erfc}(1/2-kz)]$

Unlike the standard basis, the sets presented here are not biorthogonal. However, as emphasized by Saha (1993), the only extra effort required as a result is the one-time evaluation and inversion of a moderately large matrix. Since two of the three components of our basis functions *are* biorthogonal, the matrix involved is sparse off-diagonal and its computation and inversion always amounts to a negligible overhead. Note that since k and h are continuous indices (unlike m) the radial and vertical functions are selected by specifying Δk, $k_{\max}$, Δh and $h_{\max}$ rather than simply the number of functions.

These basis sets are easy to implement: Bessel functions are available in all standard numerical libraries and the remaining factors are simple. They should, therefore, be very useful for stability studies and modeling of disk galaxies.

Acknowledgements. I am grateful to Ed Doolittle and Alar Toomre for helpful discussions. This research was supported by a Lady Davis post-doctoral fellowship.

References

Clutton-Brock, M. (1972) *Astrophys. and Space Sci.*, 16, 101–119
Kalnajs, A.J. (1977) *Astrophys. J.*, 212, 637–644
Saha P. (1993) *Mon. Not. R. astr. Soc.*, 262, 1062–1064

THE DYNAMICS OF PLANETARY NEBULAE IN THE GALAXY: EVIDENCE FOR A THIRD INTEGRAL

H. DEJONGHE
Sterrenkundig Observatorium, University of Ghent, Belgium

AND

S. DURAND, A. ACKER AND F. CHAMBAT
Observatoire Astronomique, Université Louis Pasteur, Strasbourg, France

Abstract. The dynamical modeling of various tracer populations in our galaxy is an important tool in the study of its formation and evolution. Planetary Nebulae (PNe) seem to be particularly useful for such a study. In this contribution we attempt to link the dynamics of PNe and OH/IR stars, and confirm on dynamical grounds that both classes are indeed related by stellar evolution. Moreover, we show that 2 integrals of motion are probably not sufficient to characterize the dynamical state of the PNe: the models produce a velocity dispersion which is too low, pointing at the likely presence of a third integral.

1. Introduction

Dynamical studies of the Galaxy as a whole need reasonably homogeneous samples over large volumes. At present, the OH/IR stars and the Planetary Nebulae are prime candidates for this.
We use in this work data compiled in the *Strasbourg-ESO Catalogue of Galactic PNe* [1] and recently calibrated thanks to 65 new radial velocities obtained at high resolution by Acker and Zijlstra (private communication). The radial velocities and galactic positions of about 650 PNe are now accurately known, but the selection biases of the surveys are still poorly understood. So we utilize as a projected star counts map the COBE brightness

L. Blitz and P. Teuben (eds.), Unsolved Problems of the Milky Way, 511–512.
© 1996 *International Astronomical Union.*

map of the full sky at 2.2 μm, which is commonly taken as representative for the stellar emission of Galactic populations (mainly K and M giants).

2. The modeling

The modeling consists in fitting a set of galactic orbits created by an axisymmetric Stäckel potential with a halo-disk structure [2], to the observed distribution of radial velocities, longitudes and latitudes of PNe. We use for this a Quadratic Programming method developed by H. Dejonghe [3]. The validity of the modeling is easily checked via a qualitative comparison between data and model.

3. The conclusions

- The COBE 2.2 μm map (corrected for interstellar extinction, using the method presented in [5]) is a very useful substitute for star counts in the presence of non-kinematic detection biases.
- The bulge-disk decomposition is very obvious in the density map (r,z) obtained via the 2-integral deprojection of the COBE map. Our deduced scalelengths are $h_r^B = 0.4$ Kpc for the bulge and $h_r^D = 5.8$ Kpc for the disk.
- Velocity dispersions of the OH/IR sample (about 700 stars) are globally lower that PNe ones, especially in the disk. This could indicate that the former may be indeed the progenitors of the latter. Bulge PNe on the other hand show nearly similar dispersions as the bulge OH/IR. This may be interpreted as evidence that the dynamics of bulge stars are dominated by mixing, while phase-space diffusion is more important for disk stars. Thus, the age of those disk PNe may be similar to the time-scale needed for phase-space diffusion.
- A 2-integral model does not fit the disc kinematics of the PNe well. This fact points to the presence of a third integral [6].

Acknowledgements. The COBE dataset was developed by the NASA Goddard Space Flight center under the guidance of the COBE Science Group and was provided by the NSSDC.

References

1. Acker, A., Ochsenbein, F., Stenholm, B., Tylenda, R., Marcout, J., Schon, C., 1992, *Strasbourg-ESO catalogue of galactic planetary nebulae*, ESO
2. Batsleer, P., & Dejonghe, H., 1994, A&A, 287, p.43
3. Dejonghe, H., 1989, Ap.J., 343, p.113
4. Dejonghe, H., 1993, in *IAU Symp. 153, Galactic Bulges*, eds. H. Dejonghe & H. Habing, Kluwer, p.73
5. Arendt, R. G., et al. 1994, ApJ, 425, L85
6. Durand, S., Dejonghe, H., Acker, A., 1995, A&A, in preparation

THE EXISTENCE OF MOVING GROUPS AND THE DISK HEATING PROBLEM

B. CHEN, F.FIGUERAS, J.TORRA, R.ASIAIN, C.JORDI
Departament d'Astronomia i Meteorologia
Av. Diagonal 647, E-08028 Barcelona, Spain

Abstract. A powerful moving group–finding algorithm has been developed and applied to a large sample of B, A and F main sequence stars from the Hipparcos Input Catalogue. Four moving groups near the Sun (Pleiades, Sirius, IC2391 and Hyades) have been identified without assuming any *a priori* knowledge of the properties of moving groups. This is the most convincing objective evidence for their existence. After the members of the moving groups are removed from the sample, we investigate the disk heating problem. The results show that the velocity dispersion of the local disk stars increases with age, roughly as $\sigma \propto \tau^{1/5}$.

1. Methods and Results

Distances and ages have been derived for a large sample of 2353 main sequence B, A and F stars from the $uvbyH_\beta$ photometric data, following the Figueras et al. (1991) and Asiaín (1993) algorithm. New photometric observations have been provided for more than 700 stars. The stars have distances less than 300 pc and residual velocities less than 65 Kms^{-1}. A Principal Components Analysis has been applied to the whole sample in the three dimensional velocity space (U,V,W). The first two new axes give a vertex deviation angle $\phi \sim 21^o$, whereas the third new axis remains almost perpendicular to the galactic plane. The histogram of this new first axis clearly shows a second peak on the right-hand side – identified with the Sirius moving group –, so the space velocities cannot definitively be represented by an ellipsoidal distribution.

A non-parametric technique has been applied to separate the members of moving groups. We derive the probability density function in the

L. Blitz and P. Teuben (eds.), Unsolved Problems of the Milky Way, 513–514.
© 1996 *International Astronomical Union.*

four dimensional space (U,V,W,log(age)) by using a spherical gaussian kernel estimator, and assuming that this function can be expressed as: $p(\mathbf{x}) = p_{field}(\mathbf{x}) + p_{mov}(\mathbf{x})$, the contributions of the field stars and the moving group members respectively. For the field we suppose an ellipsoidal distribution with unknown mean and covariance matrix. An iterative procedure is followed; in the first step the covariance matrix of the field is replaced by the one from the total sample. All the points $\mathbf{x}$ which have higher density than expected for the ellipsoidal distribution are isolated as members of the moving groups and the values for the field sample (mean and covariance matrix) are recomputed.

A cluster analysis applied to the moving group members allows us to identify the Pleiades, IC2391, Sirius and Hyades superclusters. After rejecting these stars, the vertex deviation for the remaining field has decreased to $\phi \sim 9^o$.

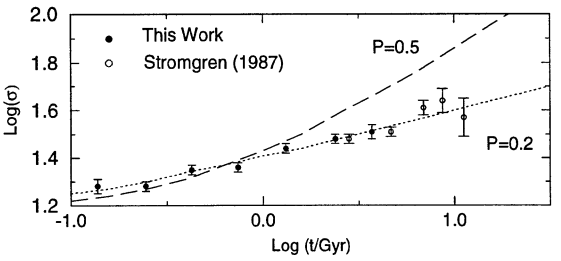

The fact that we have removed the moving group members allows a determination of the age-velocity relation for field stars younger than 3 10^9 years. The large sample used, basically from the Hipparcos Input Catalogue, implies a significant reduction of the statistical errors. In the figure, we present the total velocity dispersion ($\sigma = (\sigma_U^2 + \sigma_V^2 + \sigma_W^2)^{1/2}$) as a function of age in the solar neighbourhood. The error bars include only statistical uncertainties calculated as $\Delta(\log \sigma) = \log_{10} e/\sqrt{2N}$, where N is the number of stars in each bin. We show, for the sake of comparison, the curve $\sigma(\tau) = (\sigma_0^{1/p} + C\tau)^p$, for two sets of values p, C, and σ_0 suggested by Lacey(1991).
This work has been supported by CICYT ESP94-1311-E and DGICYT PB91-0857. BC benefits from a PIEC grant from Generalitat de Catalunya.

References

Asiaín, R. (1993), *Degree in Physics*. Universitat de Barcelona.
Figueras, F., Torra, J., Jordi, C. (1991), *A&AS* 87, pp.
Lacey, C. (1991), in *Dynamics of Disc Galaxies*, B. Sundelius (Ed.), 257
Strömgren, B. (1987), in *The Galaxy*, G. Gilmore and R. Carswell (Eds.), Reidel, 229

THE INFLUENCE OF VELOCITY DISPERSION ON DYNAMICAL FRICTION IN STELLAR DISCS

MATTIAS WAHDE
Department of Astronomy & Astrophysics,
Chalmers University of Technology, S-412 96 Göteborg, Sweden
E-mail: wahde@fy.chalmers.se

KARL JOHAN DONNER
Observatory, P.O. Box 14,
SF-00014 University of Helsinki, Finland

AND

BJÖRN SUNDELIUS
Department of Astronomy & Astrophysics,
Chalmers University of Technology, S-412 96 Göteborg, Sweden

Abstract. We have investigated the force of dynamical friction on a softened point mass orbiting inside a disc galaxy on a planar circular orbit both analytically and by means of numerical simulations. Including a velocity dispersion large enough to stabilise the disc markedly changes the physical picture of the mechanisms producing friction, whereas the numerical value of the friction is almost unaffected. Self-gravity of the disc enhances the friction only by a moderate amount.

1. Introduction and methods

A satellite galaxy orbiting inside a galactic disc will lose angular momentum due to dynamical friction. The dependence of the frictional force on several parameters has been extensively studied, but the effect of the velocity dispersion in a stellar disc has remained largely unexplored.

Using the theory developed by Lynden-Bell and Kalnajs (1972) we have derived analytical expressions for the frictional torque that are correct to second order in the velocity dispersion. We have compared these analytical

L. Blitz and P. Teuben (eds.), Unsolved Problems of the Milky Way, 515–516.
© 1996 *International Astronomical Union.*

predictions with the results from N-body simulations, carried out using the two-dimensional N-body code written by Sundelius and Thomasson (Thomasson 1991). In our simulations the galaxy consists of a disc and a rigid halo, both initially described by a Kuzmin potential. We have forced the disturber to remain on a circular orbit instead of letting it sink freely, in order to reproduce more closely the analytical assumptions (see Donner & Sundelius 1993). We vary the velocity dispersion by varying either the disc mass or Toomre's Q-parameter, keeping all other parameters fixed.

2. Results and conclusions

For non-self-gravitating simulations with small disc masses our analytical predictions agree well with the measured force. The frictional force in non-self-gravitating models depends only weakly on the velocity dispersion. We have found that the reason for this is that while the friction due to the corotation resonance is strongly reduced by velocity dispersion, this reduction is largely cancelled by a corresponding increase of the contribution from Lindblad resonances. The latter effect is related to radial displacements of the resonances due to asymmetric drift and the variation of the frequencies for non-circular stellar orbits. Both outer and inner Lindblad resonances now give a positive contribution, in contrast to the behaviour familiar from cold discs (e.g. Donner & Sundelius 1993), where the inner Lindblad resonances give rise to a negative friction, and the total effect of Lindblad resonances is to *reduce* the dynamical friction.

Finding acceptable agreement between the analytical and numerical results for small values of the velocity dispersion, we can use simulations with some confidence in order to extend our results to larger values of the velocity dispersion and to self-gravitating discs. We find that even for larger values of the velocity dispersion the friction still depends only weakly on the velocity dispersion. We also find that the inclusion of self-gravity in the simulations increases the force of dynamical friction, but only by a factor of 1.5 at the most, and that this increase is almost independent of Q. Thus the dynamical friction in a galactic disc is essentially a function of only the surface density distribution and the rotation curve. For disc masses larger than ten per cent of the total mass, the friction from the disc is much stronger than that from the halo.

Full details of this work are given in the article by Wahde et al (1994).

References

Donner, K.J. and Sundelius, B. (1993), *MNRAS*, 265, p. 88
Lynden-Bell, D. and Kalnajs, A.J. (1972), *MNRAS*, 157, p. 1
Thomasson, M. (1991), PhD Thesis, Onsala Space Observatory, Chalmers University of Technology, Göteborg, Sweden.
Wahde, M., Donner, K.J. and Sundelius, B. (1994) *MNRAS*, (submitted)

ON THE SPIRAL-INDUCED NONLINEAR DISSIPATIVE PROCESS TO THE EVOLUTION OF THE GALACTIC DISK

XIAOLEI ZHANG
Harvard-Smithsonian Center for Astrophysics
60 Garden St., MS 78, Cambridge, MA 02138, USA

1. Introduction

It is well known that in dynamical systems governed by long-range forces, the secular evolution of the system is driven predominantly by collective effects. In the current paper, we report the discovery of such a collective dissipation process induced by a self-sustained spiral density wave, which leads to important secular evolution effects in spiral galaxies.

2. Damping of the Spiral Density Wave Modes

It is found that in general there exists a phase shift between a self-consistent spiral potential and density pairs, as revealed through both the Poisson equation and the equations of motion. The sense of this phase shift is such that the potential spiral lags the density spiral in the azimuthal direction, for all trailing spirals which have radial density falloff slower than $r^{-3/2}$. For a self-sustained spiral potential-density pair, the phase shift changes sign near the corotation radius. Therefore there is a torque exerted by the potential spiral on the density spiral, and a secular transfer of energy and angular momentum from the disk mass to the density wave in the inner disk, causing the wave to be damped. The nonlinear evolution of the wave amplitude follows the Landau equation for nonequilibrium phase transition.

3. Secular Heating of the Galactic Disk and the Origin of Age-Velocity Dispersion Relation in the Solar Neighborhood

Due to the difference in the angular speed of the matter Ω and the pattern speed of the wave Ω_p, the energy released by the disk mass can not be com-

L. Blitz and P. Teuben (eds.), Unsolved Problems of the Milky Way, 517–518.
© 1996 *International Astronomical Union.*

pletely absorbed by the wave. The rest contributes to the secular heating of the disk. The space velocity diffusion coefficient of such a process is found to be

$$D = (\Omega - \Omega_p) F^2 v_c^2 \tan i \sin(m\phi_0), \tag{1}$$

where F is the fractional amplitude of the spiral wave, v_c the circular speed, i the pitch angle of the spiral, m the number of spiral arms, and ϕ_0 the equivalent phase shift. This could quantitatively explain the age-velocity dispersion relation for the solar neighborhood stars.

4. Secular Radial Mass Accretion and the Building of Disk and Bulge

The energy and angular momentum transfer from the disk mass to the density wave causes the orbit of disk stars to decay secularly. For a nearly constant orbital decay rate, the partial differential equation which governs the evolution of the disk surface density Σ admits the following self-similar solution

$$\Sigma = \Sigma_0 \frac{e^{-r/r_0}}{r/r_0} e^{\frac{-(dr/dt)_0}{r_0} t}, \tag{2}$$

where Σ_0 and r_0 are constants, and the orbital decay rate $(dr/dt)_0$ is related to the various spiral and disk parameters through

$$(\frac{dr}{dt})_0 = -\frac{1}{2} F^2 v_c \tan i \sin(m\phi_0). \tag{3}$$

In (2), the choice $r_0 = \infty$ describes a time-independent $1/r$ surface density and a constant radial flux which goes entirely to the center (building the bulge). A finite and large r_0 corresponds to a slow build up of the disk surface density. On the other hand, (2) with a small value of r_0 could also describe the self-similar build-up of the bulge itself, since the resulting density is almost identical to the de Vaucouleurs $r^{1/4}$ law. For a 20° pitch angled spiral galaxy with properties similar to our own Galaxy, the orbital decay rate is about 5 kpc in a Hubble time. A bulge size of $10^{10} M_\odot$ can thus be built up in a Hubble time.

5. Evolution Along the Hubble Sequence

As a result of the radial mass accretion in the inner disk (and excretion outside the corotation), the morphology a the disk galaxy evolves towards that of a high central concentration together with a diffused and extended envelope. The kind of spiral modes admitted by the disk thus also evolve from the open type to that of the more tightly wound. In general, the nonlinear dissipative process discussed in this paper causes a spiral galaxy to evolve along the Hubble sequence from the late to the early types.

STABILITY OF A COLLISIONLESS STELLAR DISK

E. GRIV
Department of Physics, Ben-Gurion University, Israel

The study of stability of the stellar disks of flat galaxies is the first step towards an understanding of the phenomena of spiral structure. To explain the spiral pattern, Lin and Shu (1964) further developed the Lindblad's idea of density waves by considering the spiral structure as the collective effect in a self-gravitating system. As an extension to the original Lin–Shu theory, unstable spiral modes have been obtained from an asymptotic analysis (e.g., Bertin [1980]). In such "modal theory", the Jeans-type instability (even weak) is important to the maintenance of spiral structure.

However, the hypothesis that density waves are excited by the ordinary Jeans instability in a collisionless disk of stars encounters a severe challenge. By carrying out a nonlinear stability analysis, Griv *et al.* (1994) have proved that under the influence of aperiodically growing waves of a Jeans nature, the dispersion of residual (random) velocities of stars increases. Because the Jeans instability is characterized by the critical value of dispersion, this rise in turn leads to a decrease in the growth rate of the wave amplitude and, as a result, the gravitational instability will be switched off. Thus, the Jeans-unstable spiral waves in a stellar disk have to be short-lived.

From the observational point of view, the suggestion that many spiral structures in galaxies do not appear to be organized overall grand designs has become popular recently. Accordingly, the most of spiral galaxies may be divided into two types: regular spirals and ragged, flocculent ones. As for me, the existence of regular and flocculent galaxies reflects a different nature for the spiral arms in those systems.

Below, I describe the results of the theoretical analysis which has been done mainly to understand the structure in the stellar disk of flocculent galaxies (Griv and Peter 1994, *Astrophys. J.*, submitted). We shown that in the nonlocal asymptotic approximation the generalized dispersion relation may be written as follows

L. Blitz and P. Teuben (eds.), Unsolved Problems of the Milky Way, 519–520.
© 1996 *International Astronomical Union.*

$$\epsilon^2 \frac{d^2\delta\Phi}{dr^2} + Q(\omega, k, r)\delta\Phi = 0 \ , \tag{1}$$

where $\delta\Phi$ is the amplitude of the gravity perturbation, ω is the complex eigenfrequencies of excited waves, k is the real wavenumber, r is the radial coordinate, and $\epsilon^2 \ll 1$. In analogy to plasma physics, the complex eigenvalues ω of the discrete modes that are spatially bounded are determined from (1) by means of the quasi-classical quantization rules of Bohr–Sommerfeld. The existence of discrete modes can be demonstrated by comparing (1) with the one-dimensional stationary Schrödinger equation. Assuming that $Q(\omega, k, r)$ is an almost real function, one can write relations defining the frequency and the growth rate of oscillations

$$\int_{r_2}^{r_1} \mathrm{Re}\left\{\sqrt{Q}\right\} dr = \pi(n + 1/2) \tag{2}$$

and

$$\mathrm{Im}\{\omega\} = -\frac{\int_{r_2}^{r_1} \mathrm{Im}\left\{\sqrt{Q}\right\} dr}{\int_{r_2}^{r_1} \frac{\partial}{\partial\omega}\mathrm{Re}\left\{\sqrt{Q}\right\} dr} \ , \tag{3}$$

and n is a positive number. Here the domain of integration is the range of "transparency" between the turning points r_1 and r_2 which are defined by $Q(r_1) = Q(r_2) = 0$. Equation (3) should be used only when the frequency, defined by Eq. (2), is real. Imaginary part of ω, that is, $\mathrm{Im}\{\omega\}$, which defines the Landau growth of oscillations, is equal to zero when the drift motion is neglected. In turn, that minor drifting motion, in additional to the regular circular motion, is analogous to the magnetic drift of charged particles of a plasma in an inhomogeneous magnetic field, and is related to the differential rotation of the disk (Grivnev 1988).

As it follows from (2) and (3), stellar disks of flat galaxies besides experiencing the usual gravitational Jeans instability (when the frequency from (2) is imaginary), can experience a specific *kinetic* instability of the Landau type. The etiology of this instability is the resonant interaction of drifting stars with the field of the Jeans-stable and gradient waves. The kinetic instability can be considered to be a generating mechanism for density waves, thereby leading to spiral-like patterns and dynamical relaxation in the stellar disk of disk-shaped galaxies.

References

Bertin, G. (1980) *Phys. Rep.*, 61, p. 1
Griv, E., Chiueh, Tz. and Peter, W. (1994) *Physica A*, 205, p. 299
Grivnev, E.M. (1988) *Soviet Astron.*, 32, p. 139
Lin, C.C. and Shu, F.H. (1964) *Astrophys. J.*, 140, p. 646

STABILITY OF A COLLISIONAL GALACTIC DISK

E. GRIV
Department of Physics, Ben-Gurion University, Israel

Until recently, only collisionless models have been investigated in the kinetic treatment of stellar disk stability (e.g., Fridman and Polyachenko [1984]). This is due to the fact that the frequency of ordinary binary stellar gravitational (elastic) encounters in the Galaxy is much smaller than the variation of the gravitational field for the process being studied. However, in the pioneering paper Spitzer and Schwarzschild (1951) proposed a different kind of encounter: interaction of stars with gas clouds of the interstellar medium having a mass of rougly $10^6\ M_\odot$. In recent years this hypothesis was partially confirmed by observations: it was discovered in the Galaxy a few thousand giant molecular clouds of mass $M_c \geq 10^5\ M_\odot$. Other evidence of dynamical relaxation of the star–cloud disk in the solar neighborhood was found by Grivnev and Fridman (1990); the time of relaxation was estimated equal to $\tau = (2-4) \times 10^9$ years. Hence the study of collisional star–cloud system is not only of academic interest – on the time span $t \geq 10^9$ years an actual galaxy may be a collisional ensemble of stars and clouds.

Here I report the results of the theoretical study of the dynamics of a stellar galactic disk when star–cloud collisions are taken into account (Griv and Peter 1994, *Astrophys. J.*, submitted). With respect to the physical state of our own Galaxy, the dynamics of a system with rare encounters between stars and clouds is considered when the epicyclic frequency $\kappa \simeq 10^{-8}$ encounters $\nu_c \simeq 1/\tau \sim 10^{-9}$ years^{-1}. In addition, the proper, but complicated, collision integral was replaced by an approximate model of Bhatnagar *et al.* (1954).

The dispersion relation, which connects the oscillation frequency ω and the wavenumber k, was obtained in the form

$$\frac{\kappa^2 x^2}{2\pi G\sigma_0|k|} = 1 - \sum_{l=-\infty}^{\infty} \frac{\omega_* e^{-x} I_l(x)}{\omega_* - l\kappa + i\nu_c} + 2\Omega \frac{mx^2}{rLk^2} \frac{e^{-x} I_0(x)}{\omega_* + i\nu_c} - \frac{i\nu_c \kappa^2 x^2}{2\pi G\sigma_0|k|} \frac{e^{-x} I_0(x)}{\omega_* + i\nu_c},$$

L. Blitz and P. Teuben (eds.), Unsolved Problems of the Milky Way, 521–522.
© 1996 *International Astronomical Union.*

where $x = k^2 c_r^2/\kappa^2$, c_r is the radial-velocity dispersion, σ_0 is the equilibrium surface density of the stellar disk, L is the scale of density inhomogeneity, $\omega_* = \omega - m\Omega$, m is the azimuthal mode number (the number of spiral arms), and $I_l(x)$ is the modified Bessel function.

The dispersion relation describes the Jeans and gradient branches of oscillations modified by collisions. Since in general, this relation is very complicated, in order to deal with the most interesting oscillation types I consider only some limiting cases of perturbations. Thus from the above relation, in the case of weak collisions, $\omega_*^2 \gg \nu_c^2$, the dispersion law for the Jeans branch is described by

$$\omega_{*\,1,2} \simeq \pm p|\omega_J| - \frac{\kappa^2}{2\omega_J^2 x^2}\left(i\nu_c + 2\Omega\frac{mx^2}{rLk^2}\right) , \qquad (1)$$

where $p = 1$ for perturbations with $\omega_J^2 > 0$ and $p = i$ for perturbations with $\omega_J^2 < 0$, and ω_J is the frequency of the Jeans oscillations. From (1) one concludes that Jeans-stable perturbations ($\omega_J^2 > 0$) will decay ($\mathrm{Im}\{\omega_*\} > 0$) in the presence of collisions, and Jeans-unstable perturbations ($\omega_J^2 < 0$) will undegro additional weak destabilization ($\mathrm{Im}\{\omega_*\} < 0$).

Apart from the Jeans roots (1), the dispersion relation has another root, which describes the gradient branch of oscillations

$$\omega_* \simeq \left(2\Omega\frac{mx^2}{rLk^2} + i\nu_c\right)\frac{\kappa^2}{\omega_J^2}\frac{I_0(x)}{I_1(x)} . \qquad (2)$$

Accordingly, the gradient perturbations are unstable in the presence of particle encounters in the Jeans-stable disk. In principle, this *dissipative* instability, as well as the kinetic one, can be considered as generating mechanisms for unstable short-scale spiral density waves.

I would like to acknowledge the support from the Institute of Astronomy of National Central University, Chung-Li and the NSC in Taiwan, ROC.

References

Bhatnagar, P.L., Gross, E.P. and Krook, M. (1954) *Phys. Rev.*, 94, p. 511
Fridman, A.M. and Polyachenko, V.L. (1984) *Physics of Gravitating Systems*, Vols. 1 and 2, Springer-Verlag, New York
Grivnev, E.M. and Fridman, A.M. (1990) *Soviet Astron.*, 34, p. 10
Spitzer, L. and Schwarzschild, M. (1951) *Astrophys. J.*, 114, p. 385.

GALACTIC ORBITS OF DIFFERENT GALACTIC POPULATION OBJECTS

L. P. OSSIPKOV AND S. A. KUTUZOV
St Petersburg State University,
Stary Peterhof, St Petersburg 198904, Russia

1. Introduction. It is evident that the knowledge of not only positions and velocities of objects belonging to different populations but also their osculating galactic orbits can clarify the structure and history of our Galaxy. Action variables being adiabatic invariants are especially useful for these purposes (Binney, May 1986). One of them is a usual area integral (and it can be found without any orbit calculation). The second action variable is connected with an energy integral but for 3–D orbits and arbitrary potentials it cannot be found analitically. Eccentricities resulting from orbit calculations can be used here (Lynden–Bell 1963). Comparison of eccentricities defined with different ways shown that differences between them are practically negligible (Kutuzov 1985, 1987). As for the third action variable and the corresponding third isolating integral orbit calculations can confirm its existence and control the validity of various approximations. Numerical technique allowing to find it and working at any potential is now in progress (Binney, Kumar 1993) .

2. Galactic potential and orbital elements. We used the axially symmetrical two-component model of our Galaxy (Kutuzov, Ossipkov 1989) for orbit calculations. Pericenter and apocenter cylindrical distances R_p and R_a and the maximal height of objects over the galactic plane z_m were used as orbital elements and were finding in course of orbit calculations. Two dimensionless quantities $e = (R_a - R_p)/(R_a + R_p)$, $c = 2z_m/(R_a - R_p)$ and one dimensional quantity, R_p, were considered instead of them. Sometimes we preferred to find spherical distances r_a and r_p and spherical eccentricity $e_s = (r_a - r_p)/(r_a + r_p)$.

3. Results. *3.1. Open clusters.* All orbits were found to be box ones, and the boxes were practically rectangles . The conservation of the adiabatic invariant of vertical motion $J_z = [V_z^2 + C^2(R)z^2]/[2C(R)]$, $C^2(R) = -\partial^2\Phi(R,z)/\partial z^2|_{z=0}$ (Ossipkov 1976, Villumsen, Binney 1985) has been

L. Blitz and P. Teuben (eds.), Unsolved Problems of the Milky Way, 523–524.
© 1996 *International Astronomical Union.*

checked. We found that if $J_z < 1$ (km/s)/kpc then changes of J_z do not exceed 0.01 . Mean values of orbital elements e, c, z_m are equal to to $0.06 \pm 0.01, 0.50 \pm 0.06, 0.21 \pm 0.03$ kpc respectively.

3.2. Planetary nebulae. We found that some orbits do not fill rectangle boxes and sometimes they are practically hyperbolic. Mean values of orbital elements are $< e >= (0.11; 0.16), < c >= (0.40; 0.81), < z_m >= (0.36; 0.54)$ kpc. The first values are given for Khromov's distances (1985) and the second values correspond to Cudworth's ones (1974).

3.3. Short-periodic variables . We compiled data on proper motions and radial velocities for 76 short-periodic stars . Sources used by us are given by Ossipkov, Kutuzov (1993). For RRa type stars with the period $P < 0.^d4$ we found $< R_p >= 6.65$kpc, $< e >= 0.26, < z_m >= 1.68$kpc. For stars with $0.^d4 < P < 0.^d6$ we have $< R_p >= 4.43$kpc, $< e >= 0.48, < z_m >= 5.93$kpc. If $0.^d5 < P < 0.^d6$ then $< R_p >= 3.22$kpc, $< e >= 0.56, < z_m >= 6.38$kpc. And for stars with $P > 0.^d6$ $< R_p >= 2.90$kpc, $< e >= 0.48, < z_m >= 6.80$kpc. For RRc variables $< R_p >= 2.78$ kpc, $< e >= 0.63, < z_m >= 6.58$kpc.

3.4. Globular clusters. New proper motions of globular clusters compiled by Allen, Santillan (1993) and Cudworth, Hanson (1993) were used for orbit calculations of these objects. There are some evidences of existence of three globular cluster groups forming parallel sequences on the metallicity – eccentricity diagram. Critical values of metallicity are –1.4 and –2.0.

3.5. High-velocity metal-poor stars . We have used data compiled by Allen *et al.* (1991) for orbit calculations for 40 high-velocity stars with [Fe/H] < -2.0. The sample was found to be extremely non-uniform. Orbits of 4 stars have $e_s < 0.2$ and 10 stars have $e_s > 0.9$.

References

Allen, C., Santillan, A. (1993) *Rev.Mex.Astron.Astrof.*, Vol. 25, p.39.
Allen, C., Schuster, W., Poveda, A. (1991) *AA*, Vol. 244, p. 286.
Binney, J., May, A. (1986) *MN*, Vol. 218, p. 743.
Binney, J., Kumar, S. (1993) *MN*, Vol. 261, p. 584.
Cudworth, K.M. (1974) *AJ*, Vol. 80, p.199.
Cudworth, K.M., Hanson, R.M. (1993) *AJ*, Vol. 105, p. 168.
Khromov, G.S. (1985) *Planetary Nebulae* , Nauka, Moscow.
Kutuzov, S.A. (1985) *Astronomical and Geodetical Studies* , ed. K.A.Barkhatova. Ural Univ. Press, Sverdlovsk, p.56.
Kutuzov, S.A. (1987) *Kin. i fiz. neb. tel*, Vol.3, No 4, p.11.
Kutuzov, S.A., Ossipkov, L.P. (1989) *AZh*, Vol. 66, p. 965.
Lynden-Bell, D. (1963) *Observatory*, No 932, p. 232.
Ossipkov, L.P. (1976) *Pis'ma v AZh*, Vol. 2, p. 367.
Ossipkov, L.P., Kutuzov, S.A. (1993) *Galactic Bulges*, ed. H.Dejonghe, H.J.Habing. Kluwer, Dordrecht, p.369.
Villumsen, J.V., Binney, J. (1985) *ApJ*, Vol. 295, p.388.

LOCAL VARIATIONS OF THE VELOCITY ELLIPSOID

M. MORENO
Dep. Fsica i Enginyeria Nuclear
Universitat Politècnica de Catalunya (Spain)
[manel@fen.upc.es]

J. TORRA
Dep. d'Astronomia i Meteorologia
Universitat de Barcelona (Spain)

AND

E. OBLAK
Observatoire de Besançon (France)

1. The data We have analyzed the distribution of residual velocities of nearby stars (within 200 pc of the Sun) looking for space variations on the velocity ellipsoid. We used a sample of 1071 main sequence stars of spectral types B, A and F selected from the *Hipparcos Input Catalogue* [7] with $uvbyH_\beta$ photometric data. Ages have been calculated following [1]. Six subsamples with $8.07 \leq \log(\text{age}) \leq 9.45$ have been considered.

2. Method and results The velocity distribution of stars in the solar neighborhood is described by a systematic part including the solar motion and galactic rotation, and a random part constituted by the peculiar velocities of the stars and the observational errors. The variances of peculiar velocities are expressed in terms of the velocity ellipsoid parameters that we assume to vary linearly with the position ([4], [6]). For each stellar sample, we simultaneously derive the solar motion, the velocity ellipsoid and its gradients in the galactic plane and in the z-direction. We use a new 3D extended version of the 2D algorithm developed by one of us [5].

The most remarkable results can be summarized as follows:
No dependence with age of the parameters of solar motion is found. We obtain the well known relations between the three semiaxes: $\sigma_U > \sigma_V > \sigma_W$, and the increase of their values when advancing toward older subsamples. The vertex deviation reaches its maximum values for samples number 2:

L. Blitz and P. Teuben (eds.), Unsolved Problems of the Milky Way, 525–526.
© 1996 *International Astronomical Union.*

$\phi = 20.9° \pm 6.2°$ and number 3: $\phi = 23.0° \pm 5.7°$, becoming null after twelve galactic revolutions (sample 6). The dependence of the vertex deviation on σ_U for different age samples, agrees with [2], who suggested a possible connection between the vertex deviation and a local perturbation of mass density, which could be the Orion arm.

Despite of the values obtained for the gradients are small, some of them can be considered as significant and comparable to those founded by [5]. Due to the very large error bars on derived gradients, no significant ones can be obtained but for sample 2 (table 1) and, perhaps, sample 6. Sample 2 has the greatest number of significant gradients as in [5], this is the largest sample and is constituted by relatively young stars. The dispersion of the U component decreases in the direction of the galactic center and increases in the direction of galactic rotation. The vertex deviation decreases in the direction of the galactic rotation and increases in the direction of the galactic center. The deformations and changes of orientation of the velocity ellipsoid are in good agreement with Oblak's results obtained for similar samples on the galactic plane. The gradients of the dispersion on the third component are all weak.

TABLE 1. Gradients of the velocity ellipsoid for sample 2 (321 stars, $8.37 \leq \log(\text{age}) \leq 8.67$) expressed in $km^2/s^2 \cdot pc$

$\partial\mu_{200}/\partial\xi$	$\partial\mu_{200}/\partial\eta$	$\partial\mu_{020}/\partial\xi$	$\partial\mu_{020}/\partial z$	$\partial\mu_{110}/\partial z$
$-.83 \pm .41$	$.62 \pm .34$	$.23 \pm .23$	$.43 \pm .17$	$.27 \pm .27$

Assuming the lines of constant vertex deviation as isoperturbation lines, [5] postulate the existence of a local structure oriented in the longitude direction $45° - 225°$ as an acceptable cause of this behavior (the Sun located in the inner edge of the structure). This is in acceptable agreement with the direction of the Orion arm. A similar position is adopted by [3].

This work has been supported by CICYT ESP94-1311-E and DGICYT PB91-0857.

References

1. Asian, R. (1993), *Degree in Physics*, Universitat de Barcelona
2. Mayor, M. (1970), *A&A* 6, 60
3. Menge de Freitas, S. (1982), *A&A Suppl. Ser.* 49, 687
4. Moreno, M., Torra, J. (1989), in *Errors, bias and uncertainties in Astronomy* C. Jaschek and F. Murtagh (eds.), Cambridge University Press, p. 377
5. Oblak, E. (1983), *A&A* 123, 238
6. Oblak, E., Moreno, M., Torra, J. (1993), in *Workshop on Databases for Galactic Structure*, Swarthmore (USA) (in press)
7. Turon, C. and 53 collaborators (1992), The Hipparcos Input Catalogue, *ESA SP-1136*

ESCAPE VELOCITIES FROM UNSTABLE TRIPLE STARS

J. ANOSOVA, K. TANIKAWA,
National Astronomical Observatory, Tokyo 181, Japan
J. COLIN,
Observatoire de Bordeaux, Floirac, France
AND
L. KISELEVA, P. EGGLETON
Institute of Astronomy, Cambridge CB3 0HA, UK

In order to investigate a possible origin for stars with high peculiar velocities in the thick disc of our Galaxy, the dynamical evolution of 16 000 three-dimensional triple systems which consist of a binary with equal or comparable masses of components M_1 and M_2 and a low-mass third body M_3 is considered. We examine an extensive range of initial conditions with positions of the body M_3 randomly distributed around and inside the binary orbit. M_3 was given the initial radial velocity V_0 with respect to the center of inertia of the binary. The following dynamical system of units is used in this work: the unit of distance is the semi-major axis of the binary orbit, the unit of time is the period of the binary; the universal constant of gravity is unity. In these units the total mass of the close binary is $4\pi^2$.

For all cases under consideration, before the ejection of a particle from a triple system we observe a close approach of the low-mass body to the center of inertia of the system. After this, for most cases, the small body escapes; we have here a 'gravitational slingshot'. The final velocity V_{fin} of an escaper was evaluated with respect to the center of gravity of the triple system at the time T_{esc} when the criterion of escape (Marchal, Yoshida & Sun-Yu-Sui 1983) is satisfied. The distribution and average values of final velocities and distances of escapers from the center of gravity of triple systems were obtained. They show that stars escaping by direct ejection from unstable triple systems can have large peculiar velocities with respect to field stars of the Galactic disc. Table 1 shows distributions of final distance R_{fin} and of the ratio V_{fin}/V_{crit} for the low-mass body after time $T = 40$, where V_{crit} is the critical escape velocity for M_3. These results are obtained for $R_0 = 2$,

L. Blitz and P. Teuben (eds.), Unsolved Problems of the Milky Way, 527–528.
© 1996 *International Astronomical Union.*

TABLE 1. Distributions of final velocities and distances of escapers.

V	0-1	1-2	2-4	4-6	6-8	
$f(V)$	0.178	0.179	0.231	0.162	0.097	
V	8-10	10-12	12-14	14-16	16-18	18-20
$f(V)$	0.065	0.038	0.023	0.017	0.008	0.002
R	0-5	5-35	35-70	70-105	105-140	
$f(R)$	0.028	0.139	0.187	0.196	0.180	
R	140-175	175-210	210-245	245-280	280-320	320-355
$f(R)$	0.116	0.076	0.040	0.020	0.014	0.003

TABLE 2. Final velocities in km/s for actual triple stars.

a	$1au$	$10au$	$100au$	$f(N)$
$V^* = 18V_{crit}$	$758km/s$	$232km/s$	$76km/s$	0.02%
$V^* = 15V_{crit}$	$632km/s$	$200km/s$	$63km/s$	1.8%
$V^* = 10V_{crit}$	$421km/s$	$133km/s$	$82km/s$	8.8%
$V^* = 4V_{crit}$	$168km/s$	$53km/s$	$17km/s$	41.2%

masses of components of the binary $M_2 = 0.5M_1$, initial radial velocity of low-mass body (1) $V_0 = 0.1V_{crit}$ and (2) $V_0 = 0.5V_{crit}$ (1000 initial conditions for each), and $M_3 = 10^{-2}$. For these parameters we obtained the largest final velocities of escapers. The number of escapers was 870 for case (1) and 808 for case (2). The average values of R_{fin} and V_{fin} are $< R_{fin} >= 103.87 \pm 68.50$ and $< V_{fin} >= 4.12 \pm 3.65$. At the final time, only 3% of particles have distance from the system center of $R_{fin} < 5$, but 73.0% have $R_{fin} > 50$; 47.6% of particles have $R_{fin} > 100$, 9.9% have $R_{fin} > 200$ and 1.0% have $R_{fin} > 300$. In our previous work (Kiseleva, Anosova, Colin 1994) we have shown that whan $R > 50$ the influence of the remaining binary on the escaping star is negligible.

Table 2 gives the possible values V^* of V_{fin} (in km/s) for escapers and fractions of escapers with $V_{fin} > V^*$ for different kinds of remaining binary stars. One can see that sometimes escapers with very high velocities can be produced by unstable triple stars. Thus, the dynamical evolution of close triple stars can sometimes produce high velocity stars in the Galaxy although there is no clear estimate of the number of such unstable triple stars in the initial stage of galactic formation and evolution. But at least it seems realistic enough that a certain number of highly energetic stars could be the results of escaping processes in unstable triple and multiple stars.

References

Kiseleva L., Anosova J. , Colin J. IAU 164 Proceedings, 1994,in press.

HIERARCHICAL AND NON-HIERARCHICAL TRIPLES

J. ANOSOVA,
National Astronomical Observatory, Tokyo 181, Japan
L. KISELEVA, P. EGGLETON,
Institute of Astronomy, Cambridge CB3 0HA, UK
AND
V. ORLOV
Astronomical Institute, St. Peterburgh University, St. Petersburg 198904, Russia

Triple stars and galaxies are referred to as having hierarchical or non-hierarchical structure. Thus, the dynamically stable and unstable triple systems are usually distinguished observationally by the ratio of the larger and smaller angular separation. However, (i) projection effects may hide the true configuration; and (ii) apparent hierarchical forms may occur in both types (Anosova 1986).

Numerical experiments, as well as analytical studies of dynamics of triple systems with negative total energy allowed us to formulate the general features of their evolution. One of the basic results is the following - two types of dynamics of triple systems exist:

Type I: Stable systems with non-zero angular momentum and nearly periodic orbits of bodies. The character of the motion of the bodies is conserved during the evolution of the system. These systems may be separated into classes:

Class 1: True hierarchical systems of three bodies with nearly Keplerian orbits. The minimum distance between components connects the same pair of bodies during the evolution, and the hierarchical configuration of the system is always conserved.

Class 2: True non-hierarchical stable systems of three bodies. One may separate these triple systems into three subclasses:

a) Triple systems in which the motions correspond to the Eulerian or Lagrangian analytical solutions. The ratios of the distances between the

L. Blitz and P. Teuben (eds.), Unsolved Problems of the Milky Way, 529–530.
© 1996 *International Astronomical Union.*

bodies are always constant, the rotation of the system is solid, and the initial non-hierarchical configuration is conserved during the evolution.

b) Planar true non-hierarchical triple systems of the 'dumb-bell' type, in which the minimum separation between one body and the two other alternates in strict sequence, the other two bodies not approaching one another. These triple systems have a hierarchical configuration during about 10-20% of the time, and a non-hierachical one the rest of the time.

c) Three-dimensional true non-hierarchical system of three equal-mass bodies which we call a 'toroidal' system, as the region of possible motions is a torus. The minimum separation between two bodies circulates cyclicly among the three pairs. The system has a non-hierarchical configuration during about half the time.

Type II: Unstable true non-hierarchical triple system. The minimum separation between the bodies passes from one pair of bodies to another without any definite sequence. These triple systems may have hierarchical or non-hierarchical configurations.

In the case of the random initial conditions, unstable triples occur in about 90% of cases under consideration when we study the dynamical evolution of triple systems by computer simulations (Anosova 1986; Anosova & Orlov 1994). In about 10% of cases with non-zero angular momentum, hierarchical stable systems are formed. In such systems, the motions of the bodies can be described by the superposition of two perturbed Keplerian orbits.

The stability of hierarchical systems has been studied by a number of authors (see the above reviews and also Kiseleva, Eggleton & Anosova 1994, Kiseleva, Eggleton & Orlov, 1994 and references therein). But our simulations show that most of these criteria are not very heplful, especially when ultimately unstable systems are not yet close to disruption and appear fairly stable. We compute the dynamical evolution of hierarchical triple systems in which both orbits are initially circular, and determine the lower limit to the ratio of periods (outer/inner) for which there is dynamical stability. This ranges from 6.3 to 3.4, as the distant body's mass (in units of the inner binary) ranges from 100 to 0.01. We find for some mass ratios resonance-like behaviour that occurs in a limited range of initial period ratios. A variety of types of behaviour that we find when the period ratio varies near its critical value is described.

References

Anosova J. Astrophys. Space Sci., 1986, 124, 217.
Anosova, J., Orlov V., Cel.Mech.and Dyn.Astr., 1994, 59, 327.
Kiseleva, L., Eggleton P., Anosova,J. 1994. MNRAS, 267, 161.
Kiseleva, L., Eggleton P., Orlov V. 1994. MNRAS, in press

CRITERIA OF DYNAMICAL ISOLATION OF BINARIES AND MULTIPLES

LUDMILA KISELEVA
Institute of Astronomy, Madingley Rd., Cambridge CB3 0HA, UK

AND

JOANNA ANOSOVA
National Astronomical Observatory, 2-21-1 Osawa, Mitaka, Tokyo 181, Japan

In order to obtain an objective criterion for dynamical isolation of binaries within systems of large multiplicity we study numerically the dynamical behavior and average parameters of stable hierarchical triple systems containing a close binary. Using the new criterion for hierarchical stability of triple systems with different mass ratios of components (Kiseleva, Eggleton, Anosova 1994; Kiseleva, Eggleton, Orlov 1994) the perturbing force from the outer body on the close inner binary is estimated. On this basis, the critical separations are obtained when both inner and outer orbits are practically not perturbed. Because the dispersion of masses has a very strong influence on dynamical processes in N-body systems, mass ratios of subsystems, and sometimes within subsystems, should always be taken into account. Anosova and Orlov (1989) and Anosova (1994) proposed a parameter of isolation of close pair i,j from its nearest neighbor

$$q_b = \left(\frac{m_i + m_j}{2m_l}\right)^{1/3} \frac{r_l}{r_{ij}} > q_b^* \qquad (1)$$

where l denotes the closest body besides i,j ($l = 1, 2...N; l \neq i, l \neq j$), r_ij is the separation between the components of the pair, r_l is the distance of the body l from the center mass of the pair i,j and q_b^* is an adopted critical value of q_b. This parameter q_b is the root cube of the ratio of of perturbing accelerations of one of the binary's components i or j from the other component and from the perturber l. q_b is a convenient parameter to use because it includes the mass ratio of tested subsystems. For considered

L. Blitz and P. Teuben (eds.), Unsolved Problems of the Milky Way, 531–532.
© 1996 *International Astronomical Union.*

mass rations of close and wide binaries the value of q_b is between 2.7 and 8.4.

The averages in time of values of orbital parameters for close and wide binaries for stable nearly unperturbed cases are calculated and the corresponding approximations are then made. The obtained criterion of isolation can be generalized for subsystems with larger multiplicities and also applied to multiples within clusters.

References

Anosova, J.P., Orlov, V.V. Astrophys. Space Sci.,1989, 161,209
Anosova, J.P. Astrophys. Space SCi., 1994, submitted.
Kiseleva, L.G., Eggleton, P.P., Anosova, J.P. (1994) *Mon. Not. R. Astr. Soc.*,1994, 267, 161.
Kiseleva, L.G., Eggleton, P.P., Orlov, V.V.(1994) Mon. Not. R. Astr. Soc., 1994, in press

Chapter 7

How are we to Understand the Small Scale Structure of the ISM?

THE UNSOLVED PROBLEM OF STELLAR ORIGINS

CHARLES J. LADA
Smithsonian Astrophysical Observatory
60 Garden Street
Cambridge, Massachusetts 02138 USA

1. Introduction

We now stand at the threshold of the 21st century having witnessed perhaps the greatest era of astronomical discovery in the history of mankind. During the twentieth century the subject of astronomy was revolutionized and completely transformed by technology and physics. Advances in technology that produced radio astronomy, infrared astronomy, UV, X and γ ray astronomy, large telescopes on the ground, in balloons, aircraft and space coupled with advances in nuclear, atomic and high energy physics forever changed the way in which the universe is viewed. Indeed, it is altogether likely that future historians of science will consider the twentieth century as the Golden Age of observational astronomy. As a measure of how far we have come in the last 100 years, recall that at the turn of this century the nature of spiral nebulae and of the Milky Way itself as an island universe were not yet revealed. The expansion of the universe and the microwave background were not yet discovered and exotic objects such as quasars, pulsars, gamma-ray bursters and black holes were not even envisioned by the most imaginative authors of science fiction. The interstellar medium, with its giant molecular clouds, magnetic fields and obscuring dust was unknown. Not even the nature of stars, these most fundamental objects of the astronomical universe, was understood.

Among the greatest achievements of astronomical science in the twentieth century has been the development of the theory of stellar structure and evolution. Stars derive their enormous radiant luminosities and longevities from thermonuclear reactions which fuse hydrogen, the primary product of the Big Bang, into heavier elements. The theory of stellar evolution developed in the middle of this century, provides an elegant explanation for

L. Blitz and P. Teuben (eds.), Unsolved Problems of the Milky Way, 533–549.
© 1996 *International Astronomical Union.*

this process as well as for those that occur once stars exhaust their nuclear fuel reserves in their cores. This theory has successfully accounted for the basic physical properties of stars including their size, color, composition, variability, age, and mass. It has been extended and refined to explain planetary nebulae, white dwarfs and pulsars. Yet, as we approach the end of this century, we find that this great theory is incomplete in one very critical aspect: the *origin* of stars remains a mystery. In other words, there is, as yet, no successful theory of star formation. The question of the origin of stars is one of the oldest and most fundamental problems that has challenged mankind's oldest science. The development of a theory that can elucidate how nature turns diffuse interstellar hydrogen into dense balls of gas with just the right mass to fuse hydrogen continues to be a primary goal of modern Milky Way research.

2. What We Have Learned About Star Formation

2.1. THE CONTINUING PROCESS OF STELLAR BIRTH

That the origin of stars has remained so mysterious for so long is largely due to the fact that the process of star formation has never been directly observed either with the naked eye or the with the most powerful telescopes. Moreover, prior to the twentieth century neither the energy source nor the bulk composition of stars were known. Indeed, without knowledge of the physical nature of stars it was very difficult to develop an understanding of their origin. At the end of the nineteenth century, the depth of the mystery surrounding stellar origins was nicely summed up by the fictional character Huck Finn (in the book The Adventures of Huck Finn by Mark Twain) when he observed the stars in the night sky and wondered "*...did they just happen or was they made?*" Have the stars been around since creation or were they being made in the heavens? As far as anybody could tell at dawn of this century, the entire universe consisted of a single stellar system, stars lived forever and the question of the origin of stars was a question of cosmology. As such the problem of star formation was not susceptible to detailed scientific investigation. That is, even the most basic hypotheses concerning stellar origins could not be directly tested by observation.

Over the last half century astronomical research has led to the fundamental realization that star formation has been a continuous, ongoing process throughout the history of the Galaxy and the universe. This critical fact has been demonstrated by both theory and observation. In particular, stellar evolution theory demonstrated that certain luminous stars, OB stars, burn their nuclear fuel at such prodigious rates that they can live for only a small fraction of the lifetime of our Galaxy. The existence of such stars clearly indicates that star formation is occurring in the present

epoch of Galactic history. Moreover, observations showed that OB stars were almost always members of stellar groupings called OB associations which were characterized by space densities well below the threshold for disruption by Galactic tidal forces. The dynamical ages of OB associations (10^7 yrs.) were found to be much less than the age of the Galaxy ($\sim 10^{10}$ yrs.) and comparable to the nuclear ages of the stars derived from stellar evolution theory. Such observations supplied independent confirmation that the process of star formation was active in the present epoch. The discovery of the interstellar medium of gas and dust during the early part of the twentieth century provided a crucial piece of corroborating evidence in support of the concept of ongoing Galactic star formation. Subsequent observations of interstellar material established that clouds of interstellar gas and dust had roughly stellar composition and were considerably more massive than a single star or group of stars. This revealed that the raw material to make new stars was relatively abundant in the Galaxy.

Because star formation is occurring in the present epoch, the question of the origin of stars can be investigated by direct observation. Yet, since stars form in dust shrouded cores of dark clouds, direct observation of the process of star formation has proved extremely difficult.

2.2. THE INITIAL MASS SPECTRUM OF STARS

Important clues concerning the star formation process can be gleaned from the fossil record provided by the visible, already formed stars themselves, particularly very young stars. Perhaps the most important constraint concerning the star formation process that can be derived from known properties of stars and stellar evolution theory is the Initial Mass Function (IMF). A fundamental consequence of the theory of stellar evolution is that the life history of a star is almost entirely pre-determined by its initial mass. Consequently, to understand star formation and indeed the luminosity evolution of a system of stars such as a cluster or galaxy requires a detailed knowledge of the initial distribution of stellar masses at birth. Unfortunately, stellar evolution theory by itself, is not able to predict the IMF of stars. This quantity must be derived from observations. However, to do so is not straightforward because stellar mass is not itself an observable quantity. Stellar radiant flux or luminosity is the most readily observed property of a star. However stellar evolution theory can be used to transform between luminosity and mass because of the theory's prediction of a unique mass-luminosity relation for main sequence stars. In a classic paper nearly 40 years ago Salpeter [1] used this fact and knowledge of post-main sequence stellar evolution to transform the observed luminosity function of nearby field stars into an IMF for field stars in the solar neighborhood. With the

critical assumption of a constant star formation rate through galactic history he found that the IMF was well represented by a simple power-law: $\xi(logm_*) \sim m_*^{-1.35}$ for stars with masses in the range between 1-10 solar masses. The derived sign and slope of the Salpeter IMF indicates that most stars which form in the galaxy are of low mass and moreover that most of the stellar mass in our galaxy is contained in such stars. Subsequent studies, particularly by Scalo [2, 3], extended knowledge of the field star IMF to sub-solar masses and found that the IMF has a peak at about 0.3 solar masses and therefore departs from the Salpeter power-law well above the hydrogen burning limit. This indicates that there is a characteristic stellar mass of roughly 0.3 $M_\odot$ produced as a result of the process of star formation. Implicit in Salpeter's derivation of the IMF is the assumption that the form of the IMF has remained constant through Galactic history. Subsequent studies have provided no compelling evidence to refute this remarkable notion. For example, the derived mass functions of young galactic star clusters are essentially the same as the IMF of field stars. [4, 5, 6, 7]

2.3. ASSOCIATIONS, CLUSTERS AND MULTIPLE STARS

From the stellar fossil record we also know that the birth of a star is not an isolated event. Stars form in groups over a large range of spatial scales from OB associations to clusters to binary and multiple star systems. For example, on large spatial scales, study of the spatial distribution of young OB stars indicates that all OB stars are formed in stellar groups known as OB associations [8]. The spatial extents of such associations are large (10-100 parsecs) but as mentioned earlier, the mass densities of associations are well below the limit (i.e., 0.1 $M_\odot pc^{-3}$) required for tidal stability[9]. Moreover, the typical velocity dispersion of association stars (2-4 km s^{-1}) is greater than even the escape velocity due to the mutual gravitational attraction of member stars themselves. Thus, OB associations are unbound, expanding stellar systems. OB associations contain hundreds to thousands of stars. There are considerably more low mass stars than OB stars in associations and consequently most all stars that form in the galaxy likely form in OB associations. It has long been recognized that OB associations could provide important information about the star formation process since they are so young that the individual members have not had enough time to move very far from their places of birth. For example, the present sizes of OB associations must closely reflect the sizes of the clouds which spawned them[10, 11, 12] . In addition, the structure of OB associations can provide important fossil clues about the structure and even the temporal evolution of a star forming complex. One common property of OB associations is that they are sub-structured, often consisting of sub-groupings of sequentially

differing age[9]. Such sub-structure has suggested that star formation proceeds through a star forming region in an ordered temporal sequence. The chain reaction like nature of the spatial-temporal structure of OB subgroups has led to the suggestion that OB subgroups are formed by a process of sequential triggering[12]. Within associations are contained stellar clusters. Such systems typically contain 50-500 stars, have mass densities in excess of the tidal disruption limit and sizes on the order of 1 parsec. Some of these clusters will remain bound and become field open clusters after the association itself disrupts. About 10% of all stars are believed to originate in such bound open clusters which have lifetimes on the order of 10^8 years.

On small spatial scales (1-1000 AU) the radial velocity measurements of field G dwarf stars indicate that roughly 57% of all such stars have stellar companions [13, 14]. The binary fraction does not appear to depend too strongly on spectral type as studies of both M dwarfs [15] and B stars [16] have indicated. Since some binaries may have been disrupted since formation, these fractions could be lower limits to the actual fraction of binary stars produced in the star formation process. Studies of the binary populations among pre-main sequence stars show that binary stars occur even among the youngest such stars observable, indicating that the formation of binary systems occurs prior to pre-main sequence evolution, that is, during the protostellar stage as an integral part of the star formation process [17].

2.4. GIANT MOLECULAR CLOUDS: THE SITES OF STAR FORMATION

Progress in star formation research was severely limited until observations could be made at wavelengths which could penetrate the dusty veils of obscuration and directly detect the star-forming gas and dust. By the early 1970s advances in technology began to open up the infrared, millimeter and submillimeter-wave windows for astronomical exploration. With this new instrumental capability, a direct assault on the star formation problem became possible.

Twenty-five years ago, millimeter wavelength observations (mostly of the CO molecule) provided star formation research with the fundamental discovery of giant molecular clouds (GMCs). With extents on the order of 100 parsecs GMCs are the largest objects in the Milky Way. With masses often in excess of 100,000 times the mass of the sun, GMCs rival globular clusters as the most massive objects in the Milky Way. GMCs are also among the coldest objects in the universe with gas temperatures seldom exceeding 10 K. They are composed almost entirely of molecular hydrogen, contain significant amounts of interstellar dust and are permeated by magnetic fields. The linewidths of molecular emission lines observed toward GMCs are typically on the order of a few km s^{-1} and considerably greater

that those ($\approx$ 0.2 km s^{-1}) expected from thermal motions in the very cold gas. The overall dynamical state of a GMC is therefore characterized by supersonic bulk motion which is thought to be of a turbulent nature. Such motion should be highly dissipative, yet GMCs maintain their supersonic dynamical states throughout their lifetimes. GMCs are also strongly gravitationally bound and cannot be supported from global collapse by thermal pressure alone. Since the lifetimes of GMCs are also considerably longer than their free–fall times, they must be supported by some agent other than thermal pressure. The magnetic fields which permeate molecular clouds may have important consequences for their dynamical states and their support against gravity. Field strengths on the order of 10–20 μG are believed typical for GMCs [18]. For typical gas densities, the Alfven speed (i.e., $V_A = \frac{B}{\sqrt{4\pi\rho}}$, where B is the field strength, and ρ is the gas density) is about 1 km s^{-1}. Although the dynamical states of the clouds are highly supersonic, this motion may be sub–Alfvenic and less dissipative than one might otherwise suppose [19]. Moreover, these field strengths are close in value to those needed to support clouds from gravitational collapse [20, 21].

Within the solar neighborhood virtually all known OB associations are found to be located within the immediate vicinity of a GMC. [22] Typically, the youngest subgroup of an OB association is found to excite an HII region or reflection nebula within the associated GMC, therefore demonstrating a *physical* relation with the cloud. This coupled with the facts that GMCs have dimensions which are comparable to if not larger than OB associations and have masses considerably greater than OB associations, suggests that OB associations and therefore most stars in the Galaxy are born in GMCs. The large difference between the stellar mass of an OB association and its associated GMC illustrates a fundamental property of star formation. Namely, that the star formation efficiency (SFE=stellar mass/(stellar + gaseous mass)) is low. The low efficiency of star formation in GMCs is of central importance for understanding the dynamical nature of OB associations. The unbound state of stellar associations is a natural consequence of star formation with a low conversion efficiency of gas to stars followed by a rapid removal of the unprocessed gas from the system [23, 24]. Such rapid gas removal is the expected consequence of O star formation within molecular clouds [25].

3. What We Are Learning About Star Formation

3.1. DENSE CLOUD CORES AND EMBEDDED STELLAR CLUSTERS

The mean gas density of the molecular material in a GMC is about 100–300 molecules cm^{-3}, more than 19 orders of magnitude less than that of the stars which form from it! GMCs are highly structured consisting of

numerous filaments, clumps and dense cores [30]. Somewhere between 1 and 10% of the mass in a GMC is contained in relatively dense (10^4 cm^{-3}) cores [26]. It has long been suspected that such cores are the sites of active star formation in GMCs [27]. This suspicion has been decisively confirmed by an extensive infrared survey of the nearby L1630 molecular cloud which found essentially all the recently formed stars in the cloud to be located in dense molecular gas [28].

The dense cores within a GMC have a spectrum of sizes and of masses. They range from small cores, with linear dimensions on the order of 0.1 parsecs and masses between 1-10 solar masses, to massive cores which are 100-1000 times more massive and have dimensions of a few parsecs[29, 30]. The mass spectrum of cloud cores seems to be power law in form, with a spectral index of about -1.6. Thus small low mass cores are more numerous than large, high mass cores. However, the mass spectrum of dense cores is qualitatively different from that of stars (whose mass *spectrum* has an index of -2.3) in that most of the dense gas within a GMC is contained within a few most massive cores [26]. This difference suggests that in the process of star formation, the stars themselves stars somehow affect the determination of their final mass. In addition, it suggests that most star formation in a GMC must take place in its most massive cores (where most of the dense gas is locked up).

This latter point seems to be corroborated by the large number of embedded star clusters revealed in recent infrared imaging surveys of GMCs [32, 33]. In particular, the extensive, well sampled 2μm survey of the L1630 cloud in Orion [31] indicates that more than 90% of the young stars formed over the entire cloud are located in three rich embedded star clusters which occupy only a very small fraction of the area of the cloud. Moreover these three clusters are physically associated with 3 of the cloud's 5 most massive dense cores [28]. *In GMCs most stars apparently form in rich star clusters from massive cores of dense molecular gas.* However, most of these clusters must be disrupted soon after they emerge from a GMC, otherwise there would be more (bound) open clusters in the field than are observed [32]. This, in turn, suggests that the star formation efficiency in cluster forming cores rarely reaches values as high as 50% [32, 34].

Young embedded star clusters provide unique opportunities to investigate the stellar initial mass function and its possible variation in space and time. Such young clusters are comprised of mainly low mass, pre-main sequence, stars which are brighter than at any other time in their subsequent evolution. Consequently, modern infrared imaging detectors on modest sized telescopes can readily detect stars at and below the hydrogen burning limit and thus completely sample the entire IMF of an embedded cluster. Observations of the infrared luminosity functions of nearby embed-

ded clusters have found them to be surprisingly similar in form. Modeling of the luminosity evolution of clusters consisting of mostly pre-main sequence stars suggests that this similarity can be explained if 1) the underlying mass spectra of the embedded clusters are all the same and essentially identical to the field star IMF down to the hydrogen burning limit, and 2) if star formation proceeds in a continuous fashion at a more or less uniform rate over the time the clusters are embedded in molecular gas (typically 1-7 x 10^6 yrs.) [7]. Although the mass spectra of embedded clusters appear universal in form, the star formation rate and (consequently) the duration of the embedded phase can vary by more than an order of magnitude from one cluster to another. The origin of this variation is not known but may be related to environmental factors such as the presence or absence of external star formation triggers such as shock waves produced by HII regions or supernovae [7].

3.2. PRE-MAIN SEQUENCE STARS AND CIRCUMSTELLAR DISKS

The formation and early evolution of stars can be broadly divided into three stages: I)- the *protostellar stage*, during which an embryonic young stellar object is being assembled out of molecular gas and dust, II)- the pre-hydrogen burning or *pre-main sequence stage*, during which the young stellar object is contracting in a quasi-static manner to the main sequence and III)- the zero age main sequence or *ZAMS stage*, when the star has reached the necessary internal densities and temperatures to begin a stable phase of hydrogen burning energy production. However, the exact sequence of events which governs the formation and early evolution of stars is quite different for high and low mass stars. In particular, high mass stars do not go through a significant pre-main sequence (i.e., a pre-hydrogen burning) phase. In fact such stars begin to burn hydrogen during their protostellar phase of evolution. The physical reason for this becomes apparent if one considers the timescales for protostellar collapse and pre-main sequence contraction. The timescale for the gravitational collapse of a cloud core, the free-fall time, is determined largely by ρ, the density of the cloud. For the typical mean density (n $\approx 10^4$ cm^{-3}) of a cloud core (of either low or high mass) the free–fall time is about 4 x 10^5 years. The time scale for pre-hydrogen burning evolution is the Kelvin-Helmholtz time which is very rapid for a high mass star (i.e., $\approx 10^4$ years for $M_* = 50\ M_\odot$) and relatively slow for a low mass star (i.e., $\approx 3 \times 10^7$ years for $M_* = 1\ M_\odot$). More importantly for high mass stars $\tau_{KH} < \tau_{ff}$ and these stars begin burning hydrogen and reach the main sequence before the termination of the infall or collapse phase of protostellar evolution. On the other hand, for low mass stars $\tau_{KH} > \tau_{ff}$ and these stars have an *observable* pre-main

sequence stage of stellar evolution.

Because high mass stars are extremely hot and luminous they can strongly effect their surroundings even during their protostellar stages of evolution. Moreover, since high mass stars evolve very quickly and are formed only in relatively small numbers, observing their formation is a complex and difficult task. On the other hand, low mass stars are much less destructive of their natal environments, are produced in large numbers and have relatively long formation times. Consequently, they provide unique laboratories for the investigation of star formation and much more is known about their early evolution, particularly their pre-main sequence evolution, than is known about the formative stages of OB stars.

If a low mass pre-main sequence star, such as a T Tauri star, is young enough it will still be intimately associated with gas and dust associated with its birth. In such a circumstance we expect both the stellar photosphere and the natal circumstellar gas and dust to emit radiation. Since the circumstellar material is extended over a size scale considerably larger than a stellar photosphere, the emission that emerges will be characterized by a range in temperatures and have a spectral distribution that is wider than a single blackbody. The detailed shape of the emergent spectrum will depend in part on the nature and distribution of the circumstellar material. For instance, Lynden-Bell and Pringle [35] showed that an optically thick circumstellar disk would produce a spectrum which was the superposition of a series of different blackbody functions. The shape of this composite spectrum would be power-law in form if the temperature gradient in the disk was characterized by a power-law dependence with distance from the central star. T Tauri stars were long known to emit excess near-infrared light, but it wasn't until ground-based mid-infrared and space based IRAS far-infrared observations were obtained for these stars that the true nature of their continuous spectra was evident. Such observations indicated that the spectra of most T Tauri stars were power-law in shape from visible to far-infrared (IRAS) wavelengths suggesting the presence of circumstellar disks around these stars [36, 37, 38, 39].

Additional evidence for such disks comes from optical, high resolution spectral observations of forbidden-lines from these stars which often show only blue-shifted components. The lack of red-shifted lines implicated the existence of a highly opaque and flattened distribution of material around the stars [41, 42]. More direct evidence for the presence of circumstellar disks comes from observations of optical and infrared absorption lines around stars such as FU Ori [43]. These observations indicate that the circumstellar material is differentially rotating as would be expected for a disk in Keplerian motion around a central star. These putative disks have also been detected at millimeter and submillimeter wavelengths where their

emission is optically thin and their masses can be measured (e.g., [40]). The masses typically range from 0.01 to 0.1 solar masses, comparable to that expected for a planet producing circumstellar disk. Other interesting evidence for circumstellar disks includes the detection of small ($\approx$ 100 AU) ionized structures around faint stars in the Trapezium cluster. These objects appear to best understood as the photo-evaporating atmospheres of circumstellar disks whose central stars find themselves too near the ionizing O star Θ^1C Ori [44]. Such structures have also been recently detected in space telescope images of the Orion nebula [45].

Among young stars, circumstellar disks now appear to be ubiquitous. This is one of the most important and exciting discoveries of star formation research during the last decade. For one thing this clearly indicates the importance of the role of angular momentum in the star formation process. In addition, this discovery suggests that the conditions for planet formation are prevalent around young stars and that there are hundreds of laboratories near the Sun where direct study of the conditions that lead to planet formation is now possible.

3.3. PROTOSTARS AND BIPOLAR MOLECULAR OUTFLOWS

For low mass stars the pre-main sequence phase (i.e., Stage II) of early stellar evolution begins at the end of the protostellar phase when the build up of the star by the infall/accretion of substantial amounts of molecular cloud material is essentially over. At this point the spectral energy distribution of the star is dominated by its photospheric emission and the star emerges as an observable object, which for the first time can be plotted on the HR diagram. For a star of given mass its initial position on the HR diagram corresponds to a specific size or stellar radius. In other words, a star first becomes observable as a star and first appears on the HR diagram only after it obtains a specific maximum size which is pre-determined by its prior protostellar evolution. The initial positions of stars on the HR diagram varies with stellar mass. These positions form a locus of points on the HR diagram called the "birthline" [46]. The birthline represents the initial condition for pre-main sequence (quasi-static) contraction. It is the dividing line between the protostellar and pre-main sequence stages of stellar evolution. Stellar evolution theory does not predict the existence of the birthline. The physics which determine the birthline are the mysterious physics of protostellar evolution. Understanding the nature of protostars is, at present, the major frontier of star formation research.

It has long been recognized that the greatest progress toward understanding star formation would most certainly result from the unambiguous discovery and observation of a protostar, *an object which is in the process*

of assembling into a stellar-like configuration the bulk of the material it will contain when it resides on the main sequence as a hydrogen burning star. Protostars are the Holy Grail of observational star formation research. To date no unambiguous identification of a protostar has been made. However, there exists an entire class of sources which are excellent candidates for such objects. These sources are often called "infrared protostars" because they emit almost all their radiant energy in the far-infrared. They are always found embedded in dense molecular cores and they are almost always invisible in the optical. Their infrared spectral energy distributions clearly indicate that these sources are surrounded by substantially more circumstellar gas and dust than are T Tauri stars. In fact infrared protostars and T Tauri stars appear to be at the opposite ends of a more or less continuous evolutionary sequence in which gas and dust are progressively removed from around a young star (i.e., T Tauri stars resemble infrared protostars stripped of their circumstellar envelopes; [24, 47]).

To a reasonable degree of detail, the energy distributions of many infrared protostars can be well fit by theoretical models of rotating isothermal spheres collapsing from the inside-out [50, 47] which greatly strengthens the suspicion that these objects are indeed protostellar in nature. Confirmation of their status as protostars would be definitive if infall motions in their circumstellar gas could be detected. Despite many attempts to search for such motions, only in two instances [48, 49] have molecular line spectra shown the signature expected from inside-out collapse, however in neither case is the evidence yet compelling. But far from being quiescent, the molecular gas around most infrared protostellar candidates has almost always been found to exhibit unequivocal evidence for *outflow* motions!

Fifteen years ago millimeter-wavelength CO observations of the molecular gas surrounding certain young stellar objects led to the discovery of an unanticipated phenomenon of fundamental importance for understanding star formation. In addition to their global supersonic velocity fields, molecular clouds were found to contain localized regions (0.1–3 parsecs in size) where a significant amount of gas was characterized by hypersonic bulk motion. In these regions the observed widths of molecular emission lines are found to range between 10–100 km s^{-1} ! These highly supersonic and super-Alfvenic velocities cannot be gravitationally (or magnetically) confined within the localized regions where they occur and they must represent unbound and expanding flows of cold molecular gas within the GMCs [51]. The regions containing the hypersonic outflows are almost always coincident with, if not centered on, the position of an embedded infrared source.

Well over 100 molecular outflows are now known, most within a kiloparsec of the Sun. Their properties have been extensively and thoroughly reviewed in the literature (e.g., [51, 52, 55, 53, 54]). Briefly, the masses of

such outflows are substantial, containing anywhere between 0.1 and 100 solar masses. Because of the large masses contained in the molecular outflows, it is likely that the outflowing molecular gas is swept-up ambient cloud material rather than original ejecta from the driving source. More significantly, the corresponding kinetic energies of the flows are enormous, ranging between 10^{43} and 10^{47} ergs! The dynamical timescales of the flows are estimated to be between 10^3 and 10^5 years and their local formation rate is estimated to be roughly comparable to the formation rate for stars of a solar mass or greater. Taken together, these facts suggest that molecular outflows play a fundamentally important role in the star formation process.

Perhaps the most intriguing property of the molecular outflows is their tendency to appear spatially bipolar (e.g., [56]). That is, they often consist of two spatially separate lobes of emission, with one lobe containing predominantly blueshifted gas and the other predominantly redshifted gas. Furthermore, the two separating lobes are almost always more or less symmetrically situated about an embedded infrared source, usually an infrared protostar! Bipolar molecular outflows are individually energetic enough to disrupt cloud cores and it is suspected that they are the likely agent that drives the evolution of an embedded young stellar object from the protostellar (I) stage to the pre-main sequence (II) stage of evolution.

Although molecular outflows appear to provide the mechanism which enables a protostar to remove surrounding material and in doing so evolve into a pre-main sequence star, the high frequency of association between infrared protostars and molecular outflows poses a paradox. The statistics suggest that a significant fraction of the lifetime of a protostellar object is spent in the outflow phase. Yet, if such sources are true protostars, their evolution should be characterized by the *infall* of surrounding material. How can a protostar for most of its existence be simultaneously a source of infall and outflow? How can a star form by losing mass? The answer to this question is very likely the key to understanding the basic physics of the star formation process [57].

4. What We Don't Know About Star Formation

More progress has been made toward understanding the process of star formation in the last twenty years of this century than throughout all previous history. Yet a basic theory of stellar origins still eludes us. The origin of GMCs, for instance, is a complete mystery. The overall problem of star formation can be made somewhat more manageable if we take as the initial condition the existence of a GMC. The problem can then be formulated as follows: What enables a few per cent of the otherwise dynamically stable gas and dust in a GMC to collapse and increase in density by 20 orders of mag-

nitude to form a star? This question can be further simplified by dividing it into two parts. First, how does a GMC transform roughly 10% of its mass into dense cores with the spectrum of masses and sizes we observe? Second, how does an individual dense core transform a significant fraction ($\geq$ 20%) of its mass into either a single star or a group of stars with a spectrum of masses given by the IMF? As with the question of the origin of a GMC, the physics of dense core formation is essentially unknown. Presumably for a dense core to form, the material which forms it must lose support against gravity. If this support is provided by magnetic fields, then core formation may be possible through the slow outward diffusion of magnetic fields via a process known as ambipolar diffusion [58, 59, 60, 61]. Although this mechanism appears a promising one for the formation of lower mass cores ($\sim$ 10 $M_\odot$) it is not at all obvious that it can account for the shape of the core mass spectrum and the existence of the very massive cluster forming cores in which most stars are formed. All this seems in contradiction to the opening sentence of this section. However, when the problem of star formation is yet simplified one further step, by considering the existence of a dense molecular core as the initial condition or starting point for the formation of a single low mass star, then the progress achieved in deepening our understanding of stellar origins becomes more apparent.

In order for gas in a dense core to collapse and form a star it must become gravitationally unstable and in the process lose most of its initial magnetic flux and substantially redistribute its initial angular momentum. Consider that if the magnetic fields that thread a typical dense core were to remain frozen in the gas as it collapsed and increased in density by 19 orders of magnitude to form a star, the magnetic field at the stellar surface (i.e., $B_* = B_{cloud}\ (\frac{\rho_*}{\rho_{cloud}})^{\frac{1}{2}}$) would be $\approx 10^4$ Gauss, orders of magnitude greater than that (i.e., 1 Gauss) permitted by observations of normal stars. This is usually referred to as the "magnetic flux" problem of star formation. In addition the rotational velocities of dense cores in clouds are found to be small, if observed at all (e.g., [62]). For low mass cores, which form individual stars similar in mass to the sun, the observed angular velocities are typically $\Omega \leq 3 \times 10^{-14}$ rad s^{-1}. However, the angular momentum per unit mass (i.e., $r^2\Omega$) of the slowly rotating core gas is still on the order of 10^{22} cm^2 s^{-1}, considerably in excess of that of the sun (10^{15} cm^2 s^{-1}), but not that of the outer planets of the solar system ($\sim 10^{20}$ cm^2 s^{-1}). The smooth distribution of mass in a molecular cloud core, however differs considerably from that characterizing the solar system where 99% of the mass contains less than 2% of the total angular momentum. Clearly, a significant redistribution of mass and angular momentum must occur before dense molecular cloud material can form a star. This is a modern restatement of the famous "angular momentum" problem of star formation.

During the last decade an appealing theory of low mass star formation has been in the process of development by Frank Shu and his students and collaborators [21]. This theoretical work represents the first detailed attempt to tie together the new empirical knowledge gained in the last two decades into a unified, coherent picture of stellar birth. Their scenario can be briefly outlined as follows. Star formation begins when a dense core, assumed to be supported by a magnetic field, becomes unstable as a result of the ambipolar diffusion of its field. By this attractive process both the support of the cloud and the magnetic flux of the star forming gas are largely removed, simultaneously solving two important problems. Once initiated in the central regions of the dense molecular core, the collapse proceeds in a non-homologous, inside-out fashion. Initially small amounts of low angular momentum material fall in along the core's rotational axis and quickly build up an embryonic, hydrostatic, stellar core. As a result of the conservation of angular momentum, infalling gas with even modest amounts of initial angular momentum is unable to fall directly onto the central stellar core and instead collapses into a rotating disk. In fact, in a typical rotating protostar, most of the material that ultimately ends up on the star must first fall into the disk and then be subsequently accreted onto the central stellar core. However, in order to flow through the disk and join onto the central star, accreting material must lose substantial amounts of energy and angular momentum. Indeed, during the protostellar stage the radiant output of the system should be completely dominated by accretion generated luminosity. Before attaching onto the star, accreting material must overcome a centrifugal barrier at the physical interface between the star and disk. According to the theoretical picture this is accomplished by the generation of an intense, centrifugally-driven, hydromagnetic, bipolar wind. This wind carries away a small amount of mass but a large amount of angular momentum and thus *enables a protostar to gain mass by simultaneously losing mass*, solving the key observational paradox mentioned earlier. As the protostar evolves, the outflow it generates sweeps up circumstellar matter and eventually reverses the infall, setting a limit to the amount of mass ultimately accreted by the protostar. Eventually, the outflow removes enough surrounding gas that the protostar star is revealed as a visible star with a circumstellar disk. The time from the initial collapse to the appearance of a visible young stellar object is only a few hundred thousand years or less. Over the next two to three million years of pre-main sequence evolution the circumstellar disk dissipates as most of its material either accretes onto the star or forms planets.

As impressive as this first attempt at a theory of star formation is, our understanding of stellar origins is still far from complete. For example, the questions of the formation of binary stars and the IMF are still

unanswered. The formation of high mass stars is still not yet accounted for. A compelling picture to explain the origin of bipolar flows is still missing. It is not at all clear how the formation process of stars in rich embedded clusters differs from that of single stars, although observations suggest that it must. Observations also indicate that episodic outbursts and mass loss may be important in early stellar evolution and this is not yet adequately explained or predicted by theory. We still don't know how GMCs come into being. Clearly, the current theoretical picture is a promising foundation for a comprehensive theory of star formation. Although it is still largely a work in progress, it does provide an excellent working hypothesis for ongoing and future research. At the close of the twentieth century we find star formation to be a richer, more complex and fascinating process than could have been envisioned 100 years ago. It promises to remain a major frontier of galactic research well into the next century.

5. Acknowledgements

I thank the SOC for inviting me to deliver this lecture and I am grateful to the AAS for an IAU travel grant which made my participation in this symposium possible.

References

1. E. Salpeter 1955 *Astrophys. J.*, 121, 161.
2. J. Scalo 1978 in *Protostars and Planets*, ed T. Gehrels, University of Arizona Press: Tucson, p. 265.
3. J. Scalo 1986 in *Fundamentals of Cosmic Phisics*, 11, 1.
4. L. G. Taff 1974 *Astron. J.*, 79, 1280.
5. J. Stauffer *et al.* 1989 *Astrophys. J. Letters*, 344, 21.
6. N. Reid 1993 *Monthly Notices Roy. Astron. Soc.*, 265, 785.
7. E. A. Lada and C. J. Lada 1995 *Astron. J.*, (in press).
8. M. S. Roberts 1957 *P.A.S.P.*, 69,59
9. A. Blaauw 1964 *A.R.A.A.*, 2,213.
10. A. Blaauw in *The Physics of Star Formation and Early Stellar Evolution*, eds. C.J. Lada and N.D. Kylafis, (Kluwer Academic Publishers: Dordrecht, 1991), p. 125.
11. B. G. Elmegreen and C. J. Lada 1976 *Astron. J.*, 81, 1089.
12. B. G. Elmegreen and C. J. Lada 1977 *Astrophys. J.*, 214, 725.
13. H. A. Abt and S. Levy, 1976 *Astrophys. J. Suppl. Ser.*, 30,273.
14. A. Duquennoy and M. Mayor 1991 *Astron. Astrophys.*, 248, 485.
15. D. Fischer and G. Marcy 1992 *Astrophys. J.*, 396, 178.
16. T. S. van Albada in *Birth and Evolution of Massive Stars and Stellar Groups*, eds. H. van Woerden and W. Boland, (Reidel: Dordrecht, 1985), p. 89.
17. R. Mathieu 1994 *A.R.A.A.* 32, 465.
18. C. Heiles 1987 in *Interstellar Processes* eds., D. Hollenbach and H. A. Thronson (Reidel, Dordrecht),p. 171
19. J. Arons and C. Max 1975 *Astrophys. J. Letters*, 196, 77.
20. T. Mouschovias 1976 *Astrophys. J.*, 207, 141.
21. F. H. Shu, F. C. Adams and S. Lizano 1987 *A.R.A.A.* 25, 23.

22. L. Blitz, in *Giant Molecular Clouds in the Galaxy*, eds., P. Solomon and R. Edmunds (Pergamon, Oxford, 1980), 1.
23. R Duerr, K. Imhoff and C. J. Lada 1982 *Astrophys. J.*, 261,135.
24. C. J. Lada in *I.A.U. Symposium No. 115: Star Forming Regions*, eds. M. Peimbert and J. Jugaku, (Dordrecht, Reidel, 1987), p. 1.
25. A. Whitworth, 1979 *Monthly Notices Roy. Astron. Soc.*, 186, 59.
26. E. A. Lada, J. Bally and A. Stark 1991 *Astrophys. J.*, 368,432.
27. P. C. Myers in *Protostars and Planets II*, eds. D. Black and M. S. Matthews, (University of Arizona Press: Tucson), p. 81.
28. E. A. Lada 1992 *Astrophys. J. Letters*, 393,25.
29. J. Cernicharo in *The Physics of Star Formation and Early Stellar Evolution*, eds. C.J. Lada and N.D. Kylafis, (Kluwer Academic Publishers: Dordrecht, 1991), p. 287.
30. L. Blitz in *The Physics of Star Formation and Early Stellar Evolution*, eds. C.J. Lada and N.D. Kylafis, (Kluwer Academic Publishers: Dordrecht, 1991), p. 3.
31. E. A. Lada, D. L. DePoy, N. J. Evans, and I. Gatley, 1991 *Astrophys. J.*, 371,171.
32. C. J. Lada and E. A. Lada 1991 in *The Formation and Evolution of Star Clusters*, ed. K. Janes, A.S.P. Conference Series 13, 3.
33. H. Zinnecker, M. McCaughrean and B. Wilking, in *Protostars and Planets III*, eds. G. Levy and J. Lunine, (University of Arizona Press, Tucson, 1993) p. 429
34. C. J. Lada, M. Margulis and D. Dearborn, 1984 *Astrophys. J.*, 285, 141.
35. D. Lynden-Bell and J. Pringle 1974 *Monthly Notices Roy. Astron. Soc.*, 168, 168.
36. C. J. Lada and B. A. Wilking 1984 *Astrophys. J.*, 287, 610.
37. S. M. Rucinski, 1985 *Astron. J.*, 90, 2321.
38. J. H. Beall 1987 *Astrophys. J.*, 316, 227.
39. F. C. Adams, C. J. Lada and F. Shu 1988 *Astrophys. J.*, 326, 825.
40. S.V.W. Beckwith, A. I. Sargent, R. Chini, R. Gusten 1990 *Astron. J.*, 99, 924.
41. I. Appenzeller, I. Jankovics, and R. Ostreicker 1984 *Astron. Astrophys.*, 141, 108.
42. S. Edwards, *et al.* 1987 *Astrophys. J.*, 321, 473.
43. L. Hartmann and S. Kenyon 1987 *Astrophys. J.*, 312, 243.
44. E. Churchwell, M. Felli, D. Wood and M. Massi 1987 *Astrophys. J.*, 312, 516.
45. C. R. O'Dell, W. Zheng and H. Xihai 1993 *Astrophys. J.*, 410, 696.
46. S. W. Stahler, *Astrophys. J.*, 274 (1983) 822.
47. F. C. Adams, C. J. Lada and F. Shu 1987 *Astrophys. J.*, 312, 788.
48. C. K. Walker, C. J. Lada, P. Maloney, E. Young and B. Wilking 1986 *Astrophys. J. Letters*, 309, 47.
49. S. Zhou, N. J. Evans II, C. Kompe and C. M. Walmsley 1993 *Astrophys. J.*, 404 , 232.
50. F. C. Adams and F. H. Shu 1986 *Astrophys. J.*, 308, 836.
51. C. J. Lada 1985 *Ann. Rev. Astron. Astrophys.*, 23, 267.
52. R. N. Snell in *I.A.U. Symposium No. 115: Star Forming Regions*, eds. M. Peimbert and J. Jugaku, (Dordrecht, Reidel, 1987), p. 213.
53. J. Bally and A. P. Lane in *The Physics of Star Formation and Early Stellar Evolution*, eds. C.J. Lada and N.D. Kylafis, (Kluwer Academic Publishers: Dordrecht, 1991), p. p 471.
54. R. Bachiller and J. Gomez-Gonzalez 1992 *Astr.Ap.Rev.*, 3, 257.
55. Y. Fukui *et al.* in *Protostars and Planets III*, eds. E. H. Levy and J. I. Lunine, (Arizona: Tucson), (1993) p. 603
56. R. Snell, R. Loren and R. Planbeck 1980 *Astrophys. J. Letters*, 239, 17.
57. C. J. Lada and F. H. Shu 1990 *Science* 248, 564.
58. S. Lizano and F. H. Shu 1989 *Astrophys. J.*, 342, 834.
59. R. A. Fiedler and T. Ch. Mouschovias 1993 *Astrophys. J.*, 415, 680
60. L. Mestel and L. Spitzer 1956 *Monthly Notices Roy. Astron. Soc.*, 116, 503.
61. T. Nakano 1979 *Publ. Astron. Soc. Japan*, 31, 697.
62. R. Arquilla and P. F. Goldsmith 1986 *Astrophys. J.*, 303, 356.

DISCUSSION

J. Palous: What is the evidence to your statement that inside the clouds the Angular momentum is evenly distributed?

Lada: –

H. van Woerden: How can you be sure that in the trapezium cluster the low-mass stars, too, are only 10^6 years old? Is their evolution fast enough?

Lada: The Space Telescope observations provided a very large sample of faint, low mass stars which could be placed on the HR diagram, their ages were then determined from comparison with theoretical evolutionary tracks. Their rate of evolution is entirely consistent with 10^6 year old stars.

W. Verschueren: An intriguing problem in star formation studies is the possible difference in site between low and high mass star formation. Are there cores which preferentially form low mass stars and others which form high mass stars? How would you summarize the evidence regarding this problem from all observations from the past years?

Lada: All dense cores which form stars form low mass stars. Cores which are sufficiently massive (i.e. m $\gtrsim$100 m$\odot$) can also form high mass stars. Evidently, the probability of forming a high mass star is directly related to the mass of a dense core, whereas low mass stars from in dense gas essentially independent of core mass. Consequently, there can be dense regions (of relatively low mass) which end up only producing low mass stars but it is very difficult to find a region that produces high mass stars without many low mass stars.

R. Wyse: Could you comment on the circumstances - and timescales and lengthscales - one should/could think of star formation as having positive feedback, and then on the contrary negative feedback.

Lada: First let me say that I don't think we fully understand all the physical circumstances which could result in positive and negative feedback in the star formation process. However, if we consider O stars, for example, we would predict that they simultaneously produce both positive and negative feedback via HII regions, stellar winds and supernovae. In this case the negative feedback, that is cloud destruction, is local and the timescale shorter than the positive feedback which presumably is star formation induced or triggered by shocks. These shocks need to propagate over larger distances and take longer time to sweep up sufficient material to trigger active star formation.

WHAT DO WE REALLY KNOW ABOUT CLOUD FORMATION?

BRUCE G. ELMEGREEN
IBM Research Division, T.J. Watson Research Center
P.O. Box 218, Yorktown Heights, NY 10598, USA
bge@watson.ibm.com

Abstract. Four processes of molecular cloud formation are discussed: formation in swept-up shells, coagulation of smaller clouds, condensation in larger clouds, and compression in a supersonically turbulent medium. Examples and constraints for each process are given.

1. Introduction

Most cloud formation mechanisms that have been proposed can be placed into one or more of the following four categories: (1) cloud formation by the collection of gas into a shell or ring in the ambient interstellar medium, followed by the gravitational collapse of this gas along the periphery of the shell or ring into new self-gravitating clouds; (2) cloud formation by the coagulation of smaller clouds; (3) cloud formation by condensation from larger clouds, and (4) cloud formation by compression between converging eddies in a supersonically turbulent medium. Here we review each mechanism and consider the conditions that are necessary to make a self-gravitating cloud in which stars form.

2. Cloud Formation by Collection and Collapse in Shells and Rings

There are many examples of hollow round holes, shells, or rings in the interstellar medium of our Galaxy (Heiles 1979), M31 (Brinks and Bajaja 1986), M33 (Deul and Hartog 1990), HoII (Puche et al. 1992), and a few other galaxies (e.g., Irwin 1990). These holes were presumably made by expansion away from central pressure sources that could be OB associations (Bruhweiler et al. 1980), stray supernovae, high velocity cloud impacts

L. Blitz and P. Teuben (eds.), Unsolved Problems of the Milky Way, 551–560.
© 1996 *International Astronomical Union.*

(Tenorio-Tagle 1981), and other energetic events. A review of interstellar holes and shells is in Tenorio-Tagle and Bodenheimer (1988). An extensive review of star formation in shells and rings is in Elmegreen (1992).

Small holes and shells with diameters between 1 pc and 50 pc often occur in OB associations. Occasionally there is active star formation along the periphery of these cavities (Elmegreen and Lada 1977; Thronson et al. 1985; Junkes et al. 1992; Laval et al. 1992). This star formation was presumably triggered by the expansion that made the cavity because the embedded stars along the periphery are usually much younger than the source of the high pressure, and they are sometimes moving away from the expansion center along with the rest of the gas (Thronson et al. 1985). The clouds in which these young stars form is probably residual gas from the cloud that originally made the older OB association. In that case, the triggering process is related to the rearrangement of the old cloud, not the formation of a new cloud.

Many large shells and holes are visible in HI maps of the Large Magellanic Clouds. Westerlund and Mathewson (1966), Dopita et al. (1985), Goudis and Meaburn (1978), Wang and Helfand (1991), Bruhweiler et al. (1991) and others have studied these regions. Many of these also show recent star formation along their peripheries. Sometimes these regions are again just examples of cloud rearrangement, or of the formation of new dense cores inside existing clouds, but sometimes they are regions of new cloud formation.

It is often difficult to tell the difference between cloud rearrangement and cloud formation because both can have a morphology where young stars are located on the periphery of an old expanding shell. The difference between these two cases is important however. In the first case, the process is involved with cloud destruction and the eventual cessation of star formation. The important point here is that star formation does not stop the first time a cloud is broken apart because many dense, self-gravitating fragments remain. It may take three or more generations of star formation to completely disassemble a cloud. All of the time these new stars form, the total mass of dense gas in the region can steadily decrease. In the second case, the process of expansion and cavity formation is involved with new cloud formation. Then the total mass of dense star-forming material either increases with time or remains approximately constant as old disrupted clouds are replaced by new star-forming clouds.

There are two ways in which an expanding shell can make new dense clouds, one in which the pressure from the expansion squeezes existing diffuse clouds into dense self-gravitating clouds, and another in which the accumulated material at the edge of the expansion collapses gravitationally into new clouds separated along the periphery. The first case of cloud

squeezing has been studied by Klein et al. (1985) and others. The second case of peripheral collapse has been studied by McCray and Kafatos (1987), Comeron and Torra (1994), and Elmegreen (1994b).

The time scales for expanding shells and rings to collapse along their periphery and make new self-gravitating clouds are given by the equations (Elmegreen 1994b):

$$t_{shell} = \frac{1.25}{(G\rho_0\mathcal{M})^{1/2}} \; ; \; t_{ring} = \frac{1.5}{(G\rho_0)^{1/2}\mathcal{M}} \tag{1}$$

where $\mathcal{M} = V/c$ for expansion speed V and rms speed inside the shell c. The density external to the shell is ρ_0. These equations assume the expansion proceeds as in a wind-blown bubble, as $R \propto t^{0.6}$. The resulting collapse times are rather long for the ambient medium in a typical galaxy disk. They are equal to approximately 10^8 years divided by $\mathcal{M}^{1/2}$ and $\mathcal{M}$ for shells and rings, respectively, if the density is around 1 atom cm^{-3}. For small $\mathcal{M}$, this is a longer time than the duration of the pressure that drives the expansion, so we obtain our first constraint for this mechanism of cloud formation:

CONSTRAINT 1: The expansion has to be powerful enough and long-lasting enough to make $\mathcal{M}$ large for a sufficiently long time that the collapse can occur before the shell erodes and disperses.

This means that the peripheral gas will collapse into new self-gravitating clouds if the expansion speed V is fairly large, or the internal dispersion in the swept-up gas, c, is small, or the ambient density, ρ_0, is high, or the duration of the compression is long. Thus, collapses like this are fairly common in existing molecular clouds because ρ_0 is large, making $(G\rho_0)^{-1/2}$ comparable to the lifetime of an O-type star that forms in the cloud. At low densities, however, or for very short-lived pressures, many expansions should just disperse the gas back into the ISM without any significant gravitational collapse, except possibly for very late times, even after the erosion begins, when c may drop to a low value. Then numerous tiny clouds or globules can form in the old shell.

A second condition for collapse is that the collapse time cannot be too much larger than the time for the shell or ring to shear away because of Coriolis and tidal forces in the background galaxy. If Coriolis forces are large because of a rapid galaxy rotation rate compared to $(G\rho_0)^{-1/2}$, then the expansion will just swirl around or close back up (Palous et al. 1990). This constraint can be written in terms of the Q parameter $Q = \kappa c_0/(\pi G\sigma_0)$ for epicyclic frequency κ, ambient velocity dispersion c_0, and mass column density in the disk σ_0 (Elmegreen 1994b). This leads to our second constraint:

CONSTRAINT 2: Collapse must occur before shear, requiring that

$$Q < 0.66\mathcal{M}. \tag{2}$$

This second constraint implies that molecular cloud formation is likely to occur by this mechanism in regions of galaxies where Q is low, which is where spiral structure and gravitational instabilities form molecular clouds by a competitive mechanism (Section 4). It also suggests that because κ is very high in the inner regions of galaxies, scaling approximately as $1/r$, σ has to be very high as well. This goes a long way towards accounting for the starburst phenomenon regardless of the mechanism of star formation in starburst galaxies (Elmegreen 1994a).

Another implication of constraint 1, which also applies to starburst nuclei, is that in regions where the ambient density is very high, exceeding $\sim 10^3$ cm^{-3}, the time scale for triggering is shorter than the lifetime of an O-type star for the whole interstellar medium (and not just for the cloud in which the O-star formed, as mentioned above). This implies that $\mathcal{M}$ should always be fairly large at the time of collapse, and the time scale could be significantly shorter than $(G\rho_0)^{-1/2}$. Then the formation of molecular clouds in shells and rings would be more important than their formation in ambient instabilities, which operate on the time scale $(G\rho_0)^{1/2}$.

As a result of these considerations, we make the following two predictions:

PREDICTION 1: GMC formation in giant shells should occur in about the same radial range in a galaxy disk as GMC formation in spiral arms and in giant condensations having the ambient Jeans mass (i.e., low Q).

PREDICTION 2: Starburst nuclei, where the gas density is very large, should have a high fraction of their star formation triggered in irregular shells and other swept-up debris, rather than in clouds with the ambient Jeans mass (i.e., $t_{shell} < t_{OB\ star}$).

A similar mechanism for cloud and star formation is related to the formation of shells or compressed gas structures during the collision between a high velocity cloud and the galactic plane. A recent model for this process is in Lepine and Duvert (1994), who apply it to the Orion OB association and other regions that are far from the midplane. These authors point out that an important implication of this model is that the old stars will lie ahead of the gas and young stars in the track of the colliding cloud because these old stars, having formed first, did not decelerate along with the rest of the gas after they formed in the compressed layer. A second point is that the midplane below the high latitude clouds that form this way should be relatively free of other clouds because of the clearing effect of the high velocity impact. Third, the leading, oldest stars should be relatively free of gas because the gas in which they formed was pushed back by the ram

pressure of the galactic plane at the time they were exposed. These aspects of the model appear to be true for several regions around the Sun.

3. Cloud Formation by Coagulation of Smaller Clouds

In the Oort (1954) model of cloud formation, small clouds randomly hit each other and stick together until they become large enough to collapse gravitationally. Then star formation breaks them apart and the coagulation process starts over again. This may work for diffuse cloud collisions, which Oort considered, because such collisions can be softened by magnetic fields, and because star formation does not occur in diffuse clouds until they become significantly self-gravitating. It may not work for GMC collisions, because small GMCs should form stars and disrupt before they collide with each other, and because small GMCs probably cannot stick together if they move relative to each other at the full rms speed of the interstellar medium.

Sticking collisions for equal mass clouds require a sufficiently low velocity that the collision fragments are gravitationally bound to each other after the collision is over. This implies

$$v_{rel} \leq 2.5 v_{esc} \tag{3}$$

for relative collision speed v_{rel} and cloud escape speed v_{esc} (Pumphrey and Scalo 1983). Using the size-linewidth relation for molecular clouds (Solomon et al. 1987) and the assumption that the clouds are virialized allows us to convert this relation into a mass limit for sticking, non-magnetic collisions:

$$M > 4.3 \times 10^4 \left(\frac{v_{rms}}{5 \text{ kms}^{-1}} \right)^4 \text{M}_\odot = 1.6 \times 10^6 \left(\frac{v_{SDW}}{30 \text{ kms}^{-1}} \right)^4 \text{M}_\odot \, . \tag{4}$$

The first of these expressions is useful for random collisions of clouds moving at the relative speed of $6^{1/2}$ times the observed one-dimensional rms speed, and the second is useful for collisions at spiral density wave shocks, where the relative speed is large. Evidently small GMCs (e.g., 10^3 $\text{M}_\odot$) in the Oort model are not likely to stick together if they collide with each other at the full rms speed of the interstellar medium.

Coagulation models are still reasonable, however, but they require some modifications from the original Oort picture. Most GMCs could accrete smaller clouds or diffuse clouds, which would dissipate so much energy during the collision that the velocity threshold may not apply. GMCs could also accrete other GMCs that are co-moving in space, i.e., not moving relative to each other at the full rms speed that is observed. This situation is likely to apply to turbulent models of the ISM because the relative speed between parcels of gas is small on small scales. GMCs that form in an expanding shell may coalesce too because they are co-moving.

Another possibility is that clouds collide and ultimately stick together – even at high velocities – because the cloud filling factor is nearly unity. This situation may arise in spiral arms or at the ends of the bars in barred galaxies where ISM streamlines converge and the clouds crowd together (Kenney and Lord 1991).

In addition, diffuse clouds could stick together magnetically to make a GMC, as mentioned above. In this case, the clouds would not have to touch each other physically to stick together, they need only have their magnetic field lines link up and get tangled. The cross section for such tangling is relatively large (Clifford and Elmegreen 1983) so such collisions should be frequent or even continuous.

Another aspect of cloud collisions is that even if clouds do not stick together, the collisions between them help decrease the turbulent speed in the ISM and this leads to GMC formation by macroscopic thermal instabilities. This instability is one in which a local region with, say, an excess in density, has an excess rate of cloud collisions and an excess rate of dissipation of random cloud motions. Because the average density does not change during this dissipation process, the result is a slight decrease in the turbulent pressure. The surrounding clouds continuously hit this region, however, and these impacts transfer inward-directed momentum to the cloud fragments from the collisions. This acts like an external pressure on the cooling region, which then begins to cave-in, leading to a higher density and even more cloud collisions. Eventually the region has a core with a low velocity dispersion and a high density, and it has a continuing accretion of the ambient high dispersion clouds. The core then grows arbitrarily large. Such a mechanism of cloud formation has been studied by Struck-Marcell and Scalo (1984), Tomisaka (1987), and Elmegreen (1989). It may be present in most N-body simulations with particles for clouds. When gravity is included, the instability becomes a very powerful driver for giant cloud formation.

These considerations lead to the following predictions about diffuse and molecular clouds:

PREDICTION 1: Diffuse clouds that form by the macroscopic thermal instability should appear in quiescent regions (not shells or shock fronts) with low internal rms speeds and high internal densities in approximate turbulent pressure equilibrium with the surrounding diffuse cloud population. Molecular cores and even star formation may appear in their densest self-gravitating parts.

PREDICTION 2: Orbit crowding in galactic spiral arms and near the ends of the bars in barred galaxies should make the diffuse cloud filling factor near unity, which implies ISM compression factors of around 20. This drives the coagulation of clouds into dust lanes or giant complexes, and this is a precursor to GMCs and star formation.

4. Cloud Formation by Condensation from Larger Clouds

The largest cloud complexes in spiral arms typically have masses of $\sim 10^7$ $M_\odot$ (e.g., Knapen et al. 1993; Garcia-Burillo et al. 1993), which is larger than the mass of the largest GMCs in our Galaxy. Most spiral arm GMCs are in the cores of these complexes (e.g., Grabelski et al. 1987), so they probably formed by condensation from the larger clouds (Elmegreen and Elmegreen 1983).

The 10^7 $M_\odot$ "superclouds" have a mass comparable to the Jeans' mass at the average gas density and velocity dispersion in the Galaxy. The Jeans' length and mass for disk collapse are

$$\lambda = \frac{2\hat{c}^2}{G\sigma} \approx 2.5 \text{ kpc} \quad ; \quad M = \frac{\hat{c}^4}{G^2\sigma} \approx 10^7 \text{ M}_\odot \tag{5}$$

where $\hat{c}^2 = \gamma_{eff}c^2 + v_A^2$ is an effective mean squared velocity dispersion including dissipation and magnetic fields. Here, c is the rms dispersion in 1-dimension, γ_{eff} is an effective ratio of specific heats from the energy equation, and v_A is the Alfven speed for the component of the magnetic field perpendicular to the collapse. A more complete derivation of these quantities, including an expression for γ_{eff}, is in Elmegreen (1991, 1994c).

Large cloud complexes like these are probably the result of gravitational instabilities in the spiral arms. Conditions for a spiral arm to be unstable were discussed by Elmegreen (1979, 1994c), Balbus and Cowie (1985), and Balbus (1988). The conditions can be most simply written in terms of the dimensionless parameters $G\mu/\hat{c}^2$ and $\rho_{arm}/\rho_{crit,ave}$, both of which must exceed 1, the first so that the arm is strongly self-gravitating, and the second so that the collapse time is less than the flow-through time. Here μ is the mass/length along the arm, ρ_{arm} is the gas density in the arm and $\rho_{crit,ave}$ is the average critical density at that radius in the galaxy, given by $\rho_{crit,ave} = \rho_{ave}Q$ for instability parameter $Q = \kappa\hat{c}/(\pi G\sigma)$ with epicyclic frequency κ and mass/area σ in the plane.

Spiral arms trigger this instability because the gas is dense (self-gravity is strong), the magnetic field is strong (the angular momentum of the gas is readily removed during the collapse), the rate of shear is low (the collapse proceeds in a parallel fashion along the arm, producing "pearls on a necklace" of clouds rather than spirals within spirals), and tidal forces are low (Jean-mass clouds, which necessarily have low densities after virialization because of their large mass, are not prevented from forming by Galactic tidal forces).

In a galaxy with strong spiral arms, most of the star formation occurs in the giant cloud complexes that occupy these arms. There is apparently relatively little star formation in shells or smaller isolated clouds. This

makes one suspect that the dominant mode of star formation varies from galaxy to galaxy, depending on the presence or lack of spiral waves. This observation should not be interpreted to imply that the star formation rate per unit gas mass varies in a similar way. In fact, this quantity is surprisingly constant, to within a factor of $\sim$ 5 (e.g., Kennicutt 1983; Wiklind and Henkel 1989; Thronson, et al. 1989; Devereux and Young 1991, Sage 1993). Instead it is the mode or mechanism of star formation that varies: shells and triggered star formation in spiral-less galaxies like HoII (Puche et al. 1992) replace condensation-type star formation in 10^7 $M_\odot$ clouds in spiral galaxies like NGC 4321. Apparently the high density, low shear and low tidal forces in spiral arms affords them a condition in which supercloud formation dominates all other modes of star formation. When there are no spirals, such clouds either fail to form, or form with difficulty and a slow rate, thus permitting other forms of star formation to dominate.

5. Cloud Formation by Compression in Supersonic Turbulence

The last mechanism of cloud formation considered here has received relatively little attention compared to the others, but seems now, with our generally increased attention to interstellar turbulence, to be at least as important as the others. This mechanism has clouds form randomly, spontaneously, and continuously in a supersonically turbulent medium as high speed eddies crash and compress themselves, dissipating kinetic energy and producing high densities. The intercloud medium in this model is fast-moving: it exerts a ram pressure on the surfaces of the intervening clouds that is comparable to the isotropic turbulent pressure inside the clouds.

The most obvious application of this model is to the formation of clumps inside clouds (Sasao 1973; Scalo 1990; Elmegreen 1990; Falgarone and Phillips 1990; Porter, et al. 1992; Yue et al. 1993). Such a formation mechanism presumably accounts for the fractal appearance of the cloud boundaries and the hierarchy of scales inside the clouds. Unfortunately, neither of these properties of a GMC have been demonstrated theoretically with turbulence simulations nor have they been reproduced in a laboratory. Thus the interpretation of GMC clumps in terms of structures made by supersonic turbulence is somewhat speculative at the moment, but it is extremely compelling and natural, making the arguments highly persuasive.

The point of view taken in this section is to propose that not only are the clumps inside of clouds likely to have formed by compression in supersonic turbulence, but also the whole clouds themselves. That is, whole GMCs form by compression in supersonic turbulence on extremely large scales, up to a galactic scale height or more. The gas becomes self-gravitating during the compression, as in the cloud-clump model by Elmegreen (1993),

and then GMCs form by collapse inside the turbulence-compressed layers. Diffuse clouds presumably form the same way but in smaller eddies, at slower speeds, and without enough mass to be strongly self-gravitating.

The advantage of this turbulent model is that it can account for the formation of interstellar structures on all scales that are not connected directly with either shells or superclouds from spiral arm instabilities. Turbulence can account for the IRAS cirrus clouds and high latitude clouds, molecular or atomic. It may also account for the random positions of GMCs inside superclouds, as shown, for example, by the maps in Grabelski et al. (1987). It might even account for the random positions of clouds and star formation in flocculent galaxies, which have no spiral waves.

The turbulent model makes the following predictions:

PREDICTION 1: GMC positions inside a supercloud should have the same geometric character as clump positions inside a GMC.

PREDICTION 2: Young GMCs without obvious connections to shells and direct sources of high pressure should have surrounding intercloud flows that are converging on the cloud.

PREDICTION 3: GMCs and diffuse clouds should be interconnected and part of the same turbulent structures, with GMCs representing only the self-shielded and self-gravitating regions of the larger scale complexes.

PREDICTION 4: Star formation in turbulence-compressed GMCs should have an intermittent quality in time, and a fractal quality in space.

Perhaps with these predictions, observers can find evidence for clouds that have formed this way.

References

Balbus, S.A. (1988) *ApJ*, 324, 60.
Balbus, S.A. and Cowie, L.L. (1985) *ApJ*, 297, 61.
Brinks, E. and Bajaja, E. (1986) *A&A*, 169, 14.
Bruhweiler, F.C., Gull, T.R., Kafatos, M. and Sofia, S. (1980) *ApJ*, 238, L27.
Bruhweiler, F.C., Fitzurka, M.A. and Gull, T.R. (1991) *ApJ*, 370, 551
Clifford, P. and Elmegreen, B.G. (1983) *MNRAS*, 202, 629.
Comeron, F. and Torra, J. (1994) *ApJ*, 423, 652.
Deul, E.L. and Hartog, R.H. (1990) *A&A*, 229, 362.
Devereux, N.A. and Young, J.S. (1991) *ApJ*, 371, 515.
Dopita, M.A., Mathewson, D.J. and Ford, W.L. (1985) *ApJ*, 297, 599
Elmegreen, B.G. (1979) *ApJ*, 231, 372.
Elmegreen, B.G. (1989) *ApJ*, 344, 306.
Elmegreen, B.G. (1990) *ApJ*, 361, L77.
Elmegreen, B.G. (1991) *ApJ*, 378, 139.
Elmegreen, B.G. (1992) in *Star Formation in Stellar Systems*, eds. G. Tenorio-Tagle, M. Prieto and F. Sanchez, Cambridge, Cambridge University Press, 381.
Elmegreen, B.G. (1993) *ApJ*, 419, L29.
Elmegreen, B.G. (1994a) *ApJ*, 425, L73.
Elmegreen, B.G. (1994b) *ApJ*, 427, 384.
Elmegreen, B.G. (1994c) *ApJ*, 433, 39.

Elmegreen, B.G. and Lada, C.J. (1977) *ApJ*, 214, 725.
Elmegreen, B.G. and Elmegreen, D.M. (1983) *MNRAS*, 203, 31.
Falgarone, E. and Phillips, T. (1990) *ApJ*, 359, 344.
Garcia-Burillo, S., Guelin, M. and Chernicharo, J. (1993) *A&A*, 274, 123.
Goudis, C. and Meaburn, J. (1978) *A&A*, 68, 189.
Grabelsky, D.A., Cohen, R.S., May, J., Bronfman, L. and Thaddeus, P. (1987) *ApJ*, 315, 122.
Heiles, C. (1979) *ApJ*, 229, 533.
Irwin, J.A. and Seaquist, E.R. (1990) *ApJ*, 353, 469.
Junkes, N., Fürst, E. and Reich, W. (1992) *A&A*, 261, 289.
Kenney, J.D.P. and Lord, S.D. (1991) *ApJ*, 381, 118.
Kennicutt, R.C. (1983) *ApJ*, 272, 54.
Klein, R.I., Whitaker, R.W. and Sandford, M.T., II (1985) in *Protostars and Planets II*, edS. D.C Black and M. S. Matthews, Univ. Arizona, Tucson, 33.
Knapen, J.H., Cepa, J., Beckman, J.E., Soledad Del Rio, M. and Pedlar, A. (1993) *ApJ*, 416, 563.
Laval, A., Rosado, M., Bodesteix, J., Georgelin, Y.P., Le Coarer, E., Marcelin M. and Viale, A. (1992) *A&A*, 253, 213.
Lepine, J.R.D. and Duvert, G. (1994) *A&A*, 286, 60.
McCray, R. and Kafatos, M. (1987) *ApJ*, 317, 190.
Oort, J.H. (1954) *Bull.Astr.Inst.Neth*, 12, 177.
Palouš, J., Franco J. and Tenorio-Tagle, G. (1990) *A&A*, 227, 175.
Porter, D.H., Pouquet, A. and Woodward, P.R. (1992) *Theoret.Comp Fluid Dyn.*, 4, 13.
Pumphrey, W.A. and Scalo, J.M. (1983) *ApJ*, 269, 531.
Puche, D., Westpfahl, D. and Brinks, E. (1992) *AJ*, 103, 1841.
Sage, L.J. (1993) *A&A*, 272, 123.
Sasao, T. (1973) *PASJ*, 25, 1.
Scalo, J. (1990) in *Physical Processes in Fragmentation and Star Formation*, eds. R. Capuzzo-Dolcetta, C. Chiosi and A. Di Fazio Kluwer, Dordrecht, 151.
Solomon, P.M., Rivolo, A.R., Barrett, J. and Yahil, A. (1987) *ApJ*, 319, 730.
Struck-Marcell, C. and Scalo, J.M. (1984) *ApJ*, 277, 132.
Tenorio-Tagle, G. (1981) *A&A*, 94, 338.
Tenorio-Tagle, G. and Bodenheimer, P. (1988) *ARAA*, 26, 146.
Tomisaka, K. (1987) *PASJ*, 39, 109.
Thronson, H.A., Lada, C.J. and Hewagama, T. (1985) *ApJ*, 297, 662.
Thronson, H.A., Tacconi, L., Kenney, J., Greenhouse, M.A., Margulis, M., Tacconi-Garman, L. and Young, J. (1989) *ApJ*, 344, 747.
Wang, Q. and Helfand, D. (1991) *ApJ*, 379, 327.
Westerlund, B.E. and Mathewson, D.S. (1966) *MNRAS*, 131, 371.
Wiklind, T. and Henkel, C. (1989) *A&A*, 225, 1.
Yue, Z.Y., Zhang, B., Winnewisser, G. and Stutzki, J. (1993) *Ann.Physiks*, 2, 9.

FAR-OUTER GALAXY MOLECULAR CLOUDS

And a comparison of molecular clouds across the Galaxy

J. BRAND
Istituto di Radioastronomia, CNR
Via Gobetti 101, 40129 Bologna, ITALY

AND

J.G.A. WOUTERLOOT
I. Physikalisches Institut der Univ. zu Köln
Zülpicher Str. 77, 50937 Köln, GERMANY

1. Introduction

The outer Galaxy (defined as those parts of the Galaxy with galactocentric distances $R>R_0=8.5$ kpc) in general and particularly the outermost regions ($R \gtrsim 16$ kpc; the far-outer Galaxy or FOG) has not received the attention that has been dedicated to the inner Galaxy and the solar neighbourhood.

It is however important to identify and study molecular clouds and embedded star forming regions also at large R, in order to extend our understanding of the processes that lead to the formation of clouds and stars under physical conditions that are quite different from those found in the solar neighbourhood and in the inner Galaxy.

In very general terms one could say that most things that one finds in the inner Galaxy are also present in the far-outer Galaxy, but there is much less of it: The HI and H_2 gas surface and volume densities are much smaller, and their scale-heights are larger; the star density is much smaller, there is less star formation; the interstellar radiation field (ISRF) is much weaker; there are no (known) spiral arms and fewer SNR's, so there are fewer and/or weaker external triggers for star formation; He and metal abundances are lower; the FIR emissivity is smaller, and the pressure of the intercloud medium is much smaller.

In a series of papers (Refs. [1]-[7]) we have established an observational data base of molecular clouds in the FOG, and of the detectable manifestations of star formation that goes on within them.

L. Blitz and P. Teuben (eds.), Unsolved Problems of the Milky Way, 561–566.
© 1996 *International Astronomical Union.*

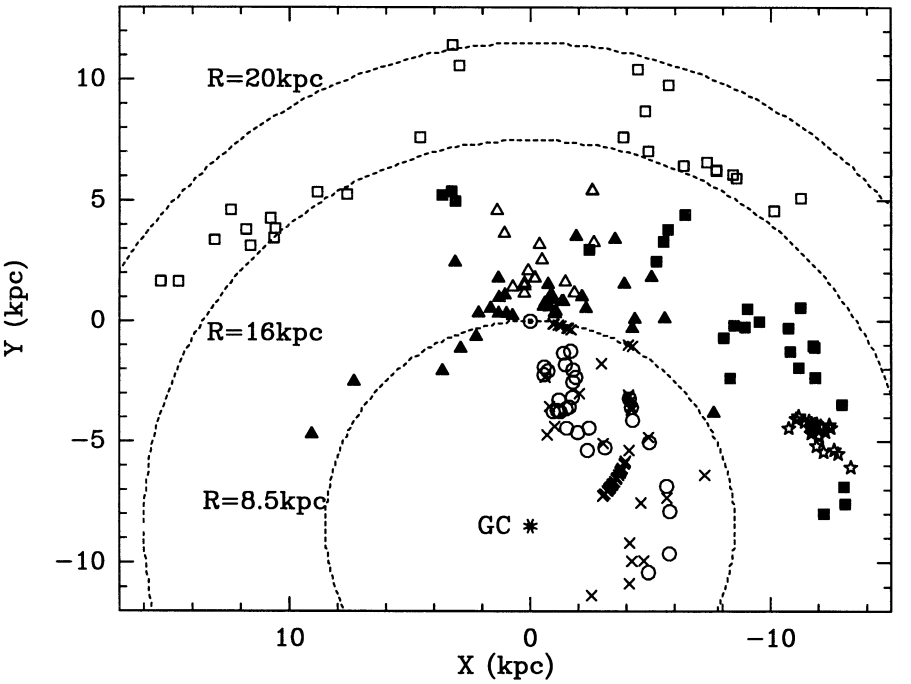

Figure 1. Distribution of the molecular clouds used in the analysis. The Sun is at (X,Y)=(0,0) and indicated by ⊙; the galactic center is at (X,Y)=(0,−8.5). Dashed circle segments indicate R = 8.5, 16, and 20 kpc respectively. The individual data sets are distinguished by different symbols: [5] (open squares), [8] (filled squares), [9] (open triangles), [10] (filled triangles), [11] (asterisks), [12] (circles), [13] (crosses).

2. Data Base

A general survey to locate sites of star formation in the outer Galaxy was made by WB89 [2], who colour-selected IRAS sources with a FIR spectral distribution typical of star-forming regions from the Point Source Catalogue, and used them as tracers for the molecular gas. For R>8.5 kpc more than 1000 molecular clouds with embedded IRAS sources were found, of which almost 200 are at R>14 kpc. BW94 [5] mapped 27 clouds from the WB89 sample in ^{12}CO(1–0), and observed several other CO isotopes and -transitions at selected positions. The clouds in this sample are at 15.7 kpc< R_{kin} <20.2 kpc, with an average R of 17.3±1.2 kpc (1σ); the median value is 16.8 kpc. We adopt R=17 kpc as a representative distance.

We analyze these data, and then compare the results with those derived

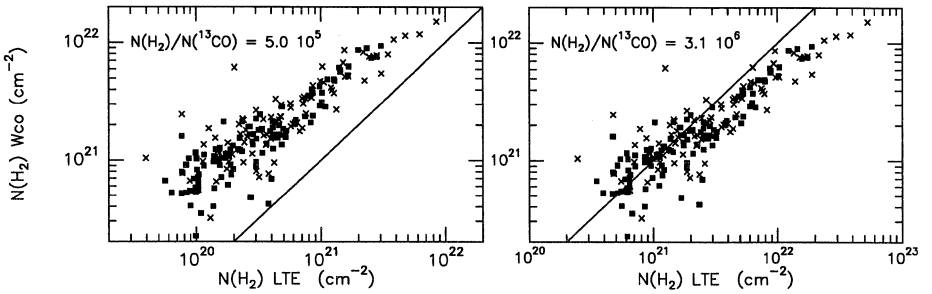

Figure 2. Comparison of column densities of H_2 calculated via $N_{Wco} = X\ W_{CO}$, with N_{lte}. The filled squares are IRAM 30-m data of the WB283 cloud and the crosses SEST data of several other FOG clouds. Left-hand panel: used local abundance ratio $N(H_2)/N(^{13}CO)$; right-hand panel: used abundance ratio at R=17 kpc, extrapolated from the gradients given by [16]. In both panels X=2.3 10^{20} $cm^{-2}(Kkms^{-1})^{-1}$, i.e. the value appropriate for the inner Galaxy, and the drawn line is for equal column densities. When taking the abundance gradients into account $N_{Wco} \approx N_{lte}$ for X in the far-outer Galaxy equal to the inner Galaxy value.

from similar observations of inner- and outer Galaxy clouds taken from the literature ([8]-[13]), and we try to use this to quantify differences (if any) in the various physical parameters (e.g. masses, kinetic temperature, and molecular abundances) between the inner- and far-outer Galaxy that could be a result of the changing environment. Figure 1 shows the galactic distribution of all molecular clouds used in the analysis. Including the literature data, we have an extended sample with parameters of 222 molecular clouds with 3<R<20 kpc, of which 130 are at R>8.5 kpc. To allow a meaningful comparison we scaled kinematic distances with the same rotation curve, X ($=N(H_2)/W_{CO}$) to 2.3 10^{20} $cm^{-2}(K\ kms^{-1})^{-1}$, and virial mass M_{vir} to $126r\Delta v^2$.

3. Conversion Factor $X = N(H_2)/W_{CO}$

BW94 have mapped their clouds completely in $^{12}CO(1–0)$, and also the majority of the literature data are of $^{12}CO(1–0)$ only. For the derivation of cloud masses we therefore depend on so-called "W_{CO}-masses", obtained from the integrated intensity $W_{CO} \equiv \int Tdv$, and the empirical fact that in the inner Galaxy there is a constant ratio $X=N(H_2)/W_{CO} \approx (2.3\pm0.3)$ 10^{20} $cm^{-2}(Kkms^{-1})^{-1}$ [14]. The resulting column density we shall denote as N_{Wco} and the mass derived from this as M_{Wco}.

For about 200 lines of sight towards molecular clouds at R>16kpc we have taken ^{13}CO data, and performed an LTE analysis to derive H_2 column densities N_{lte}.

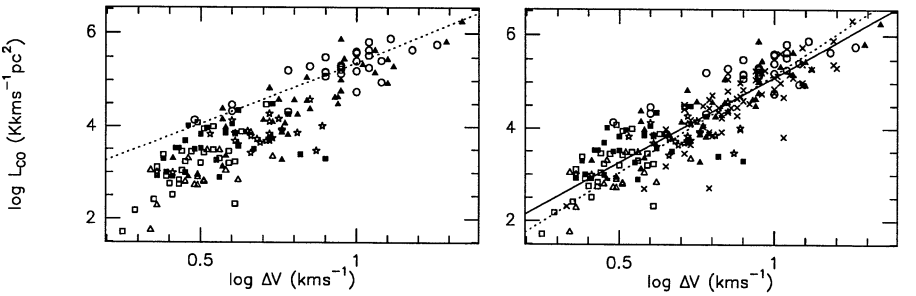

Figure 3. **a.** LogL_{CO} versus logΔv for all outer Galaxy clouds from the extended sample and the inner Galaxy clouds from [12]. The dashed line is a least-squares fit through the latter points. Symbols are as in Fig. 1. **b.** The same as **a.**, but showing all inner Galaxy clouds [12, 13]. The drawn line is a least-squares fit through the outer Galaxy data only; the dashed line fits the inner Galaxy data.

Figure 2 (*left*) shows a plot of N_{Wco} versus N_{lte}, which has been calculated using $N(H_2)/N(^{13}CO)=5.0\ 10^5$ (the value determined by [15] for local dark clouds). The drawn line indicates equal column densities. We see that $N_{lte} < N_{Wco}$; the two can be made to agree by either reducing N_{Wco}, i.e. X, or by increasing N_{lte}, i.e. $N(H_2)/N(^{13}CO)$. The existence of a galactic abundance gradient is an observational fact, and the second option is to be preferred. Extrapolating the observed and modeled [16] abundance gradients to R=17 kpc we estimate $N(H_2)/N(^{13}CO) = 3.1\ 10^6$, i.e. a ^{13}CO abundance 6 times lower than in the solar neighbourhood. Adjusting N_{lte} accordingly results in a situation where the data points are seen to scatter around the line of equal column densities (*right*), except for larger N_{lte}, which is most likely due to saturation of ^{12}CO. Averaging over all 200 lines of sight gives $X=N_{lte}/W_{CO}=(3.3\pm1.7\ [1\sigma])\ 10^{20}$ cm^{-2}(Kkms^{-1})$^{-1}$ (median $2.9\ 10^{20}$), i.e. within 30% of the inner Galaxy value.
Using the extrapolation of measured abundance gradients to the FOG one finds that using $X=2.3\ 10^{20}$=constant results in H_2 column densities close to N_{lte}.

4. Are FOG Clouds Underluminous?

In marked contrast to our conclusion in section 3, it has been argued (e.g. [8-11]) that in the outer Galaxy the value of X is 2.5 to 4 times larger than in the inner Galaxy. This is based on a comparison of a small sample of inner- and outer Galaxy clouds in a logL_{CO} versus logΔv diagram, in which the outer Galaxy clouds lie systematically lower. Because $M_{Wco} \propto X\ L_{CO}$, and assuming $M_{Wco} = M_{vir}$, it was concluded that X must be higher in

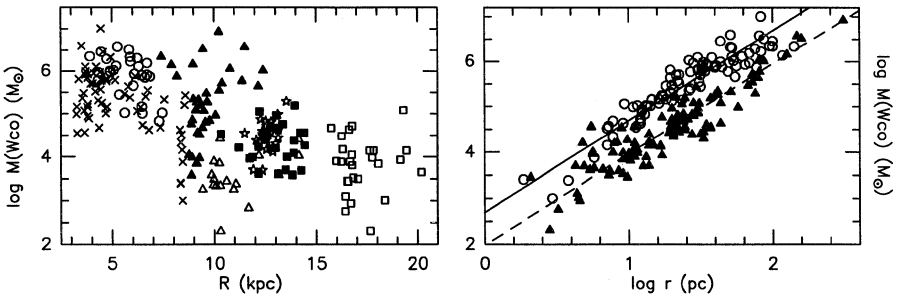

Figure 4. **a.** Plot of $\log M_{Wco}$ versus R for clouds in the extended sample. Symbols as in Fig. 1. **b.** $\log M_{Wco}$ versus logr (r=cloud radius). Inner- (circles) and outer (triangles) Galaxy clouds define relations with the same slope (2.0) but are offset from one another such that at the same mass inner Galaxy clouds are half the size of outer Galaxy clouds.

the outer Galaxy.

In Figure 3a we show a plot of cloud luminosity versus line width for all 130 clouds in the extended sample (section 2) with R>8.5 kpc. Taking only the inner Galaxy data from [12] there does seem to be a considerable difference compared to the outer Galaxy. However, adding inner Galaxy clouds from [13], the difference disappears (Fig. 3b) and fits to inner- and outer Galaxy clouds are seen to overlap. A comparison between figs. 3a and b suggests that the systematic offset in 3a is is based on a lack of small (i.e. low mass and luminosity) clouds in that inner Galaxy sample and consequently on a biased inner Galaxy fit. Figure 3b shows there is no need for a sudden change in X at R_0, consistent with our earlier conclusion.

5. Cloud Masses; Mass Spectrum

Figure 4a shows the distribution of cloud mass with R. In the inner Galaxy clouds with mass $\lesssim 3\ 10^4\ M_\odot$ are missing, probably as a result of confusion. Between R≈3 and 20 kpc the mass of the most massive cloud at a particular R decreases by about a factor of 100.

We have binned the data in mass, and assuming the mass distribution is the same at all R, we have combined the inner- and outer Galaxy samples at some intermediate mass and fitted a power-law to the resulting distribution. A fit to $M_{Wco} \geq 3.75\ 10^4\ M_\odot$ yields $dN/dM_{Wco} \propto M_{Wco}^{-1.90\pm0.11}$; a weighted fit to the outer Galaxy clouds alone gives a slope of -1.74 ± 0.05. These mass spectra are consistent with those found for samples of local and inner Galaxy clouds, as well as with those found for clumps within star-forming clouds. With a total H_2 mass in the outer Galaxy of $8\ 10^8\ M_\odot$ [3] (including

a 36% correction for He), these mass spectra imply there are about 6000 star-forming molecular clouds at R>8.5 kpc.

In Figure 4b we show the relation between M_{Wco} and cloud radius for inner- and outer Galaxy clouds. Least-squares fits to both samples have the same slope but are offset from one another such that at the same M_{Wco}, inner Galaxy clouds are half the size of outer Galaxy clouds. Taking into account that X may differ slightly between the two samples (section 3), and that some inner Galaxy clouds may have artificially higher M_{Wco} due to superposition of various clouds along the line of sight, part of the offset appears to be real. This may be caused by inner Galaxy clouds having a higher density, due for instance to increased ambient pressure.

6. Cloud Temperatures

For two FOG clouds for which we have observations in up to 5 ^{12}CO and ^{13}CO transitions we have derived a T_{kin} in the range 10–18 K, using escape probability models. This is consistent with the 10–15 K found by [17] for inner Galaxy clouds that are not located in the molecular ring. In addition we find, from a statistical analysis of antenna temperatures T_A^* of fore- and background clouds in [2], and of the envelopes of FOG clouds in [5], that the average $T_A^*[^{12}CO(1–0)]$ does not decrease with R between 9 and 16 kpc. This suggests that there is no significant gradient in T_{kin} in molecular clouds in this part of the Galaxy (see also [6]).

This work is supported in part by the Deutsche Forschungsgemeinschaft (DFG) through grant SFB-301.

References

[1] Wouterloot J.G.A., Brand J., Henkel C., 1988, A&A 191, 323
[2] Wouterloot J.G.A., Brand J., 1989, A&AS 80, 149 (WB89)
[3] Wouterloot J.G.A., Brand J., Burton W.B., Kwee K.K., 1990, A&A 230, 21
[4] Wouterloot J.G.A., Brand J., Fiegle K., 1993, A&AS 98, 589
[5] Brand J., Wouterloot J.G.A., 1994, A&AS 103, 503 (BW94)
[6] Brand J., Wouterloot J.G.A., 1995, A&A *submitted*
[7] Fiegle K., Wouterloot J.G.A., Brand J., Winnewisser G., 1995, A&A *in press*
[8] Mead K.N., Kutner M.L., 1988, ApJ 330, 399
[9] Carpenter J.M., Snell R.L., Schloerb F.P., 1990, ApJ 362, 147
[10] Sodroski J., 1991, ApJ 366, 95
[11] Digel S.W., 1991, Ph.D. Thesis, Harvard Univ.
[12] Dame T.M., Elmegreen B.G., Cohen R.S., Thaddeus P., 1986, ApJ 305, 892
[13] Solomon P.M., Rivolo A.R., Barrett J., Yahil A., 1987, ApJ 319, 730
[14] Strong A.W., Bloemen J.B.G.M., Dame T.M. et al., 1988, A&A 207, 1
[15] Dickman R.L., 1978, ApJS 37, 407
[16] Wilson T.L., Matteucci F., 1992, A&AR 4, 1
[17] Sanders D.B., Scoville N.Z., Tilanus R.P.J., Wang Z., Zhou S., 1993, in: Holt S.S. & Verter F., Back to the Galaxy, p. 311

FAR-INFRARED SPECTRAL OBSERVATIONS OF THE GALAXY BY THE FAR-INFRARED ABSOLUTE SPECTROPHOTOMETER

WILLIAM T. REACH
Universities Space Research Corporation
NASA/GSFC, Code 685, Greenbelt, MD 20771

Abstract. The Galactic continuum spectrum from 5–96 cm^{-1} is derived from COBE[1] /FIRAS observations. The spectra are dominated by warm dust emission, which may be fit with a single temperature along each line of sight in the range 16–21 K. A widespread, very cold component (4–7 K) with optical depth that is spatially correlated with the warm component is also detected. The nature of the cold component and its implications for the amount of very cold material in the Milky Way are discussed.

1. Introduction

The all-sky observations by the Far Infrared Absolute Spectrophotometer (FIRAS) aboard the Cosmic Background Explorer (*COBE*), provide the first complete coverage of the wavelength range from 4.5mm through 104μm. Here we present observations of the galactic continuum spectrum and its variation both in the galactic plane and at high galactic latitude. Full details of this work are presented in [6].

2. Observations and Method

The FIRAS has a 7° beam and it detects frequencies 2.2–96 cm^{-1} (wavelengths 4.5mm–104μm), with a spectral resolution of 0.57 cm^{-1} over the

[1]The National Aeronautics and Space Administration/ Goddard Space Flight Center (NASA/GSFC) is responsible for the design, development, and operation of the Cosmic Background Explorer (*COBE*). Scientific guidance is provided by the *COBE*Science Working Group. FSDC is also responsible for the development of the analysis software and for the production of the mission data sets.

L. Blitz and P. Teuben (eds.), Unsolved Problems of the Milky Way, 567–573.
© 1996 *International Astronomical Union.*

entire spectral range; see [3] for details. The spectra are dominated by the cosmic background radiation, interstellar medium, and zodiacal light (at high frequencies). The cosmic microwave background radiation was removed from each spectrum by subtracting a blackbody. The zodiacal light was modeled using Diffuse Infrared Background Experiment observations, to which a parameterized model of the density and temperature of interplanetary dust was fitted. Spectral lines were avoided by eliminating the appropriate frequencies.

Coaddition was necessary in order to reduce the noise in the spectra at high galactic latitude. The spectra were combined into 120 longitude bins in the galactic plane and 26 high-latitude regions. Two sample spectra, toward ($l = 45°, b = 0°$) and ($90° > l > 0°, -30° > b > -60°$) are shown in Figures 1(a) and 2(a).

The spectrum for each region was fitted by one or more modified blackbodies, with a power-law emissivity, $\epsilon_\nu = (\nu/\nu_0)^\alpha$. In the low-frequency limit, the Kramers-Kronig theorem can be used to show that α is an even positive integer [9], although it is not yet known below which frequency this limit applies. The results of using a ν^2 emissivity, a ν^α emissivity, and a ν^2 emissivity with two temperatures are shown for the two sample spectra in Figures 1(b–d) and 2(b–d).

3. Results

In the galactic plane, the FIRAS spectra cannot be modeled by a single modified blackbody with a power-law emissivity. Neither are the spectra well fitted by a continuous distribution of temperatures centered on the temperature of the dominant component at 16–21 K. Rather, the observations indicate an excess that can be reproduced by a second temperature component at much lower temperature (4–7 K). Just off the galactic plane, in the $10° < b < 30°$ zone, the very cold component is also required to match the spectra. At the highest galactic latitudes, the spectra are fit equally well by a two-temperature model or a single-temperature model with a power-law emissivity with $\alpha \simeq 1.5$. Because it is unlikely that the grain properties are significantly different at high latitude, we consider the two-component model to be valid there as well.

The optical depths of the warm and cold components are compared in Figure 3. The correlation is not exactly linear: the slope becomes steeper at fainter levels (corresponding to higher latitude). Also, the temperature of the very cold component has significant variation across the sky. In a principal components analysis of the FIRAS data, Barnes [1] identified the very cold component as an eigenspectrum with a spatial variation similar to but distinct from that of the warm dust.

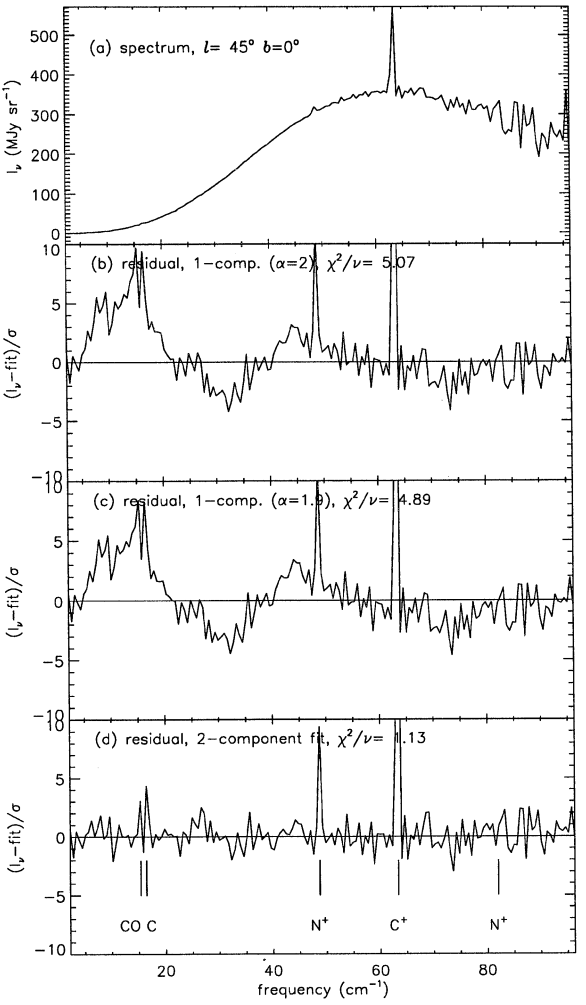

Figure 1. *(a)* Spectrum of interstellar emission in the galactic plane toward longitude $l = 45°$. Other than the identified spectral lines, the spectrum is dominated by emission from warm dust, which peaks around 65 cm^{-1} (150μm). *(b)* Residuals after a single-component modified blackbody with $\alpha = 2$ was subtracted. The residual intensity at each frequency was divided by the uncertainty at that frequency. The excess emission at 7–20 cm^{-1} (1400–500μm) is evident. *(c)* Residuals after a single component with the best-fitting emissivity index was subtracted. *(d)* Residuals after a two-component model was subtracted. The very cold emission is now adequately fit.

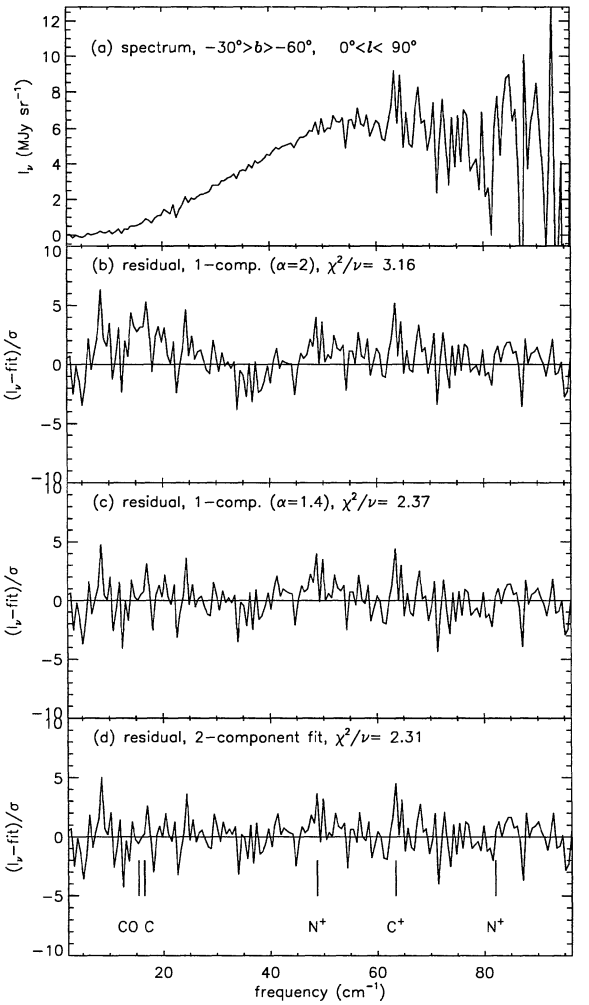

Figure 2. *(a)* Spectrum of interstellar emission in the region with $-30 > b > -60°$ and $90° > l > 0°$. Only a weak C^+ spectral line and the warm dust continuum are evident. *(b)* Residuals after a single-component modified blackbody with $\alpha = 2$ was subtracted. The excess emission at 7–20 cm^{-1} (1400–500μm) is evident. *(c)* Residuals after a single component with the best-fitting emissivity index ($\alpha = 1.4$) was subtracted. *(d)* Residuals after a two-component model was subtracted. It is not possible to clearly distinguish whether panel (c) or (d) are better fits to the data.

4. Nature of the Very Cold Component

The nature of the very cold component identified in the FIRAS spectra is of great importance, because the existence of very cold material in the

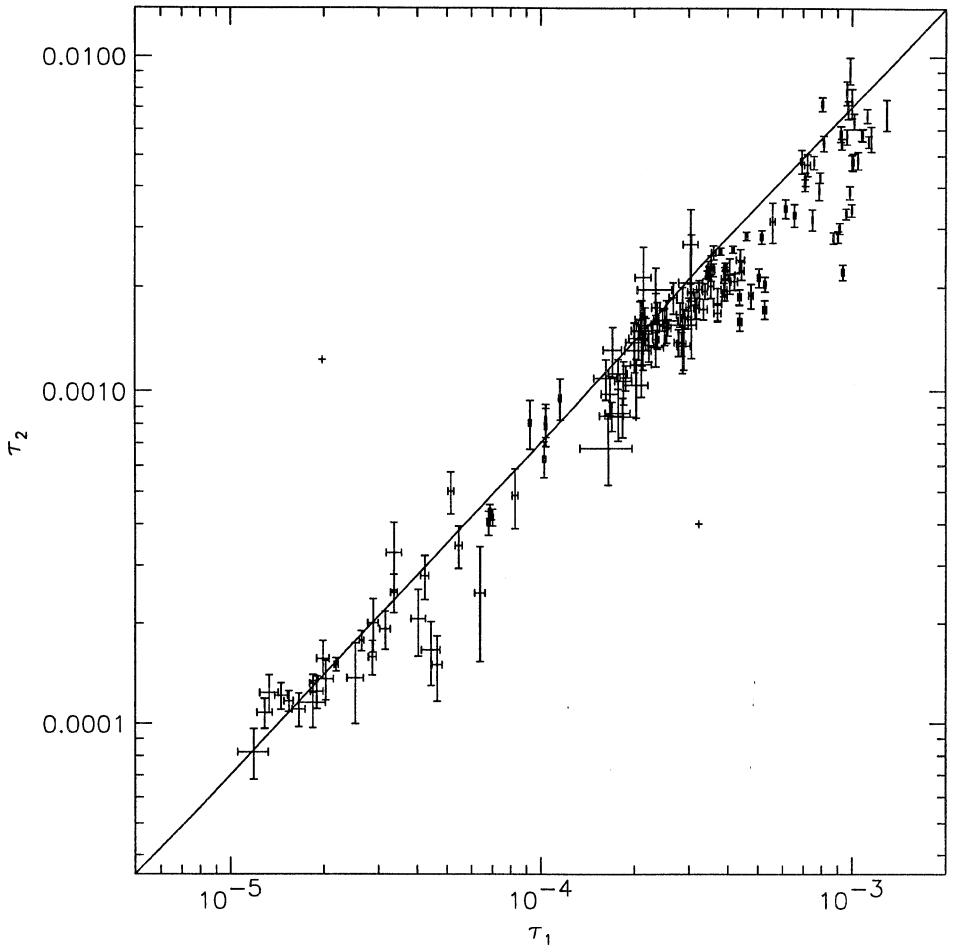

Figure 3. Comparison of the optical depths of the warm and cold components.

Milky Way has implications for the 'missing mass' problem, the composition of the halo, and the reservoir of material available for star formation. One obvious hypothesis is that the cold component is due to dust grains, similar to those that produce the warm component, but illuminated by a much-reduced radiation field. The existence of the cold component at high galactic latitude seems to preclude this hypothesis, because there are insufficient dark regions at high galactic latitude within which to shield the

dust. The strong variation of the cold component with galactic coordinates (as reflected in Figure 3) precludes its being produced exclusively in the halo, although a small halo contribution remains possible [4].

Three more hypotheses for the nature of the very cold component are emission from large grains ($\sim 10^2$ μm), very small grains (< 0.02 μm), or fractal grains. Large and fractal grains are cold because they emit relatively efficiently in the far-infrared and submillimeter, and very small grains are cold (most of the time) because they cool rapidly in between successive absorptions of photons. The large-grain hypothesis runs into abundance constraints on the heavy elements they contain, but at least one grain model has been able to incorporate relatively large grains without violating cosmic abundances [7]. The very small grain hypothesis requires some heating mechanism to keep the grains from cooling all the way to the cosmic background temperature; this issue has not been addressed yet. Fractal grains can attain a wide range of temperatures due to their geometry alone.

Another hypothesis for the cold component is that it is due to an emissivity enhancement in the submillimeter due to the optical properties of the constituent material. The variations in the cold component relative to the warm component would require that the composition change across the sky. This hypothesis is being explored further, in an attempt to determine the emissivity of interstellar dust by inverting the FIRAS spectra.

5. Implications for Cold Gas in the Milky Way

The lack of substantial power emitted by dust with temperatures in the 4–15 K range places strong constraints on the amount of very cold material in the interstellar medium. The discovery of CO absorption lines from clouds in the outer galaxy led to the suggestion that very cold molecular clouds, which would have been very difficult to detect by CO emission, may be an important, massive component of the Galaxy [5]. The power of all starlight incident on such cold clouds would be reemitted within the FIRAS bandpass. In fact, there is little power emitted besides that contained in the warm component: the cold component contains less than 0.05% of the power in the Solar neighborhood interstellar radiation field. Models for the interstellar medium including a substantial increase in the abundance of dark clouds, such as those required to harbor cold gas, must comply with the constraint that very little power is emitted by cold dust. Evidence for star formation in the far outer galaxy [2] suggests both that dust formation (in stellar outflows and supernovae) occurs there and that the radiation field will not be negligible; power absorbed from the extragalactic radiation field is also detectable.

References

1. Barnes, W. (1994), Ph. D. thesis, M.I.T.
2. De Geus, E. J., Vogel, S. N., Digel, S. W., & Gruendl, R. A. (1993), *Astrophys. J.*, 413, L97.
3. Fixsen, D. J., *et al.* (1994), *Astrophys. J.*, 420, 457.
4. Gerhard, O. E., & Silk, J. (1994), preprint.
5. Lequeux, J., Allen, R. J., & Guilloteau, S. (1993), *Astron. & Astropys.*, 280, L23.
6. Reach, W. T. *et al.*(1994), submitted to *Astrophys. J.*.
7. Rowan-Robinson, R. (1993), *Mon. Not. Roy. Astron. Soc.*, 258, 787.
8. Wright, E. L. (1991), *Astrophys. J.*, 381, 200
9. Wright, E. L. (1993), in *Back to the Galaxy*, eds. S. S. Holt & F. Verter (AIP: New York), p. 193.

THE SEARCH FOR COLD MOLECULAR GAS IN THE OUTER GALAXY

E.J. DE GEUS AND J.A. PHILLIPS
Caltech MS 105-24, Pasadena, CA 91125, USA

1. Introduction

It is well known that the rotation curves of many galaxies remain flat well outside their optical disks. This leads to the conclusion that the visible mass in galaxies is only a small fraction of the total (see *e.g.* Faber & Gallagher 1979). Although we are certain that "dark matter" exists, its composition and distribution are still unknown.

In a recent paper Pfenniger *et al.* (1994) argued strongly for the possibility that dark matter could well be in the form of cold, predominantly molecular gas in a flat distribution. To have escaped previous detection in the outer parts of our Galaxy, the gas would need to have a low temperature and thus a low emissivity. Because most substantial heating sources of gas are associated with the presence of massive stars (UV radiation and cosmic rays) this requirement may be satisfied in the Galactic plane outside the optical disk.

Support for the existence of molecular gas at large Galactic radii was obtained recently through a detection of 11 CO clouds beyond the optical disk of the Galaxy (Digel *et al.* 1994). CO(1-0), CO(2-1) and ^{13}CO (1-0) observations of the two most remote of these objects, at 22 and 28 kpc from the Galactic center, revealed kinetic temperatures similar to those of molecular gas locally and in the inner Galaxy, rather than the low temperatures proposed by Pfenniger *et al.* (1994). Subsequent Hα observations towards the cloud at 28 kpc from the center revealed the presence of ionized gas and an associated B 0.5 I star (de Geus *et al.* 1993). These observations allow us to speculate that a cold component of molecular gas might indeed exist in the outer parts of our Galaxy, which only becomes easily detectable in emission when stars form and provide a source of heating for the gas.

L. Blitz and P. Teuben (eds.), Unsolved Problems of the Milky Way, 575–581.
© 1996 *International Astronomical Union.*

Because the emissivity of the cold molecular gas is low, the best way to look for it is in absorption against a background continuum source. Absorption experiments at mm wavelengths have been successfully carried out toward the inner regions of the Galaxy (Marscher *et al.* 1991; Lucas & Liszt 1994) and, recently, Lequeux, Allen & Guilloteau (1993, hereafter LAG) detected CO absorption toward two quasars probing lines of sight through the outer Galaxy. They detected gas at Galactic radii between 8.8 and 11.5 kpc.

If we take the LAG results at face value, cold molecular gas in the outer Galaxy must be abundant. They detected absorption lines toward every quasar they observed (4 absorption lines were detected along only two lines of sight), and they argued that the gas they saw was cold, with temperatures as low as 3.5 K. To test these conclusions we have undertaken to observe as many lines of sight as possible toward mm-bright quasars to probe the outer parts of the Galactic disk. We formulated our source list as follows: We searched the NASA Extragalactic Database and the OVRO millimeter array flux history tables for extragalactic radio sources with $S(3\mathrm{mm}) \geq 1$ Jy, at low galactic latitudes in the longitude range $55° \leq l \leq 125°$. The warp in the outer parts of the Galaxy increases the useful range of Galactic latitudes to as much as $b \approx 10°$, depending on the longitude. We used the Leiden-Green bank HI maps (Burton 1985) to determine whether the line of sight to a quasar passed through the Galactic disk. Our search yielded the 6 objects listed in Table 1.

We observed each object in our sample with the Owens Valley millimeter interferometer to search for CO and HCO^+ absorption lines. The results are given in §2. We will show in this paper that the gas found in absorption is not necessarily cold, and furthermore, that the number of absorption features is significantly smaller than estimated by LAG.

2. Observations and Results

We made our observations using the Owens Valley millimeter interferometer between Oct 93 and July 94. Most of our data were collected with a five element array, but some of the HCO^+ observations of 2013+370 in July 1994 were obtained with six antennas. Table 1 summarizes the observations.

We searched for absorption at two frequencies: 115.27 GHz, which corresponds to the CO(0-1) transition, and 89.189 GHz, which is the HCO^+(0-1) transition. Although the abundance of HCO^+ is lower than that of CO in Galactic molecular clouds ($[CO]/[HCO^+] \sim 10^3$), it offers three advantages over CO: (1) the quasar fluxes are $\approx 20\%$ higher at 89 GHz, (2) HCO^+ has a larger dipole moment and thus a larger optical depth per molecule, and (3) the system temperature at 89 GHz is typically 3 times lower than

TABLE 1. Observations

Source	ℓ	b	Line	rms Jy	Δv km s^{-1}	v_{LSR} km s^{-1}	R_G kpc
1923+210	150.°38	−1.°60	CO	0.30	0.33	−102 → −18	10 → 20
2005+403	76.°82	+4.°30	CO	0.25	0.65	−152 → −36	10 → 28
			HCO^+	0.10	0.42	−144 → −36	10 → 28
2013+370	74.°87	+1.°22	CO	0.33	0.16	−65 → −45	10.7 → 12.3
			CO	0.25	0.33	−120 → −10	9 → 20
			HCO^+	0.07	0.21	−68 → −42	10.5 → 12.5
			HCO^+	0.10	0.42	−137 → −35	10 → 25
			HCO^+	0.13	0.11	−7 → +19	∼ 8.5
3C418	88.°81	+6.°04	CO	0.40	0.32	−122 → −38	10 → 19
			HCO^+	0.06	0.42	−134 → −26	10 → 22
NRAO150	150.°38	−1.°60	CO	0.25	0.33	−122 → −38	≥ 13
Cyg A 1	76.°19	+5.°77	HCO^+	0.25	0.42	−139 → −41	10 → 24
Cyg A 2	76.°19	+5.°74	HCO^+	0.25	0.42	−139 → −41	10 → 24

at 115 GHz because of a strong telluric oxygen line near 115 GHz. Figure 1 illustrates the advantage of searching for HCO^+ absorption. The HCO^+ spectrum (bottom panel) clearly shows a line close to −60 km s^{-1}, which is lost in the noise in the CO (1-0) spectrum; for the same integration time the HCO^+ spectrum has much higher signal-to-noise.

We detected absorption in only 2 objects, 3C418 and 2013+370 (Figures 1 and 2). The velocities of the lines we detected correspond to galactocentric radii between 8 and 12 kpc, formally placing them in the outer Galaxy (de Geus & Phillips 1994). We did not detect any gas in the "far outer galaxy", such as the cloud found at 28 kpc from the galactic center (Digel *et al.* 1994).

3. Discussion

The object 2013+370 was observed by us and by LAG. Their 30-m single-dish spectrum showed absorption at 4 different velocities (and thus 4 different Galactic radii). A Plateau de Bûre interferometer spectrum was also presented as confirmation of the single dish spectrum.

The OVRO mm-interferometer CO and HCO^+ spectra we are reporting here had a comparable or significantly lower rms noise level than the single dish and the interferometer spectra presented by LAG, and Figure 2 shows that we can confirm only two of the four lines they reported (one line

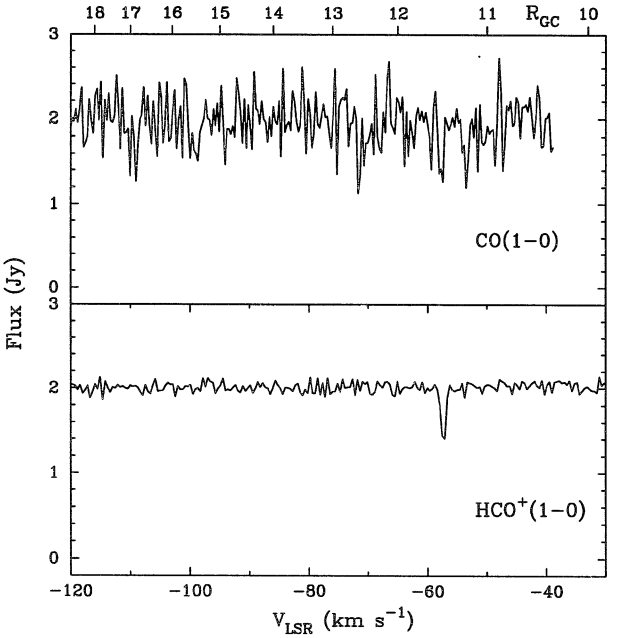

Figure 1. OVRO spectra of the low-galactic latitude quasar 3C418. The top panel shows an 8 hour track on the CO(1–0) line at 115 GHz, and the bottom panel the same integration time on the HCO^+(1–0) line.A line at a Galactic radius of 11.5 kpc is clearly detected in HCO^+ but it is hidden in the noise in the CO spectrum.

at $+6$ km s^{-1} and a closely-spaced pair near -56 km s^{-1}). The two lines that we observed close to -56 km s^{-1} have significantly different velocities and optical depths from the lines in the LAG single dish spectrum. Upon close inspection we find that LAG's interferometer spectrum is also in disagreement with their single dish spectrum, (despite their statement to the contrary) and that their interferometer spectrum (within the noise) agrees with ours. We conclude that the LAG single dish absorption spectrum is probably corrupted by inaccurate subtraction of extended CO emission.

We would like to point out that, although we have detected molecular gas in absorption along two lines of sight with the interferometer, this does not imply that the absorbing gas is necessarily cold. The standard equation of radiative transfer is:

$$T_b = T_o e^{-\tau_\nu} + T_k(1 - e^{-\tau_\nu}), \tag{1}$$

from which we see that absorption below the continuum level (T_0) may occur if the kinetic temperature of the foreground gas (T_k), which has optical depth τ_ν, is lower than the background source temperature. Hence the general conclusion that absorption implies cold gas. However, an interferometer, which has a zero response to extended emission and therefore

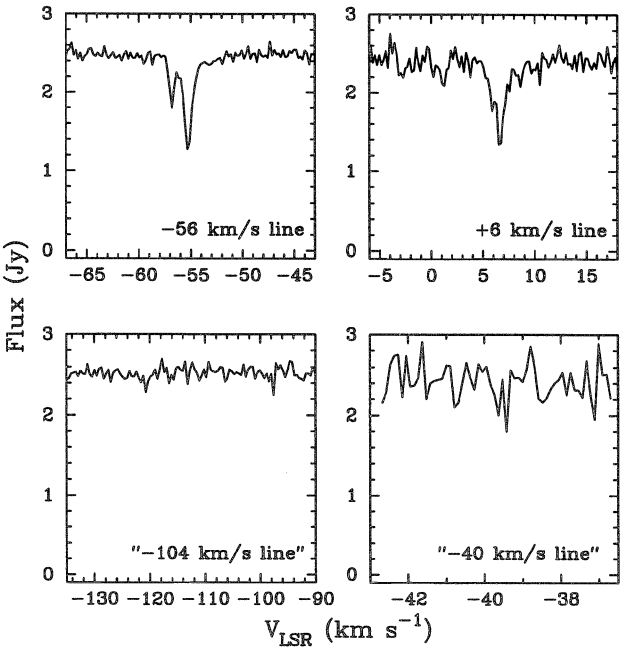

Figure 2. OVRO HCO^+ spectra of the low-galactic latitude quasar 2013+370. The four panels show the 4 different velocities at which Lequeux, Allen & Guilloteau (1993) reported the detection of absorption. We can only confirm two of those lines: the top panels show our detections of the lines at +6 km s^{-1} and the composite line at −56 km s^{-1}. The lines at −104 km s^{-1} and −40 km s^{-1} are not confirmed at higher resolution and better rms noise level than the data by LAG either at HCO^+ (bottom panels) or CO (not shown).

acts as a spatial filter, cancels the emission part of the radiative transfer equation, leaving:

$$T_b = T_o e^{-\tau_\nu}. \tag{2}$$

Ideally this equation also holds for the single dish experiment by LAG, who used the average of 4 neighboring spectra to cancel the emission from the spectrum taken toward the quasar (whether the cancelation is accurate is another issue). The foreground gas temperature does not appear in equation (2). Therefore, when using either of these techniques, the conclusion that gas is cold simply because it is seen in absorption is false.

LAG argued that gas found in emission toward 0727-115 was cold, with $T_k \approx 3.5$ K. For this conclusion they had to assume that the filling factor of CO emission in the 23″ IRAM beam was unity. However, they also noted that there were significant emission gradients in the vicinity of 0727-115. This fact indicates that the filling factor is less than unity and that the gas temperature is higher than 3.5 K. For a discussion of kinetic temperatures of gas in the outer Galaxy see also Wilson & Mauersberger (1994).

4. Conclusions

Our observations do not confirm the conclusion by LAG that a significant component of cold molecular gas resides in the outer Galaxy. However, neither do the observations exclude an abundant cold molecular component. If such a component does exist the only way to detect it is in absorption against a background source, but the small number of background sources in the 3-mm wave band severely limits the detection probability. The probability (P_n) of detecting the molecular component using a limited number (n) of (pencil-beam) lines of sight depends directly on the volume filling factor (f_V) of the gas:

$$P_n = 1 - (1 - (f_V)^{2/3})^n. \tag{3}$$

If the cold molecular gas density is $\sim$ 300 cm^{-3}, then $f_V \sim 10^{-3}$. The probability of detecting a cold cloud with six lines of sight is only $P_6 \approx 6\%$. Thus, the null results so far do not rule out the possibility of cold gas in the far outer galaxy.

Since the molecular gas is expected to have a low volume filling factor, it is essential that we sample a larger number of lines of sight. Because the number of strong quasars increases dramatically toward lower frequencies, and because the new Q-band opportunity at the VLA has made the CS(0-1) transition accessible to observation, we have obtained observing time at the VLA to search for this molecular line in absorption in the outer Galaxy. With the improved sampling possible at 49 GHz we are hopeful that statistically meaningful surveys for cold gas in the outer Galaxy are now within reach.

References

Burton, W.B. (1985) *A&A Suppl.*, 62, 365.
de Geus, E.J., Vogel, S.N., Digel, S.W. & Gruendl, R.A. (1993) *Ap. J. Letters* 413, L97.
de Geus, E.J. & Phillips, J.A. (1994) *Ap.J.* Letters submitted.
Digel, S.W., de Geus, E.J. & Thaddeus, P. (1994) *Ap.J.*, 422, 92.
Faber, S.M. & Gallagher, J.S. (1979) *Ann. Rev. Astron. Astrophys.*, 17, 135.
Lequeux, J., Allen, R.J., and Guilloteau, S. (1993) *A&A*, 280, L23.
Lucas, R., & Liszt, H.S. (1994) *A&A*, 282, L5.
Marscher, A.P., Bania, T.M. & Wang, Zh. (1991) *Ap.J.*, 371, L77.
Pfenniger, D., Combes, F.& Martinet, L. (1994) *A&A*, 285, 79.
Wilson, T. & Mauersberger, R. (1994) *A&A* 282, L 41.

DISCUSSION

R. Allen: Your suggestion that we could not have computed reliable excitation temperatures assumes that we observed only one line in absorption. In

fact, the values of excitation temperature which I gave in my paper require, and were derived from, a combination of both emission and absorption observations, in some cases even for both the 2-1 and the 1-0 transition. I would be happy to discuss the algebra involved with you during the coffee break.

de Geus: Our comment about the temperature derivation was based on the information given in Lequeux, Allen & Guilloteau (1994). There, only the temperature along the line of sight to 0727-115 is discussed, and for this object no mention is made of data other than CO (1-0) absorption and emission. Lequeux et al. (1994) then state that *because* the CO absorption line is saturated, the corresponding emission gives the excitation temperature, provided that the beam filling factor is unity. Besides arguing that the uncertainty in the beam filling factor is important and will always make the temperature estimate a lower limit, we mostly take issue with the statement that the CO line is saturated. In our data 0727-115 has revealed NO CO(1-0) absorption ($\tau < 0.65$), which implies that there is no basis for the assumption that the corresponding emission gives the excitation temperature.

HOW DOES STAR FORMATION AFFECT THE LARGE SCALE STRUCTURE OF THE ISM?

JAN PALOUŠ
Astronomical Institute
Boční II 1401, 141 31 Prague 4, Czech Republic

1. Introduction

Nearly all the star formation in the Milky Way and nearby spiral galaxies occurs in the giant molecular clouds (GMC). Inside the GMC's the units of star formation are the high density ($\geq 10^3 cm^{-3}$) and high mass ($\geq 10^3 M_\odot$) clumps (Blitz, 1991). Once a GMC is "infected" by star formation many clumps form stars producing a star forming region. The formation of massive stars induces destructive processes, such as H_2 dissociation, HI ionization, stellar winds and supernova explosions, thus self-limiting the lifetime of GMC to $\sim 3\ 10^7$ years.

Here, the star formation is discussed as a collective process happening in GMC. We describe how it influences the ambient interstellar medium and how it propagates in the Galaxy. The large scale means the size comparable to the galactic diameter.

2. Anomalous HI Features, Worms, Chimneys and Supershells

The galactic supershells, discovered by Heiles (1979), are the HI structures up to $\sim 2\ kpc$ in diameter expanding at velocities $\sim 20\ km\ s^{-1}$. They are associated with the HI holes or voids in the HI distribution. Special supershells are the galactic worms, or interstellar HI structures that lie roughly perpendicular to the galactic plane with the median width of some ~ 100 pc and the median height some ~ 180 pc. They were listed by Koo et al. (1992). Another specific version of a supershell is a "chimney": if the released energy is high enough and if the gaseous disk does not have too much of a z-extent, then a supershell blows out of the disk, forming a chimney leading the hot gas from inside the bubble into the galactic halo (Heiles, 1992).

L. Blitz and P. Teuben (eds.), Unsolved Problems of the Milky Way, 583–590.
© 1996 *International Astronomical Union.*

The supershell appearance, their shape, expansion velocities, and whether it blows out to the galactic halo and becomes a chimney, depends on the energy inserted and on the distribution of the ambient medium. The energy source can be the young and massive stars of a star forming region (Tenorio-Tagle & Bodenheimer, 1988) or the collision of a cloud with the galactic HI plane (Tenorio-Tagle, 1980, 1981). The distribution of the ambient medium influences the superbubble evolution: the low-density and sufficiently thick HI disk can suppress its blowout preventing the transport of the hot and heavy elements enriched gas from the supershell interior far out of the galactic plane. The blowouts are possible when the HI disc has a small scale height, then also the formation of chimneys may be expected (Palouš, 1990).

The local Lindblad's expanding ring of molecular clouds and the O, B stars of the Gould's belt may be the relics left after the supershell expansion (Palouš, 1987). Their motion, which distinctly deviates from the galactic differential rotation (Westin, 1985), should reflect the velocities at earlier times when the expansion has been initiated. Unfortunately, the pure expansion or the influence of the density wave give velocity fields differing from observations (Lindblad, 1980). Other scenarios, such as the collision of a high velocity cloud with the galactic plane or the expansion from a rotating cloud are also discussed (Comeron & Torra, 1992; 1994; Comeron, Torra & Gómez, 1994; Lindblad & Palouš, 1995).

New 21 cm Leiden-Dwingeloo survey by Burton and Hartmann (Burton, 1994; Hartmann, 1994) shows many anomalous-velocity HI structures (Burton et al. 1992). We compare the supershells detected in this survey with simulations: an example is given by Ehlerová et al. (1994). Comparison of the observed galactic supershells with simulations may give constrains on the z-distribution of the interstellar medium and on the energies required.

However, the interstellar medium is not just a collection of clouds and supershells expanding in smooth ambient gas and in isolation. The observations show an interconnected network of filaments with embedded amorphous density concentrations (Scalo, 1990; Elmegreen, 1993). The evolution of clumpy gas in galaxies is analyzed by Yorke et al. (1992). The expansion of superbubbles in the cloudy medium is discussed by Silich et al. (1994a, b).

3. Dissipative Cloud Collisions

The Galaxy involves diffuse, self-gravitating and unbound clouds of sizes from 1 pc to 1000 pc and masses up to $10^7 M_\odot$ (Elmegreen, 1993). About 85% of H_2 mass is contained in $\sim$ 6000 GMC larger than 22 pc in diameter with masses $> 10^5 M_\odot$ each. The cloud-to-cloud velocity dispersion is nearly

independent of mass ranging between $4-7\ km\ s^{-1}$ (Stark, 1984). With this velocity dispersion the mean free path of a GMC is $\sim 1.7\ kpc$ (Sanders, Scoville, 1987).

GMC are composed of high density clumps and interclump medium of much lower density. They do collide and we may ask if their formation can be ascribed to collisional agglomeration, or if the star formation and subsequent GMC disruption is the more ultimate result of a collision. It may depend on the relative velocity with the low velocity collision leading to agglomeration and the high velocity collision to star formation and cloud disruption.

A fraction of the energy of relative motion is dissipated in both cases. Such dissipative collisions reduce the velocity dispersion circularizing the cloud orbits. The collisional cooling is counterbalanced with heating, or increasing the noncircularity of motions, from star formation, large scale nonaxisymmetric density perturbations such as spiral arms and bars, or tidal encounters with other galaxies.

Resonances between the galactic orbital frequency and the large scale perturbation are places of increased momentum exchange between the perturbation and individual clouds. There, the orbital heating enhances higher collisional frequency and higher collisional cooling. This is why the rings of molecular clouds appear at resonances (Palouš et al. 1993; Palouš & Jungwiert 1995). Depending on the strength of perturbation, the collisions may happen at sufficiently high relative velocities inducing the ring like star formation burst (Elmegreen, 1994).

4. Propagating Star Formation

The idea that star formation at one place may initiate the star formation at another place was first proposed by Öpik (1953) and Oort (1954). An early theoretical model was developed by Mueller and Arnett (1976). The observational evidence of the sequential star formation within 1.5 kpc was reviewed by Blaauw (1991).

Here we describe two types of models: stochastic, when the propagation is given with a certain probability, and deterministic, when the propagation results from a chain of events (star formation – supershell expansion – accumulation of the ambient medium – formation of clouds) connecting the places of subsequent star formation.

4.1. STOCHASTIC MODELS

First stochastic self-propagating star formation model was developed by Seiden and Gerola (1982), Schulman & Seiden (1986) and Seiden and Schulman (1990). They introduced a finite and isotropic probability that the star

formation in one region induces star formation in a neighboring region. Another parameter is the recovery time during which the probability is lower for cells that were active recently. The galactic rotation curve and the relative size of a star forming region are other parameters of their model. Resulting patterns resemble flocculent spirals. This model particularly applies to dwarf irregular galaxies, where the star formation has the burst like nature. The galaxy has to wait until the stars begin to form, then the star formation propagates to all the disk, which is heated and the star formation turns off until the gas cools down again (Elmegreen, 1994).

The model with anisotropic probability distribution was developed by Jungwiert and Palouš (1994). The propagation probability, which depends on the direction in the galaxy, is given with an ellipse: its inclination and eccentricity are related to the galactic rotation curve, resulting in the long and well organized spiral arms. The Hubble sequence Sa - Sb - Sc - Sd - Sm - Irr may be the sequence of decreasing eccentricity and inclination of the major axis of the propagation probability ellipse, which is quite likely if this ellipse reflects the decreasing sheer along the Hubble sequence.

4.2. DETERMINISTIC MODELS

The star formation is propagating when it is able to overjump from one location in the galaxy to another. The star forming clouds can be composed from material accumulated in supershells expanding from the star forming centers. As soon as the massive stars appear they ionize the ambient medium disrupting the parental cloud. The energy from the new stellar cluster generates an expanding supershell. As it reaches large size, the mass accumulated due to the galactic sheer at the tips of elliptical supershells gets opaque to dissociating photons. The gravitational fragmentation can initiate the formation of new molecular clouds and trigger the star formation (Elmegreen, 1994). It is a self-regulating process determining the galactic star formation rate, the number of superbubbles, and the relative fraction of the disc space occupied by the hot medium (Palouš, 1989, 1993; Tenorio-Tagle, 1994).

The cloud formation in expanding supershells is the principle used in a deterministic model of propagating star formation developed by Palouš et al. (1994). It is a coherent process producing at any time of the disc evolution the non-axisymmetric large scale structures sometimes of spiral shape (Fig. 1. and 2.). The propagation organizes the star forming regions to spiral like sequences with the characteristic appearance of 'pearls on a necklace' resembling the situation noted first in observed galaxies by Walter Baade.

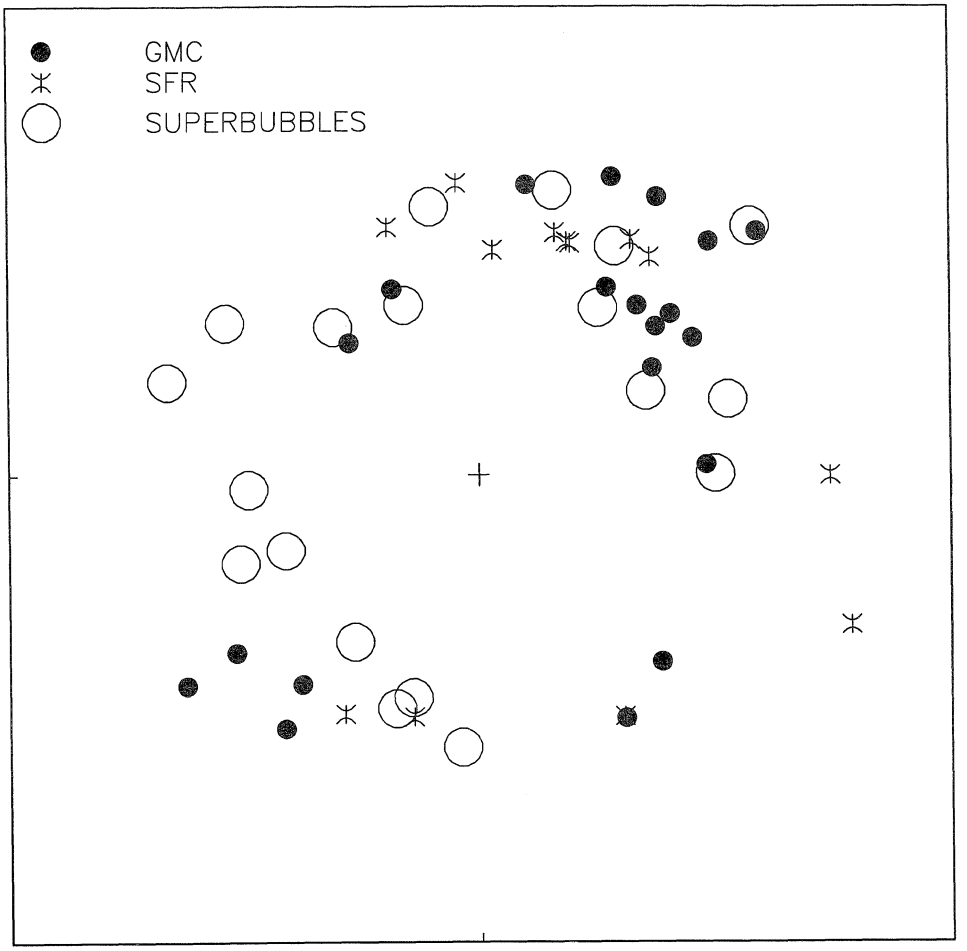

Figure 1. The self-propagating star formation model (Palouš et al., 1994). The plane distribution of massive molecular clouds ($> 10^6 M_\odot$), star forming regions (SFR) and superbubbles 1 Gyr after the first star formation was triggered in the galactic disc. The galactic center is marked with the + sign.

5. Principles of Self-Regulation

The two self-regulating mechanism should be distinguished in spiral galaxies:

1) The gravitational mechanism, which is due to the influence of the large scale non-axisymmetric features such as spiral arms and bars on the motions of individual stars. This large scale features, which form in the low velocity dispersion disc, increase the velocity dispersion of both, stars and gaseous clouds. The increase in the velocity dispersion reduces the growth

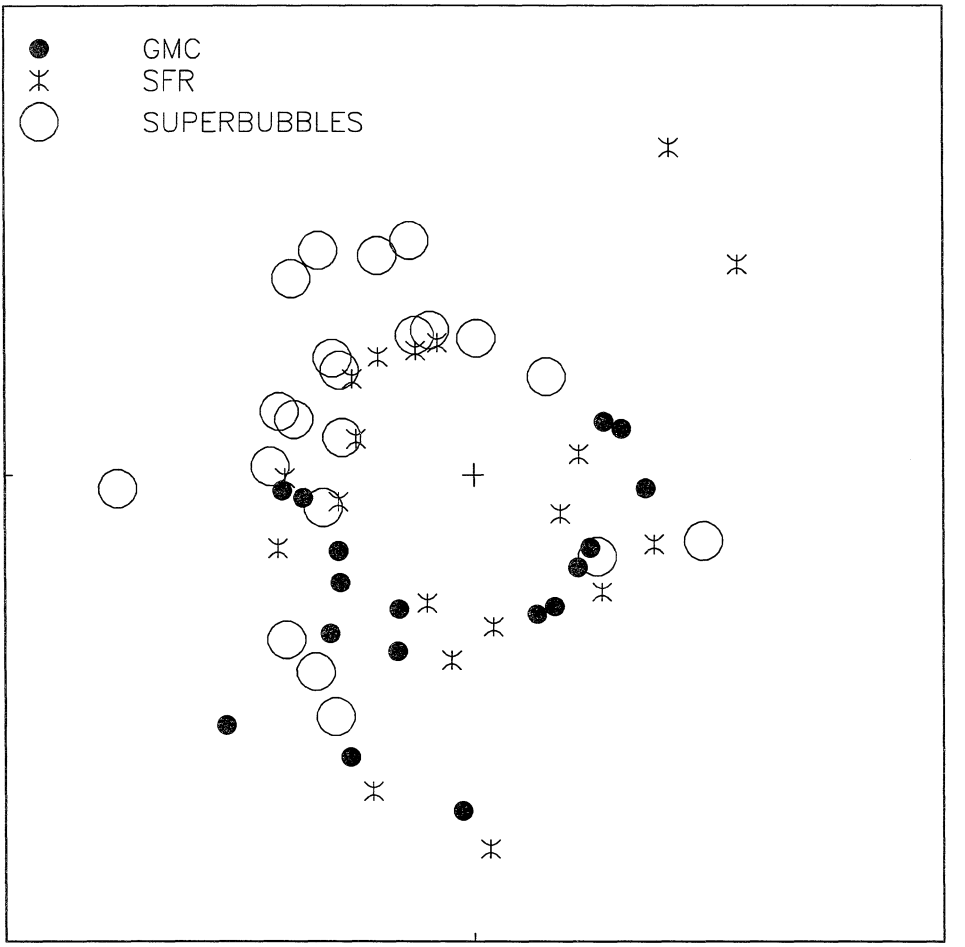

Figure 2. The self-propagating star formation model. The same as Fig. 1. 10 Gyr after the star formation was triggered in the galactic disc.

rate of non-axisymmetrical features. Without dissipation the system would rapidly become hot, stable and axisymmetric. Fortunately, the growing velocity dispersion also enhances the energy dissipation in the gaseous component decreasing its value to a critical level of marginal stability. Thus, the presence of the dissipative component keeps this mechanism in operation.

2) The mechanism related to the star formation inside the molecular clouds. The star formation heats the ambient medium prohibiting formation of further stars inside the same interstellar cloud. However, it also propagates to other places in the galaxy initiating further star formation there. This self-propagating star formation mechanism determines the galactic

star formation rate and it predicts its relation to the galactic rotation curve. This prediction should be compared with observations.

Acknowledgements

The project was supported through the grant No. 0090 of the Grant Agency of the Czech Republic.

References

Blaauw, A. (1991) *in The Physics of Star Formation and Early Stellar Evolution*, eds. C. J. Lada and N. D. Kylafis, Kluwer Academic Publishers, pp. 125 – 154
Blitz, L.(1991) in: *The Physics of Star Formation and Early Stellar Evolution*, eds. C. J. Lada and N. D. Kylafis, Kluwer Academic Publishers pp. 3 – 34
Burton, W. B. (1994) *in this proceedings*
Burton, W.B., Bania, T.M., Hartmann, D., Tang Yuan (1992) *in Evolution of Interstellar Matter and Dynamics of Galaxies*, eds. J. Palouš, W. B. Burton and P.O. Lindblad, Cambridge University Press, pp. 25 – 57
Comerón, F., Torra, J. (1992) *Astron. Astrophys.* 261, 94 – 104
Comerón, F., Torra, J. (1994) *Astron. Astrophys.* 281, 35 – 45
Comerón, F., Torra, J., Gómez, A.E. (1994) *Astron. Astrophys.* 286, 789 – 798
Dahlem, M., Dettmar, R.-J., Hummel, E. (1994) *Astron. Astrophys.*, in press
Elmegreen, B.G. (1993) *in Protostars and Planets III*, eds. E. H. Levy and J. I. Lunine, The University of Arizona Press, pp. 97 – 124
Elmegreen, B.G. (1994) *in Violent Star Formation from 30 Dor to QSOs*, ed. G. Tenorio-Tagle, Cambridge University Press, pp. 220 – 242
Elmegreen, B. G. (1994) *in The Gaseous and Stellar Disks of the Galaxy*, Astronomical Society of the Pacific Conference Series, ed. I. King, in press
Ehlerová, S., Jungwiert, B., Palouš, J. (1994) *in this proceedings*
Hartmann, D. (1994) *private communication*
Heiles, C. (1979) *ApJ*, 299, 533 – 544
Heiles, C. (1992) *in Evolution of Interstellar Matter and Dynamics of Galaxies*, eds. J. Palouš, W. B. Burton and P.O. Lindblad, Cambridge University Press, pp. 12 – 24
Jungwiert, B., Palouš, J. (1994) *Astron. Astrophys.* 287, 55 – 67
Koo, B-C. Heiles, C. and Reach, W.T. (1992) *ApJ*, 390, 108 – 132
Lindblad, P. O. (1980) *Mitt. Astron. Gesel.* 48, 151 – 159
Lindblad, P. O., Palouš, J. (1995) *in preparation*
Mueller, M. W., Arnett, W. D. (1976) *Astrophys. J.* 210, 670 – 678
Oort, J. H. (1954) *Bull. Astron. Inst. Neth.* 12, 177
Öpik, E. J. (1953) *Irish Astron. J.* 2, 219
Palouš, J. (1987) *in Evolution of Galaxies*, ed. J. Palouš, Publ. Astron. Inst. Czech. No. 69, pp. 209 – 216
Palouš, J. (1990) *IAU Symp. No. 144, Poster Proceedings*, ed. H. Bloemen, pp. 101 – 102 Palouš, J. (1989) *in Structure and Dynamics of the Interstellar Medium*, eds. G. Tenorio-Tagle, M. Moles, J. Melnik, Springer–Verlag, pp. 518 – 523
Palouš, J. (1993) *in Panchromatic View of Galaxies*, eds. G. Hensler, Ch. Theis, J. S. Gallagher, Editions Frontieres, pp. 325 – 328
Palouš, J., Franco, J., Tenorio-Tagle, G. (1990) *Astron. Astrophys.* 227, 175 – 182
Palouš, J., Jungwiert, B. (1995) *in preparation*
Palouš, J., Jungwiert, B., Kopecký, J. (1993) *Astron. Astrophys.* 274, 189 – 202
Palouš, J., Tenorio-Tagle, G., Franco, J. (1994) *Mon. Not. R. Astron. Soc.* 270, 72 – 92
Sanders, D. B., Scoville, N. Z. (1987) *in Evolution of Galaxies*, ed. J. Palouš, Publ. Astro.

Inst. Czech. No. 69, pp. 451 – 464
Scalo, J. M. (1990) *in Physical Processes in Fragmentation and Star Formation*, eds. R. Capuzzo-Dolcetta, C. Chiosi and A. Di Fazio, Dordrecht: Kluwer, pp. 151 – 177
Seiden, P. E., Gerola, H. (1982) *Fund. Cosmic. Physics* 7, 241 – 311
Schulman, L. S., Seiden, P. E. (1986) *Science*, 233, 425 – 431
Seiden, P. E., Schulman, L. S. (1990) *Advances in Physics* 39, 1 – 54
Silich, S. A., Franco, J., Palouš, J., Tenorio-Tagle, G. (1994a) *in Numerical Simulations in Astrophysics*, eds. J. Franco, S. Lizano, L. Aguilar, E. Daltabuit, Cambridge University Press, pp. 193 – 197
Silich, S. A., Franco, J., Palouš, J., Tenorio-Tagle, G. (1994b) *in Violent Star Formation*, ed. G. Tenorio-Tagle, Cambridge University Press, pp. 162 – 167
Stark, A. A. (1984) *Astrophys. J.* 281, 624 – 633
Tenorio-Tagle, G. (1980) *Astron. Astrophys.* 88, 61 – 65
Tenorio-Tagle, G. (1981) *Astron. Astrophys.* 94, 338 – 344
Tenorio-Tagle, G. (1994) *in Numerical Simulations in Astrophysics*, eds. J. Franco, S. Lizano, L. Aguilar, E. Daltabuit, Cambridge University Press, pp. 159 – 164
Tenorio-Tagle, G., Bodenheimer, P. (1988) *Ann. Rev. Astron. Astrophys.* 26, 145 – 197
Yorke, H.W., Spurzem, R., Kunze, R. (1992) *in Evolution of Interstellar Matter and Dynamics of Galaxies*, eds. J. Palouš, W.B. Burton and P.O. Lindblad, Cambridge University Press, pp. 222 – 233
Westin, T. N. G. (1985) *Astron. Astrophys. Suppl.*, 60, 99 – 134

THE STRUCTURE OF THE NEUTRAL INTERSTELLAR MEDIUM: A THEORY OF INTERSTELLAR TURBULENCE

ANTHONY WHITWORTH
Department of Physics and Astronomy,
University of Wales, Cardiff, CF2 3YB, Wales, U.K.

Abstract. We present a model for the development of density structure in the neutral interstellar medium. In this model, bulk kinetic energy is injected mainly at small scales, by jets and expanding nebulae generated by young and/or massive stars. Subsequently, this bulk kinetic energy propagates to, and is dissipated on, larger scales.

This is in contrast to standard (incompressible) Kolmogorov turbulence, where kinetic energy is injected at larger scales, then propagates to, and is dissipated on, smaller scales. The sense in which the Second Law of Thermodynamics drives the propagation of turbulent energy is reversed in the interstellar medium because virialized self-gravitating gas clumps and ensembles of clumps (clouds) have negative effective specific heat.

The model is able to explain Larson's relations (between the mass, size, and velocity-dispersion of molecular clouds and clumps; Larson 1981), the maximum masses of giant molecular cloud complexes, the velocity dispersions observed (at low resolution) in face-on spirals like the Milky Way, and the apparent scaling of the interstellar magnetic field with density.

1. Injection of turbulent energy into the interstellar medium by stars, and the generation of small-scale density structure by fragmentation of shells and layers

We assume that stars - in particular young and/or massive stars associated with jets, outflows and overpressured nebulae (HII regions, stellar wind bubbles, and supernova remnants) - are the main sources of bulk kinetic energy for the neutral gas in the interstellar medium. When a shell of dense gas is swept up by an expanding nebula, it eventually fragments

L. Blitz and P. Teuben (eds.), Unsolved Problems of the Milky Way, 591–596.
© 1996 *International Astronomical Union.*

gravitationally into clumps. Theoretical analysis (Whitworth et al. 1994) shows that, irrespective of local details, (i) the column-density of hydrogen nuclei (in all forms) through the shell at this stage is always close to the canonical value $N \sim 6 \times 10^{21} cm^{-2}$ (corresponding to a visual optical depth $\tau_V \sim 3$), and (ii) the masses of the clumps depend strongly only on the effective sound speed a_{eff}, *viz.* $M \propto a_{eff}^{\alpha}$ where $\alpha \sim 3.5 - 3.8$. Since we expect $a_{eff} \sim 0.2 - 2.0\, kms^{-1}$, clumps are created with a range of masses $5 - 5000 M_{\odot}$, but all having approximately the same column-density. If clumps formed in this way can virialize without significant dissipation, they will subscribe to Larson's relations in the form

$$R \sim 0.07\, pc\, (M/M_{\odot})^{\beta} \qquad \beta \simeq 0.5 \tag{1}$$

$$\Delta v \sim 0.24\, kms^{-1}\, (M/M_{\odot})^{\gamma} \qquad \gamma \simeq 0.25 \tag{2}$$

where R is the radius of a clump, and Δv is the velocity dispersion within a clump.

Moreover, if two such clumps collide supersonically and the resulting radiative shock produces a dense layer which has smaller internal velocity dispersion than the two original clumps, the layer will fragment gravitationally thereby generating even smaller clumps. These clumps will at their inception also have the canonical surface density; and if they virialize without too much dissipation, they will also subscribe to Larson's relations.

We conclude that the interaction between stars and the interstellar medium can inject turbulent energy into the interstellar medium and deliver density structure obeying Larson's relations, on small-to-medium scales, $< 10^4 M_{\odot}$, provided virialization occurs without too much dissipation. We now argue that this turbulent energy and density structure should evolve mainly by propagating to larger scales.

2. The consequences of the 2nd Law of Thermodynamics for the propagation and amplification of turbulent energy in an ensemble of self-gravitating gas clumps

Since the effective temperature of an ensemble of clumps (as determined by their mean random kinetic energy) greatly exceeds the effective temperature of the ambient radiation field (as determined by the mean density of electromagnetic radiation), the 2nd Law of Thermodynamics requires the ensemble of clumps to evolve in the sense which entails a net loss of heat to the ambient radiation field, *i.e.* radiative cooling. We demonstrate below that this requirement promotes an evolution in which small clumps more often amalgamate to form larger ones than *vice versa*.

To be specific, consider a virialized clump of mass M and radius R. Its self-gravitational potential energy is $-\zeta_1 GM^2/R$, (where ζ_1 is a factor of

order unity which depends on the detailed density profile of the clump). Since the clump is virialized, its net energy is half this.

Now suppose that we have a virialized ensemble of such clumps with filling factor f_{vol}, and consider the energy budget of two nearest-neighbor clumps. The bulk kinetic energy of the pair (relative to their mutual center of mass) is $f_{vol}^{(1-\beta)/(1-3\beta)}GM^2/2R$. Their mutual gravitational potential energy is $-(3f_{vol}/4\pi)^{1/3}\zeta_2(f_{vol})GM^2/R$, (where $\zeta_2(f_{vol})$ is a function which accounts for tidal interaction between the clumps and approaches unity for small values of f_{vol}.

Finally suppose that these two clumps amalgamate to form a single clump having mass $2M$, radius $2^\beta R$, and net energy $-\zeta_1 2^{1-\beta}GM^2/R$. The net energy which must be radiated away is then

$$Q = \left[\zeta_1\left(2^{(1-\beta)} - 1 + \frac{1}{2}f_{vol}^{(1-\beta)/(1-3\beta)}\right) - \left(\frac{3f_{vol}}{4\pi}\right)^{1/3}\zeta_2(f_{vol})\right]\left[\frac{GM^2}{R}\right] \tag{3}$$

Amalgamation will be the dominant sense of evolution, provided $Q > 0$, *i.e.* provided β is small (clump radius does not increase too rapidly with increasing mass) and f_{vol} is small (nearest-neighbor clumps are well separated). Observations indicate that $\delta \sim 0.5$ and that $f_{vol} \sim 0.1$; setting $\zeta_1 = \zeta_2 = 1$, these values give $Q \sim 5.13(GM^2/R)$, implying that amalgamation is thermodynamically favored over fragmentation. If we neglect the bulk kinetic energy term completely (on the assumption that the velocities of nearest neighbors are perfectly correlated), we still obtain $Q \sim 0.13(GM^2/R)$, and so amalgamation is still the thermodynamically preferred sense of evolution. Even with perfectly correlated velocities, the combinations of β and f_{vol} which must be invoked to make Q negative are untenable.

Additionally, since $dln[\Delta v]/dln[M] > 0$, amalgamation amplifies the turbulent energy. We refer to this as gravitational amplification. In other words, gravitational energy is being released both to compensate the dissipative losses going into radiation, and to increase the turbulent kinetic energy.

Basically, the negative specific heat of a virialized system means that loss of heat entails an increase in both the internal random (*i.e.* turbulent) kinetic energy and the binding energy (*i.e.* the modulus of the self-gravitational potential energy). The observed low filling factor for clumps and the observed relatively slow decline in mean clump-density with increasing clump-mass then necessitate that the turbulent energy injected into the interstellar medium on relatively small scales propagates to larger scales by amalgamation and in so doing is amplified by gravity. This is in

direct contrast to the theory of gravitational virialization proposed by Scalo & Pumphrey (1982), where clumps break up into smaller clumps.

3. Cosmic opacity and the elastic limit of interstellar gas

The lack of low-energy resonance transitions in the two most abundant atomic species in the Universe (H & He) means that the coupling between diffuse gas and radiation at low temperatures $T < T_R \sim 10^4 K$ is much weaker than at higher temperatures. At higher densities, hydrogen is mainly molecular, but even then the coupling is much weaker below $T_R \sim 3000 K$ than above. In effect, the opacity of the interstellar medium, and hence its ability to cool radiatively, increase rather abruptly as the temperature rises above T_R. The upshot is that high-velocity shocks ($v > v_R \sim 10\, kms^{-1}$) which raise the temperature of the gas above T_R will be significantly more dissipative than slower shocks. In other words v_R corresponds to an abrupt decrease in the elasticity of the interstellar medium.

[In passing, we note that this same fundamental microphysical property of cosmic matter can be held responsible for a great diversity of universal phenomena, including the origin of the cosmic microwave background and the closeness of its spectrum to that of a blackbody, thermostatic control of primordial gas in galaxy and cluster formation (Hoyle 1955), the Hayashi limit of stellar surface temperatures (Hayashi 1961), and the distribution of binary star periods (Whitworth 1994).]

4. Dissipation of turbulent energy in an ensemble of self-gravitating gas clumps, the maximum mass for giant molecular cloud complexes, and the HI velocity dispersions in face-on spiral galaxies.

The abrupt decrease in the elasticity of the interstellar medium for shock speeds exceeding v_R suggests that there is a large range of values for the rate of injection of turbulent energy into the interstellar medium over which the turbulent energy is amplified gravitationally to, but not beyond, speeds of order v_R. Substituting $\Delta v \sim v_R$ in Eqs. (2) and (1), we obtain a maximum mass $M_{max} \sim 3 \times 10^6 M_\odot$, and a maximum radius $R_{max} \sim 100\, pc$, which agree well with the values for the largest giant molecular cloud complexes observed in the Milky Way. The inference is that in these extreme complexes gravitational amplification of turbulent energy terminates because the shock velocities start to exceed v_R, and therefore become more dissipative. Presumably complexes which attempt to evolve beyond this limit undergo a disruptive episode of violent self-propagating star formation, thereby returning the residual interstellar matter to the low end of the clump mass-spectrum.

For the same reason, isolated face-on spiral galaxies observed in HI or CO, at sufficiently low resolution to sample a macroscopic portion of their interstellar media, should have velocity dispersions of order v_R at all radii. Figure 10 in Shostak & van der Kruit (1984) and Figure 10 in van der Kruit & Shostak (1984) present observations of the galaxies NGC 628 and NGC 1058 which clearly support this suggestion.

5. Shock dissipation as the the process limiting turbulent amplification of the interstellar magnetic field, and the apparent scaling of the field with density

We assume that interstellar and circumstellar magnetic fields are generated and sustained by turbulent dynamos, and that when the process operates efficiently the field is amplified to equipartition with the turbulence, so that the Alfvén speed $v_A = (4\pi\rho)^{-1/2}B$ (where the symbols have their usual identities) is comparable with the turbulent speed. As long as the process injecting turbulent energy has a coherence time-scale much longer than the ion-neutral coupling time-scale, dissipation of turbulence will be dominated by radiative shocks, and for a wide range of injection rates will set in at shock speeds of order v_R. Consequently, the largest magnetic fields observed in interstellar and circumstellar gas are likely to have $v_A \sim v_R$ or equivalently

$$B_{||} \sim (64\pi k T_R \rho/9 < m >)^{1/2} \sim C(n/cm^{-3})^{1/2} \qquad (4)$$

where $B_{||}$ is the line-of-sight component of the magnetic field, and n is the number-density of hydrogen nuclei in all forms.

Figure 1 reproduces the observational results of Fiebig & Gusten (1989), along with Eq. (4). For predominantly atomic gas, at low densities $n < 10^3 cm^{-3}$, with $T_R \sim 10^4 K$ and $< m > \sim 2.1 \times 10^{-24} g$, we have $C \sim 5.5$ microgauss. For predominantly molecular gas, at high densities $n > 10^3 cm^{-3}$, with $T_R \sim 3000 K$ and $< m > \sim 3.5 \times 10^{-24} g$, we have $C \sim 2.5$ microgauss. We see that the theoretical relationship provides a tight upper limit to the observational points.

We emphasize that the gas in which turbulent dynamo amplification of the magnetic field occurs does not have to be self-gravitating, and indeed in the circumstellar OH and H_2O maser sources contributing to Figure 1 it is most unlikely to be. Observations pertaining to self-gravitating gas are confined to the density range $10^2 - 10^4\, cm^{-3}$, where the scaling relation is not well defined. Therefore it is important to stress that we have not in this section invoked virialization.

Also, the observations may well select only the largest fields, because these are the most easily detected. In this case the inference is that these are

the only places where the injection of turbulent energy has been sufficiently vigorous to reach speeds of order v_R.

References

Fiebig, D. and Güsten, R. (1989), *Astron. & Astrophys.*, 214, 333
Hayashi, C. (1961), *Publs. astron. Soc. Japan, 13*, 450
Hoyle, F. (1953), *Astrophys. J.*, 118, 513
Larson, R.B. (1981), *Mon. Not. Roy. astron. Soc.*, 194, 809
Scalo, J.M. and Pumphrey, W.A. (1982), *Astrophys. J.*, 258, L29
Shostak, G.S. and van der Kruit, P.C. (1984), *Astron. & Astrophys.*, 132, 20
van der Kruit, P.C. and Shostak, G.S. (1984), *Astron. & Astrophys.*, 134, 258
Whitworth, A.P., (1994) *in preparation*
Whitworth, A.P., Bhattal, A.S., Chapman, S.J., Disney, M.J. and Turner, J.A. (1994), *Mon. Not. Roy. astron. Soc.*, 268, 291

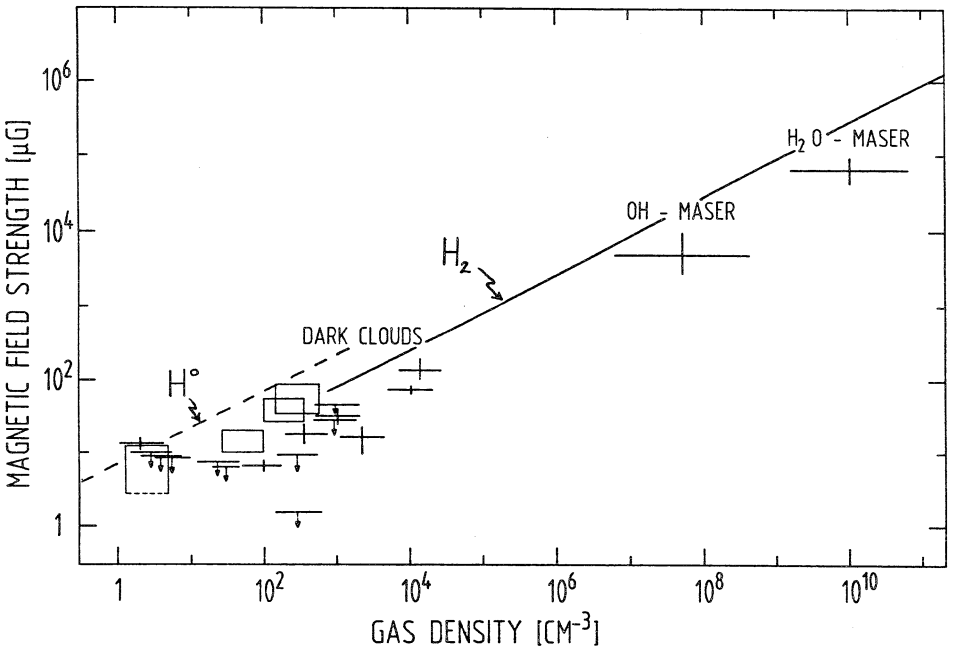

Figure 1. The variation of magnetic field strength with density, from Fiebig & Güsten (1989). The lines are the upper limits predicted by Eq. [4]. See text for details.

ARE THERE GIANT VORTICES NEAR SOLAR CIRCLE?

A.M. FRIDMAN, O.V. KHORUZHII, V.V. LYAKHOVICH AND V.S. AVEDISOVA
Institute of Astronomy, Russian Academy of Sciences
48 Pyatnitskaya St., Moscow, 109017, Russia

Abstract. The analysis of the observational line-of-sight radial velocity field of molecular clouds, connecting with young stars, has strengthened the Fridman's hypothesis (1994) on the possible existence of anticyclone in the solar neighborhood. Anticyclones are located near corotation radius of the observed spiral arms, a number of which is equal to a number of vortices. Our calculations show that the four-vortices model fits observational data fairly well.

We shall not use any theoretical conception on the nature of spiral arms generation (bar, selfgravitational or hydrodynamical mechanisms, etc.). We shall base on the treatment of the observational data.

1. Data

The observational velocity field in the visible solar neighborhood was constructed on the basis of the photometric distances to the hot stars, exciting the diffuse nebula, and the radial velocities of the molecular clouds, connecting with these nebula. For a distance determination, r, we used all available new data, concerning the photometry and spectral classification of the stars. In particular new measurements of UBV and spectral classification of LS catalogue stars were used, and also associations of HII regions with open clusters for more than 90 star forming regions. Absolute magnitudes have been derived with common calibration curve (Landolt-Bornstein, 1982). Almost all BBW nebula with distances determined by Brand and Blitz (1993) were included in the sample. The radial velocity, V_{lsr}, have been taken from the Catalogue of observational data in the galactic star-forming regions (Avedisova 1994). Fig. 1 shows the radial line-of-sight velocity field of 316 objects.

L. Blitz and P. Teuben (eds.), Unsolved Problems of the Milky Way, 597–603.
© 1996 *International Astronomical Union.*

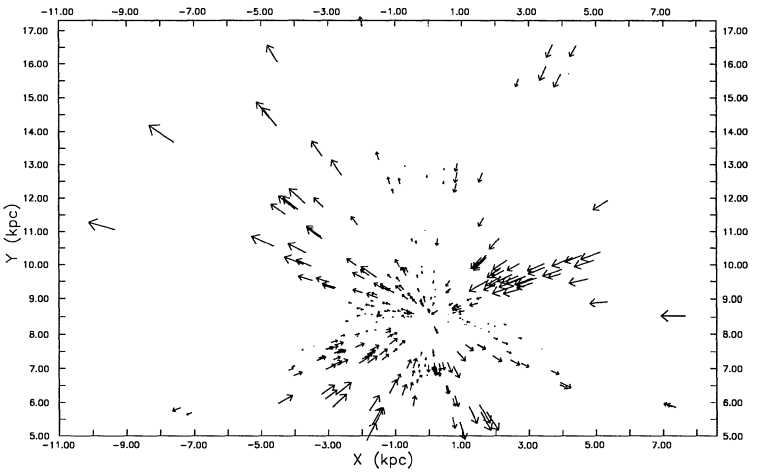

Figure 1. Line-of-sight radial velocity field of the sample of 316 objects. The Sun is at (0,8.5)

2. Model of pure circular orbits

Assuming pure circular orbits for the gas and stars, the circular rotation velocity, Θ_c, of any object with known galactocentric distance R and radial velocity V_{lsr} (Brand and Blitz 1993) is equal to

$$\Theta_c = \frac{RV_{lsr}}{R_0 \sin l \cos b} + \frac{\Theta_0 R}{R_0} \qquad (1)$$

where R_0 and Θ_0 are the galactocentric distance of the Sun and the circular rotation velocity at the position of the Sun; l and b are the galactic longitude and latitude. Below we take $R_0 = 8.5$ kpc., $\Theta_0 = 220$ km/s. Substituting our data in the right hand of (1) we find Θ_c as triangles in Figs.2-3.

3. Systematic deviations from the pure circular motion

If to overlap the rotation curve of the Northern Hemisphere (Fig. 2a) on the Southern one (Fig. 2b) we can see some discrepancy between them. Fig. 3a shows that in the azimuth range $5^o < \theta < 15^o$ cloud motions deviate from a circular rotation the most strongly. Fig. 3b shows that in the galactocentric region 9 kpc $< R <$ 11 kpc the cloud motion deviate from the circular rotation strongly. From Figs. 2-3 it follows that the strongest influence on the cloud motions is exerted by the Perseus arm. That is well known result (Burton 1966; Shane & Bieger-Schmith 1966; Rickard 1968; Kerr 1969; Humphereys 1970,1976; Brand and Blitz 1993).

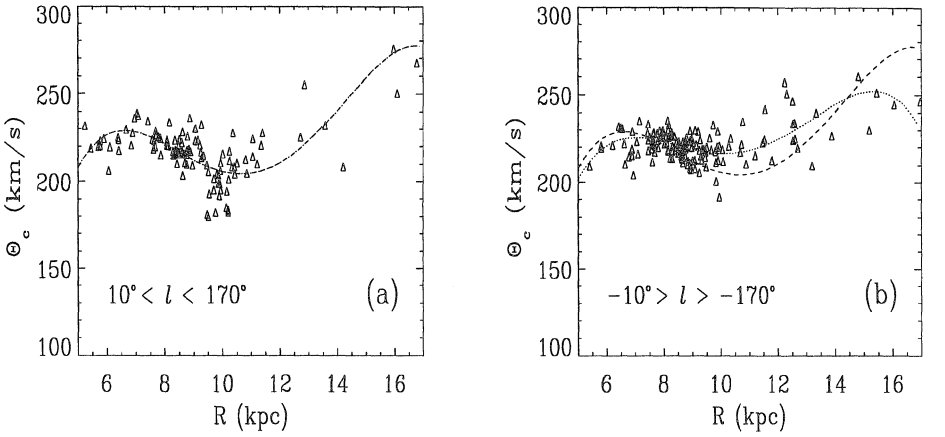

Figure 2. The circular rotation velocity Θ_c as a function of the galactocentric distance R for objects of the Northern (a) end Southern (b) Hemispheres. There are differences between the Northern (broken line) and Southern (dotted line) rotation curves

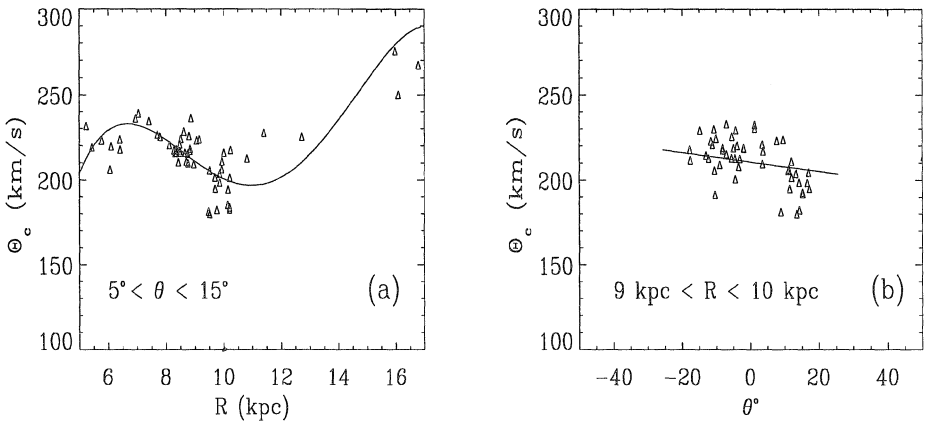

Figure 3. The circular rotation velocity Θ_c as a function of (a) the galactocentric distance R for the range of galactocentric azimuth $5^o < \theta < 15^o$, (b) the azimuth θ for the range of galactocentric distances 9 kpc $< R <$ 10 kpc

The average velocity in the direction of the galactic center ($-10^o < l < 10^o$) in the region of the Sagittarius-Carina arm is equal to $\Pi' \equiv \Pi - \Pi_0 = (-7.4 \pm 1.3)$ km/s, where Π and Π_0 are the radial galactocentric velocity of objects and LSR, respectively. The same value according to Avedisova (1986) is $\Pi' = (-6.9 \pm 2.2)$ km/s. In the anticenter direction ($170^o < l < 190^o$) in the region of the Perseus arm that is $\Pi' = (-4.4 \pm 1.7)$ km/s. The last value according to Velden (1970) is $\Pi' \approx -3.3$ km/s, Stark (1984) $\Pi' = (-3.1 \pm 1.0)$ km/s, Brand and Blitz (1993) $\Pi' = (-3.8 \pm 1.8)$ km/s.

And so we can see that the systematic deviations from the pure circular motion correlate with the location of the spiral arms. Therefore we try to explain all observed features on the base of the model which combines a circular rotation and motion in the spiral arms.

4. The average motion of clouds consists of the circular rotation and motion in spiral arms

The average (without a dispersion) motion of clouds is described by the following equation

$$\frac{V_{lsr}}{\cos b} = \left(\frac{\Theta}{R} - \frac{\Theta_0}{R_0}\right) R_0 \sin l - \frac{\Pi}{R}\left(R_0 \cos l - d\right) + \Pi_0 \cos l \qquad (2)$$

Formula (2) coincides with formula (14) of the Chapt.4 from Rohlfs (1977) (see Fig. 9), if we change $V_{lsr}/\cos b = v_r$ and $d/\cos b = r$.

Assume that the average velocity field is the superposition of the differential rotation of the Galaxy and motion in spiral waves (see Rohlfs 1977, Chapt.7 Eqs(12-13))

$$\begin{aligned} \Theta &= \Omega(R)R + A_\Theta(R)\cos(-m\Theta + F_\Theta(R)), \\ \Pi &= A_\Pi(R)\cos(-m\Theta + F_\Pi(R)) \end{aligned} \qquad (3)$$

where Ω is the average angular velocity of the rotation, A_Θ, A_Π and F_Θ, F_Π are amplitudes and phases of the azimuthal and radial velocities in spiral waves, respectively, m is number of spiral arms.

All parameters of our model were obtained by means of least-squares method (e.g. Eichhorn and Clary 1974, Jefferys 1981). In this paper we give results for m=4, which is consistent with four-arms structure of the Galaxy (see Blitz 1983, Malahova and Petrovskaya 1992).

5. The radial motion of LSR and consequence of it

In our model we obtained $\Pi_0 \approx 5$ km/s, that is consistent with that obtained by Fich et al., (1989), Brand and Blitz (1993), Fuchs, et al., (1994).

Taking into account the value Π_0 we can change from LSR frame to the galactocentric frame of reference. So we obtain, that the average velocity

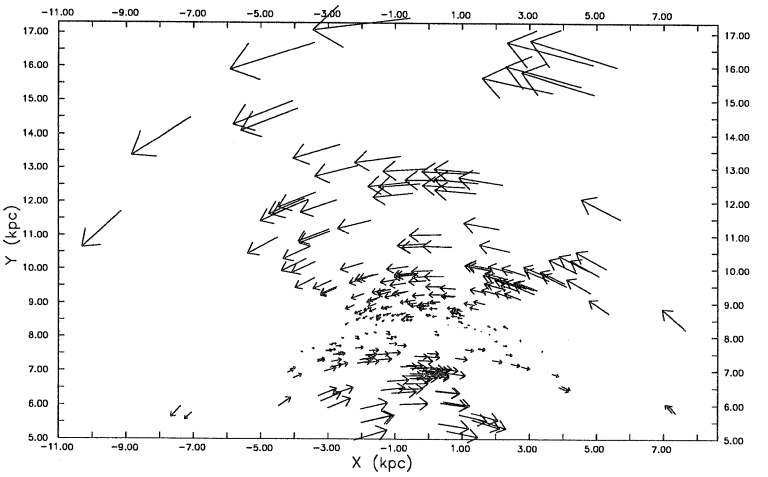

Figure 4. The full velocity field of the clouds has the form of a anticyclone with the center in the solar vicinity

$\Pi = \Pi' + \Pi_0$ in the direction of the galactic center in the region of the Sagittarius-Carina arm is equal to $\Pi \approx -2$ km/s, and in the direction of the anticenter in the region of the Perseus arm is equal to $\Pi \approx +1$ km/s.

What does it mean that we obtained the value Π with different signs for different arms?

It means that there is the corotation in the solar vicinity. Indeed, from a linear theory of spiral waves with a small pitch angle in WKB-approximation (e.g. Rohlfs 1977) we have $\Pi = -(\omega - m\Omega)\rho_1/(k\rho_0)$, where ρ_1 is the perturbation density. For trailing arms $k < 0$, $\rho_1 > 0$ we have

$$\Pi = \begin{cases} > 0, & \Omega < \omega/m, \quad R > R_c \\ < 0, & \Omega > \omega/m, \quad R < R_c \end{cases} \tag{4}$$

where R_c is the corotation radius $(\omega - m\Omega(R_c) = 0)$.

Let us show how the range of the corotation radius values depends on the range of the values Π_0:

if	$\Pi_0 < 4$ km/s	then	$R_c > 11$ kpc,
if	$\Pi_0 = 4 - 7$ km/s	then	$R_c = 11 - 7$ kpc,
if	$\Pi_0 > 7$ km/s	then	$R_c < 7$ kpc.

Fig. 4 shows the velocity field model in the system which rotates with the angular velocity of the LSR. The full vector velocity field of clouds has the form of a anticyclone with the center near the solar vicinity and between spiral arms. This picture of the velocity field qualitatively looks like that was obtained by Fuchs et al., (1994) where data of proper motions

(from PPM catalogue for objects by Brand and Blitz (1993)) were used. If the corotation radius is near the Solar distance then this anticyclone is stationary.

6. Position of anticyclone centers with respect to spiral arms

The positions of anticyclone centers with respect to spiral arms depends on the nature of the spiral generation (Lyakhovich et al., 1994). In the Table 1 we show positions of vortex centers in the observed case when $\kappa^2/2\Omega \equiv 2\Omega(R) + Rd\Omega(R)/dR > 0$, where κ is the epicyclic frequency. The first and second lines show the positions of vortex centers in the cases when a force of hydrodynamic pressure dominates a selfgravitation force and vice versa. The third line corresponds to the case when a gaseous disk is perturbed by some external perturbed force (e.g. a bar, stellar spirals, a satellite, etc.). So the location of vortex centers points to the generation mechanism of spiral arms.

TABLE 1. Centers of anticyclons

hydrodynamic	on spiral arms
selfgravitation	between spiral arms
External perturbing gravitational potential	centers of vortices have intermediate position

In our case the position of the vortex center shows that the selfgravitation force dominates the force of hydrodynamic pressure. The center of the anticyclone show a possibility of the existence of a bar structure or non-axisymmetric gravitational potential in the Milky Way.

7. Conclusion

1. Near the corotation region of the observed spiral structure, anticyclones must exist independently on the nature of the generation of spiral arms.

2. The number of anticyclones is equal to the number of spiral arms.

3. Azimuthal position of the anticyclone centers with respect to spiral arms depends on the nature of spiral generation.

4. If hydrodynamical force dominates, centers of anticyclones are located on the arms. If self-gravitating force dominates, centers of anticyclons are located between arms. Intermediate position of anticyclone centers is possible if the spiral structure is generated by external force (e.g. by a bar).

5. If the radial galactocentric velocity of LSR is in the range of 4-7 km s^{-1}, the corotation radius of the observed spiral structure lies near the solar circle.

6. The systematic deviations from the pure circular motion are observed in the solar vicinity. These deviations correlate with the location of the spiral structure.

7. The model velocity field combined the circular rotation and the motion in spiral arms describes all main peculiarities of velocity field observed in the solar vicinity.

8. In the model the anticyclone center lies near the solar vicinity.

Acknowledgements

We thank the Russian Fund of Fundamental Investigations (grant 93-02-17248) for financial support.

References

Avedisova V. S. (1994) Catalogue of observational data in galactic star-forming regions, Version 1.2 (in preparation).
Avedisova V. S. (1986) Sov. Astron. Lett. 11, 6, 378.
Blitz, L. (1983) In "Surveys of the Southern Galaxy", eds. W.B.Burton and F.P.Israel, Dordrecht, 117.
Brand, J. and Blitz, L., (1993) Astron. Asrophys. 275, 67.
Burton, W.B. (1966) Bull. Astron. Inst. Neth. 18, 247.
Fridman, A.M. (1994) In "Physics of the Gaseous and Stellar Disks of the Galaxy", ed. I.R.King, Astron. Soc. of the Pacific, 66, 15.
Fich, M., Blitz, L., Stark, A.A., (1989) ApJ 342, 272.
Fuchs, B., Frink, S., Röser, S., Wielen, R. (1994) Proceedings of the IAU Symposium 169 "Unsolved Problems of the Milky Way" held in Den Haag, the Netherland, 25-28 August.
Humphereys, R.M. (1970) AJ 75, 602.
Humphereys, R.M. (1976) ApJ 206, 114.
Jefferys, W. H., Astron. J. (1981) 86, 149.
Kerr, F.J. (1969) ARA&A 7, 39.
Landolt-Bornstein (1982) Numerical Data and Functional Relationships in Science an Technology, New Series, Group VI, 2, pp.15-18; 451; 453-455.
Lyakhovich, V.V. Fridman, A.M., Khoruzhii, O.V., (in preparation).
Malahova, Yu.N., Petrovskaya, I.V. (1992) Astron. and Astroph. Transactions, 1, 221.
Eichhorn, H.K. and Clary, W.G. (1974) Mon. Not. R. Astron. Soc. 166, 425.
Rohlfs, K. (1977) Lectures on density wave theory, Springer-Verlag, Berlin, Heidelberg, New York.
Rickard J.J. (1968) ApJ 152, 1019.
Shane, W.W., Bieger-Schmith, G.P. (1966) Astron. Inst. Neth. 18, 263.
Stark A.A. (1984) Ap. J. 281, 624.
Velden L. (1970) IAU Symp. 38, 164.

DISTANCE AND METALLICITY OF HVCS

B.P. WAKKER
University of Illinois, Urbana, USA
H. VAN WOERDEN, U.J. SCHWARZ AND R.F. PELETIER
Kapteyn Institute, Rijks Universiteit Groningen, NL
N.G. DOUGLAS
Kapteyn Institute, Rijks Universiteit Groningen, NL
AND
L. DANLY AND K.S. DE BOER
STScI, Baltimore MD, USA; Universität Bonn, Germany

Table 1 summarizes results of programs to determine distances and metallicities of high-velocity clouds (HVCs, see Wakker 1991, IAU Symp 144, 27 for a general review). Reliable absorption is reported for one stellar probe (BD+38 2182), giving a distance $D<5$ kpc for complex M. Other results are controversial (BT Dra), uncertain(HD 135485) or atypical (4 Lac). Non-detections reported by e.g. Lilienthal et al. (1990, A&A 240, 287), Danly et al. (1992, ApJS 81, 125) and de Boer et al. (1994, A&A 286, 925), yield lower limits up to 2 kpc for complexes A, C and M. Absorption by heavy elements in HVCs is reported for twelve extra-galactic probes. All absorptions reported in HVCs with $|v_{\rm LSR}|>90$ km/s are given in the table (abundances are from low-resolution H I data and thus uncertain).

With the UES on the WHT at La Palma we observed PG 1351+640. This QSO ($V=14.5$) lies projected between HVCs C III B and C III C. Absorption in the Ca H- and K-lines is detected at the HVC's H I velocity of $v_{LSR}\sim-150$ km/s. Data on elements other than Ca will be necessary to measure the actual heavy element content. Also, high-resolution H I data are required to reduce the uncertainties.

Mg II $\lambda\lambda$2796 and 2803 Å spectra were taken with the GHRS on HST for two probes of complex A. Absorption was not found in PG 0859+596 (BHB star; $B=15.9$; distance $\sim$5.5 kpc), nor in PG 0906+597 (sdB star; $B=15.2$; distance $\sim$2.5 kpc). This tentatively suggests that complex A is more distant than 5.5 kpc. This result awaits confirmation by: 1) a HST Mg II spectrum

L. Blitz and P. Teuben (eds.), Unsolved Problems of the Milky Way, 605–606.
© 1996 *International Astronomical Union.*

(still pending) of the Seyfert Mark 106; 2) high-resolution H I data; 3) a good determination of the stellar distances using intermediate-resolution spectroscopy.

TABLE 1. Detections of absorption lines in HVCs

Probe	type	HVC	Ref	v_{HVC}	$N_{H\,I}$	ion	N_{ion}	A[a]	Note
Mark 106	Sey	complex A	1	−157	$4.0{\cdot}10^{19}$	Ca^+	$6.7{\cdot}10^{11}$	0.007	
I Zw 18	dIrr	complex A	2	−165	$2.1{\cdot}10^{19}$	O	$2.9{\cdot}10^{15}$	0.16	
			2	−165	$2.1{\cdot}10^{19}$	Si^+	$6.6{\cdot}10^{13}$	0.07	
PG 1351+640	QSO	complex C	3	−154	$1.9{\cdot}10^{19}$	Ca^+	$5.7{\cdot}10^{11}$	0.014	1
PG 1259+592	QSO	complex C	4	−127	$6.2{\cdot}10^{19}$	Mg^+	—	—	2
Mark 205	Sey	complex C	5	−214	$1.9{\cdot}10^{19}$	Mg^+	$1.5{\cdot}10^{12}$	0.002	3
				−152	$1.4{\cdot}10^{18}$	Mg^+	$2.5{\cdot}10^{12}$	0.05	3
3C 351	QSO	complex C	4	−180	$9.0{\cdot}10^{18}$	Mg^+	—	—	2
BT Dra	RR Lyr	complex C	6	−136	$3.1{\cdot}10^{18}$	Ca^+	$6.0{\cdot}10^{11}$	0.09	4
			7	−133	$3.1{\cdot}10^{18}$	Na	$<1.5{\cdot}10^{10}$	<0.002	4
BD+38 2182	B3	complex M	8	−90	$3.5{\cdot}10^{18}$	Si^+	$>2.0{\cdot}10^{13}$	>0.16	5
PG 0043+039	QSO	Mag. Str.	4	−348	$1.9{\cdot}10^{18}$	Mg^+	$>9{\cdot}10^{12}$	>0.12	2
PKS 2251+11	QSO	Mag. Str.	4	−374	$4.8{\cdot}10^{18}$	Mg^+	$>1.1{\cdot}10^{13}$	>0.059	2
3C 454.3	QSO	Mag. Str.	4	−397	$1.2{\cdot}10^{18}$	Mg^+	$>1.5{\cdot}10^{13}$	>0.32	2
Fairall 9	QSO	Mag. Str.	9	+195	$2.0{\cdot}10^{20}$	Ca^+	$2.0{\cdot}10^{12}$	0.004	
HD 135485	B5 II	complex L	10	−98	$1.0{\cdot}10^{18}$	Ca^+	$1.5{\cdot}10^{11}$	0.07	6
4 Lac	B9Ia	100−7+100	11	+104	$3.0{\cdot}10^{18}$	Mg^+	$3.2{\cdot}10^{14}$	∼3	7
PKS 0837+12	QSO	242+17+106	12	+105	$1.4{\cdot}10^{19}$	Ca^+	$2.2{\cdot}10^{12}$	0.07	
NGC 3783	Sey	287+22+240	13	+240	$1.2{\cdot}10^{20}$	Ca^+	$5.5{\cdot}10^{11}$	0.002	
			14	+240	$1.2{\cdot}10^{20}$	S^+	$3.4{\cdot}10^{14}$	0.15	
			14	+240	$1.2{\cdot}10^{20}$	Si^+	$>2.6{\cdot}10^{13}$	>0.006	

[a] Abundance relative to solar abundance

REFERENCES: 1. Schwarz, Wakker, van Woerden 1994, accepted by A&A; 2. Kunth, Lequeux, Sargent, Viallefond 1994, A&A 282, 709; 3. Wakker et al. 1994 (this paper); 4. Savage et al. 1993, ApJ 413, 116; 5. Bowen, Blades 1993, ApJ 403, L55; 6. Songaila, Cowie, Weaver 1988, ApJ 329, 580; 7. Songaila, York, Cowie, Blades 1985, ApJ 293, L15; 8. Danly, Albert, Kuntz 1993, ApJ 416, L29; 9. Songaila 1981, ApJ 243, L19; 10. Albert, Blades, Morton, Lockman, Proulx, Ferrarese 1993, ApJS 88, 81. 11. Bates, Catney, Keenan 1990, MNRAS 242, 267; 12. Robertson, Schwarz, van Woerden, Murray, Morton, Hulsbosch 1991, MNRAS 248, 508; 13. West, Pettini, Penston, Blades, Morton 1985, MNRAS 215, 481; 14. Lu, Savage, Sembach 1994, ApJ 426, 563;

NOTES: 1. Preliminary value for N_{Ca}; 2. No column densities because of low velocity resolution (220 km/s); 3. Corrected values for N_{ion}; A recent WSRT map indicates N_{HI} may be $<2{\cdot}10^{18}$; 4. Disputed detections, probably spurious; 5. From line wings; detections of O and C^+ also reported; stellar distance 5 kpc; 6. Distance to star 2.4 kpc; may be circumstellar; 7. Results also given for Fe^+, Mg, O and Al^+; HVC not in the Dwingeloo survey, diameter $<<1°$; distance to star 1.2 kpc.

MOLECULAR MASS DISTRIBUTION IN THE OUTER GALAXY

SEAN J. CAREY
Rensselaer Polytechnic Institute, Troy, NY, 12180, USA
carey@charon.phys.rpi.edu

AND

KATHRYN N. MEAD AND MARC L. KUTNER
NRAO, Tucson, AZ, USA

1. Introduction

The extent and nature of molecular material in the outer Galaxy ($R > R_\odot$) has been an open, interesting question since the discovery of molecular material in the outer Galaxy (Kutner & Mead, 1981). From large scale CO surveys, two estimates of the total molecular mass have been made with the same result, $M(H_2) = 6 \times 10^8\ M_\odot$ (Wouterloot *et al.*, 1990), (Digel *et al.*, 1990). Both estimates have a strong bias towards large, star forming (warm) clouds. Wouterloot *et al.* used the IRAS point source catalog as a finder chart for their observations and the inner Galaxy mass distribution to scale their result. Digel *et al.* conducted an unbiased survey with a large (8.8 arcminute) beam which underestimated the amount of material in small clouds due to the effects of beam dilution.

Recent observations by Lequeux *et al.* (1993) have spurred interest in the amount of molecular material contained in small, cold molecular clouds. Their results based on CO absorption measurements along 2 lines of sight indicate the presence of cold molecular gas. However, their suggestion that cold molecular gas is 4-5 times more abundant than HI in the outer Galaxy is based on the tenuous assumption that the ratio of molecular to atomic column densities at a particular velocity is indicative of the ratio for all $R > R_\odot$ (Peters & Bash, 1987).

We have recently completed the most sensitive survey to date in ^{12}CO ($J = 1 \rightarrow 0$) for $R > R_\odot$ using the NRAO 12 m (Carey *et al.*, 1994). Two cloud populations, arm (at $R \sim 13$ kpc) and interarm, have been identified. The data provide us with an unbiased probe of the small and/or cold

L. Blitz and P. Teuben (eds.), Unsolved Problems of the Milky Way, 607–608.
© 1996 *International Astronomical Union.*

molecular cloud component. For the range of galactocentric radii covered, 9 kpc < R < 16 kpc, our survey is complete for clouds with $T_K \geq 5$ K and r ≥ 2 pc.

2. Correction to Total Mass Determination

Our observations have identified a small (r < 5 pc) molecular cloud component in the region surveyed. These clouds appear to be significantly CO underluminous when compared to their large, inner Galaxy counterparts. This result may be partially due to beam dilution, but it also indicates that the conversion factor (X) between CO luminosity and cloud mass is higher in the outer Galaxy (Mead & Kutner, 1988). As the X factor for these clouds is uncertain and the clouds resemble other molecular clouds which are most likely virialized, we use the virial theorem to calculate cloud masses. The breakdown of the observed mass distribution as a function of cloud size and environment is given below.

Total Mass Distribution in units of 10^5 $M_\odot$

	Cloud Size		
	r < 5 pc	r ≥ 5 pc	Total
Arm Population	1.8	6.8	8.6
Interarm Population	1.4	0.7	2.1
Total	3.2	7.5	10.7

Fully 30% of the observed mass is contained in small (cold) clouds. If the survey region is a representative sample of the outer Galaxy, then previous estimates could possibly be scaled upward by 30%; however, there is little evidence to support the suggestion of Lequeux *et al.* that cold molecular material is a gravitationally significant component of the outer Galaxy mass distribution. If small, cold clouds exist out to R ~ 25 kpc then the total molecular mass could increase by a factor of 2.

S. Carey received support from the Astronomical Society of New York and Sigma Xi, The Scientific Research Society.

References

Carey, S. J., Mead K. N., & Kutner, M. L. 1994, ApJ, in preparation
Digel, S., Bally, J., & Thaddeus, P. 1990, ApJ, 357, 29
Peters, W. L., & Bash, F. N. 1987, ApJ, 317, 646
Lequeux, J., Allen, R. J., & Guilloteau, S. 1993, A&A, 280, L23
Kutner, M. L. & Mead, K. N. 1981, ApJ, 249, L15
Mead, K. N., & Kutner, M. L. 1988, ApJ, 330, 399
Wouterloot, J. G. A., Brand, J., Burton, W. B., & Kwee K. K. 1990, A&A, 230, 21

A HYDROMAGNETIC MODEL FOR THE HIERARCHICAL STRUCTURE OF MOLECULAR CLOUDS

B.M. DEISS
Inst. f. Theor. Physik, Goethe-Universität Frankfurt, 60054 Frankfurt, Germany

AND

A. JUST
Astronomisches Rechen-Institut, 69120 Heidelberg, Germany

1. Physical System and discrete 2-scale theory

We propose a physical model of molecular clouds which is based on the idea that the back reaction of substructures of a cloud on the ambient medium maintains and stabilizes the cloud on larger scales: clumps, which are assumed to carry a magnetic moment, are coupled to the ambient medium by magnetic forces, hence continually inducing velocity fluctuations due to their random motion. The energy source is then the gravitational binding energy of the clumps in the global potential of the whole cloud.

On a given range of spatial scale we regard mol. clouds to be composed of: **i)** an ensemble of dense cores, the dynamics of which is described stellardynamically, and with the internal clump structure (mass, magnetic moment) held fixed; **ii)** a low density, partially ionized, two-component gas, the dynamics of which is treated by two-fluid magneto-hydrodynamics, where we take ambipolar diffusion into account; **iii)** a magnetic field frozen in the ionized component. In quasi-linear approximation the power spectrum of the stationary turbulent MHD velocity field reads $C^{(2)}(k) \propto B_c^2\, n\, \sigma^{-1}\, D^6\, \chi\, k$, where B_c, n, σ, D, χ denote the clumps' magnetic field, number density, velocity dispersion and size, and the ionization degree of the ambient medium, respectively. $C^{(2)}$ increases with increasing k. Integrating $C^{(2)}(k)$ over $2\pi/L \leq k \leq 2\pi/D$, where L denotes the size of the whole cloud, we obtain for the 1-dim. velocity dispersion

L. Blitz and P. Teuben (eds.), Unsolved Problems of the Milky Way, 609–610.
© 1996 *International Astronomical Union.*

$\langle V_r^2 \rangle = \left(0.22 \frac{\mathrm{km}}{\mathrm{s}}\right)^2 \left(\frac{B_c}{\mu \mathrm{G}}\right)^4 \left(\frac{n}{\mathrm{pc}^{-3}}\right) \left(\frac{\sigma}{\mathrm{km\,s}^{-1}}\right)^{-1} \left(\frac{\chi}{10^{-5}}\right)$, Examples: ρ-Oph (1.1 km/s); Taurus cloud (0.42 km/s). This is in reasonable agreement with the observed values of 1.6 km/s and 1.5 km/s, respectively.

2. Hierarchical model and scaling relation

Since clumps of a given size induce fluctuations on all larger scales, we regard $C^{(2)}(k)$ as a differential power spectrum excited by clumps dn of size D; i.e. $C^{(2)}(k) \rightarrow \mathrm{d}C(k, D)$. Integrating dC(k,D) over all scales smaller than k^{-1} yields the total spectrum $C(k) \propto k^{-e}$ with $e = 6 - c + s - 2d - a$, where we employed the observed scaling relations $\sigma \propto L^a$, $\mathrm{d}n/\mathrm{d}L \propto L^{-c}$, $B \propto L^{-d}$, $\chi \propto L^s$. The turbulent velocity amplitude $\sigma_{turb}(L)$ on a given scale L is given by the integral of $C(k)$ over all smaller scales $\pi/k \leq L$. Identifying the induced velocity fluctuations with the velocity dispersion of the substructures we find a selfconsistent power-law index α for the velocity dispersion $\sigma_{turb} \propto L^\alpha$ with $\alpha = (5 - c + s - 2d)/3$. From observations one infers $c \approx 2.3 - 3.4; s \approx 0.5 - 0.7; d \approx 0.3 - 0.7$. This yields $\alpha \approx 0.3 - 0.85$ which is in very good agreement with the observed scaling index $a \approx 0.3 - 0.7$.

3. Stability of molecular clouds

We put $p = p_{therm} + p_{turb}$ in Euler's equation and assume $p_{turb} \propto L^{2a-b}$. The (linear) criterion for gravitational stability then reads $(4\pi G\rho/c_s^2) \leq k^2[1 + (k/k_{eq})^{1-e}(b - 2a)/a]$ with the normalization $\sigma_{turb}(k = k_{eq}) = c_s$. Since $e \approx 1.6 - 2.7$, mol. clouds are stable against large-scale collapse. However, there exists a finite range of scales ($\approx$ 1 pc) which still may be gravitationally unstable, hence leading to the formation of clumps and substructures.

4. Conclusions

Our magnetized-clump model demonstrates that it is just the clumpiness of mol. clouds which leads to turbulent motions and the large-scale stabilization of the clouds. The inferred scaling relation of the induced turbulent motions is determined by scaling relations of other physical parameters of mol. clouds. This is a first step to construct a physically coherent hierarchical model. The energy source in our model is the potential energy of the whole cloud; i.e., it is an internal source. Hence, the general, hierachical structure of mol. clouds and the turbulent motions within them, seem to be an intrinsic property of selfgravitating gaseous systems.

Ref.: A. Just, S. Jacobi, B.M. Deiss 1994, Astron.Astrophys. 289, 237

GALACTIC FINE STRUCTURE AT 843 MHZ

A.J. GREEN, D. CAMPBELL-WILSON, L.E. CRAM, M.I. LARGE, B. PIESTRZYNSKI AND T. YE
University of Sydney
NSW 2006, Australia

1. Introduction

The Southern Galactic Plane surveyed by the Molonglo Observatory Synthesis Telescope (MOST) gives an unprecedented view of fine-scale structure in low frequency radio continuum emission over the area $245° \leq l \leq 355°, \mid b \mid \leq 1.5°$. The telescope operates at 843 MHz with a resolution of $43''$ and a sensitivity of approximately 2 mJy/beam for the sample region ($5° \times 3°$), centred on G317.5+0.0, presented here to illustrate significant features in the sources. This is a mosaic of 35 fields, each representing a 12 hr observation.

2. Results and Discussion

Recent work (Whiteoak 1992) has shown that thermal sources are significant 60μm infrared emitters whereas 843 MHz nonthermal sources emit weakly. Thus the ratio of 60μm to 843 MHz flux densities allows the physical origin of emission from Galactic features to be determined, a crucial step to explaining the evolution of the observed complex structures. Fig. 1 shows a grey-scale MOST image (resolution $43'' \times 43''\text{cosec}(\delta)$) overlaid by contours of the corresponding 60μm IRAS image, with a resolution of $\sim 4'$. Both images are dominated by the bright H II region, G316.8-0.1. Significant differences between the two images reveal the distribution of nonthermal sources, both Galactic and extragalactic. Statistically, it is probable that most of the isolated unresolved nonthermal sources are background galaxies. From Whiteoak and Green (1994) this region contains four published SNRs (G315.4-0.3, G315.9-0.0, G316.3-0.0, G318.9+0.4), two new SNR identifications found with the MOST (G317.3-0.2, G318.2+0.1), and two tentative MOST SNR possibilities (G317.5+0.9, G319.9-0.7).

L. Blitz and P. Teuben (eds.), Unsolved Problems of the Milky Way, 611–612.
© 1996 *International Astronomical Union.*

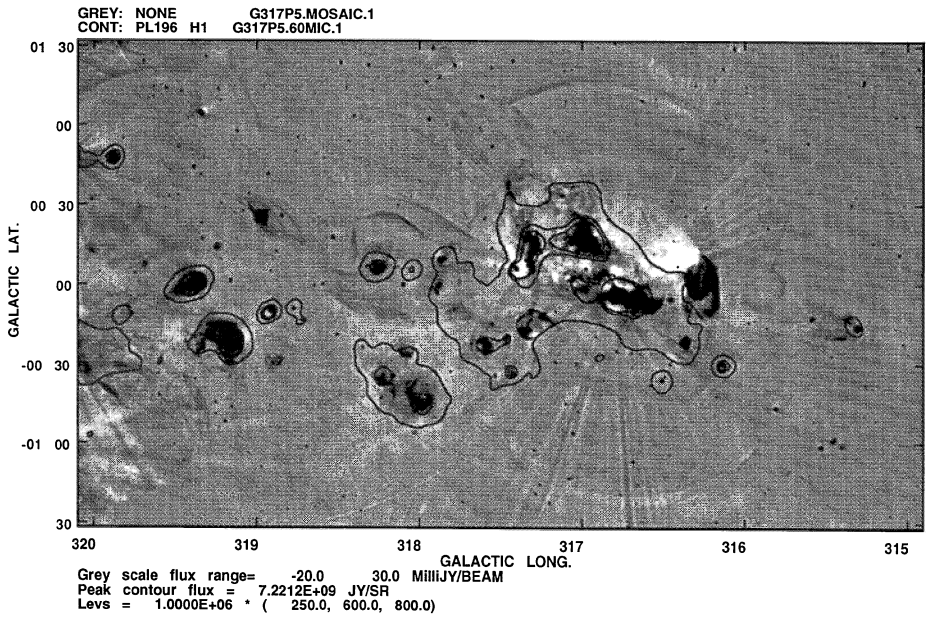

Figure 1. Grey-scale MOST image, overlaid by contours of 60μm IRAS image.

The dynamics and three-dimensional distribution of non-stellar objects in the Milky Way and how they contribute to the interstellar medium (ISM) is not well understood. The extended H II regions in the image show fibrous emission down to the sensitivity limit of the observations, while the SNRs have narrow filaments and sharp boundaries. Nevertheless, the local external environment is the dominant factor in SNR evolution, swamping any initial uniformity which might be expected from massive stars exploding. Since both SNRs and H II regions are formed by young massive stars it is surprising that their distributions are not better correlated, although different lifetimes and poor distance information for most SNRs may distort the results. The area shown has several SNRs apparently surrounding an H II complex, suggesting outward motion from a central association or propagating star formation. Observations at other frequencies are needed to elucidate the significance of the structure seen in the MOST images.

References

Whiteoak, J.B.Z. (1992) *Astron. Astrophys.*, 262, 251
Whiteoak, J.B.Z. and Green, A.J. (1994) in preparation

NEUTRAL GAS CONTRIBUTIONS TO [S II] GALACTIC BACKGROUND EMISSION

S. J. PETUCHOWSKI AND C. L. BENNETT
NASA/ Goddard Space Flight Center
spet@stars.gsfc.nasa.gov

1. Introduction

Elevated ratios of [S II]/Hα relative to those typical of H II regions have been used to identify supernova remnants (SNRs) and also characterize the diffuse Galactic background (Reynolds 1985) and gas observed on the large scale in other galaxies (e.g., Lehnert & Heckman 1994). We explore the implications for these regions of the fact that ionized sulfur may exist both in gas that is predominantly neutral as well as fully ionized.

2. Co-Occurence with [O I]

In SNRs, strong [S II] emission may arise due to the abundance of $\sim 10^4$ K electrons in shock regions. These electrons are sufficiently energetic to provide 1.85 eV excitation of S II transitions at 6716 and 6731 Å and excitation of [O I] in the same, predominantly neutral, regions.

While [O I] and [N II] emission is poorly correlated across samples of 10 SNRs in M31 (Blair, Kirshner, & Chevalier 1981) and 36 SNRs in M33 (Smith et al. 1993), we find that [S II] intensity from these regions can be decomposed into terms proportional to [O I] and [N II], as shown in Figure 1. We interpret the first term as [S II] arising within a neutral component, while the ionized component gives rise to a second term containing a factor which reflects the respective dependence of N II and S II on metallicity.

3. Excitation via Photoionization

[S II] emission may arise, additionally, in the absence of hot electrons, and unaccompanied by [O I] emission. The mechanism for sustaining [S II] ex-

L. Blitz and P. Teuben (eds.), Unsolved Problems of the Milky Way, 613–614.
© 1996 *International Astronomical Union.*

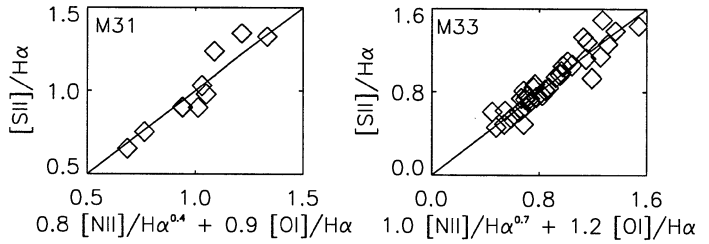

Figure 1. Fits to [S II]/Hα vs. a_{ion} ([N II]/Hα)^m + a_{neut} [O I]/Hα for SNRs in *(a)* M31 (Blair et al. 1981) and *(b)* M33 (Smith et al. 1993).

citation in cool neutral gas is that of photoionization into electronically excited states. Of those sulfur ions photoionized in a Draine (1978) spectrum of the interstellar radiation field, approximately 25% are created in the ^{2}D level, based on partial cross sections of Chapman & Henry (1971). Under typical conditions in a diffuse photodissociation region (PDR), the observed forbidden line intensity is governed by the rate of recombination.

The intercept of a fit to [S II] vs. Hα at zero Hα in the Galactic background fields observed by Reynolds (1985) suggests a contribution of (0.42 $\pm$ 0.19) Rayleighs to the [S II] flux from predominantly neutral gas. This intensity can arise in a thickness of photodissociated gas of unity optical depth within a range of temperatures between 37 and 120 K if the electron density is in the range of 1 - 5 cm^{-3} (Petuchowski & Bennett 1995). For an electron density equal to a nominal carbon density in this boundary layer, the inferred neutral hydrogen density is (8000 $\pm$ 4000) $(\frac{T}{100\ K})^{0.593}$ cm^{-3}, within the range typical of PDR interfaces of neutral clouds in the Galaxy (Hollenbach et al. 1991).

We conclude that cool neutral gas, possibly at the boundaries of fully ionized regions, constitutes a candidate medium for the origin of [S II] emission in the Galactic background.

References

Blair, W. P., Kirshner, R. P. & Chevalier, R. A. 1981, *Astrophysical Journal*, 247, p. 879.

Chapman, R. D., & Henry, R. J. 1971, *Astrophysical Journal*, 168, p. 169.

Draine, B. T. 1978, *Astrophysical Journal Supplement Series*, 36, p. 595.

Hollenbach, D. J., Takahashi, T., & Tielens, A. G. G. M. 1991, *Astrophysical Journal*, 377, p. 192.

Lehnert, M. D. & Heckman, T. M. 1994, *Astrophysical Journal Letters*, 426, p. L27.

Petuchowski, S. J., & Bennett, C. L., *Astrophysical Journal*, in press.

Reynolds, R. J. 1985, *Astrophysical Journal*, 294, p. 256.

Smith, R. C., Kirshner, R. P., Blair, W. P., Long, K. S., & Winkler, P. F. 1993, *Astrophysical Journal*, 407, p. 564.

STUDY OF THE MAGNETIC FIELD OF THE GALAXY USING CORRELATION FUNCTIONS OF THE INTENSITY OF SYNCHROTRON BACKGROUND RADIO EMISSION

V.R. SHOUTENKOV
Radioastronomy Station, Astro Space Center of Lebedev Physical Institute, Moscow, Russia

The possibility to study magnetic field of the Galaxy calculating correlation or structure functions of synchrotron background radio emission have been known long ago (Kaplan and Pikel'ner (1963); Getmantsev (1958)). But this method had not been as popular as other methods of magnetic field studies. However theoretical calculations made by Chibisov and Ptuskin (1981) showed that correlation functions of intensity of synchrotron background radio emission can give a lot of valuable information about galactic magnetic fields because of the intensity of synchrotron background radio emission depends on $H_\perp$. According to this theory correlation $C(\theta, \varphi)$ and structure $S(\theta, \varphi)$ functions of intensity, as functions of angular separation θ between two lines of sight and position angle φ on the sky between this two lines of sight, can be presented as a sum of isotropic (not dependent from angle φ) and anisotropic parts:

$$C(\theta, \varphi) = C_i(\theta) + C_a(\theta)\cos(2\varphi)$$
$$S(\theta, \varphi) = S_i(\theta) + S_a(\theta)\cos(2\varphi).$$

The anisotropy of correlation or structure functions is determined by the presence of regular component of magnetic field. Later Chibisov and Lazarian (1987) made other theoretical calculations and have essentially completed this method. They have shown the possibility to find correlation functions of random magnetic field from the amplitude of anisotropic part of correlation function $C_a(\theta)$. First observations of intensity of background radio emission have been made with Large Phased Array of Lebedev Physical Institute at 102.5 MHz and the results of analysis of correlation function of intensity have been published by Dagkesamanskii and Shoutenkov (1987) and Lazarian and Shoutenkov (1990). In this short publication I should

L. Blitz and P. Teuben (eds.), Unsolved Problems of the Milky Way, 615–616.
© 1996 *International Astronomical Union.*

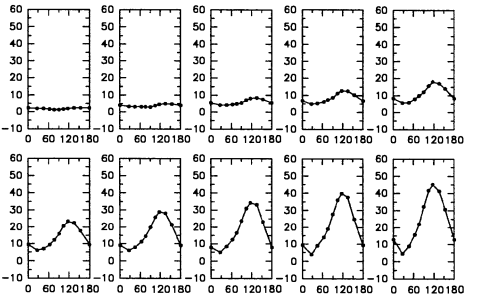

Figure 1. Structure function of intensity (Jy^2) plotted versus position angle φ for ten values of separation angle $\theta(°)$.

like to present new observational data and the results of calculations of the structure function of intensity.

The observations have been made with Large Phased Array at 102.5 MHz as part of Northern sky survey. The studied area has coordinates from 8^h00^m to 17^h00^m in right ascension and from 31° to 51° in declination. After data reduction, calibration and subtraction of discrete radio sources the contour map of intensity at 102.5 MHz have been obtained for this area. The map of this large area will be presented elsewhere.

The studied area was divided into nine smaller overlaped regions about 2^h wide. And for all these regions correlation and structure functions of intensity of background radio emission were calculated. Here I shall discuss only structure functions of background intensity. Structure function of intensity for the first region with right ascension from 8^h to 10^h is presented at Fig.1.

The cosine dependence of structure function is clearly seen on this figure. The phase of cosine determines the position angle of regular magnetic field direction in this region. The structure functions in different regions show some changes of the cosine phases and it means changes in direction of regular magnetic field. The difference between the directions of regular magnetic field for the first and last regions is about 50°.

References

Kaplan, S.A.,Pikel'ner, S.B. (1963) *The interstellar medium*. Phys. Math. Press, Moscow.
Getmantsev, G.G. (1958) *Izvestia VUZ. Radiofizica*, 1, p. 158.
Chibisov, G.V., Ptuskin, V.S. (1981) *17th Int. Cosmic Ray Conf.*, Paris, 2, p. 233.
Chibisov, G.V., Lazarian, A.L. (1987) *Preprint 283*, FIAN, Moscow.
Dagkesamanskii, R.D., Shoutenkov, V.R. (1987) *Sov. Astron. Lett.*, Vol. 13, no. 2, pp. 73–76.
Lazarian, A.L, Shoutenkov, V.R. *Sov. Astron. Lett.*, Vol. 16, no. 4, pp. 297–300.

HI BUBBLES AROUND NGC 6888

C. CAPPA DE NICOLAU
IAR, CC 5, 1894 Villa Elisa and FCAGLP, Paseo del Bosque, 1900 La Plata, Argentina

C. ROGERS
DRAO, P.O. Box 248, Penticton B.C. V2A6K3, Canada

G. DUBNER
IAFE, CC 67, 1428 Buenos Aires, Argentina

AND

N. ST.-LOUIS
U. of Montreal, Dept. of Physics, C.P. 6128, Suc. A, Montreal, Canada

1. Introduction

The interstellar bubbles are generally the result of the interaction of strong stellar winds with the surrounding material. HI voids and shells have been disclosed around several WR stars in our Galaxy (*e.g.* Niemela & Cappa de Nicolau 1991, Dubner *et al.* 1992). We report here an analysis of the interstellar medium in the vicinity of the WR star HD 192163 = WR 136 and the optical ring nebula NGC 6888 based on HI observations. Our aim is to look for the traces left in the cold interstellar gas by the action of the stellar winds of HD 192163.

2. Observations

To investigate the neutral hydrogen distribution and kinematics in the surroundings of NGC 6888 we surveyed a 2.°1 field around the nebula. The observations were carried out in July 1992, using the Synthesis Telescope of the Dominion Radio Astrophysical Observatory (DRAO) placed near Penticton, British Columbia, Canada.

L. Blitz and P. Teuben (eds.), Unsolved Problems of the Milky Way, 617–618.
© 1996 *International Astronomical Union.*

3. Main Results

A detailed analysis of the neutral hydrogen distribution at low positive velocities, compatible with the optical distance of HD 192163, and the comparison with optical and infrared emissions allowed us to identify three different HI structures with a hierarchical organization surrounding the WN6 star and its ring nebula. From inside to outside they are:

a) An inner shell: A small and elliptical almost complete HI shell is clearly seen embracing NGC 6888. The feature is detected in the velocity range +3 to +20 km $s^{-1}$and presents a complex velocity field. The shell, centred close to the position of the star, is 13×7 pc in size adopting a distance of 1.5 kpc for the WR star (Conti & Vacca 1990). The HI mass in the shell amounts to $\approx$ 200 $M_{\odot}$. The coincidence between the brightest parts of NGC 6888 and the borders of the HI emission distribution strongly suggests that the nebula is interacting with the surrounding interstellar material.

b) An outer shell: This structure, also detected in infrared emission, is best seen at +16.6 km s^{-1}. It is 30 pc in diameter at a distance of 1.5 kpc. Emission related to the shell can be detected in the velocity interval +3 to +20 km s^{-1}. The HI mass in the envelope amounts to $\approx$ 960 $M_{\odot}$. The presence of this shell in the same velocity range as the inner shell and the fact that it is centred near the position of HD 192163 lead us to the hypothesis that some relationship there exists between them.

c) An external shell: It appears as the neutral gas counterpart of the large IR shell described by Nichols–Bohlin & Fesen (1993) with a diameter of 40×47 pc. The present observational results suggest a *scenario* where the material that conforms both the inner and the outer shells was pushed out by the strong stellar wind of the WR star, expanding in an inhomogeneous interstellar medium. About 4 10^4 yr ago (Treffers & Chu 1982), the material ejected by the star originated the optical nebula. The ionized gas encountered higher density regions belonging to the outer neutral bubble and shaped the inner neutral bubble in this gas. The role of the external shell is an open question. The absence of any detectable expansion suggests that it is older than the outer shell. It might be a fossil bubble.

References

Conti, P.S., Vacca, W.D. (1990) *Astron. J.*, 100, 431.
Dubner, G., Giacani, E., Cappa de Nicolau, C., Reynoso, E. (1992) *Astron. Astrophys. Suppl.* 96, 505.
Nichols-Bohlin, J., Fesen, R.A. (1993) *Astron. J.* 105, 672.
Niemela, V., Cappa de Nicolau, C. (1991) *Astron. J.* 101, 572.
Treffers, R.R., Chu, Y.-H. (1982) *Astrophys. J.* 254, 569.

SEARCH FOR HI BUBBLES AROUND WR STARS: WR 149

C. CAPPA DE NICOLAU
Member of Carrera del Investigador, CONICET
IAR, CC 5, 1894 Villa Elisa, and FCAGLP, Paseo del Bosque, 1900 La Plata, Argentina

V.S. NIEMELA
Member of Carrera del Investigador, CIC, Prov. Buenos Aires
IAFE, CC 67, 1428 Buenos Aires, Argentina

U. HERBSTMEIER
MPIfA, Königstuhl, D-6900 Heidelberg, Germany

AND

B. KORIBALSKI
MPIfR, Auf dem Hügel 69, D-53121, Bonn, Germany
Current Address: ATNF, CSIRO, P.O.Box 76, Epping, NSW 2121, Australia

1. Introduction

The interaction of strong stellar winds with the interstellar medium creates large cavities or **interstellar bubbles** surrounded by expanding outer shells. 21-cm line (HI) observations have revealed the presence of such neutral gas bubbles around several WR stars (*e.g.* Niemela & Cappa de Nicolau 1991 and references therein; Dubner *et al.* 1992).

Continuing our search for HI bubbles around WR stars, we have analyzed the neutral hydrogen distribution in the vicinity of the Wolf-Rayet star WR 149, a highly reddened WN6-7 star located at 6.5 kpc in the direction $(l,b) = (89.^\circ53,+0.^\circ65)$.

2. Observations and Results

We have observed the surroundings of WR 149 at the λ21–cm line during January 1992 with the Effelsberg 100–m radiotelescope of the Max-Plank-

L. Blitz and P. Teuben (eds.), Unsolved Problems of the Milky Way, 619–620.
© 1996 *International Astronomical Union.*

Institut für Radioastronomie in Bonn (Germany).

TABLE 1. Main parameters of the observed HI bubbles

	Bubble A	**Bubble B**
Geometric Center *(l,b)*	89.°5,+0.°5	90.°25,+0.°5
Systemic Velocity (km s^{-1})	-47 ± 2	-47 ± 2
Kinematical Distance (kpc)	6.5 ± 0.5	6.5 ± 0.5
Radius of the Void (pc)	50	45
Radius of the Envelope (pc)	70	74
Expansion Velocity (km s^{-1})	$\simeq7$	$\simeq6$
HI mass Deficiency (10^3 $M_\odot$)	5.6	7.6
HI mass in the Envelope (10^3 $M_\odot$)	8.7	19.0
Swept-up HI Mass (10^3 $M_\odot$)	7.1	13.3
Ambient Gas Density (cm^{-3})	0.2	0.3
Kinetic Energy (10^{48} erg)	3.5	3.8

The observed HI column density distribution within the velocity interval -54 to -42 km s^{-1} is characterized by the presence of two voids partially surrounded by concentrations which form an almost complete envelope. We will refer to these structures as Bubbles A and B. WR 149 appears inside Bubble A. No obvious optical counterpart was found related to Bubble B.

The main observed and derived parameters of the bubbles are listed in Table 1. The swept-up HI mass was assumed to be a mean value between the HI mass deficiency and the HI mass in the envelope. The original ambient density was obtained by distributing the swept-up HI mass within the volume of the cavity. We note that the kinetic energy of Bubble A is less than 10% of the kinetic energy of the powerful stellar wind of the associated WR star. The parameters of these bubbles are similar to others observed around WR and O type stars.

WN6–7 type stars, as is WR 149, are often found as brightest stars in OB associations. Taking into account the high reddening of WR 149, fainter OB stars at the same distance would remain undetected. Therefore, we suggest that *both observed HI bubbles are related to undetected OB associations at the far side of the Perseus spiral arm.*

References

Dubner, G., Giacani, E., Cappa de Nicolau, C., Reynoso, E. (1992) *Astron. Astrophys. Suppl.* 96, 505.

Niemela, V.S., Cappa de Nicolau, C. (1991) *Astron. J.*, 101, 572.

GS64-01-97:

EXPANDING SUPERSHELL IN THE MILKY WAY

S. EHLEROVÁ
Astronomical Institute, Charles University
Švédská 8, 150 00 Prague 5, Czech Republic

AND

B. JUNGWIERT AND J. PALOUŠ
Astronomical Institute, Academy of Sciences
Boční II 1401, 141 31 Prague 4, Czech Republic

The expansion of shocked interstellar medium around an OB association is an example of the astrophysical blastwave (Ostriker and McKee, 1988). The thin, cold, shell-like structure expanding supersonically accumulates the ambient medium. We assume that the shell has the zero thickness at radius of the shockwave r_S and that it expands at velocity v_S. The shell is divided into elements described with equations of motion: $\frac{d}{dt}(Mv_S) = dS[(P - P_o) + n_o v_o(v_S - v_o)] - Mg(R,z)$, where M and dS are the mass and the surface of it, P, P_o are the inside and outside pressures, n_o, v_o are density and velocity of the ambient medium and $g(R,z)$ is the gravitational acceleration in the Galaxy. R,z are the galactocentric cylindrical coordinates. The mass of an element increases as long as the expansion velocity component normal to the shell, $v_\perp$, exceeds the velocity of sound in the ambient medium $\dot{M} = v_\perp n_o dS$. The 3D model using the above infinitesimally thin shell approximation was developed by Palouš (1990, 1992) and Silich (1992).

In this contribution, the 3-D numerical simulations are compared with the HI feature GS064-01-97 discovered by Heiles (1979). This structure has also been observed as a part of the Leiden–Dwingeloo 21 cm survey of the Milky Way (Hartmann, Burton, 1994). Possible energies of expansion and the distances of the structure from the galactic center are proposed. The z-distribution of the ambient medium is $n(z) = n_C e^{(-\frac{(z-z_{warp})^2}{\sigma_C{}^2})} + n_E e^{-(\frac{|z-z_{warp}|}{z_E})}$, where n_C, n_E are the volume densities and σ_C, z_E are scale heights of the gaussian and exponential components. Their values are

L. Blitz and P. Teuben (eds.), Unsolved Problems of the Milky Way, 621–622.
© 1996 *International Astronomical Union.*

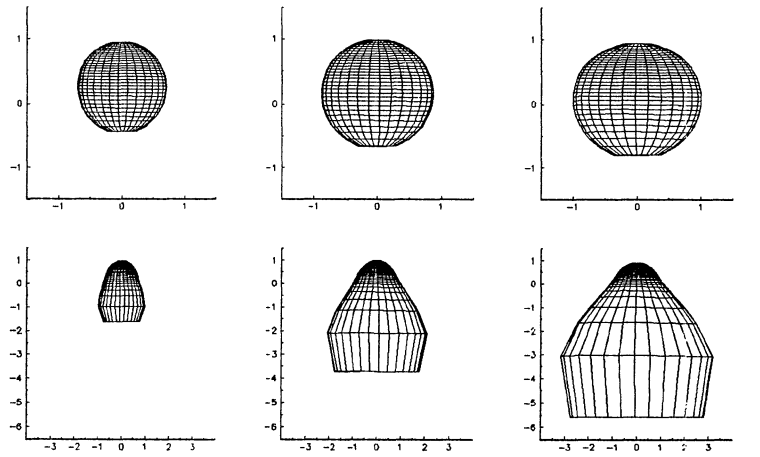

Figure 1. The supershell in the exponential (upper panel) or gaussian (lower panel) atmosphere after 10, 20 and 30 Myr of expansion.

derived from the total HI surface density $\Sigma_{\rm HI}$ and the scale height $z_{1/2}$ taken from Wouterloot et al. (1990). For the galactic HI warp we adopt $z_{warp} = 0.102\ (R - 8.075)\ cos(\phi - 85^o)$ according to Burton (1976).

Resulting initial energy is $\sim 10^{54}$ erg. With smaller or bigger values the supershell has column densities differing from observation. In the radial velocity channel maps, the angular diameter of the structure is best reproduced for the galactocentric distance 16 ± 1 kpc. In Fig. 1 we show the shape of the structure expanding in gaussian or exponential z-distribution of the ambient medium. For gaussian z-distribution the bubble blows-out to the galactic halo, which is not compatible with observation.

We conclude that the energy $\sim 10^{54}$ erg released at the galactocentric distance $\sim$ 16 kpc into the exponential HI atmosphere can produce the structure similar to GS064-01-97.

References

Burton W. B., 1976, Ann. Rev. Astron. Astrophys. 14, 275
Hartmann D., Burton B. W., 1994, private communication
Heiles, C. (1979) ApJ, 299, 533
Ostriker J.P., McKee Ch. F., 1988, Rev. Mod. Phys. 60, 1
Palouš J., 1990, IAU Symp. 144, Poster proceedings, ed. H. Bloemen, p. 101
Palouš J., 1992, in Evolution of Interstellar Matter and Dynamics of Galaxies, eds J. Palouš, W. B. Burton, and P. O. Lindblad, Cambridge University Press, p. 65
Silich S., 1992, Astrophys. Space Sci. 195, 317
Wouterloot J. G. A., Brand J., Burton, W. B., & Kwee, K. K., 1990, Astron. Astrophys. 230, 21

MULTI-WAVELENGTH STUDY OF THE GIANT BUBBLE IN CEPHEUS

L.G. BALÁZS AND P. ÁBRAHÁM
Konkoly Observatory, Budapest
Box 67, H-1525, Hungary

1. Introduction

The giant bubble in Cepheus was discovered by Kun et al. (1987) in the IRAS maps. It has an angular diameter of about 9° and connects several well-known star forming regions such as IC1396, S140, NGC7129. All these regions have nearly the same distances of about 800 pc permitting a good distance and linear size estimate for the bubble. Figure 1 shows the surface distribution of IRAS 100 μ optical depths, obtained from the 60 and 100 μ data and smoothed to the resolution of the HI survey. Although the bubble was discovered in the IRAS data base it is well pronounced in the integrated HI map obtained from the observations of Heiles & Habing (1974) and Weaver & Williams (1973). Figure 2 shows the HI line area map.

2. Results of the multivariate analysis

We analyzed the matrix built up from the mutual correlations between the HI channel maps. (We had altogether 39 channels in the -30, +10 km/s region, corresponding to a sampling frequency of 1 km/s). We used the principal components analysis to obtain non-correlated factors. (For further details of this technique see Murtagh and Heck (1987)). As a result of the principal components analysis we obtained 3 major factors describing 86 % of the variances of the observed maps.

Figure 3 shows the dependence of the factor coefficients on the radial velocity. Factor 1 peaks at large negative velocities, it can be treated as the background. Factor 2 peaks velocities close to 0, it mainly responsible for the foreground. We identified Factor 3 with the bubble itself. Figure 4 - 6 present the maps of the factor values.

L. Blitz and P. Teuben (eds.), Unsolved Problems of the Milky Way, 623–624.
© 1996 *International Astronomical Union.*

Acknowledgements

This work was supported by the National Research Found (OTKA) grant No. T4341.

References

Heiles, C., Habing, H.J. 1974, A&AS 14, 1
Kun. M., Balázs, L.G., Tóth, I. 1987, Aph. & Sp.Sc., 134, 211
Murtagh, F., Heck. A. 1987, 'Multivariate Data Analysis', *Astrophys. Space Sci. Lib.*, 131. D. Reidel Publ. Co.
Weaver, H., Williams, D.R.W. 1973, A&AS 8, 1

Figure 1

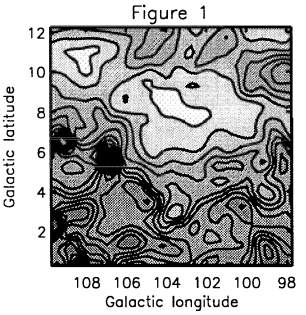

Figure 2

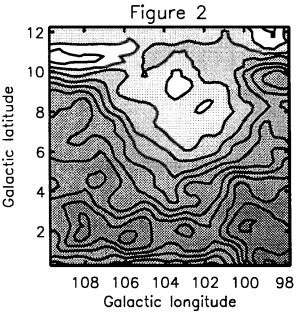

Figure 3

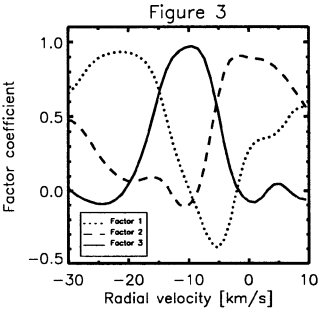

Figure 4

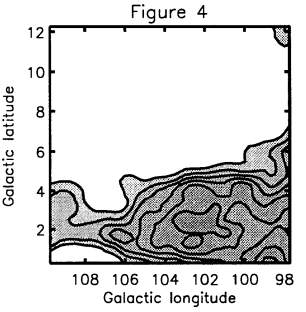

Figure 5

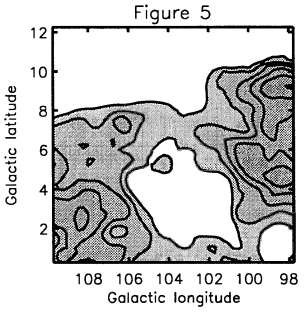

Figure 6

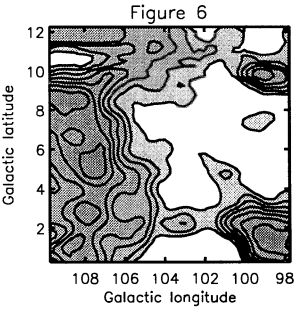

NON-THERMAL PARTICLES NEAR OB ASSOCIATIONS

ANDREI. M. BYKOV
A.F. Ioffe Institute of Physics and Technology
194021, St. Petersburg, Russia

Abstract. The observational tests to check the concept of nonthermal particle generation in the vicinity of OB associations embedded in a superbubble (SB) are discussed. Acceleration of nonthermal charged particles is expected to be very efficient due to powerful energy release by supernovae and colliding stellar winds. The distinctive features of the SB's emission spectra due to nonthermal particle interaction with gas, dust and electromagnetic fields are summarized.

1. Introduction

A study of superbubbles and supershells created by stellar winds and multiple supernova explosions in an OB association attracts great attention (see e.g. Heiles (1990), Rand & van der Hulst, (1993), Yang & Skillman, (1993)). The possibilities of acceleration of nonthermal particles in the vicinity of an OB-association have been considered in detail by Bykov (1992), Bykov & Fleishman (1993). The model of particle acceleration has been proposed where the interaction of charged particles with an ensemble of shocks and violent large scale plasma motions inside the bubble was included. The nonthermal charged particle acceleration is expected to be very efficient especially after the explosions of a few supernova in the association. The particle acceleration time is not exceed of 3×10^5 yr for typical superbubble conditions. Some tens of percent of the kinetic energy released by early type stars and supernovae can be converted to the nonthermal particles. The spectra of accelerated particles are very hard at the energy range up to a few tens of MeV per nucleon $F(p)p^2\ dp \sim N_{nth}\ p^{-1}\ dp$ and then become steeper (here F(p) - is the distribution function of energetic particles in momentum space).

L. Blitz and P. Teuben (eds.), Unsolved Problems of the Milky Way, 625–626.
© 1996 *International Astronomical Union.*

2. Nonthermal emission from OB associations

Here we present the list of expected observable consequences of the interaction of nonthermal particles with magnetic and UV radiation fields inside the SB and with gas and dust of surrounding supershell.

1) Synchrotron radio emission with flat spectrum up to a few hundreds MHz or GHz and of steeper radio spectrum (with spectral index of $\sim 0.5 - 0.8$) below. Some low degree of polarization is expected from that sources.

2) Hard continuum gamma ray emission due to nonthermal proton and electron interaction with HI shell (see Bykov & Fleishman, 1993).

3) Gamma - line emission ($0.4MeV - 10MeV$). Gamma ray in the $3 - 7\ MeV$ range has been detected recently by COMPTEL telescope from Orion complex (Bloemen et al,(1994) and could be identified with deexcitation lines from nonthermal nuclei which accelerated within bubble and interacted with dense clouds just in vicinity of SB (Bykov & Bloemen, 1994).

4) Optical emission of HeII due to recombination of doubly ionized helium and from the process $H^+ + He \rightarrow H^+ + He^{+*} + e$. Optical line of HeII λ 4686 $\mathring{A}$ will be most prominent as it is in the case of some HII regions observed by Garnett et al (1991).

5) Some distinctive spectral features of the IR emission may appear due to stochastic heating of small grains within a dense shells (or nearby clouds) by nonthermal protons and nuclei with energies up to hundreds MeV. Bozhokin & Bykov, 1995, (in preparation) calculated IR spectra due to heating of the carbon dust grains population of temperature 10 K and 25 K with MRN size distribution by nonthermal protons. We expect that the effect of dust heating by nonthermal particles is important for rather old SB without bright stars and with numerous supernova events located in the outer part of the Milky Way or in the other galaxies.

This work was supported in part by the International Science Foundation, grant NU3000 and by Russian Foundation for Fundamental Research.

References

Bloemen, H. et al., (1994). *Astron. Astrophys.* 281, L5
Bozhokin S.V., Bykov A.M. (1994), *Astron. Lett.* 20, 503
Bykov A.M. (1992). In: *Evolution of interstellar matter and dynamics of Galaxy* eds. J.Palous, W.B.Burton, P.O.Lindblad, Cambridge, p.116
Bykov A., Bloemen H. (1994), *Astron. Astrophys.* 283, L1
Bykov A.M., Fleishman G.D. (1993), *Astron. Astrophys.* 280, L27
Chu, Y.-H., Mac Low, M.M. (1990). *Astrophys. J.* 365, 510
Garnett D.R., Kennicutt R.C., Chu Y.-H., Skillman E.D. (1991), *Astrophys. J.* 373, 458
Heiles, C. (1990). *Astrophys. J.* 354, 483
Rand, R.J., van der Hulst, J.M. (1993), *Astron. J.* 105
Yang, H., Skillman, E.D. (1993), *Astron. J.* 106, 1448

G54.4−0.3 — MULTI-FREQUENCY INVESTIGATION OF AN SNR IN INTERACTION WITH THE ISM

N. JUNKES
Institut für Astronomie und Astrophysik
Universität Kiel, D-24098 Kiel, Germany

1. Introduction

G54.4−0.3 is an extended shell-type supernova remnant (SNR) in the Galactic plane. We selected this source as a candidate for the interaction of SNRs with the interstellar medium on the base of an investigation of cool IRAS point sources in the direction of SNRs. We found a statistical excess of IRAS sources with FIR spectra similar to young stellar objects ($T_{\rm d} \approx 25 - 45$ K) in the vicinity of G54.4−0.3 and a number of other SNRs in the northern hemisphere (Junkes & Fürst 1992).

This prompted us to study G54.4−0.3 in the molecular line of CO. Medium-resolution CO observations, covering the whole area of the SNR, reveal a shell-type structure in nice correlation to the radio continuum structure (Junkes et al. 1992a).

In a further investigation (Junkes et al. 1992b) we extended this study to high-resolution CO observations of selected areas across the SNR centered on the positions of IRAS point sources, and found an association with condensations or small clouds in the CO shell. One of these clouds shows a bipolar structure and self-absorption at the central position in ^{12}CO, and is probably a young stellar object (YSO) still embedded in dust.

2. ROSAT X-ray Observations

In order to investigate the hot gas in connection with the SNR, we observed G54.4−0.3 with ROSAT in four separate exposures. The extended structure in the central part of the image can be associated with the SNR. In addition, the young compact SNR G54.1+0.3 (Reich et al. 1985) shows up as a bright X-ray source in the western half of the image.

L. Blitz and P. Teuben (eds.), Unsolved Problems of the Milky Way, 627–628.
© 1996 *International Astronomical Union.*

There is a nice anti-correlation between the X-ray feature (hot thermal gas) seen in the ROSAT image and the molecular line emission in CO (cold molecular gas). The X-ray emission almost fills the gap in the CO shell. Spectral fitting of the soft X-ray emission towards G54.4−0.3 gives the following result: The best-fitting thermal plasma spectrum (Raymond & Smith 1977) shows almost complete absorption below 1.0 keV, indicating a high hydrogen column density in the direction of this SNR located directly in the Galactic plane. The results of the fit are $10^{22}\mathrm{cm}^{-2}$ for HI column density towards the source, with a plasma temperature of $\approx 2 \times 10^7$ K.

The spectral fit already indicates that the upper limit of the X-ray temperature of the SNR is too high to be reasonably determined by the ROSAT observations. In order to perform a detailed spectral analysis of the X-ray spectrum of G54.4−0.3, to investigate absorption and the hard X-ray morphology of the source, we successfully applied for observations with the Japanese ASCA satellite.

3. Final Remarks

We have investigated the SNR G54.4−0.3 and propose the following picture for this source: It is part of an extended complex of young population I objects (OB-association with associated HII-regions), the possible birthplace of the progenitor star of the supernova. An energetic stellar wind pushed molecular material ahead and condensed it to a shell. The supernova exploded inside the created cavity, and the debris expanded almost freely into the stellar wind bubble before it reached the edge of the molecular shell. Since the CO-shell was formed by the stellar wind 10^7 years ago, parts of it have been condensed and developed into protostellar or young stellar objects (YSOs). The X-ray observations trace the hot gas from inside the shell and provide another step towards the multi-frequency investigation of this SNR in interaction with the ISM.

The project is further supplemented by an investigation of the neutral gas surrounding the SNR (high-resolution HI observations) and the FIR energy distribution of the suspected YSOs (ISO proposal).

References

Caswell J.L. (1985) *Astrophys. J.*, 90, 1224

Junkes N. & Fürst E. (1992) *Evolution of Interstellar Matter and Dynamics of Galaxies*, W.B. Burton; P.O. Lindblad, J. Palous (eds.), (Cambridge University Press), p. 95

Junkes N., Fürst E., Reich W. (1992a) *Astron. Astrophys. Suppl.* 96, 1

Junkes N., Fürst E., Reich W. (1992b) *Astron. Astrophys.* 261, 289

Raymond J.C. & Smith B.W., 1977 *Astrophys. J. Suppl.* 35, 419

Reich, W., Fürst, E., Altenhoff, W.J., Reich, P., Junkes, N. (1985), *Astron. Astrophys.* 151, L10

HST SPECTROSCOPY OF THE ORION NEBULA

R.H. RUBIN
NASA/Ames
G.J. FERLAND
University of Kentucky
R.J. DUFOUR, D.K. WALTER, C.R. O'DELL
Rice University
J.A. BALDWIN
CTIO
J.J. HESTER
Arizona State University
AND
P.G. MARTIN
University of Toronto

Abstract.
From our recent Faint Object Spectrograph (FOS) observations of the Orion Nebula obtained with the Hubble Space Telescope, we present preliminary results that address the nitrogen abundance. The list of detected lines and their identifications included the first measurement of the N II] 2142 Å line in an H II region. This measurement in conjunction with [O II] 2471 Å permits a new assessment of the important N/O ratio in Orion. Unfortunately, the measurements of the N III] 1747-54 Å multiplet and the O III] 1660-66 Å multiplet have poor signal-to-noise, precluding another independent derivation of N/O.

1. Observations

Several bright regions at varying distances from θ^1 Ori C were observed during 1993 August with HST/FOS at 5–15 Å resolution. For three positions, we have total wavelength coverage from 1650–6800 Å. Additionally,

L. Blitz and P. Teuben (eds.), Unsolved Problems of the Milky Way, 629–632.
© 1996 *International Astronomical Union.*

at the three positions, we observed at $3250 < \lambda < 6800$ Å through the upper member of the 1.0″ pair of apertures (beam switching). The second member of the paired square aperture provided us with a position located 3″ from each of our primary positions with little added exposure time. This allows us to investigate small-scale variations in ionization and physical conditions in the same part of the nebula.

For the purpose of providing a preliminary list of spectral lines measured, we derive an average of the spectra taken in the three lower apertures at our positions 1, 2, and 3 – 29″, 19″, and 42″ from θ^1 Ori C. We have presented elsewhere a table listing measurements from this composite spectrum – with the measured wavelength, the vacuum rest wavelength and preliminary line identification, our measured flux in the 1″×1″ aperture (erg cm^{-2} s^{-1}), the equivalent width (Å), and the FWHM (Å) (Rubin *et al.* 1994). Because this FOS observing configuration (the 1.0″ pair of apertures) did not have proper calibration observations made until July 1994, the analysis and results presented here are subject to revision. Our Cycle 3 observations included a GHRS spectrum with the large science aperture at Position 1. This G270M exposure covered the region 2310–2360 Å and provided the first detection of Si II] 2335.3 Å emission in an HII region (Walter *et al.* 1994).

2. Discussion

We detected the N II] 2142 Å line(s) in the spectra at position 3 low only. The measurement of this line in Orion is the first in an H II region. Previously it has been seen in RR Tel (Penston *et al.* 1983), nova CrA 1981 (Williams *et al.* 1985), and the η Car S condensation (Davidson *et al.* 1986). There are two lines that arise from $^5S_2$ with lower levels $^3P_2$ (2143.45 Å) and $^3P_1$ (2139.68 Å) – in sum referred to as 2142 Å. The red component is expected to be more than twice as strong as the blue one. Preliminary analysis indicates that position 3 low has the highest T_e as measured by the combined [N II] and [O III] temperatures, which may be significant in explaining why the N II] 2142 Å line is strongest at this position. Further analysis of T_e and temperature fluctuations in the N^+ zone using this line in conjunction with the 5755 and 6584 Å lines, arising at the immediate lower levels, is underway. The measurement of N II] 2142 Å in conjunction with [O II] 2471 Å provides another measurement of the N^+/O^+ abundance ratio that is less sensitive to uncertainties in knowledge of the T_e value/distribution and to uncertainty in differential extinction compared with the more traditional optical method (see below).

Here we simply take the approach of retrofitting our two independent models of Orion (Baldwin *et al.* 1991; Rubin *et al.* 1991) to predict the

N II] 2140–43 Å line and compare with the preliminary fluxes at position 3 low. For our retrofits at this time, in order to narrow the differences in input parameters, we arbitrarily used the Rubin *et al.* ionizing spectrum for θ^1 Ori C and abundance set (whether meritorious or not). We use the same updated effective collision strengths and A-values to solve the N^+ energy level populations. Calamai & Johnson (1991) have laboratory A-values for the 2140–43 Å line. Recently calculated collision strengths affecting all 6 lowest-lying levels are from Stafford *et al.* (1994), although there is another contemporaneous set by Lennon & Burke (1994) that has somewhat different values. For our separate models, we then prorate input nitrogen abundance to force the predicted line ratio to match the extinction-corrected observed N II]2142/[O II]2471 ratio, yielding $(N/O)_{uv}$. The same is done for the [N II]6584/[O II]3727 ratio, which provides $(N/O)_{opt}$ and the observed [N III]57μm/[O III]52μm ratio, yielding $(N/O)_{ir}$. Extinction is corrected for by using A(λ) (magn.) = 2.5 C(Hβ) [1 + f(λ)], where C(Hβ) = 0.64 for our Orion position and f(λ) is from Bohlin & Savage (1981) in the UV and from Costero & Peimbert (1970) in the optical. The effect of differential extinction is to increase the observed ratio I(2142)/I(2471) by a factor of 1.20, which is less than for I(3727)/I(6584). For the $(N/O)_{ir}$ determinations, we match to I(57)/I(52) = 0.13 (Rubin *et al.* 1991) at a position which might be typical to our HST locations.

The retrofit of the Baldwin *et al.* model gives $(N/O)_{uv}$ = 0.109, $(N/O)_{opt}$ = 0.0840, and $(N/O)_{ir}$ = 0.213, while the retrofit of the Rubin *et al.* model gives respectively, 0.0843, 0.128, and 0.176. There is much that remains to be done, awaiting final calibration of our FOS spectra, in terms of reconciling these spectral region differences and model differences. This preliminary analysis is to demonstrate the expanded opportunity HST data permit in regards to just one important "unsolved problem" – deriving N/O.

Acknowledgements

We thank Patrick Harrington for information regarding his measurements of N II] 2140–43 Å in a FOS spectrum of a planetary nebula. RHR thanks Scott McNealy for providing a Sun workstation. We acknowledge NASA/Ames – Rice Univ. and NASA/Ames – Univ. of Kentucky interchanges NCC2-5008 and NCC2-5028 as well as GO.4385 from STScI.

References

Baldwin, J.A., Ferland, G.J., Martin, P.G., Corbin, M.R., Cota, S.A., Peterson, B.M., & Slettebak, A. 1991, ApJ, 374, 580

Bohlin, R.C., & Savage, B.D. 1981, ApJ, 249, 109

Calamai, A.G., & Johnson, C.E. 1991, Phys Rev A, 44, 218
Costero, R., & Peimbert, M. 1970, Bol. Obs. Ton. y Tacu., 5, 229
Davidson, K., Dufour, R.J., Walborn, N.R., & Gull, T.R. 1986, ApJ, 305, 867
Lennon, D.J. & Burke, V.M. 1994, A&AS, 103, 273
Penston, M.V., *et al.* 1983, MNRAS, 202, 833
Rubin, R.H., Simpson, J.P., Haas, M.R., & Erickson, E.F. 1991, ApJ, 374, 564
Rubin, R.H., *et al.* 1994, in *The Analysis of Emission Lines*, Proc. STScI Symp. (May 1994), Eds. R.E. Williams & M. Livio
Stafford, R.P., Bell, K.L., Hibbert, A., & Wijesundera, W.P. 1994, MNRAS, 268, 816
Walter, D.W., *et al.* 1994, in *The Analysis of Emission Lines*, Proc. STScI Symp. (May 1994), Eds. R.E. Williams & M. Livio
Williams, R.E., *et al.* 1985, MNRAS, 212, 753

Chapter 8

How do we put it together?

HOW OUGHT ONE PARAMETERIZE THE MILKY WAY?

PAUL L. SCHECHTER
Massachusetts Institute of Technology
Physics Dept. 6-206, Cambridge MA 02139, USA

1. The parameter glut

In a well known paper written a quarter century ago, cosmology was described as a search for two numbers (Sandage 1970). As those of you who have attended any of the parallel sessions of Symposium 167 surely appreciate, today's cosmologists find more than just two numbers interesting. It is likewise clear from the present symposium that the number of interesting parameters associated with the Milky Way is very much greater than two.

To illustrate the levels of complexity with which we must deal, I've constructed an incomplete chart of Milky Way structure which is something of a caricature but will still serve to make my point.

TABLE 1. Milky Way Structure

components	sub-components	sub-sub-	sub-sub-sub-
disk →	stellar →	thin →	old
	neutral ↘	thick ↘	young
	molecular ↘		
	dust ↘		
bulge →	metal rich		
	metal poor		
halo →	visible →	stellar	
	dark ↘	gaseous	
center			
ring			

Each of these components and sub-components has its associated scale lengths and multiple shape parameters. As bad as this may seem, we know

L. Blitz and P. Teuben (eds.), Unsolved Problems of the Milky Way, 633–643.
© 1996 *International Astronomical Union.*

that the situation is worse yet in other galaxies. There is a class of galaxies, the polar rings, which exhibit two disks with roughly perpendicular angular momentum axes (Schweizer *et al.* 1983). And there is a new class of galaxies (Rubin *et al.* 1992; Merrifield and Kuijken 1994) with *counter*-rotating stellar disks.

The proliferation of components is daunting. It is tempting to restrict one's attention to a single component, invoking the principle of "divide and conquer." This is a popular strategy, judging from the presentations at this symposium. But while the components may have very different shapes and enrichment histories, their dynamics are governed by a single gravitational potential. It therefore behooves us to look for a simple parameterized model of the potential.

2. Oort's parameters

In Oort's youth, when astronomy was carried out only at visible wavelengths, most of what one knew about the Milky Way was inferred from a relatively small neighborhood centered on the Sun. It made sense to approximate the mean patterns of observed proper motions and radial velocities as truncated power and Fourier series,

$$\bar{\mu} = (B + A\cos 2l - C\sin 2l) + \mathcal{O}\left(\frac{r}{R_0}\right) \quad , \quad \text{and} \qquad (1.a)$$

$$\bar{v}_{los} = r(K + A\sin 2l + C\cos 2l) + \mathcal{O}\left(\frac{r^2}{{R_0}^2}\right) \quad . \qquad (1.b)$$

This is first order in (r/R_0), where r is distance from the Sun, and second order in galactic longitude l. The four coefficients are the Oort parameters,

B: rotation about the Sun's position,
A: differential rotation,
K: Hubble-like expansion, and
C: differential expansion.

Oort's C and K are less familiar than B and A because they are usually taken to be zero on the assumption of circular orbits. The fundamentally local nature of Oort's parameterization is evident from the fact that only with the addition of higher order terms (e.g. Pont *et al.* 1994) can one derive a distance to the galactic center, R_0. Units of length are completely absent from Oort's four constants.

The addition of R_0, a global parameter, to Oort's four local parameters is esthetically unsatisfying. Moreover, as one observes stars and gas at distances r approaching R_0, one needs higher order terms in Oort's expansion (again, see Pont *et al.* 1994). Many authors (e.g. Caldwell and Coulson 1987) have used global rather than local models. Kuijken and Tremaine (1992, 1994; henceforth KT92 and KT94) introduced a non-axisymmetric global parameterization which strikes a balance between flexibility and complexity. In abandoning Oort we note that his parameterization has proven so durable precisely because local data have until now been very much better than global data.

3. Kuijken and Tremaine's parameters

The Kuijken and Tremaine model, in its full glory, involves six parameters, but for the sake of comparison with the Oort parameterization is useful to suppress one of these. It then includes

R_0	Sun's distance from the galactic center,
v_0	average circular velocity at the Sun's distance from the galactic center,
α	logarithmic derivative of the dependence of circular velocity on radius, $v \sim (R/R_0)^\alpha$,
ϵ_Ψ	ellipticity of the potential at R_0, and
ϕ_Ψ	angle between major axis of the potential and Sun-center line, positive in rotation direction.

In practice one finds that ϵ_Ψ and ϕ_Ψ usually occur in the combinations

$$c_\Psi = \epsilon_\Psi \cos 2\phi_\Psi \quad \text{and} \tag{2.a}$$

$$s_\Psi = \epsilon_\Psi \sin 2\phi_\Psi \quad . \tag{2.b}$$

These correspond to deviations from axisymmetry which are, respectively, symmetric and antisymmetric about the line from the Sun through the center of the galaxy. It is often the case that measurements of some particular kind are much more sensitive to one of these than to the other. If c_Ψ is positive, the LSR is presently at apocenter. If s_Ψ is positive, the apocenter of the LSR is in the second quadrant.

Kuijken and Tremaine adopt a "standard model" with $\alpha = 0$. This model gives a flat (constant) rotation curve and has the pleasing property that the equipotentials and closed orbits have (to first order) the same ellipticity but lie perpendicular to each other. For this model the connection

with Oort's parameters is particularly simple (KT94),

$$A = -B = \left(\frac{v_0}{2R_0}\right)(1 + c_\Psi) \quad \text{and} \tag{3.a}$$

$$C = -K = \left(\frac{v_0}{2R_0}\right) s_\Psi \quad . \tag{3.b}$$

We note that having dropped the assumption of circular orbits, it is no longer true that $A - B = \Omega$, the angular velocity of the LSR. Were we to drop the assumption that $\alpha = 0$, it would no longer be true that $A = -B$.

The interpretation of the local velocity ellipsoid is particularly straightforward using the KT parameterization. Taking ℓ_v to be the galactic longitude (in radians) of its long axis and X^2 as the squared ratio the azimuthal velocity dispersion to to the radial disperson, Kuijken and Tremaine find

$$\ell_v = -2s_\Psi \quad \text{and} \tag{4.a}$$

$$X^2 \approx \frac{1}{2} - \frac{3}{2}c_\Psi \quad , \tag{4.b}$$

where in the second equation the first term on the right hand side represents the limit of small velocity dispersion. As the velocity dispersion grows, Kuijken and Tremaine (1992) and Cuddeford and Binney (1994) find that this term is significantly greater than 1/2, particularly when the ratio of the distance to the galactic center to the scale length for the disk is greater than 2, which it would appear to be.

The sixth parameter in the KT formulation characterizes the variation of ellipticity of the potential with radius. Its effect on the observable quantities is smaller than than that of α (although of the same order). For the sake of simplicity we shall assume here that the equipotentials are similar ellipses.

4. Nature abhors a power law

The KT "standard model" has a rotation curve which remains flat as R increases. The dark and luminous components of the Milky Way, whatever they might be, surely end somewhere between here and Andromeda. It therefore makes sense to truncate our assumed power law potential at some radius, R_{cutoff}. There has been considerable discussion in the literature about where that cutoff might be (e.g. Norris and Hawkins 1991, Leonard and Tremaine 1989, Little and Tremaine 1987, Zaritsky *et al.* 1989).

Three circumstances combine to make the determination of this cutoff radius difficult. First, unlike the case of the disk of our galaxy (where even a single star can give information on the assumption that the orbit is closed or nearly closed), orbits of stars and star clusters at large galactocentric radii are likely to be far more random. Second, in the absence of proper

motion data, we can only measure one of a distant object's three velocity components, the component which is approximately radial with respect to the center of the galaxy. Finally, the numbers of objects at large galactocentric radii are small. At this point, one might reasonably ask, "If it is so hard to measure, why do we care?" We just do.

5. The acceleration perpendicular to the galactic plane

The Oort and KT parameterizations are two dimensional, and tell us nothing about the structure of the galaxy perpendicular to the plane. Just as there is a radial distribution of mass, there is also a vertical distribution. Unfortunately for our understanding, but fortunately from the point of view of constructing a simple model, it may suffice to specify only one parameter, a local surface density, Σ_{local}. If one makes the simplifying assumption that disk is infinitely thin, then its surface mass density is obtained by observing the scale height, h, and vertical velocity dispersion, σ_{zz}^2 of a tracer population with an assumed Maxwellian velocity distribution,

$$\Sigma_{local} = \frac{\sigma_{zz}^2}{2\pi G h} \quad ,$$

where we have ignored higher order terms which come into play with large dispersions perpendicular to the plane. It is instructive to compare this local determination with the surface density which would be needed if the disk were solely responsible for the radial gradient in the potential. This is particularly simple for a Mestel disk, for which

$$\Sigma_{Mestel} = \frac{{v_0}^2}{2\pi G R_0} \quad .$$

Taking the ratio of these two surface densities we have

$$\frac{\Sigma_{local}}{\Sigma_{Mestel}} = \frac{\sigma_{zz}^2}{{v_0}^2}\frac{R_0}{h} \quad .$$

Adopting values typical for stars like the Sun, $\sqrt{\sigma_{zz}^2} = 20$ km/s and $h = 300$ pc, and canonical values for v_0 and R_0 (Kerr and Lynden-Bell 1986) we get a ratio of 1/4. More realistic models give slightly larger ratios (Schechter 1992), but the the conclusion that much of the mass in the Milky Way lies elsewhere than in the disk would seem hard to escape.

6. Nuisance parameters

Sometimes, when a young radio astronomer talks about radial velocity measurements and I'm feeling mischievous, I'll ask how these have been corrected for the Sun's motion with respect to the Local Standard of Rest. In

most cases the answer is "Oh the computer corrects for it automatically." The Sun's peculiar velocity is typical of stars of its type, and of no special interest except that measurements of the parameters which *are* interesting require that we know it. The three components of the Sun's velocity therefore qualify as "nuisance" parameters. In my own experience values for these derived variously from Cepheids and carbon stars agree less well with the standard values than one would like. The Sun's distance from the galactic plane, which becomes important when considering dust and young stars at large distances, would likewise qualify as a "nuisance" parameter.

7. Bar parameters

The evidence for a barlike structure inside the solar circle is very persuasive. It is is seen photometrically in IR balloon data (Blitz and Spergel 1991), IRAS point sources (Weinberg 1993), Miras (Whitelock *et al.* 1991), COBE DIRBE maps (Arendt *et al.* 1994, and most recently in RGB clump stars (Stanek *et al.* 1994). It is seen dynamically in effects which are attributed to the rotation of a bar, including the gas motions at the center of the galaxy (Gerhard and Vietri, 1986; Binney *et al.* 1991) and the molecular (and perhaps stellar) ring at 4 kpc. Doubters may point to the significant differences in the photometrically and dynamically derived orientations for the bar, but I suspect that this discrepancy will quickly be resolved.

Such a bar adds a minimum of three parameters to our model: the bar's corotation radius, an orientation angle, ϕ_b (different from the ϕ_Ψ measured at roughly the Sun's distance from the galactic center) and a measure of the bar's strength at some fiducial radius. A fourth parameter, describing how that strength varies with radius, may also be needed.

Binney (1993) has argued that if the bar's corotation radius is at the position determined from the dynamics of galactic center gas, of order 2.4 kpc, its effect near the solar neighborhood would be negligible. We might then use the KT parameterization, since the bar can be treated as a dynamical subsystem which at large distances looks like a point mass. Conversely, at radii typical of the bar, the outer part of the Galaxy would, at worst, make itself felt through its quadrupole contributions to the potential. Not all parameters are important at all radii – they often decouple.

However Weinberg and Combes have each argued at this meeting that the bar may have a corotation radius as large as 5 kpc, in which case the the potential of the bar strongly influences the motions of stars in the Sun's neighborhood. There is always a transition region where the bar and the outer parts of the galaxy make comparable contributions to the orbits of stars. It may be our misfortune that this happens closer to the Sun's position than we would have preferred.

8. Top Ten Parameters

Ignoring our four nuisance parameters and the parameters which govern the rates at which the bar and halo quadrupole terms vary with radius, we are left with ten parameters,

R_0	Sun's distance from center,
v_0	circular velocity,
c_Ψ	symmetric ellipticity,
s_Ψ	antisymmetric ellipticity,
α	rotation curve logarithmic slope,
Σ_{local}	local surface density,
R_{cutoff}	edge of galaxy,
R_{corot}	corotation radius,
ϕ_b	bar position angle, and
b/a	bar strength.

9. Recent Results

The axis ratio of the local velocity ellipsoid as has long been a puzzle. If our galaxy had a flat rotation curve and closed orbits near the LSR were circular, the axis ratio, as measured in the plane, ought to be greater than 1/2 (KT92). It isn't. When Kuijken and Tremaine (1994) interpret the axis ratio as a deviation from axisymmetry, they find $c_\Psi = +0.12 \pm 0.04$. They find additional support for this interpretation using Merrifield's (1992) method for measuring the rotation curve.

The consequences of this conclusion are far reaching. It would imply that the circular velocity at the Sun's distance from the galactic center is smaller, by a factor of order $1 + 2c_\Psi$, than has heretofore been thought. It would also imply that distances to the galactic center, as estimated from the kinematics of stars assumed to be on circular orbits, (e.g. Caldwell and Coulson 1987; Gwinn *et al.* 1992), would be overestimated, again by a factor of order $1 + 2c_\Psi$.

Metzger (1994), in a recently completed Ph.D. thesis, has measured velocities for 8 newly discovered Cepheids toward $\ell = 300°$ (Caldwell, Keane and Schechter, 1991; Schechter *et al.* 1992) and used these to obtain a new determination of the distance to the galactic center. These eight Cepheids, *taken by themselves*, give $R_0 = 7.8 \pm 0.4$ kpc. The agreement with the "best" value given in Reid's (1993) recent review, 8.0 ± 0.5 kpc, is excellent. This would argue against a large positive value for c_Ψ.

Metzger (1994) has himself searched for new Cepheids at a complementary galactic longitude, $\ell = 60°$. Their positions, projected onto the galactic

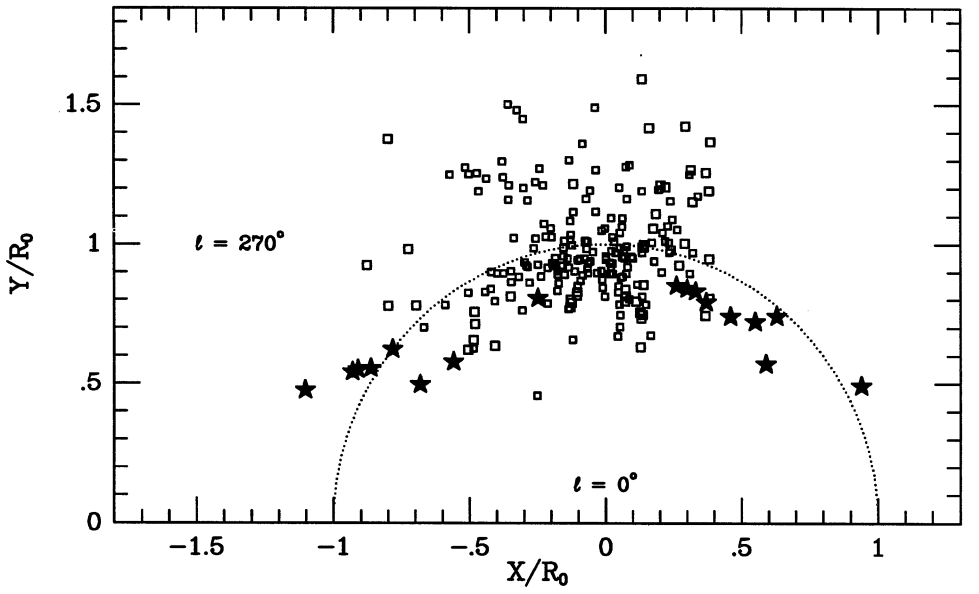

Figure 1. Newly discovered Cepheids toward $\ell = 300°$ by Caldwell, Keane and Schechter (1991) and toward $\ell = 60°$ by Metzger (1994) are shown projected onto the plane of the Galaxy as filled symbols. Previously known Cepheids are shown as open symbols.

plane, are shown in Figure 1. These are among the most heavily obscured Cepheids known, with $V - I$ colors of 4 and 5. If velocities can be measured they will provide considerable leverage on s_Ψ.

A longstanding mystery in the study of Cepheid kinematics has been their apparent net blueshift (e.g. Kraft and Schmidt 1963). The possibility that this was due to a non-zero value of Oort's K had been appreciated, but one could not rule out the possibility of a systematic error in the center of mass, "γ" velocities. Pont *et al.* (1994) have compared velocities for five Cepheids with those of their parent open clusters and find stunningly good agreement with the cluster means. Pont *et al.* find a net blueshift of 2.3 km/s for a sample of 266 Cepheids. Fitting their data to a model which allows for non-zero antisymmetric ellipticity, I find $s_\Psi = +0.037 \pm 0.017$. One can see the sense of the effect either by following the signs in equations (1b) and (3b) or by examinining Figure 2.

One of the most exciting recent results has only just been reported at this meeting, Backer and Sramek's proper motion for Sgr A* (see also Backer and Sramek 1987) , the radio source identified with the galactic center. They find a longitudinal component, $\mu_\ell = -5.83 \pm 0.4$ mas/yr. Taking R_0 to be 8.0 ± 0.5 kpc, and letting $A - B = 26.4 \pm 0.5$ km/sec/kpc (Kerr and Lynden-Bell 1986) gives $c_\Psi = +0.01 \pm 0.04$ in Kuijken and Tremaine's

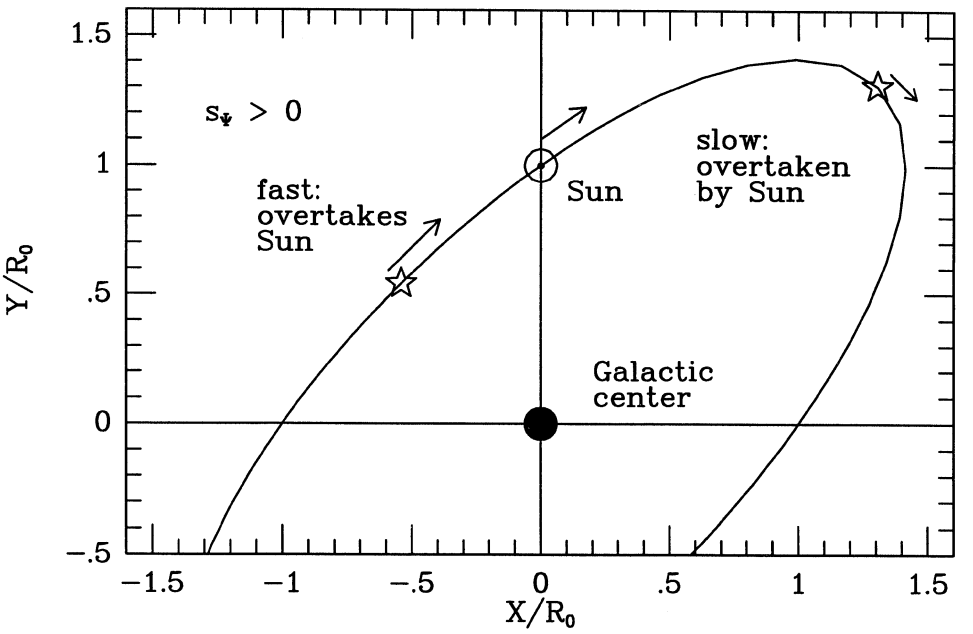

Figure 2. Closed elliptical orbits passing close to the LSR produce a net blueshift for stars in the solar neighborhood when $s_\Psi > 0$.

standard model, on the assumption that Sgr A* is at rest with respect to the center of the galaxy.

TABLE 2. Recent Results

$c_\Psi = 0.12 \pm 0.04$	velocity ellipsoid
	Kuijken and Tremaine (1994)
$R_0 = 7.8 \pm 0.4$ kpc	Cepheid velocities
	Metzger (1994)
$s_\Psi = 0.04 \pm 0.02$	Cepheid velocities
	Pont *et al.* (1994)
$\mu_\ell = -5.83 \pm 0.4$ mas/yr	Sgr A* / VLA
	Backer and Sramek (this symposium)

10. Prospects for improved parameter estimates

Both the proper motion of the Galactic center and the distance to the Galactic center would now appeaar to be measured to better than one part in 20. One of the beauties of proper motion measurements is that uncertainties continue to grow smaller until the investigators lose interest

in the problem. We are likely to see improvements soon both in the Cepheid derived value of R_0 and in the RR Lyrae value. Some of the eclipsing binaries in the bulge found by the MACHO and OGLE collaborations may ultimately yield yet better values of R_0.

The author is grateful to Mark Metzger for permission reproduce Figure 1 and to quote his results in advance of publication, and for the support of U.S. National Science Foundation Grant AST-9215736.

References

Arendt, R.G., Berriman, G.B., Boggess, N., Dwek, E., *et al.* (1994) *Astrophys.J., submitted*

Backer, D.C. and Sramek, R.A. (1987) in *The Galactic Center*, ed. D.C. Backer (New York: American Institute of Physics) p.163.

Binney, J. (1994) in *Galactic and Solar System Astrometry: Observation and Application* eds. L.V. Morrison and G.F. Gilmore (Cambridge: Cambridge University Press)

Binney,J., Gerhard, O.E., Stark, A.A., Bally, J., and Uchida, K.I. (1991) *M.N.R.A.S.* 252, 210.

Blitz, L. and Spergel, D. (1991) *Astrophys.J.* 379,631.

Caldwell, J.A.R. and Coulson, I.M. (1987) *Astr.J.* 93,1090.

Caldwell, J.A.R., Keane, M.J, and Schechter, P.L. (1991) *Astron.J.* 101,1763 .

Cuddeford, P. and Binney, J. (1994) *Mon.Not.Roy.Astr.Soc.* 266,273.

Gerhard, O.E. and Vietri, M. (1986) *Mon.Not.Roy.Astr.Soc.* 223,377.

Kerr, F.J. and Lynden-Bell, D. (1986) *Mon.Not.Roy.Astr.Soc.* 221,1023.

Kraft, R.P. and Schmidt, M. (1963) *Astrophys.J.* 137,249.

Kuijken, K. and Tremaine, S. (1992) in *The Dynamics of Disc Galaxies*, B. Sundelius, ed. (Goteborg: Chalmers University of Technology) p.71.

Kuijken, K. and Tremaine, S. (1994) *Astrophys.J.* 421,178.

Leonard, P.J.T., and Tremaine, S.D. (1989) *Astrophys.J.* 353,486.

Little, B. and Tremaine, S.D. (1987) *Astrophys.J.* 320,493.

Merrifield, M.R. (1992) *Astron.J.* 103,1552.

Merrifield, M.R. and Kuijken, K. (1994) *Astrophys.J.* 432,575.

Metzger, M.R. (1994) *unpublished Ph.D. thesis, M.I.T.*

Norris, J.E. and Hawkins, M.R. (1991) *Astrophys.J.* 380,104.

Pont, F., Mayor, M., Burki, G., (1994) *Astron. Astrophys.* 285,415.

Reid, M. (1993)*Ann.Rev.Astr.Astrophys.* 31,345.

Rubin, V.C., Graham, J.A., Kenney, J.D.P. (1992) *Astrophys.J.Letters* 394,L9

Sandage, A.R. (1970) *Physics Today* Vol. 42, No. 2, p. 34.

Schechter, P.L. (1992) in *Back to the Galaxy*, F. Verter, ed. (New York: AIP) p.571.

Schechter, P.L., Avruch, I.M., Caldwell, J.A.R. and Keane, M.J, (1992)*Astron.J.* 104,1930.

Schweizer, F., Whitmore, B.C., and Rubin, V.C. (1983) *Astron.J.* 88,909.

Stanek, K.Z., Mateo, M., Udalski, A., Szymanski, M., Kaluzny, J., and Kubiak, M. (1994) *Astrophys.J.Letters* 429,L73.

Weinberg, M.D. (1993) *Astrophys.J.* 384,81.

Whitelock, P., Feast, M., and Catchpole, R. (1991) *Mon.Not.Roy.Astr.Soc.* 248,276.

Zaritsky, D., Olszewski, E.W., Schommer, R.A., Peterson, R.C. and Aaronson, M. 1989 *Astrophys.J.* 345,759.

DISCUSSION

K. Stanek: How do the deviations from circular orbits change the distance to the galactic center as measured using the Cepheids?

Schechter: Kuijken & Tremaine tell us that with positive c_Ψ the Cepheids overestimate the distance to the center by ~20%. The apparent agreement between the Cepheid kinematic distance & other photometric distances may challenge the large positive value of c_Ψ.

DOES OUR GALAXY HAVE A MASSIVE DARK CORONA ?

K.C. FREEMAN
Mount Stromlo and Siding Spring Observatories
The Australian National University
Canberra, AUSTRALIA

Abstract. The rotation curves of spiral galaxies indicate that most of them have massive dark coronas, and it seems likely that our Galaxy also has a dark corona. Our position in the galactic disk makes it difficult to measure the galactic rotation curve beyond about 20 kpc from the galactic center, but it does allow us to use several other indicators of the total galactic mass out to very large distances. I will review some of these indicators. The conclusion is that the Galaxy does indeed have a massive dark corona: the data are consistent with the enclosed mass within radius R increasing like $M(R) \approx R(kpc) \times 10^{10}\ M_{\odot}$, out to a radius of more than 100 kpc, and a total galactic mass of at least $12 \times 10^{11}\ M_{\odot}$.

1. Introduction

The rotation curves of disk galaxies, measured from the kinematics of the interstellar gas, give a fairly direct measurement of the radial component of the gravitational field within the disk. In the inner regions of spiral galaxies (out to two or three radial scalelengths of the underlying stellar disk), the rotation curves can be well modeled by the gravitational field of the visible matter (including the gas itself). This does not work for the more extended HI rotation curves which, in many spiral galaxies, can be measured out to many disk scalelengths. In almost all such spirals, the rotation curves remain flat or rise with radius. This provides very strong evidence for the existence of a massive dark corona: see Freeman (1993) for a review. The inferred mass of this dark corona is typically 5 to 10 times the mass of the underlying stellar component. The dynamics of galactic rotation is relatively simple, and it is difficult to see how this inference about the

L. Blitz and P. Teuben (eds.), Unsolved Problems of the Milky Way, 645–650.
© 1996 *International Astronomical Union.*

existence of the massive dark coronas could be conceptually wrong, unless the adopted inverse square law of gravity is not correct in the outer regions of galaxies (eg Milgrom, 1988).

Dark coronas are detected in almost all spirals with extended rotation curves, so it seems very likely that our Galaxy also has a dark corona. The sun's position in the galactic disk makes it very difficult to measure the rotation curve of our Galaxy beyond about 20 kpc from the galactic center, so other less direct methods are needed to establish the extent and properties of the galactic dark corona.

The flat rotation curves usually seen in large spirals indicate that the galactic mass $M(R)$ enclosed within radius R increases linearly with R. We will review some of the methods that have been used to estimate the $M(R)$ distribution of the Galaxy. If the Galaxy has no dark corona, then the $M(R)$ distribution should approach the total mass of the (disk + bulge + stellar halo) for large R. So first we briefly discuss the mass of the visible components of the Galaxy.

2. The Mass of the Visible Components of the Galaxy

The mass of the visible components of the Galaxy lies mainly in its bulge and disk, with a small contribution from the metal-poor stellar halo.

- The DIRBE photometry of the galactic bulge (Dwek *et. al.*, 1994) gives a bulge mass of about $1.3 \times 10^{10}\ M_{\odot}$. This is consistent with Kent's (1992) dynamical estimates.
- The mass of the galactic disk is not well known, because (*i*) the local circular velocity, the scalelength and the local surface density of the disk are all still uncertain, and (*ii*) the parameters of the dark corona itself are uncertain, so we do not know how much the dark corona contributes to the circular velocity in the inner regions of the Galaxy. For this discussion, we adopt a circular velocity of 220 km s^{-1} near the sun, and take the radial scalelength of the disk to be 4.5 kpc (see for example Lewis and Freeman, 1989). For a bulge mass of $1.3 \times 10^{10}\ M_{\odot}$, the maximum disk mass consistent with this local circular velocity is about $11 \times 10^{10}\ M_{\odot}$, corresponding to a total surface density near the sun of about 130 $M_{\odot}$ pc^{-2}. This value for the local surface density is much higher than the recent dynamical estimates: these are mostly around 50 $M_{\odot}$ pc^{-2} (*eg.* Kuijken and Gilmore, 1989), and correspond to a total disk mass of only about $4 \times 10^{10}\ M_{\odot}$.
- Recent studies of the metal-poor stellar halo of the galaxy indicate that its mass is about $1 \times 10^{9}\ M_{\odot}$ (*eg.* Morrison, 1993); the stellar halo does not make a significant contribution to the galactic gravitational field.

We conclude that the total mass of the disk, bulge and metal-poor halo is probably in the range (5 to 12) $\times 10^{10}\ M_{\odot}$. If the correct value is at the low end of this range, then the dark corona is already making the dominant contribution to the circular velocity at the galactocentric radius of the sun.

3. The Galactic Rotation Curve

Data on the galactic rotation curve are reviewed by Fich and Tremaine (1991). For an adopted local circular velocity V_c of 220 km s^{-1} and solar radius R_o of 8.5 kpc, the mean rotation curve is roughly flat for R between about 3 kpc and 15 kpc. Beyond 15 kpc the velocity uncertainties become large and the rotation curve less secure. Merrifield (1992) extended the HI rotation curve by using the thickness of the galactic HI layer as a distance indicator: he adopts (R_o, V_c) = (7.9 kpc, 200 km s^{-1}) and finds that the rotation curve is slowly rising all the way from R = 2 kpc to the maximum extent of the measured rotation curve at 20 kpc.

The galactic rotation curve out to a radius of 20 kpc gives a total $M(20\ kpc) = 22 \times 10^{10}\ M_{\odot}$. This is at least double the estimated mass of the visible components of the Galaxy, and already provides a strong indication that the Galaxy has a dark corona. In some spirals it is possible to estimate the parameters of the dark corona (*eg.* its core radius and scale density) from the shape of the rotation curve; for the Galaxy this is difficult, because the rotation curve itself remains uncertain in the inner few kiloparsecs of the Galaxy.

4. The Escape Velocity in the Solar Neighborhood

In the solar neighborhood, stars of the metal poor stellar halo have a velocity dispersion of about 140 km s^{-1} in the radial direction: see for example Morrison *et. al.* (1990). If the halo stars in the high velocity tail of the velocity distribution are bound to the Galaxy, then their distribution of total space motions gives a lower limit on the local escape velocity V_{esc} which in turn sets a lower limit on the total galactic mass.

The mass estimates from escape velocity arguments are lower limits on the total mass because the estimated V_{esc} may be smaller than the true escape velocity in the solar neighborhood. For example, the most energetic halo stars in the solar neighborhood may be firmly bound to the Galaxy if the stars of the halo come from accreted satellites or if the velocity distribution of the halo stars has been truncated in the close approaches of the Magellanic Clouds.

Cudworth (1990) remeasured the proper motions for 9 of the highest velocity halo stars from the sample of Carney *et. al.* (1988), and found that the largest stellar space motion in the sample was about 475 km s^{-1}.

Leonard and Tremaine (1990) used a maximum likelihood analysis to estimate V_{esc} from the velocity distribution of the highest velocity stars. Their analysis included the observational biases associated with the proper motion selection criteria for high velocity stars. They found that the 90% confidence limits on V_{esc} are 450 and 650 km s^{-1}. The radial velocity alone of one particular high velocity star gives a limit of $V_{esc} > 430$ km s^{-1}.

For a simple galactic mass model (*eg.* Carney *et. al.* 1988) with $M(R) \propto R$ out to some limiting radius R_{lim} and constant for $R > R_{lim}$, the total mass M_{total} is related to the local escape velocity V_{esc} by

$$\log M_{total}/M(R_o) = (1/2)(V_{esc}/V_c)^2 - 1$$

where R_o and V_c are again the radius of the solar orbit and the circular velocity. With this model, the Leonard and Tremaine estimate of V_{esc} indicates that $M_{total} > 3 \times 10^{11}\ M_\odot$.

5. Distant Stars and Satellites

The radial velocities V_{rad} and distances d of distant stars, globular clusters and satellites can be used to provide another estimate of $M(R)$, if we assume that these objects are test particles at random orbital phases in an isolated Galaxy. The mass estimates depend on the adopted orbital properties of the tracer population (*ie.* on the isotropy or anisotropy of the velocity ellipsoid). Hartwick and Sargent (1978) derived a galactic mass $M(60kpc) = 8 \times 10^{11}$ $M_\odot$, assuming isotropic orbits for their tracer satellites. Little and Tremaine (1987) used the radial velocities and distances of distant objects to estimate the galactic mass for two approximations to the galactic mass distribution:

- for a point mass approximation, the observed distribution of (dV_{rad}^2/G) gives an estimate of the total galactic mass;
- for a very extended halo with $M(R) \propto R$, the observed distribution of V_{rad}^2 provides an estimate of the (constant) circular velocity V_c.

Zaritsky *et. al.* (1989) and Norris and Hawkins (1991) applied the Little and Tremaine method to samples of distant blue horizontal branch stars, globular clusters and satellite galaxies. The point mass approximation gives a mass $M > 11 \times 10^{11}\ M_\odot$ if the orbits of the tracers are isotropic. The extended halo approximation gives $V_c \approx 185 \pm 20$ km s^{-1} and the enclosed mass $M(50\ kpc) = 4 \times 10^{11}\ M_\odot$, again assuming isotropic orbits. Sommer-Larsen *et. al.* (1994) argue that the stellar orbits in the outer halo are probably more tangential than isotropic; if this is correct, then these mass estimates would be lower limits. Tracers with galactocentric distances between about 20 and 40 kpc give similar values for V_c.

Lin *et. al.* (1995) used the observed proper motion and radial velocity of the LMC and arguments about the dynamics of the Magellanic Stream

to constrain the mass of the Galaxy. They find that $M(100\ kpc) = (5.5 \pm 1) \times 10^{11}\ M_{\odot}$. This estimate is about half of the mass given by the timing arguments (see the next section) out to similar galactocentric distances.

6. Timing Argument

M31 lies about 710 kpc from the Galaxy and has a galactocentric radial velocity of -118 km s^{-1}. These two galaxies are the dominant objects in the Local Group. If their initial separation is small, then adopting an age for the universe and assuming radial orbits gives a lower limit on the total mass of (M31 + Galaxy) from simple Keplerian arguments (Kahn and Woltjer, 1959). For an age of 18 Gyr, this limit corresponds to a galactic mass of $(13 \pm 2) \times 10^{11}\ M_{\odot}$. (The ratio of the masses of M31 and the Galaxy is estimated from their observed rotational velocities).

Another timing estimate comes from the dwarf galaxy Leo I, at a distance of 270 kpc (Zaritsky *et. al.* 1989; Lee *et. al.* 1993). This gives a galactic mass of $(12 \pm 2) \times 10^{11}\ M_{\odot}$. The two estimates from M31 and Leo I agree remarkably well, and are consistent with a flat rotation curve ($V_c = 220$ km s^{-1}) extending out to at least 100 kpc.

More elaborate studies which include the dynamics of the angular momentum of the Local Group and interactions with nearby galaxies give similar estimates for the total galactic mass: see for example Raychaudhury and Lynden-Bell (1989). Peebles (1990) modeled the formation of the Local Group and derived a total mass of about $2 \times 10^{12}\ M_{\odot}$ for the Galaxy. Kroeker and Carlberg (1991) checked the accuracy of the timing argument mass estimates by examining binary systems identified in $\Omega = 1$ CDM simulations. They find that timing arguments (assuming radial orbits) typically underestimate the total masses by a factor of about 1.7.

7. Summary

- The mass of the known luminous components of the Galaxy is in the range (5 to 12) $\times 10^{10}\ M_{\odot}$.
- From the rotation curve of the Galaxy, $M(20\ kpc) \approx 22 \times 10^{10}\ M_{\odot}$.
- The escape velocity at the solar radius, estimated from high velocity stars in the solar neighborhood, indicates that the galactic mass $> 30 \times 10^{10}\ M_{\odot}$.
- From the kinematics of distant stars and satellites, $M(50\ kpc) \approx 40 \times 10^{10}\ M_{\odot}$.
- The timing arguments from the radial velocities and distances of M31 and Leo I give a consistent asymptotic mass estimate M_{total} of at least $120 \times 10^{10}\ M_{\odot}$.

8. Conclusion

The data are consistent with a mass distribution $M(R) \approx R(kpc) \times 10^{10}$ $M_{\odot}$ (corresponding to a flat rotation curve with $V_c \approx 220$ km s^{-1}), extending out to $R \geq 100$ kpc. The inferred ratio of the mass of the dark corona to the mass of the visible components of the Galaxy is at least 10.

References

Carney, B.W., Latham, D.W., Laird, J.B. 1988. Astron.J., 96, 560.
Cudworth, K. 1990. Astron.J., 99, 590.
Dwek, E. *et. al.* 1994. Preprint.
Fich, M., Tremaine, S. 1991. Ann.Rev.Astron.Astrophys., 29, 409.
Freeman, K.C. 1993. in Physics of Nearby Galaxies: Nature or Nurture (Paris: Editions Frontieres), p 201.
Hartwick, F.D.A., Sargent, W.L. 1978. Astrophys.J., 221, 512.
Kahn, F., Woltjer, L. 1959. Astrophys.J., 130, 705.
Kent, S. 1992. Astrophys.J., 387, 181.
Kroeker, T.L., Carlberg, R.G. 1991. Astrophys.J., 376, 1.
Kuijken, K., Gilmore, G. 1989. Mon.Not.R.Astron.Soc., 239, 605.
Lee, M.G. *et. al.* 1993. Astron.J., 106, 1420.
Leonard, P.J.T., Tremaine, S. 1990. Astrophys.J., 353, 486.
Lewis, J.R., Freeman, K.C. 1989. Astron.J., 97, 139.
Lin, D.N.C., Jones, B.F., Klemola, A.R., 1995. Astrophys.J., 439, 652.
Little, B., Tremaine, S. 1987. Astrophys.J., 320, 493.
Merrifield, M. 1992. Astron.J., 103, 1552.
Milgrom, M. 1988. Astrophys.J., 333, 689.
Morrison, H.L. 1993. Astron.J., 106, 578.
Morrison, H.L., Flynn, C., Freeman, K.C. 1990. Astron.J., 100, 1191.
Norris, J.E., Hawkins, M. 1991, Astrophys.J., 380, 104.
Peebles, P.J.E. 1990. Astrophys.J., 362, 1.
Raychaudhury, S., Lynden-Bell, D. 1989. Mon.Not.R.Astron.Soc., 240, 195.
Sommer-Larsen, J., Flynn, C., Christensen, P.R. 1994, preprint.
Zaritsky, D.*et. al.* 1989. Astrophys.J., 345, 759.

MASS NEAR THE SUN

ANDREW GOULD
Dept of Astronomy, Ohio State University
174 W. 18th Ave., Columbus, OH 43210

Abstract.

I review the dynamical measurements of mass in the solar neighborhood and show that, within 1 kpc, $\sim 40\%$ is unaccounted for by known stars and gas. I discuss several interpretations of the data including the 'standard model' where the extra mass is due to a spherical dark halo. I argue that the evidence for a radically different picture of an ultra-flat distribution is at least as compelling as the standard model.

1. Introduction

There are two basic approaches to determining the amount of mass near the Sun. The first is to take an inventory of various types of objects that may be found in the solar neighborhood such as stars, interstellar material (ISM), and dark objects. The stars (with the exception of the very late M dwarfs) are easily counted and these account for the majority of the known material. The ISM is by mass primarily gas and this is also reasonably well known. If the dark objects (which might be brown dwarfs, other baryonic compact objects, WIMPs, or other things) exist at all, they have so far escaped detection.

The second approach is to infer the local mass from its gravitational effects on the distribution of stars. If the two approaches give similar results, then the mass in the solar neighborhood is basically accounted for by the inventoried objects. If not, there is evidence for a so-far unobserved dark population. This is the problem of disk dark matter which has existed in some form for several decades.

If this comparison is carried out in the immediate solar neighborhood, say within 5 pc, then the stars are very well measured and the gas is rea-

L. Blitz and P. Teuben (eds.), Unsolved Problems of the Milky Way, 651–659.
© 1996 *International Astronomical Union.*

sonably well measured, meaning that the inventory is quite complete, at least for known classes of objects. However, the gravitational effects of this material are so small that they cannot be measured even in principle. To carry out the comparison, it is necessary to move to scales of 100s of pc. In this case, the gas is measured reasonably well, but we must *assume* that the solar-neighborhood stars are representative of the stars from a much larger region. One may show, however, that this assumption is quite reasonable.

2. Deriving the Potential from Tracer Stars

The standard approach pioneered by Oort (1932) is to measure the density and velocity of tracer stars of some specific type in a cone whose axis is perpendicular to the Galactic plane. If the stellar population is old (and hence presumably well-mixed) then the Jeans equation relates the vertical gradient of the pressure to the gravitational field, $d(\nu < v^2 >)/dz = -K\nu$. Here the tracer number density, ν, the tracer velocity dispersion $< v^2 >$, and the disk gravity K are all functions of height above the plane z. By Gauss's Law, $K(z)$ is proportional to $\Sigma(z)$ the total disk column between $-z$ and z: $K(z) = 2\pi G\Sigma(z)$. For the special case where the tracers are isothermal and where measurements are made above most of the matter in the disk, K and $< v^2 >$ are independent of height. The Jean's equation then becomes

$$\frac{d\ln\nu}{dz} = -\frac{1}{h}, \quad h \equiv \frac{< v^2 >}{2\pi\Sigma_0},$$

where Σ_0 is the total disk column.

This equation, taken together with two well known facts yields an immediate estimate of Σ_0. First, the Bahcall-Soneira model (Bahcall 1986), which predicts star counts very well to $V \sim 19$ has a disk exponential scale height of $h \sim 325$ pc for late-type dwarfs. Star counts are basically sensitive to stars that are ~ 3 scale heights above the plane since for $z < 2h$ the star-count cone has very little volume and for $z > 4h$, the stellar density is exponentially suppressed. Hence, the model scale height should reflect the true scale height at $z \sim 3h$, i.e., well above most of the known material in the disk. Second, the velocity dispersion of late-type dwarfs near the plane is measured to be $< v^2 > \sim 20\,\mathrm{km\,s^{-1}}$. One infers,

$$\Sigma_0 = \frac{1}{2\pi G}\frac{< v^2 >}{h} \sim 46\,M_\odot\,\mathrm{pc}^{-2} \quad \text{(naive)},$$

apparently in excellent agreement with the observed material in the disk (Bahcall 1984b),

$$\Sigma_{\mathrm{obs}} \sim 48\,M_\odot\,\mathrm{pc}^{-2}.$$

That is, there would appear to be no missing matter.

There are only three problems with the above analysis: the scale height is wrong, the velocity dispersion is wrong, and the observed disk column against which it is to be compared is wrong.

The scale height seems to be on exceptionally secure footing since it is embedded in a well-tested model. However, as Bahcall (1986) has taken pains to emphasize, the only claim made for star-count models is that they correctly predict star counts, not that they express the true structure of the Galaxy. In particular, the Bahcall-Soneira model uses a locally-determined color-magnitude (c-m) relation and applies this to stars at all heights. One expects that the zero point of the c-m relation changes as a function height, because more distant stars are likely to be more metal poor, and low metallicity stars are fainter at the same color. However, since changing the scale height has almost exactly the same effect as changing the zero-point, the model does not have to incorporate zero-point changes to correctly predict star counts. If stars at $\sim 1\,\mathrm{kpc}$ are $\sim 15\%$ fainter than those at the plane, then $h \sim 280\,\mathrm{pc}$.

The local velocity dispersion of late type stars is well measured. However, the relevant quantity is the dispersion at $z \sim 3h$. The local stars are not perfectly isothermal, but rather are a mixture of populations at several different dispersions. The hotter stars tend to rise well above the plane and dominate at 3 scale heights. Without offering any justification, I will simply assert that $< v^2 > \sim 25\,\mathrm{km\,s^{-1}}$ is a better estimate for the dispersion at $z \sim 3h$. Using these values for the scale height and dispersion, I find

$$\Sigma_0 = \frac{1}{2\pi G}\frac{< v^2 >}{h} \sim 82\,M_\odot\,\mathrm{pc}^{-2} \quad \text{(less naive)}.$$

Now there appears to be a great deal of dark matter. And in fact even within the standard model one expects a lot of dark matter: since the measurement is being made at $z \sim 800\,\mathrm{pc}$ above the plane there should be $2z\rho_0 \sim 14\,M_\odot\,\mathrm{pc}^{-2}$ of dark matter if the standard spherical dark halo with a local density $\rho_0 = 0.009\,M_\odot\,\mathrm{pc}^{-3}$ is correct.

The point is that the problem of measuring the local column density is much trickier than it might first appear. In addition to the problems of fixing the distance scale and velocity dispersion already mentioned, there are other systematic effects such as Malmquist bias, rotation of the velocity ellipsoid, unresolved binaries which vary as a function of height, and poor determination of the large-scale structure of the Galaxy, each of which can affect the final result at the level of tens of per cent. The bottom line is that this is a very tough measurement which requires great care.

Nevertheless, the naive estimate of $\Sigma_0 \sim 82\,M_\odot\,\mathrm{pc}^{-2}$ below 800 pc poses a few important questions. First, is the estimate roughly correct? Second, if it is roughly correct, where are the other $\sim 35\,M_\odot\,\mathrm{pc}^{-2}$ beyond what is

measured for $\Sigma_{\rm obs}$? As noted above, the standard model can account for only $\sim 15\,M_\odot\,{\rm pc}^{-2}$ of dark material.

3. Historical and Modern Determinations

Historically, the problem was first attacked by Oort (1932). It was Oort (1960) who first pointed to a factor ~ 2 discrepancy between the observed material and the gravitationally inferred mass. Bahcall (1984a) revived the investigation by developing a new method of self-consistent models and applying this method to archival data (Bahcall 1984b,c). One of Bahcall's two conclusions, that the factor ~ 2 problem remained, has been widely disseminated. However, his other principal conclusion that systematic errors were dominant over statistical errors has unfortunately received less attention. Bahcall's work stimulated several groups to acquire new samples and undertake new analyses.

Bienaymé, Robin, & Crézé (BRC 1987) inferred a local column density of $\Sigma_0 = 64 \pm 12\,M_\odot\,{\rm pc}^{-2}$ (excluding a dark halo) using a method of generalized star counts. They regarded this result as consistent with no missing matter, but if missing matter were allowed, their best fit to its scale height was $h \sim 600\,{\rm pc}$.

Kuijken & Gilmore (KG 1989, 1991) obtained a new sample of K dwarfs sensitive to mass in the range $300\,{\rm pc} < z < 2000\,{\rm pc}$ and concluded $\Sigma_0 = 46 \pm 9\,M_\odot\,{\rm pc}^{-2}$ plus $\sim 25\,M_\odot\,{\rm pc}^{-2}$ in dark halo below $z < 1.1\,{\rm kpc}$.

Kuijken (1991) added a local sample of K dwarfs to the KG cone sample making the combined sample sensitive to the range $0 < z < 300\,{\rm pc}$. He finds that the local density $\rho(0)$ is related to the no-missing-matter value by $\rho(0) = (1.02 \pm 0.15)\rho_{\rm NMM}(0)$.

Bahcall, Flynn, & Gould (BFG 1992) analyzed a cone of K giants (the first tracer sample specifically chosen to test the local mass density) and found $\Sigma_0 = 85 \pm 25\,M_\odot\,{\rm pc}^{-2}$ not including the contribution from the halo. Their study is sensitive in the range $200\,{\rm pc} < z < 500\,{\rm pc}$.

Finally, Flynn & Fuchs (1994) expanded the BFG sample in a parallel way to that used by Kuijken to expand the KG sample: they added a local sample of K giants. Like Kuijken's, their study was sensitive to $0 < z < 300\,{\rm pc}$ and they found $\Sigma_0 = 52 \pm 8\,M_\odot\,{\rm pc}^{-2}$ or $\Sigma_0 = 56 \pm 12\,M_\odot\,{\rm pc}^{-2}$ depending on assumptions and not including the dark halo.

All of these studies are subject to some criticism. The general star count method of BRC is subject to the same systematic errors that were illustrated in the simple example given above. As I will argue below, KG's results actually indicate a large amount of disk dark matter, $\Sigma_0 \sim 65\,M_\odot\,{\rm pc}^{-2}$ despite their claim to have found no disk dark matter. Kuijken's (1991) study depends on comparison of inhomogeneous data sets. This is also a

problem for the Flynn & Fuchs (1994) study although probably less so because DDO photometry allows them to select a more uniform sample. However, both Flynn & Fuchs (1994) and BFG are insensitive to mildly hot dark matter. Finally, while the BFG study is probably the most free from systematic errors, it suffers from poor statistics.

Let me now turn to a reanalysis of the KG study. The main message which has reached the community about KG is that they measured one number, the total column density of the disk, and found it to be consistent with the no-missing-mass value. In fact, KG measured two numbers, K and F, the linear and quadratic terms in the potential high above the plane,

$$\psi(z) = \text{const.} + Kz + Fz^2.$$

The measurement they made from their data alone showed,

$$F \sim 0, \qquad \frac{K}{K_{\rm obs}} = \frac{\Sigma}{\Sigma_{\rm obs}} = 1.4.$$

Roughly speaking, the linear term corresponds to the total column of the disk and the quadratic term corresponds to the local halo density. Hence, what KG actually found was that there is no halo dark matter and a large amount of disk dark matter (or alternatively an extremely flattened halo). Why then did they report the opposite: a standard dark halo, but no disk dark matter? KG assumed a standard *spherical* dark halo and then asked, given this assumption, what was the best-fit value for the disk. However, this best fit value is in conflict with their data at the 2.5 σ level. See Figures in Gould (1990).

My tentative impressions of all the results to date are

1) This is a tough problem: it is still possible that we do not understand the systematics.

2) KG tell us there is $\sim 25\,M_\odot\,{\rm pc}^{-2}$ of dark matter within 1 kpc which is consistent with our expectation of a round halo.

3) But KG also tell us that the dark matter is flatter than 1 kpc which is inconsistent with a round halo.

4) Kuijken (1991) and Flynn & Fuchs (1994) tell us the dark matter is not extremely close to the plane.

5) BFG provide systematically clean but statistically weak evidence for a substantial amount of dark matter.

A working hypothesis that is consistent with all the known data is that there is $\sim 25\,M_\odot\,{\rm pc}^{-2}$ of dark matter in a relatively flat distribution, $h \sim$ 400–700 pc. This could be either a massive thickish disk or a very flat (E10!) halo.

4. Other Evidence

I turn now to other evidence which might help constrain this picture: from star counts, from measurements of the shape of other galaxy halos, and from Macho (Massive Compact Object) detections.

Bahcall, Flynn, Gould, & Kirhakos (1994) examined a pair of deep ($\geq$ 2 hr) *Hubble Space Telescope* images of a high latitude field to a limiting magnitude of $I = 25.2$. They found no red stars $V - I > 3$. From this lack of detections, they concluded that faint red stars above the hydrogen burning limit do not contribute significantly to the mass of disk, thick disk, spheroid, or halo. If there is a substantial amount of dark matter in a flattened distribution, it must be in something other than stars.

Polar ring galaxies potentially provide information about the flatness of the mass distribution of other galaxies because the polar ring probes the potential perpendicular to the disk of the galaxy. Penny Sackett and her collaborators have spent several years acquiring new precision data on polar ring galaxies and subjecting these data to a more refined analysis than had been done previously. There are now very good constraints on two such galaxies. For NGC 4650A, Sackett et al. (1994) find an axis ratio 10:4 to 10:3, corresponding to E6–E7. For A0136-0801, Rick Pogge has obtained a spectacular Fabry-Perot velocity cube with 2700 independent data points. Preliminary analysis of these data by Sackett & Pogge (1994, in preparation) indicates the galaxy halo is E4–E5. The remarkable thing about both these flatness ratios is that, to within the errors, they are identical to the flatness ratios of the luminous disks of the respective galaxies. It is often remarked that polar ring galaxies are very special in that they have polar rings, so they might also be special in terms of the flatness of their halos. In fact, galaxies with high flatness ratios will have difficulty sustaining a polar ring unless the ring's axis occupies a very small region of parameter space. Hence, this argument would lead one to the opposite conclusion from the intended one: polar ring galaxies should actually be rounder than average. Another point which I think has more force is that the shapes of only two halos have been measured and we might therefore be the victims of unlucky statistics. However, it remains the case that the only two halos that have been measured have been found to be flat. If the Milky Way also had a dark halo distributed like its light, this halo would have an axis ratio $\sim$E10.

Finally, the detection rates of microlensing events toward the Galactic center and the Large Magellanic Cloud (LMC) also are consistent with a highly flattened mass distribution. The detection rate toward the LMC (Alcock et al. 1993; Aubourg et al. 1993) is too high to be due to known stars in the Galactic disk, thick disk, or spheroid (Bahcall et al. 1994) or stars in the LMC itself (Gould 1995), and too low to be due to Machos in

a standard spherical halo. It could, however, be due to Machos in a disk (Gould, Miralda-Escudé, & Bahcall 1994) or a thick disk (Gould 1994). The event rate measured toward the Galactic bulge by Alcock et al. (1994) and Udalski et al. (1994) is much higher than was anticipated due to a standard disk (Paczyński 1991; Griest et al. 1991) or to the Galactic bulge, even if the latter is barred (Kiraga & Paczyński 1994; Han & Gould 1994a; Zhao, Spergel, & Rich 1994). While it is still possible that the high event rate is due to statistical fluctuations (which are larger than one might naively expect – Han & Gould 1994b), recent unpublished reports (D. Bennett 1994, private communication) indicate an optical depth near the plane that is so high ($\tau \sim 7 \times 10^{-6}$) that it can scarcely be explained other than by a massive disk-like structure.

5. Conclusions

In conclusion then, there is certainly some dark matter within 1 kpc of the plane of the Milky Way. The absolute amount could be consistent with that expected from a standard spherical halo, but the internal evidence would seem to indicate that it is more flattened. In addition, we must keep in mind that the systematic errors could be large. Whatever this dark matter is, it is not hydrogen-burning stars.

The halos of the only two other galaxies that have ever been measured are both significantly flattened. There is no reason to assume that ours is any different.

The high rate and distribution of Macho detections seems to indicate an enormous amount of dark matter near the plane.

My best guess: $30 M_\odot\,\mathrm{pc}^{-2}$ of dark material near the Sun with scale height $h \sim 500\,\mathrm{pc}$.

References

Alcock, C. et al. 1993, Nature, 365, 621
Alcock, C. et al. 1994, ApJ, submitted
Aubourg, E. et al. 1993, Nature, 365, 623
Bahcall, J. N. 1984a, ApJ, 276, 156
Bahcall, J. N. 1984b, ApJ, 276, 169
Bahcall, J. N. 1984c, ApJ, 287, 926
Bahcall, J. N. 1986, Ann. Rev. 24, 577
Bahcall, J. N., Flynn, C., & Gould, A. 1992, ApJ, 389, 234 (BFG)
Bahcall, J. N., Flynn, C., Gould, A., & Kirhakos, S. 1994, ApJ Letters, in press
Bienaymé, O., Robin, A., & Crézé. M. 1987, A&A, 180, 94 (BRC)
Flynn, C. & Fuchs, B. 1994, A&A, in press
Gould, A. 1990, MNRAS, 244, 25
Gould, A. 1994, ApJ, 421, L71
Gould, A. 1995, ApJ, 441, 000
Gould, A., Miralda-Escudé, J., & Bahcall, J. N. 1994, ApJ, 423, L105

Griest, K. et al. 1991, ApJ, 372, L79
Han, C. Gould, A. 1994a, ApJ, submitted
Han, C. Gould, A. 1994b, ApJ, submitted
Kiraga, & Paczyński, B. 1994, ApJ, 430, L101
Kuijken, K. 1991, ApJ, 372, 125
Kuijken, K. & Gilmore, G. 1989, MNRAS, 239, 605 (KG)
Kuijken, K. & Gilmore, G. 1991, ApJ, 367, L9
Oort, J. H. 1932, Bull. Astron. Inst. Netherlands, 6, 249
Oort, J. H. 1960, Bull. Astron. Inst. Netherlands, 15, 45
Paczyński, B. 1991, ApJ, 371, L63
Sackett, P. D., Rix, H.-W., Jarvis, B. J., & Freeman, K. C. 1994, ApJ, 436, 000
Udalski, A. Szymański, J., Kaluzny, J., Kubiak, M., Krzemiński, W., Mateo, M., Preston, G. W., & Paczyński, B. 1993, Acta Astron., 43, 289
Zhao, H., Spergel, D. N., & Rich, R. M. 1994 ApJ Letters, submitted

DISCUSSION

J. Anderson: What would your favorite tracer population be, in terms of observable parameters like age and metal abundance? In other words, what should we (the observers) work on?

Gould: For mass, photometric surveys, I would favor K dwarfs. However, the precision photometry of F stars that you are doing will also allow isolation of an old population and will provide a very useful sample of tracer stars.

J. Binney: As Kuijken has told us, the dominant uncertainty in his study comes from the rotation of the velocity ellipsoid. I think this is an indication of a general trend: we have reached the limit of what we can learn by local analysis - another example is the problem with the observed value of $x=\sigma_\phi^2/\sigma_R^2$. It is now possible to model the Galaxy as a whole, three-dimensional object and doing so should largely eliminate many unnecessary uncertainties that plague local analyses. Of course, there will still be plenty of uncertainties left when unnecessary theoretical ones have been eliminated!

Gould: While I don't disagree with the goal of global analysis, I do think that more can be accomplished with local analyses. In particular, metallicity measurements of K dwarf would allow isolation of the disk and thick disk populations which would produce much better constraints on the potential.

K. Kuijken: I would like to emphasize that the uncertainty in the K+G analysis is largely affected by uncertainty in the velocity ellipsoid tilt at larger z. While measurement of K is affected at the 10-20 % level, F is much more uncertain, and it is very risky to take the modeled value of F too seriously.

Question: Can you be more quantitative about which bulge axis ratio is required to explain the microlensing of opt. depth?

Gould: A 3:1 axis ratio (such as measured by Dwek et al. from the COBE data) is still not adequate to explain the high observed optical depth toward the bulge.

M. Ruiz: I would like to mention one other source of dark matter, that is "cool white dwarfs", they have M/L $\sim 10^{-4}$ to 10^{-5}. In a deep proper motion survey of only three 5^0 by 5^0 areas of the sky I found 8 cool white dwarfs, contributing with $\sim 0.02\ M_\odot/pc^3$ to the density of matter in the Solar neighborhood. An extension of this survey is needed to confirm this preliminary result.

Gould: This is a very exciting result.

K. Stanek: I just want to mention that your and OGLE interpretations of OGLE results differ in that we think there is a hole in the stellar disk and also majority of lensing objects is in the bar. What we find is that if the lenses are in the disk, their average mass is $M \approx 0.6 M\odot$ - it would be difficult to hide many such stars, if lenses were in the disk.

H. van Woerden: My impression is that our galaxy offers a better chance to determine the vertical distribution of disk matter than other galaxies - but I would trade my impression for a better-educated opinion.

Gould: In principal I agree. So far, however, I don't think that the potential has been achieved.

R. Wyse: A comment on white dwarfs as candidates for dark matter in the Galaxy in significant amounts. Although white dwarfs are preferred over neutron stars by chemical evolution arguments, there are still severe problems with the elements such as Helium produced during quiescent stellar evolution of the progenitor stars. Further, should the white dwarfs be in binary systems, as may be expected on both observational and theoretical grounds, then Type Ia supernovae will most probably result, continuing on very long timescales. These of course produce further problems with chemical enrichment and should be observable in the outer halves of galaxies (ref Smecker & Wyse ApJ 1990). Thus the reason that White dwarfs are not discussed much is there are real problems, requiring continued models.

OUTER DISC ROTATION FROM CEPHEID VARIABLES

FREDERIC PONT

AND

DIDIER QUELOZ, MICHEL MAYOR AND PIERRE BRATSCHI
Geneva Observatory
1290 Sauverny
Switzerland

Abstract. We have measured radial velocities for a large number of classical cepheids of the Galaxy, particularly in the outer disc. We determine the rotation curve up to a galactocentric radius of 16 kpc. The results are then compared to similar studies using HII regions. We also consider some possible complications.

1. Introduction

Classical cepheids are bright, young stars, and both their distance and radial velocity are relatively easy to determine. This makes them ideal probes of the rotation of the Galaxy.

We present here the results of two studies of the Galactic rotation curve using classical cepheids :

– The first from a survey of faint cepheids (up to V=12 mag at $6 < R < 12$ kpc) with the CORAVEL spectrometer at ESO (Chile), begun in 1983 and completed last year (Pont et al. 1994a,b). The aim was to get a new determination of the local rotation constants A, R_0, u_0, v_0 as well as to have a closer look at some characteristics of the local velocity field.

– The second study consists of a sample of about 30 very faint cepheids of the outer disc (up to V=15 mag, $R > 11$ kpc) measured in radial velocities with CORAVEL and the ELODIE spectrometer of OHP (France). This program began in early 1994 and is ongoing. Its aim is to determine the rotation curve beyond R=11 kpc, a range in which the currently most reliable values, mainly from HII region data, are not very clear, showing a dip around R=10 kpc followed by an ambiguous rise at large R.

L. Blitz and P. Teuben (eds.), Unsolved Problems of the Milky Way, 661–667.
© 1996 *International Astronomical Union.*

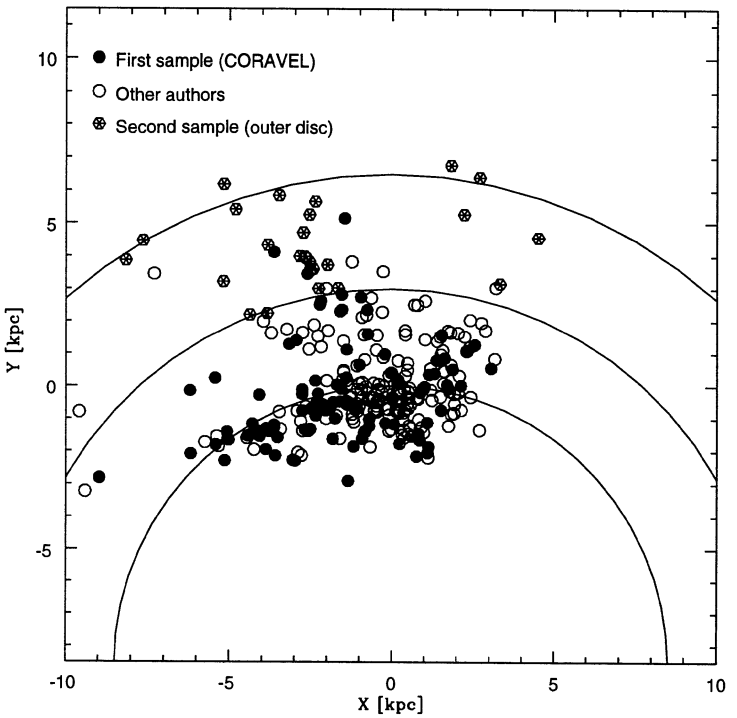

Figure 1. Position of the classical cepheids with known γ-velocities projected onto the galactic plane. The Sun is at (0,0), the galactic centre at (0,-8.5). Circles are drawn at R=8.5, 11.5 and 15 kpc. "Other authors" are mainly : Joy (1937), Stibbs (1956), Metzger et al. (1992), Moffett & Barnes (1987).

2. Observational Data

In order to use a population of stars as kinematical tracers, accurate 'distance, radial velocity' pairs are needed. Radial velocities were gathered with ELODIE or CORAVEL, and BVI photometry was complemented from La Silla (Chile) and Pic du Midi (France), or kindly communicated by Arne Henden before publication. Cepheid distances were computed from BVI photometry using period-luminosity-colour relations from Feast & Walker (1987) and Caldwell & Coulson (1987), and reddenings following Fernie (1990). Fig. 1 shows the position in the galactic plane of the considered set of classical cepheids with known γ-velocities. Notice that the outer disc sample does reach much remoter parts of the disc.

Our strategy, in order to obtain centre-of-mass radial velocities ("γ-velocities") from radial velocity pulsation curves with a minimum number of observations, was to get 5-6 measurements for every cepheid, evenly spread

over the pulsation phase, then to fit the data with the velocity curve of another cepheid of similar period. With this procedure one can recover the γ-velocity within 2-3 $\mathrm{km\,s^{-1}}$, a sufficient precision for galactic kinematics since the uncertainties are dominated by the $\sim$ 10 $\mathrm{km\,s^{-1}}$ intrinsic velocity dispersion.

3. Results

The main results are the followings :

- First, using an axisymmetric rotation model, we obtained a new set of rotation constants : $R_0 = 8.09 \pm 0.30$ kpc, $A = 15.92 \pm 0.34\ \mathrm{km\,s^{-1}\,kpc^{-1}}$ and $2\,AR_0 = 257 \pm 7\ \mathrm{km\,s^{-1}}$.
- The rotation curve is well constrained by classical cepheids between 6 and 11 kpc.
  Our data also offer strong evidence that the $\sim 3\ \mathrm{km\,s^{-1}}$ mean residual (between observed and expected velocities) long observed with cepheids is indeed a real dynamical effect and not, as sometimes proposed, an intrinsic shift between measured and actual γ-velocity (Pont et al. 1994a).
- The outer disc sample brings a strong constraint on the rotation velocity for $11 < R < 15$ kpc. Using the standard values $R = 8.5$ and $\theta_0 = 220\ \mathrm{km\,s^{-1}}$, the rotation curve beyond $R = 11$ kpc remains flat at the $\sim 200\ \mathrm{km\,s^{-1}}$ level (Fig. 2).

Comparison with HII Region Data

A comparison between Fig. 2 and Fig. 3, displaying the rotation curve for HII regions, makes it clear that the cepheid data show no evidence of the rotation velocity rise seen in the HII region data. It seems that this interesting discrepancy cannot be attributed to noise in the cepheid data, since the cepheids are quite tightly grouped around $v_{rot} \simeq 200\ \mathrm{km\,s^{-1}}$. Large errors on radial velocities are also unlikely.

Now, there could be some systematic shift in either cepheid distances or HII region distances. A distance scale change moves the points diagonally in the v_{rot} vs. R graphs (Figs. 2 and 3), the distance entering the calculation of both quantities. A better way to look at it is on the angular velocity (Ω) versus R graph (Fig. 4). The advantage of such a representation is that distance scale changes move the points horizontally. In this diagram, the HII region data would be around the 240 $\mathrm{km\,s^{-1}}$line at large R. What is to be seen in Fig. 4 is that to bring the two sets of data in agreement by adjusting the distance scale, rather large distance changes are needed. Moreover, if the cepheids were to carry all the burden of this change, they would be brought to quite unreasonable distances (14-20 kpc) which would

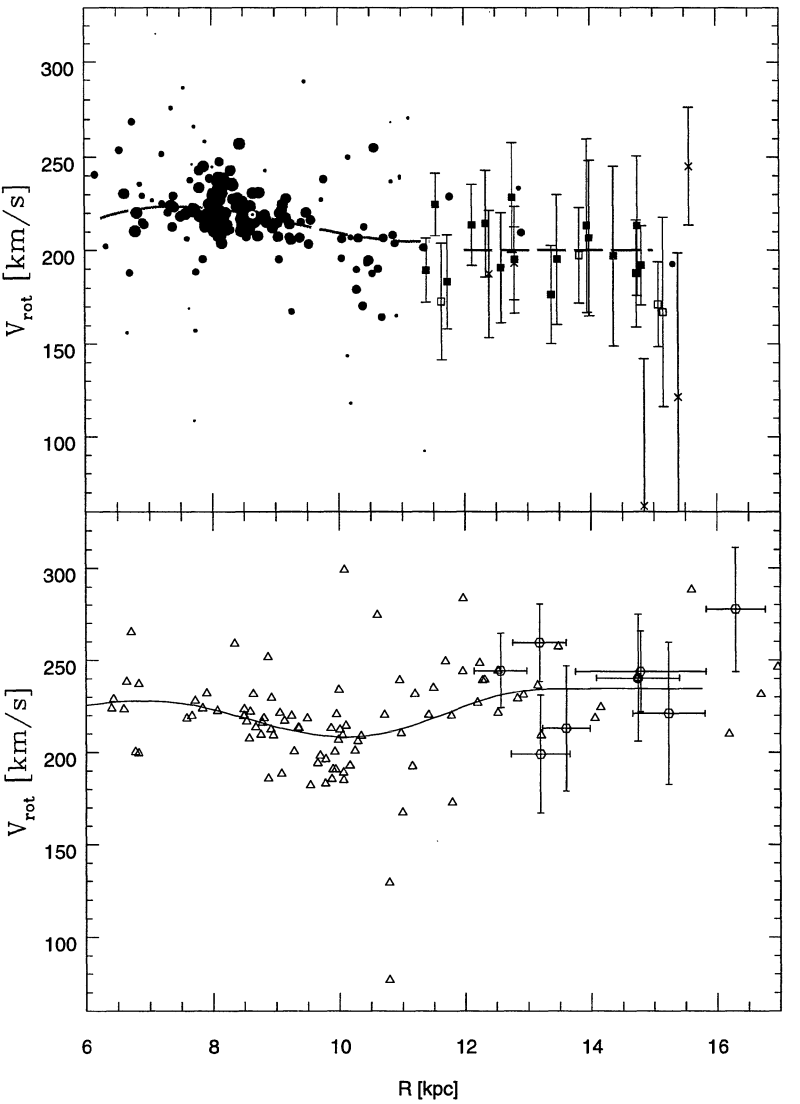

Figure 2. **(top)** Rotation curve for classical cepheids, assuming $R_0 = 8.5$ kpc and $\theta_0 = +220$ km s^{-1}. For the first sample, the dots have a size proportional to their weight in the fit (a function of galactic longitude mainly). The cepheids of the second sample are plotted as black squares, white squares if their photometry is incomplete, and crosses for possible type II cepheids. Error bars correspond to a 10 km s^{-1} kinematical velocity dispersion on the line-of-sight. The dashed line indicates the rotation curve fitted with an axisymmetric rotation model for $6 < R < 11.5$ kpc and a flat curve at 200 km s^{-1} for $R > 12$ kpc.

Figure 3. **(bottom)** Rotation curve for HII regions. Data collected from Fich et al. 1989 (triangles), Turbide & Moffat 1993 (hexagons with error bars) and Clemens 1985 (curve) on the same scale as Fig. 2. Note that while the cepheid data remains flat at 200 km s^{-1}, the HII region data rises up to $v_{rot} \simeq 240$ km s^{-1} or higher.

make their positions in the galactic plane rather unrealistic. Thus, it seems that either the rotation velocity of cepheids and HII region is different (different rotation velocity or different non-circular motion), or the HII region distance scale has to be somehow shortened.

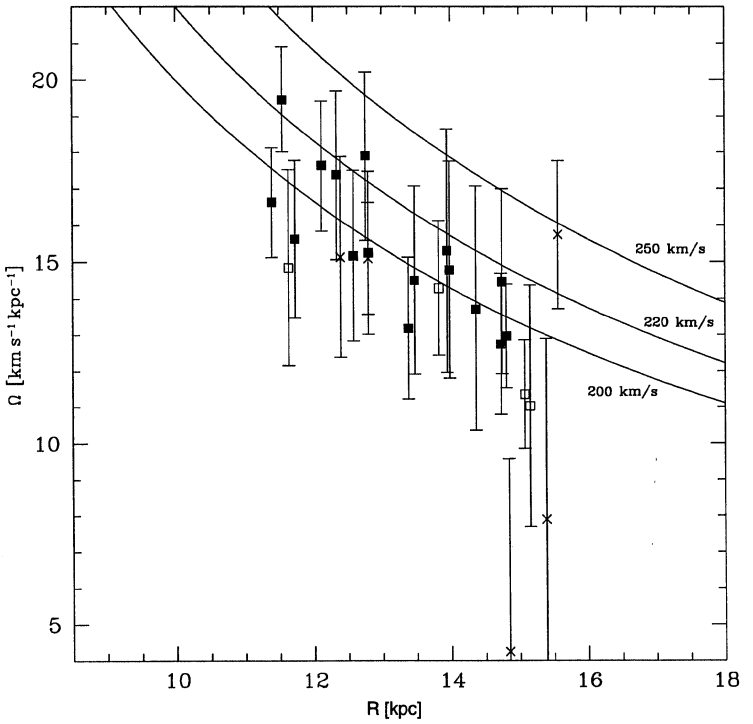

Figure 4. Angular velocity curve, Ω vs. R, for outer disc cepheids. Three lines at constant v_{rot} are indicated. Same symbols as in Fig. 2. The HII region data would be around $v_{rot} = 240$ km s^{-1} for $R > 13$ kpc. In this graph a distance scale change moves the points horizontally. Notice that bringing the cepheid data to $v_{rot} = 240$ km s^{-1} would push many of them beyond R=16 kpc.

4. Difficulties for $R > 11$ kpc Cepheids

Type II Cepheids

The most daunting problem with the outer disc cepheid sample is the possible presence of type II cepheids. For a variety of reasons, type II cepheids are even more difficult to discriminate in the outer disc than near the Sun. However, the dispersion of the final γ-velocities around that predicted by a flat rotation curve at 200 km s^{-1} is only $\sigma(v_{obs} - v_{model}) = 8$ km s^{-1}. This value is even lower than the velocity dispersion of solar neighbour-

hood cepheids (~ 10 km s^{-1}), and much lower than that expected for type II cepheids ($\sigma_{typeII} > 20 - 30$ km s^{-1} + scatter from inaccurate distances). Thus, we feel confident in expecting only a small number of type II cepheids in our sample.

Non-axisymmetric Motions

Any determination of the rotation curve from radial velocities without proper motions is vulnerable to non-axisymmetric motions, not included in the model. At first sight, the northern and southern data show no difference, which puts limits on a LSR radial motion for instance. But the sample is not large enough at present to be more specific.

Metallicity Corrections

If there is a metallicity gradient in the disc, one expects high R cepheids to be metal deficient. This affects the distance determination in two ways : it changes the coefficients of the PL or PLC relations, and it changes the reddening determinations for BVI photometry.

We used theoretical magnitudes and colours from Chiosi et al. (1993) to predict the changes introduced by metal deficiency on the cepheid distance determination. We also considered corrections proposed by Caldwell & Coulson (1985, 1987) for comparison.

It appears that the agreement between PL(V), PLC(BV) and PL(I) distances is much lowered by the corrections. More specifically, something seems to be wrong with the reddening correction. To discriminate between the possible causes of this discrepancy (insufficient photometry, lower gradient in the disc, inaccurate theoretical colours, changes in $\mathcal{R}$,..), we intend to get more photometry, and a spectroscopic indication of metallicity, for the outer disc cepheids.

References

Caldwell J. & Coulson I. 1985, MNRAS 212, 879
Caldwell J. & Coulson I. 1987, AJ 93, 1090
Chiosi C., Wood P., Capitanio N. 1993, ApJSS 86, 541
Feast M. & Walker A. 1987, ARAA 25, 345
Fernie J. 1990, ApJSS 72, 153
Fich M., Blitz L., Stark A. 1989, ApJ 342, 272
Joy A. 1937, ApJ 86, 363
Metzger M., Caldwell J., Schechter P. 1992, AJ 103, 529
Moffett T., Barnes T. 1987, PASP 99, 1206
Pont F., Mayor M., Burki G. 1994a, A&A 285, 415
Pont F., Burki G., Mayor M. 1994b, A&AS 105, 165
Stibbs D. 1956, MNRAS 116, 453
Turbide L. & Moffat A. 1993, AJ 105, 1831

DISCUSSION

Feast: Do you see any evidence of streaming motions ?

Pont: The residual velocity field exhibits local wavy fluctuations of the order of 5 km/s on a typical scale of 2 kpc, but with no obvious pattern. As for the outer disc sample, the north-south symmetry is good.

H. van Woerden: Could the difference of rotation curves between HII regions and Cepheids be caused by a difference in non-axisymmetric motions, related to a difference in age? A difference of 50-100 Myr would suffice.

Pont: In principle it could I suppose. The cepheids are still young, but there may have been enough time for them to escape the gas streaming motions. However, the HII regions studied cover a large portion of the outer disc, so that rather large-scale non-axisymmetric motions would be needed to explain the difference. If this is the case, a good knowledge of the cepheid rotation curve is important, since for most application one is interested in the *stellar* rotation curve.

WHERE DOES THE GALAXY END?

F.D.A. HARTWICK
Department of Physics and Astronomy
University of Victoria, Victoria, B.C., Canada, V8W 3P6

Abstract.

The spatial distribution of the outlying satellites of the Galaxy has been determined by fitting a three dimensional surface to the positions of 10 companion galaxies and 13 distant globular clusters. Both groups show a highly flattened distribution whose minor axes are aligned to within $\sim 5°$. The combined group of 23 objects shows a triaxial distribution with semimajor axis extending $\sim$ 400 kpc. The minor axis is inclined at $\sim 76°$ to the Galactic poles. There is a suggestion of a nested hierarchy consisting of satellite galaxies, globular clusters, and distant halo field stars, in order of decreasing spatial extension.

1. History and an Operational Definition of the Galaxy

The question posed in the title has an interesting history (*c.f.* Plaskett & Pearce 1935 for a review of early developments). Briefly, the first quantitative investigation of the Galaxy's extent was made near the end of the 18th century by W. Herschel who analyzed star counts as a function of magnitude in different areas of the sky. Herschel's Galaxy had the sun near the center of a flattened system whose major diameter, based on a modern calibration, was $\sim$ 2 kpc. Much later, Kapteyn (1922) also using the results of star counts arrived at a very similar picture (*i.e.* heliocentric, but whose size was now $\sim$ 17 kpc). Neither Herschel nor Kapteyn incorporated the distorting effects of interstellar absorption into their models. It was Shapley (1918) who used the distribution of globular clusters to define the picture of the Galaxy that we use today. The major result of Shapley's work was the demonstration that the sun was displaced from the center of

L. Blitz and P. Teuben (eds.), Unsolved Problems of the Milky Way, 669–680.
© 1996 *International Astronomical Union.*

the system by what we now believe to be $\sim$ 8 kpc. Furthermore, the size of Shapley's Galaxy as delineated by the roughly spherical distribution of globular clusters was $\sim$ 30-40 kpc.

For the purpose of this discussion we shall follow historical precedent and define the Galaxy to be the volume contained by the localized concentration of the most spatially extended light (baryonic) tracer. Such a definition is likely to result in a lower limit to the true extent of the Galaxy since the dominant component of the universe is currently believed to be non-baryonic and hence dark and dissipationless. As we discuss in the next section, the most spatially extended light tracers presently known are the satellite galaxies, and it is the spatial distribution of these objects which is the main focus of this contribution.

2. The Spatial Distribution of the Outlying Satellites

When Shapley presented his view of the Galaxy in 1918, most of the known globular clusters lay within $\sim$ 20 kpc of the Galactic center. It was nearly twenty years later when Shapley discovered the first of the family of dwarf spheroidal galaxies. It was not until the early 1950's, that a number of new relatively distant, low surface brightness satellites of the Galaxy (both dwarf spheroidal galaxies and globular clusters) were discovered on plates taken with the newly commissioned 48-inch Schmidt telescope on Mt. Palomar. Since that time other low surface brightness satellites have been discovered, primarily in the southern hemisphere. A recent compilation of globular cluster distances by Tello (1994) shows 16 clusters with distance from the Galactic center (R_g) $>$ 25 kpc while a similar compilation of local group galaxies by van den Bergh (1994) contains 11 galaxies with $R_g < 400$ kpc.

Kunkel & Demers (1976) and Lynden-Bell (1976) were the first to discuss the spatial distribution of these outlying systems. Kunkel & Demers and Kunkel (1979) drew attention to the fact that most of the outlying systems (those with $R_g > 25$ kpc) lay in a well defined plane. Lynden-Bell (1982), on the other hand, noted the tendency for certain objects (*i.e.* Ursa Minor, Draco, and Carina), to be coincident with the Magellanic Stream of neutral hydrogen. This, in turn, led him to the hypothesis that this planar system was composed of debris from a greater tidally-disrupted Magellanic galaxy. Furthermore, Lynden-Bell (1982) postulated that the tidal demise of a second (now possibly unrecognizable) 'victim' had given rise to objects defining the Fornax- Leo (I and II)-Sculptor (FLS) stream. More recently, Majewski (1994) has noted that the Phoenix and Sextans systems, as well as a number of globular clusters with the reddest horizontal branches, also populate the FLS stream and thus reinforce Lynden-Bell's hypothesis.

Inspired by this earlier work another approach has been taken here.

Rather than attempting to fit the satellites into great streams I have tried to fit a three dimensional surface to all of the outlying systems together. The surface was determined by doing a least squares solution for α, β, γ, δ, ϵ, and ϕ in the following expression:

$$\alpha x^2 + \beta y^2 + \gamma z^2 + 2\delta xy + 2\epsilon xz + 2\phi yz = 1 \quad (1)$$

where x,y,and z are rectangular Galactocentric coordinates. The cross terms in the above expression can be eliminated by rotating the coordinate system to one aligned with the principal axes x', y', z' to yield the equation for a triaxial ellipsoid:

$$\frac{x'^2}{a^2} + \frac{y'^2}{b^2} + \frac{z'^2}{c^2} = 1 \quad (2)$$

Using the above procedure a surface has been fit to a group of 23 objects: 13 globular clusters (the 16 clusters in Tello's list with $R_g > 25$ kpc minus NGC1466, NGC1841 and Recticulum which may be satellites of the LMC) and a group of 10 local group galaxies (the 11 galaxies with $R_g < 400$ kpc minus the SMC). The newly discovered dwarf spheroidal galaxy in Sagittarius (Ibata *et al.* 1994) was not included because its value of R_g appears to be less than 25 kpc. The results of the solution are shown in Fig. 1. Note that the surface is indeed triaxial with $c/a = 0.24$, $b/a = 0.52$ and that the direction of the minor axis points to $l = 306°$, $b = 14.5°$ (*i.e.* highly inclined to the Galactic pole). The uncertainties associated with each of the parameters in Fig. 1 are 90% confidence limits.

In view of these somewhat surprising results, which are based on such a small number of objects, some additional numerical experiments were carried out. The first test was to determine how often an *ellipsoidal* distribution with flattening $c/a \leq 0.24$ would occur by chance given an isotropic distribution (with allowance for the zone of avoidance) of 23 objects with the same radial distribution of distances as our sample. The result is 150 times out of 1000 trials. This ratio is reduced to 77 times out of 1000 if the additional constraint of $b/a \leq 0.52$ is also imposed. Next, having determined that the minor axis of the system of 13 globular clusters ($l = 307^{+17}_{-23}$, $b = 19.1^{+2.1}_{-21.4}$) was within $\sim 5°$ of the minor axis defined by the system of 10 satellite galaxies ($l = 305^{+39}_{-2.3}$, $b = 14.1^{+3.9}_{-6.6}$) from separate solutions of equations 1 and 2, it was found that such a situation would occur only 2 times in 1000 by chance, assuming once again an isotropic distribution of directions within each group of objects. To summarize, it is perhaps not surprising that 23 objects distributed isotropically would yield an ellipsoidal distribution as extreme as is observed in Fig. 1. It will happen by chance 8% of the time. What is much less likely to happen by chance is to have two *ellipsoidal* groups of objects with combined $c/a \leq 0.24$ whose minor axes

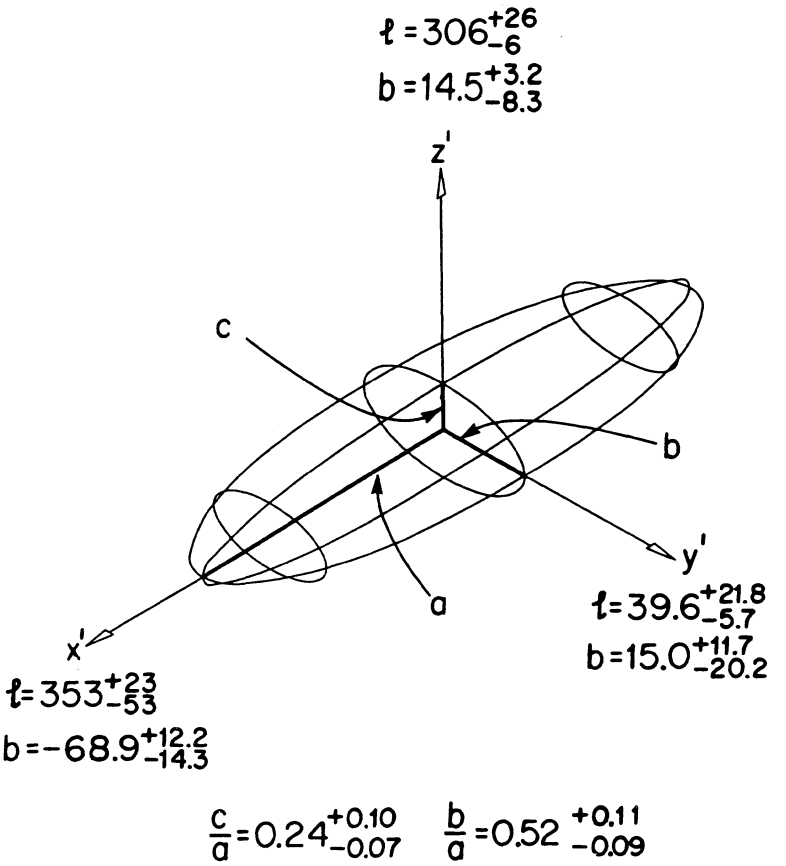

Figure 1. The orientation (in Galactic coordinates) and the shape of the surface defined by the distribution of 23 outer globular clusters and satellite galaxies.

are aligned to within 5°. The latter result appears to imply that there is a close connection between the globular clusters and the satellite galaxies.

Figure 2 shows the spatial distribution in rectangular coordinates of the 23 objects used in the solution in a coordinate system aligned with the principal axes of Fig. 1. Note that the major axis extends to nearly 800 kpc. Figure 3 shows the distribution of all of the local group galaxies in van den Bergh's (1994) compilation plotted in the same coordinate system but with reduced scale. Notice that the minor axis of the above ellipsoid points very nearly towards M31. Furthermore, there is a hint that the group of objects associated with M31 may be exhibiting a spatial distribution similar to the objects around the Galaxy. Figure 4 shows plots similar to Figs. 2 and 3 but with a projection perpendicular to the line of nodes, in order to show the effects of the zone of avoidance on the spatial distribution. If the

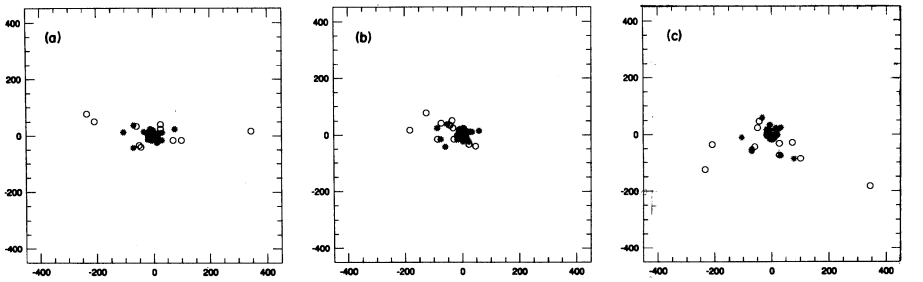

Figure 2. The spatial distribution of globular clusters (filled circles) and satellite galaxies (open circles) in the 'halo' coordinate system of Fig. 1. a) x-z projection b) y-z projection and c) x-y projection. Both scales are in kiloparsecs.

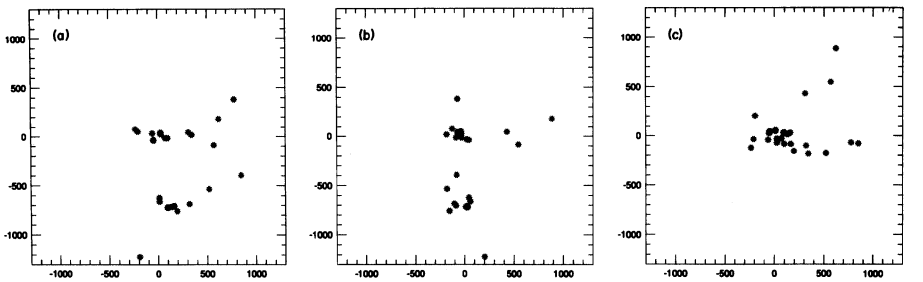

Figure 3. The local group galaxies in the same coordinates and projections as Fig. 2. Note the reduced scale.

distribution of objects around M31 is in fact similar to the Galaxy then there may be as yet undiscovered companion galaxies to M31 obscured by the Galactic plane.

3. Halo Field Star Surveys at $R_g > 25$ kpc

It seems unlikely that there are significant numbers of satellite galaxies left to be discovered around our Galaxy. Therefore, in order to make further progress in delineating the outer halo, we can look at the distribution of distant field stars. Table 1 summarizes some recent stellar surveys which extend beyond 25 kpc. The second column of the table indicates the kind of star used in the survey including RR Lyrae (RR) stars, blue-horizontal-branch (BHB) stars, carbon (C) stars and main sequence (m.s.) stars. The third and fourth columns of Table 1 give the Galactic latitude (b) and the latitude in the 'halo' coordinate system of Fig. 1 (b_h). It is not surprising

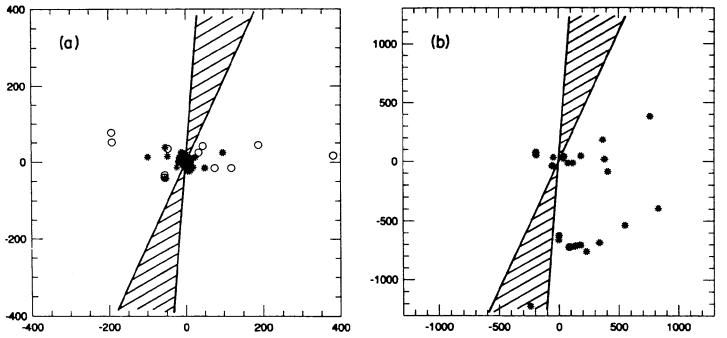

Figure 4. Same as Figs. 2 & 3 but with x-y coordinates rotated to project distributions in a plane perpendicular to the line of nodes to show the Galactic zone of avoidance (hatched area).

that most surveys have been done at relatively high Galactic latitude so that the leverage is poor for the detection of the flattening exhibited by the outlying systems. An exception is the Saha (1984) field with $b_h = -69°$. It is interesting to note that the faintest variable detected is 0.6 mag brighter than those in Saha's lower 'halo' latitude fields. The work by Bahcall *et al.* (1994) appears to be a promising way to probe the stellar halo to large distances (*e.g.* at $I = 25.3$, assuming $M_{V,TO} = 4$ and $(V - I)_{TO} = 0.6$ the limiting distance would be > 200 kpc). This assumes that the statistics are improved by looking at substantially larger areas and that unambiguous separation of faint main sequence stars from *stellar-like* extragalactic contaminants can be made.

4. The Density Profiles of the Three Luminous Components

Cursory examination of the radial extent of each of the distant components (stars, clusters and galaxies) suggests the existence of a nesting hierarchy in order of increasing spatial extension. In order to quantify this apparent tendency we have used the V/V_{max} statistic to determine the power γ in the following assumed density law:

$$\rho \propto s^{-\gamma} \tag{3}$$

where s is the distance measured along the minor axis of Fig. 1. The results are shown in Table 2 where the RR Lyrae star data is that of Saha (1984) and n is the number of objects in each solution for the indicated observed range in both R_g and s.

Clearly the results for the stellar component can and should be improved in the future. Confirmation of a nesting hierarchy could have important implications for the early evolution of the Galaxy.

TABLE 1. Field Star Surveys ($R_g > 25$ kpc)

Survey	Objects	b	b_h	Area (sq.deg)	B_{lim}	B_{faint}	R_{gfaint} (kpc)
Saha 1984	RR	24°	-25°	44	19.5	18.7	40
		30	-22	44	19.5	18.9	43
		-29	-69	44	19.5	18.1	28
Hawkins 1984	RR	-47	14	16	21.0	20.0	59
Ciardullo *et al.* 1989	RR	70	33	–	—	V=19.2	52
Sommer-Larsen&	BHB	-90	-14	18	V=18.7	V=18.6	38
Christensen 1986		-51	-12	17	V=19	V=18.4	26
Sommer-Larsen	BHB	-51	-12	17	V=19	V=18.6	31
et al. 1989		-45	22	29	V=19	V=18.4	34
Norris &	BHB	-47	14	18	20.0	20.0	70
Hawkins 1991							
Arnold &	BHB	-62	-43	33	19.5	18.5	38
Gilmore 1992		44	29	33	19.5	18.8	40
Bothun *et al.* 1991	C	±90	±20	1400	V=16	V=16	50*
Richer & Fahlman 1992	m.s.	73	-2	0.012	I=24.5	—	65
Richstone *et al.* 1992	m.s.	-89	-14	0.002	25.0	24.8	?
Bahcall *et al.* 1994	m.s.	-51	4	0.001	I=25.3	—	?

* after elimination of dwarf carbon stars (Green *et al.* 1994)

TABLE 2. Density Law Exponent

Objects	n	γ	$R_g(kpc)$	$s(kpc)$
Galaxies	10	$2.8^{+0.3}_{-0.4}$	25 – 400	24 – 101
Clusters	13	$3.3^{+0.9}_{-0.9}$	25 – 120	12 – 49
RR Lyrae	10	$7.3^{+2.7}_{-2.4}$	25 – 45	11 – 26

5. The Outer Halo and the HI Warp

A common feature of many spiral galaxies is the existence of a warp in the outer parts of the disk. Our Galaxy is no exception, and a particularly good

illustration of the warp of the Galactic HI is shown in Fig. 1 of Freudenreich *et al.* (1994) based on the data of Burton (1992). The most naive theory for producing warps has as its starting point a misalignment between the inner disk and an axisymmetric flattened outer halo. However, this naive theory has its problems which among other possibilities could be related to the existence of a triaxial outer halo (*c.f.* Binney 1992). As can be seen in Fig. 1 of Freudenreich *et al.*, the line of nodes of the Galactic warp is within $\sim 10°$ of the sun-centre line. The line of nodes determined from the distribution of outer satellites (defined by the intersection of the plane perpendicular to the minor axis of Fig. 1 and the Galactic plane) is 216°. This difference, $\sim 36°$, is probably not significant given the uncertainties in the model. Finally, we note that at least the sign of the warp is in agreement with intuitive expectation (*i.e.* above the plane in the first two quadrants and below in the last two). In summary, our understanding of the cause of warps is incomplete at present but it seems likely that there will be a close connection between the structure of the outer halo and the Galactic warp.

6. Summary and Discussion

The main results of this work can be summarized as follows. By fitting a three dimensional surface to Galaxy satellites beyond 25 kpc it is found that both the globular clusters and satellite galaxies show highly flattened spatial distributions whose minor axes are aligned to within $\sim 5°$. Such a situation which implies a close connection between the two groups of objects is extremely unlikely to have arisen by chance on the assumption that objects in both groups were drawn from an isotropic angular position distribution. The surface determined from the combined sample of 23 objects is a triaxial ellipsoid whose semimajor axis is ~ 400 kpc in extent. The orientation of the principal axes are shown in Fig. 1. The minor axis of the ellipsoid is inclined at 75.5° to the direction of the Galactic pole. When all of the local group galaxies are plotted in the new coordinate system (Fig. 3) one finds that the minor axis of the Galactic system points approximately in the direction of M31 and, in addition, the suggestion that the distribution of M31 satellites may be mimicking that of the Galaxy. A summary of recent stellar surveys to distances > 25 kpc is given. The available data are not inconsistent with the distribution found for the outer satellites but deeper surveys, especially at low Galactic latitudes, are still required. Finally, from the density profiles there is marginal evidence that the various components (*i.e.* stars, clusters, and satellite galaxies) are nested in order of increasing spatial extent. Figure 5 is a sketch along the major axis of the Galaxy and attempts to illustrate what has been found above.

Recent N-body calculations of dissipationless collapse (*e.g.* Frenk *et al.*

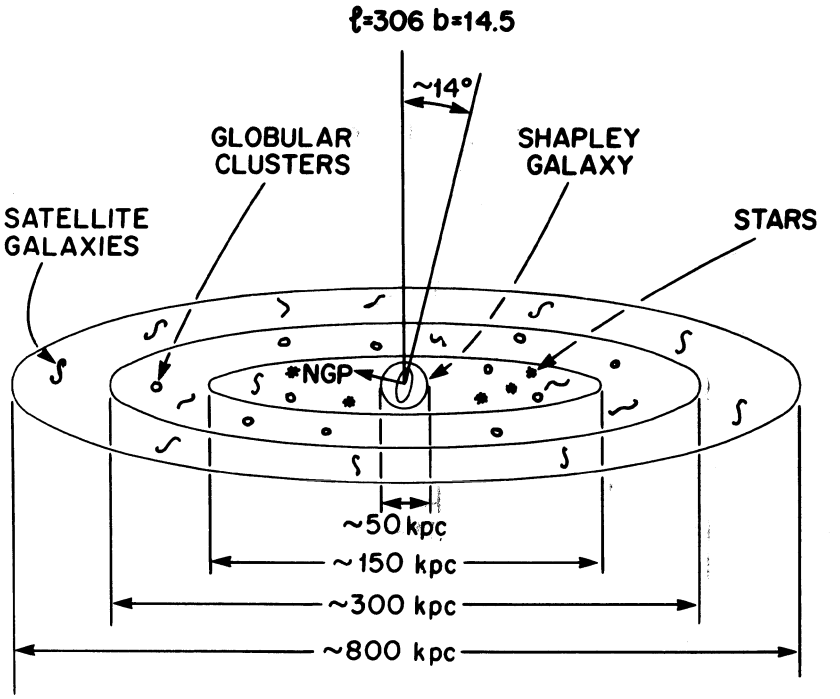

Figure 5. Summary sketch showing rough major axis dimensions of the stellar, globular cluster and satellite galaxy components. Note the orientation of the north Galactic pole (NGP).

1988; Dubinski & Carlberg 1991; Warren *et al.* 1992) show that the dark halos are triaxial with c/a$\sim$ 0.5 and b/a$\sim$ 0.7. The halos should become more oblate if a small dissipative component is included (Katz & Gunn 1991; Dubinski 1994). The fact that the ellipsoid found here has much more extreme flattening may be a reflection of the fact that *dissipational* tracers are being used to determine the shape. On the other hand, the misalignment between the Galactic disk and the minor axis, as well as the formation of a warp, seems not at all unusual in the hierarchal merging picture (*c.f.* Katz & Gunn 1991).

The outer satellites which we associate with the Galaxy extend as far away as 390 kpc. In a recent study involving the correlation in redshift of galaxies and QSO absorption line systems Lanzetta *et al.* (1994) have found in one case a Lyman α system with impact parameter 347 h^{-1} kpc. Clearly, an extended galaxy provides a rationalization for such a result. Furthermore, as the Katz & Gunn models evolve, gas collects in the cores of dark matter clumps. These structures resemble (for a time) the minihalos of Rees (1986) which have proved so successful in explaining the high

redshift Lyman α absorbers. Because of limited resolution, the fate of these minihalo-like structures in the outermost parts of the Katz & Gunn models (where collisions are rare) is not clear. However, one can imagine at least three endpoints: a) the gas cools and condenses into stars and forms what may eventually resemble a dwarf spheroidal galaxy, b) the gas is not able to condense and remains a candidate for a Lyman α absorption line observation, and c) two minihalos may occasionally collide possibly forming a globular cluster in the process. When combined with the inner stellar spheroid which *is* seen in the models (Katz 1992), one could have a natural explanation for the observed nesting hierarchy.

The author gratefully acknowledges many useful discussions with H. Vedel and C. Pritchet.

References

Arnold, R., Gilmore, G. (1992), *Mon. Not. R. astr. Soc.*, 257, 225.
Bahcall, J., Flynn, C., Gould, A., Kirhakos, S. (1994), *Astrophys. J.*, in press.
Binney, J.J. (1992), *Ann. Rev. Astron. Astrophys.*, 30, 51.
Bothun, G., Elias, J.H., MacAlpine, G. *et al.* (1991), *Astron. J.*, 101, 2220.
Burton, W.B. (1992), in *The Galactic Interstellar Medium*, ed. D. Pfenniger & P. Bartholdi (New York: Springer-Verlag), 134.
Ciardullo, R., Jacoby, G., Bond, H. (1989), *Astron. J.*, 98, 1648.
Dubinski, J. (1994), submitted to *Astrophys. J.*
Dubinski, J., Carlberg, R.G. (1991), *Astrophys. J.*, 378, 496.
Frenk, C.S., White, S.D.M., Davis, M., Efstathiou, G. (1988),*Astrophys. J.*, 327, 507.
Freudenreich, H.T., Berriman, G.B., Dwek, E. *et al.* (1994), *Astrophys. J. Lett*, 429, L69.
Green, P.J., Margon, B., Anderson, S.F., Cook, K.H. (1994), *Astrophys. J.*, in press.
Hawkins, M.R.S. (1984), *Mon. Not. R. astr. Soc.*, 206, 433.
Ibata, R.A., Gilmore, G., Irwin, M.J. (1994), *Nature*, 370, 194.
Kapteyn, J.C. (1922), *Astrophys. J.*, 55, 302.
Katz, N. (1992), *Astrophys. J.*, 391, 502.
Katz, N., Gunn, J.E. (1991), *Astrophys. J.*, 377, 365.
Kunkel, W.E. (1979), *Astrophys. J.*, 228, 718.
Kunkel, W.E., Demers, S. (1976), *R. Greenwich Obs. Bull.*, No. 182, 241.
Lanzetta,K.M., Bowen, D.V., Tytler, D., Webb, J.K. (1994), *Astrophys. J.*, in press.
Lynden-Bell, D. (1976), *R. Greenwich Obs. Bull.*, No. 182, 235.
Lynden-Bell, D. (1982), *Observatory*, 102, 202.
Majewski, S.R. (1994), *Astrophys. J. Lett*, 431, L17.
Norris, J.E., Hawkins, M.R.S. (1991), *Astrophys. J.*, 380, 104.
Plaskett, J.S., Pearce, J.A. (1935), *Publ. Dom. Astrophys. Obs.*, 5, 239.
Rees, M. (1986), *Mon. Not. R. astr. Soc.*, 218, 25P.
Richer, H.B., Fahlman, G.G. (1992), *Nature*, 358, 383.
Richstone, D., Gould, A., Guhathakurta, P., Flynn, C. (1992), *Astrophys. J.*, 388, 354.
Saha, A. (1984), *Astrophys. J.*, 283, 580.
Shapley, H. (1918), *Astrophys. J.*, 48, 154.
Sommer-Larsen, J., Christensen, P.R. (1986), *Mon. Not. R. astr. Soc.*, 219, 537.
Sommer-Larsen, J., Christensen, P.R., Carter, D. (1989), *Mon Not. R. astr. Soc.*, 238, 225.
Tello, C. (1994), *Astron. J.*, 107, 1381.
van den Bergh, S. (1994), *Astron. J.*, 107, 1328.
Warren, M.S., Quinn, P.J., Salmon, J.K., Zurek, W.H. (1992), *Astrophys. J.*, 399, 405.

DISCUSSION

J. Binney: Cen A is certainly a system in which gas on a small scale is rotating about an axis that is the long axis of the large-scale stellar distribution. Such systems seem to form often enough in the chaotic conditions of N-body models since gas and collisionless particles are subject to very different pressure. If this sort of thing is known to happen on a small scale, there seems every reason to expect its occurrence on larger scales, which have had less time to settle to an ordered state. (no reply necessary)

B. Burke: The c-axis of the "Shaply Galaxy" is nearly at right angles to the larger system that you derive. It contains most of the mass, and is triaxial, but predominantly oblate. This would dominate the potential, so the orthogonality might seem surprising (although we know of such systems). Any comment on this?

Hartwick: (*followed by Hartmann, referring to Binney's result*) So the orientation is an accident.

K. Freeman: Can you say anything about the kinematics of this outer triaxial halo system? It would be interesting to look for systematic motions in a system that is so elongated.

Hartwick: I have not yet looked at the kinematics in detail.

U. Haud: The fact that the companions of giant galaxies are preferentially concentrated to the plane, nearly perpendicular to the plane of main galaxy was first mentioned by Holmberg (1969). We have made corresponding analysis using the data on several tens of nearby groups of galaxies and confirmed such preferred concentration using both, the data on spatial distribution of companions and on their kinematics. Our results are published in A & A vol. 229, p. 47 (1990).

L. Ozernoy: You have illustrated convincingly how the size of the Milky Way Galaxy had grown in accordance with the operational definition of the Galaxy, from 2kpc to 800kpc. Bearing in mind the dark halos of the galaxies it seems possible that the dimensions of M31 and our galaxy's halos are overlapping. If the dark matter of these both galaxies is, in a sense, a common substance could we still consider the galaxies as being isolated?

Hartwick: That is possible since even the most extended light tracer may be biased i.e. may not be tracing the mass distribution.

J. Sellwood: There is a suggestion from the work of Quinn & Goodman that satellite galaxies with orbits lying close to the plane of a disc galaxy suffer more rapid dynamical friction than those which orbit over the pole. Wouldn't such an effect bias your estimate of the halo shape?

Hartwick: As I understand it, there may not be enough time for the Quinn-Goodman process to operate on the most distant objects but the question should be investigated in more detail.

HOW DO THE STELLAR DISC AND THICK DISC STOP ?

A.C. ROBIN
Observatoire de Besançon, (robin@obs-besancon.fr)

M. CRÉZÉ
Observatoire de Strasbourg, (creze@simbad.u-strasbg.fr)

AND

V. MOHAN
U.P.S.O., Manora Peak, Nainital, 263129 India

1. Abstract

As part of a stellar population sampling program, a series of photometric probes at various field sizes and depths have been obtained in a low extinction window in the galactic anticentre direction. Very deep CCD frames probe the most external parts of the disc, providing strong evidence that the galactic density scale length for the old disc population is rather short (2.5 kpc) and drops abruptly beyond 5.5-6 kpc.

Deeper frames in the I band allow to estimate photometric distances and confirm the position of the disk edge. A few stars are found at larger distances. Their number is exactly what we expect if the thick disk does not have any cutoff. We discuss the implications for the formation and evolution of the disc, for the star formation threshold, and for the origin of the thick disc population.

2. Introduction

Efforts to sample star distributions in the galactic plane should face both the problem of overcrowding and the complex structure of the absorbing layer. For these reasons the outer part of our own galactic disc is very poorly known. The radial scale length of the density decrease is controversial and we have nearly no indication what happens at the end.

L. Blitz and P. Teuben (eds.), Unsolved Problems of the Milky Way, 681–687.
© 1996 *International Astronomical Union.*

Three previous papers (Mohan et al. 1988, and Robin at al. 1992a,b) present the first results of a stellar population sampling program, including a series of photometric probes at various field sizes and depths in a low extinction window in the galactic anticentre direction. Wide field photometry in UBV in the magnitude range 12-17 is shown to interpret unambiguously in terms of extinction and stellar density. The interpretation partially uses the galactic model developed by Robin and Crézé (1986), Bienaymé et al. (1987) and Haywood et al. (1994). The model ingredients which play a role in the present investigation are the density law of the galactic disc (radially exponential) and the luminosity function from Wielen et al. (1983). Strong constraints are set on the radial structure of the disc: the galactic disc scale length is found to be 2.5 ± 0.3 kpc. Based on this scale length and assuming no dramatic change in the luminosity function one can predict what should normally happen at faintest magnitudes.

3. Deep observations towards the anticentre

Deep CCD observations in the UBVI bands have been obtained at the 3.6 meter CFH Telescope in a low extinction window at low latitude in the direction of the galactic anticentre. A detailed description of the 1987-1988 observation campaign and data analysis aspects is given elsewhere (Robin et al. 1992a). Observations cover four neighbouring fields around l=179.7deg and b=2.8 deg adding up to 29 square arcminutes. The detection limit is about magnitude 28 in V, while the completeness limit corresponding to a photometric accuracy better than 0.1 is 25 in V and 22.5 to 24 in B depending on the frame. The 1993 observation campaign allowed us to acquire V and I data complete to 25 in both bands, allowing us to have a colour index V-I down to this magnitude.

4. The edge of the old disc

The (V, B-V) distribution of stars resulting from this investigation is given in figure 1. The thin line is just a guide to compare the position of stars in both diagrams. Faint star count predictions with no cutoff in the disc deviate strongly from the observations at the faint end and there is a clear excess of blue stars in the down left part of figure 1a. The bulk of disc contributors in this magnitude range is made of disc dwarfs beyond 5.5 kpc.

All disagreements in the V, B-V diagram vanish if the stellar disc ends abruptly at 5.5 kpc as also shown in the V star counts in figure 1c, while the small number of remaining stars could own to the thick disc population (see section 5 and fig. 2).

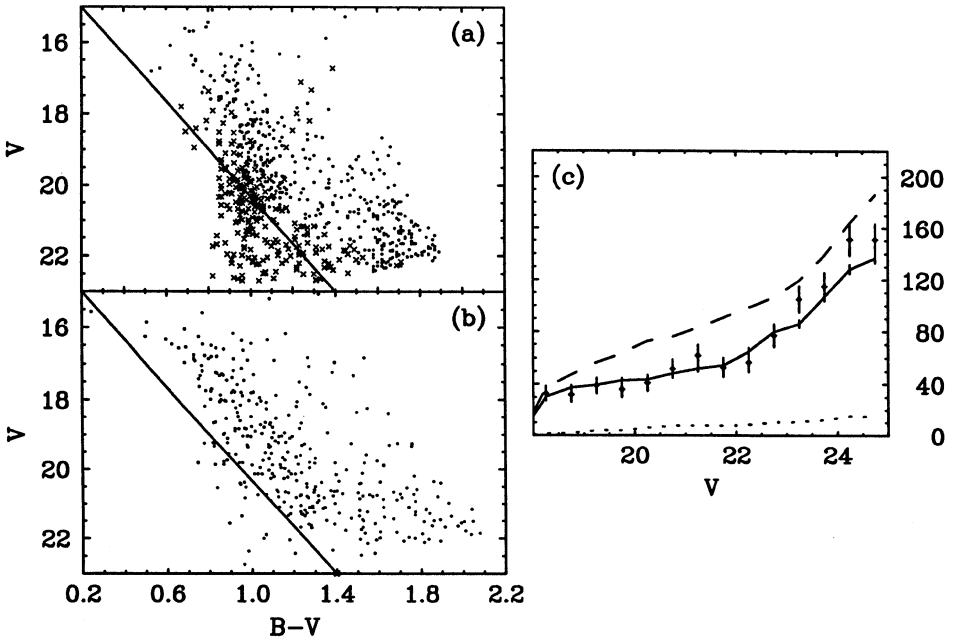

Figure 1. (V,B-V) distribution towards to the anticenter. (a) Model prediction (dots: Disc stars at distance closer than 5.5 kpc; crosses: disc stars at distance larger than 5.5 kpc. (b) Data sample. The thin line is just a guide to compare the position of stars in both diagrams. (c) V counts (Diamonds: data with 1 sigma Poisson error bars; dotted line: model with no disc cutoff; solid line: model with a disc cutoff at 5.5 kpc).

The cutoff cannot be explained by an absorbing cloud, because external galaxies, HI column density and UBV diagrams all give a maximum extinction of 1.2 to 1.4 magnitude. This is also in agreement with the fact that the fields are inside Special Area 23 selected by Kapteyn as a low extinction window.

Density distributions with scale lengths larger than the adopted 2.5 kpc would impose a still closer cutoff (at 3.5 kpc from us if $h_R = 3.5$ kpc) while shorter scale lengths are hardly compatible with the observations of bright stars in the same region (Mohan et al. 1988).

5. Where is the thick disc edge ?

Figure 1 shows that some stars are seen at distances larger than 5.5 kpc. Do these stars belong to the thick disc or old disc ?

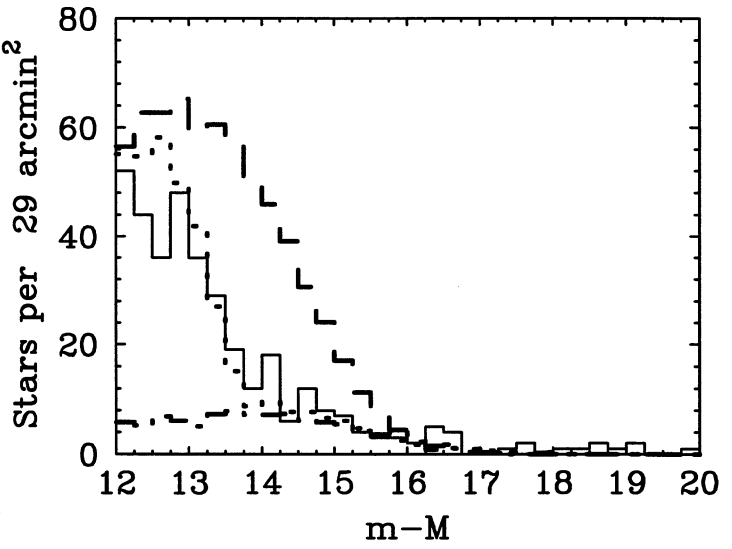

Figure 2. Histogram of distance indicator V-M_V for stars at V<24. Data: solid line. Model: All stars with disc edge at 5.5 kpc : dotted line; All stars without disc edge: dashed line; thick disc only: dotted-dashed line.

V-I colours provide a distance indicator which may be used to grossly trace the density law, although the V-I index used as luminosity indicator is slightly metal sensitive. As long as we compare distance indicators computed by the same formulae on data and on model simulations, the small error due to metallicity variations is accounted for in the model.

We compute this apparent distance indicator using a polynomial fit of the absolute V magnitude to the V-I index for disc stars from the calibrations of Bessel (1991a and b) for types earlier than M4 and Leggett (1992) for later types.

$$M_V = 2.43 + 3.80 * (V - I) - 0.0724 * (V - I)^2$$

Figure 2 shows the histogram of our indicator (V-M_V). The sample has been restricted to V<24 in order to have a more accurate distance indicator. We see that the model with a disc edge and no thick disc edge perfectly fit the data. The model without a disc edge overestimates the number of stars at m-M>13 (r≥5) by a large factor. The number of observed stars at m-M>14 corresponds exactly to model prediction for the thick disc with no cutoff.

The thick disc model results from a global investigation of the thick disc population based on magnitude and colour star count data in 19 fields well distributed in longitude and latitude (Robin et al., 1994). Such star counts turn out to tightly constrain thick disc parameters. It has a scale height of 760 pc, a local density 5.6% of the disc and a scale length of 2.5 to 3 kpc. In the present study the use of a larger scale length for the thick disc would have given too large a number of stars at m-M>14.

6. Discussion

The analysis of star counts towards the anticenter enable us to emphasize that :

- UBV data on the magnitude range 12 to 25 from Schmidt plates and CCD frames give and estimate a disc scale length of 2.5 ± 0.3 kpc.
- CCD data to magnitude 23 in B and V show the existence of a sharp cutoff in the radial distribution at 5.5 kpc from the sun (R=14 kpc).
- I band photometry allow to go deeper in magnitude and distance. A distance indicator is computed from V-I. It confirms the position of the disc cutoff. The small number of stars appearing at r>5.5 kpc is compatible with what we expect if the thick disc has no radial cutoff.

Most external disc galaxies show a radial truncation. These cutoffs seem to arise within 1 kpc or less (van der Kruit, 1988) and are found at R_{max} / h_R = 4.5 ± 1.0. In our Galaxy star counts in the anticentre (Robin et al. 1992a) give a radial scale length of 2.5 ± 0.3 kpc, rather short value but recently confirmed by the Fux and Martinet (1994) kinematic determination and close to the COBE measurement (3 kpc, Weiland et al., 1994). Together with the presently determined cutoff, it implies a ratio R_{max}/h of 5.6 ± 0.6 if $R_\odot$ = 8.5 kpc in agreement with the observed ratio in external galaxies.

Our determination of the radial extent of the old disc does not conflict with the possibly larger extent of young stars or star forming regions if an evolutionary scenario like the one of Larson (1976) is realistic (where the star formation propagates from the centre of the Galaxy to the outer part). In this case one expects to find only recent star formation in the outer part of the Galaxy and no old disc stars.

Concerning the small number of remaining stars at large distances, we have shown that their number and distance distribution coincide exactly with what we expect from the thick disc if it has no cutoff. However direct measurements of kinematics and/or metallicities of these stars would be needed. While no accurate spectra can be obtained at these magnitudes (V>23) one can get reasonably accurate proper motions from CCD on a time baseline of ten years.

Our study implies that the thick disc does not stop like the disc in the external part of the Galaxy. This fact confirms previous results showing that the thick disc is significantly different from the old thin disc. There remains at least two scenarios compatible with this result. The first emphasizes that the thick disc had formed from a merger event at the beginning of the formation of the thin disc (Quinn, Hernquist and Fullagar, 1993). These authors show that the resulting thick disc would have a slightly larger extent than the thin disc. The second scenario explains the thick disc as being formed during the collapse of the gas into the disc, stopped due to star formation (Burkert et al., 1992). In this case as well the thick disc would extend at larger radii than the thin disc, as observed in our data.

Acknowledgements

This research was partially supported by the Indo-French Centre for the Promotion of Advanced Research / Centre Franco-Indien Pour la Promotion de la Recherche Avancée.

References

Bessel M.S., 1991a, PASP 102,1181.
Bessel M.S., 1991b, AJ 101, 662
Bienaymé, O., Robin, A. C. & Crézé, M. 1987,A&A 180, 94
Burkert A., Truran J.W., Hensler G., 1992, ApJ 391, 651
Fux R. & Martinet L., 1994, A&A 287, L21
Haywood M., 1994, Thèse de doctorat, Université Paris VII.
Larson, R. B. 1976, MNRAS 176, 31
Leggett, S.K., 1992, ApJS 82, 351
Mohan, V., Bijaoui, A., Crézé, M. & Robin, A. C. 1988,A&AS 73, 85
Quinn P.J., Hernquist L. & Fullagar D.P., 1993, ApJ 403, 74
Robin, A. C. & Crézé, M. 1986,A&A 157, 71
Robin A. C., Crézé M. & Mohan V., 1992a, A&A 253, 389
Robin A. C., Crézé M. & Mohan V., 1992b, ApJ 400, L25
Robin A. C., Haywood M., Ojha D.K., Crézé M., Bienaymé O., 1994, preprint.
van der Kruit, P. C. 1988,A&A 192, 117
Weiland J. et al., 1994, ApJ 425, L81
Wielen, R. Jahreiss, H. & Krüger, R. 1983, In *The Nearby Stars and the Stellar Luminosity Function*, I.A.U Coll. 76, p. 163 , Davis Philip and Upgren (eds), L. Davis Press (Schenectady, NY).

DISCUSSION

Kraft: How did you disentangle the extinction determination (based on U-B vs B-V) from the metallicity gradient in the disk toward the anti-center?

Robin: The metallicity gradient in the disk has not the same effect as the extinction in (U-B, B-V) diagrams. The slope is steeper. We account for this gradient in model simulations in order to treat the extinction free of this effect.

P. van der Kruit: You have your disk edge at about 14kpc, while HII regions have been reported at 20-25 kpc from the center. In external galaxies stellar disks and HII region distribution always have similar extents. How do you reconcile that?

Robin: Our data show a significant truncation in the disk and not at all compatible with disk exponentially decreasing for ever. We think that the remote HII regions in the Galaxy are exceptions and probably they would not be significant in external galaxies.

PROPER MOTION STUDY OF THE GALACTIC ROTATION CURVE

B. FUCHS, S. FRINK, S. RÖSER, R. WIELEN
Astronomisches Rechen-Institut Heidelberg
Mönchhofstraße 12-14, 69120 Heidelberg, Germany

Abstract. The galactic rotation curve has been determined using the space velocities of 197 OB stars associated with 59 HII regions.

1. Introduction

The galactic rotation curve has been determined for the inner parts of the galactic disk, interior to the solar annulus, from HI measurements using the tangent point method (Burton and Gordon 1978), whereas the outer rotation curve has been determined using among other objects HII regions embedded in molecular cloud complexes (Brand and Blitz 1993). CO radial velocities are converted to circular velocities assuming that the HII regions move on circular orbits around the galactic center. Obviously proper motions of the objects provide independent information on the rotation curve. Recently the PPM catalogue (Röser and Bastian 1991, Bastian et al. 1993, Röser et al. 1994) has been compiled at the Astronomisches Rechen-Institut which is well suited as a broad data base for proper motions of high accuracy.

2. Data

We have based our analysis of the galactic rotation curve on the list of HII regions and their associated molecular cloud complexes by Brand and Blitz (1993). The exciting OB stars of the HII regions in the northern hemisphere are tabulated by Georgelin (1975) and can be identified by cross reference numbers. For the exciting OB stars of HII regions in the southern hemisphere finding charts are given by Brand (1986). Using the cross refe-

L. Blitz and P. Teuben (eds.), Unsolved Problems of the Milky Way, 689–695.
© 1996 *International Astronomical Union.*

rence numbers, spectral types, or accurate stellar positions we have tried to identify as many stars from the source list in the PPM Star Catalogue as possible. The PPM catalogue has been compiled from a comprehensive set of photographic and meridian circle catalogues and contains astrometric data of about 470 000 stars with magnitudes down to V=11. We have been able to identify 197 OB stars in the PPM catalogue which are associated with 59 HII regions. Using the positions and proper motions of the stars given in the PPM catalogue and the distances and radial velocities given by Brand and Blitz (1993), respectively, we have calculated the positions and velocities of the stars in galactic coordinates. Fig. 1 shows the projections of the positions of the HII regions onto the galactic plane.

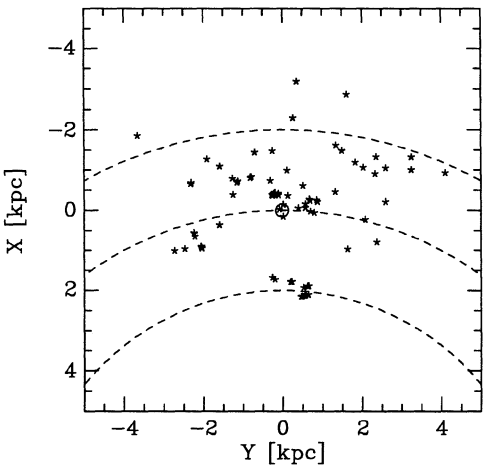

Figure 1. Projection of the positions of the HII regions onto the galactic plane. The dashed lines indicate circles around the galactic center with radii 6.5, 8.5 and 10.5 kpc. The position of the sun is indicated as ⊙.

3. Results and Discussion

3.1. ANGULAR VELOCITY OF THE LSR AND SOLAR MOTION

The proper motions of the stars are defined in the reference frame of the FK5 (Fricke et al. 1988) which represents as closely as possible an inertial frame with its origin at the position of the sun. Since the sun rotates with the local standard of rest (LSR) around the galactic center the proper motions show an apparent rotation of the stars around the LSR with the same angular velocity ω_0 as the LSR around the galactic center. Furthermore the solar motion with respect to the LSR has to be taken into account when reducing the velocity data. In order to derive these parameters we have

fitted a model of the form

$$\begin{aligned} U &= -U_\odot + \omega_0 Y - \omega_0 Y(1 - R_\odot/R), \\ V &= -V_\odot - \omega_0 X - \omega_0(R_\odot - X)(1 - R_\odot/R) \end{aligned} \quad (1)$$

to the space velocities of the stars. X, Y are the Cartesian spatial coordinates of the stars relative to the sun. The X-axis points towards the galactic center and the Y-axis into the direction of galactic rotation (cf. Fig. 1). U and V are the corresponding velocities of the stars. The first terms on the right hand sides of equation (1) describe the solar motion with respect to the LSR. The middle terms describe the rigid rotation of the reference frame described above. The rightmost terms model the differential rotation of the Galaxy. Since some of the HII regions are fairly distant from the sun we do not use Oort's approximation but adopt rigorous formulae describing a flat rotation curve. R denotes the galactocentric distance of a star. $R_\odot$ is the distance of the sun from the galactic center which we assume as 8.5 kpc throughout the present study. Deviations of the stars from the midplane are ignored. From a χ^2-fit of equation (1) to the space velocities of the 197 OB stars we find

$$\omega_0 = 5.6 \pm 0.4\ mas/a,$$
$$(U_\odot, V_\odot) = (5, 6)\ km/s.$$

The value of the angular velocity ω_0 which we find corresponds to a circular velocity of $v_c = \omega_0 R_\odot = 224$ km/s in good agreement with the IAU 1984 value. The estimated error of ω_0 has been calculated from the estimated errors given individually for the proper motions of each star in the PPM catalogue and the errors of the radial velocities and the distances of the stars given by Brand and Blitz (1993). Judging from the numerical value of χ^2 and the statistical distribution of the velocity residuals we found that the error estimates obtained this way were too low and have increased the error estimates of the proper motions by 30%. This is apparently due to systematic errors of the proper motions in the PPM catalogue which are not fully represented by the individual errors given there. The PPM is tied into the FK5 system. Lindegren (1992) has shown by a systematic comparison of the FK5 system with preliminary HIPPARCOS data that the FK5 positional system has still deficiencies, in particular in the southern hemisphere in a strip at about $\delta = -40°$. Unfortunately a number of HII regions at $\ell \approx 260°$, $b \approx 0°$ fall into this area, which we have omitted from our analysis. Furthermore it should be kept in mind that in addition to the error sources discussed so far the FK5 system might show further spurious non-physical rotations of the order of 1 mas/a (Schwan 1988).

The solar motion which we find deviates from the classical values of $(U_\odot, V_\odot) = (9,12)$ km/s (Delhaye 1965) which are rejected by our χ^2-fit

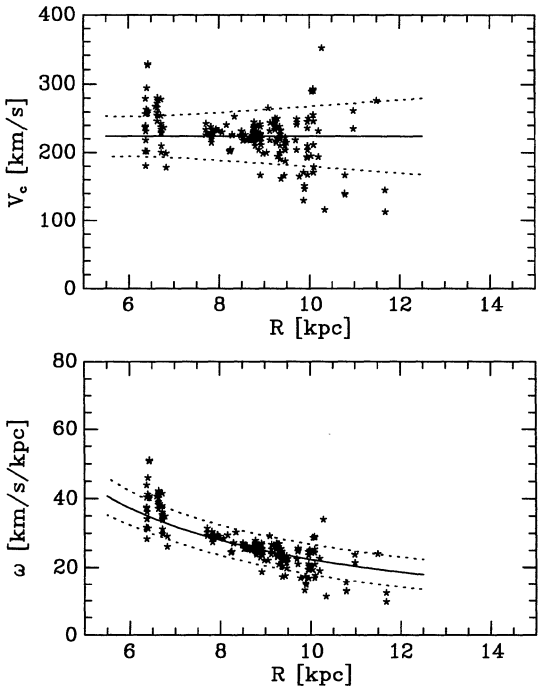

Figure 2. Rotation curve derived from the space motions of 197 OB stars associated with 59 HII regions. The lower panel shows angular velocities as function of galactocentric distance R, whereas the upper panel shows circular velocities calculated assuming $R_\odot$ = 8.5 kpc. The solid lines indicate the rotation law of a flat rotation curve. The dotted lines indicate error estimates based on the errors of the proper motions, radial velocities and distances of the stars.

to the data at a 4σ confidence level. The value of $V_\odot$ is closely related to the asymmetric drift of the sample of stars under consideration. Jahreiß and Wielen (1983) have found $V_\odot$ = 5 km/s relative to the youngest stars in the solar neighbourhood in close agreement with the value derived here. The value of $U_\odot$ = 5 km/s which we use instead of 9 km/s corresponds to the apparent inward motion of all OB stars at about 4 km/s relative to the LSR which was noted previously by Fich, Blitz and Stark (1989).This effect is usually interpreted as an outward motion of the LSR (Blitz and Spergel 1991).

3.2. ROTATION CURVE

Once the velocities have been corrected for the solar motion and the rotation of the reference frame it is straightforward to determine the circular velocity of each star. Fig. 2 shows the resulting rotation curves derived from the

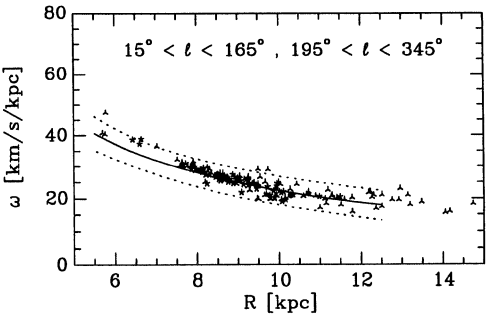

Figure 3. The rotation curve derived solely from the radial velocities of the HII regions assuming circular orbits around the galactic center. The asterisks indicate the 49 HII regions for which we could derive proper motions. The rotation law and error estimates, shown as an aid to the eye, are that of Fig. 2.

space velocities of the 197 OB stars in 59 HII regions. In Fig. 3 we show essentially the rotation curve of Brand and Blitz (1993), derived solely from the radial velocities of the HII regions assuming that they move on circular orbits around the galactic center. HII regions near $\ell = 0°$ or $\ell = 180°$ have been excluded. The limitations of proper motion studies become apparent if one realizes that we were only able to derive proper motions for 49 of the 193 HII regions. The rotation curves determined using either the full space velocities or the radial velocity components, respectively, agree very closely and are consistent with a flat shape of the rotation curve or $\omega = v_c/R$. Finally we have determined Oort's constant using stars with $|R - R_\odot| < 1$ kpc and find $A = 14.4 \pm 1.2$ km/s/kpc which agrees nicely with the flat shape of the rotation curve over larger distances intervals. The second Oort constant is according to this determination $B = -12.1 \pm 1.2$ km/s/kpc.

3.3. RESIDUAL VELOCITIES

The orientations of the velocity residuals after subtraction of the systematic velocity components due to the flat rotation curve from the space velocities of the stars are shown in Fig. 4 projected onto the galactic plane. Most of the velocity residuals are randomly orientated with the exception of the Perseus spiral arm. There is a trend of coherent motion along the spiral arm with the effect that the stars in the spiral arm tend to lag behind the general rotation of the disk. Exactly such a behaviour is predicted by the density wave theory of spiral structure for stars born recently in the shock front of the interstellar gas included by the spiral density wave (Shu et al. 1972).

Finally we have looked in our data for an apparent tilting of the galactic

plane, but found in contrast to Miyamoto et al. (1993) no significant effect.

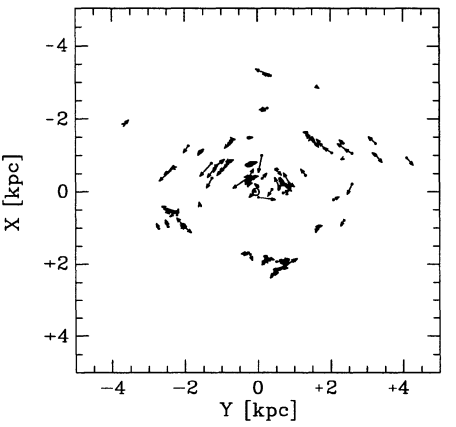

Figure 4. Velocity residuals projected onto the galactic plane after subtraction of a flat rotation curve, normalized by the errrors of the space velocities. One unit of the normalized residuals corresponds to a vector with a length of 150 pc in the diagram. Notice the aligned velocity pattern in the Perseus spiral arm in the upper right hand quadrant of the figure.

References

Bastian,U., Röser,S., Yagudin,L.I., Nesterov,V.V., Polozhentsev,D.D., Potter,Kh.I., Wielen,R., Yatskiv,Ya.S.: 1993, PPM Star Catalogue Vols. III, IV, Spektrum Akademischer Verlag, Heidelberg

Blitz,L., Spergel,D.N.: 1991, ApJ 370, 205

Brand,J.: 1986, Ph.D. thesis, Univ. of Leiden

Brand,J., Blitz,L.: 1993, AA 275, 67

Burton,W.B., Gordon,M.A.: 1978, AA 63, 7

Delhaye,J.: 1965, in "Galactic Structure", (eds.) A. Blaauw, M. Schmidt, Univ. Chicago Press, p. 61

Fich,M., Blitz,L., Stark,A.A.: 1989, ApJ 342, 272

Fricke,W., Schwan,H., Lederle,T., Bastian,U., Bien,R., Burkhardt,G., du Mont,B., Hering,R., Jährling,R., Jahreiß,H., Röser,S., Schwerdtfeger,H.M., Walter,H.G.: 1988, Veröff. Astron. Rechen-Inst. Heidelberg No. 32

Georgelin,Y.M.: 1975, Ph.D. thesis, Univ. de Provence

Jahreiß,H., Wielen,R.: 1983, IAU Coll. No. 76, 277

Lindegren,L.: 1992, in "Space Sciences with particular emphasis on High Energy Astrophysics", (eds.) T.D. Guyenne, J.J. Hunt, ESA, p. 3

Miyamoto,M., Sôma,M., Yoshizawa,M.: 1993, AJ 105, 2138

Röser,S., Bastian,U.: 1991, PPM Star Catalogue Vols. I, II, Spektrum Akademischer Verlag, Heidelberg

Röser,S., Bastian,U., Kuzmin,A.: 1994, AA Suppl. 105, 301

Schwan,H.: 1988, AA 198, 116

Shu,F.H., Milione,V., Gebel,W., Yuan,C., Goldsmith,D.W., Roberts,W.W.: 1972, ApJ 173, 557

DISCUSSION

A. Gould: The results you obtain by W_o is substantially at odds with that found by measuring the proper motion of Sgr A*. Have you considered what distortion of the galaxy might account for this?

Fuchs: –

H. van Woerden: The difference between the angular speed derived by Fuchs and that by Backer and Sramek from SgrA* is only 1.25±0.52 mas/yr, less than 3σ Taken at face value, it could be explained by a motion of SgrA* relative to the dynamic center of the Galaxy at 40 km/sec.

Fuchs: A valid point. One might add that the reference frame of the PPM Fk5 might still show non-physical rotations of the order of 1 mas/yr which will be removed once the extragalactic link is established.

THE MASS DISTRIBUTION OF THE MILKY WAY DEDUCED FROM GLOBULAR CLUSTER DYNAMICS

B. DAUPHOLE AND J. COLIN
Observatoire de Bordeaux, URA 352, CNRS/INSU, B.P. 89, F-33270 Floirac, France

AND

M. GEFFERT, M. ODENKIRCHEN AND H.-J. TUCHOLKE
Sternwarte der Universität Bonn, Auf dem Hügel 71, D-53121 Bonn, Federal Republic of Germany

Abstract. We present here a new analytical Galactic potential. We used the constraint of galactic globular cluster dynamics compared to their spatial distribution. This was done with the help of the globular clusters' proper motions. The result for the clusters dynamics show a better agreement between orbital parameters and statistical distribution of the studied globular clusters than in previous published potentials. The globular cluster dynamics constrain the mass distribution on a large scale, until 40 kpc from the centre. In this model, the total mass for the Milky Way is 7.9 10^{11} $M_{\odot}$.

1. Introduction

The mass distribution of our Galaxy and especially of the dark matter can be revealed by the dynamics of halo objects. Two categories of interesting tracers are distinguished : Globular clusters and Population II stars. Globular clusters present an advantage over halo stars: They are probably nearly all known and are distributed in the whole Galaxy, whereas catalogs of stars are often not homogeneous and biased. Moreover, globular clusters are objects widely observed due to their discernibility in the Galaxy (Webbink, 1988).

Since the pioneering work of Hartwick & Sargent (1978) on the globular cluster dynamics, many studies have been made with the help of the glob-

L. Blitz and P. Teuben (eds.), Unsolved Problems of the Milky Way, 697–702.
© 1996 *International Astronomical Union.*

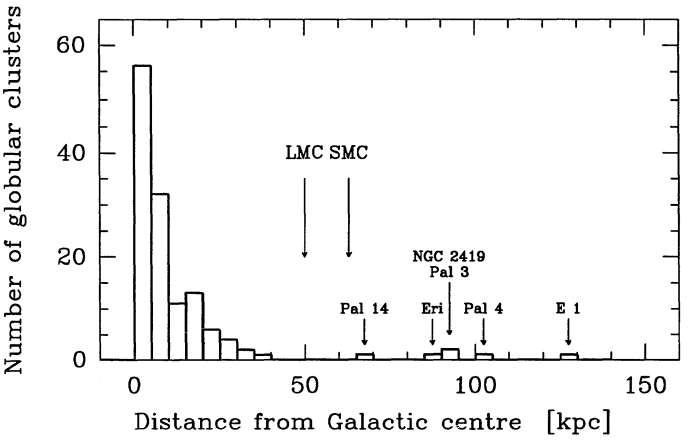

Figure 1. Distribution of observed galactocentric positions for the known globular clusters of the Galaxy. Distances are derived from Peterson (1993).

ular cluster radial velocities. These studies have shown that the mass of our Galaxy ranges between 3 10^{11} $M_\odot$ up to 13 10^{11} $M_\odot$ (e.g. Miyamoto *et al.* 1980; Frenk & White 1980; Innanen *et al.* 1983; Peterson 1985; Suntzeff *et al.* 1985; Olszewski *et al.* 1986; Little & Tremaine 1987; Thomas 1989; Zaritsky *et al.* 1989; Kulessa & Lynden-Bell 1992). But until now, these studies used the globular cluster radial velocities and distances alone.

Absolute proper motions for 26 galactic globular clusters are now known (Dauphole *et al.*, 1994). For 12 of them, proper motions were calibrated to extragalactic objects. It is therefore possible to investigate their dynamical behavior in a realistic available potential. We show here that, to be consistent with the observation of the spatial distribution, one has to constrain the mass distribution of the Milky Way at a large distance from the centre.

2. The Space Velocities of Globular Clusters : a New Constraint to the Galactic Potential

From the distances, radial velocities and proper motions of the clusters, we obtained their spatial velocities. Previous work which took into account the proper motions have shown that some of them have large apocentres, sometimes greater than 40 kpc (Allen & Martos 1988; Allen 1990; Brosche *et al.* 1991; Odenkirchen & Brosche 1992; Allen & Santillan 1993).

However, during their orbital motion these objects spend a large part of their orbital period at distances near their apocentre. An example of orbital motion and time spent by NGC 4147 is given in Odenkirchen & Brosche (1992) : This cluster is at distance greater than 40 kpc during $\approx$ 70% of its

orbital period. So, statistically, we will observe the majority of clusters at a galactocentric distance near their apocentric distance.

Remarkably, the distance from the Galactic centre of the clusters in the Milky Way presents a distribution (Fig. 1) with two groups : The first, containing 129 clusters, shows a decrease then a gap after 40 kpc, and the second one, with only 6 clusters, located beyond the Magellanic Clouds, is sparse and has probably a different nature. Since the probability to observe clusters is larger at distances near their apocentre, the distribution of the Fig. 1 indicates that the globular clusters may not have apocentres larger than the observed limit of 40 kpc. Otherwise we should observe some beyond the end of the observed distribution.

This fact imposes a new constraint to the potential of our Galaxy at large distance, *i.e.*, clusters with known spatial velocities should not have apocentric distances greater than 40 kpc.

3. The Potential Model

Previous models for the potential of our Galaxy give unrealistic orbits for the clusters, in view of their observed spatial distribution. We have built a realistic Galactic potential which reconciles the cluster motion and the statistical distribution (Dauphole & Colin, 1994). The total potential is composed of a bulge, a disc and a halo :

$$\Phi(\varpi, z) = \Phi_{\rm b}(r) + \Phi_{\rm d}(\varpi, z) + \Phi_{\rm h}(r)$$

The bulge and the halo are represented by two Plummer's spheres, and the disc by a Kuzmin's disc. The adopted analytical forms are from Miyamoto & Nagai (1975):

$$\Phi_{\rm b,h}(r) = -\frac{GM_{\rm b,h}}{\left[r^2 + b_{\rm b,h}^2\right]^{1/2}}$$

$$\Phi_{\rm d}(\varpi, z) = -\frac{GM_{\rm d}}{\left[\varpi^2 + \left[a_{\rm d} + (z^2 + b_{\rm d}^2)^{1/2}\right]^2\right]^{1/2}}$$

The adjusted constants ($M_{\rm b}$, $M_{\rm d}$, $M_{\rm h}$, $b_{\rm b}$, $b_{\rm d}$, $b_{\rm h}$ and $a_{\rm d}$) and derived parameters are presented in Tab. 1. In this model, the resulting Galactic mass is only 7.9 10^{11} $M_\odot$. The combined mass of the disc and the bulge is 9.3 10^{10} $M_\odot$. In Fig. 2 it is shown that the rotation curve derived from this model is in good agreement with the data of the work from Brand & Blitz (1993).

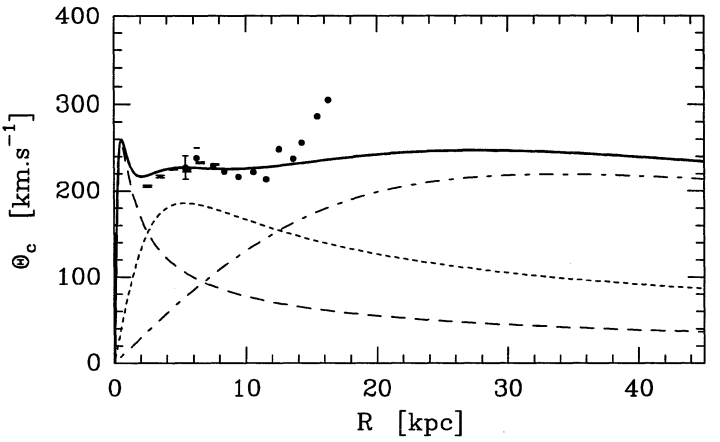

Figure 2. Rotation curve of the model (solid line) with its contributions from the bulge (dashed line), the disc (dotted line) and the halo (dashed-dotted line). Observational data with error bars are from Brand & Blitz (1993).

We computed orbital parameters for the most critical globular clusters, that is clusters with large space motion, with an integration scheme of Bulirsch-Stoer, and compared them to the ones computed in the model of Allen & Martos (1988) (hereafter AM88). Results are given in Tab. 2 along with the uncertainties on the apocentre. For each cluster we present its observed distance from the centre (column 2) and the apocentric distance reach in the AM88 model (column 3) and in our model (column 4). The errors on apocentres of the fourth column were computed as follows : We added and subtracted the measurement errors on proper motion, distance and radial velocities, then we computed the orbit and we kept the greater and the lower value obtained.

Apocentres computed in our model are smaller than in the AM88 model. However, two of them still have apocentre greater than the imposed limit, but less pronounced than in the model of Allen & Martos. Errors on the measured data can explain this disagreement. However, the global trend of this model is to reduce the apocentric distances for the clusters which have large apocentre. For clusters with smaller apocentric distances, the gain compared to other models is not really large, but our model also decreases the apocenters of these clusters. The advantage of our model is that the probability to observe them at their current position (column 2 of Tab. 2) is increased.

TABLE 1. Adjusted constants and computed local parameters.

Distance Sun-Galactic centre (adopted)	$R_\odot = 8.0$ kpc
Local circular velocity (adopted)	$V_{lsr} = 225$ km.s^{-1}
Bulge constants	$M_b = 1.3955\ 10^{10}\ M_\odot$
	$b_b = 0.35$ kpc
Disc constants	$M_d = 7.9080\ 10^{10}\ M_\odot$
	$a_d = 3.55$ kpc
	$b_d = 0.25$ kpc
Halo constants	$M_h = 6.9776\ 10^{11}\ M_\odot$
	$b_h = 24.0$ kpc
Total mass	$M_T = 7.908\ 10^{11}\ M_\odot$
Local density	$\rho_0 = 0.143\ M_\odot.pc^{-3}$
Rotation constants	$A = 14.25$ km.s^{-1}.kpc^{-1}
	$B = -13.89$ km.s^{-1}.kpc^{-1}
Local escape velocity	$v_e = 573.5$ km.s^{-1}

TABLE 2. Observed positions and apocentres reached in Allen & Martos (1988) potential and in our model. Positions are derived from Peterson's (1993) data.

Name	R_{obs} (kpc)	R_{apo} (kpc)	
		AM88	This model
NGC 4147	20.9	84.7	$52.0 \pm {}^{\infty}_{24.3}$
NGC 5466	16.2	90.1	$51.9 \pm {}^{346.9}_{21.7}$
NGC 5904	6.2	69.8	$37.3 \pm {}^{17.1}_{10.0}$
NGC 6779	9.4	53.5	$33.4 \pm {}^{148.6}_{15.8}$
NGC 6934	12.1	53.3	$31.7 \pm {}^{28.0}_{12.5}$
NGC 7078	10.5	66.6	$37.0 \pm {}^{95.4}_{19.0}$
NGC 7089	10.6	42.0	$27.7 \pm {}^{30.8}_{11.2}$

4. Conclusion

We have constructed a mass distribution model for the Milky Way in accordance with the classical observational constraints (rotation curve, local perpendicular force, local density and Oort's constants), and with the dynamics of the galactic globular clusters. This was possible due to the knowledge of the proper motions for 26 clusters. The new constraint introduced

here is a large scale constraint, until 40 kpc, since there is a deficiency of clusters beyond this limit. It can be explained if the clusters do not have apocentric distances greater than 40 kpc, otherwise we should observe some of them beyond this limit. The derived model is completely analytical and is well suited for orbit computation. Finally to constrain the dynamics of galactic globular clusters to their observed distribution, a total mass for the Galaxy of only 7.9 10^{11} $M_{\odot}$ seems to be sufficient.

Acknowledgements

We are grateful to Ch. Ducourant who checked this text, and would like to thank colleagues for their help in the typesetting.

References

Allen, C. (1990), *Rev.Mex. Astron. Astrophis.*, 20, pp. 67–72
Allen, C., Martos, M.A. (1988), *Rev.Mex. Astron. Astrophis.*, 16, pp. 25–36
Allen, C., Santillan, A. (1993), *Rev.Mex. Astron. Astrophis.*, 25, pp. 39–50
Brand, J., Blitz, L. (1993), *A&A*, 275, pp. 67–90
Brosche, P., Tucholke, H.-J., Klemola, A.R., Ninković, S., Geffert, M., Doerenkamp, P. (1991), *AJ*, 102, pp. 2022–2027
Dauphole, B., Colin, J. (1994), *A&A*, submitted.
Dauphole, B., Geffert, M., Colin, J., Ducourant, Ch., Odenkirchen, M. (1994), *A&AS*, submitted.
Frenk, C.S., White, S.D.M. (1980), *MNRAS*, 193, pp. 295–311
Hartwick, F.D.A., Sargent, W.L.W. (1978), *ApJ*, 221, pp. 512–520
Innanen, K.A., Harris, W.E., Webbink, R.F. (1983), *AJ*, 88, pp. 338–360
Kulessa, A.S., Lynden-Bell, D. (1992), *MNRAS*, 255, pp. 105–118
Little, B., Tremaine, S. (1987), *ApJ*, 320, pp. 493–501
Miyamoto, M., Nagai, R. (1975), *PASJ*, 27, pp. 533–543
Miyamoto, M., Satoh, C., Ohashi, M. (1980), *A&A*, 90, pp. 215–223
Odenkirchen, M., Brosche, P. (1992), *Astron. Nachr.*, 313, pp. 69–81
Olszewski, E.W., Peterson, R.C., Aaronson, M. (1986), *ApJ*, 302, pp. L45–L48
Peterson, R.C. (1985), *ApJ*, 297, pp. 309–313
Peterson, R.C. (1993), ESO preprint 932, pp. 13–18
Suntzeff, N., Olszewski, E., Stetson, P.B. (1985), *AJ*, 90, pp. 1481–1485
Thomas, P. (1989), *MNRAS*, 238, pp. 1319–1343
Webbink, R.F. (1988), in IAU Symposium 126, *The Harlow–Shapley Symposium on Cluster Systems in Galaxies*, J.E. Grindlay and A.G. Davis Philip, eds., Reidel, Dordrecht, pp. 49–60
Zaritsky, D., Olszewski, E.W., Schommer, R.A., Peterson, R.C., Aaronson, M. (1989), *ApJ*, 345, pp. 759–769

THE ROTATION CURVE FROM A–F SUPERGIANTS

A Progress Report

D. M. PETERSON AND D. SLOWIK
Astronomy Program
State University of New York
Stony Brook, NY 11794 USA

1. Introduction

The Galactic rotation law provides critical information for estimating the distribution of mass in the Galaxy, for tying the distance of the Sun from the Galactic center to local distance scales, and, if determined over large enough distances, for estimating the total mass of the system and the amount of nonluminous matter present. Interior to the Sun velocities are well defined by observations of the ISM, particularly HI. These techniques are not available for points exterior to the Sun and we must rely on observations of velocities of objects whose distances can be estimated. Notable among these are the Cepheids (Pont et al 1994) and the combination of CO velocities and OB cluster distances (Brand & Blitz 1993) where the two are found to coexist. Adding a new class of objects, particularly bright, relatively common objects to this effort is of importance.

Over the past few years we and a number of other investigators (Slowik & Peterson 1993, 1994, and references therein) have been involved in calibrating the strong luminosity dependence of the λ7774 triplet of OI in the A and F supergiants. Our calibration rests entirely on members of Galactic clusters, and is comparable to the Cepheid calibration in reliability. Although the primary focus of this effort is extragalactic, these objects being visible to at least 10 Mpc, its usefulness in other contexts is also apparent. We report here on the first application of this approach to determine the Galactic rotation law beyond the Solar circle.

2. The Data

For this initial effort we availed ourselves of the "queue" observing program offered by Kitt Peak National Observatory during the summer of

L. Blitz and P. Teuben (eds.), Unsolved Problems of the Milky Way, 703–706.
© 1996 *International Astronomical Union.*

1993. While a remarkable opportunity, the program came with constraints, including limitation to the equivalent of two nights of observing. In this case the instrument of choice was the Coudé Feed. As a result, none of the objects in the observing list (obtained with a SIMBAD search) exceeded 10th magnitude, and all but six were brighter than V = 9. In all, 40 objects ultimately satisfied our luminosity and color requirements. In November 1993 we were notified that approximately 100 spectra, at least one for each object in both the λ7770 and λ8600 regions were available by "ftp".

From these spectra we extract the OI equivalent widths to estimate luminosities and CaII indices to estimate reddening (Slowik & Peterson 1993, 1994). From the λ8670–8795 region we were able to derive radial velocities for each object, using a grid of synthetic spectra generated using the Kurucz programs and grid of models (Kurucz 1992). Observations of standards indicated 0.6 km s^{-1} accuracy. However, as a rule these objects all exhibit velocity variability at the few km s^{-1} level. In what follows we have adopted 10 km s^{-1} as the intrinsic uncertainty in each of these measures.

3. Discussion

Figure 1 shows the distribution on the Galactic plane of this group of objects. Although some of the objects are seen quite far from the Sun, reddening and the magnitude limits constrained the distances penetrated toward the anticenter; Galactocentric distances do not exceed 1.4 $R_\odot$. On the other hand, two objects toward l = 60° are measured at distances of 8 kpc, indicating the power of this approach.

Figure 2 shows the deduced circular velocities (assuming $v_\odot$ = 220 km s^{-1} and $R_\odot$ = 8.5 kpc) as a function of Galactocentric distance. We also show the analytic fit obtained by Brand & Blitz (1993). Clearly evident is the wave structure seen by other investigators (cf Brand & Blitz 1993, Pont et al 1994) with the circular velocity somewhat lower immediately beyond the Sun. Given the limited number of objects and angular coverage, it is premature to pursue an independent solution for the rotation law.

We are in the process of extending this effort. The original SIMBAD search indicated about 150 of these objects in the second quadrant. Rough estimates place several of them at or beyond 2 $R_\odot$, which would substantially contribute to our knowledge of the rotation law at those distances.

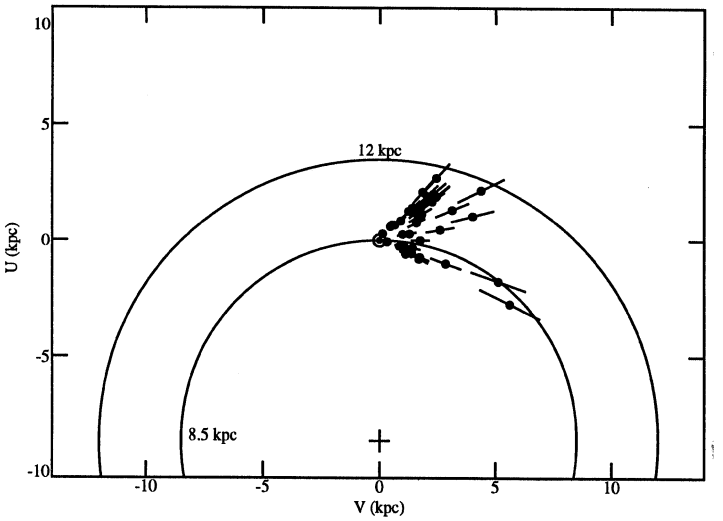

Figure 1. The distribution of the A – F supergiants, projected on the Galactic plane. Distance uncertainties are indicated.

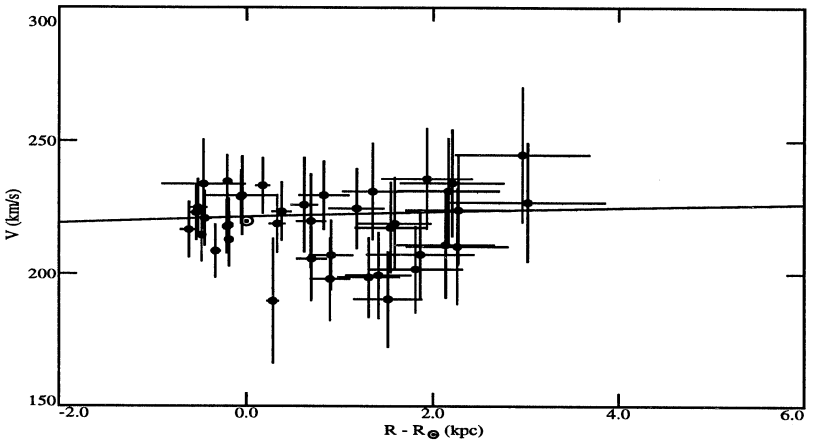

Figure 2. The velocity law defined by the current data. The solid line is from Brand & Blitz 1993.

Acknowledgements

We would like to thank the staff of the Kitt Peak National Observatory for providing the fine spectra, and acknowledge extensive use of the SIMBAD facilities located at the CDS, Strasbourg, France.

References

Brand, J. and Blitz, L. (1993) *Astron Astrophys*, 275, 67
Kurucz, R.L. (1992) in *IAU Symp. 149, Stellar Populations of Galaxies*, eds B.Barbuy and A Renzini, Dordrecht:Kluwer, 225
Pont, F., Mayor, M., and Burki, G. (1994) *Astron Astrophys*, 285, 415
Slowik, D. and Peterson, D.M. (1993) *Astron J*, 105, 1967
Slowik, D. and Peterson, D.M. (1994) *Astron J*, submitted,

THE STRUCTURAL PARAMETERS OF THE MILKY WAY

ROLAND BUSER
Astronomical Institute, University of Basel, Switzerland
AND
JIANXIANG RONG
Astronomy Department, Nanjing University, China

Abstract. A new homogeneous catalog of photographic RGU star count and three-color data in seven high-galactic latitude fields has been used to determine the structural parameter values from a large number of multi-component population models of the Galaxy. The data provide strong evidence of a *prominent thick disk component* coexisting with a canonical thin disk and a low-density spheroidal halo.

Following the definition and calibration of a *standard-RGU system* via synthetic photometry techniques [1, 2], the plate archive of the Basel-Palomar-Schmidt high-latitude survey [3] is being used to construct a homogeneous RGU-photometry data base for a reliable determination of the *larger-scale structural parameters and metallicity distributions* of the stellar population components of the Galaxy. The new catalog completed to date [4] comprises star counts and three-color distributions for about 10^4 stars in seven out of more than a dozen fields of the original survey.

We have analysed the data essentially following the methodology developed in [5] and summarized in [2]. For each field, the *observed* star counts, $N(G, G-R)$, are compared to the *expected* counts calculated from each of 12,800 multi-component models of the Galactic stellar distributions, whose *parameters* are allowed to systematically vary within plausible ranges suggested by previous work. For each model, a χ^2-estimate of goodness-of-fit to the observed data is computed for each field, whence a global χ^2-value measuring each model's simultaneous fitting to the all-survey observations in seven fields is derived, and the *globally best model* is identified by χ^2_{min}.

A χ^2-*curve* is then determined for each parameter by allowing it to vary within the adopted range while keeping all other parameters fixed at their

L. Blitz and P. Teuben (eds.), Unsolved Problems of the Milky Way, 707–708.
© 1996 *International Astronomical Union.*

TABLE 1. Optimum parameter values for combined survey of seven fields

Component		Parameter	Symbol	Unit	Optimized Value
Thin disk		local density	n_0	stars pc^{-3}	0.078
		scale length	d_1	kpc	4.01
	old	scale height dwarfs	h_1	pc	290
		scale height giants	h_2	pc	250
	young	scale height dwarfs	h_3	pc	170
Thick disk		local density	n_1	n_0	0.054
		scale length	d_2	kpc	4.25
		scale height	h_4	kpc	1.15
Halo		local density	n_2	n_0	0.0005
		effective radius	R_{eff}	kpc	2.69
		flattening	f	–	0.84

values adopted by the globally best model. In order to explore the statistical significance of the parameter values associated with χ^2_{min}, we also examine their *frequency distributions* as functions of χ^2 for all the models satisfying the condition $\chi^2 \leq \chi^2_{max} \leq \zeta\chi^2_{min}$, where $\zeta \in [1.1, 1.5]$. These distributions serve to determine the statistical weights that are applied in calculating the optimized value for each parameter, which is finally derived taking into account the possible bias induced by *parameter coupling* resulting from the preceding analysis.

Table 1 summarizes the results obtained for the combined survey of seven fields. The present data *strongly favor a thick disk component whose local density is about 5-6% of the local thin-disk density*, and which thus appears to be considerably more prominent than originally thought [6, 7], but in good agreement with more recent studies [8]. These results now also allow us to derive the *large-scale metallicity distributions* from the observed $(U - G)$ colors [9].

References

1. Buser, R. 1978, A&A 62, 411; A&A 62, 425
2. Buser, R. and Fenkart, R.P. 1990, A&A 239, 243
3. Becker, W. 1965, Z.Ap. 62, 54
4. Buser, R., Karaali, S., Topaktas, L., Karatas, Y. 1994, A&AS (in press)
5. Buser, R. and Kaeser, U. 1985, A&A 145, 1
6. Gilmore, G. 1984, MNRAS 207, 223
7. Fenkart, R.P. 1989, A&AS 78, 217; 79, 51; 80, 89; 81, 187
8. Majewski, S.R. 1993, ARA&A 31, 575
9. Buser, R. and Rong, J.X. 1994, this volume

A SYSTEM OF GALACTIC CONSTANTS BASED ON STELLAR DYNAMICS

S. NINKOVIĆ
Astronomska opservatorija
Volgina 7
11050 Beograd, Yugoslavia

Abstract. A system of galactic constants is proposed. Due to the intention of basing it on stellar dynamics, the working hypothesis is the assumption that the Galaxy is in a steady state characterized with axial symmetry. Then, as easy to see, one reaches a system containing seven independent constants typical for the present assumption. The current knowledge concerning the amounts of these constants is discussed.

1. Introduction

Among the questions where the contribution of J. H. Oort appears as essential is, certainly, the one concerning the galactic constants. The dynamical constants have been considered by the present author in an earlier paper of his (Ninković, 1987). This time a system of constants based on a given dynamical approach (steady state and axial symmetry) should be formed.

2. Formation of the System of Constants

In principle, any quantity of galactic astronomy taken at the position of the Sun may be considered as a "constant". With regard to such a variety of possibilities it is necessary to limit the scope to some kind of quantities. It is clear that the quantities concerning the spatial distribution and kinematics of galactic objects are of interest to galactic dynamics, though strictly speaking they have no dynamical nature since they do not incorporate the notion of force. On the other hand the number of necessary constants and their choice depend on the assumed dynamical approach. For example, if

L. Blitz and P. Teuben (eds.), Unsolved Problems of the Milky Way, 709–711.
© 1996 *International Astronomical Union.*

the Galaxy were spherically symmetric, then any plane connecting the Sun and the galactic center could be chosen as the plane of galactic equator, but three constants would be also necessary for transformation from the independent equatorial system to the galactic coordinates as it is the case now. In the same way the residual motion of the Sun would require three quantities to be known irrespectively of the symmetry.

Throughout this contribution it will be assumed that the Galaxy is characterized with steady state and axial symmetry. In that case, as easy to see, only two quantities are enough to describe the galactocentric position of the Sun - its distance to rotation axis and that to the galactic plane; these are the first two constants of the present system. The next will be the velocity of the local centroid, i.e. the local velocity of galactic rotation in view of the upper assumption.

These quantities, though essentially not dynamical, but important to the galactic dynamics, are followed by a group of purely dynamical quantities - the (gravitational) potential and its derivatives. As usually done, only the derivatives up to the second order are considered. Thus in the case of steady state and axial symmetry, four constants appear - the local values of the potential, itself, of the first and second radial derivatives and of the second vertical derivative. In this way one obtains a system of galactic constants, containing seven constants, based on stellar dynamics and useful for its purposes.

TABLE 1. The System of Galactic Constants

$R_\odot$	distance of the Sun to the rotation axis;
$Z_\odot$	the Sun's vertical coordinate;
$u_\odot$	the rotation velocity of the galactic disc (the centroid containing the Sun);
$\Pi_\odot$	the galactic potential;
$\left(\frac{\partial \Pi}{\partial R}\right)_\odot \left(\frac{\partial^2 \Pi}{\partial R^2}\right)_\odot \left(\frac{\partial^2 \Pi}{\partial Z^2}\right)_\odot$	

The latter five quantities are taken in the galactic plane at the distance $R_\odot$ from the galactic center; in the case of the latter three the explanations are self-evident.

3. The Actual Situation with the Constants Values

As well known, the IAU since almost ten years has been recommending the value of 8.5 *kpc* for $R_\odot$. As for $Z_\odot$, though there is no official recommendation, it is very well known that $|Z_\odot| << R_\odot$ (usually thought that $Z_\odot$

is between $+10pc$ and $+20pc$) which justifies the consideration of the other quantities mentioned above in the galactic plane instead of exactly at the Sun. The value of the local rotation velocity depends on the one of the local asymmetric drift which seems to be about 14 kms^{-1} (e. g. Ninković, 1992). The value of the galactic potential is expressed through that of the local escape velocity which seems to be significantly higher than thought earlier, perhaps even 600 kms^{-1}, or more (e. g. Ninković, 1994). The first radial derivative of the potential is expressed through the corresponding value of the circular velocity where, as well known, the IAU has been recommending 220 kms^{-1}. The second derivative can be found through the slope of the circular velocity, or through the ratio of the Oort constants, i. e. through the ratio of the local velocity dispersions (in the galactic plane) for the disc. The results seem to be discordant (e.g. Marochnik and Suchkov, 1984 - p. 235), but the disagreement can be removed so that an agreement between the locally flat rotation curve and the usual value, of about 1.6, for the velocity dispersion ratio results (Ninković, 1992). The value of the second vertical derivative depends on the problem of the local density. Since at present it is unclear how high the percentage of the local dark matter is, this question cannot be answered surely.

4. Conclusion

As a conclusion one should emphasize that the galactic constants in the present paper are considered in the framework of a system finding its basis in a given dynamical assumption. It is understandable that the next step should be the verification of the given dynamical assumption which may result in a new assumption involving additional quantities locally considered as constants. Also, one should be aware that in the actual calculations yielding the values of the constants are used samples of concrete stars where a correlation between their physical and kinematical properties, having no dynamical origin, may be of importance for the final results so that the working dynamical hypothesis may seem doubtful.

References

Marochnik, L. S. and Suchkov, A. A.:1984, Galaktika, "Nauka", glav. red. fiz.-mat. lit., Moskva.
Ninković, S.:1987, Publ. Astron. Inst. Czech. Acad. Sci., 69, 317.
Ninković, S.:1992, Astrophys. Space Sci., 187, 159.
Ninković, S.:1994, IAU Symp. 165, in press.

ESTIMATION OF GALACTIC MODEL PARAMETERS BY INTERVAL METHOD

S. A. KUTUZOV
Saint Petersburg State University, Faculty PM-PU, Stary Peterhof, 198904, Saint Petersburg, Russia

The interval method of estimating *model parameters* (*MPs*) for the Galaxy was suggested earlier (Kutuzov 1988). *Intervals* are proposed to be used both for observational estimates of *galactic parameters* (*GPs*) and for the values of *MPs*. In this work we consider a model as a tool for studying mutual interaction of *GPs*. Two-component model is considered (Kutuzov, Ossipkov 1989). We have to estimate the array $\mathbf{P}$ of eight *MPs*.

We use the following array of seven *GPs*: $\mathbf{Y} = (R_\odot, V, U, A, C, m, M)$. Here $R_\odot$ is the distance of the Sun from the centre of the Galaxy, V is the circular velocity, U is the velocity of escape, A is the Oort parameter, C is the Kuzmin parameter, m is the mass of the central parsec, M is the mass of the Galaxy. *GPs* V, U, A, C refer to vicinity of the Sun. The model allows to obtain expressions for each *GP* as a function of *MPs*: $y_i = g_i(\mathbf{P}), \quad i = 1, \ldots, k = 7$. In addition two descriptive functions are used. Data on the rotation curve of the Galaxy give us estimates just of the rotation function defined as $\Omega(x) = V(x)/x - V, \quad x = R/R_\odot$, $V(x)$ is the circular velocity function. Data on the peculiar velocity dispersion as a function of z allows to estimate the vertical acceleration $K_z(z)$. *GP* C is a slope of this curve at $z = 0$. R, z are cylindrical coordinates. Two model functions $g_8(\mathbf{P}, x)$ and $g_9(\mathbf{P}, z)$ correspond to $\Omega(x)$ and $K_z(z)$ respectively.

Observational estimates of *GPs* lie within *initial intervals* with assumed limits. We ascribe the weight w_i to the *i-th* interval which is inversely proportional to the square of its width. Now we can describe the agreement of the model with observational data by the value of the functional

$$F(\mathbf{P}, \mathbf{Y}, \Omega, K_z) = W_1 \sum_{i=1}^{k} w_i [1 - g_i(\mathbf{P})/y_i]^2 +$$

L. Blitz and P. Teuben (eds.), Unsolved Problems of the Milky Way, 713–714.
© 1996 *International Astronomical Union.*

$$+\frac{W_2}{d_2-c_2}\int_{c_2}^{d_2} w_2(x)[1-g_{k+1}(\mathbf{P},x)/\Omega(x)]^2dx+$$

$$+\frac{W_3}{d_3-c_3}\int_{c_3}^{d_3} w_3(z)[1-g_{k+2}(\mathbf{P},z)/K_z(z)]^2dz.$$

W_l are group weights given arbitrarily, $[c_l,\ d_l]$ are the ranges of corresponding functions. Weight functions $w_2(x)$, $w_3(z)$ are calculated similar to w_i. The best agreement is obtained by minimizing F with respect to $\mathbf{P}$ taking into account the constraints on *MPs*. Such a problem refers to the constrained nonlinear programming. The solution depends on assumed values of $\mathbf{Y}, \Omega, K_z$. Taking the centres of the intervals we obtain *the central solution*. Let us vary the selected *GP* or all the values of one function at once taking in turn the values of left and right limits. It gives *separate intervals*. On their basis we construct *united intervals* which include all separate ones.

We take the initial intervals of *GPs* so that they would include most of the known observational estimates of *GPs* being narrow enough. The separate intervals of *GPs* have been calculated for three variants: 1 – equipartition of *GPs* and two functions, 2 and 3 – without data on vertical acceleration and on rotation respectively. We conclude that the own variation of *GPs* have the greatest effect on the separate intervals. The separate intervals do not extend very much beyond the initial ones. The exception occurs for *GP* m in the case of variants 1 and 2 only. It means that the rotation data do not allow high value of the central parsec mass.

United intervals of the function $V(x)$ are caused most frequently by variation of *GP* M for the central part, but they are caused exclusively by variation of *GP* V for $x > 0.2$. The model circular velocity has two maxima and is flat enough outside the solar circle. United intervals of the function $K_z(z)$ are caused by variations of the acceleration itself. They coincide with the initial intervals quite satisfactorily.

So, after all the *MPs* have been estimated, and the model can be used for calculation of galactic orbits as the potential has relatively simple analytical expression.

References

Kutuzov, S.A. (1988) *Kin. i fiz. neb. tel*, 4, p. 39.
Kutuzov, S.A. and Ossipkov, L.P. (1989) *Astron. Zhurn.*, 66, p. 965.

SUBJECT INDEX

INDEX

α-elements 370
2MASS 47, 416
3-kpc arm 297

A-F-supergiants 703
accretion disk 176, 201
  fossil 175
active galactic nuclei 176
  jets 177
  UV-bump 177
AGB 15, 406, 412
age
  halo 354
age-velocity relation 433, 514, 518
age spread 377
AGN 181
Allen, David 205
aluminum 437
angular momentum transfer 87, 518
anticenter 681
Apache Point Observatory 47
arm-interarm contrast 502
ASCA 287, 628
asymmetric drift 34
asymmetry 86
axial symmetry 32
axisymmetric Jeans instability 31

Baade's window 129, 320, 405
background radio emission 615
bar 12, 32, 53, 71, 79, 93, 103, 125, 145, 147, 297, 316
  inclination 107
  potential 147
  structure 107
  viewing angle 145
basis sets 509
bending instability 32, 88
BICE 497
binary stars 531
black holes 219, 253
  binary 285
  starvation diet 178
  supermassive 169, 178
Bondi-Hoyle accretion 174
broadline clumps 314
buckling 73
bulge 42, 71, 85, 94, 103, 111, 119, 129, 329, 341, 411, 425, 429
  box-peanut 140
  boxy 73
  formation 32, 89, 403
  microlensing 93
  peanut-shaped 73

carbon stars 13, 638
CCD photometry 94
Cepheids 15, 638, 639
chaotic scenario 371
chemical inhomogeneities 373
chemo-dynamical evolution 389
chemo-dynamical model 396, 425, 429
CI 283, 469
C II 497
cloud
  filling factor 556
  formation 551
  stability 609
cluster 279
clustering

hierarchical 3
CO 297
luminosity 564
CO (J=1-0)
Columbia survey 501
CO (J=2-1)
Tokyo-NRO survey 501
COBE 51, 61
FIRAS 567
collisions
GMC 190
stellar 216
color-magnitude diagram 60, 93, 104, 112, 318
Compton Observatory 437
COMTEL 62
corotation radius 83
correlation function of intensity 615
corrugations 31, 59
cosmic rays 437
cosmic strings 257
CS (J=2-1) 265
CSHELL 112
cyclones 597

dark corona 645
dark halo 24, 651
formation 24
rotation of 6
scale-free model of 5
shape 24
dark matter 93, 575, 652
DENIS 47, 416
density waves 502, 517, 519, 521
m=1 138
differential metallicity distribution 400
diffusion of stellar orbits 431
DIRBE 51, 61
disk 52, 398, 681
asymmetry 12
dark matter 651
edge 681
ellipticity 1
evolution 681
heating 513
hot 33
lop-sided 6
mass 499
scale height 35
stability 349, 519, 521
stars 97
warp of 7
dissipationless collapse 24, 423, 676
dissipative collapse 368
distribution function 33, 351, 424
dust emission 231, 567
dwarf galaxy 98
dynamical friction 515
dynamics 79

edge-on galaxies 147
EGRET 170
electron Lorentz factor 174, 177
electrons
injection 177
secondaries 177
elliptical galaxies 32, 425
ellipticities
apparent 6
epicycle approximation 3
evolutionary processes 79
expanding molecular ring 297

F-G-dwarfs 389
Faraday rotation 271
filaments 247, 314
fine structure 613
Fokker-Planck 217
forbidden region 119

G-dwarf
distribution 400
problem 375
galactic

background 613
bar 107
center 79, 199, 205, 285, 311
"arc" 203, 263
"bridge" 203
accretion rate 174
black hole 169
mini-spiral 241
molecular clouds 282
constants 633, 707, 709
coordinates 178
dynamics 125
fine structure 611
model 681, 707, 713
potential 697
galaxies
stellar halos 39
surface photometry 39
galaxy 103
formation 1, 381, 423
inside out 376
gamma rays 437
GC 170
gas 79
dynamical simulations 145
inflow 88
kinematics 80
globular clusters 43, 99, 381, 403, 523, 524, 669, 697
age 355
proper motions 697
gravitational
focusing 220
instabilities 557
microlensing 93, 103
slingshot 527

H_2 283
CI 469
torus 285
hadronic cascades 177
halo 52, 437
elliptical 12
flattening 43
triaxial 11
heavy halo
shape of 1
He I stars 181
HI 82, 297
inner galaxy 145
scale height 479
survey 447
terminal curve 85
high-velocity clouds 605
high-velocity stars 523, 524
HII regions 689
Hipparcos 513, 525, 691
horizontal branch 368
HST 405, 605
hydro-dynamical simulations 82, 145, 147

infrared 59, 205, 232
inside out galaxy formation 376
interstellar
bubbles 618, 620
medium 613
scattering 194
turbulence 558
interval method 713
ionized
gas 613
medium 437
IRAS point sources 75, 411
iron abundance 397, 429
IRS 112
IRTF 112
ISO 628
isophote twists 6

Jeans equation 652
jets
GC spur 180
nozzle 176

K-giants 15, 329, 426, 429
Kapteyn, J.C. ix
kinematic principal axes 7
kinematics 73, 329, 341
  Baade's Window 128
  bulge 331
  Miras 411
  OH/IR stars 345
  stellar 11

Lindblad
  local expanding ring 584
  resonances 73, 83, 139, 516
local
  escape velocity 647
  mass density 499, 654
  standard of rest 119
local bubble 482
local velocity field 130
long-lived bend 36
longitude-velocity diagram 145, 147
LSR velocity 12, 600, 635, 690

M-giants 112, 347, 411
machos 656
macroscopic thermal instability 556
magnetic field 247, 263, 271, 595, 609, 615
  reconnection 254, 256, 263
maser
  H_2O 343
  SiO 119
mass 651
  distribution 697
  spectrum 565
mass-loss rates 411
massive stars 437
maximum likelihood 19
mergers
  black holes 286
  galaxies 2, 285, 358, 686
  satellite systems 408
  stars 163, 216, 279, 325
metallicity 329
  gradient 330, 368
  structure 427
microlensing 93
Milky Way 125, 341
  bulge 42
mini-spiral 241
minicavity 153
mira variable 15, 323, 333, 347, 411
model
  Kuijken and Tremaine 635
molecular
  clouds 275, 282, 437, 521
  clumps 257, 263
  gas 82, 501
    cold 575, 607
  mass 607
  ring 86, 147
  spurs 314
molecular clouds 561
monoenergetic electrons
  synchrotron emission 172
MOST 611
moving groups 513

N-body simulation 10, 32, 125, 395, 423, 676
N-body simulations 516
near-infrared
  maps 75
  photometry 80
neutral gas 613
non-circular motions 145
NTT 405
nuclear disk 119, 297, 312

OB stars 689
Ofpe/WN9 stars 226
OGLE 55, 93, 103
OH 297, 311
OH/IR stars 15, 76, 271, 285, 320, 345

link PNe 511
Oort constants 634
Oort, J.H. ix
open clusters 435, 523
orbital diffusion 372
orbit crowding 556
orbits
closed 82
closed loop 24
cusped 83
galactic 523
stochastic 5
OSIRIS 112
outer galaxy 561, 607, 669
overabundant 376
oxygen gradient 398

p-v diagrams 147
parallelogram 84
parameters
galactic model 713
pattern speed 11, 12, 14, 147
peanut bulges 88
peanut shaped 508
periodic orbits 58, 82, 135, 419, 508, 529
periodic variable stars 98
photodissociation 469
photoionization 613
pion-decay 177
planetary nebula 15, 511, 524
polar ring galaxy 24, 656
polar rings 140
Population II 24
potential-density pairs 509
proper motion 689
proton-proton collisions 177

quadratic programming 512
quasars
radio loud & radio weak 177

radial
velocity 119
velocity dispersion 34
radio jets 176
red clump stars 99, 103, 104, 105, 107
reddening 59
red giant clump stars 435
regular magnetic field 615
retrograde orbits 367
rings 139, 551
ROSAT 627
rotation curve 119, 297, 667, 689, 703
kink 505
rotation measure 271
RR Lyrae 98, 332, 361, 524, 674
Rybicki disk model 33

scale height
CO 502
HI 479
Miras 411
scattering 271
scatter of stellar metallicities 431
SDSS 47
SEST 282
Seyfert galaxies 180, 185, 189, 292
Sgr A* 169, 181, 193, 271, 285
accretion disk 175, 176
accretion rate 174, 175
bremsstrahlung 202
jet 176, 202
luminosity 170
mass 173, 174
proper motion 196
radio spectrum 169, 177, 199
source size 171, 173
spherical accretion 202
synchrotron radiation
optically thick 202
optically thin 199
variability 201

wind accretion 174
X-rays 170
shells 551
shock-acceleration
protons 178
simulations
of galaxy formation 3
SiO 119
SiO maser 333, 341
software
DoPhot 94
HRD-GST 319
MOSAIC 232
WIDTH6 389
solar neighbourhood 369
SPH 425
spherical accretion 174
spiral arms 1, 7, 59, 505
molecular 502
spiral galaxies
apparent ellipticities of 1
spiral structure 519, 521
secular evolution 517
stability 519
criterion 31
disk 349
Stäckel potentials 4
standard candle 15
star
clusters 539
counts 40, 59, 652
formation 534
GMC 583
inner disk 87
massive 205
starburst 189, 205, 279, 554
stars 651
atmospheres 279
evolution 279
starvation diet
black holes 178
stellar
collisions 216
disk shapes 24
metallicity distribution 395
populations 73, 317
structure function of intensity 615
sulfur 613
superbubble 625
superclouds 557
supernovae 625
supernova remnants 611, 613, 627
supershell 621, 625
surface density 34
SX Phenicis stars 98
synchrotron
self-absorption 172
synchrotron emission
monoenergetic electrons 172

tangent point analysis 499
thick disk 681
thickening mechanism 32
thickness of the plane 35
thick spirals 508
TIGER 138
tilt
nuclear disk 297
rotation axis 119
titanium 437
Toomre 31
Q 516
triaxiality 57, 64, 79
triple stars 527, 531
truncated disk 34
Tully–Fisher relation 1, 7
turbulence 271, 481, 591

variable stars 93
miras 404
RR Lyrae 403
velocity
dispersion 372, 423, 433, 512, 513
ellipsoid 525

velocity field
    galactic internal 7
    local 130
    residual 525, 597
vertex deviation 131, 513, 525
vertical distribution of HI 499
vertical velocity dispersion 35
violent relaxation 2, 369
VLA 272, 343, 580

warps 7, 58, 59, 140, 676
WN stars 225
WR stars 226, 279, 618, 620
WSRT 260, 606

X-ray emission 628
X factor 563, 608

young stellar objects 627

OBJECT INDEX

INDEX

0727-115 579
2013+370 577
3C418 577
47 Tuc 99, 356, 405

A0136-0801 27
AM-2 435
Arp 2 356

Cepheus 623
complex A 605

G0.08+0.15 249
G0.18-0.04 265
G317.5+0.0 611
G359.5+0.18 274
G359.54+0.18 248
G359.96+0.09 248
G54.4-0.3 627
GS64-01-97 621

HD 192163 617

IC 1396 623
IC 2006 7, 29
IC 342 139
IRS 16 181, 205, 225

Leo I 649

M0.20-0.033 265
M 101 138
M 22 330
M 31 39, 138, 165, 406, 649
M 32 351, 406
M 33 138
M 51 139
M 82 139
M 83 20
M 87 165
M 94 82, 143
Maffei 2 139

NGC 288 356
NGC 309 148
NGC 362 356
NGC 628 595
NGC 660 137, 139
NGC 720 26
NGC 891 42, 137, 139, 148, 339
NGC 1058 491, 595
NGC 1068 139
NGC 1097 137, 139
NGC 1365 20
NGC 1808 137, 139
NGC 2808 355
NGC 3079 137, 139
NGC 3115 164
NGC 3351 139
NGC 4314 139
NGC 4321 20, 134, 137, 139
NGC 4442 73
NGC 4535 14
NGC 4565 42, 88
NGC 4595 165
NGC 4650A 7, 27, 656
NGC 4945 137, 139
NGC 5236 139
NGC 5474 491
NGC 5746 73
NGC 5907 508
NGC 5927 359
NGC 5965 73
NGC 6352 359

NGC 6528 405
NGC 6553 405
NGC 6723 359
NGC 6888 617
NGC 6946 137, 139
NGC 7129 623
NGC 7479 134
NGC 7814 43

Omega Cen 99
Orion complex 437
Orion nebula 629

Pal 12 356
PG 0859+596 605
PG 0906+597 605
PG 1351+640 605

Ru 106 356

S 140 623
Sagittarius 99
Sagittarius arm 502
Sculptor 98
Scutum arm 502
Sgr C 248

Terzan 7 356

UGC 7576 27

WR 136 617
WR 149 619